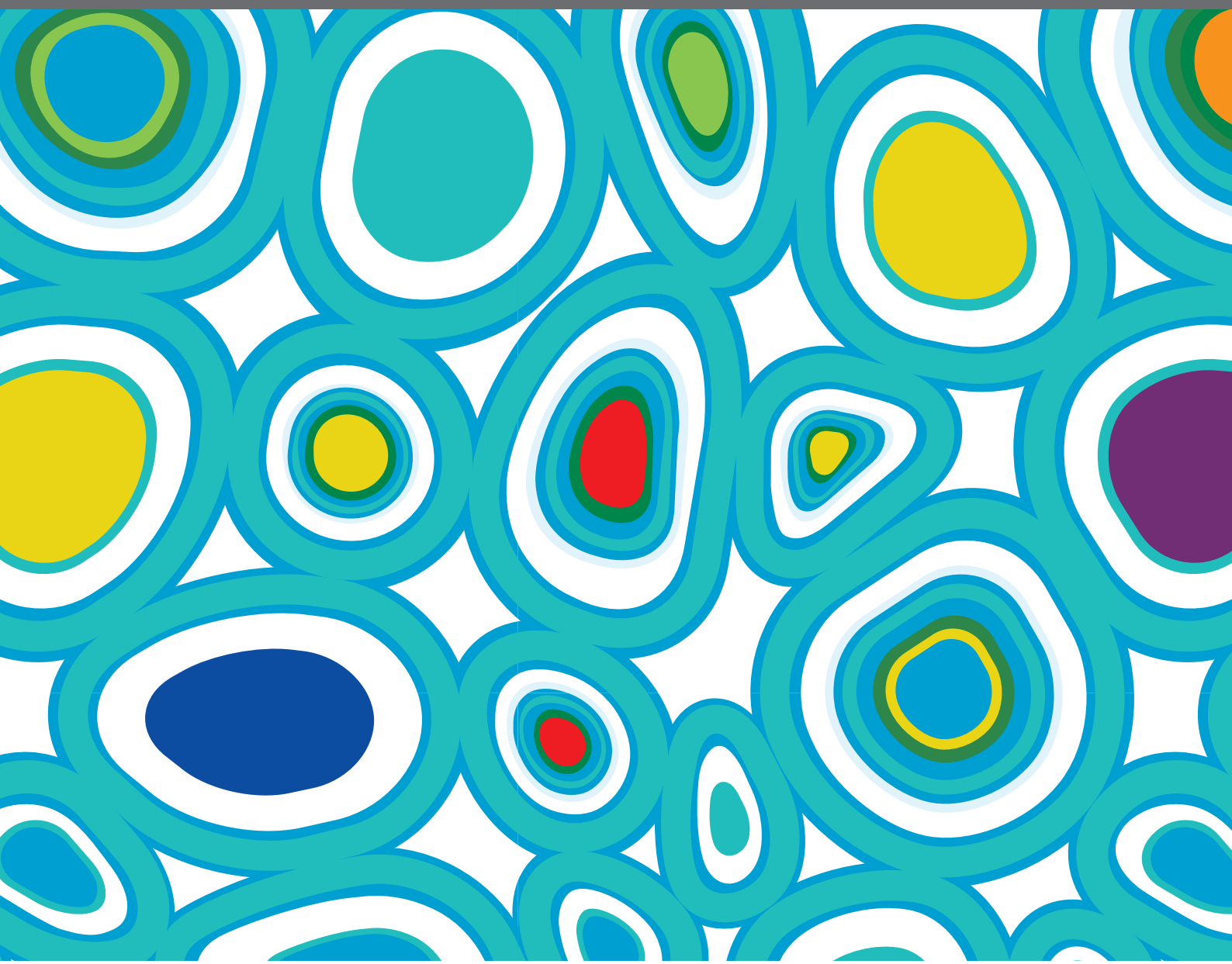
NOVEL THERAPIES FOR COMBATING BONE DISEASES THROUGH ADVANCES IN BONE REMODELING

EDITED BY: Chao Liang, Jiake Xu and Changjun Li
PUBLISHED IN: Frontiers in Cell and Developmental Biology



frontiers Research Topics

Frontiers eBook Copyright Statement

The copyright in the text of individual articles in this eBook is the property of their respective authors or their respective institutions or funders. The copyright in graphics and images within each article may be subject to copyright of other parties. In both cases this is subject to a license granted to Frontiers.

The compilation of articles constituting this eBook is the property of Frontiers.

Each article within this eBook, and the eBook itself, are published under the most recent version of the Creative Commons CC-BY licence. The version current at the date of publication of this eBook is CC-BY 4.0. If the CC-BY licence is updated, the licence granted by Frontiers is automatically updated to the new version.

When exercising any right under the CC-BY licence, Frontiers must be attributed as the original publisher of the article or eBook, as applicable.

Authors have the responsibility of ensuring that any graphics or other materials which are the property of others may be included in the CC-BY licence, but this should be checked before relying on the CC-BY licence to reproduce those materials. Any copyright notices relating to those materials must be complied with.

Copyright and source acknowledgement notices may not be removed and must be displayed in any copy, derivative work or partial copy which includes the elements in question.

All copyright, and all rights therein, are protected by national and international copyright laws. The above represents a summary only. For further information please read Frontiers' Conditions for Website Use and Copyright Statement, and the applicable CC-BY licence.

ISSN 1664-8714
ISBN 978-2-88971-827-6
DOI 10.3389/978-2-88971-827-6

About Frontiers

Frontiers is more than just an open-access publisher of scholarly articles: it is a pioneering approach to the world of academia, radically improving the way scholarly research is managed. The grand vision of Frontiers is a world where all people have an equal opportunity to seek, share and generate knowledge. Frontiers provides immediate and permanent online open access to all its publications, but this alone is not enough to realize our grand goals.

Frontiers Journal Series

The Frontiers Journal Series is a multi-tier and interdisciplinary set of open-access, online journals, promising a paradigm shift from the current review, selection and dissemination processes in academic publishing. All Frontiers journals are driven by researchers for researchers; therefore, they constitute a service to the scholarly community. At the same time, the Frontiers Journal Series operates on a revolutionary invention, the tiered publishing system, initially addressing specific communities of scholars, and gradually climbing up to broader public understanding, thus serving the interests of the lay society, too.

Dedication to Quality

Each Frontiers article is a landmark of the highest quality, thanks to genuinely collaborative interactions between authors and review editors, who include some of the world's best academicians. Research must be certified by peers before entering a stream of knowledge that may eventually reach the public - and shape society; therefore, Frontiers only applies the most rigorous and unbiased reviews.
Frontiers revolutionizes research publishing by freely delivering the most outstanding research, evaluated with no bias from both the academic and social point of view. By applying the most advanced information technologies, Frontiers is catapulting scholarly publishing into a new generation.

What are Frontiers Research Topics?

Frontiers Research Topics are very popular trademarks of the Frontiers Journals Series: they are collections of at least ten articles, all centered on a particular subject. With their unique mix of varied contributions from Original Research to Review Articles, Frontiers Research Topics unify the most influential researchers, the latest key findings and historical advances in a hot research area! Find out more on how to host your own Frontiers Research Topic or contribute to one as an author by contacting the Frontiers Editorial Office: frontiersin.org/about/contact

NOVEL THERAPIES FOR COMBATING BONE DISEASES THROUGH ADVANCES IN BONE REMODELING

Topic Editors:
Chao Liang, Hong Kong Baptist University, SAR China
Jiake Xu, University of Western Australia, Australia
Changjun Li, Central South University, China

Citation: Liang, C., Xu, J., Li, C., eds. (2021). Novel Therapies for Combating Bone Diseases Through Advances in Bone Remodeling. Lausanne: Frontiers Media SA. doi: 10.3389/978-2-88971-827-6

Table of Contents

07 ***Editorial: Novel Therapies for Combating Bone Diseases Through Advances in Bone Remodeling***
Yurui Jiao, Jiake Xu, Chao Liang and Changjun Li

10 ***Sclerostin and Its Associations With Bone Metabolism Markers and Sex Hormones in Healthy Community-Dwelling Elderly Individuals and Adolescents***
Yang Xu, Chao Gao, Jinwei He, Wenqin Gu, Chuntao Yi, Bihua Chen, Qingqing Wang, Feng Tang, Juliang Xu, Hua Yue and Zhenlin Zhang

17 ***RANKL/RANK System-Based Mechanism for Breast Cancer Bone Metastasis and Related Therapeutic Strategies***
Xiaoqiu Wu, Fangfei Li, Lei Dang, Chao Liang, Aiping Lu and Ge Zhang

31 ***Moderate Fluid Shear Stress Regulates Heme Oxygenase-1 Expression to Promote Autophagy and ECM Homeostasis in the Nucleus Pulposus Cells***
Sheng Chen, Lei Qin, Xiaohao Wu, Xuekun Fu, Sixiong Lin, Di Chen, Guozhi Xiao, Zengwu Shao and Huiling Cao

45 ***Human Umbilical Mesenchymal Stem Cells Display Therapeutic Potential in Rheumatoid Arthritis by Regulating Interactions Between Immunity and Gut Microbiota* via *the Aryl Hydrocarbon Receptor***
Xiaoya Li, Cheng Lu, Danping Fan, Xiangchen Lu, Ya Xia, Hongyan Zhao, Huihui Xu, Yongliang Zhu, Jingtao Li, Honglin Liu and Cheng Xiao

64 ***The Role of Bone-Derived Exosomes in Regulating Skeletal Metabolism and Extraosseous Diseases***
Huili Lyu, Ye Xiao, Qi Guo, Yan Huang and Xianghang Luo

81 ***Pros and Cons of Denosumab Treatment for Osteoporosis and Implication for RANKL Aptamer Therapy***
Ning Zhang, Zong-Kang Zhang, Yuanyuan Yu, Zhenjian Zhuo, Ge Zhang and Bao-Ting Zhang

90 ***Positive Effect of Gushukang on Type-H Vessel and Bone Formation***
Wantao Li, Xiaoqing Zhou, Tiejian Jiang, Hongbo He and Ting Wen

99 ***Cathepsin K: The Action in and Beyond Bone***
Rongchen Dai, Zeting Wu, Hang Yin Chu, Jun Lu, Aiping Lyu, Jin Liu and Ge Zhang

112 ***Conditional Knockout of PKC-δ in Osteoclasts Favors Bone Mass Accrual in Males Due to Decreased Osteoclast Function***
Shangfu Li, Tianwei He, Depeng Wu, Liangming Zhang, Ruiqiang Chen, Bin Liu, Jinbo Yuan, Jennifer Tickner, An Qin, Jiake Xu and Limin Rong

127 ***Functions and Clinical Significance of Super-Enhancers in Bone-Related Diseases***
Jian Qu, Zhanbo Ouyang, Wenqiang Wu, Guohua Li, Jiaojiao Wang, Qiong Lu and Zhihong Li

139 ***SLIT2 Overexpression in Periodontitis Intensifies Inflammation and Alveolar Bone Loss, Possibly via the Activation of MAPK Pathway***
Liping Wang, Jing Zheng, Janak L. Pathak, Yunxin Chen, Dongliang Liang, Luxi Yang, Haobo Sun, Mei Zhong, Lihong Wu, Li Li, Shuhua Deng, Lingyun Zheng, Yongyong Yan, Dan Hou, Lijing Wang and Linhu Ge

155 ***The Application of MSCs-Derived Extracellular Vesicles in Bone Disorders: Novel Cell-Free Therapeutic Strategy***
Shuyu Liu, Xia Xu, Shujing Liang, Zhihao Chen, Yan Zhang, Airong Qian and Lifang Hu

172 ***Multifaceted Functions and Novel Insight Into the Regulatory Role of RNA N^6-Methyladenosine Modification in Musculoskeletal Disorders***
Wenchao Zhang, Lile He, Zhongyue Liu, Xiaolei Ren, Lin Qi, Lu Wan, Wanchun Wang, Chao Tu and Zhihong Li

186 **ASPH** ***Regulates Osteogenic Differentiation and Cellular Senescence of BMSCs***
Hui Peng, Qi Guo, Ye Xiao, Tian Su, Tie-Jian Jiang, Li-Juan Guo and Min Wang

199 ***Disorders of Calcium and Phosphorus Metabolism and the Proteomics/Metabolomics-Based Research***
Meiheng Sun, Xiaoqiu Wu, Yuanyuan Yu, Luyao Wang, Duoli Xie, Zhenlin Zhang, Lin Chen, Aiping Lu, Ge Zhang and Fangfei Li

212 ***Yes-Associated Protein 1: Role and Treatment Prospects in Orthopedic Degenerative Diseases***
Wenqing Xie, Wenfeng Xiao, Kun Tang, Liyang Zhang and Yusheng Li

225 ***CircCOG8 Downregulation Contributes to the Compression-Induced Intervertebral Disk Degeneration by Targeting miR-182-5p and FOXO3***
Qian Xiang, Liang Kang, Kangcheng Zhao, Juntan Wang, Wenbin Hua, Yu Song, Xiaobo Feng, Gaocai Li, Saideng Lu, Kun Wang, Cao Yang and Yukun Zhang

241 ***Construction of a Five-Super-Enhancer-Associated-Genes Prognostic Model for Osteosarcoma Patients***
Zhanbo Ouyang, Guohua Li, Haihong Zhu, Jiaojiao Wang, Tingting Qi, Qiang Qu, Chao Tu, Jian Qu and Qiong Lu

254 ***Corrigendum: Construction of a Five-Super-Enhancer-Associated-Genes Prognostic Model for Osteosarcoma Patients***
Zhanbo Ouyang, Guohua Li, Haihong Zhu, Jiaojiao Wang, Tingting Qi, Qiang Qu, Chao Tu, Jian Qu and Qiong Lu

255 ***miR-129-5p Inhibits Bone Formation Through TCF4***
Chong Yin, Ye Tian, Yang Yu, Chaofei Yang, Peihong Su, Yipu Zhao, Xue Wang, Kewen Zhang, Jiawei Pei, Dijie Li, Zhihao Chen, Yan Zhang, Zhiping Miao and Airong Qian

270 ***A Novel Variant in*** **CLCN7** ***Regulates the Coupling of Angiogenesis and Osteogenesis***
Hui Peng, Hong-Bo He and Ting Wen

281 ***Roles of MicroRNAs in Bone Destruction of Rheumatoid Arthritis***
Hanxiao Zhao, Aiping Lu and Xiaojuan He

290 ***Medium-Intensity Treadmill Exercise Exerts Beneficial Effects on Bone Modeling Through Bone Marrow Mesenchymal Stromal Cells***
Lingli Zhang, Yu Yuan, Wei Wu, Zhongguang Sun, Le Lei, Jing Fan, Bo Gao and Jun Zou

303 ***BMSC-Derived Exosomal miR-29a Promotes Angiogenesis and Osteogenesis***
Guo-dong Lu, Peng Cheng, Ting Liu and Zhong Wang

313 ***Bone and Muscle Crosstalk in Aging***
Chen He, Wenzhen He, Jing Hou, Kaixuan Chen, Mei Huang, Mi Yang, Xianghang Luo and Changjun Li

333 ***Recent Advances of Osterix Transcription Factor in Osteoblast Differentiation and Bone Formation***
Qian Liu, Mao Li, Shiyi Wang, Zhousheng Xiao, Yuanyuan Xiong and Guangwei Wang

348 ***Antenatal Corticosteroid Therapy Attenuates Angiogenesis Through Inhibiting Osteoclastogenesis in Young Mice***
Yu Chai, Jianwen Su, Weisheng Hong, Runjiu Zhu, Caiyu Cheng, Lei Wang, Xianrong Zhang and Bin Yu

359 ***Obesity and Bone Health: A Complex Link***
Jing Hou, Chen He, Wenzhen He, Mi Yang, Xianghang Luo and Changjun Li

375 ***Communications Between Bone Marrow Macrophages and Bone Cells in Bone Remodeling***
Kaixuan Chen, Yurui Jiao, Ling Liu, Mei Huang, Chen He, Wenzhen He, Jing Hou, Mi Yang, Xianghang Luo and Changjun Li

390 ***Subchondral Bone Remodeling: A Therapeutic Target for Osteoarthritis***
Xiaobo Zhu, Yau Tsz Chan, Patrick S. H. Yung, Rocky S. Tuan and Yangzi Jiang

409 ***Regulatory Role of the RNA N^6-Methyladenosine Modification in Immunoregulatory Cells and Immune-Related Bone Homeostasis Associated With Rheumatoid Arthritis***
Danping Fan, Ya Xia, Cheng Lu, Qinbin Ye, Xiaoyu Xi, Qiong Wang, Zheng Wang, Chengyuan Wang and Cheng Xiao

423 ***Low Dose BMP2-Doped Calcium Phosphate Graft Promotes Bone Defect Healing in a Large Animal Model***
Tie Liu, Wen Fang, Gang Wu, Yining Li, Janak L. Pathak and Yuelian Liu

436 ***Downregulation of Macrophage-Specific Act-1 Intensifies Periodontitis and Alveolar Bone Loss Possibly via TNF/NF-κB Signaling***
Janak L. Pathak, Ying Fang, Yunxin Chen, Zhitong Ye, Xueqi Guo, Yongyong Yan, Jun Zha, Dongliang Liang, Xiuxian Ke, Luxi Yang, Wenchao Zhong, Lijing Wang and Liping Wang

452 ***Src Homology 2 Domain-Containing Protein Tyrosine Phosphatase Promotes Inflammation and Accelerates Osteoarthritis by Activating β-Catenin***
Tenghui Tao, Danni Luo, Chenghao Gao, Hui Liu, Zehua Lei, Wenbin Liu, Chuankun Zhou, Dahu Qi, Zhenhan Deng, Xuying Sun and Jun Xiao

467 ***CGRP Regulates the Age-Related Switch Between Osteoblast and Adipocyte Differentiation***
Hang Li, Jian Qu, Haihong Zhu, Jiaojiao Wang, Hao He, Xinyan Xie, Ren Wu and Qiong Lu

478 ***Corrigendum: CGRP Regulates the Age-Related Switch Between Osteoblast and Adipocyte Differentiation***
Hang Li, Jian Qu, Haihong Zhu, Jiaojiao Wang, Hao He, Xinyan Xie, Ren Wu and Qiong Lu

479 ***Bone-Derived Modulators That Regulate Brain Function: Emerging Therapeutic Targets for Neurological Disorders***
Hongzhen Chen, Dewei Shang, Yuguan Wen and Chao Liang

frontiers in Cell and Developmental Biology

EDITORIAL
published: 14 October 2021
doi: 10.3389/fcell.2021.766963

Editorial: Novel Therapies for Combating Bone Diseases Through Advances in Bone Remodeling

Yurui Jiao [1], Jiake Xu [2], Chao Liang [3,4]* and Changjun Li [1]**

[1] Department of Endocrinology, Endocrinology Research Center, Xiangya Hospital, Central South University, Changsha, China, [2] School of Biomedical Sciences, The University of Western Australia, Perth, WA, Australia, [3] School of Chinese Medicine, Law Sau Fai Institute for Advancing Translational Medicine in Bone and Joint Diseases, Hong Kong Baptist University, Hong Kong, Hong Kong, SAR China, [4] Department of Biology, Southern University of Science and Technology, Shenzhen, China

Keywords: bone diseases, bone remodeling, bone cells, molecular targets, translational medicine

Editorial on the Research Topic

Novel Therapies for Combating Bone Diseases Through Advances in Bone Remodeling

OPEN ACCESS

Edited and reviewed by:
Ramani Ramchandran, Medical College of Wisconsin, United States

***Correspondence:**
Changjun Li
lichangjun@csu.edu.cn
Jiake Xu
jiake.xu@uwa.edu.au
Chao Liang
liangchao512@163.com

Specialty section:
This article was submitted to Molecular and Cellular Pathology, a section of the journal Frontiers in Cell and Developmental Biology

Received: *30 August 2021*
Accepted: *21 September 2021*
Published: *14 October 2021*

Citation:
Jiao Y, Xu J, Liang C and Li C (2021) Editorial: Novel Therapies for Combating Bone Diseases Through Advances in Bone Remodeling. Front. Cell Dev. Biol. 9:766963. doi: 10.3389/fcell.2021.766963

Bone is a metabolically active organ that undergoes a constant and continuous state of remodeling throughout life, which is important for the maintenance of normal skeletal structure and function (Salhotra et al., 2020). The coordinated action between bone cells, which are composed of osteoblasts, osteoclasts, and osteocytes, is known as bone remodeling, and the imbalance between the functioning of these cells leads to bone diseases such as osteoporosis, osteoarthritis, rheumatoid arthritis, and bone tumors (Kular et al., 2012; Chen et al.). Bone marrow mesenchymal stem cells (BMSCs), bone-derived exosomes, and microRNAs (miRNAs), which are involved in the regulation of skeletal metabolism, bone remodeling, and bone diseases, have been the current focus of research in the world (Mori et al., 2019; Kalluri and LeBleu, 2020). In recent years, an increasing number of studies were enriched in the area of bone remodeling by researchers, and the most results were encouraging (Li et al., 2015, 2018). These developments, which will provide theoretical advances on bone remodeling and have a growing impact on the treatment of bone diseases in the coming years.

This editorial paper collects 9 publications aimed to explore recent developments with a focus on identifying molecular mechanisms and targets in bone remodeling as well as new therapies for bone disease and associated complications.

BONE MARROW MESENCHYMAL STEM CELLS

BMSCs display increased adipogenic with age, along with decreased osteogenic differentiation capacity. Based on this theory, one study, Peng et al. identified a differentially expressed ASPH gene, which regulates Wnt signaling mediated by Gsk3β, in middle-aged and elderly aged groups. The depletion of mouse *Asph* suppressed the capacity of osteogenic differentiation and accelerated cellular senescence in BMSCs, while the overexpression of *Asph* enhanced the capacity of osteogenic differentiation and inhibited cellular senescence. Because of the abundant expression of ASPH in a variety of malignant tumors, ASPH has been thought to be a potential therapeutic target for different cancers. Thus, they suggested that the treatment of ASPH inhibitor in patients with cancers needs to be concerned because of their potential risks of bone loss or bone fracture.

In a second study, Li et al. explored the effect of calcitonin gene-related peptide (CGRP) on the osteogenic and adipogenic differentiation potential of BMSC. In this study, they indicated that CGRP promoted the osteogenic differentiation of BMSCs while inhibiting their adipogenic differentiation. Aged and ovariectomized mice treated with CGRP showed a substantial promotion of bone formation and a reduction in fat accumulation in the bone marrow. In another study, Xie et al. summarized the significance of Yes-associated protein 1 (YAP1) in orthopedic degenerative diseases. YAP1 can regulate the osteogenic differentiation of BMSCs, as well as the activity of osteoblasts and osteoclastogenesis. Therefore, the regulation of ASPH, CGRP, and YAP1 activity is expected to become a potential intervention strategy to delay the occurrence and development of skeletal degenerative diseases.

BONE-DERIVED EXOSOMES AND MIRNAS

Emerging numbers of studies have reported miRNAs as important regulators for bone metabolism. Yin et al. focused on the function and mechanism of miR-129-5p in bone metabolism recently and found that the expression of miR-129-5p was enhanced in both aging and menopause osteoporosis models. Overexpression and down-regulation of miR-129-5p respectively inhibited or enhanced osteoblasts differentiation and bone formation by regulating downstream transcription factors of the Wnt/β-catenin pathway through targeting *Tcf4*. Moreover, bioengineered novel recombinant miR-129-5p inhibitor showed a rescue effect on osteoporosis.

Bone-derived exosomes are involved in the regulation of skeletal metabolism, bone remodeling, and pathological processes through modulating intercellular communication and the transfer of materials (Zhu et al., 2018). The founding of Lu et al. suggested that BMSC-derived exosomal miR-29a regulates angiogenesis and osteogenesis, and miR-29a-loaded BMSCs-Exosomes may serve as a robust and potential therapeutic target for osteoporosis. Besides, Lyu et al. and Liu et al. reviewed the current knowledge of exosomes and highlight the application studies of bone-derived exosomes in bone remolding and bone disorders. They summarized the role of exosomes derived from BMSCs, osteoclasts, osteoblasts, and osteocytes in skeletal metabolism, including miR-27a, miR-206a, miR-196a, miR-214, miR-30d-5p, miR-133b-3p, miR-140-3p, miR-140-5p, miR-335-3p, miR-378b, miR-218, miR-1192, miR-680, miR-302a, miR-92a-3b, miR-135b, and miR-100-5p.

OSTEOCLASTS

The interaction of receptor activator of nuclear factor-kB ligand (RANKL) and its receptor RANK is one of the fundamentals in bone remodeling. The RANK/RANKL system is well-known for regulating bone turnover by promoting the differentiation and activation of osteoclasts and has been shown to be a novel effective therapeutic target for osteoporosis. Zhang et al. focused on and summarized the advantages and disadvantages of the use of denosumab, the anti-RANKL antibody, in the treatment of postmenopausal osteoporosis. Although denosumab decreases osteoclast-mediated bone resorption and turnover, adverse events have also been reported after treatment, including skin eczema, flatulence, cellulitis, and osteonecrosis of the jaw. Considering the potential side effects of long-term medication of denosumab, aptamer has shown advantages and low toxicity and was hypothesized to be a promising candidate for therapeutic drugs targeting RANKL to counteract osteoporosis. Therefore, the determination of the three-dimensional structure of the RANKL-aptamer complex is necessary to discover the accurate binding domains and could be a crucial research basis for a functional aptamer targeting RANKL for the treatment of osteoporosis.

Protein kinase C delta (PKC-δ) functions as an important regulator in bone metabolism. Rong et al. conducted an osteoclast-specific PKC-δ knockout mouse strain to explore the function of PKC-δ in osteoclast biology. They found that ablation of PKC-δ in osteoclasts resulted in an increased bone volume in male mice, accompanied by decreased Cathepsin-K protein levels, osteoclast number, osteoclast formation, and resorption, whereas these changes were not observed in female mice. The work of this study revealed a previously unknown target for the treatment of gender-related bone diseases. In these two studies, they summarized the significance of RANKL-aptamer and PKC-δ and discuss the potential therapeutic strategies of the targeted modulation of the RANK/RANKL system and PKC-δ for bone-related diseases.

Taken together, increasing regulators have been revealed to participate in bone remodeling, which facilitates the mechanistic understanding of bone diseases and associated complications caused by disruption of bone remodeling, and provides new strategies for the treatment of bone diseases.

AUTHOR CONTRIBUTIONS

All authors listed have made a substantial, direct and intellectual contribution to the work, and approved it for publication.

FUNDING

This work was supported by National Key R&D Program of China (Grant No. 2019YFA0111900), the National Natural Science Foundation of China (Grant Nos. 81922017, 81873669, 81802209, 81930022, 91749105, 81520108008, and 81873670), Hunan Provincial Science and Technology Department (2018RS3030), and the Australian National Health and Medical Research Council (NHMRC, APP1107828, APP1127156, and APP1163933).

ACKNOWLEDGMENTS

We thank the authors of the papers published in this Research Topic for their valuable contributions.

REFERENCES

Kalluri, R., and LeBleu, V. S. (2020). The biology, function, and biomedical applications of exosomes. *Science*. 367. doi: 10.1126/science.aau6977

Kular, J., Tickner, J., Chim, S. M., and Xu, J. (2012). An overview of the regulation of bone remodelling at the cellular level. *Clin. Biochem.* 45, 863–873. doi: 10.1016/j.clinbiochem.2012.03.021

Li, C. J., Cheng, P., Liang, M. K., Chen, Y. S., Lu, Q., Wang, J. Y., et al. (2015). MicroRNA-188 regulates age-related switch between osteoblast and adipocyte differentiation. *J. Clin. Invest.* 125, 1509–1522. doi: 10.1172/JCI77716

Li, C. J., Xiao, Y., Yang, M., Su, T., Sun, X., Guo, Q., et al. (2018). Long noncoding RNA Bmncr regulates mesenchymal stem cell fate during skeletal aging. *J. Clin. Invest.* 128, 5251–5266. doi: 10.1172/JCI99044

Mori, M. A., Ludwig, R. G., Garcia-Martin, R., Brandão, B. B., and Kahn, C. R. (2019). Extracellular miRNAs: From Biomarkers to Mediators of Physiology and Disease. *Cell Metab.* 30, 656–673. doi: 10.1016/j.cmet.2019.07.011

Salhotra, A., Shah, H. N., Levi, B., and Longaker, M. T. (2020). Mechanisms of bone development and repair. *Nat. Rev. Mol. Cell Biol.* 21, 696–711. doi: 10.1038/s41580-020-00279-w

Zhu, S., Yao, F., Qiu, H., Zhang, G., Xu, H., and Xu, J. (2018). Coupling factors and exosomal packaging microRNAs involved in the regulation of bone remodelling. *Biol. Rev. Camb. Philos. Soc.* 93, 469–480. doi: 10.1111/brv.12353

Conflict of Interest: The authors declare that the research was conducted in the absence of any commercial or financial relationships that could be construed as a potential conflict of interest.

Publisher's Note: All claims expressed in this article are solely those of the authors and do not necessarily represent those of their affiliated organizations, or those of the publisher, the editors and the reviewers. Any product that may be evaluated in this article, or claim that may be made by its manufacturer, is not guaranteed or endorsed by the publisher.

Copyright © 2021 Jiao, Xu, Liang and Li. This is an open-access article distributed under the terms of the Creative Commons Attribution License (CC BY). The use, distribution or reproduction in other forums is permitted, provided the original author(s) and the copyright owner(s) are credited and that the original publication in this journal is cited, in accordance with accepted academic practice. No use, distribution or reproduction is permitted which does not comply with these terms.

frontiers in Cell and Developmental Biology

ORIGINAL RESEARCH
published: 07 February 2020
doi: 10.3389/fcell.2020.00057

Sclerostin and Its Associations With Bone Metabolism Markers and Sex Hormones in Healthy Community-Dwelling Elderly Individuals and Adolescents

Yang Xu[1], Chao Gao[1], Jinwei He[1], Wenqin Gu[2], Chuntao Yi[2], Bihua Chen[3], Qingqing Wang[3], Feng Tang[4], Juliang Xu[4], Hua Yue[1] and Zhenlin Zhang[1]**

[1] Shanghai Clinical Research Center of Bone Disease, Department of Osteoporosis and Bone Diseases, Shanghai Jiao Tong University Affiliated Sixth People's Hospital, Shanghai, China, [2] Fenglin Community Health Service Center, Shanghai, China, [3] Longhua Community Health Service Center, Shanghai, China, [4] Qixian Community Health Service Center, Shanghai, China

OPEN ACCESS

Edited by:
Chao Liang,
Hong Kong Baptist University,
Hong Kong

Reviewed by:
Xiaoguang Cheng,
Beijing Jishuitan Hospital, China
Qun Cheng,
Fudan University, China

***Correspondence:**
Hua Yue
yueyinglonghua@163.com
Zhenlin Zhang
zhangzl@sjtu.edu.cn

Specialty section:
This article was submitted to Molecular Medicine, a section of the journal Frontiers in Cell and Developmental Biology

Received: 05 November 2019
Accepted: 22 January 2020
Published: 07 February 2020

Citation:
Xu Y, Gao C, He J, Gu W, Yi C, Chen B, Wang Q, Tang F, Xu J, Yue H and Zhang Z (2020) Sclerostin and Its Associations With Bone Metabolism Markers and Sex Hormones in Healthy Community-Dwelling Elderly Individuals and Adolescents. Front. Cell Dev. Biol. 8:57. doi: 10.3389/fcell.2020.00057

Sclerostin is an important regulator of bone mass involving Wnt/β-catenin signaling pathway. We aimed to obtain the profile of serum sclerostin level and explore its associations with bone metabolism markers and sex hormones in healthy community-dwelling Chinese elderly individuals and adolescents. A cross-sectional study was performed in three communities in Shanghai. In all, 861 participants, including 574 healthy elderly individuals, and 287 healthy adolescents, were recruited. The levels of serum sclerostin, procollagen type 1 N-terminal propeptide (P1NP), β-CrossLaps of type I collagen containing cross-linked C-telopeptide (β-CTX), parathyroid hormone (PTH), 25-hydroxyvitamin D [25(OH)D], estradiol (E_2), testosterone (T), and sex hormone-binding globulin (SHBG) were measured in blood samples from all participants. Median sclerostin level was higher in males than in females and in elderly individuals than in adolescents (elderly males: 54.89 pmol/L, elderly females: 39.95 pmol/L, adolescent males: 36.58 pmol/L, adolescent females: 27.06 pmol/L; both $P < 0.05$). In elderly individuals, serum sclerostin was positively correlated with age ($\beta = 0.176$, $P < 0.001$) and T ($\beta = 0.248$, $P = 0.001$), but negatively associated to P1NP ($\beta = -0.140$, $P = 0.001$). In adolescents, circulating sclerostin was significantly and positively associated with P1NP ($\beta = 0.192$, $P = 0.003$). The directions of the association between sclerostin and P1NP were opposite in Chinese elderly individuals and adolescents, which may reflect that sclerostin plays distinct roles in different functional states of the skeleton. Our findings revealed the rough profile of circulating sclerostin level in general healthy Chinese population and its associations with bone metabolism markers and sex hormones, which may provide a clue to further elucidate the cross action of sclerostin in bone metabolism and sexual development.

Keywords: sclerostin, bone metabolism markers, sex hormones, elderly individuals, adolescents, cross-sectional study

INTRODUCTION

Sclerostin, an osteocyte-derived Wnt antagonist, inhibits the Wnt/β-catenin signaling pathway and is regarded as the important regulator of bone mass (Van Bezooijen et al., 2004). Activation of the canonical Wnt/β-catenin signaling pathway leads to increased bone formation and bone mass through promoting the maturation of osteoblasts and inhibiting the differentiation of osteoclasts (Glass et al., 2005; Krishnan et al., 2006; Baron and Rawadi, 2007). The clinical importance of sclerostin was initially highlighted by sclerosteosis and van Buchem disease, two sclerosing bone disorders caused by loss-of-function mutations of the *SOST* gene (encoding sclerostin), and further proved by the phenotypical characterization of increased bone mass and bone formation in disease-related animal models (Li et al., 2008; Van Lierop et al., 2011, 2013; Boudin et al., 2017). Based on positive results of experiments in mice and human, two monoclonal antisclerostin antibodies, romosozumab and blosozumab, have been developed as new therapies for osteoporosis and their significant effects in increasing bone mineral density (BMD) and reducing fracture risks were demonstrated (McClung et al., 2014; Recknor et al., 2015; Cosman et al., 2016; Ominsky et al., 2017; Carpenter and Ross, 2019).

Although the biological roles of sclerostin and corresponding benefits of antisclerostin antibodies have been illuminated, much epidemiological data regarding serum sclerostin levels is still unclear. Most researches about sclerostin levels are focused on special groups, and there are few studies on general healthy people from communities (He et al., 2014; Faienza et al., 2017; Hansen et al., 2019; Pekkolay et al., 2019; Singh et al., 2019; Yang et al., 2019). The associations of serum sclerostin to bone metabolism markers in different population show inconsistent results, and only a few studies have been conducted to investigate relations of serum slcerostin to sex hormones (Garnero et al., 2013; Szulc et al., 2013; Yamamoto et al., 2013; Lim et al., 2016). Exploring circulating sclerostin level in healthy population and its association with bone metabolism markers and sex hormones may provide a better understanding into the nature of sclerostin, and elucidate the cross action of sclerostin in bone metabolism and sexual development.

In this cross-sectional study, we recruited community-dwelling elderly individuals and adolescents to acquire the profile of circulating sclerostin level in general healthy Chinese population, investigate the difference of slerostin levels between elderly individuals and adolescents, and explore the associations of serum sclerostin to bone metabolism markers and sex hormones.

MATERIALS AND METHODS

Subjects

This study was approved by the Ethics Committee of the Shanghai Jiao Tong University Affiliated Sixth People's Hospital. From July to September 2016, we recruited 1107 elderly individuals (aged 65–79 years; men: 365, women: 742) from three communities of Shanghai, i.e., Fenglin, Longhua, and Qixian. All participants were evaluated by a questionnaire, physical examination and routine serum measurements including hepatic and renal function. Only 1023 can complete the questionnaire and physical examination independently. Among the 1023 participants, subjects with the following conditions were excluded: (1) abnormal laboratory measurements, including serum creatinine (Cr), uric acid (UA), alkaline phosphatase (ALP), and alanine aminotransferase (ALT); (2) secondary osteoporosis or diseases that could affect bone metabolism, including osteogenesis imperfecta, Paget's disease of bone, diabetes mellitus, primary hyperparathyroidism, rheumatoid arthritis or malignant tumors; (3) drug use that could affect bone metabolism, including the use of synthetic steroid hormones, epinephrine or anticonvulsive drugs; (4) serious primary diseases affecting the cardiovascular, pulmonary, hematopoietic, gastrointestinal, renal or nervous systems or mental state; (5) treatment with bisphosphonate, teriparatide, estrogen or other anti-osteoporosis drugs in the past 1 year; and (6) treatment with calcium >600 mg/d or VitD > 600 IU/d. Finally, 574 participants (men: 164, women: 410) were found to be in good health and enrolled in this study (**Figure 1**).

Moreover, to fill in the gap of researches on sclerostin in Chinese adolescents, and explore the role of sclerostin in different physiological states, such as different age, bone metabolism status and sex hormone levels, 292 adolescents (aged 14–18 years; men: 143, women: 149) were recruited from Fengxian high school in the Qixian community. After the same screening process as in elderly participants, 287 adolescents in good health (men: 140, women: 147) were enrolled in this study (**Figure 1**). All 861 participants were of Han ethnicity and provided written informed consent.

Biochemical Measurement

Blood samples were obtained from fasting participants in the morning from 8:00 to 10:00 and stored at −80°C. The following markers of bone metabolism and sex hormone levels were measured by electrochemiluminescence immunoassay: procollagen type 1 N-propeptide (P1NP), β-CrossLaps of type I collagen containing cross-linked C-telopeptide (β-CTX), intact parathyroid hormone (PTH), and 25-hydroxyvitamin D [25(OH)D], estradiol (E_2), testosterone (T), and sex hormone-binding globulin (SHBG). All markers were measured using the following kits (Roche Diagnostics GmbH): total P1NP kit for P1NP, β-Crosslaps kit for β-CTX, PTH kit for PTH, vitamin D total kit for 25(OH)D, estradiol III kit for E_2, testosterone II kit for T and SHBG kit for SHBG. The free androgen index (FAI) was calculated as the percentage ratio of testosterone to SHBG values (Vermeulen et al., 1999). Serum sclerostin was measured by enzyme-linked immunosorbent assay (ELISA) using polyclonal goat anti-human sclerostin as the capture antibody, biotin-labeled monoclonal mouse anti-human sclerostin as the detection antibody, and horseradish peroxidase-streptavidin and tetramethylbenzidine for the chromogenic reaction (Biomedica Medizinprodukte GmbH and Co., KG). The intra- and interassay CVs were 4–6% and 5–7%, respectively.

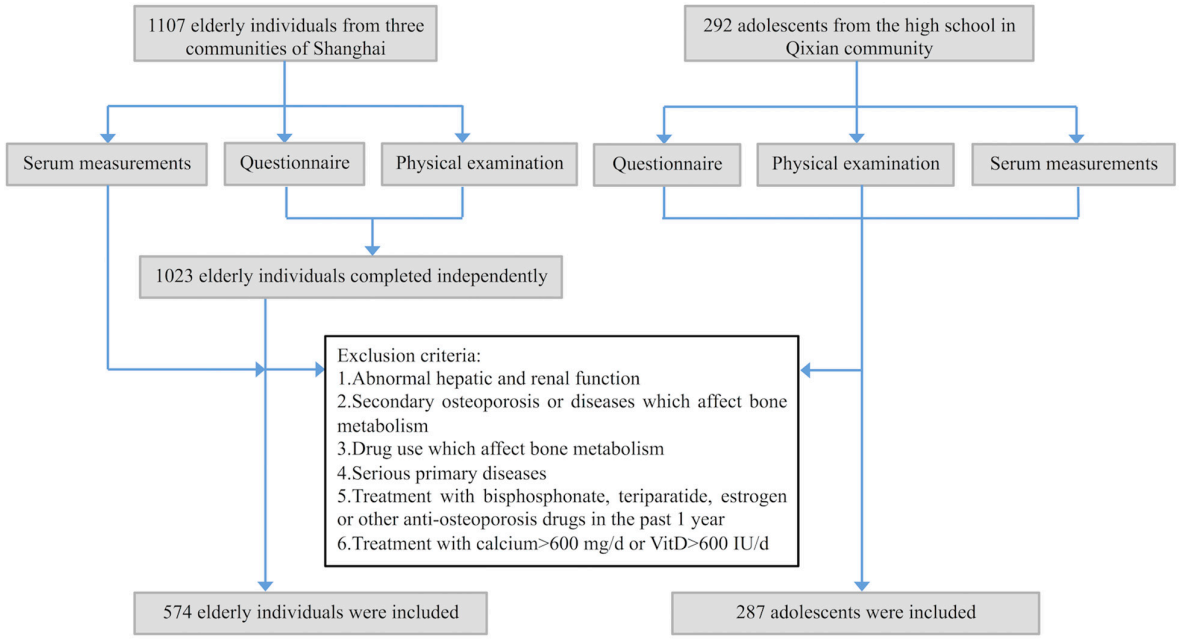


FIGURE 1 | Flowchart for recruiting process of the participants. All participants were evaluated by a questionnaire, physical examination, and routine serum measurements.

Statistical Analysis

Normally distributed data are presented as the mean ± standard deviation (SD), while non-normally distributed data are presented as the median and interquartile range. Mann–Whitney *U* test was used to determine differences of the baseline characteristics between males and females, elderly individuals and adolescents. Spearman correlation analysis was performed between sclerostin and other factors; the Spearman correlation coefficients for sex, age, BMI, bone metabolism markers and sex hormones were calculated to determine which factors would be included in the next regression analysis. Then regression analysis was used to explore associations between sclerostin and each factor, and multiple linear stepwise regression analysis was adopted to adjust for sex, age and BMI. All analyses were carried out using SPSS software, version 23 for Mac (IBM, Chicago, United States), and P values less than 0.05 were considered significant.

RESULTS

General Characteristics of the Study Population

The basic characteristics of the 861 participants were presented in **Table 1**. Elderly males had a median serum sclerostin level of 54.89 pmol/L (interquartile range: 43.34–69.88 pmol/L), while elderly females had a lower median sclerostin level of 39.95 pmol/L (interquartile range: 30.65–52.00 pmol/L). Similarly, the median sclerostin level of 36.58 pmol/L (interquartile range: 29.02–44.49 pmol/L) in adolescent males was higher than the median level of 27.06 pmol/L (interquartile range: 20.28–34.45 pmol/L) in adolescent females. The serum sclerostin level was significantly higher in males than in females ($P < 0.05$), and in elderly individuals than in adolescents ($P < 0.05$).

Correlations of Serum Sclerostin With Bone Metabolism Markers and Sex Hormones

The correlations between serum sclerostin and bone metabolism markers and sex hormones were studied in both elderly individuals and adolescents (**Table 2**). For elderly individuals, serum sclerostin was negatively correlated with sex, P1NP, β-CTX, and PTH ($r = -0.343$, $r = -0.212$, $r = -0.116$, and $r = -0.128$, respectively; $P < 0.05$), but positively correlated with age, 25(OH)D, T, FAI and E_2 ($r = 0.109$, $r = 0.143$, $r = 0.363$, $r = 0.330$, and $r = 0.257$, respectively; $P < 0.05$). For serum sclerostin in adolescents, the negative correlations with sex, 25(OH)D, SHBG, and E_2 ($r = -0.382$, $r = -0.120$, $r = -0.125$, and $r = -0.283$, respectively; $P < 0.05$), and positive correlations with P1NP, β-CTX, PTH, T, and FAI ($r = 0.333$ $r = 0.328$, $r = 0.156$, $r = 0.349$, and $r = 0.276$, respectively; $P < 0.05$) were found.

The Multiple Regression Analyses Between Sclerostin and the Correlated Factors

Factors associated with the serum sclerostin level were explored using multiple linear regression analysis (**Table 3**). In elderly individuals, serum sclerostin was positively associated with age ($\beta = 0.176$, $P < 0.001$), and after adjusting for sex, age

TABLE 1 | Basic characteristics of the 861 participants.

	Elderly individuals		Adolescents		*P* value
	Males	**Females**	**Males**	**Females**	
No. of subjects	164	410	140	147	
Age, y	70 (66–73)	70 (67–77)	16 (16–17)	16 (16–17)	<0.05[cd]
BMI, kg/m2	24.22 (22.49–26.45)	23.72 (21.64–26.17)	20.99 (19.23–22.76)	20.64 (19.36–23.01)	<0.05[cd]
P1NP, ng/mL	45.28 (36.89–57.85)	58.56 (45.66–74.15)	181.80 (141.45–277.68)	101.60 (82.97–125.60)	<0.05[abcd]
β-CTX, ng/mL	0.32 (0.23–0.43)	0.42 (0.30–0.53)	0.44 (0.34–0.62)	0.25 (0.20–0.33)	<0.05[abcd]
25(OH)D, ng/mL	26.00 (22.00–31.05)	23.81 (19.00–30.00)	18.53 (14.22–23.38)	19.66 (15.26–25.82)	<0.05[acd]
PTH, ng/L	38.15 (29.28–48.80)	38.50 (30.60–52.30)	39.00 (27.68–49.58)	32.00 (23.30–40.20)	<0.05[bd]
T, nmol/L	17.34 (13.16–22.99)	0.59 (0.38–0.91)	15.52 (12.75–18.44)	1.09 (0.76–1.43)	<0.05[abcd]
SHBG, nmol/L	59.60 (42.90–76.38)	73.30 (51.05–99.10)	27.40 (21.08–34.35)	49.40 (33.40–72.40)	<0.05[abcd]
FAI,%	31.25 (25.91–36.64)	0.82 (0.45–1.55)	58.37 (48.27–69.74)	2.21 (1.24–3.70)	<0.05[abcd]
E_2, pmol/L	119.50 (89.83–148.95)	46.17 (31.02–72.87)	82.44 (66.15–97.47)	186.40 (114.10–353.60)	<0.05[abcd]
Sclerostin, pmol/L	54.89 (43.34–69.88)	39.95 (30.65–52.00)	36.58 (29.02–44.49)	27.06 (20.28–34.45)	<0.05[abcd]

BMI, body mass index; P1NP, procollagen type 1 N-terminal propeptide; β-CTX, β-CrossLaps of type I collagen containing cross-linked C-telopeptide; 25(OH)D, 25-hydroxyvitamin D; PTH, parathyroid hormone; T, testosterone; SHBG, sex hormone-binding globulin; FAI, free androgen index; E_2, estradiol. Non-normally distributed data are shown as the median (interquartile range). [a]$P < 0.05$ when comparing the males vs. females in elderly individuals. [b]$P < 0.05$ when comparing the males vs. females in adolescents. [c]$P < 0.05$ when comparing the elderly males vs. the adolescent males. [d]$P < 0.05$ when comparing the elderly females vs. the adolescent females.

and BMI, it was still positively associated with T (β = 0.248, $P = 0.001$), but negatively associated to P1NP (β = −0.140, $P = 0.001$). In adolescents, serum sclerostin was significantly and positively associated with P1NP (β = 0.192, $P = 0.003$). After adjusting for sex, age and BMI, the association still existed. There were no associations between serum sclerostin and other bone metabolism markers or sex hormones.

DISCUSSION

In this study, the basic profile of serum sclerostin among the healthy community-dwelling Chinese population, including elderly individuals and adolescents, was first revealed. The results showed the circulating sclerostin level was significantly higher in elderly individuals than in adolescents, and serum sclerostin was positively correlated with age in elderly individuals, though the relationship was not found in adolescents. These observations correspond with previous studies (Modder et al., 2011b; Amrein et al., 2012; Coulson et al., 2017). The studies concluded that serum sclerostin levels peak early in life (∼age 10 years in girls and 14 years in boys), decline during the later stages of puberty toward a nadir at the end of puberty, and then increase over the remainder of adult life (Kirmani et al., 2012). According to its inhibitory action in osteoblast function, sclerostin is a potential candidate as the biomarker of bone formation. The increasing sclerostin level with age in elderly suggests the enhanced production may be part of the age-related impairment in bone formation. Thus, the difference of circulating sclerostin between adolescents and elderly reflects functional status of the bone, rather than total bone mass (Tsentidis et al., 2016). In addition, we also found sclerostin in males was higher than in females in both elderly individuals and adolescents. The gender difference in sclerostin levels appeared to be established during puberty, and difference in sex hormones or bone metabolism might be the cause (Kirmani et al., 2012).

Interestingly, we found serum sclerostin was positively correlated with P1NP in adolescents, but inversely associated with P1NP in elderly individuals. Although many studies have been performed to explore the correlations between sclerostin and bone metabolism markers, the results are controversial. Some studies have observed that serum P1NP and β-CTX are inversely associated with sclerostin in elderly subjects, while others have revealed no associations between them (Ardawi et al., 2011; Modder et al., 2011b; Costa et al., 2013; Durosier et al., 2013; Yamamoto et al., 2013; Catalano et al., 2014; Neumann et al., 2014). In adolescents, sclerostin levels were positively associated with P1NP and β-CTX (Kirmani et al., 2012). Even in adolescents with T1DM, sclerostin levels were still positively correlated

TABLE 2 | Correlation analyses of serum sclerostin and other parameters in elderly individuals and adolescents.

	Elderly individuals		Adolescents	
Variables	***r***	***P* value**	***r***	***P* value**
Sex	−0.343	**<0.001**	−0.382	**<0.001**
Age, y	0.109	**0.011**	0.028	0.650
BMI, kg/m^2	0.005	0.911	0.003	0.955
P1NP, ng/mL	−0.212	**<0.001**	0.333	**<0.001**
β-CTX, ng/mL	−0.116	**0.007**	0.328	**<0.001**
25(OH)D, ng/mL	0.143	**0.001**	−0.120	**0.048**
PTH, ng/L	−0.128	**0.003**	0.156	**0.010**
T, nmol/L	0.363	**<0.001**	0.349	**<0.001**
SHBG, nmol/L	−0.055	0.210	−0.125	**0.039**
FAI,%	0.330	**<0.001**	0.276	**<0.001**
E_2, pmol/L	0.257	**<0.001**	−0.283	**<0.001**

BMI, body mass index; P1NP, procollagen type 1 N-terminal propeptide; β-CTX, β-CrossLaps of type I collagen containing cross-linked C-telopeptide; 25(OH)D, 25-hydroxyvitamin D; PTH, parathyroid hormone; T, testosterone; SHBG, sex hormone-binding globulin; FAI, free androgen index; E_2, estradiol. Significant values ($P < 0.05$) are presented in bold.

TABLE 3 | Multiple linear regression analyses between sclerostin and the correlated factors.

Variables	Elderly individuals				Adolescents			
	Standardized β-coefficients	*P* Value	Standardized β-coefficients[a]	*P* Value[a]	Standardized β-coefficients	*P* Value	Standardized β-coefficients[a]	*P* Value[a]
Sex	−0.042	0.629			−0.073	0.710		
Age, y	0.176	**<0.001**			0.044	0.444		
BMI, kg/m^2	−0.026	0.575			0.106	0.103		
P1NP, ng/mL	−0.189	**0.001**	−0.140	**0.001**	0.084	0.438	0.192	**0.003**
β-CTX, ng/mL	0.082	0.162	0.079	0.161	0.070	0.484	0.055	0.567
25(OH)D, ng/mL	0.086	0.059	0.063	0.142	−0.058	0.323	−0.067	0.247
PTH, ng/L	−0.029	0.515	−0.060	0.158	0.020	0.768	0.018	0.780
T, nmol/L	0.206	**0.036**	0.248	**0.001**	0.277	0.051	0.204	0.122
SHBG, nmol/L	−0.070	0.178	−0.069	0.122	−0.014	0.853	−0.006	0.933
FAI,%	0.073	0.395	0.118	0.132	−0.164	0.331	−0.079	0.617
E_2, pmol/L	0.081	0.182	0.037	0.526	−0.128	0.051	−0.121	0.063

BMI, body mass index; P1NP, procollagen type 1 N-terminal propeptide; β-CTX, β-CrossLaps of type I collagen containing cross-linked C-telopeptide; 25(OH)D, 25-hydroxyvitamin D; PTH, parathyroid hormone; T, testosterone; SHBG, sex hormone-binding globulin; FAI, free androgen index; E_2, estradiol. Significant values ($P < 0.05$) are presented in bold. [a] Adjusted for sex, age and BMI.

with logCTX and logOsteocalcin (Tsentidis et al., 2016). The relations between scletostin and bone turnover markers were exactly opposite in elderly individuals and adolescents. In adolescents, young skeleton is submitted to growth where bone turnover might be activated to shift in a state of more gain in bone formation rather than resorption, and the metabolism is differentiated from that of elderly people (Tsentidis et al., 2016). Aline et al. proposed that the direction of the association between sclerostin and bone markers depends upon whether bone turnover is increased or decreased (Costa et al., 2013). The finding may reflect that sclerostin might play distinct roles in different functional states of the skeleton, the growing state in adolescents and the reduction of bone formation in elderly individuals (Tsentidis et al., 2016).

Regarding associations between sclerostin and sex hormones, previous studies showed that estrogen, but not testosterone, reduces circulating sclerostin levels, and the higher estrogen levels present in girls following the onset of puberty lead to their lower sclerostin levels that persist during adult life (Modder et al., 2011a; Kirmani et al., 2012). Consistent with this, Mohammed-Salleh et al. found sclerostin was negatively correlated with E_2 in both pre- and postmenopausal women, and Faryal et al. found significantly negative association between sclerostin and the free estrogen index in postmenopausal women (Mirza et al., 2010; Ardawi et al., 2011). However, in our study, we only found sclerostin was positively associated with T in elderly individuals, while no associations between sclerostin and E_2 were found. Since T was previously thought to be an anabolic factor for bone, the correlations between sclerostin and T and the biological effects of T on the circulating sclerostin level need to be determined in future studies (Riggs et al., 2002).

Some limitations of this study should be noticed. First, many other important variables were lacked, such as BMD, which is closely related to sclerostin. A positive correlation has been reported between sclerostin and BMD in many studies, however, this study did not correct for the effect of BMD. Second, the cross-sectional nature of this study may limit the statistical inference to non-causal results. Thirdly, the small sample size may have decreased the power of the statistical analyses.

In conclusion, we are the first to reveal the rough profile of the serum sclerostin level in healthy Chinese elderly individuals and adolescents from communities, and explore the associations between sclerostin with bone metabolism markers and sex hormones. The results showed the circulating sclerostin level was significantly higher in elderly individuals than in adolescents, and in males than in females. Additionally, opposite directions of the association between sclerostin and P1NP in elderly individuals and adolescents, and positive correlations between sclerostin and T in elderly individuals were revealed. Our findings may provide a clue to elucidate the cross action of sclerostin in bone metabolism and sexual development.

DATA AVAILABILITY STATEMENT

The raw data supporting the conclusions of this article will be made available by the authors, without undue reservation, to any qualified researcher.

ETHICS STATEMENT

The studies involving human participants were reviewed and approved by the Ethics Committee of the Shanghai Jiao Tong University Affiliated Sixth People's Hospital. Written informed consent to participate in this study was provided by the participants' legal guardian/next of kin.

AUTHOR CONTRIBUTIONS

YX and CG conducted the study and analyzed the data. YX wrote the draft of the manuscript. JH, WG, CY, BC, QW, FT,

and JX recruited the subjects. ZZ and HY supervised the study and revised the manuscript. All authors read and approved the final manuscript.

FUNDING

This study was supported by the National Key Research and Development Program of China (2018YFA0800801), the Science and Technology Commission of Shanghai Municipality (16411954500 and 16ZR1425700), and the National Natural Science Foundation of China (81974126 and 81770874).

ACKNOWLEDGMENTS

We are grateful to all participants and the staff from community health service centers for their supports.

REFERENCES

Amrein, K., Amrein, S., Drexler, C., Dimai, H. P., Dobnig, H., Pfeifer, K., et al. (2012). Sclerostin and its association with physical activity, age, gender, body composition, and bone mineral content in healthy adults. *J. Clin. Endocrinol. Metab.* 97, 148–154. doi: 10.1210/jc.2011-2152

Ardawi, M. S., Al-Kadi, H. A., Rouzi, A. A., and Qari, M. H. (2011). Determinants of serum sclerostin in healthy pre- and postmenopausal women. *J. Bone Miner. Res.* 26, 2812–2822. doi: 10.1002/jbmr.479

Baron, R., and Rawadi, G. (2007). Targeting the Wnt/beta-catenin pathway to regulate bone formation in the adult skeleton. *Endocrinology* 148, 2635–2643. doi: 10.1210/en.2007-0270

Boudin, E., Yorgan, T., Fijalkowski, I., Sonntag, S., Steenackers, E., Hendrickx, G., et al. (2017). The Lrp4R1170Q homozygous knock-in mouse recapitulates the bone phenotype of sclerosteosis in humans. *J. Bone Miner. Res.* 32, 1739–1749. doi: 10.1002/jbmr.3160

Carpenter, K. A., and Ross, R. D. (2019). Sclerostin antibody treatment increases bone mass and normalizes circulating phosphate levels in growing Hyp mice. *J. Bone Miner. Res.* [Epub ahead of print].

Catalano, A., Pintaudi, B., Morabito, N., Di Vieste, G., Giunta, L., Bruno, M. L., et al. (2014). Gender differences in sclerostin and clinical characteristics in type 1 diabetes mellitus. *Eur. J. Endocrinol.* 171, 293–300. doi: 10.1530/EJE-14-0106

Cosman, F., Crittenden, D. B., Adachi, J. D., Binkley, N., Czerwinski, E., Ferrari, S., et al. (2016). Romosozumab treatment in postmenopausal women with osteoporosis. *N. Engl. J. Med.* 375, 1532–1543. doi: 10.1056/NEJMoa1607948

Costa, A. G., Walker, M. D., Zhang, C. A., Cremers, S., Dworakowski, E., Mcmahon, D. J., et al. (2013). Circulating sclerostin levels and markers of bone turnover in Chinese-American and white women. *J. Clin. Endocrinol. Metab.* 98, 4736–4743. doi: 10.1210/jc.2013-2106

Coulson, J., Bagley, L., Barnouin, Y., Bradburn, S., Butler-Browne, G., Gapeyeva, H., et al. (2017). Circulating levels of dickkopf-1, osteoprotegerin and sclerostin are higher in old compared with young men and women and positively associated with whole-body bone mineral density in older adults. *Osteoporos. Int.* 28, 2683–2689. doi: 10.1007/s00198-017-4104-2

Durosier, C., Van Lierop, A., Ferrari, S., Chevalley, T., Papapoulos, S., and Rizzoli, R. (2013). Association of circulating sclerostin with bone mineral mass, microstructure, and turnover biochemical markers in healthy elderly men and women. *J. Clin. Endocrinol. Metab.* 98, 3873–3883. doi: 10.1210/jc.2013-2113

Faienza, M. F., Ventura, A., Delvecchio, M., Fusillo, A., Piacente, L., Aceto, G., et al. (2017). High sclerostin and dickkopf-1 (DKK-1) serum levels in children and adolescents with type 1 diabetes mellitus. *J. Clin. Endocrinol. Metab.* 102, 1174–1181. doi: 10.1210/jc.2016-2371

Garnero, P., Sornay-Rendu, E., Munoz, F., Borel, O., and Chapurlat, R. D. (2013). Association of serum sclerostin with bone mineral density, bone turnover, steroid and parathyroid hormones, and fracture risk in postmenopausal women: the OFELY study. *Osteoporos. Int.* 24, 489–494. doi: 10.1007/s00198-012-1978-x

Glass, D. A. II, Bialek, P., Ahn, J. D., Starbuck, M., Patel, M. S., Clevers, H., et al. (2005). Canonical Wnt signaling in differentiated osteoblasts controls osteoclast differentiation. *Dev. Cell* 8, 751–764. doi: 10.1016/j.devcel.2005.02.017

Hansen, S., Shanbhogue, V. V., Jorgensen, N. R., and Beck-Nielsen, S. S. (2019). Elevated bone remodeling markers of CTX and P1NP in addition to sclerostin in patients with X-linked hypophosphatemia: a cross-sectional controlled study. *Calcif. Tissue Int.* 104, 591–598. doi: 10.1007/s00223-019-00526-z

He, J., Zhang, H., Wang, C., Zhang, Z., Yue, H., Hu, W., et al. (2014). Associations of serum sclerostin and polymorphisms in the SOST gene with bone mineral density and markers of bone metabolism in postmenopausal Chinese women. *J. Clin. Endocrinol. Metab.* 99, E665–E673. doi: 10.1210/jc.2013-2086

Kirmani, S., Amin, S., Mccready, L. K., Atkinson, E. J., Melton, L. J. III, Muller, R., et al. (2012). Sclerostin levels during growth in children. *Osteoporos. Int.* 23, 1123–1130. doi: 10.1007/s00198-011-1669-z

Krishnan, V., Bryant, H. U., and Macdougald, O. A. (2006). Regulation of bone mass by Wnt signaling. *J. Clin. Invest.* 116, 1202–1209. doi: 10.1172/JCI28551

Li, X., Ominsky, M. S., Niu, Q. T., Sun, N., Daugherty, B., D'agostin, D., et al. (2008). Targeted deletion of the sclerostin gene in mice results in increased bone formation and bone strength. *J. Bone Miner. Res.* 23, 860–869. doi: 10.1359/jbmr.080216

Lim, Y., Kim, C. H., Lee, S. Y., Kim, H., Ahn, S. H., Lee, S. H., et al. (2016). Decreased plasma levels of sclerostin but not Dickkopf-1 are associated with an increased prevalence of osteoporotic fracture and lower bone mineral density in postmenopausal Korean women. *Calcif. Tissue Int.* 99, 350–359. doi: 10.1007/s00223-016-0160-4

McClung, M. R., Grauer, A., Boonen, S., Bolognese, M. A., Brown, J. P., Diez-Perez, A., et al. (2014). Romosozumab in postmenopausal women with low bone mineral density. *N. Engl. J. Med.* 370, 412–420. doi: 10.1056/NEJMoa1305224

Mirza, F. S., Padhi, I. D., Raisz, L. G., and Lorenzo, J. A. (2010). Serum sclerostin levels negatively correlate with parathyroid hormone levels and free estrogen index in postmenopausal women. *J. Clin. Endocrinol. Metab.* 95, 1991–1997. doi: 10.1210/jc.2009-2283

Modder, U. I., Clowes, J. A., Hoey, K., Peterson, J. M., Mccready, L., Oursler, M. J., et al. (2011a). Regulation of circulating sclerostin levels by sex steroids in women and in men. *J. Bone Miner. Res.* 26, 27–34. doi: 10.1002/jbmr.128

Modder, U. I., Hoey, K. A., Amin, S., Mccready, L. K., Achenbach, S. J., Riggs, B. L., et al. (2011b). Relation of age, gender, and bone mass to circulating sclerostin levels in women and men. *J. Bone Miner. Res.* 26, 373–379. doi: 10.1002/jbmr.217

Neumann, T., Hofbauer, L. C., Rauner, M., Lodes, S., Kastner, B., Franke, S., et al. (2014). Clinical and endocrine correlates of circulating sclerostin levels in patients with type 1 diabetes mellitus. *Clin. Endocrinol.* 80, 649–655. doi: 10.1111/cen.12364

Ominsky, M. S., Boyd, S. K., Varela, A., Jolette, J., Felx, M., Doyle, N., et al. (2017). Romosozumab improves bone mass and strength while maintaining bone quality in ovariectomized cynomolgus monkeys. *J. Bone Miner. Res.* 32, 788–801. doi: 10.1002/jbmr.3036

Pekkolay, Z., Kilinc, F., Gozel, N., Onalan, E., and Tuzcu, A. K. (2019). Increased serum sclerostin levels in patients with active acromegaly. *J. Clin. Endocrinol. Metab.* [Epub ahead of print].

Recknor, C. P., Recker, R. R., Benson, C. T., Robins, D. A., Chiang, A. Y., Alam, J., et al. (2015). The effect of discontinuing treatment with blosozumab: follow-up results of a Phase 2 randomized clinical trial in postmenopausal women with low bone mineral density. *J. Bone Miner. Res.* 30, 1717–1725. doi: 10.1002/jbmr.2489

Riggs, B. L., Khosla, S., and Melton, L. J. III (2002). Sex steroids and the construction and conservation of the adult skeleton. *Endocr. Rev.* 23, 279–302. doi: 10.1210/edrv.23.3.0465

Singh, A., Gupta, M. K., and Mishra, S. P. (2019). Study of correlation of level of expression of Wnt signaling pathway inhibitors sclerostin and dickkopf-1 with

disease activity and severity in rheumatoid arthritis patients. *Drug Discov. Ther.* 13, 22–27. doi: 10.5582/ddt.2019.01011

Szulc, P., Bertholon, C., Borel, O., Marchand, F., and Chapurlat, R. (2013). Lower fracture risk in older men with higher sclerostin concentration: a prospective analysis from the MINOS study. *J. Bone Miner. Res.* 28, 855–864. doi: 10.1002/jbmr.1823

Tsentidis, C., Gourgiotis, D., Kossiva, L., Marmarinos, A., Doulgeraki, A., and Karavanaki, K. (2016). Sclerostin distribution in children and adolescents with type 1 diabetes mellitus and correlation with bone metabolism and bone mineral density. *Pediatr. Diabetes* 17, 289–299. doi: 10.1111/pedi.12288

Van Bezooijen, R. L., Roelen, B. A., Visser, A., Van Der Wee-Pals, L., De Wilt, E., Karperien, M., et al. (2004). Sclerostin is an osteocyte-expressed negative regulator of bone formation, but not a classical BMP antagonist. *J. Exp. Med.* 199, 805–814. doi: 10.1084/jem.20031454

Van Lierop, A. H., Hamdy, N. A., Hamersma, H., Van Bezooijen, R. L., Power, J., Loveridge, N., et al. (2011). Patients with sclerosteosis and disease carriers: human models of the effect of sclerostin on bone turnover. *J. Bone Miner. Res.* 26, 2804–2811. doi: 10.1002/jbmr.474

Van Lierop, A. H., Hamdy, N. A., Van Egmond, M. E., Bakker, E., Dikkers, F. G., and Papapoulos, S. E. (2013). Van Buchem disease: clinical, biochemical, and densitometric features of patients and disease carriers. *J. Bone Miner. Res.* 28, 848–854. doi: 10.1002/jbmr.1794

Vermeulen, A., Verdonck, L., and Kaufman, J. M. (1999). A critical evaluation of simple methods for the estimation of free testosterone in serum. *J. Clin. Endocrinol. Metab.* 84, 3666–3672. doi: 10.1210/jcem.84.10.6079

Yamamoto, M., Yamauchi, M., and Sugimoto, T. (2013). Elevated sclerostin levels are associated with vertebral fractures in patients with type 2 diabetes mellitus. *J. Clin. Endocrinol. Metab.* 98, 4030–4037. doi: 10.1210/jc.2013-2143

Yang, J., Xu, S., Chen, M., Yuan, Y., Zhang, X., Ma, Y., et al. (2019). Serum sclerostin and bone morphogenetic protein-2 levels in patients with ankylosing spondylitis: a meta-analysis. *Calcif. Tissue Int.* 105, 37–50. doi: 10.1007/s00223-019-00542-z

Conflict of Interest: The authors declare that the research was conducted in the absence of any commercial or financial relationships that could be construed as a potential conflict of interest.

Copyright © 2020 Xu, Gao, He, Gu, Yi, Chen, Wang, Tang, Xu, Yue and Zhang. This is an open-access article distributed under the terms of the Creative Commons Attribution License (CC BY). The use, distribution or reproduction in other forums is permitted, provided the original author(s) and the copyright owner(s) are credited and that the original publication in this journal is cited, in accordance with accepted academic practice. No use, distribution or reproduction is permitted which does not comply with these terms.

frontiers in Cell and Developmental Biology

REVIEW
published: 11 February 2020
doi: 10.3389/fcell.2020.00076

RANKL/RANK System-Based Mechanism for Breast Cancer Bone Metastasis and Related Therapeutic Strategies

Xiaoqiu Wu[1,2,3†], Fangfei Li[1,2,3†], Lei Dang[1,2,3†], Chao Liang[1,2,3], Aiping Lu[1,2,3,4,5*] and Ge Zhang[1,2,3*]*

[1] Law Sau Fai Institute for Advancing Translational Medicine in Bone and Joint Diseases, School of Chinese Medicine, Hong Kong Baptist University, Kowloon, Hong Kong, [2] Institute of Integrated Bioinfomedicine and Translational Science, School of Chinese Medicine, Hong Kong Baptist University, Kowloon, Hong Kong, [3] Institute of Precision Medicine and Innovative Drug Discovery, HKBU Institute of Research and Continuing Education, Shenzhen, China, [4] Institute of Basic Research in Clinical Medicine, China Academy of Chinese Medical Sciences, Beijing, China, [5] Institute of Arthritis Research, Shanghai Academy of Chinese Medical Sciences, Shanghai, China

OPEN ACCESS

Edited by:
Howard Raymond Petty, University of Michigan, United States

Reviewed by:
Keith Kirkwood, University at Buffalo, United States
Xiang Hang Luo, Central South University, China

***Correspondence:**
Chao Liang
liangchao@hkbu.edu.hk
Aiping Lu
aipinglu@hkbu.edu.hk
Ge Zhang
zhangge@hkbu.edu.hk

[†] These authors have contributed equally to this work

Specialty section:
This article was submitted to Molecular Medicine, a section of the journal Frontiers in Cell and Developmental Biology

Received: *29 November 2019*
Accepted: *29 January 2020*
Published: *11 February 2020*

Citation:
Wu X, Li F, Dang L, Liang C, Lu A and Zhang G (2020) RANKL/RANK System-Based Mechanism for Breast Cancer Bone Metastasis and Related Therapeutic Strategies. Front. Cell Dev. Biol. 8:76. doi: 10.3389/fcell.2020.00076

Breast cancer remains one of the most life-threatening tumors affecting women. Most patients with advanced breast cancer eventually develop metastatic diseases, which cause significant morbidity and mortality. Approximately two-thirds of patients with advanced breast cancer exhibit osteolytic-type bone metastasis, which seriously reduce the quality of life. Therefore, development of novel therapeutic strategies for treating breast cancer patients with bone metastasis is urgently required. The "seed and soil" theory, which describes the interaction between the circulating breast cancer cells (seeds) and bone microenvironment (soil), is widely accepted as the mechanism underlying metastasis. Disruption of any step in this cycle might have promising anti-metastasis implications. The interaction of receptor activator of nuclear factor-κB ligand (RANKL) and its receptor RANK is fundamental in this vicious cycle and has been shown to be a novel effective therapeutic target. A series of therapeutic strategies have been developed to intervene in this cross-talk. Therefore, in this review, we have systematically introduced the functions of the RANKL/RANK signaling system in breast cancer and discussed related therapeutic strategies.

Keywords: RANKL, RANK, bone metastasis, breast cancer, vicious cycle, denosumab

Abbreviations: AP-1, Activator protein 1; BSP, Bone sialoprotein; c-FMS, Colony-stimulating factor 1 receptor; c-JNK, c-jun N-terminal kinase; CTCs, Circulating tumor cells; CTGF, Connective tissue growth factor; CXCR 4/12, C-X-C chemokine receptor type 4/12; DTCs, Disseminated tumor cells; EMT, epithelial mesenchymal transition; FGF, Fibroblast growth factor; IGF, Insulin-like growth factor; IL-6, Interleukin 6; LGR4, G-protein-coupled receptor 4; MAPK, Mitogen-activated protein kinase; M-CSF, Macrophage CSF; MMPs, Matrix metalloproteinases; MSC, mesenchymal stem cell; NFATc1, Nuclear factor of activated T-cells, cytoplasmic 1; NF-kB, Nuclear factor kappa-b; OCIF, Osteoclast formation inhibitor; OCPs, Osteoclast precursors; ODF, Osteoclast differentiation factor; ONJ, Osteonecrosis of the jaw; OPG, osteoprotegerin; OPGL, Osteoprotegerin ligand; PDGFs, Platelet-derived growth factors; PGE2, Prostaglandin E2; PTH, Parathyroid hormone; PTHrP, Parathyroid hormone-related protein; RANK, Receptor activator of nuclear factor-κB; RANKL, Receptor activator of nuclear factor-κB ligand; Sema3A, osteoprotective factor semaphorin 3A; SREs, skeletal-related events; TGF-β, Transforming growth factor beta 1; TNFSF11, Tumor necrosis ligand superfamily member 11; TRAF, TNF receptor-associated factor; TRAIL, TNF related apoptosis inducing ligand; TRANCE, TNF-related activation induced cytokine.

INTRODUCTION

Breast cancer is one of the most common cancers and the leading cause of mortality in females. The number of patients with breast cancer increases by approximately 1.7 million worldwide each year (Torre et al., 2015). Considering the malignant biological characteristics of breast cancer, local recurrence and distant metastasis are eventually bound to occur. In fact, most of the deaths from breast cancer are not due to the tumor in the primary site, but are the result of distant metastases in the body (Scully et al., 2012; Jin and Mu, 2015). Interestingly, metastasis of breast cancer has organ selectivity, as the lung, liver, and especially the bone are the preferred sites (Fidler, 2003). More than two-thirds of patients with advanced breast cancer eventually harbor osteolytic-type bone metastasis (Suva et al., 2009; Chen et al., 2010). Bone metastasis severely affects the quality of life of patients and indirectly limit life expectancy by inducing bone marrow aplasia, pathological osteolysis, spinal compression, bone fractures, and hypercalcemia, which are referred to as skeletal-related events (SREs) (Yoneda et al., 2013). According to statistics, the average life expectancy of patients with bone metastasis from breast cancer after diagnosis is only 2−3 years (Ibrahim et al., 2013; Cetin et al., 2015).

Most patients with breast cancer exhibit osteolytic lesions; however, osteoblastic or mixed lesions also exist. Bone is a hard tissue with mineralized bone matrix, which renders invasion by cancer cells difficult. Activation of osteoclasts is the central cellular mechanism of osteolytic bone metastasis. Accordingly, breast cancer cells that can migrate and attach to the bone surface must possess special abilities for inducing osteoclastic activation, which then destroy the hard-mineralized bone tissue. Reports show that parathyroid hormone-related protein (PTHrP) can indirectly activate osteoclastogenesis by decreasing the production of osteoprotegerin (OPG) and enhancing the expression of receptor activator of nuclear factor-κB ligand (RANKL) (Boabaid et al., 2004). In addition, the RANKL/RANK signaling system can enhance the proliferation and division of mammary epithelial cells during lobulo-alveolar morphogenesis in an autocrine or paracrine fashion, as well as promote the formation of lactating mammary glands.

Increasing evidence suggests that the RANKL/RANK signaling system is associated with nearly each step in breast cancer development, from primary oncogenesis to the establishment of secondary tumors in the bone. The interaction of breast cancer cells, osteoblasts, osteoclasts, and the bone matrix form a vicious cycle, leading to final bone metastasis. Tumor cells often modulate their gene expression to adapt to the bone microenvironment. For example, most breast cancer cells often express abundant RANK. Simultaneously, the bone also provides a unique nutrient-rich physiological microenvironment to attract tumor cells for migration and colonization in the bone. The bone matrix is rich in various growth factors and cytokines, which provide nutrition to the cancer cells. Breast cancer cells that migrate to bones express cytokines and growth factors such as interleukin (IL)-6, IL-8, IL-11, tumor growth factor (TGF)-β, prostaglandin E, or PTHrP, which can mediate RANKL expression. The up-regulated RANKL activates osteoclastogenesis, following which, many growth factors and cytokines are continually released after the turnover of the bone matrix, which in turn supports cancer cell proliferation and RANKL secretion. In addition to the rich microenvironment of the bone tissue, the abundantly secreted RANKL can also attract RANK-expressing circulating breast cancer cells to migrate into bone matrix, apart from the C-X-C chemokine receptor type (CXCR) 4/12 interaction.

Based on the critical roles of the RANK/RANKL system during the progression of initial primary breast cancer and subsequently bone metastasis, inhibition of RANKL has been developed as a novel therapeutic strategy for advanced breast cancer. Although bisphosphonates have been used for many years, denosumab, the first complete human IgG2 monoclonal antibody for RANKL, has been clinically approved for treating bone-related cancer pathologies and is being used increasingly in clinics (Rizzoli et al., 2010). Similar to OPG, denosumab binds to RANKL and then prevents it from interacting with RANK, thereby decreasing osteoclast differentiation and activation, which consequently reduces bone resorption. Furthermore, denosumab is superior to zoledronic acid in lowering the risk of SREs in patients with metastatic breast cancer and improving their quality of life (Miller, 2009; Stopeck et al., 2010).

BONE MICROENVIRONMENT

The establishment of bone metastasis is a complicated process, which involves a vicious cycle consisting of the bone microenvironment and tumor cells. Tumor cells produce adhesive molecules, which enable them to attach to the bone surface. The skeleton is composed of a complex and dynamic tissue controlled by bone-forming osteoblasts and bone-resorptive osteoclasts (Florencio-Silva et al., 2015). During bone remodeling, large quantities of growth factors and cytokines are produced, which then attract the circulating tumor cells (CTCs) to adhere to the bone surface and support metastatic tumor cells to proliferate and survive in the bone tissue (Zheng et al., 2013). Furthermore, the circulating cancer cells that enter the bone can influence bone remodeling and then modulate the bone microenvironment to render it more suitable for tumor cell colonization (Kozlow and Guise, 2005; Akhtari et al., 2008).

Bone Cells

Single nucleated osteoblasts derived from mesenchymal stem cells (MSCs) play key roles in maintaining bone homeostasis by controlling bone remodeling. Osteoblasts can not only regulate matrix mineralization, but can also affect the expression of extracellular matrix proteins, including type I collagen, osteocalcin, osteopontin, and bone sialoprotein (BSP) (Kini and Nandeesh, 2012). In addition to indirectly stimulating bone resorption by regulating osteoclast differentiation, osteoblasts can also directly attract breast cancer cells by secreting chemotactic factors and adherent molecules. CXCL12 and RANKL, cytokines that are overexpressed by osteoblast-lineage cells and circulate in the blood, can attract CXCR4 and RANK, which are highly expressed on mammary tumor cells, inducing the latter to

migrate to the bone surface. A new study regarding prostate cancer bone metastasis demonstrated that prostate cancer cells that produce exosomes can transfer pyruvate kinase M2 (PKM2) into bone marrow stromal cells and up-regulate CXCL12 in these cells (Dai et al., 2019). A similar mechanism remains to be elucidated for breast cancer bone metastasis.

After the synthesis of the new bone matrix, osteoblasts either undergo apoptosis or are embedded in the bone matrix as osteocytes. Evidence showed that the survival of osteocytes is regulated by the osteoprotective factor semaphorin 3A (Sema3A). Estrogen can induce osteocytes to express Sema3A, which acts on the receptors on osteocytes and activates GC-cGMP signaling to promote their survival (Hayashi et al., 2019). Osteocytes can affect bone remodeling by directly communicating with osteoblasts and osteoclasts via mediators that are released in the surrounding medium. For example, RANK secreted by osteocytes primarily regulates osteoclast differentiation and activity. Hence, osteocytes are considered to be mechanical sensors that indicate when and where osteoclasts or osteoblasts absorb or form bone, respectively (Boron and Boulpaep, 2005).

Osteoclasts are large cells with multiple nuclei on the bone surface. These multiple nucleated cells that originate from hematopoietic lines are fused with mononuclear osteoclast precursor cells. Osteoclasts can break down bone tissue via bone resorption (Clines and Guise, 2005). It is well known that only osteoclasts are responsible for absorbing bone (Clarke, 2008). Defects or excessive activity of osteoclasts might result in bone disease such as osteopetrosis or osteoporosis. Christian et al. reported that the iterative fusion of circulating blood monocytic cells with long-lived osteoclast syncytia maintains the function of osteoclasts (Jacome-Galarza et al., 2019). The integrin receptors on the membrane surface osteoclasts assist in binding to the bone matrix peptide; the osteoclasts then secrete acids and lysosomal enzymes to resorb the bone. Osteoclastogenesis is stimulated by two essential factors, macrophage CSF (M-CSF) and RANKL (Teitelbaum and Ross, 2003). Briefly, RANKL binds to the surface of monocytes via RANK. Together with M-CSF, RANKL promotes the fusion of multiple mononuclear cells to form multinucleated osteoclasts. M-CSF activates the signaling pathways via tyrosine kinase Src, resulting in increase in proliferation, survival, and differentiation of osteoclast precursors, which are essential for bone resorption (Clarke, 2008). Both RANKL and M-CSF are not only required for osteoclast formation but are also widely associated with monocyte/macrophage-derived cell differentiation. In addition to relying on RANKL and M-CSF, bone resorption also depends on cathepsin K, secreted by osteoclasts, and hydrogen ions. The function of osteoclasts is regulated by various hormones such as parathyroid hormone (PTH) from the parathyroid gland, which is the main meditator of the vicious cycle leading to bone metastases.

Extracellular Matrix

During bone destruction and bone formation, different types of growth factors and cytokines are produced and stored in the extracellular matrix (Hauschka et al., 1986; Guise et al., 2005). Almost 95% of the organic bone matrix is composed of collagen type I (Brodsky and Persikov, 2005). The remaining 5% consists of a series of non-collagenous proteins and proteoglycans. During bone formation, osteoblasts secrete bone morphogenetic proteins (BMPs), transforming growth factor beta 1 (TGF-β), insulin-like growth factor (IGF), and fibroblast growth factor (FGF), which are then incorporated into the bone matrix (Chirgwin and Guise, 2000; Guise, 2009). In addition, breast cancer cells can stimulate bone resorption by promoting osteoclastogenesis to release immobilized growth factors.

Growth factors and cytokines released during bone resorption can induce cancer cells to migrate to the bone and support their proliferation. IGF-1 is the most abundant growth factor in the bone extracellular matrix, followed by TGF-β (Crane and Cao, 2014). However, BMPs, FGF1, FGF2, and platelet-derived growth factor (PDGF) are scarce. Evidence shows that only TGF-β plays a direct role in promoting tumor cell metastasis to the bone (Kozlow and Guise, 2005). TGF-β is an important factor that is released during bone resorption, which stimulates tumor cells to express factors such as CTGF, IL-11 (Kang et al., 2003), and PTHrP (Yin et al., 1999), which are necessary for the metastasis of breast cancer cells to the bone. Interestingly, TGF-β mainly mediates growth inhibition at the early stages of tumorigenesis. However, most patients in the advanced stages of the disease lose TGF-β-mediated growth inhibition but still retain TGF-β-mediated regulation of their metastasis-promoting genes (Käkönen et al., 2002; Wakefield and Roberts, 2002). When breast cancer cells colonize the bone environment, molecular mechanisms controlling the interactions among osteoblasts, osteoclasts, hematopoietic stem cells, and other different types of cells are utilized to change bone homeostasis and promote the survival, dormancy, and proliferation of tumor cells (Kan et al., 2016).

RANKL/RANK/OPG SIGNALING SYSTEM

Most breast cancers with bone metastasis are osteolytic, and osteoclasts are considered to be the most effective cells for inducing bone resorption (Charles and Aliprantis, 2014). The RANKL/RANK/OPG system is well-known for regulating bone turnover by promoting the differentiation and activation of osteoclasts (Dougall and Chaisson, 2006; Boyce and Xing, 2007; Silva and Branco, 2011).

RANKL

RANKL, encoded by tumor necrosis factor superfamily 11 (*TNFSF11*), is also known as osteoprotegerin ligand (OPGL) or osteoclast differentiation factor (ODF) (Hikita et al., 2006). RANKL can be expressed in three different molecular forms: a trimeric transmembrane protein and two different secreted forms arising due to proteolytic cleavage or alternative splicing (Ikeda et al., 2001). RANKL1 is the full-length form of RANKL. RANKL2 is the shorter form of RANKL, which lacks some intracytoplasmic domains. RANKL3 is a soluble form of RANKL in which some of the amino acids at the N-terminal are missing. RANKL is highly expressed in various tissues such as lymph nodes, mammary glands, and lung, but is expressed at low levels

in the bone marrow and spleen; it is also expressed by osteoblasts, osteocytes, and activated T lymphocytes (Boyce and Xing, 2008). Although RANKL is expressed by many other cells, osteocytes are the main source of RANKL in adult bone tissue (Xiong et al., 2011). In particular, RANKL binds to RANK on myeloid cells, following which it regulates osteoclastogenesis and mediates bone resorption by promoting osteoclast activation and survival (Boyle et al., 2003; Boyce and Xing, 2008). The expression of RANKL in osteoblasts is stimulated by most known factors that stimulate osteoclastogenesis (Udagawa et al., 1999).

Recently, a new study revealed that leucine-rich repeat containing G-protein-coupled receptor 4 (LGR4, also called GPR48) is a novel receptor of RANKL (Luo et al., 2016). The osteoclasts produce LGR4, which directly interacts with RANKL and negatively regulates bone destruction via activation of Gαq/GS3K-β signaling and repression of the NFATc1 pathway during osteoclastogenesis. Mice with *Lgr4* whole body knockout and monocyte conditional knockout exhibited osteoclast hyperactivation and low bone mass. Compared to that in control mice, the number, surface area, and size of osteoclasts dramatically increased in *Lgr4* knockout mice. Furthermore, *in vitro* data showed that LGR4 competes with RANK to bind to RANKL in a dose-dependent manner and suppresses the expression and activity of a series of factors during osteoclastogenesis, attenuating osteoclast differentiation and survival.

OPG, the decoy receptor for RANKL, is secreted mainly by osteoblast lineage cells, and is a potent inhibitor of osteoclast formation, as it competes with RANK for binding to RANKL (Schoppet et al., 2002). Therefore, osteoclast formation is determined by the ratio of RANKL to OPG, rather than by the absolute levels of both molecules (Blair et al., 2006). Systemic factors such as TNF-α, PTH, and interleukins up-regulate the expression of RANKL on osteoblasts relative to that of OPG, resulting in osteoclast activation (Dougall and Chaisson, 2006). A therapeutic strategy with OPG was found to be effective in inhibiting bone resorption for humans (Mundy, 2002).

RANK

RANK, a type I homotrimeric transmembrane protein, was initially identified only on osteoclast precursors (O), mature osteoclasts, and dendritic cells (Santini et al., 2011). Later, research showed that RANK is also expressed in mammary glands and some other cancer cells with high bone metastasis potential, including breast cancer and prostate cancer (Fata et al., 2000; Chen et al., 2006; Kim et al., 2006). Vesicular RANK secreted by mature osteoclasts can trigger RANKL reverse signaling by binding to RANKL on osteoblasts to promote bone formation (Ikebuchi et al., 2018). On the other hand, RANK on the surface of osteoclast precursors interacts with osteocytic RANKL to promote osteoclastogenesis. The binding of RANKL to RANK results in receptor oligomerization, recruiting TNF receptor-associated factor (TRAF) adaptor proteins (including TRAFs 1, 2, 3, 5, and 6) to specific sites at the membrane-proximal portion of RANK (Armstrong et al., 2002; Akhtari et al., 2008). Unlike other TRAFs, TRAF6, an essential component of the RANKL-RANK signaling pathway, is one of the most critical factors in osteoclast formation and functioning. TRAF6 can activate the c-Jun N-terminal kinase (JNK) and nuclear factor kappa-b (NF-kB) pathways, thereby triggering osteoclastogenesis and bone resorption activity (Wong et al., 1998; Kobayashi et al., 2001). *Traf6* mutant mice exhibited severe osteopetrosis. The relative expression of OPG and RANKL balances this system. Currently, the ratio between RANKL and OPG is considered a therapeutic target for treating estrogen deficiency-associated osteoporosis (Rachner et al., 2011), rheumatoid arthritis (Walsh and Gravallese, 2010), Paget's disease, and bone tumors.

Osteoprotegerin (OPG)

Osteoprotegerin, the cytokine receptor of the tumor necrosis factor receptor superfamily encoded by *TNFRSF11B*, is also known as osteoclast formation inhibitor (OCIF). OPG is mainly secreted by osteoblast lineage cells, gastrointestinal epithelial cells, vascular endothelial cells, B cells, and dendritic cells (Sisay et al., 2017). The receptor was originally found to protect bones by preventing bone absorption, as it competes with RANK for binding to RANKL (Hofbauer and Heufelder, 2001). Partial deletion of *TNFRSF11B* resulted in a dramatic increase in RANKL-RANK interactions, which eventually led to juvenile Paget's disease (Whyte et al., 2002). Mice with OPG mutation show severe bone destruction (Cundy et al., 2002). Furthermore, OPG can also inhibit the apoptosis of human osteoclasts by blocking the TNF-related apoptosis-induced ligand-based signaling system (Chamoux et al., 2008).

METASTASIS OF BREAST CANCER CELLS TO THE BONE

Although osteoblastic and mixed lesions exist, most breast cancer with bone metastasis manifest as osteolytic bone metastasis, which accounts for 80−90% cases. In the case of osteolytic metastases, circulating breast cancer cells not only highly enhance osteoclast activities, but also seriously inhibit osteoblast differentiation and ultimately result in increased bone resorption and decreased bone formation, leading to higher risk of fractures. The metastasis of a primary breast cancer to the bone requires several complicated steps including: (1) proliferation at the primary breast site and acquisition of the corresponding metastatic characteristics; (2) disruption of the basement membrane; (3) invasion of the extracellular matrix; (4) intravascular infiltration and transportation; (5) adherence and retentate (6) migration to the blood vessels to form micro-metastases; (7) colonization of cancer cells and bone destruction (**Figure 1**). Inability to complete any of these steps will arrest the process (Fidler, 2003).

Invasion

The primary breast cancer cells first induce angiogenesis to supply nutrients for tumor cell proliferation. Local angiogenesis is necessary for breast cancer cells to reach a clinically detectable size. In addition, the development of new blood vessels also provides the tumor cells a pathway for entering the blood or lymphatic vessels (intravasation). After escaping from the

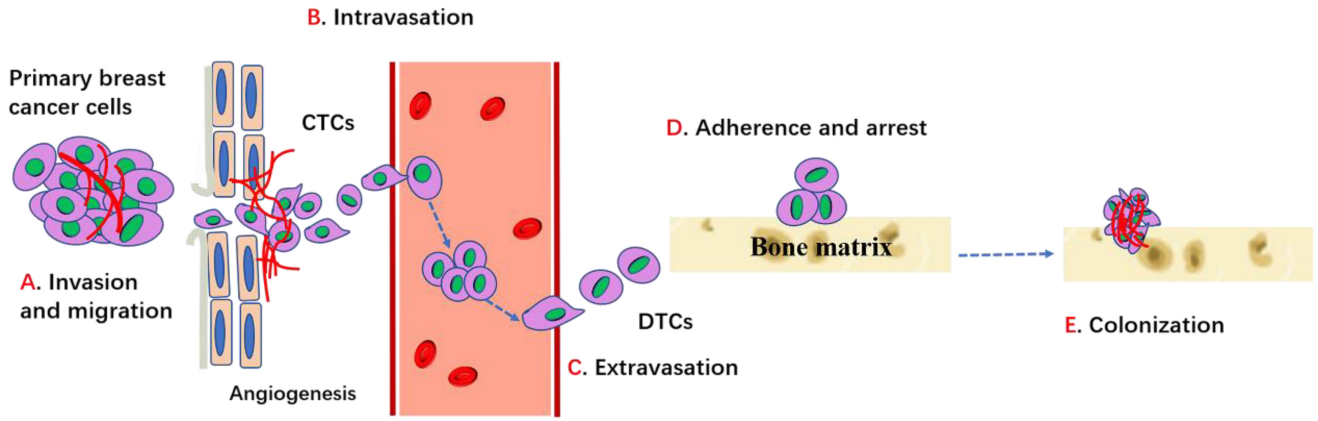


FIGURE 1 | Process of breast cancer bone metastasis. Cancer cells proliferate, invade into surrounding tissues and escape from primary site through the regulation of cadherins, MMPs, integrins and other factors. Then cancer cells enter into the circulation (intravasation) and migrate toward bone through the conduct of chemokines and other factors, etc. When cancer cells egress blood vessels (extravasation) and arrive bone target, it can adhere and bind with bone matrix and get arrest through integrins and cadherin. Then cancer cells can survive, proliferate and differentiate through the interaction with bone microenvironment which ultimately lead to the establishment of bone metastases.

primary site, the invasive breast cancer cells secrete matrix metalloproteinases (MMPs) and cathepsin-K to degrade the ECM and connective tissue and then break through the matrix barrier (Fidler, 2003; Mareel and Leroy, 2003). MMPs are a major class of proteinases necessary for tumor cell invasion. Integrins, the major receptors for extracellular matrix proteins, are also critical for cell invasion and migration. EMT is a process via which epithelioid tumor cells are transformed into mesenchymal fibroids, which show enhanced invasiveness such as mobility and distant metastasis. Evidence suggests that EMT is associated with tumor progression, as it induces proteases such as MMPs that assist in invasion and endosmosis (Bonnomet et al., 2010). Reversion of the invasive breast cancer cells into post-mitotic adipocytes may repress primary tumor invasion (Ishay-Ronen et al., 2019). Experimental results showed that high level of RANK in human mammary epithelial cells can induce EMT and increase migration (Palafox et al., 2012). Primary breast cancer cells must successfully exudate through the bone matrix to enter systemic circulation.

Migration

The breast cancer cells that enter the systemic circulation survive by evading both the host's immune response and apoptotic signals (Valastyan and Weinberg, 2011). Tumor cells that enter the systemic circulation are called circulating tumor cells (CTCs), which are disseminated to the bone through the bloodstream or lymphatic vessels. Adhesion to the vascular endothelial cells is the key for the escape of CTCs from the blood vessels. After entering the bone, the CTCs are exposed to factors in the bone microenvironment that support the growth and egress circulation (extravasation) of metastasized cells and promote colonization in the bone. These disseminated cancer cells are called disseminated tumor cells (DTCs). DTCs readily change their biological phenotype to adjust to bone environments and acquire new malignant capacities (Lambert et al., 2017). For this targeted migration, the bone also produces numerous cytokines and chemokines that attract primary tumor cells and induce them to home to the bone (Mastro et al., 2003). Human breast cancer cells express more CXCR4/RANK than normal epithelial cells, and CXCL12, the receptor of CXCR4, is highly expressed in the liver, lung, and bone marrow. Furthermore, breast cancer cells produce factors such as PTH or PTHrP, IL-1, and IL-6, which stimulate osteoblasts and stromal cells to secrete RANKL. The interactions between CXCR4 and CXCL12, RANKL, and RANK are critical for the homing of breast cancer cells to the bone marrow (Müller et al., 2001; Sun et al., 2005).

Adhesion and Survival

Adhesion is the next step after the breast cancer cells have migrated to the bone. Integrins and cadherins are major regulators for this specific adhesion. Integrin is an isodiglycan protein that mediates the interaction between breast cancer cells and the extracellular matrix. Arg-gly-asp (RGD), a tripeptide binding to αvβ3 integrin, is one of the extracellular matrix proteins present in vitronectin, osteopontin, and osteosialin, which mediates migration of tumor cells to the trabecular bone. Evidence suggests that hemocyte adhesion in the blood vessels is dependent on and is regulated by integrin activation (Felding-Habermann et al., 2001). Breast cancer cells that overexpress αvβ3 integrin are more prone to bone metastasis (Pecheur et al., 2002). The interaction of *E*-cadherin derived from tumor cells and *N*-cadherin derived from osteogenic cells activates the mTOR signaling pathway, which mediates the binding of these cancer cells to bone marrow stromal cells and then promotes homing of the breast cancer cells to the bone marrow (Wang et al., 2015).

Survival and proliferation in the bone are the next key steps underlining the success of bone metastasis after the tumor

cells have adhered to the bone tissue. The metastatic breast cancer cells overexpress a series of factors such as PTHrP to stimulate osteoblasts to highly express RANKL and reduce OPG expression. Therefore, bone resorption is promoted, which results in the release of growth factors, including BMPs, TGF-β, IGFs, FGFs, PDGFs, and calcium. These growth factors may not directly promote cancer cell proliferation but may indirectly induce angiogenesis and osteoclastogenesis to remodel the bone microenvironment for tumor cell colonization. In particular, the abundant calcium in the bone matrix can attract the calcium-sensing receptor-expressing breast cancer cells to the bone. Furthermore, Wang et al. (2018) showed that the increased intracellular calcium concentration in metastatic breast cancer cells induced by connexin 43 can disturb the osteogenic niche and promote survival (Waning et al., 2019). Furthermore, the bone microenvironment promotes breast cancer cells to transit to a migratory phenotype with new malignant capacities. For instance, compared to that in the orthotopic mammary fat pad of mice, the increased expression of Snail, a well-recognized mesenchymal marker, and the decreased expression of *E*-cadherin, a representative epithelial marker, were observed in the bone metastatic breast cancer cells, suggesting that the bone microenvironment promotes EMT of bone metastatic tumor cells. Further evidence showed that EMT is induced by TGF-β secreted during bone resorption (Heldin et al., 2012). Supported by the bone microenvironment, tumor cells successfully colonize the bone.

THE RANKL/RANK SYSTEM IS INVOLVED IN OSTEOCLAST DIFFERENTIATION AND ACTIVATION

Osteoclasts are key participants in bone remodeling, as they regulate bone structure and function in adulthood. Recently, scientists have made new breakthroughs in understanding the mechanisms underlying the differentiation and activation of osteoclasts, and the RANKL/RANK signaling system has been identified as the key regulator of osteoclastgenesis.

M-CSF and RANKL are two essential cytokines that regulate differentiation of hematopoietic lines into osteoclasts (**Figure 2**). During this process, M-CSF acts as a survival factor of early progenitor cells, whereas the RANKL-RANK signaling system acts as critical instructive osteoclast lineage signal (Nagy and Penninger, 2015). Similar to RANKL, M-CSF also originates from bone marrow stromal cells. M-CSF was originally identified to be necessary for promoting the survival of osteoclast progenitor cells and was essential for osteoclast development (Boyce and Xing, 2007). A mouse model expressing non-functional M-CSF develops osteoclast-deficient osteopetrosis, which was indicative of the key role of M-CSF in osteoclastogenesis. The interaction of M-CSF and c-FMS leads to the dimerization and phosphorylation of c-FMS, which then provides necessary signals for the proliferation and survival of osteoclast precursor cells. However, M-CSF by itself cannot complete this process. The differentiation of osteoclast precursor cells also require RANKL expression from osteoclast stromal cells and RANK expression from osteoclast precursor cells (Boyle et al., 2003). In the presence of M-CSF, RANKL binds to RANK and then activates transcription factors such as NF-κB, promoting the differentiation of osteoclast progenitors and limiting the apoptosis of mature osteoclasts. In addition to activating multiple transcription factors, RANKL also promotes osteoclast formation by stimulating all three families of mitogen-activated protein (MAP) kinases (Wada et al., 2006). Importantly, the activation of the activator protein 1 (AP-1)/nuclear factor of activated T-cells cytoplasmic 1 (NFATc1) transcription complex is a major osteoclastogenic event. RANKL produces this transcription complex by increasing the expression of the c-Fos family of proteins and promoting the nuclear translocation of Jun proteins. The dephosphorylation of NFATc1 by calcineurin in turn promotes its nuclear translocation. Dysfunction of c-Jun, c-Fos, or NFATc1 can lead to failure of osteoclast activation and cause severe osteopetrosis. Furthermore, RANKL can also promote bone destruction by inducing mature osteoclasts to generate a complex consisting of their receptor TRAF6 and c-Src, which specifically recruit cytokines to lipid rafts in the plasma membrane (Teitelbaum and Ross, 2003).

FUNCTIONS OF THE RANKL/RANK SYSTEM IN PRIMARY BREAST CANCER DEVELOPMENT AND BONE METASTASIS

To successfully survive in the primary and secondary site, breast cancer cells must possess certain unique characteristics and the bone matrix needs to provide a suitable environment.

The RANKL/RANK System Is Involved in the Initial Phases of Breast Cancer Development

In addition to the essential roles of the RANKL/RANK system in bone metabolism, reports show that RANK and RANKL act as key factors in the formation of lactating mammary glands during pregnancy (Fata et al., 2000). The expression of RANKL on mammary epithelial cells is induced by sex and pregnancy hormones. RANKL deficiency can affect the formation of the lobo-alveolar structures, which is required for lactation. RANKL expression is required for promoting the survival and proliferation of epithelial cells, as well as for lobulo-alveolar development. The dysregulation of this coordinated mechanism in transgenic mice might promote the formation of pre-neoplasias and subsequently tumor foci (Gonzalez-Suarez et al., 2010). In addition, the RANKL/RANK axis is pro-active in EMT; therefore, the RANKL/RANK system also mediates the expansion of mammary stem cells and controls the development of hormone-dependent breast cancer. Reduction in RANK expression in the mammary gland of female mice can dramatically decrease sex hormone-induced mammary cancer. Furthermore, RANK/RANKL confers resistance to γ-irradiation-induced cell death in mammary epithelial cells, changes cell

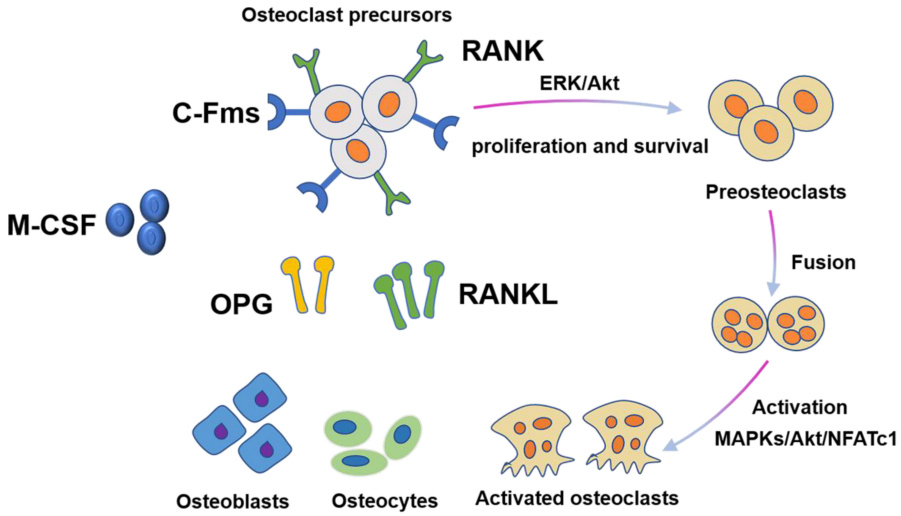


FIGURE 2 | Osteoclast differentiation is stimulated by M-CSF and RANKL. M-CSF induces the proliferation and survival of osteoclast precursor cells through activation of ERK and Akt. RANKL recruits TRAF6 to activate MAPKs, Akt, and NFATc1 to promote differentiation of osteoclast precursors to osteoclasts.

adhesion, and regulates the self-renewal capacity of tumor stem cells, contributing to the development of mammary cancer.

The RANKL/RANK System Contributes to Bone Metastasis

Direct Mechanisms

In addition to the chemotaxis caused by the interaction of CXCR4/12, RANKL in bone tissue can also attract RANK-expressing circulating breast cancer cells to the bone matrix (Jones et al., 2006; Jacob et al., 2011). Jones et al. (2006) was the first to demonstrate the chemoattractant activity of RANKL (Chawla et al., 2013). They demonstrated that the osteoblasts and bone marrow stromal cells that produced RANKL could not only attract RANK-expressing tumor cells, but also induce their migration. This mechanism is widely accepted and has been observed in many other types of cancer, including breast cancer. Current evidence suggests that around 25% breast cancer cells express RANK. Cells overexpressing RANK in intra-arterial injection showed faster tumor progression and lower overall survival rate due to enhanced bone homing and colonization than wild-type MDA-MB 231 cells. *In vitro* studies have shown that RANK overexpression in MCF-10A cells decreases intercellular contact and enhances migration (Palafox et al., 2012). RANKL-enhanced migration activates specific signaling cascades such as the MAP kinase pathways. Subsequently, the RANKL/RANK axis regulates the migration of breast cancer cells, and RANKL acts as a chemo-attractive agent on tumor cells overexpressing one of its receptors. *In vivo*, blocking of this signaling with AMG161 (IgG1 equivalent to denosumab) reduces the formation of bone marrow micro-metastasis (Sousa et al., 2018).

Indirect Mechanisms

In addition to directly attracting RANK-expressing breast cancer cells, RANKL can also modulate the microenvironment of the metastatic site. RANKL is not only expressed by the mammary epithelial cells but is also expressed on the surface of breast cancer cells. RANKL can promote both the survival and proliferation of epithelial cell precursors during breast development and simultaneously up-regulate the expression of RANK. By interacting with RANK, RANKL can facilitate neoformation of vascular tubes and then stimulate angiogenesis via the Src and phospholipase C-dependent pathway. Blood vessels provide necessary nutrients for cancer cell proliferation, and also act as one of the most prevalent means of cell migration. In addition, RANKL increases vascular permeability, which assists the breast tumor cells in escaping from the blood vessels into systematic circulation.

THE VICIOUS CYCLE OF BONE METASTASIS

More than a century ago, Stephen Paget first presented the "seed and soil" theory to describe the relationship between CTCs (seed) and metastatic sites (soil) (Langley and Fidler, 2011). Tumor cells of varying origin prefer to metastasize to different organs (Ben-Baruch, 2009). The bone is the most preferred organ for breast cancer metastasis. Although osteoblastic or mixed lesions have been observed, most breast cancer metastasis are bone lytic diseases. Osteolytic bone metastasis accounts for 80−90% cases among all patients with metastatic breast cancer (Kang et al., 2003). The exact mechanism underlying the migration of breast cancer cells to the bone remains to be elucidated, although current evidence indicates that bone metastasis is related to a crosstalk between breast cancer cells and the bone microenvironment (Azim and Azim, 2013).

Owing to the combined efforts of chemokines, circulating breast cancer cells are attracted to the bone (Sun et al., 2010). The mineralized bone matrix releases relevant growth

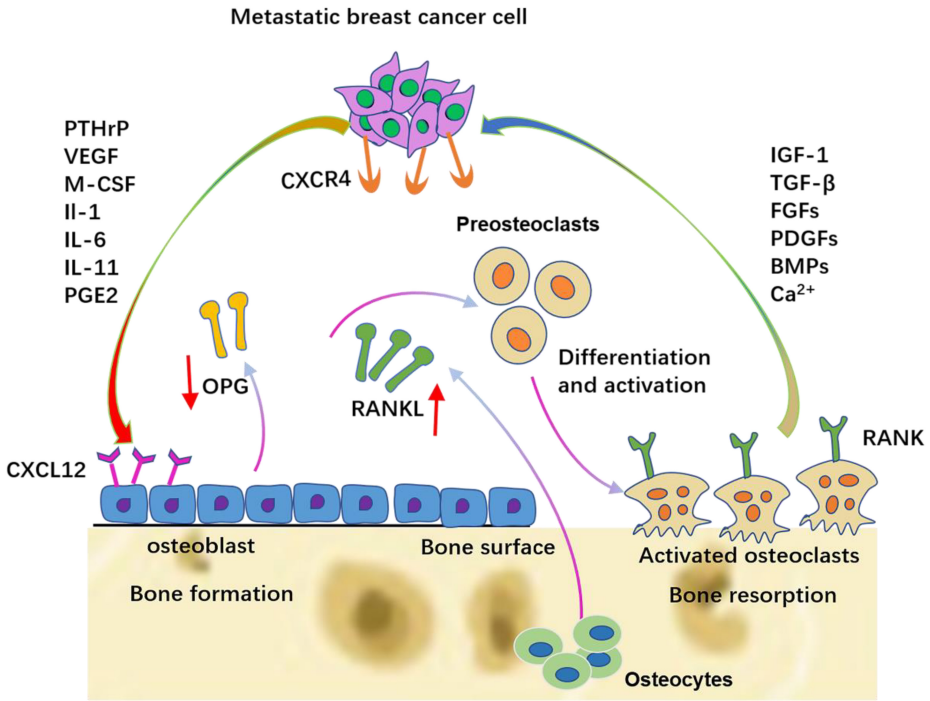


FIGURE 3 | The vicious cycle between breast cancer cells and bone. Breast cancer cells secrete soluble factors, including PTHrP, VEGF, IL-6, IL-8, and IL-11, which in the bone metastatic site act on osteoblasts/osteoclasts. The production of RANKL is increased and the production of OPG is decreased from osteoblasts. Late-stage pre-osteoclast cells respond to specific breast cancer-secreted factors by differentiation and osteolytic activation.

factors, including IGFs, TGF-β, FGFs, PDGFs, and BMPs, when interacting with metastatic breast cancer cells, and therefore, it offers a specific fertile environment for tumor cell proliferation and aggression. PDGFs, BMPs, and calcium in the bone matrix can enhance the survival of tumor cells (Sanders et al., 2000; Weilbaecher et al., 2011). Experimental evidence showed that bone-derived IGF can promote the proliferation and survival of cancer cells via the Akt/NF-κB pathway (Samani et al., 2007; Maki, 2010). As the second-most abundant growth factor in the bone extracellular matrix, TGF-β plays critical roles in inducing the vicious cycle.

After the colonization of DTCs, bone-derived TGF-β stimulates breast cancer cells to synthesize PTHrP, prostaglandin E2 (PGE2), IL-1, IL-6, and IL-11. PTHrP is one of the most important factors in mediating osteoclast activation in metastatic human breast cancer. Breast cancer cells present in the metastatic bone site produce higher amounts of PTHrP than cells in the breast or soft-tissue sites (Soki et al., 2012). These cytokines first bind to osteoblasts or stromal cells via the corresponding receptors and then up-regulate the expression of RANKL and simultaneously down-regulate the expression of OPG. The up-regulated RANKL interacts with RANK on the hematopoietic osteoclast precursors to induce mature osteoclast production. Therefore, these cytokines stimulate osteoclastic bone destruction indirectly. The resorbed bone can further release TGF-β and IGF1, thereby stimulating the proliferation of tumor cells to produce more PTHrP via Smad and the p38 MAPK signaling pathway (Le Pape et al., 2016), which in turn causes more bone resorption. This is termed the vicious cycle (**Figure 3**).

RANKL/RANK SYSTEM-BASED THERAPEUTIC STRATEGIES FOR BREAST CANCER BONE METASTASIS

Metastatic cancer cells must possess the ability to promote bone resorption to establish and grow in bone tissue. Hence, the key factors that prevent or hinder metastasis must reduce osteoclast differentiation and activation. Therefore, regulation of the main factors involved in the metastatic process, especially in the vicious cycle, should be promising.

Bisphosphonates

Currently, bisphosphonates are clinically used to treat bone complications of malignant tumors. Bisphosphonates, which include amino-bisphosphonates (ibandronate, pamidronate, and zoledronic acid) and non-amino bisphosphonates (clondronate), hinder the survival and stimulate apoptosis of mature bone-resorbing osteoclasts to suppress bone resorption. However, bisphosphonates act only on the mature, actively resorting osteoclasts, but has no effect on the residual osteoclasts (Morony et al., 2005). This might explain why zoledronic acid, which has been approved by the Food and Drug Administration (FDA) to treat patients with solid tumor bone metastasis, does not affect the patient survival rate (Coleman, 2002, 2004). Furthermore,

TABLE 1 | Some clinical trials which are involved in denosumab.

Status	Study title	Goal	Study phase	Clinical trial Gov. Identifier
Completed	Denosumab for Breast Cancer with Bone Mets	To learn if denosumab in combination with a hormonal drug can help lower the number of circulating tumor cells (CTCs) in patients with breast cancer that has spread to the bone.	Phase 2	NCT01952054
Terminated	Study of Denosumab as Adjuvant Treatment for Women with High Risk Early Breast Cancer Receiving Neoadjuvant or Adjuvant Therapy (D-CARE)	To study the effect of denosumab to see if it can prevent disease recurrence in the bone or in any other part of the body, when it is given as adjuvant therapy for women with early-stage breast cancer, who are at high risk of disease recurrence.	Phase 3	NCT01077154
Terminated	A Study to Evaluate Denosumab in Young Patients with Primary Breast Cancer	To determine if a short course of RANKL inhibition with denosumab can induce a decrease in tumor proliferation rates as determined by Ki67 immunohistochemistry (IHC) in newly diagnosed, early stage breast cancer in pre-menopausal women.	Phase 2a	NCT01864798
Completed	Denosumab (AMG 162) in Bisphosphonate Naive Metastatic Breast Cancer	To evaluate various doses and schedules for denosumab administration and characterize the safety profile in this indication.	Phase 2	NCT00091832
Completed	AMG 162 in the Treatment of Bone Loss in Subjects Undergoing Aromatase Inhibitor Therapy for Non-metastatic Breast Cancer	To evaluate AMG 162 in the treatment of bone loss in subjects undergoing Aromatase Inhibitor Therapy for Non-metastatic Breast Cancer.	Phase 3	NCT00089661
Terminated	Denosumab in Treating Patients with ER and/or PR Positive, HER2 Negative Metastatic Breast Cancer With Bone Metastases and Detectable Circulating Tumor Cells	To look at the amount of cancer cells in the blood of participants who are being treated with denosumab. To look at how long it takes for cancer to get worse when participants are being treated with denosumab.	Phase 2	NCT03070002
Completed	A Study Comparing Denosumab vs. Zoledronic Acid for the Treatment of Bone Metastases in Breast Cancer Subjects.	To determine if denosumab is non-inferior to zoledronic acid in the treatment of bone metastases in subjects with advanced breast cancer.	Phase 3	NCT00321464
Completed	RANKL Inhibition and Breast Tissue Biomarkers	To investigate the effect of RANKL inhibition with denosumab on breast tissue markers in high-risk premenopausal women with dense breasts.	Phase 1	NCT03629717
Completed	Open Label Extension to SRE Studies in United Kingdom and Czech Republic Only	To describe the safety and tolerability of denosumab administration as measured by adverse events, immunogenicity, and safety laboratory parameters in subjects who previously received either zoledronic acid (Zometa) or denosumab.	Phase 3	NCT00950911

(Continued)

TABLE 1 | Continued

Status	Study title	Goal	Study phase	Clinical trial Gov. Identifier
Completed	Study of AMG 162 in Subjects with Advanced Cancer Currently Being Treated with Intravenous (IV) Bisphosphonates	To determine the effectiveness of AMG 162 in reducing urinary N-telopeptide in advanced cancer subjects with bone metastases.	Phase 2	NCT00104650
Completed	Study of Denosumab in the Treatment of Hypercalcemia of Malignancy in Subjects with Elevated Serum Calcium	To determine the potential of denosumab to treat Hypercalcemia of Malignancy in patients with elevated serum calcium who do not respond to recent treatment with intravenous bisphosphonates by lowering corrected serum calcium < / = 11.5 mg/dL (2.9 millimoles/L) by day 10.	Phase 2	NCT00896454

many patients continue to develop SREs after bisphosphonate treatment, which warrants development of novel and effective strategies for managing these patients.

Direct and Indirect Targeting of RANKL

As previously mentioned, RANKL plays fundamental roles in the progression of primary breast cancer and bone metastasis. Hence, targeting RANKL has been an important therapeutic approach for patients with osteoclastic bone metastasis.

As OPG is one of the receptors of RANKL, interfering with RANKL function might be an efficient way of decreasing bone destruction (Morony et al., 2005). Canon et al. showed that administration of an OPG-Fc construct in a mouse model with breast cancer bone metastasis may block skeletal tumor progression and improve survival by inhibiting RANKL (Canon et al., 2008). Therefore, a genetically modified recombinant OPG-Fc construct (AMGN-0007) was developed for treating patients with bone metastases. When used for treating patients with breast cancer or multiple myeloma, AMGN-0007 has the same effect as pamidronate in reducing bone destruction (Body et al., 2003). Nevertheless, the short half-lives of several factors have prevented further research and application of this drug in clinical use. In addition, OPG can not only bind to RANKL, but can also block TNF-related apoptosis inducing ligand (TRAIL) (Emery et al., 1998). Importantly, TRAIL is considered to be a significant part of natural anticancer immunity and is the main mediator for host immune cells in inducing tumor cell death (Neville-Webbe et al., 2004).

On the other hand, a monoclonal antibody specific to human RANKL, denosumab, has shown promising clinical implications (Cummings et al., 2009). In addition, evidence shows that denosumab is efficient and safe, and is better than zoledronic acid in delaying or preventing SREs (Stopeck et al., 2010; Martin et al., 2012). Currently, denosumab has been approved by the FDA for treating treatment-induced bone loss and osteoporosis in women with high risk of fractures and metastases to bone. Denosumab acts by binding to human RANKL with high affinity and specificity and blocks its binding to RANK, thereby inhibiting RANK-medicated osteoclast formation, ultimately increasing bone volume and density (Cummings et al., 2009). Unlike OPG, denosumab not only avoids potential reactions with TRAIL, but also exerts the same beneficial effects as OPG (Abrahamsen and Teng, 2005). Denosumab is administered via subcutaneous injection and cannot be excreted via the kidney or be metabolized by the liver owing to its large molecular weight. Furthermore, unlike the mechanism of action of bisphosphonates, denosumab blocks the differentiation, activation, and survival of osteoclast precursor cells and completely eliminates osteoclasts in the treated bone tissue (Baron et al., 2011). Some clinical trials involving denosumab are shown in **Table 1**.

It is noteworthy that three clinical trials were approved for determining the effectiveness of denosumab in order to prevent the skeletal sequelae in patients with bone metastases. These clinical trials showed that denosumab caused more severe hypocalcemia than zoledronic acid (Lipton et al., 2010). Medication-related osteonecrosis of the jaw (MRONJ) involves progressive bone destruction in the jaws that occurs when anti-resorptive or anti-angiogenic drugs are used. The first case of denosumab-related ONJ was reported in a 73-year-old man diagnosed with prostatic adenocarcinoma. These clinical trials demonstrated that events of ONJ occurred more in the denosumab group than in the zoledronic acid group (2.0%, denosumab; 1.4%, zoledronic acid) (Saad et al., 2011). Therefore, whether denosumab is the best therapeutic choice for patients should be evaluated.

CONCLUSION

The common cause of death for breast cancer patients is bone metastasis, nearly 80% of which are due to osteolytic lesions. Bone metastasis always leads to devastating consequences. The life expectancy for patients with metastatic breast cancer is 2−3 years. Bone metastasis also deteriorates the quality of life by inducing severe bone pain and SREs. Therefore, the mechanism of osteolysis should be understood to design relevant therapeutic strategies. In this article, the roles of the RANKL/RANK axis in the development of primary breast cancer and secondary

establishment of bone metastasis were reviewed. The steps involved in the development of bone metastasis were also clearly described.

The RANKL/RANK system plays a critical role in breast cancer development, both during initial tumorigenesis and formation of secondary tumors in the bone. RANKL can promote the survival and proliferation of epithelial cells during the development of mammary glands and simultaneously up-regulate the expression of RANK. The RANKL/RANK system is pro-active in EMT and can promote cell migration and neovascularization (Min et al., 2003). In addition, similar to the CXCR4/12 interaction, RANKL can also attract circulating breast cancer cells to the bone matrix via the RANKL/RANK system. Therefore, targeting of RANKL has been a novel therapeutic target for treating breast cancer bone metastasis.

Currently, bone metastasis of primary breast tumors appears incurable, and disruption of the osteolytic cycle by targeting osteoclasts constitutes the main therapeutic intervention. Bisphosphonates have been used to treat patients with breast cancer bone metastasis, albeit severe side effects. Therefore, more effective therapies are urgently required. The functions of RANKL in breast cancer metastasis to bone have been described in detail in this review. Denosumab, a completely human IgG2 monoclonal antibody, was used to treat patients with osteoporosis, metastases to bone, and treatment-induced bone loss. Denosumab competitively binds to RANKL, thereby blocking the binding of RANKL to RANK and inhibiting RANK-medicated osteoclastogenesis, ultimately increasing bone volume and density. The main side effect of denosumab might be the incidence of osteonecrosis of the jaw in few patients. In addition, denosumab has no effect on the survival rate of patients with bone metastasis, which suggests that inhibition of osteoclastic resorption alone might be not sufficient for suppressing tumor dissemination. Further research is required to understand the mechanism of metastasis and develop more effective therapies directed at improving the quality of life of patients with bone metastasis.

AUTHOR CONTRIBUTIONS

XW wrote the manuscript. FL and LD helped in revising the manuscript. XW contributed in figure designing. CL contributed to the manuscript for literature research. AL and GZ revised and approved the manuscript.

FUNDING

This study was supported by the National Key R&D Program of China (2018YFA0800804) and the National Natural Science Foundation of China (81700780 and 81922081).

ACKNOWLEDGMENTS

Sincere thanks should go to the other academic and staff members in AL and GZ's group at Hong Kong Baptist University. We also thank Hong Kong Baptist University for providing critical comments and technical support. Dr. Simon Wang at the Language Centre of HKBU has helped improve the linguistic presentation of the manuscript.

REFERENCES

Abrahamsen, B., and Teng, A. (2005). Technology evaluation: denosumab, Amgen. *Curr. Opin. Mol. Ther.* 7, 604–610.

Akhtari, M., Mansuri, J., Newman, K. A., Guise, T. M., and Seth, P. (2008). Biology of breast cancer bone metastasis. *Cancer Biol. Ther.* 7, 3–9.

Armstrong, A. P., Tometsko, M. E., Glaccum, M., Sutherland, C. L., Cosman, D., and Dougall, W. C. (2002). A RANK/TRAF6-dependent signal transduction pathway is essential for osteoclast cytoskeletal organization and resorptive function. *J. Biol. Chem.* 277, 44347–44356. doi: 10.1074/jbc.m202009200

Azim, H., and Azim, H. A. Jr. (2013). Targeting RANKL in breast cancer: bone metastasis and beyond. *Expert Rev. Anticancer Ther.* 13, 195–201. doi: 10.1586/era.12.177

Baron, R., Ferrari, S., and Russell, R. G. G. (2011). Denosumab and bisphosphonates: different mechanisms of action and effects. *Bone* 48, 677–692. doi: 10.1016/j.bone.2010.11.020

Ben-Baruch, A. (2009). Site-specific metastasis formation: chemokines as regulators of tumor cell adhesion, motility and invasion. *Cell Adh. Migr.* 3, 328–333. doi: 10.4161/cam.3.4.9211

Blair, J. M., Zhou, H., Seibel, M. J., and Dunstan, C. R. (2006). Mechanisms of disease: roles of OPG, RANKL and RANK in the pathophysiology of skeletal metastasis. *Nat. Rev. Clin. Oncol.* 3, 41–49. doi: 10.1038/ncponc0381

Boabaid, F., Berry, J. E., Koh, A. J., Somerman, M. J., and McCauley, L. K. (2004). The role of parathyroid hormone−related protein in the regulation of osteoclastogenesis by cementoblasts. *J. Periodontol.* 75, 1247–1254. doi: 10.1902/jop.2004.75.9.1247

Body, J. J., Greipp, P., Coleman, R. E., Facon, T., Geurs, F., Fermand, J. P., et al. (2003). A phase I study of AMGN−0007, a recombinant osteoprotegerin construct, in patients with multiple myeloma or breast carcinoma related bone metastases. *Cancer* 97, 887–892. doi: 10.1002/cncr.11138

Bonnomet, A., Brysse, A., Tachsidis, A., Waltham, M., Thompson, E. W., Polette, M., et al. (2010). Epithelial-to-mesenchymal transitions and circulating tumor cells. *J. Mammary Gland Biol. Neoplasia* 15, 261–273. doi: 10.1007/s10911-010-9174-0

Boron, W. F., and Boulpaep, E. L. (2005). Medical physiology: a cellular and molecular approach. Philadelphia, PA: Saunders Elsevier.

Boyce, B. F., and Xing, L. (2007). Biology of RANK, RANKL, and osteoprotegerin. *Arthritis Res. Ther.* 9(Suppl. 1):S1.

Boyce, B. F., and Xing, L. (2008). Functions of RANKL/RANK/OPG in bone modeling and remodeling. *Arch. Biochem. Biophys.* 473, 139–146. doi: 10.1016/j.abb.2008.03.018

Boyle, W. J., Simonet, W. S., and Lacey, D. L. (2003). Osteoclast differentiation and activation. *Nature* 423, 337–342. doi: 10.1038/nature01658

Brodsky, B., and Persikov, A. V. (2005). Molecular structure of the collagen triple helix. *Adv. Protein Chem.* 70, 301–339. doi: 10.1016/s0065-3233(05)70009-7

Canon, J. R., Roudier, M., Bryant, R., Morony, S., Stolina, M., Kostenuik, P. J., et al. (2008). Inhibition of RANKL blocks skeletal tumor progression and improves survival in a mouse model of breast cancer bone metastasis. *Clin. Exp. Metastasis* 25, 119–129. doi: 10.1007/s10585-007-9127-1

Cetin, K., Christiansen, C. F., Sværke, C., Jacobsen, J. B., and Sørensen, H. T. (2015). Survival in patients with breast cancer with bone metastasis: a Danish population-based cohort study on the prognostic impact of initial stage of disease at breast cancer diagnosis and length of the bone metastasis-free interval. *BMJ Open* 5:e007702. doi: 10.1136/bmjopen-2015-007702

Chamoux, E., Houde, N., L'eriger, K., and Roux, S. (2008). Osteoprotegerin decreases human osteoclast apoptosis by inhibiting the TRAIL pathway. *J. Cell. Physiol.* 216, 536–542. doi: 10.1002/jcp.21430

Charles, J. F., and Aliprantis, A. O. (2014). Osteoclasts: more than 'bone eaters'. *Trends Mol. Med.* 20, 449–459. doi: 10.1016/j.molmed.2014.06.001

Chawla, S., Henshaw, R., Seeger, L., Choy, E., Blay, J.-Y., Ferrari, S., et al. (2013). Safety and efficacy of denosumab for adults and skeletally mature adolescents with giant cell tumour of bone: interim analysis of an open-label, parallel-group, phase 2 study. *Lancet Oncol.* 14, 901–908. doi: 10.1016/S1470-2045(13)70277-8

Chen, G., Sircar, K., Aprikian, A., Potti, A., Goltzman, D., and Rabbani, S. A. (2006). Expression of RANKL/RANK/OPG in primary and metastatic human prostate cancer as markers of disease stage and functional regulation. *Cancer* 107, 289–298. doi: 10.1002/cncr.21978

Chen, Y.-C., Sosnoski, D. M., and Mastro, A. M. (2010). Breast cancer metastasis to the bone: mechanisms of bone loss. *Breast Cancer Res.* 12:215. doi: 10.1186/bcr2781

Chirgwin, J. M., and Guise, T. A. (2000). Molecular mechanisms of tumor-bone interactions in osteolytic metastases. *Crit. Rev. Eukaryot. Gene Exp.* 10, 159–178.

Clarke, B. (2008). Normal bone anatomy and physiology. *Clin. J. Am. Soc. Nephrol.* 3(Suppl. 3), S131–S139. doi: 10.2215/CJN.04151206

Clines, G., and Guise, T. (2005). Hypercalcaemia of malignancy and basic research on mechanisms responsible for osteolytic and osteoblastic metastasis to bone. *Endocr. Relat. Cancer* 12, 549–583. doi: 10.1677/erc.1.00543

Coleman, R. E. (2002). Bisphosphonates for the prevention of bone metastases. *Sem. Oncol.* 29(Suppl. 21), 43–49. doi: 10.1053/sonc.2002.37415

Coleman, R. E. (2004). The role of bisphosphonates in breast cancer. *Breast* 13, 19–28. doi: 10.1016/j.breast.2004.09.004

Crane, J. L., and Cao, X. (2014). Function of matrix IGF-1 in coupling bone resorption and formation. *J. Mol. Med.* 92, 107–115. doi: 10.1007/s00109-013-1084-3

Cummings, S. R., Martin, J. S., McClung, M. R., Siris, E. S., Eastell, R., Reid, I. R., et al. (2009). Denosumab for prevention of fractures in postmenopausal women with osteoporosis. *N. Eng. J. Med.* 361, 756–765. doi: 10.1056/NEJMoa0809493

Cundy, T., Hegde, M., Naot, D., Chong, B., King, A., Wallace, R., et al. (2002). A mutation in the gene TNFRSF11B encoding osteoprotegerin causes an idiopathic hyperphosphatasia phenotype. *Hum. Mol. Genet.* 11, 2119–2127. doi: 10.1093/hmg/11.18.2119

Dai, J., Escara-Wilke, J., Keller, J. M., Jung, Y., Taichman, R. S., Pienta, K. J., et al. (2019). Primary prostate cancer educates bone stroma through exosomal pyruvate kinase M2 to promote bone metastasis. *J. Exp. Med.* 216, 2883–2899. doi: 10.1084/jem.20190158

Dougall, W. C., and Chaisson, M. (2006). The RANK/RANKL/OPG triad in cancer-induced bone diseases. *Cancer Metastasis Rev.* 25, 541–549. doi: 10.1007/s10555-006-9021-3

Emery, J. G., McDonnell, P., Burke, M. B., Deen, K. C., Lyn, S., Silverman, C., et al. (1998). Osteoprotegerin is a receptor for the cytotoxic ligand TRAIL. *J. Biol. Chem.* 273, 14363–14367. doi: 10.1074/jbc.273.23.14363

Fata, J. E., Kong, Y.-Y., Li, J., Sasaki, T., Irie-Sasaki, J., Moorehead, R. A., et al. (2000). The osteoclast differentiation factor osteoprotegerin-ligand is essential for mammary gland development. *Cell* 103, 41–50. doi: 10.1016/s0092-8674(00)00103-3

Felding-Habermann, B., O'Toole, T. E., Smith, J. W., Fransvea, E., Ruggeri, Z. M., Ginsberg, M. H., et al. (2001). Integrin activation controls metastasis in human breast cancer. *Proc. Natl. Acad. Sci. U.S.A.* 98, 1853–1858. doi: 10.1073/pnas.98.4.1853

Fidler, I. J. (2003). The pathogenesis of cancer metastasis: the'seed and soil'hypothesis revisited. *Nat. Rev. Cancer* 3, 453–458. doi: 10.1038/nrc1098

Florencio-Silva, R., Sasso, G. R. D. S., Sasso-Cerri, E., Simões, M. J., and Cerri, P. S. (2015). Biology of bone tissue: structure, function, and factors that influence bone cells. *BioMed Res. Int.* 2015:421746.

Gonzalez-Suarez, E., Jacob, A. P., Jones, J., Miller, R., Roudier-Meyer, M. P., Erwert, R., et al. (2010). RANK ligand mediates progestin-induced mammary epithelial proliferation and carcinogenesis. *Nature* 468, 103–107. doi: 10.1038/nature09495

Guise, T. A. (2009). Breaking down bone: new insight into site-specific mechanisms of breast cancer osteolysis mediated by metalloproteinases. *Genes Dev.* 23, 2117–2123. doi: 10.1101/gad.1854909

Guise, T. A., Kozlow, W. M., Heras-Herzig, A., Padalecki, S. S., Yin, J. J., and Chirgwin, J. M. (2005). Molecular mechanisms of breast cancer metastases to bone. *Clin. Breast Cancer* 5(Suppl. 2), S46–S53.

Hauschka, P., Mavrakos, A., Iafrati, M., Doleman, S., and Klagsbrun, M. (1986). Growth factors in bone matrix. Isolation of multiple types by affinity chromatography on heparin-Sepharose. *J. Biol. Chem.* 261, 12665–12674.

Hayashi, M., Nakashima, T., Yoshimura, N., Okamoto, K., Tanaka, S., and Takayanagi, H. (2019). Autoregulation of osteocyte sema3a orchestrates estrogen action and counteracts bone aging. *Cell Metab.* 29, 627.e5–637.e5. doi: 10.1016/j.cmet.2018.12.021

Heldin, C.-H., Vanlandewijck, M., and Moustakas, A. (2012). Regulation of EMT by TGFβ in cancer. *FEBS Lett.* 586, 1959–1970.

Hikita, A., Yana, I., Wakeyama, H., Nakamura, M., Kadono, Y., Oshima, Y., et al. (2006). Negative regulation of osteoclastogenesis by ectodomain shedding of receptor activator of NF-κB ligand. *J. Biol. Chem.* 281, 36846–36855. doi: 10.1074/jbc.m606656200

Hofbauer, L. C., and Heufelder, A. E. (2001). Role of receptor activator of nuclear factor-κB ligand and osteoprotegerin in bone cell biology. *J. Mol. Med.* 79, 243–253. doi: 10.1007/s001090100226

Ibrahim, T., Mercatali, L., and Amadori, D. (2013). A new emergency in oncology: bone metastases in breast cancer patients. *Oncol. Lett.* 6, 306–310. doi: 10.3892/ol.2013.1372

Ikebuchi, Y., Aoki, S., Honma, M., Hayashi, M., Sugamori, Y., Khan, M., et al. (2018). Coupling of bone resorption and formation by RANKL reverse signalling. *Nature* 561, 195–200. doi: 10.1038/s41586-018-0482-7

Ikeda, T., Kasai, M., Utsuyama, M., and Hirokawa, K. (2001). Determination of three isoforms of the receptor activator of nuclear factor-κB ligand and their differential expression in bone and thymus. *Endocrinology* 142, 1419–1426. doi: 10.1210/endo.142.4.8070

Ishay-Ronen, D., Diepenbruck, M., Kalathur, R. K. R., Sugiyama, N., Tiede, S., Ivanek, R., et al. (2019). Gain fat-lose metastasis: converting invasive breast cancer cells into adipocytes inhibits cancer metastasis. *Cancer Cell* 35, 17.e6–32.e6. doi: 10.1016/j.ccell.2018.12.002

Jacob, A., Branstetter, D., Rohrbach, K., Winters, A., Erwert, R., and Allred, S. (2011). P3-01-14: RANK and RANK Ligand (RANKL) expression in invasive breast carcinoma and human breast cancer cell lines AACR). *Cancer Res.* 71(Suppl. 24):P3-01-14–P3-01-14.

Jacome-Galarza, C. E., Percin, G. I., Muller, J. T., Mass, E., Lazarov, T., Eitler, J., et al. (2019). Developmental origin, functional maintenance and genetic rescue of osteoclasts. *Nature* 568, 541–545. doi: 10.1038/s41586-019-1105-7

Jin, X., and Mu, P. (2015). Targeting breast cancer metastasis. *Breast Cancer* 9(Suppl. 1), 23–34.

Jones, D. H., Nakashima, T., Sanchez, O. H., Kozieradzki, I., Komarova, S. V., Sarosi, I., et al. (2006). Regulation of cancer cell migration and bone metastasis by RANKL. *Nature* 440, 692–696.

Käkönen, S.-M., Selander, K. S., Chirgwin, J. M., Yin, J. J., Burns, S., Rankin, W. A., et al. (2002). Transforming growth factor-β stimulates parathyroid hormone-related protein and osteolytic metastases via Smad and mitogen-activated protein kinase signaling pathways. *J. Biol. Chem.* 277, 24571–24578. doi: 10.1074/jbc.m202561200

Kan, C., Vargas, G., Pape, F. L., and Clézardin, P. (2016). Cancer cell colonisation in the bone microenvironment. *Int. J. Mol. Sci.* 17:1674. doi: 10.3390/ijms17101674

Kang, Y., Siegel, P. M., Shu, W., Drobnjak, M., Kakonen, S. M., Cordón-Cardo, C., et al. (2003). A multigenic program mediating breast cancer metastasis to bone. *Cancer Cell* 3, 537–549. doi: 10.1016/s1535-6108(03)00132-6

Kim, N.-S., Kim, H.-J., Koo, B.-K., Kwon, M.-C., Kim, Y.-W., Cho, Y., et al. (2006). Receptor activator of NF-κB ligand regulates the proliferation of mammary epithelial cells via Id2. *Mol. Cell. Biol.* 26, 1002–1013. doi: 10.1128/mcb.26.3.1002-1013.2006

Kini, U., and Nandeesh, B. (2012). Physiology of bone formation, remodeling, and metabolism. *Radionucl. Hybrid Bone Imaging* 3, 29–57. doi: 10.1007/978-3-642-02400-9_2

Kobayashi, N., Kadono, Y., Naito, A., Matsumoto, K., Yamamoto, T., Tanaka, S., et al. (2001). Segregation of TRAF6−mediated signaling pathways clarifies its role in osteoclastogenesis. *EMBO J.* 20, 1271–1280. doi: 10.1093/emboj/20.6.1271

Kozlow, W., and Guise, T. A. (2005). Breast cancer metastasis to bone: mechanisms of osteolysis and implications for therapy. *J. Mammary Gland Biol. Neoplasia* 10, 169–180. doi: 10.1007/s10911-005-5399-8

Lambert, A. W., Pattabiraman, D. R., and Weinberg, R. A. (2017). Emerging biological principles of metastasis. *Cell* 168, 670–691. doi: 10.1016/j.cell.2016.11.037

Langley, R. R., and Fidler, I. J. (2011). The seed and soil hypothesis revisited—The role of tumor−stroma interactions in metastasis to different organs. *Int. J. Cancer* 128, 2527–2535. doi: 10.1002/ijc.26031

Le Pape, F., Vargas, G., and Clézardin, P. (2016). The role of osteoclasts in breast cancer bone metastasis. *J. Bone Oncol.* 5, 93–95. doi: 10.1016/j.jbo.2016.02.008

Lipton, A., Siena, S., Rader, M., Bilynskyy, B., Viniegra, M., and Richardson, G. (2010). Comparison of denosumab versus zoledronic acid (ZA) for treatment of bone metastases in advanced cancer patients: an integrated analysis of 3 pivotal trials. *Ann. Oncol.* 21, 380–380.

Luo, J., Yang, Z., Ma, Y., Yue, Z., Lin, H., Qu, G., et al. (2016). LGR4 is a receptor for RANKL and negatively regulates osteoclast differentiation and bone resorption. *Nat. Med.* 22, 539–546. doi: 10.1038/nm.4076

Maki, R. G. (2010). Small is beautiful: insulin-like growth factors and their role in growth, development, and cancer. *J. Clin. Oncol.* 28, 4985–4995. doi: 10.1200/JCO.2009.27.5040

Mareel, M., and Leroy, A. (2003). Clinical, cellular, and molecular aspects of cancer invasion. *Physiol. Rev.* 83, 337–376. doi: 10.1152/physrev.00024.2002

Martin, M., Bell, R., Bourgeois, H., Brufsky, A., Diel, I., Eniu, A., et al. (2012). Bone-related complications and quality of life in advanced breast cancer: results from a randomized phase III trial of denosumab versus zoledronic acid. *Clin Cancer Res.* 18, 4841–4849. doi: 10.1158/1078-0432.ccr-11-3310

Mastro, A. M., Gay, C. V., and Welch, D. R. (2003). The skeleton as a unique environment for breast cancer cells. *Clin. Exp. Metastasis* 20, 275–284.

Miller, P. D. (2009). Denosumab: anti-RANKL antibody. *Curr. Osteoporos. Rep.* 7, 18–22. doi: 10.1007/s11914-009-0004-5

Min, J.-K., Kim, Y.-M., Kim, Y.-M., Kim, E.-C., Gho, Y. S., and Kang, I.-J. (2003). Vascular endothelial growth factor up-regulates expression of receptor activator of NF-kB (RANK) in endothelial cells: Concomitant increase of angiogenic responses to RANK ligand. *J. Biol. Chem.* 278, 39548–395457.

Morony, S., Warmington, K., Adamu, S., Asuncion, F., Geng, Z., Grisanti, M., et al. (2005). The RANKL inhibitor osteoprotegerin (OPG) causes greater suppression of bone resorption and hypercalcemia compared to bisphosphonates in two models of humoral hypercalcemia of malignancy. *Endocrinology* 146, 3235–3243. doi: 10.1210/en.2004-1583

Müller, A., Homey, B., Soto, H., Ge, N., Catron, D., and Buchanan, M. E. (2001). Involvement of chemokine receptors in breast cancer metastasis. *Nature* 410, 50–56.

Mundy, G. R. (2002). Metastasis: Metastasis to bone: causes, consequences and therapeutic opportunities. *Nat. Rev. Cancer* 2, 584–593. doi: 10.1038/nrc867

Nagy, V., and Penninger, J. M. (2015). The rankl-rank story. *Gerontology* 61, 534–542. doi: 10.1159/000371845

Neville-Webbe, H., Cross, N., Eaton, C., Nyambo, R., Evans, C., Coleman, R., et al. (2004). Osteoprotegerin (OPG) produced by bone marrow stromal cells protects breast cancer cells from TRAIL-induced apoptosis. *Breast Cancer Res. Treat.* 86, 271–282. doi: 10.1023/b:brea.0000036900.48763.b3

Palafox, M., Ferrer, I., Pellegrini, P., Vila, S., Hernandez-Ortega, S., Urruticoechea, A., et al. (2012). RANK induces epithelial–mesenchymal transition and stemness in human mammary epithelial cells and promotes tumorigenesis and metastasis. *Cancer Res.* 72, 2879–2888. doi: 10.1158/0008-5472.CAN-12-0044

Pecheur, I., Peyruchaud, O., Serre, C.-M., Guglielmi, J., Voland, C., Bourre, F., et al. (2002). Integrin αvβ3 expression confers on tumor cells a greater propensity to metastasize to bone. *FASEB J.* 16, 1266–1268. doi: 10.1096/fj.01-0911fje

Rachner, T. D., Khosla, S., and Hofbauer, L. C. (2011). Osteoporosis: now and the future. *Lancet* 377, 1276–1287. doi: 10.1016/s0140-6736(10)62349-5

Rizzoli, R., Yasothan, U., and Kirkpatrick, P. (2010). *Denosumab. Nat. Rev. Drug Discov.* 9, 591–592.

Saad, F., Brown, J., Van Poznak, C., Ibrahim, T., Stemmer, S., Stopeck, A. T., et al. (2011). Incidence, risk factors, and outcomes of osteonecrosis of the jaw: integrated analysis from three blinded active-controlled phase III trials in cancer patients with bone metastases. *Ann. Oncol.* 23, 1341–1347. doi: 10.1093/annonc/mdr435

Samani, A. A., Yakar, S., LeRoith, D., and Brodt, P. (2007). The role of the IGF system in cancer growth and metastasis: overview and recent insights. *Endocr. Rev.* 28, 20–47. doi: 10.1210/er.2006-0001

Sanders, J. L., Chattopadhyay, N., Kifor, O., Yamaguchi, T., Butters, R. R., and Brown, E. M. (2000). Extracellular calcium-sensing receptor expression and its potential role in regulating parathyroid hormone-related peptide secretion in human breast cancer cell lines. *Endocrinology* 141, 4357–4364. doi: 10.1210/endo.141.12.7849

Santini, D., Schiavon, G., Vincenzi, B., Gaeta, L., Pantano, F., Russo, A., et al. (2011). Receptor activator of NF-kB (RANK) expression in primary tumors associates with bone metastasis occurrence in breast cancer patients. *PLoS One* 6:e19234. doi: 10.1371/journal.pone.0019234

Schoppet, M., Preissner, K. T., and Hofbauer, L. C. (2002). RANK ligand and osteoprotegerin: paracrine regulators of bone metabolism and vascular function. *Arterioscler. Thromb. Vasc. Biol.* 22, 549–553. doi: 10.1161/01.atv.0000012303.37971.da

Scully, O. J., Bay, B.-H., Yip, G., and Yu, Y. (2012). Breast cancer metastasis. *Cancer Genomics Proteomics* 9, 311–320.

Silva, I., and Branco, J. (2011). Rank/Rankl/opg: literature review. *Acta Reumatol. Port.* 36, 209–218.

Sisay, M., Mengistu, G., and Edessa, D. (2017). The RANK/RANKL/OPG system in tumorigenesis and metastasis of cancer stem cell: potential targets for anticancer therapy. *Onco Targets Ther.* 10, 3801–3810. doi: 10.2147/OTT.S135867

Soki, F. N., Park, S. I., and McCauley, L. K. (2012). The multifaceted actions of PTHrP in skeletal metastasis. *Future Oncol.* 8, 803–817. doi: 10.2217/fon.12.76

Sousa, S., Gineyts, E., Geraci, S., Croset, M., and Clézardin, P. (2018). "RANK-RANKL signaling inhibition delays early breast cancer bone metastasis formation. AACR)," in *Proceedings of the American Association for Cancer Research Annual Meeting.* (Chicago, IL: American Association for Cancer Research).

Stopeck, A. T., Lipton, A., Body, J.-J., Steger, G. G., Tonkin, K., De Boer, R. H., et al. (2010). Denosumab compared with zoledronic acid for the treatment of bone metastases in patients with advanced breast cancer: a randomized, double-blind study. *J. Clin. Oncol.* 28, 5132–5139.

Sun, X., Cheng, G., Hao, M., Zheng, J., Zhou, X., Zhang, J., et al. (2010). CXCL12/CXCR4/CXCR7 chemokine axis and cancer progression. *Cancer Metastasis Rev.* 29, 709–722. doi: 10.1007/s10555-010-9256-x

Sun, Y. X., Schneider, A., Jung, Y., Wang, J., Dai, J., Wang, J., et al. (2005). Skeletal localization and neutralization of the SDF−1 (CXCL12)/CXCR4 axis blocks prostate cancer metastasis and growth in osseous sites in vivo. *J. Bone Min. Res.* 20, 318–329. doi: 10.1359/jbmr.041109

Suva, L. J., Griffin, R. J., and Makhoul, I. (2009). Mechanisms of bone metastases of breast cancer. *Endocr. Rrelat. Cancer* 16, 703–713. doi: 10.1677/ERC-09-0012

Teitelbaum, S. L., and Ross, F. P. (2003). Genetic regulation of osteoclast development and function. *Nat. Rev. Genet.* 4, 638–649. doi: 10.1038/nrg1122

Torre, L. A., Bray, F., Siegel, R. L., Ferlay, J., Lortet−Tieulent, J., and Jemal, A. (2015). Global cancer statistics, 2012. *Cancer J. Clin.* 65, 87–108. doi: 10.3322/caac.21262

Udagawa, N., Takahashi, N., Jimi, E., Matsuzaki, K., Tsurukai, T., Itoh, K., et al. (1999). Osteoblasts/stromal cells stimulate osteoclast activation through expression of osteoclast differentiation factor/RANKL but not macrophage colony-stimulating factor. *Bone* 25, 517–523. doi: 10.1016/s8756-3282(99)00210-0

Valastyan, S., and Weinberg, R. A. (2011). Tumor metastasis: molecular insights and evolving paradigms. *Cell* 147, 275–292. doi: 10.1016/j.cell.2011.09.024

Wada, T., Nakashima, T., Hiroshi, N., and Penninger, J. M. (2006). RANKL–RANK signaling in osteoclastogenesis and bone disease. *Trends Mol. Med.* 12, 17–25. doi: 10.1016/j.molmed.2005.11.007

Wakefield, L. M., and Roberts, A. B. (2002). TGF-β signaling: positive and negative effects on tumorigenesis. *Curr. Opin. Gnet. Dev.* 12, 22–29. doi: 10.1016/s0959-437x(01)00259-3

Walsh, N. C., and Gravallese, E. M. (2010). Bone remodeling in rheumatic disease: a question of balance. *Immunol. Rev.* 233, 301–312. doi: 10.1111/j.0105-2896.2009.00857.x

Wang, H., Tian, L., Liu, J., Goldstein, A., Bado, I., Zhang, W., et al. (2018). The Osteogenic niche is a calcium reservoir of bone micrometastases and confers

unexpected therapeutic vulnerability. *Cancer Cell* 34:823.e7–839.e7. doi: 10.1016/j.ccell.2018.10.002

Wang, H., Yu, C., Gao, X., Welte, T., Muscarella, A. M., Tian, L., et al. (2015). The osteogenic niche promotes early-stage bone colonization of disseminated breast cancer cells. *Cancer Cell* 27, 193–210. doi: 10.1016/j.ccell.2014.11.017

Waning, D. L., Guise, T. A., and Mohammad, K. S. (2019). A "Connexin" responsible for the fatal attraction of cancer to bone. *Cell Metab.* 29, 6–8. doi: 10.1016/j.cmet.2018.12.014

Weilbaecher, K. N., Guise, T. A., and McCauley, L. K. (2011). Cancer to bone: a fatal attraction. *Nat. Rev. Cancer* 11, 411–425. doi: 10.1038/nrc3055

Whyte, M. P., Obrecht, S. E., Finnegan, P. M., Jones, J. L., Podgornik, M. N., McAlister, W. H., et al. (2002). Osteoprotegerin deficiency and juvenile Paget's disease. *N. Eng. J. Med.* 347, 175–184.

Wong, B. R., Josien, R., Lee, S. Y., Vologodskaia, M., Steinman, R. M., and Choi, Y. (1998). The TRAF family of signal transducers mediates NF-κB activation by the TRANCE receptor. *J. Biol. Chem.* 273, 28355–28359. doi: 10.1074/jbc.273.43.28355

Xiong, J., Onal, M., Jilka, R. L., Weinstein, R. S., Manolagas, S. C., and O'brien, C. A. (2011). Matrix-embedded cells control osteoclast formation. *Nat. Med.* 17, 1235-1241. doi: 10.1038/nm.2448

Yin, J. J., Selander, K., Chirgwin, J. M., Dallas, M., Grubbs, B. G., Wieser, R., et al. (1999). TGF-β signaling blockade inhibits PTHrP secretion by breast cancer cells and bone metastases development. *J. Clin. Investigat.* 103, 197–206. doi: 10.1172/jci3523

Yoneda, T., Tanaka, S., and Hata, K. (2013). Role of RANKL/RANK in primary and secondary breast cancer. *World J. Orthopedics* 4, 178–185. doi: 10.5312/wjo.v4.i4.178

Zheng, Y., Zhou, H., Dunstan, C. R., Sutherland, R. L., and Seibel, M. J. (2013). The role of the bone microenvironment in skeletal metastasis. *J. Bone Oncol.* 2, 47–57. doi: 10.1016/j.jbo.2012.11.002

Conflict of Interest: The authors declare that the research was conducted in the absence of any commercial or financial relationships that could be construed as a potential conflict of interest.

Copyright © 2020 Wu, Li, Dang, Liang, Lu and Zhang. This is an open-access article distributed under the terms of the Creative Commons Attribution License (CC BY). The use, distribution or reproduction in other forums is permitted, provided the original author(s) and the copyright owner(s) are credited and that the original publication in this journal is cited, in accordance with accepted academic practice. No use, distribution or reproduction is permitted which does not comply with these terms.

frontiers in Cell and Developmental Biology

ORIGINAL RESEARCH
published: 03 March 2020
doi: 10.3389/fcell.2020.00127

Moderate Fluid Shear Stress Regulates Heme Oxygenase-1 Expression to Promote Autophagy and ECM Homeostasis in the Nucleus Pulposus Cells

Sheng Chen[1,2], Lei Qin[2], Xiaohao Wu[2], Xuekun Fu[2], Sixiong Lin[2,3], Di Chen[4], Guozhi Xiao[2], Zengwu Shao[1] and Huiling Cao[2]**

[1] Department of Orthopaedics, Union Hospital, Tongji Medical College, Huazhong University of Science and Technology, Wuhan, China, [2] Guangdong Provincial Key Laboratory of Cell Microenvironment and Disease Research, Shenzhen Key Laboratory of Cell Microenvironment, and Department of Biology, Southern University of Science and Technology, Shenzhen, China, [3] Guangdong Provincial Key Laboratory of Orthopedics and Traumatology, Orthopedic Research Institute and Department of Spinal Surgery, The First Affiliated Hospital of Sun Yat-sen University, Guangzhou, China, [4] Department of Orthopedic Surgery, Rush University Medical Center, Chicago, IL, United States

In vertebrate, the nucleus pulposus (NP), which is an essential component of the intervertebral disk, is constantly impacted by fluid shear stress (FSS); however, molecular mechanism(s) through which FSS modulates the NP homeostasis is poorly understood. Here we show that FSS regulates the extracellular matrix (ECM) homeostasis in NP cells. A moderate dose of FSS (i.e., 12 dyne/cm^2) increases the sulfated glycosaminoglycan (sGAG) content and protein levels of Col2a1 and Aggrecan and decreases those of matrix metalloproteinase 13 (MMP13) and a disintegrin and metalloproteinase with thrombospondin motif 5 (ADMATS5) in rat NP cells, while a higher dose of FSS (i.e., 24 dyne/cm^2) displays opposite effects. Results from RNA sequencing analysis, quantitative real-time RT-PCR analysis and western blotting establish that the heme oxygenase-1 (HO-1) is a key downstream mediator of the FSS actions in NP cells. HO-1 knockdown abolishes FSS-induced alterations in ECM protein production and sGAG content in NP cells, which is reversed by HO-1 induction. Furthermore, FSS activates the autophagic pathway by increasing the LC3-II/LC3-I ratio, Beclin-1 protein level, and formation of autophagosome and autolysosome and thereby regulates ECM protein and sGAG production in a HO-1 dependent manner. Finally, we demonstrate that the intraflagellar transport (IFT) 88, a core trafficking protein of primary cilia, is critically involved in the HO-1-mediated autophagy activation and ECM protein and sGAG production in FSS-treated NP cells. Thus, we for the first time demonstrate that FSS plays an important role in maintaining ECM homeostasis through HO-1-dependent activation of autophagy in NP cells.

Keywords: nucleus pulposus cell, fluid shear stress, autophagy, heme oxygenase-1, intraflagellar transport (IFT) 88

OPEN ACCESS

Edited by:
Chao Liang,
Hong Kong Baptist University, Hong Kong

Reviewed by:
Luyuan Li,
Nankai University, China
Denghui Xie,
The Third Affiliated Hospital of Southern Medical University, China

****Correspondence:***
Zengwu Shao
szwpro@163.com
Huiling Cao
caohl@sustech.edu.cn;
xizi20042093@hotmail.com

Specialty section:
This article was submitted to Molecular Medicine, a section of the journal Frontiers in Cell and Developmental Biology

Received: *12 December 2019*
Accepted: *13 February 2020*
Published: *03 March 2020*

Citation:
Chen S, Qin L, Wu X, Fu X, Lin S, Chen D, Xiao G, Shao Z and Cao H (2020) Moderate Fluid Shear Stress Regulates Heme Oxygenase-1 Expression to Promote Autophagy and ECM Homeostasis in the Nucleus Pulposus Cells. Front. Cell Dev. Biol. 8:127. doi: 10.3389/fcell.2020.00127

INTRODUCTION

Low back pain is a common and frequently recurring musculoskeletal disorder, which causes heavy financial burden worldwide (Chen et al., 2017; Clouet et al., 2018; Ma et al., 2019). Epidemiological investigations show that over 80% of the world population will experience LBP at some point in their life, and LBP has become the leading cause of years lived with disability and the second most common reason for hospital visits (Maher et al., 2017; Henry et al., 2018; Chen et al., 2019). In the United States, the annual cost of LBP is over $100 billion, which is even more than the total cost of stroke, coronary artery disease, diabetes, rheumatoid disease and respiratory infection (Katz, 2006). Intervertebral disk degeneration is considered to be the main cause of LBP (Frapin et al., 2019), thus, it is of great importance to understand the pathophysiology of IVD.

The IVD is an avascular and fibrocartilaginous tissue, which lies between the vertebral bodies and functions as a shock absorber by distributing biomechanical loads along the spinal column (Priyadarshani et al., 2016). Each IVD can be roughly divided into three distinct regions: in the center was the gelatinous NP, encompassed by outer fibrocartilaginous AF, bordered superiorly and inferiorly by CEP (Sakai and Grad, 2015). Under normal physiological condition, although there is low cellularity in both NP and AF tissues, the resident cells, especially NP cells, synthesize and secrete the complex ECM molecules to maintain ECM homeostasis and resist the mechanical stresses, which plays a key role in the protection against IVD degeneration (Hu et al., 2016; Silagi et al., 2018; Bonnevie et al., 2019). In healthy NP tissues, ECM contains three major components: collagen type II (Col2), glycosaminoglycan (GAG) and PGs. Aggrecan, bound by massive sGAG side chains, is the most abundant PG in NP. During the process of IVD degeneration, the degradation of these ECM proteins by catabolic proteinases, such as a disintegrin and metalloproteinase with thrombospondin motif 5 (ADMATS5) and matrix metalloproteinase 13 (MMP13), is accelerated, while their biosynthesis is decreased, leading to an imbalance between the anabolic and catabolic metabolism of ECM.

Increasing evidence suggests that mechanical stresses, including FSS, hydrostatic pressure, compressive stress, tensile stress and other mechanical stresses, play a pivotal role in the regulation of ECM homeostasis in IVD (Neidlinger-Wilke et al., 2014; Chou et al., 2016). To maintain erect posture, the IVD is under compressive stress, which can induce deformation and produce hydrostatic pressure in NP. The hydrostatic pressure is then transferred to AF and induces the generation of tensile stress. During body motion and spine movement, tissue fluid within the NP flows in and out to accommodate the change of these stresses. Consequently, NP cells are constantly exposed to FSS (**Figure 1A**; Ye et al., 2018). However, whether and how FSS regulates ECM homeostasis in NP cells is poorly understood.

Autophagy is a highly conserved and adaptive process involving selectively eliminating and recycling bulk harmful cytoplasmic materials, such as misfolded proteins and damaged intracellular organelles, thereby acting as a main cytoprotective system to maintain cellular homeostasis (Towers and Thorburn, 2016; Dikic and Elazar, 2018). Generally, cells exhibit a low and basal level of autophagy. But the level of autophagy can significantly increase in response to external environment stress, including mechanical stress and nutrient deprivation, in order to provide nutrients for essential cellular functions (Gross and Graef, 2019). The HO-1, which has been identified in many tissues and organs as well as different pathophysiological scenarios, is the rate-limiting enzyme in the metabolism of heme into biliverdin, carbon monoxide and iron, and can exert cytoprotective effects against various external environment stress-induced oxidative stress, inflammation and cell death (Otterbein et al., 2016; Chiang et al., 2018). Using our recently established rat NP cell line and a Flexcell Streamer System, in the present study we demonstrate that moderate FSS maintains ECM homeostasis by promoting cell autophagy through modulation of HO-1.

MATERIALS AND METHODS

NP Cell Line Culture and FSS Experiments

An immortalized rat NP cell line used in this study was described in Oh et al. (2016). The cells were cultured in Dulbecco's Modification of Eagle's Medium (10-013-CVR; Corning, United States) containing 10% FBS (10099-141; Gibco, Australia) supplemented with 1% penicillin-streptomycin (SV30010; Hyclone, United States) at 37°C with 5% CO_2. FSS experiments were conducted as previously described (Yang et al., 2019). Cells were seeded onto collagen I-coated culture slips (75 mm × 25 mm × 1 mm; FFCS-C; Flexcell, United States) at a density of $3.0 \times 10^4/cm^2$ and incubated in a 5% CO_2 incubator at 37°C. When cells reached up to 85% confluence, the slips were then placed in a parallel plate flow chamber of Streamer® System (STR-4000; Flexcell, United States) (**Figure 1B**) and cells are exposed to 12 or 24 dyne/cm^2 FSS for 0, 1, 2, 3, and 4 h. For certain experiments, NP cells were pre-treated with 10 μM CoPP (Sigma, United States, C1900) for 1 h or 500 nM rapamycin (Selleck, United States, S1039) for 12 h before exposure to FSS.

RNA Sequencing Analysis

Total RNA was isolated from NP cells with or without FSS stimulation using a TransZol Up Plus RNA Kit (ER501-01; Transgen, China) and 3 μg RNA per sample was used as input material for the RNA sample preparations. Sequencing libraries were generated using NEBNext® UltraTM RNA Library Prep Kit (Illunina, NEB, United States) and the library quality

Abbreviations: ADAMTS5, A disintegrin and metalloproteinase with thrombospondin motif 5; AF, annulus fibrosus; CEP, cartilage endplate; Col2, collagen type II; CoPP, cobalt protoporphyrin IX; CS, chondroitin sulfate; ECM, extracellular matrix; FSS, fluid shear stress; HA, hyaluronic acid; HO-1, heme oxygenase-1; IFT, intraflagellar transport; IVD, intervertebral disk; KS, keratin sulfate; LBP, low back pain; MMP13, matrix metalloproteinase 13; NP, nucleus pulposus; PGs, proteoglycans; RAP, rapamycin; sGAG, sulfated glycosaminoglycan.

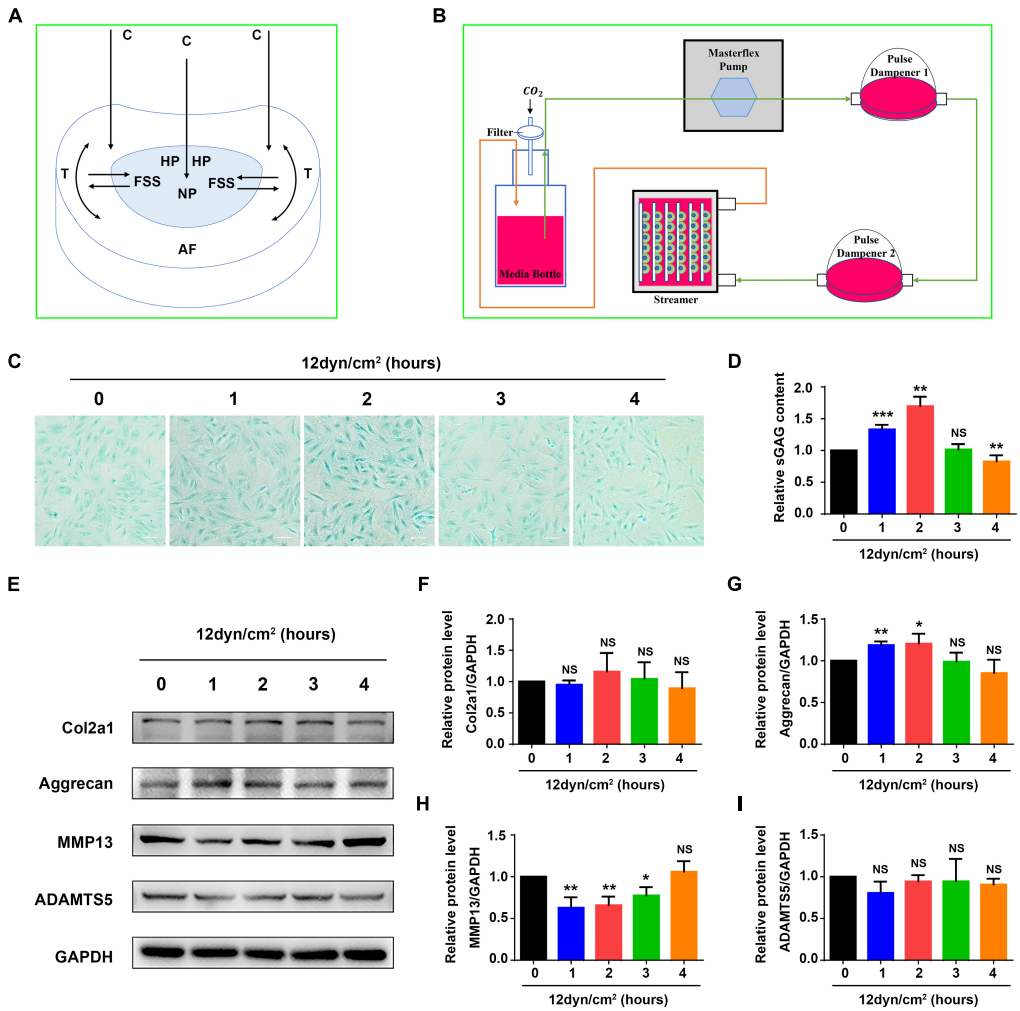


FIGURE 1 | Fluid shear stress regulates expression of ECM proteins and sGAG content in nucleus pulposus cells. **(A)** The formation of fluid shear stress (FSS) in nucleus pulposus cells (NP). Compressive stress (C), hydrostatic pressure (HP), and tensile stress (T) are indicated. **(B)** Schematic diagram of the Flexcell Streamer System. **(C)** Alcian blue staining. NP cells were treated with 12 dyne/cm^2 FSS for the indicated times. Bar, 100 μm. **(D)** sGAG content. NP cells were treated as in panel **(B)**, followed by the Blyscan Sulfated Glycosaminoglycan Assay. **(E–I)** Western blotting. NP cells were treated as in panel **(C)**, followed by Western blotting analyses for expression of Col2a1, aggrecan, MMP13, and ADAMTS5. Quantitative data from three independent experiments **(D,F–I)**. Results are expressed as mean ± standard deviation (s.d.). NS, no statistical significance, $^*P < 0.05$, $^{**}P < 0.01$, and $^{***}P < 0.001$ vs. un-treated group (0 h).

was assessed on the Agilent Bioanalyzer 2100 system. After cluster generation, the library preparations were sequenced on an Illumina Hiseq platform and 150 bp paired-end reads were generated. After quality control, reads mapping to the reference genome and quantification of gene expression level, differential expression analysis was performed by using the DESeq2 R package (1.16.1), and GO and KEGG enrichment analyses were performed by using the cluster Profiler R package. The RNASeq data have been deposited in Sequence Read Archive (SRA, PRJNA587407).

Analysis of sGAG Content

After fixed with 4% paraformaldehyde, NP cells were dehydrated by different concentrations of ethanol and xylol. The cells were then stained with alcian blue. To measure the sGAG content, cells were digested with papain extraction reagent and then the sGAG content was quantified by Blyscan Sulfated Glycosaminoglycan Assay (B1000; Biocolor, United Kingdom) according to the manufacturer's instructions.

Quantitative Real-Time Polymerase Chain Reaction (qRT-PCR) Analysis

Total RNA was extracted from NP cells using Tripure Isolation Reagent (11667165001; Roche, Germany). Reverse transcription (RT) and qRT-PCR analyses were performed as we described previously (Cao et al., 2010). Briefly, RNA was reverse transcribed into cDNA using PrimeScript^{TM} RT Master Mix (RR036A; Takara, Japan) according to the manufacturer's protocol. After reverse transcription, qRT-PCR was performed using iTaq^{TM} Universal SYBR® Green Supermix (172-5121; Bio-Rad).

The $2^{-\Delta\Delta CT}$ method was used to analyze the data, and GAPDH was used as an internal control. Primer sequences are shown in **Supplementary Table S1**.

Western Blotting Analyses

Nucleus pulposus cells were lysed with Tripure Isolation Reagent (11667165001; Roche, Germany). After centrifugation at 12,000 × *g* for 10 min at 4°C, protein pellet was isolated from the lower red organic phase by alcohol precipitation steps. Wash the protein pellet with 0.3 M guanidine hydrochloride/95% ethanol for three times and dissolve the protein pellet by adding 1% sodium dodecyl sulfate. The protein content was detected by Pierce™ BCA Protein Assay Kit (23225; ThermoFisher Scientifc, United States). Western blot analyses were performed as previously described (Cao et al., 2020). Proteins were loaded on sodium dodecyl sulfate-polyacrylamide gel for electrophoresis. After protein transfer, the membranes were blocked by 5% skimmed milk and then incubated overnight at 4°C with antibody against Col2a1 (1:1000, A1560; Abclonal Technology, China), Aggrecan (1:1000, ab36861; Abcam, United Kingdom), MMP13 (1:3000, ab39012; Abcam, United Kingdom), ADAMTS5 (1:500, ab41037; Abcam, United Kingdom), HO-1 (1:1000, 10701-1-AP; Proteintech, China), LC3-I/II (1:1000, ab62721; Abcam, United Kingdom), Beclin-1 (1:1000, 3738s; Cell Signaling Technology, United States), IFT 88 (1:500, 13967-1-AP; Proteintech, China) and GAPDH (1:2000, TA-08; ZSGB-Bio, China). After washing with TBST for three times, the membranes were incubated with secondary antibodies for 1 h at room temperature. Finally, the proteins were detected using the enhanced chemiluminescence method.

Immunofluorescence

Immunofluorescence staining was performed according to the method we previously used (Cao et al., 2020). After fixation in 4% paraformaldehyde at room temperature for 10 min, cells were permeabilized in 0.1% triton-100 for 15 min and blocked with 1% bovine serum albumin for 1 h at room temperature. Subsequently, cells were incubated overnight at 4°C with antibody against HO-1 (1:200, 10701-1-AP; Proteintech, China) and acetylated-tubulin (1:400, T6793; Sigma, United States), and then incubated for 1 h at room temperature with AlexaFluor 488-conjugated rabbit and mouse secondary antibodies (1:500, A11008 and A11001; ThermoFisher Scientifc, United States). After stained with DAPI, the cells were examined with a confocal microscope (A1R; Nikon, Japan) and analyzed with ImageJ software (Version 1.50; National Institutes of Health, United States).

Cilium Length and Prevalence Measurements

A Nikon A1R confocal microscope with an oil immersion × 100 objective was used to create maximum projection of confocal z-stacks from which cilia length was measured by ImageJ software (Version 1.50; National Institutes of Health, United States). Confocal z maximum projection was also used to determine the cilium prevalence and DAPI nuclear staining.

Transfection of Small Interfering RNA (siRNA)

The rat HO-1-siRNAs and IFT88-siRNAs were designed and manufactured by GenePharma (GenePharma Co.,Ltd., China). Transfection was performed as previously described (Cao et al., 2013). Briefly, NP cells were transfected with negative control (NC) siRNA and three independent HO-1-siRNAs and IFT88-siRNAs, respectively, the sequences are shown in **Supplementary Table S1**. The most effective target sequences for HO-1-siRNA (#2) and IFT88-siRNA (#1) were used. Cells were transfected with siRNAs at a concentration of 50 pmol/10^5 cell using Lipofectamine™ RNAiMAX Transfection Reagent (13778150; ThermoFisher Scientific, United States). 24 h later, the transfected cells were digested and seeded onto collagen I-coated culture slips for further study.

Transmission Electron Microscopy (TEM)

Harvested NP cells were washed in PBS and deionized water, and then pelleted by centrifugation. Cells were fixed with 2.5% glutaraldehyde for 2 h and 1% osmium tetroxide for 2 h, respectively. The cells were then dehydrated in ethanol and infiltrated and embedded in Embed 812. Ultrathin sections were stained with UranyLess (22409; EMS, United Kingdom) and Lead Citrate (22410; EMS, United Kingdom) and examined with a TEM (HT7700; Hitachi, Japan).

Autophagy Detection Using mRFP-GFP-LC3 Lentiviral Vector

Nucleus pulposus cells were seeded in 24 well plates (1×10^5/plate). 24 h later, cells were infected with lentiviral vector (HanBio Technology Co.,Ltd., China) according to the manufacturer's instructions. 48 h after infection, puromycin was used to screen stable NP cell line expressing mRFP-GFP-LC3. The transfected cells were then used for autophagy detection. Autophagy was determined by confocal microscope (A1R; Nikon, Japan). Autophagic flux was detected by evaluating the number of GFP and mRFP puncta. Free red dots indicated autolysosomes and yellow dots indicated autophagosomes.

Statistical Analysis

Statistical analysis was performed using GraphPad Prism 6 software (GraphPad Software Inc., United States). All experiments were carried out at least three independent experiments and the data were presented as mean ± standard deviation (s.d.). For analysis of two-group parameters, Student's *t*-tests were used. Statistical significance was set at a level of $P < 0.05$.

RESULTS

FSS Regulates ECM Protein Expression and sGAG Content in Rat NP Cells

As an initial step to explore mechanism(s) through which mechanical force regulates the homeostasis of IVD, we performed experiments to determine the effects of FSS on expression of

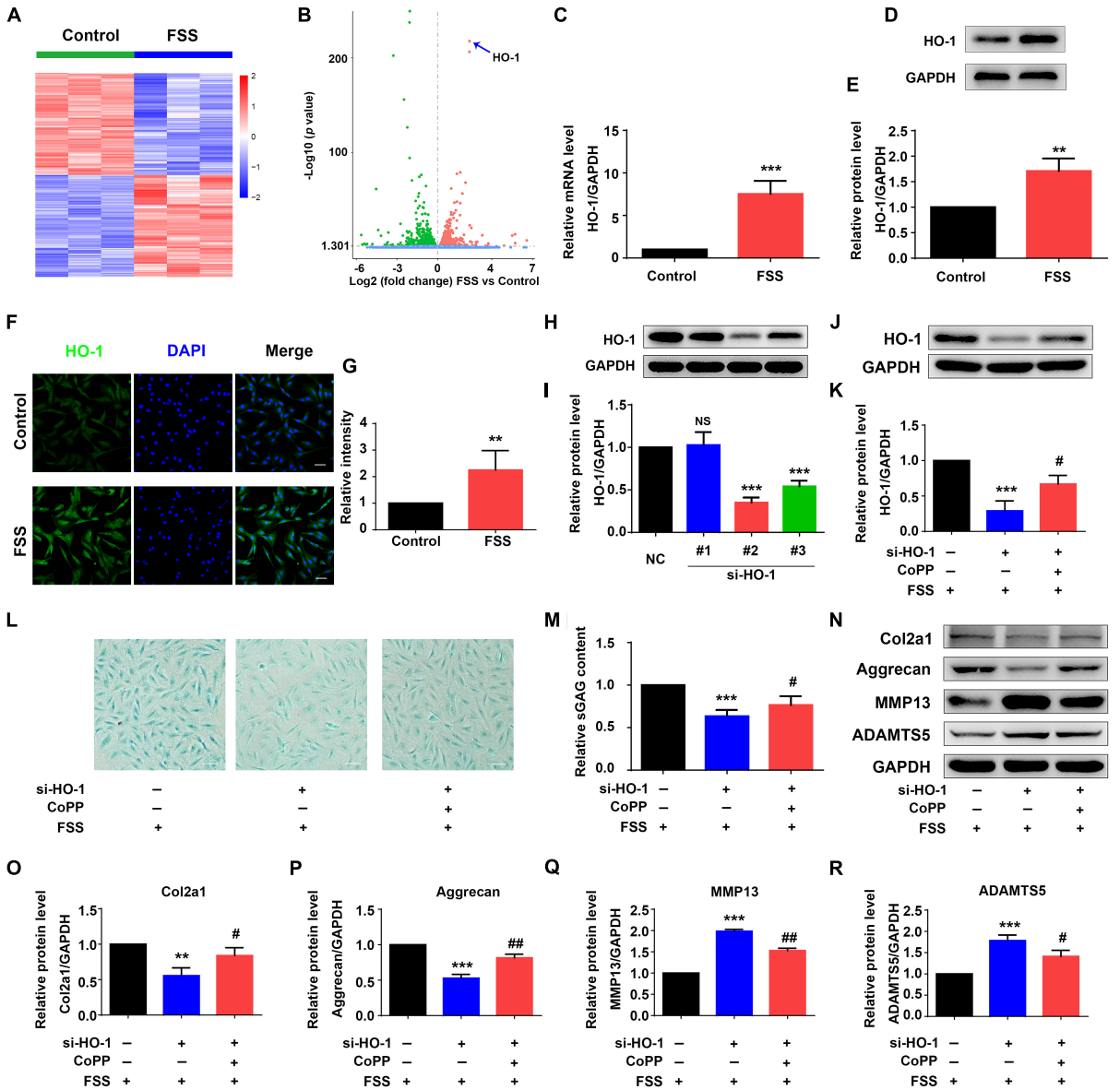


FIGURE 2 | Heme oxygenase-1 regulates FSS-mediated ECM production in NP cells. **(A)** The heat map of RNA-seq data. NP cells were treated with or without 12 dyne/cm^2 FSS for 2 h, followed by RNA-seq analysis as described in Materials and Methods. **(B)** Volcano plot of RNA-seq data. Blue arrow indicates heme oxygenase-1 (HO-1). **(C)** Quantitative real-time reverse transcriptase-polymerase chain reaction (qRT-PCR) analysis. NP cells were treated with or without 12 dyne/cm^2 FSS for 2 h, followed by qRT-PCR analysis. **(D,E)** Western blotting. NP cells were treated as in panel **(C)**, followed by western blotting. Quantitative data from three independent experiments **(E)**. **(F,G)** Immunofluorescence (IF) staining. NP cells were treated as in panel **(C)**, followed by IF staining **(E)**. Bar, 50 μm. Quantitative data from three independent experiments **(G)**. **(H,I)** HO-1 siRNA knockdown. NP cells were transfected with negative control siRNA (NC-siRNA) and three HO-1-siRNA (#1, #2, #3). Then, cells were subjected to western blotting for HO-1 **(H)**. Quantitative data from three independent experiments **(I)**. Note: #2 HO-1-siRNA showed the best knocking down effect and was used for all following experiments in this study. **(J,K)** Western blotting. NP cells were transfected with negative control siRNA (NC-siRNA) and HO-1-siRNA (#2). Then, cells were pretreated with or without HO-1 inducer cobalt protoporphyrin IX (CoPP) (10 μM) and subjected to 12 dyne/cm^2 FSS for 2 h, followed by western blotting for HO-1 **(J)**. Quantitative data from three independent experiments **(K)**. **(L,M)** sGAG content. NP cells were treated as in panel **(J)**, followed by alcian blue staining and Blyscan Sulfated Glycosaminoglycan Assay. Bar,100 μm. Quantitative data of sGAG content from three independent experiments **(M)**. **(N–R)** Western blotting. NP cells were treated as in panel **(J)**, followed by western blotting for expression of the indicated proteins. Quantitative data from three independent experiments **(O–R)**. Results are expressed as mean ± standard deviation (s.d.). NS, no statistical significance, $^{**}P < 0.05$, $^{***}P < 0.001$ vs. control, NC or FSS + NC-siRNA group; $^{\#}P < 0.01$ and $^{\#\#}P < 0.01$ vs. FSS + HO-1-siRNA group.

ECM proteins in rat NP cells. The NP cells were subjected to FSS treatment at a dose of 12 dyne/cm^2 for the indicated times (**Figure 1B**), followed by assays for sGAG content and expression of several key ECM proteins. The results showed that sGAG content and aggrecan protein level were significantly increased at 1 and 2 h of FSS treatment, and

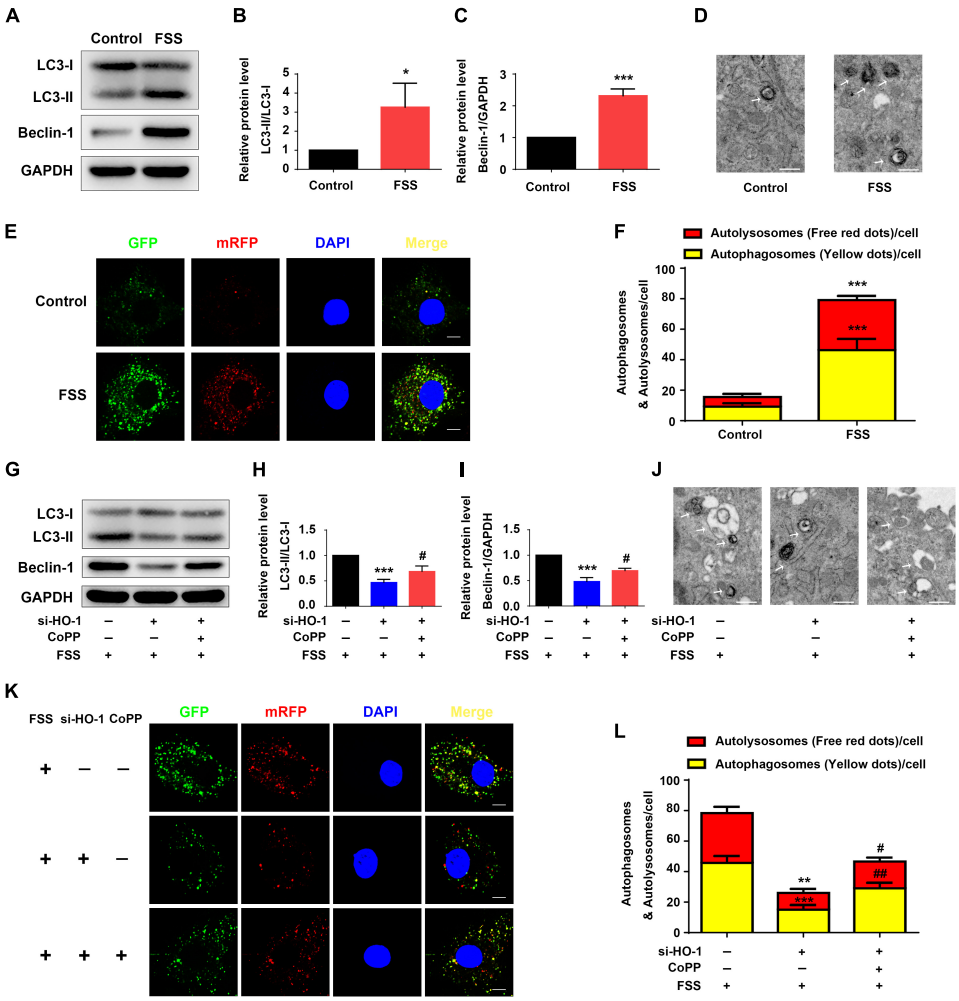


FIGURE 3 | HO-1 mediates FSS-induced autophagy in NP cells. **(A–C)** Western blotting. NP cells were treated with or without 12 dyne/cm^2 FSS for 2 h, followed by western blotting for expression of the indicated proteins. Quantification of LC3-II/LC3-I ratio **(B)** and Beclin-1 **(C)**. **(D)** Transmission Electron Microscopy (TEM). NP cells were treated as in panel **(A)**. TEM images are shown. Arrows indicate double-membrane autophagosomes and autolysosomes at various stages. Bar, 500 nm. **(E,F)** Measurements of autophagosomes and autolysosomes. NP cells were infected with lentivirus expressing a tandem mRFP-GFP-LC3 construct and treated with or without 12 dyne/cm^2 FSS for 2 h. Fluorescence images were obtained. Bar, 5 μm. Quantification of autophagosomes (yellow dots) and autolysosomes (free red dots) **(F)**. **(G–I)** Western blotting. NP cells were first treated with and without HO-1 siRNA knockdown and in the presence and absence of CoPP. Then, cells were pretreated with or without HO-1 inducer cobalt protoporphyrin IX (CoPP) (10 μM) and subjected to 12 dyne/cm^2 FSS for 2 h, followed by western blotting for expression of the indicated proteins. Quantification of LC3-II/LC3-I ratio and Beclin-1 from three independent experiments **(H,I)**. **(J)** TEM. NP cells were treated as in panel **(G)**. TEM images are shown. The arrows indicate double-membrane autophagosomes and autolysosomes. Bar, 500 nm. **(K,L)** Measurements of autophagosomes and autolysosomes. NP cells were transduced with lentivirus expressing a tandem mRFP-GFP-LC3 construct and treated as in panel **(G)**. Fluorescence images were obtained. Bar, 5 μm. Quantification of autophagosomes (yellow dots) and autolysosomes (free red dots) from three independent experiments **(L)**. $^*P < 0.05$, $^{**}P < 0.01$, and $^{***}P < 0.001$ vs. control; $^{\#}P < 0.05$ and $^{\#\#}P < 0.01$ vs. FSS + HO-1-siRNA group.

MMP13 protein level was significantly decreased at 1, 2 and 3 h of FSS treatment (**Figures 1C–E,G,H**). FSS treatment slightly increased Col2a1 expression and decreased ADAMTS5 expression (**Figures 1F,I**). However, when NP cells were exposed to 24 dyne/cm^2 FSS treatment, sGAG content and the protein levels of Col2a1 and aggrecan were decreased, while the levels of MMP13 and ADAMTS5 were increased in a time-dependent manner (**Supplementary Figure S1**). These results suggest that moderate FSS upregulates sGAG content and anabolic ECM proteins (Col2a1 and aggrecan), and downregulates catabolic ECM proteins (MMP13 and ADAMTS5) in NP cells, while high FSS exerts opposite effects. We focused our next studies to determine potential mechanism(s) through which moderate FSS (i.e., 12 dyne/cm^2 for 2 h) regulates expression of key ECM proteins and sGAG content in NP cells.

HO-1 Is Largely Upregulated by Moderate FSS in NP Cells

To identify genes that were regulated by moderate FSS treatment, NP cells were treated with or without FSS

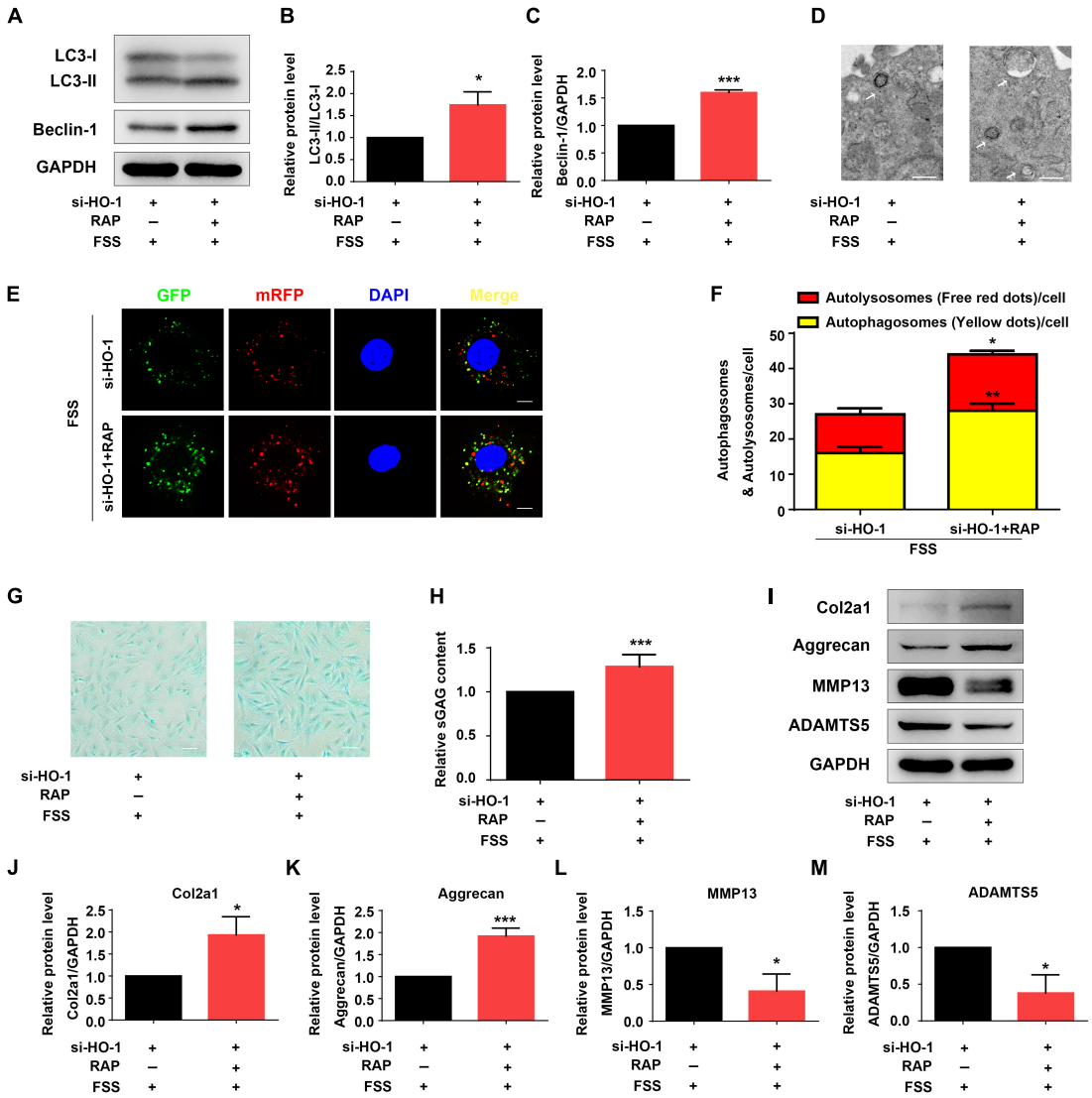


FIGURE 4 | Rapamycin regulates autophagy and ECM in NP cells. **(A–C)** Western blotting. NP cells were first transfected with HO-1 siRNA and treated with autophagy activator rapamycin (RAP, 500 nM) for 12 h. Cells were then treated with 12 dyne/cm^2 FSS for 2 h, followed by western blotting for expression of the indicated proteins. Quantification of LC3-II/LC3-I ratio and Beclin-1 from three independent experiments **(B,C)**. **(D)** Transmission Electron Microscopy (TEM). NP cells were treated as in panel **(A)**. TEM images are shown. The arrows indicate double-membrane autophagosomes and autolysosomes. Bar, 500 nm. **(E,F)** Measurements of autophagosomes and autolysosomes. NP cells were transduced with lentivirus expressing a tandem mRFP-GFP-LC3 construct and treated as in panel **(A)**. Fluorescence images were obtained. Bar, 5 μm. Quantification of autophagosomes (yellow dots) and autolysosomes (free red dots) from three independent experiments **(F)**. **(G,H)** sGAG content. NP cells were treated as in panel **(A)**, followed by alcian blue staining **(G)** and Blyscan Sulfated Glycosaminoglycan Assay **(H)**. Bar, 100 μm. **(I–M)** Western blotting. NP cells were treated as in panel **(A)**, followed by western blotting for expression of the indicated proteins **(I)**. Quantification of Col2a1, aggrecan, MMP13 and ADAMTS5 from three independent experiments **(J–M)**. Results are expressed as mean ± standard deviation (s.d.). *P < 0.05 and ***P < 0.001 vs. FSS + HO-1-siRNA group.

(12 dyne/cm^2 for 2 h). Total RNAs from both groups were isolated and subjected to RNA sequencing analysis as described in Materials and Methods. Genes upregulated (1463) or downregulated (1467) were presented in **Supplementary Table S2**. Among the upregulated genes, we found that HO-1 was significantly upregulated by FSS treatment with the lowest p value (**Figures 2A,B**). Results from qRT-PCR analysis, western blotting and immunofluorescence staining further verified that the levels of HO-1 mRNA and protein were dramatically increased by FSS treatment (**Figures 2C–G**).

HO-1 Is Critical for Moderate FSS Regulation of ECM in NP Cells

Since HO-1 was reported to regulate ECM metabolism in NP cells (Hu et al., 2016), we next determined whether HO-1 is involved in FSS regulation of ECM proteins in NP cells. To do this, NP

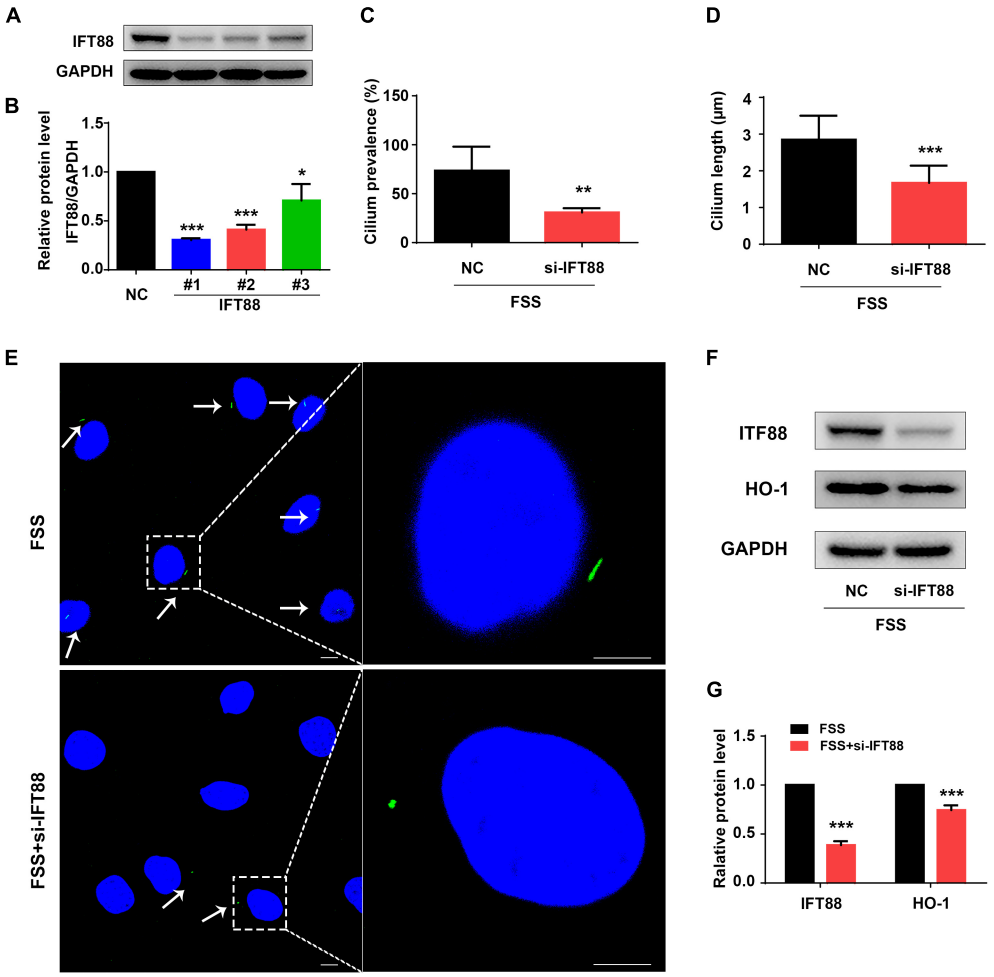


FIGURE 5 | Knockdown of IFT88 impairs cilium function and decreases expression of HO-1 in FSS-treated NP cells. **(A)** IFT88 Knockdown. NP cells were transfected with negative control siRNA (NC-siRNA) and three different IFT88-siRNA (#1, #2, #3). Then, cells were subjected to western blotting for expression of IFT88 **(A)**. Quantitative data from three independent experiments **(B)**. The #1 IFT88-siRNA was used for the following experiments in this study. **(C,D)** Qualification of cilium prevalence **(C)** and cilium length **(D)** in NP cells from three independent experiments. NP cells were transfected with negative control siRNA (NC-siRNA) and IFT88 siRNA. Then, cells were treated with 12 dyne/cm^2 FSS for 2 h. **(E)** Fluorescence images of primary cilia. Left bar, 10 μm; right bar, 5 μm. White arrows represent primary cilia. **(F,G)** Western blotting. NP cells were transfected with NC-siRNA or IFT88-siRNA (#1) and subjected to 12 dyne/cm^2 FSS for 2 h, followed by western blotting for expression of IFT88 and HO-1 **(F)**. Quantification of data from three independent experiments **(G)**. Results are expressed as mean ± standard deviation (s.d.). *P < 0.05, **P < 0.01, and ***P < 0.001 vs. NC or FSS + NC-siRNA group).

cells were transfected with negative control siRNA (NC-siRNA) and three different HO-1 siRNAs (#1, #2, and #3). We chose the #2 HO-1 siRNA for HO-1 knocking down in this study since the #2 HO-1 siRNA showed the best knocking down efficiency (**Figures 2H,I**). To determine whether HO-1 is involved in FSS regulation of ECM, NP cells were first transfected with control siRNA or HO-1-siRNA (#2). Then, cells were pretreated with or without HO-1 inducer cobalt protoporphyrin IX (CoPP) (10 μM) for 1 h and subjected to 12 dyne/cm^2 FSS for 2 h. As expected, HO-1 siRNA dramatically decreased the level of HO-1 protein, which was markedly reversed by treatment of CoPP treatment (**Figures 2J,K**). Furthermore, HO-1 siRNA significantly reduced the synthesis of sGAG, which was partially reversed by CoPP treatment (**Figures 2L,M**). Similarly, results from western blot analyses revealed that HO-1 siRNA downregulated the levels of anabolic ECM proteins (Col2a1 and aggrecan) and upregulated the levels of catabolic ECM proteins (MMP13 and ADAMTS5), which could be reversed by CoPP treatment (**Figures 2N–R**).

FSS Promotes Autophagy in NP Cells

Fluid shear stress activates autophagy in multiple cell types (Zhang et al., 2018; Yang et al., 2019). Thus, we determined whether FSS activates autophagy in NP cells. Results showed that NP cells treated with FSS displayed increased autophagy compared to untreated cells, as demonstrated by dramatic increases in the LC3-II/LC3-I ratio and Beclin-1 protein level (**Figures 3A–C**). Likewise, TEM analyses showed a marked increase in the numbers of autophagosome and autolysosome in FSS-treated cells relative to untreated cells (**Figure 3D**). Furthermore, immunofluorescence confocal microscopy analyses

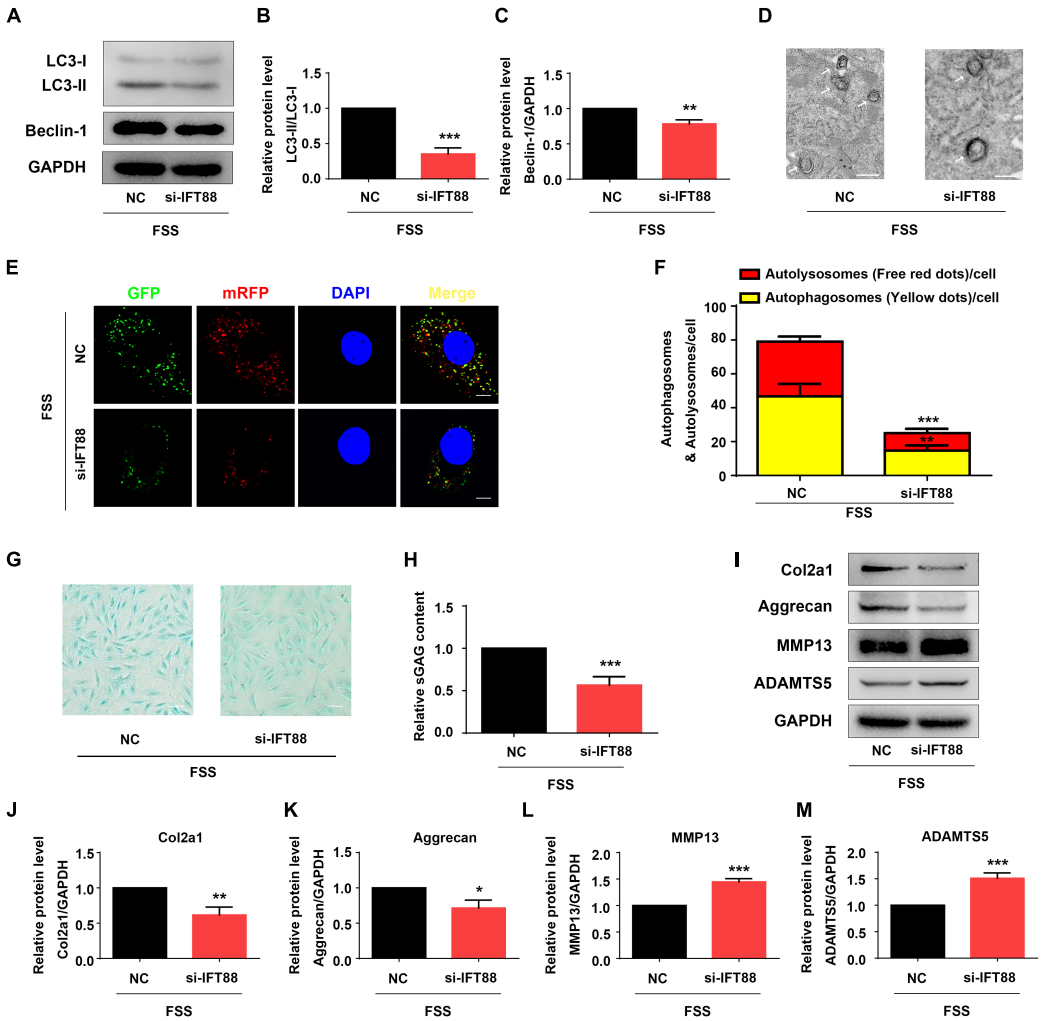


FIGURE 6 | IFT88 loss reduces autophagy and impairs ECM homeostasis in FSS-treated NP cells. **(A–C)** Western blotting. NP cells were transfected with negative control siRNA (NC-siRNA) or IFT88-siRNA (#1). Then, cells were subjected to 12 dyne/cm^2 FSS for 2 h, followed by western blotting for expression of LC3-I, LC3-II, and Beclin-1 **(A)**. Quantification of LC3-I/LC3-II ratio and Beclin-1 from three independent experiments **(B,C)**. **(D)** Transmission Electron Microscopy (TEM). NP cells were treated as in PANEL **(A)**. TEM images are shown. The arrows indicate double-membrane autophagosomes and autolysosomes. Bar, 500 nm. **(E,F)** Measurements of autophagosomes and autolysosomes. NP cells were transduced with lentivirus expressing a tandem mRFP-GFP-LC3 construct and treated as in panel **(A)**. Fluorescence images were obtained. Bar, 5 μm. Quantification of autophagosomes (yellow dots) and autolysosomes (free red dots) from three independent experiments **(F)**. **(G,H)** sGAG content. NP cells were treated as in panel **(A)**, followed by alcian blue staining **(G)** and Blyscan Sulfated Glycosaminoglycan Assay **(H)**. Bar, 100 μm. **(I–M)** Western blotting. NP cells were treated as in panel **(A)**, followed by western blotting for expression of the indicated proteins **(I)**. Quantification of expression of Col2a1, aggrecan, MMP13 and ADAMTS5 from three independent experiments **(J–M)**. Results are expressed as mean ± standard deviation (s.d.). $^*P < 0.05$, $^{**}P < 0.01$, and $^{***}P < 0.001$ vs. FSS + NC-siRNA group.

revealed that the numbers of both autophagosome (yellow dots) and autolysosome (free red dots) were dramatically increased in FSS-treated NP cells compared to those in untreated cells (**Figures 3E,F**).

HO-1 Regulates the FSS-Induced Autophagy in NP Cells

Heme oxygenase-1 was reported to activate autophagy in NP cells (Hu et al., 2016). Thus, we next determined whether HO-1 plays a role in mediation of the FSS-induced autophagy in NP cells. NP cells were treated with FSS, with or without CoPP treatment, in the presence or absence of HO-1 knockdown by siRNA. The results showed that HO-1 knockdown dramatically reduced the increases of LC3-II/LC3-I ratio and Beclin-1 expression in NP cells induced by FSS treatment, which was markedly reversed by CoPP treatment (**Figures 3G–I**). TEM analyses showed that HO-1 siRNA significantly reduced the numbers of autophagosome and autolysosome in FSS-treated NP cells compared to control siRNA/FSS-treated cells, which was largely reversed by CoPP treatment (**Figure 3J**). Similarly, immunofluorescence confocal microscopy analyses showed that the numbers of both autophagosome (yellow dots) and autolysosome (free red dots) were dramatically decreased

in HO-1 siRNA/FSS-treated NP cells compared to those in control siRNA/FSS-treated cells, which was reversed by CoPP treatment (**Figures 3K,L**).

Rapamycin Reverses HO-1 Knockdown-Induced Alterations in Autophagy and ECM Homeostasis in FSS-Treated NP Cells

Rapamycin activates autophagy in multiple cell types (Spang et al., 2014; Lopez de Figueroa et al., 2015). We next determined the effect of rapamycin treatment on autophagy suppression induced by HO-1 knockdown in FSS-treated NP cells. NP cells were first transfected with HO-1 siRNA and then pretreated with or without rapamycin for 12 h and subjected to FSS treatment for 2 h. The results showed that rapamycin treatment of the NP cells significantly increased the LC3-II/LC3-I ratio, expression level of Beclin-1 protein and formation of autophagosome and autolysosome (**Figures 4A–F**). Furthermore, rapamycin treatment also reversed the decrease of sGAG content and alterations in expression of ECM proteins induced by HO-1 knockdown in the FSS-treated NP cells (**Figures 4G–M**).

Primary Cilium Protein IFT88 Is Critical for HO-1 Regulation of Autophagy and ECM Homeostasis in FSS-Treated NP Cells

Primary cilium was reported to function as a mechano-sensor and plays an important role in mechanotransduction (He et al., 2016). As a core trafficking protein of primary cilium, IFT88 is critical for ciliary assembly and function (Coveney et al., 2018; Fu et al., 2019). We used IFT88-siRNA to knock down its expression in NP cells (**Figures 5A,B**). The #1 IFT88 siRNA displayed the best knocking down efficiency and was used in the following experiments (**Figures 5A,B**). Results showed that IFT88 knockdown significantly reduced the cilium prevalence and cilium length in FSS-treated NP cells (**Figures 5C–E**). Interestingly, IFT88 knockdown decreased the protein level of HO-1 in FSS-treated NP cells (**Figures 5F,G**). Moreover, IFT88 knockdown inhibited the autophagy activation by decreasing the LC3-II/LC3-I ratio, expression of Beclin-1 protein and formation of autophagosome and autolysosome in FSS-treated NP cells (**Figures 6A–F**). Furthermore, IFT88 knockdown decreased sGAG content and expression of anabolic proteins (Col2a1 and aggrecan) and increased expression of catabolic proteins (MMP13 and ADAMTS5) (**Figures 6G–M**).

CoPP or Rapamycin Largely Reverses IFT88 Loss-Induced Alterations in Autophagy and ECM Homeostasis in FSS-Treated NP Cells

Finally, we determined whether rapamycin or upregulation of HO-1 by CoPP can reverse the alterations in autophagy and ECM protein expression induced by IFT88 knockdown in FSS-treated NP cells. NP cells were first transfected with IFT88-siRNA. Then, cells were pretreated with CoPP (10 μM) or rapamycin (500 nM) and then subjected to FSS treatment. The results showed that both CoPP or rapamycin treatment largely reversed the IFT88 knockdown-induced alterations in LC3-II/LC3-I ratio and Beclin-1 protein level (**Figures 7A–C**), formation of autophagosome and autolysosome (**Figures 7D–F**), sGAG content (**Figures 7G,H**) and expression of anabolic and catabolic ECM proteins (**Figures 7I–M**).

DISCUSSION

In the present study, we demonstrate the effect of FSS on the regulation of ECM homeostasis in NP cells. We find that FSS regulates ECM metabolism in a loading magnitude- and time-dependent manner. When NP cells are subjected to the 24 dyne/cm^2 FSS treatment, the balance between ECM anabolism and catabolism is disrupted, as demonstrated by decreases in sGAG content and expression of Col2 and aggrecan and increase in expression of ECM-degrading proteinases MMP13 and ADAMTS5. However, when NP cells are exposed to the relatively moderate FSS (12 dyne/cm^2 for 1–2 h), FSS maintains the ECM homeostasis by promoting the ECM anabolism and inhibiting the ECM catabolism. The observed pro-anabolism and anti-catabolism effects of moderate FSS are consistent with previous studies in various cell types exposed to different mechanical stimuli. In rat fibrochondrocytes, Deschner et al. (2006) reported that dynamic tensile strain could significantly abrogate IL-1β-induced upregulation of MMPs (MMP3, MMP7, MMP8, MMP9, MMP13, MMP16, MMP17, and MMP19). In human chondrocytes, He et al. (2016) found that moderate cyclic tensile strain could reduce the protein expressions of MMP-1 and MMP-13 and exert an anti-catabolism effect to protect cartilage integrity. Results from Dai et al. (2014) demonstrated that dynamic compression could promote the synthesis of Col2 and aggrecan in adipose-derived stem cells. Our results suggested that NP cells could start an early ECM synthesis process to maintain ECM homeostasis in response to moderate FSS, and a deeper understanding of the specific mechanism by which moderate FSS regulates ECM homeostasis in NP cells might help us to seek for novel and early preventive and therapeutic targets for IVD degeneration.

Increasing evidence have revealed that HO-1 could attenuate inflammation- and oxidative stress-induced imbalance between ECM anabolism and catabolism in NP cells and chondrocytes (Guillen et al., 2008; Hu et al., 2016; An et al., 2018). In this study, we performed RNA sequencing analysis and focused on HO-1, which was significantly upregulated in NP cells exposed to moderate FSS. We found that HO-1 inhibition decreased sGAG content, downregulated ECM anabolism related proteins (Col2a1, aggrecan) and upregulated ECM catabolism related proteins (MMP13, ADAMTS5) in NP cells exposed to moderate FSS, which could be reversed by HO-1 inducer CoPP. These results suggest that HO-1 plays a critical role in the maintenance of ECM homeostasis induced by moderate FSS.

Results from different research groups indicated that FSS could induce protective autophagy in osteocytes, chondrocytes and hepatocellular carcinoma cells (Wang et al., 2018;

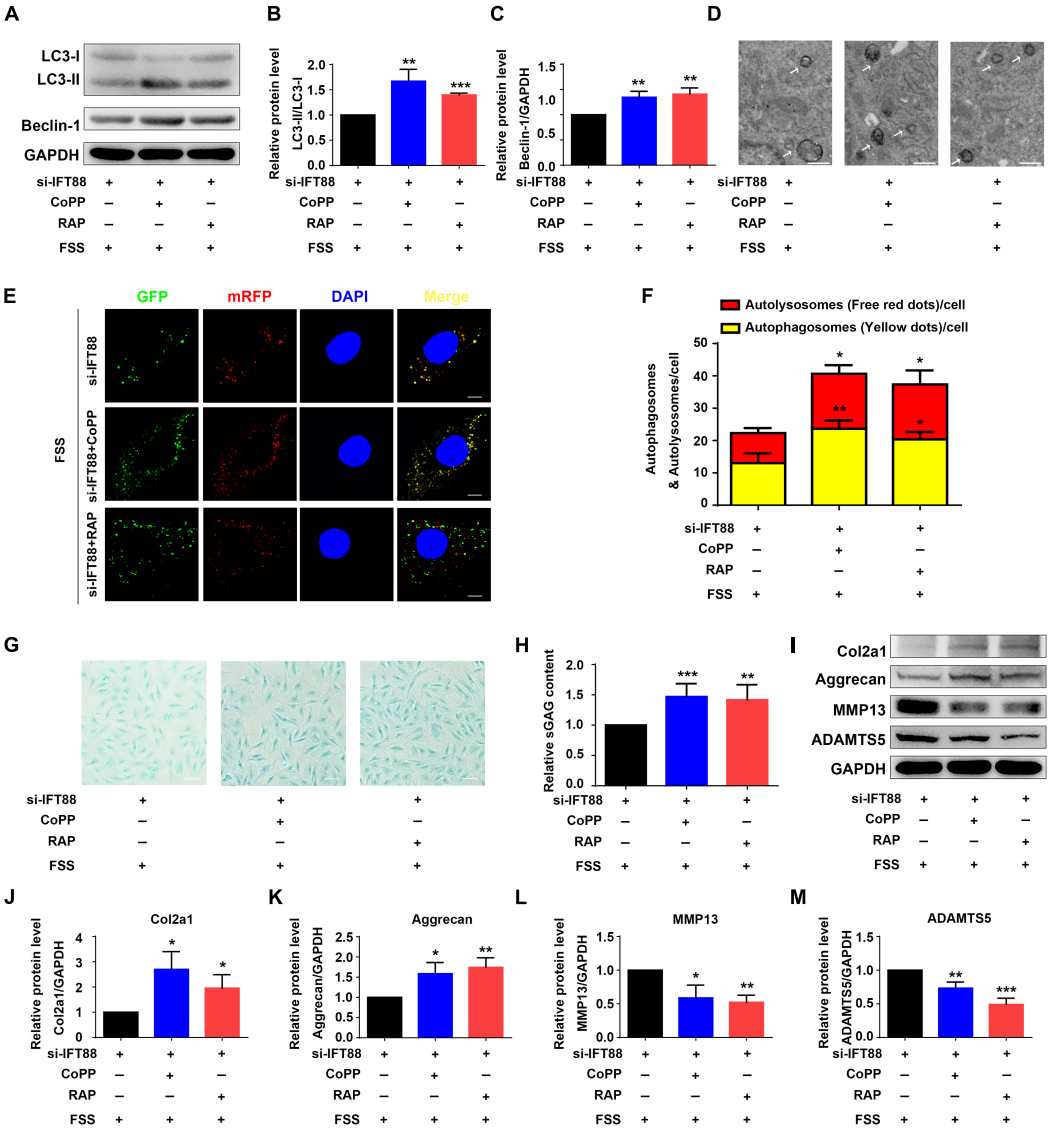


FIGURE 7 | HO-1 upregulation or rapamycin reverses IFT88 loss-induced alterations in autophagy and ECM production in FSS-treated NP cells. **(A–C)** Western blotting. NP cells were transfected with IFT88-siRNA. Then, cells were pretreated with CoPP (10 μM) or rapamycin (RAP, 500 nM) and subjected to 12 dyne/cm^2 FSS for 2 h, followed by western blotting for expression of LC3-I, LC3-II, and Beclin-1 **(A)**. Quantification of LC3-I/LC3-II ratio and Beclin-1 from three independent experiments **(B,C)**. **(D)** Transmission Electron Microscopy (TEM). NP cells were treated as in panel **(A)**. TEM images are shown. The arrows indicate double-membrane autophagosomes and autolysosomes. Bar, 500 nm. **(E,F)** Measurements of autophagosomes and autolysosomes. NP cells were transduced with lentivirus expressing a tandem mRFP-GFP-LC3 construct and treated as in panel **(A)**. Fluorescence images were obtained. Bar, 5 μm. Quantification of autophagosomes (yellow dots) and autolysosomes (free red dots) from three independent experiments **(F)**. **(G,H)** sGAG content. NP cells were treated as in panel **(A)**, followed by alcian blue staining **(G)** and Blyscan Sulfated Glycosaminoglycan Assay **(H)**. Bar, 100 μm. **(I–M)** Western blotting. NP cells were treated as in panel **(A)**, followed by western blotting for expression of the indicated proteins **(I)**. Quantification of expression of Col2a1, aggrecan, MMP13 and ADAMTS5 from three independent experiments **(J–M)**. Results are expressed as mean ± standard deviation (s.d). $^*P < 0.05$, $^{**}P < 0.01$, and $^{***}P < 0.001$ vs. FSS + IFT88-siRNA group.

Zhang et al., 2018; Yang et al., 2019). In line with previous studies, our data demonstrated that moderate FSS activated autophagy in NP cells by increasing the ratio of LC3-II to LC3-I, the protein expression of Beclin-1 and the number of autophagosomes and autolysosomes. HO-1 upregulation as a mean for autophagy induction has been reported in many diseases (Nakamura et al., 2018; Vasconcellos et al., 2018). For example, in a cadmium-induced emphysema mice model, Surolia et al. (2015) found that HO-1 mediated the activation of autophagy and protected against pulmonary endothelial cell apoptosis and development of emphysema. And in a diabetic nephropathy cell model, Dong et al. (2015) reported that HO-1 could enhance autophagy and inhibited high glucose-induced podocytes apoptosis. In this study, we demonstrated that HO-1 inhibition suppressed the FSS-induced autophagy activation, while HO-1 inducer CoPP reversed this process. Furthermore,

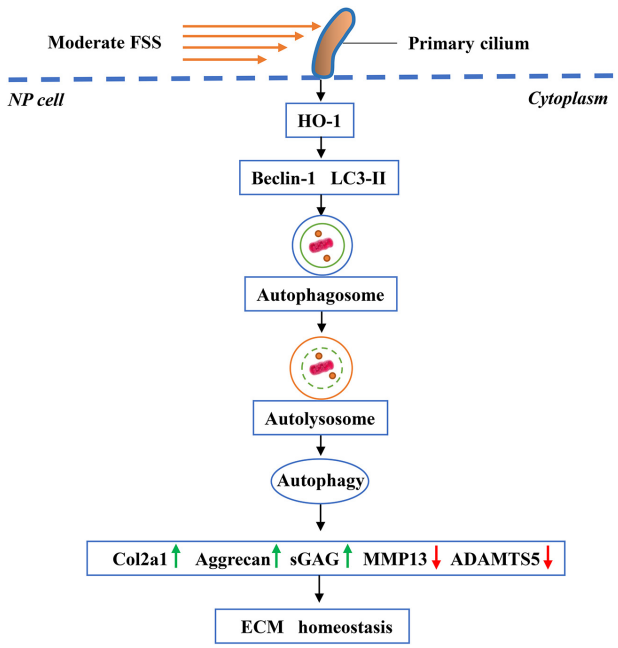


FIGURE 8 | Working model. Primary cilia sense and transmit extracellular FSS signal to NP cells, which activates HO-1 and thereby autophagy. Increased autophagy plays an important role in maintaining ECM homeostasis in NP cells.

autophagy activator rapamycin attenuated HO-1 inhibition induced disruption of FSS-induced autophagy activation and ECM homeostasis in NP cells. Collectively, these results suggest that moderate FSS maintains ECM homeostasis in NP cells, at least in part, through HO-1-mediated autophagy.

Although our results above revealed that FSS could regulate ECM homeostasis through HO-1-mediated autophagy in NP cells, how the cells sense FSS and convert it into downstream molecular signals remained unclear. Primary cilium is a microtubule-based organelle, which extends as a solitary protrusion from the surface of most mammalian cell types, including NP cells (Zheng et al., 2018; Anvarian et al., 2019). It can sense and transmit extracellular mechanical and chemical signals, to regulate various cellular processes and maintain tissue homeostasis (Hua and Ferland, 2018; Kim and Kim, 2019). Because primary cilium cannot synthesize proteins, cilium-associated trafficking proteins, such as IFT88, are therefore critical for cilium biogenesis, maintenance and function (Wang et al., 2016). Recent studies have demonstrated that hypomorphic mutation of IFT88 can result in severely stunted primary cilia and abolish the suppression effects of cyclic tensile strain on the inflammatory response to IL-1β in chondrocytes (Fu et al., 2019). Results from He et al. (2016) showed that disruption of the primary cilia in chondrocytes by IFT88-siRNA attenuated the anti-catabolism effects of moderate cyclic tensile strain. Moreover, Orhon et al. (2016) reported that hypomorphic deletion of the IFT88 impaired ciliary assembly and inhibited the FSS-induced autophagy activation in epithelial cells. Hence, we speculated that primary cilia associated with IFT88 might play a pivotal role in the mechanotransduction when NP cells were exposed to FSS. As expected, NP cells transfected with IFT88-siRNA exhibited defective primary cilia, and the disruption of primary cilia downregulated the protein expression of HO-1, inhibited the autophagy activation and destroyed the ECM homeostasis in NP cells exposed to moderate FSS. Meanwhile, we found that both CoPP and RAP partially reversed the changes. Therefore, our data suggest that primary cilium could sense and mediate moderate FSS signal to regulate HO-1 mediated autophagy activation and then maintain ECM homeostasis in NP cells (**Figure 8**).

CONCLUSION

Findings from our study indicate that moderate FSS could maintain ECM homeostasis in NP cells which requires HO-1-mediated autophagy activation in the presence of primary cilium. This study could lead us to a better understanding of moderate FSS-mediated maintenance of ECM homeostasis in NP cells, and may shed lights into developing novel strategies for early prevention and treatment of IVD degeneration.

DATA AVAILABILITY STATEMENT

The RNASeq data have been deposited in Sequence Read Archive (SRA, PRJNA587407).

AUTHOR CONTRIBUTIONS

GX, ZS, SC, and HC designed the study. SC, HC, LQ, XW, XF, and SL conducted the study and collected the data. SC and GX analyzed the data. GX, ZS, SC, DC, and HC interpreted the data. SC, HC, and GX drafted the manuscript. SC, GX, LQ, XW, XF, SL, ZS, and HC took the responsibility for the integrity of the data analysis.

FUNDING

This work was supported, in part, by the National Key Research and Development Program of China Grants (2016YFC1100100, 2019YFA0906001, and 2019YFA0906004), the National Natural Science Foundation of China Grants (91649204, 81630066, 81870532, 81972100, and 81991513), the Guangdong Provincial Science and Technology Innovation Council Grant (2017B030301018), and Science and Technology Innovation Commission of Shenzhen Municipal Government Grants (JCYJ20180302174117738, JCYJ20180302174246105, KQJSCX20180319114434843, and JSGG20180503182321166).

SUPPLEMENTARY MATERIAL

The Supplementary Material for this article can be found online at: https://www.frontiersin.org/articles/10.3389/fcell.2020.00127/full#supplementary-material

REFERENCES

An, Q. D., Li, Y. Y., Zhang, H. X., Lu, J., Yu, X. D., Lin, Q., et al. (2018). Inhibition of bromodomain-containing protein 4 ameliorates oxidative stress-mediated apoptosis and cartilage matrix degeneration through activation of NF-E2-related factor 2-heme oxygenase-1 signaling in rat chondrocytes. *J. Cell Biochem.* 119, 7719–7728. doi: 10.1002/jcb.27122

Anvarian, Z., Mykytyn, K., Mukhopadhyay, S., Pedersen, L. B., and Christensen, S. T. (2019). Cellular signalling by primary cilia in development, organ function and disease. *Nat. Rev. Nephrol.* 15, 199–219. doi: 10.1038/s41581-019-0116-9

Bonnevie, E. D., Gullbrand, S. E., Ashinsky, B. G., Tsinman, T. K., Elliott, D. M., Chao, P. G., et al. (2019). Aberrant mechanosensing in injured intervertebral discs as a result of boundary-constraint disruption and residual-strain loss. *Nat. Biomed. Eng.* 3, 998–1008. doi: 10.1038/s41551-019-0458-4

Cao, H., Yan, Q., Wang, D., Lai, Y., Zhou, B., Zhang, Q., et al. (2020). Focal adhesion protein Kindlin-2 regulates bone homeostasis in mice. *Bone Res.* 8:2. doi: 10.1038/s41413-019-0073-8

Cao, H., Yu, S., Yao, Z., Galson, D. L., Jiang, Y., Zhang, X., et al. (2010). Activating transcription factor 4 regulates osteoclast differentiation in mice. *J. Clin. Invest.* 120, 2755–2766. doi: 10.1172/JCI42106

Cao, H., Zhu, K., Qiu, L., Li, S., Niu, H., Hao, M., et al. (2013). Critical role of AKT protein in myeloma-induced osteoclast formation and osteolysis. *J. Biol. Chem.* 288, 30399–30410. doi: 10.1074/jbc.M113.469973

Chen, S., Liu, S., Ma, K., Zhao, L., Lin, H., and Shao, Z. (2019). TGF-beta signaling in intervertebral disc health and disease. *Osteoarthr. Cartil.* 27, 1109–1117. doi: 10.1016/j.joca.2019.05.005

Chen, S., Zhao, L., Deng, X., Shi, D., Wu, F., Liang, H., et al. (2017). Mesenchymal stem cells protect nucleus pulposus cells from compression-induced apoptosis by inhibiting the mitochondrial pathway. *Stem Cells Int.* 2017, 9843120. doi: 10.1155/2017/9843120

Chiang, S. K., Chen, S. E., and Chang, L. C. (2018). A dual role of heme oxygenase-1 in cancer cells. *Int. J. Mol. Sci.* 20:39. doi: 10.3390/ijms20010039

Chou, P. H., Wang, S. T., Yen, M. H., Liu, C. L., Chang, M. C., and Lee, O. K. (2016). Fluid-induced, shear stress-regulated extracellular matrix and matrix metalloproteinase genes expression on human annulus fibrosus cells. *Stem Cell Res. Ther.* 7:34. doi: 10.1186/s13287-016-0292-5

Clouet, J., Fusellier, M., Camus, A., Le Visage, C., and Guicheux, J. (2018). Intervertebral disc regeneration: from cell therapy to the development of novel bioinspired endogenous repair strategies. *Adv. Drug Deliv. Rev.* 146, 306–324. doi: 10.1016/j.addr.2018.04.017

Coveney, C. R., Collins, I., Mc Fie, M., Chanalaris, A., Yamamoto, K., and Wann, A. K. T. (2018). Cilia protein IFT88 regulates extracellular protease activity by optimizing LRP-1-mediated endocytosis. *FASEB J.* 32:fj201800334. doi: 10.1096/fj.201800334

Dai, J., Wang, H., Liu, G., Xu, Z., Li, F., and Fang, H. (2014). Dynamic compression and co-culture with nucleus pulposus cells promotes proliferation and differentiation of adipose-derived mesenchymal stem cells. *J Biomech.* 47, 966–972. doi: 10.1016/j.jbiomech.2014.01.023

Deschner, J., Rath-Deschner, B., and Agarwal, S. (2006). Regulation of matrix metalloproteinase expression by dynamic tensile strain in rat fibrochondrocytes. *Osteoarthr. Cartil.* 14, 264–272. doi: 10.1016/j.joca.2005.09.005

Dikic, I., and Elazar, Z. (2018). Mechanism and medical implications of mammalian autophagy. *Nat. Rev. Mol. Cell Biol.* 19, 349–364. doi: 10.1038/s41580-018-0003-4

Dong, C., Zheng, H., Huang, S., You, N., Xu, J., Ye, X., et al. (2015). Heme oxygenase-1 enhances autophagy in podocytes as a protective mechanism against high glucose-induced apoptosis. *Exp. Cell Res.* 337, 146–159. doi: 10.1016/j.yexcr.2015.04.005

Frapin, L., Clouet, J., Delplace, V., Fusellier, M., Guicheux, J., and Le Visage, C. (2019). Lessons learned from intervertebral disc pathophysiology to guide rational design of sequential delivery systems for therapeutic biological factors. *Adv. Drug Deliv. Rev.* 14, 49–71. doi: 10.1016/j.addr.2019.08.007

Fu, S., Thompson, C. L., Ali, A., Wang, W., Chapple, J. P., Mitchison, H. M., et al. (2019). Mechanical loading inhibits cartilage inflammatory signalling via an HDAC6 and IFT-dependent mechanism regulating primary cilia elongation. *Osteoarthr. Cartil.* 27, 1064–1074. doi: 10.1016/j.joca.2019.03.003

Gross, A., and Graef, M. (2019). Mechanisms of autophagy in metabolic stress response. *J. Mol. Biol.* 432, 28–52. doi: 10.1016/j.jmb.2019.09.005

Guillen, M., Megias, J., Gomar, F., and Alcaraz, M. (2008). Haem oxygenase-1 regulates catabolic and anabolic processes in osteoarthritic chondrocytes. *J. Pathol.* 214, 515–522. doi: 10.1002/path.2313

He, Z., Leong, D. J., Zhuo, Z., Majeska, R. J., Cardoso, L., Spray, D. C., et al. (2016). Strain-induced mechanotransduction through primary cilia, extracellular ATP, purinergic calcium signaling, and ERK1/2 transactivates CITED2 and downregulates MMP-1 and MMP-13 gene expression in chondrocytes. *Osteoarthr. Cartil.* 24, 892–901. doi: 10.1016/j.joca.2015.11.015

Henry, N., Clouet, J., Le Bideau, J., Le Visage, C., and Guicheux, J. (2018). Innovative strategies for intervertebral disc regenerative medicine: from cell therapies to multiscale delivery systems. *Biotechnol. Adv.* 36, 281–294. doi: 10.1016/j.biotechadv.2017.11.009

Hu, B., Shi, C., Xu, C., Cao, P., Tian, Y., Zhang, Y., et al. (2016). Heme oxygenase-1 attenuates IL-1beta induced alteration of anabolic and catabolic activities in intervertebral disc degeneration. *Sci. Rep.* 6:21190. doi: 10.1038/srep21190

Hua, K., and Ferland, R. J. (2018). Primary cilia proteins: ciliary and extraciliary sites and functions. *Cell Mol. Life Sci.* 75, 1521–1540. doi: 10.1007/s00018-017-2740-5

Katz, J. N. (2006). Lumbar disc disorders and low-back pain: socioeconomic factors and consequences. *J. Bone Joint Surg. Am.* 88(Suppl. 2), 21–24. doi: 10.2106/JBJS.E.01273

Kim, Y. J., and Kim, J. (2019). Therapeutic perspectives for structural and functional abnormalities of cilia. *Cell Mol. Life Sci.* 76, 3695–3709. doi: 10.1007/s00018-019-03158-6

Lopez de Figueroa, P., Lotz, M. K., Blanco, F. J., and Carames, B. (2015). Autophagy activation and protection from mitochondrial dysfunction in human chondrocytes. *Arthritis Rheumatol.* 67, 966–976. doi: 10.1002/art.39025

Ma, K., Chen, S., Li, Z., Deng, X., Huang, D., Xiong, L., et al. (2019). Mechanisms of endogenous repair failure during intervertebral disc degeneration. *Osteoarthr. Cartil.* 27, 41–48. doi: 10.1016/j.joca.2018.08.021

Maher, C., Underwood, M., and Buchbinder, R. (2017). Non-specific low back pain. *Lancet* 389, 736–747. doi: 10.1016/s0140-6736(16)30970-9

Nakamura, K., Kageyama, S., Yue, S., Huang, J., Fujii, T., Ke, B., et al. (2018). Heme oxygenase-1 regulates sirtuin-1-autophagy pathway in liver transplantation: from mouse to human. *Am. J. Transplant.* 18, 1110–1121. doi: 10.1111/ajt.14586

Neidlinger-Wilke, C., Galbusera, F., Pratsinis, H., Mavrogonatou, E., Mietsch, A., Kletsas, D., et al. (2014). Mechanical loading of the intervertebral disc: from the macroscopic to the cellular level. *Eur. Spine J.* 23(Suppl. 3), S333–S343. doi: 10.1007/s00586-013-2855-9

Oh, C.-D., Im, H.-J., Suh, J., Chee, A., An, H., and Chen, D. (2016). Rho-associated kinase inhibitor immortalizes rat nucleus pulposus and annulus fibrosus cells: establishment of intervertebral disc cell lines with novel approaches. *Spine* 41, E255–E261. doi: 10.1097/BRS.0000000000001235

Orhon, I., Dupont, N., Zaidan, M., Boitez, V., Burtin, M., Schmitt, A., et al. (2016). Primary-cilium-dependent autophagy controls epithelial cell volume in response to fluid flow. *Nat. Cell Biol.* 18, 657–667. doi: 10.1038/ncb3360

Otterbein, L. E., Foresti, R., and Motterlini, R. (2016). Heme oxygenase-1 and carbon monoxide in the heart: the balancing act between danger signaling and pro-survival. *Circ. Res.* 118, 1940–1959. doi: 10.1161/CIRCRESAHA.116.306588

Priyadarshani, P., Li, Y., and Yao, L. (2016). Advances in biological therapy for nucleus pulposus regeneration. *Osteoarthr. Carti.* 24, 206–212. doi: 10.1016/j.joca.2015.08.014

Sakai, D., and Grad, S. (2015). Advancing the cellular and molecular therapy for intervertebral disc disease. *Adv. Drug. Deliv. Rev.* 84, 159–171. doi: 10.1016/j.addr.2014.06.009

Silagi, E. S., Shapiro, I. M., and Risbud, M. V. (2018). Glycosaminoglycan synthesis in the nucleus pulposus: dysregulation and the pathogenesis of disc degeneration. *Matrix Biol.* 7, 368–379. doi: 10.1016/j.matbio.2018.02.025

Spang, N., Feldmann, A., Huesmann, H., Bekbulat, F., Schmitt, V., Hiebel, C., et al. (2014). RAB3GAP1 and RAB3GAP2 modulate basal and rapamycin-induced autophagy. *Autophagy* 10, 2297–2309. doi: 10.4161/15548627.2014.994359

Surolia, R., Karki, S., Kim, H., Yu, Z., Kulkarni, T., Mirov, S. B., et al. (2015). Heme oxygenase-1-mediated autophagy protects against pulmonary endothelial cell

death and development of emphysema in cadmium-treated mice. *Am. J. Physiol. Lung. Cell Mol. Physiol.* 309, L280–L292. doi: 10.1152/ajplung.00097.2015

Towers, C. G., and Thorburn, A. (2016). Therapeutic targeting of autophagy. *EBioMed.* 14, 15–23. doi: 10.1016/j.ebiom.2016.10.034

Vasconcellos, L. R., Siqueira, M. S., Moraes, R., Carneiro, L. A., Bozza, M. T., and Travassos, L. H. (2018). Heme Oxygenase-1 and Autophagy Linked for Cytoprotection. *Curr. Pharm. Des.* 24, 2311–2316. doi: 10.2174/1381612824666180727100909

Wang, X., Zhang, Y., Feng, T., Su, G., He, J., Gao, W., et al. (2018). fluid shear stress promotes autophagy in hepatocellular carcinoma cells. *Int. J. Biol. Sci.* 14, 1277–1290. doi: 10.7150/ijbs.27055

Wang, Z., Wann, A. K., Thompson, C. L., Hassen, A., Wang, W., and Knight, M. M. (2016). IFT88 influences chondrocyte actin organization and biomechanics. *Osteoarthri. Cartil.* 24, 544–554. doi: 10.1016/j.joca.2015.10.003

Yang, H., Wen, Y., Zhang, M., Liu, Q., Zhang, H., Zhang, J., et al. (2019). MTORC1 coordinates the autophagy and apoptosis signaling in articular chondrocytes in osteoarthritic temporomandibular joint. *Autophagy* 16, 271–288. doi: 10.1080/15548627.2019.1606647

Ye, D., Liang, W., Dai, L., and Yao, Y. (2018). Moderate fluid shear stress could regulate the cytoskeleton of nucleus pulposus and surrounding inflammatory mediators by activating the FAK-MEK5-ERK5-cFos-AP1 signaling pathway. *Dis. Markers* 2018:9405738. doi: 10.1155/2018/9405738

Zhang, B., Hou, R., Zou, Z., Luo, T., Zhang, Y., Wang, L., et al. (2018). Mechanically induced autophagy is associated with ATP metabolism and cellular viability in osteocytes in vitro. *Redox Biol.* 14, 492–498. doi: 10.1016/j.redox.2017.10.021

Zheng, L., Cao, Y., Ni, S., Qi, H., Ling, Z., Xu, X., et al. (2018). Ciliary parathyroid hormone signaling activates transforming growth factor-beta to maintain intervertebral disc homeostasis during aging. *Bone Res.* 6:21. doi: 10.1038/s41413-018-0022-y

Conflict of Interest: The authors declare that the research was conducted in the absence of any commercial or financial relationships that could be construed as a potential conflict of interest.

Copyright © 2020 Chen, Qin, Wu, Fu, Lin, Chen, Xiao, Shao and Cao. This is an open-access article distributed under the terms of the Creative Commons Attribution License (CC BY). The use, distribution or reproduction in other forums is permitted, provided the original author(s) and the copyright owner(s) are credited and that the original publication in this journal is cited, in accordance with accepted academic practice. No use, distribution or reproduction is permitted which does not comply with these terms.

frontiers in Cell and Developmental Biology

ORIGINAL RESEARCH
published: 13 March 2020
doi: 10.3389/fcell.2020.00131

Human Umbilical Mesenchymal Stem Cells Display Therapeutic Potential in Rheumatoid Arthritis by Regulating Interactions Between Immunity and Gut Microbiota *via* the Aryl Hydrocarbon Receptor

Xiaoya Li[1,2,3†], Cheng Lu[4†], Danping Fan[2,3], Xiangchen Lu[2,5], Ya Xia[2,5], Hongyan Zhao[6], Huihui Xu[6], Yongliang Zhu[7], Jingtao Li[8], Honglin Liu[2] and Cheng Xiao[1,2,3*]*

[1] Department of Emergency, China-Japan Friendship Hospital, Beijing, China, [2] Institute of Clinical Medical Sciences, China-Japan Friendship Hospital, Beijing, China, [3] Graduate School of Peking Union Medical College, Chinese Academy of Medical Sciences/Peking Union Medical College, Beijing, China, [4] Institute of Basic Research in Clinical Medicine, China Academy of Chinese Medical Sciences, Beijing, China, [5] School of Traditional Chinese Medicine, Beijing University of Chinese Medicine, Beijing, China, [6] Beijing Key Laboratory of Research of Chinese Medicine on Prevention and Treatment for Major Diseases, Experimental Research Center, China Academy of Chinese Medical Sciences, Beijing, China, [7] Department of Plant and Microbial Biology, University of California, Berkeley, Berkeley, CA, United States, [8] Department of Gastroenterology, China-Japan Friendship Hospital, Beijing, China

Background: Rheumatoid arthritis (RA) is an autoimmune disease that may be associated with gut microbiota *via* the aryl hydrocarbon receptor (AhR). Human umbilical mesenchymal stem cells (HUMSCs) have therapeutic potential against RA, but the underlying mechanism has not been fully elucidated. The purpose of this study was to explore the mechanism of action of HUMSCs in rats with collagen-induced arthritis (CIA).

Method: HUMSCs (1×10^6) were transplanted into each rat with CIA. The tissue localization of HUMSCs and the therapeutic effects in the ankles were assessed. The immune status and expression of immune-related genes and proteins in related lymphoid tissues were subsequently tested. Furthermore, the levels of immune-related factors in serum and the changes in gut microbiota in the ileum were detected, and the levels of indole and their derivatives in plasma and the levels of AhR in the ileum were evaluated.

Results: HUMSCs homed to the popliteal lymph node (PLN), mesenteric lymph node (MLN), ankle cartilage, and ileum mucosa in rats with CIA. The transplantation of HUMSCs reduced the pathology scores and the degree of bone damage in the ankles. The immune status of T regulatory cells (Tregs) and T helper (Th)17 cells and the gene expression levels of interleukin (IL)-10, transforming growth factor (TGF)-β*1*, and IL-17A were altered in the PLN, which is the lymph tissue closest to the nidus, and the MLN, which is one of the gut-associated lymphoid tissues (GALTs). The proportion and function of B cells, Tregs, and Th17 cells were regulated in other GALTs, namely,

OPEN ACCESS

Edited by:
Chao Liang,
Hong Kong Baptist University, Hong Kong

Reviewed by:
Defang Li,
Binzhou Medical University, China
William Chi-Shing Tai,
The Hong Kong Polytechnic University, Hong Kong

***Correspondence:**
Cheng Xiao
xc2002812@126.com
Honglin Liu
honglinl2003@163.com

† These authors have contributed equally to this work

Specialty section:
This article was submitted to Molecular Medicine, a section of the journal Frontiers in Cell and Developmental Biology

Received: *12 December 2019*
Accepted: *14 February 2020*
Published: *13 March 2020*

Citation:
Li X, Lu C, Fan D, Lu X, Xia Y, Zhao H, Xu H, Zhu Y, Li J, Liu H and Xiao C (2020) Human Umbilical Mesenchymal Stem Cells Display Therapeutic Potential in Rheumatoid Arthritis by Regulating Interactions Between Immunity and Gut Microbiota via the Aryl Hydrocarbon Receptor. Front. Cell Dev. Biol. 8:131. doi: 10.3389/fcell.2020.00131

Peyer's patches and the lamina propria. The gene expression of TGF-β*1* and IL-17A and protein expression of IL-10, TGF-β*1*, IL-17A, IL-22, and immunoglobulin A (IgA) were modulated in the ileum, and the serum levels of IL-10, TGF-β1, IL-17A, IL-1β, and tumor necrosis factor (TNF)-α were regulated in the rats with CIA. The relative abundances of the genera *Bacteroides* and *Bacillus* were increased in the HUMSCs-treated rat with CIA; in addition, the levels of indole, indoleacetic acid, and indole-3-lactic acid were consistently upregulated, and this upregulation was accompanied by increases in AhR gene and protein expression.

Conclusion: Our study demonstrates that HUMSCs play a therapeutic role in rats with CIA by regulating the interactions between host immunity and gut microbiota *via* the AhR.

Keywords: human umbilical mesenchymal stem cells, rheumatoid arthritis, host immunity, gut microbiota, aryl hydrocarbon receptor

INTRODUCTION

Rheumatoid arthritis (RA) is a systemic, inflammatory, and autoimmune disease characterized by immune disorders and bone dysmetabolism that ultimately leads to functional disability. RA, one of the most common autoimmune diseases, has an incidence of 0.5%–1% worldwide and is three times more common in women than in men (Smolen et al., 2016). Previous studies have revealed that the complex interplay among genotype, environmental triggers, and chance is involved in the pathogenesis and progression of RA (McInnes and Schett, 2011). In addition, in-depth research in microbiota has gradually revealed that the bidirectional influence between gut microbiota/their metabolites and host immunity might be related to RA, and alterations in the gut microbiota have been found to be involved in improving RA symptoms (Wu X. et al., 2016). RA is correlated with the inflammatory response mediated by $CD4^+$ T helper 1 (Th1) lymphocytes, T helper 17 (Th17) lymphocytes, and an imbalance between Th17 lymphocytes and T regulatory cells (Tregs) (Noack and Miossec, 2014).

Stem cells are cells with multidifferentiation capacity that exert immunomodulatory effects by modulating T and B cell proliferation and differentiation, dendritic cell maturation, and natural killer (NK) cell activity (Naik et al., 2018). In addition to their self-renewal ability, human umbilical mesenchymal stem cells (HUMSCs) exhibit minimal immune rejection and can be used for allogeneic transplantation (Ma et al., 2019). The abovementioned characteristics indicate the potential of using HUMSCs to treat autoimmune diseases (ADs), and this finding has been verified (Uccelli et al., 2008). Specifically, the use of HUMSCs in RA has shown promising results in clinical trials (Shadmanfar et al., 2018; Ghoryani et al., 2019). Basic studies have also suggested that HUMSCs can alleviate collagen-induced arthritis (CIA) partly by regulating Tregs and Th17 cells (Liu et al., 2010; Tong et al., 2015; Ma et al., 2019), but further research on the molecular mechanisms and interconnections between these different mechanisms remains rare.

The aryl hydrocarbon receptor (AhR) is a cytoplasmic receptor that responds to multiple exogenous and endogenous compounds from the diet, host metabolites, and the gut microbiota (Shinde and McGaha, 2018). Tryptophan metabolites are the main ligands of the gut microbiota (Gao et al., 2018). An increasing number of studies have shown that the AhR plays an indispensable role in the regulation of innate and adaptive immunity, including the regulation of the differentiation and function of Tregs and Th17 cells (Rothhammer and Quintana, 2019). Therefore, the AhR plays a key role in connecting immunity to the microenvironment. Although drugs that regulate Tregs and Th17 cells in CIA reportedly function through the AhR and the interaction between the AhR and the gut microbiota affects the disease status, no interaction among the gut microbiota, the AhR, Tregs/Th17 cells, and HUMSCs has been detected.

In this study, we detected the suppressive effect of HUMSCs on the differentiation of osteoclasts (OCs) in CIA. We also demonstrated that HUMSCs can regulate the immune status of the lymph tissue closest to the nidus—the popliteal lymph node (PLN). More importantly, the study showed that the immune status of gut-associated lymphoid tissues (GALTs) and the gut microbiota in the ileum were also altered by HUMSCs. In addition, the possible mechanisms underlying these effects were explored.

MATERIALS AND METHODS

Isolation and Culture of Human Umbilical Mesenchymal Stem Cells and Phenotype Identification

This study was approved by the Research Ethics Committee at the China-Japan Friendship Hospital (2019-124-K86). Fresh umbilical cord samples were obtained from the Obstetrics Department at the China-Japan Friendship Hospital after normal spontaneous full-term delivery, and written informed consent was provided by the mother. The umbilical tissue was transferred into Hanks' balanced salt solution (HBSS) (Gibco BRL Life Technologies, Grand Island, NY, United States) to remove

aggregation and blood vessels. The remaining tissue was then dissected into cubes approximately 0.5 cm^3 in size and incubated with 0.25% trypsin (Gibco) in an incubator for 15 min. The tissue was transferred to culture vessels containing high-glucose Dulbecco's modified Eagle's medium (DMEM; Gibco) with 10% fetal bovine serum (FBS; Gibco) and antibiotics (100 IU/ml penicillin, 100 μg/ml streptomycin; Gibco) at 37°C in 5% CO_2 and left undisturbed for 2 to 4 weeks to allow the migration of HUMSCs from the tissues. Once many cells surrounded the tissue, the cells were refed and passaged. After the third passage, the cells were harvested for phenotype identification through staining with antibodies against CD34, CD45, CD11b, CD19, HLA-DR, CD73, CD90, and CD105 (BD Pharmingen, San Diego, CA, United States) and analyzed with a FACS Canto II flow cytometer (FACS Canto II, Becton, Dickinson, Co., Franklin Lakes, NJ, United States). HUMSCs after the third to fifth passages were used for the experiments.

Induction of Arthritis and Arthritis Assessment

Forty male Sprague-Dawley rats (190 ± 10 g) were purchased from the National Institutes for Food and Drug Control [animal license number: SCXK (Beijing) 2014-0013]. The rats were maintained in a specific pathogen-free animal laboratory with an environment with a constant temperature of 23°C (± 2°C) and an alternating 12-h light/12-h dark cycle at the Experimental Animal Center of the Institute of Clinical Medical Sciences, China-Japan Friendship Hospital [Experiment Animal Center license number: SYXK (Beijing) 2016-0043]. Two to three rats were housed in each cage with free access to standard rodent chow and water. All the experimental procedures were examined and approved by the Institute of Clinical Medical Sciences, China-Japan Friendship Hospital, Beijing, China (No. 180207).

After the rats were subjected to adjustable feeding for 7 days, arthritis was induced as previously described (Zhao et al., 2018). Briefly, the rats were immunized on day 0 with 100 μg of bovine type II collagen (Chondrex, Inc., Redmond, WA, United States) emulsified in isopyknic incomplete Freund's adjuvant (Chondrex) *via* intradermal injection at one side of the base of the tail while avoiding the tail vein and administered booster immunization with the same preparation on day 7 on the other side of the base of the tail. The arthritis severity was examined every 3 days starting on day 1 and expressed through an arthritic index (AI) ranging from 0 to 4 points each hind leg according to conventional criteria (Zhao et al., 2018) as follows: 0 = no change, 1 = red or slight swelling, 2 = mild swelling, 3 = pronounced swelling, 4 = limb deformity and inability.

Experimental Groups and Treatments

After the onset of arthritis, the CIA model rats with no change in their AI score were excluded, and the remaining rats were randomly divided into the following three groups and started to undergo treatment on day 10: (1) normal control rats (Control group), (2) rats with CIA (CIA group), (3) CIA rats with methotrexate (MTX, Xinyi, Shanghai, China) (MTX group), and (4) CIA rats transplanted with HUMSCs (HUMSCs group). The rats in the HUMSCs group were administered 1×10^6 HUMSCs suspended in 200 μl of a 0.9% NaCl solution, and the rats belonging to the other groups were administered an equal solution of 0.9% NaCl solution *via* tail vein injection. The rats in MTX group were intragastrically administered MTX (1.5 mg/kg twice a week), and the rats in the control, CIA, and HUMSCs groups were treated with the same volume of pure water as MTX group.

Immunohistochemistry and Immunofluorescence

The rats were sacrificed on day 38 (after 28 days of treatment). For immunohistochemistry (IHC) assessment, paraffin-embedded sections (5-μm-thick) of the spleen, PLN, mesenteric lymph node (MLN), ileum, and knee joints after decalcification with 10% EDTA-Na_2 were heated in a water bath for antigen retrieval using citrate buffer (pH 6.0) or ethylenediaminetetraacetic acid (EDTA; pH 9.0) depending on the primary antibody. The sections were then incubated with 3% hydrogen peroxide (H_2O_2) for 15 min away from light. The ileum sections were incubated with the following primary antibodies: rabbit anti-rat interleukin (IL)-10 (Abcam, Cambridge, MA, United States; 1:400), rabbit anti-rat transforming growth factor (TGF)-β*1* (Abcam; 1:100), rabbit anti-rat IL-17A (Absin, Shanghai, China; 1:100), rabbit anti-rat IL-22 (Absin; 1:500), goat anti-rat immunoglobulin A (IgA; Abcam; 1:400), and rabbit anti-rat AhR (Proteintech, Rosemont, IL, United States; 1:200). Sections of the spleen, PLN, MLN, ileum, and knee joints of the HUMSCs group were incubated with primary mouse anti-human nuclear mitotic apparatus (NuMA) (Santa Cruz Biotechnology; 1:200) (a human cell-specific nuclear antigen) in antibody diluent overnight at 4°C and then with horseradish peroxidase (HRP)-linked species-specific antibodies for 20 min. The sections were subsequently stained with 3,3′-diaminobenzidine (DAB) and counterstained with hematoxylin at room temperature. Images were randomly captured using a ZEISS Axio Observer 3 microscope, and Image Pro-Plus was used to determine the positive staining area and the integral optical density of each index, which was calculated with the following formula: mean optical density = integral optical density/positive staining area. The immunofluorescence (IF) experiments involved the use of primary mouse anti-human NuMA antibody and no incubation with secondary antibody. Specifically, in the IF experiments, the samples were incubated with Alexa Fluor 555-conjugated species-specific antibodies (Cell Signaling Technology, Boston, MA, United States) for 1 h at room temperature in the dark and then sealed with mounting medium containing 4′,6-diamidino-2-phenylindole (DAPI; Invitrogen, Carlsbad, CA, United States). Images were captured randomly using a laser scanning confocal microscope (Zeiss, LSM 800).

Histopathological Evaluation and Tartrate-Resistant Acid Phosphatase Staining of Ankle Bones

The left ankle bones were decalcified and used to prepare 5-μm-thick slices, and the slices were then stained with Hematoxylin-Eosin staining (H&E). The mean inflammation

score was assessed microscopically on a scale of 0–3 according to the degree of lymphocyte infiltration, synovial hyperplasia, pannus, cartilage damage, and joint destruction (0 = normal, 1 = weak, 2 = moderate, and 3 = severe). The OCs of the ankle joints were counted by staining slices of the ankle samples with tartrate-resistant acid phosphatase (TRACP; Sigma, St. Louis, MO, United States) and were identified by the presence of multinucleated cells that stained positive for TRACP and contained at least three nuclei.

Micro-CT Analysis

A Skyscan 1174 micro-CT scanner (Bruker, Belgium) was used to scan the left ankle joints and paws of the rats, and three-dimensional (3D) images were reconstructed with the corresponding software, N-Recon, to obtain the 3D model. The corresponding CT-AN software was then used for 3D analysis to detect the following indices: bone volume (BV), bone surface (BS), and ratio of bone surface to bone volume (BS/BV).

Flow Cytometry

PLN, MLN, Peyer's patch (PP), and lamina propria lymphocyte (LPL) were evaluated according to the manufacturer's recommended protocol. Briefly, the lymph nodes and PPs of the four groups were isolated, placed in sterile normal saline solution and then ground with a 300-mesh sieve. The cell suspension was centrifuged, suspended in RPMI medium containing 10% FBS and filtered through 70-μm cell sieve. LPL was isolated as previously reported (Xiao et al., 2006), and antibodies against $CD4^+$ and $IL\text{-}17^+$ were then used to identify Th17 cells. However, cytoplasmic IL-17 was easily secreted into the extracellular space, and the concentration of IL-17 was low. Therefore, a cell stimulation cocktail with protein transport inhibitors (eBioscience, San Diego, CA, United States) was used for IL-17 stimulation overnight at 37°C prior to antibody staining. Antibodies against $CD4^+$, $CD25^+$, and $Foxp3^+$ were used to stain Tregs, and antibodies against Foxp3 were added to the cells after fixation and permeabilization using a Foxp3/Transcription Factor Staining Buffer Set (eBioscience). B cells were identified as $CD45RA^+$ and $CD3^-$ cells. The Tregs and Th17 cells in the PLN, MLN, and PP and among the LPL and the B cells in the MLN and PP and among the LPL were analyzed using a FACS Canto II flow cytometer.

Quantitative Real-Time PCR

The mRNA expression of IL-10, TGF-β1, and IL-17A in both the PLN and MLN and the mRNA expression of IL-10, TGF-β1, IL-17A, and AhR in the ileum were evaluated by quantitative real-time PCR (Q-PCR). Total RNA was extracted from the four groups using the TRIzol reagent (Invitrogen) according to the manufacturer's recommended procedure, and gDNA elimination and cDNA synthesis were then performed using a PrimeScript RT Reagent Kit with gDNA Eraser (TaKaRa, Tokyo, Japan). PCR was performed using SYBR Premix Ex Taq (Tli RNaseH Plus) (TaKaRa) with a Quant Studio 5 Real-Time PCR System (Thermo Fisher Scientific, Waltham, MA, United States). Amplification was performed using the following steps: initial denaturation at 95°C for 30 s and 40 cycles of 95°C for 15 s and 60°C for 34 s. All the experiments were performed in duplicate, and the relative mRNA expression levels were determined by the $2^{-\Delta\Delta Ct}$ method. The primers used in this analysis are shown in **Table 1**.

TABLE 1 | Specific primers used for PCR.

Gene	Forward primer	Revised primer
IL-10	5′-GATCCAGAGATCTTAGCTA-3′	5′-CTGAGGTATCAGAGGTAA-3′
TGF-β1	5′-ATCGACATGGAGCTGGTGA-3′	5′-TTGGCATGGTAGCCCTTGG-3′
IL-17A	5′-GGAGAATTCCATCCATGTGC-3′	5′-CAGAGTCCAGGGTGAAGTGG-3′
AhR	5′-CGCGGGCACCATGAGCAG-3′	5′-CTGTAACAAGAACTCTCC-3′
β-Actin	5′-CACCCGCGAGTACAACCTTC-3′	5′-CCCATACCCACCATCACACC-3′

IL, interleukin; TGF, transforming growth factor; AhR, aryl hydrocarbon receptor.

Quantitation of Serum Cytokines

The quantifications were performed according to the manufacturer's instructions. The serum levels of the inflammatory and immune-related factors IL-10, TGF-β1, IL-17A, IL-1β, and tumor necrosis factor (TNF)-α were determined by Shanghai Laizee Biotech Co., Ltd. (China) using serological Luminex multiplex cytokine analysis technology. A Bio-Plex 200 system (Bio-Rad Laboratories, Hercules, CA, United States) was used to acquire the data.

Microbiota Analysis by 16S rRNA Gene Sequencing

The ileum intestinal contents were harvested, immediately shock-frozen in liquid nitrogen, and then transferred to −80°C. A QIAamp PowerFecal DNA Kit (Qiagen, Valencia, CA, United States) was used to extract microbial DNA from the digesta according to the manufacturer's instructions. The V3–V4 region of 16S rRNA was amplified by PCR using the 16S rRNA universal primer. The PCR products were purified using a QIAquick Gel Extraction Kit (Qiagen) and quantified with the Nanodrop and Qubit systems, respectively. The purified products underwent PE250 sequencing using HiSeq 2500 according to standard protocols. After quality inspection and sequence splicing, effective sequences were obtained for further analysis. Using the Greengenes database as a reference, sequences with 97% similarity into operational taxonomic units (OTUs) were classified using the usearch61 clustering method in QIIME (v1.9.1) software, and the OTUs were annotated according to reference taxonomy in the Ribosomal Database Project (RDP) database to obtain the taxonomic assignment. The alpha diversity was analyzed using QIIME and R to obtain indices of richness (the Chao1 diversity index) and diversity (the Shannon or Simpson index). The relative abundance was estimated in terms of the phylum, genus, and species. The intestinal microbial community was analyzed *via* partial least square discriminant analysis (PLS-DA). The differences between groups at different levels of taxonomy were obtained by Lefse analyses.

Detection of Indole and Its Derivatives in Plasma

The levels of indole, indoleacetic acid (IAA), and indole-3-lactic acid (ILA) in the plasma were detected by liquid

chromatography-tandem mass spectrometry (LC-MS/MS). A standard stock solution was gradient diluted into working standard solutions with different target concentrations. Subsequently, 80 μl of the plasma samples or working standard solutions was mixed with 240 μl of precipitating agent containing 2 μg/ml 3-methyl-d3-indole. The admixture was vortexed for 5 min and then centrifuged at 13,200 rpm and 4°C for 10 min, and the supernatant was the final solution used in the LC-MS/MS system.

Chromatographic separation was achieved with an Acquity UPLC BEH C8 (1.7 μm, 2.1 mm × 100 mm) column (Waters, Milford, MA, United States) using a mobile phase of (A) 0.01% formic acid and (B) acetonitrile at a flow rate of 0.3 ml/min. The gradient elution program was as follows: 0–2.0 min, 10% B; 3.0–4.0 min, 30% B; 5.0–7.0 min, 100% B; and 7.1–9.0 min, 10% B.

MS detection was performed using an Xevo TQ-S micro spectrometer (Waters) equipped with an electrospray ionization (ESI) source in the multiple reaction monitoring (MRM) mode. The optimized MS parameters were as follows: capillary voltage, 3,000.00 V; desolvation temperature, 550°C; cone gas flow, 10 L/h; desolvation gas flow, 10.00 L/h; and target column temperature, 45°C. TargetLynx (Waters) was used for data acquisition and quantitation.

Statistical Analysis

The statistical analyses were performed with SPSS statistics 22.0 software. The significance of the differences was determined by unpaired *t*-tests (Mann–Whitney) or one-way analysis of variance (ANOVA) followed by the least significant difference (LSD) test. The non-parametric Kruskal–Wallis and Mann–Whitney *U* tests were used if the data were not normally distributed. Each data point was expressed as the mean ± *SEM* or median [interquartile range (IQR)]. $P < 0.05$ indicated significance.

RESULTS

Identification of Human Umbilical Mesenchymal Stem Cells

Cells were successfully isolated and cultured from fresh umbilical cord samples. HUMSCs were identified by harvesting cells at the third passage and analyzing them by flow cytometry. The cells were positive for the expression of CD105, CD90, and CD73 but negative for the expression of HLA-DR, CD11b, CD19, CD34, and CD45 (**Figure 1**). The results showed that the cells obtained from fresh

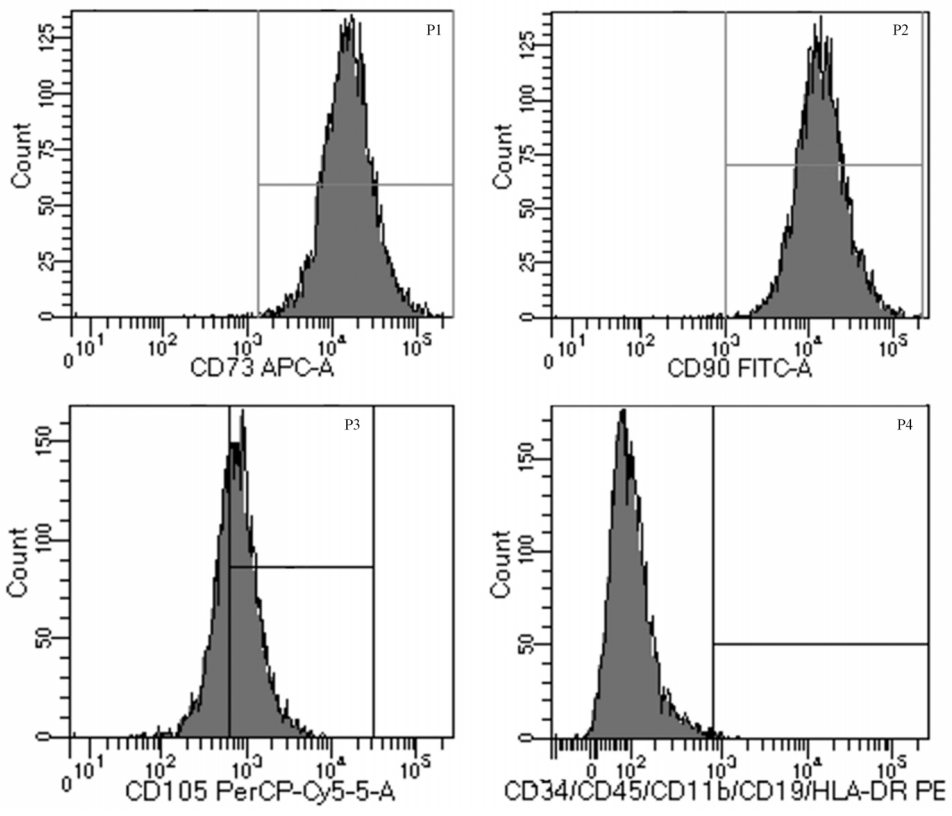


FIGURE 1 | Characteristics of human umbilical mesenchymal stem cells (HUMSCs). The cells were labeled with APC, Allophycocyanin; FITC, Fluoresein Isothiocyanate; PerCP-cy5-5, Peridinin-Chlorophyll-Protein Complex-Cyanin 5-5; PE, Phycoerythrin-conjugated anti-HUMSC surface markers and analyzed by flow cytometry.

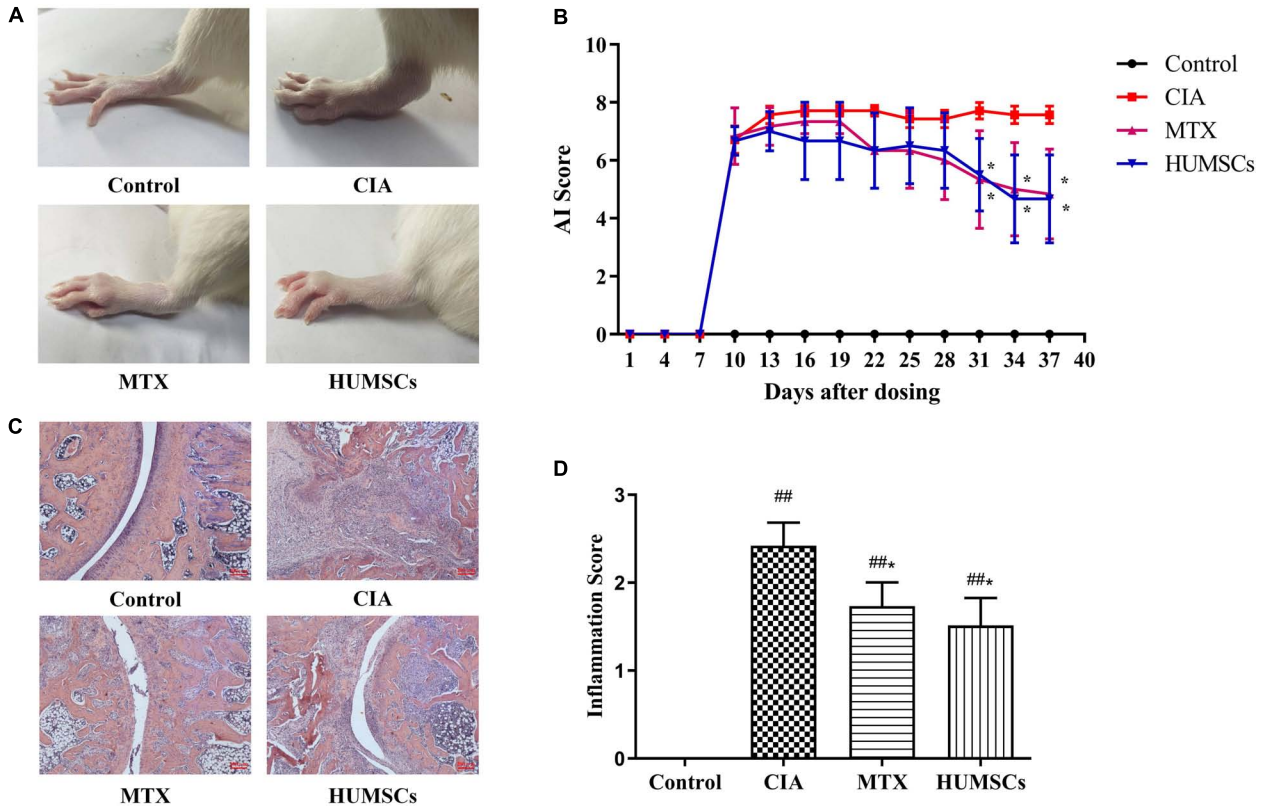


FIGURE 2 | Therapeutic effect of human umbilical mesenchymal stem cells (HUMSCs) transplantation on the rat model of collagen-induced arthritis (CIA). The rats were injected with HUMSCs *via* the tail vein (1×10^6 cells/rat, only once) or orally administered methotrexate (MTX; 1.5 mg/kg, twice a week) or pure water (both the control and CIA groups) for 28 days beginning on day 10 after primary immunization, and the arthritic index (AI) and inflammation score were then evaluated. **(A)** Representative gross lesions of the ankle joints after model development and treatments. **(B)** The arthritis severity was assessed every 3 days. Line plots show the AI score of all the groups. **(C)** Representative pathological sections of the ankle joints subjected to H&E staining. Scale bar = 200 μm. **(D)** The degree of inflammation in the ankle joints was scored according to lymphocyte infiltration, synovial hyperplasia, pannus, cartilage damage, and joint destruction based on H&E staining $N = 8$. The data are presented as the mean ± *SEM*. $^{\#\#}P < 0.01$ compared with the Control group, $^{*}P < 0.05$ compared with the CIA group. Control group = normal control group, CIA group = model group, MTX treatment group = positive control group, HUMSCs group = HUMSCs transplantation group.

umbilical cord were HUMSCs and could be used for subsequent experiments.

Effects of Human Umbilical Mesenchymal Stem Cells in Arthritis

On day 38, the CIA group exhibited severe swelling and degeneration of the ankle joints, whereas these effects were alleviated 28 days after HUMSC transplantation (**Figure 2A**). In addition, the AI of the MTX and HUMSCs groups decreased over time compared with the CIA group, and the difference was statistically significant starting at day 31 ($P < 0.05$) (**Figure 2B**). H&E staining and inflammation score revealed severe pathological changes, including lymphocyte infiltration, synovial hyperplasia, cartilage damage, joint destruction, and excessive formation of pannus in the ankles of the rats belonging to the CIA group, and MTX and HUMSC treatment of rats with CIA significantly reduced CIA joint injury and inflammation ($P < 0.05$) (**Figures 2C,D**). These findings illustrated that HUMSCs arrested the development and progression of CIA in rats.

Human Umbilical Mesenchymal Stem Cells Tissue Localization in Human Umbilical Mesenchymal Stem Cell-Transplanted Rats

To observe the homing of HUMSCs in the CIA rats, NuMA, a human cell-specific nuclear antigen, was used for the detection of HUMSCs in the PLN, MLN, ileum, and knee joints by IF and IHC. As shown in **Figures 3A,B**, extremely small numbers of protein-positive cells were found in all the observed tissues, which demonstrated that HUMSCs homed to the PLN, MLN, ankle cartilage, and ileum mucosa.

Human Umbilical Mesenchymal Stem Cells Alleviated Bone Erosion and Bone Destruction in Arthritis

The ankle joints were reconstructed in 3D and are shown in **Figure 4A**. CIA caused simultaneous and severe bone erosion of the ankle, digital joints, and metatarsal joints, and treatment with MTX and HUMSCs transplantation significantly decreased

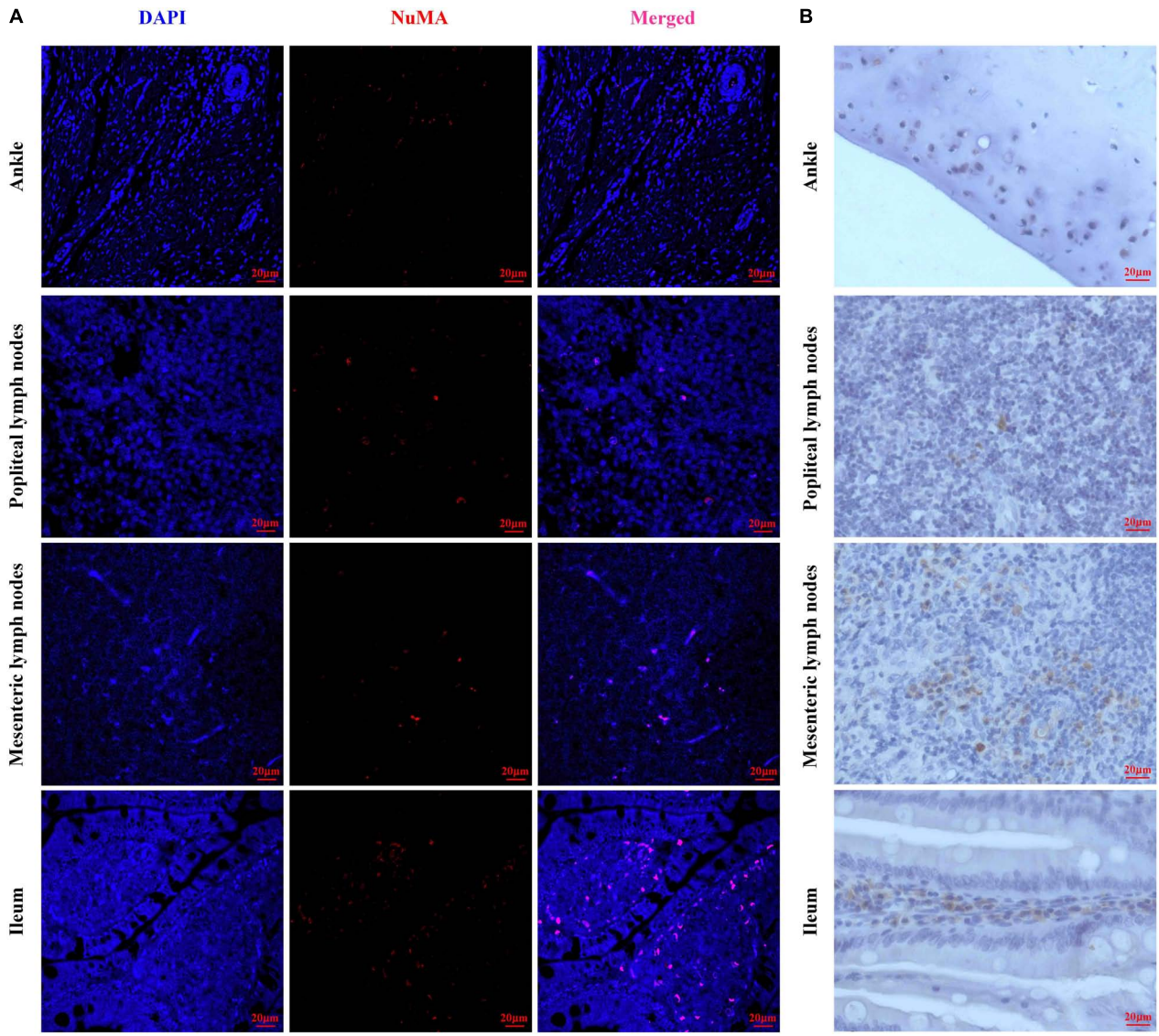


FIGURE 3 | Representative images of human umbilical mesenchymal stem cells (HUMSCs) in the different tissues examined. **(A)** Representative immunofluorescence images of NuMA protein expression in the ankle, popliteal lymph node (PLN), mesenteric lymph node (MLN), and ileum. **(B)** Representative immunohistochemical images of NuMA protein expression in the ankle, PLN, MLN, and ileum (magnification, 20×).

the degree of bone erosion in these joints. Furthermore, the BV, BS, and BS/BV were analyzed for the quantitative evaluation of bone destruction (**Figure 4B**). The BV did not differ among the Control, CIA, MTX, and HUMSC groups. In addition, the BS was obviously increased in the CIA compared with the Control group ($P < 0.01$), but MTX and HUMSCs had no effect on the BS. However, HUMSC transplantation significantly reduced the BS/BV ($P < 0.05$). The differentiation and function of OCs play a key role in bone erosion and bone destruction in both CIA and RA (Zhao et al., 2018). To determine whether the bone-protective effect of HUMSCs on joints was related to OC inhibition, TRACP staining was performed, and the ankle OCs were counted (**Figures 4C,D**). As expected, almost no OCs were found in the ankle joints in the Control group, whereas a large number of OCs were observed in the ankle joints of the CIA group. In addition, both MTX treatment and HUMSC transplantation significantly reduced the number of OCs in the ankle joints compared with those found in the CIA group ($P < 0.05$). These results suggested that the HUMSC-mediated improvement in CIA is related to inhibition of the differentiation of OCs to protect bone.

Human Umbilical Mesenchymal Stem Cells Regulated Immune Status in the Popliteal Lymph Node

The immune status in the PLN was used to represent that of the lesion site as the PLN was the closest immune tissue to

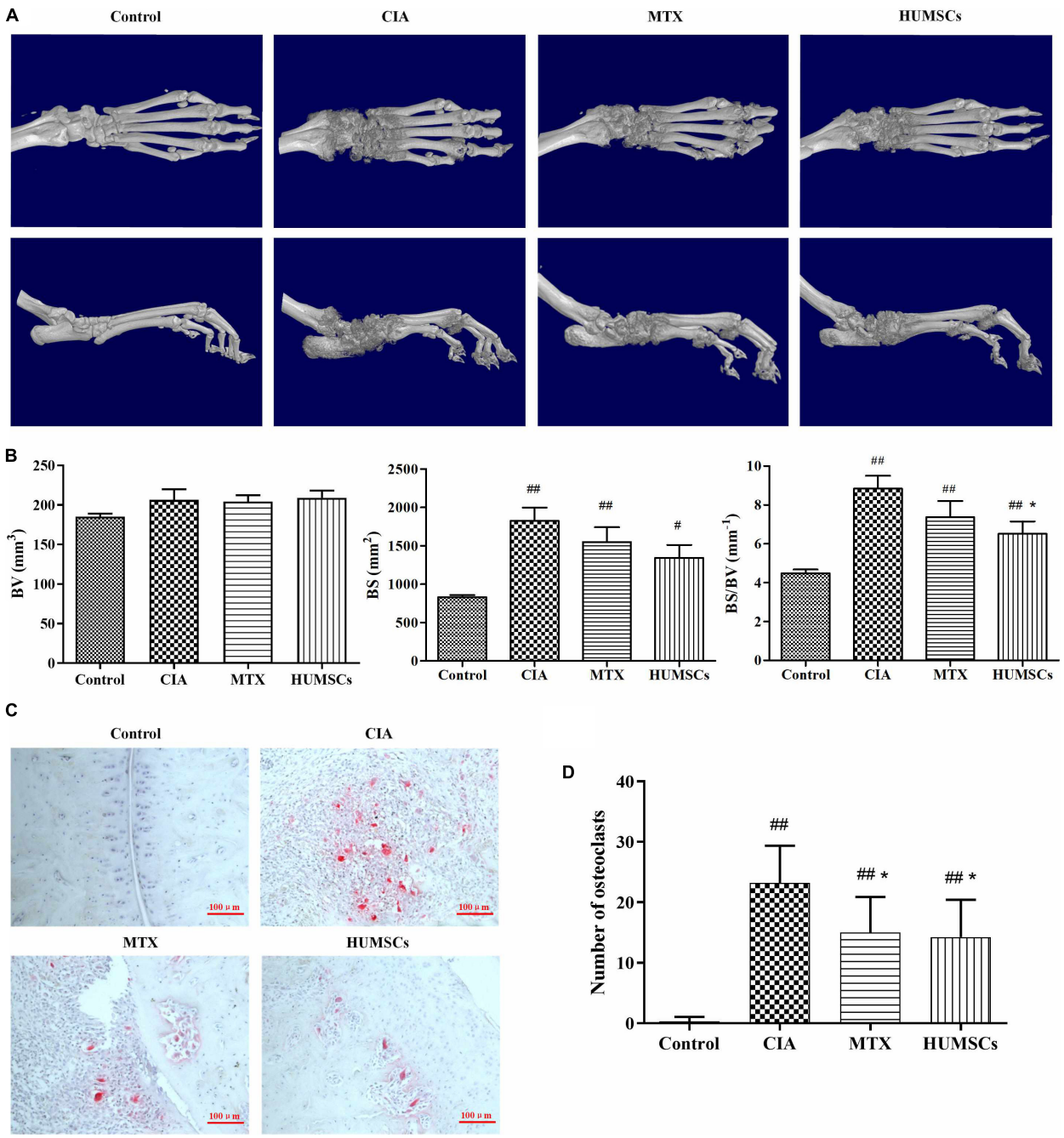


FIGURE 4 | Bone-protective effect of human umbilical mesenchymal stem cells (HUMSCs) transplantation in the ankle joints of rats with collagen-induced arthritis (CIA). Three-dimensional images of the left ankle joints and paws were reconstructed and analyzed based on micro-CT scans. The osteoclasts in the ankle joints were detected and counted after tartrate-resistant acid phosphatase (TRACP) staining. **(A)** Representative three-dimensional (3D) images of the ankle joints and paws taken from above and the side. **(B)** Bar plots showing bone volume (BV), bone surface (BS), and ratio of bone surface to bone volume (BS/BV). **(C)** Representative images of ankle joints osteoclasts detected by TRACP staining. **(D)** Bar plots showing the mean numbers of osteoclasts in the ankle joints. The data are presented as the mean ± *SEM* $N = 8$. $^{\#}P < 0.05$ compared with the Control group, $^{\#\#}P < 0.01$ compared with the Control group, $^{*}P < 0.05$ compared with the CIA group.

the lesion site. The percentages of Tregs and Th17 cells in the PLN were determined *via* flow cytometry (**Figures 5A,B**). The percentage of Tregs in the CIA group was lower than that in the Control group ($P < 0.05$). In contrast, the percentage of Tregs was higher in the HUMSC and MTX groups than in the CIA group ($P < 0.05$). The percentage of Th17 cells was higher in the CIA group than in the Control group ($P < 0.05$), while the percentage of Th17 cells in both the

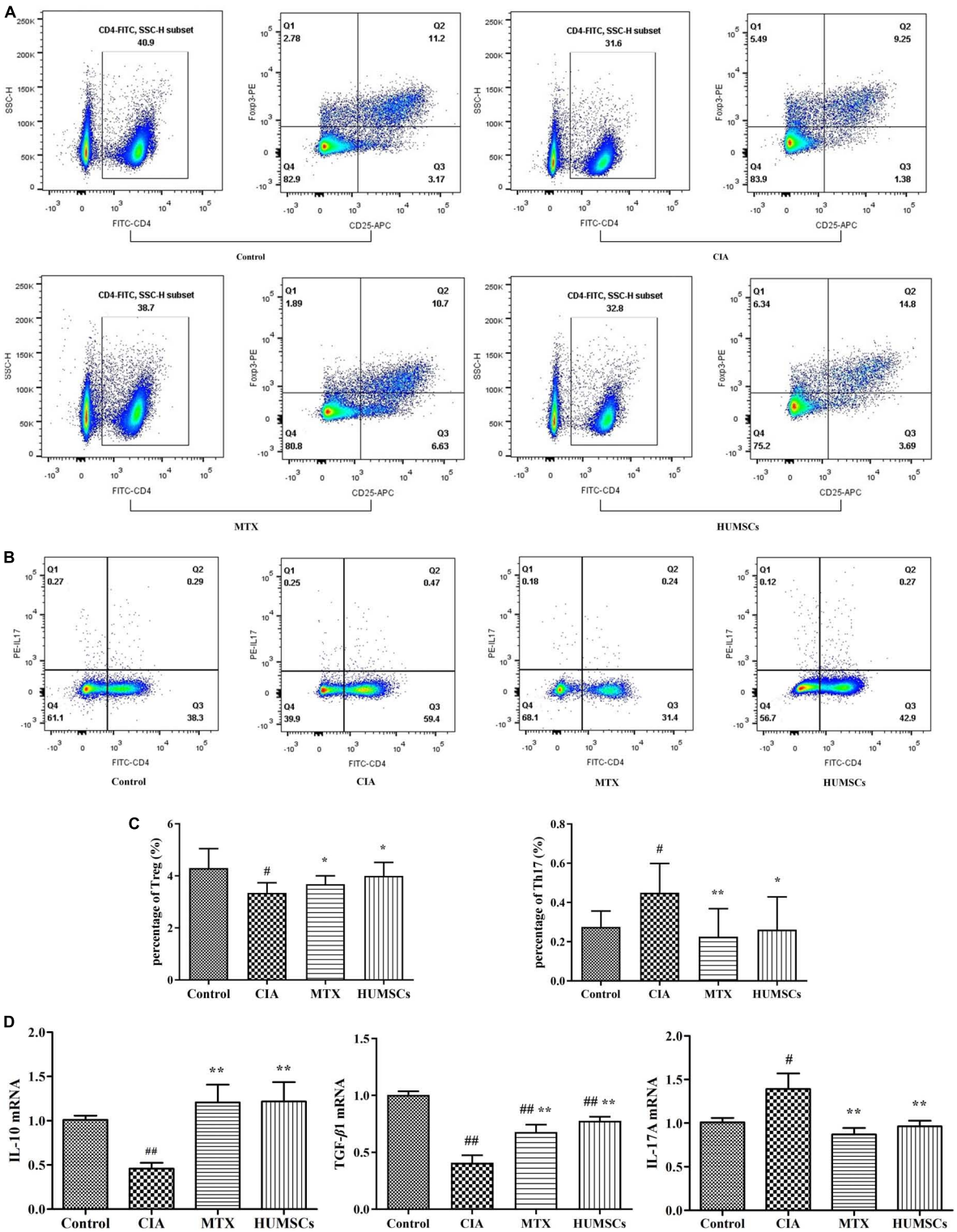


FIGURE 5 | Human umbilical mesenchymal stem cells (HUMSCs) transplantation-mediated regulation of the percentage of T regulatory cells (Tregs) and T helper (Th)17 cells and related gene expression in the popliteal lymph node (PLN) of rats with collagen-induced arthritis (CIA). The percentages of Tregs and Th17 cells were detected by flow cytometry, and the RNA expression levels of interleukin (IL)-10, transforming growth factor (TGF)-β1, and IL-17A were determined by quantitative real-time PCR (Q-PCR). **(A,B)** Representative flow cytometry images of Tregs and Th17 cells in the PLN. **(C)** Bar plots showing the percentages of Tregs and Th17 cells. **(D)** Bar plots showing the mean relative RNA expression levels of IL-10, TGF-β1, and IL-17A. The data are presented as the mean ± *SEM* $N = 8$. $^{\#}P < 0.05$ compared with the Control group, $^{\#\#}P < 0.01$ compared with the Control group, $^{*}P < 0.05$ compared with the CIA group, $^{**}P < 0.01$ compared with the CIA group.

HUMSC and MTX groups was decreased compared to that in the CIA group ($P < 0.01$, $P < 0.05$; **Figure 5C**). Additionally, as shown in **Figure 5D**, the mRNA expression of IL-10, TGF-β1, and IL-17A in the PLN was regulated by HUMSCs and MTX. The levels of both IL-10 and TGF-β1 in the CIA group were lower than those in the Control group, while the level of IL-17A was higher ($P < 0.01$, $P < 0.05$, respectively). HUMSCs and MTX enhanced the mRNA expression of IL-10 and TGF-β1 and reduced the level of IL-17A compared to those in the CIA group ($P < 0.05$). The results indicated that HUMSCs and MTX regulated the immune status and function of Tregs and Th17 cells.

Human Umbilical Mesenchymal Stem Cells Regulated the Expression of Serum Cytokines

As shown in **Figure 6**, the CIA group exhibited downregulated expression of serum IL-10 and TGF-β*1* and upregulated levels of IL-17A, IL-1β, and TNF-α compared with the Control group ($P < 0.05$, $P < 0.01$, respectively). HUMSC transplantation increased the levels of IL-10 and TGF-β*1* and decreased the levels of IL-17A, IL-1β, and TNF-α compared with those found in the CIA group ($P < 0.05$). MTX also upregulated the expression of IL-10 and TGF-β*1* ($P < 0.05$) and downregulated the expression of IL-17A and IL-1β compared with those in the CIA group ($P < 0.05$). The MTX group also showed decreased TNF-α expression compared with the CIA group, but this difference was not statistically significant. The results showed that HUMSCs can regulate not only the local but also the systemic immune state.

Human Umbilical Mesenchymal Stem Cells Modulated the Immune Status of Gut-Associated Lymphoid Tissues

To explore the effect of HUMSCs on the MLN and ileum, the percentages of Tregs and Th17 and B cells in the MLN and PP and among LPL were detected by flow cytometry (**Table 2**). CIA increased the percentage of Th17 cells in the MLN ($P < 0.05$). MTX treatment increased the percentage of only Tregs ($P < 0.05$), whereas HUMSC transplantation both increased the percentage of Tregs and decreased the percentage of Th17 cells ($P < 0.05$). Modeling and treatment did not appear to affect B cells. The proportions of the three cell subtypes in PP changed slightly with treatment, and no difference in the proportion of Tregs between the Control and CIA groups. Interestingly, the proportion of Tregs in MTX group was lower than those in the Control and CIA groups ($P < 0.05$), whereas the proportion of Tregs in the HUMSC group was higher than that in the CIA group ($P < 0.05$) and even higher than that in the Control group ($P < 0.01$). The change in the proportion of Th17 cells in PP was similar to that in the MLN, but MTX intervention also reduced the proportion of Th17 cells in PP ($P < 0.05$). Although the proportion of B cells in the MLN was not significantly different, the proportion of B cells in PP decreased after modeling ($P < 0.05$), and the proportions of B cells in the MTX and HUMSC groups increased after treatment and were higher than those in the rats belonging to the Control group ($P < 0.05$). The proportions of Tregs and Th17 cells among LPL were higher than those in the MLN and PP. The assessment of the variations in Tregs among LPL between the groups revealed a trend similar to that found in the MLN, whereas the variations

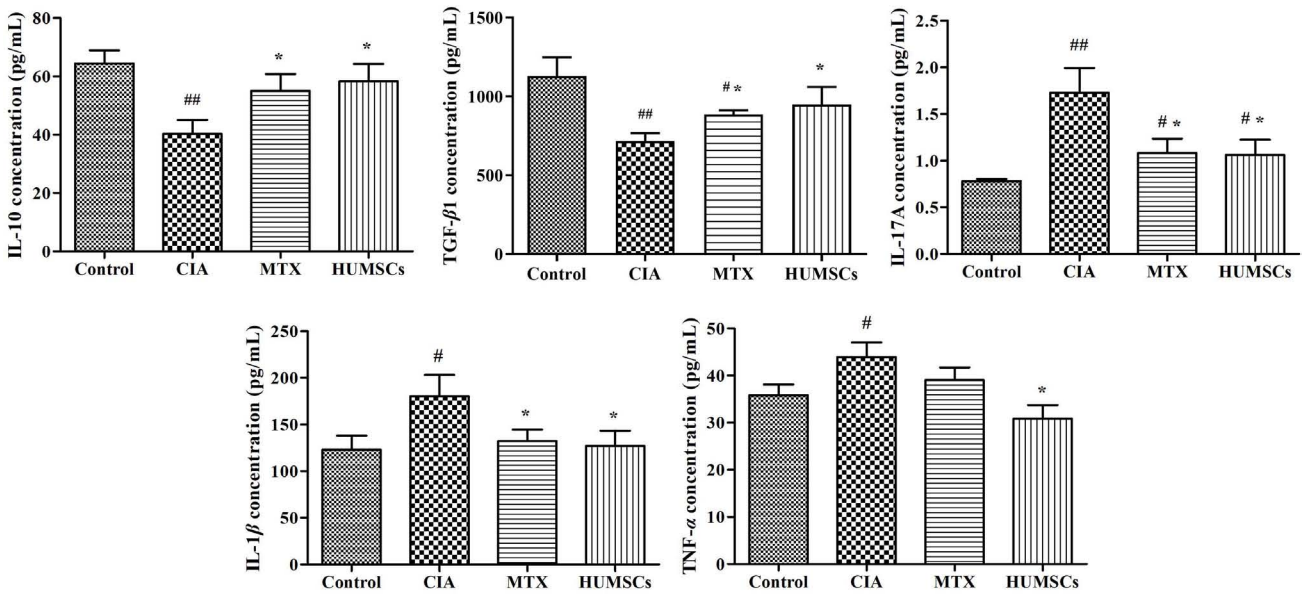


FIGURE 6 | Human umbilical mesenchymal stem cells (HUMSCs) transplantation-mediated regulation of cytokines in the collagen-induced arthritis (CIA) rats. The serum cytokine levels were measured by Luminex assays. Bar plots showing the mean levels of interleukin (IL)-10, transforming growth factor (TGF)-β1, IL-17A, IL-1β, and tumor necrosis factor (TNF)-α in all the groups $N = 8$. The data are presented as the mean ± *SEM*. $^{\#}P < 0.05$ compared with the Control group, $^{\#\#}P < 0.01$ compared with the Control group, $^{*}P < 0.05$ compared with the CIA group.

TABLE 2 | Percentages of Tregs, Th17, and B cells in gut-associated lymphoid tissues ($N = 8$).

Tissues	Group	Cell type		
		Tregs (%)	Th17 cells (%)	B cells (%)
Mesenteric lymph node	Control	6.07 ± 2.21	0.20 ± 0.12	31.50 ± 3.34
	CIA	5.41 ± 1.31	0.34 ± 0.05$^{\#}$	32.82 ± 4.18
	MTX	7.06 ± 0.80*	0.32 ± 0.08	34.34 ± 3.73
	HUMSCs	7.27 ± 0.73*	0.24 ± 0.05*	35.20 ± 5.43
Peyer's patch	Control	10.77 ± 1.62	0.67 ± 0.39	44.80 ± 5.74
	CIA	10.86 ± 1.79	1.17 ± 0.90$^{\#}$	39.23 ± 4.81$^{\#}$
	MTX	8.29 ± 1.90$^{\#}$*	0.46 ± 0.27*	55.06 ± 4.63$^{\#}$**
	HUMSCs	14.81 ± 3.09$^{\#\#}$*	0.48 ± 0.18*	54.12 ± 6.82$^{\#}$**
Lamina propria lymphocyte	Control	27.98 ± 2.89	2.57 ± 1.46	37.37 ± 2.96
	CIA	21.03 ± 5.41$^{\#}$	8.30 ± 2.02$^{\#}$	31.92 ± 3.85$^{\#}$
	MTX	31.08 ± 9.66*	3.46 ± 0.89**	46.26 ± 11.39*
	HUMSCs	28.75 ± 4.15*	3.04 ± 1.42**	49.00 ± 15.89*

The data are presented as the mean ± SEM. $^{\#}P < 0.05$ compared with the Control group, $^{\#\#}P < 0.01$ compared with the Control group, $^{*}P < 0.05$ compared with the CIA group, $^{**}P < 0.01$ compared with the CIA group. Tregs, T regulatory cells; Th17, T helper 17; CIA, collagen-induced arthritis; MTX, methotrexate; HUMSCs, human umbilical mesenchymal stem cells.

in Th17 cells and B cells followed a trend similar to those found for Th17 cells and B cells in PP, respectively, with the only difference being that the proportion of B cells after treatment was between the proportions of B cells in the Control and CIA groups. The above-described results suggested that HUMSC therapy exerts extensive immunomodulatory effects on GALTs. The most affected tissues were those closest to the intestinal contents, and these effects might be induced by metabolites or antigens related to the gut microbiota.

Furthermore, various gene and protein expression levels were detected by Q-PCR and IHC, respectively (**Figure 7**). Modeling significantly decreased the IL-10 levels in the MLN and the TGF-β1 levels in the MLN and ileum ($P < 0.05$), and treatment with MTX and HUMSC transplantation increased the expression of IL-10 and TGF-β1 to levels that were higher than that those found in the Control group ($P < 0.05$ and $P < 0.01$, respectively) (**Figures 7A,B**). The expression levels of IL-17A in the MLN and ileum were similar. The IL-17A gene expression levels were highest in the CIA group and decreased following intervention with MTX and HUMSCs ($P < 0.05$ and $P < 0.01$, respectively), and the lowest IL-17A gene level was found in the MTX group (**Figures 7A,B**). The *in situ* protein expression levels were similar to the corresponding gene expression levels (**Figures 7C,D**). Downregulated IL-10 and TGF-β1 expression and upregulated IL-17A expression were detected in the ileum of rats with CIA, and as expected, both MTX treatment and HUMSC transplantation increased the levels of IL-10 and TGF-β1 and decreased the expression of IL-17A ($P < 0.05$ and $P < 0.01$, respectively). The above-described results indicated that the levels of the major cytokines of Tregs and Th17 cells were abnormal in the MLN and ileum of rats with CIA and that MTX and HUMSCs effectively reversed Tregs and Th17 cell dysfunction. These results suggested that HUMSCs regulate the proportions and functions of Tregs and Th17 and B cells in GALTs.

We also tested the expression of IL-22 and IgA because IL-22 plays an important role in resisting pathogens and repairing the intestinal barrier by inducing intestinal epithelial cells (IECs) to produce antimicrobial peptides, and secretory IgA (SIgA) is known to regulate intestinal microorganisms. The IL-22 and IgA levels in the CIA group were significantly lower than those in the Control group ($P < 0.01$), which suggested that CIA modeling affects the mucosal immune barrier in the ileum to a certain extent and decreased the clearance of pathogenic microorganisms. MTX treatment and HUMSC transplantation affected the IL-22 and IgA levels ($P < 0.05$, $P < 0.01$, respectively) (**Figures 7C,D**), which suggested that both treatments can reshape the immune barrier and restore the regulatory effect of the intestinal tract on intestinal bacteria.

Human Umbilical Mesenchymal Stem Cells Regulated the Intestinal Microbial Community in Rats With Collagen-Induced Arthritis

The intestinal microbial diversity of the ileum was measured by determining the OTUs and the Chao1 and Shannon diversity indices (**Figures 8A–C**). The OTUs and Chao1 diversity indices in the CIA group were higher than those in the Control group ($P < 0.05$), and both of these measures were lower in the MTX and HUMSCs groups compared with the Control and CIA groups ($P < 0.01$). The analysis of the Shannon diversity index revealed no significant difference among the four groups. The results shown in **Figures 8A–C** indicated that CIA modeling and both treatments changed the rats' intestinal microbial species and the community richness but had no effect on the community diversity.

The similarity between the intestinal microbial communities was analyzed by PLS-DA. As shown in **Figure 8D**, the bacterial structures of the Control, CIA, MTX, and HUMSC groups were distributed in a counterclockwise direction. With the exception

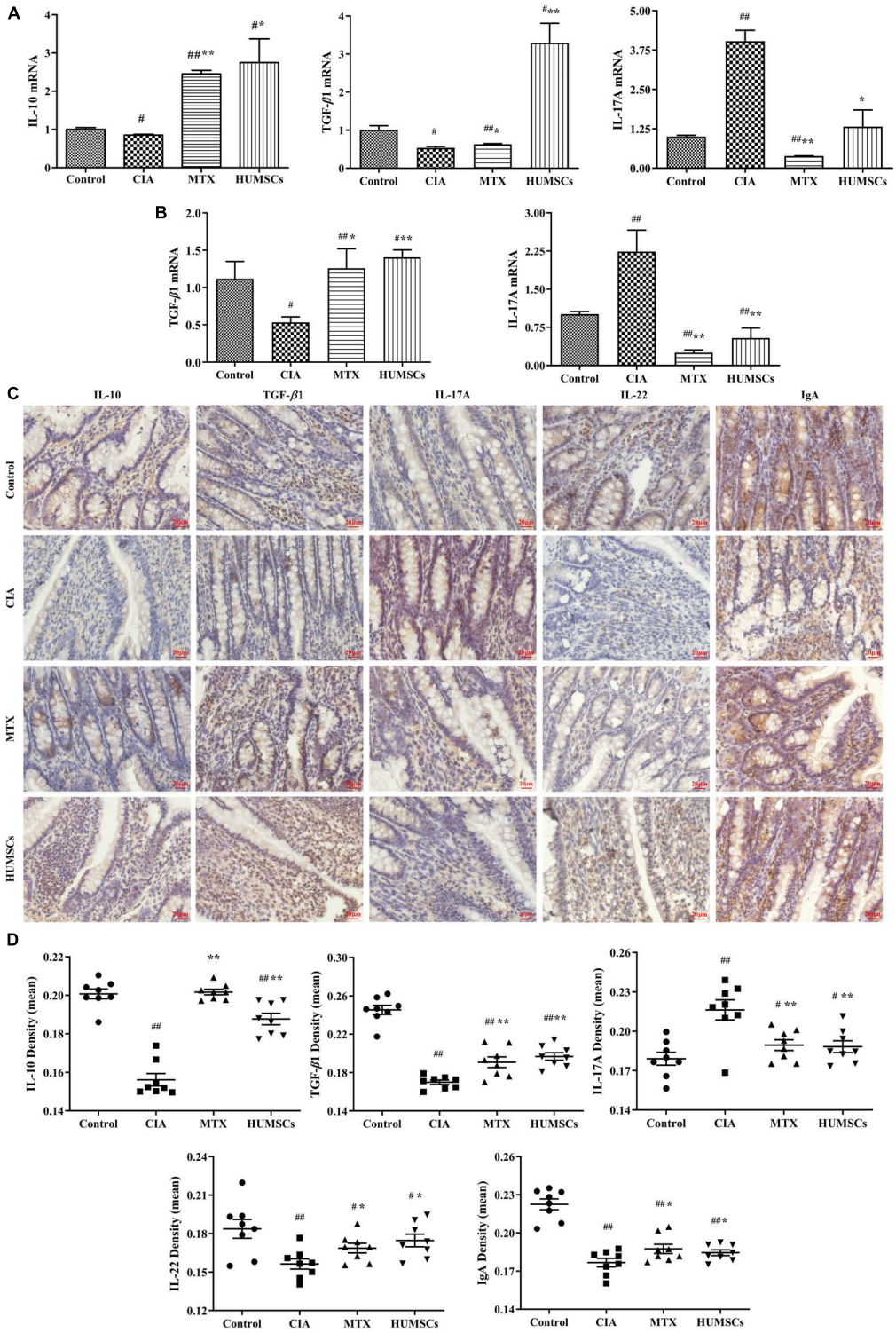


FIGURE 7 | Human umbilical mesenchymal stem cells (HUMSCs) modulate the immune status of the mesenteric lymph node (MLN) and ileum. The interleukin (IL)-10, IL-17A, and transforming growth factor (TGF)-β*1* mRNA expression levels in the MLN and the IL-17A and TGF-β*1* mRNA expression levels in the ileum were detected by quantitative real-time PCR (Q-PCR). The protein expression of IL-10, IL-17A, TGF-β*1*, IL-22, and immunoglobulin A (IgA) was determined by immunohistochemistry (IHC) assay. **(A)** Gene expression of IL-10, IL-17A, and TGF-β*1* in the MLN. **(B)** Gene expression of IL-17A and TGF-β*1* in the ileum. **(C)** Representative images of the ileum obtained by IHC (20×). **(D)** Protein expression of IL-10, IL-17A, TGF-β*1*, IL-22, and IgA in the ileum $N = 8$. The data are presented as the mean ± *SEM*. $^{\#}P < 0.05$ compared with the Control group, $^{\#\#}P < 0.01$ compared with the Control group, $^{*}P < 0.05$ compared with the CIA group, $^{**}P < 0.01$ compared with the CIA group.

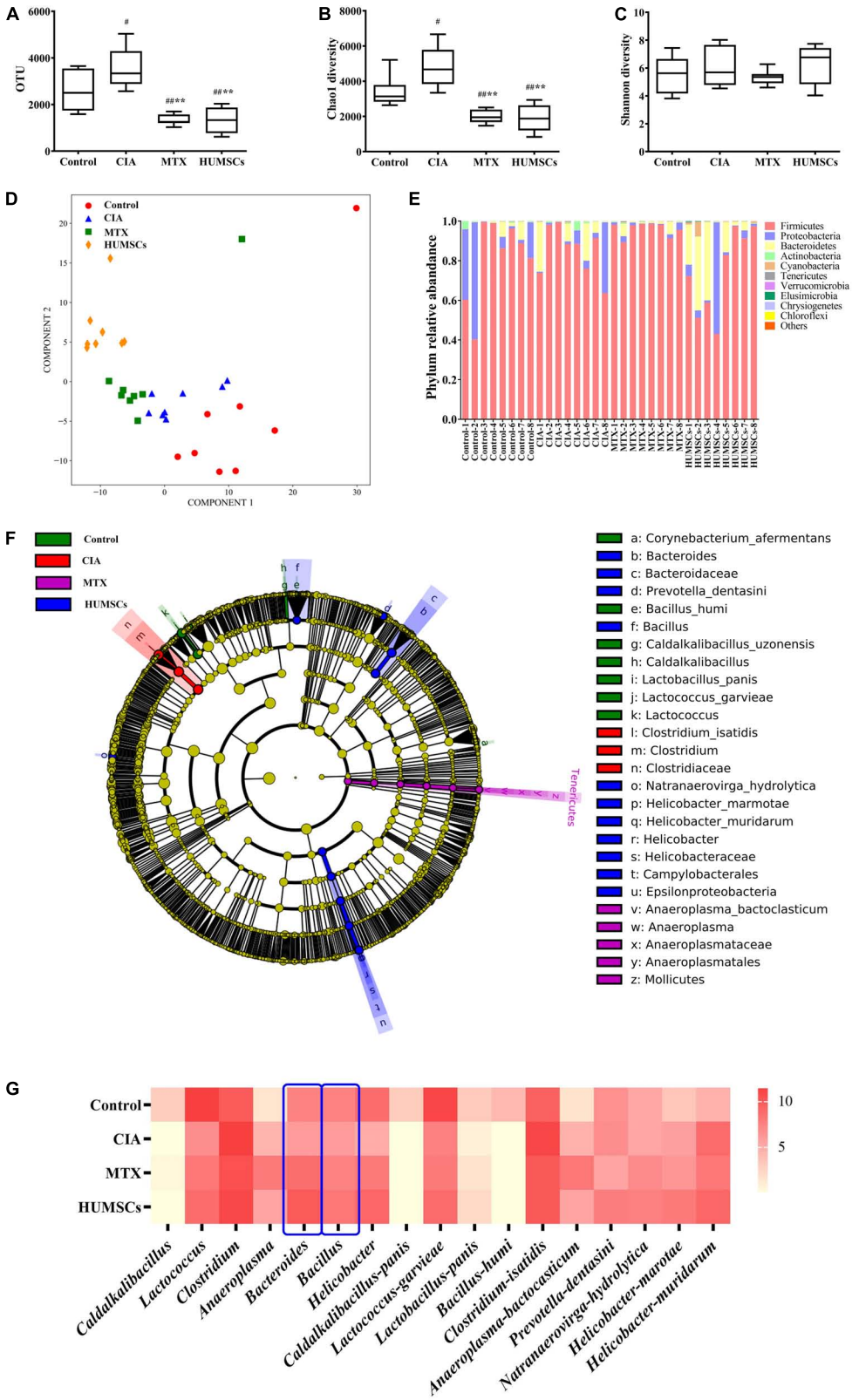


FIGURE 8 | Changes in the gut microbiota in collagen-induced arthritis (CIA), methotrexate (MTX), and human umbilical mesenchymal stem cells (HUMSCs) groups. The alpha diversity, beta diversity, and the typical bacterial genera and species were obtained by 16S sequencing. **(A–C)** Bar plots showing the mean Chao1 and

(Continued)

FIGURE 8 | Continued
Shannon diversity indices and the operational taxonomic units (OTUs) of all groups. **(D)** Relative abundance of the top 10 most abundant phyla in each sample. **(E)** The differences in the intestinal microbial communities among the groups were assessed by partial least square discriminant analysis (PLS-DA). **(F)** Taxonomical differences among the groups at the different levels. The dominant bacteria were determined by Lefse analyses. **(G)** Relative abundances among the groups at the genus and species levels $N = 8$. The data in panels **(A–C)** are presented as the medians [interquartile range (IQR)]. $^{\#}P < 0.05$ compared with the Control group, $^{\#\#}P < 0.01$ compared with the Control group, $^{*}P < 0.05$ compared with the CIA group, $^{**}P < 0.01$ compared with the CIA group.

of a few outliers, the microflora structures in each group were relatively similar, and the difference between the HUMSC rats and normal rats, between the HUMSC rats and CIA rats were the obvious, but the microbial communities of the CIA group were very similar to those of the MTX group. The results indicated that the therapeutic effect of MTX on CIA might only be slightly related to the gut microbiota, whereas the effect of HUMSCs might be largely mediated by the gut microbiota.

An overview of the gut microbiota in the four groups at the phylum level is shown in **Figure 8E**. Overall, the bacteria with the highest abundance belonged to the phylum *Firmicutes*, followed by the phyla *Proteobacteria* and *Bacteroidetes*. The abundances of the phyla *Proteobacteria* and *Bacteroidetes* among the rats varied considerably. The phyla *Chrysiogenetes* and *Chloroflexi* disappeared after treatment with MTX and HUMSCs.

The intestinal microbial species in the different groups were compared by Lefse analysis to characterize the changes in the intestinal microflora structure (**Figure 8F**). The relative abundances of two genera (*Caldalkalibacillus* and *Lactococcus*) and five species (*Caldalkalibacillus panis*, *Lactococcus garvieae*, *Lactobacillus panis, Bacillus humi*, and *Corynebacterium afermentans*) were highest in the control group. The dominant bacteria in the CIA group were relatively unitary: family *Clostridiaceae,* genus *Clostridium*, and species *Clostridium isatidis.* After MTX intervention, the relative abundance of one unit was higher than that of the other three groups from the phylum to the species level: phylum *Tenericutes*, class *Mollicutes*, order *Anaeroplasmatales*, family *Anaeroplasmataceae*, genus *Anaeroplasma*, and species *Anaeroplasma bactocasticum.* HUMSC therapy changed the most bacterial units: one class (*Epsilonproteobacteria*), one order (*Campylobacterales*), two families (*Bacteroidaceae* and *Helicobacteraceae*), three genera (*Bacteroides, Bacillus*, and *Helicobacter*), and four species (*Prevotella dentasini*, *Natranaerovirga hydrolytica*, *Helicobacter marotae*, and *Helicobacter muridarum*). The abovementioned results indicated that CIA modeling plays an important role in the changes in the gut microbiota and that HUMSCs had a greater influence on the flora than MTX.

The specific gut microbiota changes were further assessed at the genus and species levels (**Figure 8G**). CIA modeling significantly decreased the abundances of various genera, including *Caldalkalibacillus*, *Lactococcus*, *Bacteroides*, *Bacillus*, and others and various species, including *Caldalkalibacillus panis*, *Lactococcus garvieae*, *Lactobacillus panis*, and *Bacillus humi* and others, and treatment with MTX and HUMSCs increased the abundances of the genera *Lactococcus*, *Bacteroides*, and *Bacillus* and the species *Lactococcus garvieae* and *Lactobacillus panis* but did not affect the abundances of the genus *Caldalkalibacillus* and the species *Caldalkalibacillus panis* and *Bacillus humi*. Conversely, the relative abundance of the genus *Clostridium* and the species *Clostridium isatidis*, *Anaeroplasma bactocasticum*, *Helicobacter marotae*, and *Helicobacter muridarum* increased after modeling. In addition, treatment with MTX and/or HUMSCs slightly decreased the abundances of some genera and species (genus *Clostridium* and species *Clostridium isatidis* and *Helicobacter muridarum*) but increased the abundances of some bacteria (species *Anaeroplasma bactocasticum* and *Helicobacter marotae*). In addition, a few bacteria were not affected by CIA modeling but exhibited an altered abundance after treatment with MTX and HUMSCs (species *Prevotella dentasini* and *Natranaerovirga hydrolytica*). Collectively, these data indicate that although the major intestinal microbial communities exhibited differences after MTX and HUMSC treatment, the abundance of some bacteria still changed in a synchronous manner. These results indicated that MTX and HUMSCs might modulate mucosal immunity through a common mechanism involving the gut microbiota.

Gut Microbiota Regulated the Aryl Hydrocarbon Receptor Pathway Through Indole Metabolism

Based on the above-described results and those obtained in other studies, we found that *Bacteroides* and *Bacillus* can metabolize dietary tryptophan to produce indole, IAA, or ILA (Amin and Latif, 2017; Roager and Licht, 2018). Interestingly, these metabolites are AhR ligands that can stimulate the AhR and regulate intestinal mucosal immunity (Shinde and McGaha, 2018). Therefore, we detected the levels of indole, IAA, and ILA in plasma by LC-MS/MS and the AhR gene and protein expression levels in the ileum by Q-PCR and IHC, respectively. As shown in **Figure 9A**, the levels of indole, IAA, and ILA in the CIA group were significantly lower compared with those in the Control group ($P < 0.05$ and $P < 0.01$, respectively). Treatment with HUMSCs increased the levels of these three metabolites compared with those in the CIA group, and this difference was significant ($P < 0.05$). The levels of the three metabolites in the MTX group were also increased, but only the indole and ILA levels were different from those in the rats with CIA ($P < 0.05$). This result was consistent with the results from the analysis of the gut microbiota because the bacteria found at higher abundances in the HUMSC group (mainly *Lactococcus* and *Bacteroides*) can metabolize tryptophan and produce indole and other metabolites that are absorbed into the blood through the small intestine.

The assessment of the AhR expression in the ileum (**Figures 9B–D**) revealed that the AhR gene and protein expression levels in the CIA group were consistent with changes

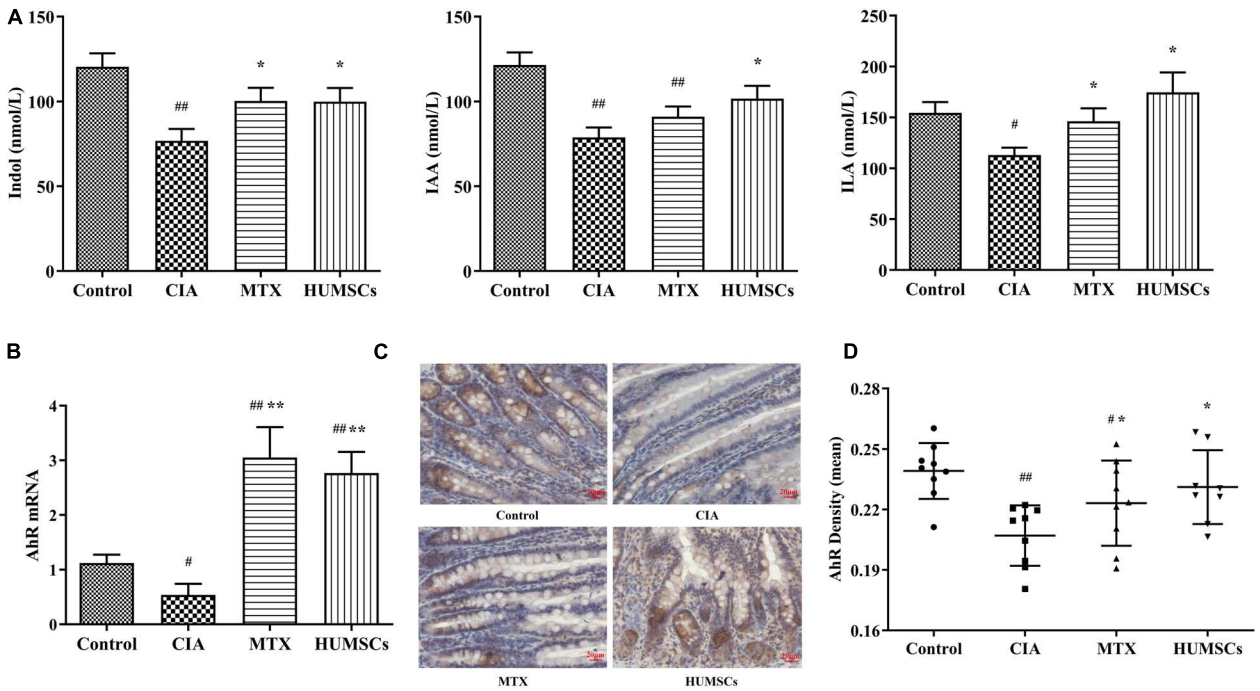


FIGURE 9 | Levels of indole and its derivatives in the plasma and aryl hydrocarbon receptor (AhR) expression in the ileum. The levels of indole, indoleacetic acid (IAA), and indole-3-lactic acid (ILA) in the plasma were detected by liquid chromatography-tandem mass spectrometry (LC-MS/MS), and the mRNA and protein expression levels of AhR were determined by quantitative real-time PCR (Q-PCR) and immunohistochemistry (IHC), respectively. **(A)** Bar plots showing the mean levels of indole, IAA, and ILA in all the groups. **(B)** AhR gene expression in the ileum. **(C)** Representative images of the ileum obtained by IHC (20×). **(D)** AhR protein expression in the ileum $N = 8$. The data are presented as the mean ± *SEM*. $^{\#}P < 0.05$ compared with the Control group, $^{\#\#}P < 0.01$ compared with the Control group, $^{*}P < 0.05$ compared with the CIA group, $^{**}P < 0.01$ compared with the CIA group.

in the levels of tryptophan metabolites, which were found at lower levels in this group compared with the Control group ($P < 0.05$ and $P < 0.01$, respectively). Treatment with MTX and HUMSCs upregulated the mRNA expression of AhR by 3-fold and more than 2-fold, respectively. However, the change in AhR protein expression was relatively minor compared with the change in its gene expression, and the AhR gene expression level in the treatment groups was between those in the Control and CIA groups but significantly differed from that in the CIA group ($P < 0.05$). These results confirms that indole, IAA, and ILA produced during bacterial decomposition activate the AhR. The regulatory effect of intestinal bacteria on mucosal immunity is likely dependent on activation of the AhR, a receptor that reportedly regulates the differentiation and function of Tregs and Th17 and B cells.

DISCUSSION

Numerous studies have explored the therapeutic effects of HUMSCs that mediate the balance between Tregs and Th17 cells in RA (Ma et al., 2019). Several researchers have explored the effect and mechanism of other drugs on RA from the perspective of the gut microbiota (Bodkhe et al., 2019). However, no researchers have linked Tregs/Th17 cells with the gut microbiota to elucidate the therapeutic mechanism of HUMSCs. Based on the tissues to which HUMSCs home, we explored the influence of HUMSCs on bone destruction in the ankle joints and the proportions and functions of Tregs and Th17 cells in the nearest lymph node—the PLN. Furthermore, we focused on functions related to Tregs and Th17 cells and the functions through which B cells regulate the gut microbiota in GALTs: the MLN, PP, and LPL. We examined the changes in the gut microbiota in the ileum in depth and found changes in most bacteria involved in the metabolism of tryptophan to indole. To validate these results, we measured the plasma levels of indole and some of its derivatives and the AhR levels in the ileum, and the results showed a key link between indole metabolism and the immune system. Based on the current results, we can confirm that HUMSCs act as a therapeutic agent in CIA by regulating the interaction between host immunity and the gut microbiota and speculate that AhR is the key link between these factors.

Several clinical and experimental studies have investigated stem cell transplantation for the treatment of RA. A clinical trial conducted in Iran found that autologous bone marrow-derived mesenchymal stem cells ameliorated the clinical symptoms of refractory RA (Ghoryani et al., 2019). Another phase 1/2 clinical trial observed that autologous bone marrow-derived mesenchymal stromal cells increase the clinical efficacy of MTX and prednisolone and reduce their use (Shadmanfar et al., 2018). Animal experiments using relatively uniform methods have also

shown that HUMSCs can be utilized to treat CIA (Cheng-Chi et al., 2012; Shin et al., 2016). Specifically, stem cells were injected at the same dose (1×10^6 cells/rat or mouse) in most studies. However, the graft sites differed (tail vein, abdominal cavity, and articular cavity), and the observation time varied from half a month to a month. Our purpose was to observe the systemic regulatory effect of HUMSCs, and based on the treatment duration used in a previous experiment (Zhao et al., 2018), 1×10^6 cells/rat were injected *via* the tail vein for one month. Some researchers have tracked the entry of stem cells into the body. Liu et al. (2010) showed that intraperitoneally injected HUMSCs could not be detected in joints, but a positive signal for HUMSCs was found in the spleen on days 3 and 7 and disappeared on day 14 after injection. In addition, Wu C. C. et al. (2016) detected the expression of HLA-A protein, which is characteristic of HUMSCs, in knee cartilage and synovial tissue on day 14 after the injection of HUMSCs into the joint. In our study, positive NuMA signaling was simultaneously detected in the knee, PLN, MLN, and ileum mucosa on day 28 after HUMSC injection. The differences in the above-described results might be due to the different transplantation methods and transplantation durations used.

Because Tregs are immunosuppressive cells, their proportion and function are crucial in the suppression of ADs. Tregs act as cytotoxic agents through cell–cell interactions and function by secreting the cytokines IL-10 and TGF-β1 (Shevach, 2009). In the intestine, Tregs play an important role in the maintenance of immune tolerance to dietary antigens and the gut microbiota (Honda and Littman, 2016). Unlike Tregs, another cell subgroup, Th17 cells, induces immune activation by secreting IL-17A to promote inflammation (Patel and Kuchroo, 2015). However, the production of IL-17A and IL-22 by Th17 cells in the gut contributes to the defense against intestinal pathogens (Ubeda and Pamer, 2012). Tregs/Th17 cells are the most studied immune cells in the peripheral blood and spleen; although the immune statuses in these two tissues reflect the immune state of the system, they are not typical (Liu et al., 2010; Ma et al., 2019). More detailed studies of this mechanism have targeted tissues to reveal the local immune status, such as targeting Tregs/Th17 cells to the MLN and PP (Tong et al., 2015). However, the involvement of HUMSCs in influencing Tregs/Th17 cells in the PLN and among LPL in CIA has not been reported. We identified the distribution of HUMSCs in CIA through their localization and then specifically determined the proportions of these two cell subtypes in HUMSC-positive tissues, namely, the PLN, MLN, PP, and LPL. In addition, SIgA plays an important role in the resistance to intestinal bacterial adhesion and endotoxin neutralization (Iijima et al., 2001). Because precursor cells secrete SIgA, we also measured the proportion of B cells in the above-listed GALTs (Reboldi et al., 2016). Our results are generally consistent with those obtained in the limited number of previous reports. HUMSC therapy significantly increased the proportion of Tregs; significantly decreased the proportion of Th17 cells in the PLN, MLN, and PP and among the LPL compared with that found in the CIA group; and significantly increased the proportion of B cells in PP and among the LPL. The abovementioned results suggested that the immune status of intestinal-associated lymphoid tissues worsened after modeling and that the homing of HUMSCs partially reversed immune disorders, and the detection of Treg-, Th17 cell-, and B cell-related factors verified the above-described results.

The importance of the gut microbiome in RA has been reported in both human patients and mouse models. Alterations to the gut microbiota are related to the risk and severity of RA, and probiotic transplantation is beneficial for RA remission. Toivanen et al. (2002) showed that patients with early RA had on average only half as many bacteria belonging to the genera *Bacteroides*, *Prevotella*, and *Porphyromonas* compared with control subjects. Another study conducted by Vaahtovuo et al. (2008) similarly found that RA patients were characterized by a different fecal diversity with a decreased abundance of bacteria belonging to the *Bacteroides–Porphyromonas–Prevotella* group, the *Bacteroides fragilis* subgroup, and the *Eubacterium rectale–Clostridium coccoides* group compared with patients with fibromyalgia. *Lactobacillus casei* has been shown to be an effective probiotic in the treatment of RA. Alipour et al. (2014) treated 22 subjects with *L. casei* and compared them with 24 subjects treated with placebo. The C-reactive protein (CRP) level, number of inflamed and painful joints, and 28-joint disease activity score (DAS-28) were significantly decreased in the 22 subjects compared with the 24 controls. In animal models, both intestinal bacteria known to be correlated with arthritis and differences in the composition of the gut microbiota between animals with CIA and normal animals and even between arthritis-susceptible and healthy or arthritic hosts were consistently detected. In the K/BxN mouse, gut-residing segmented filamentous bacteria (SFB) were found to drive the rapid development of destructive arthritis (Doube and Collins, 1988). Liu et al. (2016) revealed that the genus *Lactobacillus* was the dominant genus in mice susceptible to CIA prior to the onset of arthritis. The development of the disease increased the abundances of the families *Bacteroidaceae*, *Lachnospiraceae*, and *S24-7* in CIA-susceptible mice. Notably, germ-free mice treated with the microbiota of CIA-susceptible mice showed a higher frequency of arthritis induction than those treated with the microbiota of CIA-resistant mice. Our results showed that CIA modeling decreased the abundances of the genera *Bacteroides, Lactococcus*, and species *Lactococcus garvieae* compared with those in the Control group, which was partly consistent with the above-described findings.

The gut serves as a bridge between intestinal microorganisms and their host. Intestinal bacteria synthesize and alter multiple compounds that impact physiology and immunity (Rooks and Garrett, 2016). Numerous studies have shown that Tregs and Th17 cells are simultaneously the target cells of intestinal commensal microbiota and the key to activating the host defense against pathogens, which could result in the avoidance of other immunopathologic consequences (Bennike et al., 2017). Under conventional conditions, *Lactobacillus bifidus* induces arthritis in IL-1ra$^{-/-}$ mice, which exhibit a decreased number of Tregs and an increased number of Th17 cells (Abdollahi-Roodsaz et al., 2008). In contrast, *Bifidobacterium infantis* can induce Tregs to play an anti-inflammatory role, and *B. fragilis* polysaccharide stimulates Tregs to produce IL-10

(Abdollahi-Roodsaz et al., 2008). A study conducted by Zhang et al. (2016) revealed that the supplementation of broiler diets with *Lactococcus garvieae B301* increased the body weight and exerted a positive effect on the serum levels of immune globulins. In addition, Wang et al. (2019) showed that recombinant *Bacillus subtilis* induces a mucosal SIgA response to pseudorabies and regulates the $CD3^{+}CD4^{+}$ T cell proliferative response by IL-10. Another study showed that a mixture of two *Clostridium* strains significantly reduces the Th17/Th1 balance (Lopez et al., 2016), and infection with *Clostridium perfringens* or *Clostridium difficile* induces a pro-inflammatory response related to Th17 cells (Yacyshyn et al., 2014; Yu et al., 2017). In the current study, regarding the relative abundances of the genera *Lactococcus*, *Bacillus*, and *Bacteroides* and the species *Lactococcus garvieae*, Tregs and the related cytokines and SIgA were increased in both MTX- and HUMSC-treated rats, whereas regarding the relative abundances of the genus *Clostridium*, Th17 cells and related cytokines were upregulated in rats with CIA and reduced after the treatments, as expected. Based on the discussion and results described above, we speculated that changes in the gut microbiota caused changes in immune regulation.

A review of the literature revealed that the bacterial genera *Bacillus* and *Bacteroides* are involved in the metabolism of tryptophan into indole and its derivatives

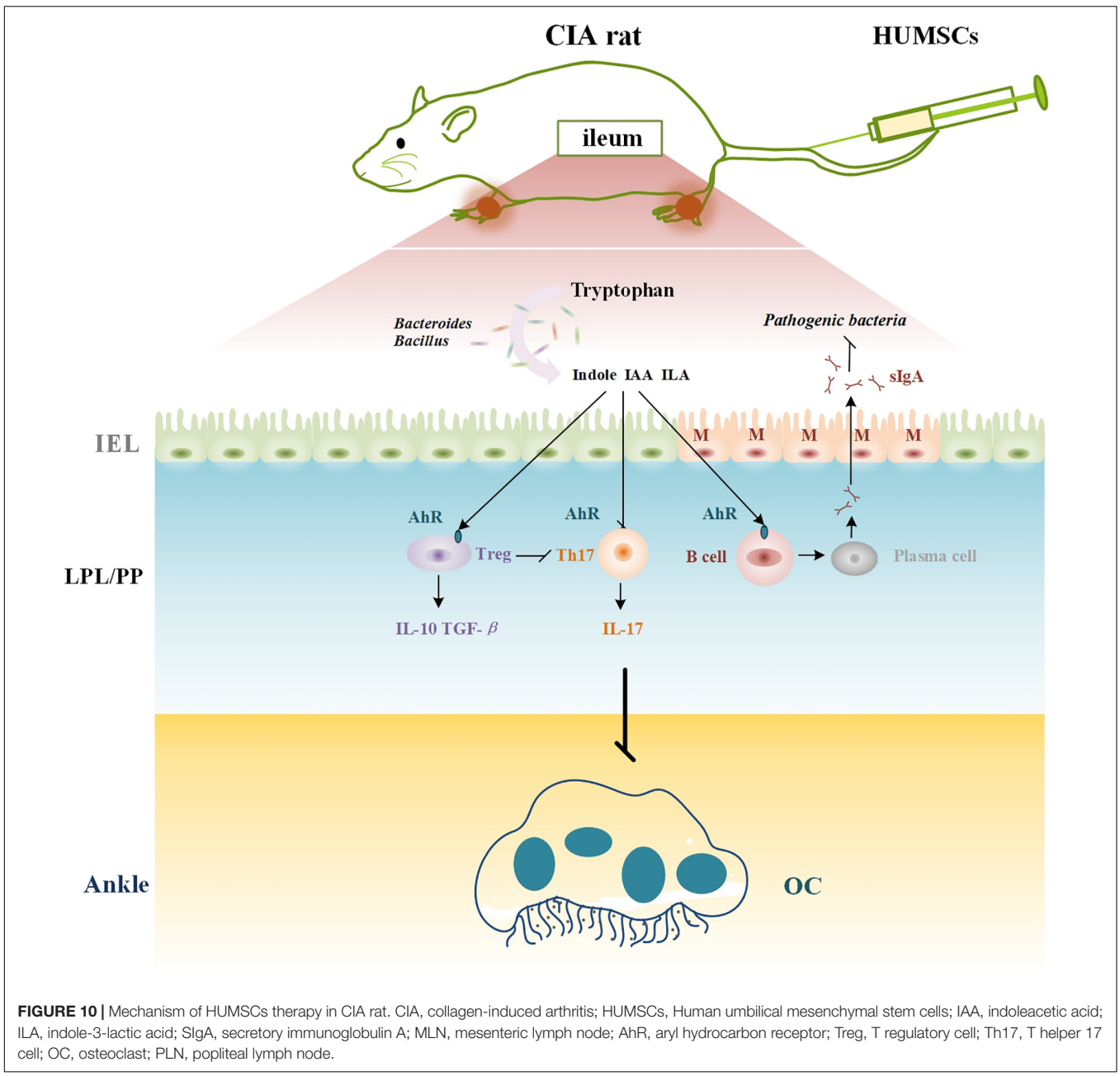


FIGURE 10 | Mechanism of HUMSCs therapy in CIA rat. CIA, collagen-induced arthritis; HUMSCs, Human umbilical mesenchymal stem cells; IAA, indoleacetic acid; ILA, indole-3-lactic acid; SIgA, secretory immunoglobulin A; MLN, mesenteric lymph node; AhR, aryl hydrocarbon receptor; Treg, T regulatory cell; Th17, T helper 17 cell; OC, osteoclast; PLN, popliteal lymph node.

(Shao et al., 2015; Roager and Licht, 2018). Interestingly, the components regulated by these bacteria, namely, indole, IAA, and ILA, are ligands of the AhR (Gao et al., 2018). The available evidence suggests that the AhR is a key sensor that allows immune cells to adapt to environmental conditions and that the inhibition of AhR activity is associated with ADs. Numerous studies have shown that activation of the AhR increases the differentiation and function of Tregs but inhibited inflammatory cytokines (Shinde and McGaha, 2018). Researchers have reported that sinomenine induces the generation of intestinal Tregs and attenuates arthritis *via* activation of the AhR even in CIA (Tong et al., 2016a). Some evidence suggests that AhR activation increases Th17 cell differentiation and the secretion of IL-17A and IL-22 (Shinde and McGaha, 2018). However, the results obtained after treatment of the CIA model consistently suggested that activation of the AhR inhibits the differentiation and function of Th17 cells (Tong et al., 2015, 2016b). This difference in results might be due to the type of ligand and animal species used and the disease type examined. In addition, Villa et al. (2017) demonstrated that intervention with 6-formylindolo[3,2-b]carbazole (FICZ), a natural agonist, increased AhR expression during B cell differentiation and the amount of AhR localized to the nucleus and significantly upregulated the expression of the downstream target gene CYP1A1 on B cells. These results imply that the AhR is involved in B cell proliferation and function. Our results demonstrated that the increased abundance of the genera *Bacteroides* and *Bacillus* might lead to increased levels of indole and its derivatives in the plasma, and these increases enhance AhR gene and protein expression in the ileum. Furthermore, activated AhR might regulate the gut microbiota by regulating Tregs and Th17 and B cells *via* a feedback loop. Although a few *Clostridium* strains, such as *Clostridium difficile* and *Clostridium sordellii*, can produce indole, IAA, or ILA (Roager and Licht, 2018), pathogenic bacteria species belonging to the genus *Clostridium* can produce toxins that induce clostridial disease. Our results showed that the genus *Clostridium* exhibited an increasing trend in the CIA group, which was in line with the function of this strain.

In summary, our results suggest that HUMSCs play a therapeutic role in CIA because these cells regulate immunity in rats with CIA and particularly immunity in GALTs. The underlying mechanism might be related to the crosstalk between immunity and the gut microbiota regulated by the AhR (**Figure 10**).

DATA AVAILABILITY STATEMENT

The datasets generated in this study are available from the corresponding author upon request. 16S sequencing data was uploaded to NCBI SRA with accession number PRJNA605946.

ETHICS STATEMENT

The study involving human participants was reviewed and approved by the Research Ethics Committee at the China-Japan Friendship Hospital (2019-124-K86). The patients/participants provided their written informed consent to participate in this study. The animal study was reviewed and approved by the Institute of Clinical Medical Sciences, China-Japan Friendship Hospital, Beijing, China (No. 180207).

AUTHOR CONTRIBUTIONS

CX and HL designed the conceptual framework of the study. XLi and CL designed the experiments and wrote the manuscript. XLi, CL, XLu, DF, YX, and JL performed the experiments. HZ, HX, and YZ analyzed the data.

REFERENCES

Abdollahi-Roodsaz, S., Joosten, L. A., Koenders, M. I., Devesa, I., Roelofs, M. F., Radstake, T. R., et al. (2008). Stimulation of TLR2 and TLR4 differentially skews the balance of T cells in a mouse model of arthritis. *J. Clin. Invest.* 118, 205–216. doi: 10.1172/JCI32639

Alipour, B., Homayouni-Rad, A., Vaghef-Mehrabany, E., Sharif, S. K., Vaghef-Mehrabany, L., Asghari-Jafarabadi, M., et al. (2014). Effects of *Lactobacillus casei* supplementation on disease activity and inflammatory cytokines in rheumatoid arthritis patients: a randomized double-blind clinical trial. *Int. J. Rheum. Dis.* 17, 519–527. doi: 10.1111/1756-185X.12333

Amin, A., and Latif, Z. (2017). Screening of mercury-resistant and indole-3-acetic acid producing bacterial-consortium for growth promotion of *Cicer arietinum* L. *J. Basic Microbiol.* 57, 204–217. doi: 10.1002/jobm.201600352

Bennike, T. B., Ellingsen, T., Glerup, H., Bonderup, O. K., Carlsen, T. G., Meyer, M. K., et al. (2017). Proteome analysis of rheumatoid arthritis Gut Mucosa. *J. Proteome Res.* 16, 346–354. doi: 10.1021/acs.jproteome.6b00598

Bodkhe, R., Balakrishnan, B., and Taneja, V. (2019). The role of microbiome in rheumatoid arthritis treatment. *Ther. Adv. Musculoskelet. Dis.* 11:1759720X19844632. doi: 10.1177/1759720X19844632

Cheng-Chi, W., Tzu-Chin, W., Fei-Lan, L., Huey-Kang, S., and Deh-Ming, C. (2012). TNF-α inhibitor reverse the effects of human umbilical cord-derived stem cells on experimental arthritis by increasing immunosuppression. *Cell Immunol.* 273, 30–40. doi: 10.1016/j.cellimm.2011.11.009

Doube, A., and Collins, A. J. (1988). Is the gut intrinsically abnormal in rheumatoid arthritis? *Ann. Rheum. Dis.* 47, 617–619. doi: 10.1136/ard.47.8.617

Gao, J., Xu, K., Liu, H., Liu, G., Bai, M., Peng, C., et al. (2018). Impact of the gut microbiota on intestinal immunity mediated by Tryptophan metabolism. *Front. Cell Infect. Microbiol.* 8:13. doi: 10.3389/fcimb.2018.00013

Ghoryani, M., Shariati-Sarabi, Z., Tavakkol-Afshari, J., Ghasemi, A., Poursamimi, J., and Mohammadi, M. (2019). Amelioration of clinical symptoms of patients with refractory rheumatoid arthritis following treatment with autologous bone marrow-derived mesenchymal stem cells: a successful clinical trial in Iran. *Biomed. Pharmacother.* 109, 1834–1840. doi: 10.1016/j.biopha.2018.11.056

Honda, K., and Littman, D. R. (2016). The microbiota in adaptive immune homeostasis and disease. *Nature* 535, 75–84. doi: 10.1038/nature18848

Iijima, H., Takahashi, I., and Kiyono, H. (2001). Mucosal immune network in the gut for the control of infectious diseases. *Rev. Med. Virol.* 11, 117–133. doi: 10.1002/rmv.307

Liu, X., Zeng, B., Zhang, J., Li, W., Mou, F., Wang, H., et al. (2016). Role of the gut microbiome in modulating arthritis progression in mice. *Sci. Rep.* 6:30594. doi: 10.1038/srep30594

Liu, Y., Mu, R., Wang, S., Long, L., Liu, X., Li, R., et al. (2010). Therapeutic potential of human umbilical cord mesenchymal stem cells in the treatment of rheumatoid arthritis. *Arthrit. Res. Ther.* 12:R210. doi: 10.1186/ar3187

Lopez, P., de Paz, B., Rodriguez-Carrio, J., Hevia, A., Sanchez, B., Margolles, A., et al. (2016). Th17 responses and natural IgM antibodies are related to gut microbiota composition in systemic lupus erythematosus patients. *Sci. Rep.* 6:24072. doi: 10.1038/srep24072

Ma, D., Xu, K., Zhang, G., Liu, Y., Gao, J., Tian, M., et al. (2019). Immunomodulatory effect of human umbilical cord mesenchymal stem cells on T lymphocytes in rheumatoid arthritis. *Int. Immunopharmacol.* 74:105687. doi: 10.1016/j.intimp.2019.105687

McInnes, I. B., and Schett, G. (2011). The pathogenesis of rheumatoid arthritis. *N. Engl. J. Med.* 365, 2205–2219. doi: 10.1056/NEJMra1004965

Naik, S., Larsen, S. B., Cowley, C. J., and Fuchs, E. (2018). Two to tango: dialog between immunity and stem cells in health and disease. *Cell* 175, 908–920. doi: 10.1016/j.cell.2018.08.071

Noack, M., and Miossec, P. (2014). Th17 and regulatory T cell balance in autoimmune and inflammatory diseases. *Autoimmun. Rev.* 13, 668–677. doi: 10.1016/j.autrev.2013.12.004

Patel, D. D., and Kuchroo, V. K. (2015). Th17 cell pathway in human immunity: lessons from genetics and therapeutic interventions. *Immunity* 43, 1040–1051. doi: 10.1016/j.immuni.2015.12.003

Reboldi, A., Arnon, T. I., Rodda, L. B., Atakilit, A., Sheppard, D., and Cyster, J. G. (2016). IgA production requires B cell interaction with subepithelial dendritic cells in Peyer's patches. *Science* 352:f4822. doi: 10.1126/science.aaf4822

Roager, H. M., and Licht, T. R. (2018). Microbial tryptophan catabolites in health and disease. *Nat. Commun.* 9:3294. doi: 10.1038/s41467-018-05470-4

Rooks, M. G., and Garrett, W. S. (2016). Gut microbiota, metabolites and host immunity. *Nat. Rev. Immunol.* 16, 341–352. doi: 10.1038/nri.2016.42

Rothhammer, V., and Quintana, F. J. (2019). The aryl hydrocarbon receptor: an environmental sensor integrating immune responses in health and disease. *Nat. Rev. Immunol.* 19, 184–197. doi: 10.1038/s41577-019-0125-8

Shadmanfar, S., Labibzadeh, N., Emadedin, M., Jaroughi, N., Azimian, V., Mardpour, S., et al. (2018). Intra-articular knee implantation of autologous bone marrow-derived mesenchymal stromal cells in rheumatoid arthritis patients with knee involvement: results of a randomized, triple-blind, placebo-controlled phase 1/2 clinical trial. *Cytotherapy* 20, 499–506. doi: 10.1016/j.jcyt.2017.12.009

Shao, J., Li, S., Zhang, N., Cui, X., Zhou, X., Zhang, G., et al. (2015). Analysis and cloning of the synthetic pathway of the phytohormone indole-3-acetic acid in the plant-beneficial *Bacillus amyloliquefaciens* SQR9. *Microb. Cell Fact* 14:130. doi: 10.1186/s12934-015-0323-4

Shevach, E. M. (2009). Mechanisms of foxp3+ T regulatory cell-mediated suppression. *Immunity* 30, 636–645. doi: 10.1016/j.immuni.2009.04.010

Shin, T. H., Kim, H. S., Kang, T. W., Lee, B. C., Lee, H. Y., Kim, Y. J., et al. (2016). Human umbilical cord blood-stem cells direct macrophage polarization and block inflammasome activation to alleviate rheumatoid arthritis. *Cell Death Dis.* 7:e2524. doi: 10.1038/cddis.2016.442

Shinde, R., and McGaha, T. L. (2018). The Aryl hydrocarbon receptor: connecting immunity to the microenvironment. *Trends Immunol.* 39, 1005–1020. doi: 10.1016/j.it.2018.10.010

Smolen, J. S., Aletaha, D., and McInnes, I. B. (2016). Rheumatoid arthritis. *Lancet* 388, 2023–2038. doi: 10.1016/S0140-6736(16)30173-8

Toivanen, P., Vartiainen, S., Jalava, J., Luukkainen, R., Möttönen, T., Eerola, E., et al. (2002). Intestinal anaerobic bacteria in early rheumatoid arthritis (RA). *Arthrit. Res.* 4:5.

Tong, B., Dou, Y., Wang, T., Yu, J., Wu, X., Lu, Q., et al. (2015). Norisoboldine ameliorates collagen-induced arthritis through regulating the balance between Th17 and regulatory T cells in gut-associated lymphoid tissues. *Toxicol. Appl. Pharmacol.* 282, 90–99. doi: 10.1016/j.taap.2014.11.008

Tong, B., Yuan, X., Dou, Y., Wu, X., Chou, G., Wang, Z., et al. (2016a). Norisoboldine, an isoquinoline alkaloid, acts as an aryl hydrocarbon receptor ligand to induce intestinal Treg cells and thereby attenuate arthritis. *Int. J. Biochem. Cell Biol.* 75, 63–73. doi: 10.1016/j.biocel.2016.03.014

Tong, B., Yuan, X., Dou, Y., Wu, X., Wang, Y., Xia, Y., et al. (2016b). Sinomenine induces the generation of intestinal Treg cells and attenuates arthritis via activation of aryl hydrocarbon receptor. *Lab. Invest.* 96, 1076–1086. doi: 10.1038/labinvest.2016.86

Ubeda, C., and Pamer, E. G. (2012). Antibiotics, microbiota, and immune defense. *Trends Immunol.* 33, 459–466. doi: 10.1016/j.it.2012.05.003

Uccelli, A., Moretta, L., and Pistoia, V. (2008). Mesenchymal stem cells in health and disease. *Nat. Rev. Immunol.* 8, 726–736. doi: 10.1038/nri2395

Vaahtovuo, J., Munukka, E., Korkeamaki, M., Luukkainen, R., and Toivanen, P. (2008). Fecal microbiota in early rheumatoid arthritis. *J. Rheumatol.* 35, 1500–1505.

Villa, M., Gialitakis, M., Tolaini, M., Ahlfors, H., Henderson, C. J., Wolf, C. R., et al. (2017). Aryl hydrocarbon receptor is required for optimal B-cell proliferation. *EMBO J.* 36, 116–128. doi: 10.15252/embj.201695027

Wang, J., Wang, Y., Zhang, E., Zhou, M., Lin, J., and Yang, Q. (2019). Intranasal administration with recombinant *Bacillus subtilis* induces strong mucosal immune responses against pseudorabies. *Microb. Cell Fact* 18:103. doi: 10.1186/s12934-019-1151-8

Wu, C. C., Liu, F. L., Sytwu, H. K., Tsai, C. Y., and Chang, D. M. (2016). CD146+ mesenchymal stem cells display greater therapeutic potential than CD146- cells for treating collagen-induced arthritis in mice. *Stem Cell Res. Ther.* 7:23. doi: 10.1186/s13287-016-0285-4

Wu, X., He, B., Liu, J., Feng, H., Ma, Y., Li, D., et al. (2016). Molecular insight into gut microbiota and rheumatoid arthritis. *Int. J. Mol. Sci.* 17:431. doi: 10.3390/ijms17030431

Xiao, C., Lu, C., Zhao, L., Liu, Z., Zhang, W., He, Y., et al. (2006). The effects of triptolide on enteric mucosal immune responses of DBA/1 mice with collagen-induced arthritis. *Planta Med.* 72, 1268–1272. doi: 10.1055/s-2006-947240

Yacyshyn, M. B., Reddy, T. N., Plageman, L. R., Wu, J., Hollar, A. R., and Yacyshyn, B. R. (2014). Clostridium difficile recurrence is characterized by pro-inflammatory peripheral blood mononuclear cell (PBMC) phenotype. *J. Med. Microbiol.* 63, 1260–1273. doi: 10.1099/jmm.0.075382-0

Yu, H., Chen, K., Sun, Y., Carter, M., Garey, K. W., Savidge, T. C., et al. (2017). Cytokines are markers of the clostridium difficile-induced inflammatory response and predict disease severity. *Clin. Vacc. Immunol.* 24:e0037-17. doi: 10.1128/CVI.00037-17

Zhang, T., Xie, J., Zhang, M., Fu, N., and Zhang, Y. (2016). Effect of a potential probiotics *Lactococcus garvieae* B301 on the growth performance, immune parameters and caecum microflora of broiler chickens. *J. Anim. Physiol. Anim. Nutr.* 100, 413–421. doi: 10.1111/jpn.12388

Zhao, H., Xu, H., Zuo, Z., Wang, G., Liu, M., Guo, M., et al. (2018). Yi Shen Juan bi pill ameliorates bone loss and destruction induced by arthritis through modulating the balance of cytokines released by different subpopulations of T cells. *Front. Pharmacol.* 9:262. doi: 10.3389/fphar.2018.00262

Conflict of Interest: The authors declare that the research was conducted in the absence of any commercial or financial relationships that could be construed as a potential conflict of interest.

Copyright © 2020 Li, Lu, Fan, Lu, Xia, Zhao, Xu, Zhu, Li, Liu and Xiao. This is an open-access article distributed under the terms of the Creative Commons Attribution License (CC BY). The use, distribution or reproduction in other forums is permitted, provided the original author(s) and the copyright owner(s) are credited and that the original publication in this journal is cited, in accordance with accepted academic practice. No use, distribution or reproduction is permitted which does not comply with these terms.

frontiers in Cell and Developmental Biology

REVIEW
published: 17 March 2020
doi: 10.3389/fcell.2020.00089

The Role of Bone-Derived Exosomes in Regulating Skeletal Metabolism and Extraosseous Diseases

*Huili Lyu, Ye Xiao, Qi Guo, Yan Huang and Xianghang Luo**

Endocrinology Research Center, Department of Endocrinology, Xiangya Hospital of Central South University, Changsha, China

Bone-derived exosomes are naturally existing nano-sized extracellular vesicles secreted by various cells, such as bone marrow stromal cells, osteoclasts, osteoblasts, and osteocytes, containing multifarious proteins, lipids, and nucleic acids. Accumulating evidence indicates that bone-derived exosomes are involved in the regulation of skeletal metabolism and extraosseous diseases through modulating intercellular communication and the transfer of materials. Following the development of research, we found that exosomes can be considered as a potential candidate as a drug delivery carrier thanks to its ability to transport molecules into targeted cells with high stability, safety, and efficiency. This review aims to discuss the emerging role of bone-derived exosomes in skeletal metabolism and extraosseous diseases as well as their potential role as candidate biomarkers or for developing new therapeutic strategies.

Keywords: exosome, skeletal metabolism, extraosseous diseases, bone tissue engineering, biomarker

OPEN ACCESS

Edited by:
Chao Liang,
Hong Kong Baptist University, Hong Kong

Reviewed by:
Guozhi Xiao,
Southern University of Science and Technology, China
ZhenLin Zhang,
Shanghai Jiao Tong University, China

****Correspondence:***
Xianghang Luo
xianghangluo@sina.com;
xianghangluo@hotmail.com

Specialty section:
This article was submitted to Molecular Medicine, a section of the journal Frontiers in Cell and Developmental Biology

Received: *11 January 2020*
Accepted: *04 February 2020*
Published: *17 March 2020*

Citation:
Lyu H, Xiao Y, Guo Q, Huang Y and Luo X (2020) The Role of Bone-Derived Exosomes in Regulating Skeletal Metabolism and Extraosseous Diseases. Front. Cell Dev. Biol. 8:89. doi: 10.3389/fcell.2020.00089

THE INTRODUCTION OF EXOSOMES

Exosomes, first discovered in the 1980s, refer to extracellular vesicles with a diameter of 30–100 nm, and they were thought to be involved in the selective release of the transferrin receptor during maturation of sheep reticulocytes (Pan and Johnstone, 1983; Johnstone et al., 1987). Despite existing in reticulocytes, exosomes were found to be released by a variety of other cells, including lymphocytes (Guay et al., 2019), dendritic cells, platelets, mast cells (Cheung et al., 2016), neurons, macrophages (Bourdonnay et al., 2015), mesenchymal stem cells (MSCs), intestinal epithelial cells (IECs), and so on (van Niel et al., 2001; Clayton et al., 2005; Taylor and Gerçel-Taylor, 2005; Raposo and Stoorvogel, 2013). Exosomes initiate formation when the inner membrane of the endosomes bud inwardly to form luminal vesicles, which then transform into multivesicular bodies (MVBs). These MVBs can either be fused with lysosomes to degrade themselves, or they can release vesicles, named exosomes, after fusion with the plasma membranes (**Figure 1**) (Simons and Raposo, 2009). It was indicated that lipids are enriched on the surfaces of exosomes, including cholesterol, sphingomyelin, and ceramides. Furthermore, exosomes contain numerous biological molecules, such as proteins, enzymes, and microRNAs (miRNAs) (Valadi et al., 2007), which mediate intercellular communication and play an important role in the physiological and pathological processes (Kowal et al., 2014; Janas et al., 2015). Exosomes secrete complex

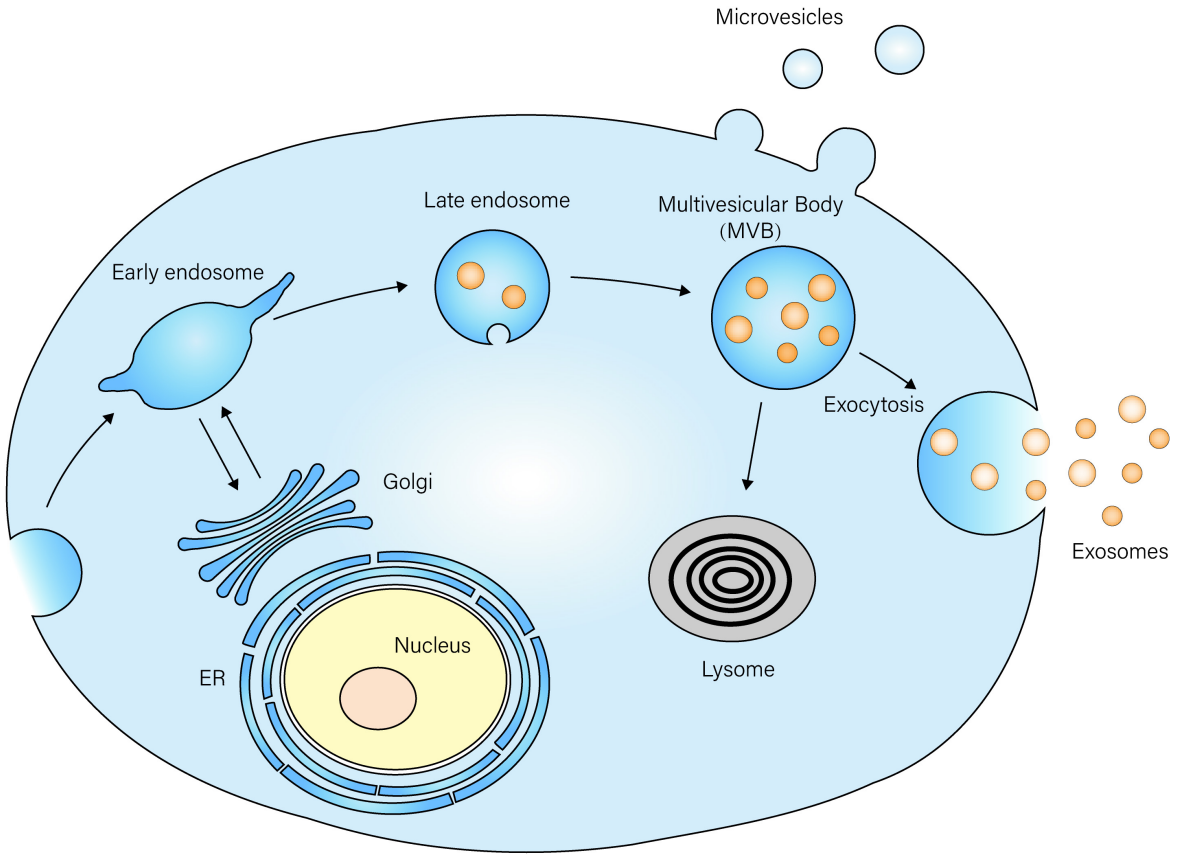


FIGURE 1 | Exosome biogenesis and secretion The membrane of the late endosome buds inwardly to form luminal vesicles, which then transform into multi-vesicle bodies (MVBs). MVBs then fuse with the plasma membrane and release vesicles named exosomes into the extracellular space. MVBs can also be fused with lysosomes, and they degrade vesicles inside.

content that depends not only on the cell type but also the microenvironment, such as mechanical properties, cellular PH, biochemical stimuli, and hypoxia (Choudhry and Harris, 2018). While previous research has shown that exosomes originating from different cells contain a specific subset of endosome-related proteins, they are involved in MVE biogenesis (e.g., Alix and Tsg101), membrane transport, and fusion (e.g., Rab GTPases, Annexins, and flotillin) (Colombo et al., 2014); among these actions, ubiquitous proteins like tetraspanins (CD9 and CD81), heat shock proteins (HSP70 and HSP90), and tumor-susceptibility gene 101 (Tsg101) are frequently used as markers of exosomes (Bjørge et al., 2017).

Exosomes have been widely investigated because of their multiple functions in diverse physiological process and diseases. As one of the most important factors in the paracrine regulation mechanism, exosomes can directly participate in signaling communication between cells. Dai et al. (2019) elucidated that prostate cancer (PCa)-derived exosomes could promote tumor growth and premetastatic niche formation in bone through transforming PKM2 into BMSCs. Alveolar macrophages (AMs) were found to secret exosomes containing the SOCS1 protein, which could be taken up by alveolar epithelial cells (AECs) and can inhibit STAT1 activation, leading to downregulation of inflammatory signaling both *in vitro* and *in vivo* (Bourdonnay et al., 2015). In addition, the microvesicles—released from primary lung epithelial cells induced by hyperoxia—containing hnRNPA2B1-associated miRNAs could be delivered into a macrophage and stimulate inflammation (Lee et al., 2019). Taken together, these experiments illustrated the essential role of exosomes in bilateral actions between AMs and AECs. Besides, the FasL-positive microvesicles released by melanoma cells were proven to induce the apoptosis of Jurkat and lymphoid cells, through which a tumor may escape from the effect of the immune system (Andreola et al., 2002). It can be seen that the exosomes derived from multiple cells are able to transfer different molecules, proteins, RNAs, and therefore have a significant effect on recipient cells.

TECHNIQUES FOR ISOLATING EXOSOMES

To optimally understand and exploit the biological action and clinical application of exosomes, it is essential to isolate them from cell culture supernatants or primary body fluids. The exosomes originate from a wealth of sources, such as whole blood

(Wu et al., 2017), menstrual blood (Dalirfardouei et al., 2018), urine (Street et al., 2017), cerebrospinal fluid (CSF) (Manek et al., 2018), milk (Leiferman et al., 2019), and so on. So far, a series of methods have been developed to isolate exosomes on the basis of size difference, molecular weight, density, certain surface markers, including differential ultracentrifugation (Raposo et al., 1996), density gradient ultracentrifugation (van der Pol et al., 2012), size based filtration, size-exclusion chromatography (Rood et al., 2010), immunoaffinity isolation (Kang et al., 2017), precipitation (Coumans et al., 2017; Li P. et al., 2017), field-flow fractionation (Zhang and Lyden, 2019), and so on. Generally speaking, every isolation technique exhibits its distinct advantages and disadvantages due to different experimental principles. Since exosomes have great potential and value in early clinical diagnosis, disease treatment, and prognosis evaluation, it is imperative to establish more user-friendly, efficient, and reliable technologies for the purpose of exosome isolation.

THE CHARACTERISTICS AND CONTENTS OF BONE-DERIVED EXOSOMES

In recent years it has been established that bone marrow stromal cells, osteoclasts, osteoblasts, and osteocytes can release exosomes that can not only regulate bone remodeling and skeletal disorders but can also participate in the progression of extraosseous diseases (Liu et al., 2017). Bone-derived exosomes contain a multitude of molecules, such as proteins and nucleic acids, that vary dynamically according to cell types as well as pathological and physiological conditions. In a recent study, researchers detected a total of 1,536 proteins contained in osteoblast-derived exosomes; they found that several valuable proteins involved in membrane trafficking and signaling pathways might be implicated in human bone diseases, including transforming growth factor beta receptor 3 (TGFBR3), lipoprotein receptor-related protein (LRP)6, bone morphogenetic protein receptor type-1 (BMPR1), and smad ubiquitylation regulatory factor-1 (SMURF1) (Ge et al., 2017). In addition, one proteomics profiling of exosomes from primary mouse osteoblasts revealed the difference in content between osteosomes under various differentiation statuses. To be more specific, 10 of the commonly expressed proteins were found to be increased more than five-fold in mineralizing (D24 osteosomes) primary mouse calvarial osteoblasts compared with proliferating osteoblasts (D0 osteosomes) (Bilen et al., 2017). Xu et al. (2014) tried to figure out the physiological role of exosomal miRNAs in osteoblast differentiation; they detected 79 miRNAs (∼8.84%) in exosomes isolated from BMSC culture supernatants and verified the presence of miRNA in exosomes during BMSCs osteogenic differentiation for the first time. Moreover, this study revealed differential expression of 14 exosomal miRNAs during osteogenic differentiation of human BMSCs; nine miRNAs (let-7a, miR-199b, miR-218, miR-148a, miR-135b, miR-203, miR-219, miR-299-5p, and miR-302b) were upregulated, and four miRNAs (miR-221, miR-155, miR-885-5p, miR-181a, and miR-320c) were downregulated (Xu et al., 2014). Another research study demonstrated that BMSC-derived exosomes could significantly reverse either S100- or LPS/ATP-induced injury in mice and hepatocytes. However, these protective effects were partly abolished with the involvement of the miR-223 inhibitor. This study firstly revealed the role of miRNA transferred by BMSCs-exo on liver injury caused by autoimmune hepatitis (Chen et al., 2018). Roccaro et al. (2013) found that BM-MSCs promoted the release and transfer of exosomes to MM (multiple myeloma) cells and detected a lower level of tumor-inhibiting factor miR-15a in MM BM-MSC versus normal BM-MSC-derived exosomes. Furthermore, a variety of oncogenic proteins and cytokines, which regulate adhesion and migration, were found to be enriched in MM BM-MSC-derived exosomes (Roccaro et al., 2013). In conclusion, the contents of bone-derived exosomes vary according to their different originators and microenvironments, which exert multiple effects on a serious of diseases, including skeletal disorders, prostate cancer, multiple myeloma, breast cancer, and so on.

THE ROLES OF BONE-DERIVED EXOSOMES IN SKELETAL METABOLISM

The skeleton is considered to be an essential support organ that protects vital organs, stores minerals, and provides a mechanical bracket for body and movement (Han et al., 2018). Osteoblast-mediated bone formation and osteoclast-mediated bone resorption maintain a dynamic balance through signaling proteins, such as asephrin-Eph, which bone remodeling process occurs throughout the lifespan to ensure the integrity of the skeleton and its multiple functions (Zhao et al., 2006; Suchacki et al., 2017). It has also been proposed that osteocytes play essential roles in bone remodeling by affecting the activities of osteoblasts and osteoclasts (Tatsumi et al., 2007).

The molecular regulation mechanism of bone remolding is affected by many factors, such as age (Ambrogini et al., 2010), genes, proteins (Ishijima et al., 2001), hormone levels (Hayashi et al., 2019), enzymes (Jin et al., 2014), amino acids (Yu et al., 2019), and cytokines (Wang et al., 2015). For example, the bone-resorbing activity of osteoclasts was negatively regulated by a signal transducer and activator of transcription 5 (Stat5), which performs its functions through suppressing MAPK activity via regulation of Dusp1 and Dusp2 (Hirose et al., 2014). Researchers found that sphingosine-1-phosphate (S1P) is able to mediate the location of osteoclast (OC) precursors (OPs) between bone and blood through its receptors, and thereby influence the osteoclastogenesis and bone remolding (Ishii et al., 2010). Glucocorticoids are shown to induce bone loss through inhibiting osteoblast function and differentiation by targeting glucocorticoid receptors and suppressing AP-1-dependent cytokines (Rauch et al., 2010). Greenblatt et al. (2015) also found a key regulator of bone turnover—charged multivesicular body protein 5 (CHMP5); it can suppress the RANK-induced NF-κB signaling in osteoclasts and thereby dampen osteoclast differentiation.

An imbalance in bone metabolism regulation can lead to many diseases, including osteoporosis, which is characterized

by age-related bone loss and increased fat formation (Moerman et al., 2004), high bone mass (HBM) resulting from abnormally increased bone formation (Yang et al., 2019), osteoarthritis, which is marked by progressive degeneration of articular cartilage (Rahmati et al., 2017), and so on. For example, the follicle-stimulating hormone (FSH) could promote activation of osteoclasts and enhance bone resorption through several signaling pathways, such as NF-kB, thus leading to a high risk of osteoporosis associated with menopause (Sponton and Kajimura, 2017). In recent years, scholars have made remarkable progress in the study of bone remodeling and related diseases as well as the role exosomes play in bone remolding, and this is attracting more and more attention.

BMSC-Derived Exosomes

There is a class of stromal stem cells with the capacity for autologous renewal in bone marrow named BMSCs. They can differentiate into osteoblasts, chondrocytes, and adipocytes (Fan et al., 2017; Li et al., 2018), and they can thereby influence bone formation, maintenance, and reconstruction (Nakajima et al., 2018). Emerging evidence suggests that BMSCs have the ability to repair bone tissue damage and promote bone regeneration, but the specific mechanism involved in this has not been clarified. It has been reported that transplanted MSCs are not able to exist *in vivo* permanently, but the therapy effect still persists even after MSCs elimination. Recently, scientists have found that this bone-protective effect may be related to paracrine vesicles, much like exosomes secreted by BMSC (Ng et al., 2015).

One study revealed that exosomes isolated from bone-marrow-derived MSCs could rescue the retardation of fracture healing in $CD9^{-/-}$ mice. The mechanism in this process is more than the recruitment of stem cells or progenitor cells by cytokines, but it also involves the induction of osteogenesis and angiogenesis partly regulated by exosomal miRNAs (Furuta et al., 2016). Fang et al. (2019) demonstrated that BMSC Exos significantly reverse the decreased osteogenic differentiation of BMSCs in steroid-induced femoral head necrosis (SFHN), and they then detected a total of 84 genes and 20 differentially expressed genes (DEGs), which consist of 11 upregulated and nine downregulated genes. Among these, DEGs, Bmps, Mmp9, and Sox9, which are related to regulating the immune system processes and the BMP/TGF-β pathway, may play important roles in the pathogenetic process of SFHN (Fang et al., 2019).

The exosomes' potential osteogenic capacity in bone regeneration was declared by Narayanan et al. (2016). They performed a series of studies to investigate how osteogenic exosomes derived from HMSCs could be endocytosed by primary HMSCs and could upregulate the expression of BMP9 and TGF-β1, which are both potent molecules in osteogenic differentiation (Luther et al., 2011; Kuroda et al., 2012). In addition, the *in vivo* experiments also indicated that both the regular exosomes and osteogenic exosomes can promote the osteogenic differentiation of HMSCs and matrix mineralization, while the osteogenic exosomes have a higher potential to induce better vascularization and calcium phosphate nucleation (Narayanan et al., 2016). Qin et al. (2016) found that exosomes isolated from BMSCs could be internalized into osteoblasts and enhance the expression of osteogenic genes. To investigate the mechanism by which exosomes promote osteogenic differentiation, they detected the miRNA in exosomes by miRNA sequencing and found highly expressed miR-27a, miR-206a, and miR-196a, among which miR-196a has the greatest potential in functional testing (Qin et al., 2016). Liu et al. (2015) indicated that transplantation of BMMSCs could rescue osteopenia in Fas-deficient-MRL/lpr mice through secreting exosomes, which were found to transfer Fas to recipient MRL/lpr BMMSCs, reduce their miR29b levels, enhance osteogenic differentiation *in vitro*, and promote bone formation *in vivo*.

Despite the critical effect in bone remolding, several studies have confirmed that BMSC-derived exosomes have the ability to reduce cartilage destruction and promote cartilage repair (Pourakbari et al., 2019). Osteoarthritis (OA) is a kind of rheumatic disease characterized by degeneration of articular cartilage and osteophyte formation (Findlay and Kuliwaba, 2016), and previous research has suggested that bone marrow-derived MSCs could be applied to treating OA and cartilage lesions in animals and humans (Nejadnik et al., 2010; Xie et al., 2012). Recently, accumulating evidence has implied that exosomes isolated from BMSCs function as vital media to elicit protective responses in cartilage. Cosenza et al. (2017) identified that BM-MSCs-derived exosomes could protect cartilage and bone from degradation through reducing apoptosis of chondrocytes, inhibiting macrophage activation, and promoting polarization of the M2 macrophage. Toh et al. (2017) proposed that the mechanism through which MSC exosomes modulate cartilage repair might rely on their ability to restore homeostasis in bioenergetics, cell number, and immunoregulation. Researchers addressed how MSCs are able to secrete miRNA-enriched exosomes to facilitate intercellular communication (Chen et al., 2010), and it is thus reasonable to conclude that exosomal miRNAs may be essential in cartilage differentiation. For instance, exosomal miRNA-23b could induce chondrogenic differentiation of hMSCs via inhibiting the expression of target PKA (Ham et al., 2012). Besides, Ning et al. (2013) found that miR-92a deficiency could cause a reduced number of chondrogenic progenitors, impaired chondrogenic differentiation, and pharyngeal cartilage defects in zebrafish. The mechanisms involved in the effect of miR-92a on chondrogenic differentiation rely on its regulation of Bmp signaling through targeting nog3 mRNA (Ning et al., 2013).

Osteoclast-Derived Exosomes

Osteoclasts are giant multinucleated cells originating from mononuclear macrophage precursor cells, and they are mainly responsible for bone resorption *in vivo* (Nevius et al., 2015). Osteoclasts participate in the occurrence and development of many bone diseases, such as osteoporosis (Novack, 2007; Hsu et al., 2011), rheumatoid arthritis, and so on. Sun et al. (2016) showed that osteoclasts could secrete miR-214-containing exosomes, which are transferred into osteoblasts via ephrinA2/EphA2 recognition to inhibit osteoblast function (**Figure 2**). Besides, the level of miR-214 is measured to be higher in the serum exosomes of osteoporotic patients and mice compared with healthy ones, which might be a potential

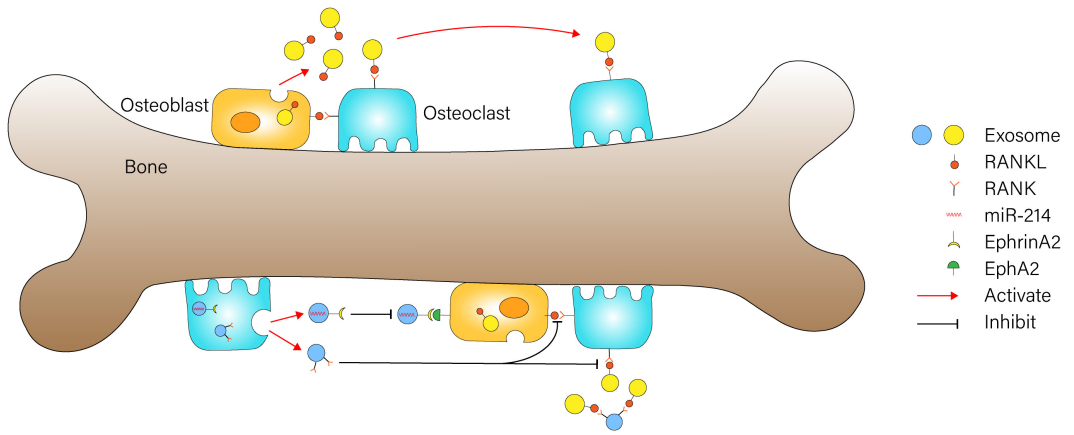


FIGURE 2 | Exosome-mediated communication between osteoblasts and osteoclasts Osteoblast-derived exosomes containing RANKL could stimulate osteoclast differentiation through binding to RANK on the surface of osteoclasts. RNAK-enriched exosomes from osteoclasts competitively bind to RANKL and prevent activation of the RANK signaling pathway in osteoclasts. miR-214-containing exosomes from osteoclasts could be transferred into osteoblasts via ephrinA2/EphA2 recognition to inhibit osteoblast function.

biomarker for osteoporosis (Sun et al., 2016). Moreover, the work of Zhao et al. (2015) demonstrated that miR-214 plays a catalytic role during RANKL-induced osteoclast differentiation through the PI3K/Akt signaling pathway by targeting phosphatase and tensin homolog (Pten). They also established Acp5-miR-214 transgenic (OC-TG214) mice to explore the effect of miR214 *in vivo*, and the results indicated that the upregulation of miR-214 in osteoclasts induced lower levels of Pten protein, higher activity of osteoclast bone resorbing, and poorer bone mineral density (BMD) (Zhao et al., 2015). Researchers tested the regulation of osteoclast formation in $1,25(OH)_2D_3$-stimulated mouse marrow; they firstly found that osteoclast precursor-derived exosomes significantly stimulated formation of osteoclasts, while exosomes from mature osteoclasts suppressed osteoclastogenesis. Next, the presence of enriched RANK was found in exosomes from osteoclasts. The RANK depletion of osteoclast-derived exosomes reduced their effect of inhibiting osteoclastogenesis. These results revealed that RNAK contained in exosomes might be the active agent that competitively binds to RANKL and prevents stimulation of the RANK signaling pathway in osteoclasts, and it thus plays a greater inhibitory role in osteoclastogenesis (**Figure 2**) (Huynh et al., 2016). Li et al. (2016) delineated the role of exosomal miR-214-3p in the intercellular communication between osteoclasts and osteoblasts, which could be transferred from osteoclasts to osteoblasts to inhibit osteoblastic bone formation. More importantly, osteoclast-targeted inhibition miR-214-3p effectively reversed the suppression of osteoblast activity and facilitated bone formation, and this is suggestive of which might be a potential therapeutic method for bone loss (Li et al., 2016).

Osteoblast-Derived Exosomes

Osteoblasts are derived from bone marrow MSCs with multidirectional differentiation potential, and they play a critical role in the synthesis, secretion, and mineralization of the bone matrix through its capacity to secrete glycoprotein and collagen. BMSCs first differentiate into osteoprogenitor cells, then turn into osteoblast precursors, and finally transform into osteoblasts (Garg et al., 2017), and this process is regulated by miRNAs (Li et al., 2009), proteins (Zou et al., 2013), signaling pathways, and so on. One *in vitro* research conducted by Cui et al. (2016) demonstrated the intercellular positive feedback mechanism between mineralizing osteoblasts (MOBs) and bone marrow stromal cells (ST2 cells). Their experiment results indicated that MOB-derived exosomes could be incorporated into ST2 cells and significantly promote their osteogenic differentiation; during this process, 91 miRNAs were detected as being overexpressed and 182 miRNAs were downregulated. Additionally, the analysis of the targeting genes and pathway networks of these miRNAs revealed that the pro-osteogenic function of MOBs-derived exosomes may partially depend on activation of the Wnt signaling pathway through downregulating Axin1 expression and upregulating β-catenin expression (Cui et al., 2016). Ge et al. (2017) identified 1,536 proteins in osteoblast-derived exosomes and sorted out several pivotal proteins that are closely related to bone diseases through network and pathway analyses. Deng et al. (2015) indicated that osteoblast-derived microvesicles can transfer RANKL proteins into osteoclast precursors and promote their differentiation into osteoclasts through activating RANKL–RANK signaling, which revealed a new mechanism involved in communication between osteoblasts and osteoclasts (**Figure 2**). Then, they conducted a series of experiments to further explore the role of microvesicles in bone metabolism by using imipramine, which was found to block microvesicles generation (Bianco et al., 2009). The *in vitro* results showed that inhibition of microvesicles generation from osteoblasts leads to significant suppression of osteoclast differentiation. Besides, the *in vivo* experiments revealed that OVX mice treated with imipramine exhibit superior properties in bone mineral density, bone volume, trabecular number, and thickness, suggesting that imipramine could prevent progression of bone loss caused by estrogen deficiency due to its function of blocking microvesicles

generation (Deng et al., 2017). Through literature review and analysis, Xie et al. (2017) summarized the role of a number of mineralizing MC3T3 cell-derived exosomes in bone remolding. To be specific, miR-30d-5p, miR-133b-3p, and miR-140-3p were found to inhibit osteoblast differentiation, while let-7, miR-335-3p, miR-378b can promote osteoblast differentiation (Xie et al., 2017).

Osteocyte-Derived Exosomes

Bone tissue is formed by the bone matrix and osteocytes originating from osteoblasts, which are widely distributed in the bone matrix and are tightly connected through the bone lacuna–tubule network system (Bonewald, 2007). Sato et al. firstly indicated the relationship between osteocyte exosomes and circulating exosomes in the serum. It was hinted that 12 miRNAs levels were significantly decreased in the circulating exosomes of OL (osteocyte less) mice plasma in contrast with control mice plasma. Therefore, it could be concluded that osteocytes release exosomes containing specific miRNAs that are transferred into circulating (Sato et al., 2017). The osteocyte-derived exosomes have been proven to mediate muscle–bone communication, and Qin et al. (2017) established that osteocyte-derived exosomes, which express the downregulation of miR-218 after myostatin treatment, can be incorporated into ostoblastic cells and suppress osteoblastic differentiation through downregulation of Wnt signaling; this can be reversed by expression of exogenous miR-218, suggesting the therapeutic potential of miR-218 in osteocytes for the treatment of bone disorders. In addition, the work of Zhang et al. (2014) confirmed the relationship between miR-218 and Wnt/β-catenin signaling in the osteogenic differentiation of human adipose tissue-derived stem cells (hASCs). Their *in vitro* experiments elucidated that overexpression of miR-218 activates the Wnt signaling pathway via directly downregulating SFRP2/DKK2 levels and then promotes hASCs osteogenic differentiation, whereas upregulation of Wnt/β-catenin signal can enhance the expression of miR-218 (Zhang et al., 2014). It has been proven that Wnt signaling acts as a positive regulator in osteoblast differentiation and regulation of bone mass (Esen et al., 2013). Taken together, miR-218 functions as a signal amplifier in the complex feed-forward regulatory circuit to activate hASCs osteogenic differentiation (Zhang et al., 2014), which further demonstrated the potential application prospect of exosomal miR-218 in bone regeneration.

THE EFFECT OF BONE-DERIVED EXOSOMES IN EXTRAOSSEOUS DISEASES

Recent studies have shown that bone-derived exosomes not only participate in regulating bone remodeling in the bone microenvironment but also act as vital communication media in multiple biological processes, including antigen presentation, apoptosis, inflammation, cancer progression, and so on (Gurunathan et al., 2019). As a result, the multiple roles of bone-derived exosomes in distant tissues and extraosseous systems attracted much attention.

Role of Bone-Derived Exosomes in Cancer

So far, people have tried many ways to explore the mechanism of cancer and conquer oncotherapy. There is no denying that we have a deeper understanding of cancer in multiple areas, such as immune responses (Fritz and Lenardo, 2019), inflammation (Ritter and Greten, 2019), lipid metabolism (Snaebjornsson et al., 2020), and so on, but there is still no proper method that could cure cancer without side effects. It is therefore interesting that bone-derived exosomes were found to participate in the progression of cancer in terms of regulating gene expression, angiogenesis, migration, and proliferation. The work of Naseri et al. (2018) indicated that BMSCs-derived exosomes (MSCs-Exo), which are loaded with LNA-anti-miR-142-3p, can deliver their cargos into 4T1 and TUBO breast cancer cells—leading to downregulation of miR-142-3p and overexpression of tumor suppressor genes—and thereby exert an efficient anti-tumor function. Additionally, their *in vivo* experiments revealed that the mice treated with LNA-miR-142-3p inhibitor-loaded MSCs-Exos showed reduced tumor volume and growth rate. These results confirmed the efficiency of transferring anti-miR molecules like LNA-anti-miR-142-3p into target tissues via MSCs-Exos and also provided new outlooks in terms of oncotherapy (Naseri et al., 2018). In another study, researchers explored how exosomes isolated from human bone marrow mesenchymal stem cells (hBMSCs) can promote migration and proliferation of osteosarcoma and gastric cancer cells through activating the Hedgehog signaling pathway (Qi et al., 2017). Additionally, it is reported that the Hedgehog signaling pathway, an essential regulator in maintaining tissue polarity and cell differentiation, plays a significant role in multiple cancers, including most basal cell carcinomas (BCCs) and extracutaneous tumors (Yang et al., 2010). Bliss et al. (2016) tried to investigate the mechanisms by which MSCs communicate with BCCs (breast cancer cells) and promote dormancy of human breast cancer cells in bone marrow. They demonstrated that MSCs primed by cancer cells can release exosomes containing miR-222/223, which in turn favor their survival and enhance drug resistance. Moreover, the treatment of MSCs transfected with anti-miR222/223 facilitated chemosensitivity of dormant BCCs in mice (Bliss et al., 2016).

Zhu et al. (2012) figured out another mechanism by which BMSCs-derived exosomes promote tumor growth *in vivo*. They detected higher expression of VEGF and CXCR4 in tumor cells treated with BMSC-exosomes, suggesting that BMSC-exosomes could enhance angiogenesis and provide tumors with a richer blood supply and therefore promote their proliferation and growth. However, the results of another experiment are different from these. Bruno et al. (2013) found that human hepatocellular carcinoma cells (HepG2), human ovarian cancer cells (Skov-3), and Kaposi's sarcoma cells incubated with BMSC-derived microvesicles exhibited lower proliferation ability, higher expression of negative regulators of the cell cycle, and an increased number of cells staying in the G0/G1 phase. They also observed the effect of microvesicles on growth of implanted tumors in mice, and the data indicated that BMSC-derived microvesicles could inhibit tumor growth and increase necrosis areas in tumors (Bruno et al., 2013). These opposing conclusions

could be derived due to the occasion of MSCs or microvesicles treatment (Klopp et al., 2011). The injection of BMSC-derived extracellular vesicles (EVs) into established tumors could inhibit tumor growth, while the growth of tumors in the early stages treated with EVs could be facilitated.

Role of Bone-Derived Exosomes in Neurologic Diseases

Researchers demonstrated that exosomes isolated from MSCs can mediate the transfer of miR-133b into astrocytes and neurons, inducing increased axonal plasticity and neurite remodeling in the ischemic boundary zone (IBZ), and thereby lead to functional recovery in rats subjected to middle cerebral artery occlusion (MCAo) (Xin et al., 2012, 2013). Besides, miR-133b + MSC treatment dramatically downregulated the expression of the connective tissue growth factor (CTGF) and the Ras homolog gene family member A (RhoA) (Xin et al., 2013), which are relevant to central nervous system (CNS) repair, post-injury restructuring (Hertel et al., 2000) and regulation of axonogenesis (Hall and Lalli, 2010). In another study, Nakano et al. (2016) found that rat BM-MSC-derived exosomes can ameliorate learning and memory impairment in STZ-diabetic mice through suppressing oxidative stress and recovering decreased synapse numbers, and this process might rely on the internalization of exosomes into astrocytes and neurons, causing recovery of damaged astrocytes and neurons. To further investigate the specific miRNAs or proteins that participated in improving diabetes-induced cognitive impairment, they conducted a series of experiments. The results proposed that the oversecretion of exosomal miR-146a due to endogenous bone marrow-derived MSCs within the condition of an enriched environment (EE) plays a key role in restraining astrocytic inflammation and preventing cognitive impairment in diabetic rats (Kubota et al., 2018). Mead and Tomarev (2017) demonstrated that BMSC-derived exosomes can be efficiently integrated into target retinal ganglion cells (RGC), thus promoting the recovery of the RGC function followed by optic nerve crush (ONC) through enhanced regeneration of RGC axons and inhibiting RGC loss in an miRNA-dependent manner. It is worth mentioning that the neuroprotective effect of BMSC-derived exosomes on RGC after ONC is significantly more potent than simple BMSC treatment (Mead et al., 2013; Mesentier-Louro et al., 2014), and this is probably due to their capacity to integrate into the retina and retain high doses. In conclusion, BMSC-derived exosomes exert a significant effect on promoting nerve repair and functional recovery, indicating their potential in the field of regeneration and remodeling of nervous system (Qing et al., 2018).

Role of Bone-Derived Exosomes in Nephropathy

It has been reported in previous researches that BM-MSCs play a key role in protecting kidney from injury (Morigi and De Coppi, 2014), although the mechanisms are not entirely elucidated. Recently, several reports have demonstrated the critical roles of BM-MSC-derived exosomes in renal injury. Wang et al. (2019b) elucidated that BMSC exosomes protect renal tubular epithelial cells (NRK-52E) against apoptosis caused by ischemia reperfusion at the early reperfusion stage through transfer of exosomal miR-199a-5p from BMSCs into NRK-52E, leading to the suppression of endoplasmic reticulum (ER) stress in target cells by targeting the binding immunoglobulin protein (BIP) (Wang et al., 2019b). In another experiment, exosomes derived from MSC-CM were found to play a significant role in preventing diabetic nephropathy by inhibiting apoptosis of tubular epithelial cells (TECs) and reversing decreased tight junction protein ZO-1, thereby enhancing the barrier function of renal tubules (Nagaishi et al., 2016). In the model of kidney injury induced by ischemia reperfusion, BMSC-derived exosomes could inhibit the apoptosis of tubular cells and enhance their proliferation, thus protecting the kidney against AKI and CKD (Gatti et al., 2011).

Bruno et al. (2009) reported that the incorporation of exosomes isolated from bone marrow MSCs into tubular epithelial cells (TECs) can exert proliferative and antiapoptotic effects *in vitro* and significantly alleviate lesions of glycerol-induced AKI in SCID mice. Moreover, they provided evidence that the effects mentioned above were completely abolished by RNase treatment, indicating that the horizontal transfer of mRNAs contained in exosomes appears to be a requirement of their protective functions (Bruno et al., 2009). Similarly, one study revealed that BM-MSC-derived exosomes have a positive effect on renal PTECs (proximal tubular epithelial cells) after ATP depletion injury, which could inhibit PTECs apoptosis and enhance transepithelial resistance (TER), at least partly, via miRNAs transfer or through transcription modulation stimulated by exosomes. The GO analysis of modulated miRNAs confirmed that several upregulated genes in the condition of ATP depletion injury were suppressed after exosome treatment, including SHC1 (Src homology 2 domain containing transforming protein 1), caspase-3, caspase-7, and SMAD4 (SMAD family member 4) genes (Lindoso et al., 2014).

Role of Bone-Derived Exosomes in Cardiac Diseases

Previous studies have proposed that BMSCs can protect cardiomyocytes from apoptosis and prevent LV (left ventricular) remodeling after MI through paracrine signaling (Uemura et al., 2006), suggesting the potential role of BMSCs in cardiac diseases. Researchers have carried out numerous experiments to investigate the underlying mechanism involved in their cardioprotective effects. Recent studies turned to focus on exosomes which are known as key transporters of paracrine factors (Gartz and Strande, 2018) and revealed the emerging role of exosomes as candidate for treatment of cardiac diseases. One research completed by Ma et al. (2018) confirmed that BMSC-derived exosomes loaded with miR-132 could be taken up by HUVECs (Human umbilical venous endothelial cells), causing overexpression of miR-132 in HUVECs, and they could thereby enhance angiogenesis *in vitro* and promote recovery of cardiac function in an AMI (acute myocardial

infarction) model. To clarify the mechanism by which miR-132 exosomes modulate angiogenesis, they further measured miR-132 target gene RASA1 (Lei et al., 2015). Their data indicated that downregulated RASA1, in response to increased miR-132, can stimulate neovascularization and maintain the cardiac function *in vivo* (Ma et al., 2018). Feng et al. (2014) demonstrated that BMSC-derived exosomes could mediate the transfer of highly expressed miR-22 in the condition of ischemic preconditioning (IPC) from BMSCs into cardiomyocytes, leading to reduced apoptosis and cardiac fibrosis after myocardial infarction by downregulating the expression level of target Mecp2. Shao et al. (2017) compared the efficiency of bone marrow-derived MSCs and MSC-Exo in myocardial infarction recovery for the first time. The results displayed that MSC-Exo gained an advantage over MSCs in preserving myocardial function after infarction through inhibiting inflammation, suppressing fibrosis, promoting proliferation, and reducing apoptosis. Moreover, the sequencing analysis of miRNA indicated that MSC-Exo and MSCs possessed a similar miRNA profile, including downregulated miR-130, miR-378, and miR-34 as well as upregulated miR-29 and miR-24, suggesting that MSC-Exo could be considered as the replacement for MSCs to develop innovative therapies for myocardial infarction.

Role of Bone-Derived Exosomes in Cutaneous Repair

During the cutaneous repair process, a variety of cells, growth factors, and the extracellular matrix cooperate to replace dead cells and reconstruct damaged tissues, in which the proliferation of fibroblasts, angiogenesis, skin cell proliferation, and re-epithelization are extremely critical (Wu et al., 2018). In a study conducted by McBride et al. (2017), Wnt3a was detected as being tethered with human BM-MSC exosomes exteriorly. Their *in vitro* results further implied that BM-MSC exosomes significantly promoted dermal fibroblast proliferation, migration, and angiogenesis, which simulative function depends heavily on CD63+ exosomes and Wnt co-receptor lipoprotein-related proteins (LRP6) (McBride et al., 2017). Shabbir et al. (2015) found that BM-MSC exosomes can be incorporated into fibroblasts and stimulate their growth and migration in a normal and diabetic chronic wound; they could also be uptaken by HUVEC cells and enhanced endothelial angiogenesis *in vitro*. Furthermore, BM-MSC exosomes can activate several pathways that play important roles in skin wound healing, such as AKT, ERK 1/2, and STAT3, and enhance the expression of various growth factors (Shabbir et al., 2015). Considering the important role of STAT3 signaling in wound healing (Dauer et al., 2005), they further investigated the content of exosomes and finally found STAT3 DNA binding activity in BMSC-derived exosomes.

Role of Bone-Derived Exosomes in Metabolic Diseases

Nowadays, patients suffering from metabolic diseases are increasingly widespread through the world, including diabetes, obesity, hyperlipidemia, and so on (Ling and Rönn, 2019; Warshauer et al., 2020). Dysfunction of metabolism is found to greatly promote the occurrence and progression of these diseases (Newgard, 2017). For example, it is already known that the function of the pancreatic islet α cell is extremely important to glucostasis, and researchers have demonstrated that the a kind of pancreatic lncRNA called Paupar could activate Pax6 α-cell target genes and help to maintain glucose homeostasis; the deletion of Paupar in mice resulted in damaged α-cell function (Singer et al., 2019). Recently, researchers have demonstrated that exosomes isolated from BM-MSCs in aged mice could be incorporated into adipocytes, myocytes, and hepatocytes and reduce their insulin sensitivity through targeting SIRT1 (sirtuin 1). They also conducted miRNA microarray analysis and detected extremely high expression of miR-29b- 3p in exosomes from BM-MSCs of old mice. The injection of nanocomplexes mediating BM-MSCs-specific inhibition of miR-29b-3p could alleviate the aging-associated insulin resistance in mice, suggesting the potential therapeutic role of exosomal miR-29b-3p in aging-associated insulin resistance (Su et al., 2019).

BONE-DERIVED EXOSOMES AS A SOURCE OF BIOMARKERS FOR DISEASE DIAGNOSIS

The content in exosomes are alterative according to the physiological and pathological state of cells; exosomes can thus reflect the physiological condition and disease development to some extent. For example, researchers analyzed human plasma EV proteomes in rest and exercise, and they found 322 differently expressed proteins, suggesting transient release of EVs into circulation in the condition of exercise (Whitham et al., 2018). Besides, exosomes can be easily collected because of their existence in blood, urine, milk, and so on (Mori et al., 2019). In previous studies, researchers have discovered the clinical value of miRNAs as potential biomarkers in some diseases. For example, the contents of two miRNAs that are elevated during osteoclastogenesis, miR16 and miR378, are found to be correspondingly higher in mice with a heavy bone metastatic tumor burden or in breast cancer patients, suggesting their potential as indicators for bone metastasis progression (Eii et al., 2013). At present, the proteins and nucleic acids contained in exosomes have been widely researched for their potential as biomarkers in clinical disease diagnosis (Wang et al., 2018).

Sato et al. (2017) firstly revealed the positive correlation between osteocytes and 12 miRNAs contained in circulating plasma exosomes, suggesting that osteocytes released exosomes that then transferred into blood. Muntión et al. (2016) isolated BM-MSC-derived exosomes from MDS patients and healthy donors (HD) and then performed microRNA expression arrays. The results demonstrated that 21 microRNAs in exosomes from MDS patients were overexpressed compared with HDs, among which the microR-10a and miR-15a were extremely high (Muntión et al., 2016). In MM patients, BMSCs release exosomes and deliver them into MM cells to regulate tumor progression. Compared with normal humans, exosomes isolated

from patients' BMSCs contain lower levels of tumor suppressor gene miR-15a and higher levels of oncogenic proteins, cytokines, and adhesion molecules (Roccaro et al., 2013). It has also been reported that elevated serum exosomal miR-214-3p is closely associated with reduced bone formation in elderly women with fractures and OVX mice, suggesting that there is great potential for the use of exosomal miR-214-3p in the diagnosis of osteoporosis (Li et al., 2016). Barrera-Ramirez et al. (2017) compared miRNA profiling of hMSC-derived exosomes from patients with acute myeloid leukemia (AML) patients and healthy people. They identified five differentially expressed miRNAs, including upregulated miR-26a-5p and miR-101-3p as well as downregulated miR-23b-5p, miR-339-3p, and miR-425-5p in AML-derived samples (Barrera-Ramirez et al., 2017); these candidate miRNAs might serve as biomarkers of AML and provide new insight into the pathogenesis and treatment of AML.

In addition, exosomes can be used as markers of diseases progression. Researchers reported exosome profiling in human ES (exudative seroma) for the first time, which was obtained from the lymphatic drainage implanted after lymphadenectomy in melanoma patients. They found that ES-derived exosomes have richer proteins compared with serum derived exosomes, including HSP90B, Annexin A1, and S100 A4, which are related to antigen presentation, the ER–phagosome pathway, and G2/M transition. In comparison with N1a patients, the number of ES-derived exosomes as well as the proteins associated with melanoma tumor cells significantly increased. Finally, they detected BRAFV600E mutation in ES-derived exosomal nucleic acids, which could serve as a factor to evaluate the risk of relapse in patients (García-Silva et al., 2019). In addition, Broggi et al. (2019) also analyzed the lymphatic exudate of metastatic melanoma patients undergoing lymphadenectomy (LAN) and demonstrated that exosomes carrying melanoma-related miRNAs or proteins could be applied as indicators of nodal metastatic spread.

APPLICATION OF MSC-DERIVED EXOSOMES IN BONE TISSUE ENGINEERING

Many clinical diseases can lead to bone defects and reduced bone formation, including fractures (Matsumoto et al., 2010), bone tumors (Waning et al., 2019), osteoporosis (Cao et al., 2012), and so on. The commonly used treatments, such as bone transplantation, are still very limited. How to promote bone formation and repair bone defects has therefore always been a challenge faced by clinicians. Based on the cytobiology and materialogy, bone tissue engineering—now a significant research problem—is focused on promoting bone tissue regeneration by using seed cells, biological scaffolds, and bioactive factors (Bose et al., 2012). Previous studies have reported the important role MSCs play in repairing damaged organs and tissues through multiple mechanisms (Caplan and Dennis, 2006; Cao et al., 2012). BMSCs are most commonly used cells in stem cell researches due to their abundant sources and convenient separation methods (Morikawa et al., 2009). Recently scientists found that MSC-derived exosomes—the microvesicles mediating intercellular communication—have great potential in bone tissue engineering.

Zhang et al. demonstrated that MSC-Exosome/β-TCP complex scaffolds have a better repair effect on rat skull defects in comparison with pure β-TCP scaffolds. They found that the MSC-Exosomes could be internalized into HMBSs and promote their proliferation, migration, and differentiation *in vitro*. They then examined the gene expression in hBMSCs induced by exosomes, and the results suggested that the underlying mechanism by which exosomes stimulate osteogenic differentiation partly rely on the activation of the PI3K/Akt pathway (Zhang et al., 2016). Qi et al. (2016) indicated that hiPSC-MSC-Exos could upregulate the expression of RUNX2, COL1, and ALP and activate the differentiation of osteoblasts *in vitro*. They also conducted an *in vivo* experiment in mice with calvarial defects, and the results showed that hiPSC-MSC-Exos could stimulate bone formation in osteoporotic conditions. Moreover, the three-dimensional micro-CT images showed higher neovascularization in β-TCP + Exos group compared with β-TCP group. Taken together, these works suggested the potential application of MSC-Exos + β-TCP scaffolds in bone defects due to their effect of facilitating angiogenesis and osteogenesis (Qi et al., 2016). In another study, researchers produced two same-sized calvarial bone defects in SD rats and treated them with hydrogel and hydrogel + exosomes; the results showed that exosomes from BMSCs could significantly enhance the bone formation in rats in the aspects of micro-CT, histological examinations, HE, and Masson staining (Qin et al., 2016).

In addition to bone remodeling, angiogenesis is also extremely important for the maintenance of bone homeostasis and bone regeneration (Saran et al., 2014; Xie et al., 2014). Angiogenesis refers to the formation of blood vessels from microvascular endothelial cells through budding, bridging, and microvascular fusion, all of which aid the transportation of necessary oxygen, nutrients, and inorganic salts to bone via extensive networks (Adams and Alitalo, 2007). Previous studies have reported that MSCs-derived exosomes play a role in promoting angiogenesis in heart (Bian et al., 2014), renal injury, cutaneous repair (Zhang et al., 2015), skeletal muscle regeneration (Nakamura et al., 2015), limb ischemia repair, and so on. Likewise, in the process of fracture healing, new blood vessels can provide nutritional support, accelerate local metabolic rate, as well as improve the efficiency of bone reconstruction and the speed of fracture healing (Deschaseaux et al., 2009; Seebach et al., 2012). For example, MSC-derived exosomes could rescue delayed fracture healing in $CD9^{-/-}$ mice and facilitate fracture healing in wild type mice; the mechanism is partly depended on the effect of MCP-1, -3, SDF-1, angiogenic factors and miRNAs (Furuta et al., 2016). In ischemic femoral head necrosis, it is also significant to promote angiogenesis and restrain ischemic necrosis areas (Glueck et al., 2007). Li H. et al. (2017) indicated that BMSC-ExosMU (exosomes secreted from HIF-1α-overexpressing BMSCs) could promote osteogenic differentiation of BMSCs through enhancing the expression of OCN and ALP *in vitro*. The MTT assay and cell-scratched wound evaluation also found that BMSC-ExosMU

could promote proliferation, migration, and tube formation of HUVECs. Next, they conducted an *in vivo* experiment, and the results revealed that the SANFH (steroid-induced avascular necrosis of femoral head) model treated with BMSC-ExosMU was detected higher vessel density and denser trabecular tissue generation compared with the control group, suggesting the significant role of BMSC-ExosMU in promoting osteogenesis and angiogenesis (Li H. et al., 2017).

EXOSOMES AS TARGETED DELIVERY VEHICLES FOR THERAPY IN SKELETAL AND EXTRAOSSEOUS DISORDERS

In recent years, the application of pharmaceutical carriers in clinical diseases has received extensive attention, and this has particularly applied to nanoscale pharmaceutical carriers, such as liposomes, microparticles, nanoparticles, etc. They have several characteristics that contribute to their high delivery efficiency, including the capacity to encapsulate hydrophobic drugs, improve drug bioavailability, transport molecules with high specificity, and so on (Tan et al., 2010). Despite the advantages mentioned above, the artificial nano drug-loading systems still face many problems. For example, the carrier molecules are easily removed by antibodies as well as complement and coagulation factors. Besides, a toxic reaction cannot be avoided due to their synthetic lipid membranes. As natural endogenous nano-microvesicles, exosomes play important roles in intercellular signal transmission and material exchange. In contrast, exosomes can overcome multiple limitations of artificial nano delivery systems and are more suitable candidates for delivery vehicles. Firstly, the exosomes have higher security because they can evade the immune detection system; in this case the immune rejection is eliminated. They also have better tolerance, which helps to protect cargo from destruction, thus leading to a longer circulating half-life. Secondly, exosomes have a natural targeting capacity depending on their cell sources. Thirdly, the membrane of exosomes can be artificially modified to enhance their functions. Finally, exosomes can penetrate cytomembranes and biological barriers easily due to their nanometer size and specific surface molecules (Ei Andaloussi et al., 2013; Jiang and Gao, 2017).

Exosome as Compounds Delivery System

At present, some chemotherapeutic drugs, such as doxorubicin and paclitaxel, can be effectively loaded into exosomes. Tian et al. (2014) indicated that exosome-encapsulated Dox (doxorubicin) can be integrated into breast cancer cells with high efficiency and significantly enhanced the therapeutic effect of Dox. They also evaluated the cardiac toxicity in tumor-bearing mice, a dose-dependent side effect of Dox (Minotti et al., 2004), and found that intravenously injected iExos-Dox has weaker cardiotoxicity compared with free Dox, suggesting that exsomes are ideal drug delivery vehicles with high safety and efficiency for targeted tumor therapy. Another study revealed that the PTX (Paclitaxel) incorporated into exosomes by mild sonication can maintain stability at various conditions for over a month and has significantly enhanced drug cytotoxicity compared with PTX alone (Kim et al., 2016). In addition to transporting chemotherapeutic drugs to target cells with high efficiency, exosomes can also greatly increase the effects of other drugs, such as anti-inflammatory agents. For example, Sun et al. (2010) found that the binding of curcumin to naturally existing nanoparticle exosomes can significantly enhance the curcumin's anti-inflammatory activity through increasing its delivery into targeted macrophages, which leads to an improved anti-shock function in mice treated with LPS.

Exosome as siRNA Delivery System

Currently, siRNA technology has been widely used in gene function research, clinical therapy, and other fields for the reason that it can induce targeted mRNA degradation and lead to post-transcriptional gene silencing (Burnett and Rossi, 2012; Crooke et al., 2018). However, siRNA-based gene treatment still faces many challenges, such as the poor cellular uptake and low stability in the circulating system. There is much evidence to suggest that the nanocarrier exosomes facilitate siRNA uptake into the targeted cells and improve its pharmacokinetics (Ozcan et al., 2015; Wang et al., 2017). It was reported that the exosome/TRPP2 siRNA complex can efficiently deliver TRPP2 (transient receptor potential polycystic 2) siRNA into FaDu cells and suppress its expression, resulting in the inhibition of the EMT (epithelial-mesenchymal transition) process and reduced invasion of FaDu cells (Wang et al., 2019a). Shokrollahi et al. (2019) treated human neuroblastoma cells (SH-SY5Y) with exosomes transfected by Hsp27 siRNA and evaluated the maturation of the human neuroblastoma cells. The data showed that the uptake of exosomes carrying siRNA HSP-27 by SH-SY5Y cells significantly inhibited their survival, clonogenic activity, and differentiation toward neuronal lineage (Shokrollahi et al., 2019). Shtam et al. (2013) used siRNA-loading exosomes to deliver RAD51-siRNA into HeLa cells and induce gene silencing, thereby inhibiting cell survival and proliferation. Exosomes can also be engineered into more suitable nanocarriers for carrying siRNA through modification. To enhance the targeting ability, Alvarez-Erviti et al. (2011) remolded the exosomes through attaching a neuron-specific RVG peptide to Lamp2b expressed on the exosomal membrane. The result revealed that the RVG exosomes were able to transport GAPDH siRNA into targeted neurons, microglia, and oligodendrocytes, and this resulted in downregulation of BACE1 gene expression, which plays a key role in Alzheimer's disease (Alvarez-Erviti et al., 2011).

Exosome as miRNA Delivery System

miRNAs are a group of non-coding single-stranded RNAs of approximately 22 nucleotides that exist in plant and animal cells (Bartel, 2004). A series of studies have shown that miRNAs can participate in cellular gene network regulation by silencing target mRNA, and they therefore play important roles in cell proliferation, differentiation, and apoptosis (Beavers et al., 2015). It has also been summarized that miRNAs play key roles in bone formation and may serve as the new breakthrough

in the treatment of skeletal diseases (Hu et al., 2010). As previously mentioned, an exosome can transfer its cargo, such as miRNAs, into targeted cells and regulate their growth and differentiation (Thomou et al., 2017). For instance, brown fat-derived exosomes carrying specific miRNA could regulate liver through targeting Fgf21 (Chen and Pfeifer, 2017). It has been proposed that the exosome can be used as a vehicle for transporting functional miRNAs and exerting therapeutic action. The miRNAs have been proven to be involved in the pathogenesis of several neurodegenerative diseases, such as Alzheimer's disease, Parkinson's disease, etc. The delivery of miRNAs packed by exosomes to central nervous system is therefore widely used for the improvement of neurological functions (Ridolfi and Abdel-Haq, 2017). Katakowski et al. (2013) obtained exosomes carrying miR-146b through plasmid transfection, and they found that miR-146b can be delivered into tumor cells via exosomes, suppressing expression of EGFR and NF-jB proteins and leading to inhibition of glioma growth *in vitro*. They also demonstrated that M146-exo can significantly reduce tumor growth in the rat brain (Katakowski et al., 2013). Chen et al. (2018) demonstrated that the miR-223 transferred by BMSCs-exo can greatly protect hepatocytes from injury in autoimmune hepatitis. One study conducted by Yu et al. (2015) revealed that anti-apoptotic miRNAs like miR-19a can be delivered into cardiomyocytes via MSC^{GATA-4} (MSC overexpressing GATA-4)-derived exosomes and promote cardiac protection, which effect is connected with the inhibition of miR-19a target PTEN as well as activation of the Akt and ERK signaling pathway.

CONCLUSION AND PERSPECTIVE

Since the first discovery of exosomes released by mature erythrocytes in 1983, this topic has attracted much attention from researchers because of their inherent properties. Exosomes are a class of extracellular vesicles sized 30–100 nm that contain cholesterol, sphingomyelin, ceramide, and other lipids on the surface that can be secreted by a variety of cells, including BMSCs, osteoclasts, osteoblasts, osteocytes, dendritic cells, epithelial cells, tumor cells, etc. In the recent years, researchers have developed various techniques to isolate exosomes based on their physical, chemical, and biological properties, and different methods have their unique advantages and disadvantages which may influence the product quality and following analysis.

With the development of molecular biotechnology, many researchers have tended to investigate the bone metabolism and skeletal disorders from a paracrine perspective, among which the exosome-mediated intercellular communication is rapidly gaining increasing attention. Bone-derived exosomes can regulate cell apoptosis, proliferation, and differentiation through multiple pathways, thus exerting important effects during physiological and pathological processes, such as bone remodeling, bone loss, fracture healing, and so on. This review has summarized the role of exosomes derived from BMSCs, osteoclasts, osteoblasts, and osteocytes in skeletal metabolism. The multiple effects of bone-derived exosomal miRNAs in bone remodeling have also been listed in **Table 1**. Besides, the bone-derived exosomes are found to participate in development of extraosseous diseases. For example, bone-derived exosomes could promote or suppress tumor growth through regulating genes expression, signaling pathways, angiogenesis, and so on. There are also numerous experiments illustrating that bone-derived exosomes are able to protect functional cells from apoptosis, thereby facilitating nerve repair, preventing nephropathy, preserving myocardial functions, and so on. It is reasonable to believe that bone-derived exosomes are highly relevant to the exploration of mechanisms of extraosseous diseases based on their ability to reach distant tissues and extraosseous systems.

In recent years, scientists have discovered the important role of exosomes in transmitting information between cells.

TABLE 1 | The role of bone-derived exosomal miRNAs in bone remolding.

Exosomal miRNA	Cells	miRNA expression	miRNA function
miR-27a miR-206a miR-196a	BMSCs	High	Promote osteogenic differentiation of osteoblasts (Qin et al., 2016)
miR-214	Osteoclasts	High	Inhibit osteoblasts function Promote RANKL induced osteoclasts differentiation (Zhao et al., 2015; Sun et al., 2016)
miR-30d-5p miR-133b-3p miR-140-3p	Mineralizing MC3T3 cells	High	Inhibit osteoblasts differentiation (Xie et al., 2017)
let-7 miR-335-3p miR-378b	Mineralizing MC3T3 cells	High	Promote osteoblasts differentiation (Xie et al., 2017)
miR-218	Osteocytes	Low	Inhibit osteoblastic differentiation (Zhang et al., 2014; Qin et al., 2017)
miR-1192 miR-680 miR-302a	Mineralizing osteoblasts (MOBs)	High	Promote bone marrow stromal cell (ST2) differentiation to osteoblasts (Cui et al., 2016)

The contents of the exosomes can reflect the physiological and pathological processes in cells, which can be released into various body fluids and microenvironments, thereby transmitting carried signals to distant tissues and cells (Yoshida et al., 2019). Exosomes can therefore be used for diseases diagnosis. In addition, the microvesicular structure of the exosomes can protect their contents from degradation, which demonstrates their stability in body fluids and enormous potential in the diagnosis and surveillance of diseases (Kourembanas, 2015). Bone-derived exosomes have become a research hotspot in the context of their use as biomarkers for clinical diseases, such as osteoporosis, MDS, AML, and so on; this provides a great opportunity for the development of a novel and sensitive diagnosis method.

BMSCs are one of the most commonly used seed cells in tissue engineering. A series of studies have shown that BMSCs have the ability to repair bone defects (Rackwitz et al., 2012), but there still exist some problems in terms of the immune response, ethics, and so on. Recently, it has been reported that BMSCs release exosomes containing signaling molecules through paracrine mechanisms to promote tissue repair (Liang et al., 2014). Therefore, scientists have started to focus on the application of BMSC-derived exosomes in bone tissue engineering. It has been found that BMSC-derived exosomes have the function of regulating osteoblasts and osteoclasts as well as promoting bone formation and neovascularization, and exosomes thus have great application prospects and research value in the field of bone tissue engineering. In addition, the potential use of exosomes as drug delivery systems for disease treatment has gained significant interest from the scientific community since they are of a nano-size and have strong penetrability and hypotoxicity as well as low immunogenicity and cell targeting properties. However, the clinical application of bone-derived exosomes still faces several challenges. The exosome extraction method currently used is not efficient enough to be applied in clinic; it is therefore imperative to design a strategy to increase the yield and purity of exosomes. Besides, the content and function of exosomes from different sources differ greatly, and the genetic information contained in exosomes is thus still not fully elucidated. There is consequently still a long way to go before exosomes can be widely used in clinic.

In summary, this article has provided an overview of the effect and mechanism of bone-derived exosomes in skeletal metabolism and extraosseous diseases, and it has opened up new perspectives for exosomes serving as biomarkers and drug delivery carriers. We have reason to believe that, with the further development of biotechnology and in-depth exploration of exosomes, the role of bone-derived exosomes in clinical diagnosis, monitoring, and treatment will be fully utilized.

AUTHOR CONTRIBUTIONS

HL wrote the manuscript and designed the figures. YX, QG, and YH revised the manuscript. XL provided critical feedback and helped to shape the manuscript. All authors listed have made a substantial contribution to the work.

REFERENCES

Adams, R. H., and Alitalo, K. (2007). Molecular regulation of angiogenesis and lymphangiogenesis. *Nat Rev. Mol. Cell Biol.* 8, 464–478. doi: 10.1038/nrm2183

Alvarez-Erviti, L., Seow, Y., Yin, H., Betts, C., Lakhal, S., and Wood, M. J. (2011). Delivery of siRNA to the mouse brain by systemic injection of targeted exosomes. *Nat. Biotechnol.* 29, 341–345. doi: 10.1038/nbt.1807

Ambrogini, E., Almeida, M., Martin-Millan, M., Paik, J. H., Depinho, R. A., Han, L., et al. (2010). FoxO-mediated defense against oxidative stress in osteoblasts is indispensable for skeletal homeostasis in mice. *Cell Metab.* 11, 136–146. doi: 10.1016/j.cmet.2009.12.009

Andreola, G., Rivoltini, L., Castelli, C., Huber, V., Perego, P., Deho, P., et al. (2002). Induction of lymphocyte apoptosis by tumor cell secretion of FasL-bearing microvesicles. *J. Exp. Med.* 195, 1303–1316. doi: 10.1084/jem.20011624

Barrera-Ramirez, J., Lavoie, J. R., Maganti, H. B., Stanford, W. L., Ito, C., Sabloff, M., et al. (2017). Micro-RNA profiling of exosomes from marrow-derived mesenchymal stromal cells in patients with acute myeloid leukemia: implications in leukemogenesis. *Stem Cell Rev.* 13, 817–825. doi: 10.1007/s12015-017-9762-0

Bartel, D. P. (2004). MicroRNAs: genomics, biogenesis, mechanism, and function. *Cell* 116, 281–297.

Beavers, K. R., Nelson, C. E., and Duvall, C. L. (2015). MiRNA inhibition in tissue engineering and regenerative medicine. *Adv. Drug Deliver. Rev.* 88, 123–137. doi: 10.1016/j.addr.2014.12.006

Bian, S., Zhang, L., Duan, L., Wang, X., Min, Y., and Yu, H. (2014). Extracellular vesicles derived from human bone marrow mesenchymal stem cells promote angiogenesis in a rat myocardial infarction model. *J. Mol. Med.* 92, 387–397. doi: 10.1007/s00109-013-1110-5

Bianco, F., Perrotta, C., Novellino, L., Francolini, M., Riganti, L., Menna, E., et al. (2009). Acid sphingomyelinase activity triggers microparticle release from glial cells. *EMBO J.* 28, 1043–1054. doi: 10.1038/emboj.2009.45

Bilen, M. A., Pan, T., Lee, Y. C., Lin, S. C., Yu, G., Pan, J., et al. (2017). Proteomics profiling of exosomes from primary mouse osteoblasts under proliferation versus mineralization conditions and characterization of their uptake into prostate cancer cells. *J. Proteome Res.* 16, 2709–2728. doi: 10.1021/acs.jproteome.6b00981

Bjørge, I. M., Kim, S. Y., Mano, J. F., Kalionis, B., and Chrzanowski, W. (2017). Extracellular vesicles, exosomes and shedding vesicles in regenerative medicine - a new paradigm for tissue repair. *Biomater. Sci. UK* 6, 60–78. doi: 10.1039/c7bm00479f

Bliss, S. A., Sinha, G., Sandiford, O. A., Williams, L. M., Engelberth, D. J., Guiro, K., et al. (2016). Mesenchymal stem cell-derived exosomes stimulate cycling quiescence and early breast cancer dormancy in bone marrow. *Cancer Res.* 76, 5832–5844. doi: 10.1158/0008-5472.can-16-1092

Bonewald, L. F. (2007). Osteocyte messages from a bony tomb. *Cell Metab.* 5, 410–411. doi: 10.1016/j.cmet.2007.05.008

Bose, S., Roy, M., and Bandyopadhyay, A. (2012). Recent advances in bone tissue engineering scaffolds. *Trends Biotechnol.* 30, 546–554. doi: 10.1016/j.tibtech.2012.07.005

Bourdonnay, E., Zasłona, Z., Penke, L. R., Speth, J. M., Schneider, D. J., Przybranowski, S., et al. (2015). Transcellular delivery of vesicular SOCS proteins from macrophages to epithelial cells blunts inflammatory signaling. *J. Exp. Med.* 212, 729–742. doi: 10.1084/jem.20141675

Broggi, M. A. S., Maillat, L., Clement, C. C., Bordry, N., Corthésy, P., Auger, A., et al. (2019). Tumor-associated factors are enriched in lymphatic exudate compared to plasma in metastatic melanoma patients. *J. Exp. Med.* 216, 1091–1107. doi: 10.1084/jem.20181618

Bruno, S., Collino, F., Deregibus, M. C., Grange, C., Tetta, C., and Camussi, G. (2013). Microvesicles derived from human bone marrow mesenchymal stem cells inhibit tumor growth. *Stem Cells Dev.* 22, 758–771. doi: 10.1089/scd.2012.0304

Bruno, S., Grange, C., Deregibus, M. C., Calogero, R. A., Saviozzi, S., Collino, F., et al. (2009). Mesenchymal stem cell-derived microvesicles protect against acute tubular injury. *J Am. Soc. Nephrol.* 20, 1053–1067. doi: 10.1681/asn.2008070798

Burnett, J. C., and Rossi, J. J. (2012). RNA-based therapeutics: current progress and future prospects. *Chem. Biol.* 19, 60–71. doi: 10.1016/j.chembiol.2011.12.008

Cao, L., Liu, G., Gan, Y., Fan, Q., Yang, F., Zhang, X., et al. (2012). The use of autologous enriched bone marrow MSCs to enhance osteoporotic bone defect repair in long-term estrogen deficient goats. *Biomaterials* 33, 5076–5084. doi: 10.1016/j.biomaterials.2012.03.069

Caplan, A. I., and Dennis, J. E. (2006). Mesenchymal stem cells as trophic mediators. *J. Cell. Biochem.* 98, 1076–1084. doi: 10.1002/jcb.20886

Chen, L., Lu, F. B., Chen, D. Z., Wu, J. L., Hu, E. D., Xu, L. M., et al. (2018). BMSCs-derived miR-223-containing exosomes contribute to liver protection in experimental autoimmune hepatitis. *Mol. Immunol.* 93, 38–46. doi: 10.1016/j.molimm.2017.11.008

Chen, T. S., Lai, R. C., Lee, M. M., Choo, A. B., Lee, C. N., and Lim, S. K. (2010). Mesenchymal stem cell secretes microparticles enriched in pre-microRNAs. *Nucleic Acids Res.* 38, 215–224. doi: 10.1093/nar/gkp857

Chen, Y., and Pfeifer, A. (2017). brown fat-derived exosomes: small vesicles with big impact. *Cell Metab.* 25, 759–760. doi: 10.1016/j.cmet.2017.03.012

Cheung, K. L., Jarrett, R., Subramaniam, S., Salimi, M., Gutowska-Owsiak, D., Chen, Y. L., et al. (2016). Psoriatic T cells recognize neolipid antigens generated by mast cell phospholipase delivered by exosomes and presented by CD1a. *J. Exp. Med.* 213, 2399–2412. doi: 10.1084/jem.20160258

Choudhry, H., and Harris, A. L. (2018). Advances in hypoxia-inducible factor biology. *Cell Metab.* 27, 281–298. doi: 10.1016/j.cmet.2017.10.005

Clayton, A., Turkes, A., Navabi, H., Mason, M. D., and Tabi, Z. (2005). Induction of heat shock proteins in B-cell exosomes. *J. Cell Sci.* 118, 3631–3638. doi: 10.1242/jcs.02494

Colombo, M., Raposo, G., and Théry, C. (2014). Biogenesis, secretion, and intercellular interactions of exosomes and other extracellular vesicles. *Annu. Rev. Cell Dev. Bi.* 30, 255–289. doi: 10.1146/annurev-cellbio-101512-122326

Cosenza, S., Ruiz, M., Toupet, K., Jorgensen, C., and Noël, D. (2017). Mesenchymal stem cells derived exosomes and microparticles protect cartilage and bone from degradation in osteoarthritis. *Sci. Rep. UK* 7:16214. doi: 10.1038/s41598-017-15376-8

Coumans, F. A. W., Brisson, A. R., Buzas, E. I., Dignat-George, F., Drees, E. E. E., Ei-Andaloussi, S., et al. (2017). Methodological guidelines to study extracellular vesicles. *Circ. Res.* 120, 1632–1648. doi: 10.1161/CIRCRESAHA.117.309417

Crooke, S. T., Witztum, J. L., Bennett, C. F., and Baker, B. F. (2018). RNA-targeted therapeutics. *Cell Metab.* 27, 714–739. doi: 10.1016/j.cmet.2018.03.004

Cui, Y., Luan, J., Li, H., Zhou, X., and Han, J. (2016). Exosomes derived from mineralizing osteoblasts promote ST2 cell osteogenic differentiation by alteration of microRNA expression. *FEBS Lett.* 590, 185–192. doi: 10.1002/1873-3468.12024

Dai, J., Escara-Wilke, J., Keller, J. M., Jung, Y., Taichman, R. S., Pienta, K. J., et al. (2019). Primary prostate cancer educates bone stroma through exosomal pyruvate kinase M2 to promote bone metastasis. *J. Exp. Med.* 216, 2883–2899. doi: 10.1084/jem.20190158

Dalirfardouei, R., Jamialahmadi, K., and Mahdipour, E. (2018). A feasible method for the isolation of mesenchymal stem cells from menstrual blood and their exosomes. *Tissue Cell* 55, 53–62. doi: 10.1016/j.tice.2018.09.010

Dauer, D. J., Ferraro, B., Song, L., Yu, B., Mora, L., Buettner, R., et al. (2005). Stat3 regulates genes common to both wound healing and cancer. *Oncogene* 24, 3397–3408. doi: 10.1038/sj.onc.1208469

Deng, L., Peng, Y., Jiang, Y., Wu, Y., Ding, Y., Wang, Y., et al. (2017). Imipramine Protects against Bone Loss by Inhibition of Osteoblast-Derived Microvesicles. *Int. J. Mol. Sci.* 18:E1013. doi: 10.3390/ijms18051013

Deng, L., Wang, Y., Peng, Y., Wu, Y., Ding, Y., Jiang, Y., et al. (2015). Osteoblast-derived microvesicles: a novel mechanism for communication between osteoblasts and osteoclasts. *Bone* 79, 37–42. doi: 10.1016/j.bone.2015.05.022

Deschaseaux, F., Sensébé, L., and Heymann, D. (2009). Mechanisms of bone repair and regeneration. *Trends Mol. Med.* 15, 417–429. doi: 10.1016/j.molmed.2009.07.002

Ei Andaloussi, S., Lakhal, S., Mäger, I., and Wood, M. J. (2013). Exosomes for targeted siRNA delivery across biological barriers. *Adv. Drug Deliver. Rev.* 65, 391–397. doi: 10.1016/j.addr.2012.08.008

Eii, B., Mercatali, L., Ibrahim, T., Campbell, N., Schwarzenbach, H., Pantel, K., et al. (2013). Tumor-induced osteoclast miRNA changes as regulators and biomarkers of osteolytic bone metastasis. *Cancer Cell* 24, 542–556. doi: 10.1016/j.ccr.2013.09.008

Esen, E., Chen, J., Karner, C. M., Okunade, A. L., Patterson, B. W., and Long, F. (2013). WNT-LRP5 signaling induces Warburg effect through mTORC2 activation during osteoblast differentiation. *Cell Metab.* 17, 745–755. doi: 10.1016/j.cmet.2013.03.017

Fan, Y., Hanai, J. I., Le, P. T., Bi, R., Maridas, D., DeMambro, V., et al. (2017). Parathyroid hormone directs bone marrow mesenchymal cell fate. *Cell Metab.* 25, 661–672. doi: 10.1016/j.cmet.2017.01.001

Fang, S., Li, Y., and Chen, P. (2019). Osteogenic effect of bone marrow mesenchymal stem cell-derived exosomes on steroid-induced osteonecrosis of the femoral head. *Drug Design Dev. Ther.* 13, 45–55. doi: 10.2147/DDDT.S178698

Feng, Y., Huang, W., Wani, M., Yu, X., and Ashraf, M. (2014). Ischemic preconditioning potentiates the protective effect of stem cells through secretion of exosomes by targeting Mecp2 via miR-22. *PLoS One* 9:e88685. doi: 10.1371/journal.pone.0088685

Findlay, D. M., and Kuliwaba, J. S. (2016). Bone-cartilage crosstalk: a conversation for understanding osteoarthritis. *Bone Res.* 4:16028. doi: 10.1038/boneres.2016.28

Fritz, J. M., and Lenardo, M. J. (2019). Development of immune checkpoint therapy for cancer. *J. Exp. Med.* 216, 1244–1254. doi: 10.1084/jem.20182395

Furuta, T., Miyaki, S., Ishitobi, H., Ogura, T., Kato, Y., Kamei, N., et al. (2016). Mesenchymal stem cell-derived exosomes promote fracture healing in a mouse model. *Stem Cells Transl Med.* 5, 1620–1630. doi: 10.5966/sctm.2015-0285

García-Silva, S., Benito-Martín, A., Sánchez-Redondo, S., Hernández-Barranco, A., Ximénez-Embún, P., Nogués, L., et al. (2019). Use of extracellular vesicles from lymphatic drainage as surrogate markers of melanoma progression and mutation. *J. Exp. Med.* 216, 1061–1070. doi: 10.1084/jem.20181522

Garg, P., Mazur, M. M., Buck, A. C., Wandtke, M. E., Liu, J., and Ebraheim, N. A. (2017). Prospective review of mesenchymal stem cells differentiation into osteoblasts. *Orthopaedic Surg.* 9, 13–19. doi: 10.1111/os.12304

Gartz, M., and Strande, J. L. (2018). Examining the Paracrine Effects of Exosomes in Cardiovascular Disease and Repair. *J. Am. Heart Assoc.* 7:e007954. doi: 10.1161/JAHA.117.007954

Gatti, S., Bruno, S., Deregibus, M. C., Sordi, A., Cantaluppi, V., Tetta, C., et al. (2011). Microvesicles derived from human adult mesenchymal stem cells protect against ischaemia-reperfusion-induced acute and chronic kidney injury. *Nephrol. Dial. Transplant.* 26, 1474–1483. doi: 10.1093/ndt/gfr015

Ge, M., Wu, Y., Ke, R., Cai, T., Yang, J., and Mu, X. (2017). Value of Osteoblast-Derived Exosomes in Bone Diseases. *J. Craniofac. Surg.* 28, 866–870. doi: 10.1097/SCS.0000000000003463

Glueck, C. J., Freiberg, R. A., Oghene, J., Fontaine, R. N., and Wang, P. (2007). Association between the T-786C eNOS polymorphism and idiopathic osteonecrosis of the head of the femur. *J. Bone Joint surg. Am. Vol.* 89, 2460–2468. doi: 10.2106/jbjs.f.01421

Greenblatt, M. B., Park, K. H., Oh, H., Kim, J. M., Shin, D. Y., Lee, J. M., et al. (2015). CHMP5 controls bone turnover rates by dampening NF-κB activity in osteoclasts. *J. Exp. Med.* 212, 1283–1301. doi: 10.1084/jem.20150407

Guay, C., Kruit, J. K., Rome, S., Menoud, V., Mulder, N. L., Jurdzinski, A., et al. (2019). Lymphocyte-derived exosomal micrornas promote pancreatic β cell death and may contribute to type 1 diabetes development. *Cell Metab.* 29, .348.e6–361.e6. doi: 10.1016/j.cmet.2018.09.011

Gurunathan, S., Kang, M. H., Jeyaraj, M., Qasim, M., and Kim, J. H. (2019). Review of the isolation, characterization, biological function, and multifarious therapeutic approaches of exosomes. *Cells* 8:307. doi: 10.3390/cells8040307

Hall, A., and Lalli, G. (2010). Rho and Ras GTPases in axon growth, guidance, and branching. *Csh. Perspect. Biol.* 2:a001818. doi: 10.1101/cshperspect.a001818

Ham, O., Song, B. W., Lee, S. Y., Choi, E., Cha, M. J., Lee, C. Y., et al. (2012). The role of microRNA-23b in the differentiation of MSC into chondrocyte by targeting protein kinase A signaling. *Biomaterials* 33, 4500–4507. doi: 10.1016/j.biomaterials.2012.03.025

Han, Y., You, X., Xing, W., Zhang, Z., and Zou, W. (2018). Paracrine and endocrine actions of bone-the functions of secretory proteins from osteoblasts, osteocytes, and osteoclasts. *Bone Res.* 6, 16. doi: 10.1038/s41413-018-0019-6

Hayashi, M., Nakashima, T., Yoshimura, N., Okamoto, K., Tanaka, S., and Takayanagi, H. (2019). Autoregulation of Osteocyte Sema3A Orchestrates Estrogen Action and Counteracts Bone Aging. *Cell Metab.* 29, 627.e5–637.e5. doi: 10.1016/j.cmet.2018.12.021

Hertel, M., Tretter, Y., Alzheimer, C., and Werner, S. (2000). Connective tissue growth factor: a novel player in tissue reorganization after brain injury? *Eur. J. Neurosci.* 12, 376–380. doi: 10.1046/j.1460-9568.2000.00930.x

Hirose, J., Masuda, H., Tokuyama, N., Omata, Y., Matsumoto, T., Yasui, T., et al. (2014). Bone resorption is regulated by cell-autonomous negative feedback loop of Stat5-Dusp axis in the osteoclast. *J. Exp. Med.* 211, 153–163. doi: 10.1084/jem.20130538

Hsu, Y. H., Chen, W. Y., Chan, C. H., Wu, C. H., Sun, Z. J., and Chang, M. S. (2011). Anti-IL-20 monoclonal antibody inhibits the differentiation of osteoclasts and protects against osteoporotic bone loss. *J. Exp. Med.* 208, 1849–1861. doi: 10.1084/jem.20102234

Hu, R., Li, H., Liu, W., Yang, L., Tan, Y. F., and Luo, X. H. (2010). Targeting miRNAs in osteoblast differentiation and bone formation. *Expert Opin. Ther. Tar.* 14, 1109–1120. doi: 10.1517/14728222.2010.512916

Huynh, N., VonMoss, L., Smith, D., Rahman, I., Felemban, M. F., Zuo, J., et al. (2016). Characterization of regulatory extracellular vesicles from osteoclasts. *J. Dent. Res.* 95, 673–679. doi: 10.1177/0022034516633189

Ishii, M., Kikuta, J., Shimazu, Y., Meier-Schellersheim, M., and Germain, R. N. (2010). Chemorepulsion by blood S1P regulates osteoclast precursor mobilization and bone remodeling in vivo. *J. Exp. Med.* 207, 2793–2798. doi: 10.1084/jem.20101474

Ishijima, M., Rittling, S. R., Yamashita, T., Tsuji, K., Kurosawa, H., Nifuji, A., et al. (2001). Enhancement of osteoclastic bone resorption and suppression of osteoblastic bone formation in response to reduced mechanical stress do not occur in the absence of osteopontin. *J. Exp. Med.* 193, 399–404. doi: 10.1084/jem.193.3.399

Janas, T., Janas, M. M., Sapoń, K., and Janas, T. (2015). Mechanisms of RNA loading into exosomes. *FEBS Lett.* 589, 1391–1398. doi: 10.1016/j.febslet.2015.04.036

Jiang, X. C., and Gao, J. Q. (2017). Exosomes as novel bio-carriers for gene and drug delivery. *Int. J. Pharmaceut.* 521, 167–175. doi: 10.1016/j.ijpharm.2017.02.038

Jin, Z., Wei, W., Yang, M., Du, Y., and Wan, Y. (2014). Mitochondrial complex I activity suppresses inflammation and enhances bone resorption by shifting macrophage-osteoclast polarization. *Cell Metab.* 20, 483–498. doi: 10.1016/j.cmet.2014.07.011

Johnstone, R. M., Adam, M., Hammond, J. R., Orr, L., and Turbide, C. (1987). Vesicle formation during reticulocyte maturation. Association of plasma membrane activities with released vesicles (exosomes). *J Biol. Chem.* 262, 9412–9420.

Kang, Y. T., Kim, Y. J., Bu, J., Cho, Y. H., Han, S. W., and Moon, B. I. (2017). High-purity capture and release of circulating exosomes using an exosome-specific dual-patterned immunofiltration (ExoDIF) device. *Nanoscale* 9, 13495–13505. doi: 10.1039/c7nr04557c

Katakowski, M., Buller, B., Zheng, X., Lu, Y., Rogers, T., Osobamiro, O., et al. (2013). Exosomes from marrow stromal cells expressing miR-146b inhibit glioma growth. *Cancer Lett.* 335, 201–204. doi: 10.1016/j.canlet.2013.02.019

Kim, M. S., Haney, M. J., Zhao, Y., Mahajan, V., Deygen, I., Klyachko, N. L., et al. (2016). Development of exosome-encapsulated paclitaxel to overcome MDR in cancer cells. *Nanomedicine* 12, 655–664. doi: 10.1016/j.nano.2015.10.012

Klopp, A. H., Gupta, A., Spaeth, E., Andreeff, M., and Marini, F. (2011). Concise review: dissecting a discrepancy in the literature: do mesenchymal stem cells support or suppress tumor growth? *Stem Cells* 29, 11–19. doi: 10.1002/stem.559

Kourembanas, S. (2015). Exosomes: vehicles of intercellular signaling, biomarkers, and vectors of cell therapy. *Annu. Rev. Physiol.* 77, 13–27. doi: 10.1146/annurev-physiol-021014-071641

Kowal, J., Tkach, M., and Théry, C. (2014). Biogenesis and secretion of exosomes. *Curr. Opin. Cell Biol.* 29, 116–125. doi: 10.1016/j.ceb.2014.05.004

Kubota, K., Nakano, M., Kobayashi, E., Mizue, Y., Chikenji, T., Otani, M., et al. (2018). An enriched environment prevents diabetes-induced cognitive impairment in rats by enhancing exosomal miR-146a secretion from endogenous bone marrow-derived mesenchymal stem cells. *PLoS One* 13:e0204252. doi: 10.1371/journal.pone.0204252

Kuroda, S., Sumner, D. R., and Virdi, A. S. (2012). Effects of TGF-β1 and VEGF-A transgenes on the osteogenic potential of bone marrow stromal cells in vitro and in vivo. *J. Tissue Eng.* 3, 2041731412459745. doi: 10.1177/2041731412459745

Lee, H., Li, C., Zhang, Y., Zhang, D., Otterbein, L. E., and Jin, Y. (2019). Caveolin-1 selectively regulates microRNA sorting into microvesicles after noxious stimuli. *J. Exp. Med.* 216, 2202–2220. doi: 10.1084/jem.20182313

Lei, Z., van Mil, A., Brandt, M. M., Grundmann, S., Hoefer, I., Smits, M., et al. (2015). MicroRNA-132/212 family enhances arteriogenesis after hindlimb ischaemia through modulation of the Ras-MAPK pathway. *J. Cell. Mol. Med.* 19, 1994–2005. doi: 10.1111/jcmm.12586

Leiferman, A., Shu, J., Upadhyaya, B., Cui, J., and Zempleni, J. (2019). Storage of extracellular vesicles in human milk, and MicroRNA profiles in human milk exosomes and infant formulas. *J. Pediatr. Gastr. Nutr.* 69, 235–238. doi: 10.1097/MPG.0000000000002363

Li, C. J., Xiao, Y., Yang, M., Su, T., Sun, X., Guo, Q., et al. (2018). Long noncoding RNA Bmncr regulates mesenchymal stem cell fate during skeletal aging. *J. Clin. Invest.* 128, 5251–5266. doi: 10.1172/JCI99044

Li, D., Liu, J., Guo, B., Liang, C., Dang, L., Lu, C., et al. (2016). Osteoclast-derived exosomal miR-214-3p inhibits osteoblastic bone formation. *Nat. Commun.* 7:10872. doi: 10.1038/ncomms10872

Li, H., Liu, D., Li, C., Zhou, S., Tian, D., Xiao, D., et al. (2017). Exosomes secreted from mutant-HIF-1α-modified bone-marrow-derived mesenchymal stem cells attenuate early steroid-induced avascular necrosis of femoral head in rabbit. *Cell Biol. Int.* 41, 1379–1390. doi: 10.1002/cbin.10869

Li, H., Xie, H., Liu, W., Hu, R., Huang, B., Tan, Y. F., et al. (2009). A novel microRNA targeting HDAC5 regulates osteoblast differentiation in mice and contributes to primary osteoporosis in humans. *J. Clin. Invest.* 119, 3666–3677. doi: 10.1172/JCI39832

Li, P., Kaslan, M., Lee, S. H., Yao, J., and Gao, Z. (2017). Progress in exosome isolation techniques. *Theranostics* 7, 789–804. doi: 10.7150/thno.18133

Liang, X., Ding, Y., Zhang, Y., Tse, H. F., and Lian, Q. (2014). Paracrine mechanisms of mesenchymal stem cell-based therapy: current status and perspectives. *Cell Transplant.* 23, 1045–1059. doi: 10.3727/096368913X667709

Lindoso, R. S., Collino, F., Bruno, S., Araujo, D. S., Sant'Anna, J. F., Tetta, C., et al. (2014). Extracellular vesicles released from mesenchymal stromal cells modulate miRNA in renal tubular cells and inhibit ATP depletion injury. *Stem Cells Dev.* 23, 1809–1819. doi: 10.1089/scd.2013.0618

Ling, C., and Rönn, T. (2019). Epigenetics in human obesity and type 2 diabetes. *Cell Metab.* 29, 1028–1044. doi: 10.1016/j.cmet.2019.03.009

Liu, J., Li, D., Wu, X., Dang, L., Lu, A., and Zhang, G. (2017). Bone-derived exosomes. *Curr. Opin. Pharmacol.* 34, 64–69. doi: 10.1016/j.coph.2017.08.008

Liu, S., Liu, D., Chen, C., Hamamura, K., Moshaverinia, A., Yang, R., et al. (2015). MSC transplantation improves osteopenia via epigenetic regulation of notch signaling in lupus. *Cell Metab.* 22, 606–618. doi: 10.1016/j.cmet.2015.08.018

Luther, G., Wagner, E. R., Zhu, G., Kang, Q., Luo, Q., Lamplot, J., et al. (2011). BMP-9 induced osteogenic differentiation of mesenchymal stem cells: molecular mechanism and therapeutic potential. *Curr. Gene Ther.* 11, 229–240.

Ma, T., Chen, Y., Chen, Y., Meng, Q., Sun, J., Shao, L., et al. (2018). MicroRNA-132, delivered by mesenchymal stem cell-derived exosomes, promote angiogenesis in myocardial infarction. *Stem Cells Int.* 2018:3290372. doi: 10.1155/2018/3290372

Manek, R., Moghieb, A., Yang, Z., Kumar, D., Kobessiy, F., Sarkis, G. A., et al. (2018). Protein Biomarkers and Neuroproteomics Characterization of Microvesicles/Exosomes from Human Cerebrospinal Fluid Following Traumatic Brain Injury. *Mol. Neurobiol.* 55, 6112–6128. doi: 10.1007/s12035-017-0821-y

Matsumoto, T., Ii, M., Nishimura, H., Shoji, T., Mifune, Y., Kawamoto, A., et al. (2010). Lnk-dependent axis of SCF-cKit signal for osteogenesis in bone fracture healing. *J. Exp. Med.* 207, 2207–2223. doi: 10.1084/jem.20100321

McBride, J. D., Rodriguez-Menocal, L., Guzman, W., Candanedo, A., Garcia-Contreras, M., and Badiavas, E. V. (2017). Bone marrow mesenchymal stem cell-derived CD63 exosomes transport wnt3a exteriorly and enhance dermal fibroblast proliferation, migration, and angiogenesis in vitro. *Stem Cells Dev.* 26, 1384–1398. doi: 10.1089/scd.2017.0087

Mead, B., Logan, A., Berry, M., Leadbeater, W., and Scheven, B. A. (2013). Intravitreally transplanted dental pulp stem cells promote neuroprotection and axon regeneration of retinal ganglion cells after optic nerve injury. *Invest. Ophth. Vis. Sci.* 54, 7544–7556. doi: 10.1167/iovs.13-13045

Mead, B., and Tomarev, S. (2017). Bone marrow-derived mesenchymal stem cells-derived exosomes promote survival of retinal ganglion cells through miRNA-dependent mechanisms. *Stem Cell. Transl. Med.* 6, 1273–1285. doi: 10.1002/sctm.16-0428

Mesentier-Louro, L. A., Zaverucha-do-Valle, C., Da Silva-Junior, A. J., Nascimento-Dos-Santos, G., Gubert, F., de Figueirêdo, A. B., et al. (2014). Distribution of mesenchymal stem cells and effects on neuronal survival and axon regeneration after optic nerve crush and cell therapy. *PLoS One* 9:e110722. doi: 10.1371/journal.pone.0110722

Minotti, G., Menna, P., Salvatorelli, E., Cairo, G., and Gianni, L. (2004). Anthracyclines: molecular advances and pharmacologic developments in antitumor activity and cardiotoxicity. *Pharmacol. Rev.* 56, 185–229. doi: 10.1124/pr.56.2.6

Moerman, E. J., Teng, K., Lipschitz, D. A., and Lecka-Czernik, B. (2004). Aging activates adipogenic and suppresses osteogenic programs in mesenchymal marrow stroma/stem cells: the role of PPAR-gamma2 transcription factor and TGF-beta/BMP signaling pathways. *Aging Cell* 3, 379–389. doi: 10.1111/j.1474-9728.2004.00127.x

Mori, M. A., Ludwig, R. G., Garcia-Martin, R., Brandão, B. B., and Kahn, C. R. (2019). Extracellular miRNAs: from biomarkers to mediators of physiology and disease. *Cell Metab.* 30, 656–673. doi: 10.1016/j.cmet.2019.07.011

Morigi, M., and De Coppi, P. (2014). Cell therapy for kidney injury: different options and mechanisms–mesenchymal and amniotic fluid stem cells. *Nephron. Exp. Nephrol.* 126:59. doi: 10.1159/000360667

Morikawa, S., Mabuchi, Y., Kubota, Y., Nagai, Y., Niibe, K., Hiratsu, E., et al. (2009). Prospective identification, isolation, and systemic transplantation of multipotent mesenchymal stem cells in murine bone marrow. *J. Exp. Med.* 206, 2483–2496. doi: 10.1084/jem.20091046

Muntión, S., Ramos, T. L., Diez-Campelo, M., Rosón, B., Sánchez-Abarca, L. I., Misiewicz-Krzeminska, I., et al. (2016). Microvesicles from mesenchymal stromal cells are involved in hpc-microenvironment crosstalk in myelodysplastic patients. *PLoS One* 11:e0146722. doi: 10.1371/journal.pone.0146722

Nagaishi, K., Mizue, Y., Chikenji, T., Otani, M., Nakano, M., Konari, N., et al. (2016). Mesenchymal stem cell therapy ameliorates diabetic nephropathy via the paracrine effect of renal trophic factors including exosomes. *Sci. Rep. UK* 6:34842. doi: 10.1038/srep34842

Nakajima, K., Kunimatsu, R., Ando, K., Ando, T., Hayashi, Y., Kihara, T., et al. (2018). Comparison of the bone regeneration ability between stem cells from human exfoliated deciduous teeth, human dental pulp stem cells and human bone marrow mesenchymal stem cells. *Biochem. Bioph. Res. Co.* 497, 876–882. doi: 10.1016/j.bbrc.2018.02.156

Nakamura, Y., Miyaki, S., Ishitobi, H., Matsuyama, S., Nakasa, T., Kamei, N., et al. (2015). Mesenchymal-stem-cell-derived exosomes accelerate skeletal muscle regeneration. *FEBS Lett.* 589, 1257–1265. doi: 10.1016/j.febslet.2015.03.031

Nakano, M., Nagaishi, K., Konari, N., Saito, Y., Chikenji, T., Mizue, Y., et al. (2016). Bone marrow-derived mesenchymal stem cells improve diabetes-induced cognitive impairment by exosome transfer into damaged neurons and astrocytes. *Sci. Rep. UK* 6:24805. doi: 10.1038/srep24805

Narayanan, R., Huang, C. C., and Ravindran, S. (2016). Hijacking the cellular mail: exosome mediated differentiation of mesenchymal stem cells. *Stem Cells Int.* 2016:3808674. doi: 10.1155/2016/3808674

Naseri, Z., Oskuee, R. K., Jaafari, M. R., and Forouzandeh Moghadam, M. (2018). Exosome-mediated delivery of functionally active miRNA-142-3p inhibitor reduces tumorigenicity of breast cancer in vitro and in vivo. *Int. J. Nanomed.* 13, 7727–7747. doi: 10.2147/IJN.S182384

Nejadnik, H., Hui, J. H., Feng Choong, E. P., Tai, B. C., and Lee, E. H. (2010). Autologous bone marrow-derived mesenchymal stem cells versus autologous chondrocyte implantation: an observational cohort study. *Am. J. Sports Med.* 38, 1110–1116. doi: 10.1177/0363546509359067

Nevius, E., Pinho, F., Dhodapkar, M., Jin, H., Nadrah, K., Horowitz, M. C., et al. (2015). Oxysterols and EBI2 promote osteoclast precursor migration to bone surfaces and regulate bone mass homeostasis. *J. Exp. Med.* 212, 1931–1946. doi: 10.1084/jem.20150088

Newgard, C. B. (2017). Metabolomics and metabolic diseases: where do we stand? *Cell Metab.* 25, 43–56. doi: 10.1016/j.cmet.2016.09.018

Ng, K. S., Kuncewicz, T. M., and Karp, J. M. (2015). beyond hit-and-run: stem cells leave a lasting memory. *Cell Metab.* 22, 541–543. doi: 10.1016/j.cmet.2015.09.019

Ning, G., Liu, X., Dai, M., Meng, A., and Wang, Q. (2013). MicroRNA-92a upholds Bmp signaling by targeting noggin3 during pharyngeal cartilage formation. *Dev. Cell* 24, 283–295. doi: 10.1016/j.devcel.2012.12.016

Novack, D. V. (2007). Estrogen and bone: osteoclasts take center stage. *Cell Metab.* 6, 254–256. doi: 10.1016/j.cmet.2007.09.007

Ozcan, G., Ozpolat, B., Coleman, R. L., Sood, A. K., and Lopez-Berestein, G. (2015). Preclinical and clinical development of siRNA-based therapeutics. *Adv. Drug Deliver. Rev.* 87, 108–119. doi: 10.1016/j.addr.2015.01.007

Pan, B. T., and Johnstone, R. M. (1983). Fate of the transferrin receptor during maturation of sheep reticulocytes in vitro: selective externalization of the receptor. *Cell* 33, 967–978. doi: 10.1016/0092-8674(83)90040-5

Pourakbari, R., Khodadadi, M., Aghebati-Maleki, A., Aghebati-Maleki, L., and Yousefi, M. (2019). The potential of exosomes in the therapy of the cartilage and bone complications; emphasis on osteoarthritis. *Life Sci.* 236:116861. doi: 10.1016/j.lfs.2019.116861

Qi, J., Zhou, Y., Jiao, Z., Wang, X., Zhao, Y., Li, Y., et al. (2017). Exosomes Derived from Human Bone Marrow Mesenchymal Stem Cells Promote Tumor Growth Through Hedgehog Signaling Pathway. *Cell. Physiol. Biochem.* 42, 2242–2254. doi: 10.1159/000479998

Qi, X., Zhang, J., Yuan, H., Xu, Z., Li, Q., Niu, X., et al. (2016). Exosomes secreted by human-induced pluripotent stem cell-derived mesenchymal stem cells repair critical-sized bone defects through enhanced angiogenesis and osteogenesis in osteoporotic rats. *Int. J. Biol. Sci.* 12, 836–849. doi: 10.7150/ijbs.14809

Qin, Y., Peng, Y., Zhao, W., Pan, J., Ksiezak-Reding, H., Cardozo, C., et al. (2017). Myostatin inhibits osteoblastic differentiation by suppressing osteocyte-derived exosomal microRNA-218: a novel mechanism in muscle-bone communication. *J. Biol. Chem.* 292, 11021–11033. doi: 10.1074/jbc.M116.770941

Qin, Y., Wang, L., Gao, Z., Chen, G., and Zhang, C. (2016). Bone marrow stromal/stem cell-derived extracellular vesicles regulate osteoblast activity and differentiation in vitro and promote bone regeneration in vivo. *Sci. Rep. UK* 6:21961. doi: 10.1038/srep21961

Qing, L., Chen, H., Tang, J., and Jia, X. (2018). Exosomes and their MicroRNA cargo: new players in peripheral nerve regeneration. *Neurorehab. Neural Re.* 32, 765–776. doi: 10.1177/1545968318798955

Rackwitz, L., Eden, L., Reppenhagen, S., Reichert, J. C., Jakob, F., Walles, H., et al. (2012). Stem cell- and growth factor-based regenerative therapies for avascular necrosis of the femoral head. *Stem Cell Res. Ther.* 3:7. doi: 10.1186/scrt98

Rahmati, M., Nalesso, G., Mobasheri, A., and Mozafari, M. (2017). Aging and osteoarthritis: central role of the extracellular matrix. *Ageing Res. Rev.* 40, 20–30. doi: 10.1016/j.arr.2017.07.004

Raposo, G., Nijman, H. W., Stoorvogel, W., Liejendekker, R., Harding, C. V., Melief, C. J., et al. (1996). B lymphocytes secrete antigen-presenting vesicles. *J. Exp. Med.* 183, 1161–1172. doi: 10.1084/jem.183.3.1161

Raposo, G., and Stoorvogel, W. (2013). Extracellular vesicles: exosomes, microvesicles, and friends. *J Cell Biol.* 200, 373–383. doi: 10.1083/jcb.201211138

Rauch, A., Seitz, S., Baschant, U., Schilling, A. F., Illing, A., Stride, B., et al. (2010). Glucocorticoids suppress bone formation by attenuating osteoblast differentiation via the monomeric glucocorticoid receptor. *Cell Metab.* 11, 517–531. doi: 10.1016/j.cmet.2010.05.005

Ridolfi, B., and Abdel-Haq, H. (2017). Neurodegenerative disorders treatment: the MicroRNA role. *Curr. Gene Ther.* 17, 327–363. doi: 10.2174/1566523218666180119120726

Ritter, B., and Greten, F. R. (2019). Modulating inflammation for cancer therapy. *J. Exp. Med.* 216, 1234–1243. doi: 10.1084/jem.20181739

Roccaro, A. M., Sacco, A., Maiso, P., Azab, A. K., Tai, Y. T., Reagan, M., et al. (2013). BM mesenchymal stromal cell-derived exosomes facilitate multiple myeloma progression. *J. Clin. Invest.* 123, 1542–1555. doi: 10.1172/jci66517

Rood, I. M., Deegens, J. K., Merchant, M. L., Tamboer, W. P., Wilkey, D. W., Wetzels, J. F., et al. (2010). Comparison of three methods for isolation of urinary microvesicles to identify biomarkers of nephrotic syndrome. *Kidney Int.* 78, 810–816. doi: 10.1038/ki.2010.262

Saran, U., Gemini Piperni, S., and Chatterjee, S. (2014). Role of angiogenesis in bone repair. *Arch. Biochem. Biophys.* 561, 109–117. doi: 10.1016/j.abb.2014.07.006

Sato, M., Suzuki, T., Kawano, M., and Tamura, M. (2017). Circulating osteocyte-derived exosomes contain miRNAs which are enriched in exosomes from MLO-Y4 cells. *Biomed. Rep.* 6, 223–231. doi: 10.3892/br.2016.824

Seebach, C., Henrich, D., Wilhelm, K., Barker, J. H., and Marzi, I. (2012). Endothelial progenitor cells improve directly and indirectly early vascularization of mesenchymal stem cell-driven bone regeneration in a critical bone defect in rats. *Cell Transplant.* 21, 1667–1677. doi: 10.3727/096368912X638937

Shabbir, A., Cox, A., Rodriguez-Menocal, L., Salgado, M., and Van Badiavas, E. (2015). Mesenchymal stem cell exosomes induce proliferation and migration of normal and chronic wound fibroblasts, and enhance angiogenesis in vitro. *Stem Cells Dev.* 24, 1635–1647. doi: 10.1089/scd.2014.0316

Shao, L., Zhang, Y., Lan, B., Wang, J., Zhang, Z., Zhang, L., et al. (2017). MiRNA-sequence indicates that mesenchymal stem cells and exosomes have similar mechanism to enhance cardiac repair. *Biomed Res. Int.* 2017:4150705. doi: 10.1155/2017/4150705

Shokrollahi, E., Nourazarian, A., Rahbarghazi, R., Salimi, L., Karbasforush, S., Khaksar, M., et al. (2019). Treatment of human neuroblastoma cell line SH-SY5Y with HSP27 siRNA tagged-exosomes decreased differentiation rate into mature neurons. *J. Cell. Physiol.* 234, 21005–21013. doi: 10.1002/jcp.28704

Shtam, T. A., Kovalev, R. A., Varfolomeeva, E. Y., Makarov, E. M., Kil, Y. V., and Filatov, M. V. (2013). Exosomes are natural carriers of exogenous siRNA to human cells in vitro. *Cell Commun. Signal.* 11:88. doi: 10.1186/1478-811X-11-88

Simons, M., and Raposo, G. (2009). Exosomes–vesicular carriers for intercellular communication. *Curr. Opin. Cell Biol.* 21, 575–581. doi: 10.1016/j.ceb.2009.03.007

Singer, R. A., Arnes, L., Cui, Y., Wang, J., Gao, Y., Guney, M. A., et al. (2019). The long noncoding RNA paupar modulates PAX6 regulatory activities to promote alpha cell development and function. *Cell Metab.* 30, 1091.e8–1106.e8. doi: 10.1016/j.cmet.2019.09.013

Snaebjornsson, M. T., Janaki-Raman, S., and Schulze, A. (2020). Greasing the wheels of the cancer machine: the role of lipid metabolism in cancer. *Cell Metab.* 31, 62–76. doi: 10.1016/j.cmet.2019.11.010

Sponton, C. H., and Kajimura, S. (2017). Burning fat and building bone by FSH blockade. *Cell Metab.* 26, 285–287. doi: 10.1016/j.cmet.2017.07.018

Street, J. M., Koritzinsky, E. H., Glispie, D. M., and Yuen, P. S. T. (2017). Urine exosome isolation and characterization. *Methods Mol. Biol.* 1641, 413–423. doi: 10.1007/978-1-4939-7172-5_23

Su, T., Xiao, Y. Z., Xiao, Y., Guo, Q., Li, C., Huang, Y., et al. (2019). Bone marrow mesenchymal stem cells-derived exosomal MiR-29b-3p regulates aging-associated insulin resistance. *ACS Nano* 13, 2450–2462. doi: 10.1021/acsnano.8b09375

Suchacki, K. J., Roberts, F., Lovdel, A., Farquharson, C., Morton, N. M., MacRae, V. E., et al. (2017). Skeletal energy homeostasis: a paradigm of endocrine discovery. *J. Endocrinol.* 234, R67–R79. doi: 10.1530/JOE-17-0147

Sun, D., Zhuang, X., Xiang, X., Liu, Y., Zhang, S., Liu, C., et al. (2010). A novel nanoparticle drug delivery system: the anti-inflammatory activity of curcumin is enhanced when encapsulated in exosomes. *Mol. Ther.* 18, 1606–1614. doi: 10.1038/mt.2010.105

Sun, W., Zhao, C., Li, Y., Wang, L., Nie, G., Peng, J., et al. (2016). Osteoclast-derived microRNA-containing exosomes selectively inhibit osteoblast activity. *Cell Discov.* 2:16015. doi: 10.1038/celldisc.2016.15

Tan, M. L., Choong, P. F., and Dass, C. R. (2010). Recent developments in liposomes, microparticles and nanoparticles for protein and peptide drug delivery. *Peptides* 31, 184–193. doi: 10.1016/j.peptides.2009.10.002

Tatsumi, S., Ishii, K., Amizuka, N., Li, M., Kobayashi, T., Kohno, K., et al. (2007). Targeted ablation of osteocytes induces osteoporosis with defective mechanotransduction. *Cell Metab.* 5, 464–475. doi: 10.1016/j.cmet.2007.05.001

Taylor, D. D., and Gerçel-Taylor, C. (2005). Tumour-derived exosomes and their role in cancer-associated T-cell signalling defects. *Brit. J. Cancer* 92, 305–311. doi: 10.1038/sj.bjc.6602316

Thomou, T., Mori, M. A., Dreyfuss, J. M., Konishi, M., Sakaguchi, M., Wolfrum, C., et al. (2017). Adipose-derived circulating miRNAs regulate gene expression in other tissues. *Nature* 542, 450–455. doi: 10.1038/nature21365

Tian, Y., Li, S., Song, J., Ji, T., Zhu, M., Anderson, G. J., et al. (2014). A doxorubicin delivery platform using engineered natural membrane vesicle exosomes for targeted tumor therapy. *Biomaterials* 35, 2383–2390. doi: 10.1016/j.biomaterials.2013.11.083

Toh, W. S., Lai, R. C., Hui, J. H. P., and Lim, S. K. (2017). MSC exosome as a cell-free MSC therapy for cartilage regeneration: implications for osteoarthritis treatment. *Semin. Cell Dev. Biol.* 67, 56–64. doi: 10.1016/j.semcdb.2016.11.008

Uemura, R., Xu, M., Ahmad, N., and Ashraf, M. (2006). Bone marrow stem cells prevent left ventricular remodeling of ischemic heart through paracrine signaling. *Circ. Res.* 98, 1414–1421. doi: 10.1161/01.res.0000225952.61196.39

Valadi, H., Ekström, K., Bossios, A., Sjöstrand, M., Lee, J. J., and Lötvall, J. O. (2007). Exosome-mediated transfer of mRNAs and microRNAs is a novel mechanism of genetic exchange between cells. *Nat. Cell Biol.* 9, 654–659. doi: 10.1038/ncb1596

van der Pol, E., Böing, A. N., Harrison, P., Sturk, A., and Nieuwland, R. (2012). Classification, functions, and clinical relevance of extracellular vesicles. *Pharmacol. Rev.* 64, 676–705. doi: 10.1124/pr.112.005983

van Niel, G., Raposo, G., Candalh, C., Boussac, M., Hershberg, R., Cerf-Bensussan, N., et al. (2001). Intestinal epithelial cells secrete exosome-like vesicles. *Gastroenterology* 121, 337–349. doi: 10.1053/gast.2001.26263

Wang, C., Chen, L., Huang, Y., Li, K., Jinye, A., Fan, T., et al. (2019a). Exosome-delivered TRPP2 siRNA inhibits the epithelial-mesenchymal transition of FaDu cells. *Oncol. Lett.* 17, 1953–1961. doi: 10.3892/ol.2018.9752

Wang, C., Zhu, G., He, W., Yin, H., Lin, F., Gou, X., et al. (2019b). BMSCs protect against renal ischemia-reperfusion injury by secreting exosomes loaded with miR-199a-5p that target BIP to inhibit endoplasmic reticulum stress at the very early reperfusion stages. *FASEB J.* 33, 5440–5456. doi: 10.1096/fj.201801821R

Wang, J., Liu, Y., Sun, W., Zhang, Q., Gu, T., and Li, G. (2018). Plasma exosomes as novel biomarker for the early diagnosis of gastric cancer. *Cancer Biomark. Sec. A of Dis. Mark.* 21, 805–812. doi: 10.3233/CBM-170738

Wang, T., Shigdar, S., Shamaileh, H. A., Gantier, M. P., Yin, W., Xiang, D., et al. (2017). Challenges and opportunities for siRNA-based cancer treatment. *Cancer Lett.* 387, 77–83. doi: 10.1016/j.canlet.2016.03.045

Wang, X., Wei, W., Krzeszinski, J. Y., Wang, Y., and Wan, Y. (2015). A liver-bone endocrine relay by igfbp1 promotes osteoclastogenesis and mediates fgf21-induced bone resorption. *Cell Metab.* 22, 811–824. doi: 10.1016/j.cmet.2015.09.010

Waning, D. L., Guise, T. A., and Mohammad, K. S. (2019). A "Connexin" responsible for the fatal attraction of cancer to bone. *Cell Metab.* 29, 6–8. doi: 10.1016/j.cmet.2018.12.014

Warshauer, J. T., Bluestone, J. A., and Anderson, M. S. (2020). New frontiers in the treatment of type 1 diabetes. *Cell Metab.* 31, 46–61. doi: 10.1016/j.cmet.2019.11.017

Whitham, M., Parker, B. L., Friedrichsen, M., Hingst, J. R., Hjorth, M., Hughes, W. E., et al. (2018). Extracellular vesicles provide a means for tissue crosstalk during exercise. *Cell Metab* 27, 237–251. doi: 10.1016/j.cmet.2017.12.001

Wu, M., Ouyang, Y., Wang, Z., Zhang, R., Huang, P. H., Chen, C., et al. (2017). Isolation of exosomes from whole blood by integrating acoustics and microfluidics. *Proc. Natl. Acad. Sci. U.S.A.* 114, 10584–10589. doi: 10.1073/pnas.1709210114

Wu, P., Zhang, B., Shi, H., Qian, H., and Xu, W. (2018). MSC-exosome: a novel cell-free therapy for cutaneous regeneration. *Cytotherapy* 20, 291–301. doi: 10.1016/j.jcyt.2017.11.002

Xie, H., Cui, Z., Wang, L., Xia, Z., Hu, Y., Xian, L., et al. (2014). PDGF-BB secreted by preosteoclasts induces angiogenesis during coupling with osteogenesis. *Nat. Med.* 20, 1270–1278. doi: 10.1038/nm.3668

Xie, X., Wang, Y., Zhao, C., Guo, S., Liu, S., Jia, W., et al. (2012). Comparative evaluation of MSCs from bone marrow and adipose tissue seeded in PRP-derived scaffold for cartilage regeneration. *Biomaterials* 33, 7008–7018. doi: 10.1016/j.biomaterials.2012.06.058

Xie, Y., Chen, Y., Zhang, L., Ge, W., and Tang, P. (2017). The roles of bone-derived exosomes and exosomal microRNAs in regulating bone remodelling. *J. Cell. Mol. Med.* 21, 1033–1041. doi: 10.1111/jcmm.13039

Xin, H., Li, Y., Buller, B., Katakowski, M., Zhang, Y., Wang, X., et al. (2012). Exosome-mediated transfer of miR-133b from multipotent mesenchymal stromal cells to neural cells contributes to neurite outgrowth. *Stem Cells* 30, 1556–1564. doi: 10.1002/stem.1129

Xin, H., Li, Y., Liu, Z., Wang, X., Shang, X., Cui, Y., et al. (2013). MiR-133b promotes neural plasticity and functional recovery after treatment of stroke

with multipotent mesenchymal stromal cells in rats via transfer of exosome-enriched extracellular particles. *Stem Cells* 31, 2737–2746. doi: 10.1002/stem.1409

Xu, J. F., Yang, G. H., Pan, X. H., Zhang, S. J., Zhao, C., Qiu, B. S., et al. (2014). Altered microRNA expression profile in exosomes during osteogenic differentiation of human bone marrow-derived mesenchymal stem cells. *PLoS One* 9:e114627. doi: 10.1371/journal.pone.0114627

Yang, L., Xie, G., Fan, Q., and Xie, J. (2010). Activation of the hedgehog-signaling pathway in human cancer and the clinical implications. *Oncogene* 29, 469–481. doi: 10.1038/onc.2009.392

Yang, M., Guo, Q., Peng, H., Xiao, Y. Z., Xiao, Y., Huang, Y., et al. (2019). Krüppel-like factor 3 inhibition by mutated lncRNA results in human high bone mass syndrome. *J. Exp. Med.* 216, 1944–1964. doi: 10.1084/jem.20181554

Yoshida, M., Satoh, A., Lin, J. B., Mills, K. F., Sasaki, Y., Rensing, N., et al. (2019). Extracellular vesicle-contained enampt delays aging and extends lifespan in mice. *Cell Metab.* 30, 329–342. doi: 10.1016/j.cmet.2019.05.015

Yu, B., Kim, H. W., Gong, M., Wang, J., Millard, R. W., Wang, Y., et al. (2015). Exosomes secreted from GATA-4 overexpressing mesenchymal stem cells serve as a reservoir of anti-apoptotic microRNAs for cardioprotection. *Int. J. Cardiol.* 182, 349–360. doi: 10.1016/j.ijcard.2014.12.043

Yu, Y., Newman, H., Shen, L., Sharma, D., Hu, G., Mirando, A. J., et al. (2019). Glutamine Metabolism Regulates Proliferation and Lineage Allocation in Skeletal Stem Cells. *Cell Metab.* 29, 966.e4–978.e4. doi: 10.1016/j.cmet.2019.01.016

Zhang, H., and Lyden, D. (2019). Asymmetric-flow field-flow fractionation technology for exomere and small extracellular vesicle separation and characterization. *Nat. Protoc.* 14, 1027–1053. doi: 10.1038/s41596-019-0126-x

Zhang, J., Guan, J., Niu, X., Hu, G., Guo, S., Li, Q., et al. (2015). Exosomes released from human induced pluripotent stem cells-derived MSCs facilitate cutaneous wound healing by promoting collagen synthesis and angiogenesis. *J. Transl. Med.* 13:49. doi: 10.1186/s12967-015-0417-0

Zhang, J., Liu, X., Li, H., Chen, C., Hu, B., Niu, X., et al. (2016). Exosomes/tricalcium phosphate combination scaffolds can enhance bone regeneration by activating the PI3K/Akt signaling pathway. *Stem Cell Res. Ther.* 7:136. doi: 10.1186/s13287-016-0391-3

Zhang, W. B., Zhong, W. J., and Wang, L. (2014). A signal-amplification circuit between miR-218 and Wnt/β-catenin signal promotes human adipose tissue-derived stem cells osteogenic differentiation. *Bone* 58, 59–66. doi: 10.1016/j.bone.2013.09.015

Zhao, C., Irie, N., Takada, Y., Shimoda, K., Miyamoto, T., Nishiwaki, T., et al. (2006). Bidirectional ephrinB2-EphB4 signaling controls bone homeostasis. *Cell Metab.* 4, 111–121. doi: 10.1016/j.cmet.2006.05.012

Zhao, C., Sun, W., Zhang, P., Ling, S., Li, Y., Zhao, D., et al. (2015). miR-214 promotes osteoclastogenesis by targeting Pten/PI3k/Akt pathway. *RNA Biol.* 12, 343–353. doi: 10.1080/15476286.2015.1017205

Zhu, W., Huang, L., Li, Y., Zhang, X., Gu, J., Yan, Y., et al. (2012). Exosomes derived from human bone marrow mesenchymal stem cells promote tumor growth in vivo. *Cancer Lett.* 315, 28–37. doi: 10.1016/j.canlet.2011.10.002

Zou, W., Greenblatt, M. B., Brady, N., Lotinun, S., Zhai, B., de Rivera, H., et al. (2013). The microtubule-associated protein DCAMKL1 regulates osteoblast function via repression of Runx2. *J. Exp. Med.* 210, 1793–1806. doi: 10.1084/jem.20111790

Conflict of Interest: The authors declare that the research was conducted in the absence of any commercial or financial relationships that could be construed as a potential conflict of interest.

Copyright © 2020 Lyu, Xiao, Guo, Huang and Luo. This is an open-access article distributed under the terms of the Creative Commons Attribution License (CC BY). The use, distribution or reproduction in other forums is permitted, provided the original author(s) and the copyright owner(s) are credited and that the original publication in this journal is cited, in accordance with accepted academic practice. No use, distribution or reproduction is permitted which does not comply with these terms.

frontiers in Cell and Developmental Biology

REVIEW
published: 14 May 2020
doi: 10.3389/fcell.2020.00325

Pros and Cons of Denosumab Treatment for Osteoporosis and Implication for RANKL Aptamer Therapy

Ning Zhang[1†], Zong-Kang Zhang[1†], Yuanyuan Yu[2], Zhenjian Zhuo[1], Ge Zhang[2] and Bao-Ting Zhang[1*]*

[1] School of Chinese Medicine, Faculty of Medicine, The Chinese University of Hong Kong, Hong Kong, China, [2] Law Sau Fai Institute for Advancing Translational Medicine in Bone and Joint Diseases, School of Chinese Medicine, Hong Kong Baptist University, Hong Kong, China

OPEN ACCESS

Edited by:
Changjun Li,
Central South University, China

Reviewed by:
Liangliang Xu,
Guangzhou University of Chinese Medicine, China
Sakamuri V. Reddy,
Medical University of South Carolina, United States

***Correspondence:**
Ge Zhang
zhangge@hkbu.edu.hk
Bao-Ting Zhang
zhangbaoting@cuhk.edu.hk

[†] These authors have contributed equally to this work

Specialty section:
This article was submitted to Molecular Medicine, a section of the journal Frontiers in Cell and Developmental Biology

Received: 01 March 2020
Accepted: 16 April 2020
Published: 14 May 2020

Citation:
Zhang N, Zhang Z-K, Yu Y, Zhuo Z, Zhang G and Zhang B-T (2020) Pros and Cons of Denosumab Treatment for Osteoporosis and Implication for RANKL Aptamer Therapy. Front. Cell Dev. Biol. 8:325. doi: 10.3389/fcell.2020.00325

Osteoporosis is age-related deterioration in bone mass and micro-architecture. Denosumab is a novel human monoclonal antibody for osteoporosis. It is a receptor activator of nuclear factor-κB ligand (RANKL) inhibitor, which binds to and inhibits osteoblast-produced RANKL, in turn reduces the binding between RANKL and osteoclast receptor RANK, therefore decreases osteoclast-mediated bone resorption and turnover. However, adverse events have also been reported after denosumab treatment, including skin eczema, flatulence, cellulitis and osteonecrosis of the jaw (ONJ). Extensive researches on the mechanism of adverse reactions caused by denosumab have been conducted and may provide new insights into developing new RANKL inhibitors that achieve better specificity and safety. Aptamers are single-stranded oligonucleotides that can bind to target molecules with high specificity and affinity. They are screened from large single-stranded synthetic oligonucleotides and enriched by a technology named SELEX (systematic evolution of ligands by exponential enrichment). With extra advantages such as high stability, low immunogenicity and easy production over antibodies, aptamers are hypothesized to be promising candidates for therapeutic drugs targeting RANKL to counteract osteoporosis. In this review, we focus on the pros and cons of denosumab treatment in osteoporosis and the implication for novel aptamer treatment.

Keywords: osteoporosis, denosumab, RANKL, aptamer, SELEX

INTRODUCTION

Osteoporosis is a disease in which the microstructure of bone deteriorates, bone mass is low, and bone fragility increases, therefore the risk of fracture increases in affected people (Black and Rosen, 2016; Eastell et al., 2016). Due to bone metabolism disorders caused by the rapid decline of estrogen levels in the body, osteoporosis is most common in postmenopausal women. Increasing bone turnover and reduced bone density result in severe bone loss and ultimately develop into osteoporosis (Deeks, 2018). The number of people who suffered from osteoporosis was approximately two hundred million in the world (Sözen et al., 2017). The female to male ratio

is 80 to 20%, while it was reported that male patients developed other clinical complications related to osteoporosis (Alswat, 2017). As a common symptom of osteoporosis, osteoporotic fractures can result in further disability and early mortality. Osteoporotic fractures occur most frequently in the vertebrae (spine), carpals, hips, pelvis and upper arms (Warriner et al., 2011). Many patients require long-term nursing home care, which would leave a huge burden on the patient's family and society. Total costs of treatment for osteoporotic fractures were estimated to be 17 billion in 2003 in the United States, and the figure is predicted to surpass 25 billion by the year 2025 (Cauley, 2013). Therefore, a lot of in-depth researches have been conducted to reveal the underlying mechanisms of osteoporosis and identify the potential therapeutic targets.

Bone morphogenesis and remodeling depend on the combined activities of osteoblasts-mediated bone formation and osteoclasts-mediated bone resorption (Zhang et al., 2014). The process is a dynamic process throughout the entire life of the individual, and plenty of systemic and local regulators of osteocytes are involved in bone remodeling (Miller, 2009). This mechanism not only protects the integrity of the bones but also makes the bones an adequate reservoir of calcium and phosphorus. According to the functions of osteoblasts and osteoclasts, bone remodeling can be divided into three primary stages. The initial stage is the differentiation of osteoclast precursor cells, activation of osteoclasts and bone resorption. Osteoclast apoptosis occurs in the intermediate stage and the meantime, osteoblasts accumulate and differentiate to form new bone in the bone lacuna. During the final stage, bone resorption is completed through osteogenesis and mineralization (Lemaire et al., 2004). Even in healthy bodies, osteoclasts-mediated bone resorption takes only a few weeks, while osteoblasts-mediated bone formation takes months (Sims and Martin, 2014). Therefore, the key to preventing bone loss is to inhibit the function of osteoclasts. The control and regulation of osteoclast activation and differentiation is achieved by a family of biologically related TNF receptor (TNFR)/TNF-like proteins: osteoprotegerin (OPG), the receptor activator of NF-κB (RANK), and RANK ligand (RANKL) (Lacey et al., 1998; Faienza et al., 2018).

Early animal experiments and clinical trials show that RANKL-targeted therapies have the potential to treat diseases relevant to osteoclast-mediated bone loss. RANKL inhibition results in a decrease in osteoclastogenesis and osteoclast activity, thereby reducing bone resorption (Bekker et al., 2004). Denosumab, a targeted antibody that binds and inhibits RANKL to reduce bone resorption, is approved by the U.S. Food and Drug Administration (FDA) for the treatment of osteoporosis in postmenopausal (PM) women with a high fracture risk (Dore, 2011; Scott and Muir, 2011). The European Medicines Agency has also declared the marketing authorization valid of denosumab for the treatment of osteoporosis in PM women at increased risk of fractures (European Medicines Agency, 2013). Apart from antibodies, some agents targeting RANKL have also been investigated to interact with RANKL specifically and interfere with its interaction with RANK (Sisay et al., 2017). Aptamers, small single-stranded oligonucleotides, are capable of binding target molecules with high affinity and specificity (Burnett and Rossi, 2012; Song et al., 2012). They are nucleotide analogs of antibodies, but it is much easier and cheaper to generate aptamers than antibodies (Kulbachinskiy, 2007; Lakhin et al., 2013). Moreover, aptamers are neither immunogenic nor toxic (Bouchard et al., 2010). Aptamer-targeted therapeutic drugs have been used in the treatment of various cancers, macular degeneration, vascular hemophilia and diabetes, which have shown excellent application prospects in the field of biomedicine (Yang et al., 2011; Cibiel et al., 2012).

This review focuses on the advantages and disadvantages of the use of the anti-RANKL antibody, denosumab, in the treatment of PM osteoporosis. Besides, the prospect and challenge of aptamers targeting RANKL as a therapeutic strategy for osteoporosis are discussed.

RANKL AS A PROMISING THERAPEUTIC TARGET FOR OSTEOPOROSIS

Receptor activator of nuclear factor-κB ligand is one of the tumor necrosis factor (TNF) superfamily members, and it is up-regulated in postmenopausal women, which can be modified mainly by estrogen supplementation (Eghbali-Fatourechi et al., 2003). RANKL is a homotrimeric transmembrane protein expressed by osteocytes, macrophages, osteoblasts, bone marrow stem cells and activated T lymphocytes (Lacey et al., 2012; Mori et al., 2013). It owns a carboxy-terminal domain that is homologous to TNF, and it is expressed on the cell surface of osteoblasts, resulting in cell-to-cell-dependent contact with osteoclast precursor cells to promote the formation of osteoclasts. RANKL also inhibits osteoclast apoptosis. RANK, the signaling receptor of RANKL, is expressed on the surface of osteoclast precursor cells, mature osteoclasts, dendritic cells and other tumor cells. It initiates osteoclastogenesis (**Figure 1**) by combining with carboxy-terminal domains of RANKL to trigger intracellular signaling cascades, which causes osteoclast precursors to evolve into multinucleated cells and differentiate into mature osteoclasts (Zaidi et al., 2003; Park et al., 2017).

Osteoprotegerin, a soluble decoy receptor, competitively binds to the trimer RANKL and negatively regulates the interaction of RANKL-RANK, thereby inhibiting the differentiation of osteoclast precursors (**Figure 1**) and inducing osteoclast apoptosis (Simonet et al., 1997). It is a soluble secreted protein lacking a transmembrane domain and a cytoplasmic domain, principally expressed by osteoblasts, bone marrow stromal cells, mature B cells and macrophages, and regulating the critical balance between bone formation and bone resorption (Yasuda et al., 1998). The amino-terminus of OPG owns a cysteine-rich region, while the carboxy-terminus forms a dimer that competitively binds to the trimer RANKL, resulting in preventing RANKL-induced generation and maturation of osteoclasts. It has been found that OPG binds RANKL approximately 500 times higher affinity than RANK (Infante et al., 2019). OPG-knockout mice resulted in a significant reduction in bone mass, while overexpression of OPG leads to a decrease in the number of osteoclasts and a noticeable increase in

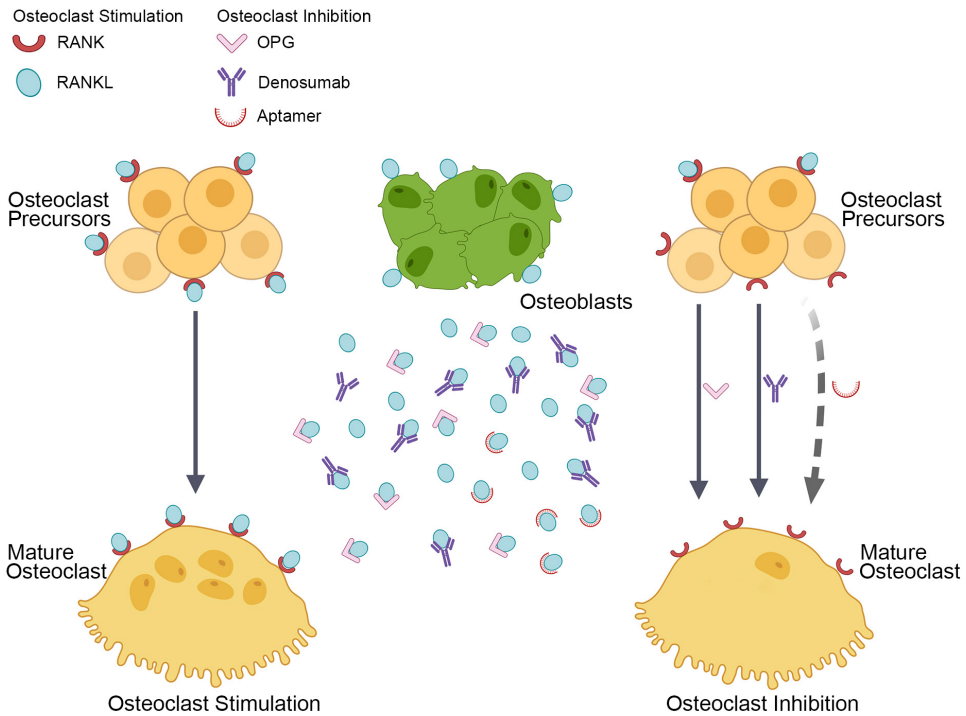


FIGURE 1 | Current and hypothetical RANKL inhibitors to suppress osteoclastogenesis. Osteoblasts produce RANKL that binds its receptor, RANK, which is located on the surface of osteoclasts and their precursors. This binding stimulates the differentiation of preosteoclasts into multinucleated and mature osteoclasts (as shown by the solid arrow in the left). The process is prevented naturally by OPG and pharmacologically by denosumab, thereby inhibiting osteoclast formation, activity, and survival (as shown by solid arrows in the right). We hypothesized a RANKL inhibitor, the aptamer, which may specifically target RANKL and inhibit osteoclastogenesis (as shown by the dotted arrow in the right).

bone mass (Nakamura et al., 2003). Therefore, the OPG/RANKL ratio is closely related to osteoclast formation and ultimately affects bone density and bone strength. Genetic mutations in the human RANKL gene and RANKL knockout mice have been associated with osteoclasts deficiency and severe osteosclerosis (Sobacchi et al., 2007; Crockett et al., 2011).

In summary, RANKL plays a vital role in the process of osteoclast differentiation. Besides, RANKL can also activate mature osteoclasts, prolong their survival time and enhance bone resorption capacity. Since the use of related antibodies, peptides and natural compounds to inhibit RANKL can prevent the formation and function of osteoclasts, RANKL is regarded as a potential target for the treatment of osteoporosis.

CURRENT THERAPEUTIC STRATEGIES TARGETING RANKL

At present, it has been found that a variety of natural and synthetic drugs can affect the function of osteoclasts through the OPG/RANK/RANKL signaling pathway, such as recombinant human osteoprotegerin, strontium compounds and human RANKL monoclonal antibodies.

Recombinant human OPG (rhOPG) was the first RANKL inhibitor that has been examined in humans (Dempster et al., 2012). It is a modified natural OPG, which makes it more biologically active and own a longer half-life. Studies have shown that rhOPG can significantly inhibit osteoclast activity and reduce bone resorption, resulting in accelerating bone maturation and increasing bone mineral density (BMD). A clinical trial demonstrated the validity of RANKL antagonization to reduce bone turnover in humans by subcutaneous injections of rhOPG (Bekker et al., 2001). RhOPG is reported to prevent bone loss diseases and participate in inhibiting alveolar bone absorption during periodontitis (Jin et al., 2007). Nonetheless, long-term medication may cause immune responses and safety concerns due to its massive molecular weight.

The trace element strontium has the dual effects of preventing bone resorption and promoting bone formation. Studies have shown that strontium mainly functions through the OPG/RANK/RANKL signaling pathway, resulting in decreased bone resorption (Mi et al., 2017). Strontium ranelate is a representative drug of strontium compounds, and it contains two strontium atoms (Cianferotti et al., 2013). The apparent increase of OPG plays a vital role in the treatment of osteoporosis with strontium ranelate and could be used as a convincing measurement to examine the therapeutic effect.

Another therapeutic strategy that explicitly targets RANKL is the use of an anti-RANKL antibody. Denosumab, a fully human monoclonal IgG2 antibody, binds with RANKL selectively and displays high affinity, which binds and neutralizes the activity of human RANKL to inhibit bone resorption and may also prevent

progression of bone erosion (Kostenuik et al., 2009). At a quite low concentration, denosumab can reduce the bone rebuilding cycle, inhibit the action of osteoclasts, and increase bone density and strength. The effect of denosumab treatment on fracture prevention in women with postmenopausal osteoporosis was evaluated in an international, multicenter, randomized, double-blind, and placebo-controlled study known as Fracture Reduction Evaluation of Denosumab in Osteoporosis Every 6 Months (FREEDOM) (Cummings et al., 2009). Denosumab was effective in reducing fracture risk in PM women with osteoporosis in the FREEDOM study.

DENOSUMAB: CLINICAL DATA AND EFFICACY EVALUATION

Denosumab is the first and only approved antagonist targeting RANKL, which can effectively block the interaction between RANKL and RANK, thereby inhibiting the formation of osteoclasts and enhancing bone strength. Denosumab could be administered once in 6 months by a subcutaneous injection of 60 mg each time. Large-scale clinical trials have shown that it can significantly improve bone turnover markers (BTM). Bone-resorption markers of collagen telopeptide of type 1 collagen (CTX) and procollagen type 1 N-terminal propeptide (PINP) were significantly reduced, while the BMD of the lumbar spine and hip joints was increased after Denosumab treatment (Cummings et al., 2009; Eastell et al., 2011). The FREEDOM study included 7,868 postmenopausal osteoporosis patients in clinical trials. According to the clinical data, denosumab significantly eliminated the risk of new vertebral fracture by 68%, non-vertebral fracture by 20% and hip fracture by 40% relative to placebo across 3 years (Cummings et al., 2009).

Similarly, another research reported that the denosumab group has a significant lower incidence of vertebral fractures and low-energy non-vertebral fractures compared to the placebo group, regardless of conditions like ages, previous fracture status and other anti-osteoporotic treatments (Palacios et al., 2015). A 7-year long-term study found that the effect of denosumab on increasing bone density had sustained through years. Patients who received long-term treatment of denosumab maintained a low incidence of fractures and reduced overall and non-vertebral fracture rates by 38 and 46% compared to placebo (Bone et al., 2017). At the end of the research, the BMD of the long-term group (up to 10 years of denosumab treatment) substantially increased from the original baseline. The increments of each site were better than those of the 7-year treatment groups (e.g., lumbar BMD increased by 21.7 and 16.5%) (Bone et al., 2017). Furthermore, bone strength increased consistently with BMD at various sites under denosumab treatment (Simon et al., 2013; Zebaze et al., 2016).

The increase in bone density could be indirectly reflected in the morphology of bone cortex and cancellous bone, which showed instant improvement. A computed tomography scanning showed that denosumab reduced the cortical porosity of patients and increased hip joint bone strength by 7.9% (Zebaze et al., 2016). The FREEDOM trial confirmed the effect of denosumab on reducing fracture rates and increasing bone density. Compared with placebo, denosumab significantly increased BMD in the lumbar spine, hip joint, femoral neck, femoral tuberosity, and distal radius 1 month after treatment, and the effect continued to increase during the subsequent 36 months. A series of controlled clinical trials showed that denosumab possessed advantages over bisphosphonates in promoting bone density in postmenopausal patients with low bone mass or osteoporosis. Denosumab has shown a gradual upward trend and long-term potential for the treatment of osteoporosis and other bone metabolic diseases (Miller et al., 2016; Anastasilakis et al., 2018). Despite numerous advantages of denosumab, it has only been on the market in recent years, and its clinical efficacy remains to be scrutinized.

THE POTENTIAL PROBLEMS RELATED TO THE ANTI-RANKL MONOCLONAL ANTIBODY, DENOSUMAB

One of the disadvantages related to denosumab is that there are some adverse reactions after medication. Since RANKL is also abundantly expressed by dendritic cells and activated T lymphocytes, the antagonistic effect caused by denosumab could affect the immune system and result in individual risk of adverse events (Walsh and Choi, 2014). In the FREEDOM study, the adverse events in the denosumab treatment group included skin eczema (3%), flatulence (2.2%), and cellulitis (0.3%) (Cummings et al., 2009; Anastasilakis et al., 2012). Although the overall incidence of adverse events in the denosumab treatment group was close to that in the placebo group, some numerical imbalances showed that the majority of adverse events was related to specific ones, including skin infections (Watts et al., 2012). Denosumab could amplify skin allergies and inflammatory responses rather than increase susceptibility to infection (Ferrari-Lacraz and Ferrari, 2011). Since the interaction between RANK and RANKL was also essential in the development of immunocytes (Anastasilakis et al., 2012), the effect of denosumab of immunogenicity should be further investigated during clinical trial, even though the higher incidence of adverse events has not been discovered thus far during long-term (7–10 years) treatment of denosumab (Bone et al., 2017).

Patients treated with denosumab are also at risk of osteonecrosis of the jaw (ONJ). A systematic review suggested that 1.7% of patients suffered ONJ during tumor treatment with denosumab (Boquete-Castro et al., 2016). A study focusing on denosumab treatment in newly diagnosed multiple myeloma patients showed that the incidence of ONJ was higher in denosumab treatment groups than in earlier solid tumor bone-related events (Morgan et al., 2010), indicating that the higher incidence might be related to more prolonged exposure to the therapies in the trial (Raje et al., 2018). Therefore, those who have undergone invasive dental surgeries, installed dentures or other implants, and have poor oral hygiene should be alerted to the risk of ONJ and are strongly advised to receive clinical examinations regularly during medication (Boquete-Castro et al., 2016). When taking denosumab, those who are already having

ONJ or who are most likely to develop ONJ should necessarily be prescribed by a dentist. Excessive dental surgery may worsen the situation. Therefore, the benefit-risk assessment can be performed according to the patient's conditions to determine whether denosumab needs to be discontinued.

Since denosumab forcefully inhibited bone turnover, serum calcium levels were evaluated carefully in FREEDOM (Dempster et al., 2012). Although the overall incidence of hypocalcemia during denosumab treatment is low (Jamal et al., 2011), for patients with renal insufficiency, blood calcium levels should be monitored and corrected during treatment. Simultaneously, an adequate supplement of calcium and vitamin D is recommended (Body et al., 2015). Other studies have shown that despite calcium supplements and calcitriol, approximately 14% of patients developed varying degrees of hypocalcemia within 6 months under denosumab treatment (Huynh et al., 2016). Severe renal insufficiency is one of the dominating risk factors.

While the mechanisms involved in the adverse effects of denosumab remains unknown so far, further research of the pathogenesis may give insights into the accurate selection of next-generation inhibitors.

APTAMER: A PROMISING THERAPEUTIC STRATEGY FOR OSTEOPOROSIS

Although the therapeutic efficacy of denosumab has been studied widely and thoroughly, the benefit/risk profile of denosumab still needs to be further studied in clinical trials. Other alternative agents targeting RANKL with low-cost and high safety for the treatment of osteoporosis and other bone-related diseases have attracted a lot of attention. Among all of these potential agents, aptamers are promising candidates due to their unique properties and promising applications.

Aptamers are small single-stranded oligonucleotides, which could specifically bind with target molecules. Aptamers are screened from oligonucleotide libraries, which generally consists of a fixed sequence at both ends of the oligonucleotide chain and a random sequence with a length of 20–60 bp in the middle, using a gold-standard methodology named SELEX (systemic evolution of ligands by exponential enrichment) (Blank and Blind, 2005). Since there are a large number of permutations and combinations of nucleotides in the intermediate sequence, different spatial conformations can be formed, thereby nearly all of the spatial structures in nature that may interact with target molecules are simulated (Tsao et al., 2017).

A comparison between aptamers and antibodies exhibited distinct advantages of aptamers. Compared to antibodies, (i) aptamers are prepared through *in vitro* screening and can be produced using cell-free chemical synthesis (ii), aptamers are not immunogenic and can be used for *in vivo* diagnosis or treatment (iii) they are smaller than antibodies and can be used for intracellular diagnosis and treatment and (iv) chemically synthesized aptamers own high accuracy, reliable repeatability, and few variations between batches in production (Song et al., 2012). Reporter genes such as fluorescein or biotin can be accurately combined with aptamers at specific sites for the research interests (Reverdatto et al., 2015). In summary, aptamers have multiple advantages over antibodies and can be promising candidates for novel therapeutic strategies for various diseases.

To date, the U.S. FDA has approved an aptamer-based drug called Mucagen, and the other ten aptamers have been studied in clinical trials (Zhou and Rossi, 2017), which demonstrates that aptamers can also be used directly as drugs. Clinical studies of Mucagen treatment in age-related macular degeneration (AMD) patients have exhibited stabilization or improvement of vision in 80% of patients at 3 months without any toxicity (Vinores, 2006). No treatment-related side effects were noted in previous phases of clinical trials, while phase III clinical trials showed endophthalmitis occurred in 1.3% of patients, traumatic injury to the lens in 0.7%, and retinal detachment in 0.6%, accounting for the most severe adverse effects (Gragoudas et al., 2004). Collectively, Mucagen has maintained an affirmative safety profile with only occasional adverse events. Other ten aptamers have undergone clinical trials for the treatment of various conditions, including macular degeneration, coagulation, oncology, and inflammation (Zhou and Rossi, 2017). Most of them have exhibited positive efficacy and non-toxicity except one aptamer, Spiegelmer, which interferes with tumor proliferation and metastasis for cancer therapy (Roccaro et al., 2014). In the phase I clinical study of Spiegelmer for multiple myeloma treatment, several mild adverse events have been reported, including headache, nasopharyngitis, contusion and rhinitis (Vater et al., 2013). A subsequent phase II clinical trial of Spiegelmer and combination with bortezomib-dexamethasone reported adverse events of thrombocytopenia, anemia, and diarrhea (Ludwig et al., 2017). Notably, the intensities of all of the adverse events were mild and no severe adverse events were reported. Nonetheless, the safety and tolerability of aptamers are still under evaluation in the following phases of clinical trials (Kaur et al., 2018). Up to now, all of the aptamers that undergone clinical trials function as antagonists, while aptamers could also act as agonists that activate target receptors and carriers that delivering drugs to target molecules and proteins (Zhou and Rossi, 2017).

Taken together, the aptamer has the potential to be the therapeutic agent targeting RANKL to counteract osteoporosis.

APTAMER TARGETING RANKL: HYPOTHETICAL POINT AND THE TECHNICAL ASPECT

The standard methodology for aptamer selection, known as SELEX, can be separated into two alternating stages. The technology firstly designs and artificially synthesizes a random single-stranded oligonucleotide library. There is a random sequence with a length of 20 to 60 bp in the middle of the oligonucleotide chain flanked by fixed sequences of 20 to 40 bp at both ends. T7 RNA polymerase promoter sequence is added to the 5′ end, and a pair of corresponding primers are designed to amplify the original oligonucleotides by a polymerase chain reaction (PCR). In the second stage, the original synthesized library is incubated with target molecules and then filtered to

isolate target molecule-nucleic acid complexes. The interacting oligonucleotides are eluted to perform PCR amplification to obtain a sub-library, which is subjected to the subsequent round of screening (Kulbachinskiy, 2007; Marimuthu et al., 2012). The screening and amplification steps mentioned above are repeated round by round until the number of the oligonucleotides that bind to target molecules no longer increases. The screening pressure increases gradually with each SELEX round. Finally, the last screening sub-library obtained is the so-called aptamer library. It is cloned and sequenced to prepare a single aptamer with high affinity for target molecules for research.

Like antibodies targeting specific proteins, aptamer generation in most situations requires the availability of purified target molecules. The whole cell-based SELEX protocol (Cell-SELEX) is used to select aptamers that recognize cell-surface proteins (Sun et al., 2011; Ye et al., 2012). Cell-SELEX allows proteins or other markers on the cell surface to be recognized at their natural conformation or in a form that has been post-translationally modified (Zhou and Rossi, 2017). According to the features of the technology, Cell-SELEX typically includes positive selection and counter selection. A negative selection could be achieved with a homologous cell type or cell line negative for the target marker. The main adverse events of denosumab derive from its ability to bind RANKL located on immune cells, which could inspire researchers to design a selection scheme to avoid those non-target cells. The generation of antibodies could not circumvent the issue, while the selection of aptamers could help overcome the obstacle by setting positive targets and negative targets. When screening aptamers targeting RANKL, aptamers binding to free RANKL in the circulatory system instead of RNAKL located on the cell surface are expected (**Figure 2**). Therefore, the combination of negative selection with RANKL on the surface of immunocytes and positive selection RANKL in the circulatory system will provide potential specific aptamers and facilitate the development of final products that we want.

Another issue about aptamers comes to their existing time in the blood system, which determines the pharmaceutical effects of these agents. Denosumab has an approximate molecular weight of 147 kDa and is produced in genetically engineered mammalian (Chinese hamster ovary) cells. While aptamers usually have a molecular weight ranging from 5 to 15 kDa, and they can be quickly metabolized by renal clearance (Lakhin et al., 2013). At present, aptamer-derived drugs are generally administered by intravenous injection, subcutaneous injection or intravitreal injection (Bouchard et al., 2010). The majority of the therapeutic targets for aptamer drugs are proteins located on cell surfaces, in blood or interstitial fluid. Unmodified aptamers are probably degraded by nucleases rapidly before reaching target cells, and released nucleosides are metabolized by endogenous purines and pyrimidines (Bouchard et al., 2010). The half-life of aptamers in the blood is as short as approximately 2 min, resulting in the pharmacokinetics of aptamer drugs has become one of the main bottlenecks in drug development (Jacobson et al., 2015). It has been demonstrated that conjugating a particular molecule with aptamers could increase the molecular weight and prolong the bloodstream circulation time. Attaching fluorine or oxygen methyls to glucosides is the most widely used modification to improve the pharmacokinetics of the aptamer (Keefe and Cload, 2008). Molecules owning high molecular weight, like polyethene glycol (PEG) or cholesterol (Burmeister et al., 2005), could also be

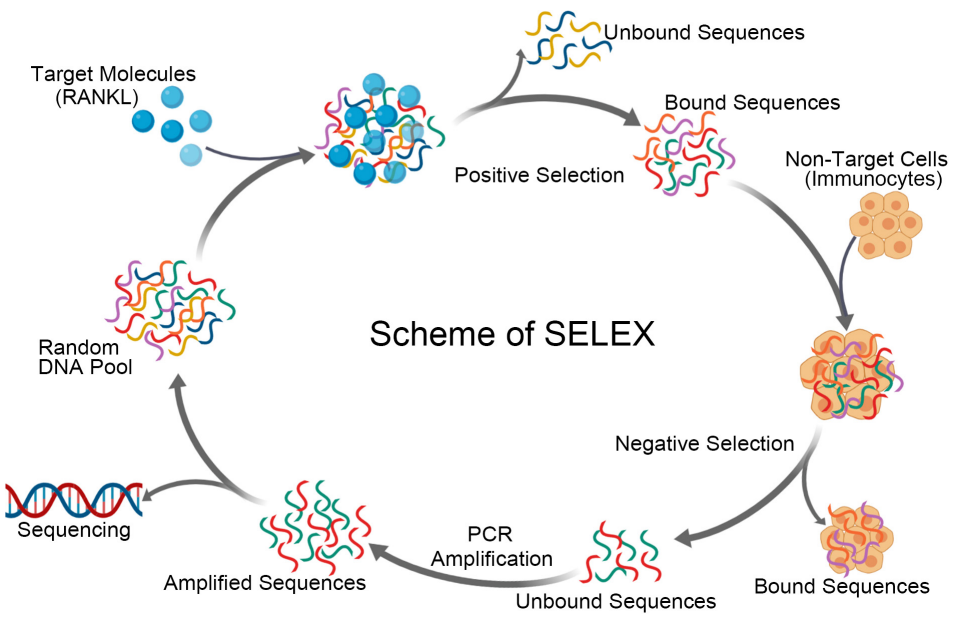


FIGURE 2 | Schematic representation of aptamer selection for RANKL using SELEX strategy. The process of screening aptamers for RANKL by SELEX includes positive selection and negative selection. A DNA library is incubated with target molecules, RANKL, in the positive selection. The bound sequences are eluted and collected, prior to be incubated with non-target cells. The bound sequences are removed and discarded in the counter selection. While the unbound sequences are amplified and used to initiate the next round of SELEX. The cycle is repeated several times, before the pool is sequenced and characterized.

used to reduce renal clearance and maintain their individualism. Besides, PEG-conjugated aptamers could improve the efficiency and accuracy of drug delivery to ensure they take effects at target tissues and organs (Boomer et al., 2005; Tan et al., 2011).

DISCUSSION AND PROSPECTS

Reducing the incidence of osteoporotic fractures is the main goal of osteoporosis treatment. Similar to other types of anti-osteoporosis drugs, discontinuation after a period of medication (drug holiday) is one of the approaches to alleviate the adverse effects (Anagnostis et al., 2017). However, discontinuation of treatment during denosumab has a strong relationship with multiple vertebral fractures, and the optimal duration of denosumab therapy has not been determined yet (Tsourdi et al., 2017). Therefore, drug cessation is generally discouraged unless appropriate and reliable alternatives are considered to replace the therapy (Tsourdi et al., 2017). Medical institutions, physicians and patients should take relevant potential risk courses before medication. Considering the potential side effects of long-term medication of denosumab, another promising agent, aptamer, has shown advantages and low toxicity according to clinical trials (Tan et al., 2011). Aptamers resemble antibodies in many ways, while they are sometimes superior to antibodies in terms of sensitivity, specificity and stability. They are simpler and cheaper to prepare, and there are few differences between batches. Meanwhile, aptamers are non-immunogenic and own intense tissue penetration, which makes them competitive agents in drug discovery and development. The screening technology has also been continuously developed to simplify the aptamer-generation process.

Despite considerable advantages of aptamers, they have not been commonly used up to now. Although the gold-standard methodology SELEX had been developed over 20 years ago, only one aptamer, Macugen, has been approved for therapeutic applications (Ferrara, 2004). While monoclonal antibodies were firstly developed in 1975, it was not until 1986 that the U.S. FDA approved the first antibody-based drug (Marks, 2012). The second antibody-derived drug entered the pharmaceutical market in 1994, and now about twenty antibody-based drugs are used in clinic (Lakhin et al., 2013; Santos et al., 2018). There were not many cases in which aptamers are currently used as drugs for the treatment or diagnosis of diseases. The aptamer screening technology has been continuously improved and developed in recent years, which has improved the efficiency of aptamer selection and improved its scope of application. The aptamers produced in quantity by chemical synthesis involves simple, controlled chemical reactions with a little batch-to-batch variation. Nonetheless, when it was firstly screened by SELEX and transformed into the application aspect, like diagnosis, usually the result may differ in aptamers' characteristics. One of the main obstacles to using aptamers in diagnosis is associated with the lack of standardized protocols. Aptamers screened for the same target in the same laboratory may have different characteristics, which may drive us to standardize the process of generating new aptamers. However, once the aptamer has been identified, the batch-to-batch variation during aptamer production is tiny.

On the other hand, through the in-depth research of the so-called Post-SELEX technology (Darmostuk et al., 2015), there are currently numerous methods to modify the aptamer, which aim to increase its specificity and affinity, enhance the nuclease resistance, and make it more effective. It should be noted that although the health risks of aptamers in the clinic have not been reported frequently, thus far, their health risks should not be ignored. The adverse events emerging in denosumab treatment, like ONJ and hypocalcemia, are supposed to be noticed and avoided by precautionary measures. Proof-of-concept studies and current clinical trials may help us better understand the function and potential risks of aptamers.

Methods of structural biology are extensively applied in the research of drug discovery. Once we obtain the potential aptamers toward RANKL, pharmacodynamic trials are undoubtedly to perform while the experiments to explore the specific binding sites between RANKL and the aptamer are equally essential to design. Therefore, the determination of the three-dimensional structure of the RANKL-aptamer complex is necessary to discover the accurate binding domains and help modify the aptamers more precisely. The result could be a crucial research basis for subsequent aptamer screening to provide a functional aptamer targeting RANKL for the treatment of osteoporosis.

AUTHOR CONTRIBUTIONS

NZ and Z-KZ did the literature research and wrote the manuscript. YY and ZZ helped in revising and polishing the manuscript. GZ and B-TZ revised and approved the manuscript.

FUNDING

This review was supported by the Hong Kong General Research Fund (14108816) and Science and Technology Innovation Commission of Shenzhen Municipality Funds (JCYJ20160229210357960).

REFERENCES

Alswat, K. A. (2017). Gender disparities in osteoporosis. *J. Clin. Med. Res.* 9, 382–387. doi: 10.14740/jocmr2970w

Anagnostis, P., Paschou, S. A., Mintziori, G., Ceausu, I., Depypere, H., Lambrinoudaki, I., et al. (2017). Drug holidays from bisphosphonates and denosumab in postmenopausal osteoporosis: EMAS position statement. *Maturitas* 101, 23–30. doi: 10.1016/j.maturitas.2017.04.008

Anastasilakis, A. D., Polyzos, S. A., and Makras, P. (2018). Therapy of endocrine disease: denosumab vs bisphosphonates for the treatment of postmenopausal osteoporosis. *Eur. J. Endocrinol.* 179, R31–R45. doi: 10.1530/EJE-18-0056

Anastasilakis, A. D., Toulis, K. A., Polyzos, S. A., Anastasilakis, C. D., and Makras, P. (2012). Long-term treatment of osteoporosis: safety and efficacy appraisal of denosumab. *Ther. Clin. Risk Manag.* 8, 295–306. doi: 10.2147/TCRM.S24239

Bekker, P. J., Holloway, D., Nakanishi, A., Arrighi, M., Leese, P. T., and Dunstan, C. R. (2001). The effect of a single dose of osteoprotegerin in postmenopausal women. *J. Bone Miner. Res.* 16, 348–360. doi: 10.1359/jbmr.2001.16.2.348

Bekker, P. J., Holloway, D. L., Rasmussen, A. S., Murphy, R., Martin, S. W., Leese, P. T., et al. (2004). A single-dose placebo-controlled study of AMG 162, a fully human monoclonal antibody to RANKL, in postmenopausal women. *J. Bone Miner. Res.* 19, 1059–1066. doi: 10.1359/jbmr.2005.20.12.2274

Black, D. M., and Rosen, C. J. (2016). Postmenopausal osteoporosis. *New Engl. J. Med.* 374, 254–262.

Blank, M., and Blind, M. (2005). Aptamers as tools for target validation. *Curr. Opin. Chem. Biol.* 9, 336–342.

Body, J.-J., Bone, H. G., De Boer, R. H., Stopeck, A., Van Poznak, C., Damião, R., et al. (2015). Hypocalcaemia in patients with metastatic bone disease treated with denosumab. *Eur. J. Cancer* 51, 1812–1821. doi: 10.1016/j.ejca.2015.05.016

Bone, H. G., Wagman, R. B., Brandi, M. L., Brown, J. P., Chapurlat, R., Cummings, S. R., et al. (2017). 10 years of denosumab treatment in postmenopausal women with osteoporosis: results from the phase 3 randomised FREEDOM trial and open-label extension. *Lancet Diabetes Endocrinol.* 5, 513–523. doi: 10.1016/S2213-8587(17)30138-9

Boomer, R. M., Lewis, S. D., Healy, J. M., Kurz, M., Wilson, C., and McCauley, T. G. (2005). Conjugation to polyethylene glycol polymer promotes aptamer biodistribution to healthy and inflamed tissues. *Oligonucleotides* 15, 183–195. doi: 10.1089/oli.2005.15.183

Boquete-Castro, A., Gómez-Moreno, G., Calvo-Guirado, J. L., Aguilar-Salvatierra, A., and Delgado-Ruiz, R. A. (2016). Denosumab and osteonecrosis of the jaw. A systematic analysis of events reported in clinical trials. *Clin. Oral Implants Res.* 27, 367–375. doi: 10.1111/clr.12556

Bouchard, P., Hutabarat, R., and Thompson, K. (2010). Discovery and development of therapeutic aptamers. *Annu. Rev. Pharmacol. Toxicol.* 50, 237–257. doi: 10.1146/annurev.pharmtox.010909.105547

Burmeister, P. E., Lewis, S. D., Silva, R. F., Preiss, J. R., Horwitz, L. R., Pendergrast, P. S., et al. (2005). Direct in vitro selection of a 2'-O-methyl aptamer to VEGF. *Chem. Biol.* 12, 25–33. doi: 10.1016/j.chembiol.2004.10.017

Burnett, J. C., and Rossi, J. J. (2012). RNA-based therapeutics: current progress and future prospects. *Chem. Biol.* 19, 60–71. doi: 10.1016/j.chembiol.2011.12.008

Cauley, J. A. (2013). Public health impact of osteoporosis. *J. Gerontol. Ser. A* 68, 1243–1251.

Cianferotti, L., D'Asta, F., and Brandi, M. L. (2013). A review on strontium ranelate long-term antifracture efficacy in the treatment of postmenopausal osteoporosis. *Ther. Adv. Musculoskel. Dis.* 5, 127–139. doi: 10.1177/1759720X13483187

Cibiel, A., Pestourie, C., and Ducongé, F. (2012). In vivo uses of aptamers selected against cell surface biomarkers for therapy and molecular imaging. *Biochimie* 94, 1595–1606. doi: 10.1016/j.biochi.2012.02.025

Crockett, J., Mellis, D., Scott, D., and Helfrich, M. (2011). New knowledge on critical osteoclast formation and activation pathways from study of rare genetic diseases of osteoclasts: focus on the RANK/RANKL axis. *Osteoporos. Int.* 22, 1–20. doi: 10.1007/s00198-010-1272-8

Cummings, S. R., Martin, J. S., McClung, M. R., Siris, E. S., Eastell, R., Reid, I. R., et al. (2009). Denosumab for prevention of fractures in postmenopausal women with osteoporosis. *New Engl. J. Med.* 361, 756–765. doi: 10.1056/NEJMoa0809493

Darmostuk, M., Rimpelova, S., Gbelcova, H., and Ruml, T. (2015). Current approaches in SELEX: an update to aptamer selection technology. *Biotechnol. Adv.* 33, 1141–1161. doi: 10.1016/j.biotechadv.2015.02.008

Deeks, E. D. (2018). Author correction to: denosumab: a review in postmenopausal osteoporosis. *Drugs Aging* 35, 261–261. doi: 10.1007/s40266-018-0535-5

Dempster, D. W., Lambing, C. L., Kostenuik, P. J., and Grauer, A. (2012). Role of RANK ligand and denosumab, a targeted RANK ligand inhibitor, in bone health and osteoporosis: a review of preclinical and clinical data. *Clin. Ther.* 34, 521–536. doi: 10.1016/j.clinthera.2012.02.002

Dore, R. K. (2011). The RANKL pathway and denosumab. *Rheum. Dis. Clin.* 37, 433–452. doi: 10.1016/j.rdc.2011.07.004

Eastell, R., Christiansen, C., Grauer, A., Kutilek, S., Libanati, C., McClung, M. R., et al. (2011). Effects of denosumab on bone turnover markers in postmenopausal osteoporosis. *J. Bone Miner. Res.* 26, 530–537. doi: 10.1080/14397595.2017.1308454

Eastell, R., O'Neill, T. W., Hofbauer, L. C., Langdahl, B., Reid, I. R., Gold, D. T., et al. (2016). Postmenopausal osteoporosis. *Nat. Rev. Dis. Primers* 2, 1–16.

Eghbali-Fatourechi, G., Khosla, S., Sanyal, A., Boyle, W. J., Lacey, D. L., and Riggs, B. L. (2003). Role of RANK ligand in mediating increased bone resorption in early postmenopausal women. *J. Clin. Invest.* 111, 1221–1230. doi: 10.1172/JCI17215

European Medicines Agency (2013). *European Medicines Agency. European Public Assessment Report: procedure no*. Amsterdam: European Medicines Agency.

Faienza, M. F., Chiarito, M., D'amato, G., Colaianni, G., Colucci, S., Grano, M., et al. (2018). Monoclonal antibodies for treating osteoporosis. *Expert Opin. Biol. Ther.* 18, 149–157. doi: 10.1080/14712598.2018.1401607

Ferrara, N. (2004). Vascular endothelial growth factor: basic science and clinical progress. *Endocr. Rev.* 25, 581–611. doi: 10.1210/er.2003-0027

Ferrari-Lacraz, S., and Ferrari, S. (2011). Do RANKL inhibitors (denosumab) affect inflammation and immunity? *Osteoporosis. Int.* 22, 435–446. doi: 10.1007/s00198-010-1326-y

Gragoudas, E. S., Adamis, A. P., Cunningham, E. T. Jr., Feinsod, M., and Guyer, D. R. (2004). Pegaptanib for neovascular age-related macular degeneration. *New Engl. J. Med.* 351, 2805–2816.

Huynh, A. L. H., Baker, S. T., Stewardson, A. J., and Johnson, D. F. (2016). Denosumab-associated hypocalcaemia: incidence, severity and patient characteristics in a tertiary hospital setting. *Pharmacoepidemiol. Drug Saf.* 25, 1274–1278. doi: 10.1002/pds.4045

Infante, M., Fabi, A., Cognetti, F., Gorini, S., Caprio, M., and Fabbri, A. (2019). RANKL/RANK/OPG system beyond bone remodeling: involvement in breast cancer and clinical perspectives. *J. Exp. Clin. Cancer Res.* 38:12. doi: 10.1186/s13046-018-1001-2

Jacobson, O., Yan, X., Niu, G., Weiss, I. D., Ma, Y., Szajek, L. P., et al. (2015). PET imaging of tenascin-C with a radiolabeled single-stranded DNA aptamer. *J. Nucl. Med.* 56, 616–621. doi: 10.2967/jnumed.114.149484

Jamal, S. A., Ljunggren, Ö., Stehman-Breen, C., Cummings, S. R., McClung, M. R., Goemaere, S., et al. (2011). Effects of denosumab on fracture and bone mineral density by level of kidney function. *J. Bone Miner. Res.* 26, 1829–1835. doi: 10.1002/jbmr.403

Jin, Q., Cirelli, J. A., Park, C. H., Sugai, J. V., Taba, M. Jr., Kostenuik, P. J., et al. (2007). RANKL inhibition through osteoprotegerin blocks bone loss in experimental periodontitis. *J. Periodontol.* 78, 1300–1308. doi: 10.1902/jop.2007.070073

Kaur, H., Bruno, J. G., Kumar, A., and Sharma, T. K. (2018). Aptamers in the therapeutics and diagnostics pipelines. *Theranostics* 8, 4016–4032. doi: 10.7150/thno.25958

Keefe, A. D., and Cload, S. T. (2008). SELEX with modified nucleotides. *Curr. Opin. Chem. Biol.* 12, 448–456. doi: 10.1016/j.cbpa.2008.06.028

Kostenuik, P. J., Nguyen, H. Q., McCabe, J., Warmington, K. S., Kurahara, C., Sun, N., et al. (2009). Denosumab, a fully human monoclonal antibody to RANKL, inhibits bone resorption and increases BMD in knock-in mice that express chimeric (murine/human) RANKL. *J. Bone Miner. Res.* 24, 182–195. doi: 10.1359/jbmr.081112

Kulbachinskiy, A. (2007). Methods for selection of aptamers to protein targets. *Biochemistry* 72, 1505–1518. doi: 10.1134/s000629790713007x

Lacey, D., Timms, E., Tan, H.-L., Kelley, M., Dunstan, C., Burgess, T., et al. (1998). Osteoprotegerin ligand is a cytokine that regulates osteoclast differentiation and activation. *Cell* 93, 165–176. doi: 10.1016/s0092-8674(00)81569-x

Lacey, D. L., Boyle, W. J., Simonet, W. S., Kostenuik, P. J., Dougall, W. C., Sullivan, J. K., et al. (2012). Bench to bedside: elucidation of the OPG–RANK–RANKL pathway and the development of denosumab. *Nat. Rev. Drug Discov.* 11, 401–419. doi: 10.1038/nrd3705

Lakhin, A., Tarantul, V., and Gening, L. (2013). Aptamers: problems, solutions and prospects. *Acta Naturae* 5, 34–43.

Lemaire, V., Tobin, F. L., Greller, L. D., Cho, C. R., and Suva, L. J. (2004). Modeling the interactions between osteoblast and osteoclast activities in bone remodeling. *J. Theor. Biol.* 229, 293–309. doi: 10.1016/j.jtbi.2004.03.023

Ludwig, H., Weisel, K., Petrucci, M. T., Leleu, X., Cafro, A. M., Garderet, L., et al. (2017). Olaptesed pegol, an anti-CXCL12/SDF-1 Spiegelmer, alone and with bortezomib-dexamethasone in relapsed/refractory multiple myeloma: a Phase IIa Study. *Leukemia* 31, 997–1000. doi: 10.1038/leu.2017.5

Marimuthu, C., Tang, T.-H., Tominaga, J., Tan, S.-C., and Gopinath, S. C. B. (2012). Single-stranded DNA (ssDNA) production in DNA aptamer generation. *Analyst* 137, 1307–1315. doi: 10.1039/c2an15905h

Marks, L. (2012). The birth pangs of monoclonal antibody therapeutics. *MAbs* 4, 403–412. doi: 10.4161/mabs.19909

Mi, B., Xiong, W., Xu, N., Guan, H., Fang, Z., Liao, H., et al. (2017). Strontium-loaded titania nanotube arrays repress osteoclast differentiation through multiple signalling pathways: in vitro and in vivo studies. *Sci. Rep*. 7:2328. doi: 10.1038/s41598-017-02491-9

Miller, P. D. (2009). Denosumab: anti-RANKL antibody. *Curr. Osteoporos. Rep*. 7, 18–22.

Miller, P. D., Pannacciulli, N., Brown, J. P., Czerwinski, E., Nedergaard, B. S., Bolognese, M. A., et al. (2016). Denosumab or zoledronic acid in postmenopausal women with osteoporosis previously treated with oral bisphosphonates. *J. Clin. Endocrinol. Metab.* 101, 3163–3170. doi: 10.1210/jc.2016-1801

Morgan, G. J., Davies, F. E., Gregory, W. M., Cocks, K., Bell, S. E., Szubert, A. J., et al. (2010). First-line treatment with zoledronic acid as compared with clodronic acid in multiple myeloma (MRC Myeloma IX): a randomised controlled trial. *Lancet* 376, 1989–1999. doi: 10.1016/S0140-6736(10)62051-X

Mori, G., D'Amelio, P., Faccio, R., and Brunetti, G. (2013). The interplay between the bone and the immune system. *Clin. Dev. Immunol.* 2013:720504. doi: 10.1155/2013/720504

Nakamura, M., Udagawa, N., Matsuura, S., Mogi, M., Nakamura, H., Horiuchi, H., et al. (2003). Osteoprotegerin regulates bone formation through a coupling mechanism with bone resorption. *Endocrinology* 144, 5441–5449. doi: 10.1210/en.2003-0717

Palacios, S., Kalouche-Khalil, L., Rizzoli, R., Zapalowski, C., Resch, H., Adachi, J. D., et al. (2015). Treatment with denosumab reduces secondary fracture risk in women with postmenopausal osteoporosis. *Climacteric* 18, 805–812. doi: 10.3109/13697137.2015.1045484

Park, J. H., Lee, N. K., and Lee, S. Y. (2017). Current understanding of RANK signaling in osteoclast differentiation and maturation. *Mol. Cells* 40, 706–713. doi: 10.14348/molcells.2017.0225

Raje, N., Terpos, E., Willenbacher, W., Shimizu, K., García-Sanz, R., Durie, B., et al. (2018). Denosumab versus zoledronic acid in bone disease treatment of newly diagnosed multiple myeloma: an international, double-blind, double-dummy, randomised, controlled, phase 3 study. *Lancet Oncol.* 19, 370–381. doi: 10.1016/S1470-2045(18)30072-X

Reverdatto, S., Burz, D. S., and Shekhtman, A. (2015). Peptide aptamers: development and applications. *Curr. Top. Med. Chem.* 15, 1082–1101. doi: 10.2174/1568026615666150413153143

Roccaro, A. M., Sacco, A., Purschke, W. G., Moschetta, M., Buchner, K., Maasch, C., et al. (2014). SDF-1 inhibition targets the bone marrow niche for cancer therapy. *Cell Rep.* 9, 118–128. doi: 10.1016/j.celrep.2014.08.042

Santos, M. L. d, Quintilio, W., Manieri, T. M., Tsuruta, L. R., and Moro, A. M. (2018). Advances and challenges in therapeutic monoclonal antibodies drug development. *Braz. J. Pharm. Sci.* 2018:54.

Scott, L. J., and Muir, V. J. (2011). Denosumab. *Drugs* 71, 1059–1069. doi: 10.2165/11207370-000000000-00000

Simon, J. A., Recknor, C., Moffett, A. H. Jr., Adachi, J. D., Franek, E., Lewiecki, E. M., et al. (2013). Impact of denosumab on the peripheral skeleton of postmenopausal women with osteoporosis: bone density, mass, and strength of the radius, and wrist fracture. *Menopause* 20, 130–137. doi: 10.1097/gme.0b013e318267f909

Simonet, W. S., Lacey, D. L., Dunstan, C. R., Kelley, M., Chang, M. S., Lüthy, R., et al. (1997). Osteoprotegerin: a novel secreted protein involved in the regulation of bone density. *Cell* 89, 309–319. doi: 10.1016/s0092-8674(00)80209-3

Sims, N. A., and Martin, T. J. (2014). Coupling the activities of bone formation and resorption: a multitude of signals within the basic multicellular unit. *Bonekey Rep.* 3:481. doi: 10.1038/bonekey.2013.215

Sisay, M., Mengistu, G., and Edessa, D. (2017). The RANK/RANKL/OPG system in tumorigenesis and metastasis of cancer stem cell: potential targets for anticancer therapy. *Onco Targets Ther.* 10, 3801–3810. doi: 10.2147/OTT.S135867

Sobacchi, C., Frattini, A., Guerrini, M. M., Abinun, M., Pangrazio, A., Susani, L., et al. (2007). Osteoclast-poor human osteopetrosis due to mutations in the gene encoding RANKL. *Nat. Genet.* 39, 960–962. doi: 10.1038/ng2076

Song, K.-M., Lee, S., and Ban, C. (2012). Aptamers and their biological applications. *Sensors* 12, 612–631.

Sözen, T., Özışık, L., and Başaran, N. Ç (2017). An overview and management of osteoporosis. *Eur. J. Rheumatol.* 4, 46–56.

Sun, W., Du, L., and Li, M. (2011). Advances and perspectives in cell-specific aptamers. *Curr. Pharm. Des.* 17, 80–91.

Tan, L., Neoh, K. G., Kang, E.-T., Choe, W. S., and Su, X. (2011). PEGylated Anti-MUC1 aptamer-doxorubicin complex for targeted drug delivery to MCF7 breast cancer cells. *Macromol. Biosci.* 11, 1331–1335. doi: 10.1002/mabi.201100173

Tsao, S.-M., Lai, J.-C., Horng, H.-E., Liu, T.-C., and Hong, C.-Y. (2017). Generation of aptamers from a primer-free randomized ssDNA library using magnetic-assisted rapid aptamer selection. *Sci. Rep.* 7, 45478–45478. doi: 10.1038/srep45478

Tsourdi, E., Langdahl, B., Cohen-Solal, M., Aubry-Rozier, B., Eriksen, E. F., Guañabens, N., et al. (2017). Discontinuation of denosumab therapy for osteoporosis: a systematic review and position statement by ECTS. *Bone* 105, 11–17. doi: 10.1016/j.bone.2017.08.003

Vater, A., Sahlmann, J., Kröger, N., Zöllner, S., Lioznov, M., Maasch, C., et al. (2013). Hematopoietic stem and progenitor cell mobilization in mice and humans by a first-in-class mirror-image oligonucleotide inhibitor of CXCL12. *Clin. Pharmacol. Ther.* 94, 150–157. doi: 10.1038/clpt.2013.58

Vinores, S. A. (2006). Pegaptanib in the treatment of wet, age-related macular degeneration. *Int. J. Nanomed.* 1, 263–268. doi: 10.1016/j.clinthera.2007.09.001

Walsh, M. C., and Choi, Y. (2014). Biology of the RANKL–RANK–OPG system in immunity, bone, and beyond. *Front. Immunol.* 5:511. doi: 10.3389/fimmu.2014.00511

Warriner, A. H., Patkar, N. M., Curtis, J. R., Delzell, E., Gary, L., Kilgore, M., et al. (2011). Which fractures are most attributable to osteoporosis? *J. Clin. Epidemiol.* 64, 46–53. doi: 10.1016/j.jclinepi.2010.07.007

Watts, N. B., Roux, C., Modlin, J. F., Brown, J. P., Daniels, A., Jackson, S., et al. (2012). Infections in postmenopausal women with osteoporosis treated with denosumab or placebo: coincidence or causal association? *Osteoporos. Int.* 23, 327–337. doi: 10.1007/s00198-011-1755-2

Yang, L., Zhang, X., Ye, M., Jiang, J., Yang, R., Fu, T., et al. (2011). Aptamer-conjugated nanomaterials and their applications. *Adv. Drug Deliv. Rev.* 63, 1361–1370. doi: 10.1016/j.addr.2011.10.002

Yasuda, H., Shima, N., Nakagawa, N., Mochizuki, S.-I., Yano, K., Fujise, N., et al. (1998). Identity of osteoclastogenesis inhibitory factor (OCIF) and osteoprotegerin (OPG): a mechanism by which opg/ocif inhibits osteoclastogenesis in vitro. *Endocrinology* 139, 1329–1337. doi: 10.1210/endo.139.3.5837

Ye, M., Hu, J., Peng, M., Liu, J., Liu, J., Liu, H., et al. (2012). Generating aptamers by cell-SELEX for applications in molecular medicine. *Int. J. Mol. Sci.* 13, 3341–3353. doi: 10.3390/ijms13033341

Zaidi, M., Blair, H. C., Moonga, B. S., Abe, E., and Huang, C. L. H. (2003). Osteoclastogenesis, bone resorption, and osteoclast-based therapeutics. *J. Bone Miner. Res.* 18, 599–609. doi: 10.1359/jbmr.2003.18.4.599

Zebaze, R., Libanati, C., McClung, M. R., Zanchetta, J. R., Kendler, D. L., Høiseth, A., et al. (2016). Denosumab reduces cortical porosity of the proximal femoral shaft in postmenopausal women with osteoporosis. *J. Bone Miner. Res.* 31, 1827–1834. doi: 10.1002/jbmr.2855

Zhang, M. S., Niu, F. W., Zhang, Y. J., and Li, K. (2014). Nobiletin acts as a potential anti-cancer agent against osteosarcoma by regulating ERK and AKT signaling pathways. *Bangladesh J. Pharmacol.* 9, 406–412.

Zhou, J., and Rossi, J. (2017). Aptamers as targeted therapeutics: current potential and challenges. *Nat. Rev. Drug Discov.* 16, 181–202. doi: 10.1038/nrd.2016.199

Conflict of Interest: The authors declare that the research was conducted in the absence of any commercial or financial relationships that could be construed as a potential conflict of interest.

Copyright © 2020 Zhang, Zhang, Yu, Zhuo, Zhang and Zhang. This is an open-access article distributed under the terms of the Creative Commons Attribution License (CC BY). The use, distribution or reproduction in other forums is permitted, provided the original author(s) and the copyright owner(s) are credited and that the original publication in this journal is cited, in accordance with accepted academic practice. No use, distribution or reproduction is permitted which does not comply with these terms.

frontiers in Cell and Developmental Biology

ORIGINAL RESEARCH
published: 21 May 2020
doi: 10.3389/fcell.2020.00265

Positive Effect of Gushukang on Type-H Vessel and Bone Formation

Wantao Li[1†], Xiaoqing Zhou[1†], Tiejian Jiang[1], Hongbo He[2] and Ting Wen[2]*

[1] Department of Endocrinology, Endocrinology Research Center, Xiangya Hospital of Central South University, Changsha, China, [2] Department of Orthopedic, Xiangya Hospital of Central South University, Changsha, China

Gushukang (GSK) is a traditional herbal compound used in Chinese medicine for the treatment of osteoporosis. Numerous studies have been conducted to elucidate the effects of GSK, but the mechanisms underlying these effects remain unclear. In the present study, we cultured osteoblasts and osteoclasts with low and high doses of GSK, and also administered 3-month-old mice with 4 and 8 g/kg/day of GSK solution. Gushukang was found to promote osteoblast differentiation and inhibit osteoclast differentiation *in vitro*. *In vivo*, mice in the GSK treatment groups showed an increase in bone mass, as measured by micro-computed tomography (Micro-CT). Tartrate resistant acid phosphatase (TRAP) staining and osteocalcin (OCN) staining experiments revealed decreased bone resorption and increased bone formation in the GSK treatment groups. In addition, we found a novel effect of GSK—it could induce type-H vessel formation in mice. The underlying mechanisms of these actions were further explored at the molecular level to investigate whether these effects were due to an overexpression of the hypoxia inducible factor-1 (HIF-1α). Our findings indicate the utility of GSK as a therapeutic for the prevention of osteoporosis.

Keywords: Gushukang, bone mass, bone formation, type-H vessel, HIF-1α

OPEN ACCESS

Edited by:
Chao Liang,
Hong Kong Baptist University, Hong Kong

Reviewed by:
ZhenLin Zhang,
Shanghai Jiao Tong University, China
Weiguo Zou,
Chinese Academy of Sciences (CAS), China

****Correspondence:***
Ting Wen
tingwen163@126.com

† These authors have contributed equally to this work

Specialty section:
This article was submitted to Molecular Medicine, a section of the journal Frontiers in Cell and Developmental Biology

Received: *19 January 2020*
Accepted: *30 March 2020*
Published: *21 May 2020*

Citation:
Li W, Zhou X, Jiang T, He H and Wen T (2020) Positive Effect of Gushukang on Type-H Vessel and Bone Formation. Front. Cell Dev. Biol. 8:265. doi: 10.3389/fcell.2020.00265

INTRODUCTION

Primary osteoporosis is a bone disease characterized by decreased bone mass and bone density, resulting from estrogen deficiency and aging (Ng et al., 2015; Wang et al., 2015; Su et al., 2019; Rendina-Ruedy and Rosen, 2020). The risk of fractures is increased in primary osteoporosis, with the potential for serious disability and increased mortality in afflicted patients (Schett and Bozec, 2014; Nevius et al., 2015; Yang et al., 2019). The current treatment for osteoporosis comprises antiresorptive and bone-forming medicines (Cao et al., 2018), including estrogens (Hayashi et al., 2019), parathyroid hormone (Fan et al., 2017), bisphosphonates (Wei et al., 2016), and drugs, which blockade follicular stimulating hormone (Sponton and Kajimura, 2017). Most of these treatments concentrate on a single aspect of the disease, and thorough assessments of their efficacy and safety is still needed (Rauch et al., 2010). Thus, an exploration of new safer and more effective therapies is warranted.

Traditional Chinese herbal medicines have recently gained interest among medical researchers due to their low cost and limited side effects, and this renewed interest includes Gushukang (GSK), a traditional medicine made up of several traditional herbs, including *Herba Epimedii, Rehmannia glutinosa*, and *Rhizoma Drynariae* (Li et al., 2015; Xiao et al., 2020). Gushukang has already been approved for listing in the Chinese Pharmacopeia for the prevention and treatment of osteoporosis.

In clinical experiments, GSK–*Herba Epimedii*, an important GSK-containing formulation, has been reported to demonstrate positive effects on bone health (Indran et al., 2016). In a pharmacological study, GSK was demonstrated to increase bone density and promote the healing of bone fractures (Wang et al., 2007). Additionally, bone loss was prevented in hens fed with GSK, and an improvement in egg production was observed (Zhou et al., 2009), which suggests that the anti-osteoporosis effect of GSK is across species. In recent studies aimed at understanding the specific mechanisms underlying this action, Li et al. (2019) revealed that GSK modulates calcium homeostasis in OVX mice and that it has a favorable effect on bone formation (Li et al., 2019). In another study, this favorable effect was demonstrated to be related to the BMP-2/Smads signaling pathway (Chai et al., 2019). In summary, GSK is beneficial for bone mass development, although details of the underlying mechanisms remain unclear. Here, we reveal a new mechanism of GSK action that may pave the way for future osteoporosis treatments.

MATERIALS AND METHODS

Experimental Animals

C57BL mice were purchased from the Experimental Animal Center of Central South University and raised in pathogen-free facilities, under a 12-h light/dark cycle as described previously (Li et al., 2018). The mice were provided with ample plastic bedding and clean water. All the experimental protocols were approved by the Subcommittee on Research and Animal Care (SRAC) of Central South University.

Tissue Collection

Drugs were administered daily at 9:00–11:00 AM for 3 months as in the study by Kondegowda et al. (2015). Next, 24, 3-month-old mice were randomly divided into three groups: the control group, the low-dose group, and the high-dose GSK treatment group. Gushukang was dissolved in PBS and then administered. Mice in the low-dose group were administered 4 g/kg/day of GSK solution, whereas mice in the high-dose group were administered 8 g/kg/day of GSK solution intragastrically each day (Li et al., 2019). Three months later, the mice were killed by euthanasia. The femurs were collected and dissected free of soft tissue, fixed in 4% paraformaldehyde solution, and maintained in PBS until micro-computed tomography (Micro-CT) analysis, histomorphometry, and immunohistochemistry (Goldberg and Dixit, 2019).

Osteoclast Differentiation

Bone marrow-derived macrophages (BMMs) were cultured as described by Schmitz et al. (2015). C57BL/6 mice aged 4 weeks were used to obtain BMMs. Cells from the bone marrow cavity were flushed with PBS and centrifuged at 1,000 rpm at 37°C. After centrifugation, the cells were cultured overnight with 100 ng/ml macrophage colony-stimulating factor (MCSF, 416-ML/CF, R&D, Minneapolis, MN, United States). Next, the unattached cells were gathered and further cultured for 48 h until sufficient BMMs were obtained. Gushukang serum was prepared as described previously (Zhao et al., 2019). Bone marrow-derived macrophages were cultured with 100 ng/ml macrophage colony-stimulating factor and 50 ng/ml receptor activator for nuclear factor-κB ligand (RANKL, 462-TR/CF, R&D, Minneapolis, MN, United States). Then, they were treated either with a low dose (20 μl/well) or a high dose (200 μl/well) of GSK serum. The osteoclasts were allowed to differentiate for 8 days, following which the effect of the GSK serum was evaluated by Tartrate resistant acid phosphatase (TRAP) staining. An osteoclast was defined as a positively stained cell with more than three nuclei (Berger et al., 2019).

Osteoblast Differentiation

Osteoblasts were cultured as described in a previous study (Yu et al., 2019). The femurs were cut into small pieces and treated with 1 mg/ml collagenase solution, containing collagenase type I and collagenase type II at 1:3 ratio (Worthington, Newark, NJ, United States). Then, bone marrow-derived mesenchymal stem cells (BMSCs) were collected and cultured in Dulbecco's Modified Eagle's Medium (Invitrogen, Carlsbad, CA, United States), to which 10% fetal bovine serum (Invitrogen, New Zealand) and 100 U/ml penicillin and streptomycin (Invitrogen) were added. The cells were cultured with 50 μM ascorbic acid, 50 mM β-glycerophosphate, 50 nM dexamethasone (Sigma, St. Louis, MO, United States), and GSK serum (a low dose of 200 μl/well or a high dose of 2 ml/well) for 14 days. Next, the cells were fixed with 4% paraformaldehyde solution and then stained with 1% Alizarin red S (pH 4.2, Sigma-Aldrich, GmbH, Munich, Germany) for 10 min. After washing with PBS three times, four visual fields were randomly selected and from each slide and analyzed. The volume of mineralized bone nodules was quantified by image J software.

Immunohistochemistry Staining

Immunohistochemical staining was performed as described in previous studies (Albrecht et al., 2011; Chen et al., 2020). Fresh femurs were obtained and fixed in 4% paraformaldehyde solution at 4°C for 24 h, and then they were placed in 10% ethylene diamine tetraacetic acid solution (pH 7.4) and decalcified for 21 days. Next, the bones were embedded in paraffin. Paraffin wax blocks were sliced into longitudinally oriented bone sections with a thickness of 4 μm. Osteocalcin staining was performed to determine the number of osteoblasts and study their surface characteristics. Tartrate resistant acid phosphatase staining was performed to determine the number of osteoclasts and study their surface characteristics. Both the staining kits were purchased from Sigma Company (St. Louis, MO, United States). The distal metaphysic area of each femur was chosen for counting the number of positive-stained cells in four random visual fields from five consecutive sections of each mouse. Then, they were normalized to the number per millimeter in the adjacent bone surface (N mm^{-1}).

Immunofluorescence Staining

Immunofluorescence staining was conducted as described in previous studies (Rached et al., 2010; Yang et al., 2017).

Fresh bone tissues were collected and fixed immediately in 4% paraformaldehyde solution at 4°C for 4 h. Subsequently, the bone tissues were placed in 0.5 M ethylene diamine tetraacetic acid solution (pH 7.4) for decalcification at 4°C for 48 h, followed by dehydration with 20% sucrose and 2% polyvinylpyrrolidone (PVP) solution for 1 day until they descended to the bottom. Next, 8% gelatin (porcine; Sigma, G2500), 20% sucrose, and 2% PVP (Sigma, PVP360) were mixed and dissolved with PBS at 60°C. Finally, the tissues were embedded as described above. Forty-micrometer-thick, longitudinally oriented bone sections were sliced and stained with primary antibodies of mouse CD31 (Abcam, ab28364, 1:100) and endomucin (Santa Cruz, V.7C7, 1:50) overnight at 4°C. Next, the sections were incubated with secondary antibodies (Jackson ImmunoResearch, 415-605-166, 1:500; 315-545-003, 1:500) at 37°C for 1 h, away from light. Polyclonal goat IgG (R&D Systems, AB-108-C) and monoclonal rat IgG2A (R&D Systems, 54447) were used as negative controls. The specimens were observed using a confocal microscope (FLUOVIEW FV300, Olympus).

Micro-Computed Tomography Analysis

Bone structure was measured by high-resolution micro-CT as described in Mills et al.'s (2016) study. The femurs were scanned at 0.5 mm under the growth plate with a voltage of 70 kV and a current of 154 mA. The following software packages were used for the three-dimensional analysis of bones: image reconstruction software (NRecon v1.6), three-dimensional model visualization software (mCTVol v2.0), and data analysis software (CTAn v1.9). Bone parameters were expressed as trabecular bone volume per tissue volume (Tb. BV/TV), trabecular number (Tb. N), trabecular thickness (Tb. Th), and trabecular separation (Tb. Sp).

Western Blotting

Protein levels were measured as described in Stier et al.'s (2018) study. The femurs were ground in a mortar after adding liquid nitrogen. The powders obtained from each bone sample were treated with a 500 μl RIPA buffer for 20 min. After centrifugation, protein lysates were obtained, which were then transferred to SDS at a ratio of 4:1 and boiled at 100°C for 10 min. The lysates were separated by 10% SDS-PAGE and blotted onto a PVDF membrane. After being blocked with milk for 60 min, the membrane was treated with primary antibodies against HIF-1α (Cell Signaling Technology, Danvers, MA, United States) overnight at 4°C and then incubated with goat antirabbit immunoglobulin (1:2,000; Santa Cruz Biotechnology) for 1 h at 37°C. Finally the bands were developed using ELC reagents.

QT-PCR

The femur and tibia were collected from each mice. mRNA levels were determined as described in Walter et al.'s (2014) study. Total RNA was extracted from bone tissues by using the TRIzol reagent (Invitrogen, Carlsbad, CA, United States); this was followed by complementary DNA (cDNA) synthesis using a cDNA Kit (Pharmacia, Piscataway, NJ, United States). QT-PCR was carried out by using a KAPA SYBR FAST qPCR Kit (KAPA Biosystems, Wilmington, MA, United States) and an ABI PRISM® 7900HT System (Applied Biosystems, Foster City, CA, United States). The primer sequence of HIF-1a was shown as follows: forward (5′–3′) TCTGGAAGGTATGTGGCATT, reverse (5′–3′) AGGGTGGGCAGAACATTTAT. mRNA expression was determined by using the $2^{-\Delta\ \Delta\ CT}$ method (Ouyang et al., 2018).

Statistical Analysis

All data are shown as mean ± SD for each group. One-way ANOVA was used for analyzing differences among the three groups (groups of control, low-dose, and high-dose GSK treatment) with PRISM, version 7.0 (GraphPad), as described in Wei et al.'s (2014) study. All experiments were conducted more than three times. Differences were considered to be significant only when $P < 0.05$.

RESULTS

GSK Promoted Bone Formation in Mice

Micro-computed tomography is a commonly used method for the measurement of bone mass density (Hirose et al., 2014). We found that the GSK-treated mice had higher values of bone mineral density (BMD) than the control group mice (**Figure 1A**). Moreover, mice treated with a low dose of GSK had a lower BMD than mice treated with a high dose of GSK. Important 3D outcomes of micro-CT analysis including BV/TV, Tb.N, and Tb.Th were higher in the GSK treatment groups than in the control group (**Figure 1B**; $P < 0.05$). Moreover, these values were lower in the low-dose GSK treatment group than in the high-dose GSK group. In contrast, trabecular separation (Tb.Sp) was lower in the GSK treatment groups (**Figure 1B**; $P < 0.05$). These results indicate that GSK treatment had a positive effect on bone formation.

GSK Increased Osteoblastogenesis *in vivo* and *in vitro*

To determine whether GSK increased bone mass by affecting the process of osteoblastogenesis, we cultured osteoblasts *in vitro*. Alizarin red staining demonstrated that formation of mineralized bone nodules was increased in cells treated with GSK compared to that in the control cells, and that the formation of additional mineralized bone nodules was dose dependent (**Figure 2A**). The optical density of the mineralized bone nodules was quantified as illustrated in **Figure 2B** ($P < 0.05$). The results obtained *in vivo* following GSK treatment are consistent with these *in vitro* results. Immunohistochemistry staining showed that the femurs from GSK-treated mice expressed a higher ratio of osteocalcin (OCN)-positive area surface to bone area than femurs from control mice. Moreover, the high-dose GSK group showed a higher ratio than the low-dose GSK group (**Figures 3A,B**; $P < 0.05$). As OCN is an important osteogenic differentiation biomarker (Li et al., 2009), the results indicate

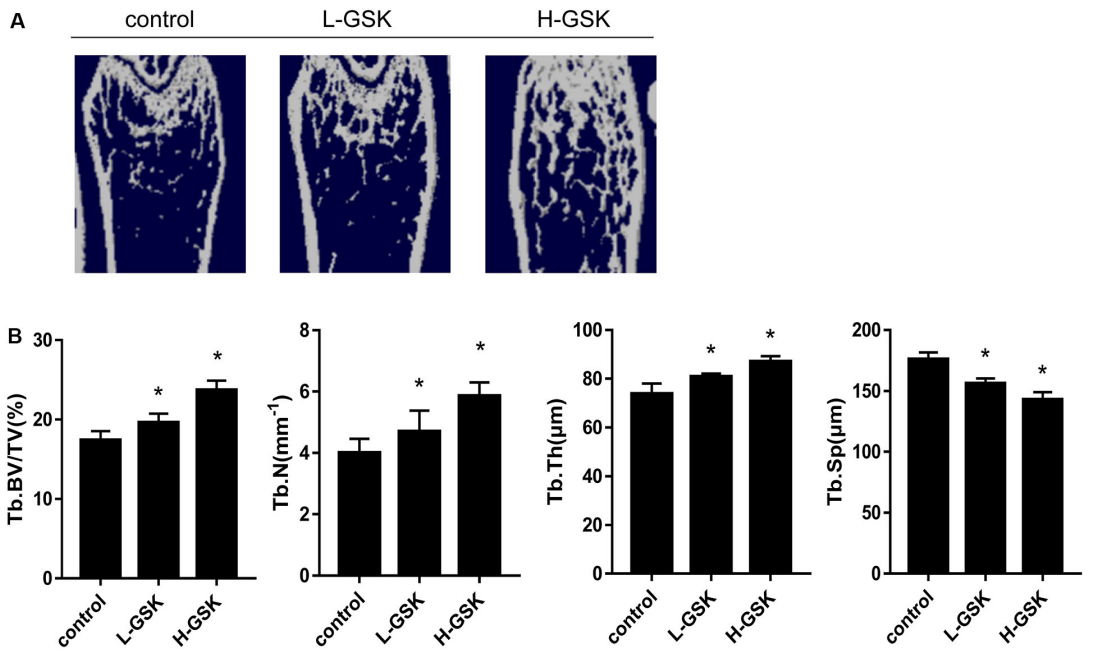


FIGURE 1 | GSK prevented bone loss in mice. **(A)** Representative μCT images of femurs collected from mice treated with low-dose (4 g/kg/day) and high-dose (8 g/kg/day) GSK or control. **(B)** Quantitation of Tb.BV/TV (trabecular bone volume per tissue volume); Tb.N (trabecular number); Tb.Th (trabecular thickness); and Tb.Sp (trabecular separation). Values were expressed as mean ± SD.*$P < 0.05$; all the assays were repeated more than three times.

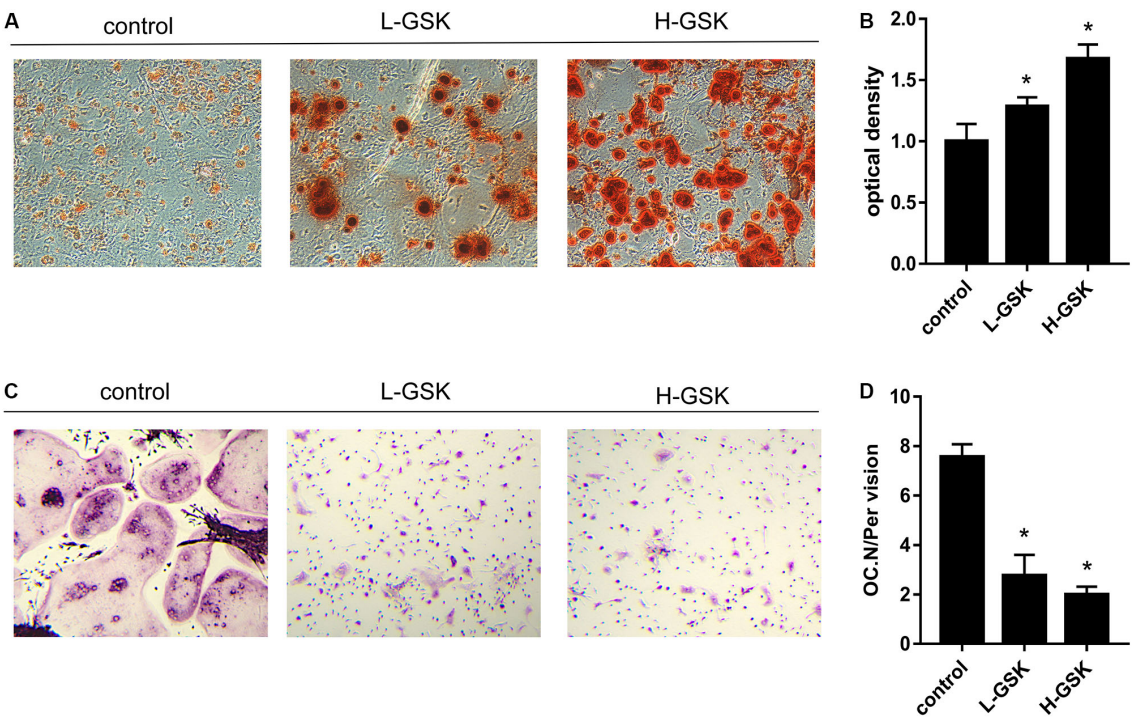


FIGURE 2 | GSK increases osteogenic differentiation and decreases osteoclast differentiation *in vitro*. **(A)** BMSCs were gathered from C57BL/6 mice (4 weeks) and cultured with GSK serum. Alizarin red staining was carried out at day 14 to assess osteogenic differentiation. Scale bar = 100 μm. **(B)** The Alizarin red staining optical density was quantified by ImageJ. *$P < 0.05$; the groups of GSK versus control. **(C)** BMMs were obtained from 4 weeks C57BL/6 mice and treated with M-CSF (100 ng/ml) and RANKL (50 ng/ml) (control), M-CSF, and RANKL added GSK serum. Osteoclast differentiation was evaluated at day 8 by TRAP staining. Scale bar = 100 μm. **(D)** The number of osteoclasts was quantified. Values were expressed as mean ± SD. *$P < 0.05$; all the assays were repeated more than three times.

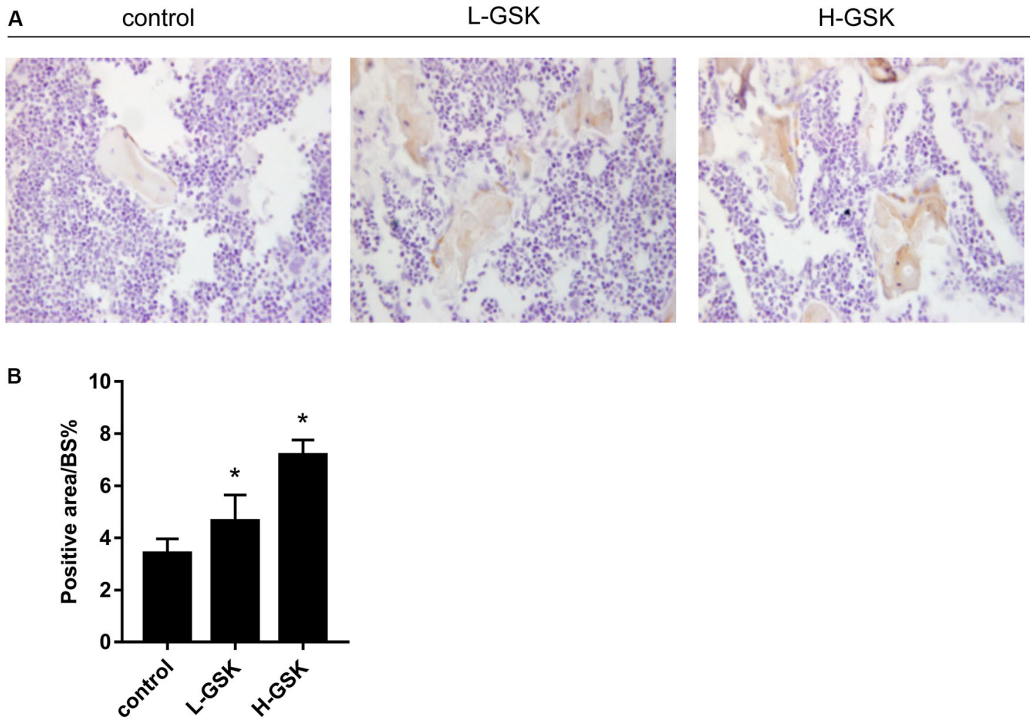


FIGURE 3 | GSK promoted the expressions of OCN in mice. **(A,B)** The protein expression of osteocalcin (OCN) of femurs gathered from mice treated with low-dose and high-dose GSK or control (saline) was determined by immunohistological staining. Scale bar = 100 μm. Values were expressed as mean ± SD. *$P < 0.05$; all the assays were repeated more than three times.

that GSK could increase bone mass partly by inducing osteoblast differentiation.

GSK Inhibited Osteoclastogenesis *in vivo* and *in vitro*

We next investigated the influence of GSK on the process of osteoclastogenesis. Osteoclasts were induced from BMMs and quantified as shown in **Figure 2D** ($P < 0.05$). We observed that the number of osteoclasts was significantly suppressed in the GSK treatment groups, and that this inhibitory capacity increased with increasing doses of GSK (**Figure 2C**). This observation was subsequently confirmed *in vivo*, since TRAP-positive osteoclasts were significantly decreased in GSK treatment groups, with high-dose GSK treatment groups showing fewer positive cells than the low-dose groups (**Figure 4A**). When the ratio of OCs to%BS and the absolute number of OCs were quantified, the GSK treatment groups showed fewer osteoclasts per area than the control groups (**Figures 4B,C**; $P < 0.05$). Thus, our findings provide evidence that GSK treatment also increases bone mass by inhibiting osteoclastogenesis.

GSK Accelerated Type-H Vessels Formation in Mice

Type-H vessels are associated with the differentiation of perivascular osteoprogenitors and bone formation (Weber et al., 2015). The type-H vessels are characterized as CD31 positive and endomucin positive (Morrison et al., 2014). The GSK treatment groups had more type-H vessels, as revealed by the number of $CD31^{hi}Emcn^{hi}$ endothelial cells, than the control group, and the formation of type-H vessels was higher in the high-dose GSK treatment group than in the low-dose group (**Figure 5A**). The ratio of type-H vessels to BS% was quantified as shown in **Figure 5B** ($P < 0.05$).

GSK Promoted the Activation of HIF-1a

The hypoxia inducible factor-1α (HIF-1α) is an important transcription factor that is activated under hypoxic conditions (Dai et al., 2019) and during the process of angiogenesis (Zhang et al., 2010). Hypoxia inducible factor-1α expression levels were increased in the GSK treatment groups, and HIF-1α expression was dependent on the GSK dose (**Figure 6A**; $P < 0.05$). These results suggest that GSK was able to upregulate the expression of HIF-1α protein. Moreover, when qRT-PCR was performed to assess the mRNA expression levels of *HIF-1α*, the GSK treatment groups showed higher levels of *HIF-1α* mRNA expression than the control group, and the high-dose group showed higher mRNA levels than the low-dose group (**Figure 6B**; $P < 0.05$). Thus, our data suggest that GSK can induce *HIF-1α* activation.

DISCUSSION

Gushukang, a traditional Chinese herbal medicine, has been used for the treatment of osteoporosis for many years, and

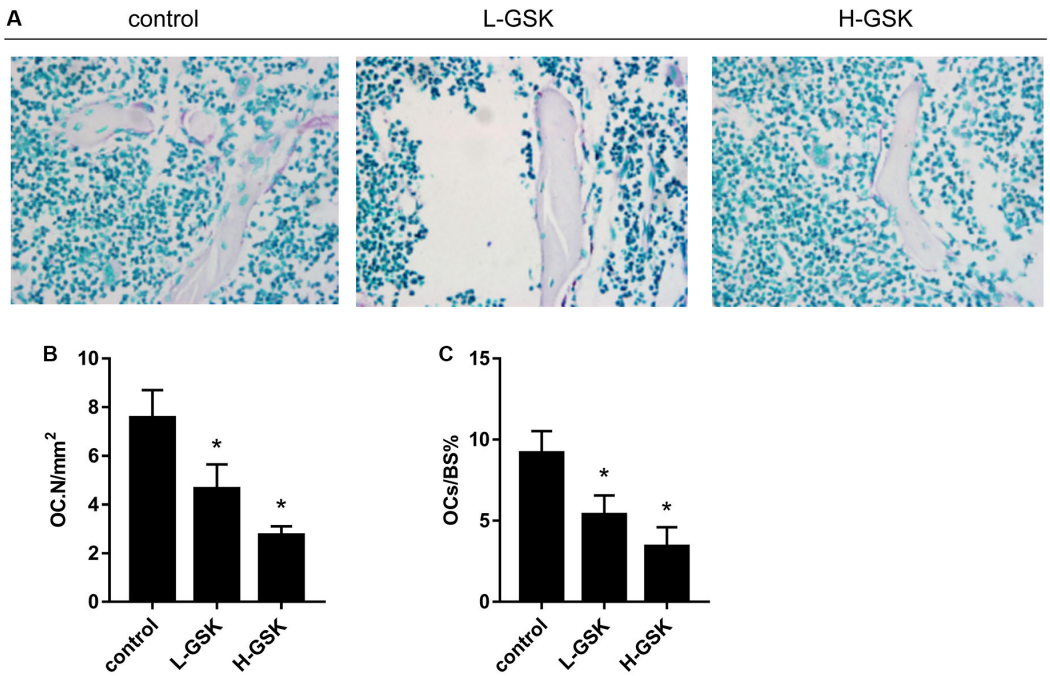


FIGURE 4 | GSK decreases the number of osteoclasts in mice. **(A)** TRAP staining was performed on femurs collected from the group of low-dose and high-dose GSK or control (saline). Scale bar = 100 μm. **(B)** Osteoclast-covered surface over bone surface (OCs/BS%) of each group was quantified. **(C)** Osteoclast number (OC.N). Values were expressed as mean ± standard deviation (SD). *$P < 0.05$; all the assays were repeated more than three times.

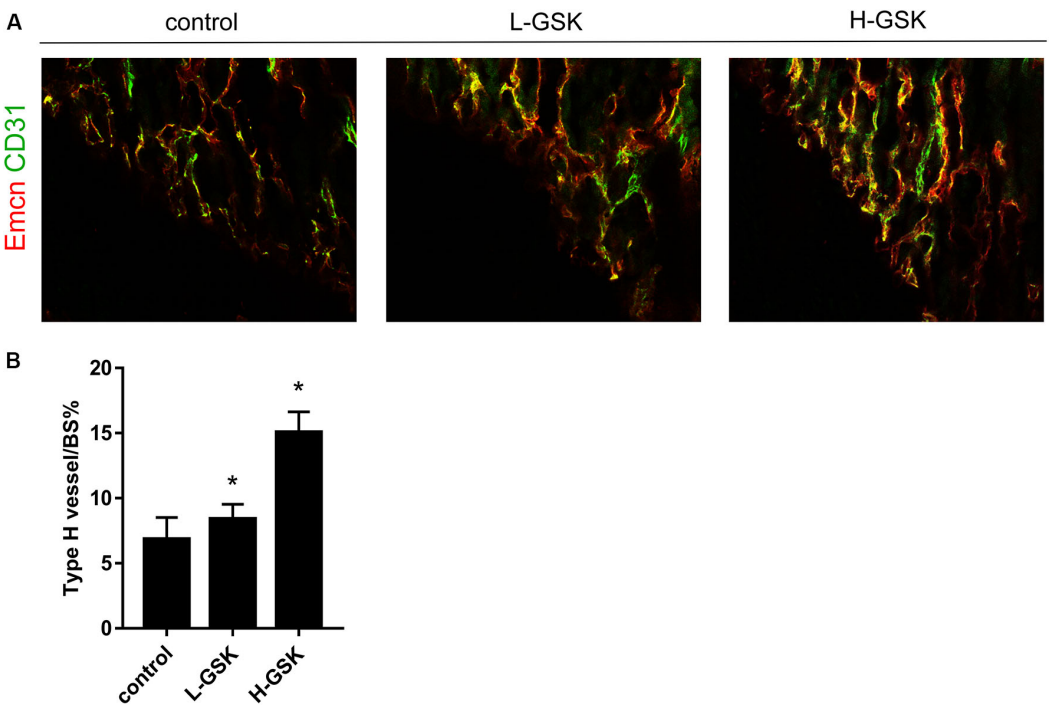


FIGURE 5 | GSK accelerated CD31hiEmcnhi vessels formation in mice. **(A)** Representative images of CD31 (green), Emcn (red) of femurs from the group of low-dose and high-dose GSK or control (saline) by immunofluorescence staining. Scale bar = 100 μm. **(B)** Type-H vessel surface was quantified. Values were expressed as mean ± SD. *$P < 0.05$; all the assays were repeated more than three times.

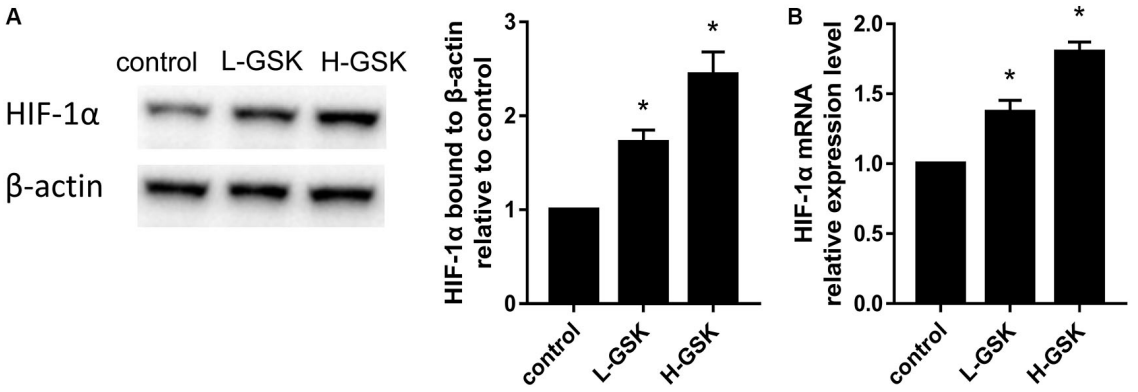


FIGURE 6 | GSK induced overexpression of HIF-1a. **(A)** Representative images of WB and quantification of the protein expression level of HIF-1a. **(B)** Quantification of the mRNA expression level of HIF-1a.Values were expressed as mean ± SD. *$P < 0.05$; all the assays were repeated more than three times.

the significant effects of this compound have been certified by clinical practices and approved by patients. Li et al. (2001) selected 197 male and female osteoporosis patients, and GSK was either administered (GSK treatment group) or not administered (control group) to patients randomly assigned to these groups (Li et al., 2001). Six months after GSK treatment, while BMD had decreased in the control group, the BMD decrease was slowed, and BMD even increased in some cases, in the GSK-treated group.

Here, we explored the underlying mechanism of GSK action and found that cells in the GSK treatment group demonstrated enhanced osteoblastogenesis during the period of osteoblast differentiation from BMSCs. In addition, the number of osteoclasts in the GSK treatment groups was lower than in the control groups, suggesting that the osteoclastogenesis ability of BMMs was inhibited by GSK. These results were found to be consistent with previous research (Wang et al., 2018). Thus, we conclude that GSK increases osteoblastogenesis and suppresses osteoclastogenesis *in vitro*.

To further understand the role of GSK *in vivo*, we evaluated bone mass and bone biochemical markers in mice. Using micro-CT, increased cortical and cancellous bone mass in the GSK treatment group could be inferred from the higher BV/TV, Tb.N, and Tb.Th and the lower Tb.Sp values observed in this group than in the control group. These results suggest that bone anabolism is greater than bone catabolism after GSK treatment, confirming that GSK enhances bone density and bone mass. Tartrate-resistant acid phosphatase, produced by osteoclasts, and OCN, secreted by osteoblasts (Booth et al., 2016; Calvier et al., 2017), levels reflect the activity of osteoclasts and osteoblasts as well as the status of bone resorption and bone formation (Long et al., 2014; Yu et al., 2015; Huang et al., 2020). In our study, TRAP and OCN staining results suggest that GSK treatment increased bone mass by activating osteoblasts and suppressing osteoclasts. Thus, bone formation was promoted and bone resorption was inhibited. This result was consistent with the results we obtained in cells, verifying the osteogenesis activity of GSK *in vivo*.

Type-H vessels are a special subtype of vessel in bone characterized by high levels of endomucin and CD31 expression (Diebold et al., 2015). Type-H vessels have recently been shown to possess the ability to induce angiogenesis and bone formation (Peng et al., 2020). Our results show that GSK-treated mice have more $CD31^{hi}Emcn^{hi}$ vessels than control mice, which suggests that GSK may have increased the abundance of type-H vessels. These results are consistent with the notion that angiogenesis and bone formation are coupled. This is the first study to report a role for GSK in angiogenesis and specifically in the formation of type-H vessels. This newfound action of GSK may find additional application in other diseases.

The mechanism underlying the effect of GSK on type-H vessels and coupling with angiogenesis were further investigated. Previous studies have shown that GSK upregulated calcium-binding protein-28k and the vitamin D receptor (Li et al., 2019), and also Osteirx and Runx2 (Wang et al., 2018). In this study, we reveal that HIF-1α, a factor produced under hypoxic conditions (Baik et al., 2019), may also play a regulatory role, with its overexpression contributing to angiogenesis and osteogenesis (Stegen et al., 2016; Hulea et al., 2018). The results of our western blot analyses show that bones from the GSK treatment group expressed higher HIF-1α protein levels and that this increase was dependent on the GSK dose. Similarly, *HIF-1α* mRNA levels measured by qRT-PCR were higher in the GSK treatment group than in the control group. These data suggest that GSK treatment may induce formation of type-H vessels and bone formation by enhancing the expression of *HIF-1α*.

CONCLUSION

In conclusion, GSK can increase bone mass by promoting bone formation and the formation of the type-H vessels, and by inhibiting bone resorption. These functions may be related to HIF-1α activity. The results of our study may advance new therapeutic treatments for the prevention of osteoporosis.

DATA AVAILABILITY STATEMENT

The datasets generated for this study are available on request to the corresponding author.

ETHICS STATEMENT

The animal study was reviewed and approved by the Subcommittee on Research and Animal Care (SRAC) of Central South University.

AUTHOR CONTRIBUTIONS

TW designed and guided the experiment. WL and XZ carried out the experiment. TJ analyzed the data. WL and HH wrote the manuscript. All authors contributed to manuscript revision and read and approved the submitted version.

ACKNOWLEDGMENTS

Gushukang was provided by Liaoningkangchen of China.

REFERENCES

Albrecht, S. C., Barata, A. G., Grosshans, J., Teleman, A. A., and Dick, T. P. (2011). In vivo mapping of hydrogen peroxide and oxidized glutathione reveals chemical and regional specificity of redox homeostasis. *Cell Metab.* 14, 819–829. doi: 10.1016/j.cmet.2011.10.010

Baik, S. H., Kang, S., Lee, W., Choi, H., Chung, S., Kim, J. I., et al. (2019). A Breakdown in Metabolic reprogramming causes microglia dysfunction in Alzheimers Disease. *Cell Metab.* 30, 493.e6–507.e6. doi: 10.1016/j.cmet.2019.06.005

Berger, J. M., Singh, P., Khrimian, L., Morgan, D. A., Chowdhury, S., Arteaga-Solis, E., et al. (2019). Mediation of the acute stress response by the skeleton. *Cell Metab.* 30, 890.e8–902.e8. doi: 10.1016/j.cmet.2019.08.012

Booth, F. W., Ruegsegger, G. N., and Olver, T. D. (2016). exercise has a bone to pick with skeletal muscle. *Cell Metab.* 23, 961–962. doi: 10.1016/j.cmet.2016.05.016

Calvier, L., Chouvarine, P., Legchenko, E., Hoffmann, N., Geldner, J., Borchert, P., et al. (2017). PPARgamma Links BMP2 and TGFbeta1 pathways in vascular smooth muscle cells, regulating cell proliferation and glucose metabolism. *Cell Metab.* 25, 1118.e7–1134.e7. doi: 10.1016/j.cmet.2017.03.011

Cao, Q., Chen, X., Wu, X., Liao, R., Huang, P., Tan, Y., et al. (2018). Inhibition of UGT8 suppresses basal-like breast cancer progression by attenuating sulfatide-alphaVbeta5 axis. *J. Exp. Med.* 215, 1679–1692. doi: 10.1084/jem.20172048

Chai, S., Wan, L., Wang, J. L., Huang, J. C., and Huang, H. X. (2019). Gushukang inhibits osteocyte apoptosis and enhances BMP-2/Smads signaling pathway in ovariectomized rats. *Phytomedicine* 64:153063. doi: 10.1016/j.phymed.2019.153063

Chen, H. J., Tas, S. W., and de Winther, M. (2020). Type-I interferons in atherosclerosis. *J. Exp. Med.* 217:e20190459. doi: 10.1084/jem.20190459

Dai, J., Escara-Wilke, J., Keller, J. M., Jung, Y., Taichman, R. S., Pienta, K. J., et al. (2019). Primary prostate cancer educates bone stroma through exosomal pyruvate kinase M2 to promote bone metastasis. *J. Exp. Med.* 216, 2883–2899. doi: 10.1084/jem.20190158

Diebold, I., Hennigs, J. K., Miyagawa, K., Li, C. G., Nickel, N. P., Kaschwich, M., et al. (2015). BMPR2 preserves mitochondrial function and DNA during reoxygenation to promote endothelial cell survival and reverse pulmonary hypertension. *Cell Metab.* 21, 596–608. doi: 10.1016/j.cmet.2015.03.010

Fan, Y., Hanai, J. I., Le, P. T., Bi, R., Maridas, D., DeMambro, V., et al. (2017). Parathyroid hormone directs bone marrow mesenchymal cell fate. *Cell Metab.* 25, 661–672. doi: 10.1016/j.cmet.2017.01.001

Goldberg, E. L., and Dixit, V. D. (2019). Bone marrow: an immunometabolic refuge during energy depletion. *Cell Metab.* 30, 621–623. doi: 10.1016/j.cmet.2019.08.022

Hayashi, M., Nakashima, T., Yoshimura, N., Okamoto, K., Tanaka, S., and Takayanagi, H. (2019). Autoregulation of osteocyte sema3a orchestrates estrogen action and counteracts bone aging. *Cell Metab.* 29, 627.e5–637.e5. doi: 10.1016/j.cmet.2018.12.021

Hirose, J., Masuda, H., Tokuyama, N., Omata, Y., Matsumoto, T., Yasui, T., et al. (2014). Bone resorption is regulated by cell-autonomous negative feedback loop of Stat5-Dusp axis in the osteoclast. *J. Exp. Med.* 211, 153–163. doi: 10.1084/jem.20130538

Huang, Y., Xiao, Y., Liu, Y., Guo, M., Guo, Q., Zhou, F., et al. (2020). MicroRNA-188 regulates aging-associated metabolic phenotype. *Aging Cell* 19:e13077. doi: 10.1111/acel.13077

Hulea, L., Gravel, S. P., Morita, M., Cargnello, M., Uchenunu, O., Im, Y. K., et al. (2018). Translational and HIF-1alpha-dependent metabolic reprogramming underpin metabolic plasticity and responses to kinase inhibitors and biguanides. *Cell Metab.* 28, 817.e8–832.e8. doi: 10.1016/j.cmet.2018.09.001

Indran, I. R., Liang, R. L., Min, T. E., and Yong, E. L. (2016). Preclinical studies and clinical evaluation of compounds from the genus Epimedium for osteoporosis and bone health. *Pharmacol. Ther.* 162, 188–205. doi: 10.1016/j.pharmthera.2016.01.015

Kondegowda, N. G., Fenutria, R., Pollack, I. R., Orthofer, M., Garcia-Ocana, A., Penninger, J. M., et al. (2015). Osteoprotegerin and denosumab stimulate human beta cell proliferation through inhibition of the receptor activator of NF-kappaB ligand pathway. *Cell Metab.* 22, 77–85. doi: 10.1016/j.cmet.2015.05.021

Li, C. J., Cheng, P., Liang, M. K., Chen, Y. S., Lu, Q., Wang, J. Y., et al. (2015). MicroRNA-188 regulates age-related switch between osteoblast and adipocyte differentiation. *J. Clin. Invest.* 125, 1509–1522. doi: 10.1172/JCI77716

Li, C. J., Xiao, Y., Yang, M., Su, T., Sun, X., Guo, Q., et al. (2018). Long noncoding RNA Bmncr regulates mesenchymal stem cell fate during skeletal aging. *J. Clin. Invest.* 128, 5251–5266. doi: 10.1172/JCI99044

Li, H., Xie, H., Liu, W., Hu, R., Huang, B., Tan, Y. F., et al. (2009). A novel microRNA targeting HDAC5 regulates osteoblast differentiation in mice and contributes to primary osteoporosis in humans. *J. Clin. Invest.* 119, 3666–3677. doi: 10.1172/JCI39832

Li, S. Q., Pei, Z. G., and Liu, Y. M. (2001). Clinical study on effect of gushukang granule in preventing and treating primary osteoporosis]. *Zhongguo Zhong Xi Yi Jie He Za Zhi* 21, 265–268.

Li, X. L., Wang, L., Bi, X. L., Chen, B. B., and Zhang, Y. (2019). Gushukang exerts osteopreserve effects by regulating vitamin D and calcium metabolism in ovariectomized mice. *J. Bone Miner. Metab.* 37, 224–234. doi: 10.1007/s00774-018-0924-1

Long, J. Z., Svensson, K. J., Tsai, L., Zeng, X., Roh, H. C., Kong, X., et al. (2014). A smooth muscle-like origin for beige adipocytes. *Cell Metab.* 19, 810–820. doi: 10.1016/j.cmet.2014.03.025

Mills, K. F., Yoshida, S., Stein, L. R., Grozio, A., Kubota, S., Sasaki, Y., et al. (2016). Long-Term administration of nicotinamide mononucleotide mitigates age-associated physiological decline in mice. *Cell Metab.* 24, 795–806. doi: 10.1016/j.cmet.2016.09.013

Morrison, A. R., Yarovinsky, T. O., Young, B. D., Moraes, F., Ross, T. D., Ceneri, N., et al. (2014). Chemokine-coupled beta2 integrin-induced macrophage Rac2-Myosin IIA interaction regulates VEGF-A mRNA stability and arteriogenesis. *J. Exp. Med.* 211, 1957–1968. doi: 10.1084/jem.20132130

Nevius, E., Pinho, F., Dhodapkar, M., Jin, H., Nadrah, K., Horowitz, M. C., et al. (2015). Oxysterols and EBI2 promote osteoclast precursor migration to bone surfaces and regulate bone mass homeostasis. *J. Exp. Med.* 212, 1931–1946. doi: 10.1084/jem.20150088

Ng, K. S., Kuncewicz, T. M., and Karp, J. M. (2015). Beyond hit-and-run: stem cells leave a lasting memory. *Cell Metab.* 22, 541–543. doi: 10.1016/j.cmet.2015.09.019

Ouyang, X., Han, S. N., Zhang, J. Y., Dioletis, E., Nemeth, B. T., Pacher, P., et al. (2018). Digoxin suppresses pyruvate kinase M2-promoted HIF-1alpha transactivation in steatohepatitis. *Cell Metab.* 27, :339.e3–350.e3. doi: 10.1016/j.cmet.2018.04.007

Peng, Y., Wu, S., Li, Y., and Crane, J. L. (2020). Type H blood vessels in bone modeling and remodeling. *Theranostics* 10, 426–436. doi: 10.7150/thno.34126

Rached, M. T., Kode, A., Xu, L., Yoshikawa, Y., Paik, J. H., Depinho, R. A., et al. (2010). FoxO1 is a positive regulator of bone formation by favoring protein synthesis and resistance to oxidative stress in osteoblasts. *Cell Metab.* 11, 147–160. doi: 10.1016/j.cmet.2010.01.001

Rauch, A., Seitz, S., Baschant, U., Schilling, A. F., Illing, A., Stride, B., et al. (2010). Glucocorticoids suppress bone formation by attenuating osteoblast differentiation via the monomeric glucocorticoid receptor. *Cell Metab.* 11, 517–531. doi: 10.1016/j.cmet.2010.05.005

Rendina-Ruedy, E., and Rosen, C. J. (2020). Lipids in the bone marrow: an evolving perspective. *Cell Metab.* 31, 219–231. doi: 10.1016/j.cmet.2019.09.015

Schett, G., and Bozec, A. (2014). Removing the bone brake. *Cell Metab.* 20, 394–395. doi: 10.1016/j.cmet.2014.08.009

Schmitz, F., Roscioni, S., and Lickert, H. (2015). Repurposing an osteoporosis drug for beta cell regeneration in diabetic patients. *Cell Metab.* 22, 58–59. doi: 10.1016/j.cmet.2015.05.024

Sponton, C. H., and Kajimura, S. (2017). Burning fat and building bone by FSH blockade. *Cell Metab.* 26, 285–287. doi: 10.1016/j.cmet.2017.07.018

Stegen, S., van Gastel, N., Eelen, G., Ghesquiere, B., D'Anna, F., Thienpont, B., et al. (2016). HIF-1alpha promotes glutamine-mediated redox homeostasis and glycogen-dependent bioenergetics to support postimplantation bone cell survival. *Cell Metab.* 23, 265–279. doi: 10.1016/j.cmet.2016.01.002

Stier, M. T., Zhang, J., Goleniewska, K., Cephus, J. Y., Rusznak, M., Wu, L., et al. (2018). IL-33 promotes the egress of group 2 innate lymphoid cells from the bone marrow. *J. Exp. Med.* 215, 263–281. doi: 10.1084/jem.20170449

Su, T., Xiao, Y., Xiao, Y., Guo, Q., Li, C., Huang, Y., et al. (2019). Bone Marrow mesenchymal stem cells-derived exosomal MiR-29b-3p regulates aging-associated insulin resistance. *ACS Nano* 13, 2450–2462. doi: 10.1021/acsnano.8b09375

Walter, K. M., Schonenberger, M. J., Trotzmuller, M., Horn, M., Elsasser, H. P., Moser, A. B., et al. (2014). Hif-2alpha promotes degradation of mammalian peroxisomes by selective autophagy. *Cell Metab.* 20, 882–897. doi: 10.1016/j.cmet.2014.09.017

Wang, Q., Zhao, Y., Sha, N., Zhang, Y., Li, C., Zhang, H., et al. (2018). The systemic bone protective effects of Gushukang granules in ovariectomized mice by inhibiting osteoclastogenesis and stimulating osteoblastogenesis. *J. Pharmacol. Sci.* 136, 155–164. doi: 10.1016/j.jphs.2018.01.007

Wang, X., Wei, W., Krzeszinski, J. Y., Wang, Y., and Wan, Y. (2015). A liver-bone endocrine relay by IGFBP1 promotes osteoclastogenesis and mediates fgf21-induced bone resorption. *Cell Metab.* 22, 811–824. doi: 10.1016/j.cmet.2015.09.010

Wang, X. J., Liang, R. X., and Zhao, L. (2007). [Progress of study on prevention and treatment of osteoporosis by compound Gushukang]. *Zhongguo Zhong Xi Yi Jie He Za Zhi* 27, 282–285.

Weber, E. W., Han, F., Tauseef, M., Birnbaumer, L., Mehta, D., and Muller, W. A. (2015). TRPC6 is the endothelial calcium channel that regulates leukocyte transendothelial migration during the inflammatory response. *J. Exp. Med.* 212, 1883–1899. doi: 10.1084/jem.20150353

Wei, W., Motoike, T., Krzeszinski, J. Y., Jin, Z., Xie, X. J., Dechow, P. C., et al. (2014). Orexin regulates bone remodeling via a dominant positive central action and a subordinate negative peripheral action. *Cell Metab.* 19, 927–940. doi: 10.1016/j.cmet.2014.03.016

Wei, W., Schwaid, A. G., Wang, X., Wang, X., Chen, S., Chu, Q., et al. (2016). Ligand activation of ERRalpha by cholesterol mediates statin and bisphosphonate effects. *Cell Metab.* 23, 479–491. doi: 10.1016/j.cmet.2015.12.010

Xiao, Y. Z., Yang, M., Xiao, Y., Guo, Q., Huang, Y., Li, C. J., et al. (2020). Reducing hypothalamic stem cell senescence protects against aging-associated physiological decline. *Cell Metab* 31, 534.e5–548.e5. doi: 10.1016/j.cmet.2020.01.002

Yang, M., Guo, Q., Peng, H., Xiao, Y. Z., Xiao, Y., Huang, Y., et al. (2019). Kruppel-like factor 3 inhibition by mutated lncRNA Reg1cp results in human high bone mass syndrome. *J. Exp. Med.* 216, 1944–1964. doi: 10.1084/jem.20181554

Yang, M., Li, C. J., Sun, X., Guo, Q., Xiao, Y., Su, T., et al. (2017). MiR-497 approximately 195 cluster regulates angiogenesis during coupling with osteogenesis by maintaining endothelial Notch and HIF-1alpha activity. *Nat. Commun.* 8:16003. doi: 10.1038/ncomms16003

Yu, V. W., Saez, B., Cook, C., Lotinun, S., Pardo-Saganta, A., Wang, Y. H., et al. (2015). Specific bone cells produce DLL4 to generate thymus-seeding progenitors from bone marrow. *J. Exp. Med.* 212, 759–774. doi: 10.1084/jem.20141843

Yu, Y., Newman, H., Shen, L., Sharma, D., Hu, G., Mirando, A. J., et al. (2019). Glutamine metabolism regulates proliferation and lineage allocation in skeletal stem cells. *Cell Metab.* 29, 966.e4–978.e4. doi: 10.1016/j.cmet.2019.01.016

Zhang, N., Fu, Z., Linke, S., Chicher, J., Gorman, J. J., Visk, D., et al. (2010). The asparaginyl hydroxylase factor inhibiting HIF-1alpha is an essential regulator of metabolism. *Cell Metab.* 11, 364–378. doi: 10.1016/j.cmet.2010.03.001

Zhao, Y., Wang, Q., Liu, S., Wang, Y., Shu, B., and Zhao, D. (2019). Preparation Of Gushukang (GSK) granules for in vivo and in vitro experiments. *J. Vis. Exp.* 9:e59171. doi: 10.3791/59171

Zhou, Z. L., Deng, Y. F., Tao, Q. S., Hu, Y. F., and Hou, J. F. (2009). Effects of Gushukang, a Chinese herbal medicine, on bone characteristics and osteoporosis in laying hens. *Poult Sci.* 88, 2342–2345. doi: 10.3382/ps.2009-00285

Conflict of Interest: The authors declare that the research was conducted in the absence of any commercial or financial relationships that could be construed as a potential conflict of interest.

Copyright © 2020 Li, Zhou, Jiang, He and Wen. This is an open-access article distributed under the terms of the Creative Commons Attribution License (CC BY). The use, distribution or reproduction in other forums is permitted, provided the original author(s) and the copyright owner(s) are credited and that the original publication in this journal is cited, in accordance with accepted academic practice. No use, distribution or reproduction is permitted which does not comply with these terms.

frontiers in Cell and Developmental Biology

REVIEW
published: 04 June 2020
doi: 10.3389/fcell.2020.00433

Cathepsin K: The Action in and Beyond Bone

Rongchen Dai[1†], Zeting Wu[2†], Hang Yin Chu[1], Jun Lu[1,3], Aiping Lyu[1], Jin Liu[1] and Ge Zhang[1*]*

[1] Law Sau Fai Institute for Advancing Translational Medicine in Bone & Joint Diseases, Hong Kong Baptist University, Hong Kong, China, [2] International Medical Service Center, The First Affiliated Hospital of Shantou University Medical College, Shantou, China, [3] School of Pharmacy, Chengdu University of Traditional Chinese Medicine, Chengdu, China

Cathepsin K (CatK) is one of the most potent proteases in lysosomal cysteine proteases family, of which main function is to mediate bone resorption. Currently, CatK is among the most attractive targets for anti-osteoporosis drug development. Although many pharmaceutical companies are working on the development of selective inhibitors for CatK, there is no FDA approved drug till now. Odanacatib (ODN) developed by Merck & Co. is the only CatK inhibitor candidate which demonstrated high therapeutic efficacy in patients with postmenopausal osteoporosis in Phase III clinical trials. Unfortunately, the development of ODN was finally terminated due to the cardio-cerebrovascular adverse effects. Therefore, it arouses concerns on the undesirable CatK inhibition in non-bone sites. It is known that CatK has far-reaching actions throughout various organs besides bone. Many studies have also demonstrated the involvement of CatK in various diseases beyond the musculoskeletal system. This review not only summarized the functional roles of CatK in bone and beyond bone, but also discussed the potential relevance of the CatK action beyond bone to the adverse effects of inhibiting CatK in non-bone sites.

Keywords: Cathepsin K, osteoclast, bone resorption, osteoporosis, osteoarthritis, Cathepsin K inhibitor, cardiovascular diseases, lung fibrosis

OPEN ACCESS

Edited by:
Changjun Li,
Xiangya Hospital, Central South University, China

Reviewed by:
Dong-Joo Cheon,
Albany Medical College, United States
Bo Gao,
Institute of Orthopaedic Surgery, Xijing Hospital, China

****Correspondence:***
Jin Liu
liujin@hkbu.edu.hk
Ge Zhang
zhangge@hkbu.edu.hk

[†]These authors share first authorship

Specialty section:
This article was submitted to Molecular Medicine, a section of the journal Frontiers in Cell and Developmental Biology

Received: *17 February 2020*
Accepted: *08 May 2020*
Published: *04 June 2020*

Citation:
Dai R, Wu Z, Chu HY, Lu J, Lyu A, Liu J and Zhang G (2020) Cathepsin K: The Action in and Beyond Bone. Front. Cell Dev. Biol. 8:433. doi: 10.3389/fcell.2020.00433

INTRODUCTION

Lysosomal cysteine proteases, firstly discovered in the 20s of the twentieth century, are generally called cathepsins nowadays. In human, there are 11 members of cathepsins (cathepsin B, C, F, H, K, L, O, S, V, W, and Z), which are distinguished by their structures, catalytic mechanisms, and which proteins they cleave (Turk et al., 2001). This big family shares a common papain-like structural fold and a conserved active site Cys-Asn-His triad of residues (Vasiljeva et al., 2007). Among them, Cathepsin K (CatK) is predominantly secreted by activated osteoclasts to degrade collagen and other matrix proteins during bone resorption (Costa et al., 2011). Human CatK is a 329-amino-acid long protein consisting of an N-terminal 15-amino-acid long signal sequence, a 99-amino-acid long propeptide and a 215-amino-acid long catalytic unit (Bromme and Okamoto, 1995). From the structural aspect, CatK has the typical three-dimensional structure of a CatL like peptidase. The active site of CatK is a V-shaped cleft located at the top of the molecule and contains the catalytic diad cysteine–histidine. It can accept a Pro residue in the P2 position, which is correlated to the high content of Pro and hydroxyproline residues in collagen (McGrath et al., 1997; Novinec and Lenarcic, 2013). Since suppression of CatK activity could prevent bone resorption without perturbing bone formation (Bromme and Lecaille, 2009; Costa et al., 2011; Garber, 2016), it has become an attractive target for anti-resorptive drug development.

Many pharmaceutical companies are working on the development of selective inhibitors for CatK, most efforts focused on the cysteine thiol moiety of CatK with reactive electrophile "warheads" to reversibly inhibit or irreversibly inactivate its proteolytic activity (Bromme and Lecaille, 2009; Wijkmans and Gossen, 2011; Lu et al., 2018). Nevertheless, there is no FDA approved drug till now. Balicatib (AAE581) developed by Novartis terminated in its Phase II trial due to cutaneous lesions such as pruritus, skin rashes and rare morphea-like skin changes (Peroni et al., 2008; Runger et al., 2012). ONO-5334, a novel synthetic inhibitor of CatK, developed by Ono Pharmaceutical Co has passed its phase I and II clinical trials (Tanaka et al., 2017). But this project was recently terminated due to some market reasons. Odanacatib developed by Merck & Co. is the only CatK inhibitor candidate which demonstrated high therapeutic efficacy in patients with postmenopausal osteoporosis in Phase III clinical trials (McClung et al., 2019). Unfortunately, due to the undesirable adverse effects in non-bone tissues, i.e., higher incidence of cardio-cerebrovascular events vs. placebo group, the development of ODN was finally stopped. CatK was previously believed to be mainly secreted by osteoclasts and active at the bone resorption surfaces (Drake et al., 1996; Costa et al., 2011). However, it becomes clear at this point that the activity of CatK has far-reaching effects throughout various organs beyond bone. Therefore, it is essential to ascertain the role of CatK in bone and non-bone sites as well as in cell types besides osteoclasts. Here, we reviewed the functional role of CatK in bone and beyond bone. We also discussed the potential relevance of the CatK action beyond bone to the adverse effects of inhibiting CatK in non-bone sites.

ROLE OF CatK IN BONE

CatK and Bone Cells

The abundant expression of CatK instead of the other cathepsins was previously identified in osteoclasts (Drake et al., 1996), the unique bone cell type responsible for absorbing bone matrix in skeletal modeling and remodeling. It has been known that CatK expression is regulated by the receptor activator of nuclear factor κB ligand (RANKL)-RANK signaling (Troen, 2006), the critical signaling pathway of osteoclastogenesis. The activation of RANKL-RANK signaling pathway in osteoclast precursors stimulates the pro-osteoclastogenic transcriptional factor NFATc1 (nuclear factor of activated T cells) to initiate the transcription of CatK (Balkan et al., 2009). Many other factors, such as tumor necrosis factor-α (TNF-α), interleukins, vitamin D, and parathyroid hormone, could also stimulate CatK expression in osteoclasts (Troen, 2006). The CatK secretion could be regulated by the interaction between the E3 ubiquitin ligase Cbl and Phosphatidylinositol-3 Kinase (PI3K) in osteoclasts (Yu et al., 2019). In the process of bone resorption, CatK are secreted from mature osteoclast into the "sealing zone," a dynamic actin-rich cell–matrix adhesion structure that defines the resorption area of bone (Takito et al., 2018), wherein the acidified milieu could dissolve the mineralized component of bone for exposing its organic matrix, which were subsequently degraded by CatK and other proteases. It is known that CatK could efficiently degrade type I collagen (Garnero et al., 1998; Kafienah et al., 1998), which constitutes approximately 90% of bone organic matrix, and extracellular matrix glycoprotein osteonectin (Bossard et al., 1996), which is among the remaining 10% constituent of bone organic matrix and is critical in supporting bone remodeling and maintaining bone mass (Delany et al., 2000). Impressively, CatK is the only osteoclast-secreted protease that is able to cleave both the triple helix and telopeptides of type I collagen fibers (Bromme and Okamoto, 1995; Garnero et al., 1998). CatK could also degrade type II collagen, the predominant matrix protein in cartilage (Kafienah et al., 1998). In addition, it was previously shown that CatK could cleave and activate the matrix-metalloproteinase-9 (MMP-9) (Christensen and Shastri, 2015), another protease necessary for bone matrix degradation. Importantly, the CatK deficient mice developed osteopetrosis while the CatK deficient osteoclasts were defective in resorbing demineralized bone (Gowen et al., 1999). Collectively, it could be concluded that CatK is indispensable for osteoclast-mediated bone resorption.

Although a previous immunoelectron microscopic study on mouse femur showed the negligible CatK expression in both osteoblasts and osteocytes (Yamaza et al., 1998), the other two important bone cell types, it is now known that CatK could be expressed and secreted by these two types of bone cells to exert its function of degrading bone matrix. The expression and secretion of CatK was found in human trabecular bone-derived osteoblasts from patients with fracture of femoral neck, which was thought to probably contribute to the maintenance of bone organic matrix and recycling of improperly processed type I collagen (Mandelin et al., 2006). On the other hand, it was recently found that osteocytes could also express and secrete CatK, which was required for the lactation-induced peri-lacunar resorption to guarantee the adequate amounts of calcium in milk for the skeletal development in offspring (Lotinun et al., 2019). In addition, it was demonstrated that mechanical loading could stimulate osteoblasts and osteocytes to express CatK whereby it could modulate modeling-based cortical bone formation by degrading periostin (Bonnet et al., 2017), the matricellular protein secreted by these two bone cell types essential for periosteal bone formation in response to mechanical loading (Bonnet et al., 2009). Intriguingly, a recent study has identified a population of periosteal stem cell (PSC) with CatK expression that could contribute to mediate intramembranous bone formation (Debnath et al., 2018). These CatK-expressing PSCs also possessed the capacity to differentiate into chondrocytes to mediate endochondral bone formation in fracture healing. However, the functional role of CatK in PSCs remains to be answered in future study.

CatK and Skeletal Diseases

The CatK function has been linked with skeletal homeostasis ever since the discovery of the mutations in CatK gene that are responsible for pycnodysostosis (Gelb et al., 1996), a rare autosomal recessive disorder characterized by osteopetrosis, bone fragility, and decreased bone turnover. *In vitro* studies revealed that the Pycnodysostosis-related mutant CatK proteins

were incapable of degrading type I collagen (Hou et al., 1999). Consistently, the urine levels of cross- linked N- and C-telopeptides of type I collagen (NTX and CTX), two bone resorption markers reflecting the degradation of type I collagen, were both decreased in the pycnodysostosis (Pycno) patients (Nishi et al., 1999), which suggests the low bone resorption activity in pycnodysostosis. Interestingly, the serum levels of Tartrate-resistent acid phosphatas (TRAP) levels, an osteoclast marker, and type I collagen carboxy-terminal propeptide (PICP) and osteocalcin, two bone formation markers reflecting bone martix synthesis, were all normal in Pycno patients (Nishi et al., 1999), suggesting that the generation of osteoclast and bone formation capacity were not affected by the lack of CatK activity in pycnodysostosis. In fact, all the CatK mutations identified in Pycno patients were loss-of-function mutations that appeared to eliminate its enzymatic activity (Hou et al., 1999; Schilling et al., 2007; Li et al., 2009; Bertola et al., 2010; Khan et al., 2010). The bone phenotype of pycnodysostosis was later reproduced in the CatK gene knockout mice, which developed mild osteopetrosis with increased trabecular and cortical bone mass due to impaired osteoclastic bone resorption (Saftig et al., 1998). In contrast, overexpression of CatK in mice resulted in the accelerated bone turnover (Kiviranta et al., 2001). Consistently, it was found that the serum CatK levels were significantly elevated in women with postmenopausal osteoporosis, while they were reduced after the patients were treated with bisphosphonates, the established anti-resorptive agents (Meier et al., 2006). Thus, all these preliminary findings lent support to the idea that targeting CatK could be a promising anti-resorptive strategy for osteoporosis. Thus far, a series of CatK inhibitors have been designed against the human CatK and developed, most of which have proved efficacious in suppressing osteoclastic bone resorption and preventing bone loss in the osteoporotic rodents or non-human primates in preclinical study. Moreover, several inhibitors have been evaluated in clinical trials to treat osteoporosis, which showed excellent efficacy on reducing bone resorption and improving trabecular bone mineral density (BMD) in osteoporotic patients. Unfortunately, despite the beneficial effect on bone, all these CatK inhibitors have currently been discontinued due to various adverse effects beyond bone in clinical trials (Drake et al., 2017).

It is noteworthy that a high bone-formation rate was also observed in the CatK-deficient ($CatK^{-/-}$) mice (Li et al., 2006), while the bone formation remains normal in patients with pycnodysostosis (Nishi et al., 1999; Chavassieux et al., 2008). Impressively, unlike the other classes of anti-resorptive agents (Baron et al., 2011), CatK inhibitors generally do not perturb bone formation (Bromme et al., 2016; Drake et al., 2017). This unexpected phenomenon suggests the uncoupling of bone resorption and bone formation under the deficiency of CatK function. The available evidence from preclinical studies have demonstrated that either CatK deficiency or inhibition did not affect the osteoclastogenesis *in vitro* (Leung et al., 2011), whereas they could maintain or led to the increased osteoclast formation in multiple preclinical animal models *in vivo* (Pennypacker et al., 2009; Duong, 2012). Accordingly, these findings indicate that CatK inhibition, contrary to other anti-resorptive strategies, does not perturb osteoclast formation and survival that are required for the osteoblastic bone formation response during remodeling (Martin and Sims, 2005). From the molecular aspect, a study by Lotinun et al. (2013) found that the CatK-deficient osteoclasts would secrete more sphingosine-1-phosphate (S1P) to enhance osteoblastic bone formation. Moreover, it was recently shown by Xie et al. (2014) that inhibition of CatK could result in the increased number of preosteoclasts, which would facilitate the secretion of platelet-derived growth factor-BB (PDGF-BB) from preosteoclasts to induce the formation of $CD31^{hi}Emcn^{hi}$ vessel subtype (highly expressing CD31 and endomucin) for stimulating bone formation.

Arthritis is a collection of joint disorders affecting the articular cartilage, bone and periarticular tissues such as synovium due to the aberrant mechanical stimulation and/or inflammation. Osteoarthritis (OA) and rheumatoid arthritis (RA) are the most common forms of arthritis, of which the primary pathological feature is the progressive cartilage matrix degradation (Pap and Korb-Pap, 2015). CatK has been implicated in cartilage matrix degradation and OA, since type II collagen, the predominant matrix protein of cartilage, are the substrates of CatK (Kafienah et al., 1998; Mort et al., 2016), while chondroitin sulfates, the glycosaminoglycans (GAGs) abundant in cartilage matrix, could specifically increase the stability and collagenolytic activity of CatK (Li et al., 2000). A recent study further demonstrated that the excess mechanical stress loading could stimulate the CatK expression in human chondrocytes (Suzuki et al., 2020). Moreover, it was shown that the CatK expression in OA cartilage increased in relation to the severity of OA (Konttinen et al., 2002). In human normal cartilage, the CatK expression was only detected in chondocytes at the deep zone of cartilage near subchondral bone, while it was detected in chondrocytes at all layers especially the superficial layer with fissures at cartilage surface in human OA cartilage as well as in human OA synovial tissues (Konttinen et al., 2002; Kozawa et al., 2016). In accordance with these findings, the collagenase-generated cleavage neoepitopes of type II collagen were found to be abundant and extended at all layers of human OA cartilage but only limited in the pericellular area of chondrocyte in human normal cartilage (Dejica et al., 2012). More importantly, the CatK-deficient mice revealed the milder cartilage degradation after anterior cruciate ligament transection (ACLT) when compared with wildtype controls (Hayami et al., 2012), whereas the CatK transgenic mice spontaneously developed synovitis and cartilage degradation (Morko et al., 2005). Taken together, these findings suggest that the increased expression and collagenase activity of CatK could contribute to the cartilage matrix degradation in OA progression. Consequently, CatK is currently among the promising therapeutic target candidates for the development of disease-modifying osteoarthritic drugs. It is encouraging to learn that CatK inhibition could exert obvious chondroprotective effect in preclinical OA models (Connor et al., 2009; McDougall et al., 2010; Hayami et al., 2012; Lindstrom et al., 2018). Furthermore, a novel selective CatK inhibitor MIV-711 by Medivir was recently reflected to reduce bone remodeling and cartilage volume loss but have no impact on pain in OA patients in a Phase-IIa trial (Conaghan et al., 2019). Nevertheless, the structural benefits by CatK inhibition

TABLE 1 | Role of CatK in bone.

Tissues	Diseases	Functions	References
Bone	Pycnodysostosis	Pycnodysostosis-related mutant CatK proteins were incapable of degrading type I collagen. All the CatK mutations identified in Pycno patients were loss-of-function mutations that appeared to eliminate its enzymatic activity.	Gelb et al., 1996; Hou et al., 1999; Nishi et al., 1999
	Postmenopausal osteoporosis	The serum CatK levels were significantly elevated in women with postmenopausal osteoporosis, while they were reduced after the patients were treated with bisphosphonates, the established anti-resorptive agents.	Meier et al., 2006
	OA	The increased expression and collagenase activity of CatK could contribute to the cartilage matrix degradation in OA progression. CatK is currently among the promising therapeutic target candidates for the development of disease-modifying osteoarthritic drugs.	Konttinen et al., 2002; Dejica et al., 2012; Kozawa et al., 2016
	RA	The serum CatK levels were increased in patients with active longstanding RA, which were significantly correlated with the severity of joint destruction. CatK deficiency largely prevented the cartilage erosion and bone destruction and reduced the joint inflammation in mice with TNF-α-mediated arthritis. Inhibition of CatK could suppress the cartilage degradation as well as the systemic and local bone loss to prevent joint destruction in preclinical RA models.	Skoumal et al., 2005; Asagiri et al., 2008; Svelander et al., 2009; Hao et al., 2015; Yamashita et al., 2018; Yamada et al., 2019

TABLE 2 | Role of CatK beyond bone.

Tissues	Disease	Functions	References
Central nervous system	AIS	CatK is required for maintaining the BBB integrity while the absence of CatK activity might result in higher risk of rtPA-induced HT after cerebral ischemia.	Zhao et al., 2019
	CA	Inhibiting CatK could inhibit the excessive ECM degradation, and thus might be beneficial for preventing CA progression.	Aoki et al., 2008
	CSDH	The CatK levels were increased while the Cystatin C levels were decreased when compared with normal controls, suggesting that CatK is highly relevant with the development of CSDH.	Tsutsumi et al., 2017
	Schizophrenia	The CatK expression was markedly upregulated in postmortem brains of patients suffering from schizophrenia who received long-term treatment with neuroleptics. This upregulation of CatK might contribute to the altered opioid levels in brains of schizophrenics probably through processing β-endorphin to release met-enkephalin.	Ko et al., 2006; Lendeckel et al., 2009
Cardiovascular system	Cardiac dysfunction	CatK deficiency are beneficial to cardiac dysfunction, including the obesity-associated cardiac hypertrophy, the pressure overload–induced cardiac hypertrophy, the diabetes-induced cardiac anomalies and the aging-induced cardiac dysfunction.	Hua et al., 2013a,b; Hua et al., 2015; Guo et al., 2017a
	MI	The CatK-deficient mice exhibited worsen post-MI cardiac function along with increased collagen deposition and fibrosis, enhanced cardiac cell death, and reduced cardiac cell proliferation than the wildtype controls.	Fang et al., 2019
	Atherosclerosis	The deficiency of CatK resulted in the reduced number of advanced lesions as well as decreased individual advanced plaque area but increased number of initial plaques in the CatK-deficient apoE$^{-/-}$ mice as compared with the CatK-intact apoE$^{-/-}$.	Lutgens et al., 2006
Respiratory system	Lung fibrosis	The pulmonary fibroblast from CatK-deficient mice showed decreased cathepsin-mediated collagenolytic activity as compared with those from wildtype mice, whereas pulmonary fibroblast from patients with lung fibrosis exhibited enhanced CatK activity.	Bühling et al., 2004
Other organs and systems	Autoimmune diseases	The lack of CatK activity could affect the innate immune response to pathogen DNA by compromising TLR9 signaling in DCs, leading to the attenuated induction of T helper 17 cells without affecting the antigen-presenting ability of DCs.	Asagiri et al., 2008
	Physiological function of thyroid	CatK is expressed by the thyroid epithelial cells and secreted into the follicular lumen for mediating the extracellular proteolysis of the prohormone TG, which is the essential process for the thyroxine liberation.	Tepel et al., 2000; Friedrichs et al., 2003; Jordans et al., 2009
	Overweight/obese	The adipogenesis was enhanced by CatK overexpression but retarded after CatK deficiency. Body weight gained after high-fat diet was remarkably decreased in mice with either genetic knockout or pharmacological inhibition of CatK when compared with the controls.	Funicello et al., 2007; Yang et al., 2008

in OA should be further evaluated and confirmed in longer and larger trials.

Apart from OA, CatK was also involved in RA progression. The high CatK expression was detected in the synovial tissues, particularly in synovial fibroblast, from RA patients (Hummel et al., 1998), as well as in osteoclasts, articular cartilage and synovial tissue in arthritic joints of cynomolgus monkey with collagen-induced arthritis (CIA) (Tanaka et al., 2016), which implies the contribution of CatK to articular bone destruction in the affected joints in RA Further, it was shown that the serum CatK levels were increased in patients with active longstanding RA, which were significantly correlated with the severity of joint destruction (Skoumal et al., 2005). By genetic approach, it was found that CatK deficiency largely prevented

the cartilage erosion and bone destruction and reduced the joint inflammation in mice with TNF-α-mediated arthritis (Hao et al., 2015). By pharmacological approach, several preclinical studies concordantly showed that inhibition of CatK could suppress the cartilage degradation as well as the systemic and local bone loss to prevent joint destruction in preclinical RA models (Asagiri et al., 2008; Svelander et al., 2009; Yamashita et al., 2018; Yamada et al., 2019). Interestingly, the efficacy of CatK inhibition on joint inflammation are contradictory among these studies. Those studies on CIA rodent models all revealed improvement in joint inflammation with CatK inhibition, whereas the study on CIA cynomolgus monkeys showed no impact on joint inflammation with CatK inhibition. This discrepancy maybe attributed to the different susceptibility and immune response to heterogenous collagen between rodents and non-human primates. Collectively, a detrimental role of CatK in RA progression could be concluded, which also suggests that targeting CatK could be a promising therapeutic strategy for RA.

Briefly, the roles of CatK in skeletal diseases are summarized in **Table 1**. Given the fundamental role in mediating bone and cartilage matrix degradation as well as the unique action to bone formation response after inhibition, CatK has become one of the most attractive therapeutic targets in bone in the past two decades. The fact is that most of the CatK inhibitors have failed in clinical trials due to adverse effects beyond bone (Bromme and Lecaille, 2009; Drake et al., 2017). Still, lessons learned from these failures not only extend our knowledge about the underlying biology of CatK and clinical efficacy of CatK inhibitors, but also prompt us to reconsider the CatK action in non-bone sites, which would be valuable for the design and development of novel CatK inhibition strategies.

ROLE OF CatK BEYOND BONE

Central Nervous System (CNS)

CatK has been found to be unevenly and widely distributed in adult rat and human brain especially in multiple neurons as well as in glial cells (Bernstein et al., 2007). Moreover, a previous study by Brix's group revealed a wide range of both molecular and cellular changes in the CNS after ablation of the CatK gene in mice (Dauth et al., 2011). It is noteworthy that an imbalance of the proteolytic network of cysteine cathepsins was found in the brains of CatK-deficient mice. Particularly, when compared with the wildtype mice, the amounts of CatB and CatL proteins in the cortex were decreased while their enzyme activities were unaltered in CatK-deficient mice. Meanwhile, the amounts of CatB and CatL proteins were increased in the striatum/mesencephalon and hippocampus in CatK-deficient mice, respectively, while their enzyme activities decreased together with the increased protein amounts of cystatin C, the endogenous cysteine protease inhibitor, in the same brain regions. These interesting findings indicate that CatK deficiency could trigger the compensative expression of CatB and CatL in brain, while the upregulated cystatin C may serve as a self-feedback mechanism in response to such compensation. Importantly, the dysregulation of CatB and CatL in cerebral cortex has been implicated with dramatic consequences in CNS, including neurodegeneration and brain atrophy (Felbor et al., 2002; Houseweart et al., 2003). Moreover, CatK-deficient mice exhibited reduced anxiety levels and both short- and long-term learning and memory deficits as compared to the wildtype mice (Dauth et al., 2011). Although two later studies by the same group have excluded the possible influence of CatK's function in thyroid and astrocytes on the brain phenotype of CatK-deficient mice (Dauth et al., 2012, 2019), the underlying molecular mechanism responsible for the CNS dysfunction in CatK-deficient mice remains elusive. Cumulatively, it indicates that the existence of CatK should be extremely vital for the development and metabolism of CNS.

The involvement of CatK has been found in various CNS diseases, including stroke, cerebral aneurysm (CA), chronic subdural hematoma (CSDH), and schizophrenia. Zhao et al. (2019) have reported a protective role of CatK in acute ischemic stroke (AIS). The recombinant tissue plasminogen activator (rtPA) is the only approved drug for the standard reperfusion treatment for AIS but could aggravate blood-brain barrier BBB disruption and increase the risk of life-threatening hemorrhagic transformation (HT) (Wardlaw et al., 2013; Khurana et al., 2017; Pena et al., 2017). The study by Zhao et al. (2019) found that CatK-deficient mice had the higher risks of HT, cerebral oedema, blood-brain barrier (BBB) disruption, neurological deficits, and infarct volume after rtPA-treated cerebral ischemia comparing with the wild types. At the molecular levels, they observed the upregulation of vascular endothelial growth factor (VEGF) and downregulation of Akt/mTOR pathway in the ischemic brain of CatK-deficient mice, which were thought to contribute to the BBB leakage in the acute ischemic brain (Zhang et al., 2000, 2017; Greenberg and Jin, 2013). Although a protective role of CatK on BBB integrity has been proposed in this study, the underlying mechanism is largely unknown and requires further study. Nevertheless, it hints that the inhibition of CatK could pose higher risk of rtPA-induced HT in patients with AIS.

The extensive breakdown of extracellular matrix (ECM) in arterial wall is a prominent pathological feature of cerebral aneurysm (CA) (Penn et al., 2011). The study by Aoki et al. (2008) attributed this aberrant change to the imbalance between cysteine cathepsins, including CatK, CatB, and CatS, and their endogenous inhibitor Cystatin C in CA development. It was found that the expression of CatK and the other two cysteine cathepsins were upregulated mainly in the late stage of CA, whereas the Cystatin C expression was downregulated with the progression of experimental CA in rats. Impressively, administration of NC-2300, an inhibitor of most of cysteine proteases, could prevent CA progression in rats by inhibiting ECM degradation in aneurysmal walls caused by cysteine cathepsins. These results suggest that inhibition of CatK might be beneficial for preventing CA progression. Intriguingly, the unusual imbalance between CatK and Cystatin C was also found to be associated with the process of chronic subdural hematoma (CSDH), another pathological conditions of CNS after head injury, according to the research by Tsutsumi et al. (2017) on a group of 42 patients with symptomatic CSDH. The results showed that both the CatK and Cystatin C levels

were concentrated in CSDH and intracranial cerebrospinal fluid (CSF). However, in peripheral venous blood of CSDH patients, the CatK levels were increased while the Cystatin C levels were decreased when compared with normal controls. The immunohistochemistry staining further revealed the diffuse CatK expression in the outer membrane of CSDH (Tsutsumi et al., 2017). This study suggests that CatK is highly relevant with the development of CSDH.

It was previously found that the CatK gene were among the very few genes that were linked to schizophrenia with various antipsychotic treatment (Ko et al., 2006), wherein its expression in rodent brain striatum was downregulated by the psychotropic substance amphetamine but was upregulated by typical and atypical neuroleptic. Consistently, Lendeckel et al. reported in a later study showing that the CatK expression was markedly upregulated in postmortem brains of patients suffering from schizophrenia who received long-term treatment with neuroleptics (Bernstein et al., 2007). By immunohistochemistry, they further identified that CatK was largely colocalized with enkephalinergic and endorphinergic innervated structures in hypothalamic nuclei (Lendeckel et al., 2009). Interestingly, they also observed a dose-dependent increase of CatK mRNA expression in dopamine receptor-expressing SH-SY5Y cells in response to the treatment of the neuroleptic agent haloperidol (Lendeckel et al., 2009), which reinforced the previous findings by Ko et al. (2006). They further demonstrated that the upregulated cerebral CatK expression by neuroleptic treatment might contribute to the altered opioid levels in brains of schizophrenics probably through processing β-endorphin to release met-enkephalin (Lendeckel et al., 2009).

Cardiovascular System

The endocardial CatK expression is regulated by RANKL (receptor activator of NFκB ligand)/RANK-NFATc1 signaling pathway (Lange and Yutzey, 2006). Although only a small amount of CatK was detected in normal heart and artery tissues (Inaoka et al., 1995; Sukhova et al., 1998), its expression was significantly upregulated in failing heart, abdominal aortic aneurysms (AAA) lesion and atherosclerotic lesions (Sukhova et al., 1998; Shi et al., 1999; Lutgens et al., 2006). Consistently, the existing evidence from a series of studies on the genetic CatK knockout mouse reveal that CatK is not essentially required for the organogenesis and postnatal development of cardiovascular system (Lange and Yutzey, 2006), but it is actively involved in the progression of various cardiovascular diseases (Lutgens et al., 2007).

The link between CatK and cardiac dysfunction has been extensively studied. Zhao and colleagues previously found that the elevated serum CatK levels were closely associated with the presence of chronic heart failure (CHF) (Zhao et al., 2015). They showed that patients with CHF who showed a low left ventricular ejection fraction (LVEF) had significantly higher serum CatK levels than those who showed a high LVEF. Consistently, in another study by Hua et al. (2013a) they detected the high CatK expression in human hearts of end-stage dilated cardiomyopathy. On the other hand, the Nair's group has reported serial studies on CatK knockout mice to authenticate the essential contribution of CatK to cardiac dysfunction, including the obesity-associated cardiac hypertrophy (Hua et al., 2013b), the pressure overload–induced cardiac hypertrophy (Hua et al., 2013a), the diabetes-induced cardiac anomalies (Guo et al., 2017a), and the aging-induced cardiac dysfunction (Hua et al., 2015). They reported several benefits of CatK deficiency to the heart including : (1) inhibiting the expression of cardiac hypertrophic proteins and apoptotic markers and partly reversing the impaired cardiomyocyte contractility associated with high-fat diet (Hua et al., 2013b), (2) attenuating the pressure overload-induced upregulation of mammalian target of rapamycin and extracellular signal-regulated kinases (ERK) signaling cascades and partly resolving the pressure overload-induced cardiac hypertrophy (Hua et al., 2013a), (3) reducing the cardiac oxidative stress and calcineurin/NFAT signaling and mitigating the cardiac dysfunction in streptozotocin-induced diabetes (Guo et al., 2017a), and (4) ameliorating the aging-related decline in cardiac function via suppressing caspase-dependent and caspase-independent cardiomyocyte apoptosis (Hua et al., 2015). Moreover, in another study on the cardiomyocyte-specific CatK-deficient mouse model by the same group, they showed that the doxorubicin-induced cardiotoxicity could be ameliorated by cardiomyocyte-specific ablation of CatK (Guo et al., 2018). Collectively, these serial studies hint the crucial role of CatK in cardiac dysfunction. Intriguingly, a recent study by Fang et al. (2019) showed that the plasma CatK levels were significantly increased in patients with coronary heart diseases (CHD) particularly in those with acute myocardial infarction (MI) when compared to non-CHD controls. They further detected the elevated CatK expression in heart from the post-MI mouse, which mainly localized to cardiomyocytes, ECs, fibroblasts, macrophages and $CD4^{+++}$ T cells as well. Surprisingly, contrary to the aforementioned protective role of CatK deficiency on cardiac function (Hua et al., 2013a,b, 2015; Guo et al., 2017a, 2018), they found that the CatK-deficient mice exhibited worsen post-MI cardiac function along with increased collagen deposition and fibrosis, enhanced cardiac cell death, and reduced cardiac cell proliferation than the wildtype controls. Moreover, they showed that CatK deficiency or inhibition increased cardiomyocyte death, whereas CatK inhibition suppressed CD4+ T-cell and macrophage death *in vitro*. These findings in turn hint a protective role of CatK on the cardiac function after MI. In addition, a research group from Japan studied the link between CatK and atrial fibrillation (AF) (Fujita et al., 2013). They found that the plasma CatK levels were higher in patients with persistent AF than those with paroxysmal AF. Moreover, the atrial CatK expression and activity were found to be also increased in the rabbits with tachypacing-induced AF, which could be attributed to the activation of Ang II (angiotensin II)/AT1R (angiotensin type 1 receptor) signaling pathway in the atrium with AF. Although the atrial CatK expression seems to be closely associated with the presence of AF, it requires further mechanistic studies to determine the effect of CatK deficiency or inhibition on AF.

Apart from cardiac dysfunction, CatK has been implicated in the pathogenesis of other cardiovascular disorders including AAA, coronary artery diseases and atherosclerosis. The

concurrent overexpression of CatK and CatS was previously identified in the human AAA lesions (Shi et al., 1999). A later study by Sun and colleagues further confirmed that CatK could play an essential role in AAA formation (Sun et al., 2012). They found that CatK knockout mice were protected from elastase perfusion-induced experimental AAA. Mechanistically, it was shown that CatK could promote T-cell proliferation, vascular SMC apoptosis, and elastin degradation to contribute to AAA formation. Cheng et al. (2013) studied the relationship between plasma circulating CatK and the prevalence of coronary artery disease (CAD), by which they showed that CatK level was an independent predictor of CAD. In this study, they found that patients with CAD had higher circulating CatK levels than the non-CAD controls. The CatK levels were positively correlated with the ratios of ICTP (cross linked carboxy-terminal telopeptide of collagen type I) /I-PINP (intact procollagen type I N-terminal propeptide), the collagen turnover-related index, indicating that the elevated circulating CatK levels were closely associated with the increased collagen turnover in CAD patients. Interestingly, among the CAD patients, the individuals with acute coronary syndrome had higher CatK levels than those with stable angina pectoris. More importantly, the CatK levels were found to be correlated positively with the percent plaque volumes and inversely with the percent fibrous volumes of coronary artery by intravascular ultrasound. These clinical findings were in line with the previous histopathological findings in human atheroma specimens showing that CatK expression was remarkably upregulated in the atherosclerotic lesions of human aorta (Sukhova et al., 1998; Lutgens et al., 2006). Specifically, the CatK expression was detected in the intima and medial SMCs of early human atherosclerotic lesions and in macrophages and SMCs of the fibrous cap in advanced atherosclerotic plaques (Sukhova et al., 1998). All these findings indicate the possible involvement of CatK in atherosclerosis. The role of CatK on the progression of atherosclerotic plaque was further investigated in the study by Lutgens and colleagues using the atherosclerosis-prone mouse model with CatK deficiency ($CatK^{-/-}apoE^{-/-}$ mice) (Lutgens et al., 2006). They found that the deficiency of CatK resulted in the reduced number of advanced lesions as well as decreased individual advanced plaque area but increased number of initial plaques in the CatK-deficient $apoE^{-/-}$ mice as compared with the CatK-intact $apoE^{-/-}$. Moreover, the atherosclerotic plaques were highly fibrotic in CatK-deficient $apoE^{-/-}$ mice, which characterizing a stable plaque phenotype. On the other hand, Platt et al. observed the increased expression and activity of CatK in mouse aortic endothelial cells (MAEC) exposed to proatherogenic oscillatory shear (OS) than the MAECs exposed to atheroprotective, unidirectional laminar shear stress (LS) (Platt et al., 2007). They further showed that knocking down CatK with small-interfering RNA (siRNA) could decreased OS-dependent elastase and gelatinase activities in MAECs. Similarly, another recent study reported that genetic knockout of CatK could mitigate the calcification, migration and proliferation of mouse aortic vascular SMCs (Guo et al., 2017b), which may contribute to the vascular calcification and intimal thickening in atherosclerosis. Collectively, these findings suggest that CatK deficiency may have a protective role in atherosclerosis by increasing plaque fibrosis and decreasing the aberrant arterial wall remodeling. Interestingly, in the aforementioned study by Lutgens et al. (2006) they also showed that CatK deficiency in $apoE^{-/-}$ mice simultaneously accelerated the formation of macrophage foam cells, the featured cell type occupying much of the lesion volume in early to intermediate atherosclerotic lesion that could lead to the progression of atherosclerosis (Rader and Pure, 2005). Both the scavenger receptor (SR)-mediated uptake of oxidized low-density lipoprotein (OX-LDL) and the storage of cholesterol esters in macrophages, as well as the lysosomal size of macrophage foam cells, were found to be increased in the absence of CatK (Lutgens et al., 2006). In addition, the CatK-deficient $apoE^{-/-}$ mice in this study showed a trend toward increased serum cholesterol, LDL cholesterol, and triglyceride levels and decreased HDL cholesterol levels (Lutgens et al., 2006), while these changes in serum lipid profile are generally considered as the clinical pro-atherogenic factor (Linton et al., 2000). Therefore, these findings not only hint a potential role of CatK in lipid metabolism, but also indicate that CatK deficiency could aggravate the formation of macrophage foam cells, which may affect the plaque stability.

Respiratory System

It is known that the lysosomal cysteine proteases play a crucial role in ECM remodeling, immunoregulation and surfactant protein processing in the lung (Buhling et al., 2004). As one of the most potent cysteine proteases, CatK has been linked with various diseases of the respiratory system. The aberrant CatK activity is closely associated with the inadequate collagen turnover in the lung.

The expression of CatK was detected in the bronchial and alveolar epithelial cells as well as alveolar macrophages in the normal lung (Buhling et al., 1999; Haeckel et al., 1999; Buhling et al., 2001). In fact, CatK plays a pivotal role in pulmonary homeostasis through collagen cleavage, which is required for the airway structural integrity (Bühling et al., 2004; Zhang et al., 2011). A previous study on CatK-deficient mice demonstrated that CatK could partly regulate mouse airway development (Zhang et al., 2011). Meanwhile, TGF-β1 was proven as an efficient substrate of CatK. This finding echoed the previous finding on the inverse correlation between the expression of CatK and TGF-β1 in lung tissues of mice with silica-induced lung fibrosis (van den Brule et al., 2005). Collectively, it indicates that the interaction between CatK and TGF-β1 might be necessary for preventing the excessive TGF-β1-driven airway remodeling, which is important for the airway development and lung homeostasis. Bühling et al. (2004) reported a protective role of CatK in lung fibrosis. They showed that CatK-deficient mice developed more pulmonary fibrosis than wildtype controls after bleomycin induction. The pulmonary fibroblast from CatK-deficient mice showed decreased cathepsin-mediated collagenolytic activity as compared with those from wildtype mice, whereas pulmonary fibroblast from patients with lung fibrosis exhibited enhanced CatK activity. Interestingly, they further showed that, comparing with nonfibrotic lung tissues, CatK expression was significantly upregulated in the fibrotic lung tissues from mice and patients with pulmonary fibrosis,

which could be dominantly contributed by the excessive CatK expression in pulmonary fibroblasts but not in bronchial epithelial cells and alveolar macrophages that were previously considered as the major cell type with CatK expression in lung (Buhling et al., 1999, 2001; Haeckel et al., 1999). The upregulated CatK expression in the fibrotic lung may reflect the self-defense mechanism in response to lung fibrosis.

Despite the protective role of CatK on lung fibrosis is univocal, the over-expression of CatK could be harmful in some other lung diseases. For example, lung emphysema, of which cigarette smoking is the major cause, was closely associated with CatK over-expression in lung (Zheng et al., 2000; Golovatch et al., 2009). The activity of CatK instead of MMPs was found to be upregulated in the lung tissues of guinea pig with cigarette smoke-induced emphysema, which may contribute to the remodeling of the lung ECM with disease progression (Golovatch et al., 2009). Additionally, a recent study done by Kubler et al. (2016) reported the negative impact of CTSK over-expression in active pulmonary tuberculosis (TB). It was observed that CatK was most abundantly expressed in cavitary lesion, which was associated with the collagen turnover of cavitation in a rabbit model of TB. They also found the increased plasma CatK levels in patients with TB when compared with healthy controls, which, as they suggested, was a feature of active pulmonary tuberculosis.

CatK has also been connected with some of the lung tumors. It was found that CatK was diffusely and strongly expressed in pulmonary perivascular epithelioid cell tumor and it maybe a potential biomarker for identification of such kind of disease (Calio et al., 2018). In addition, the expression of CatK was restricted in the LAM cells in pulmonary lymphangioleiomyomatosis (LAM), a rare disease in which LAM cells and fibroblasts form lung nodules (Chilosi et al., 2009). Dongre et al. (2017) recently reported that LAM nodule-derived CatK activity, which was thought to contribute to cyst formation and tissue damage in lung (Chilosi et al., 2009), was largely dependent on the interactions between LAM cells and lung fibroblasts.

Other Organs and Systems

CatK could play a unique role in autoimmune diseases. Researchers have previously showed that either genetic deficiency or pharmacological inhibition of CatK could suppress the autoimmune inflammation in animals with experimental autoimmune encephalomyelitis and adjuvant-induced arthritis and lupus, respectively (Asagiri et al., 2008; Zhou et al., 2017). In the study by Takayanagi's group, they demonstrated that the lack of CatK activity could affect the innate immune response to pathogen DNA by compromising Toll-like receptors 9 (TLR9) signaling in dendritic cells (DCs), leading to the attenuated induction of T helper 17 cells without affecting the antigen-presenting ability of DCs (Asagiri et al., 2008). In another study by Shi's group, they showed that CatK could contribute to autoimmune inflammation by regulating TLR7 expression, proteolytically processing TLR7, reducing the T regulatory cells (Tregs) numbers, and suppressing Treg immunosuppression activity against T effector cells (Zhou et al., 2017).

CatK is also involved in the physiological function of thyroid. It is expressed by the thyroid epithelial cells and secreted into the follicular lumen for mediating the extracellular proteolysis of the prohormone thyroglobulin (TG), which is the essential process for the thyroxine liberation (Tepel et al., 2000; Friedrichs et al., 2003; Jordans et al., 2009). Interestingly, it was found that serum CatK levels were increased by a suppressive L-thyroxine therapy but negatively correlated with aging in patients with differentiated thyroid cancer, although reasons account for this phenomenon remains unclear (Mikosch et al., 2008). On the other hand, the osteoclast-like multinucleated giant cells (MGCs) with CatK-expression were previously identified in the tumor mass of patients with anaplastic carcinoma of the thyroid gland (ACT), which were postulated to contribute to the invasive behavior of this tumor (Gaumann et al., 2001).

The CatK expression was also detected in white adipose tissue (Soukas et al., 2000; Chiellini et al., 2003), and it was markedly increased in the overweight/obese mice and peoples as compared to their controls with normal weight (Xiao et al., 2006; Yang et al., 2008). Previous studies have elegantly demonstrated that CatK could play a critical role in adipogenesis, since its expression was detected in pre-adipocytes and gradually upregulated during adipocyte differentiation (Chiellini et al., 2003), while the adipogenesis was enhanced by CatK overexpression but retarded after CatK deficiency (Funicello et al., 2007; Yang et al., 2008). In addition, body weight gained after high-fat diet was remarkably decreased in mice with either genetic knockout or pharmacological inhibition of CatK when compared with the controls (Yang et al., 2008). Moreover, the CatK-deficient mice also revealed a higher lipolytic rate in young age, an increased rate of free fatty acid oxidation after high-fat diet, and the altered serum cholesterol profiles upon the apolipoprotein E knockout, respectively, when compared with wildtype controls (Lutgens et al., 2006; Funicello et al., 2007). These findings implied the role of CatK in lipid homeostasis and metabolism.

On the other hand, the activities of CatK in skin areas is conditional. CatK gene was not detectable under normal conditions (Runger et al., 2007), but it was strongly expressed under certain circumstances, such as inflammation, scar formation and other cell-rich fibrosing processes (Quintanilla-Dieck et al., 2009). It was found that CatK expression was especially prominent in young scars and reduced with time (Quintanilla-Dieck et al., 2009). In addition to scar formation, a vital role of CatK was also suggested in primary melanomas and cutaneous melanoma metastases (Quintanilla-Dieck et al., 2008). Besides, the upregulation of CatK in the psoriatic lesions of patients with psoriasis was documented by Hirai et al. (2013). Coincidently, the upregulated CatK was found to be associated with oral squamous cell carcinoma (OSCC), in which CatK may be served as a predictive biomarker according to the study by Leusink et al. (2018).

Collectively, the roles of CatK beyond bone are summarized in **Table 2**. To sum up, based on the currently available evidence from CatK-deficient mouse model, it appears that the lack of CatK activity could bring benefits to the heart and vessels. However, results from the Phase III clinical trial of odanacatib have recorded a significantly higher incidence of

stroke, more episodes of new or recurrent atrial fibrillation or flutter and more cases of cardiovascular death in the odanacatib group as compared with placebo group (McClung et al., 2019), which highlight the cardiovascular adverse effects associated with CatK inhibition. It remains to be answered whether these cardiovascular adverse effects are attributable to the potential off-target of odanacatib or the direct inhibition of CatK in cardio-cerebrovascular tissues. Nevertheless, the inconsistency of cardiovascular impact between CatK knockout and CatK inhibition remind us that inactivation of this protease may not necessarily mimic the consequences of gene deficiency. Since inhibition of CatK with odanacatib treatment could result in the elevated CatK expression and accumulation in osteoclasts *in vitro* (Leung et al., 2011), it is plausible that CatK inhibitor could also induce the upregulation of CatK in cardio-cerebrovascular cells, which is thought to be detrimental to heart and vessels, and thus, worth further investigation. On the other hand, another CatK inhibitor Balicatib were terminated in Phase II trials due to cutaneous lesions such as pruritus, skin rashes and rare morphea-like skin changes as reported (Peroni et al., 2008; Runger et al., 2012). These dermatologic adverse events were thought to be attributed to the lysosomotropism property of this basic compound, which potentially led to the off-target inhibition of cathepsins B, L, and S expressed in skin fibroblasts. This failure in turn alerts us the importance of designing the highly selective CatK inhibitor to avoid off-target side effects.

CONCLUSION

Currently, CatK was among the most attractive targets for anti-osteoporosis drug development. This cysteine protease bears important functions in mediating bone resorption. However, the activity of CatK has far-reaching effects throughout various organs besides bone. The fact is that CatK not only demonstrates vastly distinct functional roles beyond bone, but also involves in various diseases beyond the musculoskeletal system. Nevertheless, the exact role of CatK and the underlying mechanisms in these diseases are not well-elaborated. Therefore, more in-depth mechanistic studies are urgently required to delineate the critical roles of CatK in these diseases. In another word, the sophisticated roles of CatK in various diseases beyond the musculoskeletal system would in turn pose the higher risk of adverse effects in non-bone sites after inhibiting CatK. Thus, researchers should be alerted to these risks when CatK inhibitors are developed as anti-osteoporosis drugs, while physicians should be more cautious when CatK inhibitors are prescribed for anti-osteoporosis treatment in patients with or with increased risk of developing those diseases. On the other hand, aptamer-drug conjugates (ApDC) have emerged over the past decades as a class of potential targeting agents to improve the efficacy of the traditional chemical compounds and overcome their potential side effect in off-target organs (Chen et al., 2017). Therefore, as an alternative strategy, it would be desirable to design and develop the novel "smart" CatK inhibitor chemically conjugated with bone-targeted aptamer (Zhang et al., 2012; Liu et al., 2015), by which it would facilitate the CatK inhibitor targeting bone to reduce its exposure in non-bone sites so as to prevent the potential adverse effects beyond bone.

AUTHOR CONTRIBUTIONS

RD and ZW did literature searching and prepared the manuscript. HC, JLu and AL helped in revising the manuscript. JLiu and GZ conceived the review topic and wrote most of the manuscript.

FUNDING

This work was supported by the National Key R&D Program of China (2018YFA0800804), the Hong Kong General Research Fund (HKBU12102914 to GZ, HKBU12101117 to GZ, HKBU12136616 to JLiu, and HKBU12103519 to JLiu), the National Natural Science Foundation Council of China (81702189 to JLiu and 81803374 to JLu), Shenzhen Science and Technology innovation fund (JCYJ20180302174121208 to JLu), the Science and Technology Planning Project of Shantou (190430105264372 to ZW), the Interdisciplinary Research Clusters Matching Scheme of Hong Kong Baptist University (RC-IRCs/17-18/02 to GZ), and the Quality Project of Shantou University Medical College (2019 Quality Project to ZW).

ACKNOWLEDGMENTS

Sincere thanks should go to the other academic and staff members in AL and GZ's group at the Hong Kong Baptist University.

REFERENCES

Aoki, T., Kataoka, H., Ishibashi, R., Nozaki, K., and Hashimoto, N. (2008). Cathepsin B, K, and S are expressed in cerebral aneurysms and promote the progression of cerebral aneurysms. *Stroke* 39, 2603–2610. doi: 10.1161/STROKEAHA.107.513648

Asagiri, M., Hirai, T., Kunigami, T., Kamano, S., Gober, H. J., Okamoto, K., et al. (2008). Cathepsin K-dependent toll-like receptor 9 signaling revealed in experimental arthritis. *Science* 319, 624–627. doi: 10.1126/science.1150110

Balkan, W., Martinez, A. F., Fernandez, I., Rodriguez, M. A., Pang, M., and Troen, B. R. (2009). Identification of NFAT binding sites that mediate stimulation of cathepsin K promoter activity by RANK ligand. *Gene* 446, 90–98. doi: 10.1016/j.gene.2009.06.013

Baron, R., Ferrari, S., and Russell, R. G. (2011). Denosumab and bisphosphonates: different mechanisms of action and effects. *Bone* 48, 677–692. doi: 10.1016/j.bone.2010.11.020

Bernstein, H. G., Bukowska, A., Dobrowolny, H., Bogerts, B., and Lendeckel, U. (2007). Cathepsin K and schizophrenia. *Synapse* 61, 252–253. doi: 10.1002/syn.20358

Bertola, D., Amaral, C., Kim, C., Albano, L., Aguena, M., and Passos-Bueno, M. R. (2010). Craniosynostosis in pycnodysostosis: broadening the spectrum of the cranial flat bone abnormalities. *Am. J. Med. Genet. A* 152A, 2599–2603. doi: 10.1002/ajmg.a.33609

Bonnet, N., Brun, J., Rousseau, J. C., Duong, L. T., and Ferrari, S. L. (2017). Cathepsin K controls cortical bone formation by degrading periostin. *J Bone Miner. Res.* 32, 1432–1441. doi: 10.1002/jbmr.3136

Bonnet, N., Standley, K. N., Bianchi, E. N., Stadelmann, V., Foti, M., Conway, S. J., et al. (2009). The matricellular protein periostin is required for sost inhibition and the anabolic response to mechanical loading and physical activity. *J. Biol. Chem.* 284, 35939–35950. doi: 10.1074/jbc.M109.060335

Bossard, M. J., Tomaszek, T. A., Thompson, S. K., Amegadzie, B. Y., Hanning, C. R., Jones, C., et al. (1996). Proteolytic activity of human osteoclast cathepsin K. Expression, purification, activation, and substrate identification. *J. Biol. Chem.* 271, 12517–12524. doi: 10.1074/jbc.271.21.12517

Bromme, D., and Lecaille, F. (2009). Cathepsin K inhibitors for osteoporosis and potential off-target effects. *Expert Opin. Investig. Drugs* 18, 585–600. doi: 10.1517/13543780902832661

Bromme, D., and Okamoto, K. (1995). Human cathepsin O2, a novel cysteine protease highly expressed in osteoclastomas and ovary molecular cloning, sequencing and tissue distribution. *Biol. Chem. Hoppe Seyler* 376, 379–384. doi: 10.1515/bchm3.1995.376.6.379

Bromme, D., Panwar, P., and Turan, S. (2016). Cathepsin K osteoporosis trials, pycnodysostosis and mouse deficiency models: commonalities and differences. *Expert Opin. Drug Discov.* 11, 457–472. doi: 10.1517/17460441.2016.1160884

Buhling, F., Gerber, A., Hackel, C., Kruger, S., Kohnlein, T., Bromme, D., et al. (1999). Expression of cathepsin K in lung epithelial cells. *Am. J. Respir. Cell Mol. Biol.* 20, 612–619.

Buhling, F., Reisenauer, A., Gerber, A., Kruger, S., Weber, E., Bromme, D., et al. (2001). Cathepsin K–a marker of macrophage differentiation? *J. Pathol.* 195, 375–382. doi: 10.1002/path.959

Bühling, F., Röcken, C., Brasch, F., Hartig, R., Yasuda, Y., Saftig, P., et al. (2004). Pivotal role of cathepsin K in lung fibrosis. *Am. J. Pathol.* 164, 2203–2216. doi: 10.1016/s0002-9440(10)63777-7

Buhling, F., Waldburg, N., Reisenauer, A., Heimburg, A., Golpon, H., and Welte, T. (2004). Lysosomal cysteine proteases in the lung: role in protein processing and immunoregulation. *Eur. Respir. J.* 23, 620–628. doi: 10.1183/09031936.04.00105304

Calio, A., Mengoli, M. C., Cavazza, A., Rossi, G., Ghimenton, C., Brunelli, M., et al. (2018). Cathepsin K expression in clear cell "sugar" tumor (PEComa) of the lung. *Virchows Arch.* 473, 55–59. doi: 10.1007/s00428-018-2325-1

Chavassieux, P., Asser Karsdal, M., Segovia-Silvestre, T., Neutzsky-Wulff, A. V., Chapurlat, R., Boivin, G., et al. (2008). Mechanisms of the anabolic effects of teriparatide on bone: insight from the treatment of a patient with pycnodysostosis. *J. Bone Miner. Res.* 23, 1076–1083. doi: 10.1359/jbmr.080231

Chen, K., Liu, B., Yu, B., Zhong, W., Lu, Y., Zhang, J., et al. (2017). Advances in the development of aptamer drug conjugates for targeted drug delivery. *Wiley Interdiscip. Rev. Nanomed. Nanobiotechnol.* 9:e1438. doi: 10.1002/wnan.1438

Cheng, X. W., Kikuchi, R., Ishii, H., Yoshikawa, D., Hu, L., Takahashi, R., et al. (2013). Circulating cathepsin K as a potential novel biomarker of coronary artery disease. *Atherosclerosis* 228, 211–216. doi: 10.1016/j.atherosclerosis.2013.01.004

Chiellini, C., Costa, M., Novelli, S. E., Amri, E. Z., Benzi, L., Bertacca, A., et al. (2003). Identification of cathepsin K as a novel marker of adiposity in white adipose tissue. *J. Cell. Physiol.* 195, 309–321. doi: 10.1002/jcp.10253

Chilosi, M., Pea, M., Martignoni, G., Brunelli, M., Gobbo, S., Poletti, V., et al. (2009). Cathepsin-K expression in pulmonary lymphangioleiomyomatosis. *Mod. Pathol.* 22, 161–166. doi: 10.1038/modpathol.2008.189

Christensen, J., and Shastri, V. P. (2015). Matrix-metalloproteinase-9 is cleaved and activated by cathepsin K. *BMC Res. Notes* 8:322. doi: 10.1186/s13104-015-1284-8

Conaghan, P. G., Bowes, M. A., Kingsbury, S. R., Brett, A., Guillard, G., Rizoska, B., et al. (2019). Disease-modifying effects of a novel cathepsin K inhibitor in osteoarthritis: a randomized, placebo-controlled study. *Ann. Intern. Med.* 172, 86–95. doi: 10.7326/M19-0675

Connor, J. R., LePage, C., Swift, B. A., Yamashita, D., Bendele, A. M., Maul, D., et al. (2009). Protective effects of a cathepsin K inhibitor, SB-553484, in the canine partial medial meniscectomy model of osteoarthritis. *Osteoarthr. Cartil.* 17, 1236–1243. doi: 10.1016/j.joca.2009.03.015

Costa, A. G., Cusano, N. E., Silva, B. C., Cremers, S., and Bilezikian, J. P. (2011). Cathepsin K: its skeletal actions and role as a therapeutic target in osteoporosis. *Nat. Rev. Rheumatol.* 7, 447–456. doi: 10.1038/nrrheum.2011.77

Dauth, S., Rakov, H., Sirbulescu, R. F., Ilies, I., Weber, J., Batbajar Dugershaw, B., et al. (2019). Function of Cathepsin K in the central nervous system of male mice is independent of its role in the thyroid gland. *Cell. Mol. Neurobiol.* 1–16. doi: 10.1007/s10571-019-00765-6

Dauth, S., Schmidt, M. M., Rehders, M., Dietz, F., Kelm, S., Dringen, R., et al. (2012). Characterisation and metabolism of astroglia-rich primary cultures from cathepsin K-deficient mice. *Biol. Chem.* 393, 959–970. doi: 10.1515/hsz-2012-0145

Dauth, S., Sirbulescu, R. F., Jordans, S., Rehders, M., Avena, L., Oswald, J., et al. (2011). Cathepsin K defi ciency in mice induces structural and metabolic changes in the central nervous system that are associated with learning and memory deficits. *BMC. Neurosci.* 12:74. doi: 10.1186/1471-2202-12-74

Debnath, S., Yallowitz, A. R., McCormick, J., Lalani, S., Zhang, T., Xu, R., et al. (2018). Discovery of a periosteal stem cell mediating intramembranous bone formation. *Nature* 562, 133–139. doi: 10.1038/s41586-018-0554-8

Dejica, V. M., Mort, J. S., Laverty, S., Antoniou, J., Zukor, D. J., Tanzer, M., et al. (2012). Increased type II collagen cleavage by cathepsin K and collagenase activities with aging and osteoarthritis in human articular cartilage. *Arthritis Res. Ther.* 14:R113. doi: 10.1186/ar3839

Delany, A. M., Amling, M., Priemel, M., Howe, C., Baron, R., and Canalis, E. (2000). Osteopenia and decreased bone formation in osteonectin-deficient mice. *J. Clin. Invest.* 105, 1325. doi: 10.1172/jci7039c1

Dongre, A., Clements, D., Fisher, A. J., and Johnson, S. R. (2017). Cathepsin K in lymphangioleiomyomatosis: LAM cell-fibroblast interactions enhance protease activity by extracellular acidification. *Am. J. Pathol.* 187, 1750–1762. doi: 10.1016/j.ajpath.2017.04.014

Drake, F. H., Dodds, R. A. I, James, E., Connor, J. R., Debouck, C., Richardson, S., et al. (1996). Cathepsin K, but not cathepsins B, L, or S, is abundantly expressed in human osteoclasts. *J. Biol. Chem.* 271, 12511–12516. doi: 10.1074/jbc.271.21.12511

Drake, M. T., Clarke, B. L., Oursler, M. J., and Khosla, S. (2017). Cathepsin K inhibitors for osteoporosis: biology, potential clinical utility, and lessons learned. *Endocr. Rev.* 38, 325–350. doi: 10.1210/er.2015-1114

Duong, L. T. (2012). Therapeutic inhibition of cathepsin K-reducing bone resorption while maintaining bone formation. *Bonekey Rep.* 1:67. doi: 10.1038/bonekey.2012.67

Fang, W., He, A., Xiang, M. X., Lin, Y., Wang, Y., Li, J., et al. (2019). Cathepsin K-deficiency impairs mouse cardiac function after myocardial infarction. *J. Mol. Cell. Cardiol.* 127, 44–56. doi: 10.1016/j.yjmcc.2018.11.010

Felbor, U., Kessler, B., Mothes, W., Goebel, H. H., Ploegh, H. L., Bronson, R. T., et al. (2002). Neuronal loss and brain atrophy in mice lacking cathepsins B and L. *Proc. Natl. Acad. Sci. U.S.A.* 99, 7883–7888. doi: 10.1073/pnas.112632299

Friedrichs, B., Tepel, C., Reinheckel, T., Deussing, J., von Figura, K., Herzog, V., et al. (2003). Thyroid functions of mouse cathepsins B, K, and L. *J. Clin. Invest.* 111, 1733–1745. doi: 10.1172/jci15990

Fujita, M., Cheng, X. W., Inden, Y., Shimano, M., Yoshida, N., Inoue, A., et al. (2013). Mechanisms with clinical implications for atrial fibrillation-associated remodeling: cathepsin K expression, regulation, and therapeutic target and biomarker. *J. Am. Heart Assoc.* 2:e000503. doi: 10.1161/JAHA.113.000503

Funicello, M., Novelli, M., Ragni, M., Vottari, T., Cocuzza, C., Soriano-Lopez, J., et al. (2007). Cathepsin K null mice show reduced adiposity during the rapid accumulation of fat stores. *PLoS One* 2:e683. doi: 10.1371/journal.pone.0000683

Garber, K. (2016). Two pioneering osteoporosis drugs finally approach approval. *Nat. Rev. Drug. Discov.* 15, 445–446. doi: 10.1038/nrd.2016.132

Garnero, P., Borel, O., Byrjalsen, I., Ferreras, M., Drake, F. H., McQueney, M. S., et al. (1998). The collagenolytic activity of cathepsin K is unique among mammalian proteinases. *J. Biol. Chem.* 273, 32347–32352. doi: 10.1074/jbc.273.48.32347

Gaumann, A., Hansen, T., Kohler, H. H., Kommoss, F., Mann, W., Maurer, J., et al. (2001). The expression of cathepsins in osteoclast-like giant cells of an anaplastic thyroid carcinoma with tracheal perforation. *Pathol. Res. Pract.* 197, 257–262. doi: 10.1078/0344-0338-00044

Gelb, B. D., Shi, G. P., Chapman, H. A., and Desnick, R. J. (1996). Pycnodysostosis, a lysosomal disease caused by cathepsin K deficiency. *Science* 273, 1236–1238. doi: 10.1126/science.273.5279.1236

Golovatch, P., Mercer, B. A., Lemaitre, V., Wallace, A., Foronjy, R. F., and D'Armiento, J. (2009). Role for cathepsin K in emphysema in smoke-exposed guinea pigs. *Exp. Lung Res.* 35, 631–645. doi: 10.3109/01902140902822304

Gowen, M., Lazner, F., Dodds, R., Kapadia, R., Feild, J., Tavaria, M., et al. (1999). Cathepsin K knockout mice develop osteopetrosis due to a deficit in matrix degradation but not demineralization. *J. Bone Miner. Res.* 14, 1654–1663. doi: 10.1359/jbmr.1999.14.10.1654

Greenberg, D. A., and Jin, K. (2013). Vascular endothelial growth factors (VEGFs) and stroke. *Cell. Mol. Life Sci.* 70, 1753–1761. doi: 10.1007/s00018-013-1282-8

Guo, R., Hua, Y., Ren, J., Bornfeldt, K. E., and Nair, S. (2018). Cardiomyocyte-specific disruption of Cathepsin K protects against doxorubicin-induced cardiotoxicity. *Cell Death Dis.* 9:692. doi: 10.1038/s41419-018-0727-2

Guo, R., Hua, Y., Rogers, O., Brown, T. E., Ren, J., and Nair, S. (2017a). Cathepsin K knockout protects against cardiac dysfunction in diabetic mice. *Sci. Rep.* 7:8703. doi: 10.1038/s41598-017-09037-z

Guo, R., Ren, J., and Nair, S. (2017b). Cathepsin K knockout inhibits calcification, migration and proliferation of aortic vascular smooth muscle cells. *Circulation* 136(Suppl. 1), A19464–A19464.

Haeckel, C., Krueger, S., Buehling, F., Broemme, D., Franke, K., Schuetze, A., et al. (1999). Expression of cathepsin K in the human embryo and fetus. *Dev. Dyn.* 216, 89–95. doi: 10.1002/(sici)1097-0177(199910)216:2<89::aid-dvdy1>3.0.co;2-9

Hao, L., Zhu, G., Lu, Y., Wang, M., Jules, J., Zhou, X., et al. (2015). Deficiency of cathepsin K prevents inflammation and bone erosion in rheumatoid arthritis and periodontitis and reveals its shared osteoimmune role. *FEBS Lett.* 589, 1331–1339. doi: 10.1016/j.febslet.2015.04.008

Hayami, T., Zhuo, Y., Wesolowski, G. A., Pickarski, M., and Duong, L. T. (2012). Inhibition of cathepsin K reduces cartilage degeneration in the anterior cruciate ligament transection rabbit and murine models of osteoarthritis. *Bone* 50, 1250–1259. doi: 10.1016/j.bone.2012.03.025

Hirai, T., Kanda, T., Sato, K., Takaishi, M., Nakajima, K., Yamamoto, M., et al. (2013). Cathepsin K is involved in development of psoriasis-like skin lesions through TLR-dependent Th17 activation. *J. Immunol.* 190, 4805–4811. doi: 10.4049/jimmunol.1200901

Hou, W. S., Bromme, D., Zhao, Y., Mehler, E., Dushey, C., Weinstein, H., et al. (1999). Characterization of novel cathepsin K mutations in the pro and mature polypeptide regions causing pycnodysostosis. *J. Clin. Invest.* 103, 731–738. doi: 10.1172/jci653

Houseweart, M. K., Pennacchio, L. A., Vilaythong, A., Peters, C., Noebels, J. L., and Myers, R. M. (2003). Cathepsin B but not cathepsins L or S contributes to the pathogenesis of Unverricht-Lundborg progressive myoclonus epilepsy (EPM1). *J. Neurobiol.* 56, 315–327. doi: 10.1002/neu.10253

Hua, Y., Robinson, T. J., Cao, Y., Shi, G. P., Ren, J., and Nair, S. (2015). Cathepsin K knockout alleviates aging-induced cardiac dysfunction. *Aging Cell* 14, 345–351. doi: 10.1111/acel.12276

Hua, Y., Xu, X., Shi, G. P., Chicco, A. J., Ren, J., and Nair, S. (2013a). Cathepsin K knockout alleviates pressure overload-induced cardiac hypertrophy. *Hypertension* 61, 1184–1192. doi: 10.1161/HYPERTENSIONAHA.111.00947

Hua, Y., Zhang, Y., Dolence, J., Shi, G. P., Ren, J., and Nair, S. (2013b). Cathepsin K knockout mitigates high-fat diet-induced cardiac hypertrophy and contractile dysfunction. *Diabetes* 62, 498–509. doi: 10.2337/db12-0350

Hummel, K. M., Petrow, P. K., Franz, J. K., Muller-Ladner, U., Aicher, W. K., Gay, R. E., et al. (1998). Cysteine proteinase cathepsin K mRNA is expressed in synovium of patients with rheumatoid arthritis and is detected at sites of synovial bone destruction. *J. Rheumatol.* 25, 1887–1894.

Inaoka, T., Bilbe, G., Ishibashi, O., Tezuka, K., Kumegawa, M., and Kokubo, T. (1995). Molecular cloning of human cDNA for cathepsin K: novel cysteine proteinase predominantly expressed in bone. *Biochem. Biophys. Res. Commun.* 206, 89–96. doi: 10.1006/bbrc.1995.1013

Jordans, S., Jenko-Kokalj, S., Kuhl, N. M., Tedelind, S., Sendt, W., Bromme, D., et al. (2009). Monitoring compartment-specific substrate cleavage by cathepsins B, K, L, and S at physiological pH and redox conditions. *BMC Biochem.* 10:23. doi: 10.1186/1471-2091-10-23

Kafienah, W., Bromme, D., Buttle, D. J., Croucher, L. J., and Hollander, A. P. (1998). Human cathepsin K cleaves native type I and II collagens at the N-terminal end of the triple helix. *Biochem. J.* 331(Pt 3), 727–732. doi: 10.1042/bj3310727

Khan, B., Ahmed, Z., and Ahmad, W. (2010). A novel missense mutation in cathepsin K (CTSK) gene in a consanguineous Pakistani family with pycnodysostosis. *J. Investig. Med.* 58, 720–724. doi: 10.231/JIM.0b013e3181da50bd

Khurana, D., Das, B., Kumar, A., Kumar, S. A., Khandelwal, N., Lal, V., et al. (2017). Temporal trends in intravenous thrombolysis in acute ischemic stroke: experience from a tertiary care center in India. *J. Stroke Cerebrovasc. Dis.* 26, 1266–1273. doi: 10.1016/j.jstrokecerebrovasdis.2017.01.019

Kiviranta, R., Morko, J., Uusitalo, H., Aro, H. T., Vuorio, E., and Rantakokko, J. (2001). Accelerated turnover of metaphyseal trabecular bone in mice overexpressing cathepsin K. *J. Bone Miner. Res.* 16, 1444–1452. doi: 10.1359/jbmr.2001.16.8.1444

Ko, F., Tallerico, T., and Seeman, P. (2006). Antipsychotic pathway genes with expression altered in opposite direction by antipsychotics and amphetamine. *Synapse* 60, 141–151. doi: 10.1002/syn.20287

Konttinen, Y. T., Mandelin, J., Li, T. F., Salo, J., Lassus, J., Liljestrom, M., et al. (2002). Acidic cysteine endoproteinase cathepsin K in the degeneration of the superficial articular hyaline cartilage in osteoarthritis. *Arthritis Rheum.* 46, 953–960. doi: 10.1002/art.10185

Kozawa, E., Cheng, X. W., Urakawa, H., Arai, E., Yamada, Y., Kitamura, S., et al. (2016). Increased expression and activation of cathepsin K in human osteoarthritic cartilage and synovial tissues. *J. Orthop. Res.* 34, 127–134. doi: 10.1002/jor.23005

Kubler, A., Larsson, C., Luna, B., Andrade, B. B., Amaral, E. P., Urbanowski, M., et al. (2016). Cathepsin K contributes to cavitation and collagen turnover in pulmonary tuberculosis. *J. Infect. Dis.* 213, 618–627. doi: 10.1093/infdis/jiv458

Lange, A. W., and Yutzey, K. E. (2006). NFATc1 expression in the developing heart valves is responsive to the RANKL pathway and is required for endocardial expression of cathepsin K. *Dev. Biol.* 292, 407–417. doi: 10.1016/j.ydbio.2006.01.017

Lendeckel, U., Kahne, T., Ten Have, S., Bukowska, A., Wolke, C., Bogerts, B., et al. (2009). Cathepsin K generates enkephalin from beta-endorphin: a new mechanism with possible relevance for schizophrenia. *Neurochem. Int.* 54, 410–417. doi: 10.1016/j.neuint.2009.01.011

Leung, P., Pickarski, M., Zhuo, Y., Masarachia, P. J., and Duong, L. T. (2011). The effects of the cathepsin K inhibitor odanacatib on osteoclastic bone resorption and vesicular trafficking. *Bone* 49, 623–635. doi: 10.1016/j.bone.2011.06.014

Leusink, F. K., Koudounarakis, E., Frank, M. H., Koole, R., van Diest, P. J., and Willems, S. M. (2018). Cathepsin K associates with lymph node metastasis and poor prognosis in oral squamous cell carcinoma. *BMC Cancer* 18:385. doi: 10.1186/s12885-018-4315-8

Li, C. Y., Jepsen, K. J., Majeska, R. J., Zhang, J., Ni, R., Gelb, B. D., et al. (2006). Mice lacking cathepsin K maintain bone remodeling but develop bone fragility despite high bone mass. *J. Bone Miner. Res.* 21, 865–875. doi: 10.1359/jbmr.060313

Li, H. Y., Ma, H. W., Wang, H. Q., and Ma, W. H. (2009). Molecular analysis of a novel cathepsin K gene mutation in a Chinese child with pycnodysostosis. *J. Int. Med. Res.* 37, 264–269. doi: 10.1177/147323000903700133

Li, Z., Hou, W. S., and Bromme, D. (2000). Collagenolytic activity of cathepsin K is specifically modulated by cartilage-resident chondroitin sulfates. *Biochemistry* 39, 529–536. doi: 10.1021/bi992251u

Lindstrom, E., Rizoska, B., Tunblad, K., Edenius, C., Bendele, A. M., Maul, D., et al. (2018). The selective cathepsin K inhibitor MIV-711 attenuates joint pathology in experimental animal models of osteoarthritis. *J. Transl. Med.* 16:56. doi: 10.1186/s12967-018-1425-7

Linton, M. R. F., Yancey, P. G., Davies, S. S., Jerome, W. G., Linton, E. F., Song, W. L., (eds) et al. (2000). "The role of lipids and lipoproteins in atherosclerosis," in *Endotext*, eds K. R. Feingold, B. Anawalt, A. Boyce, G. Chrousos, K. Dungan, A. Grossman, et al. (South Dartmouth, MA: MDText.com, Inc).

Liu, J., Dang, L., Li, D., Liang, C., He, X., Wu, H., et al. (2015). A delivery system specifically approaching bone resorption surfaces to facilitate therapeutic modulation of microRNAs in osteoclasts. *Biomaterials* 52, 148–160. doi: 10.1016/j.biomaterials.2015.02.007

Lotinun, S., Ishihara, Y., Nagano, K., Kiviranta, R., Carpentier, V. T., Neff, L., et al. (2019). Cathepsin K-deficient osteocytes prevent lactation-induced bone loss and parathyroid hormone suppression. *J. Clin. Invest.* 129, 3058–3071. doi: 10.1172/JCI122936

Lotinun, S., Kiviranta, R., Matsubara, T., Alzate, J. A., Neff, L., Luth, A., et al. (2013). Osteoclast-specific cathepsin K deletion stimulates S1P-dependent bone formation. *J. Clin. Invest.* 123, 666–681. doi: 10.1172/JCI64840

Lu, J., Wang, M., Wang, Z., Fu, Z., Lu, A., and Zhang, G. (2018). Advances in the discovery of cathepsin K inhibitors on bone resorption. *J. Enzyme Inhib. Med. Chem.* 33, 890–904. doi: 10.1080/14756366.2018.1465417

Lutgens, E., Lutgens, S. P., Faber, B. C., Heeneman, S., Gijbels, M. M., de Winther, M. P., et al. (2006). Disruption of the cathepsin K gene reduces atherosclerosis progression and induces plaque fibrosis but accelerates macrophage foam cell formation. *Circulation* 113, 98–107. doi: 10.1161/circulationaha.105.561449

Lutgens, S. P., Cleutjens, K. B., Daemen, M. J., and Heeneman, S. (2007). Cathepsin cysteine proteases in cardiovascular disease. *FASEB J.* 21, 3029–3041. doi: 10.1096/fj.06-7924com

Mandelin, J., Hukkanen, M., Li, T. F., Korhonen, M., Liljestrom, M., Sillat, T., et al. (2006). Human osteoblasts produce cathepsin K. *Bone* 38, 769–777. doi: 10.1016/j.bone.2005.10.017

Martin, T. J., and Sims, N. A. (2005). Osteoclast-derived activity in the coupling of bone formation to resorption. *Trends Mol. Med.* 11, 76–81. doi: 10.1016/j.molmed.2004.12.004

McClung, M. R., O'Donoghue, M. L., Papapoulos, S. E., Bone, H., Langdahl, B., Saag, K. G., et al. (2019). Odanacatib for the treatment of postmenopausal osteoporosis: results of the LOFT multicentre, randomised, double-blind, placebo-controlled trial and LOFT Extension study. *Lancet Diabetes Endocrinol.* 7, 899–911. doi: 10.1016/S2213-8587(19)30346-8

McDougall, J. J., Schuelert, N., and Bowyer, J. (2010). Cathepsin K inhibition reduces CTXII levels and joint pain in the guinea pig model of spontaneous osteoarthritis. *Osteoarthr. Cartil.* 18, 1355–1357. doi: 10.1016/j.joca.2010.07.014

McGrath, M. E., Klaus, J. L., Barnes, M. G., and Bromme, D. (1997). Crystal structure of human cathepsin K complexed with a potent inhibitor. *Nat. Struct. Biol.* 4, 105–109. doi: 10.1038/nsb0297-105

Meier, C., Meinhardt, U., Greenfield, J. R., De Winter, J., Nguyen, T. V., Dunstan, C. R., et al. (2006). Serum cathepsin K concentrations reflect osteoclastic activity in women with postmenopausal osteoporosis and patients with Paget's disease. *Clin. Lab.* 52, 1–10.

Mikosch, P., Kerschan-Schindl, K., Woloszczuk, W., Stettner, H., Kudlacek, S., Kresnik, E., et al. (2008). High cathepsin K levels in men with differentiated thyroid cancer on suppressive L-thyroxine therapy. *Thyroid* 18, 27–33. doi: 10.1089/thy.2007.0186

Morko, J., Kiviranta, R., Joronen, K., Saamanen, A. M., Vuorio, E., and Salminen-Mankonen, H. (2005). Spontaneous development of synovitis and cartilage degeneration in transgenic mice overexpressing cathepsin K. *Arthritis Rheum.* 52, 3713–3717. doi: 10.1002/art.21423

Mort, J. S., Beaudry, F., Theroux, K., Emmott, A. A., Richard, H., Fisher, W. D., et al. (2016). Early cathepsin K degradation of type II collagen in vitro and in vivo in articular cartilage. *Osteoarthr. Cartil.* 24, 1461–1469. doi: 10.1016/j.joca.2016.03.016

Nishi, Y., Atley, L., Eyre, D. E., Edelson, J. G., Superti-Furga, A., Yasuda, T., et al. (1999). Determination of bone markers in pycnodysostosis: effects of cathepsin K deficiency on bone matrix degradation. *J. Bone Miner. Res.* 14, 1902–1908. doi: 10.1359/jbmr.1999.14.11.1902

Novinec, M., and Lenarcic, B. (2013). Cathepsin K: a unique collagenolytic cysteine peptidase. *Biol. Chem.* 394, 1163–1179. doi: 10.1515/hsz-2013-0134

Pap, T., and Korb-Pap, A. (2015). Cartilage damage in osteoarthritis and rheumatoid arthritis–two unequal siblings. *Nat. Rev. Rheumatol.* 11, 606–615. doi: 10.1038/nrrheum.2015.95

Pena, I. D., Borlongan, C., Shen, G., and Davis, W. (2017). Strategies to extend thrombolytic time window for ischemic stroke treatment: an unmet clinical need. *J. Stroke* 19, 50–60. doi: 10.5853/jos.2016.01515

Penn, D. L., Komotar, R. J., and Sander Connolly, E. (2011). Hemodynamic mechanisms underlying cerebral aneurysm pathogenesis. *J. Clin. Neurosci.* 18, 1435–1438. doi: 10.1016/j.jocn.2011.05.001

Pennypacker, B., Shea, M., Liu, Q., Masarachia, P., Saftig, P., Rodan, S., et al. (2009). Bone density, strength, and formation in adult cathepsin K (-/-) mice. *Bone* 44, 199–207. doi: 10.1016/j.bone.2008.08.130

Peroni, A., Zini, A., Braga, V., Colato, C., Adami, S., and Girolomoni, G. (2008). Drug-induced morphea: report of a case induced by balicatib and review of the literature. *J. Am. Acad. Dermatol.* 59, 125–129. doi: 10.1016/j.jaad.2008.03.009

Platt, M. O., Ankeny, R. F., Shi, G. P., Weiss, D., Vega, J. D., Taylor, W. R., et al. (2007). Expression of cathepsin K is regulated by shear stress in cultured endothelial cells and is increased in endothelium in human atherosclerosis. *Am. J. Physiol. Heart Circ. Physiol.* 292, H1479–H1486.

Quintanilla-Dieck, M. J., Codriansky, K., Keady, M., Bhawan, J., and Runger, T. M. (2008). Cathepsin K in melanoma invasion. *J. Invest. Dermatol.* 128, 2281–2288. doi: 10.1038/jid.2008.63

Quintanilla-Dieck, M. J., Codriansky, K., Keady, M., Bhawan, J., and Runger, T. M. (2009). Expression and regulation of cathepsin K in skin fibroblasts. *Exp. Dermatol.* 18, 596–602. doi: 10.1111/j.1600-0625.2009.00855.x

Rader, D. J., and Pure, E. (2005). Lipoproteins, macrophage function, and atherosclerosis: beyond the foam cell? *Cell Metab.* 1, 223–230. doi: 10.1016/j.cmet.2005.03.005

Runger, T. M., Adami, S., Benhamou, C. L., Czerwinski, E., Farrerons, J., Kendler, D. L., et al. (2012). Morphea-like skin reactions in patients treated with the cathepsin K inhibitor balicatib. *J. Am. Acad. Dermatol.* 66, e89–e96. doi: 10.1016/j.jaad.2010.11.033

Runger, T. M., Quintanilla-Dieck, M. J., and Bhawan, J. (2007). Role of cathepsin K in the turnover of the dermal extracellular matrix during scar formation. *J. Invest. Dermatol.* 127, 293–297. doi: 10.1038/sj.jid.5700535

Saftig, P., Hunziker, E., Wehmeyer, O., Jones, S., Boyde, A., Rommerskirch, W., et al. (1998). Impaired osteoclastic bone resorption leads to osteopetrosis in cathepsin-K-deficient mice. *Proc. Natl. Acad. Sci. U.S.A.* 95, 13453–13458. doi: 10.1073/pnas.95.23.13453

Schilling, A. F., Mulhausen, C., Lehmann, W., Santer, R., Schinke, T., Rueger, J. M., et al. (2007). High bone mineral density in pycnodysostotic patients with a novel mutation in the propeptide of cathepsin K. *Osteoporos. Int.* 18, 659–669. doi: 10.1007/s00198-006-0311-y

Shi, G. P., Sukhova, G. K., Grubb, A., Ducharme, A., Rhode, L. H., Lee, R. T., et al. (1999). Cystatin C deficiency in human atherosclerosis and aortic aneurysms. *J. Clin. Invest.* 104, 1191–1197. doi: 10.1172/jci7709

Skoumal, M., Haberhauer, G., Kolarz, G., Hawa, G., Woloszczuk, W., and Klingler, A. (2005). Serum cathepsin K levels of patients with longstanding rheumatoid arthritis: correlation with radiological destruction. *Arthritis Res. Ther.* 7, R65–R70.

Soukas, A., Cohen, P., Socci, N. D., and Friedman, J. M. (2000). Leptin-specific patterns of gene expression in white adipose tissue. *Genes Dev.* 14, 963–980.

Sukhova, G. K., Shi, G. P., Simon, D. I., Chapman, H. A., and Libby, P. (1998). Expression of the elastolytic cathepsins S and K in human atheroma and regulation of their production in smooth muscle cells. *J. Clin. Invest.* 102, 576–583. doi: 10.1172/jci181

Sun, J., Sukhova, G. K., Zhang, J., Chen, H., Sjoberg, S., Libby, P., et al. (2012). Cathepsin K deficiency reduces elastase perfusion-induced abdominal aortic aneurysms in mice. *Arterioscler. Thromb. Vasc. Biol.* 32, 15–23. doi: 10.1161/ATVBAHA.111.235002

Suzuki, M., Takahashi, N., Sobue, Y., Ohashi, Y., Kishimoto, K., Hattori, K., et al. (2020). Hyaluronan suppresses enhanced cathepsin K expression via activation of NF-kappaB with mechanical stress loading in a human chondrocytic HCS-2/8 cells. *Sci. Rep.* 10:216. doi: 10.1038/s41598-019-57073-8

Svelander, L., Erlandsson-Harris, H., Astner, L., Grabowska, U., Klareskog, L., Lindstrom, E., et al. (2009). Inhibition of cathepsin K reduces bone erosion, cartilage degradation and inflammation evoked by collagen-induced arthritis in mice. *Eur. J. Pharmacol.* 613, 155–162. doi: 10.1016/j.ejphar.2009.03.074

Takito, J., Inoue, S., and Nakamura, M. (2018). The sealing zone in osteoclasts: a self-organized structure on the bone. *Int. J. Mol. Sci.* 19:984. doi: 10.3390/ijms19040984

Tanaka, M., Hashimoto, Y., Hasegawa, C., Deacon, S., and Eastell, R. (2017). Antiresorptive effect of a cathepsin K inhibitor ONO-5334 and its relationship to BMD increase in a phase II trial for postmenopausal osteoporosis. *BMC Musculoskelet Disord.* 18:267. doi: 10.1186/s12891-017-1625-y

Tanaka, M., Yamada, H., Nishikawa, S., Mori, H., Ochi, Y., Horai, N., et al. (2016). Joint degradation in a monkey model of collagen-induced arthritis: role of cathepsin K based on biochemical markers and histological evaluation. *Int. J. Rheumatol.* 2016:8938916. doi: 10.1155/2016/8938916

Tepel, C., Bromme, D., Herzog, V., and Brix, K. (2000). Cathepsin K in thyroid epithelial cells: sequence, localization and possible function in extracellular proteolysis of thyroglobulin. *J. Cell Sci.* 113(Pt 24), 4487–4498.

Troen, B. R. (2006). The regulation of cathepsin K gene expression. *Ann. N. Y. Acad. Sci.* 1068, 165–172. doi: 10.1196/annals.1346.018

Tsutsumi, S., Ogino, I., Miyajima, M., Nonaka, S., Ito, M., Yasumoto, Y., et al. (2017). Role of cathepsin K in the development of chronic subdural hematoma. *J. Clin. Neurosci.* 45, 343–347. doi: 10.1016/j.jocn.2017.08.021

Turk, V., Turk, B., and Turk, D. (2001). Lysosomal cysteine proteases: facts and opportunities. *EMBO J.* 20, 4629–4633. doi: 10.1093/emboj/20.17.4629

van den Brule, S., Misson, P., Buhling, F., Lison, D., and Huaux, F. (2005). Overexpression of cathepsin K during silica-induced lung fibrosis and control by TGF-beta. *Respir. Res.* 6:84.

Vasiljeva, O., Reinheckel, T., Peters, C., Turk, D., Turk, V., and Turk, B. (2007). Emerging roles of cysteine cathepsins in disease and their potential as drug targets. *Curr. Pharm. Des.* 13, 387–403. doi: 10.2174/138161207780162962

Wardlaw, J. M., Koumellis, P., and Liu, M. (2013). Thrombolysis (different doses, routes of administration and agents) for acute ischaemic stroke (Review). *Cochrane Database Syst. Rev.* 2013:CD000514.

Wijkmans, J., and Gossen, J. (2011). Inhibitors of cathepsin K: a patent review (2004 - 2010). *Expert Opin. Ther. Pat.* 21, 1611–1629. doi: 10.1517/13543776.2011.616283

Xiao, Y., Junfeng, H., Tianhong, L., Lu, W., Shulin, C., Yu, Z., et al. (2006). Cathepsin K in adipocyte differentiation and its potential role in the pathogenesis of obesity. *J. Clin. Endocrinol. Metab.* 91, 4520–4527. doi: 10.1210/jc.2005-2486

Xie, H., Cui, Z., Wang, L., Xia, Z., Hu, Y., Xian, L., et al. (2014). PDGF-BB secreted by preosteoclasts induces angiogenesis during coupling with osteogenesis. *Nat. Med.* 20, 1270–1278. doi: 10.1038/nm.3668

Yamada, H., Mori, H., Nakanishi, Y., Nishikawa, S., Hashimoto, Y., Ochi, Y., et al. (2019). Effects of the Cathepsin K Inhibitor ONO-5334 and concomitant use of ONO-5334 with methotrexate on collagen-induced arthritis in cynomolgus monkeys. *Int. J. Rheumatol.* 2019:5710340. doi: 10.1155/2019/5710340

Yamashita, T., Hagino, H., Hayashi, I., Hayashibara, M., Tanida, A., Nagira, K., et al. (2018). Effect of a cathepsin K inhibitor on arthritis and bone mineral density in ovariectomized rats with collagen-induced arthritis. *Bone Rep.* 9, 1–10. doi: 10.1016/j.bonr.2018.05.006

Yamaza, T., Goto, T., Kamiya, T., Kobayashi, Y., Sakai, H., and Tanaka, T. (1998). Study of immunoelectron microscopic localization of cathepsin K in osteoclasts and other bone cells in the mouse femur. *Bone* 23, 499–509. doi: 10.1016/s8756-3282(98)00138-0

Yang, M., Sun, J., Zhang, T., Liu, J., Zhang, J., Shi, M. A., et al. (2008). Deficiency and inhibition of cathepsin K reduce body weight gain and increase glucose metabolism in mice. *Arterioscler. Thromb. Vasc. Biol.* 28, 2202–2208. doi: 10.1161/ATVBAHA.108.172320

Yu, J., Adapala, N. S., Doherty, L., and Sanjay, A. (2019). Cbl-PI3K interaction regulates Cathepsin K secretion in osteoclasts. *Bone* 127, 376–385. doi: 10.1016/j.bone.2019.07.009

Zhang, D., Leung, N., Weber, E., Saftig, P., and Bromme, D. (2011). The effect of cathepsin K deficiency on airway development and TGF-beta1 degradation. *Respir. Res.* 12:72. doi: 10.1186/1465-9921-12-72

Zhang, G., Guo, B., Wu, H., Tang, T., Zhang, B. T., Zheng, L., et al. (2012). A delivery system targeting bone formation surfaces to facilitate RNAi-based anabolic therapy. *Nat. Med.* 18, 307–314. doi: 10.1038/nm.2617

Zhang, H. T., Zhang, P., Gao, Y., Li, C. L., Wang, H. J., Chen, L. C., et al. (2017). Early VEGF inhibition attenuates blood-brain barrier disruption in ischemic rat brains by regulating the expression of MMPs. *Mol. Med. Rep.* 15, 57–64. doi: 10.3892/mmr.2016.5974

Zhang, Z. G., Zhang, L., Jiang, Q., Zhang, R., Davies, K., Powers, C., et al. (2000). VEGF enhances angiogenesis and promotes blood-brain barrier leakage in the ischemic brain. *J. Clin. Invest.* 106, 829–838. doi: 10.1172/jci9369

Zhao, G., Li, Y., Cui, L., Li, X., Jin, Z., Han, X., et al. (2015). Increased circulating Cathepsin K in patients with chronic heart failure. *PLoS One* 10:e0136093. doi: 10.1371/journal.pone.0136093

Zhao, R., He, X. W., Shi, Y. H., Liu, Y. S., Liu, F. D., Hu, Y., et al. (2019). Cathepsin K knockout exacerbates haemorrhagic transformation induced by recombinant tissue plasminogen activator after focal cerebral ischaemia in mice. *Cell. Mol. Neurobiol.* 39, 823–831. doi: 10.1007/s10571-019-00682-8

Zheng, T., Zhu, Z., Wang, Z., Homer, R. J., Ma, B., Riese, R. J. Jr., et al. (2000). Inducible targeting of IL-13 to the adult lung causes matrix metalloproteinase- and cathepsin-dependent emphysema. *J. Clin. Invest.* 106, 1081–1093. doi: 10.1172/jci10458

Zhou, Y., Chen, H., Liu, L., Yu, X., Sukhova, G. K., Yang, M., et al. (2017). Cathepsin K deficiency ameliorates systemic lupus erythematosus-like manifestations in Fas(lpr) mice. *J. Immunol.* 198, 1846–1854. doi: 10.4049/jimmunol.1501145

Conflict of Interest: The authors declare that the research was conducted in the absence of any commercial or financial relationships that could be construed as a potential conflict of interest.

Copyright © 2020 Dai, Wu, Chu, Lu, Lyu, Liu and Zhang. This is an open-access article distributed under the terms of the Creative Commons Attribution License (CC BY). The use, distribution or reproduction in other forums is permitted, provided the original author(s) and the copyright owner(s) are credited and that the original publication in this journal is cited, in accordance with accepted academic practice. No use, distribution or reproduction is permitted which does not comply with these terms.

frontiers in Cell and Developmental Biology

ORIGINAL RESEARCH
published: 09 June 2020
doi: 10.3389/fcell.2020.00450

Conditional Knockout of PKC-δ in Osteoclasts Favors Bone Mass Accrual in Males Due to Decreased Osteoclast Function

Shangfu Li[1,2,3]†, Tianwei He[1,2,3]†, Depeng Wu[1,2,3]†, Liangming Zhang[1,2,3], Ruiqiang Chen[1,2,3], Bin Liu[1,2,3], Jinbo Yuan[4], Jennifer Tickner[4], An Qin[5], Jiake Xu[4] and Limin Rong[1,2,3]**

[1] Department of Spine Surgery, The Third Affiliated Hospital of Sun Yat-sen University, Guangzhou, China, [2] Guangdong Provincial Center for Quality Control of Minimally Invasive Spine Surgery, Guangzhou, China, [3] Guangdong Provincial Center for Engineering and Technology Research of Minimally Invasive Spine Surgery, Guangzhou, China, [4] School of Biomedical Sciences, The University of Western Australia, Perth, WA, Australia, [5] Shanghai Key Laboratory of Orthopedic Implants, Department of Orthopedic Surgery, Shanghai Ninth People's Hospital, Shanghai Jiao Tong University School of Medicine, Shanghai, China

OPEN ACCESS

Edited by:
Rajan Singh,
Charles R. Drew University of Medicine and Science, United States

Reviewed by:
John Charles Rotondo,
University of Ferrara, Italy
Colin Robert Dunstan,
University of Sydney, Australia

***Correspondence:**
Limin Rong
ronglm@mail.sysu.edu.cn
Shangfu Li
lishangfu@mail.sysu.edu.cn

† These authors have contributed equally to this work

Specialty section:
This article was submitted to Molecular Medicine, a section of the journal Frontiers in Cell and Developmental Biology

Received: 20 March 2020
Accepted: 13 May 2020
Published: 09 June 2020

Citation:
Li S, He T, Wu D, Zhang L, Chen R, Liu B, Yuan J, Tickner J, Qin A, Xu J and Rong L (2020) Conditional Knockout of PKC-δ in Osteoclasts Favors Bone Mass Accrual in Males Due to Decreased Osteoclast Function. Front. Cell Dev. Biol. 8:450. doi: 10.3389/fcell.2020.00450

Protein kinase C delta (PKC-δ) functions as an important regulator in bone metabolism. However, the precise involvement of PKC-δ in the regulation of osteoclasts remains elusive. We generated an osteoclast specific PKC-δ knockout mouse strain to investigate the function of PKC-δ in osteoclast biology. Bone phenotype was investigated using microcomputed tomography. Osteoclast and osteoblast parameters were assessed using bone histomorphometry, and analysis of osteoclast formation and function with osteoclastogensis and hydroxyapatite resorption assays. The molecular mechanisms by which PKC-δ regulated osteoclast function were dissected by Western Blotting, TUNEL assay, transfection and transcriptome sequencing. We found that ablation of PKC-δ in osteoclasts resulted in an increase in trabecular and cortical bone volume in male mice, however, the bone mass phenotype was not observed in female mice. This was accompanied by decreased osteoclast number and surface, and Cathepsin-K protein levels *in vivo*, as well as decreased osteoclast formation and resorption *in vitro* in a male-specific manner. PKC-δ regulated androgen receptor transcription by binding to its promoter, moreover, PKC-δ conditional knockout did not increase osteoclast apoptosis but increased MAPK signaling and enhanced androgen receptor transcription and expression, finally leding to significant alterations in gene expression and signaling changes related to extracellular matrix proteins specifically in male mice. In conclusion, PKC-δ plays an important role in osteoclast formation and function in a male-specific manner. Our work reveals a previously unknown target for treatment of gender-related bone diseases.

Keywords: protein kinase C delta, osteoclast, sex difference, androgen receptor, apoptosis, transcriptome sequencing

INTRODUCTION

Protein kinase C delta is a member of the highly homologous serine and threonine PKC family, it was the first novel PKC isoform to be identified by screening of mammalian cDNA libraries (Ono et al., 1988). PKC-δ is expressed ubiquitously among cells and tissues, and it is activated in a diacylglycerol and phosphatidylserine dependent but Ca^{2+} independent manner (Steinberg, 2008).

Various lines of evidence have shown that PKC-δ, activated in distinct ways, plays a critical role in regulating multiple cellular functions including growth, differentiation, apoptosis, and survival (Roffey et al., 2009).

Bone is maintained by a coupled process called bone remodeling which is characterized by the coordinated activity of bone-forming OBs and bone-resorbing OCs (Iaquinta et al., 2019), and involves a complex series of sequential steps that are highly regulated (Zaidi, 2007). In recent years, extended studies have been carried out to investigate the interrelationship between PKC-δ and skeletal diseases. It is reported that parathyroid hormone activates PKC-δ and regulates osteoblastic differentiation via a PLC-independent pathway (Yang et al., 2006). By using PKC-δ null mice, Cremasco et al. (2012) reported that PKC-δ deficiency perturbs bone homeostasis by selective uncoupling of CTSK secretion and ruffled border formation in OCs via PKC-δ-myristoylated alanine-rich C-kinase substrate (the actin bundling protein) pathway. In addition, further study revealed that global loss of PKC-δ protects against LPS-induced osteolysis owing to an intrinsic defect in osteoclastic bone resorption (Khor et al., 2013). However, the precise involvement of PKC-δ in the regulation of OC biology and bone homeostasis remains elusive.

Here, we generated a mouse strain in which PKC-δ is completely inactivated only in resorbing OCs by breeding mice carrying CTSK promoter-regulated Cre-recombinase with mice possessing loxP recombination sites flanking exon 7 of the PKC-δ gene. Our study aimed to comprehensively characterize the bone phenotype of mice with selective ablation of PKC-δ in OCs; we aimed to dissect the molecular mechanisms by which PKC-δ regulates OC differentiation and function. This study will potentially identify novel molecular targets for OC-associated bone diseases.

MATERIALS AND METHODS

Animal Procedures and Animal Care

All transgenic mice were generated on a C57BL/6J and C57BL/6N genetic background. Mice were group-housed under standard conditions: 12-h light/dark cycle, standard diet containing 1% calcium and 0.76% phosphate, and water *ad libitum* in standard cages. All mice were produced and maintained at the National Resource Center for Mutant Mice Model Animal Research Center of Nanjing University in China according to institutional guidelines. Seven mice per group for both sexes were used for the analysis of bone phenotype using Micro-CT and subsequent histology.

Abbreviations: Acta2, actin alpha 2; AR, androgen receptor; α-MEM, alpha modified Minimal Essential Medium; Bgn, biglycan; BMM, bone marrow macrophage; BV/TV, bone volume/total volume; cKO, conditional knockout; Col1a1, collagen type I alpha 1 chain; Col1a2, collagen type I alpha 2 chain; Col5a2, collagen type V alpha 2 chain; Col6a3, collagen type VI alpha 3 chain; Ct.Ar, cortical bone area; Ct.Ar/Tt.Ar, cortical area fraction; CTSK, cathepsin K; Ct.Th, cortical thickness; DMEM, Dulbecco's modified Eagle's medium; DEG, differentially expressed gene; ECM, extracellular matrix; ER, estrogen receptor; ERK, extracellular signal-regulated kinase; Fn1, fibronectin 1; GAPDH, glyceraldehyde-3-phosphate dehydrogenase; GO, Gene Ontology; IHC, Immunohistochemistry; JNK, c-Jun amino-terminal kinase; LNCaP, lymph node carcinoma of the prostate; MAPK, mitogen-activated protein kinase; MAR, mineral apposition rate; M-CSF, macrophage colony stimulating factor; Micro-CT, microcomputed tomography; Mmp12, matrix metallopeptidase 12; N.Ob/B.Pm, number of osteoblast per bone perimeter; N.Oc/B.Pm, number of osteoclasts per bone perimeter; OB, osteoblast; Ob.S/BS, osteoblast surface per bone surface; OC, osteoclast; Oc.S/BS, osteoclast surface per bone surface; PKC-δ, protein kinase C delta; RANKL, receptor activator of NF-κB ligand; Serpine 1, serpin family E member 1; Serpinh 1, serpin family H member 1; Sparc, secreted protein acidic and cysteine rich; Tb.N, trabecular number; Tb.Sp, trabecular separation; Tb.Th, trabecular thickness; Thbs1, thrombospondin 1; Tnc, tenascin C; TRAP, tartrate-resistant acid phosphatase; Tt.Ar, total cortical area.

Generation of Osteoclast-Specific PKC-δ Conditional Knockout Mice

LoxP mice were obtained from RIKEN BioResource Research Center (Stock Number: RBRC06462, Strain Name: C57BL/6-Prkcd<tm1shb>, 3-1-1 Koyadai, Tsukuba, Ibaraki, Japan). CTSK-Cre mice were kindly provided by Professor Jiake Xu from School of Biomedical Sciences, The University of Western Australia. Mice with an OC-cKO of the PKC-δ (PKC-δ cKO) were generated by crossing mice heterozygous for a floxed exon 7 PKC-δ allele (PKC-δ (ex7)$^{flox/wt}$) with CTSK-Cre mice heterozygously carrying a cyclization recombinase of which the expression is controlled by the CTSK promoter (CTSK-Cre^{+}PKC-δ$^{flox/wt}$). Offspring were genotyped and the presence of the CTSK-Cre transgene was determined on genomic DNA (gDNA) via PCR with primer sequences presented in **Supplementary Table S1**. In all the experiments described below, we analyzed CTSK-Cre^{+}PKC-δ$^{flox/flox}$ mice that lack PKC-δ in OCs, and CTSK-Cre^{-}PKC-δ$^{flox/flox}$ littermates as controls.

Micro-CT Scanning

Micro structure of bone in mice was measured by high-resolution Micro-CT using a Scanco μCT100 scanner (Brüttisellen, Zurich, Switzerland). Micro-CT analysis was performed on fixed right tibia isolated from euthanized mice scanned with a fixed isotropic voxel size of 10 μm, 100 slices, 70 kV at 200 μA and 300 ms integration time. Standard parameters were then evaluated in the trabecular region of the proximal tibia, commencing at a distance of 0.5 mm from the growth plate and extending a further 1.5 mm distally. Measured parameters included BV/TV (%), trabecular number (Tb.N, mm^{-1}), trabecular thickness (Tb.Th, mm) and trabecular separation (Tb.Sp, mm). Cortical bone was analyzed starting at a distance of 2.75 mm from the growth plate and extending 0.5 mm distally to determine total cortical area (Tt.Ar, mm^2), cortical bone area (Ct.Ar, mm^2), cortical area fraction (Ct.Ar/Tt.Ar, %) and cortical thickness (Ct.Th, μm).

Bone Histomorphometry and Immunohistochemistry

Left tibia were fixed overnight in 10% buffered formalin, decalcified with 14% EDTA for 7 days, embedded in paraffin and sectioned (3 μm) for staining. Trabecular bone and *in vivo* OB parameters were analyzed using hematoxylin and eosin (HE) stained sections, while *in vivo* OC parameters were determined from TRAP stained sections as previously described (Yao et al., 2014). Histomorphometric analysis was performed by quantifying parameters including osteoclast surface per bone surface (Oc.S/BS), number of osteoclasts per bone perimeter (N.Oc/B.Pm), osteoblast surface per bone surface (Ob.S/BS)

and number of osteoblast per bone perimeter (N.Ob/B.Pm) using an Olympus microscope and the BIOQUANT OSTEO software (BIOQUANT OSTEO 2013 Ver.13.20.6, Nashville, United States). We counted the numbers of positively stained cells in five sequential sections per mouse in each group. Safranin O Fast Green Staining, Massons trichrome staining and Von Kossa staining (in un-decalcified sections) were used to assess chondrocytes, organic and inorganic matrix components in the tibia, respectively. Cartilage thickness was measured in the middle of tibia as previously described (Tong et al., 2019) by using ImageJ software (NIH, Bethesda, MD, United States).

For the un-decalcified bone samples, femoral were dissected, fixed in 70% ethanol, dehydrated and embedded in methyl methacrylate, sagittal sections at 5 μm thickness were undergone von Kossa staining. Trabecular bone volume fraction was analyzed using ImageJ software. For dynamic histomorphometry and bone fluorescent-labeling studies, mice were injected intraperitoneally with calcein (Sigma, 20 mg/kg body weight) and alizarin red complexon (Sigma, 50 mg/kg body weight) at 9 and 2 days, respectively, before sacrifice. The MAR (μm/day) was measured in unstained sections under a fluorescence microscope (Olympus BX-63, Japan) and used to calculate the bone formation rate relative to the bone surface (BFR/BS, $\mu m^3/\mu m^2$/year) in the trabecular bone.

For CTSK IHC staining, antigen retrieval was carried out by incubating specimens with bone tissue specific antigen-retrieval solutions (SBT100013, Showbio, Shanghai, China) for 60 min at 37°C. Non-specific binding was blocked with goat serum before incubation with primary antibody against mouse CTSK (ab19027, Abcam, Cambridge, United Kingdom) at 4°C overnight. For detection, sections were treated with HRP-conjugated secondary antibody (GK500505A, Dako, Carpinteria, CA, United States) for 30 min at 37°C, followed by DAB substrate (ZLI-9017, ZSGB-Bio, Beijing, China) for 30 s, counter-stained with Maye's hematoxylin, dehydrated, and mounted. Semi-quantitative evaluation was performed as previously described (Da et al., 2009) in five random trabecular regions of each section. Two experienced pathologists scored each section which was blinded to them and the final scores were evaluated by consensus.

Macrophage Isolation From Mouse Bone Marrow, Culture, Osteoclast Differentiation, and TRAP Staining

Bone marrow macrophage from tibia and femur of WT and cKO mice were prepared as previously described (He et al., 2019). BMMs were then seeded on to 96-well plate (6×10^3 cells/well) and cultured in α-MEM supplemented with 30 ng/mL M-CSF (416-ML, R&D system, Minneapolis, MN, United States), and 100 ng/mL RANKL (462-TEC, R&D system). The media was replaced every 2 days and after 7 days of culture the cells were fixed and stained with Acid Phosphatase Staining kit (387A, Sigma-Aldrich, St. Louis, MO, United States) according to the protocol of the manufacturer. TRAP positive multinucleated cells with more than three nuclei were counted as OCs.

Western Blotting Assay

For short time course signaling pathways, BMMs at 3×10^5 cells/well were seeded into 6-well plates and incubated in complete medium with 30 ng/ml MCSF and 100 ng/ml RANKL for 4 days to allow PKC-δ deletion in OCs. In the next day, cells were starved for 4 h and then 100 ng/ml RANKL were added. Cells were harvested at the time points of 0, 5, 10, 20, 30 and 60 min. For long time periods, BMMs were stimulated with RANKL and MCSF for 0, 1, 3, 5, 7 days. Cells were lysed in RIPA buffer at indicated times for 30 min on ice for protein extraction. An equal amount of proteins (30 μg/lane) were resolved by SDS-polyacrylamide gel electrophoresis and then transferred to a polyvinylidene difluoride membrane (Millipore). The membrane was probed with the indicated primary antibody (in details in **Supplementary Table S2**), detected using horseradish peroxidase-conjugated secondary antibodies and visualized with ECL reagents (Amersham). α-tubulin was detected on the same membrane and used as a loading control.

Real-Time RT-PCR Assay

Total RNA from BMMs was extracted with RNAiso Plus (D9108A, Takara, Japan) and reverse transcription was carried out using 1 μg of total RNA with the PrimeScript RT reagent Kit and gDNA Eraser (DRR047A, Takara) in a volume of 20 μl. One microliter of cDNA was amplified with the specific primers (Invitrogen, sequences in **Supplementary Table S1**) and were quantified on a Light Cycler 480II (Roche) using SYBR green dye (DRR820A, Takara), normalizing with GAPDH. The Ct value of the reference gene GAPDH was subtracted from the Ct value of the target genes (ΔCt), and the average ΔCt value of the triplicates was taken. Relative expression levels of each gene were obtained by using the $2^{-\Delta\Delta Ct}$ method. All the experiments were repeated three times.

TUNEL Assay

Apoptosis in OCs was identified by using the *In Situ* Cell Death Detection Kit, Fluorescein (11684795910, Roche Diagnostics GmbH, Germany) according to the manufacturer's instructions. Briefly, after 5 and 7 days of RANKL induction in 35 mm and high glass bottom μ-Dish (81158, Ibidi, Germany), samples were fixed in 4% paraformaldehyde for 1 h at 20°C and permeabilized with 0.1% Triton X-100 solution for 2 min on ice. Then the TUNEL reaction mixtures were added to the samples and incubated for 60 min at 37°C in the dark. Finally the samples were visualized under confocal microscope by using an excitation wavelength of 488 nm and detection in the range of 515–565 nm (green). The actin was detected by phalloidin staining (red).

Hydroxyapatite Resorption Assay

BMMs (6×10^3 cells/well) were directly seeded into a 96 well Corning Osteo Assay Surface plate (3989, Corning Life Sciences, Tewksbury, MA, United States) to begin the differentiation process. Plates were incubated with a differentiation medium (30 ng/ml M-CSF combined 100 ng/ml RANKL), which was changed every 2 days. After 5 and 7 days, the plates were stripped with 1.2% sodium hypochlorite solution for 5 min to remove cells

and air-dried prior to imaging. Overlapping images of the entire well were taken at 20× magnification and these were then used to produce a composite image using Image Composite Editor (ICE 2.0, Microsoft, United States). The total resorption area was measured in the composite image using Image-Pro Plus (version 6.0, Media Cybernetics Company, Rockville, MD, United States).

Transfection, Transcriptional and Luciferase Assay

Prostate adenocarcinoma cell line (LNCaP, CRL1740) and 293T cell line (CRL3216) were purchased from ATCC. LNCaP cells were maintained in phenol red-free RPMI 1640 supplemented with 10% FBS. 293-T cells were maintained in DMEM supplemented with 10% FBS. Plasmids were obtained from Genomeditech Co., Ltd (Shanghai, China). Cells were transfected with AR firefly luciferase reporter (pGMAR-Lu) plasmid and control renilla luciferase reporter (pGMR-TK) plasmid using Lipofectamine^{TM} 2000 Transfection Reagent (#11668019, Life Technologies) according to the manufacturer's instruction. Cells were transferred to a 96-well plate 24 h after transfection and were further transfected with PKC-δ plasmid for another 48 h. Finally, luciferase activity was assessed using the Dural-Luciferase® Reporter Assay System (#E1910, Promega, United States) according to the manufacturer's instructions.

Transcriptome Sequencing and Bioinformatics Analysis

Total RNA was extracted using RNeasy Mini kit (QIAGEN, Germany) following the manufacturer's instructions. The quality and integrity of RNA was assessed using the RNA Nano 6000 Assay Kit of the Bioanalyzer 2100 system (Agilent Technologies, CA, United States). A total amount of 3 μg RNA per sample was used for mRNA-Seq library construction using NEBNext Ultra^{TM} RNA Library Prep Kit for Illumina (NEB, United States) according to manufacturer's recommendations. Heatmap was generated by pheatmap package in R. DEGs analysis was performed using the edgeR R package (3.18.1). The *p*-value was adjusted using the Benjamini and Hochberg method, corrected *p*-value of 0.05 and absolute fold change of 2 was set as the threshold for significantly differential expression. GO enrichment analysis of DEGs was implemented by the clusterProfiler R package, in which gene length bias were corrected, GO terms with corrected *p*-value less than 0.05 were considered significantly enriched by DEGs. KEGG database[1] was used for KEGG pathway enrichment analysis of DEGs, and clusterProfiler R package was used to test the statistical enrichment of DEGs in KEGG pathways. The RNA-seq data were analyzed by wcgene biotech (shanghai, china).

Statistical Analysis

All data was pooled from at least three independent experiments. Descriptive statistics included means and standard deviations for continuous variables and percentages for categorical ones. Normality of distribution was assessed by Kolmogorov–Smirnov test. Differences were examined by two tailed Student's *t*-test for comparing two groups and by one- or two-way analysis of variance (ANOVA) test for comparing multiple groups. When significant differences were indicated by ANOVA, Turkey's *post hoc* test was used to compare the differences between groups. All data analysis was performed with SPSS 20.0 Package (SPSS software 20.0; SPSS, Chicago, IL, United States). All statistical tests were two-sided and values of p smaller than 0.05 were considered significant.

[1]http://www.genome.jp/kegg/

RESULTS

Mice With PKC-δ cKO in Osteoclasts Exhibit Increased Bone Mass With Changes in Micro-Structure in a Sex Dependent Manner

Firstly, we confirmed the CTSK-driven PKC-δ deletion in OCs in mice. To analyze a direct effect of PKC-δ deficiency on OCs and bone homeostasis, we used the conditional PKC-δ allele in which exons 7 are flanked by loxP sites. Cre-mediated deletion of exons 7 results in a frame shift and a PKC-δ null allele (**Supplementary Figure S1A**). For specific deletion in OCs, we crossed the conditional PKC-δ allele to CTSK-Cre mice, efficiency of Cre-mediated deletion of PKC-δ exons 7 and consequent loss of PKC-δ expression in OCs was confirmed by gDNA PCR for the deleted and floxed alleles (**Supplementary Figure S1B**), together with the significant decrease of PKC-δ mRNA expression (**Supplementary Figure S1C**, BMMs stimulated with RANKL for 5 days) and protein expression (**Supplementary Figure S1D**, co-culture with RANKL for 7 days).

To determine the biological consequences of PKC-δ cKO in OCs in skeletal development, we analyzed the bone phenotype of PKC-δ cKO mice *in vivo*. Interestingly, 3-month-old male cKO mice were smaller than WT littermates, in addition, their body weight was lighter (30.5.4 ± 2.2 g vs. 26.8 ± 2.4 g) and statistical difference was found ($p < 0.05$). In contrast, there were no significant changes in female mice regarding their size and body weight (23.5 ± 2.1 g vs. 23.1 ± 2.5 g) (**Figure 1A**). We further examined the bone micro-structure using Micro-CT and found that male PKC-δ cKO mice exhibited increased trabecular and cortical bone compared to their WT littermates (**Figures 1B,C**). In the trabecular bone, with statistically significant changes ($p < 0.05$), the percentage of trabecular bone volume versus total volume was about 45% increased in male cKO mice compared to WT (BV/TV, 9.48% vs. 13.87%, **Figure 1Bii**). Moreover, there were trend of increase in trabecular number (Tb.N, 4.12/mm vs. 4.41/mm, **Figure 1Biii**) and thickness (Tb.Th, 0.047 mm vs. 0.054 mm, **Figure 1Biv**) and approximately 10% reduction in trabecular separation (Tb.Sp, 0.25 mm vs. 0.22 mm, **Figure 1Bv**). However, there were no significant changes in trabecular bone in female cKO mice when compared with the WT controls (**Figure 1B**). In the cortical bone, statistical differences of increased changes were found in male mice regarding cortical area fraction (Ct.Ar/Tt.Ar, 88.7% vs. 90.0%, **Figure 1Civ**) and cortical thickness (Ct.Th, 0.156 mm vs. 0.174 mm, **Figure 1Cv**).

While trend of increase were found in total cortical area (Tt.Ar, 0.95 mm^2 vs. 1.02 mm^2, **Figure 1Cii**) and cortical bone area (Ct.Ar, 0.85 mm^2 vs. 0.89 mm^2, **Figure 1Ciii**). As expected, the cortical changes were mild and negligible in cortical bone in female mice (**Figure 1C**). Taken together, these results revealed an increase in trabecular and cortical bone volume due to ablation of PKC-δ specifically in OCs in a sex dependent maner in male mice.

Increased Bone Fraction and Decreased Osteoclast in Trabecular Bone of PKC-δ Conditional Knockout Mice

Based on the moderate osteopetrotic phenotype observed by Micro-CT, we further explored the specific *in vivo* cellular changes at the trabecular bone surface of PKC-δ cKO mice. Because bone remodeling is highly coordinated by OC bone resorption and OB bone formation, we determined the effects of PKC-δ deletion in OCs on bone structure, OB and OC parameters. To this end, HE, TRAP and CTSK stained histological sections of tibias from 12 weeks old PKC-δ cKO and WT mice were used for histomorphometric analysis (**Figure 2**). HE staining displayed increased trabecular bone in PKC-δ cKO male mice (**Figure 2A**, indicated by yellow arrow), further confirming the Micro-CT findings (**Figure 1B**). Analysis of TRAP staining revealed a reduction in OC number and surface after PKC-δ ablation specifically in OCs (**Figures 2Bi,ii**). No significant differences were observed in OB surface and number of OBs in PKC-δ cKO mice when compared to WT littermates (**Figures 2Biii,iv**). We further verified our finding by CTSK (a specific protein expressed in mature OCs) IHC staining. As expected, semi-quantitative analysis showed decreased CTSK protein levels after inactivation of PKC-δ in OCs (**Figure 2Bv**).

It was reported that non-cannonical Wnt signaling through G protein-linked PKC-δ activation promoted bone formation (Tu et al., 2007). In addition, studies have shown that PKC-δ is an important regulator of osteochondral plasticity at the interface between articular cartilage and the osteochondral junction using PKC-δ null mice (Yang et al., 2015). To exclude the influence of osteoblast formation and cartilage changes on the bone phenotype after PKC-δ cKO in OCs, we performed bone formation and bone component analysis in the proximal tibia of 12-week-old WT and PKC-δ cKO mice. Representative images of fluorescence double labeling (**Supplementary Figures S2Ai–iv**) and histomorphometric analysis of the MAR (**Supplementary Figure S2Av**) and the bone formation rate with a bone surface referent (BFR/BS, **Supplementary Figure S2Avi**) indicated that PKC-δ cKO did not affect bone formation either in male or female mice. Bone is a dynamic organ composed of organic and inorganic elements, we used von Kossa staining (for inorganic components) and Masson's trichrome staining (for organic components) to investigate the effect of ablation of PKC-δ specifically in OCs on bone composition. Representative images showed increased inorganic contents in trabecular bone in male mice but not in female mice (**Supplementary Figure S2Bi**, indicate by yellow arrows) and semi-quantitative analysis revealed increased trabecular bone volume fraction (**Supplementary Figure S2Bii**). No changes to organic components were observed in either male or female mice (**Supplementary Figure S2C**). We examined cartilage using Safranin O Fast Green Staining (**Supplementary Figure S2Di**) and no significant differences of cartilage thickness (**Supplementary Figure S2Dii**, 126 ± 23 μm vs. 134 ± 18 μm for female and 141 ± 27 μm vs. 145 ± 22 μm for male) were found in both sexes.

Collectively, these data supported the notion that PKC-δ cKO mice exhibited moderate osteopetrosis predominately owing to changes in OC parameters.

Decreased Osteoclastogenesis and Bone Resorption in Bone Marrow Monocytes From Male PKC-δ cKO Mice

In addition to the decreased OCs observed in PKC-δ cKO male mice *in vivo*, we further investigated the effects of PKC-δ ablation selectively in OCs on osteoclastogenesis and bone resorption *in vitro*. As shown in **Figures 3A–C**, BMMs from male PKC-δ cKO produced significantly less OCs than WT littermates after stimulating with RANKL for 5 days (**Figures 3A,C**) and 7 days (**Figures 3B,C**), whereas there were no differences in OC number between female mice and WT controls (**Figures 3A–C**). Interestingly, as indicated by yellow arrows (**Figure 3A**), we found that male PKC-δ cKO OCs displayed morphology changes (be much more easily to lysis which likes a morphology change of apoptosis). Consistent with OC formation, by using Hydroxyapatite resorption assay, we demonstrated that bone resorption area was also significantly reduced in BMMs of male PKC-δ cKO after incubating with RANKL for both 5 days (**Figures 3D,F**) and 7 days (**Figures 3E,F**).

Enhanced Androgen Receptor Transcription and Expression and Increased MAPK Signaling During Osteoclastogenesis in Male PKC-δ cKO Mice

Osteoclast apoptosis is associated with cell morphology changes. As we observed obvious morphology changes in OCs during osteoclastogenesis in male PKC-δ cKO mice, we tested whether selective deletion of PKC-δ in OCs affected OC apoptosis. Interestingly, using TUNEL assay, we did not observe significant fluorescence intensity changes during osteoclastogenesis after stimulating with RANKL for 5 days (**Figures 4A,B**) and 7 days (**Figures 4C,D**) in either male or female PKC-δ cKO mice. To confirm this finding we further detected protein expression changes characteristic of apoptosis. As shown in **Figure 5A**, cleaved Caspase-3, Caspase-3, cleaved PARP and PARP protein expression levels in PKC-δ cKO mice were similar to that of WT controls during osteoclastogenesis (**Figure 5B**), further confirming that ablation of PKC-δ selectively in OC does not promote OC apoptosis.

Because AR is abundantly expressed in male OC and can potently suppress osteoclastogenesis and bone resorption (Huber et al., 2001; Kawano et al., 2003), to further explore the molecular basis for gender dependent changes during OC differentiation and function, we theorized that PKC-δ regulated

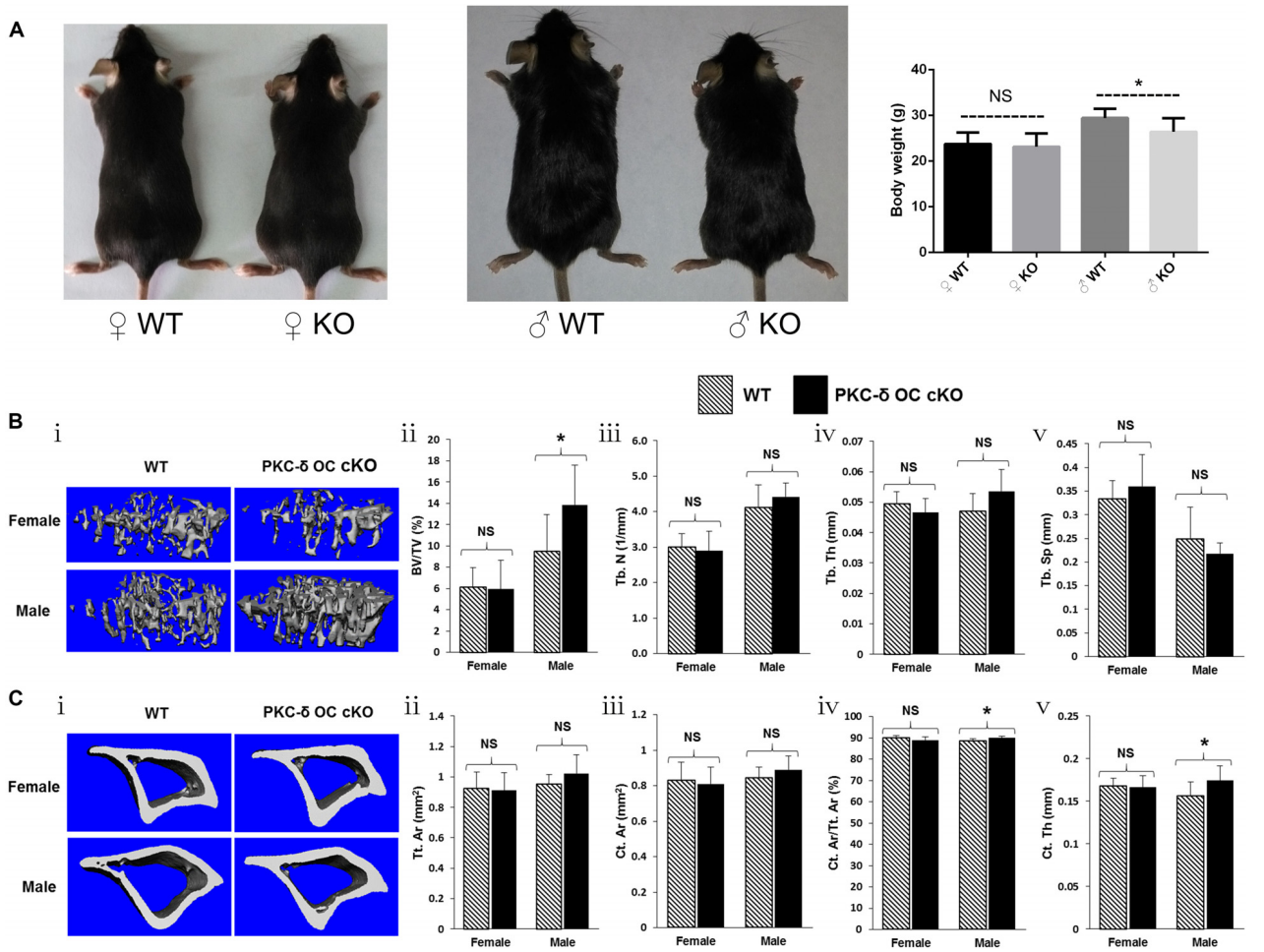


FIGURE 1 | Conditional knockout of PKC-δ in osteoclast resulted in bone mass accrual in 12-week old male mice. **(A)** Representative images and body weight of the pups at 12 weeks of age (WT wild type, KO knockout). **(B,C)** Representative 3D reconstructions of trabecular **(Bi)** and cortical **(Ci)** bone and bone parameters assessed by Micro-CT in proximal tibia in age- and sex-matched WT and PKC-δ conditional knockout mice, respectively ($n = 7$ per group). Trabecular bone parameters **(Bii–v)** are shown as trabecular bone volume fraction (BV/TV, %; **Bii**), trabecular number (Tb.N, 1/mm; **Biii**), trabecular thickness (Tb.Th, mm; **Biv**) and trabecular separation (Tb.Sp, mm; **Bv**). Micro-CT analysis of cortical bone parameters **(Cii–v)** are shown as total cortical area (Tt.Ar, mm^2; **Cii**), cortical bone area (Ct.Ar, mm^2; **Ciii**), cortical area fraction (Ct.Ar/Tt.Ar, %; **Civ**) and cortical thickness (Ct.Th, μm; **Cv**). Data are presented as mean/fold change ± SD. NS, non-significant, $^*p < 0.05$ compared with WT control group by two-way ANOVA with Tukey's *post hoc* test.

AR transcription and expression by binding to its promoter. Therefore, we firstly examined the effect of PKC-δ on AR transcriptional activity by transfection and luciferase assay. LNCaP and 293T cells were transfected with AR reporter plasmids. As expected, luciferase activity was dramatically increased after co-transfection with PKC-δ plasmid in both cell lines (**Figure 5C**), indicating that PKC-δ regulated AR transcription by binding to its promoter. Based on this finding, we further investigated the AR RNA and protein expression changes during osteoclastogenesis in PKC-δ cKO mice (**Figures 5D–F**). Interestingly, RT-PCR semi-quantification analysis revealed that selective ablation of PKC-δ in OC could greatly enhance AR transcription during osteoclastogenesis both in 3 days and 5 days after RANKL induction only in male mice (**Figure 5D**). Furthermore, optical density analysis shown that AR protein expression was also significantly elevated at all the time-points (1/3/5/7 days) following RANKL stimulation in male mice but not in female mice (**Figures 5E,F**).

Since members of the MAPK signaling (including ERK, JNK and P38) and NF-κB signaling pathways play a crucial role in OC survival, differentiation and function (Abu-Amer, 2013; Lee et al., 2018). We further investigated these signaling at 0, 5, 10, 20, 30, 60 min after RANKL stimulation in PKC-δ cKO and wild type mice. As shown in **Figure 6**, in female mice, although significant changes were found in some time points of p-P38 (0 and 5 min), p-ERK (60 min), and p-JNK (0, 5, 30, and 60 min), the trend of changes was not consistent. Moreover, no significant differences of IκB-α expression were found in cKO mice (**Figures 6A,B**). By contrast, the phosphorylation of P38 and ERK was remarkably enhanced at all the time points while the phosphorylation of JNK was significantly increased at 0, 5, 10, 20, and 60 min after RANKL treatment in male mice of PKC-δ cKO. However, the

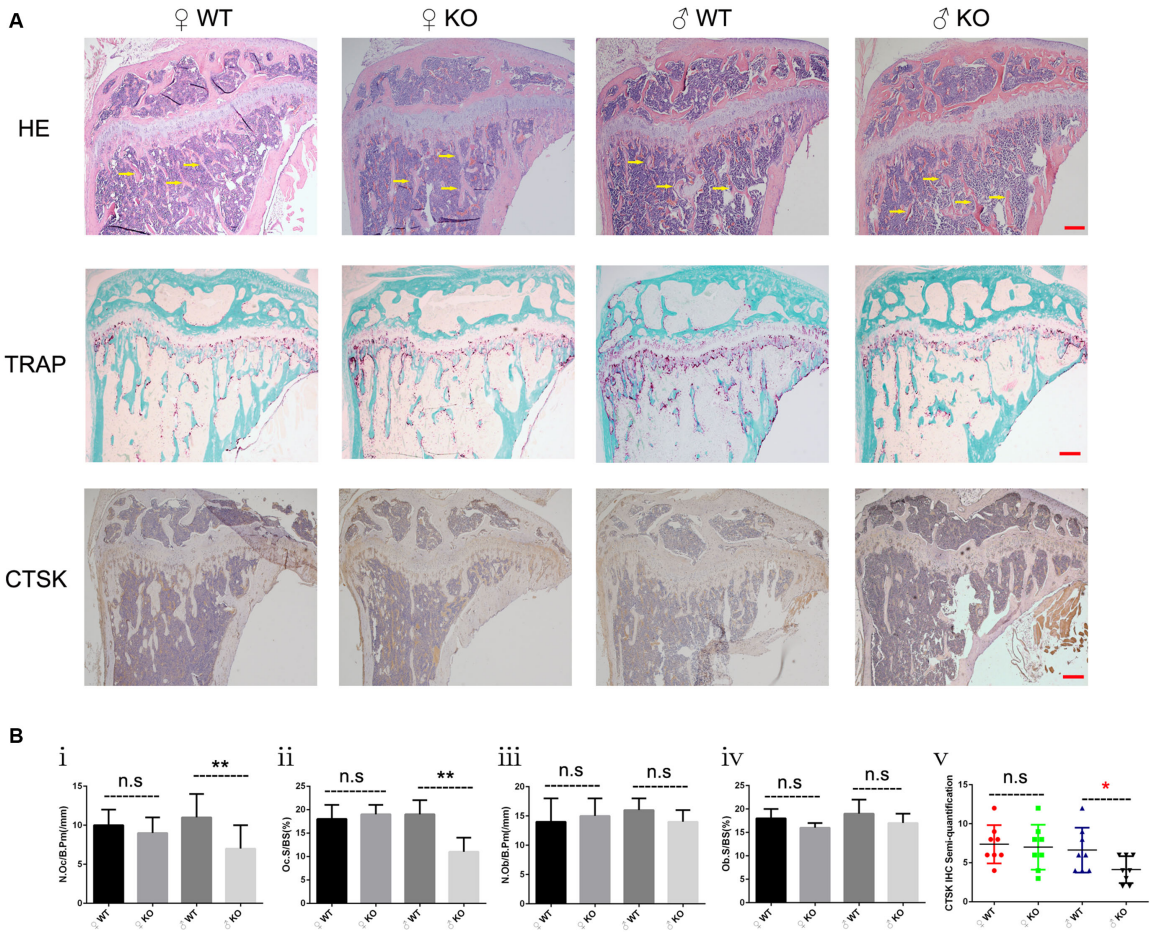


FIGURE 2 | Increased bone fraction and decreased osteoclast number in the trabecular bone of male PKC-δ cKO mice. Analysis of proximal tibia sections of 3-month-old PKC-δ cKO and age-sex matched wild type mice using histology (n = 7 per group). **(A)** Representative images of HE/TRAP/CTSK stained tibia sections. Arrows indicate trabecular bone within the tibia. Magnification = 40×, bar represents 200 μm. **(B)** Quantitative histomorphometric analysis of bone parameters: **(Bi)** Number of osteoclasts relative to bone surface (N.Oc/B.Pm, mm^{-1}); **(Bii)** Osteoclast surface relative to bone surface (Oc.S/BS, %); **(Biii)** Number of osteoblasts (N.Ob/B.Pm, mm^{-1}); **(Biv)** Osteoblast surface (Ob.S/BS, %); **(Bv)** Semi-quantification of CTSK IHC staining. Bar charts represent mean ± SD. n.s. no statistical significance, $^{*}p < 0.05$, $^{**}p < 0.01$ compared with WT control group by two-way ANOVA with Tukey's *post hoc* test.

expression levels of IκB-α were not changed (**Figures 6C,D**). These findings suggested that PKC-δ cKO enhanced the RANKL-induced MAKP signaling pathway only in male mice, especially the expression of p-P38 and p-ERK.

Taken together, our data clearly demonstrated that inactivation of PKC-δ specifically in OCs had no effect on OC apoptosis but enhanced AR transcription and expression and increased MAPK signaling during osteoclastogenesis in a sex dependent manner in male mice.

Conditional Inactivation of PKC-δ in Osteoclasts Led to Significant Gene Expression and Signaling Changes Related to Extracellular Matrix Proteins Only in Male Mice

To further address the issue of gender differences after PKC-δ cKO, we investigated the gene expression differences in BMMs after stimulating with RANKL by transcriptomics sequencing and bioinformatics analysis. RNA-seq-based expression heat map of PKC-δ cKO mice BMM-derived OCs showed that the lack of PKC-δ altered the expression of many genes much more dramatically in male mice (**Figure 7A**). We further identified the DEGs responsible for the gender differences by using Volcano plot (**Figure 7B**): There were 14 up-regulated DEGs and 2 down-regulated DEGs in male mice when compared with WT controls (**Figure 7C** and **Table 1**). In contrast, there is only one DEG in female mice (**Figure 7C**). To reveal the most likely pathways and genes responsible for the sex differences, we performed the GO enrichment analysis (**Figure 7D**). It is noticeable that most of the DEGs are located in the cellular components of extracellular region and the molecular functions are mainly collagen binding and peptidase regulator activity. We further explored the underlying molecular mechanisms for the gender differences of PKC-δ cKO on OC differentiation and function by KEGG pathway enrichment analysis (**Figures 7E,F**).

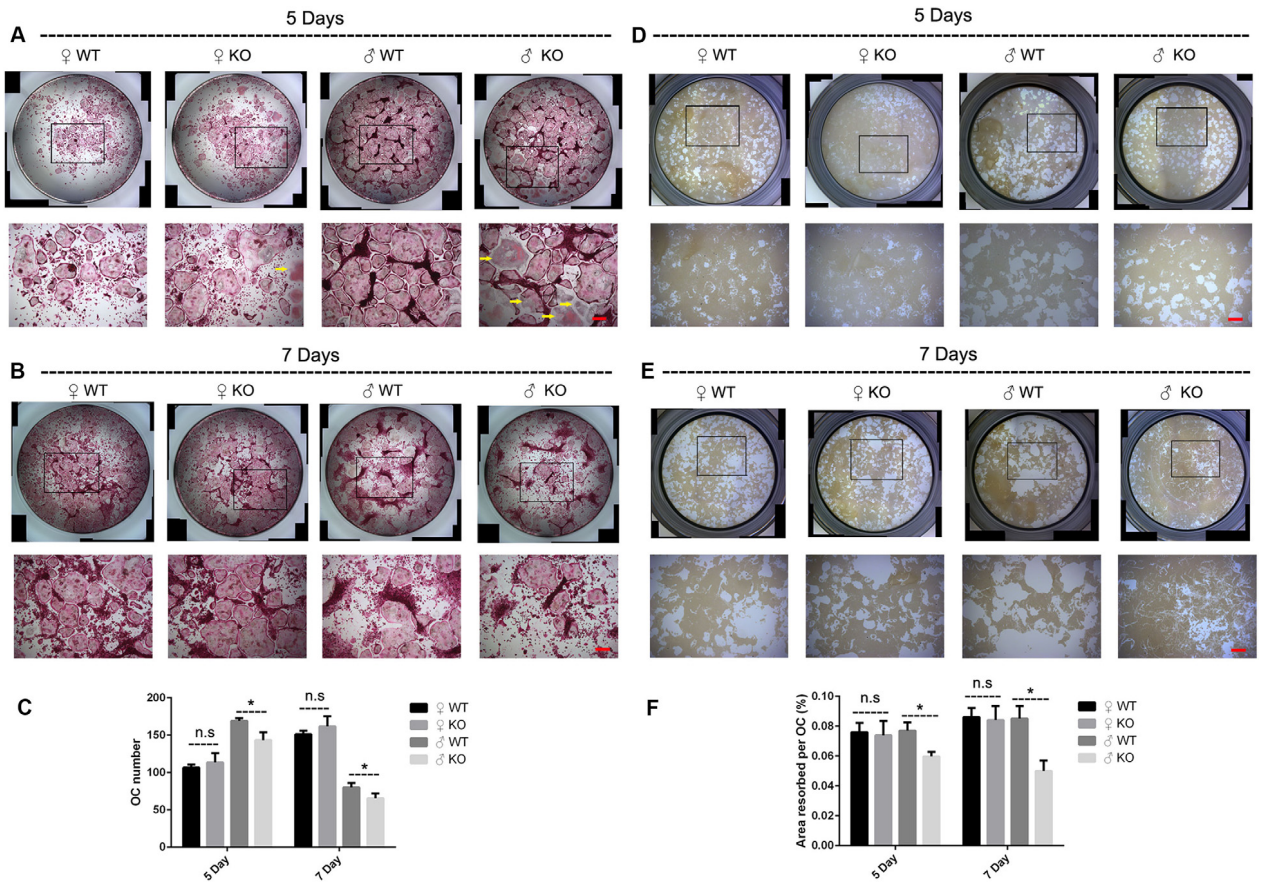


FIGURE 3 | Ablation of PKC-δ specifically in osteoclasts decreased osteoclastogenesis and bone resorption in male mice. **(A,B)** Representative images of osteoclasts with TRAP staining after RANKL (100 ng/ml) induction for 5 days **(A)** and 7 days **(B)**, the square in the upper images of each well indicated where the lower images were captured, the yellow arrow shows unusual morphology of OC in male PKC-δ cKO mice. Magnification = 50×, bar represents 200 μm. **(C)** The number of TRAP positive multinucleated cells (>3 nuclei) per well was quantified. **(D,E)** Representative images of eroded areas after RANKL (100 ng/ml) stimulation for 5 days **(D)** and 7 days **(E)**, the square in the upper images of each well indicated where the lower images were captured. Magnification = 50×, bar represents 200 μm. **(F)** Quantitative analysis of the resorbed proportion per osteoclast by measuring the area of the mineral coating removal. WT wild type, KO knockout. Experiments were carried out in triplicate and results are presented as mean ± SD. Bar represents 200 μm, n.s. no statistical significance, $^*p < 0.05$ vs. WT control group by two-way ANOVA with Tukey's *post hoc* test.

The enriched KEGG pathway scatterplot showed that most of the up-regulated DEGs were related to focal adhesion and ECM–receptor interaction (**Figure 7E**), while the down-regulated DEGs are mainly responsible for OC differentiation and lysosomes (**Figure 7F**).

Collectively, all these results indicated that deletion of PKC-δ specifically in OCs led to alteration of many DEGs and significant signaling changes only in male mice.

DISCUSSION

In this study, we found that PKC-δ deficiency in OCs favors bone mass accrual in a sex-dependent manner in male mice. Histological analysis revealed increased bone fraction and decreased OCs in the trabecular bone of male mice after cKO. Furthermore, our work suggests that PKC-δ cKO decreased osteoclastogenesis and OC function only in male mice. Finally, deletion of PKC-δ selectively in OCs did not increase OC apoptosis but enhanced AR transcription and expression and increased MAPK signaling in addition to alteration of expression of many genes and signaling changes related to ECM biology during osteoclastogenesis in male mice. Hence, these data clearly showed that ablation of PKC-δ specifically in OCs contibuted to an osteopetrotic phenotype in a sex-dependent fasion in male mice. More importantly, this work revealed the gender differences at both cellular and molecular levels. Our work displayed PKC-δ as an important regulator in OC biology and revealed a previously unknown target for treatment of sex-related bone disease.

The observed effect of loss of PKC-δ resulting in increased trabecular bone is consistent with the previous studies displayed by Cremasco et al. (2012) and Khor et al. (2013). However, there is a discrepancy that the sex differences demonstrated in

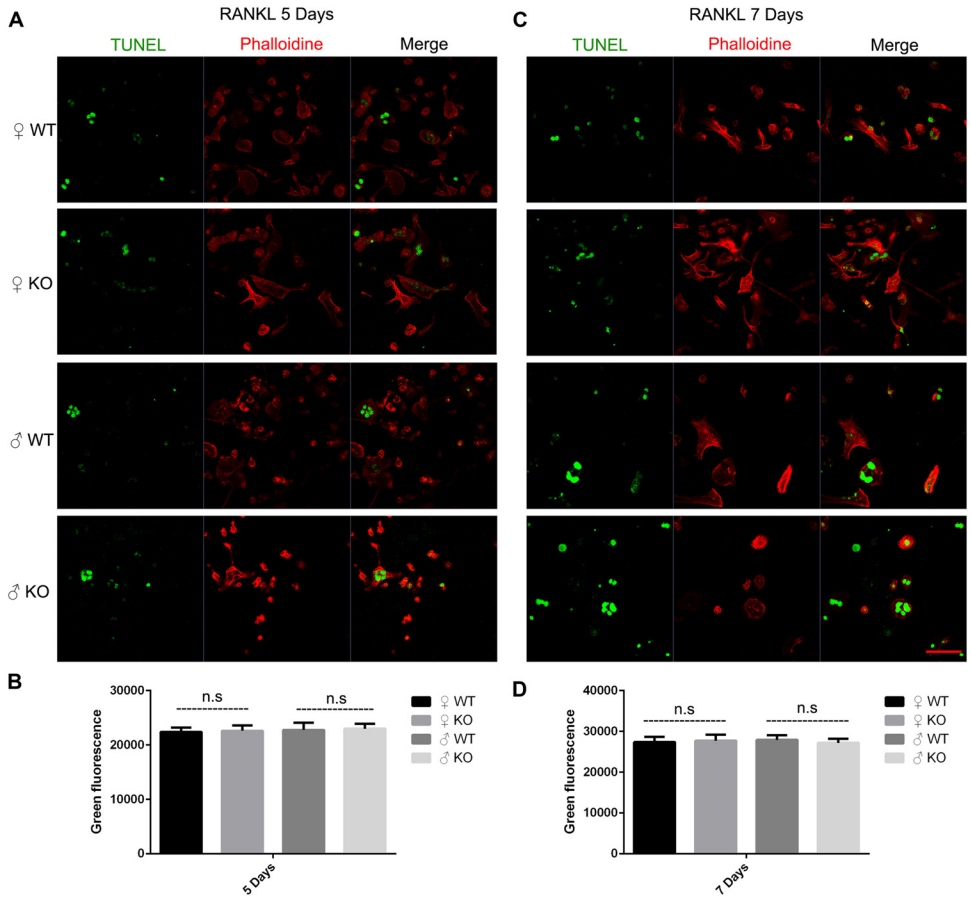


FIGURE 4 | Deletion of PKC-δ selectively in osteoclasts did not increase osteoclast apoptosis during osteoclastogenesis. **(A,C)** Osteoclasts on μ-Dish were immunofluorescently stained with TUNEL and phalloidin to visualize apoptosis and actin by confocal microscopy after RANKL induction for 5 days **(A)** and 7 days **(C)**. Magnification = 400×, bar represents 50 μm. **(B,D)** Semi-quantification of osteoclasts apoptosis was measured in a fluorescence microplate reader after stimulating with RANKL for 5 days **(B)** and 7 days **(D)**. Bar charts represent mean ± SD. Data are representative of three experiments. n.s. no statistical significance compared with WT control group by one-way ANOVA with Tukey's *post hoc* test.

our study was not observed in their papers on the global KO mice. In addition, the exact role of PKC-δ in OC formation and bone resorption is debatable. It is controversial that both PKC activators (Wang et al., 2003) and inhibitors (Yao et al., 2015) are able to inhibit osteoclastogenesis and bone resorption. PKC-δ was identified as the predominant isoform expressed in OCs among all PKC family (Khor et al., 2013), Khor et al. (2013) found enhanced osteoclastogenesis in PKC-δ null mice, and surmised that this is an attempt to compensate for an intrinsic bone resorption defect in these mice. In contrast, Cremasco et al. (2012) showed that PKC-δ deficiency did not impair OC differentiation in PKC-δ null mice. With respect to the role of PKC-δ on OC function, Cremasco et al. (2012) found that PKC-δ was required for CTSK exocytosis and genetic disruption of PKC-δ profoundly impaired OC bone resorption in bone slices and significantly decreased collagen type I fragment concentration in the culture medium. However, PKC-δ ablation did not impair ruffled border formation or trafficking of lysosomes containing v-ATPase (acidification), leading to no resorption changes in osteologic hydroxyapatite-coated slices in PKC-δ null mice. In contrast, others showed that rottlerin, a PKC-δ specific inhibitor, potently inhibited lysosomal acidification in human OCs (Sorensen et al., 2010). To investigate the exact role of PKC-δ in OC formation and function, we inactivated PKC-δ specifically in OCs by using the Cre-loxp system and found decreased osteoclastogenesis and bone resorption in PKC-δ cKO BMMs in a sex dependent manner in male mice. Consistent with our work, Khor et al. (2013) also showed that inhibition of PKC-δ and knock out of PKC-δ resulted in impaired osteoclastic bone resorption *in vitro*. These conflicting results are indicative that PKC-δ has dual roles in bone remodeling, where it may modulate both bone formation and resorption ultimately influencing the bone turnover process. Because bone is a dynamic organ with complex micro-enviroment, understanding the exact role of PKC-δ in OC biology is critical to dissecting its role in other bone cells, such as osteoblasts, osteocytes, chondrocytes and endothelial cells.

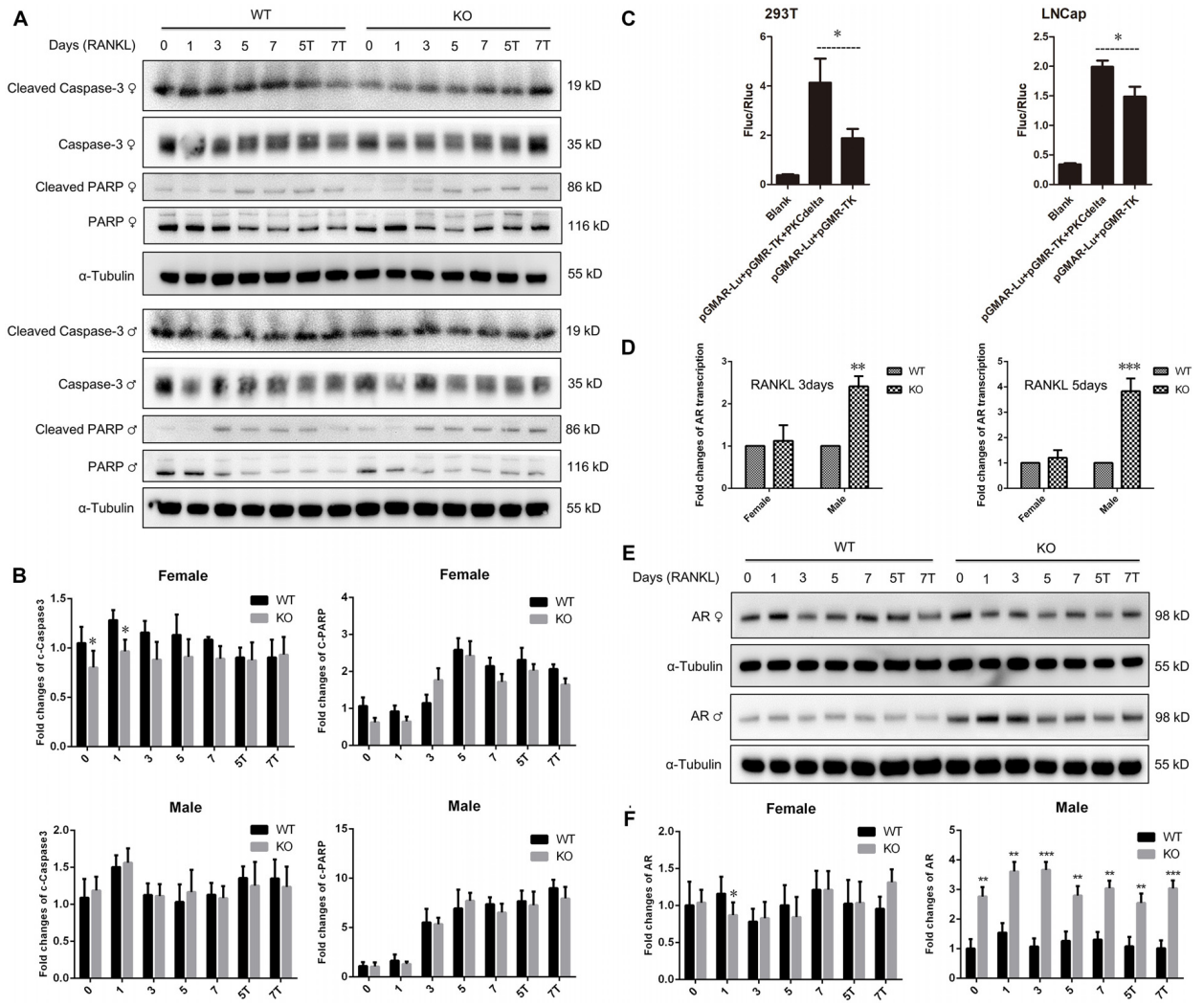


FIGURE 5 | No changes of apoptosis protein expression and significant up-regulation of androgen receptor transcription and expression in male PKC-δ deficient osteoclasts. **(A,B)** Western Blot analysis of characteristic apoptosis proteins (cleaved Caspase-3, Caspase-3, cleaved PARP and PARP) by detecting total protein from WT and PKC-δ cKO BMMs stimulated with RANKL on the indicated days **(A)**; Quantitative analysis of protein expression relative to WT littermate, as measured by densitometry of Western Blot images **(B)**. T 10^{-8} M testosterone, α-Tubulin was probed as a loading control. Statistical analysis was performed by comparing to WT in each time point for male and female, respectively. **(C)** AR transcriptional activity was significantly enhanced by PKC-δ in 293-T and LNCaP cells by transfection and luciferase assay. pGMAR-Lu AR firefly luciferase reporter, pGMR-TK control renilla luciferase reporter. **(D)** RT-PCR shown that AR transcriptional activity was significantly increased in PKC-δ cKO male mice after stimulating with 100 ng/ml RANKL for 3 days and 5 days, respectively. **(E,F)** Western Blot analysis of AR protein expression by detecting total protein from PKC-δ cKO and WT BMMs stimulated with RANKL on the indicated days **(E)**; Quantitative analysis of AR expression in cKO mice relative to WT littermate by measuring densitometry of Western Blot images **(F)**. T 10^{-8} M testosterone, α-Tubulin was probed as a loading control. Experiments were repeated three times. $^{*}p < 0.05$, $^{**}p < 0.01$, $^{***}p < 0.001$ vs. control group by two tailed Student's *t*-test **(C)** and by two-way ANOVA with Tukey's *post hoc* test **(B,D,F)**.

Another contradictory result was that the MAPK signaling was enhanced after PKC-δ ablation selectively in OCs. There may be two reasons for decreased OC differentiation and function accompanied paradoxically with increased MAPK signaling. Firstly, because ERK is responsible for OC survival (Miyazaki et al., 2000) while JNK signaling mediates an anti-apoptotic effect of RANKL in OCs (Ikeda et al., 2008). We assumed that the enhanced survival and anti-apoptotic signaling in OCs may be due to an attempt to compensate for the decreased OC function. Secondly, the MAPK signaling may be not the main signaling after PKC-δ deletion specifically in OCs.

An interesting outcome of our studies is the clear sex differences in bone phenotype and OC differentiation and function after deletion of PKC-δ selectively in OCs. It is an unknown phenomenon and not well described in the hormone-related-gene deficient mice. One example of differences between male and female mice has been found in aromatase-deficient mice, where the female aromatase-ablation mice had an increase in bone turnover resembling early postmenopausal

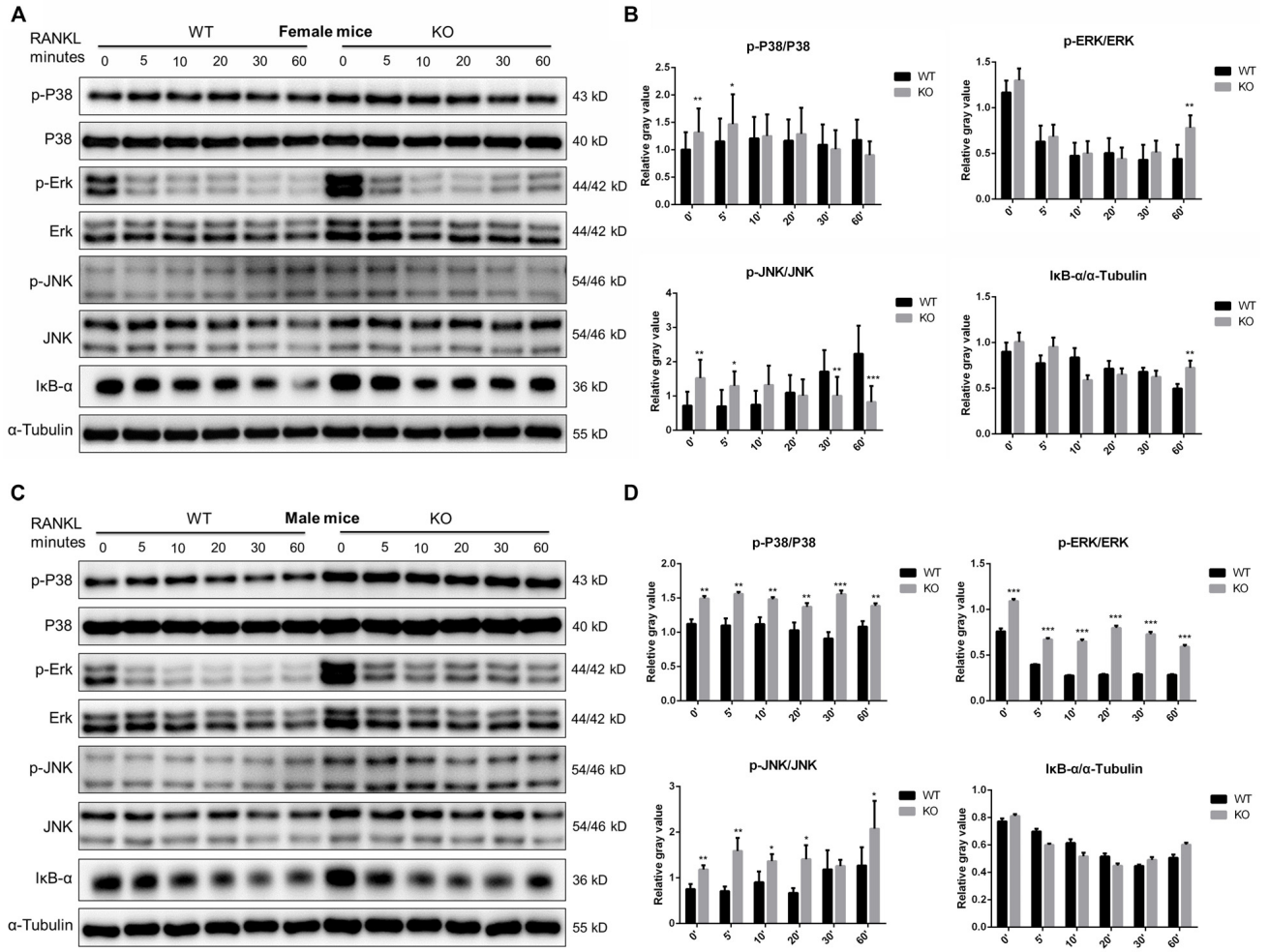


FIGURE 6 | PKC-δ conditional knockout in osteoclasts enhanced RANKL-induced MAPK signaling pathway during osteoclastogenesis in male mice. **(A,C)** Representative Western Blot images of p-JNK, JNK, p-ERK, ERK, p-P38, P-38, IκB-α and α-tubulin at 0, 5, 10, 20, 30, 60 min stimulated by 100 ng/ml RANKL in pre-osteoclasts from PKC-δ cKO and wild type female **(A)** and male **(C)** mice. **(B,D)** The relative ratios of phosphorylated proteins to unphosphorylated proteins or IκB-α to internal control were quantitatively determined in female **(B)** and male **(D)** mice, respectively. The data in the Figures represent the means ± SD. α-Tubulin was used as internal control. Experiments were carried out in triplicate. Significant differences between the cKO and wild type groups are indicated as $^{*}p < 0.05$, $^{**}p < 0.01$, $^{***}p < 0.001$ by two-way ANOVA with Tukey's *post hoc* test **(B,D)**.

osteoporosis, whereas the male aromatase-deficient mice showed decreases in both osteoblastic and osteoclastic surfaces similar to age-related osteopenia compared with WT littermates (Oz et al., 2000). Another example of a sex difference has been found in the ER knockout mice. where the female mice have decreased bone resorption and increased trabecular bone volume, whereas the bones of the male mice were unaffected by the ablation of the ER gene (Sims et al., 2002). However, we have identified two potential explanations that may account for the observed sex differences in PKC-δ cKO mice. Firstly, the presence of functional ARs in OCs (Almeida et al., 2017) indicates that OCs are able to respond directly to androgen through the AR (Pederson et al., 1999), resulting in a suppressive effect on bone resorption (Kawano et al., 2003). The sex-specific effects of androgen on gene expression in human monocyte-derived OCs indicate that AR function is indispensable for male bone formation and remodeling (Wang and Stern, 2011). Moreover, androgens regulated PKC-δ transcription and modulated its apoptotic function in prostate cancer cells (Gavrielides et al., 2006), and prenatal testosterone exposure induces hypertension in adult females via an AR-dependent PKC-δ-mediated mechanism (Blesson et al., 2015). These studies and our results suggest that PKC-δ has a direct interaction with the AR promoter. The studies above lead us to speculate that deletion of PKC-δ in OCs may suppress OC function through increasing AR expression. By using qPCR-based array, Wang and Stern (2011) showed that although OCs from both male and female mice responded to 17β-estradiol and testosterone, the effects of both estrogen and androgen differ in the two sexes, highlighting the importance

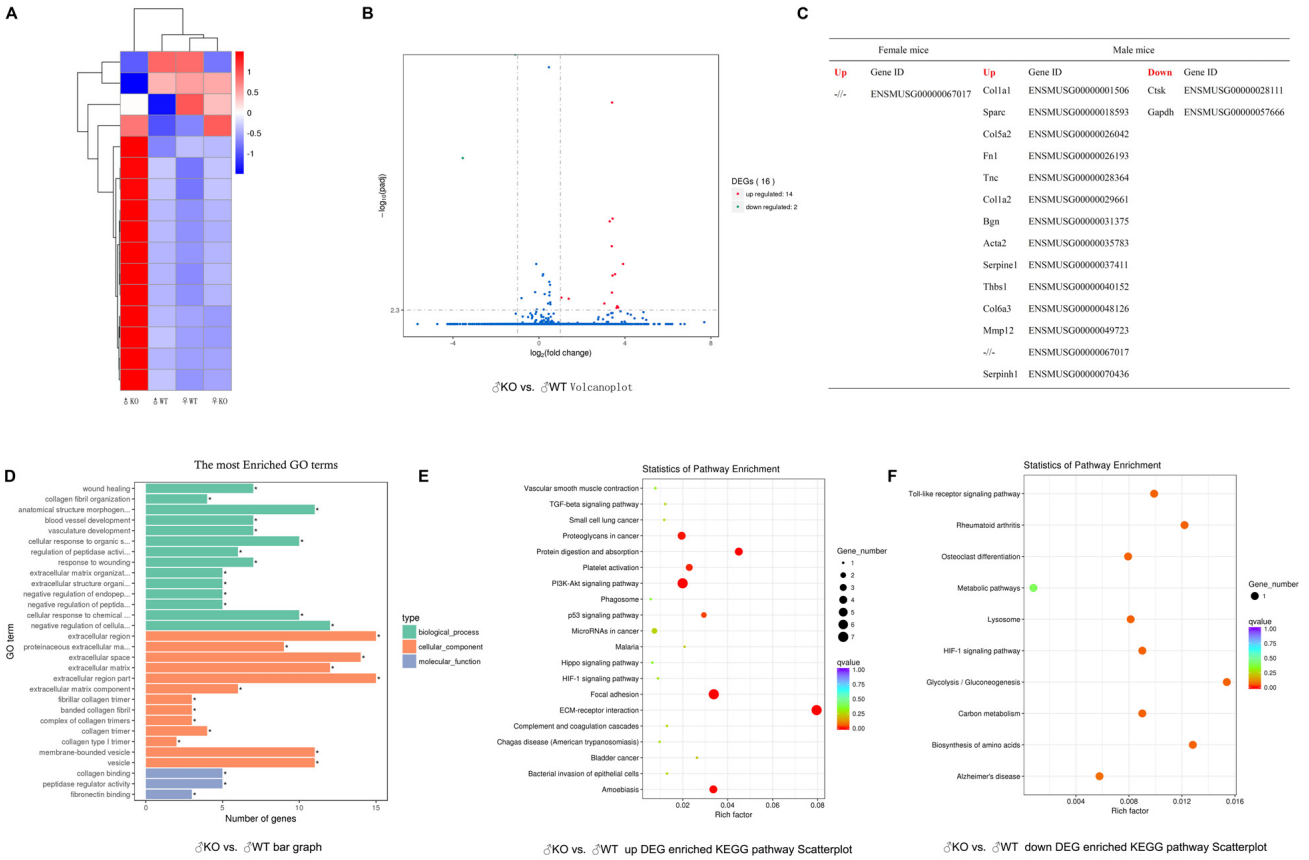


FIGURE 7 | Inactivation of PKC-δ specifically in osteoclasts led to significant alteration of differentially expressed genes (DEGs) and signaling changes only in male mice. **(A)** Heat map of DEGs up and down in 12-week-old PKC-δ cKO mice BMMs derived osteoclasts. **(B)** Volcano plot of data set showing the DEGs in the BMMs stimulating with RANKL for 3 days. Dots with red and green color represented the up-regulated and down-regulated DEGs, respectively, between PKC-δ cKO and WT male mice. **(C)** List of up-regulated and down-regulated DEGs extracted from **(A,B)** with Gene ID and presented in details in **Table 1**. **(D)** Bar graph of GO enrichment analysis of DEGs showing the most enriched GO terms compared between PKC-δ cKO and WT male mice by two tailed Student's *t*-test. **(E)** Gene set enrichment analysis of BMMs from KEGG database revealed the most likely up-regulated pathways responsible for the gender differences. **(F)** Scatterplot of KEGG pathway enrichment analysis of DEGs showed the down-regulated pathways comparing PKC-δ cKO and WT male mice. RNA-seq data from three biological replicates per group were used.

of considering gender in the design of therapeutics. This study further supports our findings of sex specific effects of PKC-δ. Secondly, transcriptome sequencing and bioinformatics analysis showed that inactivation of PKC-δ specifically in OCs led to up-regulation of only one pseudogene without function in female mice. In contrast, many genes were altered (Colla1, Colla2, Col5a2, Col6a3, Thbs1, Bgn, Tnc, Sparc, Fn1, Acta2, Serpinel, Mmp12, Serpinh1 were up-regulated while Ctsk and Gapdh were down-regulated) during osteoclastogenesis after PKC-δ ablation in male mice. It should be noted that these DEGs are mainly responsible for ECM and collagen synthesis, degradation and signaling [for example Thbs1 (Amend et al., 2015), Bgn (Shirakura et al., 2017), Sparc (Rosset and Bradshaw, 2016), Fn1 (Magnan et al., 2018), and Serpinh1 (Mimura et al., 2016)]. Interestingly, most of these DEGs play important roles in OC biology (especially Col6a3 (Mullin et al., 2018), Bgn (Bi et al., 2006; Kram et al., 2017), Thbs1 (Kukreja et al., 2009; Amend et al., 2015; Koduru et al., 2018), Tnc (Baniwal et al., 2012), Sparc (Ma et al., 2017), and Acta2 (Mullin et al., 2014)] and also displayed sexual dimorphism in regulating many cellular processes. With respect to collagen related genes, postnatal changes and sexual dimorphism were found in collagen expression in mouse skin. Col1a1 and Col1a2 mRNAs increased noticeably at day 30 and remained at high levels until day 120 in male mice, Col3a1mRNA also showed significantly high levels at day 120 in male mice as compared to female. Moreover, testosterone and its effect on collagen expression are responsible for the skin sexual dimorphism (Arai et al., 2017). Intriguingly, the Col5a1 gene is associated with increased risk of anterior cruciate ligament ruptures only in female participants (Posthumus et al., 2009). Bgn-deficient mice are resistant to OVX-induced trabecular bone loss and there is a gender difference in response to Bgn deficiency (Nielsen et al., 2003). For Fn1 and Tnc, tendon of the female mice had approximately twofold elevations in ECM proteins such as Fn1 and Tnc compared with male

TABLE 1 | Genes differentially expressed during osteoclastogenesis in male PKC-δ conditional knockout mice (n = 3).

Gene symbol	Gene name	Fold changes (cKO vs. WT, log_2)	p-value
Col1a1	Collagen type I alpha 1 chain	3.427	1.04E-21
Col1a2	Collagen type I alpha 2 chain	3.389	5.27E-17
Col5a2	Collagen type V alpha 2 chain	3.640	1.70E-06
Col6a3	Collagen type VI alpha 3 chain	3.687	2.73E-06
Sparc	Secreted protein acidic and cysteine rich	3.915	5.38E-14
Fn1	Fibronectin 1	3.404	4.37E-41
Tnc	Tenascin C	3.396	6.15E-09
Bgn	Biglycan	3.045	5.38E-07
Acta2	Actin alpha 2	3.423	6.69E-12
Serpine 1	Serpin family E member 1	3.539	3.45E-12
Thbs1	Thrombospondin 1	3.293	3.59E-21
Mmp12	Matrix metallopeptidase 12	1.042	4.71E-08
Serpinh 1	Serpin family H member 1	3.612	3.40E-06
Ctsk	Cathepsin K	−1.099	0
Gapdh	Glyceraldehyde-3-phosphate dehydrogenase	−3.541	8.60E-32

mice (Sarver et al., 2017). For Acta2, male MDR2 knockout mice tended to have a more pronounced reversal of liver fibrosis than females treated with corticosterone (Petrescu et al., 2017). For Mmp9, less elastin in the aneurysm wall in women than that in men, and the simultaneous higher level of Mmp-9, suggesting differences in the elastolytic process in abdominal aortic aneurysms between the sexes (Villard et al., 2014); in addition, male mucopolysaccharidosis type I mice have an increased incidence of aortic insufficiency associated with an increase in MMP-12 aortic arch content (Tolar et al., 2009). For CTSK, sexual dimorphism existed in MAPK-Activated protein kinase-2 regulation of RANKL-induced osteoclastogenesis in OC progenitor subpopulations (Herbert et al., 2015). Collectively, all these DEGs are closely related to the ECM and the majority display sexual dimorphism. It is reasonable to assume that the gender difference found in the studies above also could be found in other deficient mice; herein it is important to examine the phenotype of both sexes. Although the precise role of PKC-δ in ECM-related gene signaling is complex and remains to be elucidated, it is possible that PKC-δ may regulate AR activity through the DEGs above. However, the underlying molecular mechanisms of the differential expression and the role of these genes in sex related differences in OC functions need to be further investigated.

Limitations of our study should be acknowledged. First, it is reported that CTSK-Cre caused unexpected germline deletion of genes in mice which was found to be due to the expression of CTSK in both testis and ovary (Winkeler et al., 2012). This illustrates that we need to be alert to potential germline recombination which may confound our results regarding the changes of size and androgen signaling. It is reported that lack of PKC-δ (PKC-δ null mice) disrupts fertilization and embryonic development in both males and females (Ma et al., 2015). Testis and ovary dysfunction and hypogonadism are always accompanied with osteopenia (Watts et al., 2012; Karakas and Surampudi, 2018). However, in our study, we found that PKC-δ deficiency in OCs favored bone mass accrual and enhanced AR transcription and expression during osteoclastogenesis only in male mice, furthermore, the reproduction function was not affected after PKC-δ cKO in OCs (unpublished data), suggesting that the proposed effects resulting from germline deletion of PKC-δ are contradictory to our results. In addition, CTSK is mainly expressed in OCs, the expression levels of CTSK in other tissues are much lower than that in bone (Soderstrom et al., 1999). Taken together, we speculate that the CTSK expression in gonads may not confound our results. Although many of the OC-targeted Cre-deleter strains, including CTSK, TRAP and *LysM*, are imperfect and each model has its own limitations (Dallas et al., 2018), the CTSK-Cre mouse is the most widely used Cre transgenic mouse line for the *in vivo* study of OCs, their careful use will continue to provide key advances in our understanding of OC function in bone health and disease. Second, it is difficult to transfect pre-OC of the RAW264.7 cell line and BMMs with plasmids, hence the lack of evidence showing direct interaction between PKC-δ and AR in OC. However, many lines of evidence from other cell lines, such as mesenteric artery smooth muscle cells (Blesson et al., 2015), 293-T and LNCaP cells, support our findings. Clinical and genetic studies of PKC-δ gene mutations in humans are important to confirm these pre-clinical studies in mice, blood and bone samples from patients with PKC-δ deficiency will provide further information to address this issue (Belot et al., 2013; Kuehn et al., 2013; Salzer et al., 2013; Kiykim et al., 2015).

In summary, our data clearly demonstrate sex differences in the function of PKC-δ in mice. More importantly, we provide compelling evidence demonstrating that the sex differences are closely related to AR, MAPK, and ECM related signaling, unveiling an important role for PKC-δ in the pathogenesis of osteoporosis in animal models, cell culture, and molecular interactions. This work contributes to our understanding of the role of PKC-δ in OC bone resorption and might aid in the discovery of novel therapeutic targets for treatment of gender-related bone disorders.

DATA AVAILABILITY STATEMENT

The raw data supporting the conclusions of this article will be made available by the authors, without undue reservation, to any qualified researcher. The metagenomic sequencing data have been deposited into Sequence Read Archive (SRA) under accession no. PRJNA555653.

ETHICS STATEMENT

All the experiments were approved by the Institutional Animal Care and Use Committee of the Third Affiliated Hospital of Sun Yat-sen University (Approval No: IACUC-F3-18-1202) and were performed according to EU Directive 2010/63/EU.

AUTHOR CONTRIBUTIONS

SL and LR conceived the ideas. SL, JX, and AQ planned experiments. SL, TH, DW, and JY performed experiments and analyzed the data. JX and AQ contributed reagents. SL wrote the manuscript. JT and JX revised manuscript content. All authors reviewed the manuscript.

FUNDING

This study was supported by grants from the Fundamental Research Funds for the Central Universities (Grant No. 17ykpy49), the Guangdong Natural Science Foundation (Grant No. 2018A030313248), and the National Natural Science Foundation of China (Grant No. 81772398).

SUPPLEMENTARY MATERIAL

The Supplementary Material for this article can be found online at: https://www.frontiersin.org/articles/10.3389/fcell.2020.00450/full#supplementary-material

REFERENCES

Abu-Amer, Y. (2013). NF-kappaB signaling and bone resorption. *Osteoporos. Int.* 24, 2377–2386. doi: 10.1007/s00198-013-2313-x

Almeida, M., Laurent, M. R., Dubois, V., Claessens, F., O'Brien, C. A., Bouillon, R., et al. (2017). Estrogens and androgens in skeletal physiology and pathophysiology. *Physiol. Rev.* 97, 135–187. doi: 10.1152/physrev.00033.2015

Amend, S. R., Uluckan, O., Hurchla, M., Leib, D., Novack, D. V., Silva, M., et al. (2015). Thrombospondin-1 regulates bone homeostasis through effects on bone matrix integrity and nitric oxide signaling in osteoclasts. *J. Bone Miner. Res.* 30, 106–115. doi: 10.1002/jbmr.2308

Arai, K. Y., Hara, T., Nagatsuka, T., Kudo, C., Tsuchiya, S., Nomura, Y., et al. (2017). Postnatal changes and sexual dimorphism in collagen expression in mouse skin. *PLoS One* 12:e0177534. doi: 10.1371/journal.pone.0177534

Baniwal, S. K., Shah, P. K., Shi, Y., Haduong, J. H., Declerck, Y. A., Gabet, Y., et al. (2012). Runx2 promotes both osteoblastogenesis and novel osteoclastogenic signals in ST2 mesenchymal progenitor cells. *Osteoporos. Int.* 23, 1399–1413. doi: 10.1007/s00198-011-1728-5

Belot, A., Kasher, P. R., Trotter, E. W., Foray, A. P., Debaud, A. L., Rice, G. I., et al. (2013). Protein kinase cdelta deficiency causes mendelian systemic lupus erythematosus with B cell-defective apoptosis and hyperproliferation. *Arthritis Rheum.* 65, 2161–2171. doi: 10.1002/art.38008

Bi, Y., Nielsen, K. L., Kilts, T. M., Yoon, A., Karsdal, M. A., Wimer, H. F., et al. (2006). Biglycan deficiency increases osteoclast differentiation and activity due to defective osteoblasts. *Bone* 38, 778–786. doi: 10.1016/j.bone.2005.11.005

Blesson, C. S., Chinnathambi, V., Hankins, G. D., Yallampalli, C., and Sathishkumar, K. (2015). Prenatal testosterone exposure induces hypertension in adult females via androgen receptor-dependent protein kinase Cdelta-mediated mechanism. *Hypertension* 65, 683–690. doi: 10.1161/HYPERTENSIONAHA.114.04521

Cremasco, V., Decker, C. E., Stumpo, D., Blackshear, P. J., Nakayama, K. I., Nakayama, K., et al. (2012). Protein kinase C-delta deficiency perturbs bone homeostasis by selective uncoupling of cathepsin K secretion and ruffled border formation in osteoclasts. *J. Bone Miner. Res.* 27, 2452–2463. doi: 10.1002/jbmr.1701

Da, C. L., Xin, Y., Zhao, J., and Luo, X. D. (2009). Significance and relationship between Yes-associated protein and survivin expression in gastric carcinoma and precancerous lesions. *World J. Gastroenterol.* 15, 4055–4061. doi: 10.3748/wjg.15.4055

Dallas, S. L., Xie, Y., Shiflett, L. A., and Ueki, Y. (2018). Mouse cre models for the study of bone diseases. *Curr. Osteoporos. Rep.* 16, 466–477. doi: 10.1007/s11914-018-0455-7

Gavrielides, M. V., Gonzalez-Guerrico, A. M., Riobo, N. A., and Kazanietz, M. G. (2006). Androgens regulate protein kinase Cdelta transcription and modulate its apoptotic function in prostate cancer cells. *Cancer Res.* 66, 11792–11801. doi: 10.1158/0008-5472.can-06-1139

He, L., Hong, G., Zhou, L., Zhang, J., Fang, J., He, W., et al. (2019). Asiaticoside, a component of *Centella asiatica* attenuates RANKL-induced osteoclastogenesis via NFATc1 and NF-kappaB signaling pathways. *J. Cell. Physiol.* 234, 4267–4276. doi: 10.1002/jcp.27195

Herbert, B. A., Valerio, M. S., Gaestel, M., and Kirkwood, K. L. (2015). Sexual dimorphism in MAPK-activated protein kinase-2 (MK2) regulation of RANKL-induced osteoclastogenesis in osteoclast progenitor subpopulations. *PLoS One* 10:e0125387. doi: 10.1371/journal.pone.0125387

Huber, D. M., Bendixen, A. C., Pathrose, P., Srivastava, S., Dienger, K. M., Shevde, N. K., et al. (2001). Androgens suppress osteoclast formation induced by RANKL and macrophage-colony stimulating factor. *Endocrinology* 142, 3800–3808. doi: 10.1210/endo.142.9.8402

Iaquinta, M. R., Mazzoni, E., Bononi, I., Rotondo, J. C., Mazziotta, C., Montesi, M., et al. (2019). Adult stem cells for bone regeneration and repair. *Front. Cell. Dev. Biol.* 7:268. doi: 10.3389/fcell.2019.00268

Ikeda, F., Matsubara, T., Tsurukai, T., Hata, K., Nishimura, R., and Yoneda, T. (2008). JNK/c-Jun signaling mediates an anti-apoptotic effect of RANKL in osteoclasts. *J. Bone Miner. Res.* 23, 907–914. doi: 10.1359/jbmr.080211

Karakas, S. E., and Surampudi, P. (2018). New biomarkers to evaluate hyperandrogenemic women and hypogonadal men. *Adv. Clin. Chem.* 86, 71–125. doi: 10.1016/bs.acc.2018.06.001

Kawano, H., Sato, T., Yamada, T., Matsumoto, T., Sekine, K., Watanabe, T., et al. (2003). Suppressive function of androgen receptor in bone resorption. *Proc. Natl. Acad. Sci. U.S.A.* 100, 9416–9421. doi: 10.1073/pnas.1533500100

Khor, E. C., Abel, T., Tickner, J., Chim, S. M., Wang, C., Cheng, T., et al. (2013). Loss of protein kinase C-delta protects against LPS-induced osteolysis owing to an intrinsic defect in osteoclastic bone resorption. *PLoS One* 8:e70815. doi: 10.1371/journal.pone.0070815

Kiykim, A., Ogulur, I., Baris, S., Salzer, E., Karakoc-Aydiner, E., Ozen, A. O., et al. (2015). Potentially beneficial effect of hydroxychloroquine in a patient with a novel mutation in protein kinase cdelta deficiency. *J. Clin. Immunol.* 35, 523–526. doi: 10.1007/s10875-015-0178-9

Koduru, S. V., Sun, B. H., Walker, J. M., Zhu, M., Simpson, C., Dhodapkar, M., et al. (2018). The contribution of cross-talk between the cell-surface proteins CD36 and CD47-TSP-1 in osteoclast formation and function. *J. Biol. Chem.* 293, 15055–15069. doi: 10.1074/jbc.RA117.000633

Kram, V., Kilts, T. M., Bhattacharyya, N., Li, L., and Young, M. F. (2017). Small leucine rich proteoglycans, a novel link to osteoclastogenesis. *Sci. Rep.* 7:12627. doi: 10.1038/s41598-017-12651-6

Kuehn, H. S., Niemela, J. E., Rangel-Santos, A., Zhang, M., Pittaluga, S., Stoddard, J. L., et al. (2013). Loss-of-function of the protein kinase C delta (PKCdelta) causes a B-cell lymphoproliferative syndrome in humans. *Blood* 121, 3117–3125. doi: 10.1182/blood-2012-12-469544

Kukreja, A., Radfar, S., Sun, B. H., Insogna, K., and Dhodapkar, M. V. (2009). Dominant role of CD47-thrombospondin-1 interactions in myeloma-induced fusion of human dendritic cells: implications for bone disease. *Blood* 114, 3413–3421. doi: 10.1182/blood-2009-03-211920

Lee, K., Seo, I., Choi, M. H., and Jeong, D. (2018). Roles of mitogen-activated protein kinases in osteoclast biology. *Int. J. Mol. Sci.* 19:3004. doi: 10.3390/ijms19103004

Ma, J., Gao, S., Xie, X., Sun, E., Zhang, M., Zhou, Q., et al. (2017). SPARC inhibits breast cancer bone metastasis and may be a clinical therapeutic target. *Oncol. Lett.* 14, 5876–5882. doi: 10.3892/ol.2017.6925

Ma, W., Baumann, C., and Viveiros, M. M. (2015). Lack of protein kinase C-delta (PKCdelta) disrupts fertilization and embryonic development. *Mol. Reprod. Dev.* 82, 797–808. doi: 10.1002/mrd.22528

Magnan, L., Labrunie, G., Marais, S., Rey, S., Dusserre, N., Bonneu, M., et al. (2018). Characterization of a cell-assembled extracellular matrix and the effect of the devitalization process. *Acta Biomater.* 82, 56–67. doi: 10.1016/j.actbio.2018.10.006

Mimura, H., Takaya, T., Matsuda, S., Nakano, K., Muraoka, R., Tomida, M., et al. (2016). Functional role of HSP47 in the periodontal ligament subjected to occlusal overload in mice. *Int. J. Med. Sci.* 13, 248–254. doi: 10.7150/ijms.14129

Miyazaki, T., Katagiri, H., Kanegae, Y., Takayanagi, H., Sawada, Y., Yamamoto, A., et al. (2000). Reciprocal role of ERK and NF-kappaB pathways in survival and activation of osteoclasts. *J. Cell Biol.* 148, 333–342. doi: 10.1083/jcb.148.2.333

Mullin, B. H., Mamotte, C., Prince, R. L., and Wilson, S. G. (2014). Influence of ARHGEF3 and RHOA knockdown on ACTA2 and other genes in osteoblasts and osteoclasts. *PLoS One* 9:e98116. doi: 10.1371/journal.pone.0098116

Mullin, B. H., Zhu, K., Xu, J., Brown, S. J., Mullin, S., Tickner, J., et al. (2018). Expression quantitative trait locus study of bone mineral density GWAS variants in human osteoclasts. *J. Bone Miner. Res.* 33, 1044–1051. doi: 10.1002/jbmr.3412

Nielsen, K. L., Allen, M. R., Bloomfield, S. A., Andersen, T. L., Chen, X. D., Poulsen, H. S., et al. (2003). Biglycan deficiency interferes with ovariectomy-induced bone loss. *J. Bone Miner. Res.* 18, 2152–2158. doi: 10.1359/jbmr.2003.18.12.2152

Ono, Y., Fujii, T., Ogita, K., Kikkawa, U., Igarashi, K., and Nishizuka, Y. (1988). The structure, expression, and properties of additional members of the protein kinase C family. *J. Biol. Chem.* 263, 6927–6932.

Oz, O. K., Zerwekh, J. E., Fisher, C., Graves, K., Nanu, L., Millsaps, R., et al. (2000). Bone has a sexually dimorphic response to aromatase deficiency. *J. Bone Miner. Res.* 15, 507–514. doi: 10.1359/jbmr.2000.15.3.507

Pederson, L., Kremer, M., Judd, J., Pascoe, D., Spelsberg, T. C., Riggs, B. L., et al. (1999). Androgens regulate bone resorption activity of isolated osteoclasts in vitro. *Proc. Natl. Acad. Sci. U.S.A.* 96, 505–510. doi: 10.1073/pnas.96.2.505

Petrescu, A. D., Grant, S., Frampton, G., Kain, J., Hadidi, K., Williams, E., et al. (2017). Glucocorticoids cause gender-dependent reversal of hepatic fibrosis in the MDR2-knockout mouse model. *Int. J. Mol. Sci.* 18:E2389. doi: 10.3390/ijms18112389

Posthumus, M., September, A. V., O'Cuinneagain, D., van der Merwe, W., Schwellnus, M. P., and Collins, M. (2009). The COL5A1 gene is associated with increased risk of anterior cruciate ligament ruptures in female participants. *Am. J. Sports Med.* 37, 2234–2240. doi: 10.1177/0363546509338266

Roffey, J., Rosse, C., Linch, M., Hibbert, A., McDonald, N. Q., and Parker, P. J. (2009). Protein kinase C intervention: the state of play. *Curr. Opin. Cell Biol.* 21, 268–279. doi: 10.1016/j.ceb.2009.01.019

Rosset, E. M., and Bradshaw, A. D. (2016). SPARC/osteonectin in mineralized tissue. *Matrix Biol.* 52–54, 78–87. doi: 10.1016/j.matbio.2016.02.001

Salzer, E., Santos-Valente, E., Klaver, S., Ban, S. A., Emminger, W., Prengemann, N. K., et al. (2013). B-cell deficiency and severe autoimmunity caused by deficiency of protein kinase C delta. *Blood* 121, 3112–3116. doi: 10.1182/blood-2012-10-460741

Sarver, D. C., Kharaz, Y. A., Sugg, K. B., Gumucio, J. P., Comerford, E., and Mendias, C. L. (2017). Sex differences in tendon structure and function. *J. Orthop. Res.* 35, 2117–2126. doi: 10.1002/jor.23516

Shirakura, M., Kram, V., Robinson, J., Sikka, S., Kilts, T. M., Wadhwa, S., et al. (2017). Extracellular matrix mediates BMP-2 in a model of temporomandibular joint osteoarthritis. *Cells Tissues Organs* 204, 84–92. doi: 10.1159/000464102

Sims, N. A., Dupont, S., Krust, A., Clement-Lacroix, P., Minet, D., Resche-Rigon, M., et al. (2002). Deletion of estrogen receptors reveals a regulatory role for estrogen receptors-beta in bone remodeling in females but not in males. *Bone* 30, 18–25. doi: 10.1016/s8756-3282(01)00643-3

Soderstrom, M., Salminen, H., Glumoff, V., Kirschke, H., Aro, H., and Vuorio, E. (1999). Cathepsin expression during skeletal development. *Biochim. Biophys. Acta* 1446, 35–46. doi: 10.1016/s0167-4781(99)00068-8

Sorensen, M. G., Karsdal, M. A., Dziegiel, M. H., Boutin, J. A., Nosjean, O., and Henriksen, K. (2010). Screening of protein kinase inhibitors identifies PKC inhibitors as inhibitors of osteoclastic acid secretion and bone resorption. *BMC Musculoskelet. Disord.* 11:250. doi: 10.1186/1471-2474-11-250

Steinberg, S. F. (2008). Structural basis of protein kinase C isoform function. *Physiol. Rev.* 88, 1341–1378. doi: 10.1152/physrev.00034.2007

Tolar, J., Braunlin, E., Riddle, M., Peacock, B., McElmurry, R. T., Orchard, P. J., et al. (2009). Gender-related dimorphism in aortic insufficiency in murine mucopolysaccharidosis type I. *J. Heart Valve Dis.* 18, 524–529.

Tong, W., Zeng, Y., Chow, D. H. K., Yeung, W., Xu, J., Deng, Y., et al. (2019). Wnt16 attenuates osteoarthritis progression through a PCP/JNK-mTORC1-PTHrP cascade. *Ann. Rheum. Dis.* 78, 551–561. doi: 10.1136/annrheumdis-2018-214200

Tu, X., Joeng, K. S., Nakayama, K. I., Nakayama, K., Rajagopal, J., Carroll, T. J., et al. (2007). Noncanonical Wnt signaling through G protein-linked PKCdelta activation promotes bone formation. *Dev. Cell* 12, 113–127. doi: 10.1016/j.devcel.2006.11.003

Villard, C., Eriksson, P., Swedenborg, J., and Hultgren, R. (2014). Differences in elastin and elastolytic enzymes between men and women with abdominal aortic aneurysm. *Aorta* 2, 179–185. doi: 10.12945/j.aorta.2014.14-017

Wang, C., Steer, J. H., Joyce, D. A., Yip, K. H., Zheng, M. H., and Xu, J. (2003). 12-O-tetradecanoylphorbol-13-acetate (TPA) inhibits osteoclastogenesis by suppressing RANKL-induced NF-kappaB activation. *J. Bone Miner. Res.* 18, 2159–2168. doi: 10.1359/jbmr.2003.18.12.2159

Wang, J., and Stern, P. H. (2011). Sex-specific effects of estrogen and androgen on gene expression in human monocyte-derived osteoclasts. *J. Cell. Biochem.* 112, 3714–3721. doi: 10.1002/jcb.23297

Watts, N. B., Adler, R. A., Bilezikian, J. P., Drake, M. T., Eastell, R., Orwoll, E. S., et al. (2012). Osteoporosis in men: an endocrine society clinical practice guideline. *J. Clin. Endocrinol. Metab.* 97, 1802–1822. doi: 10.1210/jc.2011-3045

Winkeler, C. L., Kladney, R. D., Maggi, L. B. Jr., and Weber, J. D. (2012). Cathepsin K-Cre causes unexpected germline deletion of genes in mice. *PLoS One* 7:e42005. doi: 10.1371/journal.pone.0042005

Yang, D., Guo, J., Divieti, P., and Bringhurst, F. R. (2006). Parathyroid hormone activates PKC-delta and regulates osteoblastic differentiation via a PLC-independent pathway. *Bone* 38, 485–496. doi: 10.1016/j.bone.2005.10.009

Yang, X., Teguh, D., Wu, J. P., He, B., Kirk, T. B., Qin, S., et al. (2015). Protein kinase C delta null mice exhibit structural alterations in articular surface, intra-articular and subchondral compartments. *Arthritis Res. Ther.* 17:210. doi: 10.1186/s13075-015-0720-4

Yao, J., Li, J., Zhou, L., Cheng, J., Chim, S. M., Zhang, G., et al. (2015). Protein kinase C inhibitor, GF109203X attenuates osteoclastogenesis, bone resorption and RANKL-induced NF-kappaB and NFAT activity. *J. Cell. Physiol.* 230, 1235–1242. doi: 10.1002/jcp.24858

Yao, Z., Li, Y., Yin, X., Dong, Y., Xing, L., and Boyce, B. F. (2014). NF-kappaB RelB negatively regulates osteoblast differentiation and bone formation. *J. Bone Miner. Res.* 29, 866–877. doi: 10.1002/jbmr.2108

Zaidi, M. (2007). Skeletal remodeling in health and disease. *Nat. Med.* 13, 791–801. doi: 10.1038/nm1593

Disclosure: The funding sponsors had no role in the design of the study; in the collection, analyses, or interpretation of data; in the writing of the manuscript, and in the decision to publish the results. No benefits in any form have been or will be received from a commercial party related directly or indirectly to the subject of this article.

Conflict of Interest: The authors declare that the research was conducted in the absence of any commercial or financial relationships that could be construed as a potential conflict of interest.

Copyright © 2020 Li, He, Wu, Zhang, Chen, Liu, Yuan, Tickner, Qin, Xu and Rong. This is an open-access article distributed under the terms of the Creative Commons Attribution License (CC BY). The use, distribution or reproduction in other forums is permitted, provided the original author(s) and the copyright owner(s) are credited and that the original publication in this journal is cited, in accordance with accepted academic practice. No use, distribution or reproduction is permitted which does not comply with these terms.

frontiers in Cell and Developmental Biology

REVIEW
published: 30 June 2020
doi: 10.3389/fcell.2020.00534

Functions and Clinical Significance of Super-Enhancers in Bone-Related Diseases

Jian Qu[1,2†], Zhanbo Ouyang[1,2†], Wenqiang Wu[3], Guohua Li[1,2], Jiaojiao Wang[1,2], Qiong Lu[1,2] and Zhihong Li[2,4*]*

[1] Department of Pharmacy, The Second Xiangya Hospital, Central South University, Changsha, China, [2] Hunan Key Laboratory of Tumor Models and Individualized Medicine, The Second Xiangya Hospital, Central South University, Changsha, China, [3] Mathematical Engineering Academy of Chinese Medicine, Guangzhou University of Chinese Medicine, Guangzhou, China, [4] Department of Orthopedics, The Second Xiangya Hospital, Central South University, Changsha, China

Super-enhancers (SEs) are a large cluster of *cis*-regulatory DNA elements that contain many binding motifs, which master transcription factors and cofactors bind to with high density. SEs usually regulate the expression of genes that can control the cell identity and fate, and SEs can be used to explain the patterns of the expression of cell-specific genes. Hence, it shows great potential for application in the treatment of diseases like cancer. At present, the clinical treatments for osteosarcoma, Ewing sarcoma, and other bone-related diseases remain challenging. The poor prognosis and difficult treatment of these diseases imposes heavy economic burden on patients and society. In recent years, research on SEs with respect to bone-related diseases has attracted increasing attention. In this paper, we first review the identification and functional mechanisms of SEs. Then, we integrate the findings of the emerging studies on SEs in bone-related diseases. Finally, we summarize recent strategies for targeting SEs for the treatment of bone-related diseases. This review aims to provide comprehensive insights into the roles of SEs in bone-related diseases.

Keywords: super-enhancers, bone-related diseases, osteosarcoma, Ewing sarcoma, multiple myeloma

OPEN ACCESS

Edited by:
Changjun Li,
Xiangya Hospital, Central South University, China

Reviewed by:
Liu Yang,
Fourth Military Medical University, China
Yu Chai,
Southern Medical University, China

****Correspondence:***
Qiong Lu
christy_luq@csu.edu.cn
Zhihong Li
lizhihong@csu.edu.cn

† These authors have contributed equally to this work

Specialty section:
This article was submitted to Molecular Medicine, a section of the journal Frontiers in Cell and Developmental Biology

Received: *22 April 2020*
Accepted: *08 June 2020*
Published: *30 June 2020*

Citation:
Qu J, Ouyang Z, Wu W, Li G, Wang J, Lu Q and Li Z (2020) Functions and Clinical Significance of Super-Enhancers in Bone-Related Diseases. Front. Cell Dev. Biol. 8:534. doi: 10.3389/fcell.2020.00534

INTRODUCTION

Since the Human Genome Project was launched in 1990, our understanding of the regulatory mechanism of genes has evolved drastically. Nowadays, many scientists believe that gene transcription is controlled by types of regulatory elements known as enhancers and super-enhancers (SEs). Bulger and Groudine, 2011 proposed that enhancers are functionally defined as non-coding elements that can activate gene transcription through long-range *cis* chromatin interactions. Initially, enhancers only meant the typical enhancers (TEs). However, Hnisz et al. (2013) proposed the concept of SEs in 2013. They put forward that although TEs and SEs are similar with respect to carrying the same components such as transcription factors (TFs), cofactors, mediator complex, and RNA polymerase II (pol II) complex, SEs harbors these factors on an average 10-fold higher density than do TEs (Hnisz et al., 2013; Whyte et al., 2013; Thandapani, 2019). The difference between the function and structure of TEs and SEs are shown in **Figure 1**. SEs are a large cluster of *cis*-regulatory DNA elements densely bound by transcription factors and cofactors and play critical roles in defining cell fate and

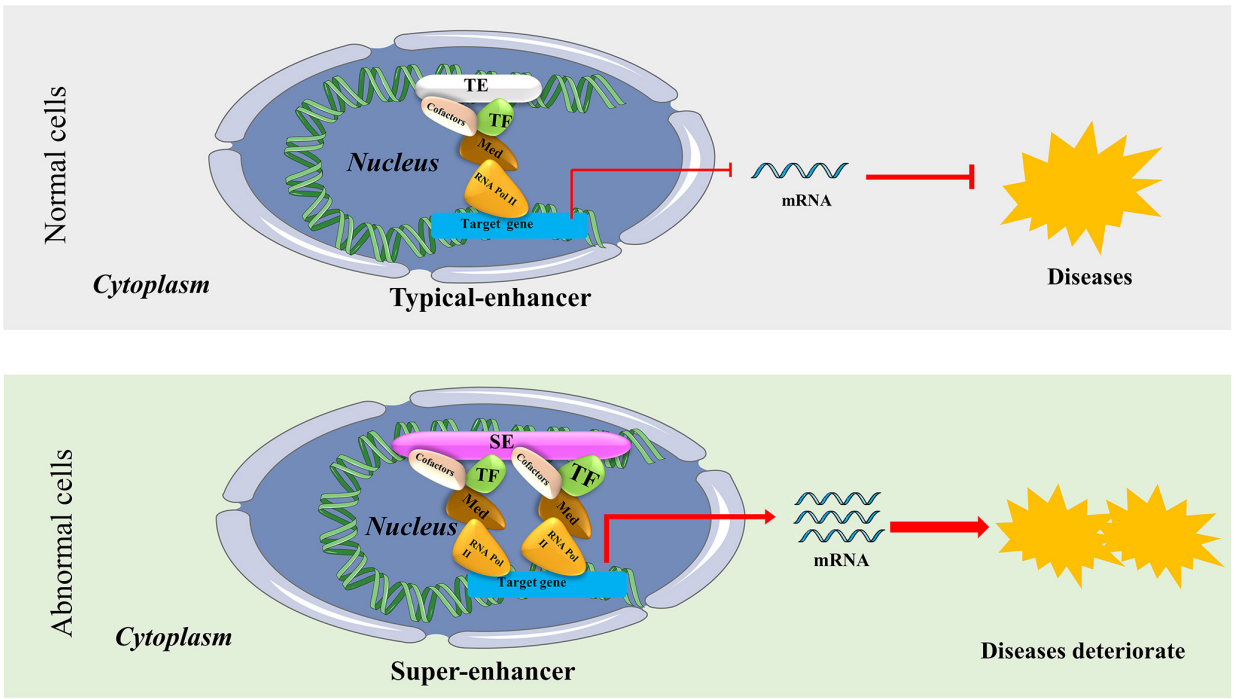


FIGURE 1 | The structure and possible functional mechanism of super-enhancers (SEs) vs. typical enhancers (TEs). SEs are a large cluster of *cis*-regulatory DNA elements densely bound by transcription factors and cofactors. SEs are often found near genes that have cell type-specific functions and genes closely associated with the progress of bone-related diseases. It usually causes diseases or accelerates the progress of diseases by regulating the expression of disease-specific genes.

identity (Hnisz et al., 2013). Histone marks such as H3K27ac, H3K4me1, and the transcription cofactor p300 are often used to define SEs (Riggi et al., 2014; Kennedy et al., 2015; Niederriter et al., 2015). Ever since their discovery, SEs have been the focus of increasing research to investigate their roles in cancers and inflammatory diseases like osteoarthritis. For example, previous research indicated that SEs frequently drive high-level expression of prominent oncogenes in cancer cells (Hnisz et al., 2013; Chipumuro et al., 2014; Kwiatkowski et al., 2014). Other groups found that SEs play a critical role in autoimmune diseases like juvenile idiopathic arthritis (Peeters et al., 2015). Shin (2018) proposed that SEs can be used as biomarkers to develop novel disease diagnostic tools and establish new directions in clinical therapeutic strategies. Hence, SEs can be considered novel targets in diseases, and targeting SEs should be a promising therapeutic strategy.

The clinical treatment of bone-related diseases such as osteosarcoma, Ewing sarcoma, osteoporosis, cartilage dysplasia, chordoma, rheumatoid arthritis, osteoarthritis, and multiple myeloma continue to remain challenging. Although the incidence of these bone-related diseases is relatively lower than cancers like lung cancer, the poor prognosis and difficult treatment imposes a heavy burden on patients and caregivers. To address this complex problem, researchers have aimed to develop high-efficiency, novel therapies based on targeting SEs to treat bone-related diseases. In recent years, the functional mechanism of SEs in these bone-related diseases has attracted increasing attention. Thus, this review will mainly focus on integrating the findings of the emerging studies on SEs (shown in **Table 1**) in bone-related diseases and summarizing the strategies of targeting SEs as a clinical treatment for bone-related diseases. We believe it can provide new insights and angles for future studies and optimum treatment strategies using SEs in bone-related diseases.

THE IDENTIFICATION OF SEs

Diseases-related cells acquire SEs through various mechanisms, including (i)mutations and genomic alterations like deletions, duplications, translocations, insertions, inversions (Mansour et al., 2014; Oldridge et al., 2015; Zhang et al., 2019); (ii) single-nucleotide polymorphisms (SNPs) (Zhu et al., 2018); (iii) chromosomal rearrangements (Affer et al., 2014; Gröschel et al., 2014; Demchenko et al., 2016); and (iv) 3D genome structural changes (Furlong and Levine, 2018). Once the SEs originated through the above mechanisms, resulting in the dysregulation of nearby SEs-target genes, which ultimately accelerates the deterioration of diseases.

With rapid developments in genetic research, many refractory diseases with complex disease mechanisms have been well studied. However, despite researchers having identified some effective treatments, osteosarcoma, Ewing sarcoma, and other bone-related diseases remain difficult to treat. The poor prognosis and difficulty in treatment impose heavy economic burden on patients and society. Although many studies have proposed

TABLE 1 | Summary of the researches about the SEs in bone-related diseases.

Diseases*	Cell/tissue*	SEs-targeted genes	Methods	Findings	References
OS	OS cell lines (U2OS/SJSA-1)	*MYC*, *STAT3*	ChIP-Seq of H3K27ac	THZ2 can inhibit the progression of osteosarcoma by targeting SE-associated genes like *MYC*, *STAT3*	Zhang et al., 2020
OS	OS cell lines (143B and SJSA1), primary OS cells (ZOS and ZOSM), and OS tissue	*LIF*	ChIP-Seq of H3K27ac	SEs function as an activator of NOTCH1 pathway through regulating LIF/STAT3 pathway in promoting the progression of osteosarcoma	Lu et al., 2020
ES	ES cell lines (A673/SKNMC)	*BCL11B*, *GLG1*	Analysis of ChIP-Seq data of H3K27ac	SEs-targeted genes *BCL11B* and *GLG1* are novel biomarkers for the diagnosis of Ewing sarcoma	Baldauf et al., 2018
ES	ES cell lines (A673/SKNMC)	*MEIS1*	ChIP-Seq of H3K27ac	SEs-associated gene *MEIS1* promotes transcriptional dysregulation in Ewing sarcoma in co-operation with EWS-FLI1	Lin et al., 2018
ES	ES cell lines (TC32/TC71)	*CCND1*	ChIP-Seq of H3K27ac	SEs-associated gene *CCND1* promotes the progression of Ewing sarcoma	Kennedy et al., 2015
ES	ES cell lines-A673 cells treated with JQ1	*EWS-FLI1*	ChIP of BRD4 and analysis of ChIP-Seq data of H3K27ac	SE-inhibitors like JQ1 can repress the progression of Ewing sarcoma through impacting *EWS-FLI1'* expression	Jacques et al., 2016
Chordoma	Chordoma cell lines and chordoma tissue	*TBXT*	ChIP-Seq of H3K27ac	The dysregulation of *TBXT* regulated by SEs is the main cause for the tumorigenesis of chordoma	Sharifnia et al., 2019
MM	Primary cells isolated from MM tissue and Myeloma cell lines	*IRF4*, *FLI1*	ChIP-Seq of H3K27ac	*IRF4* and *FLI1* showed significant overlap with SEs. They can promote the progress of MM	Jin et al., 2018
MM	MM1.S MM cells	*MYC*	ChIP-Seq of H3K27ac, BRD4, MED1	SE-inhibitors treatment like JQ1 results in preferential loss of BRD4 in *MYC*-SE, which can repress the progress of MM	Loven et al., 2013
OP	GM12878 cells/osteoblast	*RANKL*	Analysis of ChIP-Seq data of H3K27ac from ENCODE	The dysregulated expression of the SE-associated gene *RANKL* is critical for the progress of osteoporosis	Zhu et al., 2018
CD	Rat chondrosarcoma cells	*SOX9*, *SOX6*, *SOX5*	ChIP-Seq 0f H3K27ac	The dysregulation of the SE- associated genes may cause cartilage dysplasia	Liu and Lefebvre, 2015
RA	CD4 + T cell	*BACH2*	ChIP-Seq of P300 protein	SEs-associated gene *BACH2* which is critical for the progress of RA	Vahedi et al., 2015
OS	Chondrocyte cell (sw1353 and chondrocytes isolated from OA tissue)	*HMGB1*	ChIP of BRD4 and analysis of ChIP-Seq data of H3K27ac	SEs may mediate the BRD4 regulating role in the expression of *HMGB1*	Jiang et al., 2017

**OS cell, osteosarcoma cell; ES cell, Ewing sarcoma cell; OP cell, osteoporosis cell; CD cell, cartilage dysplasia cell; chordoma, RA cell, rheumatoid arthritis cell; OA cell, osteoarthritis cell; and MM cell, multiple myeloma cell.*

different treatment options for bone-related diseases, the effects of these treatments are not satisfactory. Therefore, significant research is on-going in an attempt to discover satisfactory treatment methods for these diseases.

Loven et al. (2013) and Whyte et al. (2013) first identified SEs in mouse embryonic stem cells and human cells. Since then, several publications have cited the SEs and identified its applications in different diseases (Chapuy et al., 2013; Loven et al., 2013; Whyte et al., 2013; Brown et al., 2014; Vaharautio and Taipale, 2014). Besides, an SE database—dbSUPER—in the mouse and human genome has been established by Khan and Zhang (2016). It is the first integrated and interactive database of SEs and serves as a reference for further studies related to transcriptional control of cell identity and disease. Pott and Lieb (2015) summarized the characteristics of SEs based on these publications: (i) SEs are enriched for motifs related to cell type-specific master transcription factors, and are often found near genes that have cell type-specific functions, including known master regulators; (ii) SEs are enriched for trait-associated variants; (iii) SEs overlap with previously defined large-scale regulatory domains and (iv) SEs in cancer cells are enriched in the vicinity of oncogenes. Summarizing from previous studies, abnormal SEs in disease states may form because of focal amplification, genomic regulatory elements rearrangements (Affer et al., 2014; Walker et al., 2014), and small insertions and deletions.

In recent years, research on SEs in diseases has become an important focus of clinical and basic research. As for the functional mechanism of the SEs (shown in **Figure 1**), Sengupta and George (2017) concluded that transcription factor (TF) binding to enhancers results in recruitment of the mediator complex. This, in turn, facilitates enhancer interaction with the basal transcription machinery and RNA polymerase II (Pol II) at the promoter regions in a gene-specific manner, a process mediated by "looping" of the loaded enhancer to the cognate promoter (Hnisz et al., 2016; Sur and Taipale, 2016). Thus, SEs can influence disease progression by initiating downstream transcription of the affected genes (Sengupta and George, 2017).

SEs IN BONE-RELATED DISEASES

SEs in Osteosarcoma

Osteosarcoma (OS) is the most common primary sarcoma occurring in children and adolescents. Metastasis and recurrence of osteosarcoma are the main influencing factors for the poor survival rate. The overall 5-year survival rate for patients with non-metastatic osteosarcoma is approximately 60–70%, while that for patients with metastatic and recurrent osteosarcoma is significantly reduced (Kempf-Bielack et al., 2005; Luetke et al., 2014; Kwiatkowski et al., 2014). Researchers have found that SEs play a critical role in the progression of osteosarcoma by promoting its growth and metastasis.

Chen et al. (2018) found a significant increase in *MYC* expression in metastatic osteosarcoma samples, suggesting that *MYC* may be an important therapeutic target for osteosarcoma treatment. They further tested the recently developed small-molecule SE-inhibitors of osteosarcoma and found that the SE-inhibitors were effective in inhibiting the proliferation, migration, and invasion of osteosarcoma cells. This is likely due to the inhibition of a large population of SEs containing the *MYC* target gene by THZ1 [a SE-inhibitor that also functions as a CDK7 (cyclin-dependent kinase) inhibitor] treatment. They also reported that the chosen sensitivity of some SE genes are more sensitive to THZ1 treatment than others, indicating that *MYC* binding strength, SE size and intensity, basic gene expression levels, and the activity of transcription factors and cofactors may lead to differential responses of the SEs gene to THZ1 treatment. Chen et al. (2018) have experimentally demonstrated that SE-inhibitors are promising small-molecule drugs for patients with osteosarcoma by targeting the MYC signaling pathway in osteosarcoma.

Zhang et al. (2020) found THZ2 can target SE-associated oncogenes in osteosarcoma. Using ChIP-Seq, they found that SEs are associated with oncogenic genes in osteosarcoma cells. They further reported several SE-associated genes to be sensitive to THZ2 treatment. Finally, they proved their hypothesis that THZ2 can inhibit the progression of osteosarcoma by targeting SE-associated genes such as *MYC*, *STAT3*, and *HMOX1*. These findings indicate that THZ2 has the potential to become a promising targeting drug for osteosarcoma treatment.

Morrow et al. (2018) suggested that enhancer elements can confer metastatic ability to osteosarcoma cells. They found that metastatic osteosarcoma and non-metastatic osteosarcoma have different enhancer activities for metastatic genes, and proposed a new concept of Metastatic Variant Enhancer Loci (Met-VELs). Comparing the activity of the gene with Met-VELs with the activity of SE-associated genes, they proved the existence of different Met-VELs in related metastasis genes, which lead to differences in metastatic ability between metastatic and non-metastatic osteosarcoma. Further, genes with Met-VELs were reportedly more related to osteosarcoma metastasis, while those with SE-associated genes were more related to the tumorigenesis and survival of osteosarcoma.

Lee et al. (2015) found the following phenomenon in the study of the treatment mechanism of JQ1—a bromodomain and extra terminal domain (BET) protein inhibitor—in human osteosarcoma: although the inhibition of bromodomain-containing protein 4 (BRD4) by JQ1 could inhibit the growth of osteosarcoma cells *in vitro*. They showed that the level of c-MYC protein in the cells treated with JQ1 remained unchanged. Meanwhile, some studies showed that JQ1 treatment significantly decreased the expression of *RUNX2* gene, which can be regulated by SEs with the region enriched for H3K27Ac (Encode Project Consortium, 2004; Loven et al., 2013; Whyte et al., 2013). Thus, Lee et al. (2015) suggested that the downstream target gene of JQ1 in osteosarcoma is *RUNX2* but not *MYC*, and they proved it through experiments such as ChIP-seq assay.

By profiling the epigenetic characteristics and SEs landscape of the osteosarcoma and some clinical specimens, Lu et al. (2020) found the SE-mediated regulator LIF can promote osteosarcoma stemness gene expression. Mechanistically, they found SEs function as an activator of the NOTCH1 pathway

through regulating the LIF/STAT3 pathway in promoting the progression of osteosarcoma. They believe that their findings will provide new insights for the treatments of osteosarcoma. The possible functional mechanism of SEs in osteosarcoma is shown in **Figure 2**.

SEs in Ewing Sarcoma

Ewing sarcoma is the second most common and devastating primary malignant tumor, and mainly occurs in children and adolescents. Despite advances in treatment over the past few decades, patient survival remains unsatisfactory. Thus, there is an urgent need for more effective treatments based on the molecular basis of cancer (Riggi and Stamenkovic, 2007; Mackintosh et al., 2010; Stoll et al., 2013). Several studies have shown that SEs play a critical role in the tumorigenesis, proliferation, and metastasis of Ewing sarcoma (Kennedy et al., 2015; Jacques et al., 2016; Baldauf et al., 2018; Lin et al., 2018).

Recent studies have indicated that the disease-associated fusion protein EWS-FLI1 activates or inhibits enhancer elements in Ewing sarcoma through different chromatin remodeling patterns (Riggi et al., 2014; Tomazou et al., 2015). Baldauf et al. (2018) found out that the EWSR1-ETS-targeted genes—*BCL11B* and *GLG1*—are driven by SEs through immunohistochemistry analysis. They found that both *BCL11B* and *GLG1* are more specific than *CD99* for Ewing sarcoma, suggesting that *BCL11B* and *GLG1* can be used as novel biomarkers for the diagnosis of Ewing sarcoma. Therefore, the discovery of *BCL11B* and *GLG1* may significantly reduce the number of misdiagnosed patients, thereby improving the care of patients with Ewing sarcoma.

Lin et al. (2018) used epigenetic genomics analysis to characterize transcriptional disorders in Ewing sarcoma. By focusing on SEs and its associated transcriptional regulatory mechanisms, they demonstrated that SE-associated transcripts are significantly enriched in the *EWS-FLI1* target gene, which contributes to aberrant transcription in Ewing sarcoma and mediates the specific sensitivity of Ewing sarcoma to transcriptional repression. Through comprehensive analysis, the authors identified *MEIS1* as a SE-driven oncogene that synergizes with *EWS-FLI1* in transcriptional regulation and plays a key role in pro-survival in Ewing sarcoma. Besides, they identified that the SE-related gene *APCCD1*, a downstream target of *MEIS1* and *EWS-FLI1*, was also a novel tumor-promoting factor for Ewing sarcoma.

The main known carcinogenic event in Ewing sarcoma is somatic chromosomal translocation that occurs most commonly between chromosomes 11 and 22 and results in a fusion between the 5′ region of the *EWS* gene and the 3′ region of the ETS family gene *FLI1* (Delattre et al., 1992). Kennedy et al. (2015) suggested that while direct targeting of aberrant transcription factors remains a pharmacological challenge, identifying the dependence of *EWS/FLI1* expression will provide new therapeutic avenues. They used SE analysis, near-genome shRNA assay, and small-molecule screening to identify cyclin D1 and CDK to characterize the selective dependence of Ewing sarcoma. They found that SEs regulate cyclin D1 and promote its expression in Ewing sarcoma. Moreover, Ewing sarcoma cells require CDK4 and cyclin D1 to survive and do not rely on adherent growth. Pharmacological inhibition through CDK4 with selective CDK4/6 inhibitors results in cytostasis and cell death of Ewing sarcoma cell lines *in vitro* as well as growth retardation in the Ewing sarcoma xenograft model *in vivo*. These results showed the dependence of Ewing sarcoma on CDK4 and cyclin D1; hence, CDK4/6 inhibitors can be explored further for the treatment of patients with Ewing sarcoma.

Jacques et al. (2016) focused on the *EWS-FLI1* gene, the most popular target of Ewing sarcoma, and inspired by related research, hypothesized that the expression of *EWS-FLI1* gene may be regulated by the SEs and activated by BET bromodomain activity. Based on this, they proposed that JQ1 can directly target the *EWS-FLI1* gene, releasing BRD4 from the *EWS-FLI1* promoter, thereby resulting in down-regulation of *EWS-FLI1* gene expression and inhibiting the progression and metastasis of Ewing sarcoma (Jacques et al., 2016). They proved that JQ1 can down-regulate the expression of *EWS-FLI1*, as well as inhibit the downstream gene expression of *EWS-FLI1* through a series of cell proliferation, qRT-PCR, western blotting, and CHIP analysis experiments. Hence, it was proposed as a good therapeutic drug for Ewing sarcoma. The possible functional mechanism of SEs in Ewing sarcoma is shown in **Figure 2**.

SEs in Chordoma

Chordoma is a major bone tumor that originates from the residual spinal cord tissue and occurs in the skull base, spine, and tibia (Salisbury, 1993; McMaster et al., 2001). Chordoma usually presents as a slow-growing but locally aggressive malignant tumor. There is still a recurrence tendency after surgery and radiotherapy. Given the inadequate understanding of the disease mechanism of chordoma, patients with advanced disease usually show poor prognosis because of the lack of effective therapies (Barry et al., 2011; Stacchiotti and Sommer, 2015).

Sharifnia et al. (2019) identified a SE-associated oncogenic TF named TBXT (developmental transcription factor T) with high expression in chordoma using comprehensive methods such as CRISPR-Cas9 screening, RNA-seq, and RT-qPCR. They found that CDK inhibitors can inhibit the proliferation of chordoma cells. They further demonstrated that TBXT is a SE-associated TF in chordoma. Similar to other diseases, SEs are associated with genes (*TBXT* in chordoma) that are critical for disease identity and maintenance. The dysregulation of *TBXT* regulated by SEs is the main feature of the regulatory environment in chordoma cells (Sharifnia et al., 2019). The possible functional mechanism of SEs in chordoma is shown in **Figure 2**.

SEs in Multiple Myeloma

Multiple myeloma (MM) is a malignant tumor that originates from antibody-secreting plasma cells and is driven by many genetic and epigenetic changes (Landgren et al., 2009; Weiss et al., 2009; Kuehl and Bergsagel, 2012). Research efforts have revealed the involvement of SEs-associated genes such as *IRF4* (Jin et al., 2018) and *MYC* (Loven et al., 2013; Affer et al., 2014). Studies showed that these SEs-associated genes are critical for the tumorigenesis and development of MM.

Amorim et al. (2016) proposed that bromodomain binds to the acetylated lysine residue on the histone tail, allowing the

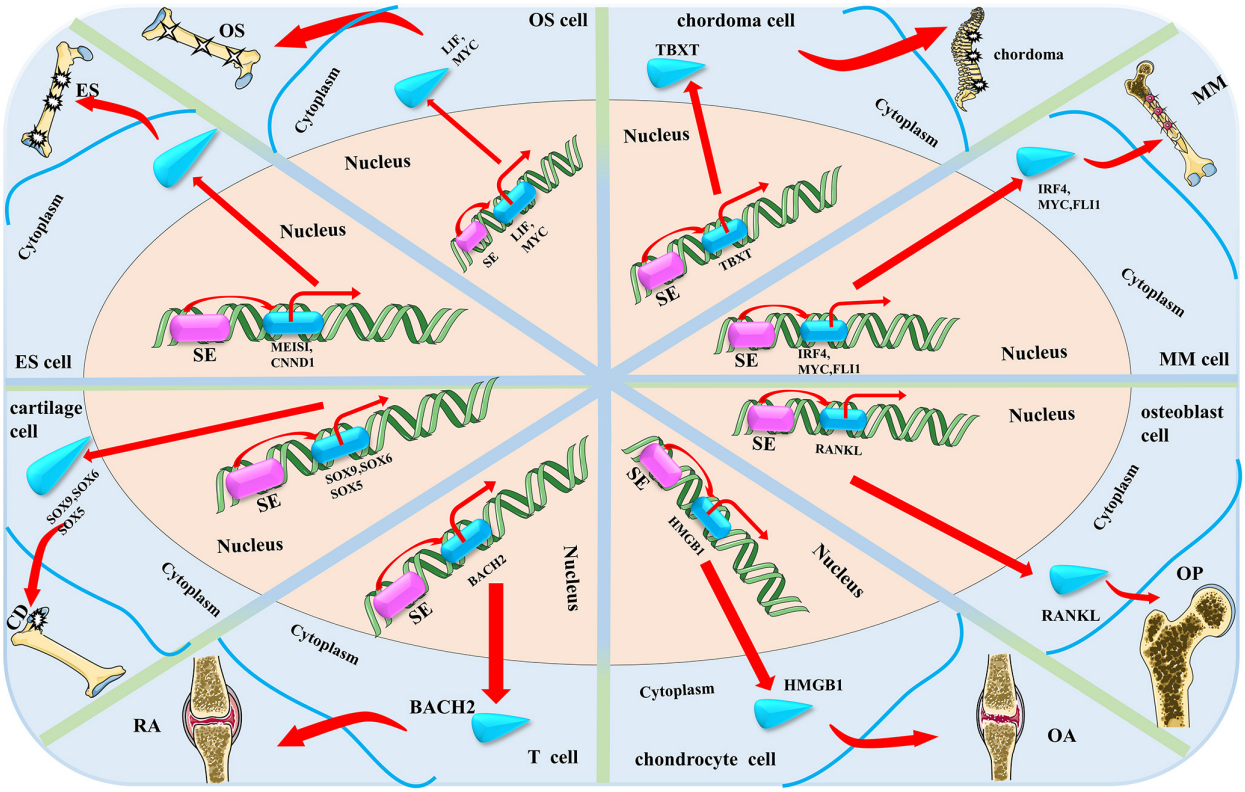


FIGURE 2 | The possible mechanism of super enhancers (SEs) in the eight main bone-related diseases discussed in this review. SE accelerates the progress of the four bone-related diseases by activating or up-regulating the expression of bone-related disease-specific genes that are near the related SEs (OS, osteosarcoma; ES, Ewing sarcoma; OP, osteoporosis; CD, cartilage dysplasia; RA, rheumatoid arthritis; OA, osteoarthritis; and MM, multiple myeloma).

extension complex that binds to the terminal portion of the protein to enter the promoter region of the gene, triggering gene transcription. Fulciniti et al. (2018) discovered that non-overlapping control of the promoter and SE-dependent transcriptomes in MM contributed to the growth and proliferation of MM. They also discovered the relationship between the transcription factor E2F and the transcriptional coactivator BRD4 in MM. They demonstrated the existence of two different regulatory pathways and showed that they can synergistically promote the growth and proliferation of MM. The discovered transcriptional regulatory mechanisms provide a theoretical basis for the development of new treatments for MM and other malignancies.

Affer et al. (2014) proposed that the *MYC* locus in MM has a loose rearrangement of enhancers and SEs that causes dysregulation of *MYC*. They proposed that rearrangement like this reposition of *MYC* nearby the genes related to SEs accelerates the progress of MM (Affer et al., 2014).

Although MM is well characterized in terms of genome and transcription, the abnormal regulatory network of the gene that supports this disease is still not well understood. Jin et al. (2018) described the regulatory elements and TF footprint in primary MM cells by RNA-seq and ChIP-seq assay. They established a SE-related TF-based regulatory network and identified several novel TFs critical for the biology of MM based on the newly established regulatory network. Their study indicated that *IRF4* and *FLI1* showed significant overlap with 92% of all SEs in MM cells and could promote the growth and proliferation of MM. These findings will provide potential therapeutic targets and new solutions for the treatment of MM.

Chromatin regulatory factors have become attractive targets for cancer therapy, but the mechanisms involved in inhibiting the gene-specific effects of tumor cells caused by these common regulatory factors are not well understood yet. Loven et al. (2013) investigated the mechanisms involved in the selective inhibition of *MYC* oncogenes in MM caused by inhibition of transcriptional coactivator BRD4. They found that treatment of MM tumor cells with the BET domain inhibitor, JQ1, resulted in preferential loss of BRD4 in *MYC*-SEs and subsequent transcriptional extension defects, which preferentially affected SE-associated genes such as *MYC*. This also consequently inhibited the progression of MM. The possible functional mechanism of SEs in MM is shown in **Figure 2**.

SEs in Osteoporosis

Osteoporosis is a metabolic disease caused by reduced bone formation and/or increased bone resorption, which results in decreased bone mass and increased bone fragility. It is characterized by reduced bone mineral density (BMD) and low bone mass. Osteoporosis has become a global health concern.

Zhu et al. (2018) found a SE-associated gene—*RANKL*—was critical for the progress of osteoporosis, by analyzing the ChIP-seq Data from ENCODE.

Some significant genome-wide association studies (GWAS) have shown that single nucleotide polymorphisms (SNPs) near *RANKL* are associated with osteoporosis on chromosome 13q14.11 (Zhang et al., 2014; Kuosmanen et al., 2016). Zhu et al. (2018) identified five BMD-associated SNPs (rs9533094, rs9533090, rs9594738, rs8001611, and rs9533095) that may be related to osteoporosis in the SEs region via bioinformatics data analysis and experimental validation. *RANKL* is a key regulator involved in bone remodeling and is critical for osteoclast differentiation, activation, survival, and enhancement of bone resorption (Lacey et al., 1998; Hsu et al., 1999; Jimi et al., 1999; Sobacchi et al., 2007). They proposed that these five SNPs up-regulate the expression of *RANKL* through long-range chromosomal interaction with SEs, thereby affecting bone metabolism and resulting in an imbalance between bone resorption and bone formation, leading to osteoporosis. These findings are critical to understanding the pathogenesis of osteoporosis. Research about *RANKL* will provide a new approach to the treatment of osteoporosis. The possible functional mechanism of SEs in osteoporosis are shown in **Figure 2**.

SEs in Cartilage Dysplasia

During the development of vertebrate embryo, chondrocytes build hundreds of vital cartilage anlagen that provide morphological and skeletal support. Their unique elongation property can rapidly drive body growth (Liu and Lefebvre, 2015). Cartilage dysplasia (CD) can seriously affect people's bone formation and growth (Warman et al., 2011). If cartilage dysplasia occurs in childhood, it will lead to lifelong defects like dwarfism or may even be fatal. Therefore, it is necessary to clarify the mechanisms related to cartilage development. Ohba et al. (2015) reported that *SOX9*-related SEs up-regulate the expression of *SOX9* gene which can promote cartilage formation. Liu and Lefebvre (2015) showed that three SOX proteins (SOX9, SOX6, and SOX5) play critical roles in chondrocyte development through SEs.

Using ChIP-seq, Ohba et al. (2015) discovered that the upstream region of key cartilage-related genes such as *SOX9* binds to a large number of enhancers and is rich in H3K27ac protein (characteristic of SEs). They found that the expression of the SEs-related genes (key cartilage-associated genes such as *SOX9*) is significantly higher than those associated with TEs. With reference to the above findings, Symon and Harley (2017) speculated that *SOX9*-related SEs up-regulate the expression of *SOX9* gene that can promote cartilage formation.

Liu and Lefebvre (2015) studied the target genes and functional modes of three SOX proteins (SOX9, SOX6, and SOX5) on chondrocytes using GWAS. They used rat chondrosarcoma (RCS) cell lines as a reliable model for chondrocytes and found that SOX6 and SOX9 bind thousands of genomic loci that are often close to each other. Although SOX proteins bind to a small number of TEs, they bind multiple sites on almost all SEs in RCS cells. These SEs are primarily associated with cartilage-specific genes. The three SOX proteins work together to activate these SEs. It is required for *in vivo* expression of their associated genes. These genes encode key regulatory factors including these three SOX proteins, as well as all essential cartilage extracellular matrix components. Chst11, Fgfr3, Runx2, and Runx3 are new targets for the three identified SOX proteins. Therefore, they proposed that these three SOX proteins closely cooperate with each other in the whole genome and effectively activate a large number of chondrocyte-specific genes through SEs, thereby realizing the unique differentiation and regulation process of chondrocytes. The possible functional mechanism of SEs in cartilage dysplasia are shown in **Figure 2**.

SEs in Rheumatoid Arthritis

Rheumatoid arthritis (RA) is a chronic inflammatory synovitis systemic disease of unknown etiology. It is characterized by multiple, symmetric, and invasive arthritis of the joints of the hands and feet, often accompanied by extra-articular involvement and serum positivity for rheumatoid factor, which can lead to joint deformity and loss of function. Vahedi et al. (2015) found a SEs-associated gene *BACH2* critical for the progress of RA.

Vahedi et al. (2015) mapped the T-cell SEs through a series of experiments. They found that many cytokines and cytokine receptor genes with SEs structure are essential for the process of RA. *BACH2*, the gene encoding the key negative regulator of effector differentiation, is the most prominent T-cell SE. This reveals a network by which SE-related genes essential for T cell biology are inhibited by *BACH2*. Immune-mediated diseases (including RA) typically occur when disease-related SNPs are highly enriched in T-cell SEs rather than TEs. Treatment of T cells with the JAK inhibitor tofacitinib disproportionately alters the expression of RA risk genes with SEs structure. Based on these findings, the depiction of SEs can accurately identify key regulatory nodes in T cells that can be preferentially regulated by pharmacological interventions. It may provide new targets for the treatment of RA or other diseases. The possible functional mechanism of SEs in RA are shown in **Figure 2**.

SEs in Osteoarthritis

Osteoarthritis is a common age-related degenerative disease that causes severe joint pain and physical dysfunction and is one of the important causes of disability in the elderly population (Xing et al., 2016). Despite its high incidence, the disease mechanism is poorly understood. Therefore, clarifying its etiology and pathogenesis can provide new drug targets for the clinical treatment of the disease. Jiang et al. (2017) found that SE inhibitor JQ1 can inhibit the progression of osteoarthritis by regulating the expression of *HMGB1*.

A growing number of studies have reported an important role for BRD4 in the pathology of inflammatory diseases which suggest its enormous potential as a drug target. Jiang et al. (2017) found that the BRD4 inhibitor, JQ1, inhibits the progression of osteoarthritis through dual effects on HMGB1 and NF-κB signaling pathways, proving that BRD4 may be a new target for the treatment of osteoarthritis. They found that BRD4 is enriched in the upstream non-promoter region of *HMGB1*

by using the ChIP assay. In addition, treatment with JQ1 induced BRD4 release from the non-promoter and binding sites of *HMGB1*. They also found abundant enrichment of H3K27ac in the *HMGB1* promoter and upstream non-promoter region. Therefore, they speculated that the SEs may mediate the regulatory role of BRD4 in the expression of HMGB1. However, they could only prove that BRD4 may be a new target for the treatment of osteoarthritis, as the mechanism of SEs on BRD4 and HMGB1 was not investigated in their study. The possible functional mechanism of SEs in osteoarthritis are shown in **Figure 2**.

TARGETING SEs FOR BONE-RELATED DISEASE THERAPY

Notably, as SEs harbor TFs binding sites with high density, a small change in the number of binding TFs can cause significant changes in associated gene transcription. Thus, disruption of the SEs structure and function should be the focus of disease therapy. Besides, as bone-related diseases prefer hijacking SEs to drive their aberrant transcription program which promotes disease processes like growth and metastasis, SEs have been exploited as a drug target with great potential for clinical treatment of bone-related diseases. Therefore, many researchers proposed that SEs can be considered as therapeutic targets. Accordingly, several types of small molecule inhibitors have been developed for the clinical treatment of bone-related diseases (shown in **Table 2**). Thus far, BET inhibitors and CDK inhibitors are the most widely used small molecule inhibitors (Jia et al., 2019). To a certain extent, drugs that target key components of SEs, such as BRD4 and CDK7, provide a novel strategy for better treatment of bone-related diseases.

BET Inhibitors Targeting SEs

The BET family proteins including BRD2, BRD3, BRD4, and BRDT play a key role in chromatin remodeling and transcriptional regulation. JQ1, the first BET inhibitor applied to target BET bromodomain was discovered by Filippakopoulos et al. (2010). Recently, many studies have shown that JQ1 has anti-proliferative activity against many cancers, and it exhibits anti-proliferative activity mainly via inhibiting c-MYC expression and up-regulating p21 expression (Delmore et al., 2011; Dang, 2012). Jia et al. (2019) concluded that JQ1 treatment displaces BRD4 preferably from histone proteins and disrupts SEs. Partly, the mechanism by which BET inhibitors like JQ1 inhibit bone-related disease progression is through repressing the SE-associated genes that are critical for bone-related diseases. As mentioned above, JQ1 treatment on MM cells decreased BRD4 binding at SEs and subsequently repressed the SE-associated genes of MM (Loven et al., 2013). It is also reported that JQ1 can inhibit the growth and disease process of osteosarcoma by repressing the SEs containing oncogenes by limiting *MYC* expression (Chen et al., 2018). However, others found that JQ1 treatment inhibits the growth and disease process of osteosarcoma by targeting *RUNX2* instead of *MYC* through influencing SEs (Lee et al., 2015). Another study initiated by

TABLE 2 | Inhibitor which targeting SEs in bone-related diseases.

Diseases	Inhibitor	Target of the inhibitor	Effect on SEs-driven transcription	Effects of SEs inhibition on diseases	References
Multiple myeloma	JQ1	BRD4	Decrease of BRD4 binding at SEs and downregulation of SEs associated genes	Repression of the progression of multiple myeloma	Loven et al., 2013
Osteosarcoma	JQ1	BRD4	Restraining of the expression of *MYC*	Inhibition of the growth and proliferation of osteosarcoma	Chen et al., 2018
Osteosarcoma	JQ1	BRD4	Restraining of the expression of *RUNX2*	Inhibition of the growth and proliferation of osteosarcoma	Lee et al., 2015
Osteosarcoma	THZ1	CDK7	Downregulation of SEs associated genes	Suppressing the proliferation, migration of osteosarcoma	Chen et al., 2018
Chordoma	THZ1	CDK7	Downregulation of SEs associated genes *TBXT*	Suppressing the proliferation of chordoma	Sharifnia et al., 2019
Osteosarcoma	THZ2	CDK7	Downregulation of SEs associated genes *LIF*, *STAT3*, *NOTCH1*	Impeding the proliferation and metastasis of osteosarcoma	Zhang et al., 2020
Ewing sarcoma	LEE011	CDK4/6	Downregulation of SEs associated genes	Impairing the progression of Ewing sarcoma	Kennedy et al., 2015
Osteoarthritis	JQ1	BRD4	Downregulation of SEs associated gene *HMGB1*	Inhibiting the progression of osteoarthritis	Jiang et al., 2017

Jacques et al. proposed that the use of JQ1 can repress the expression of *EWS-FLI1* by disrupting the *EWS-FLI1*-associated SEs and subsequently control the disease process in Ewing sarcoma (Jacques et al., 2016). Besides, Jiang et al. (2017) showed that JQ1 treatment-induced BRD4 release from the non-promoter and binding sites of *HMGB1*. They also hypothesized that it can inhibit the progression of osteoarthritis. In conclusion, SEs are sensitive to bromodomain inhibition. BET inhibitors have great therapeutic potential in bone-related diseases.

Up to now, researchers have initialed clinical trials about BET inhibitors applied in treatment for bone-related diseases. NCT03068351, one clinical trial, found that BET inhibitor RO6870810 may apply for combination therapy for MM. Another clinical trial, NCT02157636, demonstrated that BET inhibitor CPI-0610 can inhibit the progress of MM. But there aren't clinical trials related to the above SEs-inhibitors initiated. In addition, there aren't study articles about these two BET-inhibitors, with completed or registered clinical trials carried out, repress the progression of bone-related diseases through SEs reported. So, it's necessary to verify the clinical treatment effect of the above potential SEs-inhibitors of bone-related diseases through clinical trials.

CDK Inhibitors Targeting SEs

RNA Pol II, the central enzyme functioning in protein-coding gene transcription, initiation, and elongation, is particularly regulated by CDK7—one of the CDKs (Larochelle et al., 2012). CDK7 can phosphorylate the carboxyl-terminal domain of RPB1 (CTD) of RNA Pol II (RNAPIICTD), thereby regulating transcriptional initiation and pause release, as well as elongation (Palancade and Bensaude, 2003; Glover-Cutter et al., 2009; Larochelle et al., 2012). An increasing number of CDK7 inhibitors have been developed including THZ1 and THZ2. THZ1 is an advanced CDK7 inhibitor that has been reported to have the ability to target the general transcriptional elements and disrupt SEs (Kwiatkowski et al., 2014). Consistent with this, other similar findings of CDK7 inhibitor and SEs have been reported in bone-related cancers. For instance, THZ1 can suppress the proliferation, migration, and invasion of osteosarcoma cells by inhibiting the expression of important SE-containing oncogenic genes (Chen et al., 2018). Sharifnia et al. (2019) found that CDK inhibitors like THZ1 can substantially suppress the growth of chordoma by inhibiting the SEs which is critical for the expression of the important oncogene gene *TBXT* for chordoma. However, Li et al. (2017) reported that the translational significance and clinical application of THZ1 are limited by its short half-life. Compared with THZ1, THZ2 is a newly developed CDK7 inhibitor with a fivefold increase of half-life. Zhang et al. (2020) found that THZ2 can impede the proliferation and metastasis of osteosarcoma via targeting SE-associated oncogenes. Overall, CDK7 inhibition is another promising target treatment therapy for bone-related diseases. Besides CDK7 inhibitors, researchers also suggested that CDK4/6 inhibitors like LEE011 can target SEs. Kennedy et al. (2015) reported that LEE011 can impair the progression of Ewing sarcoma by inhibiting the expression of CDK4/6. In conclusion, SEs are sensitive to CDK inhibition. CDK inhibitors like THZ1, THZ2, and LEE011 also have great therapeutic potential for bone-related diseases.

To date, some clinical trials have been carried out to test the treatment effect of CDK inhibitors on bone-related diseases. For example, NCT01096342, a clinical trial carried out by Kumar et al. (2015) showed that CDK inhibitor-dinaciclib (SCH 727965) can repress the progression of MM. Based on this trial, they reported an article that demonstrates the activity of dinaciclib in relapsed MM (Kumar et al., 2015). But this article didn't demonstrate that dinaciclib can repress the progression of relapsed MM through influencing SEs in MM. Unfortunately, there aren't completed or registered clinical trials related to the above SEs-inhibitors initiated. Thus, it's necessary to verify the clinical treatment effect of the above potential CDK-inhibitors of bone-related diseases through clinical trials.

Developing New Downstream Target Genes of SEs for Bone-Related Diseases

Super-enhancers inhibitors mainly repress the progression of bone-related diseases by disrupting the SEs associated with bone-related diseases and subsequently influencing the critical oncogenes that are targeted by SEs. There are no studies yet to indicate whether SE inhibitors can be used for the potential treatment of bone-related diseases like osteoporosis, cartilage dysplasia, and RA. In the future, besides carrying out studies using the above two kinds of SEs inhibitors as a treatment approach for bone-related diseases, we should focus more on developing new downstream target genes of SEs for the diagnosis and treatment of bone-related diseases. This approach may ensure sufficient and varied treatment strategies for bone-related diseases.

SUMMARY AND PERSPECTIVE

The rapid development of bioinformatics technology has driven the study of the genetic mechanism of diseases, which has helped researchers and clinicians to better understand the underlying mechanisms of several disease conditions. Furthermore, some intractable diseases have become less difficult to treat. However, the pathogenic mechanisms of many other complex diseases remain unclear, such as osteosarcoma, Ewing sarcoma, and other bone-related diseases with poor prognosis. Multiple studies have reported novel insights of which many include SEs-associated genes such as *MYC* (Loven et al., 2013; Zhang et al., 2020) LIF, (Lu et al., 2020), and *EWS-FLI1* (Jacques et al., 2016), and SEs-inhibitors with therapeutic effects such as JQ1 (Loven et al., 2013; Lee et al., 2015; Jiang et al., 2017; Chen et al., 2018), THZ1 (Chen et al., 2018; Sharifnia et al., 2019), and THZ2 (Zhang et al., 2020) on diseases like osteosarcoma, Ewing sarcoma, MM, chordoma, and osteoarthritis. However, for osteoporosis, cartilage dysplasia, and RA, only a few therapeutic drugs have been reported that can efficiently target SEs or SEs-associated genes. Besides, there are rarely completed or registered clinical trials that investigate the clinical treatment effect of the potential SEs-inhibitors initiated. Therefore, future research should focus

more on the SEs-associated mechanism of the above bone-related diseases and it is so urgent to initiate more clinical trials that testify the potential clinical application of the above-mentioned SEs-inhibitors.

In summary, the above studies on SEs in bone-related diseases focused on the identification of disease-specific SEs and their target genes, followed by verification of the effects of the screened target gene through related *in vitro* and *in vivo* experiments. The specific stepwise method is as follows: first, identifying the bone cancer-related SEs and verifying the most related SEs by techniques such as ChIP-seq. Second, screening target genes associated with the SEs through bioinformatics analysis for building therapies for bone cancer. Finally, testing the potential and accuracy of target genes via *in vitro* and *in vivo* experiments. We believe that the findings from SEs studies will be helpful for the treatment for difficult-to-treat bone-related diseases in the future. However, to a certain degree, as the SEs-related studies most involve in cancer field, the SEs-related studies in skeleton field are rare. So, we can explore the role of SEs in skeleton field in future studies.

The discovery of SEs is a scientific and clinical breakthrough. Many studies have proven that the abnormal expression of SEs is closely related to the disease process. Therefore, research on SEs has gained immense clinical importance. By studying the expression of SEs in diseases, clarifying the pathogenesis of diseases, and finding accurate and efficient target genes, new treatment options can be developed. Thus, it is necessary to study the functions of SEs in bone-related diseases. Recent years have witnessed rapid advancements in technologies like ChIP with high-throughput sequencing (Schmidt et al., 2009) and CRISPR genome editing tool (Burgess, 2013), which offer novel insights into the function and biophysical formation of SEs, as well as the regulatory mechanisms of the targeted gene. With the accumulation of related research, the role of SEs in bone-related diseases is becoming more and more clear. However, as shown above, many studies are on the phenomenon level, and the mechanism researches such as how SEs are regulated and the detailed molecular mechanism of how SEs regulate its target genes are still insufficient. Therefore, the research on the deep and detailed mechanism needs to be strengthened in the future. Besides, the potential of the clinical application of SEs inhibitors in bone-related diseases needs to be further explored. Therefore, future studies of SEs should focus on how to better utilize SEs in the targeted therapy of bone-related diseases in clinical.

AUTHOR CONTRIBUTIONS

QL and ZL conceived of this review. ZO and JQ drafted the manuscript. WW and ZO designed the figures. GL and JW designed the tables. JQ revised the manuscript. All authors were involved in the critical revision of the manuscript and approved the final version.

FUNDING

This work was supported by grants awarded to QL by the Hunan Provincial Department of Finance Grant (Nos. 2019-93 and 2018-92).

REFERENCES

Affer, M., Chesi, M., Chen, W. G., Keats, J. J., Demchenko, Y. N., Roschke, A. V., et al. (2014). Promiscuous MYC locus rearrangements hijack enhancers but mostly super-enhancers to dysregulate MYC expression in multiple myeloma. *Leukemia* 28, 1725–1735. doi: 10.1038/leu.2014.70

Amorim, S., Stathis, A., Gleeson, M., Iyengar, S., Magarotto, V., Leleu, X., et al. (2016). Bromodomain inhibitor OTX015 in patients with lymphoma or multiple myeloma: a dose-escalation, open-label, pharmacokinetic, phase 1 study. *Lancet Haematol.* 3, e196–e204. doi: 10.1016/S2352-3026(16)00021-1

Baldauf, M. C., Orth, M. F., Dallmayer, M., Marchetto, A., Gerke, J. S., Rubio, R. A., et al. (2018). Robust diagnosis of Ewing sarcoma by immunohistochemical detection of super-enhancer-driven EWSR1-ETS targets. *Oncotarget* 9, 1587–1601. doi: 10.18632/oncotarget.20098

Barry, J. J., Jian, B. J., Sughrue, M. E., Kane, A. J., Mills, S. A., Tihan, T., et al. (2011). The next step: innovative molecular targeted therapies for treatment of intracranial chordoma patients. *Neurosurgery* 68, 231–241. doi: 10.1227/NEU.0b013e3181fd2ac5

Brown, J. D., Lin, C. Y., Duan, Q., Griffin, G., Federation, A., Paranal, R. M., et al. (2014). NF-kappaB directs dynamic super enhancer formation in inflammation and atherogenesis. *Mol. Cell* 56, 219–231. doi: 10.1016/j.molcel.2014.08.024

Bulger, M., and Groudine, M. (2011). Functional and mechanistic diversity of distal transcription enhancers. *Cell* 144, 327–339. doi: 10.1016/j.cell.2011.01.024

Burgess, D. J. (2013). Technology: a CRISPR genome-editing tool. *Nat. Rev. Genet.* 14:80. doi: 10.1038/nrg3409

Chapuy, B., McKeown, M. R., Lin, C. Y., Monti, S., Roemer, M. G., Qi, J., et al. (2013). Discovery and characterization of super-enhancer-associated dependencies in diffuse large B cell lymphoma. *Cancer Cell* 24, 777–790. doi: 10.1016/j.ccr.2013.11.003

Chen, D., Zhao, Z., Huang, Z., Chen, D., Zhu, X., Wang, Y., et al. (2018). Super enhancer inhibitors suppress MYC driven transcriptional amplification and tumor progression in osteosarcoma. *Bone Res.* 6:11. doi: 10.1038/s41413-018-0009-8

Chipumuro, E., Marco, E., Christensen, C. L., Kwiatkowski, N., Zhang, T., Hatheway, C. M., et al. (2014). CDK7 inhibition suppresses super-enhancer-linked oncogenic transcription in MYCN-driven cancer. *Cell* 159, 1126–1139. doi: 10.1016/j.cell.2014.10.024

Dang, C. V. (2012). MYC on the path to cancer. *Cell* 149, 22–35. doi: 10.1016/j.cell.2012.03.003

Delattre, O., Zucman, J., Plougastel, B., Desmaze, C., Melot, T., Peter, M., et al. (1992). Gene fusion with an ETS DNA-binding domain caused by chromosome translocation in human tumours. *Nature* 359, 162–165. doi: 10.1038/359162a0

Delmore, J. E., Issa, G. C., Lemieux, M. E., Rahl, P. B., Shi, J., Jacobs, H. M., et al. (2011). BET bromodomain inhibition as a therapeutic strategy to target c-Myc. *Cell* 146, 904–917. doi: 10.1016/j.cell.2011.08.017

Demchenko, Y., Roschke, A., Chen, W. D., Asmann, Y., Bergsagel, P. L., and Kuehl, W. M. (2016). Frequent occurrence of large duplications at reciprocal genomic rearrangement breakpoints in multiple myeloma and other tumors. *Nucleic Acids Res.* 44, 8189–8198. doi: 10.1093/nar/gkw527

Encode Project Consortium (2004). The ENCODE (ENCyclopedia Of DNA Elements) Project. *Science* 306, 636–640. doi: 10.1126/science.1105136

Filippakopoulos, P., Qi, J., Picaud, S., Shen, Y., Smith, W. B., Fedorov, O., et al. (2010). Selective inhibition of BET bromodomains. *Nature* 468, 1067–1073. doi: 10.1038/nature09504

Fulciniti, M., Lin, C. Y., Samur, M. K., Lopez, M. A., Singh, I., Lawlor, M. A., et al. (2018). Non-overlapping control of transcriptome by promoter- and super-enhancer-associated dependencies in multiple myeloma. *Cell. Rep.* 25, 3693–3705. doi: 10.1016/j.celrep.2018.12.016

Furlong, E., and Levine, M. (2018). Developmental enhancers and chromosome topology. *Science* 361, 1341–1345. doi: 10.1126/science.aau0320

Glover-Cutter, K., Larochelle, S., Erickson, B., Zhang, C., Shokat, K., Fisher, R. P., et al. (2009). TFIIH-associated Cdk7 kinase functions in phosphorylation of C-terminal domain Ser7 residues, promoter-proximal pausing, and termination by RNA polymerase II. *Mol. Cell Biol.* 29, 5455–5464.doi: 10.1128/MCB.00637-09

Gröschel, S., Sanders, M. A., Hoogenboezem, R., de Wit, E., Bouwman, B., Erpelinck, C., et al. (2014). A single oncogenic enhancer rearrangement causes concomitant EVI1 and GATA2 deregulation in leukemia. *Cell* 157, 369–381. doi: 10.1016/j.cell.2014.02.019

Hnisz, D., Abraham, B. J., Lee, T. I., Lau, A., Saint-André, V., Sigova, A. A., et al. (2013). Super-enhancers in the control of cell identity and disease. *Cell* 155, 934–947. doi: 10.1016/j.cell.2013.09.053

Hnisz, D., Day, D. S., and Young, R. A. (2016). Insulated neighborhoods: structural and functional units of mammalian gene control. *Cell* 167, 1188–1200. doi: 10.1016/j.cell.2016.10.024

Hsu, H., Lacey, D. L., Dunstan, C. R., Solovyev, I., Colombero, A., Timms, E., et al. (1999). Tumor necrosis factor receptor family member RANK mediates osteoclast differentiation and activation induced by osteoprotegerin ligand. *Proc. Natl. Acad. Sci. U.S.A.* 96, 3540–3545. doi: 10.1073/pnas.96.7.3540

Jacques, C., Lamoureux, F., Baud'Huin, M., Calleja, L. R., Quillard, T., Amiaud, J., et al. (2016). Targeting the epigenetic readers in Ewing Sarcoma inhibits the oncogenic transcription factor EWS/Fli1. *Oncotarget* 7, 24125–24140. doi: 10.18632/oncotarget.8214

Jia, Y., Chng, W. J., and Zhou, J. (2019). Super-enhancers: critical roles and therapeutic targets in hematologic malignancies. *J. Hematol. Oncol.* 12:77. doi: 10.1186/s13045-019-0757-y

Jiang, Y., Zhu, L., Zhang, T., Lu, H., Wang, C., Xue, B., et al. (2017). BRD4 has dual effects on the HMGB1 and NF-kappa B signalling pathways and is a potential therapeutic target for osteoarthritis. *Biochim. Biophys. Acta Mol. Basis Dis.* 1863, 3001–3015. doi: 10.1016/j.bbadis.2017.08.009

Jimi, E., Akiyama, S., Tsurukai, T., Okahashi, N., Kobayashi, K., Udagawa, N., et al. (1999). Osteoclast differentiation factor acts as a multifunctional regulator in murine osteoclast differentiation and function. *J. Immunol.* 163, 434–442.

Jin, Y., Chen, K., De Paepe, A., Hellqvist, E., Krstic, A. D., Metang, L., et al. (2018). Active enhancer and chromatin accessibility landscapes chart the regulatory network of primary multiple myeloma. *Blood* 131, 2138–2150. doi: 10.1182/blood-2017-09-808063

Kempf-Bielack, B., Bielack, S. S., Jurgens, H., Branscheid, D., Berdel, W. E., Exner, G. U., et al. (2005). Osteosarcoma relapse after combined modality therapy: an analysis of unselected patients in the cooperative osteosarcoma study group (COSS). *J. Clin. Oncol.* 23, 559–568. doi: 10.1200/JCO.2005.04.063

Kennedy, A. L., Vallurupalli, M., Chen, L., Crompton, B., Cowley, G., Vazquez, F., et al. (2015). Functional, chemical genomic, and super-enhancer screening identify sensitivity to cyclin D1/CDK4 pathway inhibition in Ewing sarcoma. *Oncotarget* 6, 30178–30193. doi: 10.18632/oncotarget.4903

Khan, A., and Zhang, X. (2016). dbSUPER: a database of super-enhancers in mouse and human genome. *Nucleic Acids Res.* 44, D164–D171. doi: 10.1093/nar/gkv1002

Kuehl, W. M., and Bergsagel, P. L. (2012). Molecular pathogenesis of multiple myeloma and its premalignant precursor. *J. Clin. Invest.* 122, 3456–3463. doi: 10.1172/JCI61188

Kumar, S. K., LaPlant, B., Chng, W. J., Zonder, J., Callander, N., Fonseca, R., et al. (2015). Dinaciclib, a novel CDK inhibitor, demonstrates encouraging single-agent activity in patients with relapsed multiple myeloma. *Blood* 125, 443–448. doi: 10.1182/blood-2014-05-573741

Kuosmanen, S. M., Viitala, S., Laitinen, T., Perakyla, M., Polonen, P., Kansanen, E., et al. (2016). The Effects of Sequence Variation on Genome-wide NRF2 Binding–New Target Genes and Regulatory SNPs. *Nucleic Acids Res.* 44, 1760–1775. doi: 10.1093/nar/gkw052

Kwiatkowski, N., Zhang, T., Rahl, P. B., Abraham, B. J., Reddy, J., Ficarro, S. B., et al. (2014). Targeting transcription regulation in cancer with a covalent CDK7 inhibitor. *Nature* 511, 616–620. doi: 10.1038/nature13393

Lacey, D. L., Timms, E., Tan, H. L., Kelley, M. J., Dunstan, C. R., Burgess, T., et al. (1998). Osteoprotegerin ligand is a cytokine that regulates osteoclast differentiation and activation. *Cell* 93, 165–176. doi: 10.1016/s0092-8674(00)81569-x

Landgren, O., Kyle, R. A., Pfeiffer, R. M., Katzmann, J. A., Caporaso, N. E., Hayes, R. B., et al. (2009). Monoclonal gammopathy of undetermined significance (MGUS) consistently precedes multiple myeloma: a prospective study. *Blood* 113, 5412–5417. doi: 10.1182/blood-2008-12-194241

Larochelle, S., Amat, R., Glover-Cutter, K., Sanso, M., Zhang, C., Allen, J. J., et al. (2012). Cyclin-dependent kinase control of the initiation-to-elongation switch of RNA polymerase II. *Nat. Struct. Mol. Biol.* 19, 1108–1115. doi: 10.1038/nsmb.2399

Lee, D. H., Qi, J., Bradner, J. E., Said, J. W., Doan, N. B., Forscher, C., et al. (2015). Synergistic effect of JQ1 and rapamycin for treatment of human osteosarcoma. *Int. J. Cancer* 136, 2055–2064. doi: 10.1002/ijc.29269

Li, B., Ni, C. T., Fan, Y., Madden, S. F., Klinger, R., O'Connor, A. E., et al. (2017). Therapeutic rationale to target highly expressed CDK7 conferring poor outcomes in triple-negative breast cancer. *Cancer Res.* 77, 3834–3845. doi: 10.1158/0008-5472.CAN-16-2546

Lin, L., Huang, M., Shi, X., Mayakonda, A., Hu, K., Jiang, Y. Y., et al. (2018). Super-enhancer-associated MEIS1 promotes transcriptional dysregulation in Ewing sarcoma in co-operation with EWS-FLI1. *Nucleic Acids Res.* 47, 1255–1267. doi: 10.1093/nar/gky1207

Liu, C., and Lefebvre, V. (2015). The transcription factors SOX9 and SOX5/SOX6 cooperate genome-wide through super-enhancers to drive chondrogenesis. *Nucleic Acids Res.* 43, 8183–8203. doi: 10.1093/nar/gkv688

Loven, J., Hoke, H. A., Lin, C. Y., Lau, A., Orlando, D. A., Vakoc, C. R., et al. (2013). Selective inhibition of tumor oncogenes by disruption of super-enhancers. *Cell* 153, 320–334. doi: 10.1016/j.cell.2013.03.036

Lu, B., He, Y., He, J., Wang, L., Liu, Z., Yang, J., et al. (2020). Epigenetic profiling identifies LIF as a super-enhancer-controlled regulator of stem cell-like properties in osteosarcoma. *Mol. Cancer Res.* 18, 57–67. doi: 10.1158/1541-7786.MCR-19-0470

Luetke, A., Meyers, P. A., Lewis, I., and Juergens, H. (2014). Osteosarcoma treatment - where do we stand? A state of the art review. *Cancer Treat. Rev.* 40, 523–532. doi: 10.1016/j.ctrv.2013.11.006

Mackintosh, C., Madoz-Gurpide, J., Ordonez, J. L., Osuna, D., and Herrero-Martin, D. (2010). The molecular pathogenesis of Ewing sarcoma. *Cancer Biol. Ther.* 9, 655–667. doi: 10.4161/cbt.9.9.11511

Mansour, M. R., Abraham, B. J., Anders, L., Berezovskaya, A., Gutierrez, A., Durbin, A. D., et al. (2014). Oncogene regulation. An oncogenic super-enhancer formed through somatic mutation of a noncoding intergenic element. *Science* 346, 1373–1377. doi: 10.1126/science.1259037

McMaster, M. L., Goldstein, A. M., Bromley, C. M., Ishibe, N., and Parry, D. M. (2001). Chordoma: incidence and survival patterns in the United States, 1973-1995. *Cancer Causes Control* 12, 1–11.

Morrow, J. J., Bayles, I., Funnell, A. P. W., Miller, T. E., Saiakhova, A., Lizardo, M. M., et al. (2018). Positively selected enhancer elements endow osteosarcoma cells with metastatic competence. *Nat. Med.* 24:176. doi: 10.1038/nm.4475

Niederriter, A., Varshney, A., Parker, S., and Martin, D. (2015). Super enhancers in cancers, complex disease, and developmental disorders. *Genes* 6, 1183–1200. doi: 10.3390/genes6041183

Ohba, S., He, X., Hojo, H., and McMahon, A. P. (2015). Distinct transcriptional programs underlie Sox9 regulation of the mammalian chondrocyte. *Cell Rep.* 12, 229–243. doi: 10.1016/j.celrep.2015.06.013

Oldridge, D. A., Wood, A. C., Weichert-Leahey, N., Crimmins, I., Sussman, R., Winter, C., et al. (2015). Genetic predisposition to neuroblastoma mediated by a LMO1 super-enhancer polymorphism. *Nature* 528, 418–421. doi: 10.1038/nature15540

Palancade, B., and Bensaude, O. (2003). Investigating RNA polymerase II carboxyl-terminal domain (CTD) phosphorylation. *Eur. J. Biochem.* 270, 3859–3870. doi: 10.1046/j.1432-1033.2003.03794.x

Peeters, J. G., Vervoort, S. J., Tan, S. C., Mijnheer, G., de Roock, S., Vastert, S. J., et al. (2015). Inhibition of super-enhancer activity in autoinflammatory site-derived T cells reduces disease-associated gene expression. *Cell. Rep.* 12, 1986–1996. doi: 10.1016/j.celrep.2015.08.046

Pott, S., and Lieb, J. D. (2015). What are super-enhancers? *Nat. Genet.* 47, 8–12. doi: 10.1038/ng.3167

Riggi, N., Knoechel, B., Gillespie, S. M., Rheinbay, E., Boulay, G., Suva, M. L., et al. (2014). EWS-FLI1 utilizes divergent chromatin remodeling mechanisms

to directly activate or repress enhancer elements in Ewing sarcoma. *Cancer Cell* 26, 668–681. doi: 10.1016/j.ccell.2014.10.004

Riggi, N., and Stamenkovic, I. (2007). The biology of Ewing sarcoma. *Cancer Lett.* 254, 1–10. doi: 10.1016/j.canlet.2006.12.009

Salisbury, J. R. (1993). The pathology of the human notochord. *J. Pathol.* 171, 253–255. doi: 10.1002/path.1711710404

Schmidt, D., Wilson, M. D., Spyrou, C., Brown, G. D., Hadfield, J., and Odom, D. T. (2009). ChIP-seq: using high-throughput sequencing to discover protein-DNA interactions. *Methods* 48, 240–248. doi: 10.1016/j.ymeth.2009.03.001

Sengupta, S., and George, R. E. (2017). Super-enhancer-driven transcriptional dependencies in cancer. *Trends Cancer* 3, 269–281. doi: 10.1016/j.trecan.2017.03.006

Sharifnia, T., Wawer, M. J., Chen, T., Huang, Q. Y., Weir, B. A., Sizemore, A., et al. (2019). Small-molecule targeting of brachyury transcription factor addiction in chordoma. *Nat. Med.* 25, 292–300. doi: 10.1038/s41591-018-0312-3

Shin, H. Y. (2018). Targeting super-enhancers for disease treatment and diagnosis. *Mol. Cells* 41, 506–514. doi: 10.14348/molcells.2018.2297

Sobacchi, C., Frattini, A., Guerrini, M. M., Abinun, M., Pangrazio, A., Susani, L., et al. (2007). Osteoclast-poor human osteopetrosis due to mutations in the gene encoding RANKL. *Nat. Genet.* 39, 960–962. doi: 10.1038/ng2076

Stacchiotti, S., and Sommer, J. (2015). Building a global consensus approach to chordoma: a position paper from the medical and patient community. *Lancet Oncol.* 16, e71–e83. doi: 10.1016/S1470-2045(14)71190-8

Stoll, G., Surdez, D., Tirode, F., Laud, K., Barillot, E., Zinovyev, A., et al. (2013). Systems biology of Ewing sarcoma: a network model of EWS-FLI1 effect on proliferation and apoptosis. *Nucleic Acids Res.* 41, 8853–8871. doi: 10.1093/nar/gkt678

Sur, I., and Taipale, J. (2016). The role of enhancers in cancer. *Nat. Rev. Cancer* 16, 483–493. doi: 10.1038/nrc.2016.62

Symon, A., and Harley, V. (2017). SOX9: A genomic view of tissue specific expression and action. *Int. J. Biochem. Cell Biol.* 87, 18–22. doi: 10.1016/j.biocel.2017.03.005

Thandapani, P. (2019). Super-enhancers in cancer. *Pharmacol. Ther.* 199, 129–138. doi: 10.1016/j.pharmthera.2019.02.014

Tomazou, E. M., Sheffield, N. C., Schmidl, C., Schuster, M., Schoenegger, A., Datlinger, P., et al. (2015). Epigenome mapping reveals distinct modes of gene regulation and widespread enhancer reprogramming by the oncogenic fusion protein EWS-FLI1. *Cell Rep.* 10, 1082–1095. doi: 10.1016/j.celrep.2015.01.042

Vaharautio, A., and Taipale, J. (2014). Cancer. Cancer by super-enhancer. *Science* 346, 1291–1292. doi: 10.1126/science.aaa3247

Vahedi, G., Kanno, Y., Furumoto, Y., Jiang, K., Parker, S., Erdos, M. R., et al. (2015). Super-enhancers delineate disease-associated regulatory nodes in T cells. *Nature* 520:558. doi: 10.1038/nature14154

Walker, B. A., Wardell, C. P., Brioli, A., Boyle, E., Kaiser, M. F., Begum, D. B., et al. (2014). Translocations at 8q24 juxtapose MYC with genes that harbor superenhancers resulting in overexpression and poor prognosis in myeloma patients. *Blood Cancer J.* 4:e191. doi: 10.1038/bcj.2014.13

Warman, M. L., Cormier-Daire, V., Hall, C., Krakow, D., Lachman, R., LeMerrer, M., et al. (2011). Nosology and classification of genetic skeletal disorders: 2010 revision. *Am. J. Med. Genet. A* 155A, 943–968. doi: 10.1002/ajmg.a.33909

Weiss, B. M., Abadie, J., Verma, P., Howard, R. S., and Kuehl, W. M. (2009). A monoclonal gammopathy precedes multiple myeloma in most patients. *Blood* 113, 5418–5422. doi: 10.1182/blood-2008-12-195008

Whyte, W. A., Orlando, D. A., Hnisz, D., Abraham, B. J., Lin, C. Y., Kagey, M. H., et al. (2013). Master transcription factors and mediator establish super-enhancers at key cell identity genes. *Cell* 153, 307–319. doi: 10.1016/j.cell.2013.03.035

Xing, D., Xu, Y., Liu, Q., Ke, Y., Wang, B., Li, Z., et al. (2016). Osteoarthritis and all-cause mortality in worldwide populations: grading the evidence from a meta-analysis. *Sci. Rep.* 6:24393. doi: 10.1038/srep24393

Zhang, J., Liu, W., Zou, C., Zhao, Z., Lai, Y., Shi, Z., et al. (2020). Targeting super-enhancer-associated oncogenes in osteosarcoma with THZ2, a covalent CDK7 inhibitor. *Clin Cancer Res.* 26, 2681–2692. doi: 10.1158/1078-0432.CCR-19-1418

Zhang, L., Choi, H. J., Estrada, K., Leo, P. J., Li, J., Pei, Y. F., et al. (2014). Multistage genome-wide association meta-analyses identified two new loci for bone mineral density. *Hum. Mol. Genet.* 23, 1923–1933. doi: 10.1093/hmg/ddt575

Zhang, X., Wang, Y., Chiang, H. C., Hsieh, Y. P., Lu, C., Park, B. H., et al. (2019). BRCA1 mutations attenuate super-enhancer function and chromatin looping in haploinsufficient human breast epithelial cells. *Breast Cancer Res.* 21:51. doi: 10.1186/s13058-019-1132-1

Zhu, D. L., Chen, X. F., Hu, W. X., Dong, S. S., Lu, B. J., Rong, Y., et al. (2018). Multiple functional variants at 13q14 risk locus for osteoporosis regulate RANKL expression through long-range super-enhancer. *J. Bone Miner. Res.* 33, 1335–1346. doi: 10.1002/jbmr.3419

Conflict of Interest: The authors declare that the research was conducted in the absence of any commercial or financial relationships that could be construed as a potential conflict of interest.

The handling editor declared a shared affiliation, though no other collaboration, with the authors at time of review.

Copyright © 2020 Qu, Ouyang, Wu, Li, Wang, Lu and Li. This is an open-access article distributed under the terms of the Creative Commons Attribution License (CC BY). The use, distribution or reproduction in other forums is permitted, provided the original author(s) and the copyright owner(s) are credited and that the original publication in this journal is cited, in accordance with accepted academic practice. No use, distribution or reproduction is permitted which does not comply with these terms.

frontiers in Cell and Developmental Biology

ORIGINAL RESEARCH
published: 14 July 2020
doi: 10.3389/fcell.2020.00593

SLIT2 Overexpression in Periodontitis Intensifies Inflammation and Alveolar Bone Loss, Possibly via the Activation of MAPK Pathway

Liping Wang[1†], Jing Zheng[1†], Janak L. Pathak[1†], Yunxin Chen[1], Dongliang Liang[1], Luxi Yang[1], Haobo Sun[1], Mei Zhong[1], Lihong Wu[1], Li Li[2], Shuhua Deng[2], Lingyun Zheng[2], Yongyong Yan[1], Dan Hou[1], Lijing Wang[1,2] and Linhu Ge[1]**

[1] Guangzhou Key Laboratory of Basic and Applied Research in Oral Regenerative Medicine, Affiliated Stomatology Hospital of Guangzhou Medical University, Institute of Oral Disease, Guangzhou Medical University, Guangzhou, China, [2] Vascular Biology Research Institute, School of Life Sciences and Biopharmaceutics, Guangdong Pharmaceutical University, Guangzhou, China

OPEN ACCESS

Edited by:
Chao Liang,
Hong Kong Baptist University, Hong Kong

Reviewed by:
Tomoki Maekawa,
Niigata University, Japan
Fuhua Yan,
Nanjing Stomatological Hospital (NSH), China

***Correspondence:**
Lijing Wang
2018991265@gzhmu.edu.cn
Linhu Ge
gelinhu@yeah.net

† These authors have contributed equally to this work and share first authorship

Specialty section:
This article was submitted to Molecular Medicine, a section of the journal Frontiers in Cell and Developmental Biology

Received: *14 May 2020*
Accepted: *17 June 2020*
Published: *14 July 2020*

Citation:
Wang L, Zheng J, Pathak JL, Chen Y, Liang D, Yang L, Sun H, Zhong M, Wu L, Li L, Deng S, Zheng L, Yan Y, Hou D, Wang L and Ge L (2020) SLIT2 Overexpression in Periodontitis Intensifies Inflammation and Alveolar Bone Loss, Possibly via the Activation of MAPK Pathway. Front. Cell Dev. Biol. 8:593. doi: 10.3389/fcell.2020.00593

SLIT2, a member of neuronal guidance cues, has been reported to regulate inflammation and cancer progression. Periodontitis is an oral inflammatory disease that degenerates periodontal tissue, alveolar bone and tooth. This study aims to explore the expression pattern of SLIT2 in periodontitis and its role in disease progression and bone loss. Gingival tissue of 20 periodontitis patients and 20 healthy-controls was obtained. Ligature-induced periodontitis (LIP) mice-model was developed in *Slit2-Tg* and wild-type mice. The effect of SLIT2 on inflammation, immune cell infiltration, M1 macrophage polarization, and alveolar bone loss in periodontitis was analyzed extensively. In periodontitis-affected gingival-tissue, SLIT2 expression was 4.4-fold higher compared to healthy-volunteers. LIP enhanced SLIT2 expression in mice periodontitis-affected periodontal tissue (PAPT) and blood circulation of wild-type mice by 4. 6-, and 5.0-fold, respectively. In Slit2-Tg-mice PAPT, SLIT2 expression was 1.8-fold higher compared to wild-type mice. Micro-CT and histomorphometric analysis revealed a 1.3-fold higher cement-enamel-junction to the alveolar-bone-crest (CEJ-ABC) distance and alveolar bone loss in LIP Slit2-Tg-mice compare to LIP wild-type mice. Results from RNA-sequencing, RT-qPCR, and ELISA showed a higher expression of Cxcr2, Il-18, TNFα, IL-6, and IL-1β in Slit2-Tg-mice PAPT compared to wild-type-mice. Slit2-Tg-mice PAPT showed a higher number of osteoclasts, M1 macrophages, and the upregulation of Robo1 expression. Slit2-Tg-mice PAPT showed upregulation of M1 macrophage marker CD16/32 and osteoclastogenic markers *Acp5*, *Ctsk*, and *Nfatc1*, but osteogenic markers (*Alp, Bglap*) remained unchanged. Immunohistochemistry unveiled the higher vasculature and infiltration of leucocytes and macrophages in Slit2-Tg-mice PAPT. RNA-sequencing, GO-pathway enrichment analysis, and western blot analysis revealed the activation of the MAPK signaling pathway in *Slit2*-Tg mice PAPT. In conclusion,

SLIT2 overexpression in periodontitis intensifies inflammation, immune cells infiltration, M1 macrophage polarization, osteoclastogenesis, and alveolar bone loss, possibly via activation of MAPK signaling, suggesting the role of SLIT2 on exacerbation of periodontitis and alveolar bone loss.

Keywords: SLIT2, periodontitis, alveolar bone loss, osteoclasts, MAPK signaling

INTRODUCTION

SLIT2 protein, a member of neuronal guidance cues, is also expressed in extraneuronal tissues, including kidney, lung, heart, and immune cells (Yuan et al., 1999; Wu et al., 2001; Wong et al., 2002). SLIT2 is aberrantly expressed in various cancers and plays a role in the regulation of cancer cell apoptosis, cancer metastasis, tumor-associated inflammation, and tumor progression (Wang et al., 2003, 2008; Schmid et al., 2007; Avci et al., 2008; Yang et al., 2010; Zhou et al., 2011; Chang et al., 2015; Liu et al., 2018). Moreover, the SLIT2 has been reported to aberrantly regulate the inflammation in different inflammatory diseases and cell types (Zhao et al., 2014; Zhou et al., 2017; Fernando et al., 2018). SLIT2 is a secreted protein that binds to Roundabout (ROBO) receptors, i.e., ROBO1, ROBO2, ROBO3, and ROBO4. Binding of SLIT2 with specific ROBO receptor regulates particular cell functions. SLIT2/ROBO1-axis triggers proinflammatory signaling, and SLIT2/ROBO4-axis alleviates inflammation in endothelial cells during endotoxemia (Zhao et al., 2014). Periodontitis is a 6th most common chronic inflammatory disease worldwide (Kassebaum et al., 2014), affecting periodontal tissue, alveolar bone, and oral health homeostasis (Cochran, 2008; Darveau, 2010; Hajishengallis, 2014; Richards, 2014). Polymicrobial dysbiosis disrupts oral tissue homeostasis, and host immune reaction induces local and systematic inflammation in periodontitis (Darveau, 2010). Based on the existing knowledge about biological functions of SLITs in various pathophysiological conditions, (Zhao et al., 2012) had hypothesized SLIT as an effective immunotherapeutic agent in the treatment of periodontitis. However, the expression pattern of SLIT2 in periodontal tissue during periodontitis and its' role in the pathophysiology of periodontitis is still unknown.

In periodontitis, activated proinflammatory cascade dictates the pathophysiology of the disease. Higher microvessel density (MVD) in periodontitis affected gingival tissue promotes the extravasation of inflammatory immune cells (Aspriello et al., 2009). Recruited immune cells such as macrophages and neutrophils in gingival tissue not only phagocytize the microbes but also release the proinflammatory cytokines. Enhanced macrophage infiltration in gingival tissue is frequently observed in histological images of human or animal periodontitis-affected gingival tissue sections (Yu et al., 2016). M1 macrophage polarization in periodontitis-affected gingival tissue triggers the release of proinflammatory cytokines from the immune cells and amplifies the inflammation (Yu et al., 2016; Zhou et al., 2019). Higher numbers of M1 macrophages in periodontitis-affected gingival tissue positively correlates with clinical features of chronic and aggressive periodontitis (Gonzalez et al., 2015; Yu et al., 2016; Zhou et al., 2019; Zhu et al., 2019). Neutrophil extravasates and infiltrates in periodontitis-affected gingival tissue (Zhang et al., 2020). SLIT2 has been reported to regulate neutrophil chemotaxis during lung inflammation and renal-ischemic perfusion injury (Ye et al., 2010; Chaturvedi and Robinson, 2015). However, the effect of SLIT2 on, the infiltration of leucocytes/macrophages in periodontitis-affected gingival tissue, and regulation of periodontitis-induced inflammatory cascade still need to be investigated.

Periodontitis induces periodontal tissue damage and alveolar bone resorption increasing the risk of tooth loss. Activated inflammatory cascade elevates the level of pro-inflammatory cytokines in periodontal tissue, including IL-6, IL-1β, and TNF-α. Elevated levels of pro-inflammatory cytokines in alveolar bone induce osteoclastogenesis and osteoclastogenic bone resorption (Pan et al., 2019; AlQranei and Chellaiah, 2020; Xu et al., 2020). Activation of MAPK (p38) signaling in various immune cells regulates periodontal disease progression and alveolar bone loss (Li et al., 2012; Xu et al., 2020). SLIT2 contributes to cholestatic fibrosis via activation of MAPK p38 signaling in hepatic stellate cells (Li et al., 2019). However, the effect of SLIT2 on MAPK signaling in periodontal immune cells during periodontitis is still a mystery.

In this study, we aimed to analyze the expression pattern of SLIT2 in periodontitis-affected gingival tissue, and the role of SLIT2 on the pathophysiology of periodontitis. We analyzed SLIT2 expression in the human periodontitis-affected gingival tissue and ligature-induced periodontitis (LIP)-affected mice periodontal tissue. The effect of SLIT2 on the infiltration of immune cells, M1 macrophage polarization, osteoclastogenesis, and alveolar bone loss was extensively analyzed in *Slit2*-Transgenic (Tg) periodontitis mice. Our study elucidated SLIT2 overexpression in human and mice periodontitis-affected tissue. Moreover, SLIT2 overexpression intensifies the infiltration of leucocytes/macrophages, inflammation, M1 macrophage polarization, osteoclastogenesis, alveolar bone loss, and activation of P-P38 signaling in periodontitis.

MATERIALS AND METHODS

Collection of Human Gingival Biopsies

Human gingiva, including sulcus/pocket epithelium and underlying connective tissue, were obtained from either healthy controls (n = 20) or patients with periodontitis (n = 20) with alveolar bone loss confirmed by radiography. Patients and healthy controls clinical characteristics and demographics are summarized in **Supplementary Table S1**. Written informed

consent was obtained from each patient. Human gingival tissues were used to analyze SLIT2 protein expression by ELISA. The Medical Ethics Committee of the Affiliated Stomatology Hospital of Guangzhou Medical University approved all protocols dealing with patients (approval number: KY2019032).

Animals

Total of 47 wild-type C57BL/6 and 47 *Slit2* transgenic (*Slit2-Tg*) C57BL/6 mice were used in this study. Wild-type mice were purchased from Guangdong Medical Animal Experiment Center (Guangdong, China). *Slit2-Tg* mice were obtained from Prof. Lijing Wang's lab, Vascular Biology Research Institute, School of Life Sciences and Biopharmaceutics, Guangdong Pharmaceutical University, Guangzhou, China. *Slit2-Tg* mice were generated according to the previously reported protocol (Yang et al., 2010). All the mice used were healthy and immune-normal, euthanized after their experimental periods. All studies were performed in 8-week-old male mice unless otherwise indicated. The Experimental Animal Ethics Committee of Guangzhou Medical University approved all animal care and study protocols (GY2020-004).

Primary Bone Marrow-Derived Macrophages (BMMs) Culture

Bone marrow-derived macrophages (BMMs) were harvested from the bone marrow of six C57BL/6 mice as described previously (Spiller et al., 2016). BMMs were expanded in T75 culture flasks supplemented with Gibco RPMI 1640 medium (Life Technologies, Carlsbad, CA, United States) and 10% FBS. For the *in vitro* studies cultures were supplemented with 30 ng/ml recombinant mouse macrophage colony-stimulating factor (M-CSF, CB34, Novoprotein, Shanghai, China). Cultures were used for further mRNA and protein expression analysis.

Development of Periodontitis in Mice

A ligature-induced periodontitis (LIP) model was developed in *Slit2-Tg* and wild-type mice, as described previously (Abe and Hajishengallis, 2013).

Micro-CT Analysis

Micro-CT scanned the maxilla to evaluate the morphological changes in the alveolar bone. The distance from the mesial buccal cemento-enamel junction to the alveolar bone crest (CEJ-ABC) of the second molar was measured as a reference for bone loss. The level of bone resorption was calculated as described previously (Abe and Hajishengallis, 2013).

Western Blot Analysis

Periodontitis-affected periodontal tissue (PAPT; 0.5 cm× 0.5 cm × 1.0 cm) surrounding the teeth cut from mice maxilla, including gingiva, periodontal ligament, and a part of alveolar bone, was stored at −80°C for use. Frozen periodontal tissue samples were solubilized in lysis buffer containing 10 mM of Tris–HCl, pH 7.4, 150 mM of NaCl, 1 mM of EDTA, and 1% Triton X-100 at 4°C for 20 min. The tissue lysates were subjected to centrifugation at 15000 × *g* at 4°C for 20 min. The supernatant was collected, and their protein contents were determined using Coomassie Plus Protein Assay Reagent (Pierce, Rockford, IL, United States). Cell lysate protein (50 μg) was separated by sodium dodecyl sulfate-polyacrylamide gel electrophoresis (SDS-PAGE) and transferred to polyvinylidene difluoride (PVDF) membranes. The membranes were then blocked with 5% non-fat dry milk for 1 h and incubated overnight at 4°C with primary antibodies: anti-TRAF6 (1:1000 dilution, ABclonal, Wuhan, China), anti-P38 (1:1000 dilution, ABclonal), anti-P-P38 (1:1000 dilution, Cell Signaling Technology, MA, United States), or anti-TRAP (1:1000 dilution, ABclonal). The membranes were then washed and incubated with HRP-conjugated secondary antibodies (1:5000 dilution, ABclonal) at room temperature. An enhanced chemiluminescence detection system (Thermo Scientific, MA, United States) detected the immunoreactive protein bands. Densitometry data for band intensities results were generated by analyzing the images using ImageJ software. β-actin was used as a reference housekeeping protein.

Histological Evaluation

After scanning micro-CT images, the collected maxillae were fixed in 4% formaldehyde overnight, followed by decalcification in 10% EDTA, which was exchanged every week for 1 month. The specimens were cut in 3 mm thickness along the long axis of the molars. Next, the samples were dehydrated and embedded in paraffin blocks. Serial sections of 5 μm thickness were cut and mounted on poly-l-lysine-coated slides. Hematoxylin and eosin (H&E) staining was performed separately on consecutive tissue sections. Images were captured using a microscope. The CEJ-ABC distance between the maxillary first and second molars was measured as a net bone loss on tissue sections, using Image J software (Wang et al., 2015).

Immunohistochemistry

Thick tissue sections (5 μm) were deparaffinized and rehydrated, followed by heat-induced epitope retrieval (Xiao et al., 2017). Methanol containing 3% H_2O_2 was used to block the endogenous peroxidase for 20 min. Tissue sections were then blocked with 10% bovine serum albumin (BSA) and incubated for overnight at 4°C with primary antibodies: monoclonal anti-CD34 [EP373Y], (ab81289, Abcam, Cambridge, United Kingdom), anti-CD45 (20103-1-AP, Proteintech, United States), monoclonal anti-F4/80 [BM8], (123110, BioLegend, CA, United States) or isotype controls. After washing with PBS three times, tissue sections were incubated with a corresponding goat anti-rabbit secondary antibody (SolelyBio, Beijing, China) for 30 min at 37°C. Slides were incubated with diaminobenzidine (Cell Signaling Technology, MA, United States) followed by hematoxylin counterstaining. Finally, all stained sections were dehydrated through a series of graded alcohol baths of increasing concentration, cleared in xylene, and mounted with coverslips. Stained tissue sections were visualized under a microscope (Leica, Germany), and images were captured. The visual fields between the first

molar and the second molar were photographed. The number of immunostaining-positive cells was counted in the entire area of each image.

Tartrate-Resistant Acid Phosphatase (TRAP) Staining

Tissue sections were stained using acid phosphatase (TRAP) kit (G1050, Servicebio, Wuhan, China) following the manufacturer's instructions. TRAP stained histological tissue section were examined under microscope, and images of predefined areas were captured. TRAP-positive cells appeared bright red. TRAP-positive osteoclasts, in the alveolar bone tissue section between the first molar and the second molar, were counted.

Real-Time qPCR

Periodontal tissue removed from mice maxillae (periodontitis-affected and control group) was homogenized in a mortar on liquid nitrogen, and total RNA was isolated using PureLink RNA Mini Kit (12183018A, Thermo Fisher Scientific, United States). RNA samples with 1.8 to 2.0 of the OD260/280 ratio were used for analysis, and total RNA reverse were transcribed using Takara PrimeScriptTM RT Master Mix in T100 Thermal Cycler (Bio-Rad, United States). The transcribed cDNA was used for RT-qPCR using Takara TB-Green Premix Ex Taq in LightCycler RT-PCR system (LC-480 II, Roche, Switzerland). GADPH was used as a reference housekeeping gene. The $2^{-\Delta\Delta Ct}$ method was used to analyze the relative mRNA expression levels. The primers used for RT-qPCR are listed in **Supplementary Table S2**.

Protein Expression Analysis by ELISA

ELISA analyzed the protein level in human and mice periodontal tissue protein extract, mice serum, conditioned medium of mice BMMs culture, and mice BMMs cell lysates. The procedure of periodontal tissue protein extract has been described in the Western blot analysis section above. For mice serum separation, blood samples were collected from orbital venous plexus, and the serum was separated by 5 min centrifugation at 2,000 rpm. BMMs culture conditioned medium and cell lysates were prepared as follows. On the fifth day of BMMs culture, 100 ng/ml LPS was added. After 48 h of LPS treatment, conditioned medium (CM) was collected, and attached cells in the culture harvested for cell lysate preparation. SLIT2 level in human periodontal tissue lysate was analyzed by human SLIT2 ELISA kit (Cusabio, Wuhan, China) following the manufacturer's instruction. The protein levels of IL-6, IL-1β, and TNF-a in periodontal tissue protein extract and CM were measured by mouse ELISA Standard Kit (RayBiotech, Atlanta, United States). The protein level of CD16/32 in mice periodontal tissue protein extract and the BMMs cell lysate were measured by Mouse ELISA Standard Kit (Cusabio, Wuhan, China). The protein levels of SLIT2 in mice periodontal tissue protein extract and mice serum were measured by mouse SLIT2 ELISA Kit (Cusabio, Wuhan, China) following the manufacturer's instruction.

Flow Cytometry Analysis

The cell suspension was prepared from mice periodontal tissue, including gingiva, periodontal ligament, and a part of alveolar bone for flow cytometry analysis (Mizraji et al., 2013). Prior to the test, cells were counted and cell viability was evaluated by the Zombie NIR^{TM} Fixable Viability Kit (423105, BioLegend, Beijing, China). Cells were stained with 1 μg of anti-F4/80 (123110, BioLegend, CA, United States) solution, monoclonal anti-CD11b [M1/70], (101206, BioLegend, CA, United States) or anti-rabbit IgG per 1×10^6 cells for 30 min on ice in the dark. After two times washing with PBS, the cells were resuspended in 300 μl PBS and transferred to flow tubes. Flow cytometric analysis was performed using the FACSAria III Cell Sorter (BD Biosciences, San Jose, CA, United States).

RNA Sequencing

The wild-type and Slit2-Tg periodontitis mice periodontal tissue samples without enzymatic treatment were used for RNA sequencing. Total RNA was extracted from periodontal tissue using the TRIzol kit (Invitrogen, Carlsbad, CA, United States), according to the manufacturer's protocol. The RNA concentration was determined using Qubit, and RNA amount and purity of each sample was assessed with a NanoDrop spectrophotometer (NanoDrop 2000, Wilmington, DE, United States). RNA was isolated in 40 μl of DEPC water and stored in −80°C. Briefly, RNA-seq libraries were prepared by using the Illumina TruseqTM RNA sample prep Kit and were sequenced using an Illumina HiSeq. Cutadapt was used to obtain paired-end reads (Martin, 2011). The quality of the RNA-samples used for RNA-seq is presented in **Supplementary Table S3**. The reads were aligned with Hisat2 (v 2.1.0) to GRCm38 with default parameters (Kim et al., 2015). Only the data matched to the reference genome were used for subsequent analysis. The mapped reads of each sample were assembled using StringTie (Pertea et al., 2015). Then, the transcriptomes from all samples were merged to reconstruct a comprehensive transcriptome using perl scripts. After the final transcriptome was generated, StringTie (Pertea et al., 2015) and Ballgown (Frazee et al., 2015) was used to estimate the expression levels of all transcripts. Traditional singular enrichment analysis (SEA) (Rodriguez et al., 2016) was used for the enrichment analysis of GO terms and pathways. The enrichment *P*-value calculation was performed with Fisher's exact test. RNA-sequence data are available at **Supplementary Data S1**. All raw RNA-sequencing data can be accessed from NCBI SRA database (SRA accession: PRJNA639904)[1].

Statistical Analyses

All data are presented as mean ± standard deviation (SD). Statistical analysis was performed using SPSS 19.0 statistical software (SPSS IBM, Armonk, NY, United States). For where appropriate (comparison of two groups only), two-tailed *t*-tests were done. In all cases, data from at least three independent experiments was used, and *P* value of less than 0.05 was considered to indicate a statistically significant difference.

[1]https://www.ncbi.nlm.nih.gov/bioproject/PRJNA639904/

RESULTS

Periodontitis Amplifies SLIT2 Expression in Gingival Tissue

First, we examined the SLIT2 expression in human gingival tissues of 20 periodontitis patients and 20 age and gender-matched healthy individuals. The SLIT2 protein level in periodontitis-affected human gingival tissue was 4.4-fold higher compared to healthy gingival tissue (**Figure 1A**). The SLIT2 protein level in the periodontal tissue of *Slit2*-Tg mice was 2.1-fold higher compared to wild-type mice (**Figure 1B**). The SLIT2 protein expression in wild-type mice was upregulated by 4.6-fold compared to healthy periodontal tissue (**Figure 1B**). Similarly, a 3.9-fold higher expression of SLIT2 protein was observed in *Slit2-Tg* mice PAPT compared to healthy periodontal tissue (**Figure 1B**). *Slit2-Tg* mice PAPT showed a 1.8-fold higher expression of SLIT2 protein in comparison to wild-type mice PAPT (**Figure 1B**). Additionally, the serum of wild-type periodontitis mice showed 5.0-fold higher expression of SLIT2 protein compared to wild-type healthy mice (**Figure 1C**). Our results indicate the upregulation of SLIT2 expression in gingival tissue during periodontitis in human and in PAPT of wild-type mice or *Slit2-Tg* mice. Moreover, periodontitis condition upregulates the level of serum SLIT2 in wild-type mice showing the systemic effect of periodontitis.

Higher Expression of SLIT2 Intensifies Periodontitis and Alveolar Bone Loss

We performed micro-CT scanning to analyze the effect of LIP on alveolar bone loss. Intact periodontal tissue and normal alveolar bone were observed in healthy wild-type and *Slit2*-Tg mice (**Figure 1D**). Loss of periodontal tissue and alveolar bone was observed in LIP wild-type and *Slit2-Tg* mice (**Figure 1D**). The higher CEJ-ABC distance indicates the higher effect of periodontitis on periodontal tissue damage and alveolar bone loss. CEJ-ABC distance in periodontitis wild-type mice was 1.9-fold higher compared to healthy wild-type mice (**Figure 1E**). Similarly, CEJ-ABC distance in periodontitis *Slit2-Tg* mice was 2.3-fold higher compared to healthy *Slit2-Tg* mice (**Figure 1E**). *Slit2-Tg* periodontitis mice showed a 1.3-fold higher CEJ-ABC distance compared to wild-type periodontitis mice (**Figure 1E**). This finding was corroborated by the histological images as well (**Figure 1F**). *Slit2*-Tg mice periodontitis exhibited more bone loss and bone destruction in the alveolar crest height than in wild-type mice periodontitis (**Figures 1D,E**). This effect was further corroborated by the histological images (**Figure 1F**). The histological images showed the infiltration of inflammatory immune cells in gingival epithelial and alveolar bone resorption (**Figure 1F**). Histomorphometric analysis showed 1.3-fold higher periodontitis-induced alveolar bone loss in *Slit2-Tg* mice compared to wild-type mice (**Figure 1G**). Our results indicate that the overexpressed SLIT2 in periodontitis aggravates the consequences of the disease, such as the destruction of periodontal tissue and alveolar bone loss.

SLIT2 Overexpression Amplifies Osteoclastogenesis and Inflammation in Periodontitis Milieu

Inflammatory cytokines promote osteoclastogenesis, and higher osteoclastogenesis is associated with higher bone loss. In this study, we analyzed the role of the higher SLIT2 expression in periodontitis on osteoclastogenesis. More numbers of TRAP-positive osteoclasts were visualized in the PAPT section of *Slit2-Tg* mice compared to wild type mice (**Figure 2A**). A higher degree of vasculature in gingival tissue aggravates periodontitis. In this study, we performed CD34 immunostaining in PAPT to detect microvasculatures. Higher CD34 expression was observed in PAPT *of Slit2-Tg* mice compared to wild-type mice (**Figure 2B**). Quantitative analysis showed a 1.4-fold higher number of osteoclasts in PAPT in *Slit2-Tg* mice compared to wild-type mice (**Figure 2C**). Quantitative analysis revealed 1.4-fold higher microvessel density (MVD) in PAPT of *Slit2-Tg* mice compared to wild-type mice (**Figure 2D**).

Similarly, we performed immunohistochemical staining for leukocyte specific antigen, CD45, in gingival tissue sections to analyze the effect of SLIT2 overexpression on leucocytes infiltration in PAPT. More numbers of CD45 positive cells were observed in periodontitis-affected gingival tissue of *Slit2-Tg* mice compared to wild-type mice (**Figure 2B**). Quantitative analysis results revealed a 1.2-fold higher number of CD45-positive cells in PAPT of *Slit2-Tg* mice compared to wild-type mice (**Figure 2E**). This indicates that the higher degree of leucocyte infiltration in PAPT of *Slit2-Tg* mice, possibly amplify periodontal inflammation.

RNA sequencing (RNA-seq) of mice PAPT was performed to explore the underlying mechanisms of the regulatory effects of SLIT2 on periodontitis. Among 24 common inflammatory factors, *Cxcr2*, *Il18*, and *Il1*β were differentially upregulated by more than 2-fold in PAPT of *Slit2-Tg* mice compared to wild-type mice (**Figure 3A (i)**). The heat map corroborated the differential upregulation of *Cxcr2*, *Il18,* and *Il1*β mRNA in PAPT of *Slit2-Tg* mice compared to wild-type mice (**Figure 3A (ii)**). Highly expressed pro-inflammatory cytokines in periodontal tissue abrogate periodontitis. RT-qPCR results showed 2. 3-, 1. 8-, and 1.6-fold higher expression of *Il6* (**Figure 3B**), *Il1*β (**Figure 3C**), and *Tnf* (**Figure 3D**), respectively, in PAPT of *Slit2-Tg* mice compared to wild-type mice. Protein level expression of IL-6 (**Figure 3E**), IL-1β (**Figure 3F**), and TNF-α (**Figure 3G**) were 8-, 4- and 2.6-fold higher, respectively, in PAPT of *Slit2-Tg* mice compared to wild-type mice. This result indicates that the SLIT2-overexpression intensifies the inflammation in periodontitis.

We further analyzed the differential expression of 32 osteoclastogenesis related genes in PAPT by RAN-seq. The expression of *Fosl2, Il1*β*, Mapk14, Ncf4,* and *Pik3cb,* was differentially upregulated in PAPT of *Slit2-Tg* mice compared to wild-type mice (**Figures 4A (i),(ii)**). We further analyzed the mRNA expression of the key osteoclastogenesis regulators (*Acp5, Ctsk,* and *Nfatc1*) in PAPT by RT-qPCR. Notably, the expression of *Acp5, Ctsk*, and *Nfatc1* in PAPT of *Slit2-Tg* mice was 18. 4-, 2. 2-, and 1.8-fold higher, respectively, compared to wild-type mice (**Figures 4B–D**). Additionally, the expressions

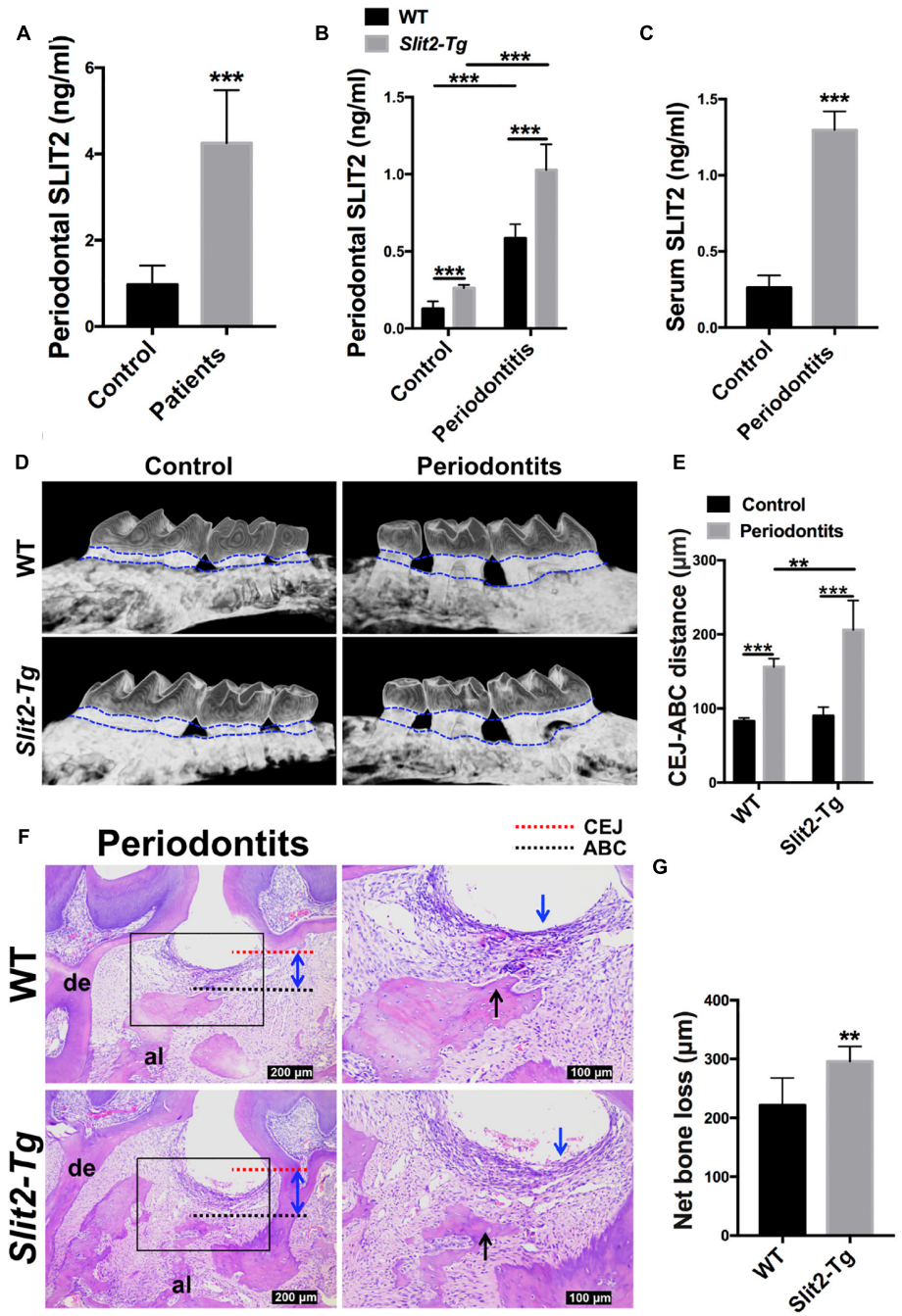


FIGURE 1 | Periodontitis-induced SLIT2 aggravates periodontitis and alveolar bone loss. Expression pattern of SLIT2 protein in, **(A)** Gingival tissue of periodontitis patients and healthy individuals (n = 20), and **(B)** periodontal tissue of healthy and periodontitis wild-type or *Slit2-Tg* mice. **(C)** Serum level of SLIT2 protein in wild-type mice (n = 5). **(D)** Micro-CT images of healthy and periodontitis-affected alveolar bone with the intact tooth of wild-type and *Slit2-Tg* mice. **(E)** Quantitative data of CEJ-ABC distance analyzed from micro-CT images. **(F)** H&E stained histological images of PAPT of wild-type and *Slit2-Tg* mice. **(G)** Quantitative data of alveolar bone loss around the periodontitis-affected tooth analyzed from histological images. Data are presented as mean ± SD (n = 6). The significant difference among the groups, $^{*}P < 0.05$, $^{**}P < 0.01$, $^{***}P < 0.001$. CEJ: cement-enamel junction, ABC: alveolar bone crest, Red dot line: CEJ level, Black dot line: ABC level, al: alveolar bone, de: dentine, blue arrow: inflammatory infiltration of the gingival epithelium, black arrow: alveolar bone resorption, double arrowhead (blue): CEJ-ABC distance, and WT: wild-type.

of the majority of osteoblastogenesis associated genes were not altered in PAPT of *Slit2-Tg* mice compared to wild-type mice. (**Figure 4E** and **Supplementary Figure S1**). These results indicate that the SLIT2 overexpression mainly triggers inflammation-induced osteoclastogenesis but might not affect the osteoblast function during periodontitis.

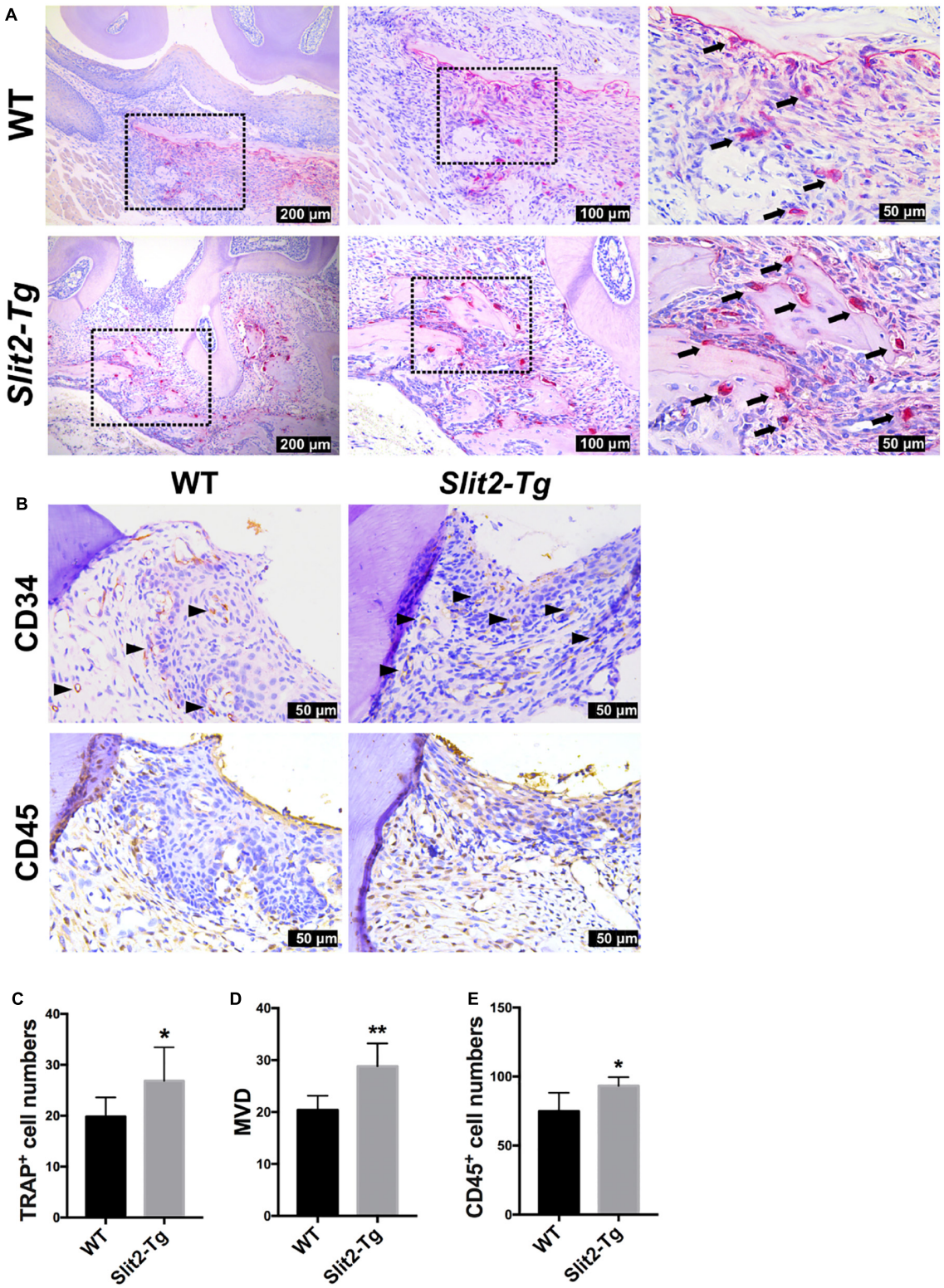


FIGURE 2 | SLIT2 overexpression augments pathological changes in both periodontal milieu soft and bone tissues during periodontitis. **(A)** Representative histological images of PAPT sections showing TRAP+ osteoclasts. **(B)** Representative CD34 and CD45 immunohistochemistry images of PAPT sections. **(C)** Quantitative analysis of osteoclasts from TRAP-stained histological tissue sections ($n = 6$). **(D)** Quantification of micro-vessel density from CD34 immunohistochemistry images ($n = 5$). **(E)** Quantification of CD45 expressing cells from CD45 immunohistochemistry images ($n = 6$). The significant difference among the groups, $^{*}P < 0.05$, $^{**}P < 0.01$. Black arrow: TRAP+ multinucleated osteoclasts. Black triangle arrowhead: microvessel. WT: wild-type.

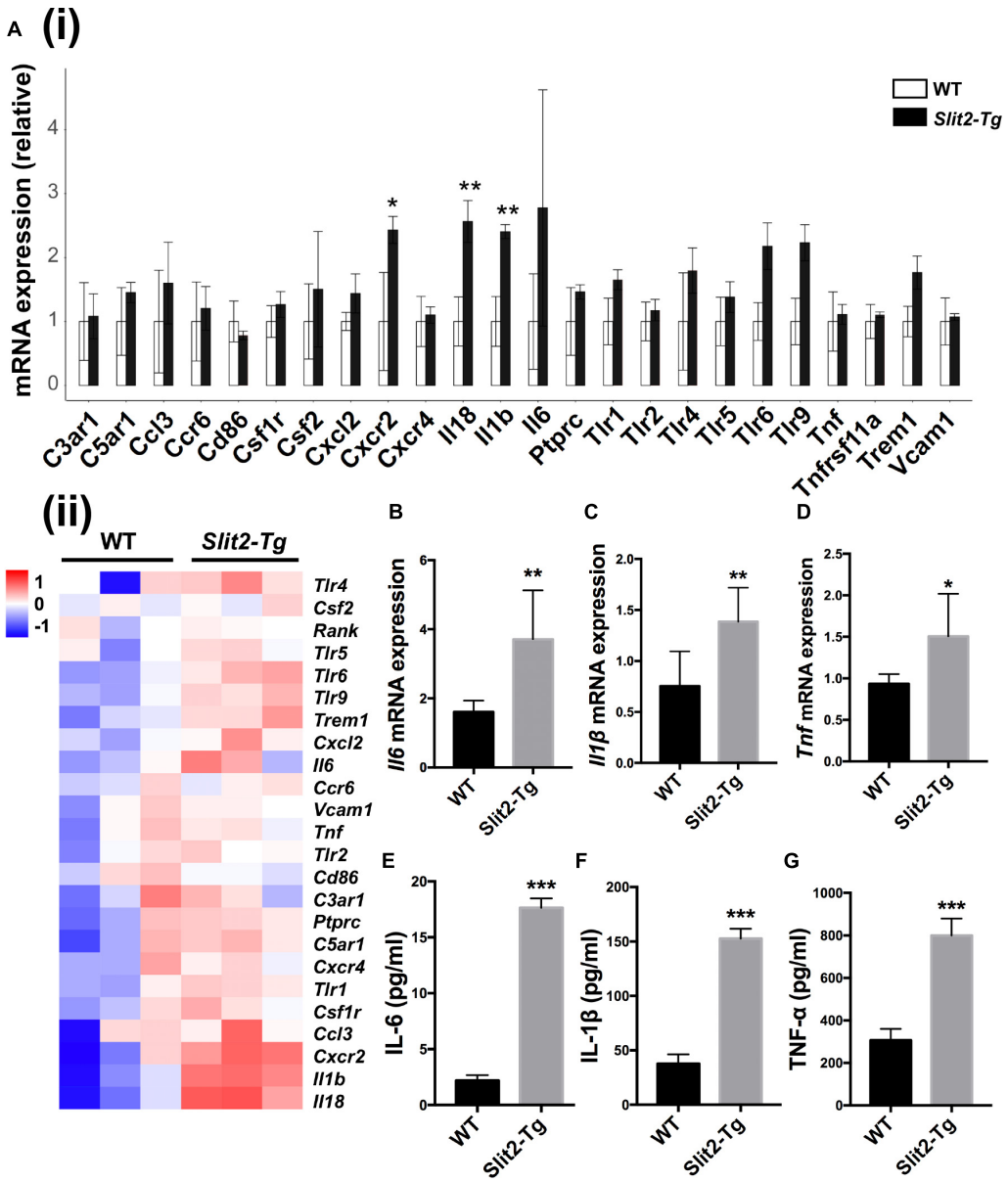


FIGURE 3 | SLIT2 overexpression triggers up-regulation of periodontal inflammatory factors. **(A (i))** Relative mRNA expression, and **(A (ii))** Heat map showing the differential expression pattern of inflammatory markers in PAPT analyzed by RNA sequencing (n = 3). Relative mRNA expression of **(B)** *Il6*, **(C)** *Il1*β, and **(D)** *Tnf*α in periodontitis-affected tissue analyzed by RT-qPCR. Protein expression of, **(E)** IL-6, **(F)** IL-1β, and **(G)** TNF-α in periodontitis-affected tissue analyzed by ELISA. Data are presented as mean ± SD (n = 6). Data are presented as mean ± SD. The significant difference among the groups, $^{*}P < 0.05$, $^{**}P < 0.01$, $^{***}P < 0.001$. Red color intensity indicates upregulation, and blue color intensity indicates the downregulation of gene expression.

SLIT2 Overexpression Enhances the Infiltration of Macrophages and M1 Macrophage Polarization in Periodontitis

More numbers of macrophages (F4/80 positive cells) were observed in the PAPT section of *Slit2-Tg* mice compared to wild-type mice (**Figure 5A (i)**). Quantitative analysis of infiltrated macrophages from immunohistochemistry images showed 1.3-fold higher numbers of macrophages in PAPT of *Slit2-Tg* mice compared to wild-type mice (**Figure 5A (ii)**). This finding was further verified by the data from flow cytometry analysis (**Figures 5B (i),(ii)**). Flow cytometry analysis revealed 1.4-fold higher numbers of CD11b+F4/80+ cells in the PAPT of *Slit2-Tg* mice compared to wild-type mice (**Figure 5B (ii)**). Prior to the test, cell viability was evaluated and above 95% viability of cells was ensured (data not shown). This finding indicates that the SLIT2 overexpression in periodontitis facilitates the infiltration of macrophages in periodontal tissue.

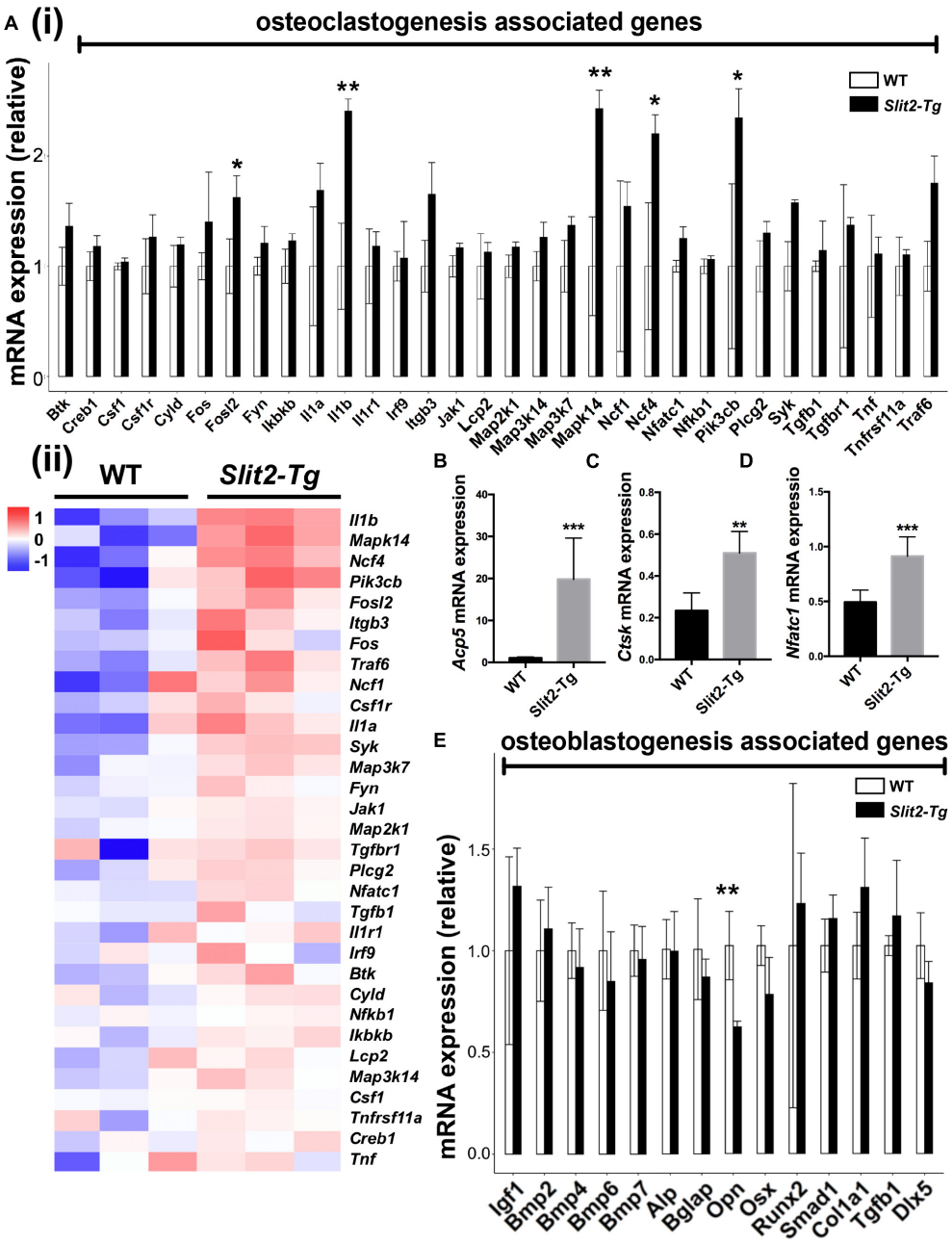


FIGURE 4 | SLIT2 overexpression activates osteoclastogenesis-related signaling pathways in periodontitis. **(A (i))** Relative mRNA expression, and **(A (ii))** Heat map showing the differential expression pattern of osteoclastogenesis related genes analyzed by RNA-seq ($n = 3$). Relative mRNA expression of **(B)** *Acp5*, **(C)** *Ctsk*, and **(D)** *Nfatc1* in periodontal tissue analyzed by RT-qPCR ($n = 6$). **(E)** Relative mRNA expression of osteoblastogenesis related genes analyzed by RNA sequencing ($n = 3$). Data are presented as mean ± SD. The significant difference among the groups, $^{*}P < 0.05$, $^{**}P < 0.01$, $^{***}P < 0.001$. WT: wild-type.

Proinflammatory cytokines trigger the M1 macrophage polarization. The relative expression of *Il1*β and *Il8* was upregulated in *Slit2-Tg* PAPT (**Figure 5C**). However, the expression of M2 macrophage polarization related cytokines (such as *Il10* and *Il4*) remained the same in *Slit2-Tg* PAPT and wild-type mice (**Figure 5D**). The protein level of CD16/32, a marker of M1 macrophage polarization, was upregulated (2.8-fold) in PAPT of *Slit2-Tg* mice compared to wild-type mice (**Figure 5E**). Similarly, under inflammatory condition (LPS treatment), cell lysate from *in vitro* cultured macrophages of *Slit2-Tg* mice expressed 4.7-fold higher CD16/32 compared to wild-type mice (**Figure 5F**). Similarly, inflammatory condition upregulated IL-6, IL-1β, and TNF-α expression in *Slit2-Tg* mice macrophages by 3. 6-, 2. 6-, and 1.9-fold, respectively, compared to wild-type mice macrophages (**Figures 5G–I**). This result indicates that SLIT2

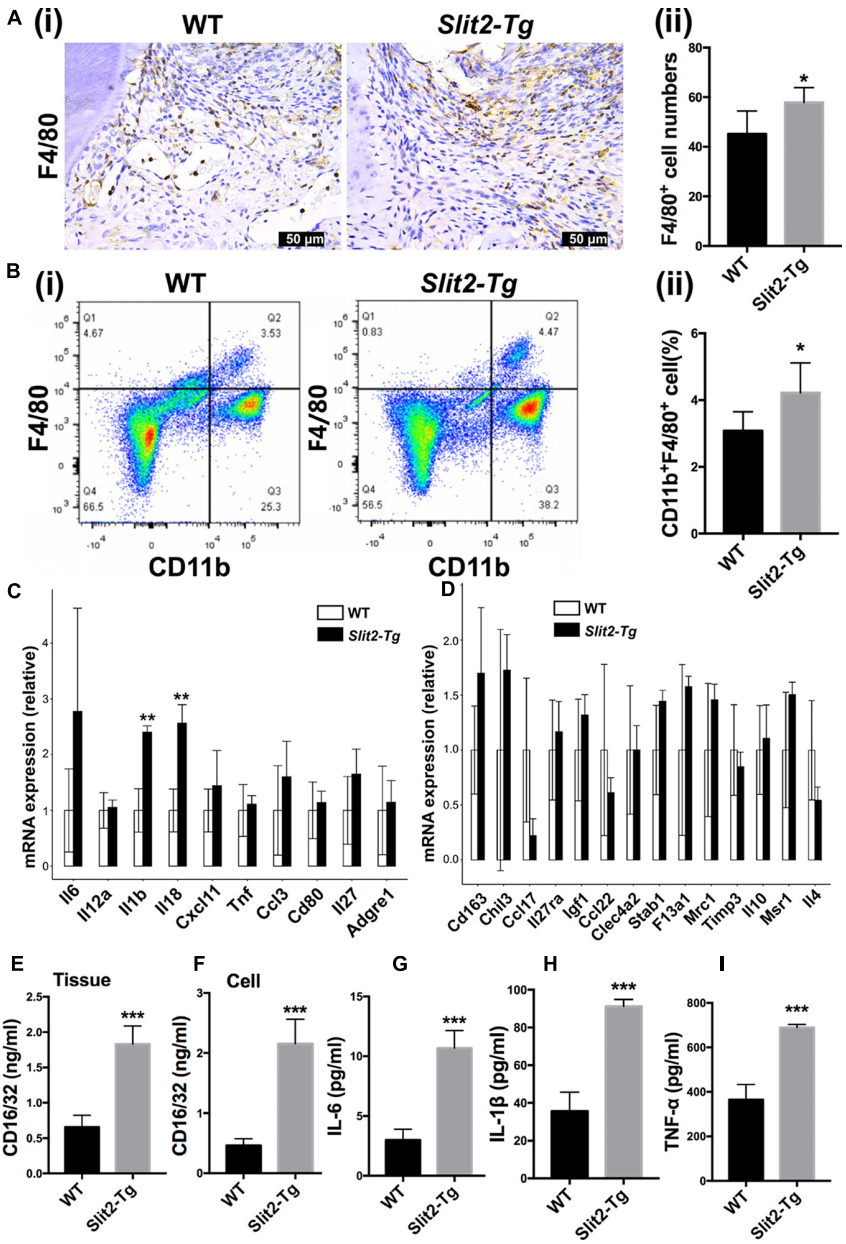


FIGURE 5 | SLIT2 overexpression induces M1 macrophage polarization in PAPT. **(A (i))** Representative F4/80 immunohistochemistry images of the PAPT section. **(A (ii))** Quantification of F4/80 expressing cells in a PAPT section from immunohistochemistry images ($n = 6$). **(B (i))** Flow cytometry analysis of F4/80 positive relative frequency of gated populations from PAPT. **(B (ii))** Quantitative analysis of F4/80+ flow cytometry data ($n = 5$). Relative mRNA expression of **(C)** M1, and **(D)** M2 macrophage polarization related genes analyzed by RNA sequencing ($n = 3$). **(E)** Protein level expression of CD16/32 in PAPT ($n = 6$). Protein level expression of, **(F)** CD16/32 in cell lysates of LPS-treated BMMs. Protein expression of **(G)** IL-6, **(H)** IL-1β, and **(I)** TNF-α in conditioned medium of LPS-treated BMMs ($n = 4$). Data are presented as mean ± SD. The significant difference among the groups, $^{*}P < 0.05$, $^{**}P < 0.01$, $^{***}P < 0.001$.

overexpression amplifies macrophage infiltration and M1 macrophage polarization in PAPT.

SLIT2 Overexpression Upregulates Its Receptor ROBO1

ROBO1, ROBO2, ROBO3, and ROBO4 are 4 receptors of SLIT2 ligand. In RNA-seq heat map, *Robo1* and *Robo2* gene expression were differentially upregulated, and *Robo3* and *Robo4* remained unchanged in *Slit2-Tg* mice PAPT (**Figures 6A–D**). Quantification of RNA-seq data showed 1.5-fold, and RT-qPCR analysis showed a 2.0-fold higher expression of Robo1 in PAPT of *Slit2-Tg* mice compared to wild type mice (**Figure 6A (ii)**). However, the expression of other receptors remained unchanged. This result indicates the possible role of the SLIT2/ROBO1 axis on SLIT2-mediated effects in periodontitis.

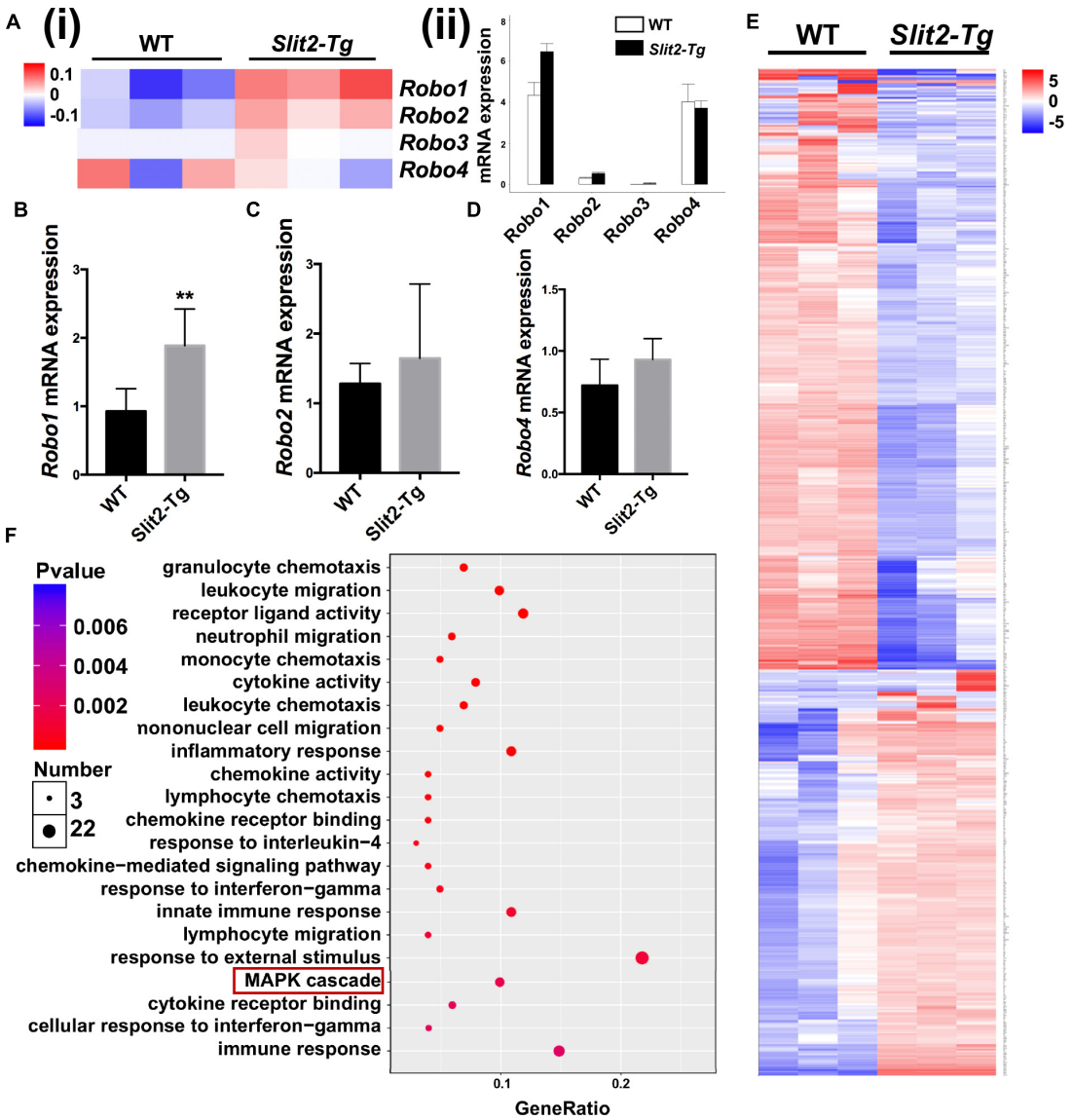


FIGURE 6 | SLIT2/ROBO1 signaling possibly regulates the SLIT2-induced inflammation in periodontitis. **(A (i))** Heat map the differential expression of Slit2 receptors *Robo1-4*, and **(A (ii))** Relative mRNA expression of *Robo1*, *Robo2*, *Robo3*, and *Robo4* in PAPT analyzed by RNA sequencing ($n = 3$). Relative mRNA expression of, **(B)** *Robo1*, **(C)** *Robo2*, and **(D)** *Robo4* in PAPT analyzed by RT-qPCR ($n = 6$). **(E)** Heat map of differentially expressed 134 mRNAs in PAPT of *Slit2-Tg* mice to wild-type mice (fdr < 0.05,| FC| > 2). **(F)** GO pathway enrichment analysis. Data are presented as mean ± SD. The significant difference among the groups, $^{*}P < 0.05$, $^{**}P < 0.01$.

Activated MAPK Signaling Might Regulates the SLIT2-Mediated Abrogation of Periodontitis

RNA sequencing data detected the expression of total of 53801 genes in mice PAPT (**Supplementary Data S1**). Among those, 134 genes were differentially expressed in *Slit2-Tg* mice. Among 134 genes, 90 were downregulated, and 44 were upregulated (**Figure 6E**). GO pathway enrichment analysis showed the significant changes in expression pattern genes associated with the 22 key signaling pathways related to inflammation, vital cell functions, and others (**Figure 6F**). We further analyzed the expression pattern of various genes associated with the MAPK pathway. RNA-seq data analysis showed a higher expression of *Dusp1, Dusp5, Flna, Hspa1a, Hspa1b, Il1β, MAPK14, Pla2g4b, Pla2g4d*, and *Pla2g4f* in *Slit2-Tg* mice PAPT (**Figure 7A**). Heat map from RNA-seq data of 20 MAPK related genes are shown in **Figure 7B**. Similarly, RT-qPCR result showed 2.1- and 1.6-fold higher expression of *Traf6* and *p38* in PAPT of *Slit2-Tg* mice compared to wild-type mice (**Figures 7B,C**). Western blot analysis showed a 2-fold higher phosphorylation p38 in PAPT of *Slit2-Tg* mice compared to wild-type mice (**Figures 7D (i–iii)**). Our finding indicates the possible role of activated MAPK pathway in SLIT2-mediated effects on periodontitis.

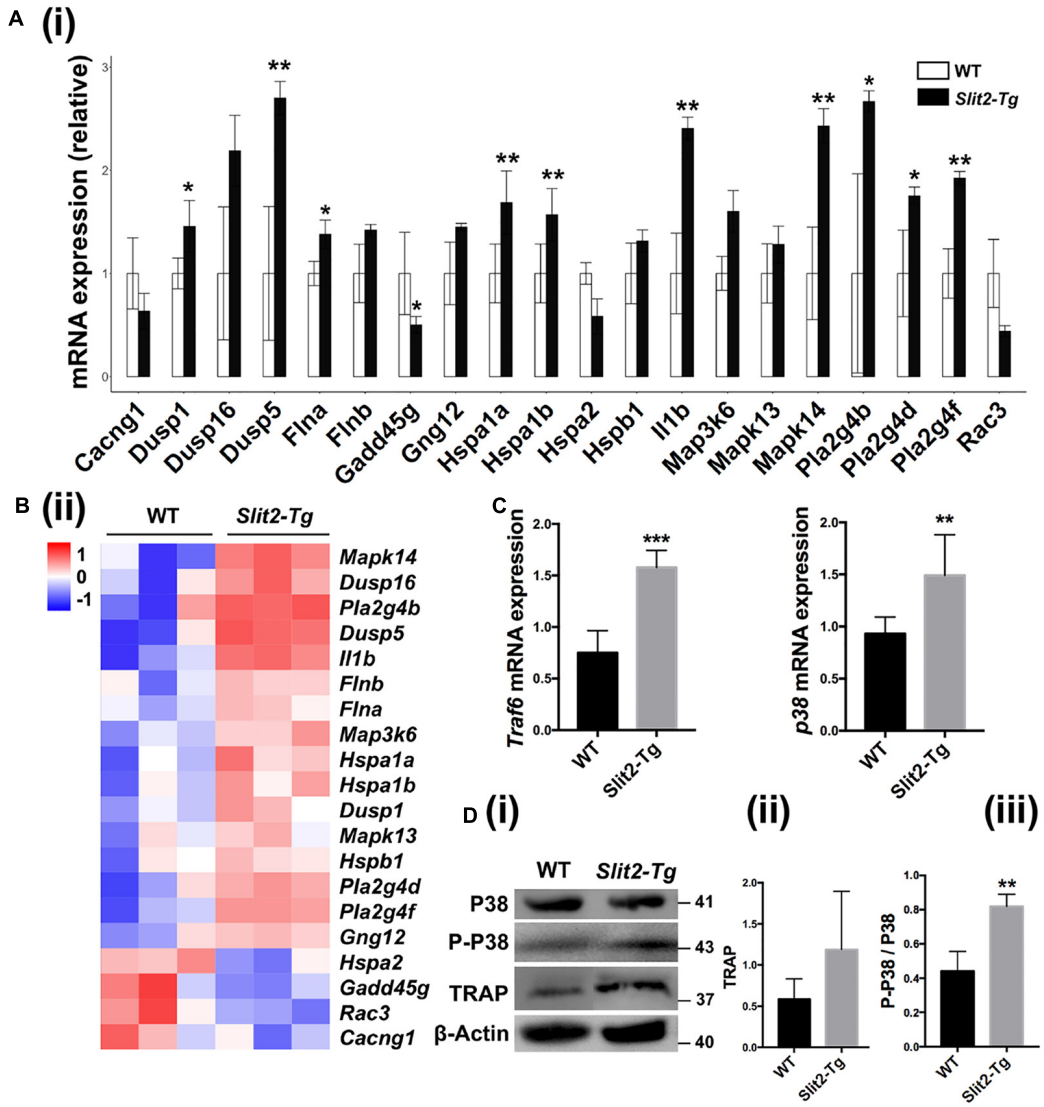


FIGURE 7 | SLIT2 overexpression activates MAPK signaling pathway in periodontitis milieu. **(A (i))** Relative mRNA expression (n = 3), and **(A (ii))** Heat map of the differential expression pattern of MAPK signaling pathway-related genes in PAPT analyzed by RNA sequencing. Relative mRNA expression of **(B)** *Traf6*, and **(C)** *p38* in PAPT analyzed by RT-qPCR (n = 6). **(D (i))** Representative western blot images of MAPK signaling related proteins. **(D (ii), (iii))** Quantitative analysis of TRAP and P-P38 (n = 4). Data are presented as mean ± SD. The significant difference among the groups, $^{*}P < 0.05$, $^{**}P < 0.01$, $^{***}P < 0.001$.

DISCUSSION

Our previous study reported that the higher expression of SLIT2 in cancer tissue of colorectal carcinoma promotes tumor metastasis (Yao et al., 2019). In this study, we found evident upregulation of SLIT2 in periodontitis-affected human gingival tissue, and PAPT of mice, as well as in the serum of periodontitis mice. SLIT2 overexpression did not initiate the periodontitis itself. However, SLIT2 overexpression aggravated the periodontitis and periodontitis-induced alveolar bone loss. SLIT2 intensified the inflammation in PAPT as indicated by higher MVD, and infiltration of leucocytes/macrophages in periodontitis *Slit2*-Tg mice compared to wild-type mice. Expression of proinflammatory markers Cxcr2, IL-18, IL-6, IL-1β, and TNFα were upregulated in PAPT of Slit2-Tg mice. Similarly, PAPT of *Slit2*-Tg mice showed upregulation of osteoclastogenic markers, higher numbers of osteoclasts, and M1 macrophage polarization. SLIT2/ROBO1 axis has been reported to induce proinflammatory properties (Zhao et al., 2014; Yao et al., 2019). ROBO1 receptor was upregulated in PAPT of *Slit2*-Tg mice compared to wild type mice. MAPK signaling is a key regulator of inflammation and osteoclastogenesis (Li et al., 2012; Xu et al., 2020). Expression of MAPK signaling related factors MAPK14 and p-p38 was upregulated in the PAPT of *Slit2*-Tg mice. For the first time, this study reported that the SLIT2 overexpression in periodontal tissue intensifies the periodontitis progression and alveolar bone loss possibly via the activation of MAPK pathway (**Figure 8**).

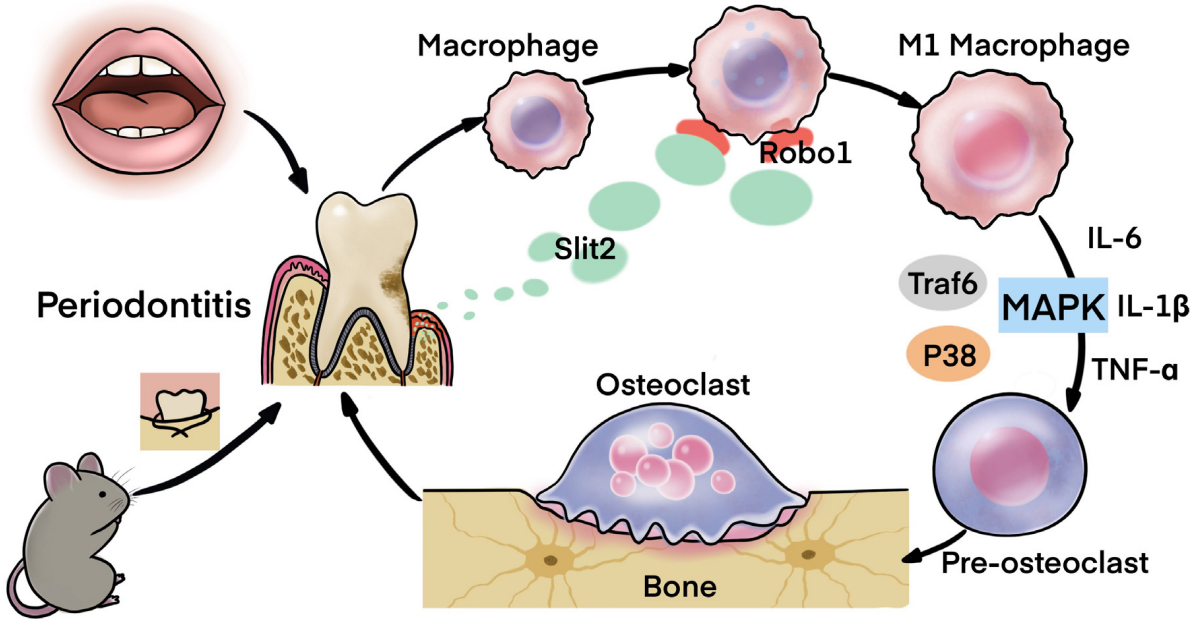


FIGURE 8 | Scheme showing the role of SLIT2 overexpression in pathophysiology of periodontitis.

Literature had reported the overexpression of SLIT2 in various cancers, including gastric, colorectal, and osteosarcoma (Shi et al., 2013; Zhao et al., 2018; Yao et al., 2019). However, the expression pattern of SLIT2 in the inflammatory oral disease periodontitis is still unknown. In this study, we unraveled the >4.0-fold upregulation of SLIT2 protein in periodontitis-affected tissue of human and mice compared to healthy tissue. Our recent study showed around 2.0-fold upregulation of SLIT serum levels in colorectal carcinoma patients (Yao et al., 2019). In the present study, serum SLIT2 level in periodontitis mice was upregulated by 5.0-fold compared to healthy mice indicating systemic upregulation. Although periodontitis is an oral inflammatory disease, it has shown various systemic effects (Papapanou, 2015). This result suggests the possible role of overexpressed SLIT2 on the systemic effects of periodontitis. SLIT2 upregulated pathological condition of hepatocellular carcinoma shows a higher expression of ROBO1. Among the 4 ROBO receptors, ROBO1 was robustly upregulated in PAPT (Avci et al., 2008). Moreover, SLIT2/ROBO4 axis has reported to exert anti-inflammatory signaling and SLIT2/ROBO1 has axis been reported to exert proinflammatory signaling (Zhao et al., 2014). In this study, we found that both SLIT2 and ROBO1 were upregulated in periodontitis, suggesting the possible role of SLIT2/ROBO1 axis on escalation of inflammation and disease progression in periodontitis.

SLIT2 promotes angiogenesis (Li et al., 2015), and the migration of specific cancer cells (Zhao et al., 2016; Yao et al., 2019). SLIT2 has been reported to inhibit neutrophil migration, but enhance eosinophil chemotaxis (Tole et al., 2009; Ye et al., 2010). In this study, SLIT2 increased the MVD and leucocyte/macrophage infiltration in PAPT. Pilling et al. (2019) recently reported the SLIT2 isoform-specific neutrophil chemorepellent and chemoattractant functions. The ∼140-kDa N-terminal Slit2 fragment (Slit2-N) enhances, and the ∼110-kDa N-terminal Slit2 fragment (Slit2-S) inhibits neutrophil migration via binding with same ROBO1 receptor. The neutrophil and macrophage chemoattractant properties of SLIT2 in periodontitis might be the act of Slit2-N fragment. However, further studies illustrating the expression pattern of Slit2-N and Slit2-S and their function on neutrophil/macrophage migration in periodontitis are needed to support this hypothesis.

Disturbed host immune reaction elevates the levels of proinflammatory cytokines such as IL-8, IL-6, IL-1β, and TNF-α in PAPT, creating inflammatory milieu (Pan et al., 2019). These cytokines trigger M1 macrophage polarization, osteoclastogenesis, and immune cell infiltration that escalate inflammation and disease progression in a vicious cycle manner. Overexpression of SLIT2 enhanced the expression of proinflammatory cytokines IL-18, IL-6, IL-1β, and TNF-α. Moreover, PAPT of *Slit2*-Tg mice showed a higher degree of M1 macrophage polarization. Higher numbers of leucocytes and macrophages were infiltrated in PAPT of *Slit2*-Tg mice. Upregulation of osteoclastogenic markers *Acp5, Ctsk* and *Nfatc1*, and higher numbers of osteoclasts were observed in PAPT of *Slit2*-Tg mice. We did not witness the direct effect of SLIT2 on osteoblast function during periodontitis. SLIT2 has been reported to inhibit osteoclastogenesis and osteoblast differentiation *in vitro* (Sun et al., 2009; Park et al., 2019). The majority of pathophysiological parameters of the periodontitis were affected by SLIT2 overexpression, indicating the vital role of SLIT2 to on periodontitis progression. Our results suggest that the SLIT2-induced inflammation-mediated osteoclastogenesis might cause alveolar bone loss in periodontitis.

SLIT2 modulates MAPK signaling to regulate the various cell functions (Li et al., 2015; Xu et al., 2018; Zhao et al., 2018). MAPK signaling is a vital regulator of inflammation and pathophysiology of periodontitis (Li et al., 2012; Xu et al., 2020). GO enrichment pathway analysis of top 134 differentially expressed mRNAs in periodontitis-affected tissue of *Slit2*-Tg mice revealed the significant upregulation of MAPK signaling related genes. We further elucidated that the P-p38 was significantly upregulated in PAPT of *Slit2*-Tg mice. Along with MAPK signaling related genes, leucocytes, monocytes, and mononuclear cell chemotaxis/migration-related genes were also significantly upregulated in PAPT of *Slit2*-Tg mice. These findings further support the possible role of MAPK signaling on SLIT2-mediated effects on periodontitis.

In this study, we unraveled the higher expression of the SLIT2 in clinical gingival tissues of periodontitis patients. We further elucidated the higher SLIT2 expression in PAPT and serum of periodontitis mice. This result suggests SLIT2 as a possible diagnostic marker of periodontitis. *Slit2*-Tg periodontitis mice model unveiled the role of SLIT2 on the escalation of disease pathophysiology. This study opens the new research direction in the role of SLIT2 on the pathophysiology of inflammatory diseases. A limitation of this study is that we did not analyze which isotope of SLIT2 regulates the pathophysiology of periodontitis and whether ROBO1 is the key receptor for SLIT2-mediated effect on periodontitis. Another limitation of this study is that we did not meticulously analyze the role of MAPK in SLIT2-mediated escalation of inflammation and osteoclastogenesis. However, our ongoing study on Robo1 knockout periodontitis mice will address these limitations.

CONCLUSION

SLIT2 was overexpressed during periodontitis. Overexpression of SLIT2 in periodontitis escalated inflammation, lymphocyte/macrophage infiltration, M1 macrophage polarization, osteoclastogenesis, alveolar bone loss, and disease progression. SLIT2 overexpression upregulated Robo1 and MAPK signaling related factors' expression in PAPT during periodontitis. Our results suggest the possible role of SLIT2/ROBO1 signaling of the pathophysiology of periodontitis via activation of MAPK p38 signaling.

DATA AVAILABILITY STATEMENT

RNAseq data was uploaded to NCBI SRA database (SRA accession: PRJNA639904), https://www.ncbi.nlm.nih.gov/bioproject/PRJNA639904/.

ETHICS STATEMENT

The studies involving human participants were reviewed and approved by The Medical Ethics Committee of the Affiliated Stomatology Hospital of Guangzhou Medical University. The patients/participants provided their written informed consent to participate in this study. The animal study was reviewed and approved by The Experimental Animal Ethics Committee of Guangzhou Medical University. Written informed consent was obtained from the individual(s) for the publication of any potentially identifiable images or data included in this article.

AUTHOR CONTRIBUTIONS

LG, LJW, LPW, JZ, and JP: study design. JZ, YC, DL, LY, HS, and MZ: experimental conduct. JZ, YC, DL, LY, HS, LHW, LL, SD, YY, and DH: animal work. JZ, JP, YC, DL, LY, and HS: data collection, analysis and interpretation. JZ and JP: manuscript preparation. All authors approved the final version of the manuscript.

FUNDING

This study was supported by the Department of Education of Guangdong Province (2018KTSCX186), Bureau of Technology Industry Business and Information of Liwan District, Guangzhou city (201804015), and the High-Level University Construction Talents of Guangzhou Medical University of China (B185006003014 and B195002003017).

SUPPLEMENTARY MATERIAL

The Supplementary Material for this article can be found online at: https://www.frontiersin.org/articles/10.3389/fcell.2020.00593/full#supplementary-material

REFERENCES

Abe, T., and Hajishengallis, G. (2013). Optimization of the ligature-induced periodontitis model in mice. *J. Immunol. Methods* 394, 49–54. doi: 10.1016/j.jim.2013.05.002

AlQranei, M. S., and Chellaiah, M. A. (2020). Osteoclastogenesis in periodontal diseases: possible mediators and mechanisms. *J. Oral. Biosci.* doi: 10.1016/j.job.2020.02.002 [Online ahead of print]

Aspriello, S. D., Zizzi, A., Lucarini, G., Rubini, C., Faloia, E., Boscaro, M., et al. (2009). Vascular endothelial growth factor and microvessel density in periodontitis patients with and without diabetes. *J. Periodontol.* 80, 1783–1789. doi: 10.1902/jop.2009.090239

Avci, M. E., Konu, O., and Yagci, T. (2008). Quantification of SLIT-ROBO transcripts in hepatocellular carcinoma reveals two groups of genes with coordinate expression. *BMC Cancer* 8:392. doi: 10.1186/1471-2407-8-392

Chang, J., Lan, T., Li, C., Ji, X., Zheng, L., Gou, H., et al. (2015). Activation of Slit2-Robo1 signaling promotes liver fibrosis. *J. Hepatol.* 63, 1413–1420. doi: 10.1016/j.jhep.2015.07.033

Chaturvedi, S., and Robinson, L. A. (2015). Slit2-Robo signaling in inflammation and kidney injury. *Pediatr. Nephrol.* 30, 561–566. doi: 10.1007/s00467-014-2825-4

Cochran, D. L. (2008). Inflammation and bone loss in periodontal disease. *J. Periodontol.* 79(8 Suppl), 1569–1576. doi: 10.1902/jop.2008.080233

Darveau, R. P. (2010). Periodontitis: a polymicrobial disruption of host homeostasis. *Nat. Rev. Microbiol.* 8, 481–490. doi: 10.1038/nrmicro2337

Fernando, R., Grisolia, A. B. D., Lu, Y., Atkins, S., and Smith, T. J. (2018). Slit2 Modulates the Inflammatory Phenotype of Orbit-Infiltrating Fibrocytes

in Graves' Disease. *J. Immunol.* 200, 3942–3949. doi: 10.4049/jimmunol.1800259

Frazee, A. C., Pertea, G., Jaffe, A. E., Langmead, B., Salzberg, S. L., and Leek, J. T. (2015). Ballgown bridges the gap between transcriptome assembly and expression analysis. *Nat. Biotechnol.* 33, 243–246. doi: 10.1038/nbt.3172

Gonzalez, O. A., Novak, M. J., Kirakodu, S., Stromberg, A., Nagarajan, R., Huang, C. B., et al. (2015). Differential gene expression profiles reflecting macrophage polarization in aging and periodontitis gingival tissues. *Immunol. Invest.* 44, 643–664. doi: 10.3109/08820139.2015.1070269

Hajishengallis, G. (2014). Immunomicrobial pathogenesis of periodontitis: keystones, pathobionts, and host response. *Trends Immunol.* 35, 3–11. doi: 10.1016/j.it.2013.09.001

Kassebaum, N. J., Bernabe, E., Dahiya, M., Bhandari, B., Murray, C. J., and Marcenes, W. (2014). Global burden of severe periodontitis in 1990-2010: a systematic review and meta-regression. *J. Dent. Res.* 93, 1045–1053. doi: 10.1177/0022034514552491

Kim, D., Langmead, B., and Salzberg, S. L. (2015). HISAT: a fast spliced aligner with low memory requirements. *Nat. Methods* 12, 357–360. doi: 10.1038/nmeth.3317

Li, C., Yang, G., Lin, L., Xuan, Y., Yan, S., Ji, X., et al. (2019). Slit2 signaling contributes to cholestatic fibrosis in mice by activation of hepatic stellate cells. *Exp. Cell Res.* 385:111626. doi: 10.1016/j.yexcr.2019.111626

Li, Q., Valerio, M. S., and Kirkwood, K. L. (2012). MAPK usage in periodontal disease progression. *J. Signal. Transduct* 2012:308943. doi: 10.1155/2012/308943

Li, S., Huang, L., Sun, Y., Bai, Y., Yang, F., Yu, W., et al. (2015). Slit2 promotes angiogenic activity via the Robo1-VEGFR2-ERK1/2 pathway in both in vivo and in vitro studies. *Invest. Ophthalmol. Vis. Sci.* 56, 5210–5217. doi: 10.1167/iovs-14-16184

Liu, J., Hou, W., Guan, T., Tang, L., Zhu, X., Li, Y., et al. (2018). Slit2/Robo1 signaling is involved in angiogenesis of glomerular endothelial cells exposed to a diabetic-like environment. *Angiogenesis* 21, 237–249. doi: 10.1007/s10456-017-9592-3

Martin, M. (2011). Cutadapt removes adapter sequences from high-throughput sequencing reads. *EMBnet.journal* 17, 10–12.

Mizraji, G., Segev, H., Wilensky, A., and Hovav, A. H. (2013). Isolation, processing and analysis of murine gingival cells. *J. Vis. Exp.* 77:e50388. doi: 10.3791/50388

Pan, W., Wang, Q., and Chen, Q. (2019). The cytokine network involved in the host immune response to periodontitis. *Int. J. Oral Sci.* 11:30. doi: 10.1038/s41368-019-0064-z

Papapanou, P. N. (2015). Systemic effects of periodontitis: lessons learned from research on atherosclerotic vascular disease and adverse pregnancy outcomes. *Int. Dent. J.* 65, 283–291. doi: 10.1111/idj.12185

Park, S. J., Lee, J. Y., Lee, S. H., Koh, J. M., and Kim, B. J. (2019). SLIT2 inhibits osteoclastogenesis and bone resorption by suppression of Cdc42 activity. *Biochem. Biophys. Res. Commun.* 514, 868–874. doi: 10.1016/j.bbrc.2019.05.046

Pertea, M., Pertea, G. M., Antonescu, C. M., Chang, T. C., Mendell, J. T., and Salzberg, S. L. (2015). StringTie enables improved reconstruction of a transcriptome from RNA-seq reads. *Nat. Biotechnol.* 33, 290–295. doi: 10.1038/nbt.3122

Pilling, D., Chinea, L. E., Consalvo, K. M., and Gomer, R. H. (2019). Different isoforms of the neuronal guidance molecule slit2 directly cause chemoattraction or chemorepulsion of human neutrophils. *J. Immunol.* 202, 239–248. doi: 10.4049/jimmunol.1800681

Richards, D. (2014). Review finds that severe periodontitis affects 11% of the world population. *Evid. Based Dent.* 15, 70–71. doi: 10.1038/sj.ebd.6401037

Rodriguez, J. C., Gonzalez, G. A., Fresno, C., Llera, A. S., and Fernandez, E. A. (2016). Improving information retrieval in functional analysis. *Comput. Biol. Med.* 79, 10–20. doi: 10.1016/j.compbiomed.2016.09.017

Schmid, B. C., Rezniczek, G. A., Fabjani, G., Yoneda, T., Leodolter, S., and Zeillinger, R. (2007). The neuronal guidance cue Slit2 induces targeted migration and may play a role in brain metastasis of breast cancer cells. *Breast Cancer Res. Treat.* 106, 333–342. doi: 10.1007/s10549-007-9504-0

Shi, R., Liu, W., Liu, B., Xu, Z., Chen, L., and Zhang, Z. (2013). Slit2 expression and its correlation with subcellular localization of beta-catenin in gastric cancer. *Oncol. Rep.* 30, 1883–1889. doi: 10.3892/or.2013.2662

Spiller, K. L., Wrona, E. A., Romero-Torres, S., Pallotta, I., Graney, P. L., Witherel, C. E., et al. (2016). Differential gene expression in human, murine, and cell line-derived macrophages upon polarization. *Exp. Cell Res.* 347, 1–13. doi: 10.1016/j.yexcr.2015.10.017

Sun, H., Dai, K., Tang, T., and Zhang, X. (2009). Regulation of osteoblast differentiation by slit2 in osteoblastic cells. *Cells Tissues Organs* 190, 69–80. doi: 10.1159/000178020

Tole, S., Mukovozov, I. M., Huang, Y. W., Magalhaes, M. A., Yan, M., Crow, M. R., et al. (2009). The axonal repellent, Slit2, inhibits directional migration of circulating neutrophils. *J. Leukoc. Biol.* 86, 1403–1415. doi: 10.1189/jlb.0609391

Wang, B., Xiao, Y., Ding, B. B., Zhang, N., Yuan, X., Gui, L., et al. (2003). Induction of tumor angiogenesis by Slit-Robo signaling and inhibition of cancer growth by blocking Robo activity. *Cancer Cell* 4, 19–29. doi: 10.1016/s1535-6108(03)00164-8

Wang, L., Guan, N., Jin, Y., Lin, X., and Gao, H. (2015). Subcutaneous vaccination with Porphyromonas gingivalis ameliorates periodontitis by modulating Th17/Treg imbalance in a murine model. *Int. Immunopharmacol.* 25, 65–73. doi: 10.1016/j.intimp.2015.01.007

Wang, L. J., Zhao, Y., Han, B., Ma, Y. G., Zhang, J., Yang, D. M., et al. (2008). Targeting Slit-Roundabout signaling inhibits tumor angiogenesis in chemical-induced squamous cell carcinogenesis. *Cancer Sci.* 99, 510–517. doi: 10.1111/j.1349-7006.2007.00721.x

Wong, K., Park, H. T., Wu, J. Y., and Rao, Y. (2002). Slit proteins: molecular guidance cues for cells ranging from neurons to leukocytes. *Curr. Opin. Genet. Dev.* 12, 583–591. doi: 10.1016/s0959-437x(02)00343-x

Wu, J. Y., Feng, L., Park, H. T., Havlioglu, N., Wen, L., Tang, H., et al. (2001). The neuronal repellent Slit inhibits leukocyte chemotaxis induced by chemotactic factors. *Nature* 410, 948–952. doi: 10.1038/35073616

Xiao, E., Mattos, M., Vieira, G. H. A., Chen, S., Correa, J. D., Wu, Y., et al. (2017). Diabetes Enhances IL-17 expression and alters the oral microbiome to increase its pathogenicity. *Cell Host Microbe* 22:120-128.e4. doi: 10.1016/j.chom.2017.06.014

Xu, R., Qin, N., Xu, X., Sun, X., Chen, X., and Zhao, J. (2018). Inhibitory effect of SLIT2 on granulosa cell proliferation mediated by the CDC42-PAKs-ERK1/2 MAPK pathway in the prehierarchical follicles of the chicken ovary. *Sci. Rep.* 8:9168. doi: 10.1038/s41598-018-27601-z

Xu, W., Chen, X., Wang, Y., Fan, B., Guo, K., Yang, C., et al. (2020). Chitooligosaccharide inhibits RANKL-induced osteoclastogenesis and ligation-induced periodontitis by suppressing MAPK/ c-fos/NFATC1 signaling. *J. Cell. Physiol.* 235, 3022–3032. doi: 10.1002/jcp.29207

Yang, X. M., Han, H. X., Sui, F., Dai, Y. M., Chen, M., and Geng, J. G. (2010). Slit-Robo signaling mediates lymphangiogenesis and promotes tumor lymphatic metastasis. *Biochem. Biophys. Res. Commun.* 396, 571–577. doi: 10.1016/j.bbrc.2010.04.152

Yao, Y., Zhou, Z., Li, L., Li, J., Huang, L., Li, J., et al. (2019). Activation of Slit2/Robo1 Signaling Promotes Tumor Metastasis in Colorectal Carcinoma through Activation of the TGF-beta/Smads Pathway. *Cells* 8:635. doi: 10.3390/cells8060635

Ye, B. Q., Geng, Z. H., Ma, L., and Geng, J. G. (2010). Slit2 regulates attractive eosinophil and repulsive neutrophil chemotaxis through differential srGAP1 expression during lung inflammation. *J. Immunol.* 185, 6294–6305. doi: 10.4049/jimmunol.1001648

Yu, T., Zhao, L., Huang, X., Ma, C., Wang, Y., Zhang, J., et al. (2016). Enhanced Activity of the Macrophage M1/M2 Phenotypes and Phenotypic Switch to M1 in periodontal infection. *J. Periodontol.* 87, 1092–1102. doi: 10.1902/jop.2016.160081

Yuan, W., Zhou, L., Chen, J. H., Wu, J. Y., Rao, Y., and Ornitz, D. M. (1999). The mouse SLIT family: secreted ligands for ROBO expressed in patterns that suggest a role in morphogenesis and axon guidance. *Dev. Biol.* 212, 290–306. doi: 10.1006/dbio.1999.9371

Zhang, Z., Yuan, W., Deng, J., Wang, D., Zhang, T., Peng, L., et al. (2020). Granulocyte colony stimulating factor (G-CSF) regulates neutrophils infiltration and periodontal tissue destruction in an experimental periodontitis. *Mol. Immunol.* 117, 110–121. doi: 10.1016/j.molimm.2019.11.003

Zhao, H., Anand, A. R., and Ganju, R. K. (2014). Slit2-Robo4 pathway modulates lipopolysaccharide-induced endothelial inflammation and its expression is dysregulated during endotoxemia. *J. Immunol.* 192, 385–393. doi: 10.4049/jimmunol.1302021

Zhao, S. J., Shen, Y. F., Li, Q., He, Y. J., Zhang, Y. K., Hu, L. P., et al. (2018). SLIT2/ROBO1 axis contributes to the Warburg effect in osteosarcoma through

activation of SRC/ERK/c-MYC/PFKFB2 pathway. *Cell Death Dis.* 9:390. doi: 10.1038/s41419-018-0419-y

Zhao, Y., Su, Y., and Ye, L. (2012). Slit-Robo: a potential way to treat periodontitis. *Med. Hypotheses* 79, 186–188. doi: 10.1016/j.mehy.2012.04.030

Zhao, Y., Zhou, F. L., Li, W. P., Wang, J., and Wang, L. J. (2016). Slit2Robo1 signaling promotes the adhesion, invasion and migration of tongue carcinoma cells via upregulating matrix metalloproteinases 2 and 9, and downregulating Ecadherin. *Mol. Med. Rep.* 14, 1901–1906. doi: 10.3892/mmr.2016.5518

Zhou, L. N., Bi, C. S., Gao, L. N., An, Y., Chen, F., and Chen, F. M. (2019). Macrophage polarization in human gingival tissue in response to periodontal disease. *Oral Dis.* 25, 265–273. doi: 10.1111/odi.12983

Zhou, W. J., Geng, Z. H., Chi, S., Zhang, W., Niu, X. F., Lan, S. J., et al. (2011). Slit-Robo signaling induces malignant transformation through Hakai-mediated E-cadherin degradation during colorectal epithelial cell carcinogenesis. *Cell Res.* 21, 609–626. doi: 10.1038/cr.2011.17

Zhou, X., Yao, Q., Sun, X., Gong, X., Yang, Y., Chen, C., et al. (2017). Slit2 ameliorates renal inflammation and fibrosis after hypoxia-and lipopolysaccharide-induced epithelial cells injury in vitro. *Exp. Cell Res.* 352, 123–129. doi: 10.1016/j.yexcr.2017.02.001

Zhu, L. F., Li, L., Wang, X. Q., Pan, L., Mei, Y. M., Fu, Y. W., et al. (2019). M1 macrophages regulate TLR4/AP1 via paracrine to promote alveolar bone destruction in periodontitis. *Oral Dis.* 25, 1972–1982. doi: 10.1111/odi.13167

Conflict of Interest: The authors declare that the research was conducted in the absence of any commercial or financial relationships that could be construed as a potential conflict of interest.

Copyright © 2020 Wang, Zheng, Pathak, Chen, Liang, Yang, Sun, Zhong, Wu, Li, Deng, Zheng, Yan, Hou, Wang and Ge. This is an open-access article distributed under the terms of the Creative Commons Attribution License (CC BY). The use, distribution or reproduction in other forums is permitted, provided the original author(s) and the copyright owner(s) are credited and that the original publication in this journal is cited, in accordance with accepted academic practice. No use, distribution or reproduction is permitted which does not comply with these terms.

frontiers in Cell and Developmental Biology

REVIEW
published: 22 July 2020
doi: 10.3389/fcell.2020.00619

The Application of MSCs-Derived Extracellular Vesicles in Bone Disorders: Novel Cell-Free Therapeutic Strategy

Shuyu Liu[1,2,3,4†], Xia Xu[1,2,3,4†], Shujing Liang[1,2,3,4†], Zhihao Chen[1,2,3,4], Yan Zhang[1,2,3,4], Airong Qian[1,2,3,4] and Lifang Hu[1,2,3,4*]*

[1] Laboratary for Bone Metabolism, Key Lab for Space Biosciences and Biotechnology, School of Life Sciences, Northwestern Polytechnical University, Xi'an, China, [2] Xi'an Key Laboratory of Special Medicine and Health Engineering, School of Life Sciences, Northwestern Polytechnical University, Xi'an, China, [3] Research Center for Special Medicine and Health Systems Engineering, School of Life Sciences, Northwestern Polytechnical University, Xi'an, China, [4] NPU-UAB Joint Laboratory for Bone Metabolism, School of Life Sciences, Northwestern Polytechnical University, Xi'an, China

OPEN ACCESS

Edited by:
Chao Liang,
Hong Kong Baptist University,
Hong Kong

Reviewed by:
Wei Seong Toh,
National University of Singapore,
Singapore
Xu Zhang,
Jiangsu University, China
Elena Jones,
University of Leeds, United Kingdom

***Correspondence:**
Airong Qian
qianair@nwpu.edu.cn
Lifang Hu
hulifang@nwpu.edu.cn

[†] These authors have contributed equally to this work

Specialty section:
This article was submitted to Molecular Medicine, a section of the journal Frontiers in Cell and Developmental Biology

Received: 09 March 2020
Accepted: 22 June 2020
Published: 22 July 2020

Citation:
Liu S, Xu X, Liang S, Chen Z, Zhang Y, Qian A and Hu L (2020) The Application of MSCs-Derived Extracellular Vesicles in Bone Disorders: Novel Cell-Free Therapeutic Strategy. Front. Cell Dev. Biol. 8:619. doi: 10.3389/fcell.2020.00619

Bone is crucial for supporting the body, protecting other organs, providing minerals, and secreting hormone to regulate other organ's function. Bone disorders result in pain and disability, severely affecting human health, reducing the quality of life and increasing costs to society. With the rapid increase in the aging population worldwide, bone disorders have become one major disease. As a result, efficacious therapies of bone disorders have become the focus of attention worldwide. Mesenchymal stem cells (MSCs) have been widely explored as a new therapeutic method for numerous diseases. Recent evidence suggests that the therapeutic effects of MSCs are mainly mediated by their extracellular vesicles (EV). MSCs-derived extracellular vesicles (MSCs-EV) is indicated as a novel cell-free alternative to cell therapy with MSCs in regenerative medicine. Here, we review the current knowledge of EV and highlight the application studies of MSCs-EV in bone disorders by focusing on osteoarthritis (OA), rheumatoid arthritis (RA), osteoporosis (OP), and bone fracture. Moreover, we discuss the key issues and perspectives of MSCs-EV as a clinical therapeutic strategy for bone diseases.

Keywords: mesenchymal stem cells, extracellular vesicles, exosomes, osteoarthritis, rheumatoid arthritis, osteoporosis, bone fracture

INTRODUCTION

Bone, one most important supportive structure of human body, plays important roles in supporting body, protecting other organs, providing minerals and secreting hormone to regulate other organs. Bone disorders have a serious impact on human health and have become common diseases among the elderly. Therefore, appropriate and effective treatment of bone diseases is one of the greatest concerns in the world today.

Mesenchymal stem cells (MSCs) are multipotent fibroblast-like cells with the potential for self-renewal and multilineage differentiation. Moreover, MSCs possess the ability to migrate to the damaged sites, where they secret anti-inflammatory factors and growth factors to promote wound healing. Thus, MSCs have become a desirable cell source in regenerative medicine and immune

therapy. MSCs transplant treatment (MSCT) is considered to be a promising therapy for a variety of human diseases and has drawn increasing attention. However, the direct use of MSCs for treating diseases faces many challenges, including genetic instability (Yoon et al., 2004; Tolar et al., 2007; Jeong et al., 2011), loss of function (Pak et al., 2003), pathogenicity (Furlani et al., 2009), and limited cell survival (Breitbach et al., 2007).

Recent evidence suggest that MSCs exert their therapeutic capabilities primarily through paracrine secretion of particles, rather than a cellular manner (Wang et al., 2015; Cosenza et al., 2017; Zhou Y. et al., 2019). The secreted particles are collectively referred to as extracellular vesicles (EV), which are usually classified as exosomes, microvesicles (MV), and apoptotic bodies based on different biogenesis way (Yáñez-Mó et al., 2015). Due to the lack of consensus on specific markers for EV subtypes, ISEV recommends the usage of EV, a collective term covering various EV subtypes (Thery et al., 2018). MSCs-derived extracellular vesicles (MSCs-EV) emerge as critical mediators of paracrine effects, with increasing evidence for their function in MSCs-mediated regeneration and immunotherapy (Li et al., 2013; Xin et al., 2013; Tan et al., 2014; Zhao et al., 2018; Biswas et al., 2019; Zhang S. et al., 2019). MSCs-EV regulate the function of recipient cells by transmitting information carried by lipids, nucleic acids and proteins, which are the main components of MSCs-EV (Yáñez-Mó et al., 2015). Compared with MSCT, MSCs-EV treatment show advantages of higher security, convenient storage, transportation and administration (Jing et al., 2018). Therefore, MSCs-EV has received increasing attention for its promising clinical application (Toh et al., 2017; Willis et al., 2018; Romanelli et al., 2019).

Here, we review the current knowledge of extracellular vesicles (EV) and MSCs-derived extracellular vesicles (MSCs-EV), and highlight the application studies of MSCs-EV for treatment of bone disorders by focusing on osteoarthritis (OA), rheumatoid arthritis (RA), osteoporosis (OP), and bone fracture. Furthermore, we discuss the key issues of MSCs-EV for clinical application.

Abbreviations: β-TCP, β-tricalcium phosphate; AD-MSCs, adipose tissue-derived mesenchymal stem cells; AFM, atomic-force microscopy; AKT, phosphorylation of protein-serine-threonine kinase; ALP, alkaline phosphatase; AMPK, adenosine 5'-monophosphate (AMP)-activated protein kinase; BFR/BS, bone formation rate per bone Surface; BMD, bone mineral density; BM-MSCs, bone marrow mesenchymal stem cells; BV/TV, bone volume/total volume; CIA, collagen-induced arthritis; Col2a1, collagen, type II, alpha 1; Dnmt1, DNA methyltransferase 1; DLS, dynamic-light scattering; ECM, extracellular matrix; ECM/GelMA/exosome, extracellular matrix/gelatin methacrylate/exosome; ERK 1/2, extracellular regulated protein kinases 1/2; ESCRT, endosomal sorting complex required for transport; EV, extracellular vesicles; FLS, fibroblast-like synoviocytes; GAPDH, glyceraldehyde-3-phosphate dehydrogenase; hESC-MSCs, human embryonic-derived mesenchymal stem cells; hiPSC, human-induced pluripotent stem cell; hMSC, human mesenchymal stem cells; HLA-DR, Antigen-antigen D Related; HSP, heat shock proteins; IL-1α, interleukin-1α; IL-1β, interleukin-1β; ILVs, intraluminal vesicles; IPFP-MSCs, infrapatellar fat pad (IPFP)-derived mesenchymal stem cells; LDHA, lactic dehydrogenase A; lncRNA, long non-coding RNA; MAPK, mitogen-activated protein kinase; MAR, mineral apposition rate; MCP-1, monocyte chemotactic protein 1; MCP-3, monocyte chemotactic protein 3; MHC, major histocompatibility complex; miRNAs, microRNAs; MMP13, matrix metalloproteinase 13; MMP14, matrix metalloproteinase 14; mRNAs, message RNAs; MSCs, mesenchymal stem cells; MSCT, MSCs transplant treatment; mtDNA, mitochondrial DNA; mTOR, mammalian target of rapamycin; MV, microvesicles; MVBs, multivesicular bodies; NTA, nanoparticle-tracking analyses; NGS, next-generation sequencing; OA, osteoarthritis; OP, osteoporosis; PGK1, phosphoglycerate kinase 1; PI3K/AKT, phosphatidylinositol-3-kinases/protein-serine-threonine kinase; PKM, protein kinase; PM, plasma membrane; PCS, photon-correlation spectroscopy; RA, rheumatoid arthritis; ROS, reactive oxygen species; Runx2, Runt-related transcription factor 2; SDF-1, stromal cell-derived factor-1; s-GAG, sulphated glycosaminoglycan; SMSCs, synovial mesenchymal stem cells; Sp1, specificity Protein 1; TGF-β1, transforming growth factor β1; TEM, transmission electron microscopy; Th1, T helper cell type 1; Th17, T helper cell type 17; Th2, T helper cell type 2; TMJ-OA, temporomandibular joint osteoarthritis; TNF-α, tumor necrosis factor-α; TRPS, tunable-resistive pulse sensing; uMSCs, umbilical cord mesenchymal stem cells; VEGF, vascular endothelial growth factor; YAP, yes-associated protein.

EXTRACELLULAR VESICLES (EV)

EV: Definition, Classification, and Function

Exosomes are a type of EV and the term "exosome" was first adopted by Trams et al. (1981) and refers to the EV formed by the endosomal system (Harding et al., 1983; Pan and Johnstone, 1983). Although the word "exosome" is commonly seen in literature, it is difficult to obtain purified exosomes, which make "exosome" ambiguous. Therefore, the International Society for Extracellular Vesicles (ISEV) has proposed minimal information for studies of extracellular vesicles 2018 (MISEV2018) in relation to the nomenclature of EV, which is defined for particles naturally released from the cell that are delimited by a lipid bilayer and cannot replicate (Thery et al., 2018). Since there is still lack of consensus on specific markers of EV subtypes, such as exosomes and ectosomes, the ISEV recommends the usage of EV, a collective term covering various subtypes of cell-released, membranous structures, called exosomes, microvesicles, microparticles, ectosomes, oncosomes, apoptotic bodies, and many other names (Thery et al., 2018). According to the uncertainty of what types of vesicles have been studied in many studies, in this review, we use the word "EV" and use the term as mentioned in the original work.

There is a different classification of EV proposed by different literature, ranging from two to six major different EV types (Cocucci et al., 2009; Thery et al., 2009; Beyer and Pisetsky, 2010; Mathivanan et al., 2010). However, due to the difficulty met in practice (e.g., the vesicles' preparations are heterogeneous) and insufficient evidence for some EV types, van der Pol et al. (2012) have proposed four different types of eukaryotic cell-derived EV: (1) endosome-origin exosomes (50–100 nm); (2) plasma membrane-derived MV (20–1000 nm); (3) plasma membrane-derived membrane particles (50–600 nm); and (4) apoptotic vesicles (1000–5000 nm) from the plasma membrane and endoplasmic reticulum. However, at present, there is still no consensus on the classification of EV as stated by ISEV (Thery et al., 2018).

As particles naturally secreted from the cell, EV has been identified as vital mediators of paracrine communication (Batiz et al., 2015; Jing et al., 2018) and demonstrated a key role in different processes, such as angiogenesis (Qi et al., 2016), antigen presentation (Shenoda and Ajit, 2016), apoptosis (Qi et al., 2019), coagulation (Fricke et al., 2017), cellular homeostasis (Takahashi et al., 2017), inflammation (Zhang S. et al., 2019).

EV is involved in numerous biological processes, including intercellular signaling, cell adhesion, waste management and protection against stress, coagulation, and vascular function and integrity, which has been summarized comprehensively by van der Pol et al. (2012).

Biogenesis and Components of EV

Different type of EV is generated through different way and contains different cargos, which depends on the cell types and the physiological conditions. The biogenesis of exosomes is well-studied, which involves the exocytosis of multivesicular endosomes (**Figure 1**). Generally, the biogenesis of exosome contains three phases: endocytosis, multivesicular body (MVB) development, and release (**Figure 1**) (Gurunathan et al., 2019). At the beginning, endocytic vesicles are produced from the plasma membrane (PM) to become early endosomes, which then develop into late endosomes via endosomal membrane budding inward to form intraluminal vesicles (ILVs). Subsequently, the late endosomes constantly bud inward and form ILVs, which keep accumulating and constitute MVBs. Finally, the MVBs may either be degraded by lysosome, or fuse with the plasma membrane to permit the ILVs to be released into the extracellular environment. The released vesicles are called exosomes (**Figure 1**) (van Niel et al., 2006; Dong et al., 2019). The exosomes play crucial roles in intercellular communication by regulating the recipient cell function. There are mainly three ways for exosomes regulating recipient cell function. First, exosomes interact with the membrane receptors of the recipient cell to activate the signaling cascade in the cell. Second, the endocytosis occurs in the recipient cell to ingurgitate the exosomes. Third, exosomes integrate own cargos with recipient cell membrane, then transfer the lipids, nucleic acids (mRNAs and miRNAs) and proteins through membrane fusion or by an endocytosis pathway, leading to numerous biological processes (**Figure 1**) (Yáñez-Mó et al., 2015).

At present, the well-known mechanism of exosome generation is driven by the endosomal sorting complex required for transport (ESCRT), which consists of approximately 30 proteins that form four complexes (ESCRT-0, ESCRT-I, ESCRT-II, ESCRT-III) with associated proteins including vacuolar protein sorting-associated protein 4 (VPS4), vesicle trafficking 1 (VTA-1), and apoptosis-linked gene 2 (ALG-2)-interacting protein X (Alix) (Hanson and Cashikar, 2012). They give the exosomes membrane a flexible state, which make exosomes be transported through the cytoplasm. Moreover, ESCRT-independent mechanism has been demonstrated for exosome biogenesis and secretion, in which way, although the four subunits of ESCRTs are silent, MVBs can still be generated (Trajkovic et al., 2008; Frydrychowicz et al., 2015). The review written by Colombo et al. (2014) provides a comprehensive understanding of the mechanism of exosome biogenesis.

Extracellular vesicles contain markers from the parent cells and therefore their subtypes can be identified and characterized. Specific markers in exosomes are mainly located at the membrane, including the tetraspanin family (CD81, CD82, CD63, and CD9), major histocompatibility complex (MHC), and lipid raft such as Flotillin-1 (**Figure 2**). Moreover, heat shock proteins (HSP) and the proteins related with MVB biogenesis are also markers for exosomes (**Figure 2**). Besides these membrane molecules, there are other proteins and nucleic acids within the exosomes. The proteins are mainly related with MVBs biogenesis (Alix, TSG101, and clathrn), cytoskeleton (actin, tubulin, syntenin, and moesin), metabolism [GAPDH (Glyceraldehyde-3-phosphate dehydrogenase), LDHA (Lactic dehydrogenase A), PGK1 (Phosphoglycerate kinase 1), aldolase, and PKM (protein kinase)], membrane transport and fusion (Rab GTPases, annexins, and flotillins), and signal transduction (kinase proteins) (Chaput and Thery, 2011; Ohno et al., 2013; Raposo and Stoorvogel, 2013). The nucleic acids in exosomes are mainly mRNA, miRNA, long non-coding RNA (lncRNA), and DNA. Besides, various lipid compounds are found in exosomes, such as ceramide, sphingomyelin, phosphatidyl choline, phosphatidylserine, phosphatidyl ethanolamine, and cholesterol (Kowal et al., 2014) (**Figure 2**). Public on-line databases of EV composition are freely accessible at Exocarta[1] and Vesiclepedia[2].

Isolation and Characterization of EV

Isolation of EV from specific tissues or cells is one important step toward further investigation and applications (**Figure 3**). Various techniques have been adopted to facilitate the isolation of EV based on different principles (**Table 1**). Traditional methods used for EV isolation are mainly based on EV properties (e.g., size and density), including ultracentrifugation, ultrafiltration, chromatography and precipitation. The ultracentrifugation process requires high centrifugal forces, up to 1,000,000 *g*. Ultracentrifugation is suitable for large sample volumes, but not for small volumes because it is time-consuming, labor-intensive and requires expensive equipment (Witwer et al., 2013). In addition, protein, aggregates, apoptotic bodies, and other non-exosomal particles may be present in EV obtained by ultracentrifugation, which is the major shortcoming of this method (Konoshenko et al., 2018). There are two types of ultracentrifugation: differential ultracentrifugation and density gradient ultracentrifugation. These two methods are used in order to increase the efficiency of particle separation and to obtain purer EV (Fernandez-Llama et al., 2010). Another isolation method is ultrafiltration, which merely depends on size or molecular weight. Ultrafiltration is rapid and does not require expensive devices, but it is difficult to remove contaminating proteins (Zeringer et al., 2015). Size-exclusion chromatography allows the separation of exosomes from proteins, but not from MV, protein aggregates, lipoparticles, macromolecules, or particulate matter (Gurunathan et al., 2019). Size-exclusion chromatography can be used in combination with ultracentrifugation for higher yields of EV (Lai et al., 2010). Precipitation isolates EV by capturing a certain size, and using simple, rapid, low-speed centrifugation on the bench top at 1,500 *g* in "polymer nets" (Gurunathan et al., 2019). Because it is easily operated

[1]http://www.exocarta.org

[2]http://www.microvesicles.org

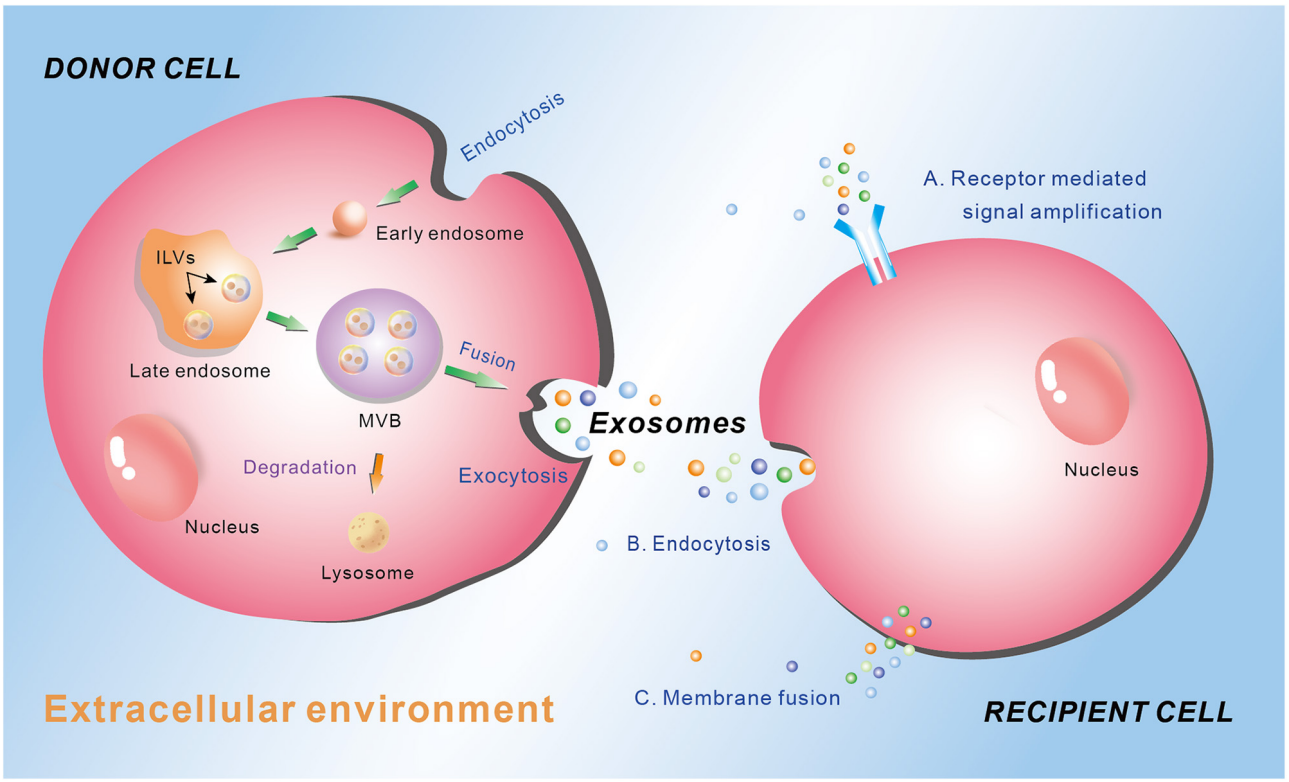


FIGURE 1 | Schematic diagram of the biogenesis and secretion of exosomes, and their function ways to the recipient cell. Donor cell plasma membrane invaginate through endocytosis to form early endosome, which subsequently develop into late endosome via endosomal membrane budding inward to form intraluminal vesicles (ILVs). The late endosome constantly buds inward and form ILVs, which keep accumulating and constitute multivesicular body (MVB). MVB can either be degraded by lysosome or fuse with the plasma membrane to permit the ILVs to be released into the extracellular environment through exocytosis as exosomes. Exosomes mediate their effects on the recipient cells through three main manners: **(A)** receptor mediated signal amplification, **(B)** endocytosis, and **(C)** membrane fusion.

and does not require specialized equipment, precipitation allows to be integrated into clinical usage and it can be applied for large sample sizes (Konoshenko et al., 2018). The disadvantage of this method is that there is no specificity for non-exosomal material, such as protein aggregates, which may be co-isolated with the exosomes resulting in low purity (Peterson et al., 2015). In addition, polymer-based precipitation is also used for EV isolation based on the changes in EV solubility and/or aggregation (Zeringer et al., 2015). *System Biosciences, LLC.* offers a proprietary reagent named ExoQuick, which can be used to purify exosomes from a wide variety of tissue culture media, and certain biofluids[3]. In order to isolate more specific EV populations, immunological methods are used based on highly specific interactions with the molecules (e.g., lipids, proteins, and polysaccharides) exposed on the EV surface. This approach is particularly useful when the protein expressed on the EV surface lacks a soluble counterpart (Gurunathan et al., 2019). Immuno-affinity is simple, rapid, and compatible with the laboratory equipment, while it is unstable and not suited for isolating EV from large quantities of biological samples (Konoshenko et al., 2018). Moreover, a new method utilizing aqueous two-phase system is adopted to isolate high-purity EV by preventing the protein contamination in the EV fraction (Kim et al., 2015). Recently, microfluidics-based technologies have become a trend for EV isolation, especially for microscale isolation, detection, and analysis of exosomes (Konoshenko et al., 2018; Gurunathan et al., 2019). Microfluidic devices utilizes the usual separation determinants and innovative sorting principles, mainly including: (a) trapping exosomes with an immune-affinity approach (microfluidic chip, "Exochip," magnetic capture beads) (Chen C. et al., 2010; Kanwar et al., 2014; Shao et al., 2015); (b) membrane-based filtration (double filtration) (Liang et al., 2017); (c) trapping exosomes on porous structures (nanowire micropillars) (Wang et al., 2013); (d) acoustics (acoustic nano-filter system); (e) lateral displacement (nanoscale lateral displacement arrays) (Wunsch et al., 2016); and (f) viscoelastic flow (field-free microfluidic sorting) (Zhou J. et al., 2019).

Characterization of EV is essential for determining their biochemical properties and biological functions. The characterization mainly includes the evaluation of the size, structure, surface biochemical markers, concentration and contents of EV. There are numerous approaches for

[3]www.systembio.com

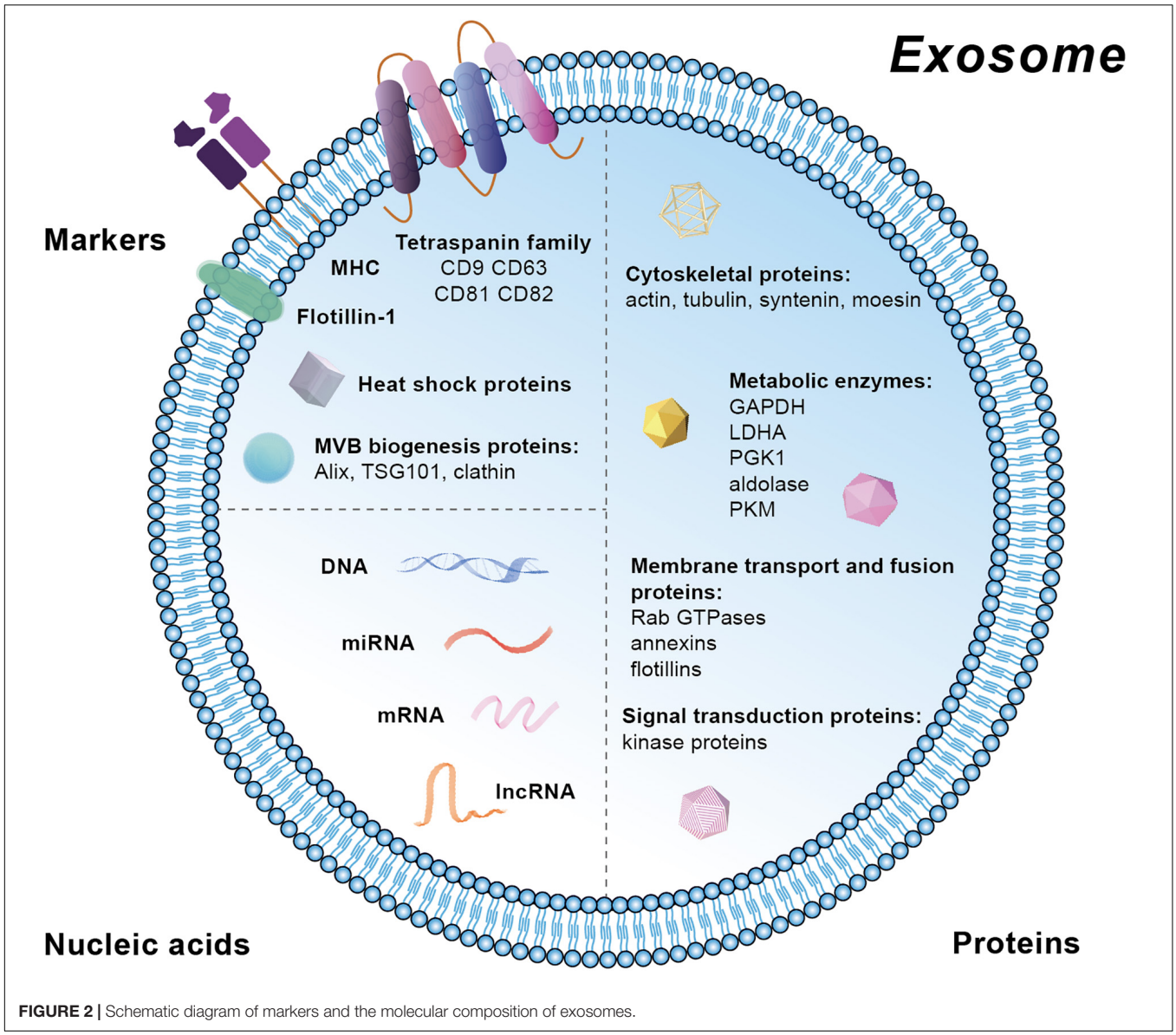


FIGURE 2 | Schematic diagram of markers and the molecular composition of exosomes.

characterizing different biochemical properties of EV. To detect EV biochemical markers, western blotting, flow cytometry, microfluidic-based technique and nanoparticle-tracking analyses (NTA) are normally used. EV components, including proteins, mRNA, miRNA, and lipid subsets can be detected by conventional test method such as western blotting, PCR and flow cytometry. As technology advances, high throughput transcriptomic studies have identified a wide range of mRNA and miRNA data sets based on microarray and next-generation sequencing (NGS) analyses leading to a comprehensive data classification. For detecting size and structure of EV, NTA, Tunable-resistive pulse sensing (TRPS), Dynamic-light scattering (DLS), Photon-correlation spectroscopy (PCS), Atomic-force microscopy (AFM), Transmission electron microscopy (TEM), Raman spectroscopy and Flow cytometry are used. Meanwhile, NTA and TRPS can be used to detect concentration.

MESENCHYMAL STEM CELLS (MSCs) and MSCs-DERIVED EV (MSCs-EV)

Mesenchymal Stem Cells (MSCs)

MSCs, also known as mesenchymal stromal cells (MSCs), are multipotent fibroblast-like cells with the potential for self-renewal and multilineage differentiation (Hu et al., 2018). The Mesenchymal and Tissue Stem Cell Committee of the International Society for Cellular Therapy (ISCT) has proposed the minimal criteria to define human MSCs (Dominici et al., 2006). First, MSCs must be plastic-adherent when maintained in standard culture conditions. Second, MSCs must express CD105, CD73, and CD90, and lack expression of CD45, CD34, CD14 or CD11b, CD79 alpha or CD19 and HLA-DR surface molecules. Third, MSCs must differentiate to osteoblasts, adipocytes and chondroblasts *in vitro*.

TABLE 1 | The isolation techniques of EV and their advantages and disadvantages.

Isolation techniques	Principle	Advantages	Disadvantages	References
Differential ultracentrifugation	Size	Conventionality, isolation from large sample volumes	Inapplicability for small sample, time-consuming, labor cost, expensive equipment-dependent	Livshits et al., 2015
Density gradient centrifugation	Density	Conventionality, isolation from large sample volumes, high purity	Inapplicable for small sample, time-consuming, labor cost, expensive instrument-dependent	Greening et al., 2015
Ultrafiltration	Size or weight	Rapidness, high purity, no limitations on sample volume	Aggressive, difficult to remove contaminating proteins	Lobb et al., 2015
Size exclusion chromatography	Size	High purity, removal of soluble proteins, preserve vesicle integrity, high sensitivity	Low yield, need of further concentration steps, limitations on sample volume and number of separated peaks	Gamez-Valero et al., 2016
Precipitation	Size	Facility, rapidness, reservation of EV integrity, no need in additional equipment, high ion concentrations	Low purity, protein contaminations	Crossland et al., 2016
Polymer precipitation	Solubility or aggregation	Preservation of EV integrity, no additional equipment, pH close to physiological range, high ion concentration	Contamination and retention of the polymer	Wang and Sun, 2014
Immuno-affinity	Membrane surface proteins	Easy, rapid, High purity, higher capture efficiency, no volume limitations	Unstable, inapplicability for large sample	Konoshenko et al., 2018
Microfluidics techniques	Membrane surface targeted markers, size, acoustics, viscoelastic flow	Rapidness, consume low volumes of sample and reagents, high purity, efficiency	High-cost, expensive equipment-dependent	Contreras-Naranjo et al., 2017

MSCs reside in almost all post-natal organs and tissues such as bone marrow, adipose, liver, lung, spleen, and muscle (da Silva Meirelles et al., 2006). MSCs have the ability to proliferate extensively and maintain the ability to differentiate into multiple cell types (e.g., osteoblasts, adipocytes, chondrocytes, and fibroblasts), which endow MSCs with stem cell nature (Pittenger et al., 1999). Besides, MSCs can migrate to the sites of damage and secrete anti-inflammatory and growth factors to maintain cellular homeostasis and promote damage repair.

With the above characteristics, MSCs are commonly used in cell therapy for regenerative medicine and immunotherapy (Squillaro et al., 2016; Galipeau and Sensebe, 2018). MSCT has caused increasing attention and is regarded as a potential new therapy for a variety of human diseases associated with brain, liver, kidney, bone, and so on (Hu et al., 2018; Chakari-Khiavi et al., 2019; Hu et al., 2019; Missoum, 2020). However, the direct use of MSCs for treating diseases encounters some problems. For example, MSCs inoculated into damage site show low survival rate and loss of function after 1 week (Pak et al., 2003; Breitbach et al., 2007; Rani et al., 2015). Besides, intraarterial MSCs administration may lead to occlusion in the distal vasculature due to their relatively large cell size (Furlani et al., 2009). In addition, MSCs may genetically unstable and undergo chromosomal abnormalities, even develop malignant tumor or generated calcification (Yoon et al., 2004; Tolar et al., 2007; Jeong et al., 2011). These issues may lower its security for treating human disease.

Recently, numerous studies demonstrate the therapeutic effect of MSCs is primarily mediated by the paracrine secretion of cytokines, growth factors and EV (Wang et al., 2015; Zhou Y. et al., 2019). MSCs-EV are identified as key mediators for the paracrine effects and gradually become the focus in regenerative medicine and disease treatment (Yang et al., 2017; Chang et al., 2018).

MSCs-EV

Over the years, of a wide array of bioactive molecules, MSCs secretions such as growth factors, cytokines and chemokines have been proved to play vital biological roles. Among these secretory products, none of them, by itself, can fully decipher the mechanism of MSCs (Meirelles Lda et al., 2009). In 2009, MSCs-derived MV were found to alleviate glycerol-induced acute tubular injury. The size of these MV ranges from 80 nm to 1 μm, with a mean value of 135 nm (Bruno et al., 2009). Subsequently, Lai et al. isolated and characterized MSCs-derived exosome for the first time from conditioned medium of human embryonic-derived MSCs (hESC-MSCs) (Lai et al., 2010). These membrane vesicles feature a diameter of 50–100 nm with an endosomal origin, housing abundant exosome-associated proteins including Alix, TSG101 and tetraspanins (Lai et al., 2010). MSCs-exosomes have special membrane binding proteins such as CD73, CD44, and CD29 compared with other EV (Lai et al., 2012). To date, more than 850 unique gene products and 150 miRNAs have been identified in MSCs-exosomes (Chen T.S. et al., 2010; Lai et al., 2012). In addition, MSCs have been demonstrated as the most prolific producer of mass exosomes (Yeo et al., 2013). They can produce large numbers of exosomes and generate permanent cell lines through cell immortalization, whose yield is not affected in

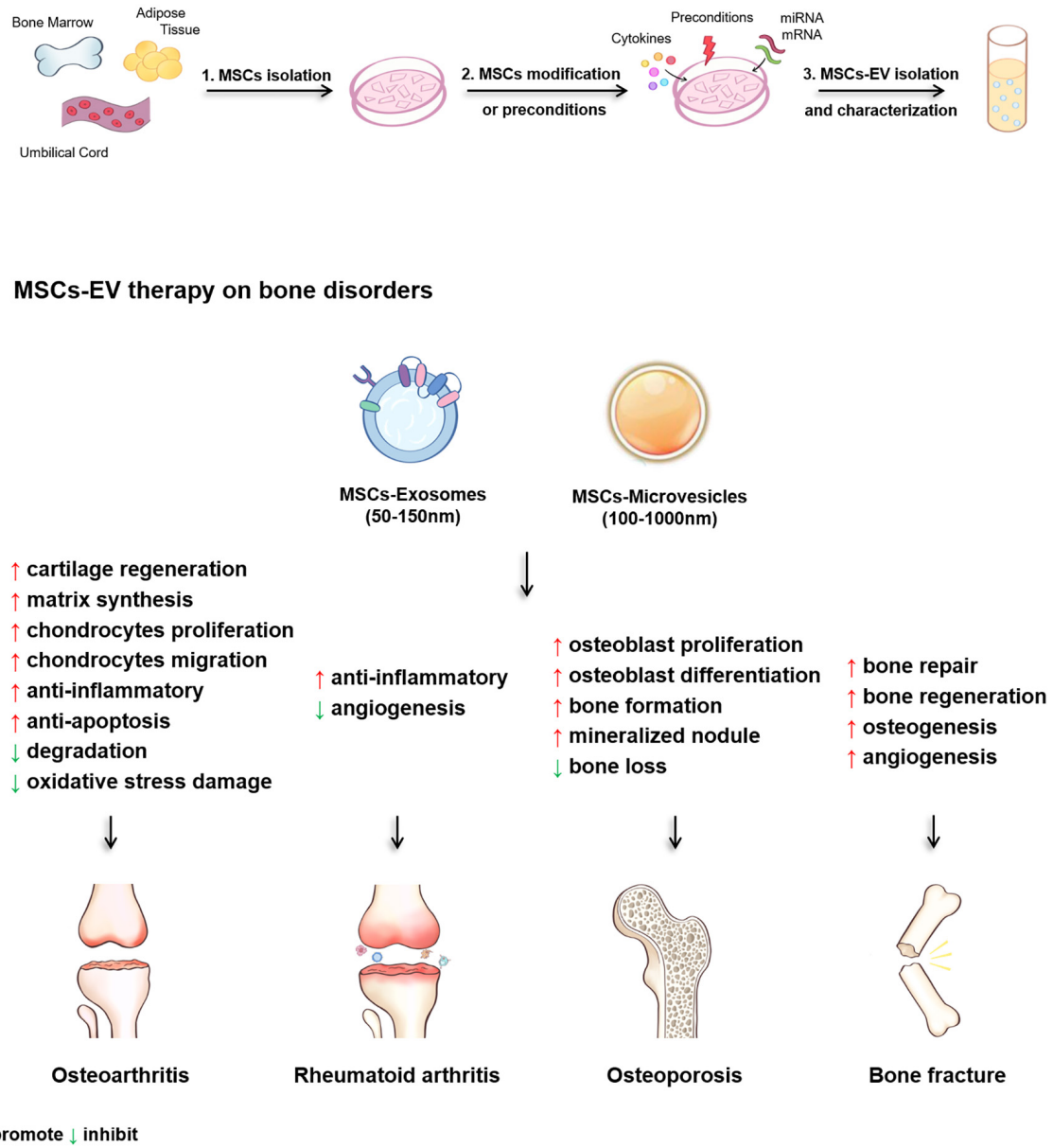


FIGURE 3 | The diagram of the MSCs-EV preparation and the therapeutic effects of MSCs-EV on osteoarthritis (OA), rheumatoid arthritis (RA), osteoporosis (OP) and bone fracture.

quantity or quality, thus ensuring a sustainable and reproducible production of exosomes from MSCs (Yeo et al., 2013).

Previous studies have shown that the function of MSCs-EV may vary depending on the source of the MSCs, thus affecting the biological effects of MSCs-EV (Baglio et al., 2015; Del Fattore et al., 2015; Lopez-Verrilli et al., 2016; Borger et al., 2017). Thus, MSCs-EV derived from different MSCs may show different clinical efficacy. It is important to determine the optimal source of MSCs. In addition, the environment of MSCs can change the content of EV derived from MSCs, thus affecting and changing the tissue environment. MSCs-EV may have the versatility and capacity to interact with multiple cell types within the immediate vicinity and remote areas to elicit appropriate cellular responses to keep the maintenance of a dynamic and homeostatic tissue microenvironment (Lai et al., 2015).

MSCs-EV AND OSTEOARTHRITIS (OA)

Osteoarthritis is the most common chronic joint disease around the world, with an incidence of 10–20% in the population over 50 years old. As the population ages and obesity increases, the incidence of OA is expected to double within the next 30 years (Blanco et al., 2011). It has become the fastest growing major health concern worldwide. OA is characterized by the degradation of the articular cartilage, the degeneration of menisci and ligaments, the thickening of the subchondral bone, and the formation of osteophytes (Loeser et al., 2012). The pathogenesis of OA is complex, involving multiple factors (e.g., age, body mass index, and genetics), multiple tissues, and processes.

There is still currently no effective treatment for OA. Most treatments are applied to manage pain, stiffness and swelling to improve joint mobility, and joint replacement is the only option for treating the entire joint dysfunction. Although the current physiotherapy or pharmacological therapy can temporarily relieve the clinical symptoms, it is difficult to fully restore joint function and also has a high risk of instability and infection (Keith, 2012; Stiehler et al., 2015; Xin-Wei et al., 2015).

The potential of MSCs to treat OA has been extensively studied (Qi et al., 2012; Vega et al., 2015; Davatchi et al., 2016). Recent studies have discovered that MSCs function in a paracrine manner by secreting cytokines, growth factors and EV (D'souza et al., 2015; Giebel et al., 2017; Fan et al., 2020) and exosomes derived from MSCs have shown the capability to protect cartilage and bone from degradation in OA through reinducing the expression of chondrocyte markers (type II collagen, aggrecan), inhibiting catabolic (MMP13 (matrix metalloproteinase 13), ADAMTS5) and inflammatory markers, inhibiting macrophage activation, and protecting chondrocytes from apoptosis, which show anti-inflammatory and cartilage protection effects (Cosenza et al., 2017).

Anti-inflammatory Effect of MSCs-EV in OA

Inflammation is an important factor in the onset and progression of OA (Nold et al., 2015; Burrello et al., 2016). In OA patients, activated macrophages and other innate immune cells release inflammatory cytokines and promote cartilage damage (Liu-Bryan, 2015). Infiltrations of B lymphocyte, T lymphocyte, plasma cells, T-helper cells, and Human Leukocyte Antigen-antigen D Related (HLA-DR)-positive dendritic-like cell were observed in the inflamed synovium (Lindblad and Hedfors, 1987). Moreover, catabolic factors [e.g., interleukin-1α (IL-1α), tumor necrosis factor-α (TNF-α)] are present in OA joints and inhibit the chondrogenesis of stem cells (Heldens et al., 2012).

Recent evidence suggest that adipose tissue-derived mesenchymal stem cells (AD-MSCs)-exosomes (size of 104 ± 19 nm) and MV (size of 279 ± 94 nm) show great potential in anti-inflammatory and preventing degeneration processes in OA (Tofiño-Vian et al., 2018). Exosomes (∼120 nm) and MV/microparticles (>150 nm) derived from bone marrow mesenchymal stem cells (BM-MSCs) show anti-inflammatory function through inhibiting T lymphocyte proliferation, stimulating macrophage polarization toward anti-inflammatory phenotype, and decreasing the percentage of $CD4^+$ and $CD8^+$ T cell subsets (Cosenza et al., 2018). In addition, BM-MSCs-exosomes (30–250 nm) induce conversion of T helper type 1 (Th1) cells into T helper type 2 (Th2) cells and reduce the potential of T cells to differentiate into interleukin 17-producing effector T cells (Th17) (Chen et al., 2016). These findings demonstrate that MSCs-EV suppress pro-inflammatory response by reducing inflammation and promoting anti-inflammatory responses that maintain the immune balance. Furthermore, in the rat model of temporomandibular joint osteoarthritis (TMJ-OA), hESC-MSCs-exosomes (size of 100–200 nm, density of 1.10–1.19 g/ml) can relieve pain and repair osteoarthritic TMJ. MSCs-exosomes increase a well-coordinated response of attenuating inflammation, enhance matrix synthesis, while reduce OA joint cellular apoptosis and matrix degradation to achieve overall joint homeostasis, which finally promote TMJ repair and regeneration (Zhang S. et al., 2019). MSCs-exosomes function through adenosine receptor-mediated adenosine activation of protein-serine-threonine kinase (AKT), extracellular regulated protein kinases (ERK) and Adenosine 5′-monophosphate (AMP)-activated protein kinase (AMPK) phosphorylation to reduce inflammation and restore matrix homeostasis in OA. These therapeutic effects were achieved by enhancing sulfated glycosaminoglycan (s-GAG) matrix synthesis impeded by interleukin-1β (IL-1β), while suppressing IL-1β-induced nitric oxide and MMP13 production (Zhang S. et al., 2019). Cosenza et al. (2017) also found that exosomes (112 ± 6.6 nm) and microparticles (223 ± 15.6 nm) from murine BM-MSCs exerted similar functional effect *in vitro* by re-establishing chondrocyte homeostatic state, protecting chondrocytes from apoptosis and stimulating macrophage polarization toward anti-inflammatory phenotype. Therefore, MSCs-EV possess the immunomodulatory properties and accelerate the recovery of cartilage and joint in OA.

Cartilage Protection and Regeneration Effect of MSCs-EV in OA

The main pathology of early stage OA is the degeneration of chondrocytes, resulting in damage to articular cartilage. Metabolic and structural changes in articular cartilage play a major role in the initiation and progression of OA. MSCs-EV exert important therapeutic effect on OA by protecting cartilage from degradation and promoting cartilage regeneration, which is now the focus of clinical therapy.

The efficacy of hESC-MSCs-exosomes (a modal size of 100 nm) on cartilage repair was firstly reported in 2016 (Zhang S. et al., 2016). After treatment with exosomes, the rat model of osteochondral defect displayed almost complete neotissue coverage with good surface regularity and complete integration with the surrounding cartilage. hESC-MSCs-exosomes accelerated neotissue filling and enhanced matrix synthesis of type II collagen and s-GAG, demonstrating the capacity of MSCs-exosomes in cartilage repair and regeneration (Zhang S. et al., 2016). It has also been demonstrated that MSCs-EV protect chondrocytes from apoptosis, balance the

anabolic and catabolic processes and re-establish chondrocyte homeostatic state via balancing the synthesis and degradation of cartilage matrix, thus protect cartilage and bone from degradation (Cosenza et al., 2017; Wang et al., 2017; Wu et al., 2019). All these observations demonstrate the therapeutic effects of MSCs-EV on OA by re-establishing cartilage homeostasis, protecting and regenerating cartilage.

Several key cargo components of MSCs-EV have shown important roles in mediating the therapeutic effects of MSCs-EV. MiRNAs, a large cargo of MSCs-EV (Chen T.S. et al., 2010), are identified as key regulators in mediating the therapeutic roles of MSCs-exosomes on OA by targeting different molecules or signaling pathways (Toh et al., 2017). AD-MSCs-EV (ranged in size from 40–50 nm to 300–400 nm) have been demonstrated to affect fibroblast-like synoviocytes (FLS) behavior in a model of chronic inflammation through direct interaction with hyaluronan matrix and miRNA release (Ragni et al., 2019). They reduced the expression of pro-inflammatory cytokines and chemokines in a chronic model of FLS inflammation. Through bioinformatics analysis, EV-embedded miRNAs regulate the main pathways, which is strictly associated with synovial inflammation in OA (Ragni et al., 2019). Further research revealed AD-MSCs-EV (50–400 nm in diameter)-embedded miRNAs alter cartilage homeostasis and macrophage polarization, supporting the protective and pro-regenerative effects in joint (Ragni et al., 2020). miR-92a-3p derived from BM-MSCs-exosomes (50–150 nm) regulates cartilage development and homeostasis through targeting Wnt5a in both chondrogenesis and OA pathogenesis as a negative regulator (Mao et al., 2018). miR-135b derived from hESC-MSCs-exosomes assists transforming growth factor β1 (TGF-β1) to promote chondrocyte proliferation by down-regulating Specificity Protein 1 (Sp1), thus promotes cartilage repair in OA (Wang et al., 2018). Infrapatellar fat pad (IPFP)-derived mesenchymal stem cells (IPFP-MSCs)-exosomes (average size of 121.9 nm) significantly enhance the autophagy level of chondrocytes via miR100-5p-mediated inhibition of mammalian target of rapamycin (mTOR) signaling pathway (Wu et al., 2019). Exosomes (30–150 nm) derived from miR-140-5p overexpressing synovial MSCs (SMSCs) activate yes-associated protein (YAP), decrease extracellular matrix (ECM) secretion, and promote proliferation and migration of articular chondrocytes via Wnt5a and Wnt5b, which in turn ameliorate OA (Tao et al., 2017). These studies demonstrate that MSCs-EV attenuate OA progression through the delivery of miRNAs, which exhibit as potential targets for future therapy (**Table 2**).

In addition to miRNA, a few lncRNAs have been found as main components of EV and to function as novel biomarkers and therapeutic targets for various diseases (Naderi-Meshkin et al., 2019). Exosomal lncRNA KLF3-AS1 derived from human MSCs (hMSCs) has been demonstrated to inhibit IL-1β induced apoptosis of chondrocytes and promote cartilage repair in a OA rat model by decreasing Runt-related transcription factor 2 (Runx2) and MMP13 expression while increasing collagen, type II, alpha 1 (Col2a1) and aggrecan expression (Liu et al., 2018). This suggests the important role of lncRNA in mediating the therapeutic effect of MSCs-exosomes on OA, demonstrating a new possible mechanism. In addition, protein components in MSCs-exosomes have been suggested to be linked with OA recovery. Zhang et al. (2018) demonstrated the therapeutic effect of vesicular CD73 in cartilage repair and regeneration (Zhang et al., 2018). hESC-MSCs-Exosomes (a modal size of 100 nm, density of 1.10–1.19 g/ml) mediated repair of osteochondral defects, which was characterized by increased cellular proliferation and infiltration, enhanced matrix synthesis and a regenerative immune phenotype. These could attribute to exosomal CD73-mediated adenosine AKT and ERK signaling (Zhang et al., 2018) (**Table 2**).

As mitochondrial dysfunction is one important cause of OA (Blanco et al., 2011) and MSCs-EV are important for intercellular mitochondria communication (Cao et al., 2020), suggesting the possibility of MSCs-EV in treating OA by regulating mitochondria function. Mitochondrial dysfunction and oxidative stress damage are associated with apoptosis, senescence and various pathological conditions, which are hallmarks of OA. In OA, chondrocytes lose their metabolic flexibility, decrease their cellular mitochondrial biogenesis, and increase their mitochondrial DNA (mtDNA) damage (Chen et al., 2019). Qi et al. (2019) have found that BM-MSCs-exosomes (50–150 nm) suppress IL-1β-induced chondrocyte apoptosis, which was partly due to mitochondrial dysfunction, through inhibiting the phosphorylation of p38 and ERK1/2, and stimulating the phosphorylation of AKT signaling pathway. Moreover, Chen et al. (2019) have reported that BM-MSCs-exosomes (40–110 nm) restore mitochondrial function and oxidative stress damage in degenerative cartilage and balance the energy metabolism, which promote cartilage regeneration. Based on these findings, they furtherly fabricated a 3D printed cartilage extracellular matrix/gelatin methacrylate/exosome (ECM/GelMA/exosome) scaffold with radially oriented channels and found it significantly facilitated the cartilage regeneration in the animal model (Chen et al., 2019).

MSCs-EV AND RHEUMATOID ARTHRITIS (RA)

Arthritis is a chronic autoimmune disease involving joints. It is characterized by persistent inflammation of joints. In RA, auto-reactive T cells and B cells are activated because of defective immune regulation. These cells proliferate and differentiate into pathological T cells and plasma B cells, which produce auto-reactive antibodies, eventually leading to inflammation and degradation of joints (Pozsgay et al., 2017). As mentioned in OA section that MSCs-EV exert anti-inflammatory effects, they have also exerted an immunomodulatory function in RA and show therapeutic effects on joint destruction (Chen et al., 2018; Cosenza et al., 2018).

Collagen-induced arthritis (CIA) is one of the most accepted animal models of RA for its capacity to simulate RA inflammatory symptoms clinically and biologically. Cosenza et al. (2018) have demonstrated that Exosomes (∼120 nm) and MV/microparticles (>150 nm) derived from BM-MSCs exert an indirect inhibitory effect on T lymphocyte and B lymphocyte proliferation in CIA

TABLE 2 | MSCs-EV cargo involved in regulation of chondrogenesis and cartilage homeostasis.

MSCs-EV cargo	Target	Effects and mechanism	References
miR-92a-3p	Wnt5a	Regulate cartilage development and homeostasis by targeting Wnt5a	Mao et al., 2018
miR-135b	Sp1[a]	Promote chondrocyte proliferation and cartilage repair in OA[b] by down-regulating Sp1[a] in chondrocyte thus affect TGF-β1[c]	Wang et al., 2018
miR-100-5p	mTOR[d]	Inhibit mTOR signaling pathway to enhance the autophagy level of chondrocytes	Wu et al., 2019
miR-140-5p	YAP[e]	Decrease ECM[f] secretion and induce proliferation and migration of articular chondrocytes via activating YAP, Wnt5a and Wnt5b	Tao et al., 2017
lnc KLF3-AS1	IL-1β[g]	Inhibit IL-1β-induced apoptosis of chondrocytes and promote cartilage repair in a rat model of OA through decreasing Runx2[h] and MMP13[i] expression while increasing Col2α1[j] and aggrecan expression	Liu et al., 2018
CD73	AKT, ERK	Osteochondral defects repair, increased cellular proliferation and infiltration, enhanced matrix synthesis and a regenerative immune phenotype, attributing to exosomal CD73-mediated adenosine activation of AKT and ERK signaling	Zhang et al., 2018

[a]Specificity protein 1; [b]Osteoarthritis; [c]Transforming growth factor β1; [d]Mammalian target of rapamycin; [e]Yes-associated protein; [f]Extracellular matrix; [g]Interleukin-1β; [h]Runt-related transcription factor 2; [i]Matrix metalloproteinase 13; [j]Collagen, type II, alpha 1.

murine model, providing the first evidence that MSCs-exosomes exert an immunomodulatory function in RA. Chen et al. (2018) have also found that BM-MSCs-exosomes show therapeutic effects on joint destruction in RA, partly due to the expression of miR-150-5p in exosomes. After being treated with MSCs-derived miR-150-5p exosomes (Exo-150), the expression of the RA markers including matrix metalloproteinase 14 (MMP14) and vascular endothelial growth factor (VEGF) in CIA mice was down-regulated. Exo-150 inhibited migration of FLS from RA, and angiogenesis *in vitro*, and alleviated arthritis in CIA mice *in vivo*. These findings indicate that EV facilitate the direct intracellular transfer of miRNAs and represent a potential therapeutic strategy for RA (Chen et al., 2018).

At present, only a few studies have reported the therapeutic effect of MSCs-EV on RA and the mechanism is unclear. As MSCs-EV play roles in immunoregulation and cartilage protection and regeneration, this may partially contribute to the therapeutic effect of MSCs-EV on RA. More research is necessary to prove the effects of MSCs-EV in treating RA.

MSCs-EV AND OSTEOPOROSIS (OP)

Osteoporosis is an age-related systemic bone disease characterized by reduced bone mass, destroyed bone microstructure, weakened bone strength, which causes increased bone brittleness and fracture risk. As one major disease worldwide, osteoporosis seriously affects people's health and increases society's financial burden. Therefore, efficient therapy of osteoporosis is one main concern of the world.

MSCs-EV have been indicated as a novel therapeutic method for osteoporosis. Qi et al. (2016) have found that exosomes (50–150 nm) secreted by human-induced pluripotent stem cell-derived mesenchymal stem cells (hiPSC-MSCs) effectively promote osteoblast proliferation, differentiation and bone formation, thus improve bone regeneration in osteoporotic rats. Zuo et al. (2019) have reported that exosomes (40–100 nm) derived from BM-MSCs alleviate radiation-induced bone loss in a rat model. After irradiation to rats, BM-MSCs-exosomes were intravenously injected into the rats immediately. The results showed that BM-MSCs-exosomes reduced intracellular reactive oxygen species (ROS) to protect cells from damage, accelerated DNA repair in the recipient BM-MSCs and partially rescued cell proliferation. Moreover, BM-MSCs-exosomes decreased the senescence-associated protein expression and restored the differentiation potential of irradiated BM-MSCs (Zuo et al., 2019). Meanwhile, BM-MSCs-exosomes reduced adipogenic gene expression and increased osteogenic gene expression of recipient BM-MSCs (Zuo et al., 2019). These results demonstrate that MSCs-EV promote bone regeneration via reducing ROS, accelerating DNA repair, restoring cell (especially osteoblast) proliferation and differentiation potential, decreasing the senescence-associated protein and adipogenic gene expression and increasing osteogenic gene expression, thus alleviate osteoporosis.

Present studies demonstrate that MSCs-EV alleviate osteoporosis by activating several signaling pathways. Wnt/β-catenin signaling is a key pathway for bone development and homeostasis (Baron and Kneissel, 2013; Zhong et al., 2014). The activation of Wnt/β-catenin signaling promotes preosteoblast to differentiate into osteoblasts. Zuo et al. (2019) have found that BM-MSCs-exosomes promotes osteogenesis, reduced the decrease in bone mass induced by irradiation by activating Wnt/β-catenin pathway in the recipient BM-MSCs. Zhao et al. (2018) found that BM-MSCs-exosomes (about 40 nm) alleviated the osteoporosis progression by promoting the osteoblast proliferation through mitogen-activated protein kinase (MAPK) signaling pathway. Moreover, Liu et al. have demonstrated the therapeutic function of BM-MSCs-exosomes on osteopenia in Fas-deficient-MRL/lpr mice (Liu et al., 2015). The Fas-deficient-MRL/lpr mice exhibit Fas-deficiency that causes elevation of intracellular miR-29b levels and downregulation of DNA methyltransferase 1 (Dnmt1) in BM-MSCs, which causes hypomethylation of the Notch1 promoter and activation of Notch signaling, thus results in impaired osteogenic differentiation. MSCs-exosomes reduce intracellular miR-29b levels by transfer Fas to the recipient MRL/lpr BM-MSCs and recover Dnmt1-mediated Notch1 promoter hypomethylation, elevate mineralized nodule formation,

expression of Runx2 and alkaline phosphatase (ALP) of MRL/lpr BM-MSCs, thus increase bone formation, trabecular bone volume, bone mineral density (BMD), bone volume/total volume (BV/TV), mineral apposition rate (MAR) and bone formation rate per bone Surface (BFR/BS) in Fas-deficient-MRL/lpr mice (Liu et al., 2015). This study demonstrates that BM-MSCs-exosomes function through Fas/miR-29b/Dnmt1/Notch epigenetic cascade to regulate the recipient cell function.

MSCs-EV AND BONE FRACTURE

Besides the critical role in alleviating osteoporosis, MSCs-EV show key roles in fracture healing. In order to ensure bone fracture healing, two basic conditions must be met: good blood transport and stable fixation. hMSCs-exosomes (80–100 mm) have been found to promote bone regeneration by enhancing angiogenesis. MSCs-exosomes increased hMSC migration, induced mineral deposition and enhanced the differentiation potential of hMSCs into osteoblasts. In addition, MSCs-exosomes enhanced the expression of osteogenesis-related and angiogenesis-related genes, such as *COL I, ALP,* and *VEGF*, and promoted bone formation *in vivo* (Takeuchi et al., 2019). The $CD9^{-/-}$ mouse, which is an established strain with low-exosome productivity, shows a significant delay in endochondral ossification and fracture healing compared with the wild-type mouse. However, injection of BM-MSCs-exosomes (approximately 80 nm) rescues the fracture healing speed in $CD9^{-/-}$ mice and increases that in the wild-type mice, indicating the potential therapeutic role of MSCs-exosomes in fracture healing (Furuta et al., 2016). In addition, MSCs-exosomes contain bone repair related cytokines such as monocyte chemotactic protein 1 (MCP-1), monocyte chemotactic protein 3 (MCP-3), stromal cell-derived factor-1 (SDF-1) and angiogenic factors, which accelerate fracture healing. Meanwhile, miRNAs derived from MSCs-exosomes are key regulators for fracture healing. miR-21 accelerates osteogenic bone formation, osteogenesis and angiogenesis, which promote fracture healing (Furuta et al., 2016). Furthermore, Zhang et al. have also demonstrated the therapeutic effect of MSCs-exosomes (approximately 100 nm) on bone fracture healing (Zhang Y. et al., 2019). They delivered umbilical cord mesenchymal stem cells (uMSCs)-exosomes carried by a HyStem-HP hydrogel to the fracture site in a rat model of femoral fracture and found that 14 days treatment significantly increased callus volumes, BMD, BV and BV/TV (Zhang Y. et al., 2019). In a separate study, hiPSC-MSCs-exosomes enhance the osteoinductivity of β-tricalcium phosphate (β-TCP) through activating the phosphatidylinositol-3-kinases/protein-serine-threonine kinase (PI3K/AKT) signaling pathway in hBMSCs. Based on the above findings, they designed hiPSC-MSCs-Exos functionalized β-TCP scaffold can effectively promote bone repair and regeneration in a rat model of calvarial bone defects (Zhang J. Y. et al., 2016). In a latest study, hypoxic uMSCs-exosomes (50–150 nm) promote fracture healing by transfering miR-126 (Liu et al., 2020). Compared with regular exosomes, hypo-exos function better in promoting angiogenesis, proliferation and migration of endothelial cells to a greater extent. Moreover, hypoxia preconditioning mediated enhanced production of exosomal miR-126 through the activation of hypoxia inducible factor 1 (HIF-1α). Hypoxia preconditioning represents a promising method for optimizing the therapeutic actions of MSC- exosomes in bone fracture healing (Liu et al., 2020). These findings verify the vital regulatory role of MSCs-EV in bone fracture healing, identifying it as a potential therapeutic method for bone fracture.

In summary, present studies demonstrate that MSCs-EV are effective for treating OA, RA, OP, and bone fracture both *in vitro* and in animal models (**Table 3** and **Figure 3**). Several regulatory pathways have been demonstrated to function in MSCs-EV treating OA, RA, OP, and bone fracture, including AKT, ERK, AMPK, mTOR-autophagy, Wnt/β-catenin, MAPK, and Notch signaling pathways. For the treatment of OA, MSCs-EV reduce inflammation by activating adenosine of AKT and ERK, and the phosphorylation of AMPK. Moreover, MSCs-EV significantly enhance the autophagy level of chondrocytes through inhibiting mTOR signaling pathway. In terms of cartilage protection and regeneration, MSCs-EV activate YAP, decrease ECM secretion, and promote articular chondrocytes proliferation and migration via Wnt5a and Wnt5b. In addition, MSCs-EV suppress IL-1β-induced chondrocyte apoptosis, and enhance s-GAG matrix synthesis through inhibiting the phosphorylation of p38 and ERK1/2 thus restore matrix homeostasis and ameliorate OA (**Table 3** and **Figure 3**). In the treatment of bone loss and fracture healing, MSCs-EV promote osteogenesis, reduced the decrease in bone mass by activating Wnt/β-catenin pathway, and alleviate the osteoporosis progression by promoting the osteoblast proliferation through MAPK signaling pathway. Furthermore, MSCs-EV recover Dnmt1-mediated Notch1 promoter hypomethylation, enhance mineralized nodule formation, elevate the expression of Runx2 and ALP, thus increase bone formation (**Table 3** and **Figure 3**). These findings suggest potential clinical application of MSCs-EV in the treatment of bone disorders and also reveal the possible regulatory pathways that can be targeted for the clinical translation of MSCs-EV in treating bone disorders (**Table 3** and **Figure 3**).

CONCLUSION AND FUTURE PERSPECTIVES

Bone is the specific organ for supporting the body, protecting other organs, and storing minerals. Bone disorders normally results in pain and disability, severely reduces the quality of life and increases the burden on society. Therefore, the efficacious therapies for bone diseases have become the major concern worldwide. More recently, MSCs-EV have been shown to mediate the therapeutic effects of MSCs in various diseases and have been applied to clinical trials for several diseases, such as type I diabetes mellitus (trial NCT02138331), macular holes (NCT03437759) and acute ischemic stroke (NCT03384433)[4]. Thus, the role of MSCs-EV in the treatment of bone diseases has

[4]www.clinicaltrials.gov

TABLE 3 | Preclinical studies on the application of MSCs-EV for treating bone disorders.

Origin of EV	Disease	Outcomes	Function way and mechanism	References
BM-MSCs[a]	OA[b]	Attenuate inflammation, promote cartilage repair and regeneration	Inhibit T lymphocyte proliferation, stimulate macrophage polarization toward anti-inflammatory phenotype, restore mitochondrial function and oxidative stress damage, balance the energy metabolism, suppress mitochondrial dysfunction apoptosis of chondrocytes through inhibiting the phosphorylation of p38 and ERK1/2[c], and stimulating of the phosphorylation of AKT[d] signaling pathway, which promote cartilage regeneration	Chen et al., 2016, 2019; Cosenza et al., 2017, 2018; Mao et al., 2018; Qi et al., 2019
AD-MSCs[e]	OA[b]	Attenuate inflammation and modulate chondrocyte metabolism	Counteract the effects of IL-1β[f]	Tofiño-Vian et al., 2018
hESC-MSCs[g]	OA[b]	Attenuate inflammation, promote cartilage repair and regeneration	Reduce inflammation through adenosine receptor-mediated AKT[d], ERK[c] and AMPK[h] phosphorylation, restore matrix homeostasis by enhancing matrix synthesis of type II collagen and s-GAG[i] matrix synthesis	Zhang S. et al., 2016; Wang et al., 2017; Zhang et al., 2018; Zhang S. et al., 2019
IPFP-MSCs[j]	OA[b]	Protect cartilage and bone from degradation and maintain cartilage homeostasis	Related to miR100-5p-regulated inhibition of mTOR[k]-autophagy pathway	Wu et al., 2019
SMSCs[l]	OA[b]	Induces chondrogenic differentiation	Activate YAP[m], decrease ECM[n] secretion, and promote proliferation and migration of articular chondrocytes via Wnt5a and Wnt5b	Tao et al., 2017
BM-MSCs[a]	RA[o]	Attenuate RA inflammatory symptoms	Inhibit T lymphocyte and B lymphocyte proliferation, migration and invasion, inhibit angiogenesis via downregulating MMP14[p] and VEGF[q]	Chen et al., 2018; Cosenza et al., 2018
hiPSC-MSC[r]	OP[s]	Improve osteoporosis, promote osteoblast proliferation, differentiation and bone formation	Up-regulate mRNA and protein expression of osteoblast-related genes	Qi et al., 2016
BM-MSCs[a]	OP[s]	Alleviate osteoporosis progression and bone loss, elevate mineralized nodule and bone formation	Accelerate DNA repair, reduce adipogenic gene expression, increase osteogenic gene expression, activating Wnt/β-catenin and MAPK[t] signaling pathway, upregulate expression of Dnmt1[u], Runx2[v] and ALP[w], downregulate expression of Notch1 and NICD	Liu et al., 2015; Zhao et al., 2018; Zuo et al., 2019
BM-MSCs[a]	Bone fracture	Promote fracture healing	Accelerate bone repair via cytokines, miRNAs such as miR-21, miR-4532, miR-125b-5p, and miR-338-3p in exosomes, promote osteogenic bone formation, osteogenesis and angiogenesis	Furuta et al., 2016; Takeuchi et al., 2019
uMSCs[x]	Bone fracture	Significantly increased callus volumes, BMD[y], BV[z] and BV/TV[aa] and enhance fracture healing, promote angiogenesis, proliferation and migration	Through HIF-1α-mediated promotion of angiogenesis and transfer of miR-126	Zhang Y. et al., 2019; Liu et al., 2020
hiPSC-MSCs[r]	Bone fracture	Promote bone repair and regeneration	Activates the PI3K/AKT[ab] signaling pathway	Zhang J. Y. et al., 2016

[a]Bone marrow mesenchymal stem cells; [b]Osteoarthritis; [c]Extracellular regulated protein kinases; [d]Phosphorylation of protein-serine-threonine kinase; [e]Adipose tissue-derived mesenchymal stem cells; [f]Interleukin-1β; [g]Human embryonic-derived mesenchymal stem cells; [h]Adenosine 5′-monophosphate (AMP)-activated protein kinase; [i]Sulfated glycosaminoglycan; [j]Infrapatellar fat pad (IPFP)-derived mesenchymal stem cells; [k]Mammalian target of rapamycin; [l]Synovial mesenchymal stem cells; [m]Yes-associated protein; [n]Extracellular matrix; [o]Rheumatoid arthritis; [p]Matrix metalloproteinase 14; [q]Vascular endothelial growth factor; [r]Human-induced pluripotent mesenchymal stem cells; [s]Osteoporosis; [t]Mitogen-activated protein kinase; [u]DNA methyltransferase1; [v]Runt-related transcription factor 2; [w]Alkaline phosphatase; [x]Umbilical cord mesenchymal stem cells; [y]Bone mineral density; [z]Bone volume; [aa]Bone volume/total volume; [ab]Phosphatidylinositol-3-kinases/Protein-serine-threonine kinase.

become a research focus. Here, we focus on the application of MSCs-EV in four major bone disorders, including OA, RA, OP, and bone fracture.

MSCs-EV, lipid-bilayer spheroids, are characterized by possessing immunomodulatory and regenerative properties, similar to their producing cells. As MSCs-EV mediate both intercellular communication and the interactions with the cellular microenvironments, they have become fascinating to be a novel cell-free therapeutic strategy for treating diseases, including bone disorders. The currently *in vitro* and *in vivo* studies reveal the efficacy of MSCs-EV in treating OA, RA, OP, and bone fracture. MSCs-EV may alleviate the pain, promote overall joint repair and regeneration in OA by suppressing inflammation, promoting cartilage repair and regeneration, and restoring joint homeostasis. They also show immunomodulatory function in RA by regulating the function of T lymphocytes and B lymphocytes and inhibiting angiogenesis via downregulating MMP14 and VEGF, exerting therapeutic effects on joint destruction of RA. Moreover, MSCs-EV improve the osteoporosis by promoting cell proliferation, osteogenic differentiation, and reducing cell

senescence of BM-MSCs or osteoblast. Furthermore, the therapeutic effect of MSCs-EV is also observed in bone fracture healing. MSCs-EV orchestrate the process of osteogenesis and angiogenesis to enhance fracture healing. Overall, the present findings suggest MSCs-EV as a new cell-free therapeutic method for bone disorders.

The findings at current stage are very encouraging; however, further research is still needed to make MSCs-EV a routine clinical treatment for bone disease. There are several critical issues to consider, including: (1) The optimal source of MSCs. Since there are many sources of MSCs (e.g., BM-MSCs and AD-MSCs) and MSCs-EV produced by different cell source contain different cargos, it is important to determine the optimal source of MSCs, which may be bioengineered for producing MSCs-EV or their specific cargos according to specific requirements. (2) Standard methods for large-scale production and isolation of MSCs-EV. Because the culture condition affects the MSCs-EV production, the production methods of MSCs-EV should be optimized and controllable for large-scale and specific type of MSCs-EV production. Moreover, there is an urgent need to develop standardized methods for the isolation and purification of MSCs-EV, although establishing a universal isolation method is unlikely due to the complexity of MSC-EV. The isolation methods should not disrupt the structure and functions of MSCs-EV. (3) Methods for rapid and accurate quantification and characterization of MSCs-EV, which are critical for MSCs-EV clinical application. (4) Safe and effective approaches to deliver MSCs-EV to the body or to target sites for treatment. (5) The pharmacokinetics (e.g., tissue distribution, half-life period) of MSCs-EV in the body. (6) Safe and optimal dosage of MSCs-EV for treating different bone diseases. MSCs-exosomes execute synergetic biological functions through combinatorial effects together with their large diverse proteomic and RNA cargo (Lai et al., 2016). It has to be taken into consideration that exosomes do not harbor many copies of miRNA molecules. On average, 100 exosomes would be needed to transfer one copy of a given abundant miRNA. In contrast, MSCs-exosomes proteins in a typical therapeutic dose have the potential to trigger a biologically relevant response (Toh et al., 2018). Moreover, as individual MSCs-EV cargo is not equally or sufficiently efficacious in ameliorating tissue injury (Lai et al., 2012), a safe and optimal dosage needs to be considered. (7) Uncovery of the action mechanisms of MSCs-EV in treating bone disorders by characterizing their functional cargos. Current available publications have demonstrated the involvement of some key molecules and signaling pathways in the therapeutic effects of MSCs-EV on bone disorders, such as Wnts, YAP, AKT, ERK, AMPK, mTOR-autophagy, Wnt/β-catenin, MAPK, and Notch signaling pathways. However, most studies have only identified the mechanism of action of MSCs-EV as a whole, without identifying their specific components. For illustrating the function and mechanism of the MSCs-EV cargo components, current available publications mainly focus on miRNAs. Therefore, the molecular mechanisms of functional components such as MSCs-EV proteins still need to be further investigated. Moreover, current findings show that MSCs-EV exert different effects on angiogenesis in the treatment of RA and bone fracture. MSCs-EV inhibit angiogenesis and the expression of VEGF in treating RA while promote angiogenesis and VEGF expression in treating bone fracture. The molecular mechanism of MSCs-EV is still unclear, further investigation is necessary to make them more suitable for clinical application. (8) The possibility of modifying MSCs and artificially synthesizing MSCs-EV or their specific cargos for treating bone diseases. Biophysical and biochemical methods can be used to modify the properties of MSCs, thereby influencing EV composition and secretion. It leaves a wide range of conditions to be explored in attempts to increase MSCs-EV yields and their therapeutic potential (Park et al., 2019). In addition, understanding the molecular mechanisms of MSCs-EV for the treatment of bone diseases will prevent some side effects and make the clinical application of MSCs-EV more precise and safer. (9) Clinical studies are needed to prove the efficacy of MSCs-EV for the treatment of bone diseased. Clarification of these key issues will make MSCs-EV a more fantastic novel cell-free therapeutic strategy for bone disorders treatment in clinics.

AUTHOR CONTRIBUTIONS

SLiu, XX, and SLia drafted the manuscript. ZC and YZ revised the manuscript. SLiu designed the figure. AQ and LH revised and approved the manuscript. All the authors contributed to the article and approved the submitted version.

FUNDING

This work was supported by the National Natural Science Foundation of China (81772017), the China Postdoctoral Science Foundation (2018T111099), Young Talent Fund of University Association for Science and Technology in Shaanxi, China (20170401), the Natural Science Foundation of Shaanxi Province (2018JM3040), and the Seed Foundation of Innovation and Creation for Graduate Students in Northwestern Polytechnical University (CX2020264).

REFERENCES

Baglio, S. R., Rooijers, K., Koppers-Lalic, D., Verweij, F. J., Perez Lanzon, M., Zini, N., et al. (2015). Human bone marrow- and adipose-mesenchymal stem cells secrete exosomes enriched in distinctive miRNA and tRNA species. *Stem Cell Res Ther.* 6:127. doi: 10.1186/s13287-015-0116-z

Baron, R., and Kneissel, M. (2013). WNT signaling in bone homeostasis and disease: from human mutations to treatments. *Nat. Med.* 19, 179–192. doi: 10.1038/nm.3074

Batiz, L. F., Castro, M. A., Burgos, P. V., Velasquez, Z. D., Munoz, R. I., Lafourcade, C. A., et al. (2015). Exosomes as novel regulators of adult neurogenic niches. *Front. Cell. Neurosci.* 9:501. doi: 10.3389/fncel.2015.00501

Beyer, C., and Pisetsky, D. S. (2010). The role of microparticles in the pathogenesis of rheumatic diseases. *Nat. Rev. Rheumatol.* 6, 21–29. doi: 10.1038/nrrheum.2009.229

Biswas, S., Mandal, G., Roy Chowdhury, S., Purohit, S., Payne, K. K., Anadon, C., et al. (2019). Exosomes produced by mesenchymal stem cells drive differentiation of myeloid cells into immunosuppressive M2-polarized macrophages in breast cancer. *J. Immunol.* 203, 3447–3460. doi: 10.4049/jimmunol.1900692

Blanco, F. J., Rego, I., and Ruiz-Romero, C. (2011). The role of mitochondria in osteoarthritis. *Nat. Rev. Rheumatol.* 7, 161–169. doi: 10.1038/nrrheum.2010.213

Borger, V., Bremer, M., Ferrer-Tur, R., Gockeln, L., Stambouli, O., Becic, A., et al. (2017). Mesenchymal stem/stromal cell-derived extracellular vesicles and their potential as novel immunomodulatory therapeutic agents. *Int. J. Mol. Sci.* 18:1450. doi: 10.3390/ijms18071450

Breitbach, M., Bostani, T., Roell, W., Xia, Y., Dewald, O., Nygren, J. M., et al. (2007). Potential risks of bone marrow cell transplantation into infarcted hearts. *Blood* 110, 1362–1369. doi: 10.1182/blood-2006-12-063412

Bruno, S., Grange, C., Deregibus, M. C., Calogero, R. A., Saviozzi, S., Collino, F., et al. (2009). Mesenchymal stem cell-derived microvesicles protect against acute tubular injury. *J. Am. Soc. Nephrol.* 20, 1053–1067. doi: 10.1681/ASN.2008070798

Burrello, J., Monticone, S., Gai, C., Gomez, Y., Kholia, S., and Camussi, G. (2016). Stem cell-derived extracellular vesicles and immune-modulation. *Front. Cell Dev. Biol.* 4:83. doi: 10.3389/fcell.2016.00083

Cao, H., Cheng, Y., Gao, H., Zhuang, J., Zhang, W., Bian, Q., et al. (2020). In vivo tracking of mesenchymal stem cell-derived extracellular vesicles improving mitochondrial function in renal ischemia-reperfusion injury. *ACS Nano* 14, 4014–4026. doi: 10.1021/acsnano.9b08207

Chakari-Khiavi, F., Dolati, S., Chakari-Khiavi, A., Abbaszadeh, H., Aghebati-Maleki, L., Pourlak, T., et al. (2019). Prospects for the application of mesenchymal stem cells in Alzheimer's disease treatment. *Life Sci.* 231:116564. doi: 10.1016/j.lfs.2019.116564

Chang, Y. H., Wu, K. C., Harn, H. J., Lin, S. Z., and Ding, D. C. (2018). Exosomes and stem cells in degenerative disease diagnosis and therapy. *Cell Transpl.* 27, 349–363. doi: 10.1177/0963689717723636

Chaput, N., and Thery, C. (2011). Exosomes: immune properties and potential clinical implementations. *Semin. Immunopathol.* 33, 419–440. doi: 10.1007/s00281-010-0233-9

Chen, C., Skog, J., Hsu, C. H., Lessard, R. T., Balaj, L., Wurdinger, T., et al. (2010). Microfluidic isolation and transcriptome analysis of serum microvesicles. *Lab Chip* 10, 505–511. doi: 10.1039/b916199f

Chen, P., Zheng, L., Wang, Y., Tao, M., Xie, Z., Xia, C., et al. (2019). Desktop-stereolithography 3D printing of a radially oriented extracellular matrix/mesenchymal stem cell exosome bioink for osteochondral defect regeneration. *Theranostics* 9, 2439–2459. doi: 10.7150/thno.31017

Chen, T. S., Lai, R. C., Lee, M. M., Choo, A. B., Lee, C. N., and Lim, S. K. (2010). Mesenchymal stem cell secretes microparticles enriched in pre-microRNAs. *Nucleic Acids Res.* 38, 215–224. doi: 10.1093/nar/gkp857

Chen, W., Huang, Y., Han, J., Yu, L., Li, Y., Lu, Z., et al. (2016). Immunomodulatory effects of mesenchymal stromal cells-derived exosome. *Immunol. Res.* 64, 831–840. doi: 10.1007/s12026-016-8798-6

Chen, Z., Wang, H. Q., Xia, Y., Yan, F. H., and Lu, Y. (2018). Therapeutic potential of mesenchymal cell-derived miRNA-150-5p-expressing exosomes in rheumatoid arthritis mediated by the modulation of MMP14 and VEGF. *J. Immunol.* 201, 2472–2482. doi: 10.4049/jimmunol.1800304

Cocucci, E., Racchetti, G., and Meldolesi, J. (2009). Shedding microvesicles: artefacts no more. *Trends Cell Biol.* 19, 43–51. doi: 10.1016/j.tcb.2008.11.003

Colombo, M., Raposo, G., and Thery, C. (2014). Biogenesis, secretion, and intercellular interactions of exosomes and other extracellular vesicles. *Annu. Rev. Cell Dev. Biol.* 30, 255–289. doi: 10.1146/annurev-cellbio-101512-122326

Contreras-Naranjo, J. C., Wu, H. J., and Ugaz, V. M. (2017). Microfluidics for exosome isolation and analysis: enabling liquid biopsy for personalized medicine. *Lab Chip* 17, 3558–3577. doi: 10.1039/c7lc00592j

Cosenza, S., Ruiz, M., Toupet, K., Jorgensen, C., and Noel, D. (2017). Mesenchymal stem cells derived exosomes and microparticles protect cartilage and bone from degradation in osteoarthritis. *Sci. Rep.* 7:16214. doi: 10.1038/s41598-017-15376-8

Cosenza, S., Toupet, K., Maumus, M., Luz-Crawford, P., Blanc-Brude, O., Jorgensen, C., et al. (2018). Mesenchymal stem cells-derived exosomes are more immunosuppressive than microparticles in inflammatory arthritis. *Theranostics* 8, 1399–1410. doi: 10.7150/thno.21072

Crossland, R. E., Norden, J., Bibby, L. A., Davis, J., and Dickinson, A. M. (2016). Evaluation of optimal extracellular vesicle small RNA isolation and qRT-PCR normalisation for serum and urine. *J. Immunol. Methods* 429, 39–49. doi: 10.1016/j.jim.2015.12.011

da Silva Meirelles, L., Chagastelles, P. C., and Nardi, N. B. (2006). Mesenchymal stem cells reside in virtually all post-natal organs and tissues. *J. Cell Sci.* 119(Pt 11), 2204–2213. doi: 10.1242/jcs.02932

Davatchi, F., Sadeghi Abdollahi, B., Mohyeddin, M., and Nikbin, B. (2016). Mesenchymal stem cell therapy for knee osteoarthritis: 5 years follow-up of three patients. *Int. J. Rheum. Dis.* 19, 219–225. doi: 10.1111/1756-185x.12670

Del Fattore, A., Luciano, R., Saracino, R., Battafarano, G., Rizzo, C., Pascucci, L., et al. (2015). Differential effects of extracellular vesicles secreted by mesenchymal stem cells from different sources on glioblastoma cells. *Expert Opin. Biol. Ther.* 15, 495–504. doi: 10.1517/14712598.2015.997706

Dominici, M., Le Blanc, K., Mueller, I., Slaper-Cortenbach, I., Marini, F., Krause, D., et al. (2006). Minimal criteria for defining multipotent mesenchymal stromal cells. The international society for cellular therapy position statement. *Cytotherapy* 8, 315–317. doi: 10.1080/14653240600855905

Dong, R., Liu, Y., Yang, Y., Wang, H., Xu, Y., and Zhang, Z. (2019). MSC-derived exosomes-based therapy for peripheral nerve injury: a novel therapeutic strategy. *Biomed. Res. Int.* 2019:6458237. doi: 10.1155/2019/6458237

D'souza, N., Rossignoli, F., Golinelli, G., Grisendi, G., Spano, C., Candini, O., et al. (2015). Mesenchymal stem/stromal cells as a delivery platform in cell and gene therapies. *BMC Medicine* 13:186. doi: 10.1186/S12916-015-0426-0

Fan, X.-L., Zhang, Y., Li, X., and Fu, Q.-L. (2020). Mechanisms underlying the protective effects of mesenchymal stem cell-based therapy. *Cell Mol. Life Sci.* 77, 2771–2794. doi: 10.1007/s00018-020-03454-6

Fernandez-Llama, P., Khositseth, S., Gonzales, P. A., Star, R. A., Pisitkun, T., and Knepper, M. A. (2010). Tamm-Horsfall protein and urinary exosome isolation. *Kidney Int.* 77, 736–742. doi: 10.1038/ki.2009.550

Fricke, A., Ullrich, P. V., Cimniak, A. F. V., Becherer, C., Follo, M., Heinz, J., et al. (2017). Levels of activated platelet-derived microvesicles in patients with soft tissue sarcoma correlate with an increased risk of venous thromboembolism. *BMC Cancer* 17:527. doi: 10.1186/s12885-017-3515-y

Frydrychowicz, M., Kolecka-Bednarczyk, A., Madejczyk, M., Yasar, S., and Dworacki, G. (2015). Exosomes - structure, biogenesis and biological role in non-small-cell lung cancer. *Scand. J. Immunol.* 81, 2–10. doi: 10.1111/sji.12247

Furlani, D., Ugurlucan, M., Ong, L., Bieback, K., Pittermann, E., Westien, I., et al. (2009). Is the intravascular administration of mesenchymal stem cells safe? Mesenchymal stem cells and intravital microscopy. *Microvasc. Res.* 77, 370–376. doi: 10.1016/j.mvr.2009.02.001

Furuta, T., Miyaki, S., Ishitobi, H., Ogura, T., Kato, Y., Kamei, N., et al. (2016). Mesenchymal stem cell-derived exosomes promote fracture healing in a mouse model. *Stem Cells Transl. Med.* 5, 1620–1630. doi: 10.5966/sctm.2015-0285

Galipeau, J., and Sensebe, L. (2018). Mesenchymal stromal cells: clinical challenges and therapeutic opportunities. *Cell Stem Cell* 22, 824–833. doi: 10.1016/j.stem.2018.05.004

Gamez-Valero, A., Monguio-Tortajada, M., Carreras-Planella, L., Franquesa, M., Beyer, K., and Borras, F. E. (2016). Size-exclusion chromatography-based isolation minimally alters extracellular Vesicles' characteristics compared to precipitating agents. *Sci. Rep.* 6:33641. doi: 10.1038/srep33641

Giebel, B., Kordelas, L., and Borger, V. (2017). Clinical potential of mesenchymal stem/stromal cell-derived extracellular vesicles. *Stem Cell Investig.* 4:84. doi: 10.21037/sci.2017.09.06

Greening, D. W., Xu, R., Ji, H., Tauro, B. J., and Simpson, R. J. (2015). A protocol for exosome isolation and characterization: evaluation of ultracentrifugation, density-gradient separation, and immunoaffinity capture methods. *Methods Mol. Biol.* 1295, 179–209. doi: 10.1007/978-1-4939-2550-6_15

Gurunathan, S., Kang, M. H., Jeyaraj, M., Qasim, M., and Kim, J. H. (2019). Review of the isolation, characterization, biological function, and multifarious therapeutic approaches of exosomes. *Cells* 8:307. doi: 10.3390/cells8040307

Hanson, P. I., and Cashikar, A. (2012). Multivesicular body morphogenesis. *Annu. Rev. Cell Dev. Biol.* 28, 337–362. doi: 10.1146/annurev-cellbio-092910-154152

Harding, C., Heuser, J., and Stahl, P. (1983). Receptor-mediated endocytosis of transferrin and recycling of the transferrin receptor in rat reticulocytes. *J. Cell Biol.* 97, 329–339. doi: 10.1083/jcb.97.2.329

Heldens, G. T. H., Blaney Davidson, E. N., Vitters, E. L., Schreurs, B. W., Piek, E., van den Berg, W. B., et al. (2012). Catabolic factors and osteoarthritis-conditioned medium inhibit chondrogenesis of human mesenchymal stem cells. *Tissue Eng. Part A* 18, 45–54. doi: 10.1089/ten.TEA.2011.0083

Hu, C., Zhao, L., and Li, L. (2019). Current understanding of adipose-derived mesenchymal stem cell-based therapies in liver diseases. *Stem Cell Res. Ther.* 10:199. doi: 10.1186/s13287-019-1310-1

Hu, L., Yin, C., Zhao, F., Ali, A., Ma, J., and Qian, A. (2018). Mesenchymal stem cells: cell fate decision to osteoblast or adipocyte and application in osteoporosis treatment. *Int. J. Mol. Sci.* 19:360. doi: 10.3390/ijms19020360

Jeong, J. O., Han, J. W., Kim, J. M., Cho, H. J., Park, C., Lee, N., et al. (2011). Malignant tumor formation after transplantation of short-term cultured bone marrow mesenchymal stem cells in experimental myocardial infarction and diabetic neuropathy. *Circ. Res.* 108, 1340–1347. doi: 10.1161/CIRCRESAHA.110.239848

Jing, H., He, X., and Zheng, J. (2018). Exosomes and regenerative medicine: state of the art and perspectives. *Transl. Res.* 196, 1–16. doi: 10.1016/j.trsl.2018.01.005

Kanwar, S. S., Dunlay, C. J., Simeone, D. M., and Nagrath, S. (2014). Microfluidic device (ExoChip) for on-chip isolation, quantification and characterization of circulating exosomes. *Lab Chip* 14, 1891–1900. doi: 10.1039/c4lc00136b

Keith, S. (2012). Osteoarthritis: diagnosis and treatment. *Am. Family Phys.* 85:49.

Kim, J., Shin, H., Kim, J., Kim, J., and Park, J. (2015). Isolation of high-purity extracellular vesicles by extracting proteins using aqueous two-phase system. *PLoS One* 10:e0129760. doi: 10.1371/journal.pone.0129760

Konoshenko, M. Y., Lekchnov, E. A., Vlassov, A. V., and Laktionov, P. P. (2018). Isolation of extracellular vesicles: general methodologies and latest trends. *Biomed. Res. Int.* 2018:8545347. doi: 10.1155/2018/8545347

Kowal, J., Tkach, M., and Théry, C. (2014). Biogenesis and secretion of exosomes. *Curr. Opin. Cell Biol.* 29, 116–125. doi: 10.1016/j.ceb.2014.05.004

Lai, R. C., Arslan, F., Lee, M. M., Sze, N. S., Choo, A., Chen, T. S., et al. (2010). Exosome secreted by MSC reduces myocardial ischemia/reperfusion injury. *Stem Cell Res.* 4, 214–222. doi: 10.1016/j.scr.2009.12.003

Lai, R. C., Tan, S. S., Teh, B. J., Sze, S. K., Arslan, F., de Kleijn, D. P., et al. (2012). Proteolytic potential of the MSC exosome proteome: implications for an exosome-mediated delivery of therapeutic proteasome. *Int. J. Proteomics* 2012:971907. doi: 10.1155/2012/971907

Lai, R. C., Tan, S. S., Yeo, R. W., Choo, A. B., Reiner, A. T., Su, Y., et al. (2016). MSC secretes at least 3 EV types each with a unique permutation of membrane lipid, protein and RNA. *J. Extracell. Vesicles* 5:29828. doi: 10.3402/jev.v5.29828

Lai, R. C., Yeo, R. W., and Lim, S. K. (2015). Mesenchymal stem cell exosomes. *Semin. Cell Dev. Biol.* 40, 82–88. doi: 10.1016/j.semcdb.2015.03.001

Li, T., Yan, Y., Wang, B., Qian, H., Zhang, X., Shen, L., et al. (2013). Exosomes derived from human umbilical cord mesenchymal stem cells alleviate liver fibrosis. *Stem Cells Dev.* 22, 845–854. doi: 10.1089/scd.2012.0395

Liang, L. G., Kong, M. Q., Zhou, S., Sheng, Y. F., Wang, P., Yu, T., et al. (2017). An integrated double-filtration microfluidic device for isolation, enrichment and quantification of urinary extracellular vesicles for detection of bladder cancer. *Sci. Rep.* 7:46224. doi: 10.1038/srep46224

Lindblad, S., and Hedfors, E. (1987). Arthroscopic and immunohistologic characterization of knee joint synovitis in osteoarthritis. *Arthritis Rheum.* 30, 1081–1088. doi: 10.1002/art.1780301001

Liu, S., Liu, D., Chen, C., Hamamura, K., Moshaverinia, A., Yang, R., et al. (2015). MSC transplantation improves osteopenia via epigenetic regulation of notch signaling in lupus. *Cell Metab.* 22, 606–618. doi: 10.1016/j.cmet.2015.08.018

Liu, W., Li, L., Rong, Y., Qian, D., Chen, J., Zhou, Z., et al. (2020). Hypoxic mesenchymal stem cell-derived exosomes promote bone fracture healing by the transfer of miR-126. *Acta Biomater.* 103, 196–212. doi: 10.1016/j.actbio.2019.12.020

Liu, Y., Zou, R., Wang, Z., Wen, C., Zhang, F., and Lin, F. (2018). Exosomal KLF3-AS1 from hMSCs promoted cartilage repair and chondrocyte proliferation in osteoarthritis. *Biochem. J.* 475, 3629–3638. doi: 10.1042/BCJ20180675

Liu-Bryan, R. (2015). Inflammation and intracellular metabolism: new targets in OA. *Osteoarthr. Cartil.* 23, 1835–1842. doi: 10.1016/j.joca.2014.12.016

Livshits, M. A., Khomyakova, E., Evtushenko, E. G., Lazarev, V. N., Kulemin, N. A., Semina, S. E., et al. (2015). Isolation of exosomes by differential centrifugation: theoretical analysis of a commonly used protocol. *Sci. Rep.* 5:17319. doi: 10.1038/srep17319

Lobb, R. J., Becker, M., Wen Wen, S., Wong, C. S. F., Wiegmans, A. P., Leimgruber, A., et al. (2015). Optimized exosome isolation protocol for cell culture supernatant and human plasma. *J. Extracell. Vesicles* 4:27031. doi: 10.3402/jev.v4.27031

Loeser, R. F., Goldring, S. R., Scanzello, C. R., and Goldring, M. B. (2012). Osteoarthritis: a disease of the joint as an organ. *Arthr. Rheumatol.* 64, 1697–1707. doi: 10.1002/art.34453

Lopez-Verrilli, M. A., Caviedes, A., Cabrera, A., Sandoval, S., Wyneken, U., and Khoury, M. (2016). Mesenchymal stem cell-derived exosomes from different sources selectively promote neuritic outgrowth. *Neuroscience* 320, 129–139. doi: 10.1016/j.neuroscience.2016.01.061

Mao, G., Zhang, Z., Hu, S., Zhang, Z., Chang, Z., Huang, Z., et al. (2018). Exosomes derived from miR-92a-3p-overexpressing human mesenchymal stem cells enhance chondrogenesis and suppress cartilage degradation via targeting WNT5A. *Stem Cell Res. Ther.* 9:247. doi: 10.1186/s13287-018-1004-0

Mathivanan, S., Ji, H., and Simpson, R. J. (2010). Exosomes: extracellular organelles important in intercellular communication. *J. Proteomics* 73, 1907–1920. doi: 10.1016/j.jprot.2010.06.006

Meirelles Lda, S., Fontes, A. M., Covas, D. T., and Caplan, A. I. (2009). Mechanisms involved in the therapeutic properties of mesenchymal stem cells. *Cytokine Growth Factor Rev.* 20, 419–427. doi: 10.1016/j.cytogfr.2009.10.002

Missoum, A. (2020). Recent updates on mesenchymal stem cell based therapy for acute renal failure. *Curr. Urol.* 13, 189–199. doi: 10.1159/000499272

Naderi-Meshkin, H., Lai, X., Amirkhah, R., Vera, J., Rasko, J. E. J., and Schmitz, U. (2019). Exosomal lncRNAs and cancer: connecting the missing links. *Bioinformatics* 35, 352–360. doi: 10.1093/bioinformatics/bty527

Nold, P., Hackstein, H., Riedlinger, T., Kasper, C., Neumann, A., Mernberger, M., et al. (2015). Immunosuppressive capabilities of mesenchymal stromal cells are maintained under hypoxic growth conditions and after gamma irradiation. *Cytotherapy* 17, 152–162. doi: 10.1016/j.jcyt.2014.10.004

Ohno, S., Ishikawa, A., and Kuroda, M. (2013). Roles of exosomes and microvesicles in disease pathogenesis. *Adv. Drug Deliv. Rev.* 65, 398–401. doi: 10.1016/j.addr.2012.07.019

Pak, H. N., Qayyum, M., Kim, D. T., Hamabe, A., Miyauchi, Y., Lill, M. C., et al. (2003). Mesenchymal stem cell injection induces cardiac nerve sprouting and increased tenascin expression in a Swine model of myocardial infarction. *J. Cardiovasc. Electrophysiol.* 14, 841–848. doi: 10.1046/j.1540-8167.2003.03124.x

Pan, B. T., and Johnstone, R. M. (1983). Fate of the transferrin receptor during maturation of sheep reticulocytes in vitro: selective externalization of the receptor. *Cell* 33, 967–978. doi: 10.1016/0092-8674(83)90040-5

Park, K. S., Bandeira, E., Shelke, G. V., Lasser, C., and Lotvall, J. (2019). Enhancement of therapeutic potential of mesenchymal stem cell-derived extracellular vesicles. *Stem Cell Res. Ther.* 10:288. doi: 10.1186/s13287-019-1398-3

Peterson, M. F., Otoc, N., Sethi, J. K., Gupta, A., and Antes, T. J. (2015). Integrated systems for exosome investigation. *Methods* 87, 31–45. doi: 10.1016/j.ymeth.2015.04.015

Pittenger, M. F., Mackay, A. M., Beck, S. C., Jaiswal, R. K., Douglas, R., Mosca, J. D., et al. (1999). Multilineage potential of adult human mesenchymal stem cells. *Science* 284, 143–147. doi: 10.1126/science.284.5411.143

Pozsgay, J., Szekanecz, Z., and Sarmay, G. (2017). Antigen-specific immunotherapies in rheumatic diseases. *Nat. Rev. Rheumatol.* 13, 525–537. doi: 10.1038/nrrheum.2017.107

Qi, H., Liu, D. P., Xiao, D. W., Tian, D. C., Su, Y. W., and Jin, S. F. (2019). Exosomes derived from mesenchymal stem cells inhibit mitochondrial dysfunction-induced apoptosis of chondrocytes via p38, ERK, and Akt pathways. *In Vitro Cell Dev. Biol. Anim.* 55, 203–210. doi: 10.1007/s11626-019-00330-x

Qi, X., Zhang, J. Y., Yuan, H., Xu, Z. L., Li, Q., Niu, X., et al. (2016). Exosomes secreted by human-induced pluripotent stem cell-derived mesenchymal stem cells repair critical-sized bone defects through enhanced angiogenesis and osteogenesis in osteoporotic rats. *Int. J. Biol. Sci.* 12, 836–849. doi: 10.7150/ijbs.14809

Qi, Y., Feng, G., and Yan, W. (2012). Mesenchymal stem cell-based treatment for cartilage defects in osteoarthritis. *Mol. Biol. Rep.* 39, 5683–5689. doi: 10.1007/s11033-011-1376-z

Ragni, E., Perucca Orfei, C., De Luca, P., Colombini, A., Vigano, M., and de Girolamo, L. (2020). Secreted factors and EV-miRNAs orchestrate the healing capacity of adipose mesenchymal stem cells for the treatment of knee osteoarthritis. *Int. J. Mol. Sci.* 21:1582. doi: 10.3390/ijms21051582

Ragni, E., Perucca Orfei, C., De Luca, P., Lugano, G., Vigano, M., Colombini, A., et al. (2019). Interaction with hyaluronan matrix and miRNA cargo as contributors for in vitro potential of mesenchymal stem cell-derived extracellular vesicles in a model of human osteoarthritic synoviocytes. *Stem Cell Res. Ther.* 10:109. doi: 10.1186/s13287-019-1215-z

Rani, S., Ryan, A. E., Griffin, M. D., and Ritter, T. (2015). Mesenchymal stem cell-derived extracellular vesicles: toward cell-free therapeutic applications. *Mol. Ther.* 23, 812–823. doi: 10.1038/mt.2015.44

Raposo, G., and Stoorvogel, W. (2013). Extracellular vesicles: exosomes, microvesicles, and friends. *J. Cell Biol.* 200, 373–383. doi: 10.1083/jcb.201211138

Romanelli, P., Bieler, L., Scharler, C., Pachler, K., Kreutzer, C., Zaunmair, P., et al. (2019). Extracellular vesicles can deliver anti-inflammatory and anti-scarring activities of mesenchymal stromal cells after spinal cord injury. *Front. Neurol.* 10:1225. doi: 10.3389/fneur.2019.01225

Shao, H., Chung, J., and Issadore, D. (2015). Diagnostic technologies for circulating tumour cells and exosomes. *Biosci. Rep.* 36:e00292. doi: 10.1042/BSR20150180

Shenoda, B. B., and Ajit, S. K. (2016). Modulation of immune responses by exosomes derived from antigen-presenting cells. *Clin. Med. Insights Pathol.* 9(Suppl. 1), 1–8. doi: 10.4137/CPath.S39925

Squillaro, T., Peluso, G., and Galderisi, U. (2016). Clinical trials with mesenchymal stem cells: an update. *Cell Transpl.* 25, 829–848. doi: 10.3727/096368915x689622

Stiehler, M., Goronzy, J., and Gunther, K. P. (2015). [Total hip arthroplasty in overweight osteoarthritis patients]. *Orthopade* 44, 523–530. doi: 10.1007/s00132-015-3094-z

Takahashi, A., Okada, R., Nagao, K., Kawamata, Y., Hanyu, A., Yoshimoto, S., et al. (2017). Exosomes maintain cellular homeostasis by excreting harmful DNA from cells. *Nat. Commun.* 8:15287. doi: 10.1038/ncomms15287

Takeuchi, R., Katagiri, W., Endo, S., and Kobayashi, T. (2019). Exosomes from conditioned media of bone marrow-derived mesenchymal stem cells promote bone regeneration by enhancing angiogenesis. *PLoS One* 14:e0225472. doi: 10.1371/journal.pone.0225472

Tan, C. Y., Lai, R. C., Wong, W., Dan, Y. Y., Lim, S. K., and Ho, H. K. (2014). Mesenchymal stem cell-derived exosomes promote hepatic regeneration in drug-induced liver injury models. *Stem Cell Res. Ther.* 5:76. doi: 10.1186/scrt465

Tao, S. C., Yuan, T., Zhang, Y. L., Yin, W. J., Guo, S. C., and Zhang, C. Q. (2017). Exosomes derived from miR-140-5p-overexpressing human synovial mesenchymal stem cells enhance cartilage tissue regeneration and prevent osteoarthritis of the knee in a rat model. *Theranostics* 7, 180–195. doi: 10.7150/thno.17133

Thery, C., Ostrowski, M., and Segura, E. (2009). Membrane vesicles as conveyors of immune responses. *Nat. Rev. Immunol.* 9, 581–593. doi: 10.1038/nri2567

Thery, C., Witwer, K. W., Aikawa, E., Alcaraz, M. J., Anderson, J. D., Andriantsitohaina, R., et al. (2018). Minimal information for studies of extracellular vesicles 2018 (MISEV2018): a position statement of the international society for extracellular vesicles and update of the MISEV2014 guidelines. *J. Extracell. Vesicles* 7:1535750. doi: 10.1080/20013078.2018.1535750

Tofiño-Vian, M., Guillén, M. I., Caz, P. D., Silvestre, A., and Alcaraz, M. J. (2018). Microvesicles from human adipose tissue-derived mesenchymal stem cells as a new protective strategy in osteoarthritic chondrocytes. *Cell. Physiol. Biochem.* 47, 11–25. doi: 10.1159/000489739

Toh, W. S., Lai, R. C., Hui, J. H. P., and Lim, S. K. (2017). MSC exosome as a cell-free MSC therapy for cartilage regeneration: implications for osteoarthritis treatment. *Semin. Cell Dev. Biol.* 67, 56–64. doi: 10.1016/j.semcdb.2016.11.008

Toh, W. S., Lai, R. C., Zhang, B., and Lim, S. K. (2018). MSC exosome works through a protein-based mechanism of action. *Biochem. Soc. Trans.* 46, 843–853. doi: 10.1042/BST20180079

Tolar, J., Nauta, A. J., Osborn, M. J., Panoskaltsis Mortari, A., McElmurry, R. T., Bell, S., et al. (2007). Sarcoma derived from cultured mesenchymal stem cells. *Stem Cells* 25, 371–379. doi: 10.1634/stemcells.2005-0620

Trajkovic, K., Hsu, C., Chiantia, S., Rajendran, L., Wenzel, D., Wieland, F., et al. (2008). Ceramide triggers budding of exosome vesicles into multivesicular endosomes. *Science* 319, 1244–1247. doi: 10.1126/science.1153124

Trams, E. G., Lauter, C. J., Salem, N. Jr., and Heine, U. (1981). Exfoliation of membrane ecto-enzymes in the form of micro-vesicles. *Biochim. Biophys. Acta* 645, 63–70. doi: 10.1016/0005-2736(81)90512-5

van der Pol, E., Böing, A. N., Harrison, P., Sturk, A., and Nieuwland, R. (2012). Classification, functions, and clinical relevance of extracellular vesicles. *Pharmacol. Rev.* 64, 676–705. doi: 10.1124/pr.112.005983

van Niel, G., Porto-Carreiro, I., Simoes, S., and Raposo, G. (2006). Exosomes: a common pathway for a specialized function. *J. Biochem.* 140, 13–21. doi: 10.1093/jb/mvj128

Vega, A., Martin-Ferrero, M. A., Del Canto, F., Alberca, M., Garcia, V., Munar, A., et al. (2015). Treatment of knee osteoarthritis with allogeneic bone marrow mesenchymal stem cells: a randomized controlled trial. *Transplantation* 99, 1681–1690. doi: 10.1097/tp.0000000000000678

Wang, D., and Sun, W. (2014). Urinary extracellular microvesicles: isolation methods and prospects for urinary proteome. *Proteomics* 14, 1922–1932. doi: 10.1002/pmic.201300371

Wang, R., Xu, B., and Xu, H. (2018). TGF-beta1 promoted chondrocyte proliferation by regulating Sp1 through MSC-exosomes derived miR-135b. *Cell Cycle* 17, 2756–2765. doi: 10.1080/15384101.2018.1556063

Wang, Y. F., Yu, D. S., Liu, Z. M., Zhou, F., Dai, J., Wu, B. B., et al. (2017). Exosomes from embryonic mesenchymal stem cells alleviate osteoarthritis through balancing synthesis and degradation of cartilage extracellular matrix. *Stem Cell Res. Ther.* 8:189. doi: 10.1186/S13287-017-0632-0

Wang, Z., Wang, Y., Wang, Z., Gutkind, J. S., Wang, Z., Wang, F., et al. (2015). Engineered mesenchymal stem cells with enhanced tropism and paracrine secretion of cytokines and growth factors to treat traumatic brain injury. *Stem Cells* 33, 456–467. doi: 10.1002/stem.1878

Wang, Z., Wu, H. J., Fine, D., Schmulen, J., Hu, Y., Godin, B., et al. (2013). Ciliated micropillars for the microfluidic-based isolation of nanoscale lipid vesicles. *Lab Chip* 13, 2879–2882. doi: 10.1039/c3lc41343h

Willis, G. R., Mitsialis, S. A., and Kourembanas, S. (2018). "Good things come in small packages": application of exosome-based therapeutics in neonatal lung injury. *Pediatr. Res.* 83, 298–307. doi: 10.1038/pr.2017.256

Witwer, K. W., Buzas, E. I., Bemis, L. T., Bora, A., Lasser, C., Lotvall, J., et al. (2013). Standardization of sample collection, isolation and analysis methods in extracellular vesicle research. *J. Extracell. Vesicles* 2:20360. doi: 10.3402/jev.v2i0.20360

Wu, J., Kuang, L., Chen, C., Yang, J., Zeng, W. N., Li, T., et al. (2019). miR-100-5p-abundant exosomes derived from infrapatellar fat pad MSCs protect articular cartilage and ameliorate gait abnormalities via inhibition of mTOR in osteoarthritis. *Biomaterials* 206, 87–100. doi: 10.1016/j.biomaterials.2019.03.022

Wunsch, B. H., Smith, J. T., Gifford, S. M., Wang, C., Brink, M., Bruce, R. L., et al. (2016). Nanoscale lateral displacement arrays for the separation of exosomes and colloids down to 20 nm. *Nat. Nanotechnol.* 11, 936–940. doi: 10.1038/nnano.2016.134

Xin, H., Li, Y., Cui, Y., Yang, J. J., Zhang, Z. G., and Chopp, M. (2013). Systemic administration of exosomes released from mesenchymal stromal cells promote functional recovery and neurovascular plasticity after stroke in rats. *J. Cereb. Blood Flow Metab.* 33, 1711–1715. doi: 10.1038/jcbfm.2013.152

Xin-Wei, L., Ying, Z., Liang-Bi, X., and Yu, W. (2015). Total hip arthroplasty: a review of advances, advantages and limitations. *Int. J. Clin. Exp. Med.* 8, 27–36.

Yáñez-Mó, M., Siljander, P. R.-M., Andreu, Z., Zavec, A. B., Borràs, F. E., Buzas, E. I., et al. (2015). Biological properties of extracellular vesicles and their physiological functions. *J. Extracell. Vesicles* 4:27066. doi: 10.3402/jev.v4.27066

Yang, Y., Ye, Y., Su, X., He, J., Bai, W., and He, X. (2017). MSCs-derived exosomes and neuroinflammation, neurogenesis and therapy of traumatic brain injury. *Front. Cell. Neurosci.* 11:55. doi: 10.3389/fncel.2017.00055

Yeo, R. W., Lai, R. C., Zhang, B., Tan, S. S., Yin, Y., Teh, B. J., et al. (2013). Mesenchymal stem cell: an efficient mass producer of exosomes for drug delivery. *Adv. Drug Deliv. Rev.* 65, 336–341. doi: 10.1016/j.addr.2012.07.001

Yoon, Y. S., Park, J. S., Tkebuchava, T., Luedeman, C., and Losordo, D. W. (2004). Unexpected severe calcification after transplantation of bone marrow cells in acute myocardial infarction. *Circulation* 109, 3154–3157. doi: 10.1161/01.CIR.0000134696.08436.65

Zeringer, E., Barta, T., Li, M., and Vlassov, A. V. (2015). Strategies for isolation of exosomes. *Cold Spring Harb. Protoc.* 2015, 319–323. doi: 10.1101/pdb.top074476

Zhang, J. Y., Liu, X. L., Li, H. Y., Chen, C. Y., Hu, B., Niu, X., et al. (2016). Exosomes/tricalcium phosphate combination scaffolds can enhance bone regeneration by activating the PI3K/Akt signaling pathway. *Stem Cell Res. Ther.* 7:136. doi: 10.1186/S13287-016-0391-3

Zhang, S., Chu, W. C., Lai, R. C., Lim, S. K., Hui, J. H., and Toh, W. S. (2016). Exosomes derived from human embryonic mesenchymal stem cells promote osteochondral regeneration. *Osteoarthr. Cartil.* 24, 2135–2140. doi: 10.1016/j.joca.2016.06.022

Zhang, S., Chuah, S. J., Lai, R. C., Hui, J. H. P., Lim, S. K., and Toh, W. S. (2018). MSC exosomes mediate cartilage repair by enhancing proliferation, attenuating apoptosis and modulating immune reactivity. *Biomaterials* 156, 16–27. doi: 10.1016/j.biomaterials.2017.11.028

Zhang, S., Teo, K. Y. W., Chuah, S. J., Lai, R. C., Lim, S. K., and Toh, W. S. (2019). MSC exosomes alleviate temporomandibular joint osteoarthritis by attenuating inflammation and restoring matrix homeostasis. *Biomaterials* 200, 35–47. doi: 10.1016/j.biomaterials.2019.02.006

Zhang, Y., Hao, Z., Wang, P., Xia, Y., Wu, J., Xia, D., et al. (2019). Exosomes from human umbilical cord mesenchymal stem cells enhance fracture healing through HIF-1alpha-mediated promotion of angiogenesis in a rat model of stabilized fracture. *Cell Prolif.* 52:e12570. doi: 10.1111/cpr.12570

Zhao, P., Xiao, L., Peng, J., Qian, Y. Q., and Huang, C. C. (2018). Exosomes derived from bone marrow mesenchymal stem cells improve osteoporosis through promoting osteoblast proliferation via MAPK pathway. *Eur. Rev. Med. Pharm. Sci.* 22, 3962–3970. doi: 10.26355/eurrev-201806-15280

Zhong, Z., Ethen, N. J., and Williams, B. O. (2014). WNT signaling in bone development and homeostasis. *Wiley Interdiscip. Rev. Dev. Biol.* 3, 489–500. doi: 10.1002/wdev.159

Zhou, J., Mukherjee, P., Gao, H., Luan, Q., and Papautsky, I. (2019). Label-free microfluidic sorting of microparticles. *APL Bioeng.* 3:041504. doi: 10.1063/1.5120501

Zhou, Y., Yamamoto, Y., Xiao, Z., and Ochiya, T. (2019). The immunomodulatory functions of mesenchymal stromal/stem cells mediated via paracrine activity. *J. Clin. Med.* 8:1025. doi: 10.3390/jcm8071025

Zuo, R., Liu, M., Wang, Y., Li, J., Wang, W., Wu, J., et al. (2019). BM-MSC-derived exosomes alleviate radiation-induced bone loss by restoring the function of recipient BM-MSCs and activating Wnt/beta-catenin signaling. *Stem Cell Res. Ther.* 10:30. doi: 10.1186/s13287-018-1121-9

Conflict of Interest: The authors declare that the research was conducted in the absence of any commercial or financial relationships that could be construed as a potential conflict of interest.

Copyright © 2020 Liu, Xu, Liang, Chen, Zhang, Qian and Hu. This is an open-access article distributed under the terms of the Creative Commons Attribution License (CC BY). The use, distribution or reproduction in other forums is permitted, provided the original author(s) and the copyright owner(s) are credited and that the original publication in this journal is cited, in accordance with accepted academic practice. No use, distribution or reproduction is permitted which does not comply with these terms.

frontiers in Cell and Developmental Biology

REVIEW
published: 02 September 2020
doi: 10.3389/fcell.2020.00870

Multifaceted Functions and Novel Insight Into the Regulatory Role of RNA N^6-Methyladenosine Modification in Musculoskeletal Disorders

Wenchao Zhang[1,2], Lile He[2,3], Zhongyue Liu[1,2], Xiaolei Ren[1,2], Lin Qi[1,2], Lu Wan[1,2], Wanchun Wang[1,2], Chao Tu[1,2] and Zhihong Li[1,2]**

[1] Department of Orthopedics, The Second Xiangya Hospital, Central South University, Changsha, China, [2] Hunan Key Laboratory of Tumor Models and Individualized Medicine, The Second Xiangya Hospital, Central South University, Changsha, China, [3] Department of Cardiovascular Surgery, The Second Xiangya Hospital, Central South University, Changsha, China

OPEN ACCESS

Edited by:
Changjun Li,
Central South University, China

Reviewed by:
Zhengwei Yan,
First Affiliated Hospital of Nanchang University, China
Amelia Eva Aranega,
University of Jaén, Spain

***Correspondence:**
Chao Tu
tuchao@csu.edu.cn
Zhihong Li
lizhihong@csu.edu.cn

Specialty section:
This article was submitted to Molecular Medicine, a section of the journal Frontiers in Cell and Developmental Biology

Received: 30 June 2020
Accepted: 11 August 2020
Published: 02 September 2020

Citation:
Zhang W, He L, Liu Z, Ren X, Qi L, Wan L, Wang W, Tu C and Li Z (2020) Multifaceted Functions and Novel Insight Into the Regulatory Role of RNA N^6-Methyladenosine Modification in Musculoskeletal Disorders. Front. Cell Dev. Biol. 8:870. doi: 10.3389/fcell.2020.00870

RNA modifications have emerged as key regulators of transcript expression in diverse physiological and pathological processes. As one of the most prevalent types of RNA modifications, N^6-methyladenosine (m^6A) has become the highlight in modulation of various diseases through interfering RNA splicing, translation, nuclear export, and decay. In many cases, the detailed functions of m^6A in cellular processes and diseases remain unclear. Notably, recent studies have determined the relationship between m^6A modification and musculoskeletal disorders containing osteosarcoma, osteoarthritis, rheumatoid arthritis, osteoporosis, etc. Herein, this review comprehensively summarizes the recent advances of m^6A modification in pathogenesis and progression of musculoskeletal diseases. Specifically, the underlying molecular mechanisms, detection technologies, regulatory functions, clinical implications, and future perspectives of m^6A in musculoskeletal disorders are discussed, with the aim to provide a novel insight into their association.

Keywords: RNA N^6-methyladenosine, METTL3, FTO, musculoskeletal disorders, epigenetics

INTRODUCTION

Currently, a growing number of studies have shed light on a new hereditary manner, the epigenetics, which refers to changes in phenotype without DNA or RNA sequences alteration (Harvey et al., 2018). Several epigenetics manners have been identified, comprising the histone modification, DNA and RNA methylation, and noncoding RNA (ncRNA) modification. Of note, there have been more than 100 modifications demonstrated within RNAs over the past few years, including the N^1-methyladenosine (m^1A), m^6A, 5-methylcytosine (m^5C), 7-methylguanosine (m^7G), m^1G, m^2G, m^6G, etc. Among them, the m^6A has received considerable attention because of its high abundance. It relates to a dynamic and reversible RNA modification that participate in a wide range of biological and pathological processes, such as the cancer progression (Lan et al., 2019) and inflammation (Zong et al., 2019). Specifically, it can manipulate the RNA splicing, export, translation, and

degradation through methylation and demethylation mediated by multiple enzymes (Cao et al., 2016).

Musculoskeletal disorders are a set of prevalent diseases characterized by dysfunction of bone and skeletal muscle, including, but not limited to, osteosarcoma (OS), osteoarthritis (OA), rheumatoid arthritis (RA), osteoporosis (OP), etc. (Madan and Grime, 2015). Several epigenetics manners have been investigated in this field (Tu et al., 2019; van Wijnen and Westendorf, 2019). Among them, the alteration of m^{6}A modification has been associated with the initiation and progression of musculoskeletal diseases.

In this review, we broadly summarize the functional repertoire of m^{6}A in various musculoskeletal disorders, aiming to expand our understanding and discuss the putative perspective for adopting m^{6}A as a novel biomarker and therapeutic target in musculoskeletal diseases.

RNA M^{6}A MODIFICATION

As aforementioned, m^{6}A modification is a dynamic and reversible epigenetic change (Zhang et al., 2020), which affects the stability and function of RNAs, thereby modulating the pathogenesis and progression of diseases (Qin et al., 2020; Wang et al., 2020; Zhu et al., 2020). M^{6}A modification has been identified in more than 7,000 human genes, and it preferentially occurred at the site of stop codons and long internal exons within the RRACH sequence (R = G or A; H = A, C, or U) (Dominissini et al., 2012). Based on current evidences, m^{6}A modification is able to interfere in RNA processing, splicing, export, degradation, and translation through the "writers," "erasers," and "readers" proteins (Chen et al., 2019). The detailed graphical description of the RNA m^{6}A mechanism is presented in **Figure 1**.

Writers refer to the RNA methyltransferases, including methyltransferase-like 3 (METTL3), methyltransferase-like 14 (METTL14), methyltransferase-like 16 (METTL16), Wilms tumor 1-associated protein (WTAP), RNA-binding motif 15, etc. They are in charge of installing m^{6}A to the RNA strand. In particular, METTL3 and METTL14 are the most studied key regulators in this process. They contain an S-adenosylmethionine–binding motif and are capable of adding methyl to the adenosine. Meanwhile, these two proteins can form a heterodimer core complex to modulate the cellular m^{6}A deposition (Liu et al., 2014), in which they adopted a class I methyltransferase fold and interacted with each other through hydrogen bonding. Additionally, biochemical analysis revealed that METTL3 principally acted as the catalytic core, whereas METTL14 mainly functioned as an RNA-binding platform (Wang et al., 2016). Besides, the cofactor WTAP itself shows no methyltransferase activity, whereas it could interplay with the core complex to mediate its localization in nuclear spots (Ping et al., 2014). Furthermore, it has been reported that WTAP protein homeostasis in turn relied on the METTL3 protein levels (Sorci et al., 2018). Therefore, these writers cooperate to exert their function of m^{6}A methylation within the specific RNA sites.

In contrast to the "writers," the "erasers" are demethylases that function in methyl removal, canonically involving the fat mass and obesity-associated protein (FTO) and alkB homolog 5 (ALKBH5). FTO can oxidize m^{6}A to generate the N(6)-hydroxymethyladenosine and N(6)-formyladenosine that have a half-life time less than 3 h (Fu et al., 2013). Generally, FTO erase methyl in either the selective or nonselective way. In the selective way, FTO recognizes and binds to the specific m^{6}A-containing motif in cells (Li et al., 2019a). Because the association between FTO and RNA is weak, the additional cellular factors can corporately work with FTO to recognize and choose the target sites (Li et al., 2019a). In addition, the m^{6}A itself can act as a "conformational marker" and interfere with the interaction between m^{6}A and FTO via altering conformational outcomes in RNAs, which is the nonselective way of FTO-mediated demethylation (Zou et al., 2016). ALKBH5 is a 2-oxoglutarate and ferrous iron–dependent nucleic acid oxygenase that induces the demethylation of multiple RNAs. It was illuminated that ALKBH5 could occupy a similar region as L1 loop of the FTO protein that was associated with the single-strand RNA selectivity (Aik et al., 2014). Taken together, FTO and ALKBH5 are both the core regulators of m^{6}A demethylation.

Readers are a group of proteins that discern the m^{6}A modification and determine the functions of RNA transcripts. YTH domain (YTHD) family members (consisting of YTHDF1, YTHDF2, YTHDF3, YTHDC1, and YTHDC2) constitute a large class of m^{6}A readers. They are located in nucleus or cytoplasm (specifically, YTHDF1 and YTHDF2 are located both in cytoplasm and nucleus, whereas YTHDF3 is only found in the cytoplasm) (Reichel et al., 2019), and characterized by containing the YT521B homology (YTH) domain that possesses an exquisite pocket with two conserved tryptophan residues (W377 and W428) for specific recognition of the methyl group (Xu et al., 2014). YTHDF1 is shown to promote translation of mRNA and enhance protein synthesis through impacting on the translation machinery, ensuring the sufficient protein generation is marked by m^{6}A (Wang et al., 2015). Conversely, YTHDF2 mediates the degradation of its target m^{6}A transcripts via reducing their stability (Li et al., 2018). Additionally, YTHDF3 participates in either promoting the protein synthesis in synergy with YTHDF1 or facilitating RNA degradation via interaction with YTHDF2. Thus, these three YTHDF proteins read the m^{6}A modification in a cooperative way (Ni et al., 2019). Moreover, the nuclear YTHDC1 is associated with the RNA splicing (Kasowitz et al., 2018) and the export of m^{6}A modified RNAs from nucleus to cytoplasm (Roundtree et al., 2017), whereas YTHDC2 engages in the elongation-promoting effect of m^{6}A methylated RNA coding region (Mao et al., 2019). In addition to the YTHD family, the family of heterogeneous nuclear ribonucleoproteins (HNRNPs) is another set of m^{6}A readers, which binds to pre-mRNA to interfere its stability and splicing (Geuens et al., 2016). HNRNPA2B1 has been well-accepted as a nuclear reader of m^{6}A, binding to the RGm^{6}AC containing sites on RNA to affect the alternative splicing and the processing of miRNAs (Alarcón et al., 2015). As to HNRNPC, because the m^{6}A residues within RNA strand can destabilize the RNA duplexes (Kierzek and Kierzek, 2003), the structure of RNA may be altered when it is m^{6}A modified. Given this, the m^{6}A has been proposed to make the UUUUU tract within RNA to become more unfolded and

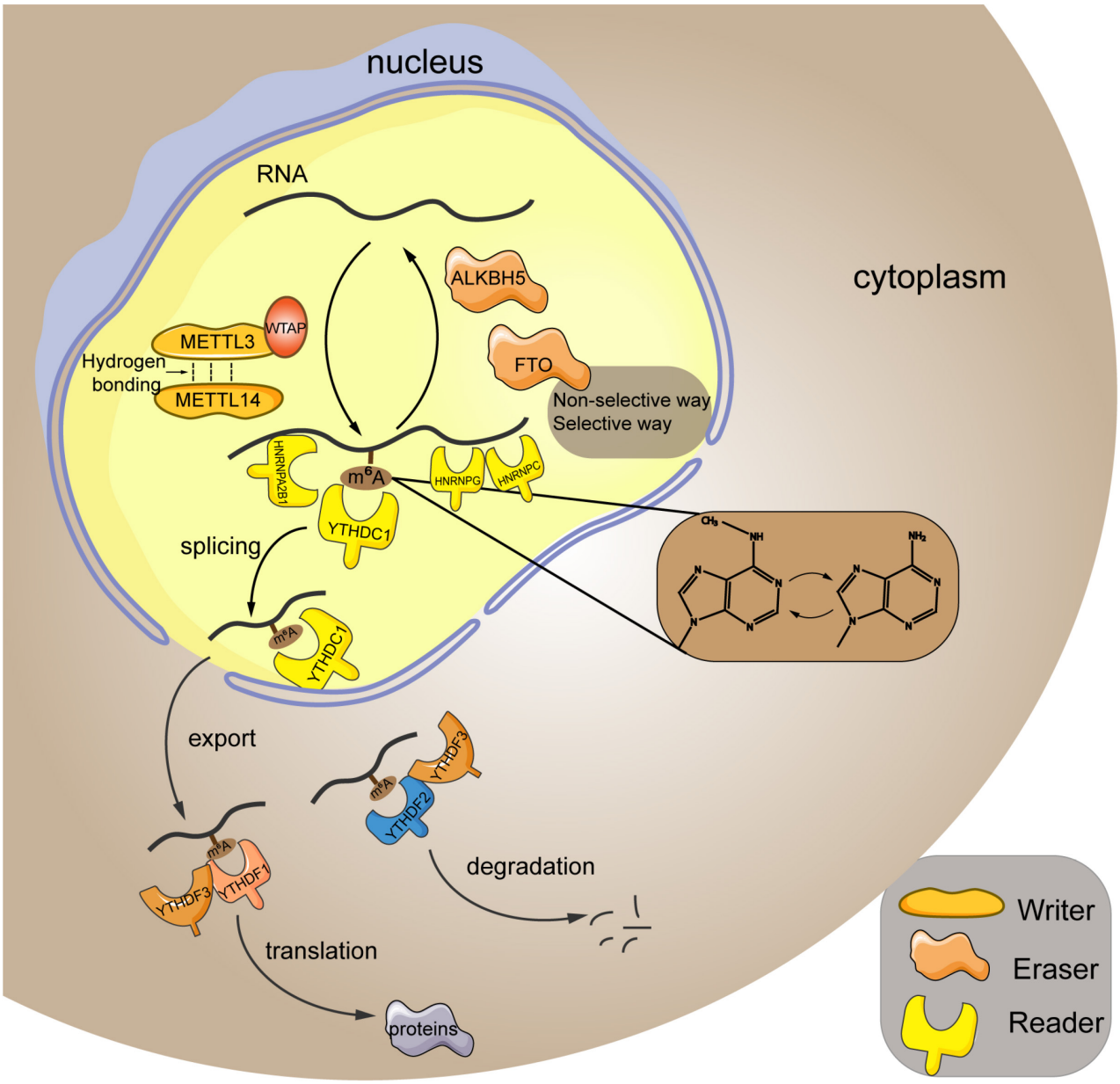


FIGURE 1 | Mechanism of m^{6}A RNA modification. M^{6}A modification is a reversible process mediated by its regulatory proteins, including the writers (MELTT3, METTL14, WTAP, etc.), erasers (FTO, ALKBH5, etc.), and readers (YTHDF1, YTHDF2, YTHDF3, etc.). METTL3, methyltransferase-like 3; METTL14, methyltransferase-like 14; WTAP, Wilms tumor 1-associated protein; FTO, fat mass and obesity-associated protein; ALKBH5, alkB homolog 5; YTHDF1, YTH domain family; member 1; HNRNPA2B1, heterogeneous nuclear ribonucleoprotein A2B1; HNRNPC, heterogeneous nuclear ribonucleoprotein C; HNRNPG, heterogeneous nuclear ribonucleoprotein G.

accessible to HNRNPC (Liu et al., 2015), which is termed as the "m^{6}A switch." Moreover, HNRNPG also recognizes the m^{6}A through "m^{6}A switch." HNRNPG has a low-complexity region that can discern a specific motif exposed by m^{6}A-mediated RNA structural change (Liu et al., 2017), subsequently modulating the cotranscriptional pre-mRNA splicing (Zhou et al., 2019). Furthermore, the insulin-like growth factor 2 mRNA-binding proteins (IGF2BPs) can target the mRNA transcripts in an m^{6}A-dependent way through recognizing their GG(m^{6}A)C sequences, subsequently stabilizing the targeted RNAs under both the normal and stress conditions (Huang et al., 2018).

ADVANCES IN TECHNOLOGIES FOR M^{6}A DETECTION

Currently, a massive number of technologies have been developed for m^{6}A detection based on the

immunohistochemistry or hybridization properties (Ovcharenko and Rentmeister, 2018). According to their detection performance, these technologies can be classified into the semiquantitative, quantitative, and precise location detection methods (Zhu et al., 2019; **Table 1**).

Semiquantitative Methods

Semiquantitative detection strategies, including the dot blot, methyl sensitivity of MazF RNA endonucleases, and immune-Northern blot, are used to determine the presence of m^{6}A modification rather than the amount. Among them, dot blot is applied to detect the global change of m^{6}A by using antibodies that specifically bind to the m^{6}A site. It is relatively simple and fast but not quantitative (Zhu et al., 2019), with low sensitivity when the m^{6}A RNA fragment is small in the samples (Nagarajan et al., 2019). A modified dot blot method has been adopted to increase the sensitivity through adding an immunoprecipitation step to enrich the m^{6}A RNA before detection (Nagarajan et al., 2019). Further, *Escherichia coli* MazF is a sequence-specific endoribonuclease, which cleave the 5′-ACA-3′ sequence but not the 5′-(m^{6}A)CA-3′ sequence within RNA strand, whereby it is an m^{6}A-sensitive RNA cleavage enzyme. Based on this technology, a new high-throughput detection method for m^{6}A has been established by researchers (Imanishi et al., 2017). Immuno-Northern blot is another way for semiquantitative detection of various types of RNA modifications. In this way, RNAs are separated and transferred onto a nylon membrane, followed by immunoblotting for measurement (Mishima et al., 2015).

Quantitative Methods

Unlike semiquantitative methods, the quantitative methods, including photo-crosslinks–based quantitative proteomics, electrochemical immunosensor method, and support vector machine–based method, can be utilized to determine the amount of m^{6}A RNA. Arguello et al. (2017) have proposed that the photo-crosslinkers, a widely used method to stabilize the protein–RNA interaction, could combine with quantitative proteomics to detect m^{6}A RNA. Meanwhile, a diazirine containing RNA probes has been recently synthesized to improve its efficiency (Arguello et al., 2017). Moreover, in the electrochemical immunosensor method (Yin et al., 2017), an anti-m^{6}A antibody has been applied to recognize and capture the m^{6}A-5′-triphosphate. Silver nanoparticles and amine-PEG3-biotin functionalized SiO_2 nanospheres (Ag@SiO_2) were used to amplify the signal, and phos-tag-biotin was employed as a bridge to connect the m^{6}ATP and Ag@SiO_2. This approach is convenient, low-cost, and of high

TABLE 1 | Technologies for m^{6}A detection.

Classification	Detection method	Mechanism	Advantages	Disadvantages	References
Semiquantitative	Dot blot	Using antibodies that specifically bind to the m^{6}A	Simplicity, speediness	Not quantitative, sensitivity is low when the m^{6}A RNA fragment is small	Nagarajan et al., 2019; Zhu et al., 2019
	Methyl sensitivity of MazF RNA endonucleases	MazF selectively cleave the 5′-ACA-3′ but not the 5′-(m^{6}A)CA-3′ sequence	Simple analyses of both m^{6}A demethylase and methyltransferase activity	Not quantitative, only able to cleave the 5′-ACA-3′ site in single-stranded RNA	Imanishi et al., 2017
	Immuno-Northern blot	Immunoblotting using antibodies against modified nucleosides	High specificity, sensitivity, and potential quantitative capability	Not quantitative	Mishima et al., 2015
Quantitative	Photo-crosslinks based quantitative proteomics	Stabilizing protein–RNA interaction and detecting via synthetic probes	Quantitative, high efficiency	Requirement of the synthesis of the probe	Arguello et al., 2017
	Electrochemical immunosensor method	Antibody–antigen interaction	Simplicity, low-cost, high specificity and sensitivity	N/A	Yin et al., 2017
	Support vector machine–based method	Computational prediction based on existent high-throughout data	Simplicity, saving the experiment cost	Relying on the existent experimental data	Chen W. et al., 2016
Gene specific location detection	MeRIP-Seq	Combination of the ChIP-Seq and RNA-Seq	High-throughput	Poor reproducibility	Meyer et al., 2012; McIntyre et al., 2020
	m^{6}A-LAIC-seq	Sequencing intact full-length RNA in both m^{6}A-positive and -negative fractions post-RIP	Detecting m^{6}A in differential RNA isoform, determining the m^{6}A levels in each gene	Cannot stoichiometrically analyze the methylation of a single modified nucleotide	Molinie et al., 2016
Nucleotide-specific location detection	HRM	Detecting the alteration of nucleic acid duplex melting properties	High-throughput, high-resolution	Relying on the previous knowledge of the modified nucleoside position at a particular RNA site	Golovina et al., 2014
	SCARLET	RNAs are cleaved, radiolabeled, digested, and analyzed by TLC	High-resolution	N/A	Liu et al., 2013
	miCLIP	Inducing specific mutational signatures to m^{6}A antibody	High-resolution	N/A	Linder et al., 2015

HRM, high-resolution melting; m^{6}A-LAIC-seq, m^{6}A level and isoform-characterization sequencing; MeRIP-Seq, methylated RNA immunoprecipitation next generation sequencing; miCLIP, m^{6}A individual nucleotide resolution cross linking and immunoprecipitation; N/A, not available; SCARLET, site-specific cleavage and radioactive labeling followed by ligation-assisted extraction and thin-layer chromatography.

specificity and sensitivity. Besides, the support vector machine–based method is a computational way to predict the m^{6}A site within RNA strand based on the existent high-throughput experiment data (Chen W. et al., 2016).

M^{6}A Location Detection Methods

To figure out the specific location of m^{6}A within RNAs, several detection methods have been further developed by researchers (Ovcharenko and Rentmeister, 2018). Generally, these techniques can be divided into two sorts, namely, the gene-specific and the nucleoside-specific detection method. The former one comprises methylated RNA immunoprecipitation next-generation sequencing (MeRIP-Seq), m^{6}A level and isoform-characterization sequencing (m^{6}A-LAIC-seq), etc. While the latter contains high-resolution melting (HRM) analysis, site-specific cleavage, and radioactive labeling followed by ligation-assisted extraction and thin-layer chromatography (SCARLET), m^{6}A individual nucleotide resolution cross-linking and immunoprecipitation (miCLIP), etc.

MeRIP-Seq combines the ChIP-Seq and RNA-Seq (Meyer et al., 2012), in which the anti-m^{6}A antibody is incubated with the RNA fragments, and the precipitated fragments then are sequenced. Hence, it can determine the origin of m^{6}A at a gene level. However, a more recent study reported that this method was of poor reproducibility because it was easily influenced by the noise (McIntyre et al., 2020). On the basis of MeRIP-seq, m^{6}A-LAIC-seq (Molinie et al., 2016) is further developed to detect the dynamic range and isoform complexity of m^{6}A content in a single gene, in which the intact full-length RNAs in both m^{6}A-positive and m^{6}A-negative fractions post-RIP are sequenced, and thus the differential isoform usages in each transcripts are detectable.

HRM (Golovina et al., 2014) is a high-throughput method for m^{6}A detection at a specific site within the RNA strand. This method works by detecting the alteration of nucleic acid duplex melting properties caused by m^{6}A modification. For instance, it has been observed that the melting temperature of RNA–DNA duplex was reduced by the presence of m^{6}A modification (Golovina et al., 2014). SCARLET (Liu et al., 2013) is a method that enables detection of m^{6}A status at any site in mRNA/long ncRNA (lncRNA), in which the m^{6}A-containing candidate sites are cleaved, radiolabeled, and site-specific ligated, followed by complete nuclease digestion. The digested m^{6}A residue is then measured by thin-layer chromatography (TLC). Moreover, MiCLIP can be used to determine the m^{6}A site at a nucleotide-specific level (Linder et al., 2015). M^{6}A antibodies bind to the m^{6}A sites within RNA strands, and the m^{6}A residues are then located by inducing specific mutational signatures after ultraviolet light–induced antibody-RNA cross-linking and reverse transcription.

RNA M^{6}A METHYLATION IN MUSCULOSKELETAL BIOLOGY

Musculoskeletal system mainly consists of skeleton and skeletal muscle, which directly participates in the motor function of human body. Diverse transcriptional factors have been reported to involve in the genesis and maintenance of musculoskeletal system. M^{6}A modification is a widely discovered and annotated epigenetic manner that takes part in the biology of musculoskeletal system. Herein, we discuss the mechanism and regulatory function of m^{6}A in this process (**Figure 2**).

M^{6}A in Bone Remodeling

Bone is a connective tissue functioning in mechanical support, mineral homeostasis, hematopoiesis, etc., which maintains its metabolic balance principally through bone remodeling, a dynamic process involved in the formation of bone matrix through osteoblasts and removal of bone mass via osteoclasts (Hadjidakis and Androulakis, 2006). Osteoblast is derived from the bone marrow mesenchymal stem cells (BMSCs) under the impact of numerous regulators, which can produce matrix to form the bone tissue. With the development of bone matrix, some osteoblasts finally reorganized and embedded into the matrix as osteocytes (Blair et al., 2017). Accordingly, osteocytes play a vital role in monitoring the bone quality and sensing the mechanotransduction, as well as secreting regulatory factors associated with bone anabolism (Tresguerres et al., 2020). By contrast, osteoclasts are multinuclear cells derived from myeloid precursors, which function in degradation and resorption of bone through secreting proteolytic enzymes and acid (Charles and Aliprantis, 2014). The osteoblasts and osteoclasts couple with each other to maintain the dynamic homeostasis of bones (Weivoda et al., 2016). Any impairment of the homeostasis under pathological condition may contribute to the bone disorder.

As an indispensable part of epigenetic regulation, m^{6}A modification is suggested as a crucial regulator participating in either the osteogenic or osteoclastogenic processes of bone. For instance, the expression of m^{6}A methyltransferases (METTL3 and METTL14) was found significantly elevated in BMSCs undergoing osteogenic induction. Accordingly, knockdown of METTL3 reduced the mRNA level of genes related to BMSC proliferation and differentiation such as the Vegfa-164 and Vegfa-188 (Tian et al., 2019). Apart from this, MYD88 gene, a vital upstream regulator of nuclear factor κB (NF-κB) signaling, was methylated by METTL3, followed by activation of NF-κB and repression of osteogenic progression. Meanwhile, the METTL3-mediated osteogenic differentiation tendency could be reversed by demethylase ALKBH5 (Yu et al., 2020). Moreover, silencing METTL3 decreased the osteogenic markers, Smad signaling, and mineralized nodules in preosteoblast MC3T3-E1 cells, indicating the reduction of osteoblast differentiation (Zhang Y. et al., 2019). Hence, the METTL3-mediated m^{6}A methylation significantly contributes to the maintenance of osteogenesis. Conversely, METTL3-mediated m^{6}A methylation was also reported to facilitate the osteoclast differentiation. METTL3 level was elevated during osteoclastogenesis, and METTL3 depletion suppressed the differentiation and bone-resorbing ability of osteoclasts. Mechanistically, Atp6v0d2 mRNA, the principal regulator of osteoclast precursor cells fusion (Kim et al., 2009) was stabilized

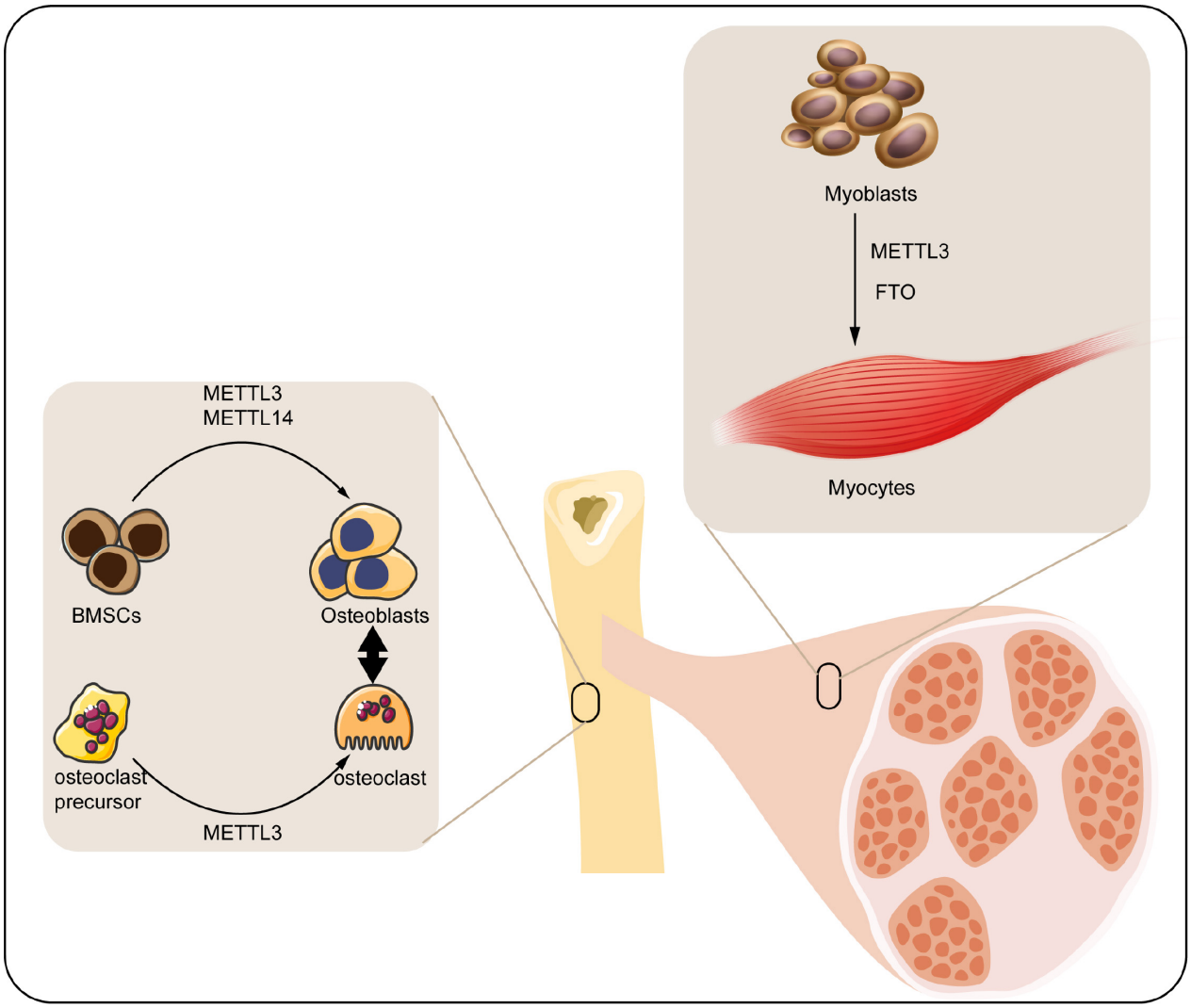


FIGURE 2 | Roles of m^{6}A modification in musculoskeletal biology. M^{6}A regulatory proteins participate in differentiation of BMSCs, osteoclast precursors, and myoblasts. METTL3, methyltransferase-like 3; METTL14, methyltransferase-like 14; FTO, fat mass and obesity-associated protein; BMSCs, bone marrow mesenchymal stem cells.

by the m^{6}A-binding protein YTHDF2 when the METTL3 was abolished (Li et al., 2020).

Taken together, the present studies have implicated the function of METTL3-mediated m^{6}A in either the osteogenic or the osteoclastogenic differentiation of bone remodeling.

M^{6}A in Skeletal Muscle Regulation

Skeletal muscle comprises almost 40% of the total body weight, which functions in both the mechanical and metabolic processes of the body such as force generation and heat production (Frontera and Ochala, 2015). Retaining skeletal muscle mass is crucial for its physiological function, which is principally determined by the size and amount of muscle fibers. Skeletal muscle fibers are generated from myoblasts via myoblasts fusion, a process named as myogenesis (Sampath et al., 2018). Epigenetic modifications involving the histone modification (Machado et al., 2017), ncRNA (Liu M. et al., 2019), DNA methylation (Miyata et al., 2015), etc. have been unraveled to play a part in this process. Among them, m^{6}A was proposed as a concernful regulator.

In the previous analyses, m^{6}A modification can modulate the activity of skeletal muscle via modifying the muscle mass and interfering with the myoblasts differentiation: (1) modifying the muscle mass. For instance, upregulation of FTO gene expression was closely associated with skeletal muscle mass increase in overweight individuals (Doaei et al., 2019). Moreover, maternal high-fat intake could even disturb the m^{6}A modification and FTO gene expression in skeletal muscle of its offspring (Li et al., 2016). Wu et al. (2017) have confirmed that activation of AMPK decreases the lipid accumulation in skeletal muscle cells through inversely regulating FTO expression

and FTO-mediated demethylation. (2) Interfering with the myoblasts differentiation. It has been elucidated that FTO downregulation inhibited the myoblasts differentiation of mice through affecting the activity of mTOR-PGC-1α-mitochondria axis, which suppressed the mitochondria biogenesis and energy production of skeletal muscle cells (Wang et al., 2017). In addition, myoblast differentiation was regulated by METTL3-promoted MyoD. Specifically, suppression of METTL3 downregulated the activation of MyoD by modifying the sites within 5' untranslated region of MyoD mRNA (Kudou et al., 2017).

ROLES OF M^{6}A IN MUSCULOSKELETAL DISORDERS

Musculoskeletal disorders refer to abnormalities of skeleton or skeletal muscle, emerging as the tumor, inflammation, trauma, etc., which may lead to disability and paralysis. Although previous work has shed light on the roles of m^{6}A in musculoskeletal disorders, the details of m^{6}A function and its involvement in the pathogenesis and progression remain unclear. Here, we summarize the current evidences concerning the pleiotropic functions of m^{6}A in musculoskeletal diseases, as presented in **Figure 3** and **Table 2**.

M^{6}A in OS

OS is the most common primary malignant bone tumor that mainly occurs in teenagers and adolescents with an annual incidence of 3.1 case per million (Gianferante et al., 2017). Although considerable advancement has been achieved in the past decades, the comprehensive mechanism network of OS has not yet been fully investigated. Currently, the standardized therapy for OS is limb salvage surgery or amputation combined with multiregimen-based chemotherapy. However, the survival rate of patients is unsatisfactory because of potential chemoresistance, lung metastasis, or tumor relapses. Recently, increasing studies have explored new therapeutic strategies for OS such as the molecular target therapy (Corre et al., 2020).

Epigenetic modification has been globally investigated in OS (Nebbioso et al., 2018). Almost all types of epigenetics, ranging from DNA methylation to histone modification, have been suggested to involve in the development and progression of OS (Cui et al., 2011). For instance, DNA methylation could downregulate miR-449c expression and eventually contributed to the tumorigenesis of OS (Li Q. et al., 2017). Meanwhile,

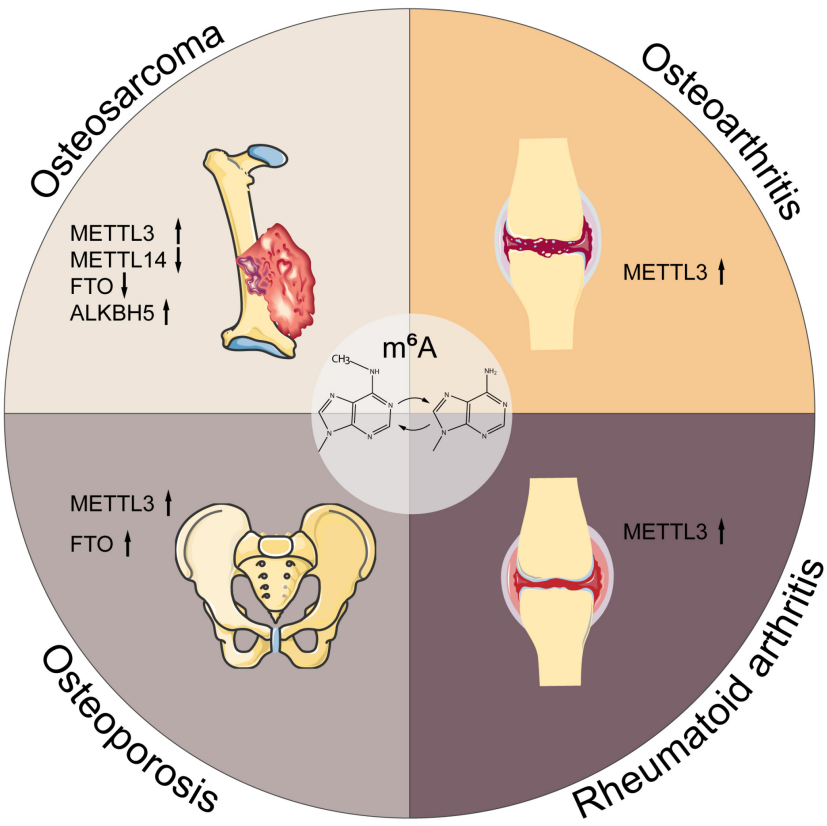


FIGURE 3 | M^{6}A in musculoskeletal disorders. M^{6}A is associated with the progression of multiple musculoskeletal diseases, including osteosarcoma, osteoarthritis, rheumatoid arthritis, and osteoporosis. METTL3, methyltransferase-like 3; METTL14, methyltransferase-like 14; FTO, fat mass and obesity-associated protein; ALKBH5, alkB homolog 5; YTHDF1, YTH domain family, member 1.

TABLE 2 | The role of m^{6}A in musculoskeletal disorders.

Diseases	M^{6}A component	Samples and condition	Function	Regulation	Target	Role in disease	References
OS	METTL14, METTL3, FTO, ALKBH5	MG63/ DXR (doxorubicin treatment)	Oncogene	↓:METTL14/FTO; ↑:METTL3/ALKBH5	Wnt signaling	Emergence and maintaining of OSCs, promoting drug resistance	Wang Y. et al., 2019
	ALKBH5	70 pairs of OS and normal tissues Osteoblast cell line and OS cell lines	Oncogene	↑	PVT1	Promoting OS cell proliferation	Chen et al., 2020
	METTL3	HOS, SAOS-2, U2OS, and MG63 cells	Oncogene	↑	ATAD2	Enhancing OS cell growth and metastasis	Zhou et al., 2020
	METTL3	28 pairs of OS cancerous and paracancerous tissues; hFOB1.19 and OS cell lines	Oncogene	↑	DRG1	Promoting OS progression	Ling et al., 2020
	METTL3	40 paired of OS tissues and adjacent tissues Osteoblast cells and OS cell lines	Oncogene	↑	LEF1	Promoting OS progression	Miao et al., 2019
OA	METTL3	ATDC5 cells	promotor	↑	NF-κB signaling	Promoting inflammatory response, collagen synthesis and degradation, and cell apoptosis in chondrocytes	Liu Q. et al., 2019
RA	METTL3	47 RA patients and 30 health controls; THP-1 cell	promotor	↑	NF-κB signaling	Promoting RA disease activity	Wang J. et al., 2019
OP	METTL3	METTL3 knock-out and knock-in mice; primary MSCs	Suppressor	↓	PTH/Pth1r signaling	Impairing bone formation	Wu et al., 2018
	METTL3	Female OP patients and control subjects; METTL3$^{+/-}$ mice	Suppressor	↓	miR320/ RUNX2	Promoting OP development	Yan et al., 2020
	FTO	44 female/male individuals with/without OP Young and aged C57BL/6J mice	promotor	↑	Pparg	Promoting the shift of osteoporotic BMSC fate to adipocyte	Shen et al., 2018
	FTO	FTO$^{flx/flx}$ (FTO$^{f/f}$) mice	Suppressor	↑	ER stress pathway	Protecting osteoblasts from genotoxic damage Maintaining bone mass	Zhang Q. et al., 2019

↑, Upregulation; ↓, Downregulation; ALKBH5, alkB homolog 5, ATAD2, ATPase family AAA domain containing 2; DRG1, GTP-binding protein 1; ER, endoplasmic reticulum; FTO, fat mass and obesity-associated protein; LEF1, lymphoid enhancer binding factor 1; METTL3, methyltransferase-like 3; METTL14, methyltransferase-like 14; NF-κB, nuclear factor κB; OA, osteoarthritis; OP, osteoporosis; OS, osteosarcoma; Pparg, peroxisome proliferator-activated receptor γ; PTH/Pth1r, parathyroid hormone /parathyroid hormone receptor-1; PVT1, plasmacytoma variant translocation 1; RA, rheumatoid arthritis; RUNX2, runt-related transcription factor 2.

histone methyltransferase has been discovered to regulate the chemosensitivity in OS (Jiang et al., 2018; He et al., 2019). Additionally, potential roles of multiple ncRNAs also have been validated in OS, such as the circRNA (Tu et al., 2020) and lncRNA (Ren et al., 2020; Xu et al., 2020). Li X. et al. (2017) reported that HOX transcript antisense intergenic RNA (HOTAIR) could enhance the development of OS via DNA methylation of CDKN2A gene. Notably, there have been some indications that m^{6}A modification exerts pivotal functions in OS.

An integrative study performed by Wang J. et al. (2019) analyzing the transcriptome-wide m^{6}A methylome enriched by chemotherapy in OS stem cells (OSCs) has revealed that several m^{6}A-related enzymes (METTL3, METTL14, FTO, ALKBH5) were altered in OS cells compared with noncancerous counterparts. The aberrantly expressed genes were associated with pluripotency regulation of the OSCs (Wang J. et al., 2019). Further, it has been shown that lncRNA plasmacytoma variant translocation 1 (PVT1) transcript was upregulated because of m^{6}A methylation decrease mediated by ALKBH5, which reduced the binding of reader protein YTHDF2 in PVT1, subsequently lessening the degradation of PVT1 and promoting tumorigenesis of OS (Chen et al., 2020). METTL3 was found localizing in both cytoplasm and nucleus of OS cells, which is also on the map of OS modulation. Downregulation of METTL3 was reported to suppress the expression of ATPase family AAA domain containing 2 (ATAD2), in conjunction with inhibition of OS cell growth and metastasis (Zhou et al., 2020). In addition, knockdown of METTL3 has been demonstrated to be associated with decreased m^{6}A methylation of GTP-binding protein (DRG) 1. Concomitant with the decreased m^{6}A methylation, the stability and expression level of DRG1 were reduced (Ling et al., 2020), resulting in suppression of the OS development, migration, and colony formation. Meanwhile, silence of METTL3 decreased the m^{6}A methylation and expression of lymphoid enhancer binding factor 1 (LEF1), followed by the advent of Wnt/β-catenin signaling pathway deactivation. Consequently, aberration of Wnt/β-catenin pathway contributed to the development of OS (Miao et al., 2019).

Collectively, based on the current evidences, the m^{6}A writers, mainly the METTL3, are found extensively involved in the tumorigenesis, progression, and migration of OS via methylating their target genes. However, the current recognition is still restricted because of the limited number and depth of studies.

M^{6}A in OA

OA is the most prevalent chronic joint disease that mainly occurs in aging and obesity population. The prevalence of OA is still in continuous growth, and it is estimated that the proportion of OA

in population 45 years or older will increase from 26.6 to 29.5% by 2032 (Hunter and Bierma-Zeinstra, 2019). Symptoms of OA typically include stiffness, pain, and movement restriction with a high risk of disability, which can bring substantial socioeconomic burden (Hunter et al., 2014). The pathogenesis of OA principally involves in degradation of cartilage matrix, which consists of collagen type II, minor collagen types IX and XI, and gel-like negatively charged proteoglycans (Kannu et al., 2009). Likewise, many inflammation-related molecules have been suggested to engage in this process such as the growth factors [transforming growth factor β, fibroblast growth factor 2 (FGF-2), and FGF-18], Wnt, β-catenin, HIF-2α, etc. (Xia et al., 2014). Targeting the inflammation pathways is regarded as a promising way for OA therapy. Particularly, epigenetic regulation has been reported to be in connection with the inflammatory factors and response (Shen et al., 2017). As an indispensable way of epigenetic regulation, m^{6}A has also been partially studied in OA.

It was expounded that METTL3 regulated OA process via enhancing inflammatory response and extracellular matrix (ECM) synthesis (Liu Q. et al., 2019). Mechanistically, silencing METTL3 inhibited the inflammatory cytokines level and nuclear factor κB signaling in OA cells, thereby deactivating the progression of OA. Meanwhile, suppression of METTL3 boosted the degradation of chondrocytes ECM through downregulating the matrix metalloprotease-13 and collagenase type X, consequently promoting the development of OA (Liu M. et al., 2019). In addition, the association between OA and FTO has also been explored in some genome-wide association studies in which they clarified that FTO-mediated overweight increased the susceptibility of OA (Zeggini et al., 2012; Panoutsopoulou et al., 2014). However, another study performed by Dai et al. (2018) showed that the FTO polymorphism (rs8044769) was not linked to OA in the Chinese Han population, and their association may be mediated by other genes. Therefore, the correlation between FTO and OA remains elusive and requires further exploration.

M^{6}A in RA

With a symptom of pain, swelling, and stiffness, RA is a common chronic inflammatory disease that primarily attacks the synovial joint (Littlejohn and Monrad, 2018). RA can bring substantial burden to both the individuals and socioeconomics because of its high morbidity and mortality (Hu et al., 2018). Besides, RA is in close linkage with the occurrence of cardiovascular diseases (Blum and Adawi, 2019). Autoimmune-mediated inflammation is a well-known cause of RA (Derksen et al., 2017), in which both the genetic regulation (Scott et al., 2010) and epigenetic regulation (Doody et al., 2017) are proposed to play indispensable roles.

The relationship between m^{6}A modification and RA has been partially unraveled in several studies. A large-scale genome-wide association study identifying the m^{6}A-associated SNPs (m^{6}A-SNPs) that affected the progression of RA has been conducted. Thirty-seven RA-related m^{6}A-SNPs were discovered, and 27 of them were verified to affect expression of 24 local genes in different RA cells or tissues, which indicated the potential roles of m^{6}A-SNPs in RA (Mo et al., 2018b). Moreover, METTL3 was validated to significantly suppress the inflammatory response of macrophages in RA. Specifically, METTL3 inhibited the generation of IL-6 and TNF-α in macrophages via restraining the phosphorylation of NF-κB. Therefore, METTL3 may serve as a potential biomarker for diagnosis of RA (Wang J. et al., 2019). However, because of the limitation of current studies, we can only hypothesize that m^{6}A can decelerate the progression of RA via regulating the inflammatory response of immune cells; studies are still needed to provide more evidences.

M^{6}A in OP

Characterizing by depletion of bone mass and impairment of bone structure, OP is mostly a condition of postmenopausal women and aging, which may lead to disastrous fracture in some cases (Armas and Recker, 2012; Boyanov et al., 2014).

Several researches have enhanced our recognition of the roles of m^{6}A modification in OP. A genome-wide identification study was indicative of the potential roles of m^{6}A-SNPs in bone mineral density. The results revealed that 138, 125, and 993 m^{6}A-SNPs were in linkage to femoral neck density disorders, lumbar spine density disorders, and heel density disorders, respectively (Mo et al., 2018a). Currently, it becomes obvious that factors associated with regulation of BMSCs differentiation are closely associated with OP. The imbalance between BMSC-derived osteoblasts and adipocytes was deemed underlying progression of OP (Chen Q. et al., 2016). It has been demonstrated that METTL3-mediated m^{6}A methylation affected the function of BMSCs through several pathways. In the first place, knockdown of m^{6}A methyltransferase METTL3 in mice induced pathological features related to the occurrence of OP via decreasing parathyroid hormone (PTH)/parathyroid hormone receptor-1 (Pth1r) signaling axis, interfering the PTH-induced osteogenic response of BMSCs (Wu et al., 2018). Moreover, downregulation of METTL3 in BMSCs inhibited the methylation of runt-related transcription factor 2 (RUNX2) and precursor (pre-) miR320 (Yan et al., 2020). RUNX2 is an essential regulator of osteoblast progenitor proliferation and osteogenic differentiation, which can enhance the bone mineralization, and multiple factors were reported to participate in the osteogenic process via targeting RUNX2 (Hou et al., 2019; Komori, 2019).

Conversely, the FTO, represented as the RNA demethylase, was reported to promote the shift of osteoporotic BMSC fate to adipocyte and impede the bone formation through a growth differentiation factor 11 (GDF11)-FTO-peroxisome proliferator-activated receptor γ (Pparg) axis, whereby high FTO expression indicated high risk of OP (Shen et al., 2018). Meanwhile, the expression of FTO could be repressed by overexpression of miR-149-3p, followed by a higher potential of BMSCs to differentiate into adipocytes (Li et al., 2019b). In addition, of SNPs in multitude utilizing the association analyses, it was shown that a FTO such as rs1421085, rs1558902 and rs1121980 were associated with bone mineral density and risk of fracture (Guo et al., 2011; Tran et al., 2014). Interestingly, although FTO inhibited the BMSCs from differentiating into osteoblasts, it could exert a protective role in differentiated osteoblasts.

Osteoblasts with FTO suppression were prone to develop cell death, which was illustrated to be caused by the interruption of DNA repair pathway. Specifically, FTO was able to stabilize the endoplasmic reticulum stress pathway components, such as Hsp70, protecting osteoblasts from genotoxic damage (Zhang Q. et al., 2019).

Taken together, m^{6}A modification is involved in the occurrence and development of OP via (1) METTL3-mediated differentiation of BMSCs to osteocyte, (2) FTO-mediated differentiation of BMSCs to adipocyte, and (3) FTO-mediated protection of osteoblasts from genotoxic damage. Herein, we assume that m^{6}A may play a dual role in OP, by which it can either promote or decelerate the progression of OP via different modifications.

CLINICAL UTILIZATIONS OF M^{6}A IN MUSCULOSKELETAL DISORDERS

RNA target therapy has become a hotspot and shown convincing prospects in treatment of many diseases with high specificity and efficacy (Crooke et al., 2018). The broad involvement of m^{6}A in musculoskeletal disorders, as outlined previously, has driven extensive research efforts at m^{6}A-based therapy. The functions of the m^{6}A regulatory proteins including FTO, METTL3, ALKBH5, etc. have been determined in OS, OA, RA, and OP as mentioned previously. As a result, the possibility is then opened for developing inhibitors or promoters of them to control the diseases.

Some natural products have been discovered showing significant activity in FTO inhibition. The natural product rhein is the first identified small-molecule inhibitor of human FTO demethylase, which competitively binds to the FTO active site and inhibit the demethylation *in vitro* (Chen et al., 2012). Additionally, by using the structure-based hierarchical virtual screening, researchers have found that entacapone directly bound to FTO and subsided its activity (Peng et al., 2019). And the natural compound radicicol also has been recognized as a potent FTO inhibitor, which suppressed the FTO demethylation activity in a dose-dependent manner (Wang et al., 2018). Besides, the meclofenamic acid (MA), a nonsteroidal anti-inflammatory drug, was identified as a specific inhibitor of FTO. Mechanically, MA competed with FTO for the binding sites within the m^{6}A modified RNA, reducing activity of FTO-mediated demethylation (Huang et al., 2015). Further, FTO may interfere the reaction of human body to other drugs. For instance, it has been elucidated that the rs7195994 variant at the FTO gene locus hereditarily impacted the TNF inhibitor response in RA patients, and the customized treatment based on the FTO genetic stratification of patients could improve the efficacy (Massey et al., 2018).

Similarly, because METTL3 up-regulation in OS, OA, and RA contributes to the progression of diseases, METTL3 may also be targeted for treatment. Although METTL3 inhibitor is not available so far, it provides us with a novel direction. The fact that several drug screening technologies for RNA-modifying enzymes such as the self-assembled monolayer desorption/ionization have been developed illustrates a promising future for METTL3-based drugs (Buker et al., 2020). Recently, the first series of small molecule inhibitors of METTL3 have been identified via high-throughput docking into the SAM binding site and protein X-ray crystallography, in which seven compounds belonging to N-substituted amide of ribofuranuronic acid analogs of adenosine or adenosine mimics with a six-member ring were uncovered to be the effective METTL3 inhibitors (Bedi et al., 2020).

In summary, m^{6}A-modifying proteins can serve as potential targets for drugs with which the FTO and METTL3 inhibitor may have great prospect in the treatment of musculoskeletal disorders.

DISCUSSION

Epigenetics has been widely illuminated in multiple diseases over the past decades, and researchers are consistently seeking for new remedy from this field (Prachayasittikul et al., 2017). Currently, a diverse set of RNA modifications has been identified and annotated. Of note, m^{6}A is the most abundant among them (Linder et al., 2015). Even though the recent advances have highlighted the crucial role of m^{6}A in a multitude of diseases, only a small percentage of them focus on the musculoskeletal disorders. In this review, we have discussed the molecular mechanisms, detection technologies, regulatory functions, and clinical implications of m^{6}A in musculoskeletal diseases. As we summarized previously, m^{6}A modification is of great potential in disease prediction and drug development, yet the current studies are insufficient.

The first issue is how to choose and optimize the laboratory used technology for m^{6}A detection in clinical practice. Although a diverse set of methods have been continually developed in experiment to detect the m^{6}A modification or analyze the m^{6}A residue locations within RNA site over the past decades, the use in clinic has not been investigated yet. Here, we envision that we can associate the disease progression with the m^{6}A presence patterns that may be presented as the presence of m^{6}A, the proportion of m^{6}A, or the specific site of m^{6}A. With the appropriate detection method, doctors will be able to figure out the situation of musculoskeletal diseases through the m^{6}A examination results.

Furthermore, it has remained a significant challenge to dissect the mechanism of m^{6}A in musculoskeletal disorders because limited studies have been performed toward it, especially for OA and RA. Meanwhile, the current studies of m^{6}A in musculoskeletal disorders focus only on the "writers" and "erasers," whereas clues toward the "readers" are scarce. As a matter of fact, roles of the "readers" have been investigated in other diseases. For instance, high YTHDF1 expression was a significant predictor of malignant tumor behaviors and poor prognosis in colorectal cancer (Nishizawa et al., 2018). IGF2BPs was demonstrated to participate in suppression of glycolysis and stemness properties of breast cancer cells via a FGF13-AS1/IGF2BPs/Myc feedback loop (Ma et al., 2019). Thus, the "readers" may also engage in the pathophysiological processes of musculoskeletal disorders.

Besides, m^{6}A-based drugs remain poorly understood. Only a limited number of FTO and METTL3 inhibitors have been identified, yet their efficacy and safety are inconclusive. Notably, there are currently no m^{6}A-based drugs developed for musculoskeletal disorders. Therefore, to address these limitations, we still have a long way to go.

CONCLUSION

As the most abundant RNA modification in eukaryotic cells, it is beyond doubt that m^{6}A is a central node of the regulatory network of diseases. The illustration of m^{6}A function has revealed its great importance in both the biological and pathological processes of bone and skeletal muscle. M^{6}A modification has been partially studied in musculoskeletal disorders, including OS, OA, RA, OP, etc. Regarding its pivotal role in regulating the progression and development of diseases, m^{6}A modification is of great potential to serve as the diagnostic biomarker or therapeutic target in musculoskeletal diseases, although more evidences are still warranted for validation in the future. Furthermore, a growing number of technologies have been developed for the m^{6}A detection, and it has become evident that m^{6}A is detectable and usable in disease prediction. Even with all of the effort over the recent years to figure out the detection methods for m^{6}A, it should be noted that there is no clear indication for selecting the most suitable detection method for clinical application. Simplified m^{6}A detection methods with high specificity/sensitivity and low costing, such as dot blot, immuno-Northern blot, and electrochemical immunosensor method, may be the promising methods to be utilized.

AUTHOR CONTRIBUTIONS

WZ and CT conceived and designed the work. WZ, LH, and ZLiu contributed to material preparation and performed data collection and analysis. WZ wrote the first draft of the manuscript. XR, LQ, LW, and WW wrote sections of the manuscript. All authors commented on previous versions of the manuscript. CT revised the manuscript. ZLi contributed to manuscript drafting, critical revision, and final approval of the version to be published. All authors read and approved the final manuscript.

FUNDING

This work was supported by the National Natural Science Foundation of China (81902745), Natural Science Foundation of Hunan Province, China (2018JJ3716), and China Scholarship Council (201806375067).

REFERENCES

Aik, W., Scotti, J. S., Choi, H., Gong, L., Demetriades, M., Schofield, C. J., et al. (2014). Structure of human RNA N^6-methyladenine demethylase ALKBH5 provides insights into its mechanisms of nucleic acid recognition and demethylation. *Nucleic Acids Res.* 42, 4741–4754. doi: 10.1093/nar/gku085

Alarcón, C. R., Goodarzi, H., Lee, H., Liu, X., Tavazoie, S., and Tavazoie, S. F. (2015). HNRNPA2B1 is a mediator of m(6)A-dependent nuclear RNA processing events. *Cell* 162, 1299–1308. doi: 10.1016/j.cell.2015.08.011

Arguello, A. E., DeLiberto, A. N., and Kleiner, R. E. (2017). RNA Chemical Proteomics Reveals the N(6)-Methyladenosine (m(6)A)-Regulated Protein-RNA Interactome. *J. Am. Chem. Soc.* 139, 17249–17252. doi: 10.1021/jacs.7b09213

Armas, L. A., and Recker, R. R. (2012). Pathophysiology of osteoporosis: new mechanistic insights. *Endocrinol. Metab. Clin. North Am.* 41, 475–486. doi: 10.1016/j.ecl.2012.04.006

Bedi, R. K., Huang, D., Eberle, S. A., Wiedmer, L., Śledź, P., and Caflisch, A. (2020). Small-molecule inhibitors of METTL3, the major human epitranscriptomic writer. *ChemMedChem* 15, 744–748. doi: 10.1002/cmdc.202000011

Blair, H. C., Larrouture, Q. C., Li, Y., Lin, H., Beer-Stoltz, D., Liu, L., et al. (2017). Osteoblast differentiation and bone matrix formation *in vivo* and *in vitro*. *Tissue Eng. Part B Rev.* 23, 268–280. doi: 10.1089/ten.TEB.2016.0454

Blum, A., and Adawi, M. (2019). Rheumatoid arthritis (RA) and cardiovascular disease. *Autoimmun. Rev.* 18, 679–690. doi: 10.1016/j.autrev.2019.05.005

Boyanov, M., Shinkov, A., Psachoulia, E., Intorcia, M., and Petkova, R. (2014). Increased bone mineral density (Bmd) in postmenopausal women with osteoporosis (Op) receiving two denosumab injections in routine clinical practice in bulgaria. *Value Health* 17:A389. doi: 10.1016/j.jval.2014.08.2662

Buker, S. M., Gurard-Levin, Z. A., Wheeler, B. D., Scholle, M. D., Case, A. W., Hirsch, J. L., et al. (2020). A mass spectrometric assay of METTL3/METTL14 methyltransferase activity. *SLAS Discov.* 25, 361–371. doi: 10.1177/2472555219878408

Cao, G., Li, H. B., Yin, Z., and Flavell, R. A. (2016). Recent advances in dynamic m6A RNA modification. *Open Biol.* 6:160003. doi: 10.1098/rsob.160003

Charles, J. F., and Aliprantis, A. O. (2014). Osteoclasts: more than 'bone eaters'. *Trends Mol. Med.* 20, 449–459. doi: 10.1016/j.molmed.2014.06.001

Chen, B., Ye, F., Yu, L., Jia, G., Huang, X., Zhang, X., et al. (2012). Development of cell-active N6-methyladenosine RNA demethylase FTO inhibitor. *J. Am. Chem. Soc.* 134, 17963–17971. doi: 10.1021/ja3064149

Chen, Q., Shou, P., Zheng, C., Jiang, M., Cao, G., Yang, Q., et al. (2016). Fate decision of mesenchymal stem cells: Adipocytes or osteoblasts? *Cell Death Differ.* 23, 1128–1139. doi: 10.1038/cdd.2015.168

Chen, S., Zhou, L., and Wang, Y. (2020). ALKBH5-mediated m(6)A demethylation of lncRNA PVT1 plays an oncogenic role in osteosarcoma. *Cancer Cell Int.* 20:34. doi: 10.1186/s12935-020-1105-6

Chen, W., Feng, P., Ding, H., and Lin, H. (2016). Identifying N (6)-methyladenosine sites in the Arabidopsis thaliana transcriptome. *Mol. Genet. Genomics* 291, 2225–2229. doi: 10.1007/s00438-016-1243-7

Chen, X. Y., Zhang, J., and Zhu, J. S. (2019). The role of m(6)A RNA methylation in human cancer. *Mol. Cancer* 18:103. doi: 10.1186/s12943-019-1033-z

Corre, I., Verrecchia, F., Crenn, V., Redini, F., and Trichet, V. (2020). The osteosarcoma microenvironment: a complex but targetable ecosystem. *Cells* 9:976. doi: 10.3390/cells9040976

Crooke, S. T., Witztum, J. L., Bennett, C. F., and Baker, B. F. (2018). RNA-Targeted Therapeutics. *Cell Metab.* 27, 714–739. doi: 10.1016/j.cmet.2018.03.004

Cui, J., Wang, W., Li, Z., Zhang, Z., Wu, B., and Zeng, L. (2011). Epigenetic changes in osteosarcoma. *Bull. Cancer* 98, E62–E68. doi: 10.1684/bdc.2011.1400

Dai, J., Ying, P., Shi, D., Hou, H., Sun, Y., Xu, Z., et al. (2018). FTO variant is not associated with osteoarthritis in the Chinese Han population: replication study for a genome-wide association study identified risk loci. *J. Orthop. Surg. Res.* 13:65. doi: 10.1186/s13018-018-0769-2

Derksen, V., Huizinga, T. W. J., and van der Woude, D. (2017). The role of autoantibodies in the pathophysiology of rheumatoid arthritis. *Semin. Immunopathol.* 39, 437–446. doi: 10.1007/s00281-017-0627-z

Doaei, S., Kalantari, N., Mohammadi, N. K., Izadi, P., Gholamalizadeh, M., Eini-Zinab, H., et al. (2019). Up-regulation of FTO gene expression was associated with increase in skeletal muscle mass in overweight male adolescents. *Arch. Med. Sci.* 15, 1133–1137. doi: 10.5114/aoms.2019.87239

Dominissini, D., Moshitch-Moshkovitz, S., Schwartz, S., Salmon-Divon, M., Ungar, L., Osenberg, S., et al. (2012). Topology of the human and mouse m6A RNA methylomes revealed by m6A-seq. *Nature* 485, 201–206. doi: 10.1038/nature11112

Doody, K. M., Bottini, N., and Firestein, G. S. (2017). Epigenetic alterations in rheumatoid arthritis fibroblast-like synoviocytes. *Epigenomics* 9, 479–492. doi: 10.2217/epi-2016-0151

Frontera, W. R., and Ochala, J. (2015). Skeletal muscle: a brief review of structure and function. *Calcif. Tissue Int.* 96, 183–195. doi: 10.1007/s00223-014-9915-y

Fu, Y., Jia, G., Pang, X., Wang, R. N., Wang, X., Li, C. J., et al. (2013). FTO-mediated formation of N6-hydroxymethyladenosine and N6-formyladenosine in mammalian RNA. *Nat. Commun.* 4:1798. doi: 10.1038/ncomms2822

Geuens, T., Bouhy, D., and Timmerman, V. (2016). The hnRNP family: insights into their role in health and disease. *Hum. Genet.* 135, 851–867. doi: 10.1007/s00439-016-1683-5

Gianferante, D. M., Mirabello, L., and Savage, S. A. (2017). Germline and somatic genetics of osteosarcoma - connecting aetiology, biology and therapy. *Nat. Rev. Endocrinol.* 13, 480–491. doi: 10.1038/nrendo.2017.16

Golovina, A. Y., Dzama, M. M., Petriukov, K. S., Zatsepin, T. S., Sergiev, P. V., Bogdanov, A. A., et al. (2014). Method for site-specific detection of m6A nucleoside presence in RNA based on high-resolution melting (HRM) analysis. *Nucleic Acids Res.* 42:e27. doi: 10.1093/nar/gkt1160

Guo, Y., Liu, H., Yang, T. L., Li, S. M., Li, S. K., Tian, Q., et al. (2011). The fat mass and obesity associated gene, FTO, is also associated with osteoporosis phenotypes. *PLoS One* 6:e27312. doi: 10.1371/journal.pone.0027312

Hadjidakis, D. J., and Androulakis, I. I. (2006). Bone remodeling. *Ann. N. Y. Acad. Sci.* 1092, 385–396. doi: 10.1196/annals.1365.035

Harvey, Z. H., Chen, Y., and Jarosz, D. F. (2018). Protein-based inheritance: epigenetics beyond the chromosome. *Mol. Cell* 69, 195–202. doi: 10.1016/j.molcel.2017.10.030

He, C., Liu, C., Wang, L., Sun, Y., Jiang, Y., and Hao, Y. (2019). Histone methyltransferase NSD2 regulates apoptosis and chemosensitivity in osteosarcoma. *Cell Death Dis.* 10:65. doi: 10.1038/s41419-019-1347-1

Hou, Z., Wang, Z., Tao, Y., Bai, J., Yu, B., Shen, J., et al. (2019). KLF2 regulates osteoblast differentiation by targeting of Runx2. *Lab. Invest.* 99, 271–280. doi: 10.1038/s41374-018-0149-x

Hu, H., Luan, L., Yang, K., and Li, S. C. (2018). Burden of rheumatoid arthritis from a societal perspective: a prevalence-based study on cost of this illness for patients in China. *Int. J. Rheum. Dis.* 21, 1572–1580. doi: 10.1111/1756-185x.13028

Huang, H., Weng, H., Sun, W., Qin, X., Shi, H., Wu, H., et al. (2018). Recognition of RNA N(6)-methyladenosine by IGF2BP proteins enhances mRNA stability and translation. *Nat. Cell Biol.* 20, 285–295. doi: 10.1038/s41556-018-0045-z

Huang, Y., Yan, J., Li, Q., Li, J., Gong, S., Zhou, H., et al. (2015). Meclofenamic acid selectively inhibits FTO demethylation of m6A over ALKBH5. *Nucleic Acids Res.* 43, 373–384. doi: 10.1093/nar/gku1276

Hunter, D. J., and Bierma-Zeinstra, S. (2019). Osteoarthritis. *Lancet* 393, 1745–1759. doi: 10.1016/s0140-6736(19)30417-9

Hunter, D. J., Schofield, D., and Callander, E. (2014). The individual and socioeconomic impact of osteoarthritis. *Nat. Rev. Rheumatol.* 10, 437–441. doi: 10.1038/nrrheum.2014.44

Imanishi, M., Tsuji, S., Suda, A., and Futaki, S. (2017). Detection of N(6)-methyladenosine based on the methyl-sensitivity of MazF RNA endonuclease. *Chem. Commun.* 53, 12930–12933. doi: 10.1039/c7cc07699a

Jiang, C., He, C., Wu, Z., Li, F., and Xiao, J. (2018). Histone methyltransferase SETD2 regulates osteosarcoma cell growth and chemosensitivity by suppressing Wnt/β-catenin signaling. *Biochem. Biophys. Res. Commun.* 502, 382–388. doi: 10.1016/j.bbrc.2018.05.176

Kannu, P., Bateman, J. F., Belluoccio, D., Fosang, A. J., and Savarirayan, R. (2009). Employing molecular genetics of chondrodysplasias to inform the study of osteoarthritis. *Arthritis Rheum.* 60, 325–334. doi: 10.1002/art.24251

Kasowitz, S. D., Ma, J., Anderson, S. J., Leu, N. A., Xu, Y., Gregory, B. D., et al. (2018). Nuclear m6A reader YTHDC1 regulates alternative polyadenylation and splicing during mouse oocyte development. *PLoS Genet.* 14:e1007412. doi: 10.1371/journal.pgen.1007412

Kierzek, E., and Kierzek, R. (2003). The thermodynamic stability of RNA duplexes and hairpins containing N6-alkyladenosines and 2-methylthio-N6-alkyladenosines. *Nucleic Acids Res.* 31, 4472–4480. doi: 10.1093/nar/gkg633

Kim, T., Ha, H. I., Kim, N., Yi, O., Lee, S. H., and Choi, Y. (2009). Adrm1 interacts with Atp6v0d2 and regulates osteoclast differentiation. *Biochem. Biophys. Res. Commun.* 390, 585–590. doi: 10.1016/j.bbrc.2009.10.010

Komori, T. (2019). Regulation of proliferation, differentiation and functions of osteoblasts by Runx2. *Int. J. Mol. Sci.* 20:1694. doi: 10.3390/ijms20071694

Kudou, K., Komatsu, T., Nogami, J., Maehara, K., Harada, A., Saeki, H., et al. (2017). The requirement of Mettl3-promoted MyoD mRNA maintenance in proliferative myoblasts for skeletal muscle differentiation. *Open Biol.* 7:170119. doi: 10.1098/rsob.170119

Lan, Q., Liu, P. Y., Haase, J., Bell, J. L., Hüttelmaier, S., and Liu, T. (2019). The critical role of RNA m(6)A methylation in cancer. *Cancer Res.* 79, 1285–1292. doi: 10.1158/0008-5472.Can-18-2965

Li, D., Cai, L., Meng, R., Feng, Z., and Xu, Q. (2020). METTL3 modulates osteoclast differentiation and function by controlling RNA stability and nuclear Export. *Int. J. Mol. Sci.* 21:1660. doi: 10.3390/ijms21051660

Li, M., Zhao, X., Wang, W., Shi, H., Pan, Q., Lu, Z., et al. (2018). Ythdf2-mediated m(6)A mRNA clearance modulates neural development in mice. *Genome Biol.* 19:69. doi: 10.1186/s13059-018-1436-y

Li, Q., Li, H., Zhao, X., Wang, B., Zhang, L., Zhang, C., et al. (2017). DNA methylation mediated downregulation of miR-449c controls osteosarcoma cell cycle progression by directly targeting oncogene c-Myc. *Int. J. Biol. Sci.* 13, 1038–1050. doi: 10.7150/ijbs.19476

Li, X., Lu, H., Fan, G., He, M., Sun, Y., Xu, K., et al. (2017). A novel interplay between HOTAIR and DNA methylation in osteosarcoma cells indicates a new therapeutic strategy. *J. Cancer Res. Clin. Oncol.* 143, 2189–2200. doi: 10.1007/s00432-017-2478-3

Li, X., Yang, J., Zhu, Y., Liu, Y., Shi, X., and Yang, G. (2016). Mouse maternal high-fat intake dynamically programmed mRNA m^{6}a modifications in adipose and skeletal muscle tissues in offspring. *Int. J. Mol. Sci.* 17:1336. doi: 10.3390/ijms17081336

Li, Y., Wu, K., Quan, W., Yu, L., Chen, S., Cheng, C., et al. (2019a). The dynamics of FTO binding and demethylation from the m(6)A motifs. *RNA Biol.* 16, 1179–1189. doi: 10.1080/15476286.2019.1621120

Li, Y., Yang, F., Gao, M., Gong, R., Jin, M., Liu, T., et al. (2019b). miR-149-3p regulates the switch between adipogenic and osteogenic differentiation of BMSCs by targeting FTO. *Mol. Ther. Nucleic Acids* 17, 590–600. doi: 10.1016/j.omtn.2019.06.023

Linder, B., Grozhik, A. V., Olarerin-George, A. O., Meydan, C., Mason, C. E., and Jaffrey, S. R. (2015). Single-nucleotide-resolution mapping of m6A and m6Am throughout the transcriptome. *Nat. Methods* 12, 767–772. doi: 10.1038/nmeth.3453

Ling, Z., Chen, L., and Zhao, J. (2020). m6A-dependent up-regulation of DRG1 by METTL3 and ELAVL1 promotes growth, migration, and colony formation in osteosarcoma. *Biosci. Rep.* 40:BSR20200282. doi: 10.1042/bsr20200282

Littlejohn, E. A., and Monrad, S. U. (2018). Early diagnosis and treatment of rheumatoid arthritis. *Prim. Care* 45, 237–255. doi: 10.1016/j.pop.2018.02.010

Liu, J., Yue, Y., Han, D., Wang, X., Fu, Y., Zhang, L., et al. (2014). A METTL3-METTL14 complex mediates mammalian nuclear RNA N6-adenosine methylation. *Nat. Chem. Biol.* 10, 93–95. doi: 10.1038/nchembio.1432

Liu, M., Li, B., Peng, W., Ma, Y., Huang, Y., Lan, X., et al. (2019). LncRNA-MEG3 promotes bovine myoblast differentiation by sponging miR-135. *J. Cell. Physiol.* 234, 18361–18370. doi: 10.1002/jcp.28469

Liu, N., Dai, Q., Zheng, G., He, C., Parisien, M., and Pan, T. (2015). N(6)-methyladenosine-dependent RNA structural switches regulate RNA-protein interactions. *Nature* 518, 560–564. doi: 10.1038/nature14234

Liu, N., Parisien, M., Dai, Q., Zheng, G., He, C., and Pan, T. (2013). Probing N6-methyladenosine RNA modification status at single nucleotide resolution in mRNA and long noncoding RNA. *RNA* 19, 1848–1856. doi: 10.1261/rna.041178.113

Liu, N., Zhou, K. I., Parisien, M., Dai, Q., Diatchenko, L., and Pan, T. (2017). N6-methyladenosine alters RNA structure to regulate binding of a low-complexity protein. *Nucleic Acids Res.* 45, 6051–6063. doi: 10.1093/nar/gkx141

Liu, Q., Li, M., Jiang, L., Jiang, R., and Fu, B. (2019). METTL3 promotes experimental osteoarthritis development by regulating inflammatory response

and apoptosis in chondrocyte. *Biochem. Biophys. Res. Commun.* 516, 22–27. doi: 10.1016/j.bbrc.2019.05.168

Ma, F., Liu, X., Zhou, S., Li, W., Liu, C., Chadwick, M., et al. (2019). Long non-coding RNA FGF13-AS1 inhibits glycolysis and stemness properties of breast cancer cells through FGF13-AS1/IGF2BPs/Myc feedback loop. *Cancer Lett.* 450, 63–75. doi: 10.1016/j.canlet.2019.02.008

Machado, L., Esteves de Lima, J., Fabre, O., Proux, C., Legendre, R., Szegedi, A., et al. (2017). *In situ* fixation redefines quiescence and early activation of skeletal muscle stem cells. *Cell Rep.* 21, 1982–1993. doi: 10.1016/j.celrep.2017.10.080

Madan, I., and Grime, P. R. (2015). The management of musculoskeletal disorders in the workplace. *Best Pract. Res. Clin. Rheumatol.* 29, 345–355. doi: 10.1016/j.berh.2015.03.002

Mao, Y., Dong, L., Liu, X. M., Guo, J., Ma, H., Shen, B., et al. (2019). m(6)A in mRNA coding regions promotes translation via the RNA helicase-containing YTHDC2. *Nat. Commun.* 10:5332. doi: 10.1038/s41467-019-13317-9

Massey, J., Plant, D., Hyrich, K., Morgan, A. W., Wilson, A. G., Spiliopoulou, A., et al. (2018). Genome-wide association study of response to tumour necrosis factor inhibitor therapy in rheumatoid arthritis. *Pharmacogenomics J.* 18, 657–664. doi: 10.1038/s41397-018-0040-6

McIntyre, A. B. R., Gokhale, N. S., Cerchietti, L., Jaffrey, S. R., Horner, S. M., and Mason, C. E. (2020). Limits in the detection of m(6)A changes using MeRIP/m(6)A-seq. *Sci. Rep.* 10:6590. doi: 10.1038/s41598-020-63355-3

Meyer, K. D., Saletore, Y., Zumbo, P., Elemento, O., Mason, C. E., and Jaffrey, S. R. (2012). Comprehensive analysis of mRNA methylation reveals enrichment in 3', UTRs and near stop codons. *Cell* 149, 1635–1646. doi: 10.1016/j.cell.2012.05.003

Miao, W., Chen, J., Jia, L., Ma, J., and Song, D. (2019). The m6A methyltransferase METTL3 promotes osteosarcoma progression by regulating the m6A level of LEF1. *Biochem. Biophys. Res. Commun.* 516, 719–725. doi: 10.1016/j.bbrc.2019.06.128

Mishima, E., Jinno, D., Akiyama, Y., Itoh, K., Nankumo, S., Shima, H., et al. (2015). Immuno-northern blotting: detection of RNA modifications by using antibodies against modified nucleosides. *PLoS One* 10:e0143756. doi: 10.1371/journal.pone.0143756

Miyata, K., Miyata, T., Nakabayashi, K., Okamura, K., Naito, M., Kawai, T., et al. (2015). DNA methylation analysis of human myoblasts during *in vitro* myogenic differentiation: de novo methylation of promoters of muscle-related genes and its involvement in transcriptional down-regulation. *Hum. Mol. Genet.* 24, 410–423. doi: 10.1093/hmg/ddu457

Mo, X. B., Zhang, Y. H., and Lei, S. F. (2018a). Genome-wide identification of m(6)A-associated SNPs as potential functional variants for bone mineral density. *Osteoporos Int.* 29, 2029–2039. doi: 10.1007/s00198-018-4573-y

Mo, X. B., Zhang, Y. H., and Lei, S. F. (2018b). Genome-Wide Identification of N(6)-Methyladenosine (m(6)A) SNPs associated with rheumatoid arthritis. *Front. Genet.* 9:299. doi: 10.3389/fgene.2018.00299

Molinie, B., Wang, J., Lim, K. S., Hillebrand, R., Lu, Z. X., Van Wittenberghe, N., et al. (2016). m(6)A-LAIC-seq reveals the census and complexity of the m(6)A epitranscriptome. *Nat. Methods* 13, 692–698. doi: 10.1038/nmeth.3898

Nagarajan, A., Janostiak, R., and Wajapeyee, N. (2019). Dot Blot Analysis for Measuring Global N(6)-Methyladenosine Modification of RNA. *Methods Mol. Biol.* 1870, 263–271. doi: 10.1007/978-1-4939-8808-2_20

Nebbioso, A., Tambaro, F. P., Dell'Aversana, C., and Altucci, L. (2018). Cancer epigenetics: moving forward. *PLoS Genet.* 14:e1007362. doi: 10.1371/journal.pgen.1007362

Ni, W., Yao, S., Zhou, Y., Liu, Y., Huang, P., Zhou, A., et al. (2019). Long noncoding RNA GAS5 inhibits progression of colorectal cancer by interacting with and triggering YAP phosphorylation and degradation and is negatively regulated by the m(6)A reader YTHDF3. *Mol. Cancer* 18:143. doi: 10.1186/s12943-019-1079-y

Nishizawa, Y., Konno, M., Asai, A., Koseki, J., Kawamoto, K., Miyoshi, N., et al. (2018). Oncogene c-Myc promotes epitranscriptome m(6)A reader YTHDF1 expression in colorectal cancer. *Oncotarget* 9, 7476–7486. doi: 10.18632/oncotarget.23554

Ovcharenko, A., and Rentmeister, A. (2018). Emerging approaches for detection of methylation sites in RNA. *Open Biol.* 8:180121. doi: 10.1098/rsob.180121

Panoutsopoulou, K., Metrustry, S., Doherty, S. A., Laslett, L. L., Maciewicz, R. A., Hart, D. J., et al. (2014). The effect of FTO variation on increased osteoarthritis risk is mediated through body mass index: a Mendelian randomisation study. *Ann. Rheum. Dis.* 73, 2082–2086. doi: 10.1136/annrheumdis-2013-203772

Peng, S., Xiao, W., Ju, D., Sun, B., Hou, N., Liu, Q., et al. (2019). Identification of entacapone as a chemical inhibitor of FTO mediating metabolic regulation through FOXO1. *Sci. Transl. Med.* 11:eaau7116. doi: 10.1126/scitranslmed.aau7116

Ping, X. L., Sun, B. F., Wang, L., Xiao, W., Yang, X., Wang, W. J., et al. (2014). Mammalian WTAP is a regulatory subunit of the RNA N6-methyladenosine methyltransferase. *Cell Res.* 24, 177–189. doi: 10.1038/cr.2014.3

Prachayasittikul, V., Prathipati, P., Pratiwi, R., Phanus-Umporn, C., Malik, A. A., Schaduangrat, N., et al. (2017). Exploring the epigenetic drug discovery landscape. *Expert Opin. Drug Discov.* 12, 345–362. doi: 10.1080/17460441.2017.1295954

Qin, L., Min, S., Shu, L., Pan, H., Zhong, J., Guo, J., et al. (2020). Genetic analysis of N6-methyladenosine modification genes in Parkinson's disease. *Neurobiol. Aging.* 93, 143.e9–143.e13. doi: 10.1016/j.neurobiolaging.2020.03.018

Reichel, M., Köster, T., and Staiger, D. (2019). Marking RNA: m6A writers, readers, and functions in Arabidopsis. *J. Mol. Cell Biol.* 11, 899–910. doi: 10.1093/jmcb/mjz085

Ren, X., He, J., Qi, L., Li, S., Zhang, C., Duan, Z., et al. (2020). Prognostic and clinicopathologic significance of long non-coding RNA opa-interacting protein 5-antisense RNA 1 in multiple human cancers. *Artif. Cells Nanomed. Biotechnol.* 48, 353–361. doi: 10.1080/21691401.2019.1709854

Roundtree, I. A., Luo, G. Z., Zhang, Z., Wang, X., Zhou, T., Cui, Y., et al. (2017). YTHDC1 mediates nuclear export of N(6)-methyladenosine methylated mRNAs. *eLife* 6:e31311. doi: 10.7554/eLife.31311

Sampath, S. C., Sampath, S. C., and Millay, D. P. (2018). Myoblast fusion confusion: the resolution begins. *Skelet. Muscle* 8:3. doi: 10.1186/s13395-017-0149-3

Scott, D. L., Wolfe, F., and Huizinga, T. W. (2010). Rheumatoid arthritis. *Lancet* 376, 1094–1108. doi: 10.1016/s0140-6736(10)60826-4

Shen, G. S., Zhou, H. B., Zhang, H., Chen, B., Liu, Z. P., Yuan, Y., et al. (2018). The GDF11-FTO-PPARγ axis controls the shift of osteoporotic MSC fate to adipocyte and inhibits bone formation during osteoporosis. *Biochim. Biophys. Acta Mol. Basis Dis.* 1864, 3644–3654. doi: 10.1016/j.bbadis.2018.09.015

Shen, J., Abu-Amer, Y., O'Keefe, R. J., and McAlinden, A. (2017). Inflammation and epigenetic regulation in osteoarthritis. *Connect Tissue Res.* 58, 49–63. doi: 10.1080/03008207.2016.1208655

Sorci, M., Ianniello, Z., Cruciani, S., Larivera, S., Ginistrelli, L. C., Capuano, E., et al. (2018). METTL3 regulates WTAP protein homeostasis. *Cell Death Dis.* 9:796. doi: 10.1038/s41419-018-0843-z

Tian, C., Huang, Y., Li, Q., Feng, Z., and Xu, Q. (2019). Mettl3 regulates osteogenic differentiation and alternative splicing of vegfa in bone marrow mesenchymal stem cells. *Int. J. Mol. Sci.* 20:551. doi: 10.3390/ijms20030551

Tran, B., Nguyen, N. D., Center, J. R., Eisman, J. A., and Nguyen, T. V. (2014). Association between fat-mass-and-obesity-associated (FTO) gene and hip fracture susceptibility. *Clin. Endocrinol.* 81, 210–217. doi: 10.1111/cen.12335

Tresguerres, F. G. F., Torres, J., López-Quiles, J., Hernández, G., Vega, J. A., and Tresguerres, I. F. (2020). The osteocyte: a multifunctional cell within the bone. *Ann. Anat.* 227:151422. doi: 10.1016/j.aanat.2019.151422

Tu, C., He, J., Chen, R., and Li, Z. (2019). The emerging role of exosomal non-coding RNAs in musculoskeletal diseases. *Curr. Pharm. Des.* 25, 4523–4535. doi: 10.2174/1381612825666191113104946

Tu, C., He, J., Qi, L., Ren, X., Zhang, C., Duan, Z., et al. (2020). Emerging landscape of circular RNAs as biomarkers and pivotal regulators in osteosarcoma. *J. Cell. Physiol.* doi: 10.1002/jcp.29754 [Epub ahead of print].

van Wijnen, A. J., and Westendorf, J. J. (2019). Epigenetics as a new frontier in orthopedic regenerative medicine and oncology. *J. Orthop. Res.* 37, 1465–1474. doi: 10.1002/jor.24305

Wang, J., Yan, S., Lu, H., Wang, S., and Xu, D. (2019). METTL3 attenuates LPS-induced inflammatory response in macrophages via NF-κB signaling pathway. *Mediators Inflamm.* 2019:3120391. doi: 10.1155/2019/3120391

Wang, R., Han, Z., Liu, B., Zhou, B., Wang, N., Jiang, Q., et al. (2018). Identification of natural compound radicicol as a Potent FTO inhibitor. *Mol. Pharm.* 15, 4092–4098. doi: 10.1021/acs.molpharmaceut.8b00522

Wang, T., Kong, S., Tao, M., and Ju, S. (2020). The potential role of RNA N6-methyladenosine in Cancer progression. *Mol. Cancer* 19:88. doi: 10.1186/s12943-020-01204-7

Wang, X., Feng, J., Xue, Y., Guan, Z., Zhang, D., Liu, Z., et al. (2016). Structural basis of N(6)-adenosine methylation by the METTL3-METTL14 complex. *Nature* 534, 575–578. doi: 10.1038/nature18298

Wang, X., Huang, N., Yang, M., Wei, D., Tai, H., Han, X., et al. (2017). FTO is required for myogenesis by positively regulating mTOR-PGC-1α pathway-mediated mitochondria biogenesis. *Cell Death Dis.* 8:e2702. doi: 10.1038/cddis.2017.122

Wang, X., Zhao, B. S., Roundtree, I. A., Lu, Z., Han, D., Ma, H., et al. (2015). N(6)-methyladenosine modulates messenger RNA translation efficiency. *Cell* 161, 1388–1399. doi: 10.1016/j.cell.2015.05.014

Wang, Y., Zeng, L., Liang, C., Zan, R., Ji, W., Zhang, Z., et al. (2019). Integrated analysis of transcriptome-wide m(6)A methylome of osteosarcoma stem cells enriched by chemotherapy. *Epigenomics* 11, 1693–1715. doi: 10.2217/epi-2019-0262

Weivoda, M. M., Ruan, M., Pederson, L., Hachfeld, C., Davey, R. A., Zajac, J. D., et al. (2016). Osteoclast TGF-β Receptor Signaling Induces Wnt1 Secretion and Couples Bone Resorption to Bone Formation. *J. Bone Miner. Res.* 31, 76–85. doi: 10.1002/jbmr.2586

Wu, W., Feng, J., Jiang, D., Zhou, X., Jiang, Q., Cai, M., et al. (2017). AMPK regulates lipid accumulation in skeletal muscle cells through FTO-dependent demethylation of N(6)-methyladenosine. *Sci. Rep.* 7:41606. doi: 10.1038/srep41606

Wu, Y., Xie, L., Wang, M., Xiong, Q., Guo, Y., Liang, Y., et al. (2018). Mettl3-mediated m(6)A RNA methylation regulates the fate of bone marrow mesenchymal stem cells and osteoporosis. *Nat. Commun.* 9:4772. doi: 10.1038/s41467-018-06898-4

Xia, B., Di, C., Zhang, J., Hu, S., Jin, H., and Tong, P. (2014). Osteoarthritis pathogenesis: a review of molecular mechanisms. *Calcif. Tissue Int.* 95, 495–505. doi: 10.1007/s00223-014-9917-9

Xu, C., Wang, X., Liu, K., Roundtree, I. A., Tempel, W., Li, Y., et al. (2014). Structural basis for selective binding of m6A RNA by the YTHDC1 YTH domain. *Nat. Chem. Biol.* 10, 927–929. doi: 10.1038/nchembio.1654

Xu, S., Gong, Y., Yin, Y., Xing, H., and Zhang, N. (2020). The multiple function of long noncoding RNAs in osteosarcoma progression, drug resistance and prognosis. *Biomed. Pharmacother.* 127:110141. doi: 10.1016/j.biopha.2020.110141

Yan, G., Yuan, Y., He, M., Gong, R., Lei, H., Zhou, H., et al. (2020). m(6)A methylation of precursor-miR-320/RUNX2 controls osteogenic potential of bone marrow-derived mesenchymal stem cells. *Mol. Ther. Nucleic Acids* 19, 421–436. doi: 10.1016/j.omtn.2019.12.001

Yin, H., Wang, H., Jiang, W., Zhou, Y., and Ai, S. (2017). Electrochemical immunosensor for N6-methyladenosine detection in human cell lines based on biotin-streptavidin system and silver-SiO(2) signal amplification. *Biosens. Bioelectron.* 90, 494–500. doi: 10.1016/j.bios.2016.10.066

Yu, J., Shen, L., Liu, Y., Ming, H., Zhu, X., Chu, M., et al. (2020). The m6A methyltransferase METTL3 cooperates with demethylase ALKBH5 to regulate osteogenic differentiation through NF-κB signaling. *Mol. Cell. Biochem.* 463, 203–210. doi: 10.1007/s11010-019-03641-5

Zeggini, E., Panoutsopoulou, K., Southam, L., Rayner, N. W., Day-Williams, A. G., Lopes, M. C., et al. (2012). Identification of new susceptibility loci for osteoarthritis (arcOGEN): a genome-wide association study. *Lancet* 380, 815–823. doi: 10.1016/s0140-6736(12)60681-3

Zhang, H., Shi, X., Huang, T., Zhao, X., Chen, W., Gu, N., et al. (2020). Dynamic landscape and evolution of m6A methylation in human. *Nucleic Acids Res.* 19:88. doi: 10.1093/nar/gkaa347

Zhang, Q., Riddle, R. C., Yang, Q., Rosen, C. R., Guttridge, D. C., Dirckx, N., et al. (2019). The RNA demethylase FTO is required for maintenance of bone mass and functions to protect osteoblasts from genotoxic damage. *Proc. Natl. Acad. Sci. U.S.A.* 116, 17980–17989. doi: 10.1073/pnas.1905489116

Zhang, Y., Gu, X., Li, D., Cai, L., and Xu, Q. (2019). METTL3 regulates osteoblast differentiation and inflammatory response via Smad Signaling and MAPK Signaling. *Int. J. Mol. Sci.* 21:199. doi: 10.3390/ijms21010199

Zhou, K. I., Shi, H., Lyu, R., Wylder, A. C., Matuszek, Ż., Pan, J. N., et al. (2019). Regulation of Co-transcriptional Pre-mRNA Splicing by m(6)A through the Low-Complexity Protein hnRNPG. *Mol. Cell* 76, 70–81.e9. doi: 10.1016/j.molcel.2019.07.005

Zhou, L., Yang, C., Zhang, N., Zhang, X., Zhao, T., and Yu, J. (2020). Silencing METTL3 inhibits the proliferation and invasion of osteosarcoma by regulating ATAD2. *Biomed. Pharmacother.* 125:109964. doi: 10.1016/j.biopha.2020.109964

Zhu, W., Wang, J. Z., Xu, Z., Cao, M., Hu, Q., Pan, C., et al. (2019). Detection of N6-methyladenosine modification residues (Review). *Int. J. Mol. Med.* 43, 2267–2278. doi: 10.3892/ijmm.2019.4169

Zhu, Z. M., Huo, F. C., and Pei, D. S. (2020). Function and evolution of RNA N6-methyladenosine modification. *Int. J. Biol. Sci.* 16, 1929–1940. doi: 10.7150/ijbs.45231

Zong, X., Zhao, J., Wang, H., Lu, Z., Wang, F., Du, H., et al. (2019). Mettl3 deficiency sustains long-chain fatty acid absorption through suppressing Traf6-dependent inflammation response. *J. Immunol.* 202, 567–578. doi: 10.4049/jimmunol.1801151

Zou, S., Toh, J. D., Wong, K. H., Gao, Y. G., Hong, W., and Woon, E. C. (2016). N(6)-Methyladenosine: a conformational marker that regulates the substrate specificity of human demethylases FTO and ALKBH5. *Sci. Rep.* 6:25677. doi: 10.1038/srep25677

Disclaimer: Figures of this review were created with the aid of Servier Medical Art (https://smart.servier.com/), reproduced under Creative Commons License attribution 3.0 Unported License.

Conflict of Interest: The authors declare that the research was conducted in the absence of any commercial or financial relationships that could be construed as a potential conflict of interest.

Copyright © 2020 Zhang, He, Liu, Ren, Qi, Wan, Wang, Tu and Li. This is an open-access article distributed under the terms of the Creative Commons Attribution License (CC BY). The use, distribution or reproduction in other forums is permitted, provided the original author(s) and the copyright owner(s) are credited and that the original publication in this journal is cited, in accordance with accepted academic practice. No use, distribution or reproduction is permitted which does not comply with these terms.

frontiers in Cell and Developmental Biology

ORIGINAL RESEARCH
published: 03 September 2020
doi: 10.3389/fcell.2020.00872

ASPH Regulates Osteogenic Differentiation and Cellular Senescence of BMSCs

*Hui Peng, Qi Guo, Ye Xiao, Tian Su, Tie-Jian Jiang, Li-Juan Guo and Min Wang**

Department of Endocrinology, Endocrinology Research Center, Xiangya Hospital of Central South University, Changsha, China

Osteogenesis and senescence of BMSCs play great roles in age-related bone loss. However, the causes of these dysfunctions remain unclear. In this study, we identified a differentially expressed *ASPH* gene in middle-aged and elderly aged groups which were obtained from GSE35955. Subsequent analysis in various databases, such as TCGA, GTEx, and CCLE, revealed that *ASPH* had positive correlations with several osteogenic markers. The depletion of mouse *Asph* suppressed the capacity of osteogenic differentiation in bone marrow mesenchymal stem cells (BMSCs). Notably, the expression of *ASPH in vitro* decreased during aging and senescence. The deficiency of *Asph* accelerated cellular senescence in BMSCs. Conversely, the overexpression of *Asph* enhanced the capacity of osteogenic differentiation and inhibited cellular senescence. Mechanistically, *ASPH* regulated Wnt signaling mediated by Gsk3β. Taken together, our data established that *ASPH* was potentially involved in the pathogenesis of age-related bone loss through regulating cellular senescence and osteogenic differentiation, which provides some new insights to treat age-related bone loss.

Keywords: *ASPH*, BMSCs, cellular senescence, osteogenesis, aging

OPEN ACCESS

Edited by:
Chao Liang,
Hong Kong Baptist University, Hong Kong

Reviewed by:
Bo Gao,
Xijing Hospital, China
Zhijun Pan,
Zhejiang University, China

***Correspondence:**
Min Wang
minwang11@126.com

Specialty section:
This article was submitted to Molecular Medicine, a section of the journal Frontiers in Cell and Developmental Biology

Received: *07 June 2020*
Accepted: *11 August 2020*
Published: *03 September 2020*

Citation:
Peng H, Guo Q, Xiao Y, Su T, Jiang T-J, Guo L-J and Wang M (2020) ASPH Regulates Osteogenic Differentiation and Cellular Senescence of BMSCs. Front. Cell Dev. Biol. 8:872. doi: 10.3389/fcell.2020.00872

INTRODUCTION

Osteoporosis is characterized by a reduction of bone mass and dysfunction of bone microarchitecture (Al Anouti et al., 2019; Yang et al., 2019). With the progressive aging of the general population, age-related osteoporosis is becoming a prevalent chronic disease in various countries. Elderly individuals are susceptible to suffer from the age-related osteoporosis because of the loss of bone mass and strength caused by skeletal aging (Li et al., 2015, 2018; Yu et al., 2018; Xiao et al., 2020). Skeletal aging-associated bone loss can be traced back to bone marrow mesenchymal stem cells (BMSCs). BMSCs play a great role in bone formation because of their potential of self-renewal and multi-lineage differentiation including osteogenic lineage (Li et al., 2018; Peng et al., 2019). During aging, BMSCs present with a reduced capacity of self-renewal and osteogenic lineage commitment, which thereby results in the aberrant age-dependent bone formation (Childs et al., 2015; Li H. et al., 2017).

Cellular senescence refers to a state of irreversible cell cycle arrest and distinct cellular alterations in response to various stress (Childs et al., 2015). This process is controlled by various types of tumor suppressors, such as $p16^{INK4A}$, $p15^{INK4b}$, Rb, and $p21^{CIP1}$ (Campisi and d'Adda di Fagagna, 2007; Childs et al., 2015; Li C. et al., 2017). Aging has been reported to be associated with increased cellular senescence. Accumulation of cellular senescence, in turn, can accelerate organismal aging

and contribute to the phenotype of aging (Childs et al., 2015). BMSCs will start the aging process early, that is, premature aging, upon stimulated by the stress. Previous studies also revealed that BMSCs underwent cellular senescence during skeletal aging and age-related modulators can cause or prevent premature aging (Lin et al., 2014; Li H. et al., 2017; Zhou et al., 2020).

Aspartate β-hydroxylase encoded by *ASPH* is a type II membrane protein, which includes several domains majorly including N-terminal cytoplasmic domain, transmembrane (TM) domain, Ca^{2+} binding domain and C-terminal catalytic domains (Treves et al., 2000; Finotti et al., 2008). *ASPH* has various isoforms because of its extensive alternative splicing. The longest *ASPH* isoform a containing C-terminal Aspartyl/Asparaginyl beta-hydroxylase catalytic domain can regulate some proteins with the epidermal growth factor (EGF)-like domains (Dinchuk et al., 2000). Based on the current studies, *ASPH* has been reported to be involved in the regulation of tumorigenesis via cell proliferation, colony formation and cellular senescence (Iwagami et al., 2016; Hou et al., 2018). Notably, a Genome-Wide Association Study (GWAS) conducted by Koller et al. (2010) described a SNP located closely with 3' region of *ASPH*. They found this SNP was conceivably associated with the lumbar spine bone mineral density in the premenopausal European-American women (Koller et al., 2010). In addition, some studies reported that *ASPH* was involved in the regulation of various signaling pathways, such as Wnt signaling, Notch signaling, IGF signaling, IRS signaling and so on (Cantarini et al., 2006; Tomimaru et al., 2013; Iwagami et al., 2016; Hou et al., 2018). It is noted that these signaling pathways are the canonical pathways during bone modeling and remodeling (Malaguarnera and Belfiore, 2014; Tu et al., 2015; Yang et al., 2017). However, the molecular network orchestrating bone formation and cellular senescence of BMSCs mediated by *ASPH* still remain unclear.

In this study, we reported that the level of *ASPH* decreased with aging or senescence. Intriguingly, *ASPH* longest isoform a facilitating the osteogenic differentiation of BMSCs, whereas preventing the process of cellular senescence. Conversely, the knockdown of *ASPH* accelerated the cellular senescence while suppressed the osteogenic differentiation. Mechanistically, these observations might be associated with aberrant Wnt signaling. Taken together, our study revealed *ASPH* promoting the process of osteogenesis while inhibiting cellular senescence through regulating Gsk3β-mediated Wnt signaling, which potentially provided new insights for aged-related bone loss.

MATERIALS AND METHODS

Differentially Expressed mRNAs Filtering and Bioinformatics Analysis

Human mRNA expression data were downloaded from Gene Expression Omnibus (GEO Accession: GEO35955)[1]. The differentially expressed mRNAs between middle-aged and elderly aged groups have been filtered using *t*-test. The R package "limma" (Ritchie et al., 2015) applied to normalize the data and identify DEGs. The DEGs was kept when adjust $p = 0.01$ and $|\log FC| = 2$. Then, kept genes have been assessed the functional enrichments, including GO (Gene Ontology) Biological Processes term and KEGG (Kyoto Encyclopedia of Genes and Genomes) pathway using the R package "Clusterprofiler"(Yu et al., 2012). All probes of the interested *ASPH* gene have been extracted from the raw data. We calculated *ASPH* expression at different coding region according to the recognition sites of probes. Its expressions at different regions then were output the violin figures using *t*-test.

Co-expression of *ASPH* With Other Genes

The raw expression data of *ASPH* and *RUNX2*, *COL1A1*, *GSK3B*, and *CTNNB1* genes were downloaded from The Cancer Genome Atlas (TCGA) project[2], the Genotype Tissue Expression (GTEx) program[3] and CCLE (Cancer Cell Line Encyclopedia) project[4]. The Pearson correlation (r) and *p*-value have been calculated using R and R Studio. The *p*-value has been marked as "0" when it is less than $1^{*}10^{-8}$.

BMSCs Culture

Mouse BMSCs (MUBMX-01001; Cyagen Biosciences) were cultured in Mouse Mesenchymal Stem Cell Growth Medium (MUBMX-90011; Cyagen Biosciences). For human BMSCs, we purified from bone marrow of participants underwent hip replacement. The gender of these subjects is male. The ages of young groups were 24, 28, 31, 27, and 32, respectively The ages in old groups were 75, 75, 78, 79, and 85, respectively.

qRT-PCR Analysis

For analysis of mRNA expression, total RNA from cultured cells was extracted using Trizol reagent (Takara). One-thousand nanograms of RNA was reverse-transcribed into first-strand cDNA using the Reverse Transcription Kit (Takara). For Human BMSCs RNA and cDNA have collected before. qPCR was performed using SYBR Green PCR Master Mix (Takara) and mRNA expression was normalized to reference genes *GAPDH*.

Western Blot

The protein was lysed using the mixture of RIPA, protease inhibitor (1:100) and phosphatase inhibitor (1:100). Western Blot was performed according to the previous described method (Li et al., 2015). The primary antibodies, GSK-3β Rabbit mAb (#9315; CST), Non-phospho (Active) β-Catenin (Ser33/37/Thr41) Rabbit mAb (#8814;CST), β-Catenin Antibody (#9562;CST), beta Actin mouse monoclonal antibody (#TA811000, ORIGENE) Phospho-GSK-3β (Ser9) Antibody (#9336; CST), and alpha-tubulin (11224-1-AP; Proteintech), were incubated overnight at 4°C, then incubated with appropriate HRP-conjugated secondary antibodies for 1 h at room temperature. The blots were visualized using ECL detection reagents.

[1]https://www.ncbi.nlm.nih.gov/geo/

[2]http://cancergenome.nih.gov/

[3]https://www.gtexportal.org/

[4]https://portals.broadinstitute.org/ccle

Immunofluorescence

For immunofluorescence, cells were washed by phosphate-buffered saline (PBS) three times. Then, cells were fixed in 4% paraformaldehyde for 15 min and followed by permeabilization and blocking with 7% FCS, 1% TritonX100 in PBS for 30 min at room temperature. Primary antibodies of total β-Catenin (#9562; CST, 1:200) and Non-phospho (Active) β-Catenin (Ser33/37/Thr41) (#8814; CST, 1:800) were incubated overnight in 7% BSA in PBS overnight at 4°C and followed by Alexa Fluor R 488 Goat Anti– rabbit (Thermo Fisher Scientific, United States) at a dilution of 1:400, and finally stained and mounted by mounting medium. Images were visualized on Olympus microscope using cellSense Dimension software.

Cell Transfection

The *Asph* siRNA, Gsk3b siRNA and the negative control (NC) were purchased from Ribibio (Guangzhou, China). The siRNAs were transfected at the concentration of 100 nM using lipofectamine RNAiMAX (Invitrogen, United States) according to manufacturer's recommendations. m*Asph* pcDNA3.1-3xFlag-C construct (GenBank:NM_004318.4) was purchased from YouBao Biology. One microgram m*Asph* (AAH) construct and negative control were transfected into BMCSs per well of 6-well-plate using Lipofectamine RNAiMAX (Invitrogen) according to manufacturer's recommendations.

Osteogenic Differentiation and Mineralization Assay

To induce osteogenic differentiation of BMSCs, BMSCs were cultured in 6-well plates at 2.5 × 106 cells per well with the mesenchymal stem cell osteogenic differentiation (MUBMX-90021; Cyagen Biosciences). At the 2rd day of osteogenic differentiation, the cell lysates were homogenized for ALP activity assay by spectrophotometric measurement of p-nitrophenol release using an Alkaline Phosphatase Assay Kit (P0321S, Beyotime). At the 7th day of osteogenic differentiation, alkaline phosphatase staining (ALP staining) was performed to evaluate the cell-matrix mineralization. We firstly washed the cells using PBS three times followed by 10% paraformaldehyde for 5 min. Then, cells were incubated in ALP incubation buffer (0.2 g barbital sodium, 0.4 g magnesium sulfate, 0.2 g calcium chloride and 0.3 g beta-glycerophosphate) at 37°C for 2 h. Next, washed cells with 2% calcium chloride and incubated with 2% cobaltous nitrate for 5 min. Then, cells were incubated in 1:80 ammonium sulfate for 10 s. At the 21st day of osteogenic differentiation, Alizarin Red staining was performed to evaluate the cell-matrix mineralization according to the manufacturer's instructions (MUBMX-90021; Cyagen Biosciences). Briefly, cells were washed using PBS three times followed by 4% paraformaldehyde for 30 min. After washed by PBS for three times, cells were stained in Alizarin red solution at 37°C for 5 min. The stained wells were imaged using the camera (ILCE-5100, SONY). Alizarin Red S released from the cell matrix into the cetyl-pyridinium chloride solution was quantified by spectrophotometry at 540 nm.

β-Galactosidase Staining

BMSCs with *Asph* siRNA interference were detected by senescence β-Galactosidase staining kit according to the manufacturer's instructions (G1580, Solarbio Life Science). Briefly, we firstly prepared the staining working solution which comprised of 10 μl β -galactosidase stain A, 10 μl β -galactosidase stain B, 930 μl β -galactosidase stain C and 50 μl X-Gal solution for each well. Then, we rinsed the cell plates with PBS followed by the fixation by 1 ml fix solution of β-galactosidase staining at room temperature for 15 min. After removal of fix solution, the plates were rinsed for three times. Then, cells were incubated with 1 ml staining working solution in incubator at 37°C overnight. Finally, the plates were visualized through Olympus microscope.

Giemsa Staining

BMSCs with *Asph* siRNA interference was detected by Giemsa staining kit according to the manufacturer's instructions (G4640, Solarbio Life Science). Briefly, we washed the cell plates with PBS followed by fixation using 1 ml methanol for 2 min. After removal of fix solution, the plates were washed three times using PBS. Then, cells were incubated in 1 ml staining solution for 15 min. Finally, the CFUs were recorded using the camera (ILCE-5100, SONY).

Statistical Analysis

Data was imported into Excel and scaled and normalized to appropriate controls. Unpaired, two-tailed Student's *t*-tests were performed for the comparisons of two groups and one-way ANOVA for comparison within multiple groups. Critical *P*-values were Bonferroni corrected and expressed as follows: ns: No significance, $^{*}P < 0.05$, $^{**}P < 0.01$, $^{**}P < 0.001$, $^{\#\#\#}P < 0.001$.

RESULTS

ASPH Is an Age-Dependent Gene in BMSCs

To identify the possible causes of age-related bone loss, we analyzed the differentially expressed genes of GSE35955 using R and R studio software (version 3.5) (Raw data was obtained from a public repository of GEO which includes human middle-aged individuals and elderly individuals) (Benisch et al., 2012). Firstly, we normalized the expression of all samples (**Figure 1A**). Secondly, we kept the deferentially expressed probes through setting the cutoff of adjust *p*-value as 0.01 and LogFC (Log FoldChange) as 2.0, respectively. A total of 152 probes (including 127 genes) have been kept. Of the differentially expressed 152 probes, the expression of 116 probes decreased while the expression of 36 probes increased in elderly aged groups in comparison to the middle-aged group (**Figures 1B,C**). Thirdly, we analyzed the top 10 enriched signaling using three sub-ontologies (BP for Biological Process, MF for Molecular Function, and CC for Cellular Component) of GO biological processes and KEGG pathway analysis (**Figures 1D,E**). KEGG analysis showed the differentially expressed genes were majorly enriched in cellular senescence, EGFR tyrosine kinase inhibitor

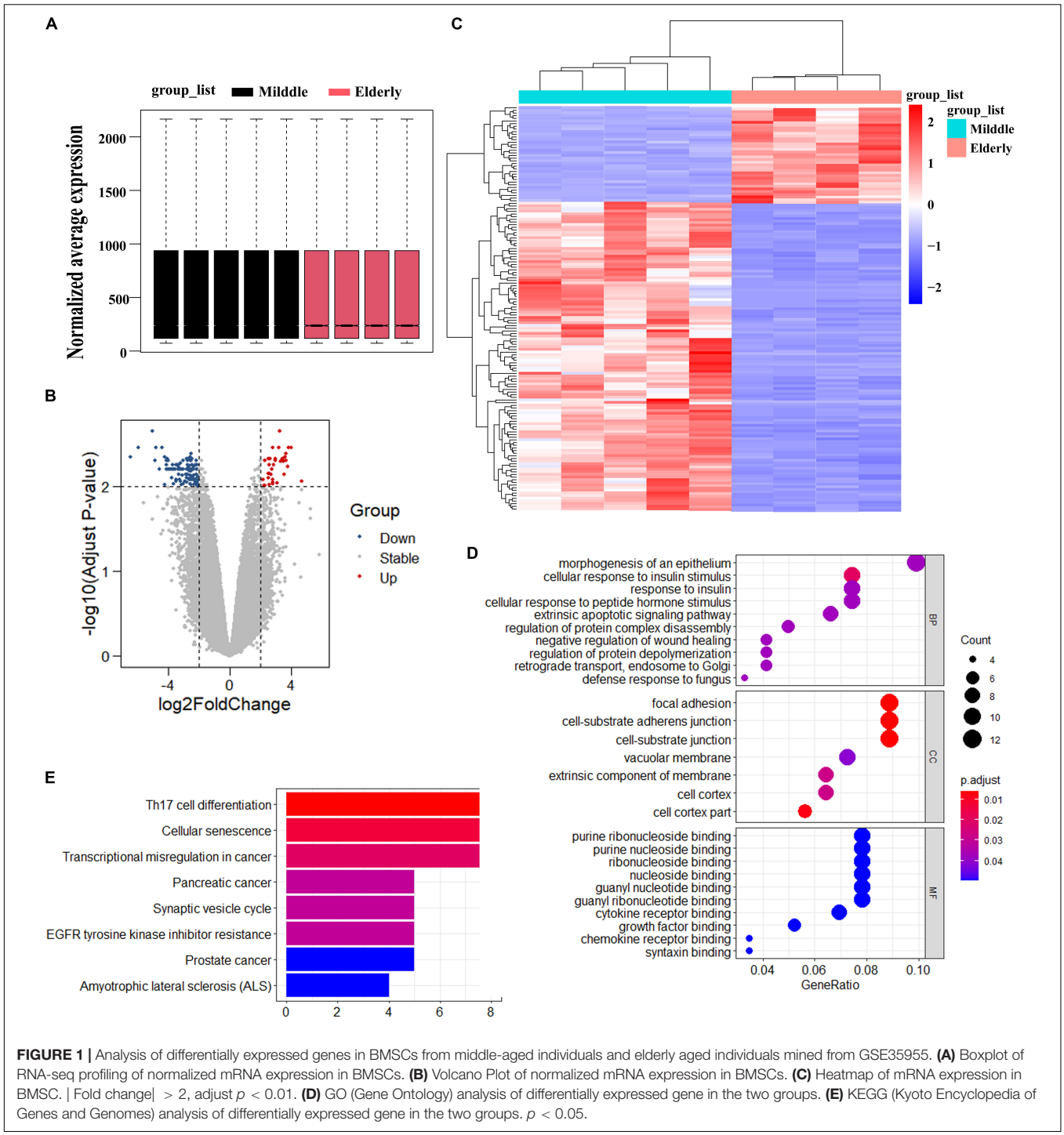


FIGURE 1 | Analysis of differentially expressed genes in BMSCs from middle-aged individuals and elderly aged individuals mined from GSE35955. **(A)** Boxplot of RNA-seq profiling of normalized mRNA expression in BMSCs. **(B)** Volcano Plot of normalized mRNA expression in BMSCs. **(C)** Heatmap of mRNA expression in BMSC. | Fold change| > 2, adjust $p < 0.01$. **(D)** GO (Gene Ontology) analysis of differentially expressed gene in the two groups. **(E)** KEGG (Kyoto Encyclopedia of Genes and Genomes) analysis of differentially expressed gene in the two groups. $p < 0.05$.

resistance and some cancer development (**Figure 1E**). Fourthly, we searched potential roles of all genes in bone formation via setting "Senescence OR Aging," "Bone," and "Gene symbol (from the differentially expressed genes)" as keywords in Pubmed database. Surprisingly, we found *ASPH* was associated with cellular senescence in cancer and possibly involved in bone health. Thus, we selected "*ASPH*" as our interested gene to conduct further studies.

ASPH Promotes Osteogenic Differentiation

Previous studies indicated *ASPH* might be associated with bone mineral density (Koller et al., 2010; Mantila Roosa et al., 2011; Benisch et al., 2012). To investigate if *ASPH* plays a role in bone formation, we analyzed the co-expression of *ASPH* with osteogenic markers such as *RUNX2* and *COL1A1* in various

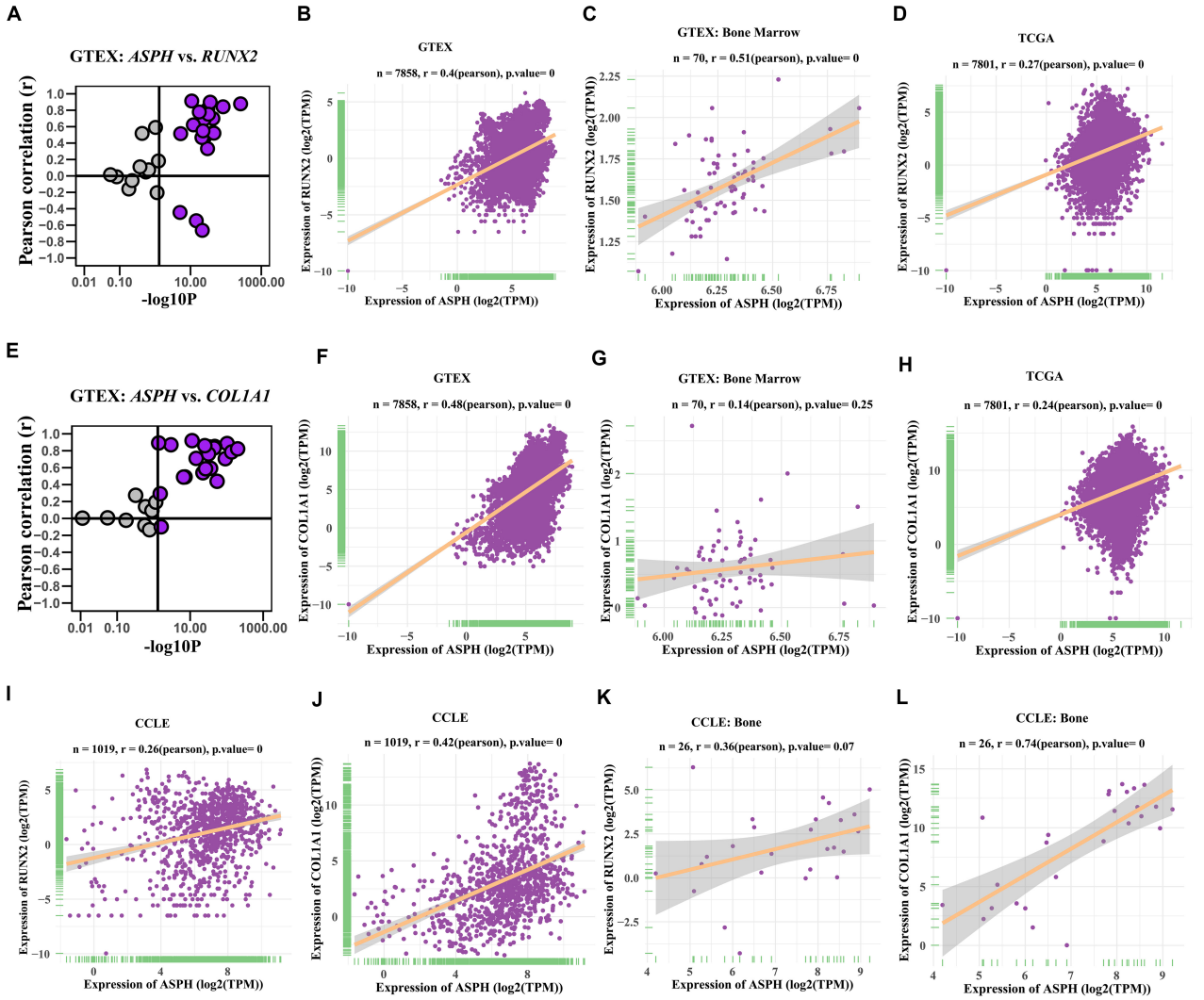


FIGURE 2 | Co-expression of *ASPH* with osteogenic markers. **(A–D)** Correlation of *ASPH* with *RUNX2* in expression in normal tissues **(A,B)**, bone marrow from normal tissues **(C)**, and cancer samples **(D)**, based on the data from Genotype Tissue Expression (GTEx) and The Cancer Genome Atlas (TCGA) databases, respectively. **(E–H)** Correlation of *ASPH* with *COL1A1* in expression in normal tissues **(E,F)**, bone marrow from normal tissues **(G)** and cancer samples **(H)**, based on the data from GTEx and databases, respectively. **(I,J)** Correlation of *ASPH* with *RUNX2* in expression in cancer cell lines **(I)** and in bone related cancer cell lines **(J)**, based on the data from Cancer Cell Line Encyclopedia (CCLE). **(K,L)** Correlation of *ASPH* with *COL1A1* in expression in cancer cell lines **(K)** and in bone related cancer cell lines **(L)**, based on the data from CCLE. The correlation coefficient (r) and *P*-value were calculated by Pearson's Correlation analysis. Note that every dot represents one tissue type **(A–C,E–G)** or one cancer type **(D,H)** or one cell line **(I–L)**.

databases. In most of normal tissues from GTEX, the correlations of *ASPH* with *RUNX2* and *COL1A1* were positive, which presented in the upper right region of **Figures 2A,E**. *ASPH* had a moderate positive correlation with *RUNX2* both in 7858 tissues (Pearson $r = 0.4$, $p = 0$) (**Figure 2B**) and specifically in 70 tissues of bone marrow (Pearson $r = 0.51$, $p = 0$) (**Figure 2C**). Similarly, *ASPH* had a positive correlation with *COL1A1* both in 7858 tissues (Pearson $r = 0.48$, $p = 0$) (**Figure 2F**) even though didn't show significant correlation with *RUNX2* in bone marrow (**Figure 2G**). In 7801 tumor tissues, *ASPH* also showed a positive correlation with *RUNX2* as well as *COL1A1* (**Figures 2D,H**). Moreover, in 1019 cancer cell lines, there were positive correlation between *ASPH* and *RUNX2* (**Figure 2I**) or *COL1A1* (**Figure 2J**). Notably, the 26 bone-related cell lines did not show significant co-expression between *ASPH* and *RUNX2* (**Figure 2K**), but showed positive correlation between *ASPH* and *COL1A1* (Pearson $r = 0.74$, $p = 0$) (**Figure 2L**). Collectively, these results partially supported that *ASPH* was positively correlated with these two genes (**Figures 2A–L**).

ASPH is an 85KD type II transmembrane protein which can generate various splicing variants including aspartyl beta-hydroxylase (AAH), junctin, and junctate (**Figure 3A**). The longest isoform a (GenBank:NM_004318.4) is comprised of several domains, majorly including N-terminal cytoplasmic domain, transmembrane (TM) domain, Ca^{2+} binding domain and C-terminal catalytic domains. We extracted the expression

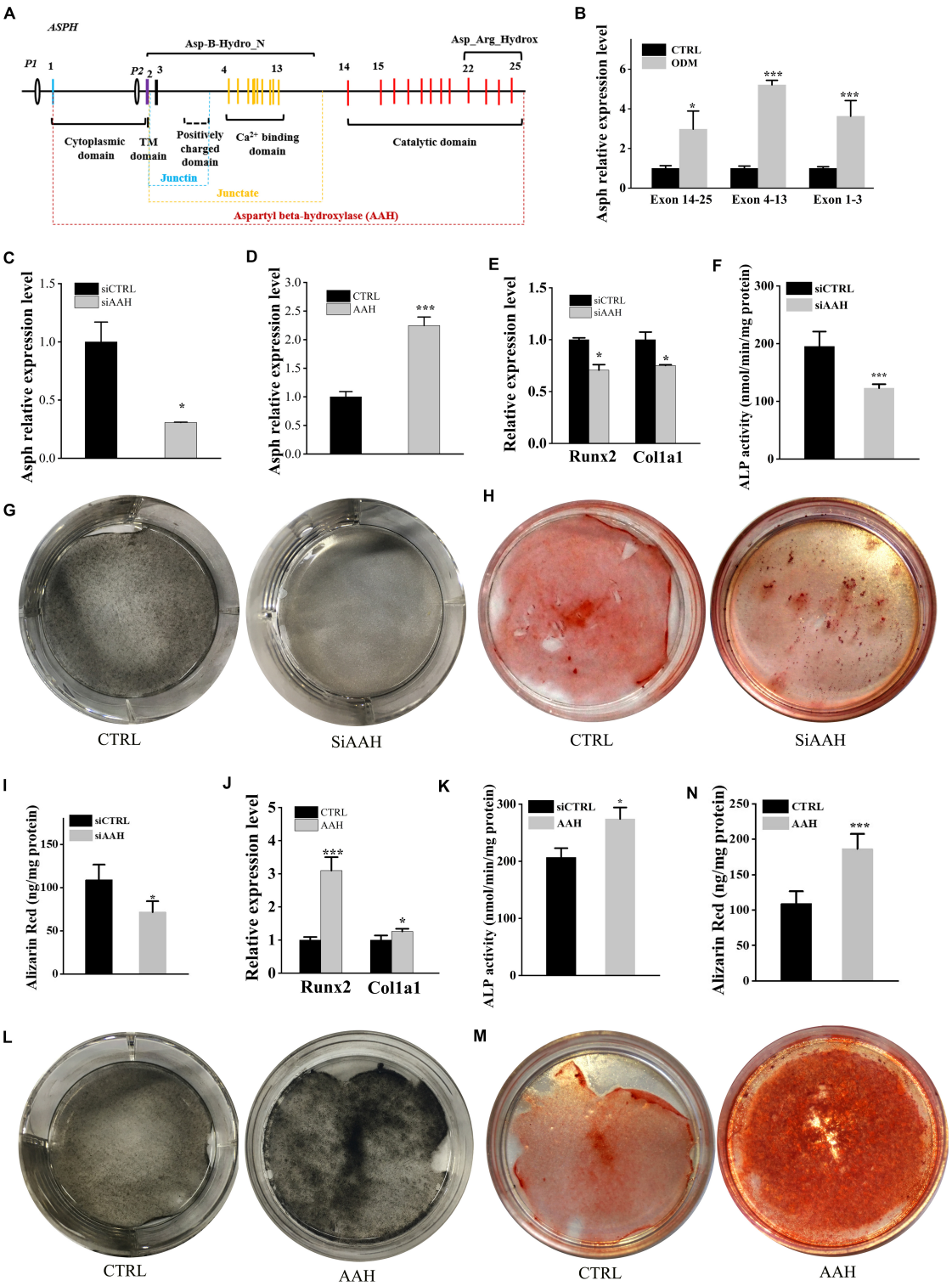


FIGURE 3 | *ASPH* promotes osteogenic differentiation. **(A)** schematic graph for *ASPH* isoforms. **(B)** qRT-PCR analysis of *ASPH* regions' expression during osteogenic differentiation. **(C)** qRT-PCR analysis of depletion of AAH. **(D)** qRT-PCR analysis of overexpression of AAH. **(E)** qRT-PCR analysis of the relative levels of *Runx2* and *Col1a1* in BMSCs with depletion of AAH. **(F)** Analysis of ALP activity in BMSCs with depletion of AAH. **(G,H)** Representative images of ALkaline Phosphatase (ALP) staining **(G)** and Alizarin red S staining **(H,I)** in BMSCs with depletion of AAH. **(J)** qRT-PCR analysis of the relative levels of *Runx2* and *Col1a1* in BMSCs with overexpression of AAH. **(K)** Analysis of ALP activity in BMSCs with overexpression of AAH. **(L,M)** Representative images of ALP staining **(L)** and Alizarin Red S staining **(M,N)** in BMSCs with overexpression of AAH. These experiments were replicated three times. Error bars show standard deviation. $^{*}P < 0.05$, $^{***}P < 0.001$.

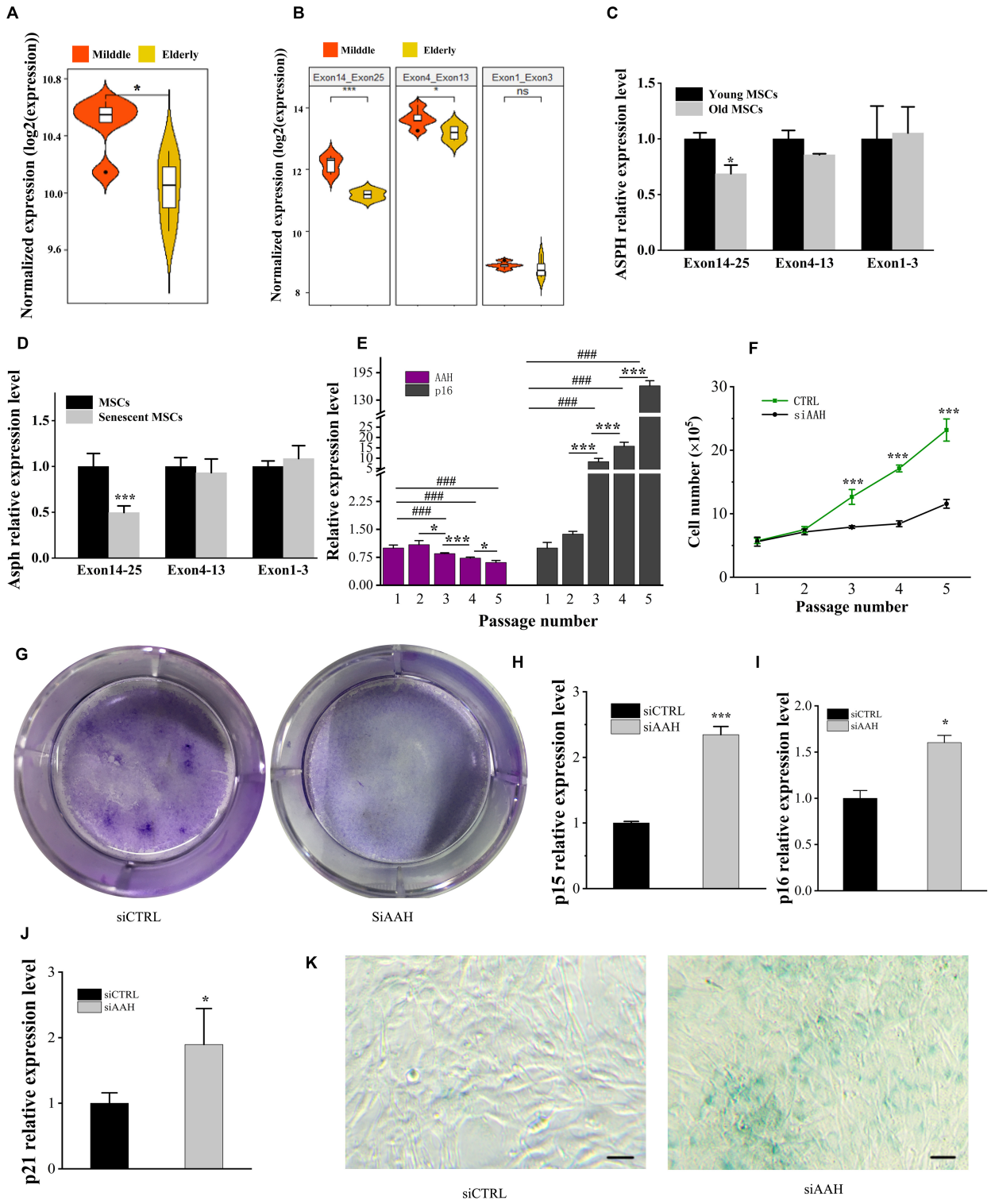


FIGURE 4 | Deficiency of *ASPH* accelerates cellular senescence in BMSCs. **(A)** Mean expression of *ASPH* in the BMSCs from middle-aged individuals and elderly aged individuals (Raw data was obtained from GSE35955). **(B)** Mean expression of different *ASPH* regions in the BMSCs from middle-aged individuals and elderly aged individuals (Raw data was obtained from GSE35955). **(C)** The expression of *ASPH* isoforms in the BMSCs from young and old individuals. **(D)** The expression of *Asph* isoforms in the young or senescent BMSCs. **(E)** The negative correlation of AAH and p16 expression during passaging (P1–P5) of BMSCs. **(F)** Doublings of BMSCs interfered with AAH siRNA *in vitro*. **(G)** Giemsa staining for the CFU-F colonies of BMSCs from BMSCs interfered with AAH siRNA *in vitro*. **(H–J)** Expression of p15 **(H)**, p16 **(I)**, and p21 **(J)** in BMSCs with depletion of AAH. **(K)** Representative images of SA-β-Gal staining of BMSCs in *Asph* siRNA transfected and control group. Scale Bar = 100 μm. These experiments were replicated three times. Error bars show standard deviation. $^{*}P < 0.05$, $^{***}P < 0.001$, $^{\#\#\#}P < 0.001$.

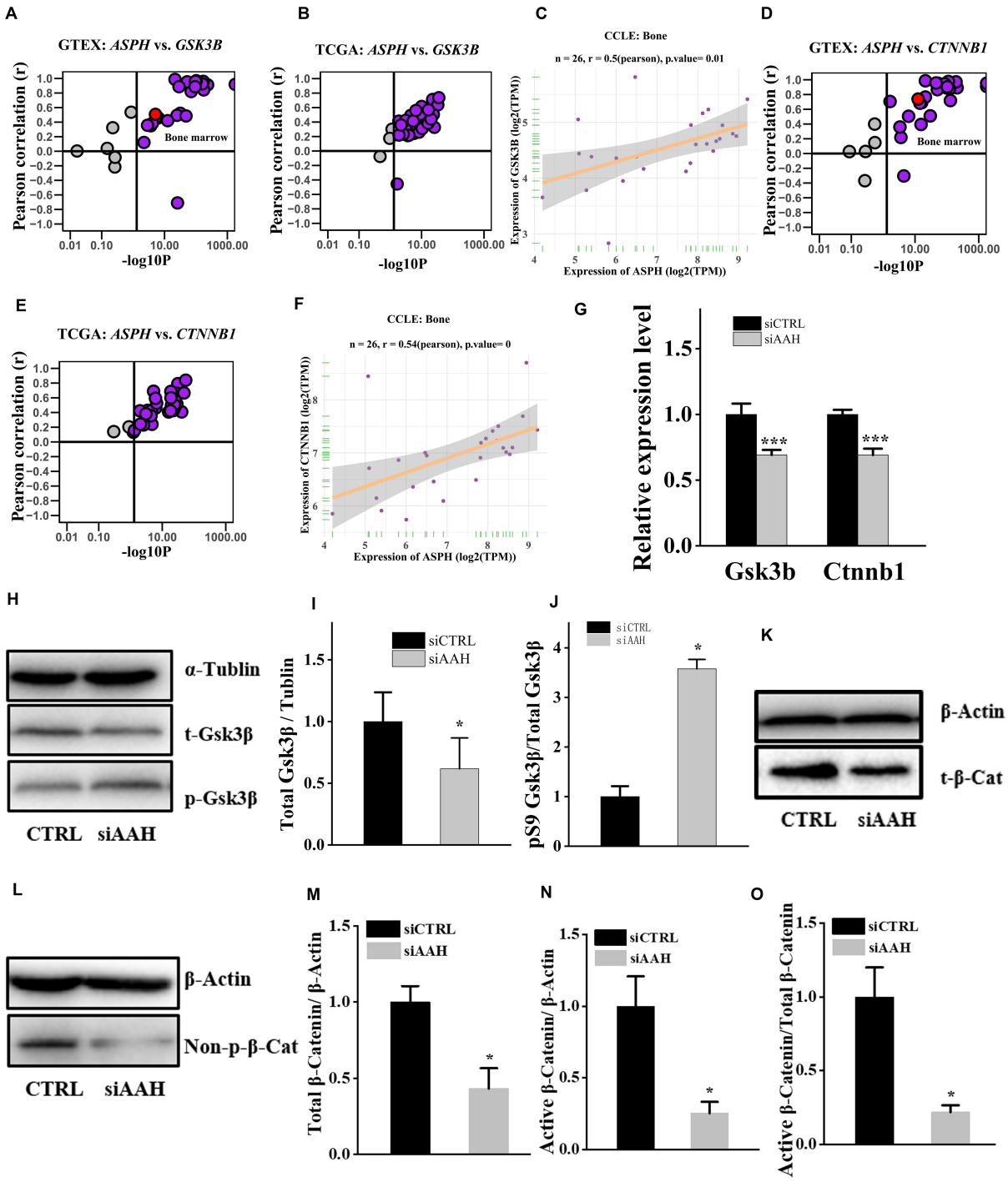


FIGURE 5 | *ASPH* regulates Gsk3β and β-Catenin. **(A–C)** Co-expression of *ASPH* with *GSK3B* in expression in normal tissues **(A)**, cancer samples **(B)**, and bone-related cell lines **(C)**, based on the data from GTEx, TCGA, and CCLE databases, respectively. **(D–F)** Co-expression of *ASPH* with *CTNNB1* in expression in normal tissues **(D)**, cancer samples **(E)**, and bone-related cell lines **(F)**, based on the data from GTEx, TCGA, and CCLE databases, respectively. The correlation coefficient (r) and *P*-value were calculated by Pearson's Correlation analysis. Note that every dot represents one tissue type **(A,D)** or one cancer type **(B,E)**. The red dots indicate tissue of bone marrow. **(G)** qRT-PCR analysis of *GSK3B* and *CTNNB1* in BMSCs interfered with *Asph* siRNA *in vitro*. **(H)** Western Blot analysis of the levels of total GSK3β and phos-Ser9 GSK3β in BMSCs transfected with *Asph* siRNA. **(I)** The ratio of total Gsk3β to α-Tublin in BMSCs transfected with *Asph* siRNA. **(J)** The ratio of phos-Ser9 GSK3β (pS9 GSK3β) to total GSK3β in BMSCs transfected with *Asph* siRNA. **(K)** Western Blot analysis of the levels of total β-Catenin (t-β-Cat) in BMSCs transfected with *Asph* siRNA. **(L)** Western Blot analysis of the levels of active β-Catenin [Non-phospho β-Catenin (Ser33/37/Thr41): Non-p-β-Cat] in BMSCs transfected with *Asph* siRNA. **(M)** The ratio of total β-Catenin to β-Actin in BMSCs transfected with *Asph* siRNA. **(N)** The ratio of active β-Catenin to β-Actin in BMSCs transfected with *Asph* siRNA. **(O)** The ratio of active β-Catenin to total β-Catenin in BMSCs transfected with *Asph* siRNA. These experiments were replicated 3 times. Error bars show standard deviation. $^{*}P < 0.05$, $^{***}P < 0.001$.

TABLE 1 | The co-expression of *ASPH* with *GSK3B*.

	Total samples	Pearson correlation(r)	*p*-value
GTEX	7858	0.59	0
GTEX: Bone marrow	70	0.51	0
TCGA	7801	0.39	0

TABLE 2 | The co-expression of *ASPH* with *CTNNB1*.

	Total samples	Pearson correlation(r)	*p*-value
GTEX	7858	0.77	0
GTEX: Bone marrow	70	0.74	0
TCGA	7801	0.48	0

of all "*ASPH*" probes and classified them into three types according to the probe-targeting positions (e.g., Exon 14–25 with C-terminal catalytic domain, Exon 4–13 with Ca^{2+} binding domain, and Exon 1–3 with a positively charged domain) (**Figure 3A**). Next, BMSCs were induced by osteogenic differentiation medium and tested its expression of different domains of *ASPH*. The qRT-PCR data showed increased expression of mouse *Asph* during osteogenesis of BMSCs (**Figure 3B**). Subsequently, BMSCs were transfected with mouse *Asph* siRNA targeting the catalytic domain (**Figure 3C**) followed by induction by osteogenic differentiation medium. qRT-PCR data suggested that downregulation of *Asph* expression was accompanied by a decline of osteogenic markers at the 7th day, including *Runx2* and *Col1a1* (**Figure 3E**). Furthermore, the matrix memorization measured by Alkaline phosphatase (ALP) activity, ALP staining and Alizarin Red staining showed a decline of AAH expression resulted in the impairment of osteogenesis in BMSCs (**Figures 3F–I**). Conversely, BMSCs were transfected with the construct of longest mouse *Asph* isoform variant 1 (GenBank:NM_023066.3) (**Figure 3D**) followed by induction by osteogenic differentiation medium. qRT-PCR suggested that up-regulation *Asph* expression was correlated with the increase of osteogenic markers, *Runx2* and *Col1a1* (**Figure 3J**). Similarly, matrix memorization measured by ALP activity, ALP staining and Alizarin Red staining showed over-expression of *Asph* resulted in the enhancement of osteogenesis in BMSCs (**Figures 3K–N**).

Ablation of *ASPH* Results in Premature Senescence of BMSCs

ASPH is known to be involved in the cellular senescence in hepatocellular carcinoma and gliomas (Iwagami et al., 2016; Sturla et al., 2016). In order to understand if *ASPH* is a cellular senescence-related gene in BMSCs, we calculated the mean *ASPH* expression and expression of different ASPH region (**Supplementary Table 1**; Peng et al., 2020a). The result suggested *ASPH* was lower in elderly aged individuals than middle-aged individuals (**Figure 4A**). The exon 4–13 and exon 14–25 of *ASPH* both decreased with aging in the two groups. However, the exon 1–3 expression locating at the common region of different *ASPH* isoforms was stable (**Figure 4B**). Then, we collected human BMSCs (hBMSCs) with different ages and tested their *ASPH* expression at different regions. As expected, compared to the aged group (age from 75 to 90), the young group (age from 24 to 32) showed a higher expression of *ASPH* longer isoforms (**Figure 4C**). Additionally, we tested the *Asph* expression in young mouse BMSCs (passage 0) and senescent mouse BMSCs (passage 5). Consistently, the expression of *Asph* longer isoforms were lower in senescent BMSCs than in young BMSCs (**Figure 4D**). These observations suggested that senescence suppressed *Asph* expression. To further test this hypothesis, we performed a series of functional analysis. qRT-PCR results demonstrated that the *Asph* expression was remarkably decreased along with cellular senescence (**Figure 4E**). Conversely, the senescence-associated p16 expression was positively correlated with cellular senescence (**Figure 4E**). Additionally, an impairment of the replicative capacity was observed in *Asph* siRNA transfected group (**Figure 4F**). CFU colonies obtained from Giemsa staining further showed the inhibition of cell proliferation in BMSCs interfered with *Asph* siRNA (**Figure 4G**). qRT-PCR results revealed that the depletion of *Asph* promoted markers of senescence, such as p15, p16, and p21 expression in BMSC (**Figures 4H–J**). Consistently, the senescence-associated β-galactosidase staining revealed that the deficiency of *Asph* promoted the cellular senescence (**Figure 4K**).

ASPH Regulates Wnt Signal Mediated by Gsk3β

It is well established that Gsk3β and β-catenin have important roles in bone formation. Based on the involvement of *ASPH* in Wnt signaling and cellular senescence in various cancers, we hypothesized that *ASPH* was involved in the bone formation and cellular senescence through regulating Gsk3β and β-catenin (Iwagami et al., 2016; Peng et al., 2020b). Thus, we analyzed the co-expression of *ASPH* with *GSK3B* and *CTNNB1* in GTEX, TACC and CCLE databases. Intriguingly, the analysis showed that *ASPH* has considerable positive correlations in mRNA expression with *GSK3B* and *CTNNB1* in most of normal/tumor tissues (**Figures 5A,B,D,E**). Furthermore, *ASPH* has a moderate or strong correlation with *GSK3B* and *CTNNB1* in the normal tissues including bone marrow from GTEX database (**Tables 1**, **2**). In bone-related cancer cell lines, *ASPH* has significant correlations with *GSK3B* (Pearson $r = 0.50$, $p = 0.01$) (**Figure 5C**) and *CTNNB1* (Pearson $r = 0.54$, $p = 0$) (**Figure 5F**). Consistent with these correlations, the expression of *GSK3B* and *CTNNB1* showed significant decrease in BMSCs with depletion of *Asph* (**Figures 5G–O**). The ratio of phos-Ser9 GSK3β to total Gsk3β has increased in the *Asph* siRNA transfected BMSCs (**Figure 5J**). *Asph* inhibition lead to the downregulation of total β-Catenin as well as active β-Catenin (**Figures 5K–O**). Consistently, cells transfected with *Asph* siRNA showed predominantly decreased distribution of the β-Catenin protein both in cytoplasm and nucleus (**Figure 6A**). The immunofluorescence analysis also suggested *Asph* inhibition ameliorated distribution of active β-Catenin in cytoplasm (**Figure 6B**). Taken together, these results suggested that *Asph* possibly regulated Gsk3β/β-catenin signaling, contributing to bone formation and preventing cellular senescence (**Figure 7**).

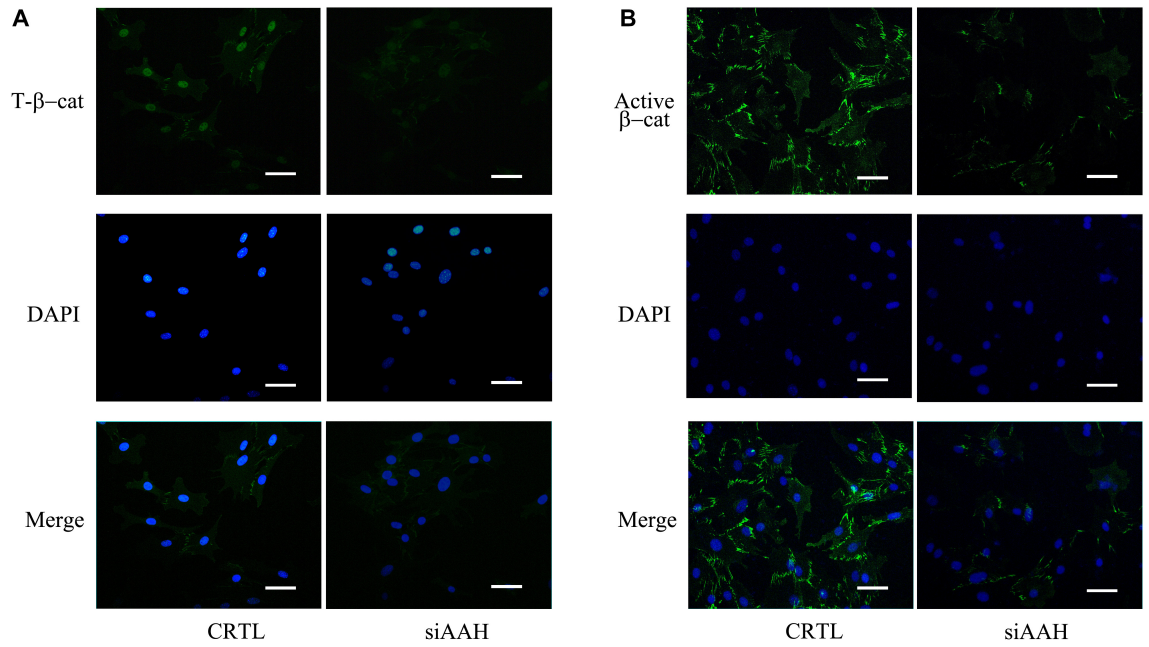


FIGURE 6 | Subcellular localization of total and active β-Catenin. **(A)** Subcellular localization of total β-Catenin protein in BMSCs transfected with *Asph* siRNA. Nuclei, DAPI (blue), total β-Catenin (green). **(B)** Subcellular localization of active β-Catenin [Non-phosph-β-Catenin (Ser33/37/Thr41)] protein in BMSCs transfected with *Asph* siRNA. Nuclei, DAPI (blue), active β-Catenin (green). Scale bar, 250 μm.

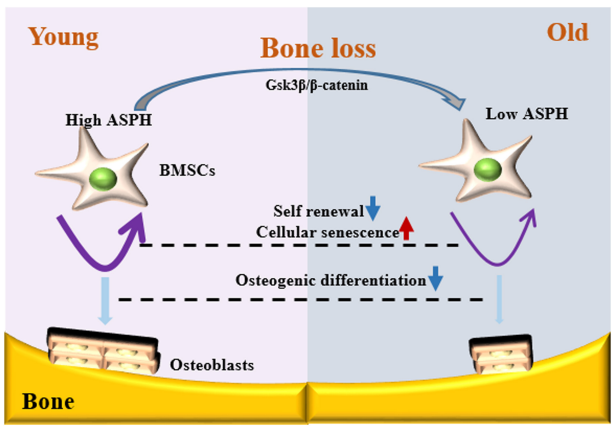


FIGURE 7 | Schematic representation of *ASPH* regulating cellular senescence and osteogenic differentiation of BMSCs during aging. Low expression of *ASPH* restrains the accumulation and activation of Gsk3β and β-Catenin to maintain the capacity of self-renewal and osteogenic differentiation. In the old individuals, the decrease of *ASPH* is companied with the cellular senescence and impaired osteogenic differentiation of BMSCs.

DISCUSSION

Osteogenesis and cellular senescence of BMSCs play great roles in bone formation (Qadir et al., 2020). In this study, our data showed *ASPH* longest isoform promoting the osteogenesis while inhibiting cellular senescence, indicating it potentially results in an elevated capacity of bone formation. Mechanistically, *ASPH* modulated the accumulation and activation of Gsk3β and β-catenin. In general, our study revealed *ASPH* was an aged-dependent modulator to regulate osteogenic differentiation and senescence in BMSCs (**Figure 6**).

Aspartate β-hydroxylase (*ASPH*) is a type II membrane protein, which is comprised of several domains, such as N-terminal cytoplasmic domain, transmembrane domain, and C-terminal catalytic domain (Finotti et al., 2008). Through data mining in GEO database, we found some genes differentially expressed in middle-aged subjects in comparison with elderly aged subjects. Through a set of filtering criteria as described in "Results" section, we finally hypothesized *ASPH* gene was partially involved in bone formation. *ASPH* is associated with the regulation of protein complex disassembly and regulation of protein depolymerization (Lee et al., 2012), which has been presented in the top 10 signaling through Go analysis (**Figure 1D**). Furthermore, KEGG analysis showed that the differentially expressed genes enriched in cellular senescence, EGFR tyrosine kinase inhibitor resistance and some cancer development. These observations gave us some clues that *ASPH* might be involved in bone modeling through regulating cellular senescence.

Accumulated evidence demonstrated that *Asph* was highly expressed during embryogenesis, which is crucial to maintain cell migration and organ development (Treves et al., 2000; Mahmood et al., 2010; Hou et al., 2018). Patel et al. (2014) performed the whole-mount *in situ* hybridization of *Asph* at embryonic day 11.5 (E11.5) and E12.5 mouse embryos.

They found a strong expression of *Asph* in snout, limbs, and eyes (Patel et al., 2014). To date, *ASPH* mutations identified in patients were established to be associated with Traboulsi syndrome which is characterized by facial dimorphism, lens dislocation, anterior segment abnormalities, and spontaneous filtering blebs (OMIM:601552) (Patel et al., 2014; Chandran et al., 2019), but does not refer to the abnormal bone mass. The knock-out *Asph* mice also replicated similar phenotypes with these patients (Dinchuk et al., 2002; Yuan et al., 2007; Patel et al., 2014). However, Peggy et al. demonstrated that *ASPH* expressed differentially in hBMSCs and was thought to be associated with the BMD and risk of bone fracture (Benisch et al., 2012). GWAS results suggested that a mutation occurred in 3' region of *ASPH* might be related to bone mass (Koller et al., 2010). In addition, the previous study suggested that *ASPH* played great roles in the other key signaling pathways like Wnt signaling, Notch signaling and so on, which are all closely involved in bone formation (Tomimaru et al., 2013; Hou et al., 2018). As expected, our study found that *ASPH* was an important modulator during osteogenesis. The correlation analysis suggested that *ASPH* had positive correlation with osteogenic markers. The expression of *Asph* was also increasing during osteogenic differentiation. Moreover, the depletion of *Asph* inhibited osteogenic differentiation while the overexpression of *Asph* promoted osteogenic differentiation. Nevertheless, Mantila Roosa et al. (2011) suggested that *Asph* was downregulated during matrix formation, which is not consistent with our results. In this study, stable expression at common region of *ASPH* (exon 1–3) and decreased expression at exon 4–25 have been showed in **Figure 3B**, which indicated that junctin has increased during aging and senescence. Thus, we suspected that *ASPH* different isoforms might be involved in the same process with opposite role.

Further study revealed that the deficiency of *Asph* in BMSCs resulting in the dysfunction of osteogenesis and cellular senescence. Conversely, overexpression of longest *Asph* variant 1 in BMSCs restored the capacity of osteogenic differentiation and prevented the cellular senescence. Gsk3β has been reported to be regulated by *ASPH* inhibitor in hepatocellular carcinoma (Iwagami et al., 2016). In addition, Gsk3β can phosphorylates the sites of β-catenin at the sites of Thr41/Ser37/Ser33 followed by the degradation of β-catenin (Wu and Pan, 2010; Peng et al., 2020b). Gsk3β-mediated Wnt signaling can promote bone formation and prevent cellular senescence (Ye et al., 2007; Seo et al., 2008; Gillespie et al., 2013). Thus, we investigated if *ASPH* regulated osteogenic differentiation and cellular senescence in BMSCs through regulating Gsk3β or β-catenin. Of note, positive correlations of *ASPH* with *GSK3B* and *CTNNB1* have been found in the normal tissues, cancer tissues as well as cancer cell lines. Furthermore, we confirmed these positive correlations *in vitro*. The deficiency of *Asph* inhibited the accumulation of Gsk3β. Nevertheless, the non-phosphorylation of β-catenin at Thr41/Ser37/Ser33 has decreased which explained the downregulation of total β-catenin. The immunofluorescence analysis supported the downregulated Wnt signaling as well.

Of note, previous studies suggested that a relatively low level of *ASPH* expression in normal mature tissues, while abundant expression of *ASPH* in a variety of malignant tumors (Lavaissiere et al., 1996; Lin et al., 2019). Thus, *ASPH* has been thought to be a potential therapeutic target for different cancers (Shimoda et al., 2012; Dong et al., 2015; Sturla et al., 2016). However, according to our current data *in vitro*, it suggested that the treatment of *ASPH* inhibitor in patients with cancer need to be concerned because of their potential risks of bone loss or bone fracture.

DATA AVAILABILITY STATEMENT

Publicly available datasets were analyzed in this study. This data can be found here: the GEO database (Accession number: GSE35955; https://www.ncbi.nlm.nih.gov/geo/query/acc.cgi?acc~=~GSE35955).

ETHICS STATEMENT

The studies involving human participants were reviewed and approved by the Ethics Committee of Xiangya Hospital of Central South University. The patients/participants provided their written informed consent to participate in this study. The animal study was reviewed and approved by the Xiangya Hospital of Central South University Ethics Committee.

AUTHOR CONTRIBUTIONS

HP designed this study, carried out most of the experiments, and wrote the manuscript. QG, TS, YX, T-JJ, and L-JG helped to collect samples. MW supervised the experiments, analyzed results, and proofread the manuscript. All authors contributed to the article and approved the submitted version.

FUNDING

This work was supported by the Grant No. 81873670 from the National Natural Science Foundation of China (NSFC).

ACKNOWLEDGMENTS

We gratefully acknowledge Prof. Stephen P. Robertson and Dr. Zandra A. Jenkins at the University of Otago for helping to form the hypothesis.

SUPPLEMENTARY MATERIAL

The Supplementary Material for this article can be found online at: https://www.frontiersin.org/articles/10.3389/fcell.2020.00872/full#supplementary-material

REFERENCES

Al Anouti, F., Taha, Z., Shamim, S., Khalaf, K., Al Kaabi, L., and Alsafar, H. (2019). An insight into the paradigms of osteoporosis: from genetics to biomechanics. *Bone Rep.* 11:100216. doi: 10.1016/j.bonr.2019.100216

Benisch, P., Schilling, T., Klein-Hitpass, L., Frey, S. P., Seefried, L., Raaijmakers, N., et al. (2012). The transcriptional profile of mesenchymal stem cell populations in primary osteoporosis is distinct and shows overexpression of osteogenic inhibitors. *PLoS One* 7:e45142. doi: 10.1371/journal.pone.0045142

Campisi, J., and d'Adda di Fagagna, F. (2007). Cellular senescence: when bad things happen to good cells. *Nat. Rev. Mol. Cell Biol.* 8, 729–740. doi: 10.1038/nrm2233

Cantarini, M. C., de la Monte, S. M., Pang, M., Tong, M., D'Errico, A., Trevisani, F., et al. (2006). Aspartyl-asparagyl β hydroxylase over-expression in human hepatoma is linked to activation of insulin-like growth factor and notch signaling mechanisms. *Hepatology* 44, 446–457. doi: 10.1002/hep.21272

Chandran, P., Chermakani, P., Venkataraman, P., Thilagar, S. P., Raman, G. V., and Sundaresan, P. (2019). A novel 5 bp homozygous deletion mutation in ASPH gene associates with Traboulsi syndrome. *Ophthalm. Genet.* 40, 185–187. doi: 10.1080/13816810.2019.1605390

Childs, B. G., Durik, M., Baker, D. J., and van Deursen, J. M. (2015). Cellular senescence in aging and age-related disease: from mechanisms to therapy. *Nat. Med.* 21, 1424–1435. doi: 10.1038/nm.4000

Dinchuk, J. E., Focht, R. J., Kelley, J. A., Henderson, N. L., Zolotarjova, N. I., Wynn, R., et al. (2002). Absence of post-translational aspartyl β-hydroxylation of epidermal growth factor domains in mice leads to developmental defects and an increased incidence of intestinal neoplasia. *J. Biol. Chem.* 277, 12970–12977. doi: 10.1074/jbc.M110389200

Dinchuk, J. E., Henderson, N. L., Burn, T. C., Huber, R., Ho, S. P., Link, J., et al. (2000). Aspartyl β-Hydroxylase (Asph) and an evolutionarily conserved isoform of asph missing the catalytic domain share exons with junctin. *J. Biol. Chem.* 275, 39543–39554. doi: 10.1074/jbc.M006753200

Dong, X., Lin, Q., Aihara, A., Li, Y., Huang, C.-K., Chung, W., et al. (2015). Aspartate β-hydroxylase expression promotes a malignant pancreatic cellular phenotype. *Oncotarget* 6, 1231–1248. doi: 10.18632/oncotarget.2840

Finotti, A., Treves, S., Zorzato, F., Gambari, R., and Feriotto, G. (2008). Upstream stimulatory factors are involved in the P1 promoter directed transcription of the AbetaH-J-J locus. *BMC Mol. Biol.* 9:110. doi: 10.1186/1471-2199-9-110

Gillespie, J. R., Bush, J. R., Bell, G. I., Aubrey, L. A., Dupuis, H., Ferron, M., et al. (2013). GSK-3β function in bone regulates skeletal development, whole-body metabolism, and male life span. *Endocrinology* 154, 3702–3718. doi: 10.1210/en.2013-1155

Hou, G., Xu, B., Bi, Y., Wu, C., Ru, B., Sun, B., et al. (2018). Recent advances in research on aspartate β-hydroxylase (ASPH) in pancreatic cancer: a brief update. *Bosn. J. Basic Med. Sci.* 18, 297–304. doi: 10.17305/bjbms.2018.3539

Iwagami, Y., Huang, C.-K., Olsen, M. J., Thomas, J.-M., Jang, G., Kim, M., et al. (2016). Aspartate β-hydroxylase modulates cellular senescence through glycogen synthase kinase 3β in hepatocellular carcinoma. *Hepatology* 63, 1213–1226. doi: 10.1002/hep.28411

Koller, D. L., Ichikawa, S., Lai, D., Padgett, L. R., Doheny, K. F., Pugh, E., et al. (2010). Genome-Wide association study of bone mineral density in premenopausal european-american women and replication in african-american women. *J. Clin. Endocrinol. Metab.* 95, 1802–1809. doi: 10.1210/jc.2009-1903

Lavaissiere, L., Jia, S., Nishiyama, M., de la Monte, S., Stern, A. M., Wands, J. R., et al. (1996). Overexpression of human aspartyl(asparaginyl)beta-hydroxylase in hepatocellular carcinoma and cholangiocarcinoma. *J. Clin. Invest.* 98, 1313–1323. doi: 10.1172/JCI118918

Lee, K. W., Maeng, J.-S., Choi, J. Y., Lee, Y. R., Hwang, C. Y., Park, S. S., et al. (2012). Role of junctin protein interactions in cellular dynamics of calsequestrin polymer upon calcium perturbation. *J. Biol. Chem.* 287, 1679–1687. doi: 10.1074/jbc.M111.254045

Li, C., Chai, Y., Wang, L., Gao, B., Chen, H., Gao, P., et al. (2017). Programmed cell senescence in skeleton during late puberty. *Nat. Commun.* 8:1312. doi: 10.1038/s41467-017-01509-0

Li, H., Liu, P., Xu, S., Li, Y., Dekker, J. D., Li, B., et al. (2017). FOXP1 controls mesenchymal stem cell commitment and senescence during skeletal aging. *J. Clin. Invest.* 127, 1241–1253. doi: 10.1172/JCI89511

Li, C., Cheng, P., Liang, M., Chen, Y., Lu, Q., Wang, J., et al. (2015). MicroRNA-188 regulates age-related switch between osteoblast and adipocyte differentiation. *J. Clin. Invest.* 125, 1509–1522. doi: 10.1172/JCI77716

Li, C., Xiao, Y., Yang, M., Su, T., Sun, X., Guo, Q., et al. (2018). Long noncoding RNA Bmncr regulates mesenchymal stem cell fate during skeletal aging. *J. Clin. Invest.* 128, 5251–5266. doi: 10.1172/JCI99044

Lin, Q., Chen, X., Meng, F., Ogawa, K., Li, M., Song, R., et al. (2019). ASPH-notch axis guided exosomal delivery of prometastatic secretome renders breast cancer multi-organ metastasis. *Mol. Cancer* 18:156. doi: 10.1186/s12943-019-1077-0

Lin, S. P., Chiu, F. Y., Wang, Y., Yen, M. L., Kao, S. Y., and Hung, S. C. (2014). RB maintains quiescence and prevents premature senescence through upregulation of DNMT1 in mesenchymal stromal cells. *Stem Cell Rep.* 3, 975–986. doi: 10.1016/j.stemcr.2014.10.002

Mahmood, A., Harkness, L., Schrøder, H. D., Abdallah, B. M., and Kassem, M. (2010). Enhanced differentiation of human embryonic stem cells to mesenchymal progenitors by inhibition of TGF-β/activin/nodal signaling using SB-431542. *J. Bone Miner. Res.* 25, 1216–1233. doi: 10.1002/jbmr.34

Malaguarnera, R., and Belfiore, A. (2014). The emerging role of insulin and insulin-like growth factor signaling in cancer stem cells. *Front. Endocrinol.* 5:10. doi: 10.3389/fendo.2014.00010

Mantila Roosa, S. M., Liu, Y., and Turner, C. H. (2011). Gene expression patterns in bone following mechanical loading. *J. Bone Miner. Res.* 26, 100–112. doi: 10.1002/jbmr.193

Patel, N., Khan, A. O., Mansour, A., Mohamed, J. Y., Al-Assiri, A., Haddad, R., et al. (2014). Mutations in ASPH cause facial dysmorphism, lens dislocation, anterior-segment abnormalities, and spontaneous filtering blebs, or traboulsi syndrome. *Am. J. Hum. Genet.* 94, 755–759. doi: 10.1016/j.ajhg.2014.04.002

Peng, H., Guo, Q., Xiao, Y., Su, T., Jiang, T., Guo, L., et al. (2020a). ASPH regulates osteogenic differentiation and cellular senescence of BMSCs. *Figshare Dataset.* doi: 10.6084/m9.figshare.12436757.v1

Peng, H., Jenkins, Z. A., White, R., Connors, S., Hunter, M. F., Ronan, A., et al. (2020b). An activating variant in CTNNB1 is associated with a sclerosing bone dysplasia and adrenocortical neoplasia. *J. Clin. Endocrinol. Metab.* 105, 688–695. doi: 10.1210/clinem/dgaa034

Peng, H., Yang, M., Guo, Q., Su, T., Xiao, Y., and Xia, Z.-Y. (2019). Dendrobium officinale polysaccharides regulate age-related lineage commitment between osteogenic and adipogenic differentiation. *Cell Prolif.* 52, 1–10. doi: 10.1111/cpr.12624

Qadir, A., Liang, S., Wu, Z., Chen, Z., Hu, L., and Qian, A. (2020). Senile osteoporosis: the involvement of differentiation and senescence of bone marrow stromal cells. *Int. J. Mol. Sci.* 21:349. doi: 10.3390/ijms21010349

Ritchie, M. E., Phipson, B., Wu, D., Hu, Y., Law, C. W., Shi, W., et al. (2015). limma powers differential expression analyses for RNA-sequencing and microarray studies. *Nucleic Acids Res.* 43:e47. doi: 10.1093/nar/gkv007

Seo, Y.-H., Jung, H.-J., Shin, H.-T., Kim, Y.-M., Yim, H., Chung, H.-Y., et al. (2008). Enhanced glycogenesis is involved in cellular senescence via GSK3/GS modulation. *Aging Cell* 7, 894–907. doi: 10.1111/j.1474-9726.2008.00436.x

Shimoda, M., Tomimaru, Y., Charpentier, K. P., Safran, H., Carlson, R. I., and Wands, J. (2012). Tumor progression-related transmembrane protein aspartate-β-hydroxylase is a target for immunotherapy of hepatocellular carcinoma. *J. Hepatol.* 56, 1129–1135. doi: 10.1016/j.jhep.2011.12.016

Sturla, L.-M., Tong, M., Hebda, N., Gao, J., Thomas, J.-M., Olsen, M., et al. (2016). Aspartate-β-hydroxylase (ASPH): a potential therapeutic target in human malignant gliomas. *Heliyon* 2:e00203. doi: 10.1016/j.heliyon.2016.e00203

Tomimaru, Y., Koga, H., Yano, H., de la Monte, S., Wands, J. R., and Kim, M. (2013). Upregulation of T-cell factor-4 isoform-responsive target genes in hepatocellular carcinoma. *Liver Int.* 33, 1100–1112. doi: 10.1111/liv.12188

Treves, S., Feriotto, G., Moccagatta, L., Gambari, R., and Zorzato, F. (2000). Molecular cloning, expression, functional characterization, chromosomal localization, and gene structure of junctate, a novel integral calcium binding protein of Sarco(endo)plasmic reticulum membrane. *J. Biol. Chem.* 275, 39555–39568. doi: 10.1074/jbc.M005473200

Tu, X., Delgado-Calle, J., Condon, K. W., Maycas, M., Zhang, H., Carlesso, N., et al. (2015). Osteocytes mediate the anabolic actions of canonical Wnt/β-catenin signaling in bone. *Proc. Natl. Acad. Sci. U.S.A.* 112, E478–E486. doi: 10.1073/pnas.1409857112

Wu, D., and Pan, W. (2010). GSK3: a multifaceted kinase in Wnt signaling. *Trends Biochem. Sci.* 35, 161–168. doi: 10.1016/j.tibs.2009.10.002

Xiao, Y.-Z., Yang, M., Xiao, Y., Guo, Q., Huang, Y., Li, C.-J., et al. (2020). Reducing hypothalamic stem cell senescence protects against aging-associated physiological decline. *Cell Metab.* 31, 534–548.e5. doi: 10.1016/j.cmet.2020.01.002

Yang, M., Guo, Q., Peng, H., Xiao, Y.-Z., Xiao, Y., Huang, Y., et al. (2019). Krüppel-like factor 3 inhibition by mutated lncRNA Reg1cp results in human high bone mass syndrome. *J. Exp. Med.* 216, 1944–1964. doi: 10.1084/jem.20181554

Yang, M., Li, C.-J., Sun, X., Guo, Q., Xiao, Y., Su, T., et al. (2017). MiR-497 195 cluster regulates angiogenesis during coupling with osteogenesis by maintaining endothelial Notch and HIF-1α activity. *Nat. Commun.* 8, 1–11. doi: 10.1038/ncomms16003

Ye, X., Zerlanko, B., Kennedy, A., Banumathy, G., Zhang, R., and Adams, P. D. (2007). Downregulation of Wnt signaling is a trigger for formation of facultative heterochromatin and onset of cell senescence in primary human cells. *Mol. Cell* 27, 183–196. doi: 10.1016/j.molcel.2007.05.034

Yu, B., Huo, L., Liu, Y., Deng, P., Szymanski, J., Li, J., et al. (2018). PGC-1α controls skeletal stem cell fate and bone-fat balance in osteoporosis and skeletal aging by inducing TAZ. *Cell Stem Cell* 23, 193–209.e5. doi: 10.1016/j.stem.2018.06.009

Yu, G., Wang, L.-G., Han, Y., and He, Q.-Y. (2012). clusterProfiler: an R package for comparing biological themes among gene clusters. *Omi. A J. Integr. Biol.* 16, 284–287. doi: 10.1089/omi.2011.0118

Yuan, Q., Fan, G.-C., Dong, M., Altschafl, B., Diwan, A., Ren, X., et al. (2007). Sarcoplasmic reticulum calcium overloading in junctin deficiency enhances cardiac contractility but increases ventricular automaticity. *Circulation* 115, 300–309. doi: 10.1161/CIRCULATIONAHA.106.654699

Zhou, X., Hong, Y., Zhang, H., and Li, X. (2020). Mesenchymal stem cell senescence and rejuvenation: current status and challenges. *Front. Cell Dev. Biol.* 8:364. doi: 10.3389/fcell.2020.00364

Conflict of Interest: The authors declare that the research was conducted in the absence of any commercial or financial relationships that could be construed as a potential conflict of interest.

Copyright © 2020 Peng, Guo, Xiao, Su, Jiang, Guo and Wang. This is an open-access article distributed under the terms of the Creative Commons Attribution License (CC BY). The use, distribution or reproduction in other forums is permitted, provided the original author(s) and the copyright owner(s) are credited and that the original publication in this journal is cited, in accordance with accepted academic practice. No use, distribution or reproduction is permitted which does not comply with these terms.

frontiers in Cell and Developmental Biology

REVIEW
published: 10 September 2020
doi: 10.3389/fcell.2020.576110

Disorders of Calcium and Phosphorus Metabolism and the Proteomics/Metabolomics-Based Research

Meiheng Sun[1,2,3,4†], Xiaoqiu Wu[1,2,3†], Yuanyuan Yu[1,2,3], Luyao Wang[1,2,3], Duoli Xie[1,2], Zhenlin Zhang[5], Lin Chen[6], Aiping Lu[1,2,3,7,8], Ge Zhang[1,2,3] and Fangfei Li[1,2,3]**

[1] Law Sau Fai Institute for Advancing Translational Medicine in Bone and Joint Diseases, School of Chinese Medicine, Hong Kong Baptist University, Kowloon Tsai, Hong Kong, [2] Institute of Integrated Bioinfomedicine and Translational Science, School of Chinese Medicine, Hong Kong Baptist University, Kowloon Tsai, Hong Kong, [3] Institute of Precision Medicine and Innovative Drug Discovery, HKBU Institute for Research and Continuing Education, Shenzhen, China, [4] Jiangsu Key Laboratory of Xenotransplantation, School of Basic Medical Science, Nanjing Medical University, Nanjing, China, [5] Shanghai Clinical Research Center of Bone Disease, Department of Osteoporosis and Bone Disease, Shanghai Jiao Tong University Affiliated Sixth People's Hospital, Shanghai, China, [6] Department of Wound Repair and Rehabilitation Medicine, State Key Laboratory of Trauma, Burns and Combined Injury, Trauma Center, Research Institute of Surgery, Daping Hospital, Army Medical University, Chongqing, China, [7] Institute of Basic Research in Clinical Medicine, China Academy of Chinese Medical Sciences, Beijing, China, [8] Institute of Arthritis Research, Shanghai Academy of Chinese Medical Sciences, Shanghai, China

OPEN ACCESS

Edited by:
Changjun Li,
Central South University, China

Reviewed by:
Qiong Lu,
Central South University, China
Lori O'Brien,
The University of North Carolina at Chapel Hill, United States

***Correspondence:**
Ge Zhang
zhangge@hkbu.edu.hk
Fangfei Li
fangfeili@hkbu.edu.hk

†These authors share first authorship

Specialty section:
This article was submitted to Molecular Medicine, a section of the journal Frontiers in Cell and Developmental Biology

Received: 25 June 2020
Accepted: 20 August 2020
Published: 10 September 2020

Citation:
Sun M, Wu X, Yu Y, Wang L, Xie D, Zhang Z, Chen L, Lu A, Zhang G and Li F (2020) Disorders of Calcium and Phosphorus Metabolism and the Proteomics/Metabolomics-Based Research. Front. Cell Dev. Biol. 8:576110. doi: 10.3389/fcell.2020.576110

Since calcium and phosphorus play vital roles in a multitude of physiologic systems, disorders of calcium and phosphorus metabolism always lead to severe consequences such as skeletal-related and cardiovascular morbidity, or even life-threatening. Physiologically, the maintenance of calcium and phosphorus homeostasis is achieved via a variety of concerted actions of hormones such as parathyroid hormone (PTH), vitamin D, and fibroblast growth factor (FGF23), which could be regulated mainly at three organs, the intestine, kidney, and bone. Disruption of any organ or factor might lead to disorders of calcium and phosphorus metabolism. Currently, lacking of accurate diagnostic approaches and unknown molecular basis of pathophysiology will result in patients being unable to receive a precise diagnosis and personalized treatment timely. Therefore, it is urgent to identify early diagnostic biomarkers and develop therapeutic strategies. Fortunately, proteomics and metabolomics offer promising tools to discover novel indicators and further understanding of pathological mechanisms. Therefore, in this review, we will give a systematic introduction on PTH-1,25$(OH)_2$D-FGF23 axis in the disorders of calcium and phosphorus metabolism, diagnostic biomarkers identified, and potential altered metabolic pathways involved.

Keywords: disorders of calcium and phosphorus metabolism, PTH-1,25$(OH)_2$D-FGF23 axis, proteomics, metabolomics, biomarkers

INTRODUCTION

Disorders of calcium and phosphorus metabolism occur when calcium and phosphorus levels in the body deviate from basal condition, which could be classified into hypercalcemia, hypocalcemia, hyperphosphatemia, and hypophosphatemia. In the view of biological characteristics of this disease, changes in calcium, phosphate, alkaline phosphatase (ALP) and hormone levels such as parathyroid hormone (PTH), vitamin D, and fibroblast growth factor (FGF23) will eventually

occur, which could severely influence the life quality of patients and even indirectly shorten life expectancy by inducing growth retardation, osteomalacia, skeletal and dental anomalies, muscle spasms, nephrolithiasis, hypocalcemia convulsions, etc., since calcium and phosphorus are essential components in bone mineralization (Takeda et al., 2004; van Abel et al., 2005; Civitelli and Ziambaras, 2011). In addition, they could also play critical roles in a multitude of physiological processes. For instance, calcium is involved in hormones secretion, the blood-clotting, and the nerve excitement, while phosphorus is required for energy metabolism, cell signaling, and the stabilization of phospholipid content on cell membrane (Takeda et al., 2004; Lambers et al., 2006). Therefore, the regulation of calcium and phosphate ions within narrow limits is critical in maintaining normal physiological activity. It tightly relies on three target organs: intestine, kidney, and bone.

Accumulating evidence suggests that a variety of concerted actions of hormones, including parathyroid hormone (PTH), vitamin D, and fibroblast growth factor (FGF23) associate with nearly each target organ in maintaining the calcium and phosphorus homeostasis (Renkema et al., 2008; Peacock, 2010). On the one hand, when the ionized calcium concentration rises, the thyroid gland increases the secretion of calcitonin, a polypeptide hormone that could reduce the flow of PTH (Talmage et al., 1980; Austin and Heath, 1981). Therefore, the resulting down-regulated PTH inhibits removal of calcium from the bone, increases the loss of calcium in the urine and reduces intestinal calcium absorption through inhibiting the production of vitamin D active form $1,25(OH)_2D$, the chief mediator for calcium absorption at intestine (Khundmiri et al., 2016). Notably, PTH has a more significant effect on enhancing the excretion of phosphate ions in the urine. Since phosphates could combine with calcium ions to form insoluble salts, and then remove them from the serum exchangeable pool. As a consequence, reduced PTH corrects the high calcium concentration toward the average level. On the other hand, the reduction of ionized calcium concentration could be detected by the calcium-sensing receptor (CaSR) located in parathyroid cells, which will improve the rapid release of PTH accordingly. The up-regulated PTH and $1,25(OH)_2D$ corrects ionized calcium concentration through the same route. Also, FGF23 could decrease the phosphate levels through reducing the renal phosphate reabsorption and intestinal absorption by inhibiting the production of $1,25(OH)_2D$ (Shimada et al., 2004; Martin et al., 2012; Razali et al., 2015).

Based on the detailed understanding of calcium and phosphorus metabolism, we could better explore many genetic or non-hereditary factors that will cause disorders of calcium and phosphorus metabolism via impairing the functions of organs or concentrations of the related hormones, respectively. For example, hyperparathyroidism and hypoparathyroidism could induce the imbalance of calcium and phosphorus via influencing the levels of PTH. Vitamin D deficiency or hereditary factors resulting in changes of $1,25(OH)_2D$, PTH, and FGF23 levels could cause genetic or non-hereditary rickets. Additionally, malignancy is also a common cause for disorders of calcium and phosphorus metabolism via direct invasion of bone in Local Osteolytic Hypercalcemia (LOH), enhancing the flow of parathyroid hormone-related protein (PTHrP), which has the similar function with PTH, or increased synthesis of $1,25(OH)_2D$ in various lymphoid tumors (Guise et al., 1996). Acute or chronic kidney disease could disrupt the phosphorus balance through phosphate excretion failure and impair calcium metabolism through a loss of vitamin synthesis capacity. Although there are some clinical methods identified to diagnose the disorders of calcium and phosphorus metabolism, including blood tests, bone density scan, radiography, and bone biopsy, they are not universally applicable due to great trauma, high price, and low specificity (Nickolas and Jamal, 2015). Therefore, it is necessary to explore novel diagnostic biomarkers valuable to detect this disease.

For the in-depth understanding of the disorders of calcium and phosphorus metabolism, omics help a lot, especially proteomics and metabolomics. Proteomics generally refers to analysis of a wide range of proteins, which vary with time and different states the organism undergoes (Anderson and Anderson, 1998; Blackstock and Weir, 1999). While metabolomics, an emerging technology to study metabolites, the small molecule substrates, provides a direct readout of organism state (Nicholson, 2006). An essential focus of proteomics and metabolomics is the identification of novel biomarkers, which could detect disease quickly. For instance, immunoglobulin heavy constant alpha 2 was identified by Kang et al. (2012) as a potential breast cancer metastasis indicator for diagnosis, also, Nicholson et al. (2011) suggested the branched-chain amino acids such as isoleucine might be a valuable biomarker associated with Type 2 diabetes. Another focus is the elucidation of pathogenesis and the discovery of personalized and precision treatment relies on the molecular characteristics associated with a disease (Vaidyanathan, 2012). For example, Jamshidi et al. (2011) found nitric oxide synthase pathway altered significantly in a patient with Hereditary Hemorrhagic Telangiectasia (HHT) by metabolomics studies. Accordingly, the patient' health has been improved by treating with bevacizumab, an anti-VEGF drug that associated with nitric oxide production. We will also provide current examples of proteomics and metabolomics applications in the disorders of calcium and phosphorus metabolism at the end of this review.

CALCIUM METABOLISM

Calcium is the most abundant ion in the body, which plays a pivotal role in cell membrane function and intracellular signaling. More than 99% of total calcium is located in bone, acting structurally as supporting material in the form of calcium hydroxyapatite $[Ca_{10}(PO_4)_6(OH)_2]$ (Peacock, 2010). In contrast, less than 1% disperses in extracellular fluids, and intracellular calcium levels are extremely low. Calcium in extracellular fluids, intracellular fluids, and bone are balanced by the calcium absorbed in the diet at the small intestine. Calcium exchange between extracellular fluids and bone is an essential dynamic part of bone remodeling via a rapidly exchangeable pool. Urinary excretion is also involved in achieving the calcium homeostasis (Parfitt, 1976a,b; Kumar, 1991).

Calcium in extracellular fluids is present in three fractions. About 40% bound to proteins in the blood, primarily albumin, which could not be filterable by the kidney, whereas an additional 10% of calcium circulates as soluble components combing with various organic anions. The remaining, the most critical form of calcium in extracellular fluids exists as an active free ionized fraction, which determines the physiological effect of calcium (Bushinsky and Monk, 1998), because it interacts directly with cell membranes, with calcium channels, and with the calcium-sensing receptor (CaSR).

Calcium-sensing receptor is abundantly in the parathyroid cells, where it represents the molecular mechanism by which parathyroid cells detect a tiny reduction of ionized calcium concentration and modulate the rapid release of PTH accordingly (Brown et al., 1993; Brown et al., 1995; Hebert, 1996). Briefly, decreased plasma calcium concentration will inactivate CaSR, leading to increased flow of PTH, which has a direct effect on the renal calcium reabsorption and bone absorption through the interaction with the receptorPTH1R (van Abel et al., 2005; Peacock, 2010). Persistent changes in PTH concentration will also enhance intestinal calcium absorption through promoting 25-hydroxyvitamin D3-1α-hydroxylase activity to manufacture vitamin D active form $1,25(OH)_2D$, or calcitriol, the central mediator for calcium absorption at intestine (Burnett-Bowie et al., 2009). Physiological concentration of $1,25(OH)_2D$ could enter target cells to interact with its nuclear receptor VDR. The complex then heterodimerizes with the retinoic acid × receptor (RXR), which subsequently interacts with the vitamin D response element (VDRE) on the target gene to control its expression (Hendy et al., 2006; Christakos et al., 2016). Note that although the $1,25(OH)_2D$ manufacture in the kidney could be promoted by PTH, itself plays an inhibitory role in the synthesis and secretion of PTH, which might be explained by a feedback loop (Demay et al., 1992). Conversely, when the calcium levels rise, the thyroid gland will increase the flow of calcitonin, another polypeptide hormone, which could reduce the secretion of PTH, resulting in the opposite direction (Talmage et al., 1980; Austin and Heath, 1981).

Intestinal handling of calcium is tightly regulated by $1,25(OH)_2D$ and occurs in a passive route or an energy-dependent transcellular pathway (Pérez et al., 2008). The paracellular route depends on the concentration gradient of calcium along the tight junction in the intestinal epithelium. While, the active pathway for intestinal calcium absorption is subject to rather strict transcriptional control of $1,25(OH)_2D$, which represents a pivotal adaptive mechanism under calcium deficiency.

In the active pathway, the intestinal calcium channels TRPV (Transient receptor potential channels, and "V" for vanilloid), primarily TRPV6 but also TRPV5, are responsible for calcium entry (Hoenderop et al., 1999; Hoenderop et al., 2001). Once absorbed, the transcellular movement of calcium in the cytosol to the opposite side is completed under the help of calbindin, a vitamin D-dependent protein. Then the egress of calcium is mediated by the Na^+/Ca^+ exchanger (NCX1) through using energy provided by Ca-ATPase or Ca^+ pump (PMCA1b) (Pérez et al., 2008). Recently, a study discovered a critical role of a channel kinase, TRPM7 ("M" for melastatin), for mineral homeostasis. Mittermeier et al. (2019) showed that TRPM7 depletion resulted in a sharply decline in calcium concentration, suggesting in addition to the factors discussed above, TRPM7 is also necessary for the massive calcium absorption at the intestine, representing another path that need more in-depth exploration. Therefore, the whole process is carefully controlled by $1,25(OH)_2D$ via its properties of gene transcription regulation of the essential proteins including TRPVs, TRPM7, calbindin, PMCA1b, and NCX1 (Malloy et al., 1999; Fleet et al., 2002; Song et al., 2003). The paracellular route might also be mediated by $1,25(OH)_2D$ partly, but it remains unknown (Chirayath et al., 1998).

In the kidney, approximately 70% will be reabsorbed via a passive route driven by concentration gradient. In contrast, 25–27% will be reabsorbed in the thick ascending limb of the loop of Henle and in the distal convoluted tubule and collecting tubule by active pathway, mirroring the intestinal calcium absorption described previously (Hoenderop et al., 2005; van de Graaf et al., 2007; de Groot et al., 2008; Renkema et al., 2008). Note that PTH has a more significant influence on the urinary excretion of phosphate ions than calcium (Blaine et al., 2015). Since phosphates could combine with calcium ions to form insoluble complexes, more phosphate removal will ultimately raise the serum ionized calcium levels. It is worth mentioning that the kidney could also influence the plasma calcium concentration through processing vitamin D into calcitriol under the influence of high PTH levels.

Since bone contains 99% of the total calcium, it serves as an essential storage organ for calcium. It is a complicated and dynamic tissue mediated by bone-absorptive osteoclasts and bone-forming osteoblasts (Martin and Sims, 2005; Florencio-Silva et al., 2015). Studies have shown that calcium removal from bone is not only regulated by PTH and $1,25(OH)_2D$, under whose influence on the receptor activator of NF-κB ligand (RANKL) to promote maturation of osteoclasts (Boyle et al., 2003; Hamann and Lane, 2006; Bilezikian, 2008; Boyce and Xing, 2008; Blaine et al., 2015), but also could be directly affected by changes in local calcium concentration independent of the above factors, although the molecular basis is not well studied (Dvorak and Riccardi, 2004).

PHOSPHORUS METABOLISM

Phosphorus is critical for many normal biological activities, including muscle contraction, cell signaling, and stabilization of membranes. Similar to calcium, phosphorus is also found predominantly in mineralized bone in the form of hydroxyapatite, approximately 10% exists in soft tissues, and the remaining 2–3% circulates in the extracellular fluids, constituting a phosphate pool that could be rapid exchangeable. Plasma phosphorus balance is the result of phosphate uptake at intestine and reabsorption in the kidney. Both two approaches are regulated by sodium-dependent phosphate cotransporters (Na^+/Pi-cotransporters) belonging to the *SLC34* (NaPi-IIa, NaPi-IIc, and NaPi-IIb) or *SLC20* gene families of solute carriers,

although the latter has been proved to contributes less (Virkki et al., 2007; Biber et al., 2013; Wagner et al., 2014).

Intestinal phosphorus absorption occurs predominantly in the passive paracellular pathway through the luminal concentration of phosphorus. A small energy-dependent transcellular route occurs through NaPi-IIb across the apical brush-border membrane. When the phosphorus concentration decreases, 1α-hydroxylase in the kidney will be activated to manufacture $1,25(OH)_2D$ (Hughes et al., 1975), which could increase the expression levels of NaPi-IIb, resulting in enhanced phosphorus absorption at intestine (Katai et al., 1999; Xu et al., 2002).

Phosphate reabsorption in the kidney is mediated primarily by NaPi-IIa channels, while NaPi-IIc play a lesser role (Beck et al., 1998). There is a variety of hormones that influence the renal handling of phosphorus through NaPi-II cotransporters. The most well studied is PTH, which could reduce protein trafficking of the NaPi-II cotransporters to the membrane via endocytosis (Traebert et al., 2000a,b; Yang et al., 2004). Fibroblast growth factor 23 (FGF23), another critical hormone that reduces the phosphorus levels, also has been shown to decrease NaPi-II cotransporters expression in the proximal tubule (Schiavi, 2006; Razzaque and Lanske, 2007; Farrow et al., 2009). Also, the phosphorus-reducing effect of FGF23 could also be achieved via its inhibitory role on $1,25(OH)_2D$ (Shimada et al., 2004; Martin et al., 2012; Razali et al., 2015). It is noteworthy that increased $1,25(OH)_2D$ concentration appears to promote FGF23 release, suggesting that the inhibitory role of FGF23 on $1,25(OH)_2D$ is likely part of a negative feedback loop on phosphorus balance (Kolek et al., 2005; Masuyama et al., 2006). Intriguingly, FGF23 could also inhibit PTH in an alpha-klotho (KL)-dependent manner (Ben-Dov et al., 2007). However, PTH appears to stimulate the synthesis of FGF23 via mechanisms involving PKA/Wnt pathway (Lavi-Moshayoff et al., 2010).

Under average conditions, adults have a net skeletal phosphorus balance close to zero through adjusting the amount of phosphate absorption and urinary excretion. Several essential factors, including phosphatonins, the phosphate-regulating genes associated with endopeptidase (PHEX), etc., that could contribute to the changes in levels of FGF23, which is involved in vitamin D metabolism, also have been identified as indirect factors participating in phosphorus metabolism in bone (Quarles, 2003). However, the comprehensive understanding of phosphorus metabolism in bone still remains elusive, which needs further investigation.

In conclusion, maintenance of calcium and phosphate ions within narrow range tightly relies on three organs: intestine, kidney, and bone. And the organs' functions are principally regulated via several hormones, including PTH, vitamin D, and FGF23. Among them, PTH maintains calcium and phosphorus homeostasis by (1) enhancing the intestinal calcium and phosphate absorption through promoting the manufacture of $1,25(OH)_2D$; (2) increasing phosphorus excretion through its internalization effect on NaPi-II cotransporters and interaction with PTH1R in the kidney; (3) increasing bone absorption. The most important function of vitamin D is to promote the absorption of calcium and phosphorus at intestine. In addition, it could also act on osteoclasts to release calcium ions by promoting RANKL system. FGF23 could reduce phosphorus levels by inhibitory role on NaPi-II cotransporters in the kidney and promote the phosphorus uptake into the bone indirectly. Also, the identification of the vital TRPV, TRPM7, VDR, NaPi cotransporters, and CaSR all have further advanced our understanding of calcium and phosphorus homeostasis and even the disorders of mineral metabolism (shown in **Figure 1**).

DISORDERS OF CALCIUM AND PHOSPHORUS METABOLISM

Hypercalcemia

Hypercalcemia occurs in approximately 1 in 500 among the general adult population (Waters, 2009). Malignancy and hyperparathyroidism are the two most common causes (Bilezikian and Silverberg, 2004; Stewart, 2005). Up to 20–30% of cancer patients are reported to have symptoms of hypercalcemia due to (1) direct invasion of bone in Local Osteolytic Hypercalcemia (LOH); (2) Humoral hyperkalemia of malignancy (HHM); Or (3) increased synthesis of $1,25(OH)_2D$ (Insogna and Broadus, 1987). In patients with LOH, the hypercalcemia results from a variety of osteoclast activating factors, which are responsible for the significant increase in osteoclast absorption (Roodman, 2004), while HHM is caused by considerable flow of parathyroid hormone-related protein (PTHrP) derived from malignant cells (Guise et al., 1996). Although PTHrP bears similarity to PTH only in the initial eight amino acids, its capacity to bind to the PTH receptor is basically the same, which promotes bone absorption and increases renal reabsorption of calcium (Stewart et al., 1982; Burtis et al., 1988). Various lymphoid tumors, the most well-known Hodgkin's lymphoma, have been shown to promote intestinal absorption and renal reabsorption of calcium through secreting vast amounts of $1,25(OH)_2D$ (Seymour et al., 1994).

Hyperparathyroidism could also be classified into three categories: (1) primary hyperparathyroidism, which is primarily caused by adenomas of parathyroid glands; (2) secondary hyperparathyroidism, which is caused by resultant hyperplasia of parathyroid glands in response to hypocalcemia; (3) tertiary hyperparathyroidism, a term used to describe progressive stage of secondary hyperparathyroidism along with unresponsive flow of PTH. Patients with hyperparathyroidism will show increased synthesis of $1,25(OH)_2D$ as a subsequent result of the elevation of PTH levels. Therefore, the promotion of renal reabsorption of calcium by PTH and increased osteoclast and intestinal calcium absorption by $1,25(OH)_2D$ lead to the occurrence of hypercalcemia.

Also, patients with Familial hypocalciuric hypercalcemia (FHH), a rare inherited disease with mutation in CaSR, could also result in hypercalcemia because the inactive CaSR in the parathyroid gland will lead to a slight elevation of PTH, similar to the hyperparathyroidism discussed above (Carroll and Schade, 2003). Furthermore, sarcoidosis, a multisystem granulomatous disorder, the cause of which is still not elucidated, could also result in hypercalcemia because of the elevated levels of $1,25(OH)_2D$ (Iannuzzi et al., 2007).

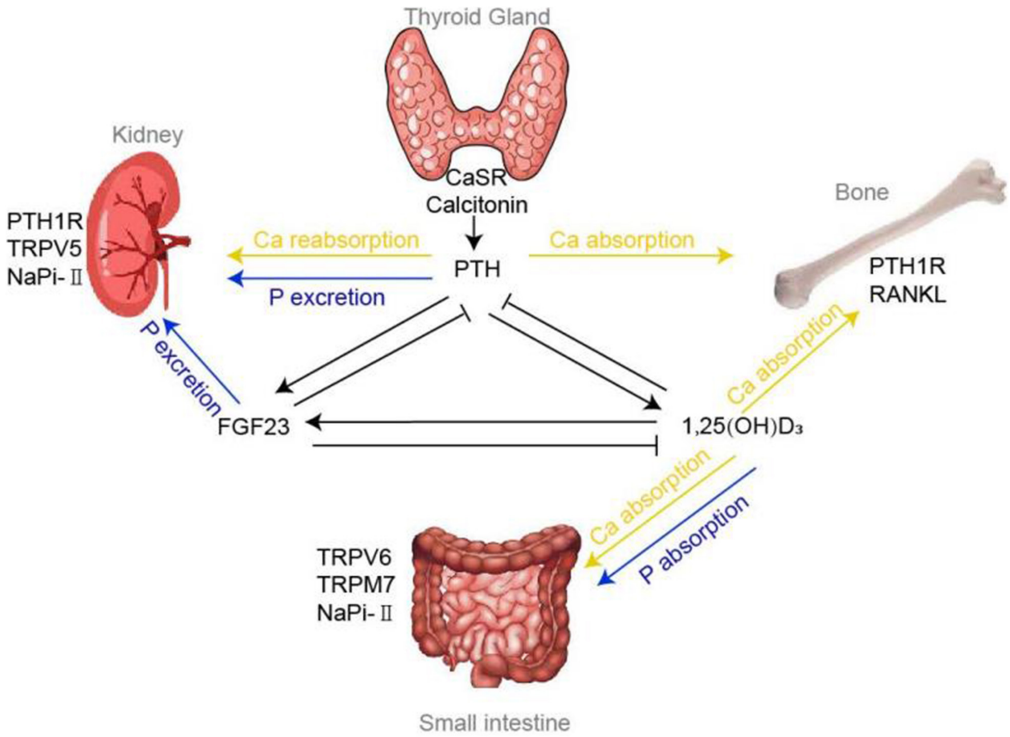


FIGURE 1 | Calcium and phosphorus homeostasis. Regulation of calcium and phosphorus homeostasis tightly relies on a variety of concerted actions of three target organs: intestine, kidney and bone, whose functions are principally regulated by a panel of hormones, including PTH, vitamin D, FGF23 and various factors. Tiny changes in calcium could be sensed by CaSR and Calcitonin located in the thyroid gland, thereby modulating the flow of PTH accordingly. Under the influence of effectors of TRPVs, NaPi-II cotransporters, PTH1R, etc., PTH mediates the absorption and reabsorption of calcium and phosphorus in the bones and kidneys. $1,25(OH)_2D$, the chief mediator for calcium and phosphorus absorption at intestine, could also regulate the bone calcium absorption via RANKL system. FGF23, another critical hormone that promote phosphorus urinary excretion, has been shown to decrease NaPi-II cotransporters expression in the proximal tubule.

Hypocalcemia

Also, the common causes of hypocalcemia are PTH related, or vitamin D described (Zivin et al., 2001). Contrary to hyperparathyroidism, hypoparathyroidism, which refers to the impaired secretion of PTH due to the irreversible parathyroidectomy, radiation damage, and congenital disabilities, is the leading cause of chronic hypocalcemia. A similar disease term called pseudohypoparathyroidism (PsHP), showing resistant to PTH, is also characterized by hypocalcemia. In addition, the lack of vitamin D caused by UV exposure deficiency or kidney dysfunction, could also result in hypocalcemia (Cooper and Gittoes, 2008).

Hyperphosphatemia

Because the organs that regulate phosphorus balance are principally the intestine, kidney, and some other tissues, hyperphosphatemia will occur when intestinal absorption rises, renal excretion in acute or chronic kidney disease reduces, or tissue release of phosphorus to extracellular fluids enhances. It is noteworthy that in addition to the hypocalcemia resulting from kidney disease because of impaired vitamin D synthesis, hyperphosphatemia could also occur in chronic kidney disease (CKD) caused by the phosphorus excretion failure. Since phosphates could combine with calcium ions to form insoluble complexes, hyperphosphatemia-induced calcium deposits in the soft tissues will ultimately lead to abnormalities in bone morphology such as bone mineralization and calcification of blood vessels (Fukagawa et al., 2017). At the 2006 Spanish Mineral Metabolism and Bone Disease Conference, the Kidney Disease Improving Global Outcomes (KDIGO) officially named it as chronic kidney disease-mineral and bone disorder (CKD-MBD), while the hyperphosphatemia is an essential biochemical feature (Khwaja, 2010; Bover et al., 2016; Ketteler et al., 2017). Hypoparathyroidism-related hyperphosphatemia refers to the low levels of PTH, which typically promotes phosphate excretion. Therefore, PTH insufficiency could result in more phosphate remaining in the blood. Also, increased tissue release of phosphorus could also occur in tumor lysis syndrome, rhabdomyolysis, hemolysis, hyperthermia, acute leukemia, etc. (Voelkl et al., 2019).

Hypophosphatemia

Similar to the factors causing hyperphosphatemia, hypophosphatemia will occur when there is inadequate phosphorus intake at intestine or excessive renal wasting resulting from rickets or Fanconi's syndrome.

Rickets is a metabolic bone disease, which refers to inadequate mineralization of growing bones caused by abnormal metabolism

of calcium, phosphorus, and/or vitamin D. It could be divided into nutritional rickets and hereditary rickets due to different pathogenesis.

Hereditary rickets could be classified into two categories due to different types of gene variations: (1) vitamin D-dependent rickets (Miller, 2017); and (2) hereditary hypophosphatemic rickets (HP) (Beck-Nielsen et al., 2012). Moreover, vitamin D-dependent rickets might be further classified into type 1A (VDDR1A) and type 1B (VDDR1B) associated with vitamin D synthesis, and type 2A (VDDR2A) and type 2B (VDDR2B) pertaining to vitamin D receptor activity in more detail. Therefore, its typical biochemical characteristics are hypocalcemia and hypophosphatemia caused by vitamin D deficiency. VDDR1A is due to the deletion of 1-alpha hydroxylase enzyme caused by mutations in the *CPY27B1* gene. While VDDR1B results from the deletion of first-step enzyme, 25-hydroxylase, caused by the mutations in the *CYP2R1* gene. Due to variations in the vitamin D receptor (*VDR*) gene, VDDR2A shows resistance to $1,25(OH)_2D$. However, unlike VDDR2A, the function of VDR is normal in VDDR2B, which prevents the binding of VDR-RXR heterodimer to VDR element (VDRE), resulting in abnormal vitamin D transcriptional function (Fraser et al., 1973).

Hereditary hypophosphatemic rickets (HR) is a rare group of renal phosphate wasting disorders. Hypophosphatemia and average calcium concentration are their typical biochemical characteristics. It is a type of hereditary rickets caused by the variations in phosphoproteins or cotransporters, which are necessary for renal phosphate reabsorption (Guven et al., 2017). So far, a panel of genetic causes has been identified. Some genetic mutations lead to increased serum FGF23 concentration (FGF23-dependent HR), while others influence phosphate transporters without affecting serum FGF23 levels (FGF23-independent HR). Although these two types could be distinguished by FGF23 concentration easily, the diseases within the group need to be differentiated by further molecular testing.

X-linked dominant HR (XLDHR) caused by *PHEX* gene mutation is the most common type of FGF23-dependent HR. *PHEX* gene product does not seem to regulate FGF23 clearance directly, but to encode a membrane endopeptidase, which could promote the removal of FGF23 (Rowe, 2012). Therefore, *PHEX* mutation could result in elevated FGF23, which is unable to degrade. High levels of FGF23 could also occur in Autosomal Dominant Hypophosphatemic Rickets (ADHR), which is caused by the inactive mutation in the proteolytic cleavage domain (RXXR cleavage motif) in FGF23, therefore the variation renders FGF23 resistant to proteolytic cleavage (Shimada et al., 2002). Also, increasing serum FGF23 concentration could also result from the Autosomal Recessive Hypophosphatemic Rickets (ARHR), including 1) Autosomal Recessive Hypophosphatemic Rickets Type 1 (ARHR1), which is caused by inactive mutation in the dentin matrix acidic phosphoprotein (DMP1) gene acting on the inhibition of FGF23 expression, and 2) Autosomal Recessive Hypophosphatemic Rickets Type 2 (ARHR2), which is caused by ectonucleotide pyrophosphatase/phosphodiesterase 1 (ENPP1) inactive mutation (Lorenz-Depiereux et al., 2006). Furthermore, a rare disease termed Hypophosphatemic Rickets with Hyperparathyroidism caused by a balanced translocation adjacent to the KL gene, whose product is FGF23's necessary cofactor alpha-Klotho, could lead to an increase of circulating alpha-Klotho. As a result, since alpha-Klotho could stimulate the expression of FGF23, it might explain the up-regulation of FGF23 (Brownstein et al., 2008). Other rare genetic diseases involving osteoglophonic dysplasia, McCune–Albright syndrome, Raine syndrome, opsismodysplasia, etc., could also cause hypophosphatemia through influencing FGF23 concentration (Acar et al., 2017).

In addition to changes in FGF23 levels, cotransporters and PTH receptor variations could also induce hypophosphatemia via disrupted phosphorus reabsorption metabolism. Hereditary Hypophosphatemic Rickets with Hypercalciuria (HHRH) and Hypophosphatemic Rickets with Nephrolithiasis and Osteoporosis Type 1 (NPHLOP1), which are caused by the inactive mutations in *SLC34A3* (also known as NaPi-IIc) and *SLC34A1* (also known as NaPi-IIa) respectively, could result in hypophosphatemia through the abnormal renal reabsorption process (Tencza et al., 2009). Hypophosphatemic Rickets with Nephrolithiasis and Osteoporosis Type 2 (NPHLOP2), caused by an inactive mutation of *SLC9A3R1* (also known as NHERF1), which encodes an adaptor protein that regulates several G protein-coupled receptors including PTH1R. Moreover, Dent Disease is the result of mutations in the *CLCN5* or *OCRL* gene, which is characterized by renal dysfunction, thereby eventually resulting in calcium and phosphorus disorders (Devuyst and Thakker, 2010).

In addition to hereditary rickets, nutritional rickets is also a serious global public health problem, which refers to abnormal bone mineralization caused by vitamin D deficiency. Furthermore, both genetic and acquired Fanconi's syndrome could also lead to renal phosphate wasting in urine due to defects in the proximal tubule (Izzedine et al., 2003). The classification of disorders of calcium and phosphorus metabolism is summarized in **Table 1**.

APPLICATION OF PROTEOMICS/METABOLOMICS IN DISORDERS OF CALCIUM AND PHOSPHORUS METABOLISM

Proteomics and Metabolomics/Metabonomics are essential branches of system biology. Although all proteins are based on DNA, post translational modifications render gene analysis alone is impossible to define the abundance of proteins. The proteome consists of all proteins present in particular cell types or tissues, while the metabolome consists of small molecules known as metabolites (Blackstock and Weir, 1999; Hollywood et al., 2006). They are technologies that comprehensively characterize the protein and metabolic levels of cells or organisms to study the roles of proteins and the metabolic profiles in biological and pathological systems (Nicholson et al., 1999). Therefore, they are promising approaches to identify biomarkers or unmask perturbations and signal pathways associated with

TABLE 1 | Classification of disorders of calcium and phosphorus metabolism.

Type	Causes
Hypercalcemia	Malignancy Hyperparathyroidism Familial hypocalciuric hypercalcemia (FHH) Sarcoidosis, etc.
Hypocalcemia	Hypoparathyroidism Pseudohypoparathyroidism (PsHP) Vitamin D deficiency
Hyperphosphatemia	Kidney disease Hypoparathyroidism Tumor lysis syndrome Rhabdomyolysis Hemolysis Hyperthermia Acute leukemia, etc.
Hypophosphatemia	Hereditary rickets: Vitamin D-dependent rickets: (VDDR1A, VDDR1B, VDDR2A, VDDR2B). Hereditary hypophosphatemic rickets: (XLDHR, ADHR, ARHR, Hypophosphatemic Rickets with Hyperparathyroidism, McCune-Albright syndrome, Raine syndrome, Opsismodysplasia, HHRH, NPHLOP1, NPHLOP2, Dent Disease) Nutritional rickets Fanconi's syndrome

disease through available biological samples, such as urine (Want et al., 2010; Cheng et al., 2012), plasma, etc. (Qiu et al., 2009). Also, a rapidly growing body of proteomics and metabolomics related work has promoted the development of precision medicine and has been widely concerned (Suhre et al., 2011). To illustrate the current status of the applications of proteomics and metabolomics in disorders of calcium and phosphorus metabolism, we discuss here the advances that used these technologies to investigate novel biomarkers and disturbed pathways related with this disease.

PROTEOMICS/METABOLOMICS STUDIES ON PRIMARY HYPERPARATHYROIDISM

Primary hyperparathyroidism (PHPT) is characterized by hypercalcemia and abnormal excessive flow of PTH. To unveil the pathophysiology of PHPT, molecular details about parathyroid hyperplasia and adenoma, two similar causes contributing to the PHPT, must be revealed. Therefore, Akpinar et al. (2017) performed a study to differentiate these two diseases through comparative proteomics. Forty novel dysregulated proteins of interest were identified, of which 14 were up-regulated in hyperplasia and 26 were overexpressed in adenoma. It is worth mentioning that most of the up-regulated proteins in hyperplasia identified are mitochondrial proteins, involving cytochrome b-c1 complex subunit 1, enoyl-CoA hydratase, 60 kDa heat shock protein, etc., suggesting the importance of abnormal mitochondrial activity in the pathogenesis of PHPT. Although this research could not create a biomarker panel, the changes in mitochondrial proteins expression yield important direction for future studies to differentiate parathyroid hyperplasia and adenoma, which remained a significant challenge to dissolve (Akpinar et al., 2017). Although parathyroid adenomas account for approximately 85% cases of PHPT (Carling, 2001), its pathogenesis is only partially understood. Varshney et al. (2014) showed that 15 differentially expressed proteins involving in diverse cellular functions were found between adenomatous and healthy parathyroid tissues through proteomics. Although functional categorization of dysregulated proteins did not focus on a certain signaling, the services of the identified proteins associate with a massive number of pathways, including the regulation of programed cell death, transcription, and signal transduction, etc. Among them, ATP synthase subunit d protein is also reported in the research by Akpinar et al. (2017). However, majority of the identified proteins are different with the earlier study by Giusti et al. (2011) which might be explained by the different disease severity and ethnicity (Asian Indian vs. Caucasian), that needs further validation. Therefore, the characterized proteins might provide new directions for the in-depth exploration of molecular details of the disease and novel therapeutic options that target at the differentially expressed proteins (Varshney et al., 2014).

On the one hand, evidence shows that parathyroid adenomas might consist of chief cells, oxyphilic cells, or a mixture of both cells (Williams, 1974). To differentiate different cell types within parathyroid adenomas, Lu et al. (2018) identified a series of proteins that altered significantly between chief and oxyphilic cell adenomas, and p53 pathway might be involved through proteomics analysis, since the higher expression of LMO3 and S100B in oxyphilic cells, which could inhibit the transcription of the *TP53* gene. Intriguingly, lower expression of nuclear receptor TR4 was reported in oxyphilic cells compared to chief cells. Evidence has shown that mitochondria accumulation was observed in TR4–/– mice, implicating decreased TR4 level might contribute to the oxyphilic cells transformation and formation, which is characterized by high mitochondrial content. In addition, compared to cytoplasm and nuclei subcellular location of TR4 in normal parathyroid, it mainly localized in the nuclei of adenomas, implying different roles of TR4 in adenomas that remains elusive, which needs further investigation. On the other hand, PHPT could also be classified into two different groups based on their relative responsiveness to ambient calcium. Koh et al. (2018) identified a set of candidate genes expressed differently between the calcium-sensitive and calcium-resistant parathyroid tumors by RNA seq and proteomics analysis. Notably, based on the results of studies by Akpinar et al. (2017) elevated expression of mitochondrial genes such as *COX7B*, *CYCS*, and *APT5G3* were observed in calcium-resistant group, providing a potential relationship between calcium-resistant (mitochondria-rich) and hyperplasia, which needs additional research to address. In calcium-sensitive group, ECM and trafficking genes, *TNXB* and *LIN7A*, which are necessary for CaSR-mediated signaling, showed significant high levels. Hence, the results suggest that the different PHPT clinical presentation, provenance and outcome might be caused by different molecular basis, which remains unknown (Koh et al., 2018).

A single gland disease (SGD), which is caused by a single parathyroid adenoma, and multiglandular disease (MGD), which is recognized with multiple adenomas or multiglandular hyperplasia, both could result in PHPT; however, there are no biomarkers available to differentiate these two types. Therefore, Battini et al. (2016) aimed to compare the tissue metabolome profiles between SGD and MGD in PHPT to investigate the difference, and eventually identified a multitude of metabolites which could accurately predict SGD from MGD. For instance, compared with MGD, elevated levels of succinate and fumarate were observed in SGD, which involved in the tricarboxylic acid cycle, while a higher expression of glutamate, GSH, and ascorbate serving as antioxidants in MGD. However, due to the limited samples, data should be validated in further research (Battini et al., 2016).

Normocalcemic primary hyperparathyroidism (NC-PHPT), the first subclinical phase of PHPT, is a new clinical stage characterized by average serum calcium concentration and elevated PTH levels. In contrast, the second stage of termed hypercalcemic primary hyperparathyroidism (HC-PHPT) is typically characterized by a hypercalcemic phase. Notably, emerging evidence has shown that PHPT is typically accompanied by cardiovascular morbidity (Lundgren et al., 2001). However, it is unclear whether NC-PHPT and HC-PHPT share the same risk factors associated with cardiovascular events. Recently, Yener Ozturk et al. (2016) suggested that patients with NC-PHPT have similar metabolome profiles compared with the HC-PHPT group. Therefore, due to the unknown molecular mechanism, NC-PHPT should be further explored in the future for valuable early diagnosis (Yener Ozturk et al., 2016). The above differentially expressed proteins, metabolites, and involving metabolic pathways are shown in **Table 2**.

PROTEOMICS/METABOLOMICS STUDIES ON CKD-MBD

Based on the status of bone turnover, CKD-MBD could be classified into two groups: (1) High Turnover Bone Disease (HTBD), which is followed by secondary hyperparathyroidism; and (2) Low Turnover Bone Disease (LTBD), which is associated with osteoporosis. In addition, based on evidence suggesting that adipose tissue calcification might originate from the differentiation of stem cells, the exploration of stem cells extracted from adipose tissue of different bone status might provide important clues for the soft tissue calcification mechanism. Recently, a proteomic study performed by Kasap et al. (2015) identified a total of 32 regulated proteins in stem cells and analyzed the potential relationship between different proteins and bone turnover status, suggesting their essential roles in distinguishing HTBD with LTBD. For example, two structural proteins, F-acting-capping protein and keratin, and type 1 cytoskeleton 10, attract our attention due to their significant abundances in HTBD compared to LTBD, indicating the novel roles in determining the bone turnover status. Although the exact functions of them in stem cells are poorly understood, the data offers important source for further discoveries (Kasap et al., 2015).

Although CKD-MBD patients have a considerable mortality and disability rate, the current biomedical predicators are lagging and not sensitive enough. Therefore, according to the guidelines that clinicians should focus more on serum biochemical indicators for diagnosis, which is given by the Kidney Disease Improving Global Outcomes (KDIGO), it is crucial to identify novel early diagnostic biomarkers valuable. Recently, Wu et al. (2015) have identified a set of metabolic biomarkers for CKD-MBD by employing metabolomics. After validating the potential biomarkers, a total of 32 potential biomarkers were identified (Wu et al., 2015). For example, elevated dopamine glucuronide is a promising biomarker for onset of CKD-MBD because dopamine level is positively correlated with phosphate concentration, the high level of which is a typical characteristic of CKD-MBD. In addition, up-regulated glycylprolylhydroxyproline and glutaminyl-hydroxyproline are metabolic products of hydroxyproline, which could act as a bone biomarker that also may be a potential biomarker for CKD-MBD. However, the substrates of TCA cycle intermediates, glutamyl-glutamate and *N*-acetylaspartylglutamic acid, could not

TABLE 2 | Proteomics/Metabolomics studies on PHPT.

Proteins/metabolites	Comparision	Biological process	References
Nucleophosmin, peroxiredoxin-2, Bcl-2-like protein-10, DNAJC2 protein (Hsp40), ATP synthase subunit day, aconitase 2, elongation factor Tu (p43), phosphatidylinositol transfer protein, MED26 protein (isoform-2), fibronectin type III, vacuole membrane protein 1 (HSPC292), prohibitin, nuclear receptor binding factor 2, zinc finger protein 394, Ras-related protein Rab-7b	Parathyroid adenomas vs. normal	Regulation of programed cell death cell organization and transcription, miscellaneous proteins, Ras protein signal transduction	Varshney et al., 2014
Nuclear receptor subfamily 2 group C member 2 (TR4), LIM domain only protein 3 (LMO3), calcium-binding protein B (S100B)	Oxyphilic cell vs. chief cell in parathyroid adenoma	p53 pathway	Lu et al., 2018
Ubiquinone oxidoreductase core subunit V1, cytochrome C oxidase subunit 7B, cytochrome C, ATP synthase, lin-7 homolog A, tenascin, etc.	Calcium-sensitive vs. calcium-resistant parathyroid tumors	Redox metabolism, GPCR trafficking, GPCR signal transduction, PI3 kinase signaling	Koh et al., 2018
Phosphorylcholine, choline, glycerophosphocholine, fumarate, succinate, lactate, glucose, glutamine, ascorbate, etc.	Single gland disease vs. multiglandular disease in PHPT	Tricarboxylic acid cycle	Battini et al., 2016
60 kDa heat shock protein, ubiquitin carboxyl-termial hydrolase, lamin-A/C, heterogeneous nuclear ribonucleo-proteins A2/B1, etc.	Parathyroid hyperplasia vs. adenoma	Energy metabolism, redox metabolism, protein folding etc.	Akpinar et al., 2017

be valuable biomarkers because they are involved in a variety of diseases and not specific. Furthermore, the results suggest that metabolic pathway patterns also shift, involving routes of protein synthesis, amino acid metabolism, and steroid hormone metabolism in addition to the established metabolic pathways associated with phosphorus, calcium, PTH, and vitamin D (Levin et al., 2007), with evident promise for better understanding of the pathogenesis in CKD-MBD.

Another similar article performed by Shen et al. (2019) also found various biomarkers correlated to PTH in SHPT. However, in contrast to the above study, which mainly focused on the altered metabolites in CKD-MBD, this study primarily focused on those correlated with PTH. The results indicated that five differential metabolites, allyl isothiocyanate, L-phenylalanine, D-Aspartic acid, indoleacetaldehyde, and D-galactose correlated with PTH could serve as potential biomarkers to diagnose SHPT with good sensitivity and accuracy (Shen et al., 2019). Among them, L-phenylalanine is an activator of CaSR, which shows inhibitory role on PTH secretion, might be an explanation for its diagnostic value as a biomarker for SHPT (Gensure et al., 2003). Additionally, a proteomics study also identified a multitude of mediators of inflammation (IL-6 and TNF-α) and mineral and bone disorders biomarkers (OPG, OPN, OCN, FGF23, and Fetuin-A) as a multiplexed panel to improve early CKD diagnosis. OPG, OPN, and FGF23 could also reflect vascular severity, the leading complication of CKD. Therefore, these studies provide a novel tool for clinical evaluation for CKD staging and therapeutic response (Mihai et al., 2016).

Evidence has shown that the proliferation of oxyphil cell might involve in SHPT development, however, the mechanism is not clarified (Sumida et al., 2011). Therefore, to identify the critical regulatory factors of oxyphil cell proliferation might be helpful to unravel the pathogenesis and therapeutic target of SHPT. Recently, Li et al. (2018) aimed to identify proteins expressed differently in oxyphil compared with chief cells, and eventually found that mitochondrial proteins, consistent with the above results discussed, and metabolisms involving protein synthesis and cell cycle regulation were significantly altered in oxyphil cell. Generally, active vitamin D is used as treatment option but sometime resistance occurs. In this study, down-regulated vitamin D binding protein (DBP) might be a potential explanation in the calcitriol treatment resistance by impairing transportation of vitamin D. The critical MIF-CUL1 axis that associated with ubiquitin mediated proteolysis might participate in the proliferation of oxyphil cell due to their significantly altered expression. The results shed light on mitochondria dysfunction in proliferation mechanisms of oxyphil cells, which accelerates the SHPT progression (Li et al., 2018).

Generally, hyperphosphatemia is a well-known promoter of cardiovascular dysfunction, a severe complication of CKD, which is the leading cause of poor prognosis (Block et al., 2004). Therefore, a metabolomics study aiming to define the molecular basis underlying hyperphosphatemia-induced vascular endothelial dysfunction performed by Zhou et al. (2016) identified 36 metabolites, which were significantly altered in human umbilical vein endothelial cells (HUVECs), involving vast metabolic pathways such as urea cycle, energy metabolism, etc. Among them, ornithine increased significantly. Further study demonstrated that the up-regulation of ornithine might result from the elevated arginase 2, which mediates the hydrolysis of arginine to form ornithine. Therefore, the results point that arginase 2 might serve as a therapeutic target for cardiovascular abnormalities caused by hyperphosphatemia (Zhou et al., 2016). However, further clinical samples analysis from patients to understand the comprehensive changes is necessary due to the limitations of cell models. Proteins and metabolites that expressed differently, and related pathways defined above are summarized in **Table 3**.

PROTEOMICS/METABOLOMICS STUDIES ON NUTRITIONAL RICKETS

For the diagnosis of nutritional rickets, although there are several serum biochemical tests, such as 25(OH)D, calcium, phosphate,

TABLE 3 | Proteomics/Metabolomics studies on CKD-MBD.

Protein/metabolite	Comparision	Biological process	References
N-(1-Deoxy-1-fructosyl) tryptophan, *N*-acetylaspartylglutamic acid, glycylprolylhydroxyproline, (R)-pantothenic acid 4′-*O*-b-D-glucoside, aminohippuric acid, etc.	CKD-MBD vs. normal	Protein synthesis and amino acid metabolism, energy metabolism, and steroid hormone metabolism	Wu et al., 2015
Allyl isothiocyanate, L-phenylalanine, D-Aspartic acid, indoleacetaldehyde, and D-galactose corrected with PTH	SHPT vs. normal	Amino acid metabolism	Shen et al., 2019
Cullin-1, 5′-AMP-activiated protein kinase subunit beta-2, Carnitine palmitoyltransferase 1B, protein, E3 ubiquitin-protein ligase CBL, etc.	Oxyphil cell modules vs. Chief cell modules	Wnt signaling, TGF-β, ubiquitin mediated proteolysis, cell cycle regulation, protein synthesis	Li et al., 2018
Total 36 metabolites, especially ornithine	hyperphosphatemia- associated cardiovascular vs. normal	Urea cycle, arginine-, proline-, metabolism etc.	Zhou et al., 2016
IL-6, TNF-α, OPG,OPN,OCN,FGF-23, Fetuin-A	CKD stage vs. normal	RANK/RANKL/OPF signaling pathway, energy metabolism	Mihai et al., 2016
Vimentin, F-acting-capping protein subunit beta-alfa-1, WD repeat-containing protein 1, prelamin A/C, DnaJ homolog subfamily B member 11, 78kDa glucose-regulated protein, endoplasmin, stress-70 protein, protein disulfide-isomerase A, peroxiredoxin, etc.	High Turnover Bone disease vs. Low Turnover Bone Disease	Redox metabolism, protein biosynthesis degradation, transcription, energy and amino acid metabolism	Kasap et al., 2015

alkaline phosphatase (ALP) and PTH, clinical symptoms and radiography, there are still defects in sensitivityand specificity (Faerk et al., 2002). Therefore, to investigate nutritional rickets-related urinary biomarkers, an unbiasedglobal urinary metabolomics analysis performed by Wang et al. (2014) defined a panel of altered metabolic profiles associated with nutritional rickets. 31 differentially expressed proteins were identified, and five candidate biomarkers for clinical diagnosis were screened. To further improve accuracy, a combination of several biomarkers was employed, such as phosphate and sebacic acid, which could predict nutritional rickets with high sensitivity. Therefore, based on the pathway analysis of biomarkers, the urinary metabolomics analysis gives new insights into the pathophysiology of nutritional rickets (Wang et al., 2014).

DISCUSSION AND FUTURE PERSPECTIVES

Since calcium and phosphorus metabolism play vital roles in a multitude of physiologic systems, disorders of calcium and phosphorus metabolism, as a systemic disease, always lead to destructive consequences such as skeletal-related events or even life-threatening. Therefore, it is necessary to understand the calcium and phosphorus metabolism for early diagnosis and corresponding therapeutic strategies. In this paper, the roles of PTH-1,25$(OH)_2$D-FGF23 axis in the calcium and phosphorus metabolism were described. And the pathological causes and various categories of this disease were also clearly discussed.

PTH-1,25$(OH)_2$D-FGF23 system is critical in the whole process of calcium and phosphorus metabolism. PTH and FGF23 could mediate calcium and phosphorus concentration within tight limits via a rapidly exchangeable pool between bone and extracellular fluids and urinary mineral excretion. Under the influence of PTH, 1,25$(OH)_2$D could promote calcium and phosphorus absorption at intestine. Therefore, disorders of calcium and phosphorus metabolism could be caused by the disturbance on PTH-1,25$(OH)_2$D-FGF23 system and each impaired function of related organs.

Based on the detailed understanding of the PTH-1,25$(OH)_2$D-FGF23 axis, we could better summarize vast types of genetic or no-hereditary disorders of calcium and phosphorus metabolism. On the one hand, changes in PTH concentration are induced by hyperparathyroidism or hypoparathyroidism. On the other hand, rickets, which is caused by vitamin D deficiency or hereditary factors resulting in disturbed levels of PTH or FGF23, has become a global health problem, especially the Hereditary Diseases/Disorders of Calcium and Phosphorus Metabolism (HDCPM). Their early diagnosis and therapy have become an urgent challenge around the world. Also, malignancy is a common cause for disorders of calcium and phosphorus metabolism via direct invasion of bone or up-regulated 1,25$(OH)_2$D, whereas acute or chronic kidney disease could disrupt the mineral homeostasis due to phosphate excretion failure or impaired 1,25$(OH)_2$D synthesis capacity.

Proteomics and metabolomics, the comprehensive technologies to study the altered proteins and metabolic pathways by systematically characterizing the changes in the proteome and metabolome profiles in a disease state, play essential roles in identifying biomarkers and elucidation of pathological mechanisms. Some proteomics and metabolomics studies have identified a series of valuable biomarkers and potential signaling pathways associated with disorders of calcium and phosphorus metabolism. For example, studies on PHPT found a set of disturbed proteins and metabolites, which could provide new directions for the molecular basis exploration of this disease and better discrimination of different groups of PHPT. In the search for the biomarkers of CKD-MBD and associated calcification complication, biomarkers that could be used for early diagnosis and altered metabolic pathways have been identified. These studies not only shed light on clinical diagnosis and prognosis for CKD-MBD, but also hint the potential therapeutic targets for the cardiovascular morbidity caused by hyperphosphatemia. For the metabolomics analysis of nutritional rickets, a panel of urinary biomarkers with high accuracy and specificity are defined, which could provide new clues into the pathophysiology of this disease. However, a limited number of samples, cell models, etc. need further validation series, and the exact roles of altered proteins/metabolites and metabolic pathways remains a need for in-depth investigation. Although some studies have applied this technology to biomarkers discovery and exploration of molecular mechanisms, there are still many metabolic pathways and clinical diagnostic biomarkers for disorders of calcium and phosphorus metabolism that have not yet been discovered, especially for Hereditary Diseases/Disorders of Calcium and Phosphorus Metabolism (HDCPM), the most common genetic metabolic diseases in newborns. Currently, the omics study on it is still blank; therefore more in-depth omics studies associated with this disease are required in the future.

AUTHOR CONTRIBUTIONS

MS wrote the manuscript. FL and XW helped in revising the manuscript. FL, AL, and GZ supervised the preparation of the manuscript. All authors contributed to the article and approved the submitted version.

FUNDING

This study was supported by the National Key Research and Development Program of China (2018YFA0800804), the Interdisciplinary Research Matching Scheme Hong Kong Baptist University (RC-IRMS/15-16/01), the Hong Kong General Research Fund (12101018, 12102518), and the National Natural Science Foundation Council of China (81703049). Sincere thanks should go to the other academic and staff members in AL and GZ's group at Hong Kong Baptist University. We also thank Hong Kong Baptist University for providing critical comments and technical support.

REFERENCES

Acar, S., Demir, K., and Shi, Y. (2017). Genetic causes of rickets. *J. Clin. Res. Pediatr. Endocrinol.* 9(Suppl. 2), 88–105. doi: 10.4274/jcrpe.2017.S008

Akpinar, G., Kasap, M., Canturk, N. Z., Zulfigarova, M., Islek, E. E., Guler, S. A., et al. (2017). Proteomics analysis of tissue samples reveals changes in mitochondrial protein levels in parathyroid hyperplasia over adenoma. *Cancer Genom. Proteom.* 14, 197–211. doi: 10.21873/cgp.20031

Anderson, N. L., and Anderson, N. G. (1998). Proteome and proteomics: new technologies, new concepts, and new words. *Electrophoresis* 19, 1853–1861. doi: 10.1002/elps.1150191103

Austin, L. A., and Heath, H. (1981). Calcitonin: physiology and pathophysiology. *N. Engl. J. Med.* 304, 269–278. doi: 10.1056/nejm198101293040505

Battini, S., Imperiale, A., Taïeb, D., Elbayed, K., Cicek, A. E., Sebag, F., et al. (2016). High-resolution magic angle spinning (1)H nuclear magnetic resonance spectroscopy metabolomics of hyperfunctioning parathyroid glands. *Surgery* 160, 384–394. doi: 10.1016/j.surg.2016.03.002

Beck, L., Karaplis, A. C., Amizuka, N., Hewson, A. S., Ozawa, H., and Tenenhouse, H. S. (1998). Targeted inactivation of Npt2 in mice leads to severe renal phosphate wasting, hypercalciuria, and skeletal abnormalities. *Proc. Natl. Acad. Sci. U.S.A.* 95, 5372–5377. doi: 10.1073/pnas.95.9.5372

Beck-Nielsen, S. S., Brixen, K., Gram, J., and Brusgaard, K. (2012). Mutational analysis of PHEX, FGF23, DMP1, SLC34A3 and CLCN5 in patients with hypophosphatemic rickets. *J. Hum. Genet.* 57, 453–458. doi: 10.1038/jhg.2012.56

Ben-Dov, I. Z., Galitzer, H., Lavi-Moshayoff, V., Goetz, R., Kuro-o, M., Mohammadi, M., et al. (2007). The parathyroid is a target organ for FGF23 in rats. *J. Clin. Invest.* 117, 4003–4008.

Biber, J., Hernando, N., and Forster, I. (2013). Phosphate transporters and their function. *Annu. Rev. Physiol.* 75, 535–550. doi: 10.1146/annurev-physiol-030212-183748

Bilezikian, J. P. (2008). Combination anabolic and antiresorptive therapy for osteoporosis: opening the anabolic window. *Curr. Osteopor. Rep.* 6, 24–30. doi: 10.1007/s11914-008-0005-9

Bilezikian, J. P., and Silverberg, S. J. (2004). Clinical practice. Asymptomatic primary hyperparathyroidism. *N. Engl. J. Med.* 350, 1746–1751.

Blackstock, W. P., and Weir, M. P. (1999). Proteomics: quantitative and physical mapping of cellular proteins. *Trends Biotechnol.* 17, 121–127. doi: 10.1016/s0167-7799(98)01245-1

Blaine, J., Chonchol, M., and Levi, M. (2015). Renal control of calcium, phosphate, and magnesium homeostasis. *Clin. J. Am. Soc. Nephrol.* 10, 1257–1272. doi: 10.2215/CJN.09750913

Block, G. A., Klassen, P. S., Lazarus, J. M., Ofsthun, N., Lowrie, E. G., and Chertow, G. M. (2004). Mineral metabolism, mortality, and morbidity in maintenance hemodialysis. *J. Am. Soc. Nephrol.* 15, 2208–2218. doi: 10.1097/01.asn.0000133041.27682.a2

Bover, J., Ureña-Torres, P., Górriz, J. L., Lloret, M. J., da Silva, I., Ruiz-García, C., et al. (2016). Cardiovascular calcifications in chronic kidney disease: potential therapeutic implications. *Nefrologia* 36, 597–608. doi: 10.1016/j.nefro.2016.05.023

Boyce, B. F., and Xing, L. (2008). Functions of RANKL/RANK/OPG in bone modeling and remodeling. *Archiv. Biochem. Biophys.* 473, 139–146. doi: 10.1016/j.abb.2008.03.018

Boyle, W. J., Simonet, W. S., and Lacey, D. L. (2003). Osteoclast differentiation and activation. *Nature* 423, 337–342. doi: 10.1038/nature01658

Brown, E. M., Gamba, G., Riccardi, D., Lombardi, M., Butters, R., Kifor, O., et al. (1993). Cloning and characterization of an extracellular Ca(2+)-sensing receptor from bovine parathyroid. *Nature* 366, 575–580. doi: 10.1038/366575a0

Brown, E. M., Pollak, M., and Hebert, S. C. (1995). Sensing of extracellular Ca2+ by parathyroid and kidney cells: cloning and characterization of an extracellular Ca(2+)-sensing receptor. *Am. J. Kidney Dis.* 25, 506–513. doi: 10.1016/0272-6386(95)90118-3

Brownstein, C. A., Adler, F., Nelson-Williams, C., Iijima, J., Li, P., Imura, A., et al. (2008). A translocation causing increased alpha-klotho level results in hypophosphatemic rickets and hyperparathyroidism. *Proc. Natl. Acad. Sci. U.S.A.* 105, 3455–3460. doi: 10.1073/pnas.0712361105

Burnett-Bowie, S.-A. M., Henao, M. P., Dere, M. E., Lee, H., and Leder, B. Z. (2009). Effects of hPTH(1-34) infusion on circulating serum phosphate, 1,25-dihydroxyvitamin D, and FGF23 levels in healthy men. *J. Bone Min. Res.* 24, 1681–1685. doi: 10.1359/jbmr.090406

Burtis, W. J., Wu, T. L., Insogna, K. L., and Stewart, A. F. (1988). Humoral hypercalcemia of malignancy. *Ann. Intern. Med.* 108, 454–457.

Bushinsky, D. A., and Monk, R. D. (1998). Electrolyte quintet: calcium. *Lancet* 352, 306–311.

Carling, T. (2001). Molecular pathology of parathyroid tumors. *Trends Endocrinol. Metab.* 12, 53–58. doi: 10.1016/s1043-2760(00)00345-3

Carroll, M. F., and Schade, D. S. (2003). A practical approach to hypercalcemia. *Am. Fam. Phys.* 67, 1959–1966.

Cheng, Y., Xie, G., Chen, T., Qiu, Y., Zou, X., Zheng, M., et al. (2012). Distinct urinary metabolic profile of human colorectal cancer. *J. Proteom. Res.* 11, 1354–1363. doi: 10.1021/pr201001a

Chirayath, M. V., Gajdzik, L., Hulla, W., Graf, J., Cross, H. S., and Peterlik, M. (1998). Vitamin D increases tight-junction conductance and paracellular Ca2+ transport in Caco-2 cell cultures. *Am. J. Physiol.* 274, G389–G396. doi: 10.1152/ajpgi.1998.274.2.G389

Christakos, S., Dhawan, P., Verstuyf, A., Verlinden, L., and Carmeliet, G. (2016). Vitamin D: metabolism, molecular mechanism of action, and pleiotropic effects. *Physiol. Rev.* 96, 365–408. doi: 10.1152/physrev.00014.2015

Civitelli, R., and Ziambaras, K. (2011). Calcium and phosphate homeostasis: concerted interplay of new regulators. *J. Endocrinol. Invest.* 34(7 Suppl.), 3–7.

Cooper, M. S., and Gittoes, N. J. L. (2008). Diagnosis and management of hypocalcaemia. *BMJ* 336, 1298–1302. doi: 10.1136/bmj.39582.589433.BE

de Groot, T., Bindels, R. J. M., and Hoenderop, J. G. J. (2008). TRPV5: an ingeniously controlled calcium channel. *Kidney Intern.* 74, 1241–1246. doi: 10.1038/ki.2008.320

Demay, M. B., Kiernan, M. S., DeLuca, H. F., and Kronenberg, H. M. (1992). Sequences in the human parathyroid hormone gene that bind the 1,25-dihydroxyvitamin D3 receptor and mediate transcriptional repression in response to 1,25-dihydroxyvitamin D3. *Proc. Natl. Acad. Sci. U.S.A.* 89, 8097–8101. doi: 10.1073/pnas.89.17.8097

Devuyst, O., and Thakker, R. V. (2010). Dent's disease. *Orphanet. J. Rare Dis.* 5:28. doi: 10.1186/1750-1172-5-28

Dvorak, M. M., and Riccardi, D. (2004). Ca2+ as an extracellular signal in bone. *Cell Calcium* 35, 249–255. doi: 10.1016/j.ceca.2003.10.014

Faerk, J., Peitersen, B., Petersen, S., and Michaelsen, K. F. (2002). Bone mineralisation in premature infants cannot be predicted from serum alkaline phosphatase or serum phosphate. *Arch. Dis. Child Fetal Neonatal. Edn.* 87, F133–F136. doi: 10.1136/fn.87.2.f133

Farrow, E. G., Davis, S. I., Summers, L. J., and White, K. E. (2009). Initial FGF23-mediated signaling occurs in the distal convoluted tubule. *J. Am. Soc. Nephrol.* 20, 955–960. doi: 10.1681/ASN.2008070783

Fleet, J. C., Eksir, F., Hance, K. W., and Wood, R. J. (2002). Vitamin D-inducible calcium transport and gene expression in three Caco-2 cell lines. *Am. J. Physiol.* 283, G618–G625.

Florencio-Silva, R., Sasso, G. R. D. S., Sasso-Cerri, E., Simões, M. J., and Cerri, P. S. (2015). Biology of bone tissue: structure, function, and factors that influence bone cells. *Biomed. Res. Intern.* 2015:421746. doi: 10.1155/2015/421746

Fraser, D., Kooh, S. W., Kind, H. P., Holick, M. F., Tanaka, Y., and DeLuca, H. F. (1973). Pathogenesis of hereditary vitamin-D-dependent rickets. An inborn error of vitamin D metabolism involving defective conversion of 25-hydroxyvitamin D to 1 alpha,25-dihydroxyvitamin D. *N. Engl. J. Med.* 289, 817–822. doi: 10.1056/nejm197310182891601

Fukagawa, M., Inaba, M., Yokoyama, K., Shigematsu, T., Ando, R., and Miyamoto, K. I. (2017). An introduction to CKD-MBD research: restart for the future. *Clin. Exp. Nephrol.* 21(Suppl. 1), 1–3. doi: 10.1007/s10157-016-1372-7

Gensure, R. C., Shimizu, N., Tsang, J., and Gardella, T. J. (2003). Identification of a contact site for residue 19 of parathyroid hormone (PTH) and PTH-related protein analogs in transmembrane domain two of the type 1 PTH receptor. *Mol. Endocrinol.* 17, 2647–2658. doi: 10.1210/me.2003-0275

Giusti, L., Cetani, F., Ciregia, F., Da Valle, Y., Donadio, E., Giannaccini, G., et al. (2011). A proteomic approach to study parathyroid glands. *Mol. Biosyst.* 7, 687–699. doi: 10.1039/c0mb00191k

Guise, T. A., Yin, J. J., Taylor, S. D., Kumagai, Y., Dallas, M., Boyce, B. F., et al. (1996). Evidence for a causal role of parathyroid hormone-related protein in the pathogenesis of human breast cancer-mediated osteolysis. *J. Clin. Invest.* 98, 1544–1549. doi: 10.1172/jci118947

Guven, A., Al-Rijjal, R. A., BinEssa, H. A., Dogan, D., Kor, Y., Zou, M., et al. (2017). Mutational analysis of PHEX, FGF23 and CLCN5 in patients with hypophosphataemic rickets. *Clin. Endocrinol.* 87, 103–112. doi: 10.1111/cen.13347

Hamann, K. L., and Lane, N. E. (2006). Parathyroid hormone update. *Rheum. Dis. Clin. N. Am.* 32, 703–719.

Hebert, S. C. (1996). Extracellular calcium-sensing receptor: implications for calcium and magnesium handling in the kidney. *Kidney Intern.* 50, 2129–2139. doi: 10.1038/ki.1996.539

Hendy, G. N., Hruska, K. A., Mathew, S., and Goltzman, D. (2006). New insights into mineral and skeletal regulation by active forms of vitamin D. *Kidney Intern.* 69, 218–223. doi: 10.1038/sj.ki.5000091

Hoenderop, J. G., van der Kemp, A. W., Hartog, A., van de Graaf, S. F., van Os, C. H., Willems, P. H., et al. (1999). Molecular identification of the apical Ca2+ channel in 1, 25-dihydroxyvitamin D3-responsive epithelia. *J. Biol. Chem.* 274, 8375–8378. doi: 10.1074/jbc.274.13.8375

Hoenderop, J. G., Vennekens, R., Müller, D., Prenen, J., Droogmans, G., Bindels, R. J., et al. (2001). Function and expression of the epithelial Ca(2+) channel family: comparison of mammalian ECaC1 and 2. *J. Physiol.* 537(Pt 3), 747–761. doi: 10.1113/jphysiol.2001.012917

Hoenderop, J. G. J., Nilius, B., and Bindels, R. J. M. (2005). Calcium absorption across epithelia. *Physiol. Rev.* 85, 373–422. doi: 10.1152/physrev.00003.2004

Hollywood, K., Brison, D. R., and Goodacre, R. (2006). Metabolomics: current technologies and future trends. *Proteomics* 6, 4716–4723. doi: 10.1002/pmic.200600106

Hughes, M. R., Brumbaugh, P. F., Hussler, M. R., Wergedal, J. E., and Baylink, D. J. (1975). Regulation of serum 1alpha,25-dihydroxyvitamin D3 by calcium and phosphate in the rat. *Science* 190, 578–580. doi: 10.1126/science.1188357

Iannuzzi, M. C., Rybicki, B. A., and Teirstein, A. S. (2007). Sarcoidosis. *N. Engl. J. Med.* 357, 2153–2165.

Insogna, K. L., and Broadus, A. E. (1987). Hypercalcemia of malignancy. *Annu. Rev. Med.* 38, 241–256.

Izzedine, H., Launay-Vacher, V., Isnard-Bagnis, C., and Deray, G. (2003). Drug-induced Fanconi's syndrome. *Am. J. Kidney Dis.* 41, 292–309.

Jamshidi, N., Miller, F. J., Mandel, J., Evans, T., and Kuo, M. D. (2011). Individualized therapy of HHT driven by network analysis of metabolomic profiles. *BMC Syst. Biol.* 5:200. doi: 10.1186/1752-0509-5-200

Kang, S., Maeng, H., Kim, B. G., Qing, G. M., Choi, Y. P., Kim, H. Y., et al. (2012). In situ identification and localization of IGHA2 in the breast tumor microenvironment by mass spectrometry. *J. Proteom. Res.* 11, 4567–4574. doi: 10.1021/pr3003672

Kasap, M., Yeğenağa, I., Akpinar, G., Tuncay, M., Aksoy, A., and Karaoz, E. (2015). Comparative proteome analysis of hAT-MSCs isolated from chronic renal failure patients with differences in their bone turnover status. *PLoS One* 10:e0142934. doi: 10.1371/journal.pone.0142934

Katai, K., Miyamoto, K., Kishida, S., Segawa, H., Nii, T., Tanaka, H., et al. (1999). Regulation of intestinal Na+-dependent phosphate co-transporters by a low-phosphate diet and 1,25-dihydroxyvitamin D3. *Biochem. J.* 343(Pt 3), 705–712. doi: 10.1042/0264-6021:3430705

Ketteler, M., Block, G. A., Evenepoel, P., Fukagawa, M., Herzog, C. A., McCann, L., et al. (2017). Executive summary of the 2017 KDIGO chronic kidney disease-mineral and bone disorder (CKD-MBD) guideline update: what's changed and why it matters. *Kidney Intern.* 92, 26–36. doi: 10.1016/j.kint.2017.04.006

Khundmiri, S. J., Murray, R. D., and Lederer, E. (2016). PTH and Vitamin D. *Comprehen. Physiol.* 6, 561–601. doi: 10.1002/cphy.c140071

Khwaja, A. (2010). Chronic kidney disease-mineral and bone disorder KDIGO guidelines. *Nephron. Clin. Pract.* 116, c25–c26. doi: 10.1159/000314546

Koh, J., Hogue, J. A., Roman, S. A., Scheri, R. P., Fradin, H., Corcoran, D. L., et al. (2018). Transcriptional profiling reveals distinct classes of parathyroid tumors in PHPT. *Endocrine Relat. Cancer* 25, 407–420. doi: 10.1530/ERC-17-0470

Kolek, O. I., Hines, E. R., Jones, M. D., LeSueur, L. K., Lipko, M. A., Kiela, P. R., et al. (2005). 1alpha,25-Dihydroxyvitamin D3 upregulates FGF23 gene expression in bone: the final link in a renal-gastrointestinal-skeletal axis that controls phosphate transport. *Am. J. Physiolo.* 289, G1036–G1042.

Kumar, R. (1991). Vitamin D and calcium transport. *Kidney Intern.* 40, 1177–1189. doi: 10.1038/ki.1991.332

Lambers, T. T., Bindels, R. J. M., and Hoenderop, J. G. J. (2006). Coordinated control of renal Ca2+ handling. *Kidney Intern.* 69, 650–654. doi: 10.1038/sj.ki.5000169

Lavi-Moshayoff, V., Wasserman, G., Meir, T., Silver, J., and Naveh-Many, T. (2010). PTH increases FGF23 gene expression and mediates the high-FGF23 levels of experimental kidney failure: a bone parathyroid feedback loop. *Am. J. Physiol.* 299, F882–F889. doi: 10.1152/ajprenal.00360.2010

Levin, A., Bakris, G. L., Molitch, M., Smulders, M., Tian, J., Williams, L. A., et al. (2007). Prevalence of abnormal serum vitamin D, PTH, calcium, and phosphorus in patients with chronic kidney disease: results of the study to evaluate early kidney disease. *Kidney Int.* 71, 31–38. doi: 10.1038/sj.ki.5002009

Li, S., Mao, J., Wang, M., Zhang, M., Ni, L., Tao, Y., et al. (2018). Comparative proteomic analysis of chief and oxyphil cell nodules in refractory uremic hyperparathyroidism by iTRAQ coupled LC-MS/MS. *J. Proteom.* 179, 42–52. doi: 10.1016/j.jprot.2018.02.029

Lorenz-Depiereux, B., Bastepe, M., Benet-Pagès, A., Amyere, M., Wagenstaller, J., Müller-Barth, U., et al. (2006). DMP1 mutations in autosomal recessive hypophosphatemia implicate a bone matrix protein in the regulation of phosphate homeostasis. *Nat. Genet.* 38, 1248–1250. doi: 10.1038/ng1868

Lu, M., Kjellin, H., Fotouhi, O., Lee, L., Nilsson, I.-L., Haglund, F., et al. (2018). Molecular profiles of oxyphilic and chief cell parathyroid adenoma. *Mol. Cell. Endocrinol.* 470, 84–95. doi: 10.1016/j.mce.2017.10.001

Lundgren, E., Lind, L., Palmér, M., Jakobsson, S., Ljunghall, S., and Rastad, J. (2001). Increased cardiovascular mortality and normalized serum calcium in patients with mild hypercalcemia followed up for 25 years. *Surgery* 130, 978–985. doi: 10.1067/msy.2001.118377

Malloy, P. J., Pike, J. W., and Feldman, D. (1999). The vitamin D receptor and the syndrome of hereditary 1,25-dihydroxyvitamin D-resistant rickets. *Endocr. Rev.* 20, 156–188. doi: 10.1210/edrv.20.2.0359

Martin, A., David, V., and Quarles, L. D. (2012). Regulation and function of the FGF23/klotho endocrine pathways. *Physiol. Rev.* 92, 131–155. doi: 10.1152/physrev.00002.2011

Martin, T. J., and Sims, N. A. (2005). Osteoclast-derived activity in the coupling of bone formation to resorption. *Trends Mol. Med.* 11, 76–81. doi: 10.1016/j.molmed.2004.12.004

Masuyama, R., Stockmans, I., Torrekens, S., Van Looveren, R., Maes, C., Carmeliet, P., et al. (2006). Vitamin D receptor in chondrocytes promotes osteoclastogenesis and regulates FGF23 production in osteoblasts. *J. Clin. Invest.* 116, 3150–3159. doi: 10.1172/jci29463

Mihai, S., Codrici, E., Popescu, I. D., Enciu, A.-M., Rusu, E., Zilisteanu, D., et al. (2016). Proteomic biomarkers panel: new insights in chronic kidney disease. *Dis. Mark.* 2016:3185232.

Miller, W. L. (2017). Genetic disorders of Vitamin D biosynthesis and degradation. *J. Steroid. Biochem. Mol. Biol.* 165(Pt A), 101–108. doi: 10.1016/j.jsbmb.2016.04.001

Mittermeier, L., Demirkhanyan, L., Stadlbauer, B., Breit, A., Recordati, C., Hilgendorff, A., et al. (2019). TRPM7 is the central gatekeeper of intestinal mineral absorption essential for postnatal survival. *Proc. Natl. Acad. Sci. U.S.A.* 116, 4706–4715. doi: 10.1073/pnas.1810633116

Nicholson, J. K. (2006). Global systems biology, personalized medicine and molecular epidemiology. *Mol. Syst. Biol.* 2:52. doi: 10.1038/msb4100095

Nicholson, J. K., Lindon, J. C., and Holmes, E. (1999). 'Metabonomics': understanding the metabolic responses of living systems to pathophysiological stimuli via multivariate statistical analysis of biological NMR spectroscopic data. *Xenobiotica* 29, 1181–1189. doi: 10.1080/004982599238047

Nicholson, J. K., Wilson, I. D., and Lindon, J. C. (2011). Pharmacometabonomics as an effector for personalized medicine. *Pharmacogenomics* 12, 103–111. doi: 10.2217/pgs.10.157

Nickolas, T. L., and Jamal, S. A. (2015). Bone kidney interactions. *Rev. Endoc. Metab. Disord.* 16, 157–163. doi: 10.1007/s11154-015-9314-3

Parfitt, A. M. (1976a). The actions of parathyroid hormone on bone: relation to bone remodeling and turnover, calcium homeostasis, and metabolic bone disease. Part I of IV parts: mechanisms of calcium transfer between blood and bone and their cellular basis: morphological and kinetic approaches to bone turnover. *Metabolism* 25, 809–844. doi: 10.1016/0026-0495(76)90151-7

Parfitt, A. M. (1976b). The actions of parathyroid hormone on bone: relation to bone remodeling and turnover, calcium homeostasis, and metabolic bone diseases. II. PTH and bone cells: bone turnover and plasma calcium regulation. *Metabolism* 25, 909–955. doi: 10.1016/0026-0495(76)90124-4

Peacock, M. (2010). Calcium metabolism in health and disease. *Clin. J. Am. Soc. Nephrol.* 5(Suppl. 1), S23–S30. doi: 10.2215/CJN.05910809

Pérez, A. V., Picotto, G., Carpentieri, A. R., Rivoira, M. A., Peralta López, M. E., and Tolosa de Talamoni, N. G. (2008). Minireview on regulation of intestinal calcium absorption. Emphasis on molecular mechanisms of transcellular pathway. *Digestion* 77, 22–34. doi: 10.1159/000116623

Qiu, Y., Cai, G., Su, M., Chen, T., Zheng, X., Xu, Y., et al. (2009). Serum metabolite profiling of human colorectal cancer using GC-TOFMS and UPLC-QTOFMS. *J. Proteome Res.* 8, 4844–4850. doi: 10.1021/pr9004162

Quarles, L. D. (2003). FGF23, PHEX, and MEPE regulation of phosphate homeostasis and skeletal mineralization. *Am. J. Physiol. Endocrinol. Metab.* 285, E1–E9.

Razali, N. N., Hwu, T. T., and Thilakavathy, K. (2015). Phosphate homeostasis and genetic mutations of familial hypophosphatemic rickets. *J. Pediatr. Endocrinol. Metab.* 28, 1009–1017. doi: 10.1515/jpem-2014-0366

Razzaque, M. S., and Lanske, B. (2007). The emerging role of the fibroblast growth factor-23-klotho axis in renal regulation of phosphate homeostasis. *J. Endocrinol.* 194, 1–10. doi: 10.1677/joe-07-0095

Renkema, K. Y., Alexander, R. T., Bindels, R. J., and Hoenderop, J. G. (2008). Calcium and phosphate homeostasis: concerted interplay of new regulators. *Ann. Med.* 40, 82–91. doi: 10.1080/07853890701689645

Roodman, G. D. (2004). Mechanisms of bone metastasis. *N. Engl. J. Med.* 350, 1655–1664.

Rowe, P. S. N. (2012). Regulation of bone-renal mineral and energy metabolism: the PHEX, FGF23, DMP1, MEPE ASARM pathway. *Crit. Rev. Eukaryot. Gene Expr.* 22, 61–86. doi: 10.1615/critreveukargeneexpr.v22.i1.50

Schiavi, S. C. (2006). Fibroblast growth factor 23: the making of a hormone. *Kidney Intern.* 69, 425–427. doi: 10.1038/sj.ki.5000168

Seymour, J. F., Gagel, R. F., Hagemeister, F. B., Dimopoulos, M. A., and Cabanillas, F. (1994). Calcitriol production in hypercalcemic and normocalcemic patients with non-Hodgkin lymphoma. *Ann. Intern. Med.* 121, 633–640. doi: 10.7326/0003-4819-121-9-199411010-00001

Shen, Q., Xiang, W., Ye, S., Lei, X., Wang, L., Jia, S., et al. (2019). Plasma metabolite biomarkers related to secondary hyperparathyroidism and parathyroid hormone. *J. Cell Biochem.* 120, 15766–15775. doi: 10.1002/jcb.28846

Shimada, T., Hasegawa, H., Yamazaki, Y., Muto, T., Hino, R., Takeuchi, Y., et al. (2004). FGF-23 is a potent regulator of vitamin D metabolism and phosphate homeostasis. *J. Bone Min. Res.* 19, 429–435. doi: 10.1359/jbmr.0301264

Shimada, T., Muto, T., Urakawa, I., Yoneya, T., Yamazaki, Y., Okawa, K., et al. (2002). Mutant FGF-23 responsible for autosomal dominant hypophosphatemic rickets is resistant to proteolytic cleavage and causes hypophosphatemia in vivo. *Endocrinology* 143, 3179–3182. doi: 10.1210/endo.143.8.8795

Song, Y., Peng, X., Porta, A., Takanaga, H., Peng, J.-B., Hediger, M. A., et al. (2003). Calcium transporter 1 and epithelial calcium channel messenger ribonucleic acid are differentially regulated by 1,25 dihydroxyvitamin D3 in the intestine and kidney of mice. *Endocrinology* 144, 3885–3894. doi: 10.1210/en.2003-0314

Stewart, A. F. (2005). Clinical practice. Hypercalcemia associated with cancer. *N. Engl. J. Med.* 352, 373–379.

Stewart, A. F., Vignery, A., Silverglate, A., Ravin, N. D., LiVolsi, V., Broadus, A. E., et al. (1982). Quantitative bone histomorphometry in humoral hypercalcemia of malignancy: uncoupling of bone cell activity. *J. Clin. Endocrinol. Metab.* 55, 219–227. doi: 10.1210/jcem-55-2-219

Suhre, K., Shin, S. Y., Petersen, A. K., Mohney, R. P., Meredith, D., Wägele, B., et al. (2011). Human metabolic individuality in biomedical and pharmaceutical research. *Nature* 477, 54–60. doi: 10.1038/nature10354

Sumida, K., Nakamura, M., Ubara, Y., Marui, Y., Tanaka, K., Takaichi, K., et al. (2011). Histopathological alterations of the parathyroid glands in haemodialysis patients with secondary hyperparathyroidism refractory to cinacalcet hydrochloride. *J. Clin. Pathol.* 64, 756–760. doi: 10.1136/jclinpath-2011-200100

Takeda, E., Yamamoto, H., Nashiki, K., Sato, T., Arai, H., and Taketani, Y. (2004). Inorganic phosphate homeostasis and the role of dietary phosphorus. *J. Cell. Mol. Med.* 8, 191–200. doi: 10.1111/j.1582-4934.2004.tb00274.x

Talmage, R. V., Grubb, S. A., Norimatsu, H., and Vanderwiel, C. J. (1980). Evidence for an important physiological role for calcitonin. *Proc. Natl. Acad. Sci. U.S.A.* 77, 609–613. doi: 10.1073/pnas.77.1.609

Tencza, A. L., Ichikawa, S., Dang, A., Kenagy, D., McCarthy, E., Econs, M. J., et al. (2009). Hypophosphatemic rickets with hypercalciuria due to mutation in SLC34A3/type IIc sodium-phosphate cotransporter: presentation as hypercalciuria and nephrolithiasis. *J. Clin. Endocrinol. Metab.* 94, 4433–4438. doi: 10.1210/jc.2009-1535

Traebert, M., Roth, J., Biber, J., Murer, H., and Kaissling, B. (2000a). Internalization of proximal tubular type II Na-P(i) cotransporter by PTH: immunogold electron microscopy. *Am. J. Physiol. Renal Physiol.* 278, F148–F154.

Traebert, M., Völkl, H., Biber, J., Murer, H., and Kaissling, B. (2000b). Luminal and contraluminal action of 1-34 and 3-34 PTH peptides on renal type IIa Na-P(i) cotransporter. *Am. J. Physiol. Renal Physiol.* 278, F792–F798.

Vaidyanathan, G. (2012). Redefining clinical trials: the age of personalized medicine. *Cell* 148, 1079–1080. doi: 10.1016/j.cell.2012.02.041

van Abel, M., Hoenderop, J. G. J., van der Kemp, A. W. C. M., Friedlaender, M. M., van Leeuwen, J. P. T. M., and Bindels, R. J. M. (2005). Coordinated control of renal Ca(2+) transport proteins by parathyroid hormone. *Kidney Intern.* 68, 1708–1721. doi: 10.1111/j.1523-1755.2005.00587.x

van de Graaf, S. F. J., Bindels, R. J. M., and Hoenderop, J. G. J. (2007). Physiology of epithelial Ca2+ and Mg2+ transport. *Rev. Physiol. Biochem. Pharmacol.* 158, 77–160. doi: 10.1007/112_2006_0607

Varshney, S., Bhadada, S. K., Arya, A. K., Sharma, S., Behera, A., Bhansali, A., et al. (2014). Changes in parathyroid proteome in patients with primary hyperparathyroidism due to sporadic parathyroid adenomas. *Clin. Endocrinol.* 81, 614–620. doi: 10.1111/cen.12479

Virkki, L. V., Biber, J., Murer, H., and Forster, I. C. (2007). Phosphate transporters: a tale of two solute carrier families. *Am. J. Physiol. Renal Physiol.* 293, F643–F654.

Voelkl, J., Lang, F., Eckardt, K.-U., Amann, K., Kuro-O, M., Pasch, A., et al. (2019). Signaling pathways involved in vascular smooth muscle cell calcification during hyperphosphatemia. *Cell. Mol. Life Sci.* 76, 2077–2091. doi: 10.1007/s00018-019-03054-z

Wagner, C. A., Hernando, N., Forster, I. C., and Biber, J. (2014). The SLC34 family of sodium-dependent phosphate transporters. *Pflug. Archiv. Eur. J. Physiol.* 466, 139–153. doi: 10.1007/s00424-013-1418-6

Wang, M., Yang, X., Ren, L., Li, S., He, X., Wu, X., et al. (2014). Biomarkers identified by urinary metabonomics for noninvasive diagnosis of nutritional rickets. *J. Proteom. Res.* 13, 4131–4142. doi: 10.1021/pr500517u

Want, E. J., Wilson, I. D., Gika, H., Theodoridis, G., Plumb, R. S., Shockcor, J., et al. (2010). Global metabolic profiling procedures for urine using UPLC-MS. *Nat. Protoc.* 5, 1005–1018. doi: 10.1038/nprot.2010.50

Waters, M. (2009). Hypercalcaemia. *InnovAiT Educ. Inspirat. Gen. Pract.* 2, 698–701. doi: 10.1093/innovait/inp143

Williams, E. D. (1974). Pathology of the parathyroid glands. *Clin. Endocrinol. Metab.* 3, 285–303.

Wu, Q., Lai, X., Zhu, Z., Hong, Z., Dong, X., Wang, T., et al. (2015). Evidence for chronic kidney disease-mineral and bone disorder associated with metabolic pathway changes. *Medicine* 94:e1273. doi: 10.1097/md.0000000000001273

Xu, H., Bai, L., Collins, J. F., and Ghishan, F. K. (2002). Age-dependent regulation of rat intestinal type IIb sodium-phosphate cotransporter by 1,25-(OH)(2) vitamin D(3). *Am. J. Physiol.* 282, C487–C493.

Yang, L. E., Maunsbach, A. B., Leong, P. K. K., and McDonough, A. A. (2004). Differential traffic of proximal tubule Na+ transporters during hypertension or PTH: NHE3 to base of microvilli vs. *NaPi2* to endosomes. *Am. J. Physiol. Renal Physiol.* 287, F896–F906.

Yener Ozturk, F., Erol, S., Canat, M. M., Karatas, S., Kuzu, I., Dogan Cakir, S., et al. (2016). Patients with normocalcemic primary hyperparathyroidism may have similar metabolic profile as hypercalcemic patients. *Endocr. J.* 63, 111–118. doi: 10.1507/endocrj.EJ15-0392

Zhou, R., Kang, X., Tang, B., Mohan, C., Wu, T., Peng, A., et al. (2016). Ornithine is a key mediator in hyperphosphatemia-mediated human umbilical vein endothelial cell apoptosis: insights gained from metabolomics. *Life Sci.* 146, 73–80. doi: 10.1016/j.lfs.2016.01.003

Zivin, J. R., Gooley, T., Zager, R. A., and Ryan, M. J. (2001). Hypocalcemia: a pervasive metabolic abnormality in the critically ill. *Am. J. Kidney Dis.* 37, 689–698. doi: 10.1016/s0272-6386(01)80116-5

Conflict of Interest: The authors declare that the research was conducted in the absence of any commercial or financial relationships that could be construed as a potential conflict of interest.

Copyright © 2020 Sun, Wu, Yu, Wang, Xie, Zhang, Chen, Lu, Zhang and Li. This is an open-access article distributed under the terms of the Creative Commons Attribution License (CC BY). The use, distribution or reproduction in other forums is permitted, provided the original author(s) and the copyright owner(s) are credited and that the original publication in this journal is cited, in accordance with accepted academic practice. No use, distribution or reproduction is permitted which does not comply with these terms.

frontiers in Cell and Developmental Biology

REVIEW
published: 15 October 2020
doi: 10.3389/fcell.2020.573455

Yes-Associated Protein 1: Role and Treatment Prospects in Orthopedic Degenerative Diseases

Wenqing Xie[1,2†], Wenfeng Xiao[1,2†], Kun Tang[3], Liyang Zhang[4] and Yusheng Li[1,2]**

[1] Department of Orthopedics, Xiangya Hospital, Central South University, Changsha, China, [2] National Clinical Research Center for Geriatric Disorders, Xiangya Hospital, Central South University, Changsha, China, [3] Discipline Construction Office, Xiangya Hospital, Central South University, Changsha, China, [4] Department of Neurosurgery, Xiangya Hospital, Central South University, Changsha, China

OPEN ACCESS

Edited by:
Chao Liang,
Hong Kong Baptist University,
Hong Kong

Reviewed by:
James Pritchett,
Manchester Metropolitan University,
United Kingdom
Min Zhang,
Shanghai Children's Medical Center,
China
Huiling Cao,
Southern University of Science
and Technology, China
Xiao Lv,
Johns Hopkins Medicine,
United States
Zeyu Huang,
Duke University, United States

***Correspondence:**
Yusheng Li
liyusheng@csu.edu.cn
Liyang Zhang
zhangliyang@csu.edu.cn

† These authors have contributed equally to this work

Specialty section:
This article was submitted to Molecular Medicine, a section of the journal Frontiers in Cell and Developmental Biology

Received: 17 June 2020
Accepted: 25 September 2020
Published: 15 October 2020

Citation:
Xie W, Xiao W, Tang K, Zhang L and Li Y (2020) Yes-Associated Protein 1: Role and Treatment Prospects in Orthopedic Degenerative Diseases. Front. Cell Dev. Biol. 8:573455. doi: 10.3389/fcell.2020.573455

The Hippo/yes-associated protein 1 signaling pathway is an evolutionarily conserved signaling pathway. This signaling pathway is primarily involved in the regulation of stem cell self-renewal, organ size and tissue regeneration by regulating cell proliferation, differentiation and apoptosis. It plays an important role in embryonic development and tissue organ formation. Yes-associated protein 1 (YAP1) is a key transcription factor in the Hippo signaling pathway and is negatively regulated by this pathway. Changes in YAP1 expression levels affect the occurrence and development of a variety of tumors, but the specific mechanism associated with this phenomenon has not been thoroughly studied. Recently, several studies have described the role of YAP1 in osteoarthritis (OA). Indeed, YAP1 is involved in orthopedic degenerative diseases such as osteoporosis (OP) in addition to OA. In this review, we will summarize the significance of YAP1 in orthopedic degenerative diseases and discuss the potential of the targeted modulation of YAP1 for the treatment of these diseases.

Keywords: yes-associated protein 1, osteoarthritis, osteoporosis, chondrocyte, mesenchymal stem cells

INTRODUCTION

YAP1, a connexin and transcriptional co-activator that plays an important role in cells, was first discovered by Sudol (1994) in 1994 and is the core factor of the Hippo signaling pathway (Huang et al., 2005; Dong et al., 2007). In mammalian cells, the primary members of Hippo/YAP1 signaling pathway include mammalian sterile 20-like kinase 1/2 (MST1/2), savlador family WW domain containing protein 1 (SAV1), large tumor suppressor homolog kinases 1/2 (LATS1/2), Mps one binder 1 (MOB1), YAP1, transcriptional co-activator with PDZ-binding motif (TAZ), and the TEAD family of transcription factors (TEAD1-4) (Kodaka and Hata, 2015). It is worth noting that YAP1 protein is regarded as the analog of TAZ. It has 488 amino acids, about half of the oxygen acid sequence of it are identical to TAZ and it has the same topological structure as TAZ (Low et al., 2014). The functions of YAP1 and TAZ are often redundant, which are generally referred to as YAP1/TAZ. However, YAP1 and TAZ can also function independently, and YAP1 has stronger influence than TAZ (Low et al., 2014; Plouffe et al., 2018). In terms of function, YAP1 and TAZ are mainly transcription co activators and multifunctional intracellular connexins, which participate in intracellular signal transduction and transcriptional co-activation of their downstream target factors (Hong and Guan, 2012). The Hippo/YAP1 signaling pathway exerts its functions through regulation of the above mentioned signaling pathway members. In a series

of enzymatic cascade reactions that occur when the Hippo pathway is activated, MST1/2 first binds to SAV to undergo protein kinase phosphorylation, which then phosphorylates LATS1/2 and MOB1, and finally YAP1/TAZ effector factors are phosphorylated, allowing them to bind to intracytoplasmic 14-3-3 proteins and decompose together, forcing YAP1/TAZ to remain in the cytoplasm and be degraded by the protease system (Zhao et al., 2011). When the Hippo signaling pathway is blocked, unphosphorylated YAP1/TAZ will be transported into the nucleus to promote the transcription of downstream target genes, such as connective tissue growth factor (*CTGF*) and cysteine-rich angiogenic inducer 61 (*CYR61*) (Van Haele et al., 2019). YAP1/TAZ regulates various physiological processes, and its dysfunction has been implicated in an increasing number of human diseases (Zheng and Pan, 2019). By inhibiting YAP1 and TAZ transcriptional co-activators, the Hippo pathway regulates cell proliferation, apoptosis, and stemness in response to a variety of extracellular and intracellular signals, including cell-to-cell contact, cell polarity, mechanical cues, G-protein ligand-coupled receptors, and cellular energy status (Yu et al., 2015). In addition to the typical Hippo signaling pathway, mechanical cues can also mediate YAP1 activity independently of the Hippo signaling pathway. Thus, mechanical cues and Hippo signaling represent two parallel inputs converging on YAP1/TAZ regulation (Dupont et al., 2011; Wada et al., 2011). YAP1/TAZ can also act as on-off mechanosensing switches by sensing changes in the composition and mechanics of the extracellular matrix (ECM). The regulation of their activity has been described by a hierarchical model in which elements of Hippo pathway are controlled by focal adhesions (FAs) (Nardone et al., 2017).

Many musculoskeletal diseases are the result of long-term degeneration and often occur in the late stages of the disease (Ehrlich, 2017). As most degenerative diseases, such as OA, OP and degenerative disc disease, occur in the elderly, the global aging challenge may increase the prevalence of these diseases and their burden on society (Li and Chen, 2019). OA is the most common motor system degenerative disease in middle-aged and elderly individuals, with a survey showing that the prevalence of symptomatic OA in men and women over 60 years old was 18.0 and 9.6%, respectively. Among these individuals, 80% of patients had limited movement and 25% could not complete daily activities independently (Glyn-Jones et al., 2015). The European Society for Clinical and Economic Aspects of Osteoporosis and Osteoarthritis (ESCEO) has indicated that the cost of treating OA accounts for 1.0–2.5% of the gross domestic product of developed countries (Hiligsmann et al., 2013). In 2017, The Lancet, one of the four major medical journals, published that OA has become one the top 10 diseases leading to years lived with disability (YLDs) in China (Disease et al., 2017). OP can be divided into primary osteoporosis and secondary osteoporosis, where primary osteoporosis is more common in the clinic, and the main incidence population is the elderly and postmenopausal women (Rachner et al., 2011). OP has a high incidence worldwide (Fujiwara, 2016; Clynes et al., 2020), with the latest survey showing that the number of OP patients worldwide exceeds 200 million, and its prevalence has leaped to the seventh most common and frequently occurring disease. Studies have shown (Lin et al., 2015) that with the aging of the population, Chinese OP patients will account for more than half of the global OP patients by 2020. OP is a disease associated with aging, and as the global elderly population increases, the incidence will be greatly increased, and the associated adverse consequences will be more serious.

Thus, orthopedic degenerative diseases (OA and OP) pose great challenges to human health. Over the past decade, more and more studies have highlighted the importance of YAP1 in many diseases, including OA and OP. Because YAP1 has been less studied in degenerative disc diseases, this article reviews the role of YAP1 in orthopedic degenerative diseases (OA and OP).

BASIC STRUCTURE AND FUNCTIONS OF YAP1

YAP1 was first discovered and named by Sudol et al. (1995). Sudol et al. (1995) identified, characterized and cloned a new protein with a molecular weight of 65 Kd, it binds to the homolog Src homology domain 3 (SH3) region of the non-receptor tyrosine kinase YES. The *YAP1* gene product has two subtypes, named YAP1-1 and YAP1-2, which are distinguished by an additional 38 amino acids encoding the WW domain. The YAP1-1 subtype contains a single proline and is named Yes-associated protein (YAP65) because it binds to the proto-oncogene Yes (Sudol, 1994). Mammalian ortholog is YAP1, which has one (YAP1-1) or 2 (YAP1-2) WW domains (Sudol et al., 1995; Gaffney et al., 2012). YAP1 is primarily composed of a transcription activator binding domain (TID), a double tryptophan domain (WW domain) and a transcription activation domain (TAD). Some isomers contain an SH3 binding domain (SH3-BM) and a leucine zinc finger structure (Sudol et al., 1995). There is a proline-rich region at the N-terminus of the YAP1 protein, followed by a TEAD transcription factor interacting domain (TID) and a WW domain (Vassilev et al., 2001). The TID domain is used to recruit and bind transcriptional co-activators to regulate target gene expression together with YAP1. There is a SH3-BM behind the WW domain, followed by the TAD domain and the (PDZ domain binding motif (PDZ-BM), which primarily bind to and initiate the transcriptional expression of specific genes (Ren et al., 1993; Mohler et al., 1999). And because of the differences in regulation of transcription stage, translation level and modification level, YAP1 exhibits different functions in different types of cells. Modular structure of YAP1 protein is shown in **Figure 1**.

The primary function of YAP1 is to regulate stem cell self-renewal, tissue regeneration and organ size (Zhao et al., 2011; Mo et al., 2014). Under physiological conditions, YAP1 plays an important role in promoting cell proliferation, inhibiting cell apoptosis, and maintaining the multidirectional differentiation potential of stem cells, while under pathological conditions, YAP1 overexpression can easily lead to the occurrence of malignant tumors. In recent years, research on YAP1 has increased, especially with respect to tumors. YAP1 has been confirmed to be overexpressed in a variety of tumors, including gastric tumors (An et al., 2020), liver tumors (Bisso et al., 2020), ovarian cancer

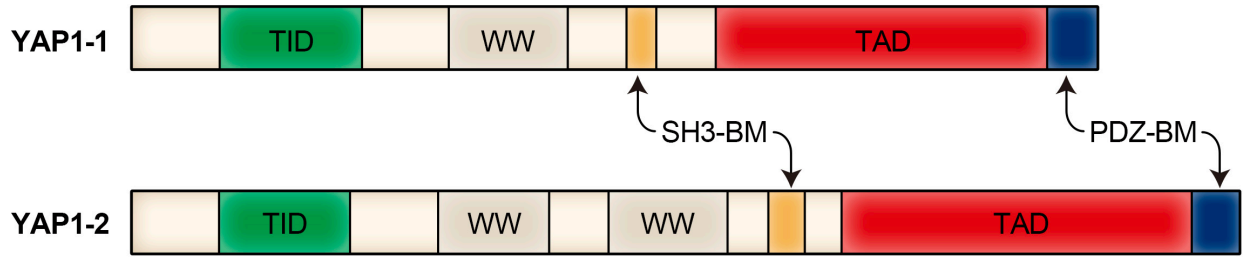


FIGURE 1 | Modular structure of YAP1 protein.

(Munoz-Galvan et al., 2020), and breast cancer (Song et al., 2018), suggesting that YAP1 has a role as a candidate oncogene in tumorigenesis. In addition, YAP1 also plays an important role in the migration and invasion of melanoma and osteosarcoma (Zucchini et al., 2019; Luo et al., 2020). However, the role of YAP1 in carcinogenesis is complex, with a recent study showing that the activation of YAP1 in peritumoral tissues has an inhibitory effect in cancer (Moya et al., 2019). It is noteworthy that YAP1 appears to play a tumor suppressive role in hematological cancers (Cottini et al., 2014), which contrasts with its oncogenic function in most solid tumors. YAP1 gene loci are frequently deleted in hematological cancers, and YAP1 expression or inhibition of MST1 results in inhibited growth and increased apoptosis. Therefore, additional studies are still needed to confirm the role of YAP1 in different types of tumors at different stages.

Recent studies have shown that YAP1 can regulate transcription factors critical for bone homeostasis, such as runt-related transcription factor 2 (RUNX2) (Zaidi et al., 2004), signal transducer and activator of transcription factor 3 (STAT3) (Huang et al., 2016) and β-catenin (Pan et al., 2018). And YAP1 also plays an important role in the cellular and molecular mechanisms of bone development and disease. YAP1 regulates the differentiation of chondrocyte progenitor cells (Jung et al., 2016) and interacts with several transcription factors to control gene expression in osteoblasts and chondrocytes (Deng et al., 2016). Therefore, YAP1 is essential for the proliferation and differentiation of both osteocytes and chondrocytes. In addition, YAP1/TAZ also affects the stemness development of marrow-derived mesenchymal stem cells (MSCs), which can affect the differentiation of osteoblasts (OBs), osteoclasts (OCs) and adipocytes (Wang et al., 2019). As precursor cells of chondrocytes, osteoblasts and adipocytes, MSCs are gradually becoming a potential cell source for the treatment of a variety of inflammatory, degenerative and autoimmune diseases (Su et al., 2017). The ability of MSCs to differentiate into chondrocytes provides a new approach for the repair of cartilage defects in cartilage degenerative diseases, such as OA, which has great potential for application in the repair of articular cartilage damage. When the balance between adipogenesis and osteogenesis of MSCs and the maintenance of chondrocyte phenotype is disrupted, bone and cartilage diseases such as OA and OP may occur. Therefore, YAP1 can affect the occurrence and development of orthopedic degenerative diseases (OA and OP) through multiple pathways, and this finding also provides a potential important target for the treatment of OA and OP.

ROLE OF YAP1 IN OA

OA is the most common degenerative joint disease and is characterized by deterioration of cartilage integrity, chondrocytopenia, subchondral sclerosis, and low-grade synovial inflammation (Hawker, 2019). Chondrocytes are the only cell type present in mature cartilage, where they are dispersed in the extracellular matrix of cartilage, playing an important role in maintaining the integrity and the biological function of cartilage and having a significant role in the degeneration process of OA cartilage (Markstedt et al., 2015). Interestingly, YAP1 is involved in chondrocyte differentiation as well as phenotype maintenance and is overexpressed in OA tissues (Zhong et al., 2013a; Karystinou et al., 2015).

YAP1 Is an Important Promoter of OA

Several studies have confirmed that YAP1 is overexpressed in OA animal model tissues, and the YAP1 content increases with the severity of OA (Nie et al., 2019; Zhang et al., 2019; Kania et al., 2020). Gong et al. (2019) reached the same conclusion in studies with an OA mouse model and human OA tissue: (1) YAP1 transcription was upregulated in knee chondrocytes of OA mice by RT-qPCR analysis; (2) YAP1 levels detected in articular chondrocytes of OA mice were upregulated by Western blot analyses; (3) and YAP1 mRNA and protein levels were increased in human chondrocytes of OA compared with normal human cartilage. This overexpression is mainly focused on the expression of the nucleus. Recent studies observed that the number of nuclear YAP1-expressing cells (52.43%) in OA cartilage was significantly higher than that detected in normal cartilage (8.39%), while the localization of cytoplasmic YAP1 was significantly lower than that observed in normal cartilage (20.02% in OA and 76.39% in normal cartilage) (Zhang et al., 2020). The level of YAP1 protein in the synovial fluid of patients with knee OA was observed to be significantly higher than that of a control group, suggesting that YAP1 protein may be an important factor in the pathogenesis of knee OA (Hwang et al., 2019). These results showed that YAP1 is significantly expressed at high levels in the OA model, suggesting that it may be involved in the development of OA

and that inhibiting YAP1 expression may aid in inhibiting the development of OA.

Inflammatory mediators produced by chondrocytes play a key role in the development of OA, interleukin-1β (IL-1β) and tumor necrosis factor-α (TNF-α), which are the two most effective catabolic factors, with IL-1β having a stronger inhibitory effect on chondrogenesis than TNF-α (Heldens et al., 2012). After 24 h of treatment with IL-1β (10 ng/ml) in mouse articular chondrocytes, IL-1β was observed to significantly increase the expression of YAP1, which in turn increased the expression of matrix metalloproteinase-13 (MMP-13) and A disintegrin and metalloproteinase with thrombospondin motifs 5 (ADAMTS5) (Gong et al., 2019). ADAMTS5 and MMP-13 are well known to be important factors in cartilage degeneration associated with OA, and their expression can degrade type II collagen and proteoglycans, which leads to the excessive degradation of ECM, promoting the occurrence and development of OA (Song et al., 2007; Little et al., 2009; Scanzello, 2017). Inhibition of YAP1 expression can reverse ECM degradation and chondrocyte apoptosis induced by IL-1β (Gong et al., 2019).

However, there are a few studies showing that YAP1 plays a protective role in the progression of OA. These results of these studies suggest that YAP1 can delay the progression of OA and may allow for the treatment of OA by upregulating YAP1 (Luo et al., 2017; Deng et al., 2018; Fu et al., 2019). A recently published study by Deng et al. (2018) showed that YAP1 activation by transgene overexpression or deletion of its upstream inhibitory kinase Mst1/2 can protect the integrity of articular cartilage, while the loss of YAP1 in chondrocytes may promote cartilage destruction. It is also believed that the inflammatory reaction triggered by YAP1 by inhibiting the NF-κB signal is necessary and sufficient for delaying OA progression (Deng et al., 2018). However, in the study by Deng et al., Col2-CreER^{T2}; Yap1$^{fl/fl}$ conditional knockout mice were induced from the embryonic stage, not before the onset of OA. Furthermore, focusing only on the total expression of YAP1 in human patient samples and mouse joints without detecting the nuclear localization of YAP1 may have an impact on the final results. Therefore, YAP1 can be considered as an important promoter of OA.

High YAP1 Expression Inhibits Chondrocyte Differentiation in OA

The pathological process of OA includes chronic inflammation and the progressive degeneration of cartilage (Vinatier et al., 2018). Studies have shown that the imbalance of chondrocyte homeostasis is associated with the development of OA (Ma et al., 2019). Therefore, it is particularly important to prevent articular cartilage degeneration and maintain the homeostasis and health of chondrocytes. In the process of chondrogenic differentiation, sex-determining region Y-type high mobility group box protein 9 SOX9) is one of the primary regulators of early chondrocyte differentiation and interacts with the transcription factors SOX5 and SOX6 to promote the proliferation and differentiation of chondrocytes, subsequently promoting the expression of chondrocyte matrix components, including aggrecan and type II collagen (Darling and Athanasiou, 2005). YAP1 has been reported to be a negative regulator of chondrogenesis, and the level of YAP1 expression has been shown to be a key element in maintaining chondrocyte function *in vitro* (Karystinou et al., 2015; Kania et al., 2020). Zhang et al. (2019) observed through qPCR and Western blotting analyses that YAP1 overexpression significantly downregulates the expression of Runx2, osteocalcin, and collagen I related to ATDC5 cell differentiation, while inhibition of YAP1 significantly enhances the expression of Runx2, osteocalcin, and collagen I. Notably, YAP1 also promotes early chondrocyte proliferation by regulating SOX6 expression and inhibiting collagen type X (COL10A1) expression by interacting with Runx2 during chondrocyte maturation, thereby inhibiting chondrocyte maturation (Deng et al., 2016; Ying et al., 2018). YAP1 negatively regulates chondrocyte differentiation by activating the β-catenin signaling pathway, and YAP1 overexpression enhances chondrocyte proliferation but inhibits chondrocyte differentiation (Yang et al., 2017). In another study of cartilage differentiation (Nie et al., 2019), dasatinib treatment was observed to significantly upregulate the serine phosphorylation of YAP1 and downregulate the protein expression of YAP1 and TAZ in a dose-dependent manner, promoting cartilage gene differentiation of MSCs by promoting the serine phosphorylation of YAP1. Goto et al. (2018) also showed that YAP1/TAZ activation in chondrogenesis can inhibit chondrocyte differentiation and maturation, leading to chondrodysplasia through a mechanism in which the activation of YAP1 or TAZ leads to decreased Sox9 expression. These findings suggest that YAP1 overexpression may play a role in the pathophysiology of OA by inhibiting chondrocyte differentiation.

Downregulation of YAP1 Favors the Maintenance of Chondrocyte Phenotype in OA

When cartilage tissue is chronically degenerated or acutely damaged, its self-repair ability is poor, and there is little possibility of self-recovery (Buckwalter and Mankin, 1998), which ultimately leads to the occurrence of OA. The transplantation of chondrocyte biomaterials is a commonly used method to reconstruct cartilage tissue (Brittberg, 2010). However, when cultured *in vitro*, chondrocytes often fail to maintain their phenotypic stability and lose SOX9 and cartilage-specific marker expression (type II collagen and aggrecan) (Schnabel et al., 2002; Goessler et al., 2004, 2005; De Croos et al., 2006), which is not conducive to cartilage tissue reconstruction. However, promoting the maintenance of the cartilage phenotype and inducing the re-expression of cartilage-specific markers to ensure the regeneration of cartilage tissue with biochemical and mechanical functions remains a difficult challenge.

Interestingly, Zhong et al. (2013a) reported for the first time that downregulation of YAP1 expression was associated with maintenance of chondrogenic phenotype *in vitro*. In his study, high type I collagen expression in chondrocytes was observed to be accompanied by the YAP1 aggregation in the nucleus, while type II collagen expression was accompanied by the cytoplasmic localization of YAP1 (Zhong et al., 2013a). Chondrocytes are well-recognized stiffness-sensitive cells, and

the establishment of an appropriate physical microenvironment of the extracellular matrix plays an important role in maintaining the chondrogenic lineage. The culturing of chondrocytes on a stiff matrix accelerates the loss of the differentiation phenotype, which appears to be well maintained on a softer matrix (Schuh et al., 2010; Allen et al., 2012). However, when YAP1/TAZ was depleted, both the proliferation rate of chondrocytes cultured on hard substrates and the expression levels of chondrogenic markers behaved as if the chondrocytes had been cultured on soft substrates (Zhong et al., 2013a). Therefore, inhibiting YAP1 in chondrocytes is beneficial to maintain the chondrocyte phenotype. In the absence of YAP1, chondrocytes can maintain their phenotype on stiff substrates. G-protein coupled receptor (GPCR) and its downstream Rho GTPase can activate YAP1/TAZ (Miller et al., 2012; Yu et al., 2012). Cell adhesion to matrix induces YAP1 localization into nucleus by activating Rho GTPase or FAK-SRC-PI3K pathway (Zhao et al., 2012). Interfering with the formation of F-actin blocked the effect of extracellular matrix on nuclear localization of YAP1. Rho GTPase and F-actin microfilaments play an important role in the regulation of YAP1/TAZ by mechanical environment. The mechanical environment includes intercellular contact, matrix adhesion, extracellular matrix hardness, basal area, etc. YAP1 has been noted to be affected by fluid shear stress in MSCs and chondrocytes, and the maintenance of the primary chondrocyte phenotype is associated with the exclusion of YAP1 from the nucleus, which may involve mechanical and cytoskeletal cues or the Hippo pathway (Zhong et al., 2013b). A recent study (Zhang et al., 2020) also observed a corresponding increase in YAP1 nuclear expression in cartilage matrix stiffness and the expression of CTGF, the most highly characteristic YAP1 target, in OA patients compared with that observed in normal patients. Finally, it was concluded that a substrate with a similar physiological hardness partially contributes to the maintenance of the chondrocyte phenotype *in vitro* through YAP1 cytoplasmic retention (Zhang et al., 2020). In summary, downregulation of YAP1 levels contributes to the maintenance of the chondrocyte phenotype, which may be associated with YAP1 mediating mechanical cues. Therefore, the phenotype of chondrocytes can be regulated by fine-tuning the expression of YAP1 to obtain the best conditions for cell implantation and facilitate the reconstruction of cartilage tissue.

In summary, YAP1 is an important promoter of OA and regulates the differentiation and phenotypic maintenance of chondrocytes in OA. More research should focus on the *in vivo* studies of YAP1 in patients with OA, which will help to apply YAP1 in the clinical treatment of OA. The specific signaling pathways of YAP1 promoting the occurrence and development of OA are shown in **Figure 2**.

ROLE OF YAP1 IN OP

OP is a systemic metabolic bone disease characterized by reduced bone mass and degenerative changes in bone microstructure, resulting in increased bone fragility and fracture prone (Kendler, 2011; Siris et al., 2014). OP is a major threat to the health of women and the elderly, even leading to paralysis, and it has become a chronic disease that seriously affects the health of the middle-aged and elderly population (Lin et al., 2015; Miller, 2016; Kanis et al., 2019). The Hippo signaling pathway regulates the physiological activities of osteoblasts, osteoclasts, chondrocytes and other cells through a molecular regulatory network composed of the core molecule YAP1/TAZ. Disruption of the balance of environmental or other signaling molecules causes abnormal bone metabolism and leads to bone metabolic diseases such as OP. The role of YAP1 in OP is briefly discussed below.

Regulation of the Osteogenic Differentiation of MSCs

Adipogenesis and osteogenesis are mutually exclusive processes during MSC differentiation, and the proper balance between these processes is key to maintaining the balance of the bone marrow environment (Chen et al., 2016). Once this precisely regulated balance is disrupted, various metabolic-related diseases, including OP, may develop. Osteoinductive factors such as Runx2 have been demonstrated to inhibit adipogenesis, while peroxisome proliferator-activated receptor γ (PPARγ) stimulates adipogenesis and inhibits osteogenesis (Ge et al., 2016). Runx2 and PPARγ are subtly regulated to determine the alternating cell fate of MSCs (Fakhry et al., 2013). Other studies have also identified YAP1/TAZ as a major regulator of cell fate that promotes osteogenesis and adipogenesis in MSCs (Hong et al., 2005; Tang and Weiss, 2017). Zhong et al. (2013b) observed that with the increase of the intensity of hydrodynamic stimulation, the expression of YAP1 increased in the nucleus, which promoted the osteogenesis of MSCs, inhibited their adipogenic differentiation, and led to the dedifferentiation of chondrocytes. Another study observed that YAP1 could bind to RUNX2 and PPARγ in the nucleus, promote osteogenic differentiation of MSCs, inhibiting adipogenic differentiation and that the degree of osteogenic differentiation was positively correlated with cytoskeletal density (Pan et al., 2017). Moreover, YAP1/TAZ can reverse MMP14-induced bone loss (Tang et al., 2013).

YAP1/TAZ has recently been recognized as a key regulator that promotes osteogenesis and inhibits adipogenesis through the Smad4 or β-catenin signaling pathways to maintain mouse bone homeostasis (Pan et al., 2018; Jia et al., 2019; Park et al., 2019). Pan et al. (2018) elucidated the underlying mechanism by which YAP1 regulates bone homeostasis. Through *in vivo* studies and cell culture experiments, they found that YAP1 is necessary to promote the proliferation and differentiation of mouse OB-lineage cells and to inhibit the adipogenic potential of MSCs, thereby maintaining the quality of trabecular bone. They also showed that YAP1 is required in OB-lineage cells to maintain cytoplasmic and nuclear pools of β-catenin (Pan et al., 2018). The same conclusion was reached in another study on human MSCs (Lorthongpanich et al., 2019). Studies have shown that (1) the level of YAP1 expression during human MSC differentiation is crucial for adipogenic osteogenic differentiation; (2) the ability of osteoblasts to differentiate can be enhanced by increased YAP1 levels (through drug treatment or genetic manipulation)

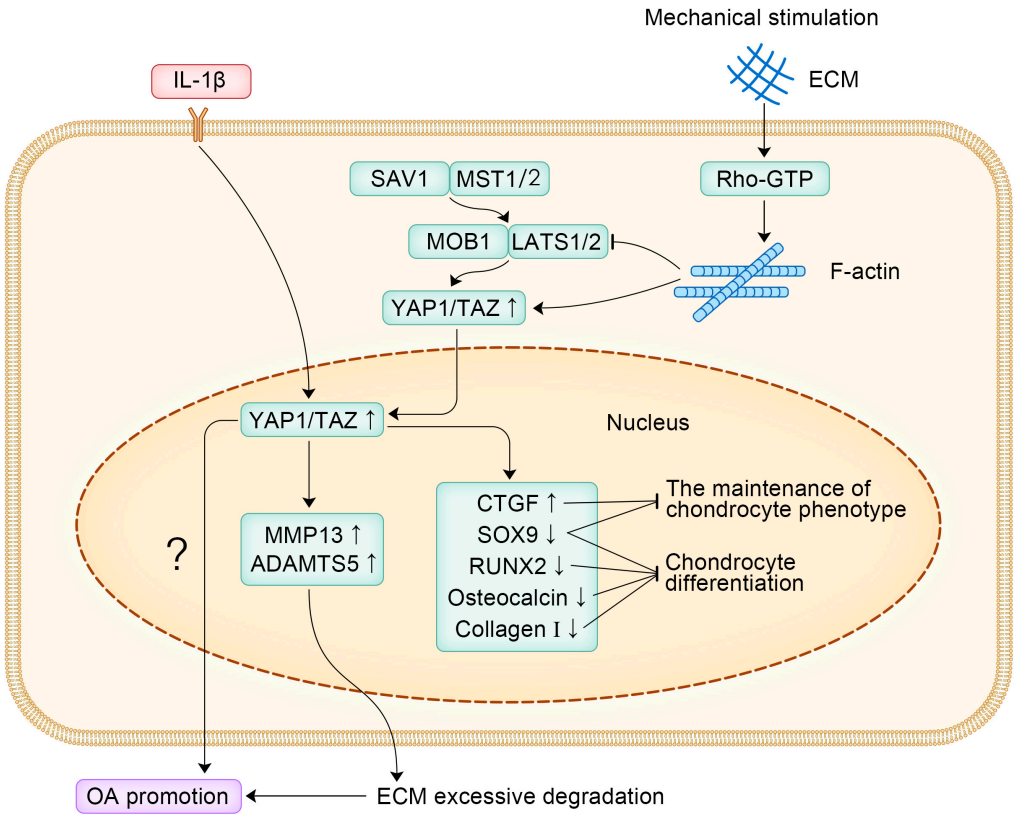


FIGURE 2 | The specific signaling pathways of YAP1 promoting the occurrence and development of OA.

and inhibit their differentiation into adipocytes, even if the cells are cultured in a cytokine-rich medium capable of promoting and supporting adipogenic differentiation; and (3) low YAP1 levels promotes adipogenic differentiation but inhibits osteogenic differentiation (Lorthongpanich et al., 2019). Consistent with these findings, Guo et al. (2018) also observed that in hMSCs lacking kindlin-2, YAP1 or TAZ overexpression largely restored the ability of MSCs to differentiate into osteocytes and reversed adipogenic differentiation caused by kindlin-2 deletion. Kindlin-2 is essential for regulating the osteogenic differentiation of MSCs, which increases during osteogenic differentiation and decreases during adipogenic differentiation. The regulatory role of YAP1/TAZ in the osteogenic and adipogenic differentiation of MSCs is shown in **Figure 3**. YAP1 regulates the balance between the adipogenic and osteogenic differentiation of MSCs and is expected to be a potential target for therapeutic intervention in OP, but additional studies are still needed to elucidate the specific mechanism by which YAP1 directs the fate of MSCs.

Role of YAP1 in Mediating the Ability of Other Substances to Play Potential Therapeutic Roles in OP

In addition to regulating the osteogenic differentiation of MSCs, YAP1 can also mediate the ability of other substances (genes, proteins, etc.) to play a role in the treatment of OP. In the rat model of disuse osteoporosis (DOP), exosomes derived from human umbilical cord mesenchymal stem cells (HUCMSC-Exos) can reduce the apoptosis of MSCs in DOP rats through the miR-1263/Mob1/Hippo signaling pathway (Yang et al., 2020). The specific mechanism involves the miR-1263-mediated inhibition of Mob1 expression, which activates YAP1 and inhibits apoptosis. In the ovariectomized osteoporosis nude mouse model, YAP1 can mediate the therapeutic effect of melatonin toward OP, while the YAP1 inhibitor VP can attenuate the therapeutic effect of melatonin against OP (Wang et al., 2019). Another study showed that myocardin-related transcription factors (MRTFs) can regulate the balance between the adipogenic and osteogenic differentiation of MSCs, which promotes the osteogenic activity of YAP1/TAZ by maintaining the production of smooth muscle actin (SMA) in MSCs (Bian et al., 2016). Therefore, MRTF can be considered to be a novel regulator of bone homeostasis and may be a potential target for the therapeutic intervention of OP. Adequate vitamin D is important to ensure the effective prevention and treatment of OP, but vitamin D supplementation alone cannot promote calcium absorption, as it requires vitamin D receptor (VDR) to promote its biological effects (Fleet and Schoch, 2010; Shang and Sun, 2017). Recent *in vitro* studies have shown that propionic acid promotes VDR expression by activating YAP1 (Lin et al., 2020), which may be a potential pharmacological strategy for the treatment of OP.

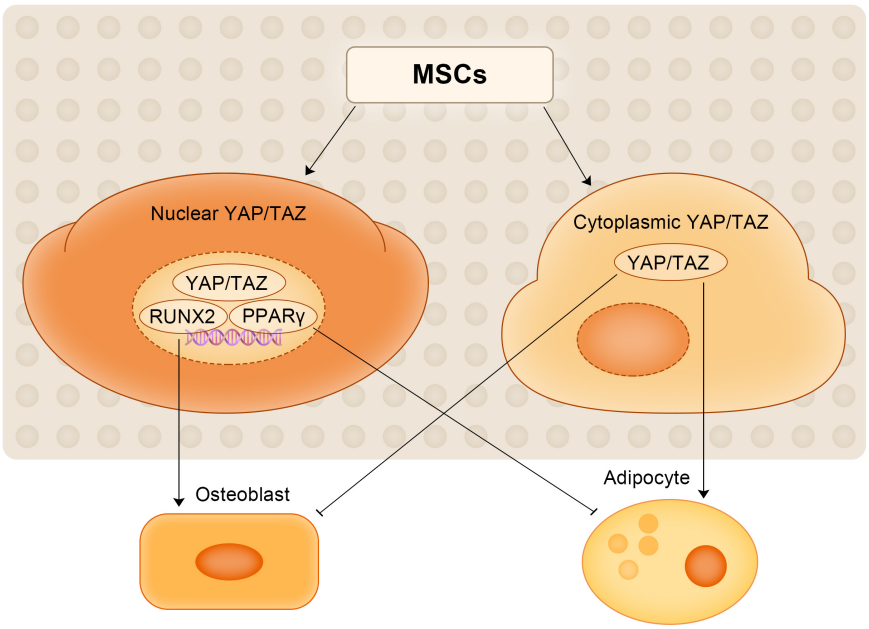


FIGURE 3 | The regulatory role of YAP1/TAZ in the osteogenic and adipogenic differentiation of MSCs.

Mechanical signals play a key role in bone growth and homeostasis (Yuan et al., 2017; Miyazaki et al., 2019). Mechanical stimulation increases bone mass by stimulating the activity and production of osteoblasts (Klein-Nulend et al., 2012; Meakin et al., 2014), and YAP1 is considered to be a mediator of mechanical signaling responses in a variety of cell types (Dupont et al., 2011; Hansen et al., 2015). Recent studies have shown that Piezo1 is a mechanically sensitive ion channel that is highly expressed in osteocytes, and its expression and activity are increased under the action of fluid shear stress (Li et al., 2019). Studies have shown that Piezo channels work through Ca2+ signaling pathways (He et al., 2018). The opening of the Piezo channels can lead to Ca2+ entry into cells, which may trigger intracellular Ca2+ signaling pathways and act as a differentiation regulator (Pathak et al., 2014). YAP1 and TAZ are necessary for WNT1 stimulation by fluids or Yoda1 (a Piezo1 agonist), demonstrating that mechanical activation of Piezo1 stimulates WNT1 expression in osteocytes, at least in part, by activating YAP1 and TAZ (Li et al., 2019). YAP1 can exert biological effects in OP by mediating the activities of other substances (genes, proteins, etc.), and other YAP1-mediated pathways, including the Piezo1-YAP1 pathway, may be a potential method to treat OP.

Role of YAP1 in OBs and OCs Activity

The normal metabolism of bone tissue depends on the dynamic balance of OBs and OCs, which is also the basis for maintaining normal bone remodeling processes. Bone reconstruction includes the OC-mediated removal of old or damaged bone (bone resorption) and the subsequent replacement of new bone formed by OBs (bone formation) (Chen et al., 2018). OP occurs when bone formation by OBs is insufficient to combat the bone remodeling by OCs. YAP1 has been shown to play an important role in OBs and OCs.

OBs are bone-forming cells derived from mesenchymal stem cells. Kegelman et al. (2018) established a *YAP1/TAZ* gene knockout mouse model and confirmed the synergistic effect of YAP1 and TAZ at the gene level, which were shown to promote bone development by regulating the activity of OBs and the generation of OCs. However, after an individual is born, YAP1/YAZ exhibits a more complex regulatory mechanism for the OB lineage. Xiong et al. (2018) observed that YAP1/YAZ inhibits the differentiation of OB precursor cells and inhibits the transcriptional activity of RUNX2 to some extent, whereas in mature OBs and osteocytes, YAP1/YAZ promoted bone formation and inhibited bone resorption. Therefore, the regulation of OB by YAP1/TAZ is closely associated with the developmental stage of individuals and the differentiation state of cells. OC is the terminal differentiated cell of hematopoietic stem cells (HSCs) stimulated by receptor activator of nuclear factor-kappa B ligand (RANKL), which is prone to promote OP when its activity is too high (Novack and Teitelbaum, 2008). In osteoclasts, RANKL acts with cytokines in the cytoplasm to phosphorylate downstream protein kinase B (PKB/AKT) and promote osteoclastogenesis (Okamoto et al., 2017). At the same time, the effector molecule YAP1 can induce AKT phosphorylation (Jiang et al., 2017), suggesting that YAP1 may promote osteoclast formation. When YAP1 activity is inhibited by verteporfin, a small molecule drug that prevents YAP1 from binding to the TEAD domain, osteoclast formation would also be inhibited, and OC generation and bone resorption activity are inversely correlated with drug dose (Liu-Chittenden et al., 2012; Zhao et al., 2018). And as a response to mechanical stimulation, Piezo1 in osteoblasts promotes the expression of

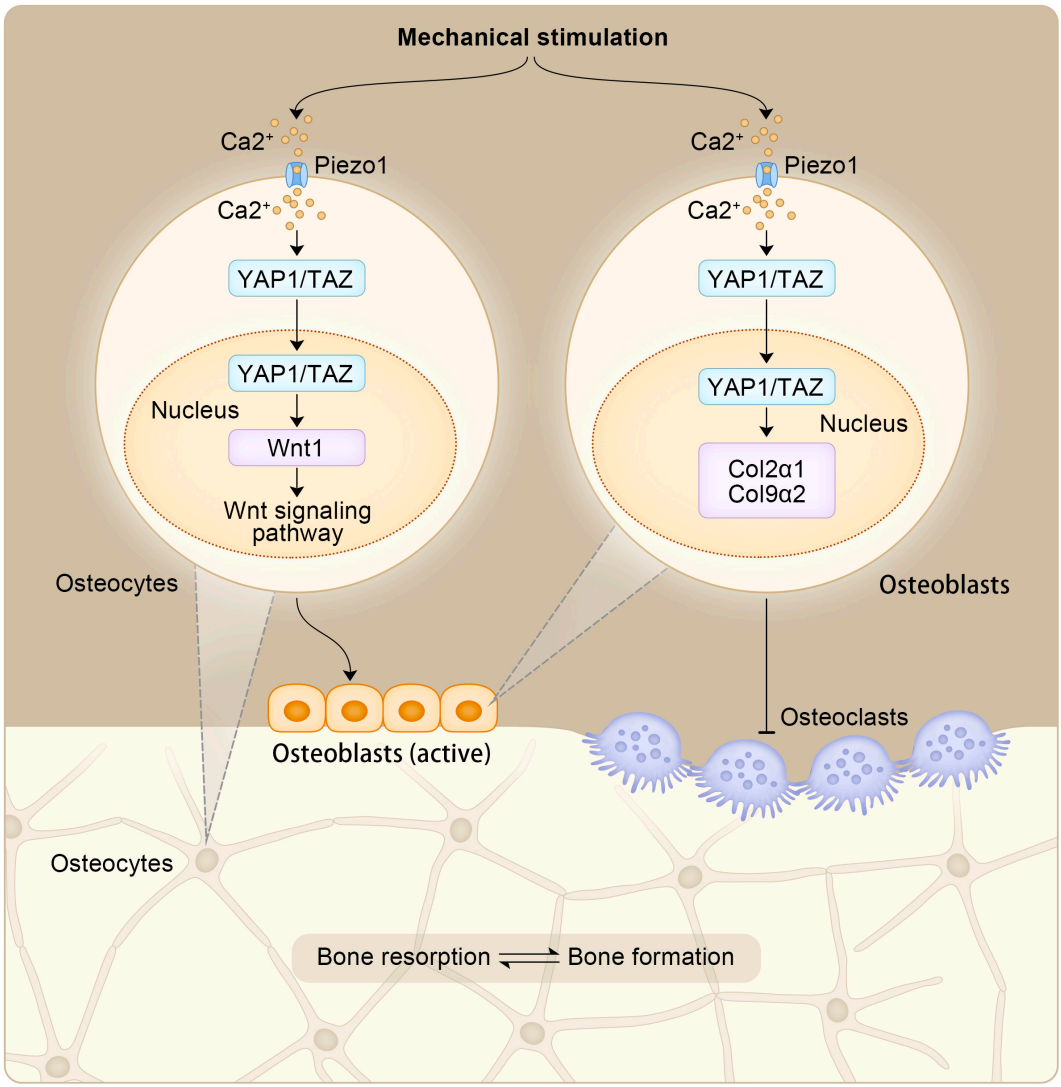


FIGURE 4 | The effects of Piezo1 mediated mechanical stimulation in OB and OC.

COL2α1 and COL9α2 in osteoblast cell lines through YAP1. In turn, these collagen isoforms regulate OC differentiation (Wang et al., 2020). Moreover, in osteocytes, increased Wnt1 expression resulting from Piezo1 mediated mechanical stimulation through YAP1/TAZ can activate the Wnt signaling pathway, which stimulates OBs to form new bone (Li et al., 2019). YAP1 can play a role in the occurrence and development of OP by regulating the activity of OB and promoting the generation of OC, and its role in OB and OC can also provide new ideas for the treatment of OP. The effects of Piezo1 mediated mechanical stimulation in OB and OC is shown in **Figure 4**.

In summary, the role of YAP1 in OP is to regulate the osteogenic differentiation of MSCs, mediate the ability of other substances (genes, proteins, etc.) to play a potential therapeutic role in OP, regulate the activity of OBs and promote the generation of OCs. More research should be focused on how to regulate the expression of the YAP1 gene and YAP1 activity to treat and prevent OP. The role of YAP1 in different cell types is shown in **Table 1**.

Targeting YAP1 in Orthopedic Degenerative Diseases (OA and OP)

Since YAP1 is a promoter in the development of OA, and downregulation of YAP1 contributes to chondrocyte differentiation and the maintenance of the chondrocyte phenotype in OA, the downregulation of YAP1 activity may be an effective way to treat OA. Interestingly, commonly used anti-OA drugs can inhibit YAP1 expression in different ways in OA mouse models, including paracetamol, diacerein, 99Tc-MDP, DSG, O3, vitamin C, and rapamycin (Zhang et al., 2019). Verteporfin, an inhibitor of YAP1, is also a good choice, as it can disrupt the YAP1-TEAD interaction and thereby inhibit YAP1 activity (Brodowska et al., 2014). Studies have shown that

TABLE 1 | The role of YAP1 in different cell types.

Model	Function	References
Human articular chondrocytes	The number of nuclear YAP1-expressing cells in OA cartilage is significantly higher than that detected in normal cartilage	Zhang et al., 2020
Human MSCs	YAP1 is a negative regulator of chondrogenesis in mesenchymal stem cells	Karystinou et al., 2015
Mouse MSCs	YAP1 promotes early chondrocyte proliferation by regulating SOX6 expression	Ying et al., 2018
ATDC5 cell line	YAP1 negatively regulates chondrocyte differentiation by activating the β-catenin signaling pathway	Yang et al., 2017
Mouse articular chondrocytes	The downregulation of YAP1 expression is associated with maintenance of chondrogenic phenotype *in vitro*	Zhong et al., 2013a
Mouse MSCs and articular chondrocytes	The maintenance of the primary chondrocyte phenotype is associated with the exclusion of YAP1 from the nucleus; the increased expression of YAP1 in the nucleus promotes the osteogenic effects of MSCs, inhibits their adipogenic differentiation, and leads to dedifferentiation of chondrocytes	Zhong et al., 2013b
Mouse embryonic fibroblasts and primary MSCs	YAP1/TAZ is the major regulator of cell fate that promotes osteogenesis and adipogenesis in MSCs	Hong et al., 2005
Mouse MSCs	YAP1 can bind to RUNX2 and PPARγ in the nucleus to promote osteogenic differentiation of MSCs and inhibit their adipogenic differentiation	Pan et al., 2017
Human MSCs	Low YAP1 levels promotes adipogenic differentiation but inhibits osteogenic differentiation	Lorthongpanich et al., 2019
Human MSCs	YAP1 or TAZ overexpression largely restores the ability of MSCs to differentiate into osteocytes and reverses adipogenic differentiation caused by kindlin-2 deletion.	Guo et al., 2018
Mouse MSCs	The increased expression of YAP1 in the nucleus promotes the osteogenesis of MSCs, inhibits their adipogenic differentiation, and leads to dedifferentiation of chondrocytes	Bian et al., 2016
Mouse osteoblast	The regulation of OB by YAP1/TAZ is closely associated with the developmental stage of individuals and the differentiation state of cells	Xiong et al., 2018
Mouse osteoblast	Piezo1 in osteoblasts promotes the expression of COL2α1 and COL9α2 in osteoblast cell lines through YAP1	Wang et al., 2020
Mouse osteoclast	YAP1 is an essential regulator for osteoclast differentiation and activity	Zhao et al., 2018

the intra-articular injection of verteporfin, a selective inhibitor of YAP1, can significantly maintain cartilage homeostasis in a mouse OA model and that a sustained-release system consisting of chitosan microspheres and verteporfin has significant anti-OA effects (Zhang et al., 2020). Another YAP1 activity inhibitor, dasatinib, can also perform a similar function (Nie et al., 2019). Dasatinib can significantly inhibit YAP1 expression, promote cartilage differentiation and repair cartilage defects. Furthermore, its effect is more significant in the sustained release system composed with GelMA hydrogel. In addition to drug inhibition, YAP1 activity can also be inhibited at the gene level. SiRNA can activate RNA interference to specifically achieve mRNA degradation by complementary binding sequences with target mRNAs (Setten et al., 2019). Inhibition of *YAP1* by *YAP1* siRNA can reduce cartilage damage and chondrocyte apoptosis as well as reduce abnormal subchondral bone formation (Gong et al., 2019). Since the WW domain is essential for YAP1 to regulate biological processes such as apoptosis and autophagy (Chen et al., 2019), the activity of YAP1 may also be inhibited to some extent by deleting the WW domain.

Because YAP1 can regulate the osteogenic differentiation of MSCs and mediate the ability of a variety of substances to play a potential therapeutic role in OP, the upregulation of YAP1 activity has a positive effect on the treatment of OP. From this point of view, some YAP1 agonists may have great application prospects in the treatment of OP. The transcription factor IRF3 is a YAP1 agonist that can interact with YAP1 and TEAD4 in the nucleus to enhance their interaction and promote the nuclear translocation and activation of YAP1 (Jiao et al., 2018). Because the stimulation of glucocorticoid receptor (GR) can lead to increased protein levels and nuclear accumulation of YAP1 and promote its transcriptional activity *in vitro* and *in vivo*, glucocorticoids (GCs) can also act as YAP1 agonists (Sorrentino et al., 2017). In addition, ethacridine can also activate YAP1 and enhance TEAD-responsive reporter activity in the presence of YAP1 (Kawano et al., 2015). However, none of these YAP1 agonists have been studied in OP, and their efficacy against OP remains unknown. In addition to YAP1 agonists, YAP1 can also mediate the therapeutic effects of the genes or proteins mentioned above in OP (Bian et al., 2016; Li et al., 2019; Wang et al., 2019; Lin et al., 2020; Yang et al., 2020).

Therefore, interfering with the activity of YAP1 through drug inhibition or the modification of gene expression is a promising method for the treatment of OA, which can provide a reference for treatment strategies of OA. In OP, upregulation of YAP1 activity by YAP1 agonists or through the biological

effects of other substances mediated by YAP1 also appear to be an effective therapeutic option worthy of further study. However, there are still many problems for YAP1 to become a potential disease-modifying OA drug (DMOAD), such as the selection of the optimal dose, the determination of treatment course and withdrawal indication, whether YAP1 can be combined with other DMOADs, etc.

CONCLUSION

Aging alters the integrity of cells, tissues and systems, which results in a decrease in the function of the muscular system of bones and joints, this change increases the risk of developing degenerative diseases in orthopedics. However, the occurrence and development of orthopedic degenerative diseases is not an inevitable process, and if appropriate measures are taken, it is possible to restore the function of middle-aged and elderly patients. To date, there is no satisfactory drug or treatment for orthopedic degenerative diseases such as OA and OP. YAP1 has the functions of promoting cell proliferation, inhibiting cell apoptosis and maintaining the multidirectional differentiation potential of stem cells, and it has unique prospects in OA and OP. On the one hand, YAP1 is an important promoter of OA, and its high expression inhibits chondrocyte differentiation in OA, whereas its downregulation is beneficial to the maintenance of chondrocyte phenotype in OA. On the other hand, YAP1 in OP can regulate the osteogenic differentiation of MSCs and can mediate other substances (genes, proteins, etc.) to play a potential therapeutic role in OP, as well as regulate the activity of OBs and promote the generation of OCs. Therefore, the regulation of YAP1 activity through various means is expected to become a promising intervention strategy to delay the occurrence and development of orthopedic degenerative diseases. Although some progress has been made in the research of YAP1 in orthopedic degenerative diseases, many mechanisms associated with its effects remain unclear, and additional research and clinical trials are needed to elucidate the specific role of YAP1 in orthopedic degenerative diseases (such as OA and OP).

AUTHOR CONTRIBUTIONS

WQX and WFX conceptualized this review, decided on the content, and wrote the manuscript. KT prepared the figures. LZ and YL revised this review. All authors approved the final version of the manuscript and agreed to be accountable for all aspects of the work.

FUNDING

This review was supported by the National Key R&D Program of China (2019YFA0111900), the National Natural Science Foundation of China (Nos. 81874030 and 81902253), the Provincial Natural Science Foundation of Hunan (No. 2020JJ3060), the Innovation-Driven Project of Central South University (No. 2020CX045), the Undergraduate Innovation Training Program of Central South University (Nos. XCX20190545 and XCX20190606), the Key program of Health Commission of Hunan Province (No. 20201902), and the CMA·Young and Middle-aged Doctors Outstanding Development Program–Osteoporosis Specialized Scientific Research Fund Project (No. G-X-2019-1107-12).

REFERENCES

Allen, J. L., Cooke, M. E., and Alliston, T. (2012). ECM stiffness primes the TGFbeta pathway to promote chondrocyte differentiation. *Mol. Biol. Cell* 23, 3731–3742. doi: 10.1091/mbc.e12-03-0172

An, L., Nie, P., Chen, M., Tang, Y., Zhang, H., Guan, J., et al. (2020). MST4 kinase suppresses gastric tumorigenesis by limiting YAP activation via a non-canonical pathway. *J. Exp. Med.* 217:e20191817. doi: 10.1084/jem.20191817

Bian, H., Lin, J. Z., Li, C., and Farmer, S. R. (2016). Myocardin-related transcription factor A (MRTFA) regulates the fate of bone marrow mesenchymal stem cells and its absence in mice leads to osteopenia. *Mol. Metab.* 5, 970–979. doi: 10.1016/j.molmet.2016.08.012

Bisso, A., Filipuzzi, M., Gamarra Figueroa, G. P., Brumana, G., Biagioni, F., Doni, M., et al. (2020). Cooperation between MYC and β-catenin in liver tumorigenesis requires Yap/Taz. *Hepatology* doi: 10.1002/hep.31120 [Epub ahead of print].

Brittberg, M. (2010). Cell carriers as the next generation of cell therapy for cartilage repair: a review of the matrix-induced autologous chondrocyte implantation procedure. *Am. J. Sports Med.* 38, 1259–1271. doi: 10.1177/0363546509346395

Brodowska, K., Al-Moujahed, A., Marmalidou, A., Meyer Zu Horste, M., Cichy, J., Miller, J. W., et al. (2014). The clinically used photosensitizer Verteporfin (VP) inhibits YAP-TEAD and human retinoblastoma cell growth in vitro without light activation. *Exp. Eye Res.* 124, 67–73. doi: 10.1016/j.exer.2014.04.011

Buckwalter, J. A., and Mankin, H. J. (1998). Articular cartilage: degeneration and osteoarthritis, repair, regeneration, and transplantation. *Instr. Course Lect.* 47, 487–504.

Chen, Q., Shou, P., Zheng, C., Jiang, M., Cao, G., Yang, Q., et al. (2016). Fate decision of mesenchymal stem cells: adipocytes or osteoblasts? *Cell Death Differ.* 23, 1128–1139. doi: 10.1038/cdd.2015.168

Chen, X., Wang, Z., Duan, N., Zhu, G., Schwarz, E. M., and Xie, C. (2018). Osteoblast-osteoclast interactions. *Connect. Tissue Res.* 59, 99–107. doi: 10.1080/03008207.2017.1290085

Chen, Y. A., Lu, C. Y., Cheng, T. Y., Pan, S. H., Chen, H. F., and Chang, N. S. (2019). WW domain-containing proteins YAP and TAZ in the hippo pathway as key regulators in stemness maintenance, tissue homeostasis, and tumorigenesis. *Front. Oncol.* 9:60. doi: 10.3389/fonc.2019.00060

Clynes, M. A., Harvey, N. C., Curtis, E. M., Fuggle, N. R., Dennison, E. M., and Cooper, C. (2020). The epidemiology of osteoporosis. *Br. Med. Bull.* 133, 105–117. doi: 10.1093/bmb/ldaa005

Cottini, F., Hideshima, T., Xu, C., Sattler, M., Dori, M., Agnelli, L., et al. (2014). Rescue of Hippo coactivator YAP1 triggers DNA damage-induced apoptosis in hematological cancers. *Nat. Med.* 20, 599–606. doi: 10.1038/nm.3562

Darling, E. M., and Athanasiou, K. A. (2005). Rapid phenotypic changes in passaged articular chondrocyte subpopulations. *J. Orthop. Res.* 23, 425–432. doi: 10.1016/j.orthres.2004.08.008

De Croos, J. N., Dhaliwal, S. S., Grynpas, M. D., Pilliar, R. M., and Kandel, R. A. (2006). Cyclic compressive mechanical stimulation induces sequential catabolic and anabolic gene changes in chondrocytes resulting in increased extracellular matrix accumulation. *Matrix Biol.* 25, 323–331. doi: 10.1016/j.matbio.2006.03.005

Deng, Y., Lu, J., Li, W., Wu, A., Zhang, X., Tong, W., et al. (2018). Reciprocal inhibition of YAP/TAZ and NF-κB regulates osteoarthritic cartilage degradation. *Nat. Commun.* 9:4564. doi: 10.1038/s41467-018-07022-2

Deng, Y., Wu, A., Li, P., Li, G., Qin, L., Song, H., et al. (2016). Yap1 regulates multiple steps of chondrocyte differentiation during skeletal development and bone repair. *Cell Rep.* 14, 2224–2237. doi: 10.1016/j.celrep.2016.02.021

Disease, G. B. D., Injury, I., and Prevalence, C. (2017). Global, regional, and national incidence, prevalence, and years lived with disability for 328 diseases and injuries for 195 countries, 1990-2016: a systematic analysis for the Global Burden of Disease Study 2016. *Lancet* 390, 1211–1259. doi: 10.1016/S0140-6736(17)32154-2

Dong, J., Feldmann, G., Huang, J., Wu, S., Zhang, N., Comerford, S. A., et al. (2007). Elucidation of a universal size-control mechanism in *Drosophila* and mammals. *Cell* 130, 1120–1133. doi: 10.1016/j.cell.2007.07.019

Dupont, S., Morsut, L., Aragona, M., Enzo, E., Giulitti, S., Cordenonsi, M., et al. (2011). Role of YAP/TAZ in mechanotransduction. *Nature* 474, 179–183. doi: 10.1038/nature10137

Ehrlich, G. D. (2017). Novel genetic markers for common degenerative orthopedic diseases. *Genet. Test. Mol. Biomarkers* 21:577. doi: 10.1089/gtmb.2017.29036.gde

Fakhry, M., Hamade, E., Badran, B., Buchet, R., and Magne, D. (2013). Molecular mechanisms of mesenchymal stem cell differentiation towards osteoblasts. *World J. Stem Cells* 5, 136–148. doi: 10.4252/wjsc.v5.i4.136

Fleet, J. C., and Schoch, R. D. (2010). Molecular mechanisms for regulation of intestinal calcium absorption by vitamin D and other factors. *Crit. Rev. Clin. Lab. Sci.* 47, 181–195. doi: 10.3109/10408363.2010.536429

Fu, L., Hu, Y., Song, M., Liu, Z., Zhang, W., Yu, F. X., et al. (2019). Up-regulation of FOXD1 by YAP alleviates senescence and osteoarthritis. *PLoS Biol.* 17:e3000201. doi: 10.1371/journal.pbio.3000201

Fujiwara, S. (2016). [Epidemiology of respiratory diseases and osteoporosis.] *Clin. Calcium* 26, 1387–1392.

Gaffney, C. J., Oka, T., Mazack, V., Hilman, D., Gat, U., Muramatsu, T., et al. (2012). Identification, basic characterization and evolutionary analysis of differentially spliced mRNA isoforms of human YAP1 gene. *Gene* 509, 215–222. doi: 10.1016/j.gene.2012.08.025

Ge, C., Cawthorn, W. P., Li, Y., Zhao, G., Macdougald, O. A., and Franceschi, R. T. (2016). Reciprocal control of osteogenic and adipogenic differentiation by ERK/MAP kinase phosphorylation of Runx2 and PPARγ transcription factors. *J. Cell. Physiol.* 231, 587–596. doi: 10.1002/jcp.25102

Glyn-Jones, S., Palmer, A. J., Agricola, R., Price, A. J., Vincent, T. L., Weinans, H., et al. (2015). Osteoarthritis. *Lancet* 386, 376–387. doi: 10.1016/S0140-6736(14)60802-3

Goessler, U. R., Bieback, K., Bugert, P., Naim, R., Schafer, C., Sadick, H., et al. (2005). Human chondrocytes differentially express matrix modulators during in vitro expansion for tissue engineering. *Int. J. Mol. Med.* 16, 509–515.

Goessler, U. R., Bugert, P., Bieback, K., Baisch, A., Sadick, H., Verse, T., et al. (2004). Expression of collagen and fiber-associated proteins in human septal cartilage during in vitro dedifferentiation. *Int. J. Mol. Med.* 14, 1015–1022. doi: 10.3892/ijmm.14.6.1015

Gong, Y., Li, S. J., Liu, R., Zhan, J. F., Tan, C., Fang, Y. F., et al. (2019). Inhibition of YAP with siRNA prevents cartilage degradation and ameliorates osteoarthritis development. *J. Mol. Med.* 97, 103–114. doi: 10.1007/s00109-018-1705-y

Goto, H., Nishio, M., To, Y., Oishi, T., Miyachi, Y., Maehama, T., et al. (2018). Loss of *Mob1a/b* in mice results in chondrodysplasia due to YAP1/TAZ-TEAD-dependent repression of SOX9. *Development* 145:dev159244. doi: 10.1242/dev.159244

Guo, L., Cai, T., Chen, K., Wang, R., Wang, J., Cui, C., et al. (2018). Kindlin-2 regulates mesenchymal stem cell differentiation through control of YAP1/TAZ. *J. Cell Biol.* 217, 1431–1451. doi: 10.1083/jcb.201612177

Hansen, C. G., Moroishi, T., and Guan, K. L. (2015). YAP and TAZ: a nexus for Hippo signaling and beyond. *Trends Cell Biol.* 25, 499–513. doi: 10.1016/j.tcb.2015.05.002

Hawker, G. A. (2019). Osteoarthritis is a serious disease. *Clin. Exp. Rheumatol.* 37(Suppl. 120), 3–6.

He, L., Si, G., Huang, J., Samuel, A. D. T., and Perrimon, N. (2018). Mechanical regulation of stem-cell differentiation by the stretch-activated Piezo channel. *Nature* 555, 103–106. doi: 10.1038/nature25744

Heldens, G. T., Blaney Davidson, E. N., Vitters, E. L., Schreurs, B. W., Piek, E., van den Berg, W. B., et al. (2012). Catabolic factors and osteoarthritis-conditioned medium inhibit chondrogenesis of human mesenchymal stem cells. *Tissue Eng. Part A* 18, 45–54. doi: 10.1089/ten.TEA.2011.0083

Hiligsmann, M., Cooper, C., Arden, N., Boers, M., Branco, J. C., Luisa Brandi, M., et al. (2013). Health economics in the field of osteoarthritis: an expert's consensus paper from the European Society for Clinical and Economic Aspects of Osteoporosis and Osteoarthritis (ESCEO). *Semin. Arthritis Rheum.* 43, 303–313. doi: 10.1016/j.semarthrit.2013.07.003

Hong, J. H., Hwang, E. S., McManus, M. T., Amsterdam, A., Tian, Y., Kalmukova, R., et al. (2005). TAZ, a transcriptional modulator of mesenchymal stem cell differentiation. *Science* 309, 1074–1078. doi: 10.1126/science.1110955

Hong, W., and Guan, K. L. (2012). The YAP and TAZ transcription co-activators: key downstream effectors of the mammalian Hippo pathway. *Semin. Cell Dev. Biol.* 23, 785–793. doi: 10.1016/j.semcdb.2012.05.004

Huang, J., Wu, S., Barrera, J., Matthews, K., and Pan, D. (2005). The Hippo signaling pathway coordinately regulates cell proliferation and apoptosis by inactivating Yorkie, the *Drosophila* Homolog of YAP. *Cell* 122, 421–434. doi: 10.1016/j.cell.2005.06.007

Huang, Z., Wang, Y., Hu, G., Zhou, J., Mei, L., and Xiong, W. C. (2016). YAP is a critical inducer of SOCS3, preventing reactive astrogliosis. *Cereb. Cortex* 26, 2299–2310. doi: 10.1093/cercor/bhv292

Hwang, J. H., Han, U., Yang, M., Choi, Y., Choi, J., Lee, J. M., et al. (2019). Artificial cellular nano-environment composed of collagen-based nanofilm promotes osteogenic differentiation of mesenchymal stem cells. *Acta Biomater.* 86, 247–256. doi: 10.1016/j.actbio.2018.12.044

Jia, L., Zhang, Y., Ji, Y., Xiong, Y., Zhang, W., Wen, Y., et al. (2019). YAP balances the osteogenic and adipogenic differentiation of hPDLSCs in vitro partly through the Wnt/β-catenin signaling pathway. *Biochem. Biophys. Res. Commun.* 518, 154–160. doi: 10.1016/j.bbrc.2019.08.024

Jiang, J., Chang, W., Fu, Y., Gao, Y., Zhao, C., Zhang, X., et al. (2017). SAV1 represses the development of human colorectal cancer by regulating the Akt-mTOR pathway in a YAP-dependent manner. *Cell Prolif.* 50:e12351. doi: 10.1111/cpr.12351

Jiao, S., Guan, J., Chen, M., Wang, W., Li, C., Wang, Y., et al. (2018). Targeting IRF3 as a YAP agonist therapy against gastric cancer. *J. Exp. Med.* 215, 699–718. doi: 10.1084/jem.20171116

Jung, K. H., McCarthy, R. L., Zhou, C., Uprety, N., Barton, M. C., and Beretta, L. (2016). MicroRNA regulates hepatocytic differentiation of progenitor cells by targeting YAP1. *Stem Cells* 34, 1284–1296. doi: 10.1002/stem.2283

Kania, K., Colella, F., Riemen, A. H. K., Wang, H., Howard, K. A., Aigner, T., et al. (2020). Regulation of *Gdf5* expression in joint remodelling, repair and osteoarthritis. *Sci. Rep.* 10:157. doi: 10.1038/s41598-019-57011-8

Kanis, J. A., Cooper, C., Rizzoli, R., Reginster, J. Y., and Scientific Advisory Board of the European Society for Clinical and Economic Aspects of Osteoporosis (2019). European guidance for the diagnosis and management of osteoporosis in postmenopausal women. *Osteoporos. Int.* 30, 3–44. doi: 10.1007/s00198-018-4704-5

Karystinou, A., Roelofs, A. J., Neve, A., Cantatore, F. P., Wackerhage, H., and De Bari, C. (2015). Yes-associated protein (YAP) is a negative regulator of chondrogenesis in mesenchymal stem cells. *Arthritis Res. Ther.* 17:147. doi: 10.1186/s13075-015-0639-9

Kawano, S., Maruyama, J., Nagashima, S., Inami, K., Qiu, W., Iwasa, H., et al. (2015). A cell-based screening for TAZ activators identifies ethacridine, a widely used antiseptic and abortifacient, as a compound that promotes dephosphorylation of TAZ and inhibits adipogenesis in C3H10T1/2 cells. *J. Biochem.* 158, 413–423. doi: 10.1093/jb/mvv051

Kegelman, C. D., Mason, D. E., Dawahare, J. H., Horan, D. J., Vigil, G. D., Howard, S. S., et al. (2018). Skeletal cell YAP and TAZ combinatorially promote bone development. *FASEB J.* 32, 2706–2721. doi: 10.1096/fj.201700872R

Kendler, D. (2011). Osteoporosis: therapies now and in the future. *Climacteric* 14, 604–605.

Klein-Nulend, J., Bacabac, R. G., and Bakker, A. D. (2012). Mechanical loading and how it affects bone cells: the role of the osteocyte cytoskeleton in maintaining our skeleton. *Eur. Cell Mater.* 24, 278–291. doi: 10.22203/ecm.v024a20

Kodaka, M., and Hata, Y. (2015). The mammalian Hippo pathway: regulation and function of YAP1 and TAZ. *Cell. Mol. Life Sci.* 72, 285–306. doi: 10.1007/s00018-014-1742-9

Li, B., and Chen, D. (2019). Degenerative musculoskeletal diseases: pathology and treatments. *J. Orthop. Translat.* 17, 1–2. doi: 10.1016/j.jot.2019.05.001

Li, X., Han, L., Nookaew, I., Mannen, E., Silva, M. J., Almeida, M., et al. (2019). Stimulation of Piezo1 by mechanical signals promotes bone anabolism. *eLife* 8:e49631. doi: 10.7554/eLife.49631

Lin, H., Huang, Y., Tian, T., Wang, P., and Li, Y. (2020). Propionate promotes vitamin D receptor expression via yes-associated protein in rats with short bowel syndrome. *Biochem. Biophys. Res. Commun.* 523, 645–650. doi: 10.1016/j.bbrc.2019.12.127

Lin, X., Xiong, D., Peng, Y. Q., Sheng, Z. F., Wu, X. Y., Wu, X. P., et al. (2015). Epidemiology and management of osteoporosis in the People's Republic of China: current perspectives. *Clin. Interv. Aging* 10, 1017–1033. doi: 10.2147/CIA.S54613

Little, C. B., Barai, A., Burkhardt, D., Smith, S. M., Fosang, A. J., Werb, Z., et al. (2009). Matrix metalloproteinase 13-deficient mice are resistant to osteoarthritic cartilage erosion but not chondrocyte hypertrophy or osteophyte development. *Arthritis Rheum.* 60, 3723–3733. doi: 10.1002/art.25002

Liu-Chittenden, Y., Huang, B., Shim, J. S., Chen, Q., Lee, S. J., Anders, R. A., et al. (2012). Genetic and pharmacological disruption of the TEAD-YAP complex suppresses the oncogenic activity of YAP. *Genes Dev.* 26, 1300–1305. doi: 10.1101/gad.192856.112

Lorthongpanich, C., Thumanu, K., Tangkiettrakul, K., Jiamvoraphong, N., Laowtammathron, C., Damkham, N., et al. (2019). YAP as a key regulator of adipo-osteogenic differentiation in human MSCs. *Stem Cell Res. Ther.* 10:402. doi: 10.1186/s13287-019-1494-4

Low, B. C., Pan, C. Q., Shivashankar, G. V., Bershadsky, A., Sudol, M., and Sheetz, M. (2014). YAP/TAZ as mechanosensors and mechanotransducers in regulating organ size and tumor growth. *FEBS Lett.* 588, 2663–2670. doi: 10.1016/j.febslet.2014.04.012

Luo, C., Balsa, E., Perry, E. A., Liang, J., Tavares, C. D., Vazquez, F., et al. (2020). H3K27me3-mediated PGC1α gene silencing promotes melanoma invasion through WNT5A and YAP. *J. Clin. Invest.* 130, 853–862. doi: 10.1172/jci130038

Luo, H., Yao, L., Zhang, Y., and Li, R. (2017). Liquid chromatography-mass spectrometry-based quantitative proteomics analysis reveals chondroprotective effects of astragaloside IV in interleukin-1β-induced SW1353 chondrocyte-like cells. *Biomed. Pharmacother.* 91, 796–802. doi: 10.1016/j.biopha.2017.04.127

Ma, F., Li, G., Yu, Y., Xu, J., and Wu, X. (2019). MiR-33b-3p promotes chondrocyte proliferation and inhibits chondrocyte apoptosis and cartilage ECM degradation by targeting DNMT3A in osteoarthritis. *Biochem. Biophys. Res. Commun.* 519, 430–437. doi: 10.1016/j.bbrc.2019.09.022

Markstedt, K., Mantas, A., Tournier, I., Martinez Avila, H., Hagg, D., and Gatenholm, P. (2015). 3D bioprinting human chondrocytes with nanocellulose-alginate bioink for cartilage tissue engineering applications. *Biomacromolecules* 16, 1489–1496. doi: 10.1021/acs.biomac.5b00188

Meakin, L. B., Galea, G. L., Sugiyama, T., Lanyon, L. E., and Price, J. S. (2014). Age-related impairment of bones' adaptive response to loading in mice is associated with sex-related deficiencies in osteoblasts but no change in osteocytes. *J. Bone Miner. Res.* 29, 1859–1871. doi: 10.1002/jbmr.2222

Miller, E., Yang, J., DeRan, M., Wu, C., Su, A. I., Bonamy, G. M., et al. (2012). Identification of serum-derived sphingosine-1-phosphate as a small molecule regulator of YAP. *Chem. Biol.* 19, 955–962. doi: 10.1016/j.chembiol.2012.07.005

Miller, P. D. (2016). Management of severe osteoporosis. *Expert Opin. Pharmacother.* 17, 473–488. doi: 10.1517/14656566.2016.1124856

Miyazaki, T., Zhao, Z., Ichihara, Y., Yoshino, D., Imamura, T., Sawada, K., et al. (2019). Mechanical regulation of bone homeostasis through p130Cas-mediated alleviation of NF-κB activity. *Sci. Adv.* 5:eaau7802. doi: 10.1126/sciadv.aau7802

Mo, J. S., Park, H. W., and Guan, K. L. (2014). The Hippo signaling pathway in stem cell biology and cancer. *EMBO Rep.* 15, 642–656. doi: 10.15252/embr.201438638

Mohler, P. J., Kreda, S. M., Boucher, R. C., Sudol, M., Stutts, M. J., and Milgram, S. L. (1999). Yes-associated protein 65 localizes p62(c-Yes) to the apical compartment of airway epithelia by association with EBP50. *J. Cell Biol.* 147, 879–890. doi: 10.1083/jcb.147.4.879

Moya, I. M., Castaldo, S. A., Van den Mooter, L., Soheily, S., Sansores-Garcia, L., Jacobs, J., et al. (2019). Peritumoral activation of the Hippo pathway effectors YAP and TAZ suppresses liver cancer in mice. *Science* 366, 1029–1034. doi: 10.1126/science.aaw9886

Munoz-Galvan, S., Felipe-Abrio, B., Verdugo-Sivianes, E. M., Perez, M., Jimenez-Garcia, M. P., Suarez-Martinez, E., et al. (2020). Downregulation of *MYPT1* increases tumor resistance in ovarian cancer by targeting the Hippo pathway and increasing the stemness. *Mol. Cancer* 19:7. doi: 10.1186/s12943-020-1130-z

Nardone, G., Oliver-De La Cruz, J., Vrbsky, J., Martini, C., Pribyl, J., Skládal, P., et al. (2017). YAP regulates cell mechanics by controlling focal adhesion assembly. *Nat. Commun.* 8:15321. doi: 10.1038/ncomms15321

Nie, P., Li, Y., Suo, H., Jiang, N., Yu, D., and Fang, B. (2019). Dasatinib promotes chondrogenic differentiation of human mesenchymal stem cells via the Src/Hippo-YAP signaling pathway. *ACS Biomater. Sci. Eng.* 5, 5255–5265. doi: 10.1021/acsbiomaterials.9b00618

Novack, D. V., and Teitelbaum, S. L. (2008). The osteoclast: friend or foe? *Annu. Rev. Pathol.* 3, 457–484. doi: 10.1146/annurev.pathmechdis.3.121806.151431

Okamoto, K., Nakashima, T., Shinohara, M., Negishi-Koga, T., Komatsu, N., Terashima, A., et al. (2017). Osteoimmunology: the conceptual framework unifying the immune and skeletal systems. *Physiol. Rev.* 97, 1295–1349. doi: 10.1152/physrev.00036.2016

Pan, H., Xie, Y., Zhang, Z., Li, K., Hu, D., Zheng, X., et al. (2017). YAP-mediated mechanotransduction regulates osteogenic and adipogenic differentiation of BMSCs on hierarchical structure. *Colloids Surf. B Biointerfaces* 152, 344–353. doi: 10.1016/j.colsurfb.2017.01.039

Pan, J. X., Xiong, L., Zhao, K., Zeng, P., Wang, B., Tang, F. L., et al. (2018). YAP promotes osteogenesis and suppresses adipogenic differentiation by regulating β-catenin signaling. *Bone Res.* 6:18.

Park, J. S., Kim, M., Song, N. J., Kim, J. H., Seo, D., Lee, J. H., et al. (2019). A reciprocal role of the Smad4-Taz axis in osteogenesis and adipogenesis of mesenchymal stem cells. *Stem Cells* 37, 368–381. doi: 10.1002/stem.2949

Pathak, M. M., Nourse, J. L., Tran, T., Hwe, J., Arulmoli, J., Le, D. T., et al. (2014). Stretch-activated ion channel Piezo1 directs lineage choice in human neural stem cells. *Proc. Natl. Acad. Sci. U.S.A.* 111, 16148–16153. doi: 10.1073/pnas.1409802111

Plouffe, S. W., Lin, K. C., Moore, J. L. III, Tan, F. E., Ma, S., Ye, Z., et al. (2018). The Hippo pathway effector proteins YAP and TAZ have both distinct and overlapping functions in the cell. *J. Biol. Chem.* 293, 11230–11240. doi: 10.1074/jbc.RA118.002715

Rachner, T. D., Khosla, S., and Hofbauer, L. C. (2011). Osteoporosis: now and the future. *Lancet* 377, 1276–1287.

Ren, R., Mayer, B. J., Cicchetti, P., and Baltimore, D. (1993). Identification of a ten-amino acid proline-rich SH3 binding site. *Science* 259, 1157–1161. doi: 10.1126/science.8438166

Scanzello, C. R. (2017). Role of low-grade inflammation in osteoarthritis. *Curr. Opin. Rheumatol.* 29, 79–85. doi: 10.1097/BOR.0000000000000353

Schnabel, M., Marlovits, S., Eckhoff, G., Fichtel, I., Gotzen, L., Vecsei, V., et al. (2002). Dedifferentiation-associated changes in morphology and gene expression in primary human articular chondrocytes in cell culture. *Osteoarthritis Cartil.* 10, 62–70. doi: 10.1053/joca.2001.0482

Schuh, E., Kramer, J., Rohwedel, J., Notbohm, H., Muller, R., Gutsmann, T., et al. (2010). Effect of matrix elasticity on the maintenance of the chondrogenic phenotype. *Tissue Eng. Part A* 16, 1281–1290. doi: 10.1089/ten.TEA.2009.0614

Setten, R. L., Rossi, J. J., and Han, S. P. (2019). The current state and future directions of RNAi-based therapeutics. *Nat. Rev. Drug Discov.* 18, 421–446. doi: 10.1038/s41573-019-0017-4

Shang, M., and Sun, J. (2017). Vitamin D/VDR, probiotics, and gastrointestinal diseases. *Curr. Med. Chem.* 24, 876–887. doi: 10.2174/0929867323666161202150008

Siris, E. S., Adler, R., Bilezikian, J., Bolognese, M., Dawson-Hughes, B., Favus, M. J., et al. (2014). The clinical diagnosis of osteoporosis: a position statement from the National Bone Health Alliance Working Group. *Osteoporos. Int.* 25, 1439–1443. doi: 10.1007/s00198-014-2655-z

Song, H., Wu, T., Xie, D., Li, D., Hua, K., Hu, J., et al. (2018). WBP2 downregulation inhibits proliferation by blocking YAP transcription and the EGFR/PI3K/Akt signaling pathway in triple negative breast cancer. *Cell. Physiol. Biochem.* 48, 1968–1982. doi: 10.1159/000492520

Song, R. H., Tortorella, M. D., Malfait, A. M., Alston, J. T., Yang, Z., Arner, E. C., et al. (2007). Aggrecan degradation in human articular cartilage explants is mediated by both ADAMTS-4 and ADAMTS-5. *Arthritis Rheum.* 56, 575–585. doi: 10.1002/art.22334

Sorrentino, G., Ruggeri, N., Zannini, A., Ingallina, E., Bertolio, R., Marotta, C., et al. (2017). Glucocorticoid receptor signalling activates YAP in breast cancer. *Nat. Commun.* 8:14073. doi: 10.1038/ncomms14073

Su, N., Gao, P. L., Wang, K., Wang, J. Y., Zhong, Y., and Luo, Y. (2017). Fibrous scaffolds potentiate the paracrine function of mesenchymal stem cells: a new dimension in cell-material interaction. *Biomaterials* 141, 74–85. doi: 10.1016/j.biomaterials.2017.06.028

Sudol, M. (1994). Yes-associated protein (YAP65) is a proline-rich phosphoprotein that binds to the SH3 domain of the Yes proto-oncogene product. *Oncogene* 9, 2145–2152.

Sudol, M., Bork, P., Einbond, A., Kastury, K., Druck, T., Negrini, M., et al. (1995). Characterization of the mammalian YAP (Yes-associated protein) gene and its role in defining a novel protein module, the WW domain. *J. Biol. Chem.* 270, 14733–14741. doi: 10.1074/jbc.270.24.14733

Tang, Y., Rowe, R. G., Botvinick, E. L., Kurup, A., Putnam, A. J., Seiki, M., et al. (2013). MT1-MMP-dependent control of skeletal stem cell commitment via a beta1-integrin/YAP/TAZ signaling axis. *Dev. Cell* 25, 402–416. doi: 10.1016/j.devcel.2013.04.011

Tang, Y., and Weiss, S. J. (2017). Snail/Slug-YAP/TAZ complexes cooperatively regulate mesenchymal stem cell function and bone formation. *Cell Cycle* 16, 399–405. doi: 10.1080/15384101.2017.1280643

Van Haele, M., Moya, I. M., Karaman, R., Rens, G., Snoeck, J., Govaere, O., et al. (2019). YAP and TAZ heterogeneity in primary liver cancer: an analysis of its prognostic and diagnostic role. *Int. J. Mol. Sci.* 20:638. doi: 10.3390/ijms20030638

Vassilev, A., Kaneko, K. J., Shu, H., Zhao, Y., and DePamphilis, M. L. (2001). TEAD/TEF transcription factors utilize the activation domain of YAP65, a Src/Yes-associated protein localized in the cytoplasm. *Genes Dev.* 15, 1229–1241. doi: 10.1101/gad.888601

Vinatier, C., Dominguez, E., Guicheux, J., and Carames, B. (2018). Role of the inflammation-autophagy-senescence integrative network in osteoarthritis. *Front. Physiol.* 9:706. doi: 10.3389/fphys.2018.00706

Wada, K., Itoga, K., Okano, T., Yonemura, S., and Sasaki, H. (2011). Hippo pathway regulation by cell morphology and stress fibers. *Development* 138, 3907–3914. doi: 10.1242/dev.070987

Wang, L., You, X., Lotinun, S., Zhang, L., Wu, N., and Zou, W. (2020). Mechanical sensing protein PIEZO1 regulates bone homeostasis via osteoblast-osteoclast crosstalk. *Nat. Commun.* 11:282. doi: 10.1038/s41467-019-14146-6

Wang, X., Liang, T., Qiu, J., Qiu, X., Gao, B., Gao, W., et al. (2019). Melatonin reverses the loss of stemness induced by TNF-α in human bone marrow mesenchymal stem cells through upregulation of YAP expression. *Stem Cells Int.* 2019:6568394. doi: 10.1155/2019/6568394

Xiong, J., Almeida, M., and O'Brien, C. A. (2018). The YAP/TAZ transcriptional co-activators have opposing effects at different stages of osteoblast differentiation. *Bone* 112, 1–9. doi: 10.1016/j.bone.2018.04.001

Yang, B., Sun, H., Song, F., Yu, M., Wu, Y., and Wang, J. (2017). YAP1 negatively regulates chondrocyte differentiation partly by activating the beta-catenin signaling pathway. *Int. J. Biochem. Cell Biol.* 87, 104–113. doi: 10.1016/j.biocel.2017.04.007

Yang, B. C., Kuang, M. J., Kang, J. Y., Zhao, J., Ma, J. X., and Ma, X. L. (2020). Human umbilical cord mesenchymal stem cell-derived exosomes act via the miR-1263/Mob1/Hippo signaling pathway to prevent apoptosis in disuse osteoporosis. *Biochem. Biophys. Res. Commun.* 524, 883–889. doi: 10.1016/j.bbrc.2020.02.001

Ying, J., Wang, P., Zhang, S., Xu, T., Zhang, L., Dong, R., et al. (2018). Transforming growth factor-beta1 promotes articular cartilage repair through canonical Smad and Hippo pathways in bone mesenchymal stem cells. *Life Sci.* 192, 84–90. doi: 10.1016/j.lfs.2017.11.028

Yu, F. X., Zhao, B., and Guan, K. L. (2015). Hippo pathway in organ size control, tissue homeostasis, and cancer. *Cell* 163, 811–828. doi: 10.1016/j.cell.2015.10.044

Yu, F. X., Zhao, B., Panupinthu, N., Jewell, J. L., Lian, I., Wang, L. H., et al. (2012). Regulation of the Hippo-YAP pathway by G-protein-coupled receptor signaling. *Cell* 150, 780–791. doi: 10.1016/j.cell.2012.06.037

Yuan, Y., Zhang, L., Tong, X., Zhang, M., Zhao, Y., Guo, J., et al. (2017). Mechanical stress regulates bone metabolism through MicroRNAs. *J. Cell. Physiol.* 232, 1239–1245. doi: 10.1002/jcp.25688

Zaidi, S. K., Sullivan, A. J., Medina, R., Ito, Y., van Wijnen, A. J., Stein, J. L., et al. (2004). Tyrosine phosphorylation controls Runx2-mediated subnuclear targeting of YAP to repress transcription. *EMBO J.* 23, 790–799. doi: 10.1038/sj.emboj.7600073

Zhang, Q., Fang, X., Zhao, W., and Liang, Q. (2019). The transcriptional coactivator YAP1 is overexpressed in osteoarthritis and promotes its progression by interacting with Beclin-1. *Gene* 689, 210–219. doi: 10.1016/j.gene.2018.11.068

Zhang, X., Cai, D., Zhou, F., Yu, J., Wu, X., Yu, D., et al. (2020). Targeting downstream subcellular YAP activity as a function of matrix stiffness with Verteporfin-encapsulated chitosan microsphere attenuates osteoarthritis. *Biomaterials* 232:119724. doi: 10.1016/j.biomaterials.2019.119724

Zhao, B., Li, L., Wang, L., Wang, C. Y., Yu, J., and Guan, K. L. (2012). Cell detachment activates the Hippo pathway via cytoskeleton reorganization to induce anoikis. *Genes Dev.* 26, 54–68. doi: 10.1101/gad.173435.111

Zhao, B., Tumaneng, K., and Guan, K. L. (2011). The Hippo pathway in organ size control, tissue regeneration and stem cell self-renewal. *Nat. Cell Biol.* 13, 877–883. doi: 10.1038/ncb2303

Zhao, L., Guan, H., Song, C., Wang, Y., Liu, C., Cai, C., et al. (2018). YAP1 is essential for osteoclastogenesis through a TEADs-dependent mechanism. *Bone* 110, 177–186. doi: 10.1016/j.bone.2018.01.035

Zheng, Y., and Pan, D. (2019). The hippo signaling pathway in development and disease. *Dev. Cell* 50, 264–282. doi: 10.1016/j.devcel.2019.06.003

Zhong, W., Li, Y., Li, L., Zhang, W., Wang, S., and Zheng, X. (2013a). YAP-mediated regulation of the chondrogenic phenotype in response to matrix elasticity. *J. Mol. Histol.* 44, 587–595. doi: 10.1007/s10735-013-9502-y

Zhong, W., Tian, K., Zheng, X., Li, L., Zhang, W., Wang, S., et al. (2013b). Mesenchymal stem cell and chondrocyte fates in a multishear microdevice are regulated by Yes-associated protein. *Stem Cells Dev.* 22, 2083–2093. doi: 10.1089/scd.2012.0685

Zucchini, C., Manara, M. C., Cristalli, C., Carrabotta, M., Greco, S., Pinca, R. S., et al. (2019). ROCK2 deprivation leads to the inhibition of tumor growth and metastatic potential in osteosarcoma cells through the modulation of YAP activity. *J. Exp. Clin. Cancer Res.* 38:503. doi: 10.1186/s13046-019-1506-3

Conflict of Interest: The authors declare that the research was conducted in the absence of any commercial or financial relationships that could be construed as a potential conflict of interest.

Copyright © 2020 Xie, Xiao, Tang, Zhang and Li. This is an open-access article distributed under the terms of the Creative Commons Attribution License (CC BY). The use, distribution or reproduction in other forums is permitted, provided the original author(s) and the copyright owner(s) are credited and that the original publication in this journal is cited, in accordance with accepted academic practice. No use, distribution or reproduction is permitted which does not comply with these terms.

frontiers in Cell and Developmental Biology

ORIGINAL RESEARCH
published: 21 October 2020
doi: 10.3389/fcell.2020.581941

CircCOG8 Downregulation Contributes to the Compression-Induced Intervertebral Disk Degeneration by Targeting miR-182-5p and FOXO3

*Qian Xiang†, Liang Kang†, Kangcheng Zhao†, Juntan Wang, Wenbin Hua, Yu Song, Xiaobo Feng, Gaocai Li, Saideng Lu, Kun Wang, Cao Yang and Yukun Zhang**

Department of Orthopaedics, Union Hospital, Tongji Medical College, Huazhong University of Science and Technology, Wuhan, China

OPEN ACCESS

Edited by:
Chao Liang,
Hong Kong Baptist University, Hong Kong

Reviewed by:
Halesha Dhurvigere Basavarajappa,
Beckman Research Institute, City of Hope, United States
Hui Liu,
First Affiliated Hospital of Sun Yat-sen University, China

***Correspondence:**
Yukun Zhang
zhangyukuncom@126.com

† These authors have contributed equally to this work

Specialty section:
This article was submitted to Molecular Medicine, a section of the journal Frontiers in Cell and Developmental Biology

Received: *10 July 2020*
Accepted: *22 September 2020*
Published: *21 October 2020*

Citation:
Xiang Q, Kang L, Zhao K, Wang J, Hua W, Song Y, Feng X, Li G, Lu S, Wang K, Yang C and Zhang Y (2020) CircCOG8 Downregulation Contributes to the Compression-Induced Intervertebral Disk Degeneration by Targeting miR-182-5p and FOXO3. Front. Cell Dev. Biol. 8:581941. doi: 10.3389/fcell.2020.581941

Circular RNAs (circRNAs) have been increasingly demonstrated to play critical roles in the pathogenesis of various human diseases. Intervertebral disk degeneration (IDD) is recognized as the major contributor to lower back pain, and mechanical stress is a predominant trigger for IDD. However, little is known about the part that circRNAs play in the involvement of mechanical stress during IDD development. In the present study, we identified a novel circRNA and examined the role of this circRNA in a compression loading-induced IDD process. We detected the expression pattern of circCOG8 and observed its function in disk NP cells under mechanical stress. We conducted bioinformatics analysis, RNA immunoprecipitation experiment, and reporter gene assay to unveil the mechanism of the circCOG8 downregulation mediated IVD degeneration. Results showed that the circCOG8 expression was obviously down-regulated by the mechanical stress in disk NP cells. CircCOG8 attenuated NP cells apoptosis, intracellular ROS accumulation, and ECM degradation *in vitro* and *ex vivo*. CircCOG8 directly interacted with miR-182-5p and, thus, modulated the FOXO3 expression to affect the compression-induced IDD progression. Altogether, the present study revealed that the circCOG8/miR-182-5p/FOXO3 pathway was an important underlying mechanism in the involvement of compression during the IDD progression. Intervention of circCOG8 is a new therapeutic strategy for IDD treatment.

Keywords: nucleus pulposus cell, intervertebral disk degeneration, mechanical stress, circular RNA, circCOG8, microRNA sponge

INTRODUCTION

Lower back pain is a global health problem with a high morbidity and it is the leading cause of job disability in the modern society (Hoy et al., 2014). Although there are various initiating contributors associated with lower back pain, it is widely accepted that the intervertebral disk degeneration (IDD) is the major reason (Hughes et al., 2012). However, the pathogenesis and etiology of IDD have not been explicitly clarified yet. Physiologically, the intervertebral disk (IVD) comprises the

inner gelatinous nucleus pulposus (NP), the surrounding collagenous annulus fibrosus (AF), as well as the cartilaginous endplates (EP), and the disks act as the most important load-bearing structure of the spine (Roberts et al., 2006). Disk NP cells are in the center of IVD and play a crucial part in maintaining the balance between the NP extracellular matrix (ECM) catabolism and anabolism. The abundance of ECM, including the proteoglycans and type II collagen generated by the NP cells, make important contributions to the physiological structure and function of IVD (Roughley, 2004). And, IVD degeneration is typically characterized by the aberrant conditions of NP cells that the ECM catabolism exceeds anabolism, cell apoptosis rates are abnormally increased, and reactive oxygen species (ROS) generation and antioxidant defense get out of balance to cause oxidative stress (Zhao et al., 2007; Risbud and Shapiro, 2014; Feng et al., 2017). Deep research into the underlying mechanism of these aberrant activities of the NP cells can help clinicians get a better understanding of the IDD pathogenesis and, thus, provide new strategies for the IDD treatment (Hughes et al., 2012; Sakai and Grad, 2015).

Mechanical stress is a critical etiological factor that provokes IVD degeneration (Setton and Chen, 2006; Neidlinger-Wilke et al., 2014). The pressure of the human IVD ranges from 0.1 to 1.1 MPa *in vivo* depending on the postures and the disk is also subjected to various non-physiological mechanical loading, which, in return, contributes significantly to the disk damage (Wilke et al., 1999; Adams and Roughley, 2006). Studies have reported that mechanical loads could induce the ECM degradation via shifting the balance of the ECM metabolism homeostasis toward catabolism, accompanied by an elevated expression of catabolic genes, such as disintegrin and metalloproteinase with thrombospondin motifs (ADAMTS), as well as, matrix metalloproteinases (MMP) (Yurube et al., 2012; Holguin and Silva, 2018). Meanwhile, it was demonstrated that mechanical compression contributed to excessive ROS accumulation to promote oxidative stress in NP cells (Li et al., 2017). In our previous work, we elucidated that applying a static compression of 1.0 MPa to human NP cells obviously induced programmed cell death by which it was deeply involved in disk injury (Li et al., 2018). Furthermore, we also unveiled that mechanical loading could effectively induce various pathological responses of disk cells in an *ex vivo* organ-cultured rat IVD model (Wu et al., 2019).

Accumulating evidence have revealed that non-coding RNAs, including microRNAs (miRNAs) and circular RNAs (circRNAs), functionally participate in the pathophysiological process of IDD (Li et al., 2015, 2019). MiRNAs are highly conserved, short, and single stranded endogenous RNAs which can regulate the target mRNA expression via associating with AGO proteins (Bartel, 2004). For instance, miR-7 was found to be a critical contributor to the IDD by targeting GDF5 in disk NP cells, as reported in our previous work (W. Liu et al., 2016). In the present study, results revealed that miR-182-5p contributed to the compression-induced damage in NP cells which was obviously upregulated under compression stress. CircRNAs are another type of understudied non-coding RNAs and they have a closed continuous loop which enables them to be more stable compared to the linear RNAs and resistant to degradation by exonucleases or RNase R (Han et al., 2018). In regard to the biological function of circRNAs, evidence has claimed that a number of circRNAs can sequester miRNAs to indirectly regulate the corresponding target genes expression which was also called "miRNA sponge" (Memczak et al., 2013). The most representative miRNA sponge is that the Cdr1as, an antisense transcript of cerebellar degeneration-related protein 1, harbors 74 conserved binding sites for miR-7 (Hansen et al., 2013). It has been reported that circRNAs exerted significant effects on the initiation and development of degenerative disk diseases by functioning as competing endogenous RNAs and consequently modulating target mRNAs levels (Cheng et al., 2018; Song et al., 2018). However, little is known about the part circRNAs play in the IDD progression induced by mechanical stress. Therefore, this study was aimed to explore a possible role of circRNAs in the mechanisms leading to IDD by examining their expression in disk NP cells under mechanical stress. We identified a novel circular RNA circCOG8 based on the circRNA microarray and bioinformatics analysis and systemically investigated the role of this circRNA in the progression of compression-loading-induced IDD.

RESULTS

CircCOG8 Was Significantly Down Regulated in the Disk NP Cells Under Mechanical Stress

To uncover the potential role of circRNAs in the progression of IDD induced by mechanical loading, we examined the effects of compression on human disk NP cells in three different samples. Compression treatment significantly increased the NP cell apoptosis and intracellular ROS accumulation, increased the expression of Bax, ADAMTS-4, ADAMTS-5 as well as MMP-13, and inhibited the expression of Bcl-2, Aggrecan as well as Type II collagen (**Figures 1A–C**). It was suggested that the compression treatment resulted in elevated cell apoptosis, ROS accumulation, and ECM degradation in human disk NP cells. Then, we performed circRNAs microarray assays using three pairs of disk cells samples treated by 1.0 MPa mechanical loading for 36 h. Data revealed that a total of 1,784 circRNAs were significantly dysregulated, among which, 1,498 gene items were downregulated by mechanical loading compared with the control. **Figure 1D** showed the top 100 most significantly down-regulated circRNAs. Since most of the differentially expressed circRNAs were down-regulated in the compression treatment group, we then selected seven out of the top 100 remarkably down-regulated circRNAs for the validation in three different pairs of cell samples by real-time qPCR analysis and these seven circRNAs were all rich in miRNA binding sites. The log2 fold-changes of microarray data and RT-qPCR data were both calculated and we found that, of the seven circRNAs, the circCOG8 showed the highest fold-change (**Figure 1E**). As a result, the circCOG8 was chosen as the subject for further experiments. CircCOG8 (hsa_circ_0040060)

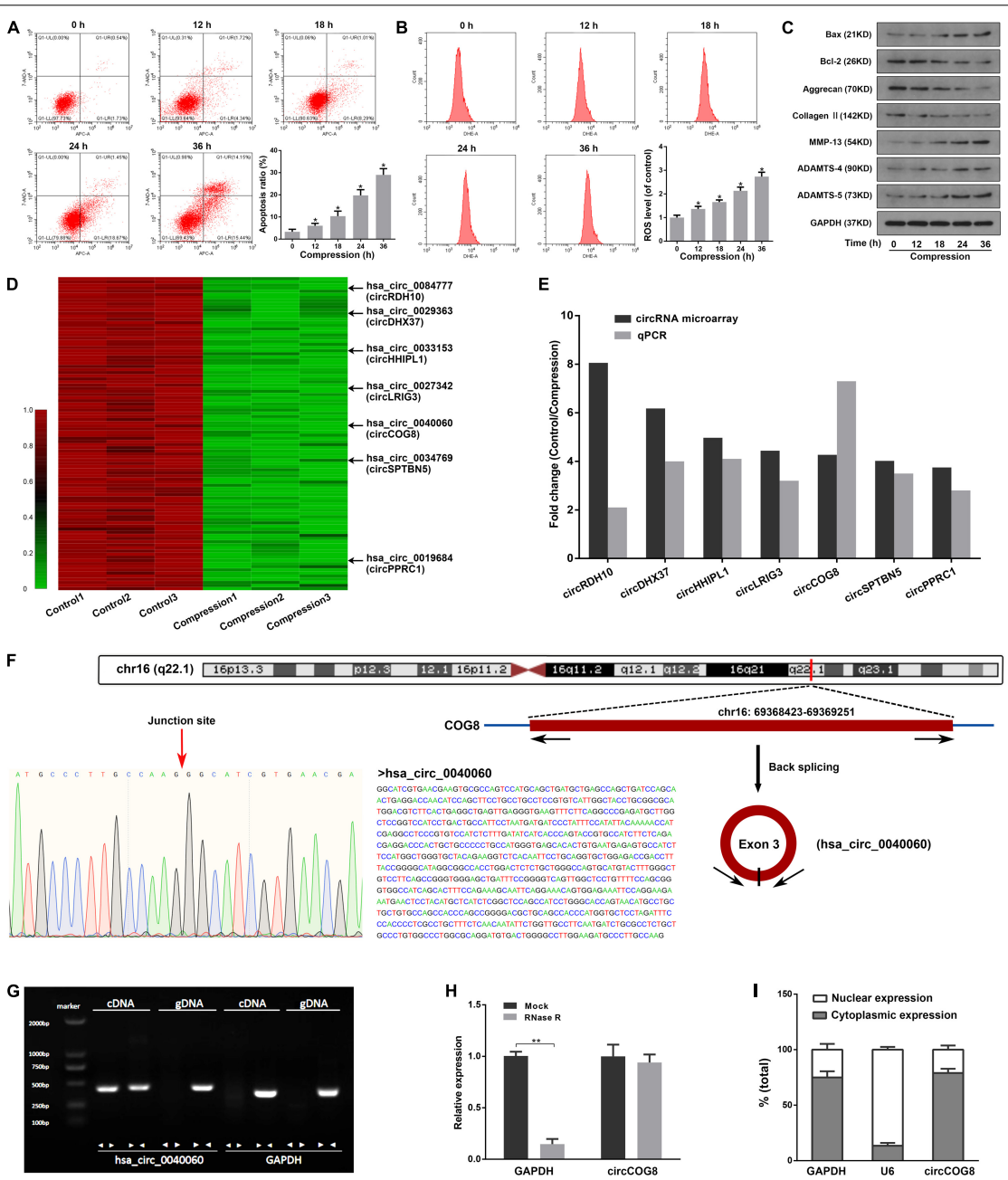


FIGURE 1 | CircCOG8 was significantly down-regulated in the compression-treated human NP cells. **(A)** The human NP cells were treated with 1 MPa compression for the indicated time points (0, 12, 18, 24, and 36 h), and the cell apoptosis was determined by the Annexin V-APC and 7-AAD double-staining with subsequent flow cytometry analysis. Data were represented as mean ± SD. 0 h group served as a control, $^{*}p < 0.05$ versus control, $n = 3$ (ANOVA with Tukey's post-test). **(B)** The intracellular ROS production of the NP cells with compression for indicated time points were examined by the ROS-specific fluorescent probe DHE and measured by the flow cytometry analysis. Data were represented as mean ± SD. 0 h group served as a control, $^{*}p < 0.05$ versus control, $n = 3$ (ANOVA with Tukey's post-test). **(C)** Western blot analysis was used to detect the protein expression level of ECM anabolism markers (Aggrecan, Type II collagen), ECM catabolism enzymes (MMP-13, ADAMTS-4, ADAMTS-5), and apoptosis-associated markers (Bax, Bcl-2). Data were normalized to the GAPDH control. The GAPDH band served as a common internal loading control for Bax, Bcl-2, Aggrecan, Type II collagen, MMP-13, ADAMTS-4, and ADAMTS-5. **(D)** Clustered heat map showed the top 100 significantly down-regulated circRNAs in three samples of the compression treated human NP cells and three control samples. The arrows indicated the seven candidate circRNAs which were further validated using a real-time qPCR analysis. **(E)** Comparison of the fold changes for the seven candidate circRNAs from the circRNA array and real-time qPCR validation. **(F)** The genomic loci of the COG8 gene and circCOG8. The expression of circCOG8 was validated by the Sanger sequencing. **(G)** The products amplified using the divergent or convergent primers were verified by agarose gel electrophoresis. Divergent primers were used to amplify circCOG8 in cDNA but not in genomic DNA (gDNA). Convergent primers could amplify both the circCOG8 and linear RNA GAPDH. **(H)** The RT-qPCR analysis of circCOG8 and linear control GAPDH mRNA after treatment with RNase R in the disk NP cells. $^{**}p < 0.05$, $n = 3$. **(I)** RT-qPCR assay in nuclear and cytoplasmic fractions showed the levels of nuclear control transcript (U6), cytoplasmic control transcript (GAPDH), and circCOG8.

is generated from back-spliced exon 3 of COG8 which is located on chromosome 16q22.1 (chr16:69368423-69369251), as annotated in the circBase online database using the human reference genome GRCh37/hg19 (**Figure 1F**). The length of the circCOG8 is 828 nt (nucleotide). The PCR assay suggested that divergent primers could amplify the circular circCOG8 in cDNA but not in gDNA, and convergent primers could amplify both the circCOG8 and linear control GAPDH (**Figure 1G**). Sanger sequencing was performed to confirm the amplified products using divergent primers, as shown in **Figure 1F**. CircCOG8 was resistant to RNase R exonuclease digestion, further supporting the notion that this type of RNA was circular (**Figure 1H**). Moreover, the circCOG8 was primarily distributed in the cytoplasm, as examined by the cytoplasmic and nuclear RNA isolation followed by RT-qPCR in disk NP cells (**Figure 1I**).

Overexpression of CircCOG8 Protected Disk NP Cells From Mechanical Stress-Induced Cellular Damage

Next, we transfected the disk NP cells with the circCOG8 expression adenovirus vector to overexpress circCOG8, or with shRNA targeting the junction site of circCOG8 to knockdown circCOG8. As revealed in **Figure 2A**, the NP cells transfected with the circCOG8 overexpression vector showed a higher

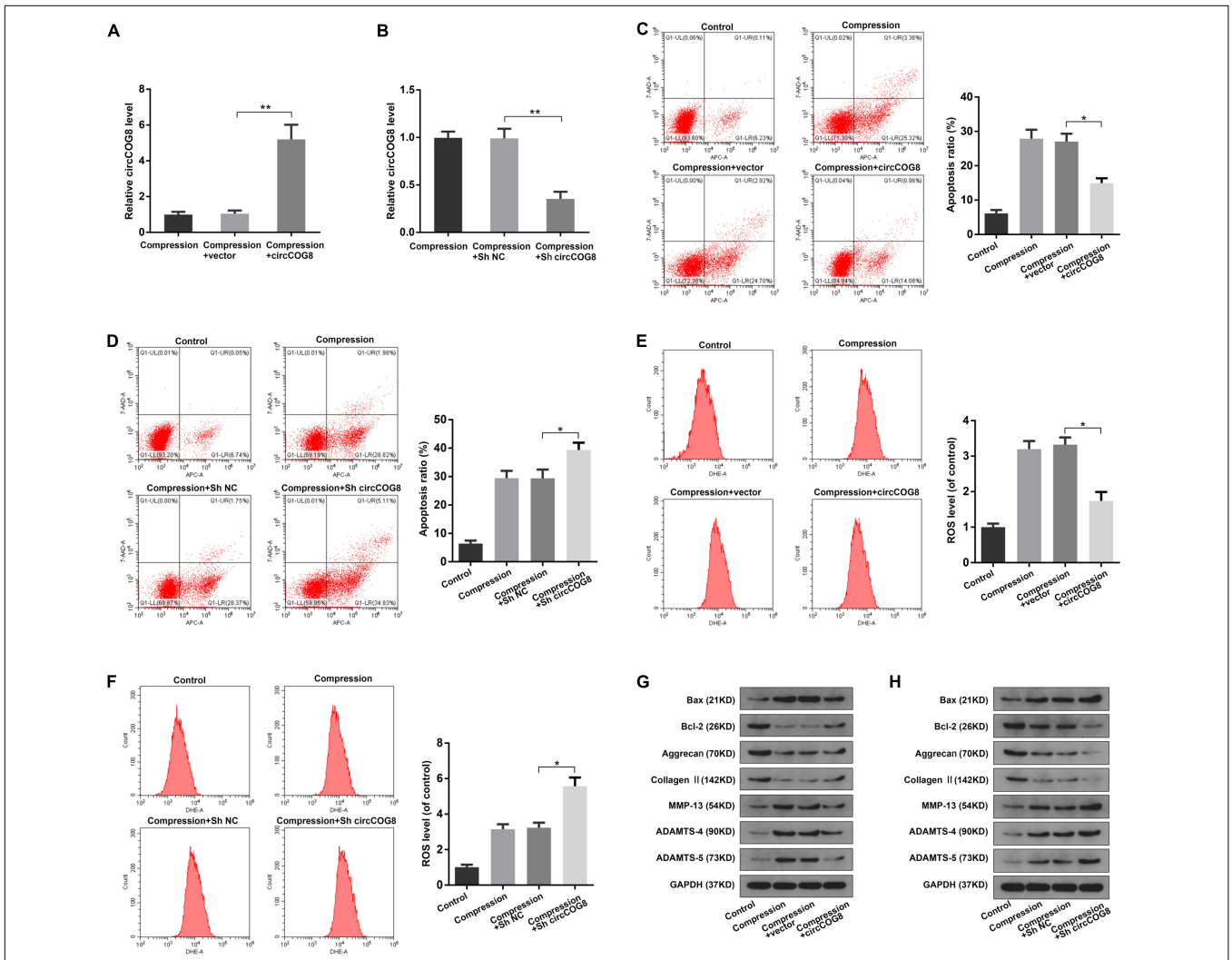


FIGURE 2 | Function of circCOG8 in disk NP cells under mechanical stress. **(A,B)** The human NP cells under compression treatment were transfected with the circCOG8 overexpression vector or circCOG8 shRNA, and the circCOG8 RNA level was examined using the RT-qPCR analysis. **(C,D)** The apoptosis ratio of the NP cells transfected with the circCOG8 overexpression vector or circCOG8 shRNA was determined by the flow cytometry analysis after the Annexin V-APC and 7-AAD double-staining. **(E,F)** The intracellular ROS levels of the NP cells transfected with the circCOG8 overexpression vector or circCOG8 shRNA were detected by DHE and measured by the flow cytometry analysis. **(G,H)** Human NP cells under compression were treated with the circCOG8 overexpression or circCOG8 shRNA, and the protein levels of Bax, Bcl-2, Aggrecan, Type II collagen, MMP-13, ADAMTS-4, and ADAMTS-5 were determined by the western blot analysis. The corresponding GAPDH band served as a common internal loading control for Bax, Bcl-2, Aggrecan, Type II collagen, MMP-13, ADAMTS-4, and ADAMTS-5. Data were represented as mean ± SD. $^{*}p < 0.05$, $^{**}p < 0.01$, $n = 3$ (Student's t-test).

circCOG8 expression level under the compression treatment. In contrast, the circCOG8 shRNA obviously resulted in the circCOG8 downregulation (**Figure 2B**). Then, we used flow cytometry analysis by Annexin V/PI dual staining to evaluate the circCOG8's effect on the NP cells apoptosis under compression. We found that the circCOG8 overexpression obviously decreased the apoptosis incidence of NP cells (**Figure 2C**) and circCOG8 knockdown increased the apoptosis rate of NP cells under compression (**Figure 2D**). The intracellular ROS level were examined using the fluorescent probe DHE and flow cytometry which indicated that circCOG8 could markedly inhibit the ROS production of NP cells (**Figure 2E**) and the circCOG8 shRNA could promote the ROS production of disk NP cells induced by mechanical loading (**Figure 2F**). Western blot analysis suggested that the circCOG8 knockdown increased the protein level of ADAMTS-4, ADAMTS-5, MMP-13 as well as Bax and decreased the expression of Type II collagen, aggrecan as well as Bcl-2 while the circCOG8 overexpression partially counteracted the effects of mechanical loading on these gene expression (**Figures 2G,H**). The results above demonstrated that circCOG8 could alleviate the effect of mechanical stress on disk NP cells.

CircCOG8 Functioned as miR-182-5p Sponge to Inhibit Its Expression

Considering the circular RNAs can interact with microRNAs to function as microRNA sponges, circCOG8 might target a critical microRNA to regulate its activity. Firstly, we used the StarBase online tool and Circular RNA Interactome online database to predict the targeting miRNAs of circCOG8, and found that there were eight candidate miRNAs identified by overlapping the predicting results from these two databases (**Figure 3A**). Then, we used real-time qPCR analysis to determine whether these predicted miRNAs were dysregulated in the disk NP cells under mechanical stress. Results showed that the miR-182-5p was the only significantly upregulated miRNA with a fold change > 2 (**Figure 3B**). According to the StarBase online database, there was a potential binding site between the circCOG8 and miR-182-5p seed region (**Figure 3C**). Next, we performed the subsequent experiments to investigate the ability of the circCOG8 to directly interact with the miR-182-5p in disk NP cells. We transfected the disk NP cells with the circCOG8 shRNA to inhibit the circCOG8 expression, with the results proving that the miR-182-5p level was obviously enhanced after the circCOG8 knockdown (**Figure 3D**). Then, we conducted the Argonaute-2 (AGO2) immunoprecipitation by RT-qPCR to examine whether the AGO2 was associated with the miR-182-5p transcripts which could bind circCOG8. We found that both the circCOG8 and miR-182-5p were highly enriched by the anti-AGO2 antibodies (**Figure 3E**). Furthermore, the pMIR-REPORT luciferase reporter plasmids with mutant (MUT) or wild type (WT) circCOG8 fragment which possessed miR-182-5p complementary binding sequence were co-transfected to the HEK293T cells with miR-182-5p. Results revealed that the relative Luc/R-luc ratio of WT luciferase reporter was obviously lower in the miR-182-5p mimic group compared to the negative control (**Figure 3F**). In summary, the above data demonstrated that circCOG8 functioned as an miR-182-5p sponge to suppress its expression in the disk NP cells.

MiR-182-5p Facilitated Mechanical Stress-Induced Cellular Damage of Disk NP Cells

Since miR-182-5p is the circCOG8-targeted microRNA, we speculated that miR-182-5p could have crucial regulating effects on the disk NP cells with compression loading. To test our hypothesis, we carried out the following experiments. Using the RT-qPCR assay, we found that miR-182-5p was elevated in the disk NP cells after the compression stimulation; the miR-182-5p expression was markedly inhibited after the miRNA inhibitor treatment and increased after the miRNA mimic treatment (**Figures 4A,E**). As revealed in **Figures 4B–D**, the miR-182-5p inhibitor markedly inhibited the up-regulation of apoptosis rate, ROS production, and ECM degradation in disk NP cells induced by mechanical stress. Conversely, these changes in NP cells induced by compression stress were enhanced when co-treated with the miR-182-5p overexpression (**Figures 4F–H**). The above data revealed the critical role of miR-182-5p in promoting cell apoptosis, oxidative stress, and ECM degradation in the disk NP cells under mechanical stress.

MiR-182-5p Functioned in Disk NP Cells via Interacting With FOXO3

It has been reported that the transcription factors of the Forkhead box O class (FOXOs) played important regulating roles in the intervertebral disk maturation and homeostasis (Alvarez-Garcia et al., 2018; Penolazzi et al., 2018). Using the TargetScan online tool, we found that the Forkhead box O3 (FOXO3) possessed complementary sequence to the miR-182-5p seed region (**Figure 5A**). Then, we performed the luciferase analysis to validate that the miR-182-5p could directly target FOXO3. Luciferase reporter vector with mutant (MUT) or wild type (WT) FOXO3 3′-UTR, which possessed the miR-182-5p binding sites, were transfected to the HEK293T cells treated with miR-182-5p. As expected, miR-182-5p markedly suppress the luciferase activity of the WT-FOXO3 3′-UTR reporter while there was no significant difference in the MUT-FOXO3 3′-UTR reporter activity between the miR-182-5p mimic and control group (**Figure 5B**). Next, we performed the western blotting analysis in the disk NP cells to further validate the above findings. It was illustrated that miR-182-5p markedly suppressed the FOXO3 protein level (**Figure 5C**). Conversely, the miR-182-5p knockdown dramatically promoted the FOXO3 protein level (**Figure 5D**). The above results suggested that miR-182-5p could bind to FOXO3 3′-UTR to repress its expression. Then, we carried out the western blot analysis to explore the role of interaction between miR-182-5p and FOXO3 in the disk NP cells under mechanical stress. It was suggested that the level of FOXO3 protein was obviously decreased under the compression loading (**Figures 5E,F**). Overexpressing miR-182-5p could facilitate the inhibitive effect of mechanical stress on FOXO3 expression (**Figure 5E**) and the miR-182-5p inhibitor could mitigate the inhibitive effect of compression on the FOXO3 protein level

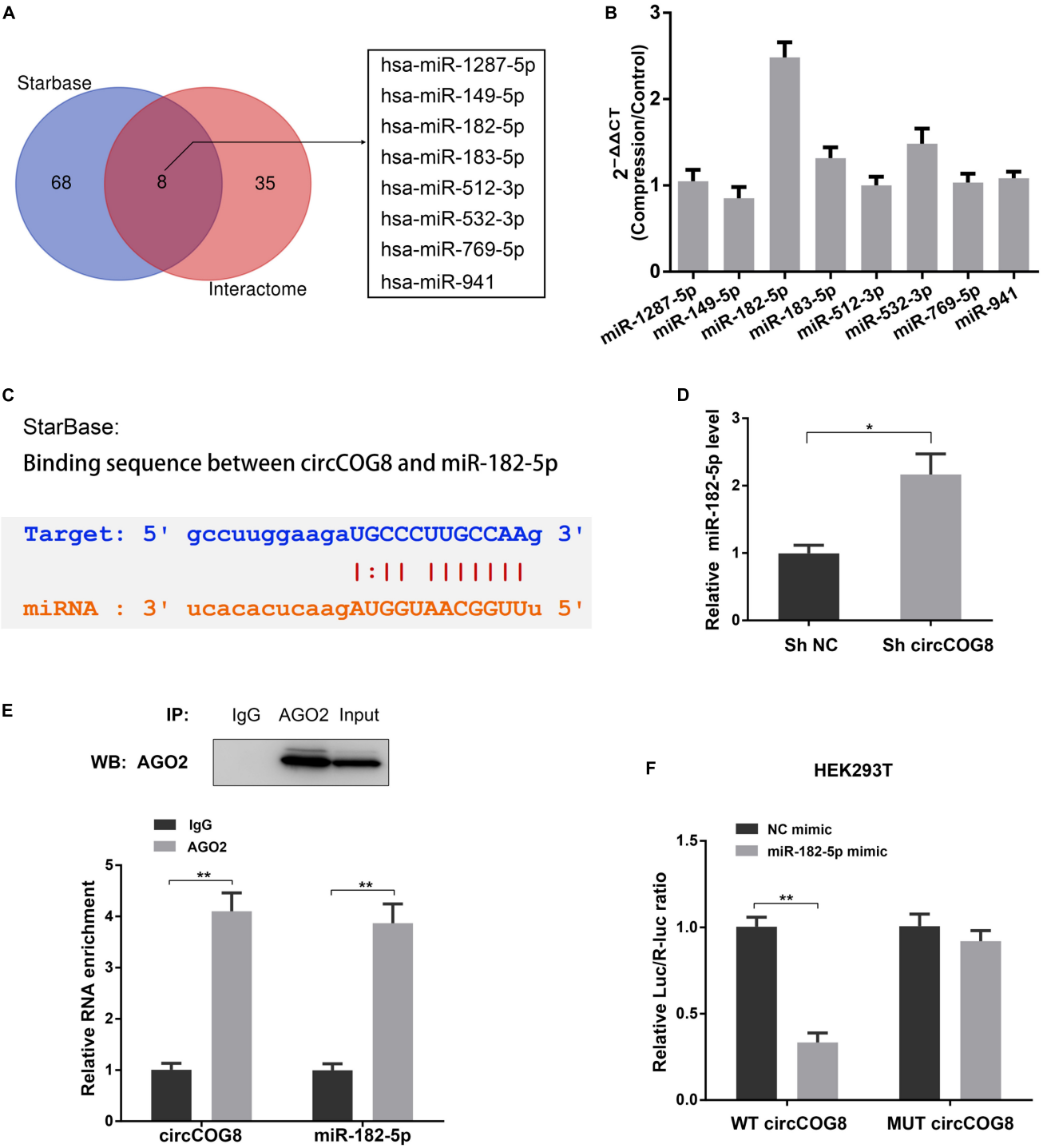


FIGURE 3 | CircCOG8 acted as a sponge for miR-182-5p to inhibit its expression. **(A)** The Veen diagram revealed the eight candidate circCOG8-targeting miRNAs identified using the StarBase online tool and the Circular RNA Interactome online database. **(B)** The expression pattern of these eight candidate miRNAs in the disk NP cells under mechanical stress were determined by the real-time qPCR analysis. The upregulated magnitudes of these eight miRNAs were shown as fold changes of the compression treated cell samples to control cell samples. **(C)** Schematic of the binding sequence between circCOG8 and miR-182-5p based on the StarBase online database. **(D)** The expression level of miR-182-5p in the disk NP cells transfected with the circCOG8 shRNA or control was examined by the real-time qPCR analysis. **(E)** The RNA immunoprecipitation (RIP) assay was used to detect circCOG8 and miR-182-5p enrichment. The AGO2 protein level was examined by the IP-western blot analysis (upper) and co-precipitated circCOG8 and miR-182-5p RNA levels were examined using the qRT-PCR analysis (lower). **(F)** Wild-type (WT) or mutant (MUT) circCOG8 luciferase reporter vectors were co-transfected with the miR-182-5p mimic or NC mimic into HEK-293T cells. The relative luciferase activity was determined as the ratio of firefly luciferase/Renilla luciferase (Luc/R-luc). Data were represented as mean ± SD. $^{*}p < 0.05$, $^{**}p < 0.01$, $n = 3$ (Student's *t*-test).

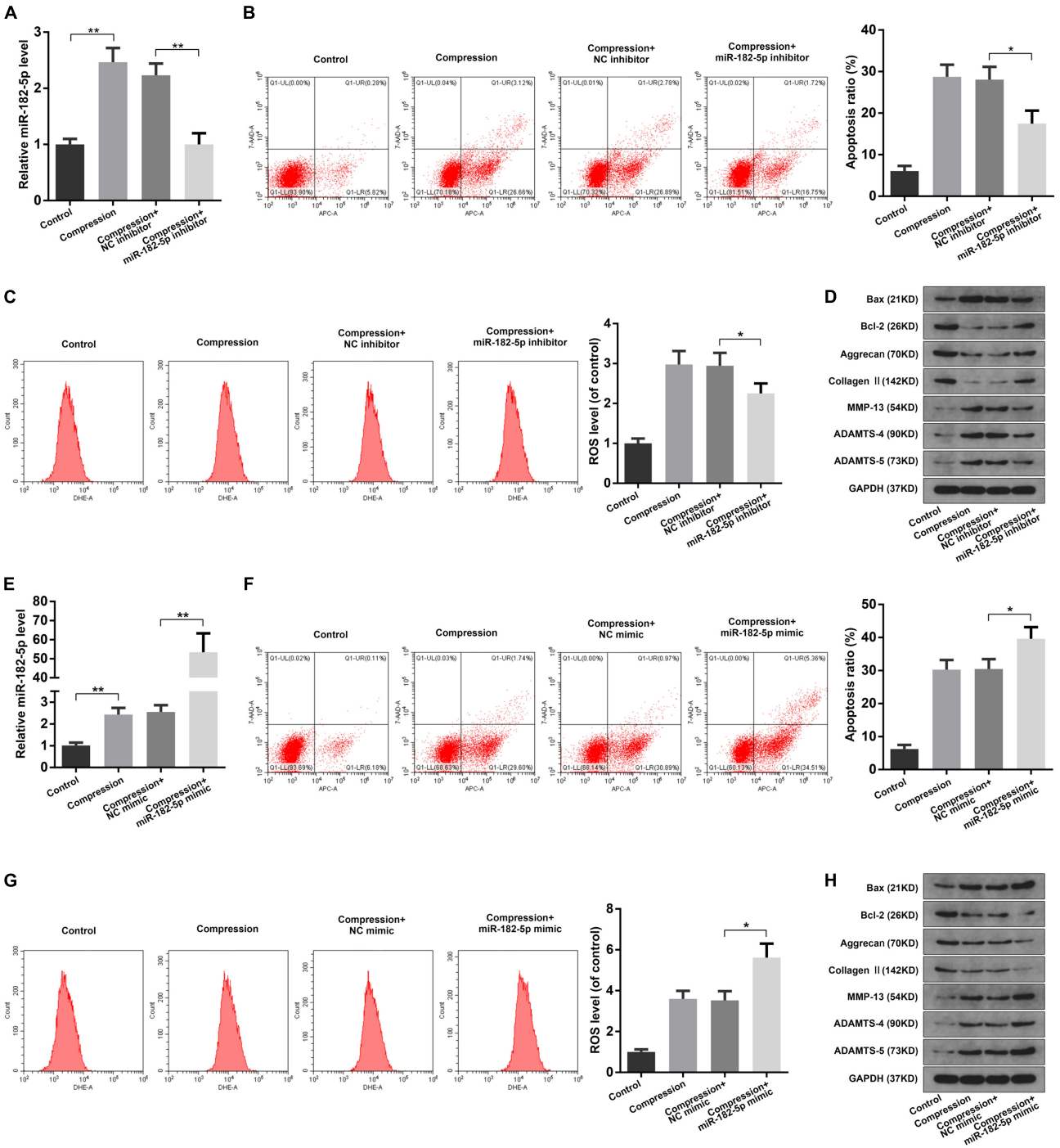


FIGURE 4 | Function of miR-182-5p in disk NP cells under mechanical stress. **(A)** The human NP cells under compression were transfected with the miR-182-5p inhibitor and the miR-182-5p expression level was examined using the RT-qPCR analysis. **(B)** The apoptosis ratio of the NP cells with the miR-182-5p inhibitor treatment was evaluated using the Annexin V-APC and 7-AAD double-staining with subsequent flow cytometry analysis. **(C)** The intracellular ROS accumulation of the NP cells with the miR-182-5p inhibitor treatment were detected by DHE and measured by the flow cytometry analysis. **(D)** The protein expression levels of Bax, Bcl-2, Aggrecan, Type II collagen, MMP-13, ADAMTS-4, and ADAMTS-5 were determined by the western blot analysis. The GAPDH band served as a common internal loading control for Bax, Bcl-2, Aggrecan, Type II collagen, MMP-13, ADAMTS-4, and ADAMTS-5. **(E)** The human NP cells under compression were transfected with the miR-182-5p mimic and the miR-182-5p level was determined by the RT-qPCR analysis. **(F)** The apoptosis ratio of the NP cells with miR-182-5p mimic treatment. **(G)** The intracellular ROS levels of the NP cells transfected with the miR-182-5p mimic. **(H)** The protein levels of Bax, Bcl-2, Aggrecan, Type II collagen, MMP-13, ADAMTS-4, and ADAMTS-5 were determined by the western blot analysis. The GAPDH band served as a common internal loading control for Bax, Bcl-2, Aggrecan, Type II collagen, MMP-13, ADAMTS-4, and ADAMTS-5. Data were represented as mean ± SD. $^{*}p < 0.05$, $^{**}p < 0.01$, $n = 3$ (Student's *t*-test).

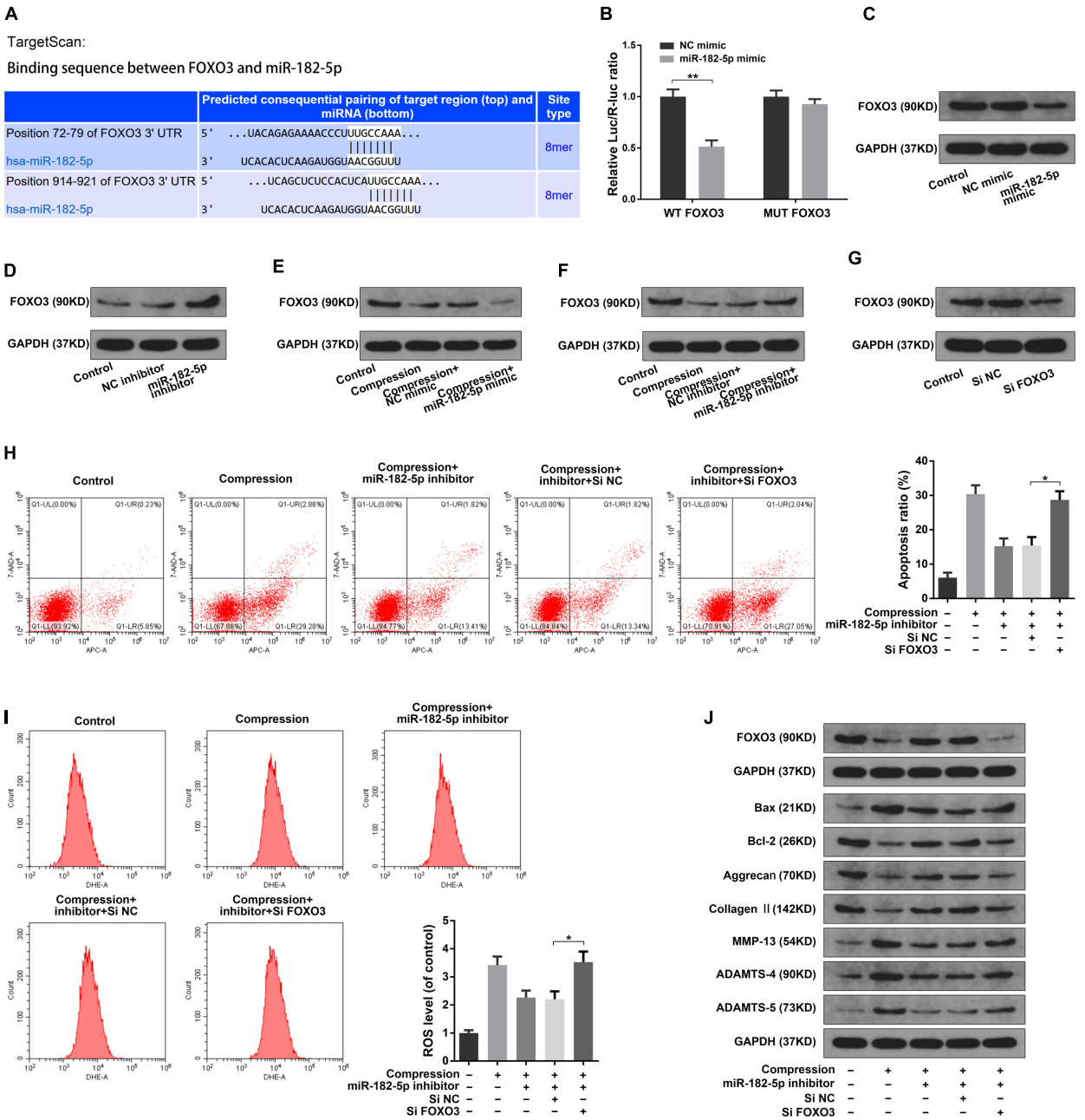


FIGURE 5 | MiR-182-5p functioned in disk NP cells via targeting FOXO3. **(A)** Schematic of the binding sequence between the 3′ UTR of FOXO3 and miR-182-5p based on the TargetScan online database. **(B)** WT or MUT FOXO3 luciferase reporter vectors were co-transfected into the HEK-293T cells with the miR-182-5p mimic or NC mimic, and the luciferase reporter activity was presented as the relative Luc/R-Luc ratio. **(C,D)** The human NP cells were transfected with the miR-182-5p mimic or miR-182-5p inhibitor, the FOXO3 expression level was were determined by the western blot analysis. **(E,F)** The human NP cells under the compression treatment were transfected with the miR-182-5p mimic or miR-182-5p inhibitor, the FOXO3 expression level was were determined by the western blot analysis. **(G)** The FOXO3 protein expression level in the disk NP cells treated with the FOXO3 siRNA or siNC. **(H)** The Annexin V-APC and 7-AAD double-staining results indicating the apoptosis ratio of the NP cells. **(I)** The intracellular ROS levels in the NP cells were detected by DHE with the flow cytometry analysis. **(J)** The protein levels of FOXO3, Bax, Bcl-2, Aggrecan, Type II collagen, MMP-13, ADAMTS-4, and ADAMTS-5 were determined by the western blot analysis. The upper GAPDH band served as an internal loading control for FOXO3; the lower GAPDH band served as a common internal loading control for Bax, Bcl-2, Aggrecan, Type II collagen, MMP-13, ADAMTS-4, and ADAMTS-5. Data were represented as mean ± SD. $^{*}p < 0.05$, $^{**}p < 0.01$, $n = 3$ (Student's t-test).

(**Figure 5F**). Subsequently, the FOXO3 siRNA was used to further validate the critical role of FOXO3 (**Figure 5G**). It was revealed that the FOXO3 siRNA could partially counteract the effect of the miR-182-5p knockdown on human NP cells (**Figures 5H–J**). The above results demonstrated that miR-182-5p functioned in the disk NP cells through interacting with FOXO3.

CircCOG8 Functioned in Disk NP Cells via Targeting miR-182-5p and FOXO3

To further examine the effects of circCOG8 on the FOXO3 expression with the involvement of miR-182-5p, we then carried out the following experiments. The luciferase activity assay revealed that miR-182-5p markedly repressed the WT-FOXO3 luciferase activity while circCOG8 could partially reverse this inhibitory effect (**Figure 6A**). Western blotting analysis also revealed that the repressive function of miR-182-5p on the FOXO3 expression level could be neutralized by the circCOG8 upregulation (**Figure 6B**). It was suggested that circCOG8 could function as the miR-182-5p sponge to modulate the FOXO3 expression. Subsequently, we found that the up-regulation of cell death rate, ROS production as well as the ECM catabolic activity in the disk NP cells caused by miR-182-5p could be counteracted by the circCOG8 overexpression (**Figures 6C–E**). Moreover, using the siRNA-mediated FOXO3 knockdown, we found that the absence of FOXO3 evidently abolished the protective effect of the circCOG8 overexpression in the disk NP cells under mechanical stress (**Figures 6F–H**). The above results revealed that circCOG8 exerted its functions by targeting miR-182-5p and FOXO3.

CircCOG8 Overexpression Attenuated Compression-Induced IDD *ex vivo*

To further test the function of circCOG8 exhibited on the compression-induced IDD progression, we established the *ex vivo* organ-cultured rat disk model. The modeled rat IVDs *ex vivo* were injected with the adenovirus circCOG8 or control vector. Then, the IVD specimens were harvested and subjected to histopathological analysis (**Figures 7A,B**). In the control groups, the round-shaped NP tissues occupied more than half area of the disk as examined by the HE staining, and abundant proteoglycan matrix was confirmed in the NP area as indicated by the Safranin-O staining (**Figure 7A**). In the compression-induced IDD groups, the NP tissues area in the disk was obviously smaller with the collapsed disk height and the proteoglycan matrix volume was markedly decreased. Conversely, the circCOG8 overexpression could alleviate these disk degenerative changes induced by the compression when comparing with the IDD groups. The statistical data also suggested that the histological grades in the IDD groups were higher than that in the circCOG8 overexpression groups (**Figure 7B**). The TUNEL assay showed that the NP cell apoptosis ratio was elevated in the compression-induced IDD groups and markedly decreased after co-treatment of the circCOG8 overexpression (**Figures 7C,D**). Furthermore, compared to the IDD groups, the ROS level in IVD tissues indicated by H_2O_2 content was obviously decreased in the circCOG8 overexpression groups (**Figure 7E**). Lastly, the western blot analysis revealed that circCOG8 could alleviate the FOXO3 reduction, ECM degradation, and apoptotic response in the *ex vivo* organ-cultured model (**Figure 7F**). Collectively, the above results indicated that the circCOG8 overexpression could attenuate the compression-induced IDD *ex vivo*.

DISCUSSION

Previous studies have demonstrated that IVD degeneration was a complicated disease involving numerous pathologic processes during which the nucleus pulposus cells residing in the IVD center has played a key role (Sakai et al., 2012). The impairment of the structural and functional integrity of the NP is a classical character of IDD progression, including the imbalanced metabolism of the ECM, NP cell apoptosis, and excessive ROS accumulation (Roberts et al., 2006; Zhao et al., 2007; Feng et al., 2017). The IVD is an important load-bearing structure and it is under various degrees of mechanical stress during which the NP could counteract and distribute the mechanical loads in the spine (Wilke et al., 1999; Gilchrist et al., 2011). Accumulating evidences have corroborated that mechanical stress was a predominant initiating factor for IDD and abnormal mechanical stress induced various pathological cellular responses within the IVD (MacLean et al., 2005; Li S. et al., 2018). Recently, research demonstrated that the compression treatment on NP cells could lead to the activation of the NF-κB pathway, MAPK pathway, and the deactivation of the PI3K/Akt pathway (Jiang et al., 2018; Li et al., 2018; Glaeser et al., 2020; Huang et al., 2020), which provided new insights into the association between mechanical stress and IDD. In this study, we found that applying a static mechanical load of 1.0 MPa could induce ECM degradation, cell apoptosis, and excessive ROS production in NP cells, which was consistent with the previous findings (Li et al., 2017; Lin et al., 2017; Chen et al., 2018; Wu et al., 2019). Moreover, we also applied an *ex vivo* IDD model induced by mechanical stress in this study. Compared with the *in vitro* analysis, the *ex vivo* system provided a better model to uncover the pathogenesis of IDD, with the intervertebral disk structure and native ECM intact, which were important to further investigate the involvement of mechanical loading in IVD degeneration (Lee et al., 2006; Koerner et al., 2016; Wu et al., 2019). In the *ex vivo* model, the imbalance between the ECM deposition and degradation, the increased NP cell apoptosis, and overproduction of ROS were also detected. However, the precise molecular mechanism of the involvement of mechanical stress during IDD progression remains unclear and more efforts should be made to develop novel therapeutic targets for IDD.

Recently, evidence increasingly reported that circRNAs played crucial roles during the physiology and pathology of various human diseases (Zhao and Shen, 2017; Chen et al., 2018; Kleaveland et al., 2018; Liu et al., 2018). CircRNAs are single-stranded non-coding RNA molecules without 5′–3′ polarities and polyadenylated tails as a result of the circular structure generated by back splicing of introns, exons, or intergenic regions. With the following characteristics including the exceptional stability, conservation across species, and cell and tissue-specific expression patterns, circRNAs have been found involved in many crucial cellular processes and the dysregulation of circRNAs resulted in the initiation and development of a broad range of diseases. CircRNAs could directly bind to microRNAs and sequester them from the cytoplasm and, thus, counteract the inhibitory effect of miRNAs on their targeting mRNA (Li et al., 2018). The most representative circRNA Cdr1as

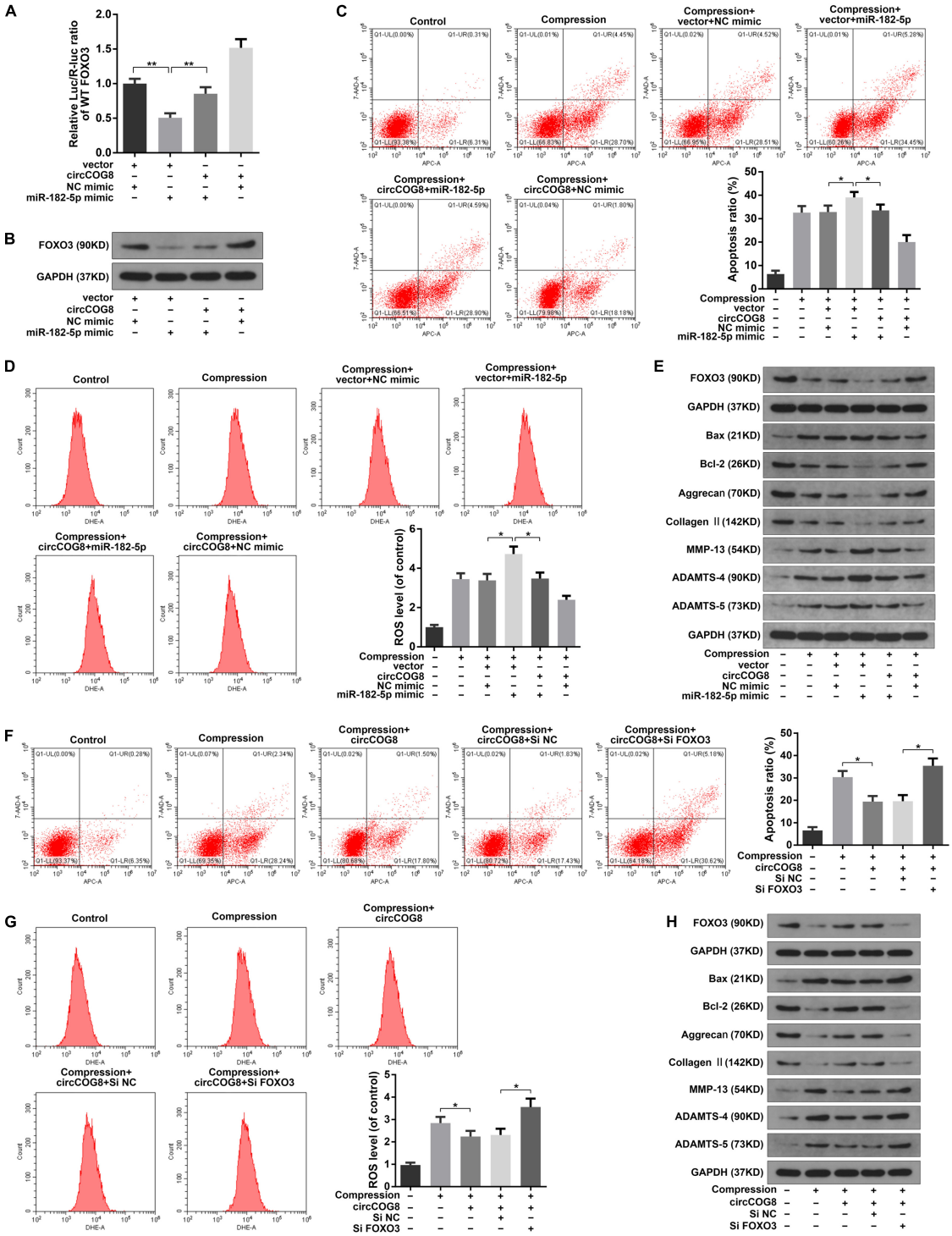


FIGURE 6 | CircCOG8 functioned in the disk NP cells by targeting miR-182-5p and FOXO3. **(A)** WT FOXO3 luciferase reporter vector was co-transfected into the HEK-293T cells with the miR-182-5p mimic or NC mimic, thecircCOG8 overexpression or control vector, and the luciferase reporter activity was presented as the relative Luc/R-Luc ratio. **(B)** The FOXO3 protein expression levels of the human NP cells under compression in corresponding groups were examined by the western blot analysis. **(C)** The apoptosis ratio in the NP cells was detected by Annexin V-APC and 7-AAD double-staining. **(D)** The intracellular ROS levels in the NP cells were detected by DHE with the flow cytometry analysis. **(E)** The protein levels of FOXO3, Bax, Bcl-2, Aggrecan, Type II collagen, MMP-13, ADAMTS-4, and ADAMTS-5 were determined by the western blot analysis. The upper GAPDH band served as an internal loading control for FOXO3; the lower GAPDH band served as a common internal loading control for Bax, Bcl-2, Aggrecan, Type II collagen, MMP-13, ADAMTS-4, and ADAMTS-5. **(F)** The Annexin V-APC and 7-AAD double-staining results indicating the apoptosis ratio of the NP cells. **(G)** The intracellular ROS production in the NP cells was detected by DHE with flow cytometry analysis. **(H)** The protein levels of FOXO3, Bax, Bcl-2, Aggrecan, Type II collagen, MMP-13, ADAMTS-4, and ADAMTS-5 were examined by the western blot analysis. The upper GAPDH band served as an internal loading control for FOXO3; the lower GAPDH band served as a common internal loading control for Bax, Bcl-2, Aggrecan, Type II collagen, MMP-13, ADAMTS-4, and ADAMTS-5. Data were represented as mean ± SD. $^*p < 0.05$, $^{**}p < 0.01$, $n = 3$ (Student's t-test).

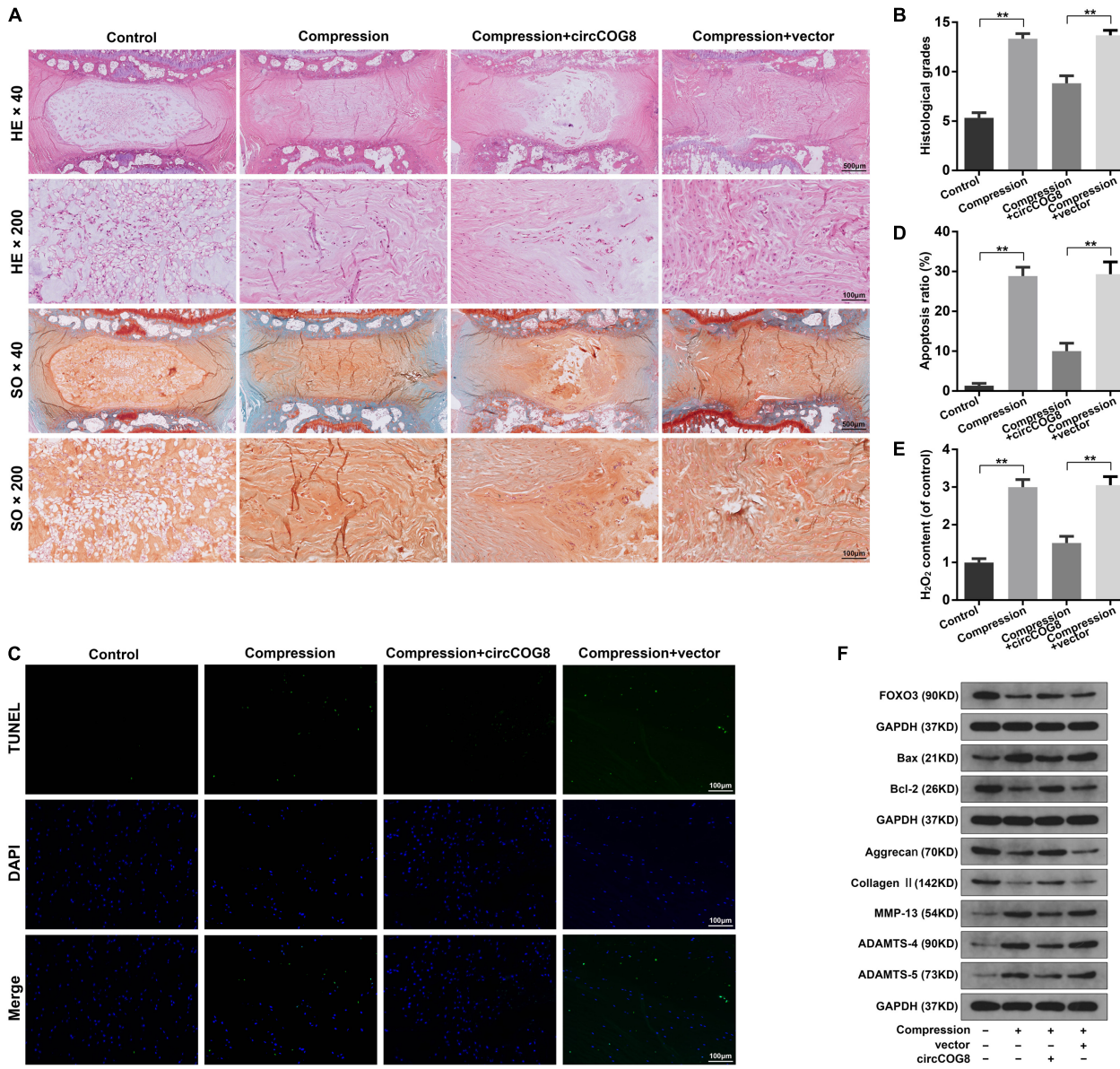


FIGURE 7 | CircCOG8 overexpression attenuated the compression-induced IDD *ex vivo*. **(A)** Representative photograph of the rat IVD tissues stained with HE and SO. The images were scanned at × 40 magnification (scale bar = 500 μm) and × 200 magnification (scale bar = 100 μm). **(B)** The histological grades of the disk samples evaluated by the histological grading scale. **(C)** Representative photograph of the TUNEL analysis to examine the NP cell apoptosis (scale bar = 100 μm). **(D)** Quantitative analysis of the TUNEL-positive cells indicating the apoptosis ratio. **(E)** The H_2O_2 content in the IVD tissues indicating the ROS level. **(F)** Western blot analysis was used to determine the protein expression level of FOXO3, Bax, Bcl-2, Aggrecan, Type II collagen, MMP-13, ADAMTS-4, and ADAMTS-5. The upper GAPDH band served as an internal loading control for FOXO3; the middle GAPDH band served as a common internal loading control for Bax and Bcl-2; the lower GAPDH band served as a common internal loading control for Aggrecan, Type II collagen, MMP-13, ADAMTS-4, and ADAMTS-5. Data were represented as mean ± SD. $^{*}p < 0.05$, $^{**}p < 0.01$, $n = 6$ IVDs per group (Student's *t*-test).

possesses more than 70 miR-7-binding sites and emerging evidence indicates that the interactions between Cdr1as and its targeting miRNAs are closely associated with the pathology of some human diseases, such as neuropsychiatric disorders, melanoma invasion and metastasis, and β-cell dysfunction in diabetic conditions (Piwecka et al., 2017; Stoll et al., 2018; Hanniford et al., 2020). A previous research by Liu et al. (2017) reported that a dysregulated circular RNA named circRNA-MSR participated in the chondrocyte ECM degradation through binding to miRNAs and, thus, regulating the TNF-α expression during osteoarthritis progression. Emerging evidence has shown several upregulated or downregulated circRNAs in the degenerated disks played an important part in the IDD pathogenesis. For example, a circular RNA hsa_circ_001653 was upregulated in the degenerated disk tissues with close relation to the IVD degeneration degrees. This circRNA could

inhibit the NP cell proliferation and ECM synthesis through targeting miR-486-3p to modulate CEMIP, which contributed significantly to the IDD development (Cui and Zhang, 2020). It was reported that a critical circRNA named circVMA21 was downregulated during IDD. CircVMA21 obviously inhibited inflammatory cytokines-induced disk cells apoptosis and ECM degradation by functioning as competing endogenous RNAs to bind to miR-200c and, thus, regulate the targeting gene XIAP (Cheng et al., 2018). There were also several other identified circRNAs reported to participate in the pathogenesis of IDD in the past few years (Li et al., 2019). However, it remains undetermined how circRNAs play a part functionally in the involvement of mechanical loads during the IVD degeneration development.

Although an increasing number of circRNAs have been identified across different eukaryotic species from microorganisms to animals, only a minor fraction of them have been researched for the biological implications (Conn et al., 2015). The circRNA identified in this study was a novel circRNA which played a critical role during the IDD progression involving mechanical stress. We showed that the circCOG8 expression in the disk NP cells was markedly downregulated by mechanical loading as determined by the microarray and RT-qPCR assays. CircCOG8 overexpression significantly alleviated the NP cell ECM degradation, cell apoptosis, and ROS accumulation induced by compression. And, downregulating circCOG8 could aggravate these effects of compression on the disk NP cells. Functionally, the critical microRNA miR-182-5p might mediate the effects of circCOG8 exerted on the disk cells. Using the bioinformatics prediction, the RNA immunoprecipitation assay and reporter gene analysis, we unveiled that circCOG8 could directly interact with miR-182-5p. Interestingly, miR-182-5p was found markedly upregulated in the disk NP cells under mechanical loading in this study. We showed that miR-182-5p facilitated the elevated apoptosis, oxidative stress as well as ECM degradation in the disk NP cells induced by mechanical loading. Inhibiting miR-182-5p markedly attenuated these cellular damages induced by compression loading. Generally, the regulatory function of a microRNA mainly is achieved by interacting with 3′-UTR of targeting mRNA to negatively regulate the gene expression. Using the online miRNA binding predicting tool, we found FOXO3 was an important miR-182-5p targeting gene and we further verified the interaction between them. FOXO3, known as FOXO3a or FKHR-L1, is among the Forkhead box O (FOXO) family of transcription factors which plays a crucial part in the normal physiological structure and function of IVD (Alvarez-Garcia et al., 2018). Previous study revealed that the FOXO3 expression level was obviously downregulated in severe degenerated human IVDs, contributing to the major histopathological changes during IDD progression (Penolazzi et al., 2018). In the present study, we observed that the FOXO3 expression in the NP cells was repressed by compression loading. FOXO3 was identified as the key targeting gene for miR-182-5p and their interaction accounted for a crucial part in the involvement of compression during IVD degeneration. Moreover, circCOG8 evidently neutralized the repressive function of miR-182-5p exerted on FOXO3, suggesting the role of circCOG8 as an miR-182-5p sponge to modulate the FOXO3 expression. We further validated that the absence of FOXO3 could counteract the protective effect of circCOG8 on human NP cells under compression loading by using the siRNA-mediated FOXO3 knockdown. However, the underlying mechanism by which circCOG8 and miR-182-5p could respond to mechanical stress still needed further investigation. Taken together, this study revealed that circCOG8 attenuated the mechanical stress induced damage in NP cells via restoring the FOXO3 expression achieved by sponging the miR-182-5p.

Collectively, the major findings from our study can be summarized as the following. (1) CircCOG8, derived from the third exon of COG8 gene, is a novel identified circRNA that functionally participates in the involvement of mechanical stress during IDD progression. (2) CircCOG8 can directly interact with miR-182-5p and, thus, modulate the FOXO3 expression in NP cells. (3) Compression-induced circCOG8 downregulation is an important underlying mechanism in the NP cell ECM degradation, cell apoptosis, and ROS accumulation via regulating the miR-182-5p/FOXO3 axis. In conclusion, the present study suggested that targeting the circCOG8/miR-182-5p/FOXO3 pathway provides a new therapeutic strategy for IDD treatment.

MATERIALS AND METHODS

Patient Samples

The present study was supervised by the Clinical Research Ethics Committee of Tongji Medical College, Huazhong University of Science and Technology, and all methods were used in strict adherence with the approved guidelines. The IVD tissue specimens were obtained from patients with idiopathic scoliosis who underwent spinal surgery. Informed consents were obtained from all subjects. Patients' medical records were collected and the IVD degeneration degrees were assessed by the Pfirrmann MRI-grading system (Pfirrmann et al., 2001). Generally, six disk tissue specimens were collected from two males and four females, aged 17–26 years old (mean: 21.3 years). The Pfirrmann grades of these disk samples were generally evaluated as Grade I or II. Among these specimens, three NP tissues were used to isolate the disk NP cells for the circRNA microarray assay and the other three were used for further *in vitro* experiments.

Primary Cells Culture

The disk NP tissue samples were dissected and digested using 0.25% pronase for 0.5 h and 0.2% type II collagenase for 4 h at 37°C. After filtering through a 70 μm pore size mesh, the NP cells were transferred to Dulbecco's modified Eagle medium (DMEM; Gibco, United States) with 15% fetal bovine serum (FBS; Gibco, United States), streptomycin (100 mg/ml; Gibco, United States) as well as penicillin (100 units/ml; Gibco, United States). The NP cells were cultured at 37°C in a CO_2 incubator with a controlled humidified atmosphere composed of 95% air and 5% CO_2. The culture medium was replaced

every 3 days. The second-generation cells were used in this study. For the compression treatment, the disk NP cells were treated by a previously described compression device to provide 1 MPa static mechanical loading (Wu et al., 2019). Briefly, the stainless pressure vessel allowed for pumping compressed gas into it to form a closed high-pressure environment which was monitored with a barometer. The pressure vessel was pumped into the mixed 0.5% CO_2 and 99.5% compressed air and the cells were placed in cell culture plates under humidified atmosphere at 37°C. Unless otherwise specified in the figures, the NP cells were treated under mechanical stress for 36 h.

Western Blotting

Samples were lysed by a radio immunoprecipitation lysis buffer and their protein contents were determined by an Enhanced BCA Protein Assay Kit (Beyotime, China). After centrifugation, the lysates were run by sodium dodecyl sulfate-polyacrylamide gel electrophoresis gels and transferred onto the polyvinylidene fluoride membranes. Then, the membranes were blocked for 1 h at 25°C with 5% non-fat dried milk in TBST, incubated overnight at 4°C with primary antibody. The membranes were subsequently incubated with the HRP-conjugated secondary antibody (dilution 1:2,000; Abcam). Protein bands were detected with enhanced chemiluminescence reagents (Amersham). The primary antibodies used are as follows: Bax (ab32503, Abcam), Bcl-2 (ab196495, Abcam), ADAMTS-4 (ab185722, Abcam), ADAMTS-5 (ab41037, Abcam), MMP-13 (ab39012, Abcam), aggrecan (13880-1-AP, Proteintech), Type II collagen (ab34712, Abcam), and FOXO3 (ab23683, Abcam). GAPDH (#5174, Cell Signaling Technology) was used as controls.

Flow Cytometry Analysis

The NP cell samples after various treatments were harvested and the apoptosis rates were examined by the dual-staining with Annexin V-APC and 7-AAD (KeyGen Biotech). Cell samples were washed twice by PBS and resuspended with the binding buffer then doubly stained with annexin-V and 7-AAD. And, the intracellular ROS production were examined by an ROS-specific fluorescent probe dihydroethidium (DHE, Beyotime). The stained cells from each experiment were analyzed by the FACSCalibur flow cytometer (Becton Dickinson).

RNA Extraction and qPCR Assay

Total cellular RNA extraction was performed with the TRIzol method following the merchant guide. The NE-PER Nuclear and Cytoplasmic Extraction Reagents (Thermo Scientific) were applied to isolate the nuclear and cytoplasmic fractions, following manufacturer's protocols. The first-strand cDNA was obtained from total RNA via a PrimeScript RT reagent kit (Takara Bio). The qPCR was carried out using SYBR Green Supermix (BioRad) and All-in-One miRNA RT-qPCR Kit (GeneCopoeia, Inc.). GAPDH was used as the internal control for mRNA and circRNA, and U6 was used to normalize miRNA level. Primers used in this study are as follows: *circCOG8* F, TTCAATGATCTGCGCCTCTG; *circCOG8* R, TTGGTCCTCAGTTGCTGGAT; *GAPDH* F, GTCTTCACCACCATGGAGAA; *GAPDH* R, TAAGC AGTTGGTGGTGCAG; *U6* F, CTCGCTTCGGCAGCACA; *U6* R, AACGCTTCACGAATTTGCGT; *MiR-182-5p stem-loop primer*, GTCGTATCCAGTGCAGGGTC CGAGGTATTCGCACTGGATACGACAGTGTG. *Divergent-circCOG8* F, ATGCTCATCTCGGCTCCAG; *Divergent-circCOG8* R, AGGAATGGCAGTCAGGATGG; *Convergent-circCOG8* F, CCATCCTGACTGCCATTCCT; *Convergent-circCOG8* R, CTGGAGCCGAGATGAGCAT; *Divergent-GAPDH* F, CACTTTGTCAAGCTCATTTCC; *Divergent-GAPDH* R, TTGGCAGTGGGGACACGGAAG; *Convergent-GAPDH* F, TCCATGCCATCACTGCCAC; and *Convergent-GAPDH* R, GTGGTCGTTGAGGGCAATG.

Circular RNA Microarray and Bioinformatics Analysis

Total cellular RNA from mechanical loading treated the disk NP cells or corresponding control cells was isolated to carry out the microarray assay. And, the circRNAs microarray assay was performed by the CapitalBio Corporation (Beijing, China) according to standard procedures. The GeneSpring GX software was used to analyze the microarray data. The thresholds were set as follows: fold change > 2, P-value < 0.05 evaluated using the Student's t-test. Clustered heat map was made to present the significantly down-regulated gene items in mechanical loading treated disk cells. The targeting miRNA of circCOG8 was predicted using the StarBase online database[1] and the Circular RNA Interactome online database[2]. And, the targeting genes of miR-182-5p were predicted based on the TargetScan online tool[3] as well as the miRDB[4]. Microarray raw data used in this study were available from the corresponding author upon reasonable request.

RNase R Treatment

Total cellular RNA (2 μg) extracted from the human disk NP cells was treated with 3 unit/μg of RNase R and the samples were incubated for 0.5 h at 37°C. GAPDH mRNA was used as the linear control group. Three independent experiments were performed with triplicate samples.

Luciferase Reporter Assay

The HEK-293T cells were cultured in 24-well plates to 60% confluence. Then, the cells were co-transfected with a luciferase reporter construct and miR-182-5p overexpression construct. The corresponding reporter construct of the WT pMIR-REPORT-circCOG8 as well as the MUT pMIR-REPORT-circCOG8 and the WT pMIR-REPORT-FOXO3-3′ UTR as well as the MUT

[1]http://starbase.sysu.edu.cn
[2]http://circinteractome.nia.nih.gov
[3]http://www.targetscan.org
[4]http://www.mirdb.org

pMIR-REPORT-FOXO3-3'UTR were obtained from the Obio Technology, Corp. 48 h after the transfection by lipofectamine 3000, the cells were assayed with the dual-luciferase reporter assay system (Promega), and measurements were performed on the Beckman–Coulter DTX880. Relative luciferase activity was presented as the Luc/R-Luc ratio by dividing the firefly luciferase (Luc) value by the *Renilla* luciferase (R-Luc) value.

RNA-Binding Protein Immunoprecipitation (RIP)

The RIP analysis was carried out by using a Magna RIP RNA-Binding Protein Immunoprecipitation Kit (EMD Millipore Corporation, Billerica, MA, United States) combined with the human anti-AGO2 antibody (#2897, Cell signaling), according to the merchant guide. Briefly, after pelleting and re-suspending by RIP lysis buffer, the cells extract was treated with the RIP buffer containing A/G magnetic beads conjugated with an anti-AGO2 antibody or corresponding control IgG. Co-precipitated circCOG8, as well as miR-182-5p, was subsequently examined using the RT-qPCR assay.

Cell Transfection

For the circCOG8 overexpression, exon 3 of human COG8 gene (828 bp) with approximate 1 kb flanking introns containing complementary Alu elements were amplified to construct the recombinant adenovirus vector (Obio Technology, Shanghai, China), as described previously (Zhang et al., 2014). For the lentiviral circCOG8 shRNA construction, oligonucleotides with the circCOG8 targeting sequences were inserted to the pLKD-CMV-G&PR-U6-shRNA vector (Obio Technology, Shanghai, China). Targeting sequence for circCOG8: CCAAGGGCATCGTGAACGA, negative control sequence: TTCTCCGAACGTGTCACGT. MiR-182-5p mimic, miR-182-5p inhibitor, as well as their corresponding negative controls, were produced by the GenePharma, Corp. FOXO3 siRNA (targeting sequence: GCATGTTCAATGGGAGCTTGGA) and its control siRNA was purchased from the Obio Technology, Corp. The NP cells were cultured with six-well plates to 70–80% confluence and then, the cell transfection was achieved by the Lipofectamine 3000 transfection reagent (Invitrogen, United States), according to the merchant guide.

IVD Organ Model Culture

Rat IVDs of Co6/7 and Co7/8 were collected from Sprague-Dawley rats of 3 months, with an approval from the Animal Experimentation Committee of Huazhong University of Science and Technology. Interact disks were meticulously isolated and cultured by the DMEM (Gibco, United States) with 15% FBS (Gibco, United States), streptomycin (100 mg/ml; Gibco, United States) as well as penicillin (100 units/ml; Gibco, United States), according to our previous study (Wu et al., 2019). The IVDs were cultured at 37°C and the medium was replaced every 3 days. For the compression treatment, the IVD organ model was placed on the culture plates in the compression device which could provide 1 MPa static compression, as described above. According to the classic air-pressure principle, the custom-made compression apparatus was applied, as previously described, to expose the IVDs to static high pressure (Hutton et al., 1999; Wu et al., 2019). And, the IVDs were treated under continuous mechanical loading except for the time when the culture medium was replaced.

CircRNA Injection Into *ex vivo* Cultured IVD Models

The adeno-associated virus (AAV) vector overexpressing circCOG8 and the control vector were constructed and packaged by the Obio Technology (Shanghai, China). The *ex vivo* IVD organs were randomly divided into four groups: control group (n = 6), compression group (n = 6), circCOG8 injection with compression group (n = 6), and control vector injection with compression group (n = 6). The *ex vivo* disks were injected with a 2 μl solution containing the experimental virus vector overexpressing circCOG8 or the control virus vector by using the 33-G needle. Then, the cultured IVDs were treated under a static mechanical loading for 4 weeks.

Histological Evaluation, TUNEL Staining, and ROS Measurement in *ex vivo* Cultured IVD Models

The rat disk tissues were collected and rinsed using PBS. Disk samples were fixed by formalin and decalcified using EDTA. Then, the disks were embedded in paraffin, sectioned, and stained using the hematoxylin-eosin, as well as the safranin O. Histological evaluation grades were determined according to a previous study (Mao et al., 2011). The *in situ* apoptotic activity was examined by the TUNEL Apoptosis Assay Kit (C1088, Beyotime, China). The specimens were overlaid by the Vectashield Hard Set mounting medium containing DAPI. TUNEL positive cells were counted from three different fields of disk NP and the ratio of positive cells relative to total was determined. The ROS level in IVD tissues was measured by the Hydrogen Peroxide assay kit (NJJCbio, Nanjing, China), following the merchant guide.

Statistical Analysis

The data were expressed as a mean value ± standard deviation (SD). Each experiment was repeated independently for three times, unless otherwise indicated. All data in the study were processed by the GraphPad Prism 7.0 software. Statistical significance was analyzed using the Student's t-test for two-group comparisons, one-way analysis of variance (ANOVA) with Tukey's post-test for multiple group comparisons. Significance levels were set as $^{*}p < 0.05$, $^{**}p < 0.01$.

DATA AVAILABILITY STATEMENT

All datasets generated for this study are included in the article/**Supplementary Material.**

ETHICS STATEMENT

The animal study was reviewed and approved by the Animal Experimentation Committee of Huazhong University of Science and Technology.

AUTHOR CONTRIBUTIONS

QX and LK designed the study protocol. QX, LK, KZ, JW, WH, YS, XF, and SL performed the experiments. KZ, GL, and KW collected and analyzed data. QX, LK, and KZ wrote the manuscript. CY and YZ reviewed and revised the manuscript. YZ supported and supervised the study. All authors contributed to the article and approved the submitted version.

FUNDING

This study was supported by the grants from the National Natural Science Foundation of China (81772391, 81974348, and 81902260).

SUPPLEMENTARY MATERIAL

The Supplementary Material for this article can be found online at: https://www.frontiersin.org/articles/10.3389/fcell.2020.581941/full#supplementary-material

REFERENCES

Adams, M. A., and Roughley, P. J. (2006). What is intervertebral disc degeneration, and what causes it? *Spine* 31, 2151–2161. doi: 10.1097/01.brs.0000231761.73859.2c

Alvarez-Garcia, O., Matsuzaki, T., Olmer, M., Miyata, K., Mokuda, S., Sakai, D., et al. (2018). FOXO are required for intervertebral disk homeostasis during aging and their deficiency promotes disk degeneration. *Aging Cell* 17:e12800. doi: 10.1111/acel.12800

Bartel, D. P. (2004). MicroRNAs: genomics, biogenesis, mechanism, and function. *Cell* 116, 281–297.

Chen, B., Wei, W., Huang, X., Xie, X., Kong, Y., Dai, D., et al. (2018). circEPSTI1 as a prognostic marker and mediator of triple-negative breast cancer progression. *Theranostics* 8, 4003–4015. doi: 10.7150/thno.24106

Chen, S., Lv, X., Hu, B., Zhao, L., Li, S., Li, Z., et al. (2018). Critical contribution of RIPK1 mediated mitochondrial dysfunction and oxidative stress to compression-induced rat nucleus pulposus cells necroptosis and apoptosis. *Apoptosis* 23, 299–313. doi: 10.1007/s10495-018-1455-x

Cheng, X., Zhang, L., Zhang, K., Zhang, G., Hu, Y., Sun, X., et al. (2018). Circular RNA VMA21 protects against intervertebral disc degeneration through targeting miR-200c and X linked inhibitor-of-apoptosis protein. *Ann. Rheum. Dis.* 77, 770–779. doi: 10.1136/annrheumdis-2017-212056

Conn, S. J., Pillman, K. A., Toubia, J., Conn, V. M., Salmanidis, M., Phillips, C. A., et al. (2015). The RNA binding protein quaking regulates formation of circRNAs. *Cell* 160, 1125–1134. doi: 10.1016/j.cell.2015.02.014

Cui, S., and Zhang, L. (2020). circ_001653 silencing promotes the proliferation and ECM synthesis of NPCs in IDD by downregulating miR-486-3p-mediated CEMIP. *Mol. Ther. Nucleic Acids* 20, 385–399. doi: 10.1016/j.omtn.2020.01.026

Feng, C., Yang, M., Lan, M., Liu, C., Zhang, Y., Huang, B., et al. (2017). ROS: crucial intermediators in the pathogenesis of intervertebral disc degeneration. *Oxid. Med. Cell. Longev.* 2017:5601593. doi: 10.1155/2017/5601593

Gilchrist, C. L., Darling, E. M., Chen, J., and Setton, L. A. (2011). Extracellular matrix ligand and stiffness modulate immature nucleus pulposus cell-cell interactions. *PLoS One* 6:e27170. doi: 10.1371/journal.pone.0027170

Glaeser, J. D., Salehi, K., Kanim, L. E. A., NaPier, Z., Kropf, M. A., Cuéllar, J. M., et al. (2020). NF-κB inhibitor, NEMO-binding domain peptide attenuates intervertebral disc degeneration. *Spine J.* 20, 1480–1491. doi: 10.1016/j.spinee.2020.04.025

Han, B., Chao, J., and Yao, H. (2018). Circular RNA and its mechanisms in disease: from the bench to the clinic. *Pharmacol. Ther.* 187, 31–44. doi: 10.1016/j.pharmthera.2018.01.010

Hanniford, D., Ulloa-Morales, A., Karz, A., Berzoti-Coelho, M. G., Moubarak, R. S., Sánchez-Sendra, B., et al. (2020). Epigenetic silencing of CDR1as drives IGF2BP3-mediated melanoma invasion and metastasis. *Cancer Cell* 37, 55.e15–70.e15. doi: 10.1016/j.ccell.2019.12.007

Hansen, T. B., Jensen, T. I., Clausen, B. H., Bramsen, J. B., Finsen, B., Damgaard, C. K., et al. (2013). Natural RNA circles function as efficient microRNA sponges. *Nature* 495, 384–388. doi: 10.1038/nature11993

Holguin, N., and Silva, M. J. (2018). In-vivo nucleus pulposus-specific regulation of adult murine intervertebral disc degeneration via Wnt/Beta-catenin signaling. *Sci. Rep.* 8:11191. doi: 10.1038/s41598-018-29352-3

Hoy, D. G., Smith, E., Cross, M., Sanchez-Riera, L., Buchbinder, R., Blyth, F. M., et al. (2014). The global burden of musculoskeletal conditions for 2010: an overview of methods. *Ann. Rheum. Dis.* 73:982. doi: 10.1136/annrheumdis-2013-204344

Huang, D., Peng, Y., Ma, K., Qing, X., Deng, X., Li, Z., et al. (2020). Puerarin relieved compression-induced apoptosis and mitochondrial dysfunction in human nucleus pulposus mesenchymal stem cells via the PI3K/Akt pathway. *Stem Cells Int.* 2020:7126914. doi: 10.1155/2020/7126914

Hughes, S. P., Freemont, A. J., Hukins, D. W., McGregor, A. H., and Roberts, S. (2012). The pathogenesis of degeneration of the intervertebral disc and emerging therapies in the management of back pain. *J. Bone Joint Surg. Br.* 94, 1298–1304. doi: 10.1302/0301-620x.94b10.28986

Hutton, W. C., Elmer, W. A., Boden, S. D., Hyon, S., Toribatake, Y., Tomita, K., et al. (1999). The effect of hydrostatic pressure on intervertebral disc metabolism. *Spine* 24:1507. doi: 10.1097/00007632-199908010-00002

Jiang, Y., Dong, G., and Song, Y. (2018). Nucleus pulposus cell senescence is alleviated by resveratrol through regulating the ROS/NF-κB pathway under high-magnitude compression. *Biosci. Rep.* 38:BSR20180670. doi: 10.1042/bsr20180670

Kleaveland, B., Shi, C. Y., Stefano, J., and Bartel, D. P. (2018). A network of noncoding regulatory RNAs acts in the mammalian brain. *Cell* 174, 350.e17–362.e17. doi: 10.1016/j.cell.2018.05.022

Koerner, J. D., Markova, D. Z., Schroeder, G. D., Rihn, J. A., Hilibrand, A. S., Vaccaro, A. R., et al. (2016). The effect of substance p on an intervertebral disc rat organ culture model. *Spine* 41, 1851–1859. doi: 10.1097/brs.0000000000001676

Lee, C. R., Iatridis, J. C., Poveda, L., and Alini, M. (2006). In vitro organ culture of the bovine intervertebral disc: effects of vertebral endplate and potential for mechanobiology studies. *Spine* 31, 515–522. doi: 10.1097/01.brs.0000201302.59050.72

Li, P., Hou, G., Zhang, R., Gan, Y., Xu, Y., Song, L., et al. (2017). High-magnitude compression accelerates the premature senescence of nucleus pulposus cells via the p38 MAPK-ROS pathway. *Arthritis Res. Ther.* 19:209. doi: 10.1186/s13075-017-1384-z

Li, S., Hua, W., Wang, K., Gao, Y., Chen, S., Liu, W., et al. (2018). Autophagy attenuates compression-induced apoptosis of human nucleus pulposus cells via MEK/ERK/NRF1/Atg7 signaling pathways during intervertebral disc degeneration. *Exp. Cell Res.* 370, 87–97. doi: 10.1016/j.yexcr.2018.06.012

Li, X., Yang, L., and Chen, L. L. (2018). The biogenesis, functions, and challenges of circular RNAs. *Mol. Cell.* 71, 428–442. doi: 10.1016/j.molcel.2018.06.034

Li, Z., Chen, X., Xu, D., Li, S., Chan, M. T. V., and Wu, W. K. K. (2019). Circular RNAs in nucleus pulposus cell function and intervertebral disc degeneration. *Cell. Prolif.* 52:e12704. doi: 10.1111/cpr.12704

Li, Z., Yu, X., Shen, J., Chan, M. T., and Wu, W. K. (2015). MicroRNA in intervertebral disc degeneration. *Cell. Prolif.* 48, 278–283. doi: 10.1111/cpr.12180

Lin, H., Ma, X., Wang, B. C., Zhao, L., Liu, J. X., Pu, F. F., et al. (2017). Edaravone ameliorates compression-induced damage in rat nucleus pulposus cells. *Life Sci.* 189, 76–83. doi: 10.1016/j.lfs.2017.09.024

Liu, G., Huang, K., Jie, Z., Wu, Y., Chen, J., Chen, Z., et al. (2018). CircFAT1 sponges miR-375 to promote the expression of Yes-associated protein 1 in osteosarcoma cells. *Mol. Cancer* 17:170. doi: 10.1186/s12943-018-0917-7

Liu, Q., Zhang, X., Hu, X., Yuan, L., Cheng, J., Jiang, Y., et al. (2017). Emerging roles of circRNA related to the mechanical stress in human cartilage degradation of osteoarthritis. *Mol. Ther. Nucleic Acids* 7, 223–230. doi: 10.1016/j.omtn.2017.04.004

Liu, W., Zhang, Y., Xia, P., Li, S., Feng, X., Gao, Y., et al. (2016). MicroRNA-7 regulates IL-1beta-induced extracellular matrix degeneration by targeting GDF5 in human nucleus pulposus cells. *Biomed. Pharmacother.* 83, 1414–1421. doi: 10.1016/j.biopha.2016.08.062

MacLean, J. J., Lee, C. R., Alini, M., and Iatridis, J. C. (2005). The effects of short-term load duration on anabolic and catabolic gene expression in the rat tail intervertebral disc. *J. Orthop. Res.* 23, 1120–1127. doi: 10.1016/j.orthres.2005.01.020

Mao, H. J., Chen, Q. X., Han, B., Li, F. C., Feng, J., Shi, Z. L., et al. (2011). The effect of injection volume on disc degeneration in a rat tail model. *Spine* 36, E1062–E1069. doi: 10.1097/BRS.0b013e3182027d42

Memczak, S., Jens, M., Elefsinioti, A., Torti, F., Krueger, J., Rybak, A., et al. (2013). Circular RNAs are a large class of animal RNAs with regulatory potency. *Nature* 495, 333–338. doi: 10.1038/nature11928

Neidlinger-Wilke, C., Galbusera, F., Pratsinis, H., Mavrogonatou, E., Mietsch, A., Kletsas, D., et al. (2014). Mechanical loading of the intervertebral disc: from the macroscopic to the cellular level. *Eur. Spine J.* 23(Suppl. 3), S333–S343. doi: 10.1007/s00586-013-2855-9

Penolazzi, L., Lambertini, E., Bergamin, L. S., Roncada, T., De Bonis, P., Cavallo, M., et al. (2018). MicroRNA-221 silencing attenuates the degenerated phenotype of intervertebral disc cells. *Aging* 10, 2001–2015. doi: 10.18632/aging.101525

Pfirrmann, C. W., Metzdorf, A., Zanetti, M., Hodler, J., and Boos, N. (2001). Magnetic resonance classification of lumbar intervertebral disc degeneration. *Spine* 26, 1873–1878. doi: 10.1097/00007632-200109010-00011

Piwecka, M., Glažar, P., Hernandez-Miranda, L. R., Memczak, S., Wolf, S. A., Rybak-Wolf, A., et al. (2017). Loss of a mammalian circular RNA locus causes miRNA deregulation and affects brain function. *Science* 357:eaam8526. doi: 10.1126/science.aam8526

Risbud, M. V., and Shapiro, I. M. (2014). Role of cytokines in intervertebral disc degeneration: pain and disc content. *Nat. Rev. Rheumatol.* 10, 44–56. doi: 10.1038/nrrheum.2013.160

Roberts, S., Evans, H., Trivedi, J., and Menage, J. (2006). Histology and pathology of the human intervertebral disc. *J. Bone Joint Surg. Am.* 88(Suppl. 2), 10–14. doi: 10.2106/jbjs.F.00019

Roughley, P. J. (2004). Biology of intervertebral disc aging and degeneration: involvement of the extracellular matrix. *Spine* 29, 2691–2699. doi: 10.1097/01.brs.0000146101.53784.b1

Sakai, D., and Grad, S. (2015). Advancing the cellular and molecular therapy for intervertebral disc disease. *Adv. Drug Deliv. Rev* 84, 159–171. doi: 10.1016/j.addr.2014.06.009

Sakai, D., Nakamura, Y., Nakai, T., Mishima, T., Kato, S., Grad, S., et al. (2012). Exhaustion of nucleus pulposus progenitor cells with ageing and degeneration of the intervertebral disc. *Nat. Commun.* 3:1264. doi: 10.1038/ncomms2226

Setton, L. A., and Chen, J. (2006). Mechanobiology of the intervertebral disc and relevance to disc degeneration. *J. Bone Joint Surg. Am.* 88(Suppl. 2), 52–57. doi: 10.2106/jbjs.F.00001

Song, J., Wang, H. L., Song, K. H., Ding, Z. W., Wang, H. L., Ma, X. S., et al. (2018). CircularRNA_104670 plays a critical role in intervertebral disc degeneration by functioning as a ceRNA. *Exp. Mol. Med.* 50:94. doi: 10.1038/s12276-018-0125-y

Stoll, L., Sobel, J., Rodriguez-Trejo, A., Guay, C., Lee, K., Venø, M. T., et al. (2018). Circular RNAs as novel regulators of β-cell functions in normal and disease conditions. *Mol. Metab.* 9, 69–83. doi: 10.1016/j.molmet.2018.01.010

Wilke, H. J., Neef, P., Caimi, M., Hoogland, T., and Claes, L. E. (1999). New in vivo measurements of pressures in the intervertebral disc in daily life. *Spine* 24, 755–762. doi: 10.1097/00007632-199904150-00005

Wu, X., Liao, Z., Wang, K., Hua, W., Liu, X., Song, Y., et al. (2019). Targeting the IL-1beta/IL-1Ra pathways for the aggregation of human islet amyloid polypeptide in an ex vivo organ culture system of the intervertebral disc. *Exp. Mol. Med.* 51:110. doi: 10.1038/s12276-019-0310-7

Yurube, T., Takada, T., Suzuki, T., Kakutani, K., Maeno, K., Doita, M., et al. (2012). Rat tail static compression model mimics extracellular matrix metabolic imbalances of matrix metalloproteinases, aggrecanases, and tissue inhibitors of metalloproteinases in intervertebral disc degeneration. *Arthritis Res. Ther.* 14:R51. doi: 10.1186/ar3764

Zhang, X. O., Wang, H. B., Zhang, Y., Lu, X., Chen, L. L., and Yang, L. (2014). Complementary sequence-mediated exon circularization. *Cell* 159, 134–147. doi: 10.1016/j.cell.2014.09.001

Zhao, C. Q., Wang, L. M., Jiang, L. S., and Dai, L. Y. (2007). The cell biology of intervertebral disc aging and degeneration. *Ageing Res. Rev.* 6, 247–261. doi: 10.1016/j.arr.2007.08.001

Zhao, Z. J., and Shen, J. (2017). Circular RNA participates in the carcinogenesis and the malignant behavior of cancer. *RNA Biol.* 14, 514–521. doi: 10.1080/15476286.2015.1122162

Conflict of Interest: The authors declare that the research was conducted in the absence of any commercial or financial relationships that could be construed as a potential conflict of interest.

Copyright © 2020 Xiang, Kang, Zhao, Wang, Hua, Song, Feng, Li, Lu, Wang, Yang and Zhang. This is an open-access article distributed under the terms of the Creative Commons Attribution License (CC BY). The use, distribution or reproduction in other forums is permitted, provided the original author(s) and the copyright owner(s) are credited and that the original publication in this journal is cited, in accordance with accepted academic practice. No use, distribution or reproduction is permitted which does not comply with these terms.

frontiers in Cell and Developmental Biology

ORIGINAL RESEARCH
published: 30 October 2020
doi: 10.3389/fcell.2020.598660

Construction of a Five-Super-Enhancer-Associated-Genes Prognostic Model for Osteosarcoma Patients

Zhanbo Ouyang[1], Guohua Li[1], Haihong Zhu[1], Jiaojiao Wang[1], Tingting Qi[1], Qiang Qu[2], Chao Tu[3], Jian Qu[1] and Qiong Lu[1]**

[1] Department of Pharmacy, The Second Xiangya Hospital, Central South University; Institute of Clinical Pharmacy, Central South University, Changsha, China, [2] Department of Pharmacy, Xiangya Hospital, Central South University, Changsha, China, [3] Department of Orthopaedics, The Second Xiangya Hospital, Central South University, Changsha, China

OPEN ACCESS

Edited by:
Changjun Li,
Xiangya Hospital, Central South University, China

Reviewed by:
Lanxiang Wu,
Chongqing Medical University, China
Xiaolong Tang,
Shenzhen University Health Science Centre, China
Donna Fu,
University of California, San Francisco, United States

***Correspondence:**
Jian Qu
qujianstanley@csu.edu.cn
Qiong Lu
christy_luq@csu.edu.cn

Specialty section:
This article was submitted to Molecular Medicine, a section of the journal Frontiers in Cell and Developmental Biology

Received: *25 August 2020*
Accepted: *05 October 2020*
Published: *30 October 2020*

Citation:
Ouyang Z, Li G, Zhu H, Wang J, Qi T, Qu Q, Tu C, Qu J and Lu Q (2020) Construction of a Five-Super-Enhancer-Associated-Genes Prognostic Model for Osteosarcoma Patients. Front. Cell Dev. Biol. 8:598660. doi: 10.3389/fcell.2020.598660

Osteosarcoma is a malignant tumor most commonly arising in children and adolescents and associated with poor prognosis. In recent years, some prognostic models have been constructed to assist clinicians in the treatment of osteosarcoma. However, the prognosis and treatment of patients with osteosarcoma remain unsatisfactory. Notably, super-enhancer (SE)-associated genes strongly promote the progression of osteosarcoma. In the present study, we constructed a novel effective prognostic model using SE-associated genes from osteosarcoma. Five SE-associated genes were initially screened through the least absolute shrinkage and selection operator (Lasso) penalized Cox regression, as well as univariate and multivariate Cox regression analyses. Meanwhile, a risk score model was constructed using the expression of these five genes. The excellent performance of the five-SE-associated-gene-based prognostic model was determined via time-dependent receiver operating characteristic (ROC) curves and Kaplan–Meier curves. Inferior outcome of overall survival (OS) was predicted in the high-risk group. A nomogram based on the polygenic risk score model was further established to validate the performance of the prognostic model. It showed that our prognostic model performed outstandingly in predicting 1-, 3-, and 5-year OS of patients with osteosarcoma. Meanwhile, these five genes also belonged to the hub genes associated with survival and necrosis of osteosarcoma according to the result of weighted gene co-expression network analysis based on the dataset of GSE39058. Therefore, we believe that the five-SE-associated-gene-based prognostic model established in this study can accurately predict the prognosis of patients with osteosarcoma and effectively assist clinicians in treating osteosarcoma in the future.

Keywords: osteosarcoma, super-enhancer, prognostic model, Lasso, weighted gene co-expression network analysis, overall survival

Abbreviations: AIC, Akaike information criterion; AUC, area under the ROC; C-index, concordance index; GEO, Gene Expression Omnibus; GS, gene significance; HR, hazard ratio; IGV, Integrative Genomics Viewer; K–M, Kaplan–Meier; Lasso, least absolute shrinkage and selection operator; MM, module membership; OS, overall survival; ROC, receiver operating characteristic; SE, super-enhancer; TCGA, The Cancer Genome Atlas; WGCNA, weighted gene co-expression network analysis.

INTRODUCTION

Osteosarcoma, the most common primary bone tumor, is most commonly arising in children and adolescents (Bielack et al., 2009). The survival rate of patients with osteosarcoma is markedly low due to the tendency of osteosarcoma for early metastasis and rapid progression (Kempf-Bielack et al., 2005). The overall 5-year survival rate of patients with non-metastatic osteosarcoma is approximately 60–70%, while the survival rate of osteosarcoma patients with metastatic symptoms is only 20–30% (Kempf-Bielack et al., 2005; Luetke et al., 2014; Meazza and Scanagatta, 2016). Moreover, high-grade patients comprise nearly 80–90% of those diagnosed with osteosarcoma; the treatment of these patients is challenging (Bielack et al., 2009). Furthermore, despite advancements in treatment in recent years, the therapeutic outcomes remain unsatisfactory. Although numerous traditional predictive factors, such as age, necrosis, recurrence, and clinical stage, are important contributors to clinical outcome, they are less effective in predicting the survival status due to the complex molecular mechanisms of osteosarcoma progression. Thus, it is urgent to investigate novel effective molecular biomarkers for the more precise prediction of the prognosis of patients with osteosarcoma.

Super-enhancer is a large cluster of *cis*-regulatory DNA elements densely bound by transcription factors and cofactors, playing vital roles in defining cell fate and identity (Hnisz et al., 2013). Histone marks (H3K27ac, H3K4me1, and H3K4me3), cofactor (p300), and mediators (CDK7 and BRD4) are common biomarkers used to define SE (Lovén et al., 2013; Hnisz et al., 2015; Ma et al., 2019); among them, H3K27ac is the most efficient biomarker for identifying SE (Creyghton et al., 2010; Hnisz et al., 2013; Whyte et al., 2013). Therefore, we used H3K27ac, H3K4me1, and H3K4me3 as SE biomarkers in this study based on the ChIP–seq profiles data from Cistrome. Moreover, SE plays a critical role in the progression of osteosarcoma through activating the expression of its downstream target oncogenes, such as *MYC*, *LIF*, and *STAT3* (Chen et al., 2018; Lu et al., 2020; Zhang et al., 2020). Furthermore, SE inhibitors (e.g., JQ1, THZ1, and THZ2), which were developed for the treatment of osteosarcoma, could restore the expression levels of these genes (Lee et al., 2015; Chen et al., 2018; Zhang et al., 2020). Thus, screening and identifying hub oncogenes driven by SE will provide novel insights into the diagnosis, prognosis, and treatment of osteosarcoma.

The Lasso penalized Cox regression analysis, designed by Tibshirani (1997), is an accurate statistical method frequently used for the selection of variables in the Cox regression model. It can remarkably improve the accuracy of the model it generates compared with the stepwise regression method, as it involves fewer variables and produces more interpretable models (Tibshirani, 1997; Xiong et al., 2019). The reason for Lasso screening fewer variables is that it can regularize the impact of some variables by shrinking their coefficients to zero (Zhang et al., 2018). Nowadays, Lasso is widely used in constructing prognostic models for the prediction of survival based on complicated high-throughput genomic data (Zhang et al., 2013; Lu et al., 2019; Wang et al., 2019; Wu et al., 2019). Based on this advantage, we applied the Lasso regression method to the construction of a prognostic model of osteosarcoma.

Weighted gene co-expression network analysis (WGCNA) is a system bioinformatics method involving molecular interaction mechanism analysis and construction of correlation gene networks (Zhang and Horvath, 2005). WGCNA has been frequently utilized in identifying probable oncogenes and in screening candidate targets for various cancers (Udyavar et al., 2013). Using WGCNA, Tian et al. (2018) showed that the insulin-like growth factor-binding-associated genes may play a critical role in osteosarcoma metastasis progression. Guan et al. (2020) defined four key genes (*ALOX5AP*, *HLA-DMB*, *HLA-DRA*, and *SPINT2*) as prognostic markers for osteosarcoma metastasis. We adapted WGCNA to identify the five screened genes from SE-associated genes that were crucial hub genes of osteosarcoma. Prognostic models based on some cancer-related genes (Long et al., 2018; Zuo et al., 2019), long non-coding RNAs (Liu et al., 2020; Yang et al., 2020; Zhang et al., 2020), or other biomarkers (Park et al., 2017; Elwood et al., 2018) for improving patient prognosis attract considerable attention. For instance, Zhu et al. (2020) constructed a seven-gene signature associated with osteosarcoma energy metabolism for predicting the prognosis of osteosarcoma through WGCNA and Lasso Cox regression analysis. Dong et al. (2019) constructed a risk score model based on eight genes for predicting the metastasis of osteosarcoma mainly through Lasso logistic regression analysis. Thus, we attempted to perform WGCNA for osteosarcoma and screen hub genes related to clinical traits of this disease. Nomograms are interactive tools developed in recent years, which have been widely used to predict the probability of survival (Wang et al., 2018; Yap et al., 2018; Pan et al., 2019; Xiao et al., 2019; Zhang et al., 2019). Similarly, we constructed a prognostic model and a visualized nomogram based on this model to improve the prognosis of patients with osteosarcoma.

In this study, Lasso penalized Cox regression analysis was initially performed using 349 selected SE-associated genes. A gene cluster containing five SE-associated genes, namely, *AMN1*, *LIMS1*, *SAMD4A*, *SPARC*, and *ZP3*, was screened. Subsequently, a risk score model based on these five genes was constructed and verified using training and validation datasets. Meanwhile, univariate and multivariate Cox regression analyses and ROC curve analysis were also used to assess the predictive ability of the model. We further screened module genes related to clinical traits of patients with osteosarcoma via WGCNA. The five SE-associated genes were also part of the module genes linked to survival and recurrence of osteosarcoma. Finally, an interactive nomogram was constructed based on the risk score model including the five-gene risk group and clinical traits. The five-SE-associated-gene-based prognostic model developed in this study will provide promising inspiration for the clinical therapy of patients with osteosarcoma.

MATERIALS AND METHODS

Data Collection and Expression Matrix Preparation

We downloaded the osteosarcoma dataset GSE39058 as training data from the National Center for Biotechnology Information GEO[1]. The 20,819 genes in 42 samples of osteosarcoma were annotated according to the probe information from Illumina HumanHT-12 WG-DASL V4.0 R2 Expression BeadChip (GPL14951) (Kelly et al., 2013). We processed the raw data of the expression matrix by transformation of log2– via the R package "limma." The clinical information was organized into a matrix and is shown in **Table 1**. One sample (GSM954821) was excluded due to the lack of information on the survival status. The validation dataset Target-osteosarcoma (Target-OS) was downloaded from the publicly available database of TCGA[2]. The 434 SE-associated genes from the osteosarcoma cell line U2OS were obtained from the website of the SE database (version 1.03[3]). Following the intersection of SE-associated genes and 20,819 genes from GSE39058, 349 SE-associated genes were used for the subsequent analysis. Chromatin immunoprecipitation (ChIP) signals of H3K27ac-seq, H3K4me1-seq, and H3K4me3-seq in U2OS were also downloaded from Cistrome[4] and visualized using the IGV (Thorvaldsdottir et al., 2013).

Lasso Penalized Cox Proportional Hazard Regression Model

Lasso penalized Cox regression analysis was performed to screen important prognostic genes for predicting the OS of patients with osteosarcoma using R package "glmnet" (Friedman et al., 2010; Simon et al., 2011; Tibshirani et al., 2012). The shrinking penalty was identified based on the tuning parameter lambda (λ), which was identified based on 10-fold cross-validation. Two optimal λ values (λ_{min} and λ_{lse}) were highlighted by the vertical lines with a minimizing mean-square error. To determine the optimal λ value, we performed the Wilcoxon test and ROC curve analysis for the comparison of λ_{min} and λ_{lse} values. These two λ values were used to construct a new fitted Lasso model, and two lists of genes were generated.

[1]https://www.ncbi.nlm.nih.gov/geo/

[2]https://cancergenome.nih.gov/

[3]http://www.licpathway.net/sedb

[4]http://cistrome.org/db/#/

TABLE 1 | The clinical information of 41 OS patients from dataset GSE39058.

Variable		Number
Gender	Male	21
	Female	20
Necrosis	Low	14
	High	27
Recurrence	No	21
	Yes	20
Death	No	29
	Yes	12

Cox Proportional Hazard Regression Model

Univariate and multivariate Cox proportional hazard regression analyses were performed to validate the associations between the expression levels of selected genes and OS of the patients via the R package "survival" and "survminer." The regression coefficient (β-value) and HR were predicted. Harrell's C-index, likelihood ratio test, and Wald test were also calculated, and the results are presented in the forest plot. Survival analysis of the single gene in the prognostic model was performed using the K–M survival curve and log-rank test via the R package "survival" and "survminer." Time-dependent ROC curve analysis was calculated to evaluate the predictive capability of OS of the prognostic model via the R package "timeROC."

Polygenic Risk Score Model for Prognostic Prediction

To further investigate the prognostic model based on the gene group, a polygenic risk score model was constructed used the following forum RiskScore = $\Sigma\beta i * Xi$. Xi is the level of gene expression and βi is the regression coefficient. The risk score model was defined as the linear combination of the expression levels of selected genes. The patients with osteosarcoma in the two datasets were divided into high- and low-risk groups according to the risk score. We verified the power of the polygenic risk score model through single-gene expression status analysis, event distribution analysis, K–M survival analysis, and time-dependent ROC curve analysis.

Predictive Nomogram for Prognostic Prediction

A nomogram based on independent prognostic factors of clinical traits and the polygenic risk score was constructed to predict the probability of 1-, 3-, and 5-year OS of patients with osteosarcoma. Subsequently, the discrimination of the nomogram was verified using the C-index obtained through a bootstrap method with 1,000 resamples. Calibration curves were plotted to compare the nomogram-predicted and ideal probabilities against the observed rates. Total points were calculated according to the parameters of prognostic factors using the R package "nomogramEx." Each variable of the nomogram yields points, and their sum represents the total points that a patient receives. Finally, we developed the interactive nomogram for predicting the probability of OS of patients with osteosarcoma using the R package "replot."

WGCNA

Weighted gene co-expression network analysis was performed to screen SE-associated hub genes linked to clinical traits using the dataset GSE39058. The analysis was performed as previously described (Ma et al., 2019). The optimal soft-thresholding value was estimated based on scale independence and mean connectivity analysis. Clinical traits-related genes were clustered into different modules. Moreover, the correlation between

modules and clinical traits was highlighted in the heatmap. The relationship between the clinically significant MM and GS was displayed in the scatter plots.

Protein–Protein Interaction Analysis and Pathway Enrichment Analysis

Eigengenes within clinically significant modules and SE-associated genes were intersected using the Venn plot and produced a list of hub genes. An interaction network between hub genes and drugs was also constructed to identify some drugs related with these hub genes via "NetworkAnalyst 3.0" (Zhou et al., 2019). Subsequently, Kyoto Encyclopedia of Genes and Genomes (KEGG) pathway analysis was performed using these hub genes. The top 10 items of the enriched pathway were selected and shown in the dot plot.

RESULTS

Establishment and Validation of the Lasso Penalized Cox Regression Model

The flowchart shows our analysis procedures for the construction of the SE-associated gene-based prognostic model of osteosarcoma (**Figure 1**). The 349 SE-associated genes based on the dataset of GSE39058 were selected to perform the Lasso penalized Cox regression analysis. Firstly, to identify the best-fit parameter of the λ parameter, two important optional λ values ($\log\lambda_{min} = -1.91$ and $\log\lambda_{lse} = -1.48$) were calculated from the vertical lines with a minimizing mean-square error and further used to select two groups of genes (**Figures 2A–C**). Moreover, Lasso models were reconstructed according to the λ_{min} and λ_{lse}, and survival probabilities were further estimated based on two gene lists (**Figure 2D**). As shown in **Figure 2D**, the use of the five gene-based prognostic model based on the λ_{min} (Wilcoxon test, $p = 1.4e{-}05$) facilitated the obvious distinction of survival probabilities between samples obtained from living and expired patients. However, when a two-gene-based prognostic model was used based on the λ_{lse}, there was no statistically significant difference observed (Wilcoxon test, $p > 0.05$). Similarly, the outcome of ROC curve analysis showed that the area under the curve minimum (AUC_{min}) was 0.92, implying that the five-gene-based Lasso model performed well in predicting the probability of OS of patients with osteosarcoma (**Figure 2E**).

Validation of Independent Prognostic Factors by the Cox Regression Model

For the validation of the Lasso penalized Cox regression model, we performed univariate and multivariate Cox regression analyses to determine whether these genes were independent

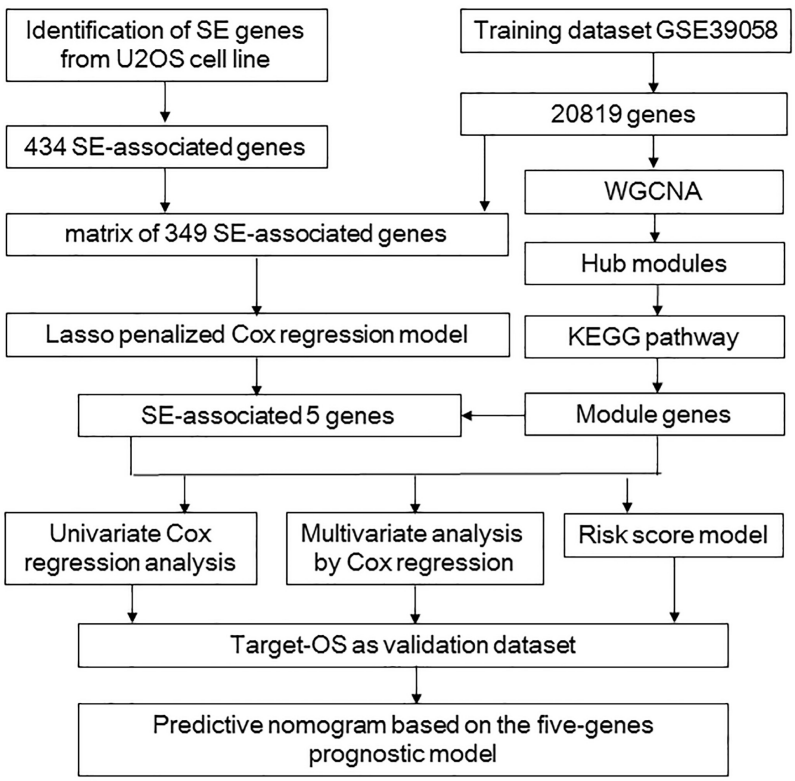


FIGURE 1 | The procedure workflow used to establish and certify the SE-associated gene-based prognostic model for patients with osteosarcoma. KEGG, Kyoto Encyclopedia of Genes and Genomes; Lasso, least absolute shrinkage and selection operator; Target-OS, Target-osteosarcoma; SE, super-enhancer; WGCNA, weighted gene co-expression network analysis.

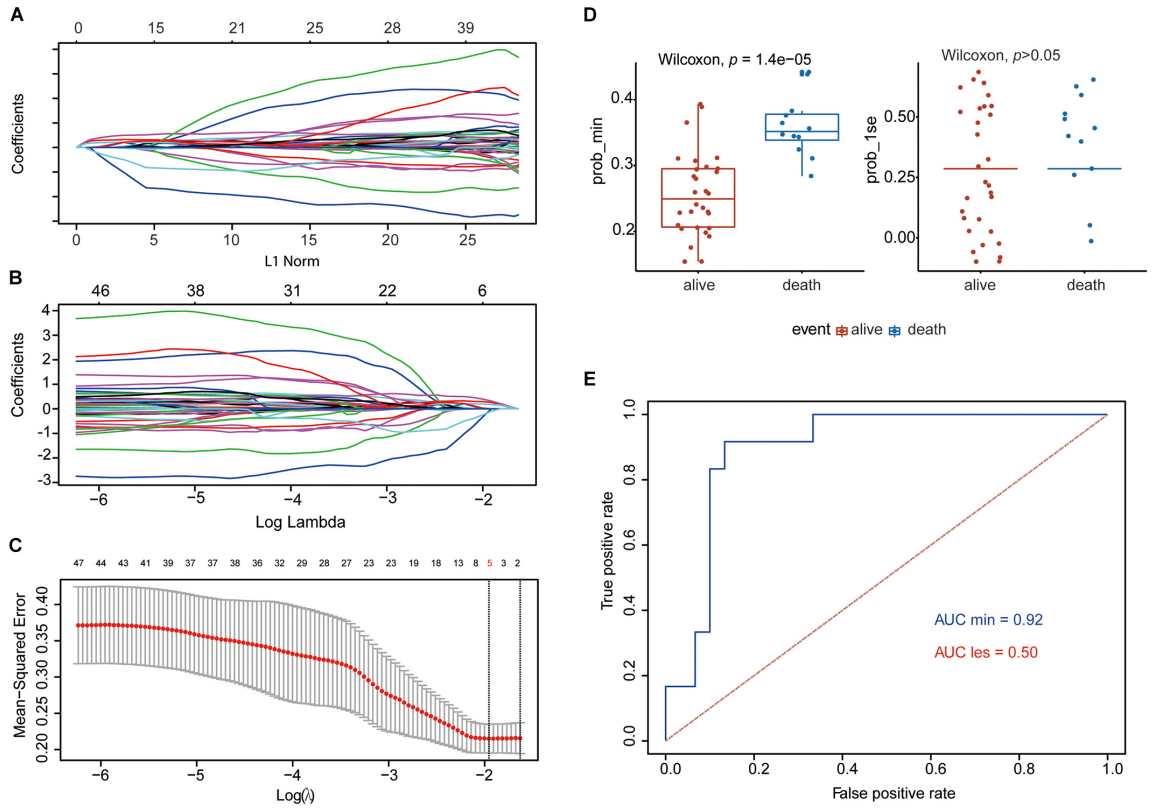


FIGURE 2 | Establishment of the five-gene prognostic model by Lasso regression analysis based on the 349 SE-associated genes from data downloaded from SEdb. **(A,B)** Lasso coefficient profiles of the 349 SE-associated genes. **(C)** Two optimal lambda (λ) values (λ_{min} and λ_{lse}) were estimated according to the vertical lines with a minimizing mean-square error. The vertical axis represents the mean-square error, while the horizontal axis represents the value of log(λ). **(D)** The scatter plot of survival status of patients with osteosarcoma based on the five-gene model (left, λ_{min}, $p = 1.4e{-}05$) or two-gene model (right, λ_{lse}, $p > 0.05$) using the Wilcoxon test. **(E)** ROC curves of the two prognostic models based on λ_{min} and λ_{lse}. The values of AUC were included in the figure. AUC, area under the curve; Lasso, least absolute shrinkage and selection operator; ROC, receiver operating characteristic; SE, super-enhancer; SEdb, super-enhancer database.

prognostic factors for the OS of patients with osteosarcoma. In the univariate Cox regression analysis, all log-rank *p*-values of these five genes were <0.05 (**Figure 3A**). Following multivariate Cox regression analysis, the global *p*-value (log-rank test) of the five-gene prognostic model was only 0.000171 (**Figure 3B**). The AIC was 59.74, and the C-index was 0.89, indicating that these five genes may be favorable prognostic factors for the OS of patients with osteosarcoma. Moreover, the outcome of K–M survival analysis was consistent with that of the univariate Cox regression analysis (**Figure 3C**). Furthermore, *AMN1* and *ZP3* may be protective factors in osteosarcoma (HR: 1.26e−36 and 1.13e−07, respectively), whereas *LIMS1*, *SAMD4A*, and *SPARC* appear to be harmful factors in this setting (HR: 699.2, 167, and 298.7, respectively). Thus, a Lasso penalized Cox regression model including five SE-associated genes may be used to predict the OS of patients with osteosarcoma.

Establishment and Validation of the Polygenic Risk Score Model

We integrated the expression data of the five genes and corresponding coefficient derived from the above multivariate regression analysis to establish the risk score model. All patients in the training dataset of GSE39058 ($N = 41$) were divided into high-risk (risk score > 0) and low-risk groups (risk score < 0) (**Figure 4A**). As shown in **Figure 4B**, survival was more commonly observed in the low-risk group, whereas death was more frequent in the high-risk group. *LIMS1*, *SAMD4A*, and *SPARC* tended to upregulated, whereas *AMN1* and *ZP3* were downregulated in patients of the high-risk group (**Figure 4C**). The K–M OS analysis predicted an inferior outcome of OS in the high-risk group (log-rank test, $p = 0.0006$) (**Figure 4D**). Meanwhile, the AUCs of a time-dependent ROC curve calculated using the five-gene-based risk score model were >0.8 (**Figure 4E**), indicating that the forecast model had high sensitivity and specificity.

The Target-OS dataset was further used to verify the predictive values of the polygenic risk score. Following the multivariate Cox regression analysis, the global *p*-value (log-rank test) of the five-gene prognostic model for the Target-OS dataset was <0.05 (**Supplementary Figure S1A**). A total of 88 patients were classified into the low- and high-risk groups using the optimal cutoff value of the risk score (**Supplementary Figures S1B–D**). The K–M curves of two groups based on risk scores were

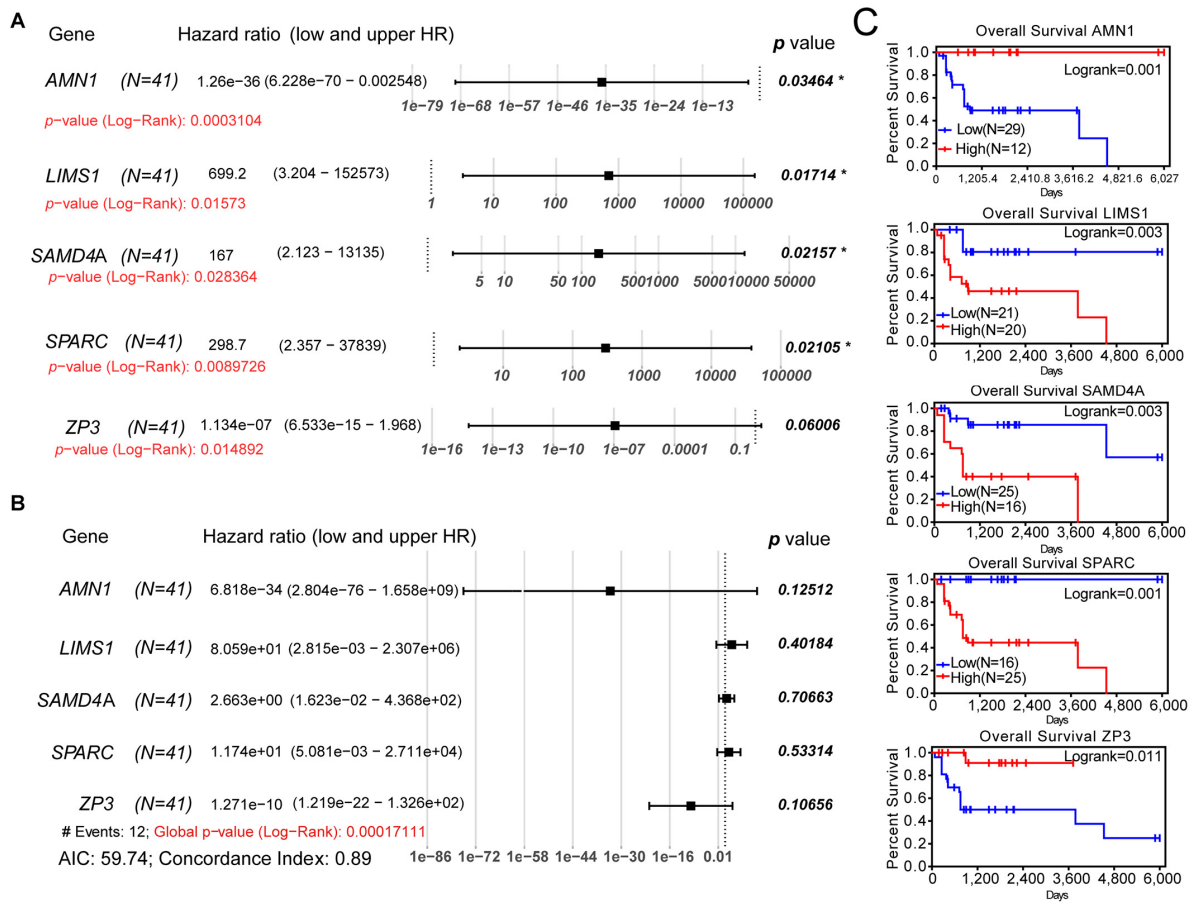


FIGURE 3 | Univariate and multivariate Cox regression analyses and K–M survival analysis of the five-gene prognostic model. **(A)** Univariate Cox regression analysis of each gene of the model. **(B)** Multivariate Cox regression analysis of the five-gene model. **(C)** K–M survival curves showing the difference in OS between the relative high- and low-expression groups for each gene according to the median of expression levels. K–M, Kaplan–Meier; AIC, Akaike information criterion; OS, overall survival.

significantly different (log-rank test, $p < 0.05$), and AUCs of time-dependent ROC curves also showed that the five-gene risk model could be a favorable approach to predicting the OS of patients with osteosarcoma (**Supplementary Figures S1E,F**).

Construction of the Predictive Nomogram Based on the Risk Score Model for Prognostic Prediction

To visualize the Cox regression model, a nomogram was constructed for predicting the 1-, 3-, and 5-year OS probability for patients with osteosarcoma in the GSE39058 dataset ($N = 41$). The predictors of the nomogram included age, sex, necrosis, recurrence, and risk group (**Figure 5A**). The calibration plot shown in **Figure 5B** illustrates the performance of the nomogram. The calibration plots were close to the ideal prediction gray line (45° line), indicating that our nomogram performed well in predicting survival probability (**Figure 5B**). To assess the predictive effect of the risk group as an indicator of OS, we applied the nomogram to a specific patient (GSM954850) in GSE39058 (**Figures 5C,D**). The patient GSM954850 expired at 750 days. According to the model containing the risk group, the predicted probability of death at 1,095 days was 0.815; this value was markedly higher than that obtained for the model lacking the risk group (0.659). This finding implies that the predictive model containing the risk group as a parameter is more accurate than that lacking the risk group.

Identification of SE-Related Hub Genes in Osteosarcoma Using WGCNA and a Protein–Protein Interaction Network

Weighted gene co-expression network analysis is another bioinformatics method for the analysis of clinical traits linked to the levels of gene expression. Cluster analysis was performed to display the heatmap of clinical traits (**Figure 6A**). As shown in **Figure 6B**, $\beta = 9$ was selected as the best soft-thresholding value via prediction of the scale independence and mean connectivity (**Figure 6B**) to construct the gene co-expression network. Subsequently, eigengenes were divided into different colored modules, producing 17 different modules. A module–trait relationship heatmap was developed according to Pearson's

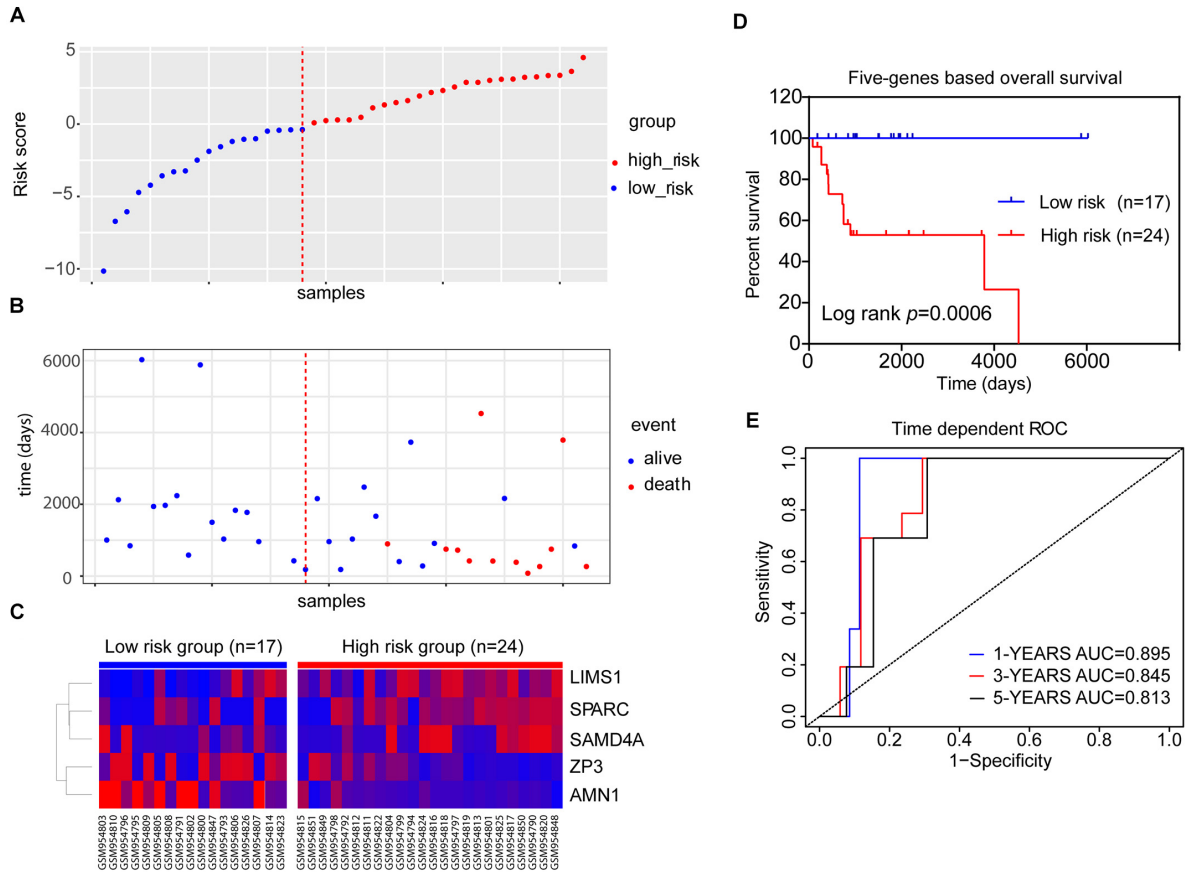


FIGURE 4 | The five-gene risk score model for the GSE39058 dataset ($N = 41$). **(A)** Scatter plot displaying the risk score of each patient in the GSE39058 dataset. Patients were divided into high- or low-risk groups according to the risk score. The blue plots represent the patients in the low-risk group (risk score ≤ 0), while the red plots represent patients in the high-risk group (risk score > 0). **(B)** The survival status distribution of patients with osteosarcoma in the high- or low-risk groups. **(C)** The expression status of the five prognostic genes in 41 patients with osteosarcoma in the GSE39058 dataset. **(D)** K–M survival curves showing the difference in OS between high- and low-risk patients (41 patients) (log-rank test, $p = 0.0006$). **(E)** Time-dependent ROC curve analysis for the prediction of survival using the five-gene prognostic model. The AUCs of 1-, 3-, and 5-year OS are shown in the figure. AUC, area under the curve; K–M, Kaplan–Meier; OS, overall survival; ROC, receiver operating characteristic.

correlation coefficient (**Figure 6C**). Three modules presented higher correlation with clinical traits: MEgray60 with recurrence ($r = 0.37$, $p = 0.01$); MEblue with death ($r = 0.33$, $p = 0.03$); and MEpink with survival time ($r = 0.47$, $p = 0.002$) (**Figure 6C**). A scatter plot also showed that the MM of these three modules was positively correlated with GS (**Figure 6D**). A Venn plot of SE-associated genes derived from the SE-associated gene matrix was drawn, and the genes within three modules were intersected (**Figure 6E**). There were 13, 70, and 16 interaction genes between module gray60, blue, pink, and SE-associated genes. The interaction genes were enriched in numerous cancer-related pathways, such as proteoglycans in cancer and transcriptional misregulation in cancer (**Figure 6F**). In addition, we constructed a gene–drug interaction network using the five genes and related drugs (**Supplementary Figure S2**). All five genes interacted with JQ1 (an established SE inhibitor). The network depicted that these five genes were probably regulated by SE to a certain extent. Finally, we displayed the signal tracks for the H3K27ac, H3K4me1, and H3K4me3 ChIP–seq profiles of the five genes (**Figure 7**). We observed five predicted SEs near these five genes. These data suggest that the expression of the five genes is regulated by SE. In addition, the SE inhibitor JQ1 may regulate the expression pattern in U2OS cells.

DISCUSSION

Notably, there is a lack of effective target treatment regimens in clinical practice, except for the traditional method of surgical resection. Recently, prognostic models based on some disease-related genes or other biomarkers for improving the prognosis of osteosarcoma have attracted considerable attention. The Lasso regression Cox model, gene risk score model, and univariate and multivariate Cox regression models are widely used for the screening and mining of hub genes related to survival and other clinical characteristics. Particularly, the Lasso model can be applied to solve "curse of dimensionality" (small sample size combined with a very large number of genes) when large amounts

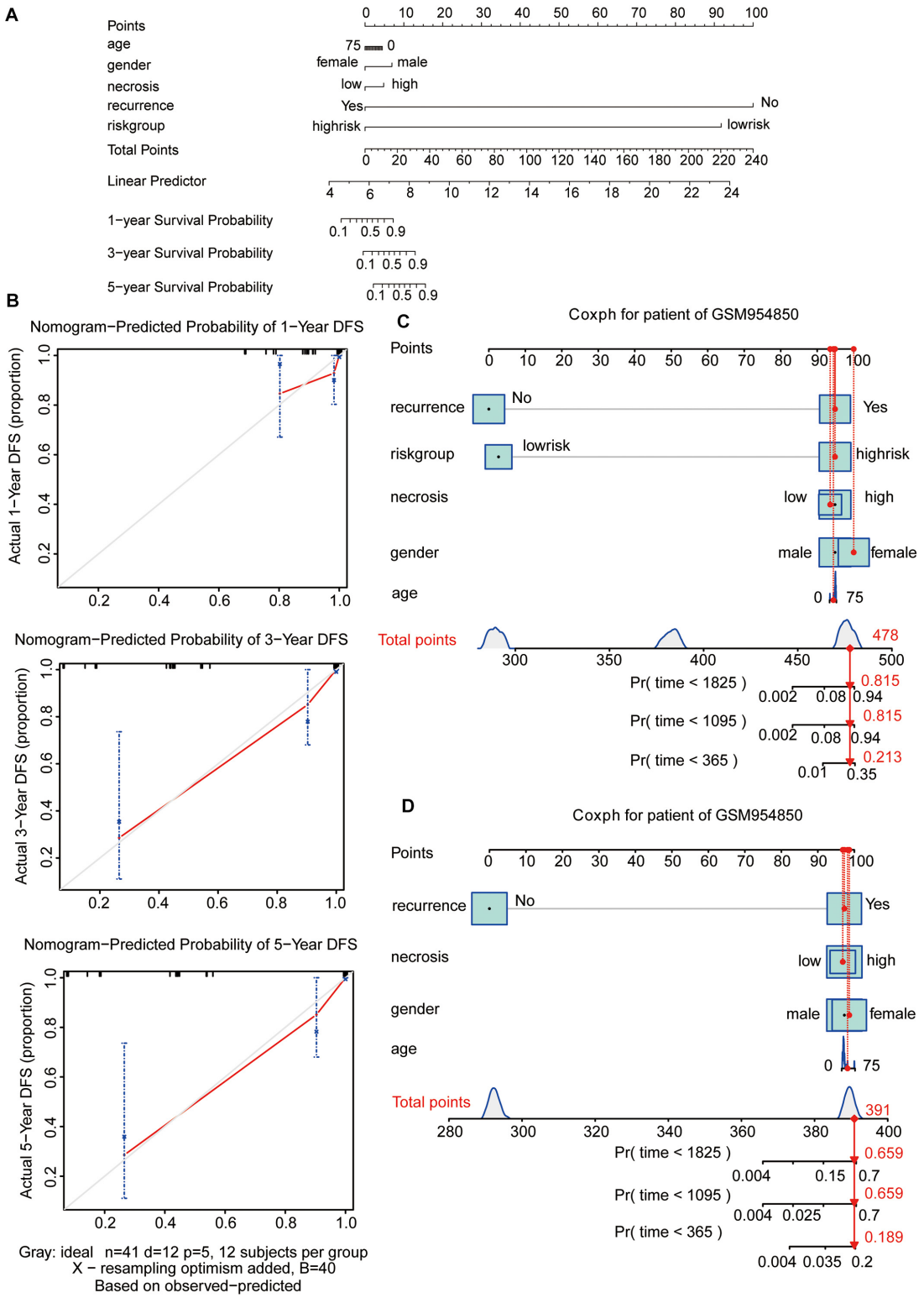


FIGURE 5 | Nomogram predicting the probability of 1-, 3-, and 5-year OS in patients with osteosarcoma. **(A)** Nomogram adding up the points identified on the points scale (the upward line) for each variable. The total points projected on the bottom scales indicate the probability of 1-, 3-, and 5-year OS. **(B)** Calibration plot for predicting the 1-, 3-, and 5-year OS. The gray line represents the ideal condition. **(C,D)** The nomograms predicting the probability of 1-, 3-, and 5-year OS for the specific patient GSM954850 based on the model containing or not containing the risk group in the GSE39058 dataset. OS, overall survival; DFS, disease-free survival.

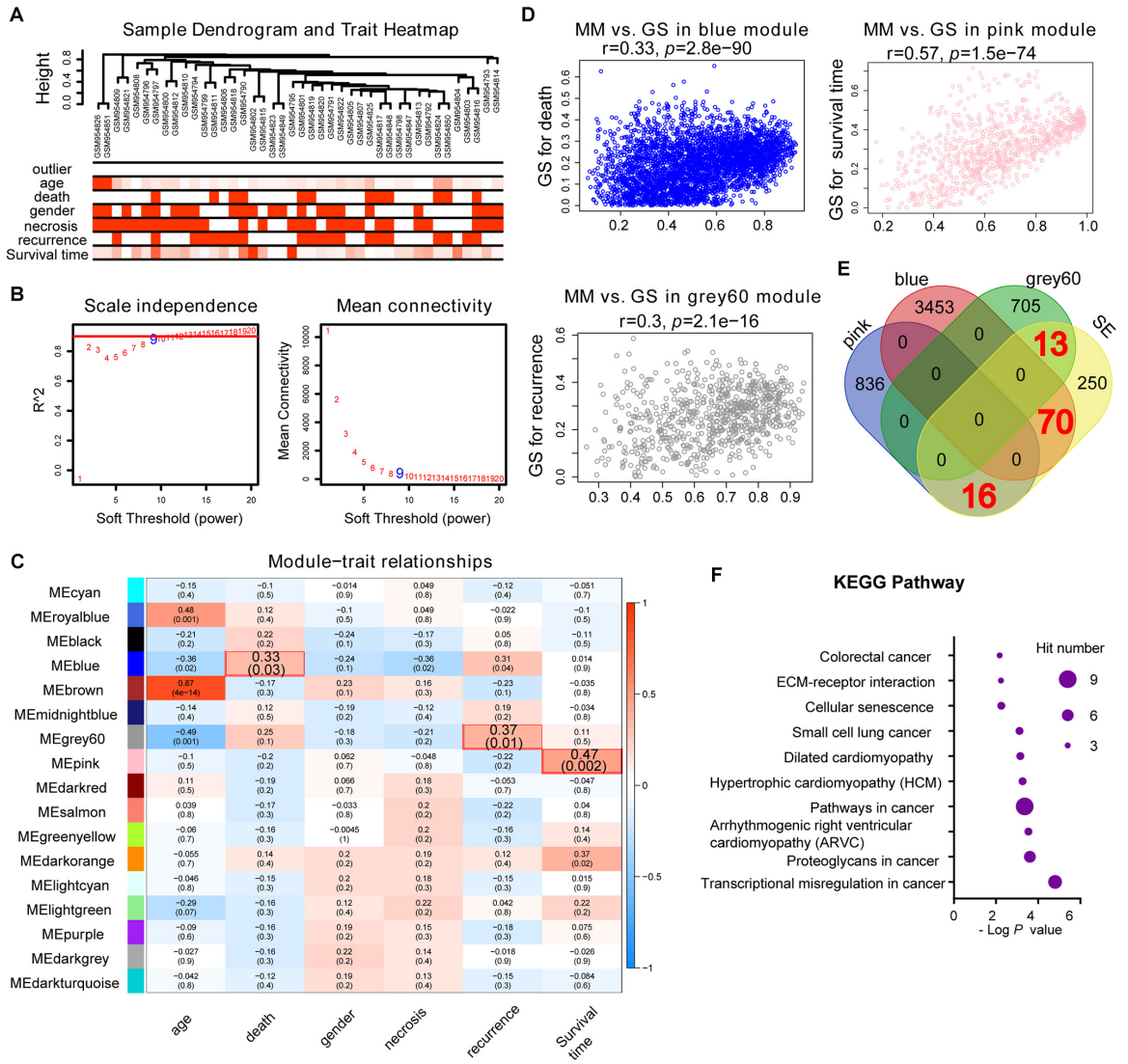


FIGURE 6 | Identification of SE-related hub genes in osteosarcoma based on the GSE39058 dataset through WGCNA analysis. **(A)** Cluster analysis between the gene expression in the GSE39058 dataset and sample outliers or clinical traits. Color intensity was proportional to sample outliers, age, gender, necrosis, recurrence, and survival time. **(B)** Analysis of the scale independence and mean connectivity (vertical axis) for various soft-thresholding powers (β value of horizontal axis). **(C)** Heatmap of the correlation between modules and clinical traits of osteosarcoma; *p*-values in the table specify the correlation between modules and clinical traits. Three modules had high correlation with clinical traits: MEgray60 with recurrence ($r = 0.37$, $p = 0.01$); MEblue with death ($r = 0.33$, $p = 0.03$); and MEpink with survival time ($r = 0.47$, $p = 0.002$). **(D)** Scatterplot showing the MM versus GS of module genes related to death in the blue module, recurrence in the gray60 module, or survival time in the pink module (horizontal axis: MM means module membership, vertical axis: GS means gene significance). **(E)** Venn plot of SE-related genes and eigengenes in the blue, gray60, and pink modules. There are 70, 13, and 16 correlated genes, respectively. **(F)** KEGG pathway analysis of the above-correlated genes in the Venn plot. KEGG, Kyoto Encyclopedia of Genes and Genomes; SE, super-enhancer; WGCNA, weighted gene co-expression network analysis.

of throughput biological data are processed. Recently, Lasso and WGCNA were used to construct a nomogram of radiomics of diagnostic computed tomography for predicting the survival of patients with high-grade osteosarcoma, which showed favorable performance (Wu et al., 2018). Another study also identified a seven-gene signature as a predictive biomarker for energy metabolism in osteosarcoma by Lasso and multivariate Cox regression (Zhu et al., 2020). Lasso coefficient profiles of the genes associated with the metastasis of osteosarcoma were established. These profiles were used to construct a risk score model for the prediction of metastasis of osteosarcoma (Dong et al., 2019). These findings imply that prognostic models based on different clinical traits and gene expression levels may help to potentiate the personalized treatment of patients with osteosarcoma.

In the present study, we constructed a five-SE-associated-gene-based nomogram prognostic model to improve the prognosis of patients with osteosarcoma. We first constructed an SE-associated gene expression matrix based on the 349



FIGURE 7 | Signal tracks for H3K27ac (red), H3K4me1 (purple), and H3K4me3 (green) ChIP–seq profiles of the five-SE-associated hub genes visualized using IGV. The regions of SE are shown in a pink bar upon the signal tracks. ChIP–seq, chromatin immunoprecipitation–sequencing; SE, super-enhancer; IGV, Integrative Genomics Viewer.

genes derived from the intersection of SE-associated genes and 20,819 genes from the GSE39058 dataset. According to this expression matrix, Lasso penalized Cox regression analysis was performed to screen a gene cluster containing *AMN1*, *LIMS1*, *SAMD4A*, *SPARC*, and *ZP3*, which was used to construct the risk score model based on the expression levels of five genes. Considering the group risk score as an independent indicator for prognosis, the K–M curve and log-rank test showed that a high risk score was correlated to augmented death ratio. We assessed the capability of the five-gene prognostic model in the GSE39058 dataset and also in the validation dataset Target-OS via univariate and multivariate Cox regression analyses and ROC curve analysis. The AUCs of the prognostic model for predicting the 1-, 3-, and 5-year OS were 0.895, 0.845, and 0.813, respectively, for the GSE39058 dataset and 0.549, 0.721, and 0.724, respectively, for the Target-OS dataset. The AUCs and C-index also showed that the five-gene prognostic model had a great performance for the prediction of survival and could be a robust and efficient model of prognosis. An interactive nomogram based on the risk score model and other clinical traits was constructed and identified using the calibration plots. To determine the predictive effect of the risk group as an indicator of OS, we also applied the nomogram to a specific patient (GSM954850) in the GSE39058 dataset. The predictive model containing the risk group as a parameter is more accurate compared with the nomogram model lacking the risk group. Through this approach, the prognosis of patients in the high-risk group may improve following the adjustment of individual treatment regimens for these patients.

The WGCNA of the 20,819 genes from the GSE39058 dataset revealed that the above five SE-associated genes also belonged to module genes. The KEGG analysis showed that the module genes associated with SE were enriched in numerous cancer-related pathways, such as proteoglycans in cancer and transcriptional misregulation in cancer. *LIMS1* functions as an oncogene to promote the survival of pancreatic cancer cells under oxygen–glucose deprivation conditions (Huang et al., 2019). The protein LIMS1 (also known as PINCH1) encoded by LIMS1 acts as an adaptor protein which contains five LIM domains or double zinc fingers (Hobert et al., 1999). LIMS1 can be involved in integrin signaling through interacting with integrin-linked kinase mediated by its LIM domain. Besides, LIMS1 can bind to integrin-linked kinase and parvin, which forms a protein complex, which is critical for the cell extracellular matrix adhesion (Ito et al., 2010). High expression of LIMS1 is associated with poor prognosis in human laryngeal carcinomas (Tsinias et al., 2018). Inhibition of LIMS1 through knockdown of LIMS1 can inhibit cell proliferation of neuroblastoma cells (Saeki et al., 2018). Thus, *LIMS1* may be considered as a biomarker for osteosarcoma. Secreted protein acidic and rich in cysteine (*SPARC*) encodes a cysteine-rich acidic

matrix-associated protein, which is essential for extracellular matrix synthesis and epithelial–mesenchymal transition that promotes migration and invasion of many cancers (Sun et al., 2018; Jiang et al., 2019; López-Moncada et al., 2019). In particular, overexpression of *SPARC*, which was critical for the growth and maintenance of osteosarcoma, was found in 51 of 55 osteosarcoma tumor samples (Dalla-Torre et al., 2006). Overexpression of *SPARC* also mediated the suppressing effect of *TP53INP1* on the migration of pancreatic cancer cells and promoted the progression of malignant cancers (Seux et al., 2011). Therefore, it is convincing that *SPARC* can serve as a biomarker or treatment target for osteosarcoma. SAMD4A, encoded by the sterile alpha motif domain containing 4A (*SAMD4A*), was reported to involve in processes such as maternal RNA destabilization, translational repression, and early embryo development in the role of a posttranscriptional regulator (Smibert et al., 1996; Baez et al., 2011). Although studies about the function of *SAMD4A* in cancer are still rare, we believe that *SAMD4A* will become a novel biomarker for predicting the prognosis of osteosarcoma based on the findings of this study. Antagonist of the mitotic exit network 1 (*AMN1*) is essential for mitotic checkpoints and chromosome stability; the protein encoded by AMN1 is involved in the progression of cell cycle (Wang et al., 2003; Xie et al., 2019). Although there are no relative studies about the role of *ZP3* in osteosarcoma, even if in cancer, combined with the findings of our study, we should also pay attention to *AMN1* and *ZP3* in osteosarcoma in a certain extent. In the present study, the gene–drug interaction network of the five genes showed that all genes interacted with JQ1 (an established SE inhibitor). Moreover, according to the ChIP–seq signal of H3K27ac, H3K4me1, and H3K4me3, we detected strong signals of SEs around these five genes. These data support that the expression of the five genes may be regulated by SE, while JQ1 as an SE inhibitor probably regulated the expression pattern in U2OS cells. Further molecular mechanism studies are warranted to recover the relationship between expression and SE in the future.

In conclusion, this was the first study that used the Lasso model to screen prognostic indicators from the profile of SE-associated genes. The five-gene-based interactive nomogram may be used as a clinical tool for improving the prognosis of patients with osteosarcoma, offering novel insights into personalized therapy in this setting.

DATA AVAILABILITY STATEMENT

All datasets presented in this study are included in the article/ **Supplementary Material**.

AUTHOR CONTRIBUTIONS

JQ and QL conceived and designed the theme of this study. ZO drafted the manuscript. TQ, GL, HZ, JW, and CT provided some helpful advice in several statistic methods. JQ and QQ revised the manuscript. The manuscript was revised critically by all authors involving in this study and all authors approved the final version with one accord.

FUNDING

This work was supported by grants awarded to QL by the Hunan Provincial Department of Finance Grant (Nos. 2019-93 and 2018-92) and to CT by the National Scientific foundation of China (No. 81902745).

SUPPLEMENTARY MATERIAL

The Supplementary Material for this article can be found online at: https://www.frontiersin.org/articles/10.3389/fcell.2020.598660/full#supplementary-material

Supplementary Figure 1 | Multivariate Cox regression analysis and risk score model analysis of the validation dataset Target-OS ($N = 88$). **(A)** Multivariate Cox regression analysis of dataset Target-OS based on the five-gene model. **(B)** Scatterplot displaying the risk score of each patient in the Target-OS dataset. The patients were divided into the high- or low-risk groups according to the risk score. The blue plots represent the patients in the low-risk group (risk score ≤ 0), while the red plots represent those in the high-risk group (risk score > 0). **(C)** Survival status distribution of the high- or low-risk groups in the Target-OS dataset. **(D)** The expression status of the five prognostic genes for patients in the Target-OS dataset. **(E)** K–M survival curves showing the difference in OS between high- and low-risk patients in the Target-OS dataset (log-rank test, $p = 0.0438$). **(F)** Time-dependent ROC curves analysis of survival prediction for patients in the Target-OS dataset using the five-gene prognostic model. The AUCs for 1-, 3-, and 5-year OS are shown in the figure. AUC, area under curve; K–M, Kaplan–Meier; ROC, receiver operating characteristic; Target-OS, Target-osteosarcoma, OS, overall survival; AIC, Akaike information criterion.

Supplementary Figure 2 | Gene–drug interaction network analysis of the five genes and drugs.

REFERENCES

Baez, M. V., Luchelli, L., Maschi, D., Habif, M., Pascual, M., Thomas, M. G., et al. (2011). Smaug1 mRNA-silencing foci respond to NMDA and modulate synapse formation. *J. Cell. Biol.* 195, 1141–1157. doi: 10.1083/jcb.201108159

Bielack, S., Carrle, D., and Casali, P. G. (2009). Osteosarcoma: ESMO clinical recommendations for diagnosis, treatment and follow-up. *Ann. Oncol.* 20(Suppl. 4), 137–139. doi: 10.1093/annonc/mdp154

Chen, D., Zhao, Z., Huang, Z., Chen, D.-C., Zhu, X.-X., Wang, Y.-Z., et al. (2018). Super enhancer inhibitors suppress MYC driven transcriptional amplification and tumor progression in osteosarcoma. *Bone Res.* 6:11.

Creyghton, M. P., Cheng, A. W., Welstead, G. G., Kooistra, T., Carey, B. W., Steine, E. J., et al. (2010). Histone H3K27ac separates active from poised enhancers and predicts developmental state. *Proc. Natl. Acad. Sci. U.S.A.* 107, 21931–21936. doi: 10.1073/pnas.1016071107

Dalla-Torre, C. A., Yoshimoto, M., Lee, C. H., Joshua, A. M., de Toledo, S. R., Petrilli, A. S., et al. (2006). Effects of THBS3, SPARC and SPP1 expression on biological behavior and survival in patients with osteosarcoma. *BMC Cancer* 6:237. doi: 10.1186/1471-2407-6-237

Dong, S., Huo, H., Mao, Y., Li, X., and Dong, L. (2019). A risk score model for the prediction of osteosarcoma metastasis. *FEBS Open Biol.* 9, 519–526. doi: 10.1002/2211-5463.12592

Elwood, J. M., Tawfiq, E., TinTin, S., Marshall, R. J., Phung, T. M., Campbell, I., et al. (2018). Development and validation of a new predictive model for breast cancer survival in New Zealand and comparison to the Nottingham prognostic index. *BMC Cancer* 18:897. doi: 10.1186/s12885-018-4791-x

Friedman, J., Hastie, T., and Tibshirani, R. (2010). Regularization paths for generalized linear models via coordinate descent. *J. Stat. Softw.* 33, 1–22.

Guan, X., Guan, Z., and Song, C. (2020). Expression profile analysis identifies key genes as prognostic markers for metastasis of osteosarcoma. *Cancer Cell. Int.* 20:104.

Hnisz, D., Abraham, B. J., Lee, T. I., Lau, A., Saint-André, V., Sigova, A. A., et al. (2013). Super-enhancers in the control of cell identity and disease. *Cell* 155, 934–947. doi: 10.1016/j.cell.2013.09.053

Hnisz, D., Schuijers, J., Lin, C. Y., Weintraub, A. S., Abraham, B. J., Lee, T. I., et al. (2015). Convergence of developmental and oncogenic signaling pathways at transcriptional super-enhancers. *Mol. Cell.* 58, 362–370. doi: 10.1016/j.molcel.2015.02.014

Hobert, O., Moerman, D. G., Clark, K. A., Beckerle, M. C., and Ruvkun, G. (1999). A conserved LIM protein that affects muscular adherens junction integrity and mechanosensory function in *Caenorhabditis elegans*. *J. Cell. Biol.* 144, 45–57. doi: 10.1083/jcb.144.1.45

Huang, C., Li, Y., Li, Z., Xu, Y., Li, N., Ge, Y., et al. (2019). LIMS1 promotes pancreatic cancer cell survival under oxygen-glucose deprivation conditions by enhancing HIF1A protein translation. *Clin. Cancer Res.* 25, 4091–4103. doi: 10.1158/1078-0432.ccr-18-3533

Ito, S., Takahara, Y., Hyodo, T., Hasegawa, H., Asano, E., Hamaguchi, M., et al. (2010). The roles of two distinct regions of PINCH-1 in the regulation of cell attachment and spreading. *Mol. Biol. Cell.* 21, 4120–4129. doi: 10.1091/mbc.E10-05-0459

Jiang, X., Liu, F., Wang, Y., and Gao, J. (2019). Secreted protein acidic and rich in cysteine promotes epithelial-mesenchymal transition of hepatocellular carcinoma cells and acquisition of cancerstem cell phenotypes. *J. Gastroenterol. Hepatol.* 34, 1860–1868. doi: 10.1111/jgh.14692

Kelly, A. D., Haibe-Kains, B., Janeway, K. A., Hill, K. E., Howe, E., Goldsmith, J., et al. (2013). MicroRNA paraffin-based studies in osteosarcoma reveal reproducible independent prognostic profiles at 14q32. *Genome Med.* 5:2. doi: 10.1186/gm406

Kempf-Bielack, B., Bielack, S. S., Jurgens, H., Branscheid, D., Berdel, W. E., Exner, G. U., et al. (2005). Osteosarcoma relapse after combined modality therapy: an analysis of unselected patients in the cooperative osteosarcoma study group (COSS). *J. Clin. Oncol.* 23, 559–568. doi: 10.1200/jco.2005.04.063

Lee, D. H., Qi, J., Bradner, J. E., Said, J. W., Doan, N. B., Forscher, C., et al. (2015). Synergistic effect of JQ1 and rapamycin for treatment of human osteosarcoma. *Int. J. Cancer* 136, 2055–2064. doi: 10.1002/ijc.29269

Liu, Y., Gou, X., Wei, Z., Yu, H., Zhou, X., and Li, X. (2020). Bioinformatics profiling integrating a four immune-related long non-coding RNAs signature as a prognostic model for papillary renal cell carcinoma. *Aging* 12, 15359–15373. doi: 10.18632/aging.103580

Long, J., Zhang, L., Wan, X., Lin, J., Bai, Y., Xu, W., et al. (2018). A four-gene-based prognostic model predicts overall survival in patients with hepatocellular carcinoma. *J. Cell. Mol. Med.* 22, 5928–5938. doi: 10.1111/jcmm.13863

López-Moncada, F., Torres, M. J., Castellón, E. A., and Contreras, H. R. (2019). Secreted protein acidic and rich in cysteine (SPARC) induces epithelial-mesenchymal transition, enhancing migration and invasion, and is associated with high Gleason score in prostate cancer. *Asian J. Androl.* 21, 557–564. doi: 10.4103/aja.aja_23_19

Lovén, J., Hoke, H. A., Lin, C. Y., Lau, A., Orlando, D. A., Vakoc, C. R., et al. (2013). Selective inhibition of tumor oncogenes by disruption of super-enhancers. *Cell* 153, 320–334. doi: 10.1016/j.cell.2013.03.036

Lu, B., He, Y., He, J., Wang, L., Liu, Z., Yang, J., et al. (2020). Epigenetic profiling identifies LIF as a super-enhancer-controlled regulator of stem cell-like properties in osteosarcoma. *Mol. Cancer Res.* 18, 57–67. doi: 10.1158/1541-7786.mcr-19-0470

Lu, L., Wu, Y., Feng, M., Xue, X., and Fan, Y. (2019). A novel seven-miRNA prognostic model to predict overall survival in head and neck squamous cell carcinoma patients. *Mol. Med. Rep.* 20, 4340–4348. doi: 10.3892/mmr.2019.10665

Luetke, A., Meyers, P. A., Lewis, I., and Juergens, H. (2014). Osteosarcoma treatment - where do we stand? A state of the art review. *Cancer Treat. Rev.* 40, 523–532. doi: 10.1016/j.ctrv.2013.11.006

Ma, H., Qu, J., Luo, J., Qi, T., Tan, H., Jiang, Z., et al. (2019). Super-enhancer-associated hub genes in chronic myeloid leukemia identified using weighted gene co-expression network analysis. *Cancer Manag. Res.* 11, 10705–10718. doi: 10.2147/CMAR.S214614

Meazza, C., and Scanagatta, P. (2016). Metastatic osteosarcoma: a challenging multidisciplinary treatment. *Expert Rev. Anticancer Ther.* 16, 543–556. doi: 10.1586/14737140.2016.1168697

Pan, X., Yang, W., Chen, Y., Tong, L., Li, C., and Li, H. (2019). Nomogram for predicting the overall survival of patients with inflammatory breast cancer: a SEER-based study. *Breast* 47, 56–61. doi: 10.1016/j.breast.2019.05.015

Park, H. S., Park, J. S., Chun, Y. J., Roh, Y. H., Moon, J., Chon, H. J., et al. (2017). Prognostic factors and scoring model for survival in metastatic biliary tract cancer. *Cancer Res. Treat.* 49, 1127–1139. doi: 10.4143/crt.2016.538

Saeki, N., Saito, A., Sugaya, Y., Amemiya, M., Ono, H., Komatsuzaki, R., et al. (2018). Chromatin immunoprecipitation and DNA sequencing identified a LIMS1/ILK pathway regulated by LMO1 in neuroblastoma. *Cancer Genomics Proteomics* 15, 165–174. doi: 10.21873/cgp.20074

Seux, M., Peuget, S., Montero, M. P., Siret, C., Rigot, V., Clerc, P., et al. (2011). TP53INP1 decreases pancreatic cancer cell migration by regulating SPARC expression. *Oncogene* 30, 3049–3061. doi: 10.1038/onc.2011.25

Simon, N., Friedman, J., Hastie, T., and Tibshirani, R. (2011). Regularization paths for Cox's proportional hazards model via coordinate descent. *J. Stat. Softw.* 39, 1–13. doi: 10.18637/jss.v039.i05

Smibert, C. A., Wilson, J. E., Kerr, K., and Macdonald, P. M. (1996). smaug protein represses translation of unlocalized nanos mRNA in the *Drosophila embryo*. *Genes Dev.* 10, 2600–2609. doi: 10.1101/gad.10.20.2600

Sun, W., Feng, J., Yi, Q., Xu, X., Chen, Y., and Tang, L. (2018). SPARC acts as a mediator of TGF-β1 in promoting epithelial-to-mesenchymal transition in A549 and H1299 lung cancer cells. *Biofactors* 44, 453–464. doi: 10.1002/biof.1442

Thorvaldsdottir, H., Robinson, J. T., and Mesirov, J. P. (2013). Integrative Genomics Viewer (IGV): high-performance genomics data visualization and exploration. *Brief. Bioinform.* 14, 178–192. doi: 10.1093/bib/bbs017

Tian, H., Guan, D., and Li, J. (2018). Identifying osteosarcoma metastasis associated genes by weighted gene co-expression network analysis (WGCNA). *Medicine* 97:e10781. doi: 10.1097/md.0000000000010781

Tibshirani, R. (1997). The lasso method for variable selection in the Cox model. *Stat. Med.* 16, 385–395. doi: 10.1002/(sici)1097-0258(19970228)16:4<385::aid-sim380>3.0.co;2-3

Tibshirani, R., Bien, J., Friedman, J., Hastie, T., Simon, N., Taylor, J., et al. (2012). Strong rules for discarding predictors in lasso-type problems. *J. R. Stat. Soc. Ser. B Stat. Methodol.* 74, 245–266. doi: 10.1111/j.1467-9868.2011.01004.x

Tsinias, G., Nikou, S., Papadas, T., Pitsos, P., Papadaki, H., and Bravou, V. (2018). High PINCH1 expression in human laryngeal carcinoma associates with poor prognosis. *Anal. Cell. Pathol.* 2018:2989635. doi: 10.1155/2018/2989635

Udyavar, A. R., Hoeksema, M. D., Clark, J. E., Zou, Y., Tang, Z., Li, Z., et al. (2013). Co-expression network analysis identifies spleen tyrosine kinase (SYK) as a candidate oncogenic driver in a subset of small-cell lung cancer. *BMC Syst. Biol.* 7(Suppl. 5):S1. doi: 10.1186/1752-0509-7-S5-S1

Wang, L., Shi, J., Huang, Y., Liu, S., Zhang, J., Ding, H., et al. (2019). A six-gene prognostic model predicts overall survival in bladder cancer patients. *Cancer Cell. Int.* 19:229. doi: 10.1186/s12935-019-0950-7

Wang, S., Yang, L., Ci, B., Maclean, M., Gerber, D. E., Xiao, G., et al. (2018). Development and validation of a nomogram prognostic model for SCLC patients. *J. Thorac. Oncol.* 13, 1338–1348. doi: 10.1016/j.jtho.2018.05.037

Wang, Y., Shirogane, T., Liu, D., Harper, J. W., and Elledge, S. J. (2003). Exit from exit: resetting the cell cycle through Amn1 inhibition of G protein signaling. *Cell* 112, 697–709. doi: 10.1016/s0092-8674(03)00121-1

Whyte, W. A., Orlando, D. A., Hnisz, D., Abraham, B. J., Lin, C. Y., Kagey, M. H., et al. (2013). Master transcription factors and mediator establish super-enhancers at key cell identity genes. *Cell* 153, 307–319. doi: 10.1016/j.cell.2013.03.035

Wu, M., Li, X., Zhang, T., Liu, Z., and Zhao, Y. (2019). Identification of a nine-gene signature and establishment of a prognostic nomogram predicting overall survival of pancreatic cancer. *Front. Oncol.* 9:996. doi: 10.3389/fonc.2019.00996

Wu, Y., Xu, L., Yang, P., Lin, N., Huang, X., Pan, W., et al. (2018). Survival prediction in high-grade osteosarcoma using radiomics of diagnostic computed tomography. *EBioMedicine* 34, 27–34. doi: 10.1016/j.ebiom.2018.07.006

Xiao, Z., Shi, Z., Hu, L., Gao, Y., Zhao, J., Liu, Y., et al. (2019). A new nomogram from the SEER database for predicting the prognosis of gallbladder cancer

patients after surgery. *Ann. Transl. Med.* 7, 738. doi: 10.21037/atm.2019.11.112

Xie, B., Becker, E., Stuparevic, I., Wery, M., Szachnowski, U., Morillon, A., et al. (2019). The anti-cancer drug 5-fluorouracil affects cell cycle regulators and potential regulatory long non-coding RNAs in yeast. *RNA Biol.* 16, 727–741. doi: 10.1080/15476286.2019.1581596

Xiong, Y., Ling, Q. H., Han, F., and Liu, Q. H. (2019). An efficient gene selection method for microarray data based on LASSO and BPSO. *BMC Bioinformatics* 20(Suppl. 22):715. doi: 10.1186/s12859-019-3228-0

Yang, S., Wang, Y., Ren, J., Zhou, X., Cai, K., Guo, L., et al. (2020). Identification of diagnostic and prognostic lncRNA biomarkers in oral squamous carcinoma by integrated analysis and machine learning. *Cancer Biomark.* [Epub ahead of print]. doi: 10.3233/cbm-191215

Yap, W. K., Shih, M. C., Kuo, C., Pai, P. C., Chou, W. C., Chang, K. P., et al. (2018). Development and validation of a nomogram for assessing survival in patients with metastatic lung cancer referred for radiotherapy for bone metastases. *JAMA Netw. Open* 1:e183242. doi: 10.1001/jamanetworkopen.2018.3242

Zhang, B., and Horvath, S. (2005). A general framework for weighted gene co-expression network analysis. *Stat. Appl. Genet. Mol. Biol.* 4:17.

Zhang, D., Zeng, S., and Hu, X. (2020). Identification of a three-long noncoding RNA prognostic model involved competitive endogenous RNA in kidney renal clear cell carcinoma. *Cancer Cell. Int.* 20:319. doi: 10.1186/s12935-020-01423-4

Zhang, F., Tapera, T. M., and Gou, J. (2018). Application of a new dietary pattern analysis method in nutritional epidemiology. *BMC Med. Res. Methodol.* 18:119. doi: 10.1186/s12874-018-0585-8

Zhang, J., Fan, J., Yin, R., Geng, L., Zhu, M., Shen, W., et al. (2019). A nomogram to predict overall survival of patients with early stage non-small cell lung cancer. *J. Thorac. Dis.* 11, 5407–5416. doi: 10.21037/jtd.2019.11.53

Zhang, J., Liu, W., Zou, C., Zhao, Z., Lai, Y., Shi, Z., et al. (2020). Targeting super-enhancer-associated oncogenes in osteosarcoma with THZ2, a covalent CDK7 inhibitor. *Clin. Cancer Res.* 26, 2681–2692. doi: 10.1158/1078-0432.CCR-19-1418

Zhang, J. X., Song, W., Chen, Z. H., Wei, J. H., Liao, Y. J., Lei, J., et al. (2013). Prognostic and predictive value of a microRNA signature in stage II colon cancer: a microRNA expression analysis. *Lancet Oncol.* 14, 1295–1306. doi: 10.1016/s1470-2045(13)70491-1

Zhou, G., Soufan, O., Ewald, J., Hancock, R. E. W., Basu, N., and Xia, J. (2019). NetworkAnalyst 3.0: a visual analytics platform for comprehensive gene expression profiling and meta-analysis. *Nucleic Acids Res.* 47, W234–W241. doi: 10.1093/nar/gkz240

Zhu, N., Hou, J., Ma, G., Guo, S., Zhao, C., and Chen, B. (2020). Co-expression network analysis identifies a gene signature as a predictive biomarker for energy metabolism in osteosarcoma. *Cancer Cell. Int.* 20:259. doi: 10.1186/s12935-020-01352-2

Zuo, S., Wei, M., Zhang, H., Chen, A., Wu, J., Wei, J., et al. (2019). A robust six-gene prognostic signature for prediction of both disease-free and overall survival in non-small cell lung cancer. *J. Transl. Med.* 17:152. doi: 10.1186/s12967-019-1899-y

Conflict of Interest: The authors declare that the research was conducted in the absence of any commercial or financial relationships that could be construed as a potential conflict of interest.

Copyright © 2020 Ouyang, Li, Zhu, Wang, Qi, Qu, Tu, Qu and Lu. This is an open-access article distributed under the terms of the Creative Commons Attribution License (CC BY). The use, distribution or reproduction in other forums is permitted, provided the original author(s) and the copyright owner(s) are credited and that the original publication in this journal is cited, in accordance with accepted academic practice. No use, distribution or reproduction is permitted which does not comply with these terms.

frontiers in Cell and Developmental Biology

CORRECTION
published: 19 January 2021
doi: 10.3389/fcell.2020.631453

Corrigendum: Construction of a Five-Super-Enhancer-Associated-Genes Prognostic Model for Osteosarcoma Patients

Zhanbo Ouyang[1], Guohua Li[1], Haihong Zhu[1], Jiaojiao Wang[1], Tingting Qi[1], Qiang Qu[2], Chao Tu[3], Jian Qu[1] and Qiong Lu[1]**

[1] Department of Pharmacy, The Second Xiangya Hospital, Central South University; Institute of Clinical Pharmacy, Central South University, Changsha, China, [2] Department of Pharmacy, Xiangya Hospital, Central South University, Changsha, China, [3] Department of Orthopaedics, The Second Xiangya Hospital, Central South University, Changsha, China

Keywords: osteosarcoma, super-enhancer, prognostic model, Lasso, weighted gene co-expression network analysis, overall survival

OPEN ACCESS

Approved by:
Frontiers Editorial Office, Frontiers Media SA, Switzerland

***Correspondence:**
Jian Qu
qujianstanley@csu.edu.cn
Qiong Lu
christy_luq@csu.edu.cn

Specialty section:
This article was submitted to Molecular Medicine, a section of the journal Frontiers in Cell and Developmental Biology

Received: *20 November 2020*
Accepted: *30 December 2020*
Published: *19 January 2021*

Citation:
Ouyang Z, Li G, Zhu H, Wang J, Qi T, Qu Q, Tu C, Qu J and Lu Q (2021) Corrigendum: Construction of a Five-Super-Enhancer-Associated-Genes Prognostic Model for Osteosarcoma Patients. Front. Cell Dev. Biol. 8:631453. doi: 10.3389/fcell.2020.631453

A Corrigendum on

Construction of a Five-Super-Enhancer-Associated-Genes Prognostic Model for Osteosarcoma Patients

by Ouyang, Z., Li, G., Zhu, H., Wang, J., Qi, T., Qu, Q., et al. (2020). Front. Cell Dev. Biol. 8:598660. doi: 10.3389/fcell.2020.598660

In the published article, there were errors in the AUTHOR CONTRIBUTIONS section. Corrections have been made to **AUTHOR CONTRIBUTIONS**:

"JQ and QL conceived and designed the theme of this study. ZO drafted the manuscript. TQ, GL, HZ, JW, and CT provided some helpful advice in several statistic methods. JQ and QQ revised the manuscript. The manuscript was revised critically by all authors involving in this study and all authors approved the final version with one accord."

The authors apologize for this error and state that this does not change the scientific conclusions of the article in any way. The original article has been updated.

Copyright © 2021 Ouyang, Li, Zhu, Wang, Qi, Qu, Tu, Qu and Lu. This is an open-access article distributed under the terms of the Creative Commons Attribution License (CC BY). The use, distribution or reproduction in other forums is permitted, provided the original author(s) and the copyright owner(s) are credited and that the original publication in this journal is cited, in accordance with accepted academic practice. No use, distribution or reproduction is permitted which does not comply with these terms.

frontiers in Cell and Developmental Biology

ORIGINAL RESEARCH
published: 06 November 2020
doi: 10.3389/fcell.2020.600641

miR-129-5p Inhibits Bone Formation Through TCF4

*Chong Yin[1†], Ye Tian[1†], Yang Yu[2], Chaofei Yang[1], Peihong Su[1], Yipu Zhao[1], Xue Wang[1], Kewen Zhang[1], Jiawei Pei[1], Dijie Li[1], Zhihao Chen[1], Yan Zhang[1], Zhiping Miao[1] and Airong Qian[1]**

[1] *Lab for Bone Metabolism, Xi'an Key Laboratory of Special Medicine and Health Engineering, Key Lab for Space Biosciences and Biotechnology, Research Center for Special Medicine and Health Systems Engineering, NPU-UAB Joint Laboratory for Bone Metabolism, School of Life Sciences, Northwestern Polytechnical University, Xi'an, China,* [2] *Tianjin Key Laboratory on Technologies Enabling Development Clinical Therapeutics and Diagnostics (Theranostics), School of pharmacy, Tianjin Medical University, Tianjin, China*

Osteoporosis is a frequently occurring bone disease in middle-aged and aged men and women. However, current therapies on this disease are still not ideal. MicroRNAs (miRNAs) are a class of endogenous non-protein-coding RNA with a length of 18–25 nucleotides. miRNAs have been identified as important regulators for development, metabolism, carcinogenesis, and bone formation. miR-129-5p has been reported as a regulator of cancer and neuroscience, whereas studies about its function on bone formation is still limited. In this study, we investigated the function and mechanism of miR-129-5p on osteoblast differentiation and bone formation. We have assessed the expression of miRNAs in bone mesenchymal stem cells from aging and menopause osteoporosis C57BL6 mice. The expression of miR-129-5p was altered in all osteoporosis models. Besides, the expression of miR-129-5p was negatively correlated with osteoblastic differentiation markers in the femur tissues of C57BL/6 mice of different ages. We further demonstrated that overexpression of miR-129-5p inhibited osteoblast differentiation in MC3T3-E1 cell line, as well as bone formation of C57BL/6 mice. On the other hand, down-regulation of miR-129-5p enhanced osteoblast differentiation and bone formation. We also found that miR-129-5p inhibited Wnt/β-catenin pathway in osteoblast. The target gene of miR-129-5p has been forecasted and proved as *Tcf4*. We further found that plasmid containing *Tcf4*–3′ UTR sequence enhanced osteoblast differentiation, as well as Wnt/β-catenin pathway in MC3T3-E1 cells. To further investigate the rescue effect of miR-129-5p inhibitor, we manufactured bioengineered novel recombinant miR-129-5p inhibitor through *Escherichia coli* system and then tested its function. The results showed that the novel recombinant miR-129-5p inhibitor promoted osteoblast differentiation and greatly ameliorated menopause osteoporosis in C57BL6 mice. In conclusion, we have discovered miR-129-5p as an inhibitor of bone formation. miR-129-5p inhibited downstream transcription factors of Wnt/β-catenin pathway through targeting *Tcf4*. Moreover, novel recombinant miR-129-5p inhibitor showed rescue effect on osteoporosis. This study has revealed a new mechanism of osteogenic differentiation and provided novel therapeutic strategies for treatment of skeletal disorders.

Keywords: osteoporosis, osteoblast, miR-129-5p, TCF4, recombinant RNA

OPEN ACCESS

Edited by:
Chao Liang,
Hong Kong Baptist University, Hong Kong

Reviewed by:
Gang Li,
Houston Methodist Research Institute, United States
Ancuta Jurj,
Iuliu Hatieganu University of Medicine and Pharmacy, Romania

***Correspondence:**
Airong Qian
qianair@nwpu.edu.cn

† These authors have contributed equally to this work

Specialty section:
This article was submitted to Molecular Medicine, a section of the journal Frontiers in Cell and Developmental Biology

Received: *30 August 2020*
Accepted: *14 October 2020*
Published: *06 November 2020*

Citation:
Yin C, Tian Y, Yu Y, Yang C, Su P, Zhao Y, Wang X, Zhang K, Pei J, Li D, Chen Z, Zhang Y, Miao Z and Qian A (2020) miR-129-5p Inhibits Bone Formation Through TCF4. Front. Cell Dev. Biol. 8:600641. doi: 10.3389/fcell.2020.600641

INTRODUCTION

Osteoporosis is a high-incident bone disease in middle-aged and aged men and women, with symptoms identified as declined bone mass and bone strength, deteriorated bone microarchitecture, and increased risk of fracture (Hendrickx et al., 2015). The causes of osteoporosis are multiple and complex. Among those, declined osteoblast differentiation, which leads to discouraged bone formation, was proved as one of the major causes of osteoporosis (Jabbar et al., 2011; Gennari et al., 2016). Osteoblast differentiation could be affected by multiple signaling pathways and osteogenic factors, including microRNAs (miRNAs), which were proved to be highly correlated with osteoblast differentiation and osteoporosis.

MicroRNAs are a class of endogenous non-protein-coding RNA with 18–25 nucleotides in length. miRNAs have been known as important regulators for development, metabolism, carcinogenesis, and bone formation (Bartel, 2009; Rigoutsos and Furnari, 2010; Chen et al., 2017). Emerging numbers of studies have reported miRNAs as regulators for osteoblast differentiation and bone formation, such as miR-21, miR-214, miR-188, miR-148-3p, miR-422a, etc. (Wang et al., 2013; Cao et al., 2014; Li et al., 2015, 2017; Yuan et al., 2019). These studies suggested that the functional and mechanism researches on osteogenic miRNAs would be helpful to develop potential therapeutic strategies for osteoporosis. miR-129-5p has been reported as a regulator of cancer and neural disease (Li G. et al., 2019; Zeng et al., 2019), whereas studies on its function in bone formation are relatively limited. Shi et al. (2020) reported that hsa-miR-129-5p inhibited osteogenic differentiation of adipose-derived stem cells via Wnt/β-catenin pathway, which implied that miR-129-5p may also be an inhibitor of bone formation. Therefore, the reduction of miR-129-5p level in bone tissue might be a potential anabolic strategy for ameliorating osteoporosis.

Biological approaches have been made to use live cells to bioengineer natural RNA molecules that are ready to use as RNAi agents (Ponchon et al., 2009; Huang et al., 2013; Chen et al., 2015; Ho and Yu, 2016). These recombinant RNA technologies provided a novel way for fast production of large quantities of chimeric RNAs in a cost-effective manner. As benefit from this technological progress, we used an improved ncRNA carrier (nCAR; Ho et al., 2018) for production of recombinant miR-129-5p inhibitor (nCAR/anti129). This bioengineered nCAR/anti129 may better capture the activity of natural RNAs and thus have greater potential for clinical application.

In this study, we have identified miR-129-5p as an inhibitor for osteoblast differentiation and bone formation. We found that miR-129-5p blocked downstream transcript factors of Wnt/β-catenin pathway by targeting *Tcf4*. In addition, novel recombinant miR-129-5p inhibitor that was manufactured through *Escherichia coli* system was applied to *in vivo* study to further figure out its rescue effect on postmenopausal osteoporosis. The study has discovered a novel mechanism regulating osteoblast differentiation and bone formation and provided new ideas for the translational medical research of osteogenic miRNAs on osteoporosis.

RESULTS

miR-129-5p Was Associated With Bone Formation Reduction

We detected miR-129-5p expression level in bone marrow mesenchymal stem cells (BMSCs) of both male and female aging mice femur tissue. Reverse transcriptase-polymerase chain reaction (RT-PCR) results showed that in 21-month-old male and female mice, the expression level of miR-129-5p was enhanced by 218.3% ($P < 0.001$) and 70.7% ($P < 0.001$), respectively, compared to 6-month-old control mice (**Figure 1A**). These results implied that during the aging process, the expression of miR-129-5p is up-regulated in bone tissue and osteogenic cells.

To further prove the correlation between miR-129-5p and osteogenesis, correlation analysis was performed. The results showed that miR-129-5p expression was negatively correlated with the expression of osteogenic transcript factor *Osterix* and *Runx2* (runt-related transcription factor 2) in the femur tissue of different ages of C57BL/6 mice (**Figures 1B,C**). These results suggested that the expression level of miR-129-5p was negatively correlated with osteogenesis.

miR-129-5p Inhibited Osteoblast Differentiation and Bone Formation

The functions of miR-129-5p on osteoblast differentiation and bone formation were investigated. miR-129-5p mimic and inhibitor were synthesized to manipulate miR-129-5p expression in MC3T3-E1 cells and calvaria of C57BL/6 mice. Mimic-NC and inhibitor-NC were used as control.

In MC3T3-E1 cells, the expression level of miR-129-5p was increased by 123.7% ($P < 0.001$) compared to negative control after mimic-129-5p transfection (**Supplementary Figure S1A**) and was decreased by 37.8% ($P < 0.001$) when inhibitor-129-5p was transfected (**Supplementary Figure S1B**). RT-PCR results revealed that the expression level of osteogenic transcript factor *Osterix* and *Runx2* was decreased by 73% ($P < 0.001$) and 51.8% ($P < 0.05$), respectively when cells were exposed to mimic-129-5p (**Figure 2B**). Moreover, the alkaline phosphatase (ALP)-positive blue–violet complexes and alizarin red-stained mineralized nodules were both significantly decreased (**Figure 2A** and **Supplementary Figure S2A**). As for inhibitor-129-5p transfection, expression levels of *Osterix* and *Runx2* were enhanced by 135.5% ($P < 0.01$) and 42.4% ($P < 0.001$), respectively (**Figure 2D**). ALP-positive blue–violet complexes and alizarin red-stained mineralized nodules were also significantly enhanced (**Figure 2C** and **Supplementary Figure S2B**). The results confirmed that miR-129-5p inhibited osteoblast differentiation.

Then miR-129-5p mimic and inhibitor were implemented in calvaria of C57BL/6 mice by transfection reagent (Entranster^{TM} *In vivo* Transfection Reagent) to determine the function of miR-129-5p *in vivo*. The expression levels of miR-129-5p in mice calvarias were significantly enhanced by mimic-129-5p (**Supplementary Figure S1C**, $P < 0.001$) and decreased by inhibitor-129-5p (**Supplementary Figure S1D**, $P < 0.001$) 3 days after the injection. Mineral apposition rate (MAR, an assessment

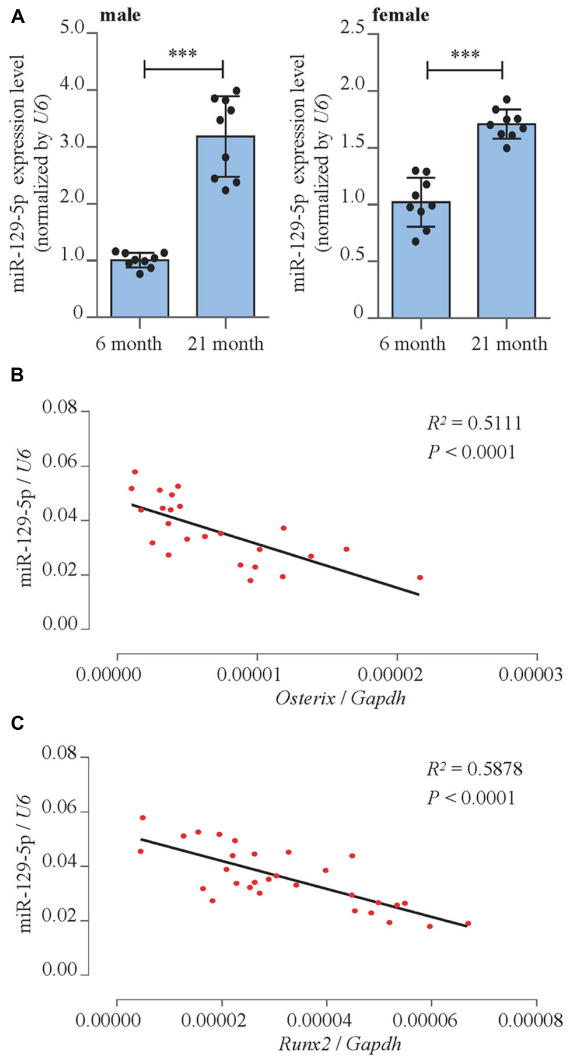


FIGURE 1 | miR-129-5p was associated with bone formation reduction. **(A)** Expression levels of miR-129-5p in BMSCs of 6- and 21-month male (left) and female (right) C57BL/6 mice, as detected by reverse transcriptase-polymerase chain reaction (RT-PCR; mean ± SD, ***$P < 0.001$). **(B,C)** Correlation analysis between miR-129-5p level and *Osterix* or *Runx2* mRNA levels in femur tissues from C57BL/6 mice, respectively, as detected by RT-PCR.

of bone formation) of calvarial bone in mimic-129-5p transfected mice was decreased by 32.2% (**Figure 2E**, $P < 0.01$), whereas calvarial MAR in mice treated by inhibitor-129-5p was enhanced by 75.1% (**Figure 2F**, $P < 0.001$). The *in vitro* and *in vivo* results proved that miR-129-5p would inhibit both osteoblast differentiation and bone formation.

miR-129-5p Inhibited Downstream Transcript Factors of Wnt/β-Catenin Pathway

We moved forward to investigate the mechanism of the inhibitory effect of miR-129-5p on osteoblast differentiation. The correlation between miR-129-5p expression and essential osteogenic transcript factors in the femur tissue of different ages of C57BL/6 mice was investigated. The expression of transcript factor *Hes1*, *Smad2*, and *Hif1a* showed no significant correlation with miR-129-5p (**Supplementary Figure S3**). While *Tcf7* and *Lef1*, downstream transcript factors of Wnt/β-catenin pathway, showed negative correlation with miR-129-5p (**Figures 3A,B** and **Supplementary Figure S4**). Wnt/β-catenin pathway is one of the most essential pathways that regulate osteoblast differentiation and bone formation through its downstream transcript factors TCF7 and LEF1 (Maria et al., 2007; Hu et al., 2018). These results implied that miR-129-5p might inhibit downstream transcript factors of Wnt/β-catenin pathway.

The expression levels and activities of TCF7 and LEF1 in miR-129-5p mimic- or inhibitor-treated MC3T3-E1 cells were further determined. Results demonstrated that mRNA expression levels of *Tcf7* and *Lef1* were both significantly inhibited by the overexpression of miR-129-5p (**Figures 3C,D**; $P < 0.001$) and elevated by the knockdown of miR-129-5p (**Figures 3F,G**; $P < 0.01$, $P < 0.001$). Moreover, the negative influence of miR-129-5p on TCF7/LEF1 was confirmed by luciferase reporter assay. The luciferase reporter plasmid containing TCF7/LEF1 binding site was constructed and co-transfected into MC3T3-E1 cells along with miR-129-5p mimic or inhibitor. Results showed that after mimic or inhibitor-129-5p exposures, TCF7/LEF1 activities were evidently reduced (approximately 47.4%, **Figure 3E**, $P < 0.001$) or enhanced (45.4%, **Figure 3H**, $P < 0.01$). These data demonstrated that miR-129-5p had inhibitory effect on both the expressions and the activities of the downstream transcript factors of Wnt/β-catenin pathway, which suggested that the regulation of miR-129-5p on osteoblast differentiation was probably through the inhibition of these transcription factors.

miR-129-5p Inhibited Osteoblast Differentiation and Wnt/β-Catenin Downstream Transcript Factors *via* Targeting *Tcf4*

We have forecasted that miR-129-5p targeted *Tcf4* (**Table 1**), and TCF4 has been reported as an important conducting transcriptional factor in Wnt/β-catenin pathway (Reinhold and Naski, 2007). In this study, we for the first time determined the regulatory effect of miR-129-5p on TCF4. We discovered that mimic-129-5p significantly down-regulated TCF4 mRNA and protein expressions (**Figure 4A**), which were up-regulated by inhibitor-129-5p (**Figure 4B**). The binding effect of miR-129-5p to *Tcf4* -3′ UTR was also investigated by luciferase reporter assay. The luciferase reporter plasmids that either have a wild-type *Tcf4*–3′ UTR (Luc-WT) or a *Tcf4*–3′ UTR containing mutant sequences (Luc-mut) of the miR-129-5p binding site were constructed and transfected into MC3T3-E1 cells along with mimic-129-5p or inhibitor-129-5p. Results revealed that luciferase activities were significantly decreased by mimic-129-5p in cells transfected by Luc-WT (**Figure 4C**) and enhanced by inhibitor-129-5p (**Supplementary Figure S5**).

To further confirm the role of TCF4 as a mediator between miR-129-5p and osteoblast differentiation, we constructed *Tcf4*-UTR plasmid that contained *Tcf4*–3′ UTR embodied miR-129-5p

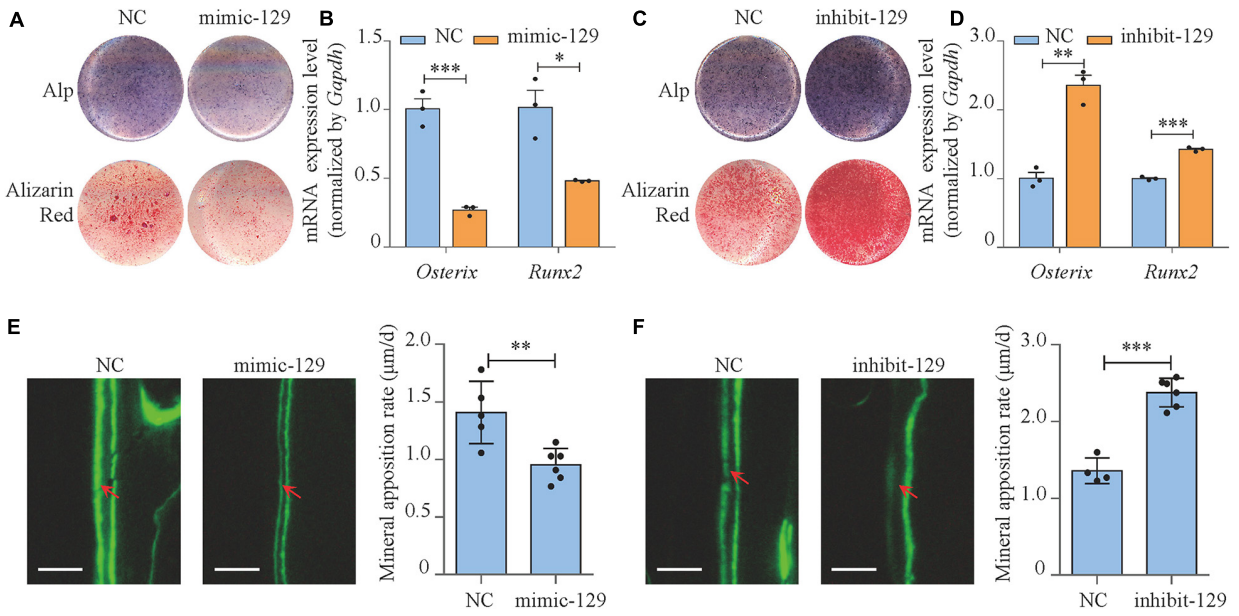


FIGURE 2 | miR-129-5p inhibited osteoblast differentiation and bone formation. **(A)** Alp and alizarin red staining of MC3T3-E1 cells treated with mimic-129-5p (compared to mimic-NC), as detected by Alp staining and alizarin red staining. Alp, results of Alp staining; alizarin red, results of alizarin red staining; NC, mimic-NC; mimic-129, mimic-129-5p. **(B)** *Osterix* and *Runx2* expression levels of MC3T3-E1 cells treated with mimic-129-5p, as detected by reverse transcriptase-polymerase chain reaction (RT-PCR; mean ± SD, $^{*}P < 0.05$, $^{***}P < 0.001$). **(C)** Alp and alizarin red staining of MC3T3-E1 cells treated with inhibitor-129-5p (compared to inhibitor-NC), as detected by Alp staining and alizarin red staining. NC: inhibitor-NC. inhibit-129: inhibitor-129-5p. **(D)** *Osterix* and *Runx2* expression levels of MC3T3-E1 cells treated with inhibitor-129-5p, as detected by RT-PCR (mean ± SD, $^{**}P < 0.01$, $^{***}P < 0.001$). **(E)** Calvarial bone mineral apposition rate of C57BL/6 mice treated with mimic-129-5p (mean ± SD, $^{**}P < 0.01$). Scale bar: 10 μm. **(F)** Calvarial bone mineral apposition rate of C57BL/6 mice treated with inhibitor-129-5p (mean ± SD, $^{***}P < 0.001$). Scale bar: 10 μm.

binding sequence. The control plasmid was also established that contained the mutant binding sequence (mutant) of miR-129-5p. *Tcf4*-UTR and mutant plasmid were transfected to MC3T3-E1 cells along with mimic-129-5p or inhibitor-129-5p. For MC3T3-E1 cells transfected with mimic-NC, osteoblast differentiation marker *Osterix* was up-regulated by 31.9% ($P < 0.01$) after treatment with *Tcf4*–3′ UTR, as compared to cells treated with mutant *Tcf4*–3′ UTR. In high-expression miR-129-5p cells induced by mimic-129-5p, *Osterix* was up-regulated by a more drastic level of 132.8% ($P < 0.001$) after *Tcf4*–3′ UTR treatment compared to mutant *Tcf4*–3′ UTR (**Figure 4E**). For *Runx2*, the similar patterns were observed as *Osterix*: *Tcf4*–3′ UTR enhanced its expression by 91.9% ($P < 0.001$) in cells transfected with mimic-NC, which was enhanced by a higher degree of 220% ($P < 0.001$) in mimic-129-5p-treated MC3T3-E1 cells (**Figure 4F**). Alp activities and mineralized nodules were also enhanced by *Tcf4*–3′ UTR, which were more significant in mimic-129-5p–treated cells (**Figure 4D** and **Supplementary Figures S6A,B**). On the other hand, in low miR-129-5p cells induced by inhibitor-129-5p, the expression levels of *Osterix* and *Runx2*, along with Alp activities and mineralized nodules were only slightly enhanced by *Tcf4*–3′ UTR as compared to cells with normal miR-129-5p level (**Figures 4G–I** and **Supplementary Figures S6C,D**). These results demonstrated that *Tcf4*–3′ UTR would alleviate the inhibitory effect of miR-129-5p on osteoblast differentiation and proved that miR-129-5p inhibited osteoblast differentiation via targeting *Tcf4*.

Moreover, we also investigated the expressions and the activities of the downstream transcript factors of Wnt/β-catenin pathway in *Tcf4*-UTR transfected MC3T3-E1 cells. The treatment of *Tcf4*-UTR up-regulated mRNA expression levels of *Tcf7* and *Lef1* by 76.4% ($P < 0.001$) and 104.3% ($P < 0.001$), respectively in mimic-NC-treated cells. However, in high-expression miR-129-5p cells, *Tcf4*-UTR up-regulated *Tcf7* and *Lef1* level up to 180% ($P < 0.001$) and 215.3% ($P < 0.001$), respectively (**Figures 5A,B**). The activity of TCF7/LEF1 was enhanced by 108.9% ($P < 0.001$) through *Tcf4*-UTR treatment in cells with normal miR-129-5p level and reached 223.8% ($P < 0.001$) in high miR-129-5p cells (**Figure 5C**). Meanwhile, after inhibitor-129-5p treatment, *Tcf4*-UTR enhanced both expressions and activities of TCF7 and LEF1 by a minor extent than that in cells with normal miR-129-5p level (**Figures 5D–F**). All these results indicated that miR-129-5p inhibited osteoblast differentiation and downstream transcript factors of Wnt/β-catenin pathway through targeting *Tcf4*.

Rescue Effect of miR-129-5p Inhibitor on Postmenopausal Osteoporosis

We moved forward to investigate the rescue effect of miR-129-5p inhibitor on osteoporosis. Postmenopausal osteoporosis mouse model was constructed by ovariectomization. The transfection of inhibitor-129-5p was implemented into calvarias of OVX mice as previously described (Yin et al., 2019). Expression levels of miR-129-5p in calvarias were significantly enhanced

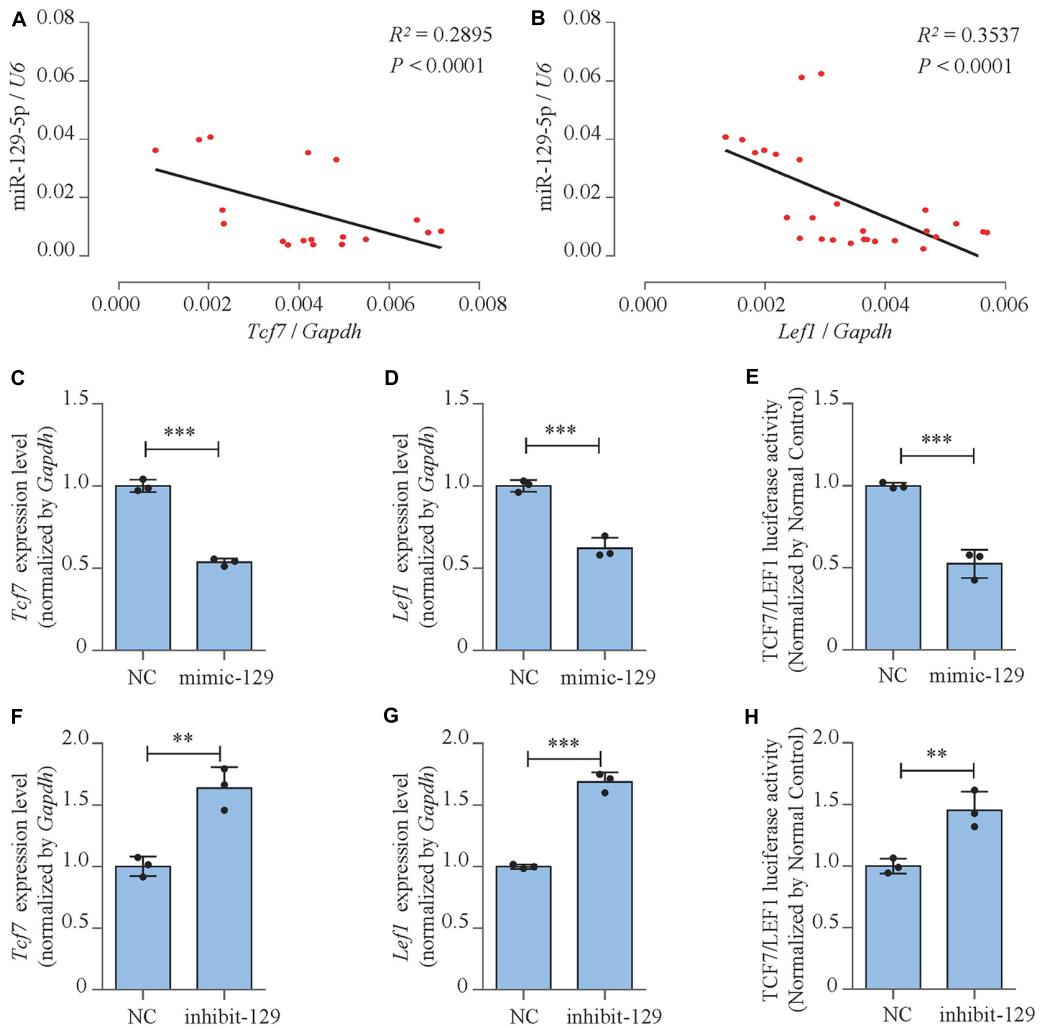


FIGURE 3 | miR-129-5p inhibited downstream transcript factors of Wnt/β-catenin pathway. **(A,B)** Correlation analysis between miR-129-5p and *Tcf7* or *Lef1* mRNA levels in femur tissues from C57BL/6 mice, respectively, as detected by reverse transcriptase-polymerase chain reaction (RT-PCR). **(C,D)** *Tcf7* and *Lef1* expression levels of MC3T3-E1 cells treated with mimic-129-5p, as detected by RT-PCR (mean ± SD, ***$P < 0.001$). NC, mimic-NC; mimic-129, mimic-129-5p. **(E)** TCF7/LEF1 activities of MC3T3-E1 cells treated with mimic-129-5p, as detected by luciferase reporter assay (mean ± SD, ***$P < 0.001$). **(F,G)** *Tcf7* and *Lef1* expression levels of MC3T3-E1 cells treated with inhibitor-129-5p, as detected by RT-PCR (mean ± SD, **$P < 0.01$, ***$P < 0.001$). NC, inhibitor-NC; inhibit-129, inhibitor-129-5p. **(H)** TCF7/LEF1 activities of MC3T3-E1 cells treated with inhibitor-129-5p, as detected by luciferase reporter assay (mean ± SD, **$P < 0.01$).

by OVX surgery and were significantly down-regulated upon transfection (**Figure 7A**). Mineral apposition rate in the OVX mice was decreased by 48.2% ($P < 0.001$) and increased by 107.3% ($P < 0.001$) after treatment with inhibitor-129-5p (**Figures 6A,B**). Moreover, the expression levels of osteogenic factors OCN and OSTREIX, along with miR-129-5p target gene TCF4, were all down-regulated after OVX surgery, which were rescued by inhibitor-129-5p treatment. mRNA expression level of transcript factors *Tcf7* and *Lef1* also exhibited similar tendency (**Figures 6C–H**, **7B–F**). The results proved the rescue effect of inhibitor-129-5p on postmenopausal osteoporosis, and further implied that miR-129-5p might serve as a potential therapeutics target for osteoporosis.

TABLE 1 | Bonding sequence of miR-129-5p to *Tcf4* -3′UTR.

Sequences	Folding Energy (-Lcal/mol)
GTAA—-ACA—-AAGCAAAAAA | : | | || | | | | | | | CGTTCGGGTCTGGCGTTTTTC	−6.10

Bioengineered Recombinant miR-129-5p Inhibitor Enhanced Osteoblast Differentiation and Rescued Postmenopausal Osteoporosis

To further achieve the translational medical application of miR-129-5p with higher efficiency and lower cost, bioengineered novel recombinant miR-129-5p inhibitor was manufactured

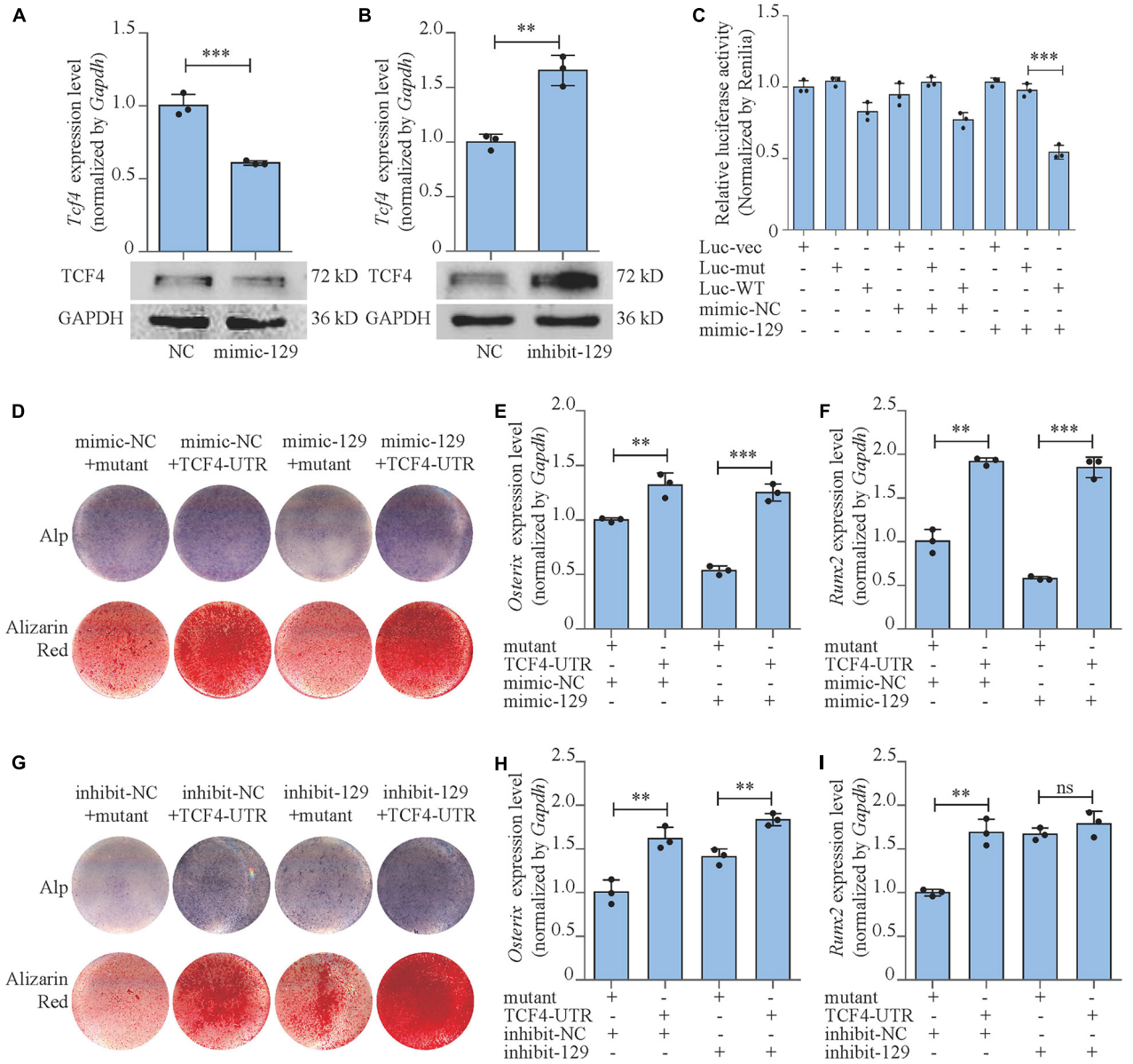


FIGURE 4 | miR-129-5p inhibited osteoblast differentiation via targeting *Tcf4*. **(A,B)** TCF4 expression levels of MC3T3-E1 cells treated with mimic or inhibitor-129-5p, as detected by reverse transcriptase-polymerase chain reaction (RT-PCR) and Western blot (mean ± SD, $^{***}P < 0.001$). NC, mimic-NC or inhibitor-NC; mimic-129, mimic-129-5p; inhibit-129, inhibitor-129-5p. **(C)** Binding effect of miR-129-5p and *Tcf4*–3′ UTR, as detected by luciferase reporter assay (mean ± SD, $^{***}P < 0.001$). Luc-vec: empty luciferase reporter plasmid. Luc-mut: luciferase reporter plasmid containing mutant *Tcf4*–3′ UTR. Luc-WT: luciferase reporter plasmid containing wild-type *Tcf4*–3′ UTR. **(D)** Alp and alizarin red staining of MC3T3-E1 cells treated with *Tcf4*–3′ UTR plasmid and mimic-129-5p. Alp, results of Alp staining; alizarin red, results of alizarin red staining. Mutant: expression plasmid containing mutant miR-129-5p binding site sequence of *Tcf4*–3′ UTR. TCF4-UTR: expression plasmid containing wild-type miR-129-5p binding site sequence of *Tcf4*–3′ UTR. **(E,F)** *Osterix* or *Runx2* expression levels of MC3T3-E1 cells treated with *Tcf4*–3′ UTR plasmid and mimic-129-5p, as detected by RT-PCR (mean ± SD, $^{**}P < 0.01$, $^{***}P < 0.001$). **(G)** Alp and alizarin red staining of MC3T3-E1 cells treated with *Tcf4*–3′ UTR plasmid and inhibitor-129-5p. **(H,I)** *Osterix* or *Runx2* expression levels of MC3T3-E1 cells treated with *Tcf4*–3′ UTR plasmid and inhibitor-129-5p, as detected by RT-PCR (mean ± SD, $^{**}P < 0.01$).

through *E. coli* system (**Supplementary Figure S7**), and its function was further determined. The recombinant miR-129-5p inhibitor efficiently decreased miR-129-5p level in MC3T3-E1 cells (approximately 56%, **Figure 8A**, $P < 0.01$). The Alp activities and mineralized nodules, along with *Osterix* and *Runx2* expression level, were all significantly enhanced, indicating that the recombinant miR-129-5p inhibitor promoted osteoblast differentiation (**Figures 8B,C** and **Supplementary Figure S8**). TCF and LEF1 presented a significant increment in both mRNA expressions and activities (**Figures 8D–F**). Expression of miR-129-5p target gene TCF4 was also significantly increased (**Figure 8G**), demonstrating that recombinant miR-129-5p

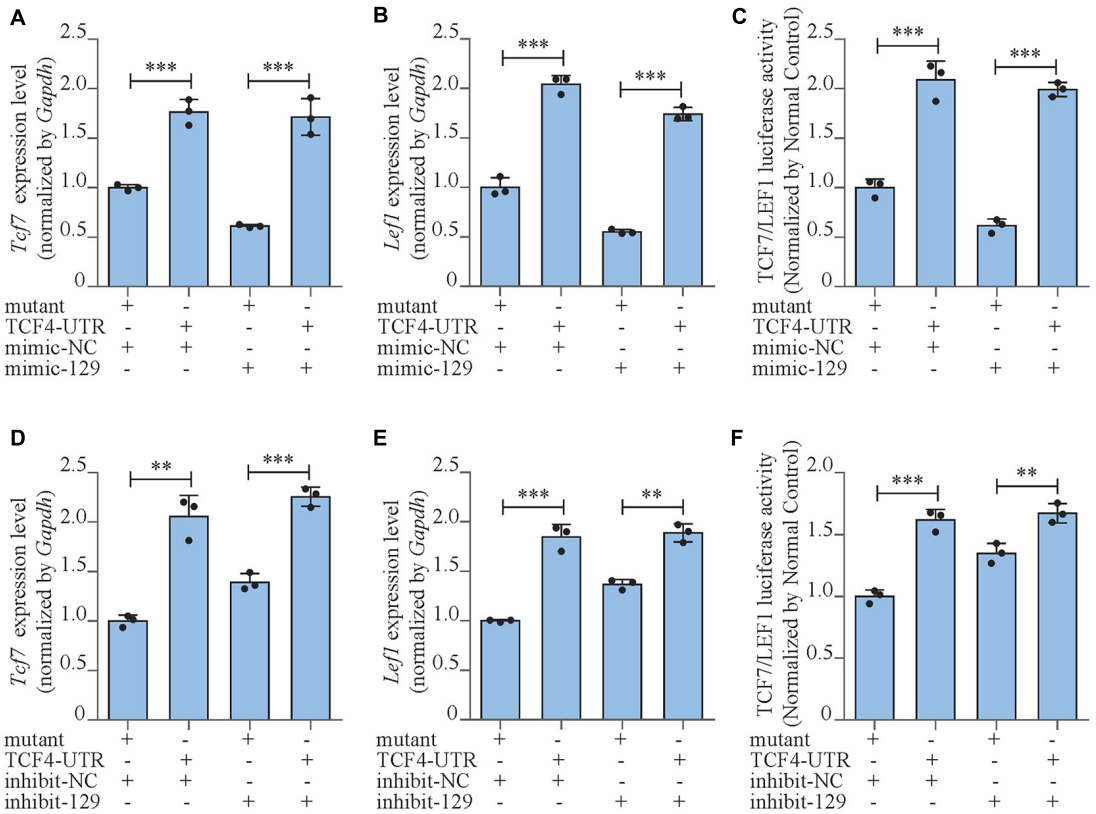


FIGURE 5 | miR-129-5p inhibited Wnt/β-catenin downstream transcript factors via targeting *Tcf4*. **(A,B)** *Tcf7* and *Lef1* expression levels of MC3T3-E1 cells treated with *Tcf4*–3′ UTR plasmid and mimic-129-5p, as detected by reverse transcriptase-polymerase chain reaction (RT-PCR; mean ± SD, ***$P < 0.001$). Mutant/TCF4-UTR: expression plasmid containing mutant/wild-type miR-129-5p binding site sequence of *Tcf4*–3′ UTR. **(C)** TCF7/LEF1 activities of MC3T3-E1 cells treated with *Tcf4*–3′ UTR plasmid and mimic-129-5p, as detected by luciferase reporter assay (mean ± SD, ***$P < 0.001$). **(D,E)** *Tcf7* and *Lef1* expression levels of MC3T3-E1 cells treated with *Tcf4*–3′ UTR plasmid and inhibitor-129-5p, as detected by RT-PCR (mean ± SD, **$P < 0.01$, ***$P < 0.001$). **(F)** TCF7/LEF1 activities of MC3T3-E1 cells treated with *Tcf4*–3′ UTR plasmid and inhibitor-129-5p, as detected by luciferase reporter assay (mean ± SD, **$P < 0.01$, ***$P < 0.001$).

inhibitor enhanced TCF4 level and downstream transcript factors of Wnt/β-catenin pathway. Moreover, recombinant miR-129-5p inhibitor was also implemented in calvarias of OVX mice. The mineral apposition rate was decreased by 56.3% ($P < 0.001$) in the OVX mice, but was increased by 100.2% ($P < 0.001$) upon recombinant miR-129-5p inhibitor treatment (**Figures 8H–I**). The *in vitro* and *in vivo* results have proved the prospect that recombinant miR-129-5p inhibitor may be used as a potential therapeutic drug for osteoporosis.

DISCUSSION

Osteoporosis has become an emerging threat to elderly population because of its high incidence. The patients would suffer from bone mass reduction, bone microstructure deterioration, hunchback, muscle spasms, myasthenia, pain, and increased risk of fracture. Many factors contribute to osteoporosis, including genetic diseases, hormonal disruption, malnutrition, drug side effects, disuse, etc. (Georgiou et al., 2012). Among all reasons, one of the most essential causes of osteoporosis is the deterioration of osteoblast differentiation, which decreased bone formation and further led to osteoporosis.

The differentiation of osteoblast is a long-term physiological process that could be impacted by many genetic and epigenetic factors. miRNAs are a sort of non-coding RNA with 18 to 25 nucleotides in length. miRNAs are widely expressed in eukaryotes and have been known as important regulators for multiple physiological and pathological processes (Bartel, 2009; Rigoutsos and Furnari, 2010; Chen et al., 2017). miRNAs played an important role in regulating osteoblast differentiation and bone formation. Wang et al. revealed that miR-214 inhibited bone formation *via* targeting *Atf4* (Wang et al., 2013). Li et al. (2015) have reported that miR-188 inhibited osteogenic differentiation of BMSCs and consequently promoted BMSC adipogenic differentiation, which further mediated aging-related osteoporosis. Zuo et al. (2015) discovered miR-103a, which was sensitive to mechanical stimulation and mediated disuse osteoporosis by targeting *Runx2*. Wang et al. (2018, 2020) recently discovered that miR-139-3p inhibited osteoblast function and bone formation through *Elk1*. These studies demonstrated the important role of miRNAs on bone formation and implied that translational medical research of osteogenic

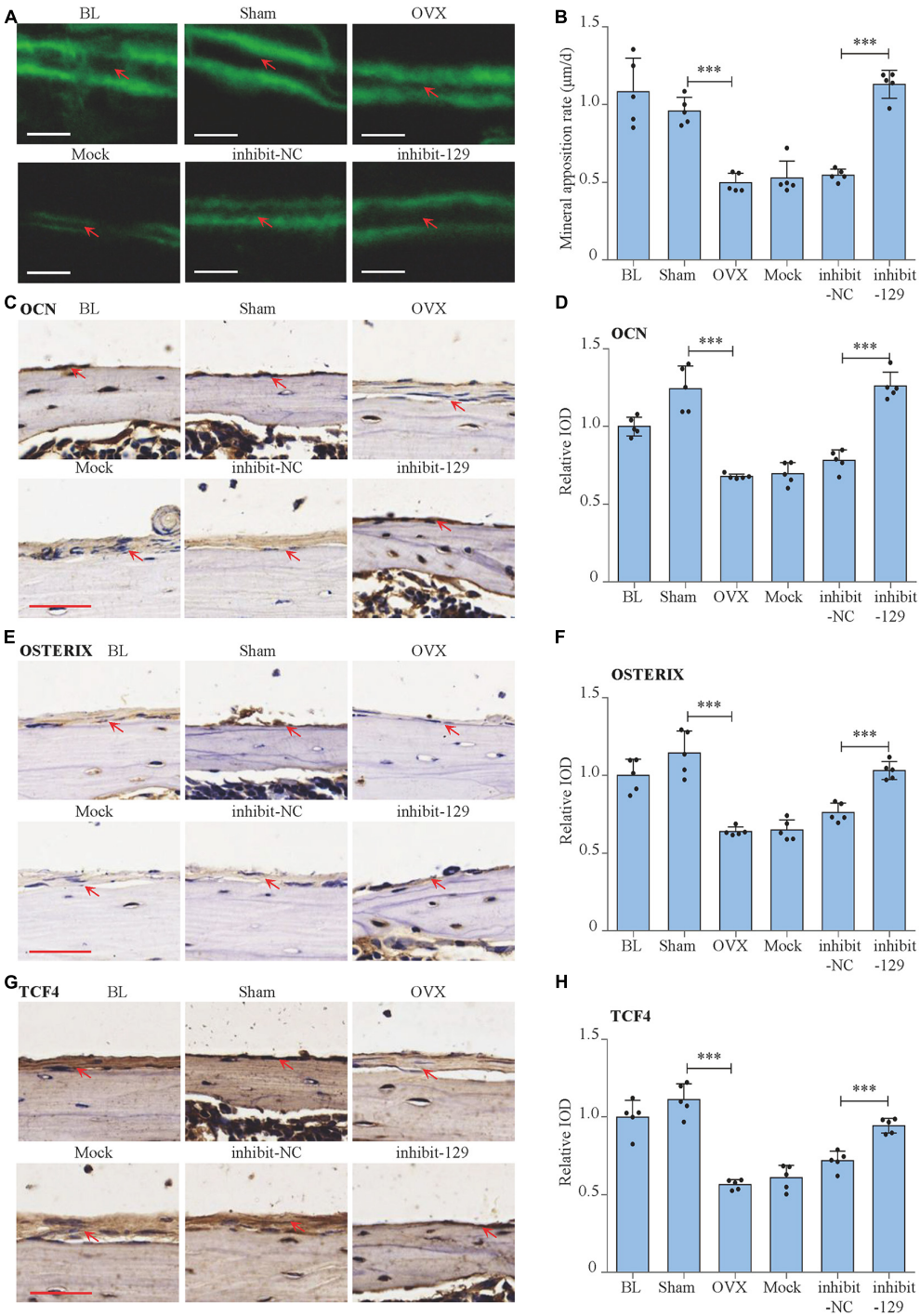


FIGURE 6 | Rescue effect of miR-129-5p inhibitor on postmenopausal osteoporosis. **(A)** Representative images showing calvarial mineral apposition rate of C57BL/6 mice after OVX and inhibitor-129-5p treatment. Scale bar: 10 μm. BL (baseline): sacrifice before RNA treatment. Sham: sham OVX operation group. OVX: OVX group. Mock: transfection reagent control group. inhibit-NC: inhibitor-NC–treated group. inhibit-129: inhibitor-129-5p–treated group. **(B)** Calvarial mineral apposition rates of C57BL/6 mice after OVX and inhibitor-129-5p treatment (mean ± SD, ***$P < 0.001$). **(C)** Expression of OCN in calvarial tissues of C57BL/6 mice after OVX and inhibitor-129-5p treatment, as detected by immunohistochemical staining. Scale bar: 50 μm. **(D)** Quantification of relative integrated optical density (IOD) values of OCN immunostaining using Image-Pro Plus 6.0 software (mean ± SD, ***$P < 0.001$). **(E)** Expression of OXTERIX in calvarial tissues of C57BL/6 mice after OVX and inhibitor-129-5p treatment, as detected by immunohistochemical staining. Scale bar: 50 μm. **(F)** Quantification of relative IOD values of OXTERIX immunostaining using Image-Pro Plus 6.0 software (mean ± SD, ***$P < 0.001$). **(G)** Expression of RUNX2 in calvarial tissues of C57BL/6 mice after OVX and inhibitor-129-5p treatment, as detected by immunohistochemical staining. Scale bar: 50 μm. **(H)** Quantification of relative IOD values of RUNX2 immunostaining using Image-Pro Plus 6.0 software (mean ± SD, ***$P < 0.001$).

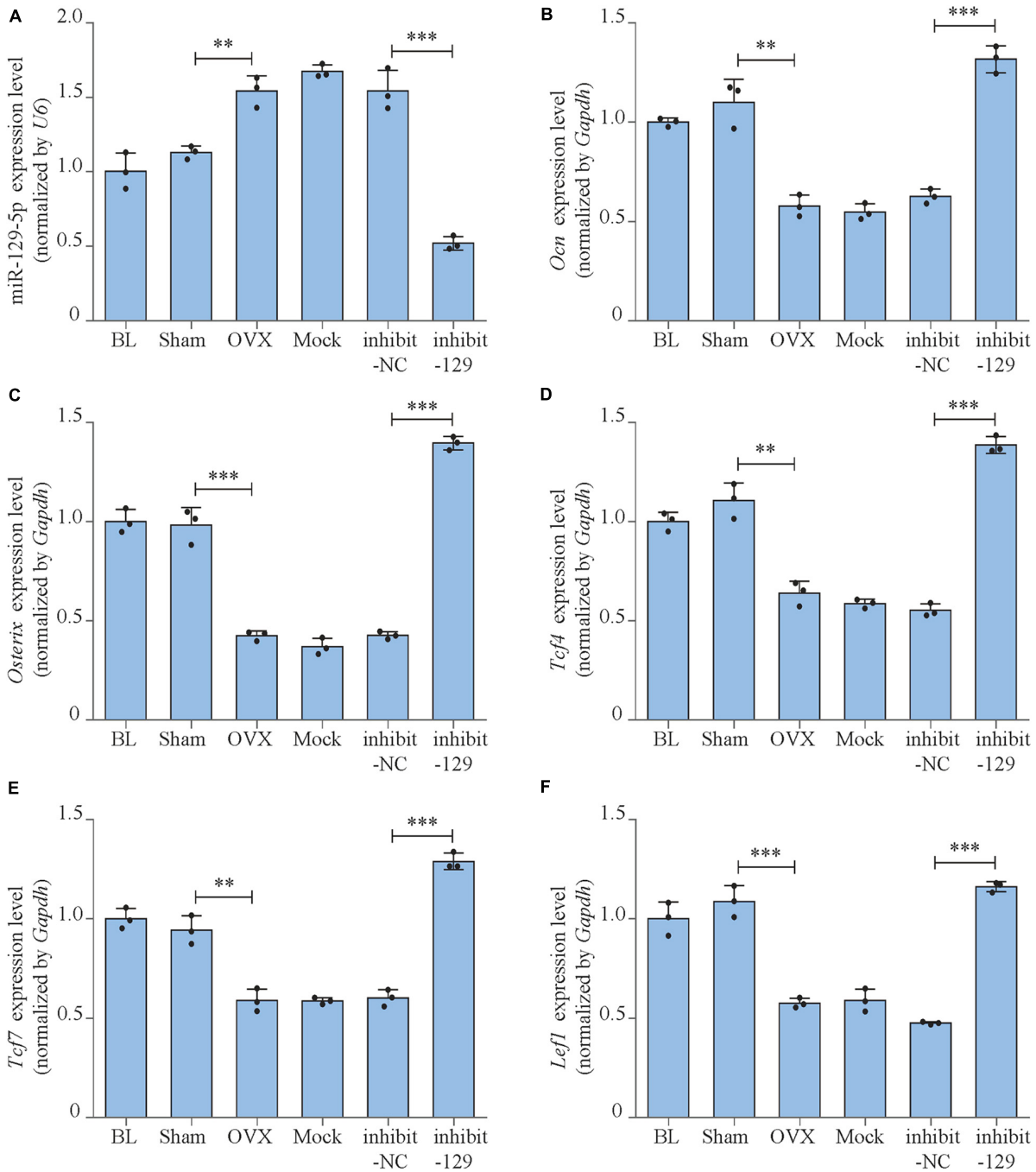


FIGURE 7 | miR-129-5p and osteogenic transcript factor expression levels of OVX mice after inhibitor-129-5p treatment. **(A)** miR-129-5p level in calvarial tissue of C57BL/6 mice after OVX and inhibitor-129-5p treatment, as detected by reverse transcriptase-polymerase chain reaction (RT-PCR; mean ± SD, $^{**}P < 0.01$, $^{***}P < 0.001$). BL (baseline): sacrifice before RNA treatment. Sham: sham OVX operation group. OVX: OVX group. Mock: transfection reagent control group. inhibit-NC: inhibitor-NC–treated group. inhibit-129: inhibitor-129-5p–treated group. **(B–F)** *Ocn*, *Osterix*, *Tcf4*, *Tcf7*, and *Lef1* expression levels in calvarial tissue of C57BL/6 mice after OVX and inhibitor-129-5p treatment, as detected by RT-PCR (mean ± SD, $^{**}P < 0.01$, $^{***}P < 0.001$).

miRNAs would be helpful to discover potential treatment for osteoporosis.

miR-129-5p is a miRNA that has been reported as a regulator of cancer development and Alzheimer disease (Li G. et al., 2019; Zeng et al., 2019). Shi et al. found hsa-miR-129-5p inhibited osteogenic differentiation of adipose-derived stem cells (Shi et al., 2020), while its function on bone formation is still unexplored. To further reveal the correlation between miR-129-5p and osteoporosis, in this study, we have stimulated aging-related osteoporosis in male aging mice model and menopause

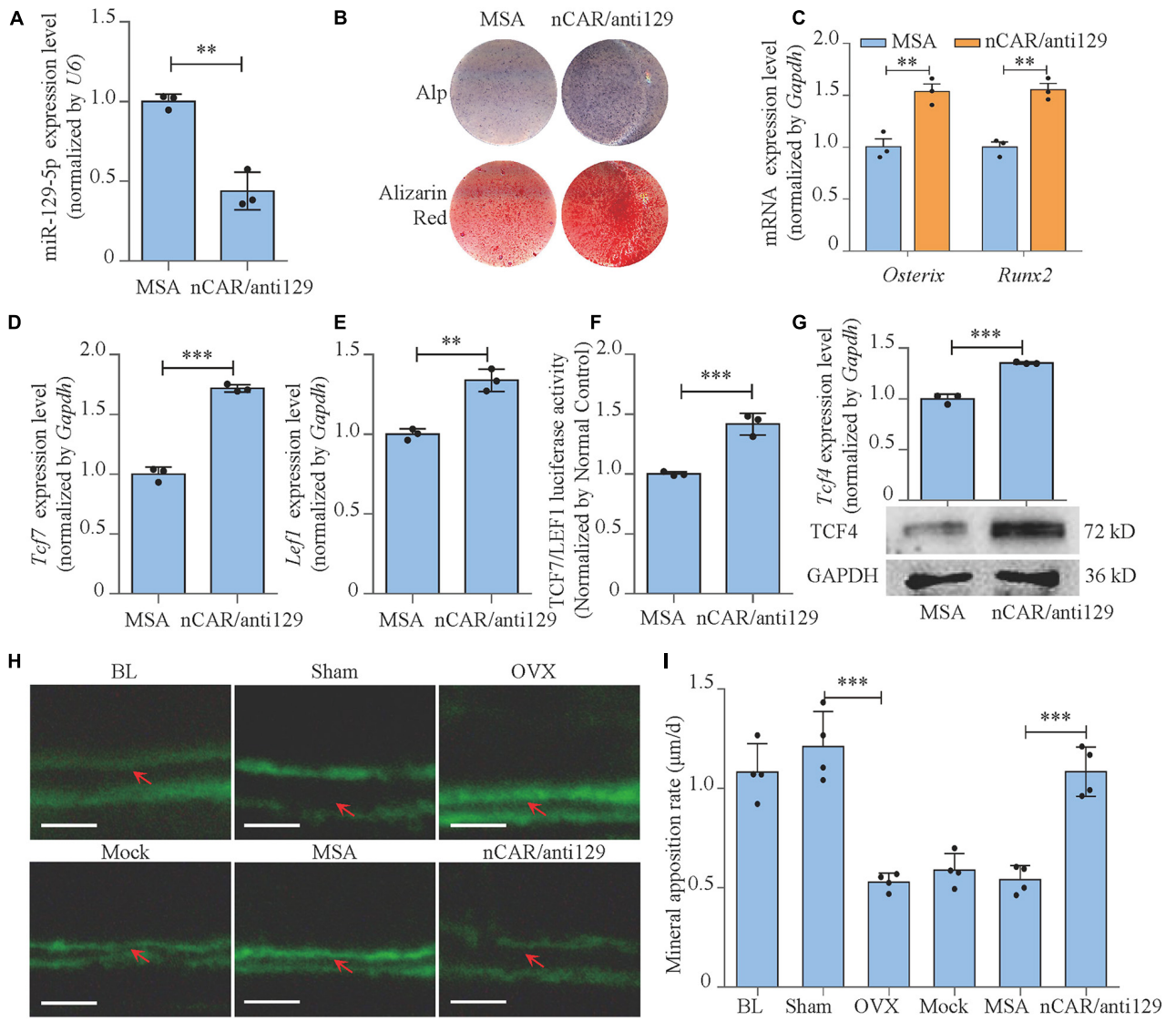


FIGURE 8 | Bioengineered recombinant miR-129-5p inhibitor enhanced osteoblast differentiation and rescued postmenopausal osteoporosis. **(A)** miR-129-5p expression levels of MC3T3-E1 cells treated with recombinant miR-129-5p inhibitor, as detected by reverse transcriptase-polymerase chain reaction (RT-PCR; mean ± SD, $^{**}P < 0.01$). MSA: $tRNA^{Met}$ fused Sephadex aptamer. nCAR/anti129: novel recombinant miR-129-5p inhibitor. **(B)** Alp and alizarin red staining of MC3T3-E1 cells treated with recombinant miR-129-5p inhibitor, as detected by Alp staining and alizarin red staining. Alp: results of Alp staining. alizarin red: results of alizarin red staining. **(C)** *Osterix* and *Runx2* expression levels of MC3T3-E1 cells treated with recombinant miR-129-5p inhibitor, as detected by RT-PCR (mean ± SD, $^{**}P < 0.01$). **(D,E)** *Tcf7* and *Lef1* expression levels of MC3T3-E1 cells treated with recombinant miR-129-5p inhibitor, as detected by RT-PCR (mean ± SD, $^{**}P < 0.01$, $^{***}P < 0.001$). **(F)** TCF7/LEF1 activities of MC3T3-E1 cells treated with recombinant miR-129-5p inhibitor, as detected by luciferase reporter assay (mean ± SD, $^{***}P < 0.001$). **(G)** TCF4 expression levels of MC3T3-E1 cells treated with recombinant miR-129-5p inhibitor, as detected by RT-PCR and Western blot (mean ± SD, $^{***}P < 0.001$). **(H)** Representative images showing calvarial mineral apposition rate of C57BL/6 mice after OVX and recombinant miR-129-5p inhibitor treatment. Scale bar: 10 μm. BL (baseline): sacrifice before RNA treatment. Sham: sham OVX operation group. OVX: OVX group. Mock: transfection reagent control group. MSA: empty recombinant tRNA treated group. nCAR/anti129: novel recombinant miR-129-5p–inhibitor treated group. **(I)** Calvarial mineral apposition rates of C57BL/6 mice after OVX and recombinant miR-129-5p inhibitor treatment (mean ± SD, $^{***}P < 0.001$).

osteoporosis in female aging menopause mice model. The expression of miR-129-5p in BMSC demonstrated that miR-129-5p expression was enhanced in both osteoporosis models. Moreover, correlation analysis also proved that miR-129-5p negatively correlated with osteogenic marker gene in different ages of mice (**Figure 1**). We further proved the inhibitory effect of miR-129-5p on osteoblast differentiation and bone formation (**Figure 2**). The results proved that miR-129-5p is an important regulatory factor to osteoblast differentiation and bone formation.

MicroRNA inhibited the translation of target gene by binding to its 3′ UTR region (Lai, 2002). In Shi et al.'s (2020) study, hsa-miR-129-5p inhibited Wnt/β-catenin pathway via targeting *Grm5*. In Li et al. (2013); Zhang et al. (2017),

and Cao et al. (2018), hsa-miR-129-5p inhibited Wnt/β-catenin pathway via targeting *Apc*, *Sox4*, and *Wnt5a*, respectively. Wnt/β-catenin pathway is one of the most essential pathways regulating bone formation, which activates multiple osteogenic factors by TCF7 and LEF1 (Maria et al., 2007; Georgiou et al., 2012). In our study, we have first proved that miR-129-5p inhibited the expression and activity of downstream transcription factors of Wnt/β-catenin pathway TCF7 and LEF1 (**Figure 3**). However, *Tcf7* and *Lef1* were not target genes of miR-129-5p (predicted by miRDB, http://www.mirdb.org/, Chen and Wang, 2020), so we turned our attention to the regulator of *Tcf7* and *Lef1*. Because multiple TCFs within wnt signaling pathway played essential roles on regulating *Tcf7* and *Lef1*. Therefore, we used miRDB to screen the targeting effect of miR-129-5p on TCFs and found the 3′UTR of Tcf4 had 6 binding sites of miR-129-5p. TCF4 has been reported as an important regulatory factor of wnt/β-catenin pathway, and therefore promoted osteogenic differentiation (Reinhold and Naski, 2007). On this basis, we confirmed the targeting effect of miR-129-5p on *Tcf4*. Moreover, the 3′UTR sequence of *Tcf4* was also proved to enhance both osteoblast differentiation and downstream transcription factors of wnt/β-catenin pathway (**Figures 4**, **5**). All these results illustrated that miR-129-5p promoted osteoblast differentiation and bone formation through inhibiting downstream transcription factors of wnt/β-catenin pathway by targeting *Tcf4*. However, besides TCF4, other unknown mechanisms may also exist for the inhibition of osteoblast differentiation by miR-129-5p.

Based on the finding that miR-129-5p inhibited bone formation, we have further proved that the inhibitor of miR-129-5p ameliorated menopausal osteoporosis (**Figures 6**, **7**). However, until now, most RNA-based therapeutic drugs were still manufactured by chemical synthesis, which resulted in very high cost on synthesis and the unclear biosafety. The novel RNA bioengineering system that can express functional miRNA and siRNA by *E. coli* was recently established (Ho et al., 2018; Li X. et al., 2019), which could manufacture recombinant RNA with extremely low cost (multi-mg RNA in 1L *E. coli*), along with high safety and high efficiency. Using this technique, the novel recombinant miR-129-5p inhibitor was manufactured, and its effects on osteoblast have been proved as good as chemical synthesized miR-129-5p inhibitor. Moreover, the novel recombinant miR-129-5p inhibitor also proved its high efficiency on rescuing menopausal osteoporosis at much lower dose (four times less) compared to chemical synthesized miR-129-5p inhibitor (**Figure 8**). These results have proved that the novel recombinant miR-129-5p inhibitor may serve as a promising drug for osteoporosis treatment.

Taken together, we have identified miR-129-5p that inhibited osteoblast differentiation and bone formation. miR-129-5p targeted *Tcf4* and thus inhibited downstream transcription factors of Wnt/β-catenin pathway. miR-129-5p inhibitor ameliorated menopausal osteoporosis, and the novel recombinant miR-129-5p inhibitor showed its high efficiency on promoting osteoblast differentiation and rescuing osteoporosis. The study illuminated a new mechanism regulating bone formation and also provided novel therapeutic strategies for the treatment of osteoporosis.

MATERIALS AND METHODS

Cell Culture and Mouse Model

Murine preosteoblast MC3T3-E1 cell line was generously provided by Dr. Hong Zhou (The University of Sydney, Sydney, Australia). MC3T3-E1 cells were cultured in osteoblast culture medium containing α modified eagle medium (α-MEM, Gibco, 11900-024, Carlsbad, CA) supplemented with 10% fetal bovine serum (FBS; Biological Industries, 04-001-1A, Kibbutz Beit Haemek, Israel), 1% L-glutamine (Sigma, G8540, St. Louis, MO, United States), 1% penicillin (Amresco, 0242, Solon, OH, United States), and streptomycin (Amresco, 0382, Solon, OH, United States). Cell cultures were maintained at a humidified 37°C, 5% CO_2 incubator (Thermo Fisher Scientific, Waltham, MA, United States). Murine mesenchymal stem cell line C3H10 T1/2 was purchased from Runde Biotechnology Co., Ltd. (Xi'an, China). C3H10 T1/2 cells were cultured in mesenchymal stem cell culture medium containing Dulbecco modified eagle medium (DMEM, Gibco, 12800-017) supplemented with 10% FBS, 1% L-glutamine, 1% penicillin, and streptomycin. Cell cultures were maintained at a humidified 37°C, 5% CO_2 incubator.

Aging and ovariectomized (OVX) mice were adopted to construct the osteoporosis model. All mice were purchased from the Laboratory Animal Center of the Fourth Military Medical University (Xi'an, China). For aging mice model, 12 male and 12 female 6-month-old male C57BL/6 mice were maintained under standard animal housing conditions (12-h light, 12-h dark cycles and free access to food and water). Six male mice and six female mice which, were kept until 21 months old, were selected as aging group, whereas the other mice were used as control group. Mice were euthanized, and femurs were collected and processed for RNA-seq or BMSCs isolation for RT-PCR.

For OVX mouse model, sixty-six 2-month-old female C57BL/6 mice were maintained under standard animal housing conditions. The mice were ovariectomized or sham-operated at 3 months of age. Mice were euthanized 38 days after surgery (4 months of age), and the calvarias were collected to investigate the therapeutic effects of miR-129-5p inhibitor and recombinant miR-129-5p inhibitor. Euthanasia was performed using CO_2. All animal experiments were performed in accordance with the recommendation of the Guiding Principles for the Care and Use of Laboratory Animals (the Institutional Experimental Animal Committee of Northwestern Polytechnical University, Xi'an, China), and all animal studies were reviewed and approved by the Institutional Experimental Animal Committee of Northwestern Polytechnical University, Xi'an, China. For all procedures involving animals, all efforts were made to reduce the number of the mice used and their suffering.

Isolation of BMSCs

Mouse BMSCs were isolated to investigate the expression levels of miR-129-5p in male and female aging mice. Mouse femurs were immediately harvested, and attached soft tissues were removed.

Bone marrow was washed and collected by phosphate-buffered saline (PBS) using a 25-gauge syringe needle. The collected PBS with bone marrow was centrifuged (1,200*g*, 8 min) and dissociated by culture medium using a 29-gauge syringe needle. The suspension was cultured in a 60-mm plate for 3 h (37°C, 5% CO_2), and culture medium was changed. Cells were cultured for another 36 h with culture medium changed every 12 h. The cells were transferred into a new plate as the first-passage cells. Third-passage cells were used for RT-PCR detection.

Real-Time PCR

Real-Time PCR was used to assess expression levels of miR-129-5p and selected mRNAs. Total RNA was extracted from mouse femur and calvarial tissues or culture cells using Trizol reagent (Invitrogen, 15596018). Mouse femur and calvaria were harvested and grinded with liquid nitrogen and then digested by Trizol reagent; 1 μg of total RNA was used for cDNA synthesis using one-step PrimeScript RT reagent kit (TaKaRa, RR037A, Dalian, China). Quantitative PCR amplification was performed using the Thermal Cycler C-1000 Touch system (BIO-RAD CFX Manager, Hercules, CA) and SYBR Premix Ex TaqII kit (TaKaRa, RR820A). For mRNA, *Gapdh* was used as internal control gene. For miR-129-5p, *U6* was used as internal control. The quantitative PCR reaction conditions included initial denaturation step at 95°C for 30 s, followed by 42 cycles at 95°C for 10 s, 60°C for 30 s, and 72°C for 5 s. Data were calculated using the comparative Ct method ($2^{-\Delta\ \Delta\ Ct}$) and expressed as fold change compared to corresponding control. Primers (for sequences, see **Table 2**) were synthesized by Sangon Biotech Co., Ltd. (Shanghai, China).

TABLE 2 | Primer Sequences for qRT-PCR.

Target gene	Sequences (5′→3′)
miR-129-5p-Forward	CTTTTTGCGGTCTGGGCTTGC
miR-129-5p-Reverse	AGTGCAGGGTCCGAGGTATT
miR-129-5p-RT	GTCGTATCCAGTGCAGGGTCCGAGGTATTCGCA CTGGATACGACGCAAGC
Osterix-Forward	CCCTTCCCTCACTCATTTCC
Osterix- Reverse	CAACCGCCTTGGGCTTAT
Runx2-Forward	CGCCCCTCCCTGAACTCT
Runx2-Reverse	TGCCTGCCTGGGATCTGTA
Tcf4-Forward	ATCGCAGACGCAAGAGGTTTCAG
Tcf4-Reverse	ACATACCGCTTCGCACATTCAGAG
Tcf7-Forward	CAGAATCCACAGATACAGCA
Tcf7-Reverse	CAGCCTTTGAAATCTTCATC
Lef1-Forward	GATCCCCTTCAAGGACGAAG
Lef1-Reverse	GGCTTGTCTGACCACCTCAT
Ocn-Forward	GAAGGCAACAGTCGATTCACC
Ocn-Reverse	GACTGTCTTGCCCCAAGTTCC
Gapdh-Forward	TGCACCACCAACTGCTTAG
Gapdh- Reverse	GGATGCAGGGATGATGTTC
U6-Forward	GTGCTCGCTTCGGCAGCACATAT
U6-Reverse	AAAATATGGAACGCTTCACGAA

Transfection of the miR-129-5p Mimic and Inhibitor

miR-129-5p mimic and inhibitor (Genepharma, Shanghai, China) transfection was performed to manipulate miR-129-5p expression. For transfection *in vitro*, MC3T3-E1 or C3H10 T1/2 cells were seeded in a 24-well plate at 3.2×10^4 cells per well and were transfected with miR-129-5p mimic or inhibitor by Lipofectamine™ 2000 (Invitrogen, 11668-030) according to the manufacturer's instructions (40 nM), using mimic-NC or inhibitor-NC as normal control, respectively. The overexpression or knockdown of miR-129-5p in cells was confirmed by RT-PCR 36 h after the transfection.

For *in vivo* transfection, 32 female C57BL/6 mice (4-month-old) were randomly divided into four groups (mimic-NC, mimic-129-5p, inhibitor-NC, inhibitor-129-5p). For each group, mice were injected subcutaneously over the calvarial surface with plasmids formulated with Entranster™ *In Vivo* Transfection Reagent (Engreen, 18668-11-2, Beijing, China) at the dosage of 40 μL (including 4.8 μg RNA) according to the manufacturer's instructions. All mice received the same standard diet during the experimental period. Three mice from each group were euthanized 3 days after treatment, and calvarias from mice were processed for RT-PCR (n = 3/group). All other mice were euthanized 21 days after treatment, and calvarias were processed for histomorphometric analyses (n = 5/group; Yin et al., 2019).

Alkaline Phosphatase Staining and Alizarin Red Staining

For osteogenic differentiation treatment, MC3T3-E1 cells at confluence of 100% were induced by osteogenic medium with α-MEM, 10% FBS, 1% β-glycerophosphate (Sigma, G9422), 1% ascorbic acid (Sigma, A7631), 1% penicillin/streptomycin, and 1% L-glutamine. The cell cultures were maintained at 37°C with 5% CO_2, and medium was replaced every 2 days. As for C3H10 T1/2 cells, osteogenic medium was made by DMEM, 20% FBS (ExCell Bio, FND500, Moorebank, Australia), 1% β-glycerophosphate, 1% ascorbic acid, 1% penicillin/streptomycin, 1% L-glutamine, and 1 mM dexamethasone (Sigma, D4902).

Alp staining and alizarin red staining were performed to determine osteoblast differentiation. ALP of osteoblasts was stained 3 days after having been induced by osteogenic medium. The staining was performed by 5-bromo-4-chloro-3-indolyl phosphate (BCIP)/ nitro blue tetrazolium (NBT) Alkaline Phosphatase Color Development Kit (Beyotime Biotechnology, C3206, Shanghai, China) according to the manufacturer's instruction. Briefly, cells were washed with PBS (pH7.4) and fixed in 10% buffered formaldehyde. Formaldehyde was washed with PBS, and then cells were stained with BCIP/NBT solution. The staining was stopped by immersing into distilled water. After staining, the plates were dried and scanned with CanoScan 9000F Mark II scanner (Canon, Tokyo, Japan). For MC3T3-E1 cells, alizarin red staining was carried out after having been induced by osteogenic medium for 21 days. As for C3H10 T1/2 cells, alizarin red staining was carried out after 10 days' treatment of osteogenic medium. The

cells were washed with PBS and then stained with 0.5% alizarin red S (pH 4.0, Sigma, A5533) for 30 min. After immersion into tap water for 30 min, the plates were dried and scanned with CanoScan 9000F Mark II scanner and analyzed by Image-Pro Plus 6.0 software (National Institutes of Health, Bethesda, MD) to determine the ALP and alizarin red staining intensities.

Western Blot

For detection of protein levels, Western blot analysis was performed as previously described (Yin et al., 2018). Protein samples from cultural cells were extracted. Cells were washed three times by cold PBS and then digested by cell lysis buffer (Beyotime, P0013, Haimen, China) with 1% protease inhibitor cocktail (Calbiochem, 539134, Darmstadt, Germany). Protein concentrations were analyzed by bicinchoninic acid protein assay kit (Thermo Fisher Scientific, 23225); 100 ng of proteins for each sample was subjected to sodium dodecyl sulfate–polyacrylamide gel electrophoresis (PAGE) using 5% stacking gel and 12% separating gel, 140 V, 30 min, and transferred (400 mA, 1 h) to nitrocellulose filter membranes (Pall, 66485, Port Washington, NY, United States). Membranes were blocked with 4% skimmed milk (BD Biosciences, 232100, Franklin Lakes, NJ, United States) for 1 h at room temperature and then incubated with primary antibodies at 4°C overnight with the following primary antibodies: TCF4 (Rabbit pAb, 1:1,000, Proteintech, 22337-1-AP, Rosemont, IL, United States) and GAPDH (Rabbit pAb, 1:1,000; Proteintech, 10494-1-AP). Blots were then incubated with horseradish peroxidase (HRP)–labeled secondary antibody (1:2,000; CWBIO, CW0103, Beijing, China) and visualized using chemiluminescence detection system (Thermo Fisher Scientific, NCI5080). Protein bands were scanned by a chemiluminescence imaging system (Tanon, 4600SF, Shanghai, China). GAPDH was adopted as internal control.

Bone Histomorphometric Analyses

Bone histomorphometric analysis was performed to investigate the effect of miR-129-5p on bone formation. To measure mineral appositional rate, double-calcein labeling was performed by intraperitoneal injection with calcein green (20mg/kg body weight, Sigma, C0875) in the time sequence of 10 and 3 days before euthanasia for specimen collection. Collected calvarial samples were directly embedded in OCT (Leica, 14020108926, Wetzlar, Germany). Transverse cryosections (4 μm in thickness) were made by a freezing-microtome (Leica, CM1100), and slides were examined with a fluorescent microscope (NEXCOPE NIB900, Ningbo, China). Bone dynamic histomorphometric analyses for mineral apposition rate were performed using image analysis software (Image J, National Institutes of Health, Bethesda, MD, United States; Ushiku et al., 2010).

Immunohistochemical Staining

To investigate the rescue effect of miR-129-5p inhibitor on osteogenic gene and TCF4 levels in mice calvarias, immunohistochemical staining analysis was performed as previously described (Yin et al., 2019). Mouse calvarias were dissected and fixed in 4% paraformaldehyde, decalcified in 17% ethylenediaminetetraacetic acid (Sigma, E9884) for 21 days, and embedded in paraffin (Huayong, Shanghai, China). Sections (5 μm in thickness) were dewaxed, immersed in the distilled water, blocked in 5% goat serum (CWBIO, CW0130) in PBS, and then incubated overnight at 4°C with primary antibodies against OCN (Rabbit pAb, 1:200, Santa Cruz Biotech, sc-365797, Dallas, TX, United States), OSTERIX (Rabbit pAb, 1:50; Proteintech, 12593-1-AP), and TCF4 (Rabbit pAb, 1:100, Proteintech, 22337-1-AP), respectively. Following three washes in PBS, the sections were labeled with HRP-labeled secondary antibody 1.5 h at room temperature and developed for color reaction using diaminobenzidine (CWBIO, CW2068) and hematoxylin counterstain. Slides were scanned by Aperio AT2 Digital Pathology Scanner (Leica), and protein immunostaining intensities on top surface of the calvarias were analyzed by Image-Pro Plus 6.0 software.

Luciferase Reporter Assay

To analyze the function of miR-129-5p in regulating TCF7/LEF1 activity in MC3T3-E1 cells, TCF7/LEF1 luciferase reporter plasmid was constructed by inserting eight repeats of TCF7/LEF1 binding motif sequence (AGATCAAAGG) to the promoter region of nanoluc luciferase gene sequence in PNL1.1 plasmid (N1351, Promega, Fitchburg, WI). MC3T3-E1 cells were seeded in a 6-well plate at 1×10^5 cells per well, and TCF7/LEF1 luciferase reporter plasmid was transfected by Engreen Entranster^{TM} H4000 Reagent according to the manufacturer's instructions. Six hours after transfection, the medium was replaced by antibiotic-free culture medium. After 3-h culture, the cells were transfected with miR-129-5p mimic or inhibitor (40 nM) with its relative mimic-NC or inhibitor-NC as negative control. A luciferase reporter assay was performed 72 h after the transfection using the Nano-Glo® Luciferase Assay System (Promega, N1120, Fitchburg, WI, United States) according to the manufacturer's instruction. Briefly, 100 μL cell culture medium was collected into a microplate, and then 100 μL diluted Nano-Glo® Luciferase Assay Substrate was added. Nanoluc luciferase luminescent signals were quantified by a microplate reader (Synergy, United States) at 460 nm, and each value from the nanoluc luciferase constructs was normalized by a normal control.

To detect interaction between miR-129-5p and *Tcf4*, wild-type binding sequence of miR-129-5p in *Tcf4*–3′ UTR (Luc-WT, with binding site sequence "GCAAAAAA") and its relative mutant binding sequence (Luc-mut, with binding site sequence "TAGGGGGG") were designed and were synthesized by TsingKe Biotech Co., Ltd. (Beijing, China) and then inserted into pMIR-Report Luciferase plasmid (miaolingbio, P0471,Wuhan, China), respectively, with empty pMIR-Report Luciferase plasmid (Luc-vec) as control. Internal control pRL-TK Renilla plasmid was generously provided by Dr. Pengsheng Zheng (Xi'an Jiaotong University, Xi'an, China). The reporter plasmids were co-transfected with pRL-TK Renilla plasmid into MC3T3-E1 cells, and miR-129-5p mimic/inhibitor transfection was performed as mentioned above. Luciferase reporter assays were performed with the dual-luciferase reporter assay system

(Promega, E1910, Fitchburg, WI, United States) according to the manufacturer's instruction. Luminescent signals were quantified, and each value from the firefly luciferase was normalized by Renilla luciferase.

Therapeutic miR-129-5p Inhibitor in OVX Mice

To investigate therapeutic effect of miR-129-5p inhibitor on osteoporosis, 48 OVX mice were randomly divided into seven groups (baseline, sham, OVX, mock, inhibitor-NC, inhibitor-129-5p). The transfection was performed at 8 and 15 days after OVX, respectively. And mice were injected subcutaneously over the calvarial surface with inhibitor-129-5p or inhibitor-NC formulated with Entranster^{TM} *In vivo* Transfection Reagent twice per day, at the dosage of 40 μL (including 4.8 μg RNA) according to the manufacturer's instructions. In the mock group, mice were injected with the same volume of normal saline mixed with transfection reagent. The mice in OVX group received no treatment. All mice were given the same standard diet during the experimental period. All mice of the baseline group and three mice from other groups were euthanized 11 days after OVX treatment, and calvarias were used for RT-PCR (n = 3/group). All the other mice were euthanized 35 days after OVX, and calvarias were used for immunohistochemical staining and histomorphometric analyses (n = 3/group; Yin et al., 2019).

Manufacture and Transfection of Recombinant miR-129-5p Inhibitor

Recombinant miR-129-5p inhibitors were manufactured to achieve the translational medical application of miR-129-5p with high efficiency and low cost. The production was performed as previously described (Ho et al., 2018; Li X. et al., 2019). In brief, sequence of inhibitor-129-5p was designed and synthesized and then inserted into plasmid pBSMrnaSeph. The edited plasmid was transformed into *E. coli* (HST08). Total RNA of *E. coli* was extracted and purified by fast protein liquid chromatography. The purity of recombinant miR-129-5p inhibitors were checked by denaturing urea 8% PAGE. The whole manufacture process was performed by RQCON Biological Technology Co., Ltd. (Xi'an, China).

In vitro transfection of recombinant inhibitor-129-5p (nCAR/anti129) was performed by Lipofectamine^{TM} 2000 according to the manufacturer's instructions (10 nM), using empty tRNA scaffold (tRNA^{Met} fused Sephadex aptamer, MSA) as control. As for *in vivo* transfection of recombinant miR-129-5p inhibitor, 18 OVX mice were randomly divided into five groups (baseline, sham, OVX, mock, MSA, nCAR/anti129). The transfection was performed at 8 and 15 days after OVX, respectively. Mice were injected subcutaneously over the calvarial surface with recombinant miR-129-5p inhibitor or MSA formulated with Entranster^{TM} *In vivo* Transfection Reagent twice per day, at the dosage of 40 μL (including 1.2 μg RNA) according to the manufacturer's instructions. In the mock group, mice were injected with normal saline mixed with transfection reagent, and the OVX group was given no treatment. All mice received the same standard diet during the experimental period. The mice in the baseline group were sacrificed at 11 days after OVX treatment; all other mice were killed 35 days after OVX, and calvarias were processed for histomorphometric analyses (n = 3/group).

Statistical Analysis

The statistical analyses of the data were performed with GraphPad Prism version 6.0 software (GraphPad Software, Inc., La Jolla, CA, United States), and a Student t-test was used. The data are presented as mean ± standard deviation (SD). $P < 0.05$ was considered statistically significant for all comparisons. Correlation between miR-129-5p and other genes was exhibited by linear regression and Pearson correlation coefficient.

DATA AVAILABILITY STATEMENT

The original contributions presented in the study are included in the article/**Supplementary Material**, further inquiries can be directed to the corresponding author.

ETHICS STATEMENT

The animal study was reviewed and approved by the Institutional Experimental Animal Committee of Northwestern Polytechnical University, Xi'an, China.

AUTHOR CONTRIBUTIONS

CYi, YT, and AQ designed the experiments. CYi, YT, YY, CYa, PS, YZ, XW, KZ, JP, and DL performed the experiments and analyzed the data. CYi, YT, and YY wrote the manuscript. All authors read and approved the final manuscript.

FUNDING

This work was supported by the National Natural Science Foundation of China (81801871 and 32000924), the China Postdoctoral Science Foundation (2019T120947), Shaanxi Provincial Key R&D Program (2018KWZ-10), Special fund for technological innovation of Shaanxi Province (2019QYPY-207), the Shaanxi Provincial Postdoctoral Science Foundation (2017BSHEDZZ13), the Fundamental Research Funds for the Central Universities (3102019smxy003).

SUPPLEMENTARY MATERIAL

The Supplementary Material for this article can be found online at: https://www.frontiersin.org/articles/10.3389/fcell.2020.600641/full#supplementary-material

REFERENCES

Bartel, D. P. (2009). MicroRNAs: target recognition and regulatory functions. *Cell* 136, 215–233. doi: 10.1016/j.cell.2009.01.002

Cao, J. Y., Wang, Q. C., Wu, G., Li, S. S., and Wang, Q. (2018). miR-129-5p inhibits gemcitabine resistance and promotes cell apoptosis of bladder cancer cells by targeting Wnt5a. *Int. Urol. Nephrol.* 50, 1811–1819. doi: 10.1007/s11255-018-1959-x

Cao, Z., Moore, B. T., Wang, Y., Peng, X. H., Lappe, J. M., Recker, R. R., et al. (2014). miR-422a as a potential cellular microRNA biomarker for postmenopausal osteoporosis. *PLoS One* 9:e97098. doi: 10.1371/journal.pone.0097098

Chen, Q. X., Wang, W. P., Zeng, S., Urayama, S., and Yu, A. M. (2015). A general approach to high-yield biosynthesis of chimeric RNAs bearing various types of functional small RNAs for broad applications. *Nucleic Acids Res.* 43, 3857–3869. doi: 10.1093/nar/gkv228

Chen, Y. H., and Wang, X. W. (2020). miRDB: an online database for prediction of functional microRNA targets. *Nucleic Acids Res.* 48, D127–D131. doi: 10.1093/nar/gkz757

Chen, Z. H., Zhang, Y., Liang, C., Chen, L., Zhang, G., and Qian, A. R. (2017). Mechanosensitive miRNAs and bone formation. *Int .J .Mol. Sci.* 18:1684. doi: 10.3390/ijms18081684

Gennari, L., Rotatori, S., Bianciardi, S., Nuti, R., and Merlotti, D. (2016). Treatment needs and current options for postmenopausal osteoporosis. *Expert Opin. Pharmacother.* 17, 1141–1152. doi: 10.1080/14656566.2016.1176147

Georgiou, K. R., Hui, S. K., and Xian, C. J. (2012). Regulatory pathways associated with bone loss and bone marrow adiposity caused by aging, chemotherapy, glucocorticoid therapy and radiotherapy. *Am. J. Stem Cell* 1, 205–224.

Hendrickx, G., Boudin, E., and Van Hul, W. (2015). A look behind the scenes: the risk and pathogenesis of primary osteoporosis. *Nat. Rev. Rheumatol.* 11, 462–474. doi: 10.1038/nrrheum.2015.48

Ho, P. Y., Duan, Z. J., Chen, H. W., and Yu, A. M. (2018). Bioengineered noncoding RNAs selectively change cellular miRNome profiles for cancer therapy. *J. Pharmacol. Exp. Ther.* 365, 494–506. doi: 10.1124/jpet.118.247775

Ho, P. Y., and Yu, A. M. (2016). Bioengineering of noncoding RNAs for research agents and therapeutics. *Wiley Interdiscip. Rev. RNA* 7, 186–197. doi: 10.1002/wrna.1324

Hu, L. F., Su, P. H., Yin, C., Zhang, Y., Li, R. Z., Yan, K., et al. (2018). Microtubule actin crosslinking factor 1 promotes osteoblast differentiation by promoting β-catenin/TCF1/Runx2 signaling axis. *J. Cell. Physiol.* 233, 1574–1584. doi: 10.1002/jcp.26059

Huang, L., Jin, J., Deighan, P., Kiner, E., McReynolds, L., and Lieberman, J. (2013). Efficient and specific gene knockdown by small interfering RNAs produced in bacteria. *Nat. Biotechnol.* 31, 350–356. doi: 10.1038/nbt.2537

Jabbar, S., Drury, J., Fordham, J. N., Datta, H. K., Francis, R. M., and Tuck, S. P. (2011). Osteoprotegerin, RANKL and bone turnover in postmenopausal osteoporosis. *J. Clin. Pathol.* 64, 354–357. doi: 10.1136/jcp.2010.086595

Lai, E. C. (2002). MicroRNAs are complementary to 3′ UTR sequence motifs that mediate negative post-transcriptional regulation. *Nat. Genet.* 30, 363–364. doi: 10.1038/ng865

Li, C. J., Cheng, P., Liang, M. K., Chen, Y. S., Lu, Q., Wang, J. Y., et al. (2015). MicroRNA-188 regulates age-related switch between osteoblast and adipocyte differentiation. *J. Clin. Invest.* 125, 1509–1522. doi: 10.1172/JCI77716

Li, C. X., Talele, N. P., Boo, S., Anne, K., Ericka, K. W., Jenna, L. B., et al. (2017). MicroRNA-21 preserves the fibrotic mechanical memory of mesenchymal stem cells. *Nat. Mater.* 16, 379–389. doi: 10.1038/nmat4780

Li, G., Xie, J. H., and Wang, J. H. (2019). Tumor suppressor function of miR-129-5p in lung cancer. *Oncol Lett.* 17, 5777–5783. doi: 10.3892/ol.2019.10241

Li, M. H., Tian, L. L., Wang, L., Yao, H. C., Zhang, J. R., Lu, J. G., et al. (2013). Down-regulation of miR-129-5p inhibits growth and induces apoptosis in laryngeal squamous cell carcinoma by targeting APC. *PLoS One* 8:e77829. doi: 10.1371/journal.pone.0077829

Li, X., Tian, Y., Tu, M. J., Ho, P. Y., Batra, N., and Yu, A. M. (2019). Bioengineered miR-27b-3p and miR-328-3p modulate drug metabolism and disposition via the regulation of target ADME gene expression. *Acta Pharm. Sin. B* 9, 639–647. doi: 10.1016/j.apsb.2018.12.002

Maria, A., Li, H., Marta, M. M., Charles, A. O., and Stavros, C. M. (2007). Oxidative stress antagonizes Wnt signaling in osteoblast precursors by diverting beta-catenin from T cell factor- to forkhead box O-mediated transcription. *J. Biol. Chem.* 282, 27298–27305. doi: 10.1074/jbc.M702811200

Ponchon, L., Beauvais, G., Nonin-Lecomte, S., and Dardel, F. (2009). A generic protocol for the expression and purification of recombinant RNA in *Escherichia coli* using a tRNA scaffold. *Nat. Protoc.* 4, 947–959. doi: 10.1038/nprot.2009.67

Reinhold, M. I., and Naski, M. C. (2007). Direct interactions of Runx2 and canonical Wnt signaling induce FGF18. *J. Biol. Chem.* 282, 3653–3663. doi: 10.1074/jbc.M608995200

Rigoutsos, I., and Furnari, F. (2010). Gene-expression forum: decoy for microRNAs. *Nature* 465, 1016–1017. doi: 10.1038/4651016a

Shi, Z. L., Zhang, H., Fan, Z. Y., Ma, W., Song, Y. Z., Li, M., et al. (2020). Long noncoding RNA LINC00314 facilitates osteogenic differentiation of adipose-derived stem cells through the hsa-miR-129-5p/GRM5 axis via the Wnt signaling pathway. *Stem Cell Res Ther.* 11:240. doi: 10.1186/s13287-020-01754-z

Ushiku, C., Adams, D. J., Jiang, X., Wang L. P., and Rowe, D. W. (2010). Long bone fracture repair in mice harboring GFP reporters for cells within the osteoblastic lineage. *J. Orthop. Res.* 28, 1338–1347. doi: 10.1002/jor.21105

Wang, X. G., Guo, B. S., Li, Q., Peng, J., Yang, Z. J., Wang, A. Y., et al. (2013). miR-214 targets ATF4 to inhibit bone formation. *Nat. Med.* 19, 93–100. doi: 10.1038/nm.3026

Wang, Y. X., Wang, K., Hu, Z. B., Zhou, H., Zhang, L. J., Wang, H., et al. (2018). MicroRNA-139-3p regulates osteoblast differentiation and apoptosis by targeting ELK1 and interacting with long noncoding RNA ODSM. *Cell Death Dis.* 9:1107. doi: 10.1038/s41419-018-1153-1

Wang, Y. X., Wang, K., Zhang, L. J., Tan, Y. J., Hu, Z. B., Dang, L., et al. (2020). Targeted overexpression of the long noncoding RNA ODSM can regulate osteoblast function in vitro and in vivo. *Cell Death Dis.* 11:133. doi: 10.1038/s41419-020-2325-3

Yin, C., Tian, Y., Yu, Y., Wang, H. Y., Wu, Z. X., Huang, Z. Z., et al. (2019). A novel long noncoding RNA AK016739 inhibits osteoblast differentiation and bone formation. *J. Cell. Physiol.* 234, 11524–11536. doi: 10.1002/jcp.27815

Yin, C., Zhang, Y., Hu, L. F., Tian, Y., Chen, Z. H., Li, D. J., et al. (2018). Mechanical unloading reduces microtubule actin crosslinking factor 1 expression to inhibit β-catenin signaling and osteoblast proliferation. *J. Cell. Physiol.* 233, 5405–5419. doi: 10.1002/jcp.26374

Yuan, H. R., Xu, X. W., Feng, X., Zhu, E. D., Zhou, J., Wang, G. N., et al. (2019). A novel long noncoding RNA PGC1β-OT1 regulates adipocyte and osteoblast differentiation through antagonizing miR-148a-3p. *Cell Death. Differ.* 26, 2029–2045. doi: 10.1038/s41418-019-0296-7

Zeng, Z. L., Liu, Y. J., Zheng, W., Liu, L. B., Yin, H. L., Zhang, S. M., et al. (2019). MicroRNA-129-5p alleviates nerve injury and inflammatory response of Alzheimer's disease via downregulating SOX6. *Cell Cycle* 18, 3095–3110. doi: 10.1080/15384101.2019.1669388

Zhang, P., Li, J. F., Song, Y. Z., and Wang, X. (2017). MiR-129-5p inhibits proliferation and invasion of chondrosarcoma cells by regulating SOX4/Wnt/β-catenin signaling pathway. *Cell Physiol. Biochem.* 42, 242–253. doi: 10.1159/000477323

Zuo, B., Zhu, J., Li, J., Wang, C. D., Zhao, X. Y., Cai, G. Q., et al. (2015). microRNA-103a functions as a mechanosensitive microRNA to inhibit bone formation through targeting Runx2. *J. Bone Miner Res.* 30, 330–345. doi: 10.1002/jbmr.2352

Conflict of Interest: The authors declare that the research was conducted in the absence of any commercial or financial relationships that could be construed as a potential conflict of interest.

Copyright © 2020 Yin, Tian, Yu, Yang, Su, Zhao, Wang, Zhang, Pei, Li, Chen, Zhang, Miao and Qian. This is an open-access article distributed under the terms of the Creative Commons Attribution License (CC BY). The use, distribution or reproduction in other forums is permitted, provided the original author(s) and the copyright owner(s) are credited and that the original publication in this journal is cited, in accordance with accepted academic practice. No use, distribution or reproduction is permitted which does not comply with these terms.

frontiers in Cell and Developmental Biology

ORIGINAL RESEARCH
published: 16 November 2020
doi: 10.3389/fcell.2020.599826

A Novel Variant in *CLCN7* Regulates the Coupling of Angiogenesis and Osteogenesis

Hui Peng[1], *Hong-Bo He*[2] *and Ting Wen*[2]*

[1] Department of Endocrinology, Endocrinology Research Center, Xiangya Hospital of Central South University, Changsha, China, [2] Department of Orthopedic, Xiangya Hospital of Central South University, Changsha, China

Autosomal dominant osteopetrosis type II (ADO II), characterized by increased bone mass and density, is caused by mutations in the chloride channel 7 (*CLCN7*) gene. In this study, a novel missense variant in *CLCN7* (c.1678A > G; p.Met560Val) was identified in three symptomatic subjects and one carrier of a Chinese family with ADO II. Notably, bone formation markers, including osteocalcin and total procollagen type N-terminal propeptide, have increased or presented at the upper limit of the normal range in the three patients. Serum factors secreted by osteoclast lineage cells and affecting the $CD31^{hi}EMCN^{hi}$ vessel formation, such as tartrate-resistant acid phosphatase 5b, platelet-derived growth factor-BB, vascular endothelial growth factor, and SLIT3, had a higher expression in three ADO II subjects than in 15 healthy age-matched and sex-matched controls. Moreover, the conditioned medium was obtained from preosteoclast induced from the ADO II patients' peripheral blood mononuclear cells. It was found to promote the $CD31^{hi}EMCN^{hi}$ vessel formation of human microvascular endothelial cells and osteogenic differentiation of bone marrow-derived stem cells. Taken together, our finding revealed a novel *CLCN7* variant associated with ADO II and suggested that the sclerotic bone was potentially associated with the increase of the $CD31^{hi}EMCN^{hi}$ vessel formation and bone formation.

Keywords: autosomal dominant osteopetrosis type II, *CLCN7*, variant, $CD31^{hi}Emcn^{hi}$ vessel formation, bone formation

OPEN ACCESS

Edited by:
Chao Liang,
Hong Kong Baptist University, Hong Kong

Reviewed by:
Li Hui,
Shaanxi Provincial People's Hospital, China
Peng Cheng,
Nanjing Medical University, China

***Correspondence:**
Ting Wen
tingwen163@126.com

Specialty section:
This article was submitted to Molecular Medicine, a section of the journal Frontiers in Cell and Developmental Biology

Received: *28 August 2020*
Accepted: *20 October 2020*
Published: *16 November 2020*

Citation:
Peng H, He H-B and Wen T (2020) A Novel Variant in CLCN7 Regulates the Coupling of Angiogenesis and Osteogenesis. Front. Cell Dev. Biol. 8:599826. doi: 10.3389/fcell.2020.599826

INTRODUCTION

Autosomal dominant osteopetrosis type II (ADO II; OPTA2, Online Mendelian Inheritance in Man: 166600), also known as "Albers Schönberg disease," is the most common type of osteopetrosis with an estimated prevalence of 2.5/100,000 (Bénichou et al., 2000; Del Fattore et al., 2008). It is characterized by segmentary osteosclerosis, predominantly involving in the vertebral endplates ("rugger-jersey spine"), iliac wings ("bone within bone" sign), and the skull base. Previous studies revealed that ADO II was a phenotypically heterogeneous disease whose clinical spectrums ranged from unaffected radiography mutation carriers to affected skeletal patients yet asymptomatic to severe manifestations including fracture, osteomyelitis, visual loss, and bone marrow failure (Bénichou et al., 2000; Waguespack et al., 2007).

The bone homeostasis was maintained by balancing osteoclast-mediated resorption and osteoblast-mediated formation (Wang et al., 2018; Hayashi et al., 2019; Rodriguez-Laguna et al., 2019). The disrupted bone mass and structure of osteopetrosis resulted from the impaired

osteoclast-mediated bone resorption caused by genetic factors (Tolar et al., 2004; Sobacchi et al., 2013). Bénichou et al. (2001) previously considered that ADO II was genetically homogeneous with a single disease-causing gene on 16p13.3. Accumulated studies showed that roughly 70% of patients harbored heterozygous missense mutations of the *CLCN7* gene in a dominant-negative form (Cleiren et al., 2001). To date, more than 40 mutations in *CLCN7* has been identified in different osteopetrosis families (Leisle et al., 2011; Pang et al., 2016). *CLCN7* (Online Mendelian Inheritance in Man: 602727) is a multi-pass membrane protein that acts as a Cl-/H + exchanger by voltage gate (Leisle et al., 2011). It mainly resides in the late endosomes, lysosomes, and the ruffled membrane of osteoclasts. In osteoclasts, the ruffled border contains Cl-channels that are inserted by exocytotic fusion together with the H + -ATPase to ensure the acidification of extracellular resorption lacuna. Pathogenic mutations in *the CLCN7* gene impairing acidification of extracellular resorption lacuna were assumed to prevent degradation of the calcified and organic matrix of bone (Weinert et al., 2010). Furthermore, some studies suggested that chloride channels could be a drug target for osteopetrosis (Capulli et al., 2015). Mattia et al. demonstrated that *CLCN7* mutant-specific small interfering RNAs silenced dominant-negative *CLCN7* transcripts and subsequently ameliorated the bone phenotype in ADO II (Verkman and Galietta, 2009). Recent research also demonstrated that the specific small interfering RNA therapy normalized extra-skeletal manifestations on the ADO II mouse (Maurizi et al., 2019).

Some studies suggested that *CLCN7* mutations regulate bone formation in patients with osteopetrosis (Barvencik et al., 2014; Coudert et al., 2014). The vessels in the bone niche were reported to play great roles in bone formation (Abarrategi et al., 2018; Hao et al., 2019). A specific endothelium in the murine skeletal system, termed type H, strongly positive for CD31 and endomucin, is crucial in bone formation and regeneration (Kusumbe et al., 2014; Ramasamy et al., 2014; Langen et al., 2017). Accumulated evidence suggests that the type H vessels exert on bone formation in many aspects, ranging from mediating local growth of the vasculature, to providing a necessary microenvironment for perivascular osteoprogenitors, and coupling angiogenesis to osteogenesis (Yang et al., 2017). Previous findings revealed that platelet-derived growth factor-BB (PDGF-BB) secreted by preosteoclast could induce $CD31^{hi}Emcn^{hi}$ vessels subtype subsequently prevented bone loss in osteoporosis and bone-loss diseases (Xie et al., 2014). Furthermore, we recently found a mutation in *Reg1cp* involved in high bone mass syndrome through promoting angiogenesis (Yang et al., 2019). However, whether the bone accrual is associated with the coupling between angiogenesis and osteogenesis or not remains unclear.

Here, we ascertained a missense variant in *CLCN7* in a Chinese family. This is the first description genetically confirmed with this heterozygous missense mutation (c.1678A > G; p. Met560Val) responsible for ADO II. Additionally, these results indicated that the mutation might be associated with the dysfunction of the angiogenesis and osteogenesis, which further explained the elevated bone formation markers in this ADO II family.

MATERIALS AND METHODS

Family Collection

The Chinese family who suffered from ADO II was recruited from Xiangya Hospital Central South University. There were three affected individuals (II3, II7, and III2 in **Figure 1A**) in this family, and all of the affected subjects were not born of consanguineous parents. The patients underwent a series of clinical evaluation including laboratory and radiography examination in Xiangya Hospital, such as blood route, liver function test, renal function test, serum calcium (Ca), phosphate (P), alkaline phosphatase (ALP), β-Cross Laps of type I collagen containing cross-linked C-telopeptide, osteocalcin (OC), total procollagen type N-terminal propeptide (TPINP), and intact parathyroid hormone (PTH). Additionally, the patients were carried out with bone mineral density of the total body measured by a dual-energy X-ray absorptiometry densitometer and X-ray of bilateral hip joints and lumbar. The study was approved by the Ethics Committee of Xiangya Hospital Central South University. All subjects involved in this study signed informed consent documents before participating in the project.

Whole-Genome Sequence

Genomic DNA was collected and extracted from peripheral whole blood samples using Qiagen DNA kits. The genomic DNA met the sequencing requirements of the purity (optical density 260/280 > 1.8) and concentration (50 ng/ml) of each sample. Whole-genome sequencing was conducted by Annoroad Gene Technology by using Illumina/TruSeq Nano DNA HT Library Preparation Kit for capture and Illumina sequencing platforms for data generation (150-bp paired-end, 300 cycles). Sequencing was performed with 150-bp paired-end reads on the Illumina NovaSeq 6000 sequencing platform. The mean coverage was 40×.

Variant Filtering and Analysis

Sequence alignment was performed with the Burrows–Wheeler Aligner mem using human genome assembly hg19 as the reference, then produce called variants with RTG tools Hyplotype Caller. Annotation of gene context was carried out with annovar using Single Nucleotide Polymorphism Database, Refseq gene as the reference.

Sanger Sequence

The variant was amplified by using DNA polymerase [MIX (GREEN), TSINGKE, China], and the former and reverse primers are CTTGAGGAGTCCACACCCAC and CTGGGAGCAGGTGGATGG, respectively. Forward and reverse sequencing reactions were performed with the Big Dye Terminator Cycle Sequencing Ready Reaction Kit (PE Applied Biosystems), and the products were analyzed on an ABI 3730XL automated sequencer (PE Applied Biosystems).

Enzyme-Linked Immunosorbent Assay

Serum was obtained from peripheral blood using 4,000 rpm for 5 min. Then, we used the ELISA kits to test the expression of tartrate-resistant acid phosphatase 5b (TRAP-5b), PDGF-BB, vascular endothelial growth factor (VEGF; R&D Systems), and

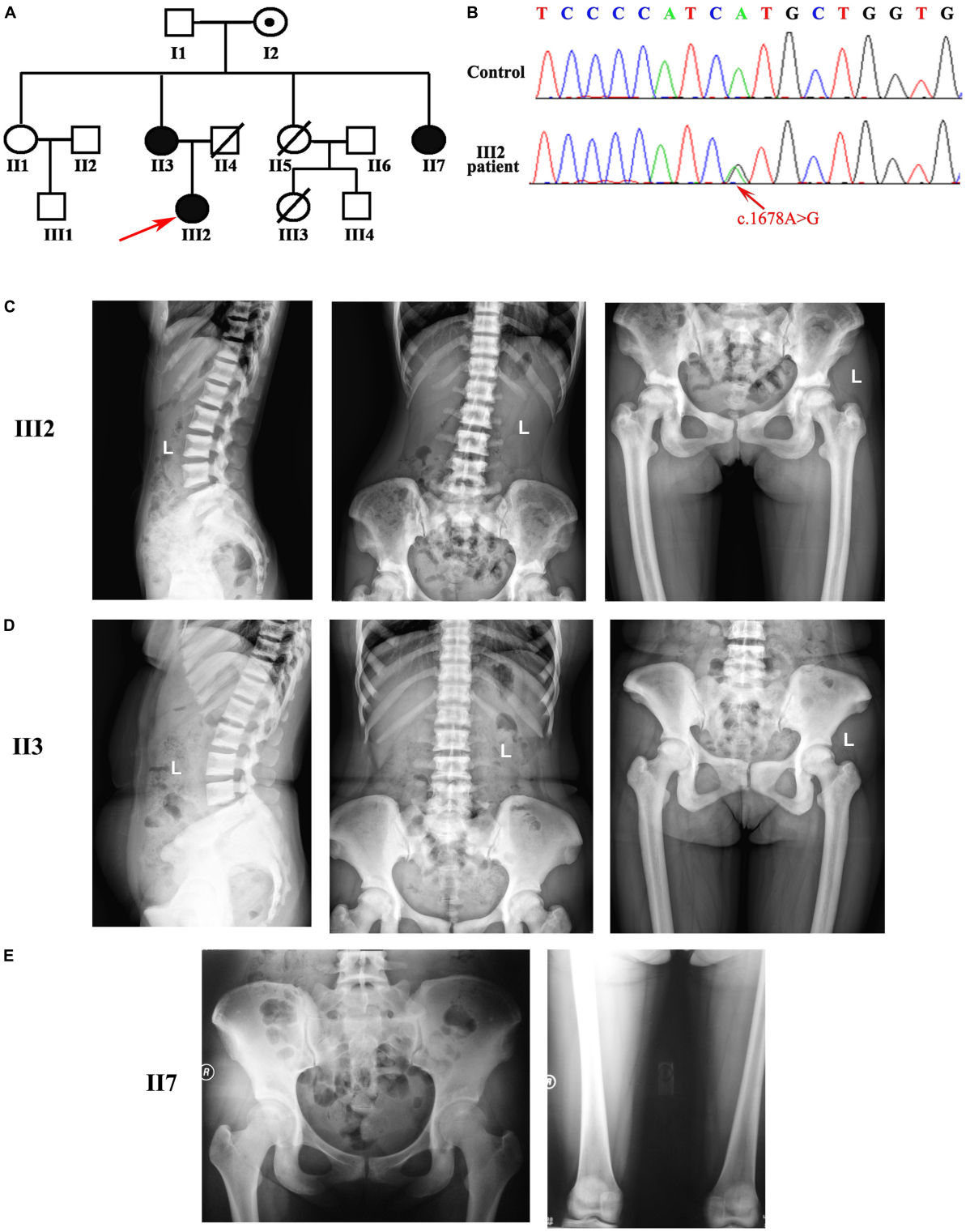


FIGURE 1 | Pedigree of the osteopetrosis family was associated with the mutation in *CLCN7*. **(A)** Pedigree of a Chinese family with osteopetrosis. Squares represent males, and circles represent females. Red arrow indicates the proband in this family. White symbols represent unaffected subjects, and black symbols indicate affected subjects. Symbols with an embedded black dot represent asymptomatic carriers. Symbols with a diagonal line represent deceased subjects. **(B)** Sanger sequence chromatograms from the proband and unaffected II1. c.1678A > G transition is indicated by the red arrow. **(C–E)** Radiographic image reveals osteosclerosis in three affected patients (radiographic images of III2 in the top row, images of II3 in the second row, and images of II7 in the bottom row). Images showed vertebral endplates ("rugger-jersey spine"; III2 and II3) and osteosclerosis of the pelvis and femoral (III2, II3, and II7).

SLIT3 (SED353Mi) in serum according to the manufacturers' instructions. The ELISA was replicated three times for the affected patients, and the mean values were used.

Cell Culture

A total of 15 ml of heparin anti-coagulated peripheral blood was obtained from every subject, including all members of this family and healthy age- and sex-matched controls. Then, peripheral blood mononuclear cells (PBMCs) were washed using phosphate-buffered saline twice and cultured in minimum essential medium Eagle-α containing 10% fetal bovine serum, 100 U ml^{-1} penicillin, 100 μg ml^{-1} streptomycin sulfate, and 50 ng ml^{-1} macrophage colony-stimulating factor (M-CSF; R&D Systems Inc.). Non-adherent cells were incubated with M-CSF (50 ng ml^{-1}) to obtain pure monocytes and macrophages. Then, PBMCs were cultured in 24-well plates at 1×10^5 cells per well with 50 ng ml^{-1} of M-CSF and 100 ng ml^{-1} receptor activator of nuclear factor-kappa-B ligand. Cells became preosteoclasts after a 3-day culture. We collected serum-containing conditioned medium from the preosteoclasts. After centrifugation (2,500 rpm for 10 min at 4°C), we aliquoted conditioned media and stored them at −80°C. Human BMSCs (HUXMA-0100; Cyagen Biosciences) were cultured in a human mesenchymal stem cell growth medium (HUXMA-90011; Cyagen Biosciences). To induce osteogenic differentiation of BMSCs, BMSCs were cultured in 48-well using the serum-containing conditioned medium. Then, we collected protein to test ALP activity on day 2, RNA on the 3rd day, and performed the ALP staining on day 7. Human microvascular endothelial cells (HMECs) were cultured with MCDB131 medium (Gibco) supplemented 10% fetal bovine serum, 100 U ml^{-1} penicillin, and 100 μg ml^{-1} streptomycin.

Real-Time Quantitative Polymerase Chain Reaction

Quantitative PCR analysis was performed as described previously (Xiao et al., 2020). Briefly, we extracted RNA from cells using Trizol reagent (Takara). Then, 1,000-ng RNA was reverse-transcribed into first-strand complementary DNA using the Reverse Transcription Kit (Takara). Quantitative PCR was performed using SYBR Green PCR Master Mix (Takara), and messenger RNA expression was normalized to reference genes *GAPDH*.

Tube Formation Assay

The Matrigel (BD Biosciences) was plated in 48-well plates and then incubated at 37°C for 45 min. HMECs were seeded in 48-well plates at 5×10^4 cells per well on polymerized Matrigel. The cells were cultured in the preosteoclast-conditioned medium collected from patients or control individuals for 4 h incubation at 37°C. Then, the tube formation was observed through microscopy, and the number of tube branches was quantified in four random microscope visual fields of each well.

Alkaline Phosphatase Activity

On the second day of osteogenic differentiation, the cell lysates were homogenized for ALP activity assay by spectrophotometric measurement of *p*-nitrophenol release using an ALP Assay Kit (P0321S, Beyotime) according to the manufacturer's instructions.

Alkaline Phosphatase Staining

The cells were washed using phosphate-buffered saline for three times, followed by 10% paraformaldehyde for 5 min. Then, cells were incubated in ALP incubation buffer (0.2-*g* barbital sodium, 0.4-*g* magnesium sulfate, 0.2-*g* calcium chloride, and 0.3-*g* beta-glycerophosphate) at 37°C for 2 h. Next, cells were washed with 2% calcium chloride and incubated with 2% cobaltous nitrate for 5 min. Finally, cells were incubated in 1:80 ammonium sulfate for 10 s. The ALP staining was observed through a microscope.

Statistical Analysis

Data were imported into Excel and scaled and normalized to appropriate controls. Unpaired, two-tailed Student's *t*-tests were performed for the comparisons of two groups. Critical *P*-values were Bonferroni corrected and expressed as follows: $^*P < 0.05$. $^{**}P < 0.01$.

RESULTS

Clinical Characteristics of Patients

A Chinese patient, aged 22 years, was admitted to the Department of Endocrinology with a history of bone pain for 6 years. There was a family history of a similar disease of her mother (II3) and aunt (II7) shown in **Figure 1A**. All these three patients had a mild phenotype of osteopetrosis only with bone pain on hip joints and back. The proband also had a history of fracture in the hip. On examination, we did not find poor nutritional status, short stature, malformed craniofacial appearance, hepatosplenomegaly, and intellectual disability in the proband and other affected patients in this family.

Laboratory findings of the three patients showed that the hematopoietic function, liver function, kidney function, total serum calcium, and total serum phosphorus were within the normal ranges except for a slight increase of aspartate transaminase of II3 (**Table 1**). For bone turnover markers, β cross-linked C-telopeptide of type 1 collagen and ALP have not detected any abnormalities in this family (**Table 2**). However, markers of bone formation in the proband, such as OC and TPINP, were both found at the upper limit of the normal range (**Table 2**). Moreover, the levels of OC, TPINP, and PTH (parathormone) were found to be elevated in her mother (II3). The level of OC in her aunt (II7) also slightly increased. Thus, we hypothesized that bone formation in these patients had been elevated (**Table 2**).

The total bone mineral density values of the three patients at lumbar and hip sites, measured by dual-energy X-ray absorptiometry, are shown in **Table 3**. The three affected patients were all with regular menstruation. The *Z* values at different sites of the three patients were significantly higher than the those of the sex-matched and age-matched

TABLE 1 | Hematopoietic, hepatorenal, and serum electrolytic data of ADO II subjects.

Parameters	III2	II3	II7	Normal range
WBC ($10^9 \cdot L^{-1}$)	4.2	5.3	5.46	3.5–9.5
Hb ($g \cdot L^{-1}$)	124	126	126	115–150
RBC ($10^{12} \cdot L^{-1}$)	4.52	4.34	4.19	3.80–5.10
PLT ($10^9 \cdot L^{-1}$)	295	240	146	125–350
ALT (μ/L)	9.3	21.6	20.4	7.0–40.0
AST (μ/L)	32.4	46.5	22.5	13.0–35.0
BUN (mmol/L)	4.58	5.56	6.95	2.60–7.50
Cre (μmol/L)	55	69	53	41.0–111.0
UA (μmol/L)	287.5	289.5	246	155.0–357.0
Na (mmol/L)	140	142.8	142	137.0–147.0
K (mmol/L)	4.54	4.22	3.6	3.50–5.30
Cl (mmol/L)	103.4	107.8	105.6	99.0–110.0
Ca (mmol/L)	2.45	2.28	2.22	2.00–2.60
Mg (mmol/L)	0.91	0.84	0.98	0.66–1.07
P (mmol/L)	1.41	1.45	1.25	0.86–1.78

WBC, white blood cells; RBC, red blood cells; Hb, hemoglobin; PLT, platelet; ALT, alanine transaminase; AST, aspartate transaminase; BUN, blood urea nitrogen; Cre, creatinine; and UA, uric acid.

TABLE 2 | Bone biomarker of ADO II subjects.

	III2	II3	II7	Normal range
ALP (μ/L)	55.3	64.5	46.8	45.0–125.0
OC (ng/ml)	20.44	26.79	45	4.11–21.87
TPINP (ng/ml)	58.37	131.4	NA	8.53–64.32
PTH (pg/ml)	44.8	83.8	59.85	15.0–68.3
β-CTX (pg/ml)	290.5	243.5	572	68–680

ALP, alkaline phosphatase; OC, osteocalcin; TPINP, total procollagen type N-terminal propeptide; PTH, parathormone; β-CTX, β cross-linked C-telopeptide of type 1 collagen; and NA, not available.

TABLE 3 | Bone mass density of the ADO II subjects.

Subjects	Age	Total		Lumbar		Left hip	
		Total BMD (g/cm^2)	*Z* value	Total BMD (g/cm^2)	*Z* value	Total BMD (g/cm^2)	*Z* value
III2	21	1.611	5.8	2.221	12.1	1.591	6.9
II 3	42	2.063	8.0	2.304	12.7	1.918	9.6
II7	29	1.973	7.6	2.245	11.2	1.855	8.3

BMD, Bone mineral density.

controls (**Table 3**). Radiological features of the three patients revealed diffused osteosclerosis, predominantly at the vertebral endplates ("rugger-jersey spine"). The superior ramus of the pubis, sacral vertebrae, femoral head, and greater trochanter of femur also presented diffuse osteosclerosis. The boundaries among cancellous bone, cortical bone, and bone medullary disappeared (**Figures 1C–E**). Based on their clinical and radiological assessment, the family was diagnosed with ADO II.

Genetic Analysis With Whole-Genome Sequencing and Identification of the Pathogenic Variant

We performed the whole-genome sequence in the three affected patients. Firstly, we filtered the common variants, which were unlikely to cause the rare heritable disorder (allele frequency greater than 0.1% in the 1000 Genomes database and Exome Variant Server). Then, we excluded the variants with low confidence and the putative impact. Next, we tried to find the shared variant in the three patients. Interestingly, a heterozygous missense variant (c.1678A > G, p.Met560Val) in *CLCN7* segregated with osteopetrosis among three affected patients. We then performed the Sanger sequence in all members of this family and found the variant occurred in three patients and a non-penetrant carrier (I2 in **Figure 1A** was asymptomatic and did not present abnormal bone phenotype as well as laboratory findings; **Figure 1B**).

Various mutations in *CLCN7* have been reported to be involved in the pathogenesis of osteopetrosis (**Figure 2**). In gnomAD database, the PopMax Allele Frequency and allele count of this variant were 0.00000900058 and 1, respectively, (the total Allele number was 245442). Moreover, this variant was not found in East Asian with 17228 Allele number in total. Pro560 in *CLCN7*, which is substituted to a Valine in three patients, is phylogenetically highly conserved among both vertebrates and invertebrates (**Figure 3**) [Phylop] score of 6.111 and [PhastCons] score of 1. *CLCN7* gene was also predicted to be intolerant whose Residual Variation Intolerance Score is 7.0381% (**Table 4**). Furthermore, the effect of missense mutation Met560Val in *CLCN7* was predicted by different variant effect prediction software (PolyPhen-2, MutationTaster, CADD, MPC). It suggested that the Met560Val substitution is likely to be deleterious (PolyPhen score of 0.991, probably damaging; MutationTaster score of 0.999, disease-causing; CADD score of 24.3, damaging; MPC score of 1.0788, possibly damaging; **Table 4**). Based on the genetic analysis, this study revealed that the heterozygous missense mutation was possibly responsible for the ADO II.

CLCN7 Mutation Induces the Type H Vessel Formation and Osteogenic Differentiation *in vitro*

The cross-talks between osteoclasts and other cells, including osteoblasts, endothelium cells, have been well established (Phan et al., 2004; Ramasamy et al., 2014; Xie et al., 2014; Yang et al., 2017, 2019; Chen et al., 2018; Li et al., 2019). Additionally, PDGF-BB secreted by preosteoclasts could result in elevated bone mass through inducing angiogenesis during coupling with osteogenesis (Xie et al., 2014). To investigate if the osteosclerotic bone of these patients was associated with the coupling between angiogenesis and osteogenesis, we collected the serum from ADO II individuals and 15 normal controls for further studies. TRAP-5b is well-established to be secreted by osteoclasts, and PDGF-BB, VEGF, and SLIT3 can also be secreted by osteoclasts/preosteoclasts, which were reported to be

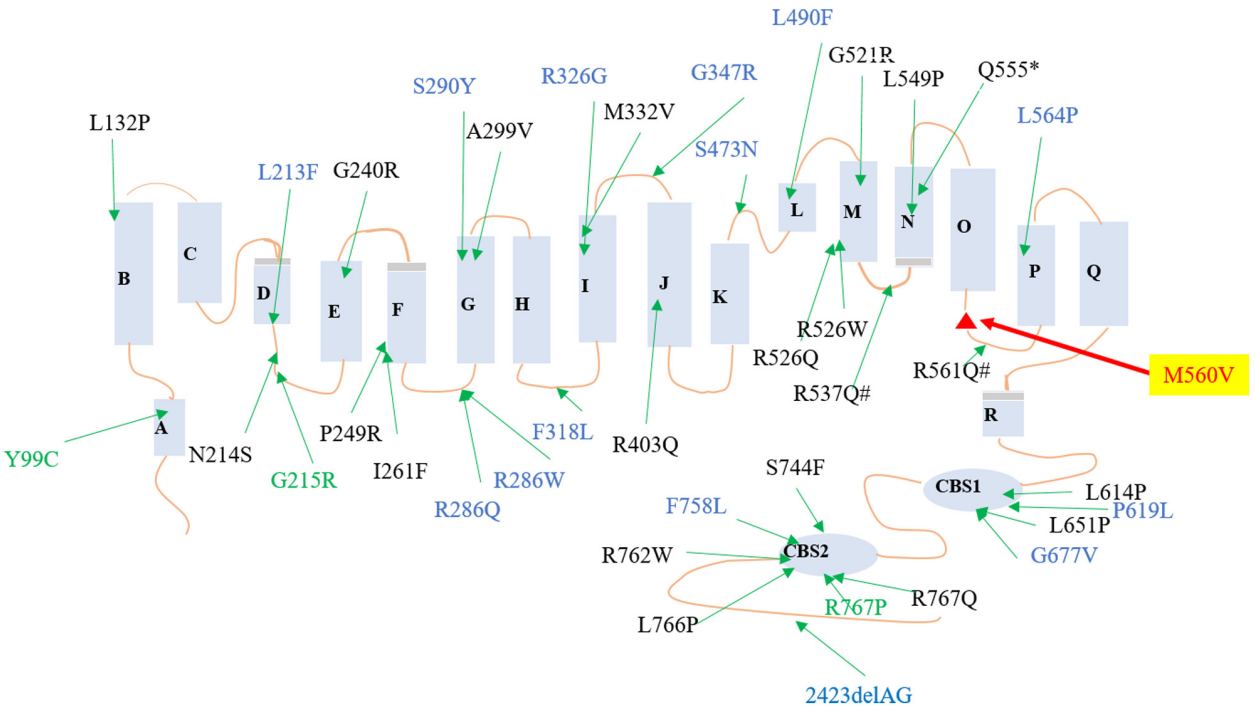


FIGURE 2 | Reported mutations of *CLCN7* in osteopetrosis family. Red mutation was found in this family. Black mutations were reported to cause osteopetrosis autosomal recessive 4, blue mutations were reported to cause ADO II, and green mutations were reported to cause different types of osteopetrosis.

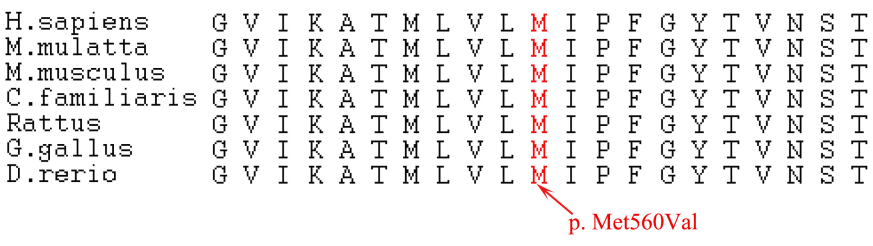


FIGURE 3 | Conservation of the mutated amino acids. Alignment of the *CLCN7* proteins, showing the conservation of the mutated residues among different species. p. Met560Val transition is indicated by the red arrow.

TABLE 4 | Summary of the *CLCN7* mutation in this family with ADO II.

Variant (Missense)	Numbers		Rarity in gnomAD		Conservation (Extremely conserved)		Pathogenic prediction (Damaging)			
	Patients	Carrier	PopMax AF	Allele count	Phylop score	PhastCon score	MutationT-aster score	MPC	CADD score Phred	RVIS%
c.1678A > G p.Met560Val	3	1	9.00058E-06	1	6.111	1	0.999	1.0788	24.3	7.04%

PopMax AF, Maximum allele frequency in any one population; MPC, mutant prevention concentration; CADD, Combined Annotation Dependent Depletion; and RVIS, Residual Variation Intolerance Score.

involved in the type H formation (Bollerslev et al., 2013; Sivaraj and Adams, 2016; Kim et al., 2018; Peng et al., 2020). Thus, we selected them to see if they have been altered in ADO II patients. Surprisingly, the level of TRAP-5b, PDGF-BB, VEGF, and SLIT3 showed a remarkable increase in ADO II patients compared with the 15 control groups with matched age and sex (**Figures 4A–D**). To further confirm the possible effect of type H vessels in this kindred, we purified the PBMCs from the patients and control normal subjects. Then, the collected preosteoclast condition medium from osteoclastic-induced PBMCs has been

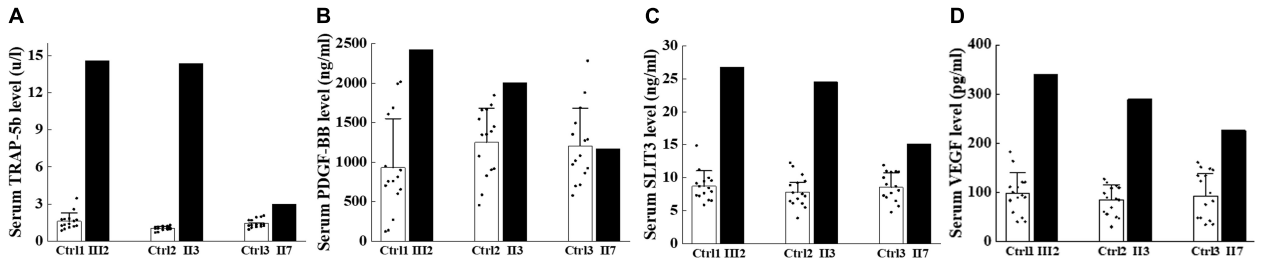


FIGURE 4 | Expression of factors secreted by osteoclast lineage cells elevated in the affected patients. Serum analysis of ADO II subjects and age-matched and sex-matched. **(A)** Expression of serum TRAP-5b. **(B)** Expression of serum PDGF-BB. **(C)** Expression of serum SLIT3. **(D)** Expression of serum VEGF. Number of controls = 15. Data are shown as mean ± SD.

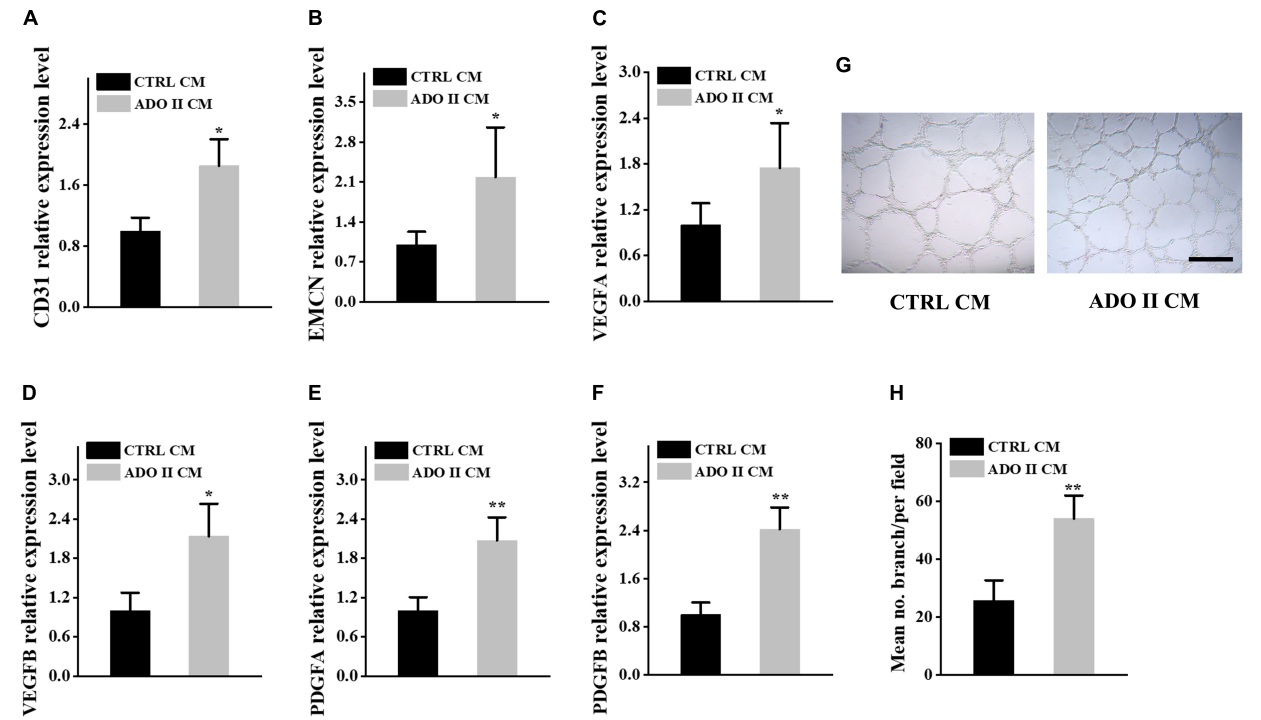


FIGURE 5 | Preosteoclast-conditioned medium from ADO II patients promotes vessel formation *in vitro*. HMECs were treated with a preosteoclast-conditioned medium from ADO II patients or control groups. **(A,B)** qRT–PCR analysis of the relative levels of *CD31* **(A)**, *EMCN* **(B)**, *VEGFA* **(C)**, *VEGFB* **(D)**, *PDGFA* **(E)**, and *PDGFB* **(F)** in HMECs. **(G)** Representative images of tube formation. **(H)** Quantification of tube branch numbers per field. CTRL CM, control conditioned medium; ADO II CM, ADO II conditioned medium. These experiments were replicated three times. Data are shown as mean ± SD. **P* < 0.05 and ***P* < 0.01.

used to culture the HMECs. As expected, the expression of *CD31*, *EMCN*, and vessel growth factors, including *VEGFA*, *VEGFB*, *PDGFA*, and *PDGFB,* has increased in the cells treated with preosteoclast-conditioned medium from ADO II cells compared with the cells from control individuals (**Figures 5A–F**). Moreover, the tube formation also has been promoted by the ADO II-conditioned medium (**Figures 5G,H**). Even the expression of *RUNX2* was not altered by the conditioned medium from patients; other osteogenic markers in hBMSCs, such as *ALPL* and *SP7,* elevated (**Figures 6A–C**). Consistent with these results, both ALP activity and ALP staining showed a significant difference between the two groups (**Figures 6D,E**). Together, these data suggested that the *CLCN7* mutation might cause the bone accrual partially because of the elevated coupling of bone formation with type H formation.

DISCUSSION

Osteopetrosis is a rare genetic condition of increased bone mass and density generally due to a defect of bone resorption. The common complications are confined to the skeleton, including bone fracture, bone pain, osteomyelitis, and rare bone marrow failure (Bénichou et al., 2000). Bone pain on the back was described in three affected patients and fracture on the hip of the proband. Their prominent radiographic signatures of vertebral

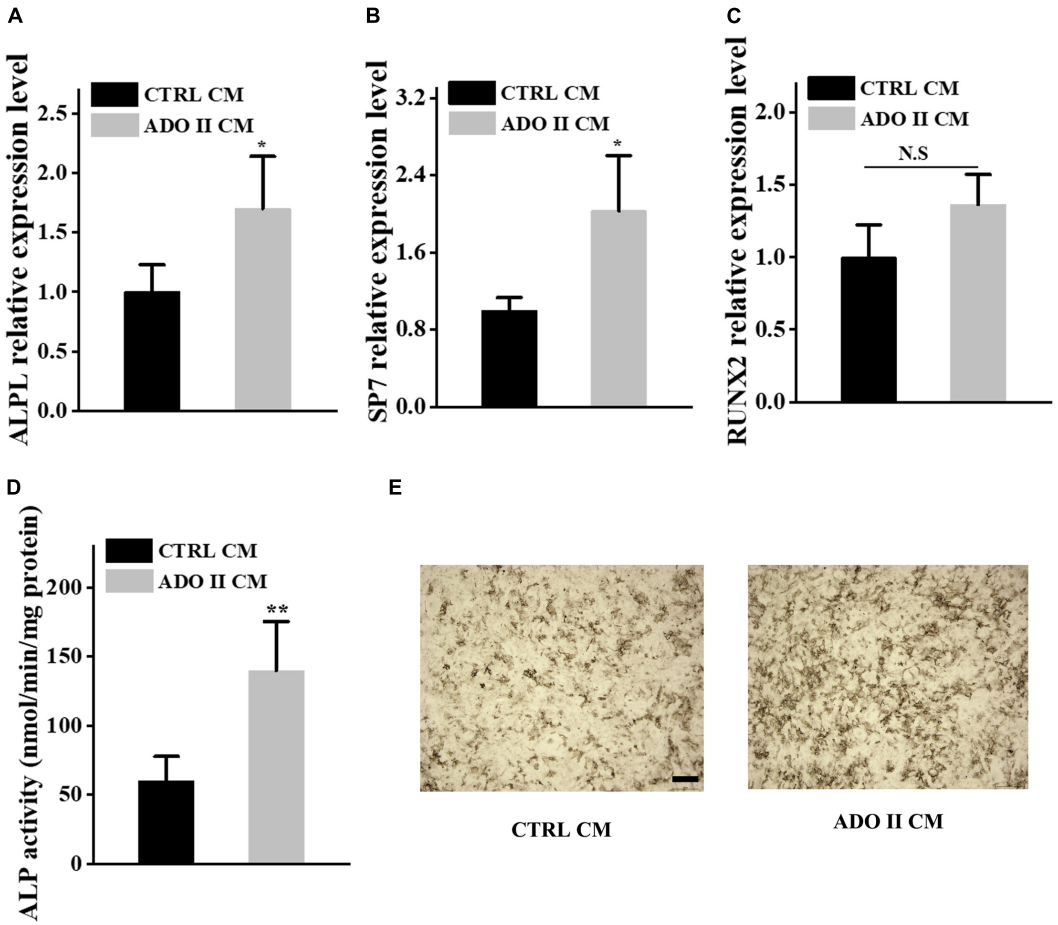


FIGURE 6 | Preosteoclast-conditioned medium from ADO II patients enhances osteoblastic differentiation *in vitro*. BMSCs were treated with a preosteoclast-conditioned medium from ADO II patients or control groups. **(A–C)** qRT–PCR analysis of the relative levels of *ALPL* **(A)**, *SP7* **(B)**, and *RUNX2* **(C)** in BMSCs. **(D)** ALP activity in BMSCs. **(E)** Representative images of ALP staining in BMSCs. Scale bar = 300 μm. These experiments were replicated three times. Data are shown as mean ± SD. $^{*}P < 0.05$ and $^{**}P < 0.01$.

endplates ("rugger-jersey spine") and diffused bone sclerosis were found in three affected patients.

The mutation analysis in this family was in agreement with the clinical diagnosis of ADO-II. Previous studies that reported several mutations in *CLCN7* could result in severe recessive, dominant, and intermediate osteopetrosis (Frattini et al., 2003). Currently, genetic and molecular diagnoses were available for patients with ADO II, especially to the missense mutations in the *CLCN7* gene (Bollerslev et al., 2013). Above 70% of patients harbored heterozygous dominant-negative mutations of the *CLCN7* gene (Cleiren et al., 2001). These *CLCN7*-related mutations are usually located in different structures of its protein, such as intramembrane α helices, extracellular loops, Cl-binding sites, and CBS domains (Pang et al., 2016; Jentsch and Pusch, 2018). We identified a heterozygous variant p.Met560Val located in the loop between helix N and helix O in three patients and an unaffected carrier. There was only one allele of the identified mutation in gnomAD and was not presented in East Asian populations. Additionally, Steven et al. have estimated the penetrance of ADO II to be approximately 66% (62 clinically affected individuals/94 subjects with the gene mutation), which means among the individuals with *CLCN7* mutations, one third were asymptomatic gene carriers without osteopetrosis-related signs in clinical, biochemical, and radiological results (Waguespack et al., 2003). Thus, the carrier did not present the related osteosclerotic bone associated with the incomplete penetrance. The phenotypical and genetic heterogeneity and incomplete penetrance remain unclear in skeletal dysplasia (Alam et al., 2017; Chen et al., 2020). It is likely to be related to the environmental factors, methylated gene modification, the complex interaction between other genes and *CLCN7*, and even some unidentified loci (Zhang et al., 2009; Leisle et al., 2011; Boudin et al., 2016), which need more further studies to elucidate.

The previous investigation indicated that ADO was one of the osteoclast-rich forms of osteopetrosis (Bollerslev et al., 2013). The bone biopsies from patients with ADO showed increased size and number of osteoclasts (Bollerslev et al., 1993). Chen et al. revealed that c.1856C > T mutation in *CLCN7* identified in an ADO II case resulted in enhanced but hypofunctional osteoclastogenesis (Chen et al., 2016). Besides, previous studies

showed that the serum TRAP-5b was significantly elevated in osteoclast-rich ADO II mice and patients (Chen et al., 2016; Alam et al., 2017). Consistent with these studies, the elevated serum TRAP-5b was also found in these patients with ADO II (Alatalo et al., 2004). The prominently elevated biochemical measurements of TRAP-5b suggested that the variant affected the function of osteoclast and indicated the molecular feature to be osteoclast-rich osteopetrosis in this family.

Osteopetrosis is a clinically heterogenetic disorder. In this Chinese family with the *CLCN7* variant, the serum bone formation markers (OC, TPINP, and PTH) were at the upper limit range in the proband. They also elevated in the proband's mother (II3), and the level of OC increased remarkably in the aunt (II7). The variable level of bone formation markers in the three affected patients might be associated with the characterization of clinical heterogeneity or some factors, such as age, lifestyle, and other environmental stimulus (Lundberg et al., 2018; Chevalier et al., 2020). Taken together, the upregulated or upper limit range of serum bone formation markers implied that the bone formation increased. It is extensively reported that the coupling of angiogenesis with osteogenesis plays a great role in bone modeling and remodeling (Phan et al., 2004; Ramasamy et al., 2014; Xie et al., 2014; Yang et al., 2017, 2019; Chen et al., 2018; Li et al., 2018). Previous findings revealed that PDGF-BB secreted by preosteoclasts could stimulate angiogenesis during coupling with osteogenesis (Xie et al., 2014). Furthermore, we demonstrated that *Reg1cp* mutation potentially caused high bone mass syndrome by regulating the coupling of angiogenesis with osteogenesis (Yang et al., 2019). Other studies revealed that the secret factors, including VEGF and SLIT3 by osteoclast lineage cells, could regulate type H formation during bone regeneration (Xu et al., 2018; Peng et al., 2020). Based on these findings, we investigated if this *CLCN7* mutation contributed to the increased bone mass by regulating the process of angiogenesis and osteogenesis. Intriguingly, we found that the levels of PDGF-BB, VEGF, and SLIT3 were increased in ADO II individuals. Of note, the conditioned medium from PBMCs of ADO II patients promoted vessel formation of HMECs as well as osteogenic differentiation of hBMSCs. These results gave some new insights into the pathogenesis in this family.

In this study, we identified a novel missense variant (p.Met560Val) in *CLCN7* through whole-genome sequencing and detected it in all affected family members by Sanger sequence. The rarity, conservation, and pathogenic predication all supported that this *CLCN7* mutation might be a disease-causing one. Furthermore, the *in vitro* experiments showed that the variant promoted the vessel formation and osteogenic differentiation in this family. To conclude, we presented a novel heterozygous mutation (p.Met560Val) in *CLCN7* segregated with ADO II in this Chinese family and revealed that it might be associated with the increased type H vessel formation and bone formation.

DATA AVAILABILITY STATEMENT

The whole-genome sequencing data were deposited on the Genbank (Sequence Read Archive) database with the accession no. PRJNA669897.

ETHICS STATEMENT

The studies involving human participants were reviewed and approved by Ethics Committee of the Xiangya Hospital of Central South University. The patients/participants provided their written informed consent to participate in this study. Written informed consent was obtained from the individual(s) for the publication of any potentially identifiable images or data included in this article.

AUTHOR CONTRIBUTIONS

HP designed the experiments, performed whole-genome sequencing analysis, carried out most of the experiments, and drafted the manuscript. TW and H-BH recruited the patients. TW supervised the experiments, analyzed results, and proofread the manuscript. All authors were involved in the final approval of the submitted version.

ACKNOWLEDGMENTS

The authors would like to thank the family for their participation in this study. The authors gratefully acknowledge Prof. Stephen P. Robertson at the University of Otago, providing the platform and the method of genetic analysis.

REFERENCES

Abarrategi, A., Mian, S. A., Passaro, D., Rouault-Pierre, K., Grey, W., and Bonnet, D. (2018). Modeling the human bone marrow niche in mice: from host bone marrow engraftment to bioengineering approaches. *J. Exp. Med.* 215, 729–743. doi: 10.1084/jem.20172139

Alam, I., McQueen, A. K., Acton, D., Reilly, A. M., Gerard-O'Riley, R. L., Oakes, D. K., et al. (2017). Phenotypic severity of autosomal dominant osteopetrosis type II (ADO2) mice on different genetic backgrounds recapitulates the features of human disease. *Bone* 94, 34–41. doi: 10.1016/j.bone.2016.10.016

Alatalo, S. L., Ivaska, K. K., Waguespack, S. G., Econs, M. J., Väänänen, K., and Halleen, J. M. (2004). Osteoclast-derived serum tartrate-resistant acid phosphatase 5b in Albers-Schonberg disease (type II autosomal dominant osteopetrosis). *Clin. Chem.* 50, 883–890. doi: 10.1373/clinchem.2003.029355

Barvencik, F., Kurth, I., Koehne, T., Stauber, T., Zustin, J., Tsiakas, K., et al. (2014). CLCN7 and TCIRG1 mutations differentially affect bone matrix mineralization in osteopetrotic individuals. *J. Bone Miner. Res.* 29, 982–991. doi: 10.1002/jbmr.2100

Bénichou, O., Cleiren, E., Gram, J., Bollerslev, J., de Vernejoul, M.-C., and Van Hul, W. (2001). Mapping of autosomal dominant osteopetrosis type II (Albers-Schönberg disease) to chromosome 16p13.3. *Am. J. Hum. Genet.* 69, 647–654. doi: 10.1086/323132

Bénichou, O. D., Laredo, J. D., and de Vernejoul, M. C. (2000). Type II autosomal dominant osteopetrosis (Albers-Schönberg disease): clinical and radiological

manifestations in 42 patients. *Bone* 26, 87–93. doi: 10.1016/S8756-3282(99)00244-6

Bollerslev, J., Henriksen, K., Frost Nielsen, M., Brixen, K., and Van Hul, W. (2013). Autosomal dominant osteopetrosis revisited: lessons from recent studies. *Eur. J. Endocrinol.* 169, R39–R57. doi: 10.1530/EJE-13-0136

Bollerslev, J., Marks, S. C. Jr., Pockwinse, S., Kassem, M., and Brixen, K. (1993). Ultrastructural investigations of bone resorptive cells in two types of autosomal dominant osteopetrosis. *Bone* 14, 865–869. doi: 10.1016/8756-3282(93)90316-3

Boudin, E., Fijalkowski, I., Hendrickx, G., and Van Hul, W. (2016). Genetic control of bone mass. *Mol. Cell. Endocrinol.* 432, 3–13. doi: 10.1016/j.mce.2015.12.021

Capulli, M., Maurizi, A., Ventura, L., Rucci, N., and Teti, A. (2015). Effective small interfering RNA therapy to treat CLCN7-dependent autosomal dominant osteopetrosis type 2. *Mol. Ther. Nucleic Acids* 4:e248. doi: 10.1038/mtna.2015.21

Chen, X., Wang, Z., Duan, N., Zhu, G., Schwarz, E. M., and Xie, C. (2018). Osteoblast–osteoclast interactions. *Connect. Tissue Res.* 59, 99–107. doi: 10.1080/03008207.2017.1290085

Chen, X., Zhang, K., Hock, J., Wang, C., and Yu, X. (2016). Enhanced but hypofunctional osteoclastogenesis in an autosomal dominant osteopetrosis type II case carrying a c.1856C>T mutation in CLCN7. *Bone Res.* 4:16035. doi: 10.1038/boneres.2016.35

Chen, Y.-H., Grigelioniene, G., Newton, P. T., Gullander, J., Elfving, M., Hammarsjö, A., et al. (2020). Absence of GP130 cytokine receptor signaling causes extended Stüve-Wiedemann syndrome. *J. Exp. Med.* 217:e20191306. doi: 10.1084/jem.20191306

Chevalier, C., Kieser, S., Çolakoğlu, M., Hadadi, N., Brun, J., Rigo, D., et al. (2020). Warmth prevents bone loss through the gut microbiota. *Cell Metab.* 32, 575.e7–590.e7. doi: 10.1016/j.cmet.2020.08.012

Cleiren, E., Bénichou, O., Van Hul, E., Gram, J., Bollerslev, J., Singer, F. R., et al. (2001). Albers-Schonberg disease (autosomal dominant osteopetrosis, type II) results from mutations in the ClCN7 chloride channel gene. *Hum. Mol. Genet.* 10, 2861–2867. doi: 10.1093/hmg/10.25.2861

Coudert, A. E., Del Fattore, A., Baulard, C., Olaso, R., Schiltz, C., Collet, C., et al. (2014). Differentially expressed genes in autosomal dominant osteopetrosis type II osteoclasts reveal known and novel pathways for osteoclast biology. *Lab. Investig.* 94, 275–285. doi: 10.1038/labinvest.2013.140

Del Fattore, A., Cappariello, A., and Teti, A. (2008). Genetics, pathogenesis and complications of osteopetrosis. *Bone* 42, 19–29. doi: 10.1016/j.bone.2007.08.029

Frattini, A., Pangrazio, A., Susani, L., Sobacchi, C., Mirolo, M., Abinun, M., et al. (2003). Chloride channel ClCN7 mutations are responsible for severe recessive, dominant, and intermediate osteopetrosis. *J. Bone Miner. Res.* 18, 1740–1747. doi: 10.1359/jbmr.2003.18.10.1740

Hao, X., Gu, H., Chen, C., Huang, D., Zhao, Y., Xie, L., et al. (2019). Metabolic imaging reveals a unique preference of symmetric cell division and homing of leukemia-initiating cells in an endosteal niche. *Cell Metab.* 29, 950.e6–965.e6. doi: 10.1016/j.cmet.2018.11.013

Hayashi, M., Nakashima, T., Yoshimura, N., Okamoto, K., Tanaka, S., and Takayanagi, H. (2019). Autoregulation of osteocyte sema3a orchestrates estrogen action and counteracts bone aging. *Cell Metab.* 29, 627.e5–637.e5. doi: 10.1016/j.cmet.2018.12.021

Jentsch, T. J., and Pusch, M. (2018). CLC chloride channels and transporters: structure, function, physiology, and disease. *Physiol. Rev.* 98, 1493–1590. doi: 10.1152/physrev.00047.2017

Kim, B. J., Lee, Y. S., Lee, S. Y., Baek, W. Y., Choi, Y. J., Moon, S. A., et al. (2018). Osteoclast-secreted SLIT3 coordinates bone resorption and formation. *J. Clin. Invest.* 128, 1429–1441. doi: 10.1172/JCI91086

Kusumbe, A. P., Ramasamy, S. K., and Adams, R. H. (2014). Coupling of angiogenesis and osteogenesis by a specific vessel subtype in bone. *Nature* 507, 323–328. doi: 10.1038/nature13145

Langen, U. H., Pitulescu, M. E., Kim, J. M., Enriquez-Gasca, R., Sivaraj, K. K., Kusumbe, A. P., et al. (2017). Cell-matrix signals specify bone endothelial cells during developmental osteogenesis. *Nat. Cell Biol.* 19, 189–201. doi: 10.1038/ncb3476

Leisle, L., Ludwig, C. F., Wagner, F. A., Jentsch, T. J., and Stauber, T. (2011). ClC-7 is a slowly voltage-gated 2Cl−/1H+-exchanger and requires Ostm1 for transport activity. *EMBO J.* 30, 2140–2152. doi: 10.1038/emboj.2011.137

Li, C., Xiao, Y., Yang, M., Su, T., Sun, X., Guo, Q., et al. (2018). Long noncoding RNA Bmncr regulates mesenchymal stem cell fate during skeletal aging. *J. Clin. Invest.* 128, 5251–5266. doi: 10.1172/JCI99044

Li, X., Sun, X., and Carmeliet, P. (2019). Hallmarks of endothelial cell metabolism in health and disease. *Cell Metab.* 30, 414–433. doi: 10.1016/j.cmet.2019.08.011

Lundberg, J. O., Carlström, M., and Weitzberg, E. (2018). Metabolic effects of dietary nitrate in health and disease. *Cell Metab.* 28, 9–22. doi: 10.1016/j.cmet.2018.06.007

Maurizi, A., Capulli, M., Curle, A., Patel, R., Ucci, A., Côrtes, J. A., et al. (2019). Extra-skeletal manifestations in mice affected by Clcn7-dependent autosomal dominant osteopetrosis type 2 clinical and therapeutic implications. *Bone Res.* 7:17. doi: 10.1038/s41413-019-0055-x

Pang, Q., Chi, Y., Zhao, Z., Xing, X., Li, M., Wang, O., et al. (2016). Novel mutations of CLCN7 cause autosomal dominant osteopetrosis type II (ADO-II) and intermediate autosomal recessive osteopetrosis (IARO) in Chinese patients. *Osteoporos. Int.* 27, 1047–1055. doi: 10.1007/s00198-015-3320-x

Peng, Y., Wu, S., Li, Y., and Crane, J. L. (2020). Type H blood vessels in bone modeling and remodeling. *Theranostics* 10, 426–436. doi: 10.7150/thno.34126

Phan, T. C. A., Xu, J., and Zheng, M. H. (2004). Interaction between osteoblast and osteoclast: impact in bone disease. *Histol. Histopathol.* 19, 1325–1344. doi: 10.14670/HH-19.1325

Ramasamy, S. K., Kusumbe, A. P., Wang, L., and Adams, R. H. (2014). Endothelial Notch activity promotes angiogenesis and osteogenesis in bone. *Nature* 507, 376–380. doi: 10.1038/nature13146

Rodriguez-Laguna, L., Agra, N., Ibañez, K., Oliva-Molina, G., Gordo, G., Khurana, N., et al. (2019). Somatic activating mutations in PIK3CA cause generalized lymphatic anomaly. *J. Exp. Med.* 216, 407–418. doi: 10.1084/jem.20181353

Sivaraj, K. K., and Adams, R. H. (2016). Blood vessel formation and function in bone. *Development* 143, 2706–2715. doi: 10.1242/dev.136861

Sobacchi, C., Schulz, A., Coxon, F. P., Villa, A., and Helfrich, M. H. (2013). Osteopetrosis: genetics, treatment and new insights into osteoclast function. *Nat. Rev. Endocrinol.* 9, 522–536. doi: 10.1038/nrendo.2013.137

Tolar, J., Teitelbaum, S. L., and Orchard, P. J. (2004). Osteopetrosis. *N. Engl. J. Med.* 351, 2839–2849. doi: 10.1056/NEJMra040952

Verkman, A. S., and Galietta, L. J. V. (2009). Chloride channels as drug targets. *Nat. Rev. Drug Discov.* 8, 153–171. doi: 10.1038/nrd2780

Waguespack, S. G., Hui, S. L., DiMeglio, L. A., and Econs, M. J. (2007). Autosomal dominant osteopetrosis: clinical severity and natural history of 94 subjects with a chloride channel 7 gene mutation. *J. Clin. Endocrinol. Metab.* 92, 771–778. doi: 10.1210/jc.2006-1986

Waguespack, S. G., Koller, D. L., White, K. E., Fishburn, T., Carn, G., Buckwalter, K. A., et al. (2003). Chloride channel 7 (ClCN7) gene mutations and autosomal dominant osteopetrosis, type II. *J. Bone Miner. Res.* 18, 1513–1518. doi: 10.1359/jbmr.2003.18.8.1513

Wang, C., Hockerman, S., Jacobsen, E. J., Alippe, Y., Selness, S. R., Hope, H. R., et al. (2018). Selective inhibition of the p38α MAPK–MK2 axis inhibits inflammatory cues including inflammasome priming signals. *J. Exp. Med.* 215, 1315–1325. doi: 10.1084/jem.20172063

Weinert, S., Jabs, S., Supanchart, C., Schweizer, M., Gimber, N., Richter, M., et al. (2010). Lysosomal pathology and osteopetrosis upon loss of H+-driven lysosomal Cl-accumulation. *Science* 328, 1401–1403. doi: 10.1126/science.1188072

Xiao, Y.-Z., Yang, M., Xiao, Y., Guo, Q., Huang, Y., Li, C.-J., et al. (2020). Reducing hypothalamic stem cell senescence protects against aging-associated physiological decline. *Cell Metab.* 31, 534.e5–548.e5. doi: 10.1016/j.cmet.2020.01.002

Xie, H., Cui, Z., Wang, L., Xia, Z., Hu, Y., Xian, L., et al. (2014). PDGF-BB secreted by preosteoclasts induces angiogenesis during coupling with osteogenesis. *Nat. Med.* 20, 1270–1278. doi: 10.1038/nm.3668

Xu, R., Yallowitz, A., Qin, A., Wu, Z., Shin, D. Y., Kim, J.-M., et al. (2018). Targeting skeletal endothelium to ameliorate bone loss. *Nat. Med.* 24, 823–833. doi: 10.1038/s41591-018-0020-z

Yang, M., Guo, Q., Peng, H., Xiao, Y.-Z., Xiao, Y., Huang, Y., et al. (2019). Krüppel-like factor 3 inhibition by mutated lncRNA Reg1cp results in human

high bone mass syndrome. *J. Exp. Med.* 216, 1944–1964. doi: 10.1084/jem.20181554

Yang, M., Li, C.-J., Sun, X., Guo, Q., Xiao, Y., Su, T., et al. (2017). MiR-497 195 cluster regulates angiogenesis during coupling with osteogenesis by maintaining endothelial Notch and HIF-1α activity. *Nat. Commun.* 8, 1–11. doi: 10.1038/ncomms16003

Zhang, Z., He, J., Zhang, H., Hu, W., Fu, W., Gu, J., et al. (2009). Identification of the CLCN7 gene mutations in two Chinese families with autosomal dominant osteopetrosis (type II). *J. Bone Miner. Metab.* 27, 444–451. doi: 10.1007/s00774-009-0051-0

Conflict of Interest: The authors declare that the research was conducted in the absence of any commercial or financial relationships that could be construed as a potential conflict of interest.

Copyright © 2020 Peng, He and Wen. This is an open-access article distributed under the terms of the Creative Commons Attribution License (CC BY). The use, distribution or reproduction in other forums is permitted, provided the original author(s) and the copyright owner(s) are credited and that the original publication in this journal is cited, in accordance with accepted academic practice. No use, distribution or reproduction is permitted which does not comply with these terms.

frontiers in Cell and Developmental Biology

REVIEW
published: 19 November 2020
doi: 10.3389/fcell.2020.600867

Roles of MicroRNAs in Bone Destruction of Rheumatoid Arthritis

Hanxiao Zhao[1,2], *Aiping Lu*[3,4]* *and Xiaojuan He*[1]*

[1] Institute of Basic Research in Clinical Medicine, China Academy of Chinese Medical Sciences, Beijing, China, [2] The Second Clinical College of Guangzhou University of Chinese Medicine, Guangzhou, China, [3] Law Sau Fai Institute for Advancing Translational Medicine in Bone and Joint Diseases, School of Chinese Medicine, Hong Kong Baptist University, Kowloon Tong, Hong Kong, [4] Shanghai GuangHua Hospital of Integrated Traditional Chinese and Western Medicine, Institute of Arthritis Research, Shanghai Academy of Chinese Medical Sciences, Shanghai, China

As an important pathological result of rheumatoid arthritis (RA), bone destruction will lead to joint injury and dysfunction. The imbalance of bone metabolism caused by increased osteoclast activities and decreased osteoblast activities is the main cause of bone destruction in RA. MicroRNAs (MiRNAs) play an important role in regulating bone metabolic network. Recent studies have shown that miRNAs play indispensable roles in the occurrence and development of bone-related diseases including RA. In this paper, the role of miRNAs in regulating bone destruction of RA in recent years, especially the differentiation and activities of osteoclast and osteoblast, is reviewed. Our results will not only help provide ideas for further studies on miRNAs' roles in regulating bone destruction, but give candidate targets for miRNAs-based drugs research in bone destruction therapy of RA as well.

Keywords: microRNAs, rheumatoid arthritis, bone destruction, osteoclast, osteoblast

OPEN ACCESS

Edited by:
Changjun Li,
Central South University, China

Reviewed by:
Zhang Peng,
Chinese Academy of Sciences (CAS), China
Runyue Huang,
Guangzhou University of Chinese Medicine, China

***Correspondence:**
Aiping Lu
aipinglu@hkbu.edu.hk
Xiaojuan He
hxj19@126.com

Specialty section:
This article was submitted to Molecular Medicine, a section of the journal Frontiers in Cell and Developmental Biology

Received: *31 August 2020*
Accepted: *26 October 2020*
Published: *19 November 2020*

Citation:
Zhao H, Lu A and He X (2020) Roles of MicroRNAs in Bone Destruction of Rheumatoid Arthritis. Front. Cell Dev. Biol. 8:600867. doi: 10.3389/fcell.2020.600867

INTRODUCTION

Rheumatoid arthritis (RA) is the most common systemic inflammatory arthritis. As one of the major public health challenges in the world, the standardized prevalence rate of RA is 240 per 100,000 population, and its prevalence and morbidity are currently on the rise (Safiri et al., 2019). Bone destruction is a hallmark of this disease and occurs in the following forms: focal bone at the edge of the joint and subchondral erosion, bone loss around joints and systemic bone loss (osteoporosis) (Goldring, 2015). It occurs in the early stage of RA and develops with time, leading to joint damage and functional impairment in patients, which is an important prognostic indicator in RA (Panagopoulos and Lambrou, 2018). Bone homeostasis relies on the balance between osteoclasts-mediated bone absorption and osteoblasts-mediated bone formation (Guo Q. et al., 2018). Bone destruction in RA is an imbalance of this relationship, which is the result of inducing osteoclasts and inhibiting osteoblasts (Panagopoulos and Lambrou, 2018).

MicroRNAs (MiRNAs) are an endogenous, small (about 22 nucleotides long), non-coding and functional RNA families. MiRNAs are differentially expressed and deregulated in RA, and participate in the pathogenesis of RA by regulating target genes (Li et al., 2019). The association between changes in miRNAs expression and pathogenesis of RA has been previously demonstrated (Sugatani et al., 2011). Because miRNAs have multiple functions and extensive regulatory functions, they also play important roles in bone pathophysiology. MiRNAs have become an important regulator of osteoclastogenesis, osteoblasts growth and differentiation

(Chen et al., 2015; Baum and Gravallese, 2016; Liu J. et al., 2019). In experimental arthritis models, miRNAs analogs and antagonists have shown encouraging results as experimental treatments (Hou et al., 2019).

Therefore, the purpose of this article is to comprehensively review recently reported miRNAs in osteoclastogenesis and osteoblastogenesis, highlighting their pathogenetic mechanisms leading to the development of bone destruction in RA. We searched Medline database through PubMed for English language original articles from 2016 to 2020 using keywords as the following: rheumatoid arthritis and miRNAs and bone destruction, rheumatoid arthritis and osteoclast and miRNAs, rheumatoid arthritis and osteoblast and miRNAs, rheumatoid arthritis and miRNAs and bone, osteoclast differentiation and miRNAs, osteoblast differentiation and miRNAs, osteoclastogenesis and miRNAs, and osteoblastogenesis and miRNAs. The miRNA-target interaction proposed by bioinformatics alone were not be discussed here. Reviews and articles in other languages were excluded. Bone damage caused by other factors and diseases, changes in miRNAs caused by drugs or other factors, as well as indirect effects of miRNAs on osteoclasts and osteoblasts on bone damage were excluded.

BONE DESTRUCTION IN RA

The cores of bone destruction in RA lie in excessive bone absorption and insufficient bone reconstruction. Osteoclasts play a key role in the bone destruction of RA. Monocytes of the monocyte/macrophage lineage are precursors of osteoclasts, which enter the inflamed joints and synovium and differentiate into osteoclasts (Karmakar et al., 2010). Osteoclasts differentiation can be regulated through receptor activator for nuclear factor-κ B ligand (RANKL), which binds to its receptor activator for nuclear factor-κB (RANK), and macrophage colony-stimulating factor (M-CSF), which binds to its receptor colony stimulating factor 1 receptor (CSF1R, also known as M-CSFR) (Lozano et al., 2019). Osteoblasts, synovial fibroblasts (FLS) and other cells express RANKL, and RANKL binds with its receptor RANK, which activates osteoclasts to generate signals (Ono et al., 2020). Driven by RANKL receptor activator, the activation of nuclear factor of activated T cells (NFATc1) and tumor necrosis factor receptor-related factor 6 (TRAF6) can further promote the activation and expression of other transcription factors, signal pathways and genes required for osteoclast differentiation (Chen X. et al., 2018; Hrdlicka et al., 2019). Leucine rich repeat containing G protein-coupled receptor 4 (LGR4) is another receptor of RANKL, which competes with RANK to bind RANKL and inhibits the typical RANKL signal during osteoclast differentiation (Luo et al., 2016). Osteoprotegerin (OPG) is a receptor for RANKL and competitively inhibits RANK/RANKL binding. In RA, the ratio of RANKL and OPG can affect this disease progression (Panagopoulos and Lambrou, 2018). M-CSFR, the receptor encoded by c-fms gene, is dimerized, phosphorylated, and activated by M-CSF, which triggers the activation of serine/threonine kinase family called mitogen-activated protein kinase (MAPK) and phosphatidylinositol 3 kinase (PI3K). The activation of PI3K stimulates the activation of protein kinase B (PKB, or AKT) and mammalian target of rapamycin (mTOR). This process plays a role of proliferation and survival in osteogenesis (Anesi et al., 2019).

The microenvironment of RA can not only promote the production and activation of osteoclasts, but also inhibit the function of the osteoblasts (Gravallese, 2017). Due to the limited repair capacity of bone erosion, the inhibition of osteoblasts differentiation and function may cause to impaired bone formation in RA. There are two main pathways required for osteoblasts differentiation from mesenchymal precursors: Wnt and bone morphogenetic protein (BMP) pathway (Gravallese, 2017). In addition, systemic hormones, fibroblast growth factor, as well as other signaling factors are also involved (Valenti et al., 2018). Several evidences support that Wnt signaling plays a role in bone loss and new bone formation in RA (Cici et al., 2019). In the absence of Wnt stimulation, β-catenin is phosphorylated by the glycogen synthase kinase 3β (GSK-3β) complex and further degraded in the cytoplasm after ubiquitination. While Wnt proteins stimulation inhibit GSK-3β, induce β-catenin accumulation in the cytoplasm, promote β-catenin to enter the nucleus and induce target gene expression (Maeda et al., 2019). Wnt pathway can activate target genes, promote differentiation in pre-osteoblasts, up-regulate OPG expression and down-regulate RANKL expression in osteoblasts (Cici et al., 2019). Wnt signaling is regulated by different inhibitors, such as the secreted frizzled-related protein, the Wnt inhibitory factor 1, sclerostin and the Dickkopf (Dkk) family of secreted proteins. Bone destruction caused by RA may be related to over-production of Wnt inhibitors such as Dkk-1 (Adami et al., 2016). Bone morphogenetic proteins (BMPs) belong to the transforming growth factor-β (TGF-β) super-family. BMP pathway, including canonical drosophila mothers against decapentaplegic protein (Smad) signaling and non-Smad signaling (Sanchez-Duffhues et al., 2015), regulates the proliferation, differentiation, maturation and activity of osteoblasts in bone formation. Inflammatory cytokines in inflamed joints can regulate BMP signaling, and altered BMP signaling is essential for osteoblasts and their progenitors (Lukac et al., 2020). Therefore, targeting the BMP pathway may become a potential treatment for bone destruction in RA (He X. et al., 2019).

EFFECTS OF MIRNAS ON BONE DESTRUCTION IN RA

MiRNAs Regulate Osteoclasts

RANK/RANKL/OPG Signal Pathway

RANK/RANKL/OPG signal pathway plays an important role in osteoclast differentiation. One study showed that the expression level of miR-145-5p in peripheral blood mononuclear cells and synovial tissue of patients with RA increased. During the differentiation of mouse monocyte/macrophage RAW264.7 cells, overexpressed miR-145-5p directly targeted OPG and promoted osteoclast differentiation. MiR-145-5p significantly reduced the

expression of OPG, while inhibiting miR-145-5p had the opposite effect. Overexpression of miR-145-5p also up-regulated the expression of RANK and RANKL. In the collagen-induced arthritis (CIA) mice, 4 weeks after intravenous injection of mir-145-5p agomir, the bone erosion of ankle joint became worse (Chen Y. et al., 2018). Changes in miR-124 have been found in many inflammatory and immune diseases (Qin et al., 2016). The expression of miR-124 is reduced in various human tumors and has a tumor suppressing effect (Jia et al., 2019; Moghadasi et al., 2020). Ohnuma et al.'s (2019) research found that overexpression of miR-124 inhibited osteoclast differentiation and bone resorption by inhibiting the level of NFATc1 in mouse bone marrow-derived macrophages (BMMs) induced by tumor necrosis factor-α (TNF-α), interleukin 6 (IL-6), OPG and M-CSF. Besides, Nakamachi et al. (2016) discovered that the expression of miR-124 was significantly down-regulated in the joints of adjuvant-induced arthritis (AIA) rats (Nakamachi et al., 2016). Treated with precursor-miR-124 significantly alleviated bone destruction, and also reduced the expression of RANKL, NFATc1 and integrin β1 in AIA rats. *In vitro*, both rat NFATc1 and human NFATc1 were the direct targets of miR-124 to inhibit osteoclast differentiation (Nakamachi et al., 2016). So far, several other studies had shown that miR-146a inhibited osteoclast differentiation in CIA mice (Ammari et al., 2018), which may be related to the expression of proteins related to the RANK/RANKL/OPG signal pathway. Tao et al. (2017) found that the expression of endogenous miR-106b increased in inflammatory mouse joints. Inhibition of miR-106b significantly alleviated the development of arthritis in CIA mice, decreased RANKL:OPG ratio as well as the number and formation of osteoclasts (Tao et al., 2017).

In addition, many other studies showed that miR-338-3p (Niu et al., 2019) and miR-340 (Zhao et al., 2017a) inhibited the differentiation of osteoclasts by targeting the factors related to RANK/RANKL/OPG signaling pathway, while miR-34c (Cong et al., 2017), miR-182 (Miller et al., 2016), and miR-346-3p (Mao et al., 2020) promoted the formation of osteoclasts by participating in the regulation of the expression of genes and proteins related to this pathway. However, these studies were only carried out *in vitro*, lacking the further verification from animal experiments.

Actually, a miRNA could not only regulate the activities of osteoclasts, some other cells that involved in the development of bone destruction in RA, such as FLS, could also influenced by the same miRNA. Wang et al. showed that miR-21 was up-regulated during the osteoclast formation of RAW264.7 cells induced by RANKL, and up-regulation of miR-21 promoted osteoclast differentiation and bone resorption. Overexpression of miR-21 decreased the expression level of PTEN protein and increased the expression of p-AKT and NFATc1 (Wang S. et al., 2020). One study indicated that the level of miR-21 was increased in FLS of CIA rats, and upregulated miR-21 could promote FLS proliferation by facilitating NF-κB nuclear translocation (Chen et al., 2016). However, another research showed that after intraperitoneal injection of miR-21 lentivirus, the paw volume and arthritis index of CIA rats were lower than those of CIA model group. MiR-21 inhibited the expression of IL-6, IL-8, and Wnt protein in synovial tissue of CIA rats. Overexpression of miR-21 alleviated the symptoms of RA by down-regulating Wnt signaling pathway (Liu X. G. et al., 2019). The different conclusions of miR-21 *in vivo* and *in vitro* may be due to the more complex internal environment of RA model, or the differential regulation of miR-21 in different cells. Therefore, these assumptions need to be confirmed by further experiments.

M-CSF Related Pathway

M-CSF pathway also plays a key role in the process of osteoclast differentiation. Activated by the combination of M-CSF and M-CSFR, PI3K/AKT pathway can enhance the survival and proliferation of osteoclast precursors (Kim and Kim, 2016). MiR-142 existed in hematopoietic cells and played an important role in inflammation and immune response (Sharma, 2017) and negatively regulated the differentiation and conversion of monocytes and macrophages into osteoclasts (Fordham et al., 2016). Moreover, the expression of miR-142-3p was up-regulated in synovial tissue of RA patients (Qiang et al., 2019). Another study in CIA mice showed that after injection of miR-17-5p mimic, the number of osteoclasts reduced by directly reducing the expression of signal transducer and activator of transcription 3 (STAT3) and janus kinase-1 (JAK1) (Najm et al., 2020). However, the role and function of miRNAs in RA animal models as well as RA patients still need further studies.

MiRNAs Regulate Other Factors in Osteoclasts

In addition, as a key cytokine in the pathophysiology of RA, TNF can stimulate osteoclast differentiation (Noack and Miossec, 2017). Anti-TNF drugs may improve the condition of patients with RA (Bek et al., 2017). MiR-125a-5p, known as a tumor suppressor, participates in cancer development and progression by regulating cell proliferation, migration, invasion and metastasis. Studies had shown that the concentration of miR-125a-5p in peripheral blood of patients with RA was obviously increased (Ormseth et al., 2015; Churov et al., 2015). Sun et al. (2019) found that miR-125a-5p increased significantly during the differentiation of RAW 264.7 cells stimulated by M-CSF and RANKL. Overexpression of miR-125a-5p up-regulated the expression levels of translating ribosome affinity purification (TRAP), matrix metalloproteinase-2 (MMP-2), MMP-9 and cathepsin K, inhibited the expression of TNF receptor superfamily member 1B (TNFRSF1B) and promoted the differentiation of osteoclasts (Sun et al., 2019). MiRNA-1225 is regarded as a modulator in the development of cancers and other biological reactions. A research found that the expression of miR−1225 decreased in the differentiation of BMMs stimulated by RANKL. By regulating the axis of Keap1-Nrf2-TNF-α, miR-1225 inhibited the differentiation of osteoclasts, and then regulated the production of reactive oxygen species (Reziwan et al., 2019). However, more *in vivo* experiments still urgently needed to provide further evidences. As anti-TNF drugs have been applied in clinical practice, whether miRNAs-based therapy could act synergistically with anti-TNF therapy on RA may be one of the research trends. In addition, miR-506 could partially target Sirtuin 1 (SIRT1). After inhibiting the expression of miR-506 (Yan et al., 2019), osteoclast formation was inhibited. MiR-199a-5p (Guo K. et al., 2018) promoted

osteoclast differentiation by regulating Mafb. Whereas miR-192-5p could inhibit osteoclast formation by negatively regulating the expression of ras-related C3 botulinum toxin substrate 2 (RAC2) in CIA rats (Zheng et al., 2020).

MiRNAs Regulate Osteoblasts

Wnt Pathway

Wnt pathway is one of the important pathways in osteoblast differentiation. β-catenin is the key factor of Wnt pathway, and many miRNAs work directly or indirectly through β-catenin. Lin et al. considered that miR-92a-1-5p was significantly down-regulated during the osteogenic differentiation of mouse osteoblast precursor cell line MC3T3-E1 induced by BMP2. MiR-92a-1-5p was a negative regulator of osteogenic differentiation. The expression of β-catenin was negatively regulated by miR-92a-1-5p, and the inhibition of miR-92a-1-5p on β-catenin was weakened by Wnt signal activator or GSK-3β knockout (Lin Z. et al., 2019). In addition, by regulating the expression of Wnt pathway related factors such as β -catenin, miR-26b-3p (Lin Y. et al., 2019), miR-193a (Wang S. N. et al., 2018; Wang W. et al., 2018), miR-4739 (Elsafadi et al., 2017), miR-150-3p (Wang N. et al., 2016), and miR-23a (Li et al., 2016) could also inhibit osteoblast differentiation but miR-101 (Wang H. et al., 2016) and miR-199b-5p (Zhao et al., 2016) could promote osteoblast differentiation.

Besides regulating β-catenin, some miRNAs could also influence Wnt pathway inhibitors. As a Wnt antagonist, DKK2 inhibits osteoblast activity by binding low-density-lipoprotein receptor-related proteins 5/6 (LRP5/6), thus preventing the formation of Wnt-FZD-LRP complex. Additionally, Myd88 signal can inhibit proliferation, migration and differentiation of BMSCs by inhibiting AKT/β-catenin/GSK-3β signal pathway (Martino et al., 2016). Xia et al. (2019) pointed out that overexpressed miR-200c enhanced the osteoblast differentiation of human BMSCs. Overexpressed miR-200c enhanced the levels of BMP2, Runx2, RANKL, Osterix(Osx), Osteocalcin (OCN), Osteopontin (OPN) and collagen type I by directly decreasing Myd88, as well as the expression of β-catenin, AKT and phosphorylated AKT. After inhibiting miR-200c, the effect was opposite (Xia et al., 2019).

BMP Pathway

Another important pathway of osteoblast differentiation is BMP pathway. Members of TGF-β superfamily transmit intracellular signals through Smad complex or MAPK cascade. In Smad-dependent signaling, phosphorylated Smad2/3 or phosphorylated Smad1/5/8 is complexed with Smad4 and co-located in the nucleus, where they regulated the expression of downstream target genes (Wu M. et al., 2016). Chen et al. (2020) pointed out that the differentiation and mineralization of primary osteoblasts isolated from a RA patient were inhibited after co-culture with exosomes of fibroblast-like synoviocytes from synovial tissues. Exosomes treated with miR-486-5p mimic promoted osteoblast differentiation, and increased BMP2 expression and Smad1/5/8 phosphorylation by decreasing Tob1 expression. In CIA mice, the exosomes of synovial fibroblasts also confirmed the same results (Chen et al., 2020). However, the role of miR-486-5p in RA animal models still need further investigation.

There are also miRNAs that affect Samd7 which negatively regulates BMP pathway. He G. et al. (2019) showed that miR-877-3p promoted the osteogenic differentiation and mineralization of MC3T3-E1 cells induced by TGF-β1, and inhibited the expression of Smad7 gene. MiR-877-3p promoted the expression of osteogenic genes such as Runx2, Osx, collagen type I alpha 1, p-Smad2, and p-Smad3, but this promotion was significantly inhibited by Smad7. The expression of Smad7 was up-regulated and the levels of p-Smad2 and p-Smad3 were decreased by inhibiting miR-877-3p (He G. et al., 2019). Additionally, by regulating the translation and expression of BMP pathway related factors, miR-144-3p (Huang C. et al., 2016), miR-217 (Zhu et al., 2017), miR-92a (Yan et al., 2018), and miR-765 (Wang T. et al., 2020) also inhibited osteoblast differentiation.

MiRNAs Regulate Other Factors in Osteoblasts

In addition to Wnt and BMP pathways, osteoblast differentiation is also regulated by many other factors. Many miRNAs inhibited the osteogenic differentiation of cells in various ways. For example, miR-383 (Tang et al., 2018) directly regulated Satb2, miR-27a (Gong et al., 2016) reduced the protein and gene expression level of Sp7, miR-10b (Yang et al., 2017) overexpression up-regulated the expression of signal transducer and activator of transcription 1 (STAT1) and blocked the nuclear translocation of Runx2, miR-23a-5p (Ren et al., 2018; Yang et al., 2020) directly targeted and inhibited the expression of Runx2 and MAPK13, miR-206 suppressed the glutamine metabolism (Chen et al., 2019), miR-320a (Huang J. et al., 2016) negatively regulated homeobox a10 (HOXA10), miR-214 (Guo et al., 2017) participates in the inhibition of the c-jun n-terminal kinase (JNK) and p38 pathways, miR-495 (Tian et al., 2017) directly targeted the high-mobility group A2 gene (HMGA2), miR-125a-3p negatively regulated G-protein-coupled receptor kinase interacting protein-1 (GIT1) (Tu et al., 2016), and after miR-223 (Zhang et al., 2018) and miR-23a cluster (Godfrey et al., 2018) inhibition, short-chain dehydrogenase/reductase 3 (DHRS3) and HoxA cluster were respectively targeted to promote osteogenic differentiation.

On the contrary, there are also many other miRNAs that can promote the osteogenic differentiation of cells. MiR-1-3p (Zhou et al., 2020) directly targeted and inhibited the expression of hypoxia-inducible factor 1-alpha inhibitor (HIF1AN), miR-5100 (Wang et al., 2017) directly inhibited the expression of Tob2, miR-7-5p (Chen B. et al., 2018) directly targeted chemokine-like receptor 1 (CMKLR1), miR-590-3p (Wu S. et al., 2016) directly inhibited the expression of adenomatous polyposis coli (APC), and miR-98 promoted osteogenic differentiation via targeting HMGA2 in human BMSCs (Gao et al., 2018).

Liu et al. (2018) Interestingly, in one study, miR-98-5p negatively regulated the expression of casein kinase 2 interacting protein-1 (CKIP-1) gene and protein to promote the osteogenic differentiation of MC3T3-E1 cells (Liu et al., 2018). But another study in three types of cells (MC3T3-E1 cells, mouse and human BMSCs), miR-98-5p inhibited osteogenic differentiation by targeting HMGA2 (Zheng et al., 2019). And for miR-224, it

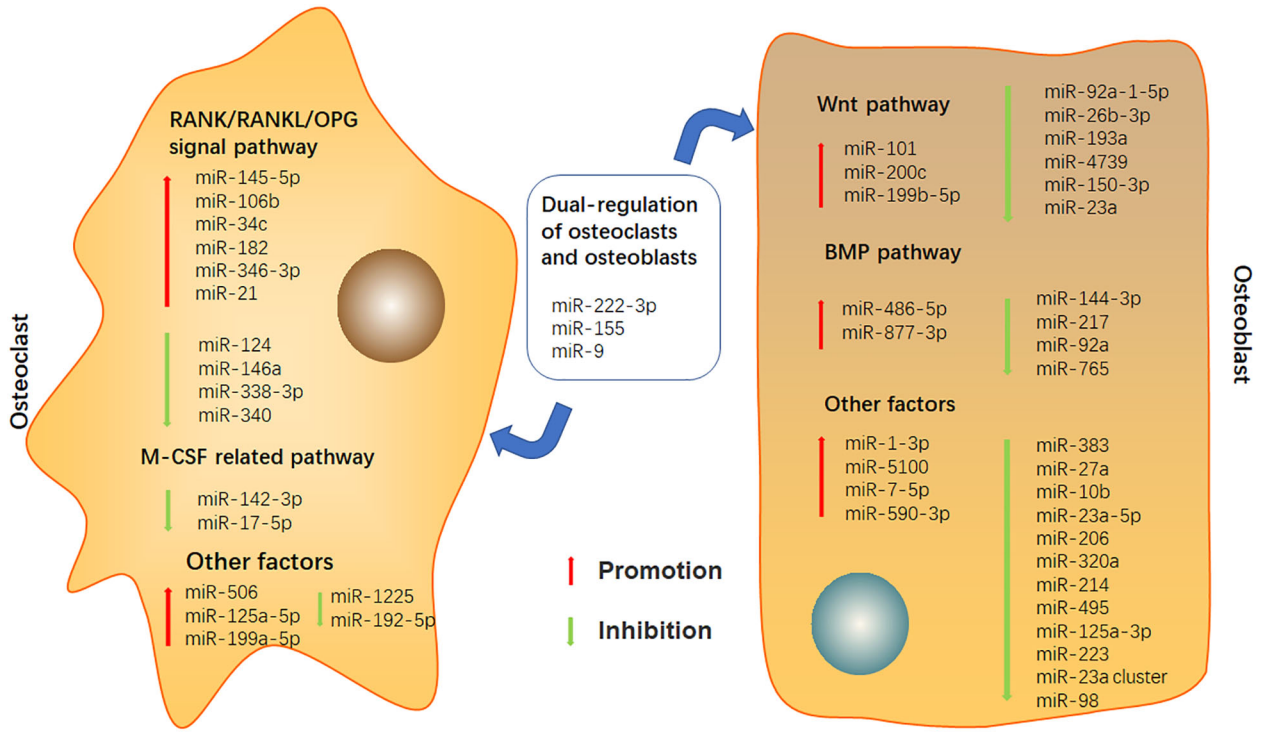


FIGURE 1 | Effects of miRNAs on osteoclast and osteoblast.

inhibited osteoblast differentiation in mesenchymal stem cells by directly targeting Smad4 (Luo et al., 2018), but miR-224 regulated the expression of Rac1 to promoted osteogenic differentiation in human mesenchymal stem cells (Cai et al., 2019).

MiRNAs Dual-Regulate Osteoclasts and Osteoblasts

With the deepening of the studies, researchers found that some miRNAs not only act on a single pathway or a kind of cell. They can simultaneously regulate osteoclasts and osteoblasts as well.

Takigawa et al. (2016) held that miR-222-3p, as an inhibitory regulator of osteoclast generation, inhibited the up-regulation of TRAP and cathepsin K in RAW264.7 cells. MiR-222-3p significantly down-regulated the gene level of NFATc1. Yan et al. (2016) manifested that miR-222-3p inhibited the osteogenic differentiation of human BMSCs. Overexpression of miR-222-3p inhibited Smad5 and Runx2 protein levels, while miR-222-3p had the opposite inhibitory effect and stimulated the phosphorylation of Smad1/5/8 (Yan et al., 2016).

Zhao et al. (2017b) discussed that in mouse BMMs cells, TGF-β1 up-regulated the expression of miR-155 and inhibited osteoclast differentiation, while silencing Smad4 reversed the effect of TGF-β1. MiR-155 inhibited osteoclast differentiation by targeting two regulators of osteoclast generation, suppressor of cytokine signaling and microphthalmia-associated transcription factor (Zhao et al., 2017b). MiR-155 not only inhibited osteoclast differentiation, but also inhibited osteoblast differentiation. Gu et al. (2017) showed that in MC3T3-E1 cells induced by BMP2, miR-155 was down-regulated. The gene and protein expression of p-Smad5 and Smad5 was blocked after miR-155 overexpression. Overexpression of Smad5 reversed the inhibitory effect of miR-155 on osteogenesis (Gu et al., 2017).

Lee et al. (2020) indicated that intraarticular injection of miR-9 not only reduced the clinical arthritis score and erosion score, but also significantly decreased inflammatory exudate, inflammation rate and pannus formation, and inhibited osteoclast formation in CIA rats. Qu et al. (2016) thought that miR-9 promoted osteogenic differentiation in MC3T3-E1 cells induced by BMP2. Overexpression of miR-9 up-regulated the concentration of p-adenosine monophosphate-activated protein kinase (p-AMPK) and promoted the protein expression of p-AMPK to increase significantly (Qu et al., 2016).

Therefore, a miRNA may inhibit or promote osteoclast and osteogenesis at the same time, or it may have an opposite effect on osteoclasts and osteoblasts. Maybe the concentration, action time and microenvironment can partly explain the diversity of miRNAs' action.

CONCLUSION AND PROSPECT

In RA, the cure rate of bone destruction is low and the disability rate is high, which seriously threatens the daily life of RA patients. Conventional synthetic disease-modified antirheumatic drugs (csDMARDs), as the first-line drugs recommended by domestic and foreign guidelines, can effectively alleviate the

progress of RA and control clinical symptoms, but they are not effective for all RA patients (Schett et al., 2016). The effects of csDMARDs on bone destruction caused by RA are not as expected. The emergence and application of biological agents has brought a major breakthrough in the treatment of bone destruction in RA. Although the use of drugs can alleviate clinical symptoms to a certain extent, it cannot completely repair bone destruction. In the current studies of treatment methods, researchers mainly focus on inflammation control and osteoclast inhibition. However, for the bone destruction caused by RA, this is not enough. The repair of bone destruction and new bone formation may be an important part of the future treatment plan. Additionally, although the ability of miRNAs to target multiple genes in the process of osteoclast and osteoblast differentiation makes them a promising target for developing drugs to treat bone destruction in RA, most of the current researches on miRNAs regulating bone destruction were mainly *in vitro* experiments, lacking enough evidences from animal experiments and clinical trials. Therefore, further animal and clinical researches will be the focus of the next studies. However, the complex role of miRNAs makes further animal experiments and clinical trials face great challenges. As mentioned above, the role of miRNAs may be influenced by different time of action and different concentrations in different microenvironments. Our understanding of miRNAs is still far from enough. How to better and faster make miRNAs-based drugs play a role in the treatment of RA bone destruction is a question we need to carefully think about. Due to the complexity of the role of miRNAs in different pathways, different cells and different microenvironment, some technologies such as omics, systemic biology and biological computing need to be jointly introduced in in-depth studies. In addition, since the ultimate purposes of basic researches are to apply and serve the clinical practices, we should also consider more miRNAs supported by clinical data (Wang M. et al., 2020) in future studies, so as to continuously improve our understanding of miRNAs in bone destruction of RA.

In this article, we summarized the potential of miRNAs involved in bone destruction, provided the latest overview of miRNAs in bone metabolism, and demonstrated the role of miRNAs in osteoclast and osteoblast differentiation of RA (**Figure 1** and **Supplementary Table 1**). Although a large number of further studies are still needed to discover the complete miRNAs information network regulating bone balance, targeting miRNAs can be considered as a potential candidate for the treatment of bone destruction caused by RA in future.

AUTHOR CONTRIBUTIONS

HZ wrote the manuscript. AL and XH revised and approved the manuscript. All authors contributed to the article and approved the submitted version.

FUNDING

This work was supported by the National Key Research and Development Program of China (2018YFC1705205).

SUPPLEMENTARY MATERIAL

The Supplementary Material for this article can be found online at: https://www.frontiersin.org/articles/10.3389/fcell.2020.600867/full#supplementary-material

REFERENCES

Adami, G., Orsolini, G., Adami, S., Viapiana, O., Idolazzi, L., Gatti, D., et al. (2016). Effects of TNF Inhibitors on Parathyroid Hormone and Wnt Signaling Antagonists in Rheumatoid Arthritis. *Calcif. Tissue Int.* 99, 360–364. doi: 10.1007/s00223-016-0161-3

Ammari, M., Presumey, J., Ponsolles, C., Roussignol, G., Roubert, C., Escriou, V., et al. (2018). Delivery of miR-146a to Ly6C(high) monocytes inhibits pathogenic bone erosion in inflammatory arthritis. *Theranostics* 8, 5972–5985. doi: 10.7150/thno.29313

Anesi, A., Generali, L., Sandoni, L., Pozzi, S., and Grande, A. (2019). From osteoclast differentiation to osteonecrosis of the jaw: molecular and clinical insights. *Int. J. Mol. Sci.* 20:4925. doi: 10.3390/ijms20194925

Baum, R., and Gravallese, E. M. (2016). Bone as a Target organ in rheumatic disease: impact on osteoclasts and osteoblasts. *Clin. Rev. Allergy. Immunol.* 51, 1–15. doi: 10.1007/s12016-015-8515-6

Bek, S., Bojesen, A. B., Nielsen, J. V., Sode, J., Bank, S., Vogel, U., et al. (2017). Systematic review and meta-analysis: pharmacogenetics of anti-TNF treatment response in rheumatoid arthritis. *Pharmacogenom. J.* 17, 403–411. doi: 10.1038/tpj.2017.26

Cai, Q., Zheng, P., Ma, F., Zhang, H., Li, Z., Fu, Q., et al. (2019). MicroRNA-224 enhances the osteoblastic differentiation of hMSCs via Rac1. *Cell Biochem. Funct.* 37, 62–71. doi: 10.1002/cbf.3373

Chen, B., Meng, J., Zeng, Y. T., Du, Y. X., Zhang, J., Si, Y. M., et al. (2018). MicroRNA-7-5p regulates osteogenic differentiation of hMSCs via targeting CMKLR1. *Eur. Rev. Med. Pharmacol. Sci.* 22, 7826–7831. doi: 10.26355/eurrev_201811_16407

Chen, X., Wang, Z., Duan, N., Zhu, G., Schwarz, E. M., and Xie, C. (2018). Osteoblast-osteoclast interactions. *Connect. Tissue Res.* 59, 99–107. doi: 10.1080/03008207.2017.1290085

Chen, Y., Wang, X., Yang, M., Ruan, W., Wei, W., Gu, D., et al. (2018). miR-145-5p increases osteoclast numbers in vitro and aggravates bone erosion in collagen-induced arthritis by targeting osteoprotegerin. *Med. Sci. Monit.* 24, 5292–5300. doi: 10.12659/MSM.908219

Chen, J., Liu, M., Luo, X., Peng, L., Zhao, Z., He, C., et al. (2020). Exosomal miRNA-486-5p derived from rheumatoid arthritis fibroblast-like synoviocytes induces osteoblast differentiation through the Tob1/BMP/Smad pathway. *Biomater. Sci.* 8, 3430–3442. doi: 10.1039/c9bm01761e

Chen, X. M., Huang, Q. C., Yang, S. L., Chu, Y. L., Yan, Y. H., Han, L., et al. (2015). Role of Micro RNAs in the pathogenesis of rheumatoid arthritis: novel perspectives based on review of the literature. *Medicine* 94:e1326. doi: 10.1097/MD.0000000000001326

Chen, Y., Xian, P. F., Yang, L., and Wang, S. X. (2016). MicroRNA-21 promotes proliferation of fibroblast-like synoviocytes through mediation of NF-kappaB nuclear translocation in a rat model of collagen-induced rheumatoid arthritis. *Biomed. Res. Int.* 2016:9279078. doi: 10.1155/2016/9279078

Chen, Y., Yang, Y. R., Fan, X. L., Lin, P., Yang, H., Chen, X. Z., et al. (2019). miR-206 inhibits osteogenic differentiation of bone marrow mesenchymal stem cells by targetting glutaminase. *Biosci. Rep.* 39:BSR20181108. doi: 10.1042/bsr20181108

Churov, A. V., Oleinik, E. K., and Knip, M. (2015). MicroRNAs in rheumatoid arthritis: altered expression and diagnostic potential. *Autoimmun. Rev.* 14, 1029–1037. doi: 10.1016/j.autrev.2015.07.005

Cici, D., Corrado, A., Rotondo, C., and Cantatore, F. P. (2019). Wnt signaling and biological therapy in rheumatoid arthritis and spondyloarthritis. *Int. J. Mol. Sci.* 20:5552. doi: 10.3390/ijms20225552

Cong, F., Wu, N., Tian, X., Fan, J., Liu, J., Song, T., et al. (2017). MicroRNA-34c promotes osteoclast differentiation through targeting LGR4. *Gene* 610, 1–8. doi: 10.1016/j.gene.2017.01.028

Elsafadi, M., Manikandan, M., Alajez, N. M., Hamam, R., Dawud, R. A., Aldahmash, A., et al. (2017). MicroRNA-4739 regulates osteogenic and adipocytic differentiation of immortalized human bone marrow stromal cells via targeting LRP3. *Stem Cell Res.* 20, 94–104. doi: 10.1016/j.scr.2017.03.001

Fordham, J. B., Guilfoyle, K., Naqvi, A. R., and Nares, S. (2016). MiR-142-3p is a RANKL-dependent inducer of cell death in osteoclasts. *Sci. Rep.* 6:24980. doi: 10.1038/srep24980

Gao, X. L., Cao, M. G., Ai, G. G., and Hu, Y. B. (2018). Mir-98 reduces the expression of HMGA2 and promotes osteogenic differentiation of mesenchymal stem cells. *Eur. Rev. Med. Pharmacol. Sci.* 22, 3311–3317. doi: 10.26355/eurrev_201806_15150

Godfrey, T. C., Wildman, B. J., Beloti, M. M., Kemper, A. G., Ferraz, E. P., Roy, B., et al. (2018). The microRNA-23a cluster regulates the developmental HoxA cluster function during osteoblast differentiation. *J. Biol. Chem.* 293, 17646–17660. doi: 10.1074/jbc.RA118.003052

Goldring, S. R. (2015). Inflammatory signaling induced bone loss. *Bone* 80, 143–149. doi: 10.1016/j.bone.2015.05.024

Gong, Y., Lu, J., Yu, X., and Yu, Y. (2016). Expression of Sp7 in Satb2-induced osteogenic differentiation of mouse bone marrow stromal cells is regulated by microRNA-27a. *Mol. Cell. Biochem.* 417, 7–16. doi: 10.1007/s11010-016-2709-y

Gravallese, E. M. (2017). Bone Wasn't Built in a day: destruction and formation of bone in the rheumatic diseases. *Trans. Am. Clin. Climatol. Assoc.* 128, 24–43.

Gu, Y., Ma, L., Song, L., Li, X., Chen, D., and Bai, X. (2017). miR-155 Inhibits Mouse Osteoblast Differentiation by Suppressing SMAD5 Expression. *Biomed. Res. Int.* 2017:1893520. doi: 10.1155/2017/1893520

Guo, K., Zhang, D., Wu, H., Zhu, Q., Yang, C., and Zhu, J. (2018). MiRNA-199a-5p positively regulated RANKL-induced osteoclast differentiation by target Mafb protein. *J. Cell Biochem.* doi: 10.1002/jcb.27968 [Online ahead of print]

Guo, Q., Wang, Y., Xu, D., Nossent, J., Pavlos, N. J., and Xu, J. (2018). Rheumatoid arthritis: pathological mechanisms and modern pharmacologic therapies. *Bone Res.* 6:15. doi: 10.1038/s41413-018-0016-9

Guo, Y., Li, L., Gao, J., Chen, X., and Sang, Q. (2017). miR-214 suppresses the osteogenic differentiation of bone marrow-derived mesenchymal stem cells and these effects are mediated through the inhibition of the JNK and p38 pathways. *Int. J. Mol. Med.* 39, 71–80. doi: 10.3892/ijmm.2016.2826

He, G., Chen, J., and Huang, D. (2019). miR-877-3p promotes TGF-β1-induced osteoblast differentiation of MC3T3-E1 cells by targeting Smad7. *Exp. Ther. Med.* 18, 312–319. doi: 10.3892/etm.2019.7570

He, X., Liu, J., Liang, C., Badshah, S. A., Zheng, K., Dang, L., et al. (2019). Osteoblastic PLEKHO1 contributes to joint inflammation in rheumatoid arthritis. *EBioMedicine* 41, 538–555. doi: 10.1016/j.ebiom.2019.02.009

Hou, C., Wang, D., and Zhang, L. (2019). MicroRNA-34a-3p inhibits proliferation of rheumatoid arthritis fibroblast-like synoviocytes. *Mol. Med. Rep.* 20, 2563–2570. doi: 10.3892/mmr.2019.10516

Hrdlicka, H. C., Lee, S. K., and Delany, A. M. (2019). MicroRNAs are critical regulators of osteoclast differentiation. *Curr. Mol. Biol. Rep.* 5, 65–74. doi: 10.1007/s40610-019-0116-3

Huang, C., Geng, J., Wei, X., Zhang, R., and Jiang, S. (2016). MiR-144-3p regulates osteogenic differentiation and proliferation of murine mesenchymal stem cells by specifically targeting Smad4. *FEBS Lett.* 590, 795–807. doi: 10.1002/1873-3468.12112

Huang, J., Meng, Y., Liu, Y., Chen, Y., Yang, H., Chen, D., et al. (2016). MicroRNA-320a regulates the osteogenic differentiation of human bone marrow-derived mesenchymal stem cells by targeting HOXA10. *Cell Physiol. Biochem.* 38, 40–48. doi: 10.1159/000438607

Jia, X., Wang, X., Guo, X., Ji, J., Lou, G., Zhao, J., et al. (2019). MicroRNA-124: an emerging therapeutic target in cancer. *Cancer Med.* 8, 5638–5650. doi: 10.1002/cam4.2489

Karmakar, S., Kay, J., and Gravallese, E. M. (2010). Bone damage in rheumatoid arthritis: mechanistic insights and approaches to prevention. *Rheum. Dis. Clin. North Am.* 36, 385–404. doi: 10.1016/j.rdc.2010.03.003

Kim, J. H., and Kim, N. (2016). Signaling pathways in osteoclast differentiation. *Chonnam. Med. J.* 52, 12–17. doi: 10.4068/cmj.2016.52.1.12

Lee, W. S., Yasuda, S., Kono, M., Kudo, Y., Shimamura, S., Kono, M., et al. (2020). MicroRNA-9 ameliorates destructive arthritis through down-regulation of NF-κB1-RANKL pathway in fibroblast-like synoviocytes. *Clin. Immunol.* 212:108348. doi: 10.1016/j.clim.2020.108348

Li, T., Li, H., Wang, Y., Li, T., Fan, J., Xiao, K., et al. (2016). microRNA-23a inhibits osteogenic differentiation of human bone marrow-derived mesenchymal stem cells by targeting LRP5. *Int. J. Biochem. Cell Biol.* 72, 55–62. doi: 10.1016/j.biocel.2016.01.004

Li, W., Wang, X., Chang, L., and Wang, F. (2019). MiR-377 inhibits wear particle-induced osteolysis via targeting RANKL. *Cell Biol. Int.* 43, 658–668. doi: 10.1002/cbin.11143

Lin, Y., Xiao, L., Zhang, Y., Li, P., Wu, Y., and Lin, Y. (2019). MiR-26b-3p regulates osteoblast differentiation via targeting estrogen receptor α. *Genomics* 111, 1089–1096. doi: 10.1016/j.ygeno.2018.07.003

Lin, Z., Tang, Y., Tan, H., and Cai, D. (2019). MicroRNA-92a-1-5p influences osteogenic differentiation of MC3T3-E1 cells by regulating β-catenin. *J. Bone. Miner. Metab.* 37, 264–272. doi: 10.1007/s00774-018-0935-y

Liu, J., Dang, L., Wu, X., Li, D., Ren, Q., Lu, A., et al. (2019). microRNA-mediated regulation of bone remodeling: a brief review. *JBMR Plus* 3:e10213. doi: 10.1002/jbm4.10213

Liu, X. G., Zhang, Y., Ju, W. F., Li, C. Y., and Mu, Y. C. (2019). MiR-21 relieves rheumatoid arthritis in rats via targeting Wnt signaling pathway. *Eur. Rev. Med. Pharmacol. Sci.* 23, 96–103. doi: 10.26355/eurrev_201908_18635

Liu, Q., Guo, Y., Wang, Y., Zou, X., and Yan, Z. (2018). miR-98-5p promotes osteoblast differentiation in MC3T3-E1 cells by targeting CKIP-1. *Mol. Med. Rep.* 17, 4797–4802. doi: 10.3892/mmr.2018.8416

Lozano, C., Duroux-Richard, I., Firat, H., Schordan, E., and Apparailly, F. (2019). MicroRNAs: key regulators to understand osteoclast differentiation? *Front. Immunol.* 10:375. doi: 10.3389/fimmu.2019.00375

Lukac, N., Katavic, V., Novak, S., Sucur, A., Filipovic, M., Kalajzic, I., et al. (2020). What do we know about bone morphogenetic proteins and osteochondroprogenitors in inflammatory conditions? *Bone* 137:115403. doi: 10.1016/j.bone.2020.115403

Luo, J., Yang, Z., Ma, Y., Yue, Z., Lin, H., Qu, G., et al. (2016). LGR4 is a receptor for RANKL and negatively regulates osteoclast differentiation and bone resorption. *Nat. Med.* 22, 539–546. doi: 10.1038/nm.4076

Luo, Y., Cao, X., Chen, J., Gu, J., Zhao, J., and Sun, J. (2018). MicroRNA-224 suppresses osteoblast differentiation by inhibiting SMAD4. *J. Cell. Physiol.* 233, 6929–6937. doi: 10.1002/jcp.26596

Maeda, K., Kobayashi, Y., Koide, M., Uehara, S., Okamoto, M., Ishihara, A., et al. (2019). The regulation of bone metabolism and disorders by Wnt signaling. *Int. J. Mol. Sci.* 20:5525. doi: 10.3390/ijms20225525

Mao, Y., Chen, Y., Fu, Y., Guan, J., Liang, M., Zhu, Y., et al. (2020). miR-346-3p promotes osteoclastogenesis via inhibiting TRAF3 gene. *In Vitro Cell Dev. Biol. Anim.* 56, 533–542. doi: 10.1007/s11626-020-00479-w

Martino, M. M., Maruyama, K., Kuhn, G. A., Satoh, T., Takeuchi, O., Müller, R., et al. (2016). Inhibition of IL-1R1/MyD88 signalling promotes mesenchymal stem cell-driven tissue regeneration. *Nat. Commun.* 7:11051. doi: 10.1038/ncomms11051

Miller, C. H., Smith, S. M., Elguindy, M., Zhang, T., Xiang, J. Z., Hu, X., et al. (2016). RBP-J-Regulated miR-182 Promotes TNF-alpha-Induced Osteoclastogenesis. *J. Immunol.* 196, 4977–4986. doi: 10.4049/jimmunol.1502044

Moghadasi, M., Alivand, M., Fardi, M., Moghadam, K. S., and Solali, S. (2020). Emerging molecular functions of microRNA-124: cancer pathology and therapeutic implications. *Pathol. Res. Pract.* 216:152827. doi: 10.1016/j.prp.2020.152827

Najm, A., Masson, F. M., Preuss, P., Georges, S., Ory, B., Quillard, T., et al. (2020). miR-17-5p reduces inflammation and bone erosions in collagen induced arthritis mice and directly targets the JAK-STAT pathway in rheumatoid

arthritis fibroblast-like synoviocytes. *Arthritis Rheumatol.* doi: 10.1002/art.41441 [Online ahead of print]

Nakamachi, Y., Ohnuma, K., Uto, K., Noguchi, Y., Saegusa, J., and Kawano, S. (2016). MicroRNA-124 inhibits the progression of adjuvant-induced arthritis in rats. *Ann. Rheum. Dis.* 75, 601–608. doi: 10.1136/annrheumdis-2014-206417

Niu, D., Gong, Z., Sun, X., Yuan, J., Zheng, T., Wang, X., et al. (2019). miR-338-3p regulates osteoclastogenesis via targeting IKKβ gene. *In Vitro Cell Dev. Biol. Anim.* 55, 243–251. doi: 10.1007/s11626-019-00325-8

Noack, M., and Miossec, P. (2017). Selected cytokine pathways in rheumatoid arthritis. *Semin. Immunopathol.* 39, 365–383. doi: 10.1007/s00281-017-0619-z

Ohnuma, K., Kasagi, S., Uto, K., Noguchi, Y., Nakamachi, Y., Saegusa, J., et al. (2019). MicroRNA-124 inhibits TNF-alpha- and IL-6-induced osteoclastogenesis. *Rheumatol. Int.* 39, 689–695. doi: 10.1007/s00296-018-4218-7

Ono, T., Hayashi, M., Sasaki, F., and Nakashima, T. (2020). RANKL biology: bone metabolism, the immune system, and beyond. *Inflamm. Regen.* 40:2. doi: 10.1186/s41232-019-0111-3

Ormseth, M. J., Solus, J. F., Vickers, K. C., Oeser, A. M., Raggi, P., and Stein, C. M. (2015). Utility of Select Plasma MicroRNA for disease and cardiovascular risk assessment in patients with rheumatoid arthritis. *J. Rheumatol.* 42, 1746–1751. doi: 10.3899/jrheum.150232

Panagopoulos, P. K., and Lambrou, G. I. (2018). Bone erosions in rheumatoid arthritis: recent developments in pathogenesis and therapeutic implications. *J. Musculoskeletal Neuronal Interact.* 18, 304–319.

Qiang, J., Lv, T., Wu, Z., and Yang, X. (2019). Down-regulation of microRNA-142-3p inhibits the aggressive phenotypes of rheumatoid arthritis fibroblast-like synoviocytes through inhibiting nuclear factor-κB signaling. *Biosci. Rep.* 39:BSR20190700. doi: 10.1042/bsr20190700

Qin, Z., Wang, P.-Y., Su, D.-F., and Liu, X. (2016). miRNA-124 in immune system and immune disorders. *Front. Immunol.* 7:406. doi: 10.3389/fimmu.2016.00406

Qu, J., Lu, D., Guo, H., Miao, W., Wu, G., and Zhou, M. (2016). MicroRNA-9 regulates osteoblast differentiation and angiogenesis via the AMPK signaling pathway. *Mol. Cell. Biochem.* 411, 23–33. doi: 10.1007/s11010-015-2565-1

Ren, G., Sun, J., Li, M. M., Zhang, Y. D., Li, R. H., and Li, Y. M. (2018). MicroRNA-23a-5p regulates osteogenic differentiation of human bone marrow-derived mesenchymal stem cells by targeting mitogen-activated protein kinase-13. *Mol. Med. Rep.* 17, 4554–4560. doi: 10.3892/mmr.2018.8452

Reziwan, K., Sun, D., Zhang, B., and Zhao, Z. (2019). MicroRNA-1225 activates Keap1-Nrf2-HO-1 signalling to inhibit TNFα-induced osteoclastogenesis by mediating ROS generation. *Cell Biochem. Funct.* 37, 256–265. doi: 10.1002/cbf.3394

Safiri, S., Kolahi, A. A., Hoy, D., Smith, E., Bettampadi, D., Mansournia, M. A., et al. (2019). Global, regional and national burden of rheumatoid arthritis 1990-2017: a systematic analysis of the Global Burden of Disease study 2017. *Ann. Rheum. Dis.* 78, 1463–1471. doi: 10.1136/annrheumdis-2019-215920

Sanchez-Duffhues, G., Hiepen, C., Knaus, P., and Ten Dijke, P. (2015). Bone morphogenetic protein signaling in bone homeostasis. *Bone* 80, 43–59. doi: 10.1016/j.bone.2015.05.025

Schett, G., Emery, P., Tanaka, Y., Burmester, G., Pisetsky, D. S., Naredo, E., et al. (2016). Tapering biologic and conventional DMARD therapy in rheumatoid arthritis: current evidence and future directions. *Ann. Rheum. Dis.* 75, 1428–1437. doi: 10.1136/annrheumdis-2016-209201

Sharma, S. (2017). Immunomodulation: a definitive role of microRNA-142. *Dev. Comp. Immunol.* 77, 150–156. doi: 10.1016/j.dci.2017.08.001

Sugatani, T., Vacher, J., and Hruska, K. A. (2011). A microRNA expression signature of osteoclastogenesis. *Blood* 117, 3648–3657. doi: 10.1182/blood-2010-10-311415

Sun, L., Lian, J. X., and Meng, S. (2019). MiR-125a-5p promotes osteoclastogenesis by targeting TNFRSF1B. *Cell Mol. Biol. Lett.* 24, 23. doi: 10.1186/s11658-019-0146-0

Takigawa, S., Chen, A., Wan, Q., Na, S., Sudo, A., Yokota, H., et al. (2016). Role of miR-222-3p in c-Src-Mediated Regulation of Osteoclastogenesis. *Int. J. Mol. Sci.* 17:240. doi: 10.3390/ijms17020240

Tang, J., Zhang, Z., Jin, X., and Shi, H. (2018). miR-383 negatively regulates osteoblastic differentiation of bone marrow mesenchymal stem cells in rats by targeting Satb2. *Bone* 114, 137–143. doi: 10.1016/j.bone.2018.06.010

Tao, Y., Wang, Z., Wang, L., Shi, J., Guo, X., Zhou, W., et al. (2017). Downregulation of miR-106b attenuates inflammatory responses and joint damage in collagen-induced arthritis. *Rheumatology* 56, 1804–1813. doi: 10.1093/rheumatology/kex233

Tian, Z., Zhou, H., Xu, Y., and Bai, J. (2017). MicroRNA-495 Inhibits New Bone Regeneration via Targeting High Mobility Group AT-Hook 2 (HMGA2). *Med. Sci. Monit.* 23, 4689–4698. doi: 10.12659/msm.904404

Tu, X. M., Gu, Y. L., and Ren, G. Q. (2016). miR-125a-3p targetedly regulates GIT1 expression to inhibit osteoblastic proliferation and differentiation. *Exp. Ther. Med.* 12, 4099–4106. doi: 10.3892/etm.2016.3874

Valenti, M. T., Dalle Carbonare, L., and Mottes, M. (2018). Role of microRNAs in progenitor cell commitment and osteogenic differentiation in health and disease (Review). *Int. J. Mol. Med.* 41, 2441–2449. doi: 10.3892/ijmm.2018.3452

Wang, H., Cui, Y., Luan, J., Zhou, X., Li, C., Li, H., et al. (2017). MiR-5100 promotes osteogenic differentiation by targeting Tob2. *J. Bone. Miner. Metab.* 35, 608–615. doi: 10.1007/s00774-016-0799-y

Wang, H., Meng, Y., Cui, Q., Qin, F., Yang, H., Chen, Y., et al. (2016). MiR-101 Targets the EZH2/Wnt/β-Catenin the Pathway to Promote the Osteogenic Differentiation of Human Bone Marrow-Derived Mesenchymal Stem Cells. *Sci. Rep.* 6:36988. doi: 10.1038/srep36988

Wang, N., Zhou, Z., Wu, T., Liu, W., Yin, P., Pan, C., et al. (2016). TNF-α-induced NF-κB activation upregulates microRNA-150-3p and inhibits osteogenesis of mesenchymal stem cells by targeting β-catenin. *Open Biol.* 6:150258. doi: 10.1098/rsob.150258

Wang, M., Mei, L., Liu, Z., Tang, X., Wu, X., Chen, X., et al. (2020). The mechanism of Chinese herbal formula HQT in the treatment of rheumatoid arthritis is related to its regulation of lncRNA uc.477 and miR-19b. *J. Leukoc. Biol.* 108, 519–529. doi: 10.1002/jlb.3ma0620-441rrrr

Wang, S., Liu, Z., Wang, J., Ji, X., Yao, Z., and Wang, X. (2020). miR21 promotes osteoclastogenesis through activation of PI3K/Akt signaling by targeting Pten in RAW264.7 cells. *Mol. Med. Rep.* 21, 1125–1132. doi: 10.3892/mmr.2020.10938

Wang, T., Zhang, C., Wu, C., Liu, J., Yu, H., Zhou, X., et al. (2020). miR-765 inhibits the osteogenic differentiation of human bone marrow mesenchymal stem cells by targeting BMP6 via regulating the BMP6/Smad1/5/9 signaling pathway. *Stem Cell Res. Ther.* 11:62. doi: 10.1186/s13287-020-1579-0

Wang, S. N., Zhao, X. Q., Yu, B., and Wang, B. W. (2018). miR-193a inhibits osteogenic differentiation of bone marrow-derived stroma cell via targeting HMGB1. *Biochem. Biophys. Res. Commun.* 503, 536–543. doi: 10.1016/j.bbrc.2018.05.132

Wang, W., Chen, J., Hui, Y., Huang, M., and Yuan, P. (2018). Down-regulation of miR-193a-3p promotes osteoblast differentiation through up-regulation of LGR4/ATF4 signaling. *Biochem. Biophys. Res. Commun.* 503, 2186–2193. doi: 10.1016/j.bbrc.2018.08.011

Wu, M., Chen, G., and Li, Y. P. (2016). TGF-beta and BMP signaling in osteoblast, skeletal development, and bone formation, homeostasis and disease. *Bone Res.* 4:16009. doi: 10.1038/boneres.2016.9

Wu, S., Liu, W., and Zhou, L. (2016). MiR-590-3p regulates osteogenic differentiation of human mesenchymal stem cells by regulating APC gene. *Biochem. Biophys. Res. Commun.* 478, 1582–1587. doi: 10.1016/j.bbrc.2016.08.160

Xia, P., Gu, R., Zhang, W., Shao, L., Li, F., Wu, C., et al. (2019). MicroRNA-200c promotes osteogenic differentiation of human bone mesenchymal stem cells through activating the AKT/β-Catenin signaling pathway via downregulating Myd88. *J. Cell. Physiol.* 234, 22675–22686. doi: 10.1002/jcp.28834

Yan, J., Guo, D., Yang, S., Sun, H., Wu, B., and Zhou, D. (2016). Inhibition of miR-222-3p activity promoted osteogenic differentiation of hBMSCs by regulating Smad5-RUNX2 signal axis. *Biochem. Biophys. Res. Commun.* 470, 498–503. doi: 10.1016/j.bbrc.2016.01.133

Yan, S., Miao, L., Lu, Y., and Wang, L. (2019). MicroRNA-506 upregulation contributes to sirtuin 1 inhibition of osteoclastogenesis in bone marrow stromal cells induced by TNF-α treatment. *Cell Biochem. Funct.* 37, 598–607. doi: 10.1002/cbf.3436

Yan, X., Wang, H., Li, Y., Jiang, Y., Shao, Q., and Xu, W. (2018). MicroRNA-92a overexpression promotes the osteogenic differentiation of bone mesenchymal stem cells by impeding Smad6-mediated runt-related transcription factor 2 degradation. *Mol. Med. Rep.* 17, 7821–7826. doi: 10.3892/mmr.2018.8829

Yang, J., Wang, S., Wang, F., Mu, X., Qu, Y., Zhao, Z., et al. (2017). Downregulation of miR-10b promotes osteoblast differentiation through targeting Bcl6. *Int. J. Mol. Med.* 39, 1605–1612. doi: 10.3892/ijmm.2017.2955

Yang, J. X., Xie, P., Li, Y. S., Wen, T., and Yang, X. C. (2020). Osteoclast-derived miR-23a-5p-containing exosomes inhibit osteogenic differentiation by regulating Runx2. *Cell. Signal.* 70:109504. doi: 10.1016/j.cellsig.2019.109504

Zhang, S., Liu, Y., Zheng, Z., Zeng, X., Liu, D., Wang, C., et al. (2018). MicroRNA-223 Suppresses Osteoblast Differentiation by Inhibiting DHRS3. *Cell Physiol. Biochem.* 47, 667–679. doi: 10.1159/000490021

Zhao, H., Zhang, J., Shao, H., Liu, J., Jin, M., Chen, J., et al. (2017a). miRNA-340 inhibits osteoclast differentiation via repression of MITF. *Biosci. Rep.* 37:BSR20170302. doi: 10.1042/bsr20170302

Zhao, H., Zhang, J., Shao, H., Liu, J., Jin, M., Chen, J., et al. (2017b). Transforming Growth Factor β1/Smad4 signaling affects osteoclast differentiation via regulation of miR-155 expression. *Mol. Cells* 40, 211–221. doi: 10.14348/molcells.2017.2303

Zhao, R., Li, Y., Lin, Z., Wan, J., Xu, C., Zeng, Y., et al. (2016). miR-199b-5p modulates BMSC osteogenesis via suppressing GSK-3β/β-catenin signaling pathway. *Biochem. Biophys. Res. Commun.* 477, 749–754. doi: 10.1016/j.bbrc.2016.06.130

Zheng, F., Wang, F., and Xu, Z. (2019). MicroRNA-98-5p prevents bone regeneration by targeting high mobility group AT-Hook 2. *Exp. Ther. Med.* 18, 2660–2666. doi: 10.3892/etm.2019.7835

Zheng, J., Zhu, L., Iok In, I., Chen, Y., Jia, N., and Zhu, W. (2020). Bone marrow-derived mesenchymal stem cells-secreted exosomal microRNA-192-5p delays inflammatory response in rheumatoid arthritis. *Int. Immunopharmacol.* 78:105985. doi: 10.1016/j.intimp.2019.105985

Zhou, L., Qiu, M., Yang, L., Yang, L., Zhang, Y., Mu, S., et al. (2020). MicroRNA-1-3p enhances osteoblast differentiation of MC3T3-E1 cells by interacting with hypoxia-inducible factor 1 α inhibitor (HIF1AN). *Mech. Dev.* 162:103613. doi: 10.1016/j.mod.2020.103613

Zhu, Y. L., Wang, S., Ding, D. G., Xu, L., and Zhu, H. T. (2017). miR-217 inhibits osteogenic differentiation of rat bone marrow-derived mesenchymal stem cells by binding to Runx2. *Mol. Med. Rep.* 15, 3271–3277. doi: 10.3892/mmr.2017.6349

Conflict of Interest: The authors declare that the research was conducted in the absence of any commercial or financial relationships that could be construed as a potential conflict of interest.

Copyright © 2020 Zhao, Lu and He. This is an open-access article distributed under the terms of the Creative Commons Attribution License (CC BY). The use, distribution or reproduction in other forums is permitted, provided the original author(s) and the copyright owner(s) are credited and that the original publication in this journal is cited, in accordance with accepted academic practice. No use, distribution or reproduction is permitted which does not comply with these terms.

frontiers in Cell and Developmental Biology

ORIGINAL RESEARCH
published: 24 November 2020
doi: 10.3389/fcell.2020.600639

Medium-Intensity Treadmill Exercise Exerts Beneficial Effects on Bone Modeling Through Bone Marrow Mesenchymal Stromal Cells

Lingli Zhang[1], Yu Yuan[1], Wei Wu[1], Zhongguang Sun[1], Le Lei[1], Jing Fan[2], Bo Gao[2] and Jun Zou[1]**

[1] School of Kinesiology, Shanghai University of Sport, Shanghai, China, [2] Institute of Orthopedic Surgery, Xijing Hospital, Fourth Military Medical University, Xi'an, China

OPEN ACCESS

Edited by:
Changjun Li,
Central South University, China

Reviewed by:
Rui Shao,
Shanghai Jiao Tong University, China
Shaoting Fu,
Shanghai Normal University, China
Shoutao Qiu,
Shanghai Jiao Tong University, China

***Correspondence:**
Bo Gao
gaobofmmu@hotmail.com
Jun Zou
junzou@sus.edu.cn

Specialty section:
This article was submitted to Molecular Medicine, a section of the journal Frontiers in Cell and Developmental Biology

Received: *30 August 2020*
Accepted: *28 October 2020*
Published: *24 November 2020*

Citation:
Zhang L, Yuan Y, Wu W, Sun Z, Lei L, Fan J, Gao B and Zou J (2020) Medium-Intensity Treadmill Exercise Exerts Beneficial Effects on Bone Modeling Through Bone Marrow Mesenchymal Stromal Cells. Front. Cell Dev. Biol. 8:600639. doi: 10.3389/fcell.2020.600639

As a type of multipotential cells, bone marrow mesenchymal stromal cells (BMMSCs) can differentiate into chondrocytes, osteoblasts, and adipocytes under different loading condition or specific microenvironment. Previous studies have shown that BMMSCs and their lineage-differentiated progeny (for example, osteoblasts), and osteocytes are mechanosensitive in bone. The appropriate physical activity and exercise could help attenuate bone loss, effectively stimulate bone formation, increase bone mineral density (BMD), prevent the progression of osteoporosis, and reduce the risk of bone fractures. Bone morphogenetic protein (BMP) is originally discovered as a protein with heterotopic bone-inducing activity in the bone matrix that exerts a critical role in multiple stages of bone metabolism. In the present study, the medium-intensity treadmill exercise enhanced bone formation and increased *osteocalcin (OCN)* and *osteopontin (OPN)* mRNA expression as well as activation of the BMP-Smad signaling pathway *in vivo*. In order to investigate the effect of a BMP-Smad signaling pathway, we injected mice with activated enzyme inhibitors (LDN-193189HCL) and subjected the mice to treadmill exercise intervention. LDN-193189HCL attenuated the BMD and bone mass mediated by medium-intensity exercise and BMP-Smad signaling pathway.

Keywords: treadmill exercise, bone morphogenetic protein, BMP-Smad signaling pathway, bone marrow mesenchymal stromal cell, bone formation, enzyme inhibitor

INTRODUCTION

Bone is critical for the sports system. The existence and structure of bone depends completely on the formation, quantity, and activity of bone cells that are regulated by several factors, such as mechanical and chemical stimuli, receptor and signal transduction, transcription and translation, heredity, nutrition, and endocrines (Rodan, 1998). Exercise or mechanical stimulation is one of the main factors affecting bone mass; it does not

completely inhibit the loss of bone mineral content with increasing age and menopause and has a positive effect on several circulational index of bone metabolism (Smith et al., 2014). The appropriate physical activity and exercise could help attenuate bone loss, effectively stimulate bone formation, increase bone mineral density (BMD), prevent the progression of osteoporosis, and reduce the risk of bone fractures (Smith and Gilligan, 1991). The exercise can also reduce the risk of falls and increase the bone strength, flexibility, balance, and reaction time (Smith and Gilligan, 1991). Thus, exercise is known to improve bone health based on two aspects primarily by increasing the growth period of peak bone mass (PBM) in children and adolescents and maintaining or slowing down the aging (especially emphasizes the premenopausal women) with respect to bone absorption rate (Sumida et al., 2014; Winther et al., 2014; Tucker et al., 2015). Long-time high-intensity exercise or physical activity were bad for bone healthy, such as soldiers and marathon runners.

Recent studies have greatly expanded the knowledge of mechanoresponse of mesenchymal stem cells and their roles on the maintenance of bone homeostasis (Potier et al., 2010). Many studies in the mechanosensibility of bone marrow mesenchymal stromal cells (BMMSCs) have indicated central roles of BMMSCs in locomotion induced bone mass increase (Casazza et al., 2012; Shin et al., 2013; Monika et al., 2015). As a type of multipotential cells, BMMSCs can differentiate into chondrocytes, osteoblasts, and adipocytes under different loading condition (Zhang et al., 2016) or specific microenvironment. Previous studies have shown that BMMSCs and their lineage-differentiated progeny (for example, osteoblasts), and osteocytes are mechanosensitive in bone (Wang et al., 2020). And it is suggested that constant loading in an appropriate intensity is able to switch the differentiation direction of BMMSCs from adipogenesis to osteoblastogenesis (Casazza et al., 2012; Monika et al., 2015). Besides, the increase of BMMSC proliferation induced by fluid shear stress also contributes to the number of total bone cell population (Riddle et al., 2005). Accordingly, a direct connection between locomotion and enhancement of bone quality is built in light of the mechanical ability of BMMSCs. It is still unclear how these ubiquious signals arising from mechanical stimulation are perceived by BMMSCs and then how the cells respond to them. The key regulatory signals are generated during exercise and that these factors are first and foremost mechanical in nature.

The differentiation of BMMSCs toward an osteogenic lineage relies on various of signaling pathways including: Bone morphogenetic protein (BMP), IGF, NOTCH, Hedgehog and Wnt signaling (James, 2013). BMP is originally discovered as a protein with heterotopic bone-inducing activity in the bone matrix. BMPs are multi-functional growth factors that belong to the transforming growth factor beta (TGF-β) superfamily (Di et al., 2003). The signaling transduction by BMPs occurs specifically via both canonical Smad-dependent pathways (TGF-β/BMP ligands, receptors and Smads) and non-canonical Smad-independent signaling pathway (MAPK pathway) (Chen et al., 2012). Mechanical load can stimulate the activation of osteoblasts. Effective osteogenesis differentiation is highly dependent on the growth factor signals and mechanical load. It is still unclear how exercise type, intensity, duration, and frequency affect bone mass and strength. Hitherto, exercise and mechanical load promoted the expression of BMP-related target genes in osteoblasts and improved the morphological structure and mechanical properties of bone.

In order to investigate the effect of a BMP-Smad signaling pathway, we injected mice with activated enzyme inhibitors (LDN-193189HCL) and subjected the mice to treadmill exercise intervention. BMD, bone mass, the content of osteoblasts and osteoclasts, and the index of serum and urine were tested. In this study, we aimed to investigate the influence of exercise on bone metabolism in mice with or without the inhibition of BMP-Smad signaling pathway.

MATERIALS AND METHODS

Treatment of Animals

Twelve 2-month-old C57BL/6 male mice were randomly divided into two groups with six mice in each group: control group (Control), and exercise group (Exercise) in part one experiment. Exercise group was assigned treadmill running for 5 weeks, 6 days per week. The exercise program was adapted from previous studies (Mehl et al., 2005; Ferreira et al., 2007). Briefly, the mice were trained on a treadmill (**Figure 1A**). The speed of exercise group was equivalent to 85% maximal oxygen uptake (VO_{2max}).

Seventy-two 7-week-old C57BL/6 male mice were divided into four groups in accordance with weight and BMD of mice with 18 mice in each group: control group (C), exercise group (E), LDN group (LDN+C), and exercise with LDN group (LDN+E) in part two experiment. Mice in the exercise group and exercise with LDN group were assigned treadmill running exercise at intensities for 6 weeks, 6 days per week (**Figure 2A**).

All mice were maintained at five mice per cage, and provided food and water *ad libitum*. All mice were housed in an environment maintained on a 12-h light–dark cycle at 22 ± 2°C. All the mice were anesthetized with ether inhalation the animals were euthanized by cervical vertebra dislocation.

LDN-193189HCL Injection

Mice in the LDN groups were injected with LDN (LDN-193189HCL, Selleckchem) on Wednesday from the third to sixth week by intraperitoneal injection (Yu et al., 2008a; Lee et al., 2011; Katagiri and Tsukamoto, 2013). LDN (3 mg/kg body weight) was mixed with DMSO and slowly added this DMSO liquor into physiological saline. LDN powder was completely dissolved using water bath ultrasonic and dissolved by 0.22 μm filter. Each mouse was weighed before injecting and the doses of LDN were adjusted.

Calcein Injection

A 20.0 mg calcein was mixed with 5 ml 4% $NaHCO_3$ (PH: 8.0–8.5) and 5 ml stroke-physiological saline solution. Mouse bones were labeled with subcutaneously injected calcein (5 μl/g) at day 1 and 8 before the mice were killed at day 9.

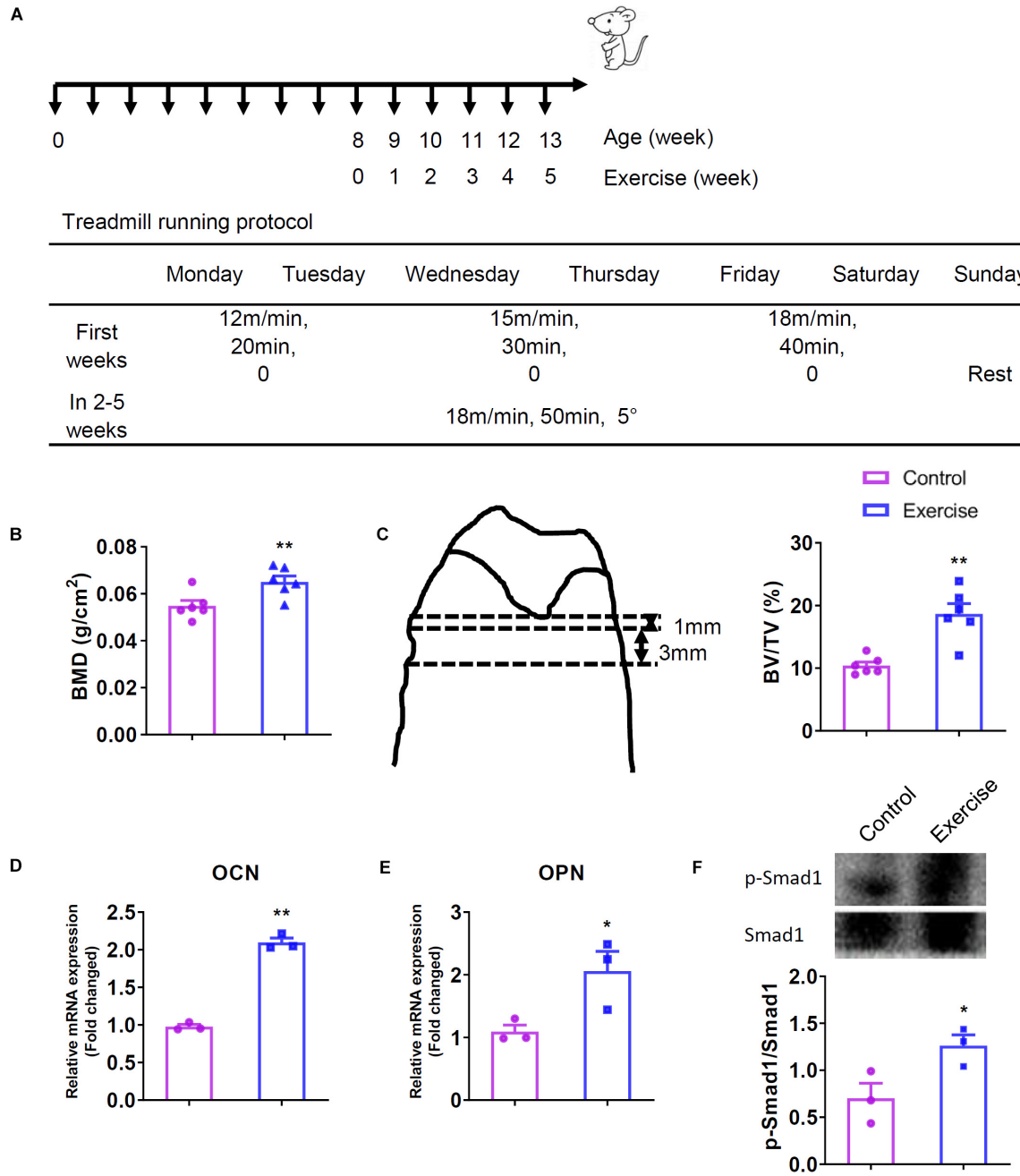
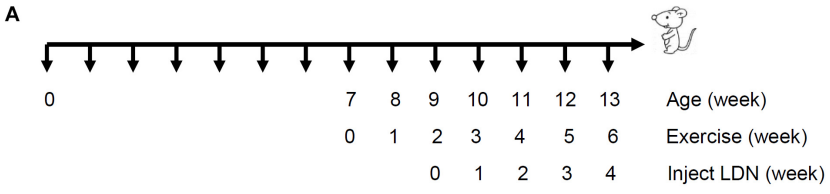


FIGURE 1 | Exercise increased bone mineral density (BMD) and trabecular bone volume (BV/TV) of the femurs and activated bone morphogenetic protein signaling (BMPS) pathway. Mice were exercised for 5 weeks and then killed. The femurs of these mice were used for BMD and bone mass determination, and tibias were used for evaluating the mRNA expression and protein activation. **(A)** Treadmill running protocol. **(B)** BMD values of mice ($n = 6$). **(C)** The area of bone histomorphometry was used for calculating the bone mass and BV/TV values of mice ($n = 6$). **(D)** *OCN* mRNA expression of mice ($n = 3$). **(E)** *OPN* mRNA expression of mice ($n = 3$). **(F)** Activation of Smad1 proteins in mice ($n = 3$). $^*P < 0.05$, $^{**}P < 0.01$ as compared to the control group.

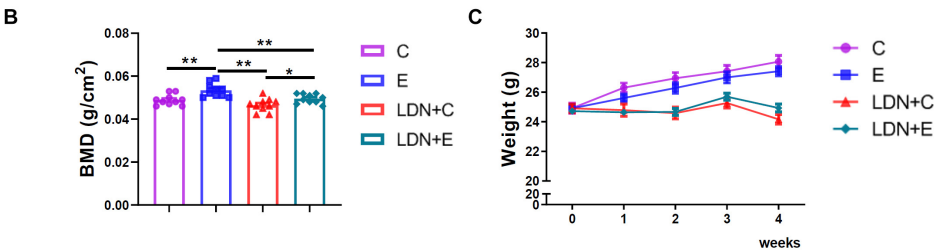
BMMSCs Cultures and ALP Staining

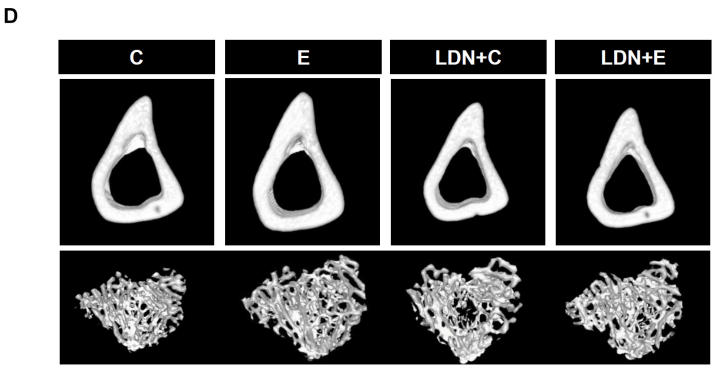
The femurs of mice were used for BMMSCs extraction and culture. The bone marrow cells were washed out with α-MEM (HyClone, United States). After being centrifuged at 1000 rpm for 10 min, the pellets were resuspended in α-MEM supplemented with 10% fetal bovine serum (FBS) (Gibco, United States), and 1% penicillin-streptomycin (Invitrogen, United States). The cells were seeded at a density of 5×10^6 cells/well in 12-well plates. Alkaline phosphatase (ALP) staining was performed 7 days after seeding (Sigma-Aldrich ALP stain kit, United States), and images were captured using a microscope (Nikon Eclipse 90i and Nikon Elements AR 3



Treadmill running protocol

	Wednesday	Thursday	Friday	Saturday	Sunday	Monday	Tuesday
In 1-2 weeks	12m/min, 20min, 0		15m/min, 30min, 0		18m/min, 40min, 0		Rest
In 3-6 weeks	18m/min, 50min, 5°						





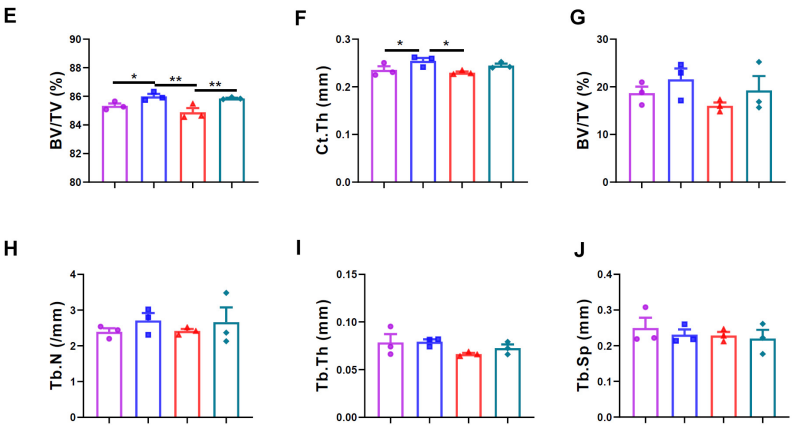


FIGURE 2 | Effects of exercise and LDN injection on mouse body weight and bone mineral density (BMD) of the femurs. Exercise increased cortical bone volume (BV/TV), and cortical thickness (Ct.Th) of tibia. Mice were exercised for 6 weeks in the presence or absence of LDN and then killed. The femurs of these mice were used for BMD determination. Body weights of mice in the four groups were recorded every week during the exercise. **(A)** Treadmill running protocol. **(B)** BMD values of mice (n = 10). **(C)** Average body weight was shown (n = 18). **(D)** Representative μCT images showed two-dimensional cortical and trabecular architecture in mouse tibia (n = 3). **(E)** Cortical bone volume per tissue volume (BV/TV). **(F)** Cortical thickness (Ct.Th). **(G)** Trabecular bone volume per tissue volume (BV/TV). **(H)** Trabecular number (Tb.N). **(I)** Trabecular thickness (Tb.Th). **(J)** Trabecular separation (Tb.Sp). $^{*}P < 0.05$, $^{**}P < 0.01$.

software, Japan). Colony-forming units (CFUs) were calculated from those images.

BMD Measurement of Total Femurs

The left femurs were used for BMD. Special attention was paid to avoiding damage of the bone cortex when removing the skin, muscles, and connective tissues. Before testing, the specimens were observed under a microscope to make sure all specimens were intact. The dual energy X-ray absorptiometry method was used for measurement of BMD (Osteocore3 Digital 2D, France) of the total left femurs.

Bone Histomorphometry

The right femurs were isolated, fixed in 4% paraformaldehyde (PFA) after washing with PBS, and then dehydrated in 70% ethanol. The specimens were dehydrated sequentially in ascending concentrations of ethanol (95%, 100%) and xylene, and then embedded in methyl methacrylate. The femurs were cut at 4-μm thickness using a microtome (Leica RM2265, Germany), transferred onto gelatin-coated slides, and dried overnight in an oven at 60°C. After the slices were stained using Masson's method, the digitizing morphometric system (Osteomeasure High Resolution Color Subsystem) was used to measure the bone histomorphometric parameters. In the present study, the region of cancellous bone measured was 1–4 mm distal to the lower margin of the growth plate in the proximal femur (**Figure 1C**). The measured parameters for cancellous bone included bone volume (BV), the total tissue volume (TV), bone surface (BS), single-labeled surfaces (sLS), double-labeled surfaces (dLS) and so on. These data were used to calculate the percent cancellous mineral apposition rate (MAR), bone formation rate/bone volume (BFR/BV), bone formation rate/total tissue volume (BFR/TV), bone formation rate/bone surface (BFR/BS), bone volume (BV/TV), trabecular number (Tb.N), trabecular thickness (Tb.Th), and trabecular separation (Tb.Sp).

μCT for BMD and Bone Histomorphometry

The right tibias were observed under a microscope to ensure all specimens were intact. After fixation with 4% PFA and dehydrated in 70% ethanol, the specimens were scanned by a μCT scanner (Skyscan 1174; Bruker, Kontich, Belgium) with acquisition settings of: 40 kVp, 555 uA, filter AL 0.5 mm, and 9 micron isotropic resolution. Bone microarchitecture parameters of cortical bone and trabecular bone were measured using the built-in software as follows: bone volume (BV/TV), cortical thickness (Ct.Th), Tb.N, Tb.Th, and Tb.Sp.

Methods for Bone Biomechanics Measurement

The three-point bending method was performed for biomechanics analysis (Reger RGM-2020, China) immediately after BMD measurement. Then, a vernier caliper was used for measurement of femoral short axis, and minor axis in the central part of the direction of Tb.Th. When testing, the proximal and distal ends of the femur were fixed on the machine pedestal, with a 12-mm span and specimens in horizontal position. The probe moved continuously down at a speed of 1 mm/min for bending test with no preload. Data including maximum load, yield stress, and elastic modulus were automatically calculated by a computer program.

Real-Time PCR

The total RNA was isolated from the left tibias of mice using TRIzol (Sigma, United States) and reverse-transcription (Revert Aid first strand cDNA Synthesis Kit, Cat.#:K1622, Thermo Scientific, United States) was conducted using 1 μg of total RNA with oligo-dT primers at 42°C for 1 h. All PCRs were performed using 2 μg of respective cDNA with SYBR Green qPCR Master Mix (Roche, Switzerland). *Osteocalcin (OCN)* mRNA, *osteopontin (OPN)* mRNA, *Osterix (OSX)* mRNA, *runt related transcription factor 2 (Runx2)* mRNA, *msh homeobox-2 (MSX2)* mRNA, *distal-less homeobox 5 (DLX5)* mRNA, and *GAPDH* mRNA were measured by quantitative testing. Quantification of mRNA was performed using Step One Plus™ Sequencing Detection System (Life Technologies, United States). The mouse primers used in this study are presented in **Table 1**.

Western Blot Assay

The total proteins were extracted from other tibias with RIPA Lysis Buffer (Biyuntian, China) containing a protease inhibitor cocktail (Roche, Switzerland). Proteins were separated by 10% SDS-PAGE with 80 to 120 V, and then transferred onto a 0.45 μm PVDF membrane (Millipore, United States) with 300 mA for 2 h. The blotting membranes were blocked with 5% skim milk powder in 1 × TBS-Tween (TBST) for 1 h. After washing with 1 × TBST three times for 10 min once, the blotting membranes incubated with phospho-Smad1 (CST, #9553), Smad1 (CST, #9743), phospho-p44/42 MAPK (CST, #5726), p44/42 MAPK (CST, #9102), phospho-p38 MAPK (CST, #9211), p38 MAPK (CST, #9212), and β-Actin (CST, #5057). The molecular weight and gray value of the target strip were analyzed by the Image J system.

TABLE 1 | RT-PCR primer Sequences.

mRNA	Primer	Sequences (5′–3′)
OCN	Forward	AGCAGGAGGGCAATAAGGTAGT
	Reverse	ACCGTAGATGCGTTTGTAGGC
OPN	Forward	CAGCCTGCACCCAGATCCTA
	Reverse	GCGCAAGGAGATTCTGCTTCT
OSX	Forward	TGGTACAAGGCAGGCATCCA
	Reverse	GGAGCAAAGTCAGATGGGTAAGT
Runx2	Forward	TTTAGGGCGCATTCCTCATC
	Reverse	TGTCCTTGTGGATTAAAAGGACTTG
MSX2	Forward	AACACAAGACCAACCGGAAG
	Reverse	GCCGTATATGGATGCTGCTT
DLX5	Forward	CACCACCCGTCTCAGGAATC
	Reverse	GCTTTGCCATAAGAAGCAGAGG
GAPDH	Forward	CCACAGTCCATGCCATCAC
	Reverse	CATACCAGGAAATGAGCTTGAC

Serum and Urine Biochemical Maker Analysis

Massage technique was used to obtain urine samples, which were stored at −80°C until further analysis. All the mice were anesthetized with ether inhalation; after blood samples were collected, the animals were euthanized by cervical vertebra dislocation. The serum samples were collected from the blood. The levels of serum calcium and phosphorus were measured by colorimetric assays (Total Calcium LiquiColor kit: Stanbio, TX, United States; inorganic phosphorus mensuration reagent kit: Shanghai, China). Urinary deoxypyridinoline (DPD) levels were measured by enzyme-linked immunosorbent assay (DPD EIA kit; METRA, San Diego, CA, United States). Urinary carboxy-terminal collagen cross-linking telopeptide of type I collagen (CTX-I) levels were measured by enzyme-linked immunosorbent assay (RatLaps^{TM} CTX-I EIA kit; Boldon, United Kingdom). Urinary creatinine (UCr) levels were measured by creatinine colorimetric assay using a creatinine mensuration reagent kit (Hubei, China).

Serum Starvation

The mouse embryo fibroblasts (MEFs) were extracted from embryo of C57BL/6 mice (Anna et al., 2014), 14–16 days pregnant. Embryo washed three times with PBS. After being detached with 0.25% trypsin-EDTA (Gibco, United States) for 30 min, the pellets were resuspended in high-MEM supplemented with 10% FBS (Gibco, United States), and 1% penicillin-streptomycin (Invitrogen, United States) at 37°C in 5%CO_2 incubator. The cells were seeded in six-well plates. When cells reached 80–90% confluence, the essential medium was changed to high-MEM supplemented 1% penicillin-streptomycin without FBS for 4 h. After 4 h, four six-well plates were divided into four groups with six wells in each group, then supplemented with 1% penicillin-streptomycin and mice serum in different groups, respectively. After 30 min, the cells were collected and used for measuring the phospho-Smad1, Smad1, and β-Actin. After 1 h, another cells were collected and used for measuring the phospho-p44/42 MAPK, p44/42 MAPK, phospho-p38 MAPK, p38 MAPK, and β-Actin.

Statistical Analysis

All the data were expressed as mean ± SEM. Two-way analysis of variance (ANOVA) was performed, and statistical differences were calculated using independent sample *T*-test. Values of $P < 0.05$ were considered statistically significant. All statistical analysis was performed by statistical software SPSS 13.0 for Windows (version 13, SPSS, Chicago, IL, United States).

RESULTS

Treadmill Exercise Increases BMD, Bone Volume of 2-Month-Old Male Mice and Activates BMP-Smad Signaling Pathway

In the present study, 2-month-old male mice undergo 5-week treadmill exercise were analyzed for BMD and bone histomorphometry. We found that treadmill exercise significantly improved bone mass and quality including BMD and BV/TV compared to control littermates (**Figures 1B,C**), and was efficient to up-regulated the expression of *OCN* and *OPN* (**Figures 1D,E**). Mechanistically, western blot analysis showed that exercise activated the Smad1 protein phosphorylation (**Figure 1F**).

Treadmill Exercise Increases BMD, Cortical Bone BV/TV and Ct.Th of Tibia, and LDN Injection Shows a Significant Effect on Mouse Body Weight

To further investigate the role of BMP signaling in treadmill exercise-induced bone formation, 7-week-old male mice were performed a 6-week round exercise and injected specific BMP singnaling inhibitor – LDN. The mice ran at the speed of 18 m/min on a 5° slope, which is categorized as medium-intensity exercise. We found that 6 weeks of medium-intensity exercise significantly increased mice BMD. BMD in the E group was significantly higher than that in the C group ($P < 0.01$), and BMD in the LDN+E group was higher than that in the LDN+C group ($P < 0.05$); four times inhibition of BMP signaling decreased the BMD that was significantly lower in the LDN+E group than that in the E group ($P < 0.01$) (**Figure 2B**). Mouse body weight was measured every week during exercise and inhibition of BMP signaling (**Table 2** and **Figure 2C**). Inhibition of BMP signaling decreased the mouse body weight; however, the exercise did not show a significant effect on mouse body weight during Inhibition of BMP signaling for 3 weeks. These results suggested that medium-intensity exercise increased the BMD in mice, whereas LDN attenuated the BMD.

Next, exercise was found to increase the cortical bone BV/TV and Ct.Th of tibia (**Figure 2D**): cortical bone BV/TV in the E group was higher than that in the C group ($P < 0.05$), cortical bone BV/TV in the LDN+E group was significantly higher than that in the LDN+C group ($P < 0.01$) (**Figure 2E**); whereas, the Ct.Th in the E group was higher than that in the C group ($P < 0.05$) (**Figure 2F**). Inhibition of BMP signaling alone did not have any effect on the bone mass of tibia (**Figures 2G–J**). The data of three-point bending experiment including maximum load, yield stress, and elastic modulus were no difference between groups (**Supplementary Figures S1A–C**).

Medium-Intensity Exercise Increases Bone Formation and Inhibits Bone Resorption, and LDN Injection Inhibits the Exercise–Mediated Bone Formation and Promotes Bone Resorption

Mouse bones were labeled with subcutaneously injected calcein (5 μL/g) at days 1 and 8. After the slices were made, the bone volume was examined using bone histomorphometry (**Figure 3A**). We found that exercise increased the bone formation and LDN injection inhibited the exercise-based improvement in the bone formation. In addition, exercise

TABLE 2 | Effects of exercise and LDN on mouse body weight.

Group	*N*	Weight (g)				
		0	1	2	3	4
C	18	24.92 ± 1.43	26.31 ± 1.33	26.94 ± 1.62	27.42 ± 1.68	28.07 ± 1.73
E	18	24.92 ± 1.13	25.61 ± 1.09	26.28 ± 1.46	27.00 ± 1.55	27.41 ± 1.24
LDN+C	18	24.91 ± 1.18	24.79 ± 1.68**	24.58 ± 1.63**	25.27 ± 1.45**	24.17 ± 1.39**$^{\Delta\Delta}$
LDN+E	18	24.72 ± 0.33	24.64 ± 0.57$^{\Delta\Delta}$	24.67 ± 0.95$^{\Delta\Delta}$	25.70 ± 0.97$^{\Delta}$	24.93 ± 1.13**$^{\Delta\Delta}$

$^{**}P < 0.01$ as compared to the C group. $^{\Delta}$ $P < 0.05$, $^{\Delta\Delta}$ $P < 0.01$ as compared to the E group.

increased the bone formation of femur: BV/TV and Tb.N in the LDN+E group were higher than those in the LDN+C group (**Figures 3B,C**), Tb.Sp in the LDN+E group was lower than that in the LDN+C group (**Figure 3E**), BFR/TV and BFR/BS in the E group were higher than those in the C group (**Figures 3H,I**). Also, we found that LDN injection inhibited the exercise-improved bone formation: BFR/BV, BFR/TV, and BFR/BS were lower in the LDN+E group than the E group ($P < 0.05$) (**Figures 3G,I**). Mice that were exercised for 6 weeks or injected with LDN alone revealed that BV/TV, Tb.N, and BFR/TV in the LDN+C group were lower than those in the E group (**Figures 3B,C,H**), while Tb.Sp in the LDN+C group was higher than that in the E group (**Figure 3E**). Tb.Th and MAR were no statistical differences (**Figures 3D,F**).

After the slices were stained using Masson's method, the femur bones of 6 mice were used for bone histomorphometry analysis (**Figure 3J**). Consequently, exercise could increase the bone formation of femur: BV/TV and Tb.N in the E group were higher than those in the C group (**Figures 3K,L**), while Tb.Sp in the E group was lower than that in the C group (**Figure 3N**). Moreover, BV/TV in the LDN+C group was lower than that in the E group (**Figure 3K**), while Tb.Sp in the LDN+C group was higher than that in the E group (**Figure 3N**) when mice were exercised for 6 weeks or injected with LDN alone. Tb.Th was no statistical difference (**Figure 3M**).

We measured the calcium and phosphorus levels in the serum and found that inhibition of BMP signaling increased these levels. The serum calcium level in the LDN+C group was significantly higher than that in the C group ($P < 0.01$) (**Figure 3O**), while the serum calcium and phosphorus levels were significantly higher in the LDN+E group than that in the E group ($P < 0.01$) (**Figures 3O,P**). The serum calcium level in the LDN+E group was significantly higher than that in the LDN+C group ($P < 0.05$) (**Figure 3O**). Importantly, we found that medium-intensity exercise significantly decreased circulating DPD and CTX-I level, indicating the inhibition effect of bone resorption potency. Moreover, Inhibition of BMP signaling could attenuate the inhibitory effect of medium-intensity exercise, indicating BMP signaling as the key modulator of treadmill exercise-induced bone remoldling. Also, the urinary DPD and CTX-I levels, two *in vivo* bone resorption markers, were measured. Exercise led to a decrease in the urine CTX-I levels, while Inhibition of BMP signaling promoted the bone resorption. DPD/Ucr in the LDN+C group was significantly higher than that in the C group ($P < 0.01$) (**Figure 3Q**); DPD/Ucr and CTX-I levels were higher in the LDN+E group than the E group ($P < 0.05$) (**Figures 3Q,R**).

Treadmill Exercise Activates Smad1 Protein Phosphorylation, and LDN Injection Inhibits the Expression of Osteoblast–Related Genes in Tibia

The mRNA expression of *OCN* was lower in the LDN+E group than the E group ($P < 0.05$) (**Figure 4A**). The mRNA expression of OSX, Runx2, MSX2, DLX5 were no statistical differences (**Figures 4B–E**). The left tibias were used for the evaluation of protein activation (**Figure 4F**). Western blot analysis with antibodies to p-Smad1 and Smad1 showed that p-Smad1 expression was higher in the E group than in the C group ($P < 0.05$) (**Figure 4G**), indicating that exercise could activate the Smad1 protein phosphorylation. Also, Smad1 expression was higher in the LDN+E group than the LDN+C group ($P < 0.05$) (**Figure 4H**), suggesting that exercise improves Smad1 protein expression. ERK expression was lower in the E group than the C group ($P < 0.05$) (**Figure 4J**). The ERK and P38 protein phosphorylation, P38 expression were no statistical differences (**Figures 4I,K,L**).

Medium Level of Exercise Increases Osteogenic Differentiation of BMMSCs and Activates Smad1 Protein Phosphorylation, and LDN Injection Inhibits Smad1 Protein Phosphorylation

To further test whether medium level treadmill exercise have impact on BMMSCs, we isolated BMMSCs followed by previously described protocal and analyzed their colony-forming and osteogenic ability. ALP staining showed that medium level treadmill exercise markedly increase osteogenic differentiation potential. What's more, inhibition of BMP signaling significantly attenuated. The ALP-positive CFU was measured, which indicated the number of osteogenic BMMSCs in the bone marrow. The medium level of exercise increased the number of osteogenic BMMSCs (**Figures 5A,B**).

Mouse embryo fibroblasts were extracted from embryo of C57BL/6 mice, 14–16 days pregnant. The essential medium was changed to high-MEM without FBS for 4 h, supplemented with mice serum in different groups, respectively. After 30 min, the cells were used for measuring the protein activity (**Figure 5C**). Exercise activated Smad1 protein phosphorylation, whereas LDN injection inhibited the Smad1 protein phosphorylation (**Figures 5D,E**). In addition, Inhibition of BMP signaling did

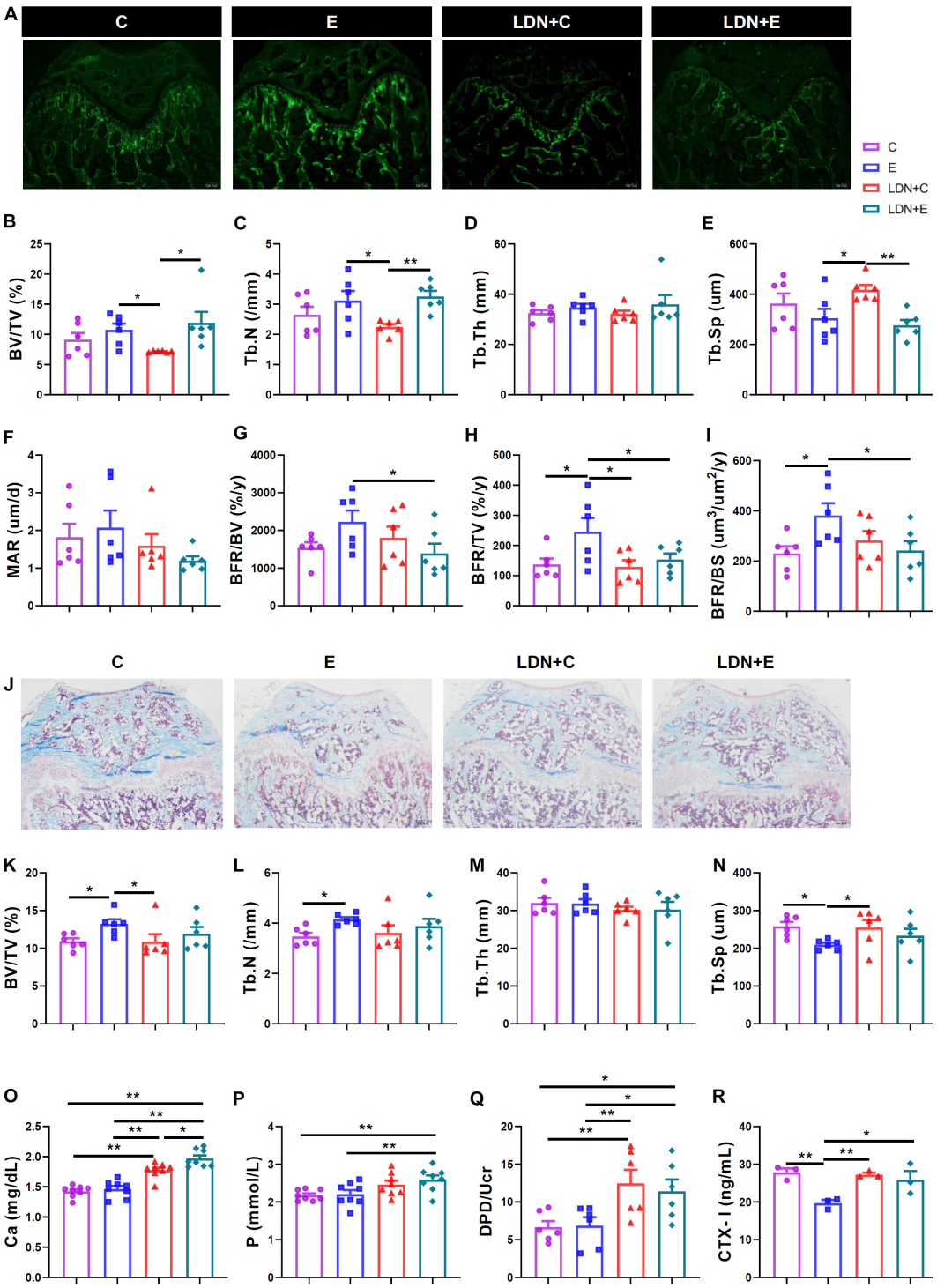


FIGURE 3 | Medium-intensity exercise increased bone formation and inhibited bone resorption, and LDN injection inhibited the exercise–mediated bone formation and promoted bone resorption. Mice were exercised for 6 weeks in the presence or absence of LDN and then killed. **(A)** Mouse bones were labeled with subcutaneously injected calcein (5 μl/g) at days 1 and 8 (n = 6). **(B)** Trabecular bone volume (BV/TV). **(C)** Trabecular number (Tb.N). **(D)** Trabecular thickness (Tb.Th). **(E)** Trabecular separation (Tb.Sp). **(F)** Mineral apposition rate (MAR) values of the four groups of mice. **(G)** Bone formation rate/bone volume (BFR/BV) values of the four groups of mice. **(H)** Bone formation rate/total tissue volume (BFR/TV) values of the four groups of mice. **(I)** Bone formation rate/bone surface (BFR/BS) values of the four groups of mice. **(J)** After the slices were stained using Masson's method, the femur bones of six mice were used for bone histomorphometry analysis (n = 6). The photos of the masson staining. **(K)** Trabecular bone volume (BV/TV). **(L)** Trabecular number (Tb.N). **(M)** Trabecular thickness (Tb.Th). **(N)** Trabecular separation (Tb.Sp). **(O)** The serum calcium level (n = 8). **(P)** The serum phosphorus level (n = 8). **(Q)** The urinary deoxypyridinoline (DPD) level (n = 6). **(R)** The urinary carboxy-terminal collagen cross-linking telopeptide of type I collagen (CTX-I) level (n = 3). $^{*}P < 0.05$, $^{**}P < 0.01$.

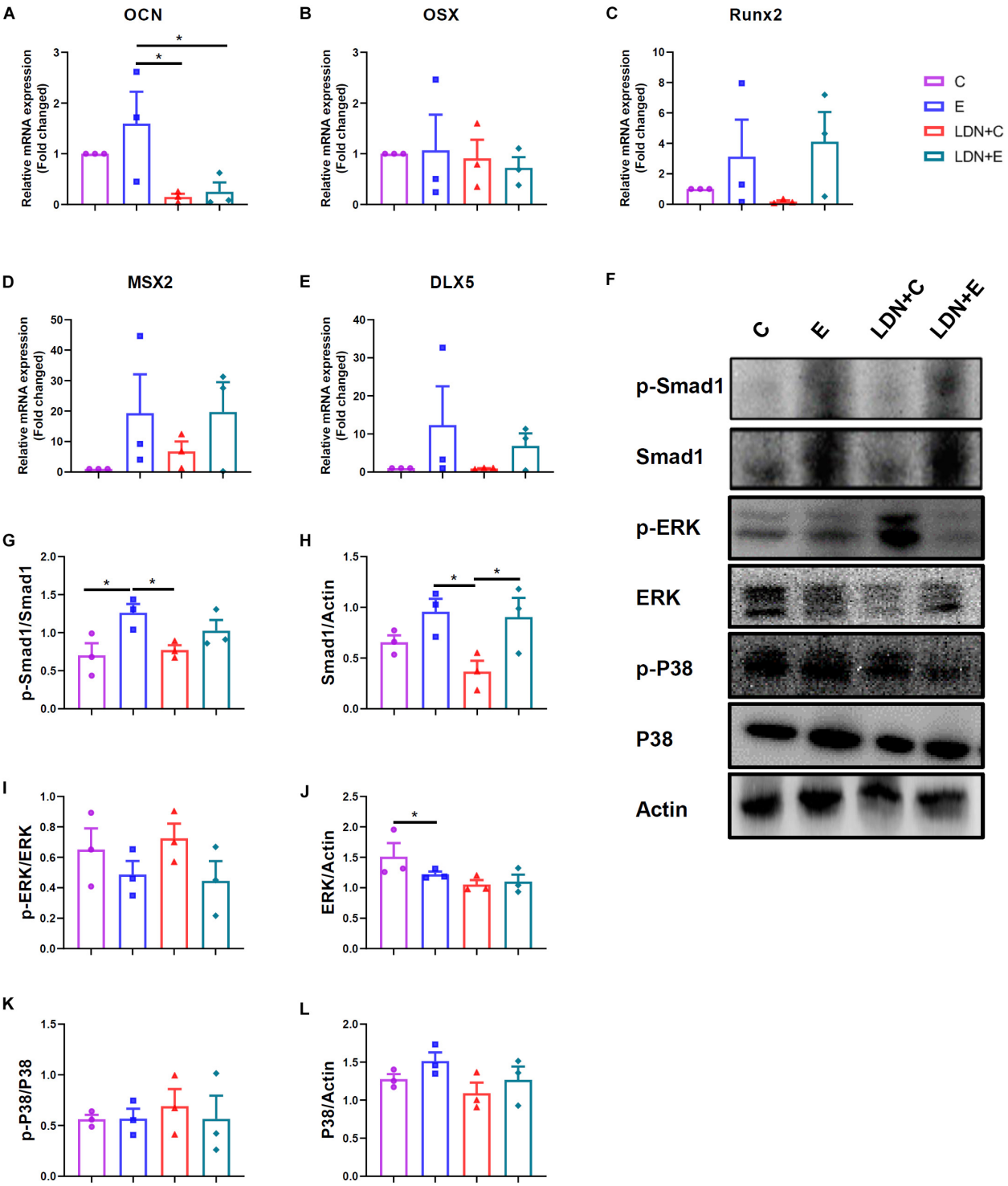


FIGURE 4 | Exercise could active Smad1 protein, and LDN injection inhibited the expression of osteoblast–related genes in tibia. Mice were exercised for 6 weeks in the presence or absence of LDN and then killed. The left tibias were used for the evaluation of gene expression and protein activation. **(A)** The mRNA expression of *OCN* ($n = 4$). **(B)** The mRNA expression of *OSX* ($n = 4$). **(C)** The mRNA expression of *Runx2* ($n = 4$). **(D)** The mRNA expression of *MSX2* ($n = 4$). **(E)** The mRNA expression of *DLX5* ($n = 4$). **(F)** Representative images of protein expression by Western blot. **(G,H)** Western blot analysis with antibodies to p-Smad1 and Smad1 ($n = 4$). **(I,J)** Western blot analysis with antibodies to p-ERK and ERK ($n = 4$). **(K,L)** Western blot analysis with antibodies to p-P38 and P38 ($n = 4$). *$P < 0.05$.

not affect the phosphorylation of P38 and ERK proteins (**Figures 5F–I**).

DISCUSSION

The medium level exercise increased BMD and BV/TV of the femurs of 2-month-old male mice, in addition, increased the expression of osteoblast-related genes (*OCN* and *OPN*), and activated the BMP-Smad signaling pathway *in vivo*. OCN collagen constitutes osteoblast synthesis and secretion and is a specific marker of bone formation (Magni et al., 2016). OPN can stimulate the osteoblast proliferation and calcification, promote the adhesion of osteoclasts and bone matrix, and improve the bone resorption (Zhang et al., 2018). BMP signaling is one of the essential pathways involved in osteogenic differentiation of BMMSCs and regulation of bone formation (Huang et al., 2018). Therefore, we hypothesized that BMP-Smad signaling pathway mediates the treadmill exercise that can regulate BMMSCs to osteoblast differentiation in mice.

Mice were exercised for 6 weeks. Firstly, at the end of 2-week exercise training, the mice body weight of the four groups did not differ significantly. This exercise training was categorized as medium-intensity exercise, and the strength was about 85% VO_{2max} (Droste et al., 2003; Kramer et al., 2006; Petzinger et al., 2013). The results

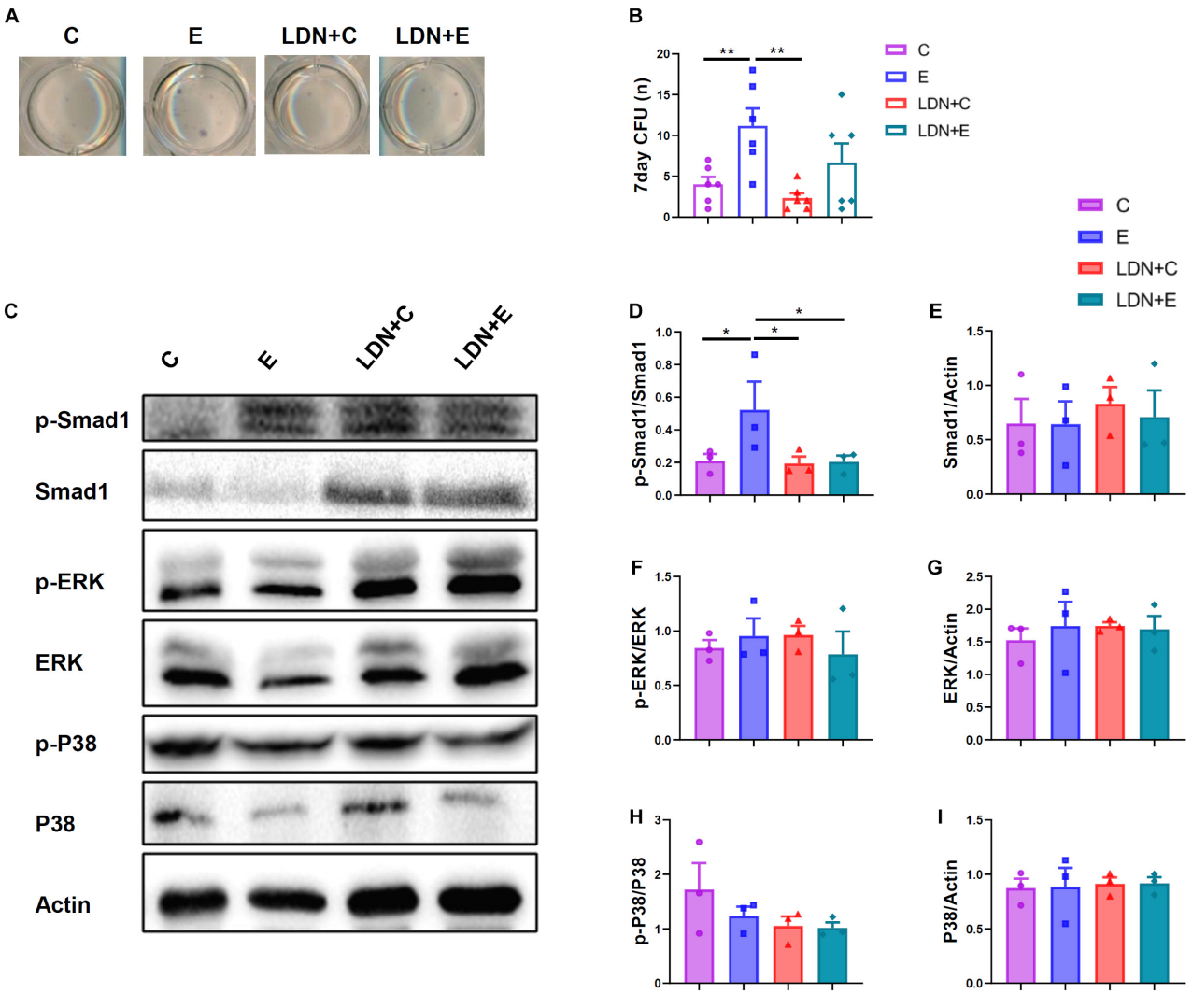


FIGURE 5 | Effects of exercise and LDN injection on the number of BMMSCs, and exercise activated Smad1 protein phosphorylation, and LDN injection inhibited Smad1 protein phosphorylation. Mice were exercised for 6 weeks in the presence or absence of LDN and then killed. The bone marrow cells were flushed out, plated, and cultured for 10 days, and then stained for ALP. **(A)** Representative images of colony-forming units (CFU) staining. **(B)** ALP quantitation results ($n = 6$). **(C)** The mouse embryo fibroblasts (MEF) were extracted from embryo of C57BL/6 mice, 14–16 days pregnant. The essential medium was changed to high-MEM without FBS, supplemented with mice serum in different groups, respectively. After 30 min, the cells were used for measuring the protein activity. Representative images of protein expression by Western blot. **(D,E)** Western blot analysis with antibodies to p-Smad1 and Smad1. **(F,G)** Western blot analysis with antibodies to p-ERK and ERK. **(H,I)** Western blot analysis with antibodies to p-P38 and P38. $^{*}P < 0.05$, $^{**}P < 0.01$.

suggested that the mice can adapt to medium-intensity treadmill exercise for 4 weeks, which is similar to that reported previously (Zhang et al., 2017). In addition, the medium level of exercise could activate Smad1 protein phosphorylation from serum starvation experiment *in vitro*; the experimental results were in agreement with previous studies. However, it did not activate P38 and ERK protein phosphorylation.

Previous studies have shown that resistance exercise stimulates bone formation and only slightly affects bone resorption (Smith et al., 2008, 2014) as exercise renders muscle tension via the mechanical stress pathways and stimulates the bone formation. But running exercise could increase the BMD of growing mice (Huang et al., 2003). After 6 weeks of exercise, the medium level of exercise significantly increased the BMD, the cortical bone volume, and Ct.Th of tibia. Furthermore, bone histomorphometry showed that the medium level of exercise led to an increase in BFR/TV, BFR/BS, trabecular bone volume, and Tb.N, accompanied by a decrease in bone separation. These results are consistent with those from previous studies, which showed that medium-intensity exercise enhanced the bone formation (Ronga et al., 2013; Smith et al., 2014; Iura et al., 2015; Li et al., 2015). There was no significant difference in maximum load, yield stress, and elastic modulus of femurs between groups, which may be due to the stable biomechanical properties of bone. Bone strength mainly includes bone mass and bone quality. Although bone mass determines about 80% of bone biomechanical strength, recent data show that BMD can't completely provide bone biomechanical index (Hasegawa et al., 2001). In addition to bone mass, it is related to the internal structure of bone such as the three-dimensional architecture of bone and the connectivity between trabeculae. Due to the stability of bone biomechanical properties, the effect of external intervention is not significant.

In addition, the ALP-positive CFU, an indication of the number of osteogenic BMMSCs in the bone marrow. Mouse ALP is frequently measured and used as a bone marker in mammalian bone research (Halling et al., 2013). The osteoblasts activity is improved with increased ALP secretion (Shen et al., 2007). Exercise stimulates the ALP production by osteogenic cells in order to increase the mineralization of the newly forming bone (Roussignol et al., 2012; Wang et al., 2018). Supposedly, the increase in bone formation and the number of osteoblasts may be mediated by the increase in the number of osteogenic BMMSCs (Zhang et al., 2017). Osteoclasts constantly resorb old bone, and osteoblasts form osteoid that is converted into mineralized bone. The urinary levels of DPD and CTX-I were bone resorption markers *in vivo* (Woitge et al., 1998; Vesper et al., 2002; Carvalho et al., 2006), and exercise leads to a decrease in the urinary levels of CTX-I. Previous studies have shown that exercise decreases the bone resorption (O'Kane et al., 2006; Kishimoto et al., 2012; Pacheco-Costa et al., 2018). These results indicated that medium level exercise suppressed bone resorption, which contributed to the increase in bone mass.

Bone morphogenetic proteins exert their diverse biological effects through two types of transmembrane receptors: BMP receptor type I (BMPR-I) and type II (BMPR-II) possess intrinsic serine/threonine kinase activity (Heldin et al., 1997). Type I and II BMP receptors are highly homologous transmembrane serine/threonine kinases. Only when two type I and two type II receptors form the heterogeneous dimers in the BMP family, they exhibit a high affinity toward the ligand. An allele-specific RNAi has been established for the mutant type I receptor, ALK2 (Lowery and Rosen, 2012). LDN-193189HCL as a BMP signaling inhibitor have been developed for the specific inhibition of BMP type I receptor-Smad1/5/8 signaling axis (Katagiri and Tsukamoto, 2013; Yu et al., 2017), inhibited the kinase ALK2 (the amino acid sequence of ALK2 login NP001103675) in mice (Lowery and Rosen, 2012). Consecutively, LDN-193189 is a potent derivative of dorsomorphin, the first chemical inhibitor explicitly identified for the receptor-induced phosphorylation of Smad1/5/8s but not the MAP kinase pathway (Yu et al., 2008b; Katagiri and Tsukamoto, 2013).

Inhibition of BMP-Smad signaling reduced the body weight in mice. Thus, LDN injection might potentially lead to weight loss by reducing bone mass. Because LDN-193189 has been shown to reduce the heterotopic bone formation in a transgenic mouse model carrying a mutant *ALK2* gene (Yu et al., 2008a; Katagiri and Tsukamoto, 2013). Furthermore, the pharmacological dose of LDN led to a slight decrease in BMD. The LDN injection further decreased the BFR/BV, BFR/TV, and BFR/BS in combination with the medium level of exercise in young mice. Moreover, the injection also decreased the osteoblast-related *OCN* mRNA expression. Activated Smads regulate the expression of transcriptional factors and transcriptional co-activators vital for osteoblasts differentiations (DLX5, Runx2, and OSX) (Chen et al., 2012). Herein, we have identified the altered expression of the BMP/Smad target gene, *DLX5*, which is an osteoblast-specific and BMP signaling specific transcription factor (Lee et al., 2003), critical for skeletal tissue development (Komori, 2019) and osteoblast differentiation (Tadic et al., 2002). Msx2 is the BMP/Smad target gene (Jovanovic et al., 2018), a homeodomain transcription factor relevant to osteoblast survival, programming (Tong and Lee, 2013), and orthotopic craniofacial bone formation (Jabs et al., 1993). The trend of *MSX2* gene expression was similar to that of *DLX5* and did not differ significantly. In addition, inhibition of BMP signaling increased the serum calcium and phosphorus levels, the bone absorption may be enhanced. The serum calcium and phosphorus levels were critical bone mineral components of the blood (Lin et al., 2012; Orcy et al., 2014). When bone is decomposed or resorbed, it releases calcium, phosphorus, and other minerals in the blood circulation. Injecting LDN could enhance bone resorption, but not significantly decrease the number of osteogenic BMMSCs. Simultaneously, it downregulates the level of Smad1 protein.

Furthermore, we found that the medium level exercise attenuated the decreasing BMD, cortical bone volume, trabecular bone volume, Tb.N, and serum calcium levels caused by LDN injection. Different intensities of exercise training affected the serum calcium levels differentially. The medium level of exercise combined with LDN injection also increased the Smad1 protein expression as compared to LDN injection alone.

DATA AVAILABILITY STATEMENT

The original contributions presented in the study are included in the article/**Supplementary Material** inquiries can be directed to the corresponding authors.

ETHICS STATEMENT

These mice in the study were purchased from the Second Military Medical University Animal Centre (Shanghai SLAC Laboratory Animal Co.) according to the protocols (Approval Number: 2007000563539) authorized by the Ethical Committee of Shanghai University of Sport on the Care and Use of Animal Subjects. We have complied with all relevant ethical regulations for animal testing and research.

AUTHOR CONTRIBUTIONS

JZ designed this study. LZ, WW, ZS, LL, and JF did the experiments. LZ and YY analyzed the experimental data. LZ and BG were responsible for manuscript writing. JZ revised the manuscript and supervised this entire program. All authors approved the final version of this manuscript.

FUNDING

This work was supported by National Natural Science Foundation of China (Nos. 81871835 and 81572242) and Shanghai Key Laboratory of Human Sport Competence Development and Maintenance (Shanghai University of Sport) (No. 11DZ2261100). The funders had no role in study design, data collection and analysis, decision to publish, or preparation of the manuscript.

SUPPLEMENTARY MATERIAL

The Supplementary Material for this article can be found online at: https://www.frontiersin.org/articles/10.3389/fcell.2020.600639/full#supplementary-material

Supplementary Figure 1 | Biomechanical parameters of bone. **(A)** Maximum load. **(B)** Yield stress. **(C)** elastic modulus.

REFERENCES

Anna, L., Xuechun, X., James, Y., Huiyi, K., Huijuan, L., Yuji, M., et al. (2014). Pdgf-aa promotes osteogenic differentiation and migration of mesenchymal stem cell by down-regulating pdgfrα and derepressing bmp-smad1/5/8 signaling. *PLoS One* 9:e113785. doi: 10.1371/journal.pone.0113785

Carvalho, D. C., Garlipp, C. R., Bottini, P. V., Afaz, S. H., Moda, M. A., and Cliquet Jr, A. (2006). Effect of treadmill gait on bone markers and bone mineral density of quadriplegic subjects. *Braz. J. Med. Biol. Res.* 39, 1357–1363. doi: 10.1590/s0100-879x2006001000012

Casazza, K., Hanks, L. J., Hidalgo, B., Hu, H. H., and Affuso, O. (2012). Short-term physical activity intervention decreases femoral bone marrow adipose tissue in young children: a pilot study. *Bone* 50, 0–27.

Chen, G., Deng, C., and Li, Y. P. (2012). Tgf-β and bmp signaling in osteoblast differentiation and bone formation. *Int. J. Biol. Sci.* 8, 272–288. doi: 10.7150/ijbs.2929

Di, C., Ming, Z., and Mundy, G. R. (2003). Bone morphogenetic proteins. *Growth Fact.* 22, 233–241.

Droste, S. K., Gesing, A., Ulbricht, S., Müller, M. B., Linthorst, A. C., and Reul, J. M. (2003). Effects of long-term voluntary exercise on the mouse hypothalamic-pituitary-adrenocortical axis. *Endocrinology* 144, 3012–3023. doi: 10.1210/en.2003-0097

Ferreira, J. C., Rolim, N. P., Bartholomeu, J. B., Gobatto, C. A., Kokubun, E., and Brum, P. C. (2007). Maximal lactate steady state in running mice: effect of exercise training. *Clin. Exp. Pharmacol. Physiol.* 34, 760–765. doi: 10.1111/j.1440-1681.2007.04635.x

Halling, L. C., Englund, U. H., Narisawa, S., Millán, J. L., and Magnusson, P. (2013). Isozyme profile and tissue-origin of alkaline phosphatases in mouse serum. *Bone* 53, 399–408. doi: 10.1016/j.bone.2012.12.048

Hasegawa, Y., Schneider, P., and Reiners, C. (2001). Age, sex, and grip strength determine architectural bone parameters assessed by peripheral quantitative computed tomography (pQCT) at the human radius. *J. Biomech.* 34, 497–503. doi: 10.1016/s0021-9290(00)00211-6

Heldin, C. H., Miyazono, K., and Ten, D. P. (1997). Tgf-beta signalling from cell membrane to nucleus through smad proteins. *Nature* 390, 465–471. doi: 10.1038/37284

Huang, H., Dou, L., Song, J., and Luo, J. (2018). Cbfa2t2 is required for bmp-2-induced osteogenic differentiation of mesenchymal stem cells. *Biochem. Biophys. Res. Commun.* 496, 1095–1101. doi: 10.1016/j.bbrc.2018.01.144

Huang, T. H., Lin, S. C., Chang, F. L., Hsieh, S. S., Liu, S. H., and Yang, R. S. (2003). Effects of different exercise modes on mineralization, structure, and biomechanical properties of growing bone. *J. Appl. Physiol.* 95, 300–307. doi: 10.1152/japplphysiol.01076.2002

Iura, A., Mcnerny, E. G., Zhang, Y., Kamiya, N., Tantillo, M., Lynch, M., et al. (2015). Mechanical loading synergistically increases trabecular bone volume and improves mechanical properties in the mouse when bmp signaling is specifically ablated in osteoblasts. *PLoS One* 10:e0141345. doi: 10.1371/journal.pone.0141345

Jabs, E. W., Müller, Ulrich, Li, Xiang, et al. (1993). A mutation in the homeodomain of the human msx2 gene in a family affected with autosomal dominant craniosynostosis. *Cell* 75, 443–450. doi: 10.1016/0092-8674(93)90379-5

James, A. W. (2013). Review of signaling pathways governing msc osteogenic and adipogenic differentiation. *Scientifica* 2013, 1–17. doi: 10.1155/2013/684736

Jovanovic, V., Salti, A., Tilleman, H., Zega, K., Jukic, M., Zou, H., et al. (2018). Bmp/smad pathway promotes neurogenesis of midbrain dopaminergic neuronsin vivoand in human induced pluripotent and neural stem cells. *J. Neuroence* 38, 1540–1517.

Katagiri, T., and Tsukamoto, S. (2013). The unique activity of bone morphogenetic proteins in bone: a critical role of the smad signaling pathway. *Biol. Chem.* 394, 703–714. doi: 10.1515/hsz-2012-0310

Kishimoto, K., Lynch, R. P., Reiger, J., and Yingling, V. R. (2012). Short-term jump activity on bone metabolism in female college-aged nonathletes. *J. Sports Sci. Med.* 11, 31–38.

Komori, T. (2019). Regulation of Proliferation, Differentiation and Functions of Osteoblasts by Runx2. *Int. J. Mol. Sci.* 20:1694. doi: 10.3390/ijms20071694

Kramer, H. F., Witczak, C. A., Fujii, N., Jessen, N., Taylor, E. B., Arnolds, D. E., et al. (2006). Distinct signals regulate as160 phosphorylation in response to insulin, aicar, and contraction in mouse skeletal muscle. *Diabetes* 55, 2067–2076. doi: 10.2337/db06-0150

Lee, M. H., Kim, Y. J., Kim, H. J., Park, H. D., Kang, A. R., and Kyung, H. M. (2003). Bmp-2-induced runx2 expression is mediated by dlx5, and tgf-beta 1 opposes the bmp-2-induced osteoblast differentiation by suppression of dlx5 expression. *J. Biol. Chem.* 278, 34387–34394. doi: 10.1074/jbc.m211386200

Lee, Y. C., Cheng, C. J., Bilen, M. A., Lu, J. F., Satcher, R. L., Yu-Lee, L. Y., et al. (2011). Bmp4 promotes prostate tumor growth in bone through osteogenesis. *Cancer Res.* 71, 5194–5203. doi: 10.1158/0008-5472.can-10-4374

Li, M., Wu, W., Tan, L., Mu, D., Zhu, D., Wang, J., et al. (2015). Low-magnitude mechanical vibration regulates expression of osteogenic proteins

in ovariectomized rats. *Biochem. Biophys. Res. Commun.* 465, 344–348. doi: 10.1016/j.bbrc.2015.07.154

Lin, C. F., Huang, T. H., Tu, K. C., Lin, L. L., Tu, Y. H., and Yang, R. S. (2012). Acute effects of plyometric jumping and intermittent running on serum bone markers in young males. *Eur. J. Appl. Physiol.* 112, 1475–1484. doi: 10.1007/s00421-011-2108-8

Lowery, J. W., and Rosen, V. (2012). Allele-specific rna interference in fop silencing the fop gene. *Gene Therapy* 19, 701–702. doi: 10.1038/gt.2011.190

Magni, P., Macchi, C., Sirtori, C. R., and Corsi Romanelli, M. M. (2016). Osteocalcin as a potential risk biomarker for cardiovascular and metabolic diseases. *Clin. Chem. Lab. Med.* 54, 1579–1587.

Mehl, K. A., Davis, J. M., Clements, J. M., Berger, F. G., Pena, M. M., and Carson, J. A. (2005). Decreased intestinal polyp multiplicity is related to exercise mode and gender in apcmin/+ mice. *J. Appl. Physiol.* 98, 2219–2225. doi: 10.1152/japplphysiol.00975.2004

Monika, M., Smieszek, A., Klaudia, C., Katarzyna, B., and Krzysztof, M. (2015). Physical activity increases the total number of bone-marrow-derived mesenchymal stem cells, enhances their osteogenic potential, and inhibits their adipogenic properties. *Stem Cells Int.* 2015, 1–11. doi: 10.1155/2015/379093

O'Kane, J. W., Hutchinson, E., Atley, L. M., and Eyre, D. R. (2006). Sport-related differences in biomarkers of bone resorption and cartilage degradation in endurance athletes. *Osteoarthr. Cartil.* 14, 71–76. doi: 10.1016/j.joca.2005.08.003

Orcy, R., Antunes, M. F., Schiller, T., Seus, T., and Böhlke, M. (2014). Aerobic exercise increases phosphate removal during hemodialysis: a controlled trial. *Hemodial. Int.* 18, 450–458. doi: 10.1111/hdi.12123

Pacheco-Costa, R., Davis, H. M., Atkinson, E. G., Dilley, J. E., Byiringiro, I., Aref, M. W., et al. (2018). Reversal of loss of bone mass in old mice treated with mefloquine. *Bone* 114, 22–31. doi: 10.1016/j.bone.2018.06.002

Petzinger, G. M., Walsh, J. P., Akopian, G., Hogg, E., Abernathy, A., Arevalo, P., et al. (2013). Effects of treadmill exercise on dopaminergic transmission in the 1-methyl-4-phenyl-1,2,3,6-tetrahydropyridine-lesioned mouse model of basal ganglia injury. *J. Neurosci.* 27, 5291–5300. doi: 10.1523/jneurosci.1069-07.2007

Potier, E., Noailly, J., and Ito, K. (2010). Directing bone marrow-derived stromal cell function with mechanics. *J. Biomech.* 43, 807–817. doi: 10.1016/j.jbiomech.2009.11.019

Riddle, R. C., Taylor, A. F., Genetos, D. C., and Donahue, H. J. (2005). Map kinase and calcium signaling mediate fluid flow-induced human mesenchymal stem cell proliferation. *AJP Cell Physiol.* 290, C776–C784.

Rodan, G. A. (1998). Bone homeostasis. *Proc. Natl. Acad. Sci. U S A.* 95, 13361–13362.

Ronga, M., Fagetti, A., Canton, G., Paiusco, E., Surace, M. F., and Cherubino, P. (2013). Clinical applications of growth factors in bone injuries: experience with bmps. *Inj. Int. J. Care Inj.* 44, S34–S39.

Roussignol, X., Currey, C., Duparc, F., and Dujardin, F. (2012). Indications and results for the exogen^{TM} ultrasound system in the management of non-union: a 59-case pilot study. *Orthopaed. Traumatol. Surg. Res.* 98, 206–213. doi: 10.1016/j.otsr.2011.10.011

Shen, C. L., Williams, J. S., Chyu, M. C., Paige, R. L., Stephens, A. L., Chauncey, K. B., et al. (2007). Comparison of the effects of tai chi and resistance training on bone metabolism in the elderly: a feasibility study. *Am. J. Chin. Med.* 35, 369–381. doi: 10.1142/s0192415x07004898

Shin, J. W., Swift, J., Ivanovska, I., Spinler, K. R., Buxboim, A., and Discher, D. E. (2013). Mechanobiology of bone marrow stem cells: from myosin-ii forces to compliance of matrix and nucleus in cell forms and fates. *Differentiation* 86, 77–86. doi: 10.1016/j.diff.2013.05.001

Smith, E. L., and Gilligan, C. (1991). Physical activity effects on bone metabolism. *Calcified Tissue Int.* 49, S50–S54.

Smith, S. M., Abrams, S. A., Davisstreet, J. E., Heer, M., O'Brien, K. O., Wastney, M. E., et al. (2014). Fifty years of human space travel: implications for bone and calcium research. *Annu. Rev. Nutr.* 34, 377–400. doi: 10.1146/annurev-nutr-071813-105440

Smith, S. M., Zwart, S. R., Heer, M., Lee, S. M. C., Baecker, N., Meuche, S., et al. (2008). Wise-2005: supine treadmill exercise within lower body negative pressure and flywheel resistive exercise as a countermeasure to bed rest-induced bone loss in women during 60-day simulated microgravity. *Bone* 42, 572–581. doi: 10.1016/j.bone.2007.11.015

Sumida, S., Iwamoto, J., Uenishi, K., and Otani, T. (2014). One-year changes in bone mineral density and bone turnover markers in premenopausal amateur runners: a prospective study. *Keio J. Med.* 63, 43–51. doi: 10.2302/kjm.2013-0010-oa

Tadic, T., Dodig, M., Erceg, I., Marijanovic, I., Mina, M., Kalajzic, Z., et al. (2002). Overexpression of dlx5 in chicken calvarial cells accelerates osteoblastic differentiation. *J. Bone Miner. Res.* 17, 1008–1014. doi: 10.1359/jbmr.2002.17.6.1008

Tong, M. L., and Lee, E. H. (2013). Transcriptional regulatory cascades in runx2-dependent bone development. *Tissue Engine. Part B Rev.* 19, 254–263. doi: 10.1089/ten.teb.2012.0527

Tucker, L. A., Strong, J. E., Lecheminant, J. D., and Bailey, B. W. (2015). Effect of two jumping programs on hip bone mineral density in premenopausal women: a randomized controlled trial. *Am. J. Health Promot.* 29, 158–164. doi: 10.4278/ajhp.130430-quan-200

Vesper, H. W., Demers, L. M., Eastell, R., Garnero, P., Kleerekoper, M., Robins, S. P., et al. (2002). Assessment and recommendations on factors contributing to preanalytical variability of urinary pyridinoline and deoxypyridinoline. *Clin. Chem.* 48, 220–235. doi: 10.1093/clinchem/48.2.220

Wang, L., You, X., Lotinun, S., Zhang, L., Wu, N., and Zou, W. (2020). Mechanical sensing protein PIEZO1 regulates bone homeostasis via osteoblast-osteoclast crosstalk. *Nat. Commun.* 11:282.

Wang, Y., Newman, M. R., and Benoit, D. S. W. (2018). Development of controlled drug delivery systems for bone fracture-targeted therapeutic delivery: a review. *Eur. J. Pharmaceut. Biopharmaceut.* 127, 223–236. doi: 10.1016/j.ejpb.2018.02.023

Winther, A., Dennison, E., Ahmed, L. A., Furberg, A. S., Grimnes, G., Jorde, R., et al. (2014). The tromsø study: fit futures: a study of norwegian adolescents' lifestyle and bone health. *Arch. Osteopor.* 9:185.

Woitge, H. W., Friedmann, B., Suttner, S., Farahmand, I., Müller, M., Schmidt-Gayk, H., et al. (1998). Changes in bone turnover induced by aerobic and anaerobic exercise in young males. *J. Bone Miner. Res.* 13, 1797–1804. doi: 10.1359/jbmr.1998.13.12.1797

Yu, P. B., Deng, D. Y., Lai, C. S., Hong, C. C., Cuny, G. D., Bouxsein, M. L., et al. (2008a). Bmp type i receptor inhibition reduces heterotopic [corrected] ossification. *Nat. Med.* 14, 1363–1369. doi: 10.1038/nm.1888

Yu, P. B., Hong, C. C., Sachidanandan, C., Babitt, J. L., Deng, D. Y., Hoyng, S. A., et al. (2008b). Dorsomorphin inhibits bmp signals required for embryogenesis and iron metabolism. *Nat. Chem. Biol.* 4, 33–41. doi: 10.1038/nchembio.2007.54

Yu, Y., Lin, Y., Yang, G., and Tian, L. (2017). The interplay between tgf-β/smad and bmp/smad signaling pathways in the epithelial mesenchymal transition of a549 cells induced by silica. *Toxicol. Mech. Methods* 28, 286–292. doi: 10.1080/15376516.2017.1407978

Zhang, J., Cai, L., Tang, L., Zhang, X., Yang, L., Zheng, K., et al. (2018). Highly dispersed lithium doped mesoporous silica nanospheres regulating adhesion, proliferation, morphology, alp activity and osteogenesis related gene expressions of bmscs. *Colloids Surf. B Biointerfaces* 170, 563–571. doi: 10.1016/j.colsurfb.2018.06.038

Zhang, L., Chen, X., Wu, J., Yuan, Y., Guo, J., Biswas, S., et al. (2017). The effects of different intensities of exercise and active vitamin D on mouse bone mass and bone strength. *J. Bone Miner. Metab.* 35, 265–277. doi: 10.1007/s00774-016-0764-9

Zhang, L., Liu, W., Zhao, J., Ma, X., Shen, L., Zhang, Y., et al. (2016). Mechanical stress regulates osteogenic differentiation and rankl/opg ratio in periodontal ligament stem cells by the wnt/β-catenin pathway. *Biochimica Biophysica Acta* 1860:2211–2219. doi: 10.1016/j.bbagen.2016.05.003

Conflict of Interest: The authors declare that the research was conducted in the absence of any commercial or financial relationships that could be construed as a potential conflict of interest.

Copyright © 2020 Zhang, Yuan, Wu, Sun, Lei, Fan, Gao and Zou. This is an open-access article distributed under the terms of the Creative Commons Attribution License (CC BY). The use, distribution or reproduction in other forums is permitted, provided the original author(s) and the copyright owner(s) are credited and that the original publication in this journal is cited, in accordance with accepted academic practice. No use, distribution or reproduction is permitted which does not comply with these terms.

frontiers in Cell and Developmental Biology

ORIGINAL RESEARCH
published: 09 December 2020
doi: 10.3389/fcell.2020.608521

BMSC-Derived Exosomal miR-29a Promotes Angiogenesis and Osteogenesis

Guo-dong Lu[1†], Peng Cheng[2†], Ting Liu[3] and Zhong Wang[1*]*

[1] Department of Cardiology, The First Affiliated Hospital of Shihezi University Medical College, Shihezi, China, [2] Division of Geriatric Endocrinology, The First Affiliated Hospital, Nanjing Medical University, Nanjing, China, [3] Department of Endocrinology, Changsha Central Hospital, Changsha, China

Angiogenesis and osteogenesis are tightly coupled during bone modeling and remodeling processes. Here we reported that bone marrow mesenchymal stem cell (BMSC)-derived exosomal miR-29a promotes angiogenesis and osteogenesis *in vitro* and *in vivo*. BMSC-derived exosomes (BMSCs-Exos) can be taken up by human umbilical vein endothelial cells (HUVECs) and promote the proliferation, migration, and tube formation of HUVECs. MiRNA-29a level was high in BMSCs-Exos and can be transported into HUVECs to regulate angiogenesis. VASH1 was identified as a direct target of miR-29a, mediating the effects of BMSC-derived exosomal miR-29a on angiogenesis. More interestingly, miR29a-loaded exosomes from engineered BMSCs (miR-29a-loaded BMSCs-Exos) showed a robust ability of promoting angiogenesis and osteogenesis *in vivo*. Taken together, these findings suggest that BMSC-derived exosomal miR-29a regulates angiogenesis and osteogenesis, and miR-29a-loaded BMSCs-Exos may serve as a potential therapeutic target for osteoporosis.

Keywords: BMSCs-exosomes, miRNA-29a, angiogenesis, osteogenesis, osteoporosis

OPEN ACCESS

Edited by:
Changjun Li,
Central South University, China

Reviewed by:
Bo Gao,
Fourth Military Medical University, China
Yu Chai,
Southern Medical University, China

****Correspondence:***
Ting Liu
2649547299@qq.com
Zhong Wang
wangzhong2014@163.com

[†]These authors have contributed equally to this work

Specialty section:
This article was submitted to Molecular Medicine, a section of the journal Frontiers in Cell and Developmental Biology

Received: *21 September 2020*
Accepted: *04 November 2020*
Published: *09 December 2020*

Citation:
Lu G, Cheng P, Liu T and Wang Z (2020) BMSC-Derived Exosomal miR-29a Promotes Angiogenesis and Osteogenesis. Front. Cell Dev. Biol. 8:608521. doi: 10.3389/fcell.2020.608521

INTRODUCTION

Bone undergoes sustained modeling and remodeling processes throughout life to ensure the integrity and structure of the skeleton (Wu et al., 2010). Angiogenesis is tightly coupled with bone formation and regeneration for proper bone homeostasis (Hui et al., 2014; Kusumbe et al., 2014; Yang et al., 2017). Recently, extracellular vesicles (EVs), such as exosomes and microvesicles, have been attracting a strong research interest for use as natural drug delivery systems (Chen et al., 2018; Tang and Wang, 2020). Mesenchymal stem cell (MSC)-derived exosomes have been reported to be involved in multiple physiology and pathology activities including osteogenesis, bone regeneration, osteoarthritis, cardiomyoblast hypoxia–reperfusion, cognitive impairment, inflammation, stroke, sepsis, and tumorigenesis (Zheng et al., 2018; Huang et al., 2020; Jin et al., 2020; Nakano et al., 2020; Tan et al., 2020; Venkat et al., 2020; Xu et al., 2020; Zou et al., 2020). Jia et al. (2020) report that exosomes secreted by young MSCs promote osteogenesis and bone formation in older rats. Liu et al. (2020) find that MSC-derived exosomes promote bone fracture healing by transferring miR-126. Zuo et al. (2019) report that bone marrow MSC (BMSC)-derived exosomes alleviate radiation-induced bone loss by activating Wnt/β-catenin signaling. However, the effects of BMSC-derived exosomes (BMSCs-Exos), especially the key microRNAs within the BMSCs-Exos, on angiogenesis and osteogenesis are not well studied.

MicroRNAs are a class of small non-coding RNAs of 19–22 nucleotides and involved in almost all cellular processes as a negative mediator of mRNA translational efficiency (Li et al., 2015). MicroRNAs post-transcriptionally decrease targeted gene expression through binding the sequence in the 3′ untranslated region (UTR) of the target mRNAs (Li et al., 2015). Recently, miRNAs were reported to be secreted and delivered into distal or local tissue and cells through circulation within exosomes (Hu et al., 2018; Vilaca-Faria et al., 2019; Song et al., 2020; Sun et al., 2020). Exosomes are EVs, with sizes arranged from 30 to 150 nm, released from multiple cell types. The functions of containing and transporting of bioactive protein, mRNAs, and miRNAs to other cells make exosomes a research hotspot of intracellular communications (Li and Tang, 2020). Recent studies report that exosomes from MSCs (Gong et al., 2017), smooth muscle cells (Zheng et al., 2017), tumor cells (Zhang et al., 2016), leukemia cells, and macrophages (Li M. et al., 2019) mediate angiogenesis. MSC-derived exosomes containing miR-30b, miR-30c, and miR-424 promote angiogenesis through targeting DLL4 (Ghosh et al., 2010; Bridge et al., 2012; Gong et al., 2017). Exosomal miR-301 derived from MSCs inhibits myocardial autophagy to protect myocardial infarction (Li Y. et al., 2019). MiR-155 within exosomes from smooth muscle cells induces endothelial injury and promotes atherosclerosis (Zheng et al., 2017). In gastric carcinoma, cell-derived microvesicles delivered miR-29a/c to suppress angiogenesis (Zhang et al., 2016). Li M. et al. (2019) report that macrophage-derived exosomes suppress the inflammation and promote the proliferation and migration of endothelial cells during wound healing. Li's group reported that human induced pluripotent stem cell-derived exosomes promote bone defect repair through enhancing angiogenesis and osteogenesis in ovariectomy-induced osteoporotic rat model (Qi et al., 2016). However, the exact molecular mechanisms responsible for the effects of BMSCs-Exos on angiogenesis and osteogenesis remain elusive.

In this study, we reported that BMSCs-Exos can be transported into endothelial cells and promote the proliferation, migration, and tube formation of endothelial cells. MiRNA-29a level was high in BMSCs-Exos and promoted angiogenesis. VASH1 was identified as a direct target of miR-29a, mediating the effects of BMSC-derived exosomal miR-29a on angiogenesis. Moreover, miR-29a-loaded BMSCs-Exos showed a strong ability to promote angiogenesis and osteogenesis *in vivo*.

MATERIALS AND METHODS

Animals and Treatment

Three-month-old male C57BL/6J mice were injected with miR-29a-loaded BMSCs-Exo, BMSCs-Exo, or phosphate-buffered saline (PBS) control *via* the tail vein (100 μg exosomes dissolved with 100 μl PBS or an equal volume of PBS) twice per week for 2 months. Then, the femurs were collected for analysis of angiogenesis and osteogenesis by immunostaining and micro-CT analysis. Animal care and experimental protocol were approved by the Animal Care and Use Committees of the Laboratory Animal Research Center at Shihezi University First Affiliated Hospital. The animals were maintained in a pathogen-free facility of the Laboratory Animal Research Center at Shihezi University First Affiliated Hospital, with free access to food and water prior to the initiation of experiments.

BMSC-Derived Exosome Isolation and Characterization

We isolated BMSC exosomes based on the protocols described previously (Ying et al., 2017). Briefly, we dissected femora from C57BL/6J mice. Then, we crushed and digested the femurs with collagenase II at 37°C for 15 min to make a single-cell suspension. The BMSCs were FACS-sorted using (Sca-$1^+CD29^+CD45^-CD11b^-$) strategy and cultured in exosome-free medium for 72 h. We collected the medium of BMSCs and centrifuged such to remove dead cells or debris. The collected medium was subjected to ultracentrifugation at 100,000 *g* for 4-6 h at 4°C after filtration with a 0.22-μm filter. The exosome-containing pellet was washed and resuspended with PBS. We characterized the exosomes by detecting the expression of exosome-specific markers syntenin 1 and TSG101 by western blot, concentration by NanoSight analysis (Particle Metrix), and size distribution and morphology by transmission electron microscopy imaging (Hitachi H7500 TEM). For the *in vitro* experiments, exosomes (2 μg of exosomes per 1×10^5 recipient cells) were added to the culture medium for 12 h, and then tube formation was measured.

Tube Formation Assay

Fifty microliters of Matrigel (BD Biosciences) was plated in 96-well culture plates and then incubated at 37°C. Human umbilical vein endothelial cells (HUVECs) were cultured on Matrigel with different exosomes or other treatments. After incubation at 37°C for 4 h, tube formation was visualized under microscopy and analyzed by measuring the cumulative tube lengths.

MTS Assay

The tetrazolium-dye-based MTS assay was used to evaluate cell growth rate as described previously (Zheng et al., 2017). In brief, 1×10^4 cells per well were seeded in triplicate into 96-well plates for 24 h. Then, the cells were treated with different treatments according to design. After treatment, the cells were washed twice with PBS and treated with 2 mg/ml Hank's buffer and incubated for 1 h. Then, the dark blue crystal should be seen under light microscopy. The crystals were dissolved in dimethyl sulfoxide, and the absorbance was measured with a Thermo Fluoroscan Ascent spectrometer at 570 nm.

Wound-Healing Assay

A total of 5×10^5 HUVECs were seeded in six-well plates. Scratch wounds were created using 100-ml sterile pipette tips when the cells grew to 95% confluence. The plates were washed twice with PBS to remove the suspended cells. Images were captured in three defined fields at 0 and 48 h, respectively.

Immunoblotting

We performed western blotting analysis as previously described (Li et al., 2016b; Li C. et al., 2017). Exosome lysates were

separated by SDS-PAGE blotted on polyvinylidene fluoride membranes (Millipore). The membranes were incubated with primary antibodies against syntenin 1(PA5-28826), TSG101 (ab125011), and VASH1 (EPR17420). All the primary antibodies were incubated at 4°C overnight, and specific proteins were visualized by enhanced chemiluminescence (ECL Kit; Amersham Biosciences).

qRT-PCR Analysis

The total RNAs were extracted by Trizol (Thermo Fisher Scientific). Qiagen miRNeasy Mini Kit was used to extract exosomal miRNAs. cDNA was prepared using the SuperScript First-Strand Synthesis System (Invitrogen) for qRT-PCR analysis by SYBR GreenMaster Mix (Qiagen). 2-CT method was used to calculate the relative expression after normalization with GAPDH and U6 (Li et al., 2016a).

Luciferase Activity Assay

Luciferase activity assays were conducted as reported previously (Yang et al., 2017). We constructed the wild-type and mutated VASH1 3′ UTR luciferase reporter plasmids with the potential binding site of miR-29a-3p and co-transfected them with miR-29a-3p mimics or miR-NC into HEK293 cells, respectively. Renilla luciferase reporter plasmids were used as internal control. The luciferase activities were measured by a Dual-Glo Luciferase Assay Kit (Promega).

Quantification and Statistical Analysis

All data are presented as mean ± SEM. For comparisons between two groups, a two-tailed Student's *t*-test was used. Comparisons between multiple groups were made using ANOVA, followed by Bonferroni post-test. All experiments were repeated at least three times, and representative experiments are shown. $p < 0.05$ was considered statistically significant.

RESULTS

BMSC-Derived Exosomes Promoted Angiogenesis

To obtain BMSCs-Exos, BMSCs were isolated from C57BL/6J mice by fluorescence-activated sorting (Sca-1^+CD29^+CD45^-CD$11b^-$) and then cultured with exosome-free medium for 72 h. The BMSCs-Exos were isolated by ultracentrifugation after the removal of dead cells and debris from the conditional medium. The exosomes were round-shaped vesicles with a bilayer membrane structure, as observed by electron microscopy (**Figure 1A**). The concentration of exosomes was around 1 to 2 × 10^{10} particles/ml, and the diameter predominantly ranged from 30 to 150 nm (**Figure 1B**). The exosome-specific protein markers (syntenin 1 and TSG 101) were highly expressed in these exosomes as evidenced by Western blotting analysis (**Figure 1C**).

Next, we tested the effects of BMSCs-Exos on angiogenesis. BMSCs-Exos and PBS control were added to the culture medium of HUVECs, respectively, for tube-like structure formation assay. The cumulative tube length was significantly longer in HUVECs treated with BMSCs-Exos compared to those treated with PBS control (**Figures 1D,E**). Furthermore, the proliferation and migration of BMSCs-Exos-treated HUVECs were dramatically increased compared to the PBS-treated control (**Figures 1F,G**). These data indicated that BMSCs-Exos promoted the proliferation and migration of endothelial cells and thus enhanced angiogenesis.

BMSC-Derived Exosomal miR-29a Transported Into Endothelial Cells

Exosomes contain and transport bioactive proteins, mRNAs, and microRNAs into distal and nearby cells. Next, we measured the angiogenesis-related miRNA (miR-19b, miR-21, miR-27, miR-29a, miR-125b, miR-126b, and miR-214) expression in BMSCs-Exos. A qPCR analysis revealed that miR-29a-3p, but not miR-29a-5p, was the most highly expressed microRNA among the detected miRNAs within BMSCs-Exos (**Figure 2A**). Thus, we chose miR-29a-3p to study. Our previous study found that exosomal miR-29a could be taken up by adipocytes, myocytes, and hepatocytes and then regulate insulin resistance (Liu T. et al., 2019). In this study, we tested whether exosomal miR-29a could be transferred into endothelial cells to affect angiogenesis. First, we tested whether BMSCs-Exos can be transferred into endothelial cells. The BMSCs-Exos were labeled with the fluorescent dye PKH26 and then added into the culture medium of HUVECs. The red fluorescence staining showed that HUVECs exhibited an efficient uptake of BMSCs-Exos (**Figure 2B**). Furthermore, after culturing with BMSCs-Exos, the miR-29a level in these recipient HUVECs was significantly higher than those cultured with PBS control (**Figure 2C**).

BMSCs-Exosomal miR-29a Promoted Angiogenesis

Next, we tested whether BMSCs-Exosomal miR-29a could regulate angiogenesis. First, miR-29a mimic was transfected into HUVECs to measure the effects of miR-29a on angiogenesis. MiR-29a level was dramatically increased in HUVECs transfected with miR-29a mimic compared to the control mimic group, indicating successful and effective transfection (**Figure 3A**). A tube-like structure formation assay showed that the cumulative tube length was significantly longer in miR-29a mimic-transfected HUVECs, in contrast to the control group (**Figures 3B,C**). As expected, HUVECs with the overexpression of miR-29a showed an enhanced ability of proliferation and migration in contrast to the control group (**Figures 3D,E**). Furthermore, BMSCs-Exos with miR-29a deficiency obtained from BMSCs with transfection of antagomir-29a were added into the culture medium of HUVECs. Consistently, BMSCs-Exos dramatically promoted tube-like structure formation, proliferation, and migration of HUVECs compared to those treated with the PBS control. However, the effects of BMSCs-Exos on angiogenesis were blunted with miR-29a deficiency in BMSCs-Exos (**Figures 3F–J**). These data indicated that miR-29a within exosomes played a key role in promoting angiogenesis by BMSCs-Exos.

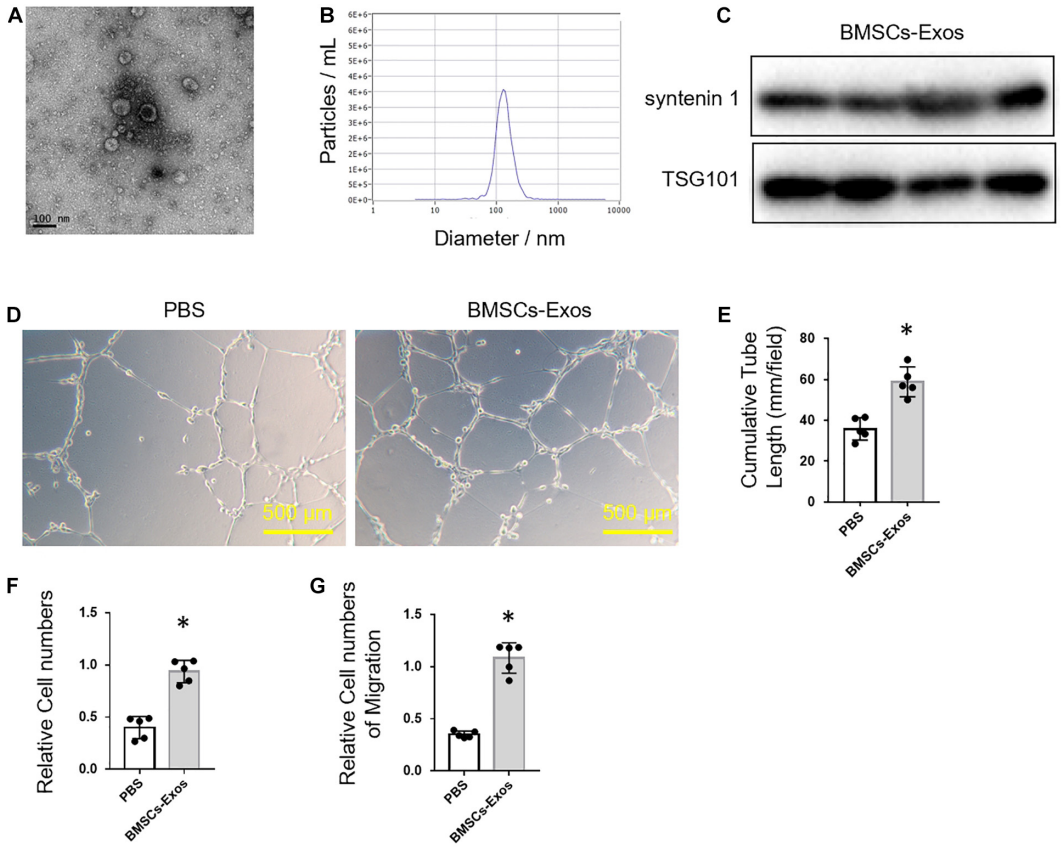


FIGURE 1 | Bone marrow mesenchymal stem cell (BMSC)-derived exosomes promoted angiogenesis. **(A)** Representative picture of BMSC-derived exosomes collected by ultracentrifugation. Scale bar: 100 nm. **(B)** Size distribution profile of BMSC-derived exosomes. **(C)** Western blot analysis of exosome-specific markers, syntenin 1 and TSG101. Representative images of tube formation **(D)** and quantitative data of cumulative tube length **(E)** of human umbilical vein endothelial cell (HUVEC) cultured with phosphate-buffered saline control or BMSCs-Exos. Scale bars, 500 μm. **(F)** MTS assay was used to detect the proliferation of HUVECs. **(G)** Wound-healing assay was used to detect the migration of HUVECs; $N = 5$. Data are presented as mean ± SEM. $^*P < 0.05$ as determined by Student's *t*-test.

BMSCs-Exosomal miR-29a Regulated Angiogenesis *via* VASH1

miRNAs bind to the amino acid coding sequence or 3′ UTRs of target genes to regulate gene expression. Target Scan was used to identify the targets of miR-29a. Among the predicted genes, we chose VASH1 for further study (**Figure 4A** and **Supplementary Table S1**). The reason that we chose VASH1 to study is that, among these target genes of miR-29a, VASH1 is a robust negative regulator of angiogenesis. Thus, we speculate that miR-29a might promote angiogenesis through post-transcriptional inhibition of VASH1. We have also listed the target genes that associated with osteogenesis and angiogenesis in **Supplementary Table S1**. The mRNA and protein levels of VASH1 were measured in HUVECs treated with miR-29a mimic or control by qPCR and western blotting analysis. miR-29a mimics downregulated VASH1 protein level but not mRNA level, indicating the post-transcriptional regulation of miR-29a on VASH1 gene (**Figures 4B,C**). A sequence analysis revealed that the binding site of miR-29a in the 3′UTR of VASH1 was from position 2244 to 2250 (**Figure 4A**). The direct binding of miR-29a on the seed region of VASH1 3′UTR was confirmed by luciferase reporter assay. Luciferase reporter constructs with wild-type 3′UTR of VASH1 (pGL3-VASH1$^{WT-3'UTR}$) was generated and transfected into HEK293 cells with co-transfection of miR-29a mimics. The analysis of luciferase enzyme activity showed that miR-29a mimics significantly suppressed the luciferase activity of VASH1 3′UTR reporter gene. However, the mutation of two nucleotides in the putative binding sites in 3′UTR of VASH1 completely abolished these effects (**Figure 4D**). Furthermore, whether VASH1 mediates the effects of miR-29a on angiogenesis was tested. HUVECs transfected with miR-29a mimics were replenished with rVASH1, and a tube-like structure formation assay was conducted. Interestingly, the effect of miR-29a mimics on tube formation was blunted with the replenishment of rVASH1 (**Figures 4E,F**). These data indicated that VASH1, as a direct target, mediated the regulation of miR-29a on angiogenesis.

BMSCs-miR-29a Exosomes Promoted Angiogenesis and Osteogenesis *in vivo*

These above *in vitro* lead us to test the effects of BMSCs-Exos and miR-29a-loaded BMSCs-Exos on angiogenesis and

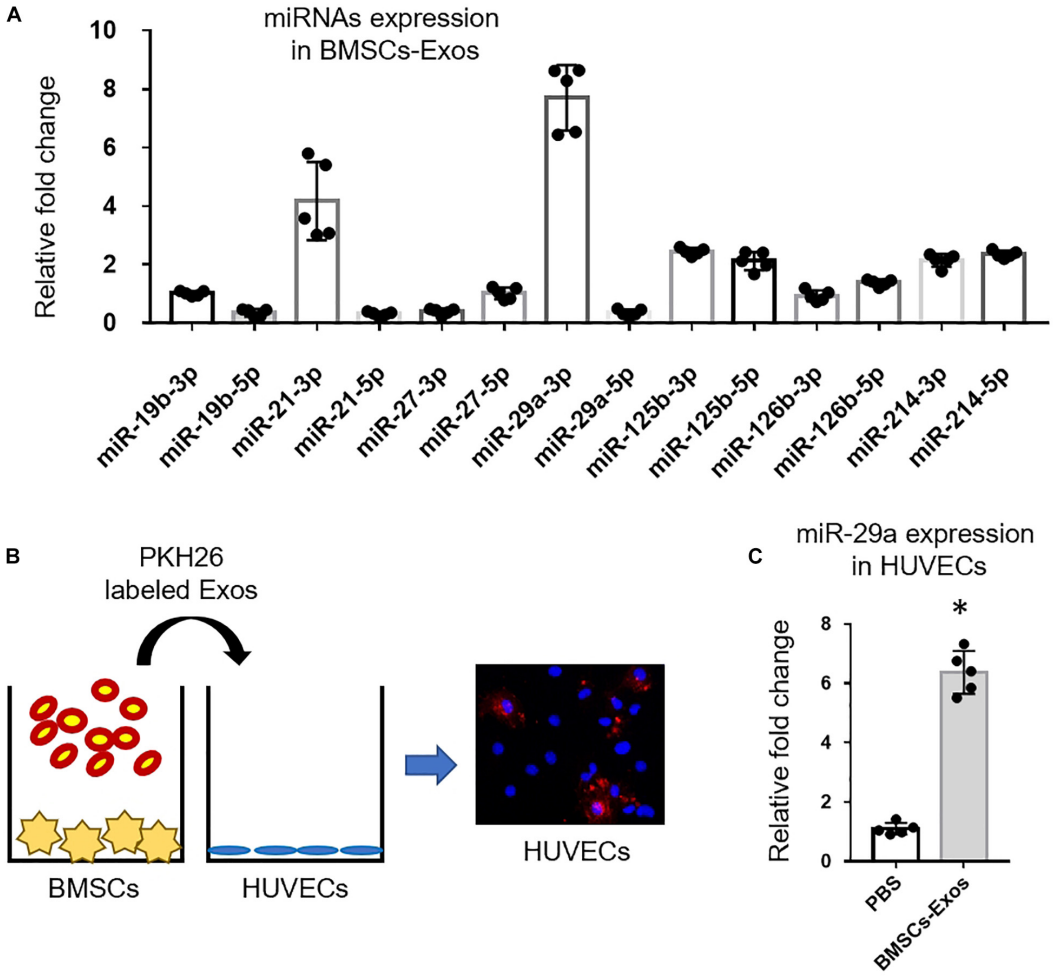


FIGURE 2 | miR-29a was increased in bone marrow mesenchymal stem cells (BMSCs)-Exo and transported into endothelial cells. **(A)** qPCR analysis of angiogenesis-related miRNA expression in BMSCs. **(B)** Exos from BMSCs were labeled with PKH26 and then added to human umbilical vein endothelial cell (HUVEC) cultures. **(C)** After treatment of BMSCs-Exos for 24 h, the levels of miR-29a in HUVECs were measured by qPCR analysis. Data are presented as mean ± SEM; $N = 5$ per group. $^*p < 0.05$, Student's *t*-test.

osteogenesis *in vivo*. First, we isolated BMSCs-Exos from an age-related osteoporotic mouse model to measure the miR-29a level within exosomes. We found that the miR-29a level was dramatically decreased in aged BMSCs-Exo compared to young BMSCs-Exo, implying that the decreased level of miR-29a in aged exosome might contribute to age-related bone loss (**Figures 5A,B**). Next, BMSCs transfected with miR-29a mimics were subjected to collect the miR-29a-loaded BMSCs-Exos. The 3-month-old mice were treated with miR-29a-loaded BMSCs-Exos, BMSCs-Exos, or PBS control for 2 months. An immunostaining analysis revealed that the number of CD31-positive endothelial cells increased in mice treated with BMSCs-Exos compared to the PBS-treated control. More interestingly, mice with treatment of miR-29a-loaded BMSCs-Exos showed a greater number of endothelial cells than BMSCs-Exo-treated mice (**Figures 5C,D**) as angiogenesis is tightly coupled with osteogenesis. Next, we measured the effects of miR-29a-loaded BMSCs-Exos on osteogenesis. As expected, mice treated with miR-29a-loaded BMSCs-Exos have a greater number of osteocalcin-positive osteoblasts in bone surface compared with BMSCs-Exos- or PBS-treated mice (**Figures 5E,F**).

miR-29a-Loaded BMSCs-Exos Increased Trabecular Bone Mass

Next, we tested the function of miR-29a-loaded BMSCs-Exos on bone mass. The 3-month-old mice were treated with miR-29a-loaded BMSCs-Exos, BMSCs-Exos, or PBS control for 2 months. A micro-CT analysis revealed that mice with treatment of BMSCs-Exos showed increased bone mineral density (BMD), trabecular bone volume (BV/TV), trabecular bone number (Tb.N), and lower trabecular separation (Tb. Sp) in contrast to the PBS-treated control. Moreover, the miR-29a-loaded BMSCs-Exos-treated mice showed additive elevation in BMD, BV/TV, and Tb.N when compared to BMSCs-Exos-treated mice (**Figures 6A–F**). We have also measured the effects of miR-29a-loaded BMSCs-Exos on cortical

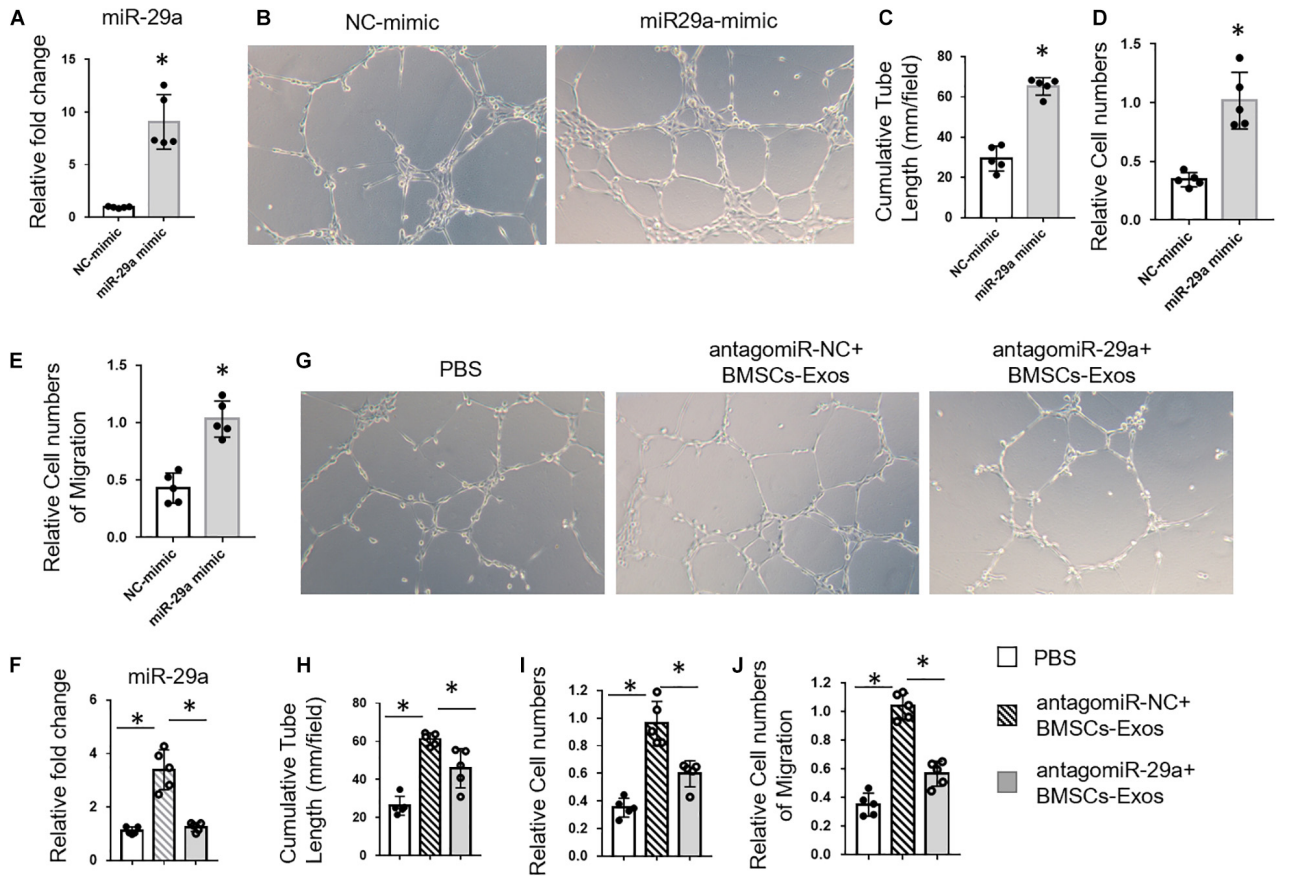


FIGURE 3 | Bone marrow mesenchymal stem cells (BMSCs)-exosomal miR-29a promoted angiogenesis. **(A)** qPCR analysis of miR-29a expression in human umbilical vein endothelial cells (HUVECs) transfected with miR-29a mimic. Representative images of tube formation **(B)** and quantitative data of cumulative tube length **(C)** of HUVECs transfected with miR-29a or control mimics. **(D)** MTS assay was used to detect the proliferation of HUVECs. **(E)** Wound-healing assay was used to detect the migration of HUVECs. **(F)** qPCR analysis of miR-29a expression in exosomes collected from BMSCs with transfection of antagomir-29a. Representative images of tube formation **(G)** and quantitative data of cumulative tube length **(H)** of HUVECs with different treatments as indicated. **(I)** MTS assay was used to detect the proliferation of HUVECs. **(J)** Wound-healing assay was used to detect the migration of HUVECs; $N = 5$. Data are presented as mean ± SEM. $^*P < 0.05$, Student's *t*-test for **(A–E)** and ANOVA for **(F–J)**.

bone phenotype. However, we did not observe a significant change in cortical bone thickness in miR-29a-loaded BMSCs-Exos-treated mice compared to BMSCs-Exos- or PBS-treated mice (**Figures 6G,H**). These data indicate that miR-29a-loaded BMSCs-Exos have a robust ability of increasing bone mass in mice.

DISCUSSION

In this study, we have shown that BMSCs-Exos promote angiogenesis and osteogenesis. BMSCs-Exos can be taken up by endothelial cells and regulate angiogenesis. BMSCs-Exos promoted the tube-like structure formation, proliferation, and migration of HUVECs. We found that the miR-29a level was high in BMSCs-Exos and played key roles in regulating angiogenesis. Downregulation of miR-29a level in BMSCs-Exos showed blunted effects on promoting angiogenesis. Furthermore, we identified that VASH1, as a direct target of miR-29a, mediated the effects of BMSCs-Exos on angiogenesis. miR-29a-loaded BMSCs-Exos have a robust ability of increasing bone mass in mice. More interestingly, we found that miR-29a level was dramatically decreased in aged BMSCs-Exos compared to young BMSCs-Exos, implying that the decreased level of miR-29a in aged exosome might contribute to age-related bone loss, and miR-29a-loaded BMSCs-Exo might be a potential way to treat age-related osteoporosis. It is worthwhile to investigate the effect of miR-29a-loaded BMSCs-Exo in aged mice in a future study.

miR-29a belongs to miR-29 family which has been reported to regulate angiogenesis (Li Z. et al., 2017). miR-29a mimics regulate the angiogenesis of gastric carcinoma cells and downregulate VEGF level (Zhang et al., 2016). Besides the endogenous regulation, miR-29a/c can be secreted into microvesicles and transported into endothelial cells to affect angiogenesis. Zhang et al. (2016) found that upregulation of miR-29a/c level in microvesicles by transfection of miR-29a/c mimics in HEK293 cells suppresses VEGF expression and angiogenesis in gastric carcinoma cells. We found that BMSCs-exosomal miR-29a

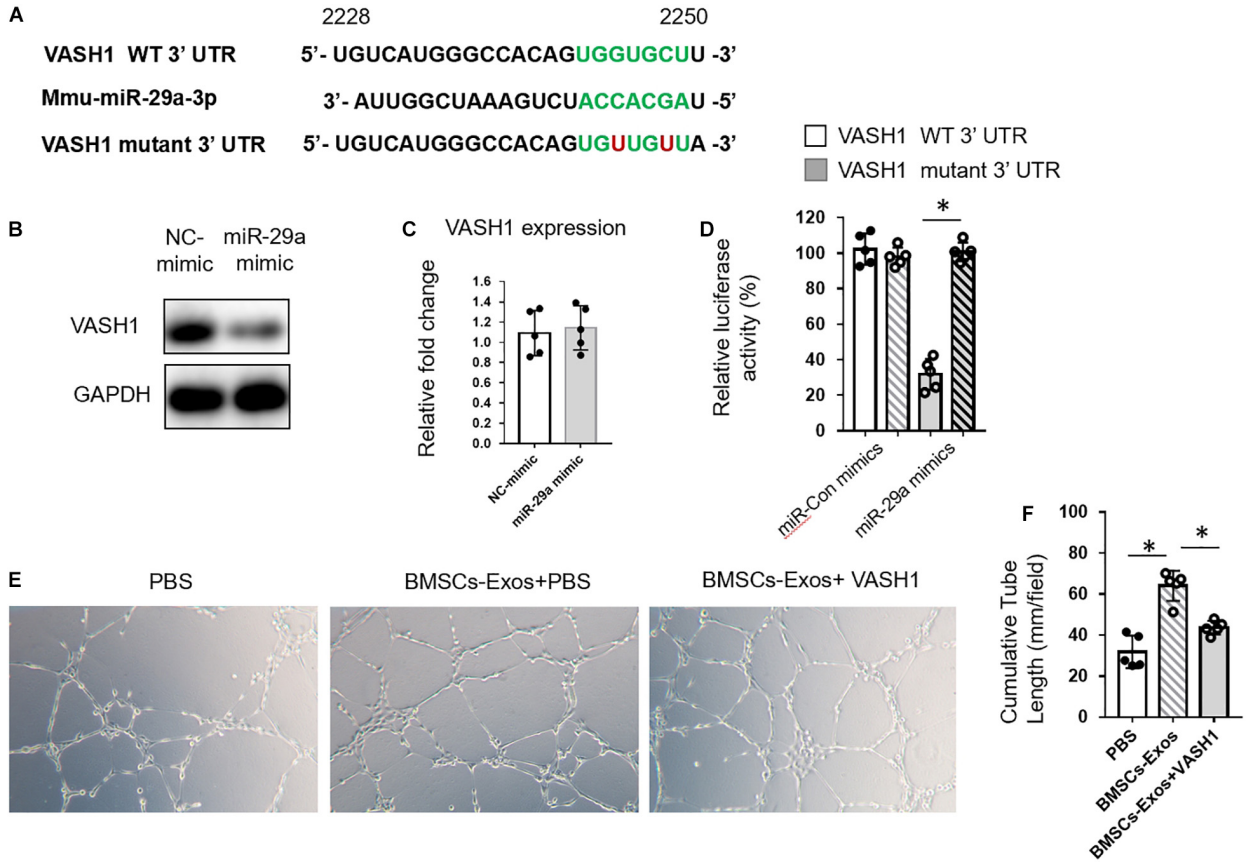


FIGURE 4 | BMSCs-exosomal miR-29a regulated angiogenesis *via* VASH1. **(A)** The miR-29a targets were predicted using TargetScan. Western blot analysis **(B)** and qPCR analysis **(C)** of VASH1 in human umbilical vein endothelial cells (HUVECs) transfected with miR-29a or control mimics. **(D)** The impact of miR-29a mimics on WT-VASH1; the mutant-VASH1 luciferase activity in 293T cells is shown. Representative images of tube formation **(E)** and quantitative data of cumulative tube length **(F)** of HUVECs with different treatments as indicated; $N = 5$. Data are presented as mean ± SEM. $^*P < 0.05$ as determined by Student's *t*-test for **(C)** and ANOVA for **(D,F)**.

promoted angiogenesis. Although we found that miR-29a within BMSCs-Exos plays a vital role in regulating angiogenesis, we cannot exclude the possibilities that other microRNAs or small molecules within exosomes also contribute to the regulation of BMSCs-Exos on angiogenesis. Zheng et al. (2017) found that miR-155 mediates endothelial injury and atherosclerosis. MSC-derived exosomes promote endothelial cell angiogenesis by transferring miR-125a (Gong et al., 2017). Thus, screening other potential components in BMSCs-Exos regulating angiogenesis is worthy of future study.

Other than MSCs, other cell types, such as smooth muscle cells, adipose tissue macrophages, and tumor cells, also secret exosomes to mediate angiogenesis. Exosomal miR-155 from smooth muscle cells has been reported to induce endothelial injury and promote atherosclerosis (Zheng et al., 2017). Ovarian cancer cell-derived PKR1-positive exosomes promote migration and tube formation of HUVECs *in vitro* (Zhang et al., 2020). Adipocytes can secret exosomes to regulate angiogenesis in diabetic mice (Wang et al., 2018). The reason we chose BMSCs to study is that as functionally and numerically dominant in bone marrow, BMSCs show robust abilities of regulating angiogenesis and osteogenesis (Li et al., 2013, 2016a, 2018; Li C. et al., 2017). The effects of BMSCs-Exos and the key components within exosome on angiogenesis and osteogenesis in mice are not well studied. Thus, in this study, we tested the function of BMSCs-Exos on angiogenesis and osteogenesis.

Type H vessel has been reported to be coupled with osteogenesis in recent years. In this study, we found that miR-29a within BMSCs-Exos promoted angiogenesis. However, among the predicted target genes of miR-29a, there is no gene reported to be involved in the signaling or pathway associated with type H vessel formation. Thus, we did not test the effects of BMSC-derived exosomal miR-29a on type H vessel formation, whereas there is a possibility that miR-29a might regulate type H vessel formation through undefined signaling or pathway. It is worthwhile to test this hypothesis in a future study.

In our study, we observed increased bone mass in mice with the treatment of miR-29a-loaded BMSCs-Exos. In this study, we focus on the effects of miR-29a-loaded BMSCs-Exos on angiogenesis. We speculate that the increased angiogenesis may contribute to the increased bone mass in response

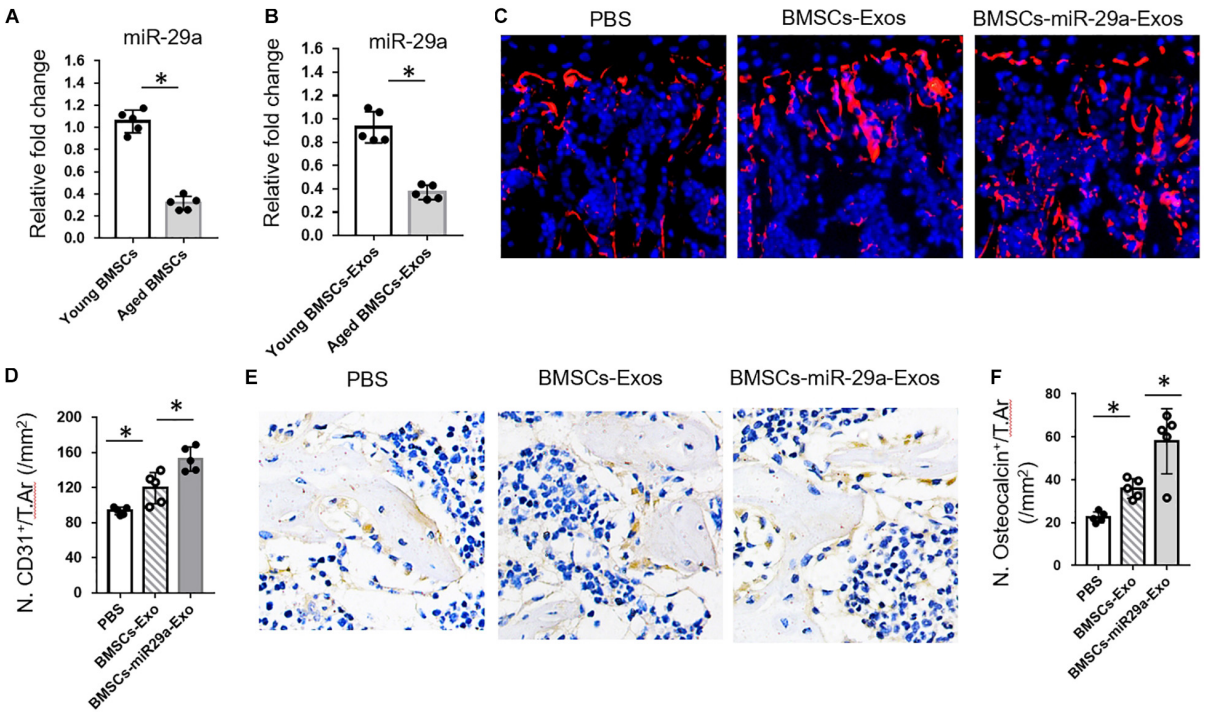


FIGURE 5 | Bone marrow mesenchymal stem cells (BMSCs)-miR-29a exosomes promoted angiogenesis and osteogenesis. **(A**,**B)** qPCR analysis of miRNA-29a-3p expression in young (3 months) and aged (18 months) BMSCs and of exosomes isolated from young and aged BMSCs. The 3-month-old mice were injected with BMSCs-Exos, BMSCs-miR29a-Exos, or phosphate-buffered saline for 2 months. **(C)** Representative images of CD31 (red) immunostaining. Nuclei, 4′,6-diamidino-2-phenylindole (blue). **(D)** Quantitative analysis of $CD31^+$ endothelial cells in distal femora. **(E)** Representative images of osteocalcin immunostaining. **(F)** Quantitative analysis of $osteocalcin^+$ osteoblasts in distal femora ($N = 5$ mice in each group). Data are mean ± SD. $^*P < 0.05$ as determined by ANOVA.

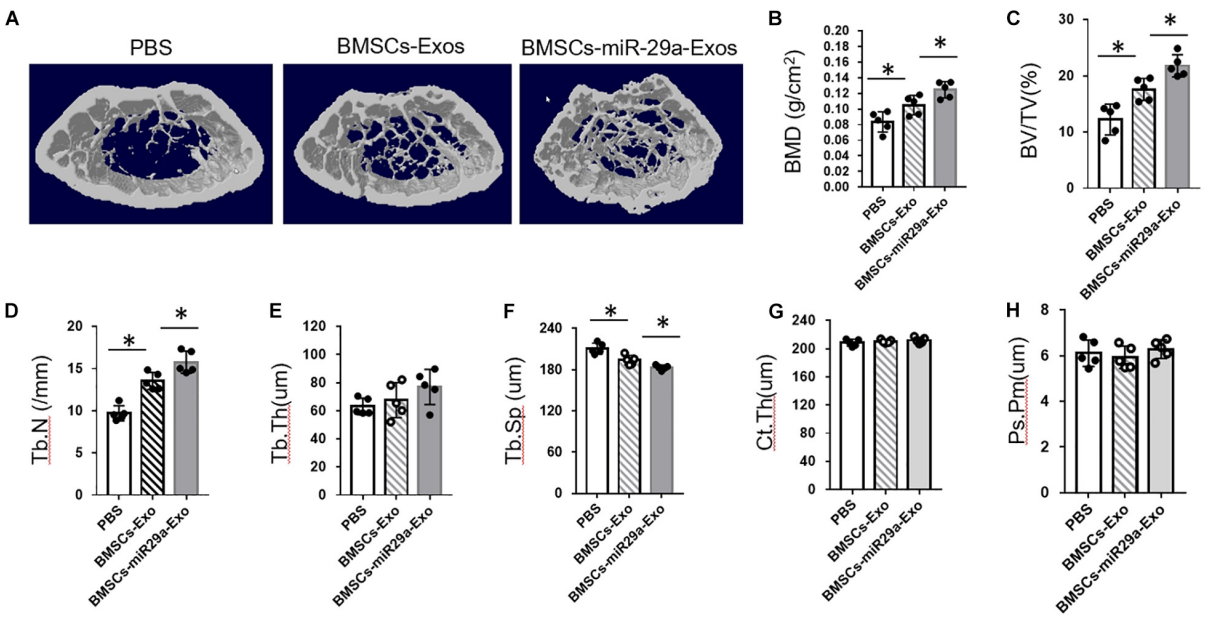


FIGURE 6 | miR-29a-loaded bone marrow mesenchymal stem cells (BMSCs)-exosomes increased trabecular bone mass. The 3-month-old female mice were injected with BMSCs-Exos, BMSCs-miR29a-Exos, or phosphate-buffered saline for 2 months. Representative micro-CT images **(A)** and quantitative micro-CT analysis **(B**–**H)** of bone mineral density, trabecular bone volume (BV/TV), trabecular bone number (Tb.N), trabecular thickness (Tb. Th), trabecular separation (Tb. Sp), cortical thickness (Ct. Th), and periosteal perimeter (Ps. Pm) in femurs ($N = 5$ mice in each group). Data are mean ± SD (ANOVA). $^*P < 0.05$ as determined by ANOVA.

to miR-29a-loaded BMSCs-Exos. However, miR-29a-loaded BMSCs-Exos may have direct effects on osteogenesis and/or osteoclastogenesis. Recent studies reported that microRNA-29a can repress osteoclastogenesis to counteract glucocorticoid-induced bone loss (Wu et al., 2019). Lian et al. (2019) found that miR-29a regulates PCAF-mediated RANKL and CXCL12 to repress osteoclast formation. MiR-29a has also been reported to regulate osteoblast differentiation of BMSCs in a high-fat environment through modulating Frizzled 4 (Liu F. et al., 2019). Thus, miR-29a-loaded BMSCs-Exos may have multiple effects on angiogenesis, osteogenesis, and osteoclastogenesis.

We did not observe a significant increase in cortical bone from mice treated with miR-29a-loaded BMSCs-Exos in contrast to those from PBS-treated mice. This may be because of the way and period of administration of exosomes. Previous studies reported that majority of exosomes accumulated in the liver and lung through tail vein injection as measured by fluorescence molecular tomography imaging system. Xie's group reported that BMSC-specific aptamer conjugated exosomes have a high efficiency of bone tissue accumulation (Luo et al., 2019). Whereas they did not show the effects of BMSC-specific aptamer conjugated exosomes' effect on cortical bone, the effects of bone tissue-targeted delivery of exosomes with a prolonged treatment time on cortical bone are an attractive topic for future study.

In this study, we found that miR29a-loaded BMSCs-Exos promote angiogenesis and osteogenesis. BMSCs-Exos promote the proliferation, migration, and tube formation of HUVECs. MiRNA-29a level was high in BMSCs-Exos and can be transported into HUVECs to regulate angiogenesis in a VASH1-dependent way. More interestingly, miR29a-loaded BMSCs-Exos have a robust ability of promoting angiogenesis and osteogenesis in mice. Thus, these findings suggest that BMSC-derived exosomal miR-29a regulates angiogenesis and osteogenesis, and miR-29a-loaded BMSCs-Exos may serve as a potential therapeutic target for osteoporosis.

DATA AVAILABILITY STATEMENT

The original contributions presented in the study are included in the article/**Supplementary Material**. Further inquiries can be directed to the corresponding author/s.

ETHICS STATEMENT

Animal care and experimental protocol were approved by the Animal Care and Use Committees of the Laboratory Animal Research Center at Shihezi University First Affiliated Hospital.

AUTHOR CONTRIBUTIONS

ZW and TL designed the experiments, supervised the experiments, analyzed results, and wrote the manuscript. GL and PC carried out most of the experiments. All authors contributed to the article and approved the submitted version.

FUNDING

This work was supported by Hunan Health Committee Scientific Research Fund of China (Grant C2019132).

SUPPLEMENTARY MATERIAL

The Supplementary Material for this article can be found online at: https://www.frontiersin.org/articles/10.3389/fcell.2020.608521/full#supplementary-material

REFERENCES

Bridge, G., Monteiro, R., Henderson, S., Emuss, V., Lagos, D., Georgopoulou, D., et al. (2012). The microRNA-30 family targets DLL4 to modulate endothelial cell behavior during angiogenesis. *Blood* 120, 5063–5072. doi: 10.1182/blood-2012-04-423004

Chen, C. Y., Rao, S. S., Ren, L., Hu, X. K., Tan, Y. J., Hu, Y., et al. (2018). Exosomal DMBT1 from human urine-derived stem cells facilitates diabetic wound repair by promoting angiogenesis. *Theranostics* 8, 1607–1623. doi: 10.7150/thno.22958

Ghosh, G., Subramanian, I. V., Adhikari, N., Zhang, X., Joshi, H. P., Basi, D., et al. (2010). Hypoxia-induced microRNA-424 expression in human endothelial cells regulates HIF-α isoforms and promotes angiogenesis. *J. Clin. Invest.* 120, 4141–4154. doi: 10.1172/jci42980

Gong, M., Yu, B., Wang, J., Wang, Y., Liu, M., Paul, C., et al. (2017). Mesenchymal stem cells release exosomes that transfer miRNAs to endothelial cells and promote angiogenesis. *Oncotarget* 8, 45200–45212. doi: 10.18632/oncotarget.16778

Hu, Y., Rao, S. S., Wang, Z. X., Cao, J., Tan, Y. J., Luo, J., et al. (2018). Exosomes from human umbilical cord blood accelerate cutaneous wound healing through miR-21-3p-mediated promotion of angiogenesis and fibroblast function. *Theranostics* 8, 169–184. doi: 10.7150/thno.21234

Huang, C. C., Kang, M., Lu, Y., Shirazia, S., Diaza, J. I., Cooper, L. F., et al. (2020). Functionally engineered extracellular vesicles improve bone regeneration. *Acta Biomater.* 109, 182–194. doi: 10.1016/j.actbio.2020.04.017

Hui, X., Zhuang, C., Long, W., Xia, Z., Hu, Y., Xian, L., et al. (2014). PDGF-BB secreted by preosteoclasts induces angiogenesis during coupling with osteogenesis. *Nat. Med.* 20, 1270–1278. doi: 10.1038/nm.3668

Jia, Y., Qiu, S., Xu, J., Kang, Q., and Chai, Y. (2020). Exosomes secreted by young mesenchymal stem cells promote new bone formation during distraction osteogenesis in older rats. *Calcif. Tissue Int.* 106, 509–517. doi: 10.1007/s00223-019-00656-4

Jin, Z., Ren, J., and Qi, S. (2020). Exosomal miR-9-5p secreted by bone marrow-derived mesenchymal stem cells alleviates osteoarthritis by inhibiting syndecan-1. *Cell Tissue Res.* 381, 99–114. doi: 10.1007/s00441-020-03193-x

Kusumbe, A. P., Ramasamy, S. K., and Adams, R. H. (2014). Coupling of angiogenesis and osteogenesis by a specific vessel subtype in bone. *Nature* 507, 323–328. doi: 10.1038/nature13145

Li, C., Chai, Y., Wang, L., Gao, B., Chen, H., Gao, P., et al. (2017). Programmed cell senescence in skeleton during late puberty. *Nat. Commun.* 8:1312.

Li, C., Wang, W., Xie, L., Luo, X., Cao, X., and Wan, M. (2016a). Lipoprotein receptor-related protein 6 is required for parathyroid hormone-induced Sost suppression. *Ann. N. Y. Acad. Sci.* 1364, 62–73. doi: 10.1111/nyas.12750

Li, C., Xing, Q., Yu, B., Xie, H., Wang, W., Shi, C., et al. (2013). Disruption of LRP6 in osteoblasts blunts the bone anabolic activity of PTH. *J. Bone Miner. Res.* 28, 2094–2108. doi: 10.1002/jbmr.1962

Li, C., Zhen, G., Chai, Y., Xie, L., Crane, J. L., Farber, E., et al. (2016b). RhoA determines lineage fate of mesenchymal stem cells by modulating CTGF-VEGF complex in extracellular matrix. *Nat. Commun.* 7:11455.

Li, C. J., Cheng, P., Liang, M. K., Chen, Y. S., Lu, Q., Wang, J. Y., et al. (2015). MicroRNA-188 regulates age-related switch between osteoblast and adipocyte differentiation. *J. Clin. Invest.* 125, 1509–1522. doi: 10.1172/jci77716

Li, C. J., Xiao, Y., Yang, M., Su, T., Sun, X., Guo, Q., et al. (2018). Long noncoding RNA Bmncr regulates mesenchymal stem cell fate during skeletal aging. *J. Clin. Invest.* 128, 5251–5266. doi: 10.1172/jci99044

Li, M., Wang, T., Tian, H., Wei, G., Zhao, L., and Shi, Y. (2019). Macrophage-derived exosomes accelerate wound healing through their anti-inflammation effects in a diabetic rat model. *Artif. Cells Nanomed. Biotechnol.* 47, 3793–3803. doi: 10.1080/21691401.2019.1669617

Li, X., and Tang, M. (2020). Exosomes released from M2 macrophages transfer miR-221-3p contributed to EOC progression through targeting CDKN1B. *Cancer Med.* 9, 5976–5988. doi: 10.1002/cam4.3252

Li, Y., Yang, R., Guo, B., Zhang, H., Zhang, H., Liu, S., et al. (2019). Exosomal miR-301 derived from mesenchymal stem cells protects myocardial infarction by inhibiting myocardial autophagy. *Biochem. Biophys. Res. Commun.* 514, 323–328. doi: 10.1016/j.bbrc.2019.04.138

Li, Z., Jiang, R., Yue, Q., and Peng, H. (2017). MicroRNA-29 regulates myocardial microvascular endothelial cells proliferation and migration in association with IGF1 in type 2 diabetes. *Biochem. Biophys. Res. Commun.* 487, 15–21. doi: 10.1016/j.bbrc.2017.03.055

Lian, W. S., Ko, J. Y., Chen, Y. S., Ke, H.-J., Hsieh, C.-K., Kuo, C.-W., et al. (2019). MicroRNA-29a represses osteoclast formation and protects against osteoporosis by regulating PCAF-mediated RANKL and CXCL12. *Cell Death Dis.* 10:705.

Liu, F., Wang, Z. F., Liu, F. F., Xu, J. Z., Liu, Q., and Lan, J. (2019). [MicroRNA-29a-3p regulates osteoblast differentiation and peri-implant osseointegration in a rat model of hyperlipidemia by modulating Frizzled 4 expression]. *Hua Xi Kou Qiang Yi Xue Za Zhi* 37, 200–207.

Liu, T., Sun, Y. C., Cheng, P., and Shao, H. G. (2019). Adipose tissue macrophage-derived exosomal miR-29a regulates obesity-associated insulin resistance. *Biochem. Biophys. Res. Commun.* 515, 352–358. doi: 10.1016/j.bbrc.2019.05.113

Liu, W., Li, L., Rong, Y., Qian, D., Chen, J., Zhou, Z., et al. (2020). Hypoxic mesenchymal stem cell-derived exosomes promote bone fracture healing by the transfer of miR-126. *Acta Biomater.* 103, 196–212. doi: 10.1016/j.actbio.2019.12.020

Luo, Z. W., Li, F. X., Liu, Y. W., Rao, S. S., Yin, H., Huang, J., et al. (2019). Aptamer-functionalized exosomes from bone marrow stromal cells target bone to promote bone regeneration. *Nanoscale* 11, 20884–20892. doi: 10.1039/c9nr02791b

Nakano, M., Kubota, K., Kobayashi, E., Chikenji, T. S., Saito, Y., Konari, N., et al. (2020). Bone marrow-derived mesenchymal stem cells improve cognitive impairment in an Alzheimer's disease model by increasing the expression of microRNA-146a in hippocampus. *Sci. Rep.* 10:10772.

Qi, X., Zhang, J., Yuan, H., Xu, Z., Li, Q., Niu, X., et al. (2016). Exosomes secreted by human-induced pluripotent stem cell-derived mesenchymal stem cells repair critical-sized bone defects through enhanced angiogenesis and osteogenesis in osteoporotic rats. *Int. J. Biol. Sci.* 12, 836–849. doi: 10.7150/ijbs.14809

Song, W., Chen, Y., Zhu, G., Xie, H., Yang, Z., and Li, L. (2020). Exosome-mediated miR-9-5p promotes proliferation and migration of renal cancer cells both in vitro and in vivo by targeting SOCS4. *Biochem. Biophys. Res. Commun.* 529, 1216–1224. doi: 10.1016/j.bbrc.2020.06.114

Sun, W., Zhao, P., Zhou, Y., Xing, C., Zhao, L., Li, Z., et al. (2020). Ultrasound targeted microbubble destruction assisted exosomal delivery of miR-21 protects the heart from chemotherapy associated cardiotoxicity. *Biochem. Biophys. Res. Commun.* 532, 60–67. doi: 10.1016/j.bbrc.2020.05.044

Tan, S. H. S., Wong, J. R. Y., Sim, S. J. Y., Tjio, C. K. E., Wong, K. L., Chew, J. R. J., et al. (2020). Mesenchymal stem cell exosomes in bone regenerative strategies-a systematic review of preclinical studies. *Mater. Today Bio* 7:100067. doi: 10.1016/j.mtbio.2020.100067

Tang, T. T., and Wang, B. (2020). Extracellular vesicle-encapsulated IL-10 as novel nanotherapeutics against ischemic AKI. *Sci. Adv.* 6:eaaz0748. doi: 10.1126/sciadv.aaz0748

Venkat, P., Zacharek, A., Landschoot-Ward, J., Wang, F., Culmone, L., Chen, Z., et al. (2020). Exosomes derived from bone marrow mesenchymal stem cells harvested from type two diabetes rats promotes neurorestorative effects after stroke in type two diabetes rats. *Exp. Neurol.* 334:113456. doi: 10.1016/j.expneurol.2020.113456

Vilaca-Faria, H., Salgado, A. J., and Teixeira, F. G. (2019). Mesenchymal stem cells-derived exosomes: a new possible therapeutic strategy for Parkinson's disease? *Cells* 8:118. doi: 10.3390/cells8020118

Wang, F., Chen, F. F., Shang, Y. Y., Li, Y., Wang, Z. H., Han, L., et al. (2018). Insulin resistance adipocyte-derived exosomes aggravate atherosclerosis by increasing vasa vasorum angiogenesis in diabetic ApoE(-/-) mice. *Int. J. Cardiol.* 265, 181–187. doi: 10.1016/j.ijcard.2018.04.028

Wu, R. W., Lian, W. S., Chen, Y. S., Kuo, C. W., Ke, H. C., Hsieh, C. K., et al. (2019). MicroRNA-29a counteracts glucocorticoid induction of bone loss through repressing TNFSF13b modulation of osteoclastogenesis. *Int. J. Mol. Sci.* 20:5141. doi: 10.3390/ijms20205141

Wu, X., Pang, L., Lei, W., Lu, W., Li, J., Li, Z., et al. (2010). Inhibition of Sca-1-positive skeletal stem cell recruitment by alendronate blunts the anabolic effects of parathyroid hormone on bone remodeling. *Cell Stem Cell* 7, 571–580. doi: 10.1016/j.stem.2010.09.012

Xu, Y., Liu, N., Wei, Y., Zhou, D., Lin, R., Wang, X., et al. (2020). Anticancer effects of miR-124 delivered by BM-MSC derived exosomes on cell proliferation, epithelial mesenchymal transition, and chemotherapy sensitivity of pancreatic cancer cells. *Aging (Albany NY)* 12, 19660–19676. doi: 10.18632/aging.103997

Yang, M., Li, C. J., Sun, X., Guo, Q., Xiao, Y., Su, T., et al. (2017). MiR-497 approximately 195 cluster regulates angiogenesis during coupling with osteogenesis by maintaining endothelial Notch and HIF-1alpha activity. *Nat. Commun.* 8:16003.

Ying, W., Riopel, M., Bandyopadhyay, G., Dong, Y., Birmingham, A., Seo, J. B., et al. (2017). Adipose tissue macrophage-derived exosomal miRNAs can modulate in vivo and in vitro insulin sensitivity. *Cell* 171, 372–384.e12.

Zhang, H., Bai, M., Deng, T., Liu, R., Wang, X., Qu, Y., et al. (2016). Cell-derived microvesicles mediate the delivery of miR-29a/c to suppress angiogenesis in gastric carcinoma. *Cancer Lett.* 375, 331–339. doi: 10.1016/j.canlet.2016.03.026

Zhang, X., Sheng, Y., Li, B., Wang, Q., Liu, X., and Han, J. (2020). Ovarian cancer derived PKR1 positive exosomes promote angiogenesis by promoting migration and tube formation in vitro. *Cell Biochem. Funct.* doi: 10.1002/cbf.3583 [Epub ahead of print].

Zheng, B., Yin, W. N., Suzuki, T., Zhang, X. H., Zhang, Y., Song, L. L., et al. (2017). Exosome-mediated miR-155 transfer from smooth muscle cells to endothelial cells induces endothelial injury and promotes atherosclerosis. *Mol. Ther.* 25, 1279–1294. doi: 10.1016/j.ymthe.2017.03.031

Zheng, G., Huang, R., Qiu, G., Ge, M., Wang, J., Shu, Q., et al. (2018). Mesenchymal stromal cell-derived extracellular vesicles: regenerative and immunomodulatory effects and potential applications in sepsis. *Cell Tissue Res.* 374, 1–15. doi: 10.1007/s00441-018-2871-5

Zou, L., Ma, X., Wu, B., Chen, Y., Xie, D., and Peng, C. (2020). Protective effect of bone marrow mesenchymal stem cell-derived exosomes on cardiomyoblast hypoxia-reperfusion injury through the miR-149/let-7c/Faslg axis. *Free Radic. Res.* 15, 1–19. doi: 10.1080/10715762.2020.1837793

Zuo, R., Liu, M., Wang, Y., Li, J., Wang, W., Wu, J., et al. (2019). BM-MSC-derived exosomes alleviate radiation-induced bone loss by restoring the function of recipient BM-MSCs and activating Wnt/beta-catenin signaling. *Stem Cell Res. Ther.* 10:30.

Conflict of Interest: The authors declare that the research was conducted in the absence of any commercial or financial relationships that could be construed as a potential conflict of interest.

Copyright © 2020 Lu, Cheng, Liu and Wang. This is an open-access article distributed under the terms of the Creative Commons Attribution License (CC BY). The use, distribution or reproduction in other forums is permitted, provided the original author(s) and the copyright owner(s) are credited and that the original publication in this journal is cited, in accordance with accepted academic practice. No use, distribution or reproduction is permitted which does not comply with these terms.

frontiers in Cell and Developmental Biology

REVIEW
published: 10 December 2020
doi: 10.3389/fcell.2020.585644

Bone and Muscle Crosstalk in Aging

*Chen He[1], Wenzhen He[1], Jing Hou[1], Kaixuan Chen[1], Mei Huang[1], Mi Yang[1], Xianghang Luo[1,2,3] and Changjun Li[1,2,3]**

[1] Department of Endocrinology, Endocrinology Research Center, Xiangya Hospital of Central South University, Changsha, China, [2] National Clinical Research Center for Geriatric Disorders, Xiangya Hospital of Central South University, Changsha, China, [3] Key Laboratory of Organ Injury, Aging and Regenerative Medicine of Hunan Province, Changsha, China

Osteoporosis and sarcopenia are two age-related diseases that affect the quality of life in the elderly. Initially, they were thought to be two independent diseases; however, recently, increasing basic and clinical data suggest that skeletal muscle and bone are both spatially and metabolically connected. The term "osteosarcopenia" is used to define a condition of synergy of low bone mineral density with muscle atrophy and hypofunction. Bone and muscle cells secrete several factors, such as cytokines, myokines, and osteokines, into the circulation to influence the biological and pathological activities in local and distant organs and cells. Recent studies reveal that extracellular vesicles containing microRNAs derived from senescent skeletal muscle and bone cells can also be transported and aid in regulating bone-muscle crosstalk. In this review, we summarize the age-related changes in the secretome and extracellular vesicle-microRNAs secreted by the muscle and bone, and discuss their interactions between muscle and bone cells during aging.

Keywords: bone, muscle, crosstalk, aging, osteosarcopenia

OPEN ACCESS

Edited by:
Rebecca Ann Wingert, University of Notre Dame, United States

Reviewed by:
Sonia Alonso-Martin, Biodonostia Health Research Institute (IIS Biodonostia), Spain
Mark Hamrick, Augusta University, United States

****Correspondence:***
Changjun Li
lichangjun@csu.edu.cn

Specialty section:
This article was submitted to Molecular Medicine, a section of the journal Frontiers in Cell and Developmental Biology

Received: *21 July 2020*
Accepted: *09 November 2020*
Published: *10 December 2020*

Citation:
He C, He W, Hou J, Chen K, Huang M, Yang M, Luo X and Li C (2020) Bone and Muscle Crosstalk in Aging. Front. Cell Dev. Biol. 8:585644. doi: 10.3389/fcell.2020.585644

INTRODUCTION

With increasing aging populations, studies regarding aging have become an emerging field. Aging is the process of tissue deterioration coupled with an enormous economic burden. Osteosarcopenia is an age-related pathological condition characterized by porous and fragile bone and sarcopenia (a disease exhibiting low muscle mass and function), recognized as a "hazardous duet," which induces fragile bones and increased risk of fractures, thus leading to high mortality rates and global financial threat. Binkley and Buehring (2009) first coined Sarco-Osteopenia to diagnose simultaneous bone and muscle weakness, calling for scientists to investigate specific mechanisms of the co-existence of osteoporosis and sarcopenia. Fat infiltration is a common character of aged bone and muscle; besides, osteoporosis and sarcopenia share several genetic, developmental, and endocrine factors. Endocrine factors have become a hot spot for studying the pathogenesis of osteosarcopenia, especially regarding myokines and osteokines.

Myokines, defined as soluble molecules expressed and released by muscle fibers, regulate the biological and pathological activities of local and distant cells and organs. McPherron et al. (1997) identified the first myokine, i.e., myostatin, which is expressed in developing and mature muscle and negatively regulates muscle mass. Steensberg et al. (2000) reported that contracting muscle releases interleukin-6 into the bloodstream, and realized that muscle could function as an endocrine organ. Moreover, with the development of modern sequencing and analytic technology, about 672 myokines were identified (Grube et al., 2018). They are composed mainly of peptides, such as growth factors, cytokines, and some small organic acids. Various myokines in the circulation

work together to maintain homeostasis via muscle-organ crosstalk (Das et al., 2020). For example, contracting muscle secretes brain-derived neurotrophic factors to improve the memory and learning capacity, and exercise-induced irisin was reported to promote thermogenesis and increase bone mass (Vaynman et al., 2004; Boström et al., 2012; Colaianni et al., 2015; Severinsen and Pedersen, 2020).

Osteokines, a combination of two Greek words ("osteo" meaning "bone" and "kino" meaning "movement"), represent bone cell-derived factors, which influence local and systemic metabolism. The bone marrow microenvironment is complex and comprises diverse cells. Cells that participate in bone metabolism include bone marrow mesenchymal stem cells (BMSCs), osteoblasts, osteocytes, osteoclasts, and their precursor cells. The most widely studied osteokines are of osteoblast, osteocyte, and osteoclast origin. For instance, receptor activator of nuclear factor kappa B ligand (RANKL) and osteoprotegerin (OPG) from osteoblasts, sclerostin (SOST), fibroblast growth factor 23 (FGF23), and RANKL from osteocytes, and receptor activator of nuclear factor kappa B (RANK) from osteoclasts etc. Unlike skeletal muscle, from which over 600 myokines were identified, bone was not recognized as an endocrine organ until 2007 (Lee et al., 2007). In addition, the research regarding bone-derived factors mediating bone-muscle crosstalk is limited.

Besides the cytokines, growth factors and proteases released by aging cells, which are defined as the senescence-associated secretory phenotype (SASP), are harmful to musculoskeletal function. The nuclear acid changes in aging cells reportedly induce dysfunction in their parent cells (Yang et al., 2017; Li et al., 2018; Xiao Y.Z. et al., 2020). Recently, extracellular vesicles holding the above factors shed from senescent cells have also been recognized as another type of SASP (Alibhai et al., 2020).

Extracellular vesicles play an important role in cell-to-cell communication, as they can circulate in blood and dock into distant target cells to exert regulatory roles. Extracellular vesicles (EVs) can be divided into many types depending on their size, synthesis, and secretion mechanisms. Current methods cannot isolate profoundly pure subsets; therefore, we prefer the umbrella term "extracellular vesicles." Two main subtypes of EVs exist, including exosomes, which are "cup shaped" membranous vesicles between 30 and 150 nm released by late endosome fusion with plasma membranes, and microvesicles, irregularly shaped vesicles measuring 100–1,000 nm, which originate directly from cell membranes. EVs hold microRNAs, proteins, mRNAs, lipids, etc., bind with or are endocytosed by recipient cells, transport their cargo to target cells to modulate biological activities. Recently, many articles describe the regulatory effects of senescent cell-released EVs in various pathologic conditions. Kadota et al. (2018) had reviewed the effects that senescent-cell-EVs exert on age-related lung diseases. In addition, enhanced miR-29b-3p expression in senescent-BMSC-EVs accounts for insulin resistance during aging (Su et al., 2019). However, there are few researches investigating the effects of EVs released from aging cells on musculoskeletal homeostasis. For instance, researchers found that raising miR-31 in aged BMSC and endothelial cell EVs suppress bone formation and enhance bone resorption, likewise increased miR-31 could inhibit dystrophin response to loading, and cause muscles of aged rats more susceptible to injury after disuse (Weilner et al., 2016; Hughes et al., 2018; Xu R. et al., 2018).

There are many reviews regarding musculoskeletal communication for osteosarcopenia, but they mainly focus on simple bone-muscle crosstalk; aging and nutrition are included as additional factors to emphasize that dysfunction of skeletal muscle and bone always occur together (Reginster et al., 2016; Li et al., 2019). In this review, we focus on bone-muscle crosstalk during aging, briefly describe several classical and new myokines and osteokines (**Tables 1**, **2** and **Figure 1**), discuss how EV-microRNAs change with age (**Table 3** and **Figure 2**), and finally point out the shortcomings of present studies and provide prospects of the potential field in age-related musculoskeletal diseases.

PROTEOME ALTERED WITH AGE IN BONE-MUSCLE CROSSTALK

Myokine

Irisin

Irisin, a polypeptide comprising 112 amino acids, is a messenger derived from skeletal muscle to regulate metabolism. Boström et al. (2012) revealed that irisin, a proteolytic product with amino terminal residues of fibronectin type III domain containing 5 (FNDC5), acts as an exercise-induced myokine to promote thermogenesis by browning white fat. Besides, Boström et al. (2012) revealed that irisin might function in glucolipid metabolism. Lately, it has been confirmed to rescue obesity in high-fat diet animal models and improve insulin resistance by targeting genes involved in glucose transport and utilization, such as solute carrier family 2, member 4 (*Glut4*) and phosphoenolpyruvate carboxykinase (*Pck*) (Xin et al., 2016). In addition, irisin was reported to promote pancreatic β cell proliferation and protect it from apoptosis to directly maintain pancreatic function. Exercise increases serum irisin level, furthermore, exercise is of great benefit to bone remodeling. Therefore, irisin was chosen for further investigation to determine whether it is engaged in muscle-bone communication *in vitro* and *in vivo*.

The effects of irisin on BMSCs

Colaianni et al. (2014) reported that irisin is continuously released at a basal level by muscle and enhanced during exercise. BMSCs cultured in myoblast conditioned medium exhibit more alkaline phosphatase (ALP)-positive colonies (Colaianni et al., 2014). Furthermore, they found that recombinant irisin injection in young male mice once a week at a low dose of 100 μg/kg for 4 weeks increases cortical bone mass and stimulates osteoblastic bone formation without altering energy metabolism, indicating that irisin promotes expression of activating transcription factor 4 (*Atf4*), which subsequently enhances the biological activity of runt-related transcription factor 2 (RUNX2) and a series of osteogenic transcription factors, enabling BMSCs to develop into the osteogenic lineage (Colaianni et al., 2015). In addition, irisin can improve the colony formation ability of BMSCs and enhance

TABLE 1 | Myokines altered with age in bone-muscle crosstalk.

	Target organ/cell and age-related bone-muscle crosstalk	Main physiology function
Myokines		
Irisin	BMSCs	Increase ALP positive colonies (Colaianni et al., 2014). Promote BMSCs develop into osteogenic lineage via ATF4-dependent RUNX2 activation (Colaianni et al., 2015). Rescue colony formation and ALP, Collagen I expression of BMSCs from suspended mice (Colaianni et al., 2017).
	Osteoblasts	Promote osteoblast proliferation and differentiation via MAPK pathway (Colaianni et al., 2015; Qiao et al., 2016). Reduce osteoblast apoptosis (Xu et al., 2020). Preserve osteoblast differentiation via β-Catenin in suspended mice (Chen et al., 2020). Polarize Macrophages into M2 phenotype via AMPK pathway then promote osteoblast differentiation (Ye et al., 2020).
	Osteocytes	Assist osteocyte-related osteocytic osteolysis and increase sclerostin expression (Kim et al., 2018). Downregulate SOST expression (Storlino et al., 2020). Inhibit the apoptosis of osteocytes under oxidative stress and/or microgravity via decreasing mitochondrial pathway of cell death (Storlino et al., 2020). Regulate osteoclast formation and activities via modulating OPG expression (Colaianni et al., 2017).
	Osteoclasts	Reduce expression of Cathepsin K, *Rank* and *Nfatc1* mRNA level (Ma et al., 2018). Promote proliferation and decrease differentiation of osteoclast precursors through p38, JNK and RANKL-induced NF-κB pathway separately (Ma et al., 2018).
	Muscle	Enhance the mRNA level of muscle growth-related gene like *Igf1* and *Pgc1α4* through ERK signaling pathway and suppress the expression of myostatin (Huh et al., 2014). Improve the proliferation and fusion of myoblasts; enhance protein synthesis via activation of AKT and ERK; activate satellite cells pool; increase expression of *Il-6*, then facilitate myogenesis (Reza et al., 2017b). Improve sarcolemmal stability or increase phosphorylation of FOXO3α and attenuate chymotrypsin-like enzyme activity (Reza et al., 2017a; Chang and Kong, 2020). Promote proliferation of C2C12 cells via increasing chemokine (C-C motif) ligand 7 (Lee et al., 2019).
	Age-related bone-muscle crosstalk	Negatively correlated with age (Huh et al., 2012; Rana et al., 2014). Increase with age (Mahmoodnia et al., 2016; Ruan et al., 2019). Use as a biomarker to predict pre-sarcopenia and sarcopenia (Chang et al., 2017). Positive association with bone mineral status and low irisin level is related to increased hip fracture risk (Yan et al., 2018).
Myostatin	BMSCs	Promote mesenchymal multipotent cells differentiate toward adipocytes (Hamrick et al., 2007). Induce the expression of *Pparγ* and *C/EBPα* (Rebbapragada et al., 2003). Decrease the mechanosensitivity of BMSCs (Hamrick et al., 2007).
	Osteoblasts	Inhibit expression of *Alp*, osteocalcin, osterix and *Runx2* (Chen et al., 2017; Zhang et al., 2020). Decrease the number of osteoblasts on bone surface (Chen et al., 2017). Low-intensity pulsed ultrasound inhibits myostatin to enhance the proliferation of osteoblasts (Sun et al., 2019).
	Osteocytes	Increase the expression of Wnt pathway inhibitor SOST, DKK1, besides, promote RANKL expression in osteocytes (Qin et al., 2017). Reduce the miR-218 expression in osteocytes-derived exosomes and then impairs osteoblastic differentiation via Wnt pathway (Qin et al., 2017).
	Osteoclasts	Increase the expression of *Nfatc1* and the number of TRAP + multinucleated giant cells (Chen et al., 2017). Enhance expression of integrin αv, integrin β3 and calcitonin receptor via enhancing SMAD2-dependent NFATc1 nuclear translocation (Dankbar et al., 2015).
	Muscle	Myostatin-null mice show muscle hypertrophy (Shan et al., 2013). Myostatin inhibition by GASP-2 can promote proliferation and differentiation of myoblasts (Perie et al., 2016). Downregulate *Pax7* to suppress activation and self-renew of quiescent satellite cells; arrest C2C12 myoblasts in G1 phase through promoting P21 expression; decrease *Pax3*, *Myod1*, and *Myf5* expression to suppress differentiation (Rodriguez et al., 2014). Enhance ribosome biogenesis through activating S6K and rpS6 (Rodriguez et al., 2014). Decrease protein synthesis via inhibiting eEF2K-eEF2 after AMPK phosphonation (Deng et al., 2017). Promote the gene expression of *Murf-1*, enhance the proteasome activity of 26S and increase the expression of autophagy-related genes, such as *Atg3, Atg12*, etc. (Wang D.T. et al., 2015).
	Age-related bone-muscle crosstalk	Increase with age until 57 years old, then it exhibits a decrease trend (Szulc et al., 2012). Myostatin level is periodic, and exhibit the highest concentration in spring (Szulc et al., 2012). Increase or decrease with age (Bowser et al., 2013; Poggioli et al., 2016). Myostatin in fast muscle fiber ensued with aging (Shibaguchi et al., 2018). *Mstn* deficiency improve muscle atrophy and reduced muscle capacity in aging mice (Siriett et al., 2006). Myostatin inhibitor can be used to treat age-related sarcopenia (White and LeBrasseur, 2014). High myostatin level is related to low BMD subjects in Chinese elderly (Wu et al., 2018). Myostatin inhibition enhance osteogenesis induced by aged myofibers and myoblast cell line (Zhang et al., 2020).

(Continued)

TABLE 1 | Continued

	Target organ/cell and age-related bone-muscle crosstalk	Main physiology function
FGF21	BMSCs	Favor BMSCs commitment into adipocytes over osteoblast lineage via PPARγ-FGF21 feed-forward regulatory pathway (Wei et al., 2012).
	Osteoclasts	Bone resorption enhanced in *Fgf21* transgenic mice possibly via increasing the expression level of RANKL in osteocytes (Wei et al., 2012). Promote RANKL-induced osteoclastogenesis via promoting IGFBP1 release by liver then combination with Integrin β1 receptor in osteoclasts (Wang X. et al., 2015). MiR-100 overexpression causes reduced FGF21 level thus inhibit osteoclasts-mediated bone resorption and partially restore the bone phenotype in OVX-operated mice (Zhou et al., 2019).
	Muscle	Dispensable for muscle mass maintenances in normal condition and necessary to induce muscle atrophy and weakness in starvation state via enhancing BNIP3 activation (Oost et al., 2019). Reduction of OPA1 is related to aging-related muscle atrophy, while *Fgf21* deletion is reported to partially rescue the muscle loss caused by OPA1 deficiency (Tezze et al., 2017). Induce cell cycle exit in C2C12 myoblasts through suppressing the cell cycle-related protein sequential to activation of p21 induced by p53 (Liu S. et al., 2017; Liu et al., 2017b. Enhance myogenesis via activating PAX3, and promote formation of smaller aerobic myofibers during fasting via the FGF21-SIRT1-AMPK-PGC1α pathway (Liu S. et al., 2017; Liu et al., 2017a,b)
	Age-related bone-muscle crosstalk	Increase with age (Hao et al., 2018; Lee et al., 2020). Negative associated with BMD (Hao et al., 2018; Lee et al., 2020). Positive relevant with the sarcopenia (Hanks et al., 2015; Tezze et al., 2017).
BAIBA	Osteoblasts	Promote proliferation or enhance the expression of *Runx2, Opg,* osteopontin, and *Alp* via moderate ROS induced by NAD(P)H oxidase 4 (Zhu X.W. et al., 2018).
	Osteocytes	Protect young osteocytes from ROS induced cell death via protecting the mitochondrial morphology and function (Kitase et al., 2018).
	Muscle	BAIBA can prevent loss of EDL and soleus muscle function in unloading hindlimb male mice (Jung et al., 2015). BAIBA prevent hyperlipidemia-induced insulin resistance and palmitate-induced inflammation in C2C12 myoblast cell line (Kitase et al., 2018).
	Age-related bone-muscle crosstalk	The protective effect of BAIBA on osteocytes decreasing with age due to reduction of BAIBA receptor-MRGPRD in osteocytes (Kitase et al., 2018). Aged skeletal muscle produces more BAIBA (Kitase et al., 2018).
METRNL	Osteoblasts	Inhibit mineralized nodule formation (Gong et al., 2016).
	Muscle	Wait to explore.
	Age-related bone-muscle crosstalk	Wait to explore.

the expression of previously impaired genes, such as *Alp* and collagen I, in hind-limb suspended mice (Colaianni et al., 2017).

The effects of irisin on osteoblasts

Increased bone formation not only can be realized by BMSC osteogenic bias but also promoted by enhanced osteoblast proliferation and differentiation. Mitogen-activated protein kinase (MAPK) signaling pathways mainly regulate cell proliferation and differentiation, with no exception regarding its role in osteoblasts. Qiao et al. (2016) illustrated that after treatment with irisin, basal MAPK14 (p38) and total MAPK1 (ERK) remain constant in osteoblasts, but expression levels of phosphorylated p38 and phosphorylated ERK increase and peak 5-20 min after stimulus. Pretreatment of primary rat osteoblasts and MC3T3-E1 cells with p38 inhibitor SB203580, or ERK inhibitor U0126 eliminate the effect of irisin on proliferation and differentiation (Qiao et al., 2016). Consistent with that, Colaianni et al. (2015) reported that irisin enhances ERK phosphorylation in cultured osteoblasts. Furthermore, irisin can reduce the number of apoptotic osteoblasts in an osteoporosis rat model, and protect against decreased osteoblast differentiation by increasing β-catenin levels (Chen et al., 2020; Xu et al., 2020). Except for its direct effect on osteoblasts, irisin can indirectly promote osteogenesis by polarizing macrophages to the M2 phenotype via the adenosine monophosphate-activated protein kinase (AMPK) pathway (Ye et al., 2020).

The effects of irisin on osteocytes

Kim et al. (2018) first discovered the irisin receptor, αV Integrin, in osteocytes. They reported that an osteocyte-related direct bone resorption model, ovariectomy (OVX)-induced Osteocytic osteolysis, requires *Fndc5* and sclerostin to induce bone resorption. Moreover, sclerostin, a protein specifically expressed in osteocytes, appears increased in a dose-dependent manner after culture with irisin (Kim et al., 2018). Nevertheless, Colaianni et al. (2015) showed that irisin level is negatively correlated with sclerostin. Kim et al. (2018) hypothesized that irisin plays a bidirectional role depending on its exposure mode, like the parathyroid hormone (PTH). Lately, Storlino et al. (2020) demonstrated that SOST expression is downregulated by intermittent irisin administration, while continuous irisin exposure doesn't modify SOST expression. Moreover, they found

TABLE 2 | Osteokines altered with age in bone-muscle crosstalk.

	Target organ/cell and age-related bone-muscle crosstalk	Main physiology function
Osteokines		
Osteocalcin	Muscle	Improve the ability of muscle to utilize glucose and fatty acids and form a feed-forward axis to amplify the role in adaption to exercise (Mera et al., 2016a). Necessary to maintain muscle mass in old mice via promoting protein synthesis (Mera et al., 2016b). Enhance C2C12 myoblast cell proliferation and myogenic differentiation thorough activation of the Pl3K/Akt, p38 and GPRC6A-ERK1/2 signaling pathway separately (Liu S. et al., 2017). Positive associated with muscle mass or function (Levinger et al., 2014; Harslof et al., 2016; Lin et al., 2016).
	Bone	Marker of bone formation, but *Ocn*$^{-/-}$ mice exhibit an increased bone mass (Li J. et al., 2016). Suppress bone formation when coupled to a Gi-protein in human osteoblast cell line (Bodine and Komm, 1999). Promote bone mineral mature in an *Ocn* knockout mice and hydroxyapatite crystal growth was suppressed by OCN in certain studies (Neve et al., 2013). Recruit osteoclasts and promote osteoclastogenesis or enhance its chemotaxis (Neve et al., 2013; Li J. et al., 2016). Enhanced RANKL-dependent bone resorption mediated by muscle released IL-6 (Mera et al., 2016a).
	Age-related bone-muscle crosstalk	Decrease with age (Mera et al., 2016a; Diemar et al., 2020). Negative association with BMD (Kim et al., 2010; Ling et al., 2016). Maintain muscle mass and improve the muscle phenotype of aged mice (Mera et al., 2016a,b)
Sclerostin	Muscle	*Sost* $^{-/-}$ mice exhibit an increasing trend of lean body mass fraction and overexpress sclerostin by an adeno-associated virus showing a significant reduction in lean body mass (Kim S.P. et al., 2017). Sclerostin is higher in low muscle mass subjects than healthy controls (Kim et al., 2019). Suppress Wnt3a mediated crosstalk between the MLO-Y4 osteocytes and muscle cells C2C12 via regulating Wnt/β-catenin pathway (Huang et al., 2017). Sclerostin inhibition restore muscle function in cancer induced muscle weakness (Hesse et al., 2019). Cannot prevent soleus muscle atrophy in rodents after spinal cord injury, probably because minimally expression of *Lrp5*/*Lrp6* in the rat soleus (Phillips et al., 2018).
	Bone	Various modifications in or near *SOST* can cause abnormal bone mineral density such as Sclerosteosis and Van Buchem disease (Holdsworth et al., 2019). Sclerostin transgenic mice exhibit osteopenia (Winkler et al., 2003). Regulate differentiation and mineralization of osteogenic lineage cell via a MEPE-ASARM dependent mechanism (Atkins et al., 2011). Sclerostin inhibition could reactive quiescent bone lining cells (Kim S.W. et al., 2017).
	Age-related bone-muscle crosstalk	Ensues with aging (Mirza et al., 2010; Ota et al., 2013). Lower sclerostin level in osteoporosis patients (Reppe et al., 2015). Ablation of *Sost* showed an increasing trend of lean body mass in elderly animals (Kim S.P. et al., 2017). A positive relevance between sclerostin and sarcopenia in type 2 diabetes mellitus (Medeiros et al., 2020).
OPG/RANKL/RANK	Muscle	RANKL-RANK interaction activates NF-κB, a pro-inflammation pathway which can inhibit myogenic differentiation and enhance the expression of ubiquitin proteasome system to induce muscle atrophy. Anti-RANKL protect muscle from chronic inflammation and improve its mechanical properties through shifting macrophages into M2 phenotype and inhibit the activation of NF-κB (Hamoudi et al., 2019). Dystrophic mdx mice specifically knockout *Rank* in muscle rescue its maximum specific force, while full-length OPG-Fc treatment activates sarco/endoplasmic reticulum Ca^{2+} ATPase to regulate Ca^{2+} homeostasis in dystrophic EDL through another pathway (Dufresne et al., 2018). RANKL inhibitor Dmab can rescue muscle function in human (Bonnet et al., 2019). *Opg* knockout mice displayed selective atrophy of fast-twitch-type IIb myofibers atrophy and C2C12 myotube exhibited reduced cross section area when exposure to RANKL (Hamoudi et al., 2020).
	Bone	RANKL-RANK activate major molecules in downstream pathway signaling, like nuclear factor NF-κB and colony stimulating factor 1 receptor et al., thereby driven pre-osteoclasts to differentiate into osteoclasts (Chung et al., 2014). *Opg* ablated mice showed increased adipocytes and BMSCs from these mice prefer to adipogenesis via enhanced expression of adipogenic transcription marker, *Pparγ* (Zhang et al., 2016). RANK in osteoclasts derived exosomes induce reverse RANKL signaling leading to increased osteogenesis and mineralization (Ikebuchi et al., 2018).
	Age-related bone-muscle crosstalk	RANKL/OPG ratio, a preferable harmful determinant of bone mass, increase with age (Chung et al., 2014; Zhang et al., 2016; Piemontese et al., 2017). IL-3 can improve the RANKL/OPG ratio and act as a potent medicine to treat osteoporosis (Singh et al., 2018). RANKL inhibitor Dmab can rescue muscle function in postmenopausal women, and also in osteo-sarcopenic *Pparb*$^{-/-}$ mice (Bonnet et al., 2019).

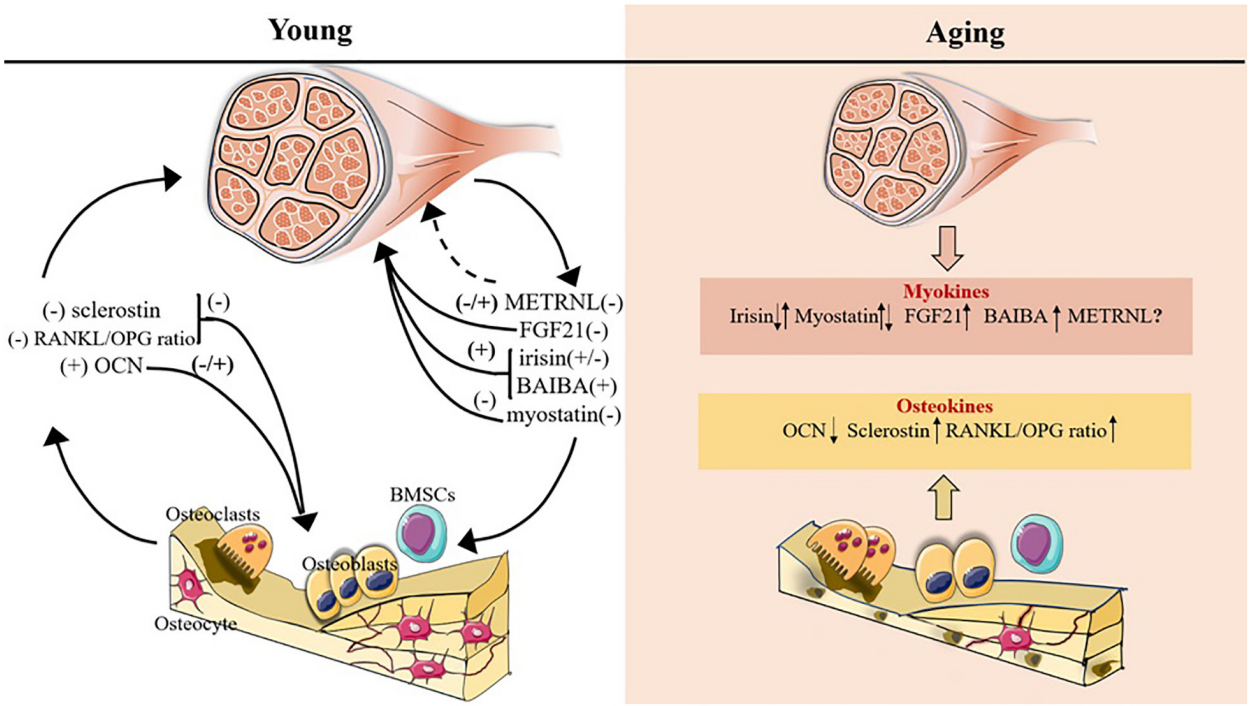


FIGURE 1 | Myokines and osteokines altered with age in bone-muscle crosstalk. The plus symbol indicates positive association with bone/muscle mass; minus symbol indicates negative association with bone/muscle mass; upward and downward arrows indicate expression increase and decrease, respectively; question mark and the dotted line indicate that the function on bone/muscle is unclear.

TABLE 3 | Potentially different expression of senescence-EVs-microRNAs in bone-muscle crosstalk.

	Target organ/cell and age-related bone-muscle crosstalk	Main physiology function
EVs-microRNAs from skeletal muscle	Bone	MiR-27a-3p in muscle-EVs promote MC3T3-E1 osteogenic differentiation via β-catenin signaling pathway (Takafuji et al., 2020). Negative effect on osteoclast formation and its mitochondrial metabolism (Fulzele et al., 2019).
	Muscle	EVs-miR-27 might be an active player, and wait to explore.
	Age-related bone-muscle crosstalk	MiR-34a is highly express in aged mouse skeletal muscle and oxidative stress treated C2C12 cells, then these EVs home to bone marrow leading to BMSCs senescence via repressing SIRT1 expression (Yang et al., 2020). Role of EV-miR-1, miR-133a, miR-27, miR-29b-3p, and miR-34a in osteosarcopenia wait to explore.
EVs-microRNAs from bone cells	Bone	Osteocytes-derived EVs miR-218 can be suppressed by myostatin, then taken up by osteoblasts inhibiting osteoblastic differentiation (Qin et al., 2017).
	Muscle	Wait to explore.
	Age-related bone-muscle crosstalk	Aged BMSCs express high level of miR-31a-5p leading to bias lineage fate of BMSCs to adipocytes through SATB2, and it release exosomes with high level of miR-31a-5p, then increase the number and function of osteoclasts via Rho pathway (Xu R. et al., 2018). Aged osteoclasts were found to liberate EVs unloading enhanced expression of miR-214-3p, increasing miR-214-3p not only promote osteoclast formation but also embracing in osteoclasts-derived EVs then lead to impaired bone formation (Li D. et al., 2016). MiR-183-5p increase with age in bone-derived EVs and endocytosed by BMSCs to suppress osteogenic differentiation and lead to senescence (Davis et al., 2017). Role of miR-15b, miR-17, miR-183, miR-186, miR-188, miR-20a, miR-214, miR-221, miR-24, miR-31, miR-328, miR-365, and miR-374, and miR-99b etc. in aged bone cells-EVs in osteosarcopenia wait to explore.

that irisin inhibits the apoptosis of osteocytes under oxidative stress and/or microgravity (Storlino et al., 2020). Apoptosis inhibition can be explained by the decreased mitochondrial (intrinsic) pathway of cell death. Specifically, irisin can enhance the expression of mitochondrial transcription factor A and increase the ratio of B cell leukemia 2 (BCL2)/BCL2-associated

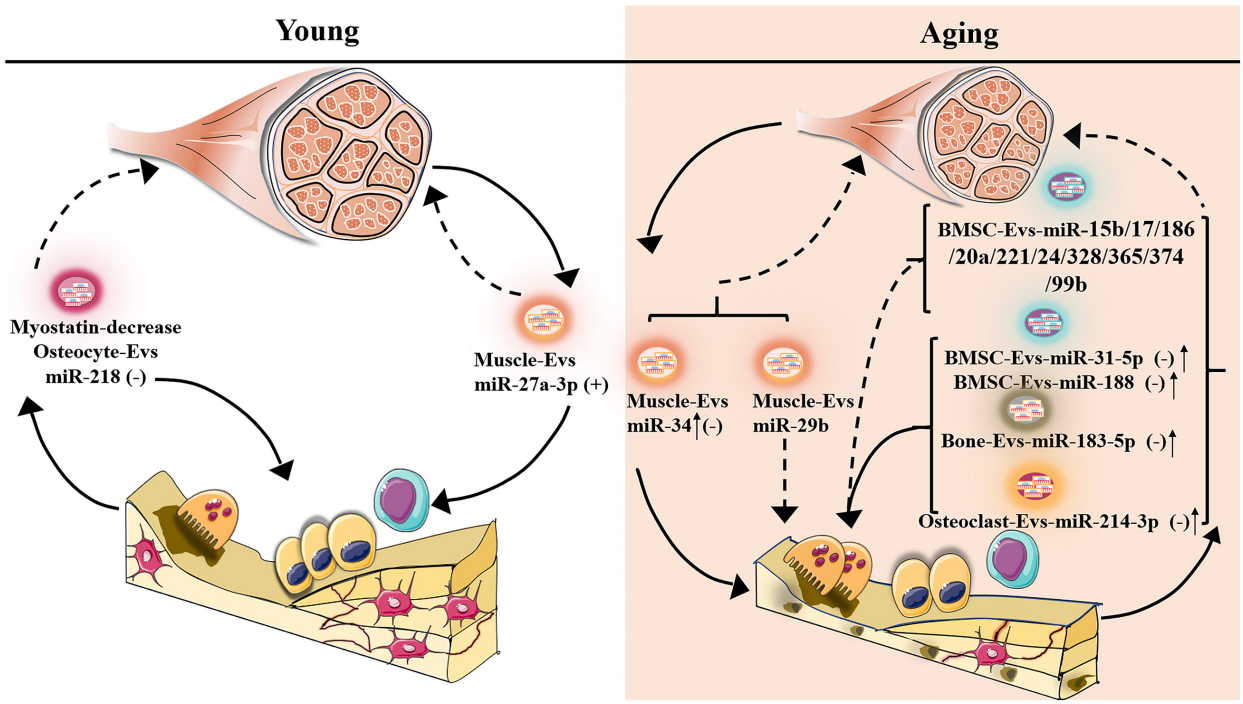


FIGURE 2 | Potentially different expression of senescent-EV-microRNAs in bone-muscle crosstalk. The plus symbol indicates positive association with bone/muscle mass; minus symbol indicates negative association with bone/muscle mass; upward arrow indicates expression increase; the dotted line indicates that the function on bone/muscle is unclear.

X protein (BAX), while high BCL2 level can impair BAX initiating autoactivation of caspase-9, then block the activation of the executioner, caspase-3. Besides, it can improve the expression of Podoplanin and Connexin 43, genes important for osteocyte dendrite and gap junction channel formation, respectively (Storlino et al., 2020). In addition, irisin may target osteocytes first, then modulates OPG expression, thus decreasing the RANKL/OPG ratio to regulate osteoclast formation and activities (Colaianni et al., 2017).

The effects of irisin on osteoclasts

Besides the effects on BMSCs and osteoblasts etc., Colaianni et al. (2015) also found that irisin-treated mice exhibit significantly lower number of osteoclasts. Consistent with the above result, irisin was found to reduce the phosphatase acid tartrate resistant (TRAP)-positive multinucleated cells induced by disuse, and it can reduce expression of Cathepsin K, *Rank*, and nuclear factor of activated T cells cytoplasmic 1 (*Nfatc1*) mRNA levels significantly (Ma et al., 2018). The detailed mechanism may be explained by the fact that irisin promotes proliferation and decreases differentiation of osteoclast precursors through the p38, c-Jun amino terminal kinase (JNK) signaling pathways and the RANKL-induced nuclear factor kappa B (NF-κB) pathway (Ma et al., 2018). Furthermore, Ibanez et al. (2014) and Xu et al. (2020) found that irisin could upregulate nuclear factor E2-related factor 2 (NRF2) expression levels, while *Nrf2* knockout increases the survival rate of osteoclasts. This indicates that irisin might decrease the survival of osteoclasts via *Nrf2* modification.

The effects of irisin on muscle

Besides paracrine and endocrine functions, irisin has also been shown to promote myogenesis via autocrine function. Huh et al. (2014) demonstrated that irisin expression increases during myogenic differentiation, furthermore, irisin exposure enhances mRNA levels of muscle growth-related genes, such as insulin-like growth factor 1 (*Igf1*) and peroxisome proliferative activated receptor gamma coactivator 1 alpha4 (*Pgc1α4*) through the ERK signaling pathway, and suppresses myostatin expression (Huh et al., 2014). An *in vivo* study conducted by Reza et al. (2017b) showed that irisin injection in normal and pathogenic circumstances cause significant skeletal muscle hypertrophy, accompanied with enhanced grip strength. The underlying mechanisms include (1) irisin improves proliferation and fusion activity of myoblasts; (2) enhances protein synthesis by promoting activation of AKT and ERK; (3) expands the activated satellite cells pool; (4) increases expression of exercise-related genes, such as interleukin-6, thereafter facilitating myogenesis (Reza et al., 2017b). In addition, irisin can partially restore muscle atrophy caused by various etiologies by improving sarcolemmal stability or increasing phosphorylation of forkhead box O3 alpha (FOXO3α) and attenuating chymotrypsin-like enzyme activity (Reza et al., 2017a; Chang and Kong, 2020). Moreover, irisin administration can enhance C2C12 myoblasts expressing FNDC5, suggesting that irisin might amplify its positive effect on myogenesis through a regeneration feedback loop (Colaianni et al., 2015). Furthermore, irisin promote C2C12 proliferation via increased

chemokine (C-C motif) ligand 7 of active downstream ERK pathway (Lee et al., 2019). However, further investigation is required regarding irisin receptors in muscle cells to understand the mechanisms behind the activation of different signaling pathways.

Irisin in bone-muscle crosstalk during aging

During aging, decreased mobility and loss of muscle may reduce irisin expression. This hypothesis laid a foundation for follow-up studies investigating the relationship between irisin and aging together with age-related musculoskeletal diseases. The relationship between irisin and age is controversial, with irrelevant, positive, and negative correlation. Huh et al. (2012) reported that irisin level is negatively correlated with age, and it may be induced by age-related muscle loss. Consistent with these results, multiple regression analysis models using backward elimination showed that telomere length is inversely proportional to age and positively associated with plasma irisin level. Telomere length can be predicted by plasma irisin level, and this suggested that age may be negatively associated with irisin level (Rana et al., 2014). Likewise, many epidemiological studies refer to circulating irisin levels growing with age (Mahmoodnia et al., 2016; Ruan et al., 2019). The paradoxical results may be due to researchers using different ELISA kits, which produce varying results, or the inclusion and exclusion criteria set by the researchers differ. More attention should be paid to confirm the genuine relationship between these parameters. In addition, irisin level is positively correlated to human biceps circumference, and irisin was confirmed to use as a biomarker to predict pre-sarcopenia and sarcopenia (Huh et al., 2012; Chang et al., 2017). Furthermore, irisin level is positively associated with bone mineral status, while low irisin level is related to increased hip fracture risk, further corroborating that age-related decreases in muscle and bone may be explained by decreased irisin level, but the detailed mechanism of action remains to be elucidated (Yan et al., 2018).

Myostatin

Myostatin, also known as growth differentiation factor 8 (GDF8), is a transforming growth factor-beta (TGFβ) superfamily protein mainly secreted from muscle fibers. Myostatin is released in an inactive form, then undergoes a series of proteolytic cleavage by bone morphogenetic protein 1/tolloid family of metalloproteinases, and finally produces a mature polypeptide. The hydrolysates N-terminal prodomain can interact with the mature homodimer, counteracting myostatin binding to activin type IIB receptor and activin-like kinase 4 (ALK4) or activin-like kinase 5 (ALK5) heterodimer. Furthermore, follistatin can also combine with myostatin and competitively inhibit myostatin binding to the receptor (Rebbapragada et al., 2003; White and LeBrasseur, 2014). Myostatin is a negative regulator of muscle and strength, and genetic mutation or ablation of the myostatin (*Mstn*) leads to muscle hypertrophy, enhanced strength, and improved bone architecture (Dankbar et al., 2015). The elaborate biological functions of myostatin in the musculoskeletal system are described below.

The effects of myostatin on BMSCs

The "colony switch" refers to the fact that once bone marrow stromal cells favor osteogenic differentiation, adipogenesis will be adversely affected. Hamrick et al. (2007) illustrated that BMSCs cultured within an osteogenic medium (obtained from *Mstn* knockout mice) exhibit more pronounced ALP and alizarin red staining than WT controls, and myostatin exposure induces mesenchymal multipotent cells differentiation toward adipocytes. Consistent with that, Rebbapragada et al. (2003) demonstrated that myostatin induces the expression of adipogenic transcription factors peroxisome proliferator-activated receptor gamma (*Pparγ*) and CCAAT enhancer binding protein alpha (*C/EBPα*). Although myostatin ablation promotes osteogenic bias, it cannot restore unloading-induced bone catabolism, which may be due to myostatin-reduced osteogenic differentiation via decreased mechanosensitivity of BMSCs (Hamrick et al., 2007).

The effects of myostatin on osteoblasts

Unsurprisingly, *in vitro* exogenous GDF8 can inhibit the expression of *Alp*, osteocalcin, and two important osteogenic transcription factors, osterix and *Runx2*, while alizarin red staining is also restrained. Moreover, *in vivo*, recombinant myostatin decreases the number of osteoblasts on the bone surface, while its neutralizing antibody reverses this effect (Chen et al., 2017). Myostatin inhibition can rescue the ALP signal and RUNX2 expression in aged primary myofiber- and C2C12 cell line-treated MC3T3-E1 (Zhang et al., 2020). This occurs because the myostatin inhibitor combines with myostatin to reduce negative effects from aged muscle on osteogenic differentiation. Recently, Sun et al. (2019) find that low-intensity pulsed ultrasound could improve bone healing by regulating the myostatin signaling pathway, they deduced that low-intensity pulsed ultrasound promote osteoblast proliferation via inhibiting Smad3-induced β-catenin stabilization through compromised myostatin signaling pathway.

The effects of myostatin on osteocytes

Research has reported that myostatin directly affects osteocytes. Osteocytes, comprising 90% of total bone cells, are deeply embedded in the bone matrix, thus the research on primary osteocytes is limited. Qin et al. (2017) used Osteocytic (Ocy454) cells as an osteocyte-study model, and revealed that myostatin could increase the expression of Wnt pathway inhibitor SOST, dickkopf Wnt signaling pathway inhibitor 1 (DKK1), while promoting the osteoclastogenesis gene *Rankl* in osteocytes. Moreover, myostatin can reduce miR-218 expression in osteocyte-derived EVs and its parent cells, while miR-218 was reported to promote the Wnt pathway by inhibiting SOST expression. Specifically, EVs released by myostatin-treated Ocy454 cells can be taken up by osteoblasts and osteoclast precursor cells during cultured within a medium, and then it can impair osteoblastic differentiation via the Wnt pathway, but exert no effect on osteoclastic differentiation (Qin et al., 2017). This conclusion was made based on *in vitro* results, and *in vivo* study is required further.

The effects of myostatin on osteoclasts

Besides affecting the expression of RANKL in osteocytes, myostatin can also directly increase the expression of osteoclast differentiation-related genes. Myostatin incubation with RANKL and macrophage colony stimulating factor (M-CSF) treated macrophages increases the number of $TRAP^+$ multinucleated giant cells, while it also increases the expression of NFATc1 in a dose-dependent manner (Chen et al., 2017). Likewise, bone surface osteoclasts appeared reduced in myostatin antibody-administrated mice (Chen et al., 2017). Recently, Dankbar et al. (2015) demonstrate that *Mstn* knockout mice display lower osteoclast number and smaller osteoclast size, but it seems like myostatin exerts no effect on osteoclast function *per se*, they also report that myostatin enhances the expression of genes engaged in RANKL-induced osteoclastogenesis, such as Integrin αv, Integrin β3, and calcitonin receptor, via enhancing SMAD2-dependent NFATc1 nuclear translocation, which is independent from the ERK pathway.

The effects of myostatin on muscle

Shan et al. (2013) revealed that myostatin-null mice show muscle hypertrophy. Inhibiting the myostatin canonical pathway by growth and differentiation factor-associated serum protein 2 (GASP-2) was shown to promote proliferation and differentiation of myoblasts (Perie et al., 2016). Regulation of myostatin in myogenesis is profoundly complicated. Rodriguez et al. (2014) elaborated on the mechanism via two schematic illustrations. First, myostatin downregulates paired box 7 (*Pax7*) to suppress activation and self-renewal of quiescent satellite cells. Second, C2C12 myoblasts are arrested in the G1 phase through promotion of p21 expression and inhibition of phosphorylated cyclin dependent kinases 2 (CDK2) and cyclin dependent kinases 4 (CDK4). Third, myostatin suppresses differentiation by reducing myogenic genes, such as *Pax3*, myogenic differentiation 1 (*Myod1*), and myogenic factor 5 (*Myf5*), through downregulation of the MEK/ERK1/2 MAPK pathway and/or the AKT/mTORC1 signaling pathway (Rodriguez et al., 2014). Besides affecting the number of muscle fibers, myostatin also decreases its cytoplasmic volume by disrupting the balance between protein synthesis and degradation. Specifically, besides sequential activation of transcription factors eukaryotic translation initiation factor 4E (eIF4E) and eukaryotic translation initiation factor 4E binding protein 1 (4E-BP1) in the PI3K/Akt/mTOR pathway, myostatin inhibition was found to affect translation efficiency and ability by enhancing ribosome biogenesis via the activation of ribosomal protein S6 kinase (S6K) and ribosomal protein S6 (rpS6) (Rodriguez et al., 2014). In addition, myostatin can decrease protein synthesis through inhibition of eukaryotic translation elongation factor 2 kinase (eEF2K)-eukaryotic translation elongation factor 2 (Eef2) after AMPK phosphonation (Deng et al., 2017). As for protein degradation, it was reported that myostatin not only promotes gene expression in ubiquitin proteasome, such as tripartite motif-containing 63 (*Murf-1*), and enhances the proteasome activity of 26S; but also increases the expression of autophagy-related 3 (*Atg3*), *Atg12,* etc., which are autophagy-related genes (Wang D.T. et al., 2015).

Myostatin in bone-muscle crosstalk during aging

Shibaguchi et al. (2018) showed that myostatin increases with age in fast muscle fibers, while myostatin and its receptors in slow muscle are less responsive. This may explain why fast muscle fiber atrophy is characteristic of aging muscle. Opposing results may be explained by species differences (Bowser et al., 2013). Moreover, muscle atrophy and reduced muscle capacity are improved in aging *Mstn*-deficient mice compared to WT littermates (Siriett et al., 2006). Further, evidence indicates that the myostatin inhibitor can treat age-related sarcopenia (White and LeBrasseur, 2014). Nevertheless, the relevance between age and myostatin is ambiguous. Different opinions exist, with some reporting that circulating myostatin level increases with age until 57 years old, and decreases thereafter, while others implied that serum myostatin increases or decreases with age continuously (Szulc et al., 2012; Bowser et al., 2013; Poggioli et al., 2016). Interestingly, Szulc et al. (2012) found that myostatin level exhibits circannual variation, with greater concentrations observed during spring. These various opinions may due to a highly homologous amino acid sequence-growth and differentiation factor 11 (GDF11), to date no effective method can distinguish GDF11 from GDF8, furthermore, many studies examined circulating total myostatin, including the inactive and active forms, but only biologically active forms are functional. Circulating myostatin levels do not reflect the actual amount in special tissues (Szulc et al., 2012; Shibaguchi et al., 2018; Wu et al., 2018). Moreover, western blot analysis may not reflect true levels of myostatin, as other proteins may appear at the same molecular weight (Poggioli et al., 2016). Regarding the relationship between altered myostatin level and bone status, a cross-sectional study illustrated that high mature myostatin level is significantly related to low bone mineral density (BMD) in elderly Chinese subjects (Wu et al., 2018). Meanwhile, aged myofibers and myoblast cell line enhance osteogenesis upon exposure to myostatin propeptides, which indicates that myostatin may be a potential target to treat osteosarcopenia. Initially, the safety of the myostatin inhibitor was controversial, but later Morissette et al. (2009) dispelled fears that using myostatin inhibitor could cause heart enlargement and showed that it improves insulin sensitivity and bone density (Zhang et al., 2020). In addition, Ran et al. (2020) revealed that anchoring the propeptide to the second extracellular loop of the exosome surface marker CD63 could assist the impaired administration efficacy due to low biological activity and stability. Further research is required to promote myostatin inhibitor as a promising prospect for patients with osteosarcopenia.

Other Myokines

Other myokines, such as fibroblast growth factor 21 (FGF21), β-aminoisobutyric acid (BAIBA), and Meteorin-like (METRNL), have been discovered in recent years and reported to affect osteogenesis, myogenesis, and bone-muscle crosstalk during aging. Here, we briefly describe their roles in bone and muscle, and their effects on age-related crosstalk.

Fibroblast growth factor 21

Fibroblast growth factor 21, abbreviated as FGF21, is weakly expresses in healthy muscle, and it increases with age, starvation,

and mitochondrial dysfunction (Oost et al., 2019). FGF21 belongs to the FGF family, scientists have found 23 FGF proteins to date, most FGF family proteins regulate cell proliferation, while FGF21 mainly affects metabolism (Itoh, 2014). Despite expressed in muscle, it is also referred to as a hepatokine and adipokine, as the primary organ releasing FGF21 depends on different stimuli (Itoh, 2014). The function of FGF21 on metabolism is controversial, as scientists found that *Fgf21* knockout prevents high-fat ketogenic diet-induced insulin resistance in mice, but others confirmed the benefits of FGF21 on glucolipid metabolism (Itoh, 2014). Also, the relationship between FGF21 and bone and muscle is intriguing.

The effects of FGF21 on osteogenesis. Wei et al. (2012) firstly identified FGF21 as a skeletal metabolism regulator in 2012, they reported that either FGF21 pharmacological exposure or genetic gain-of-function, causes significantly low bone mass phenotype, moreover, PPARγ-FGF21 forms a feed-forward regulatory pathway, which favors BMSCs commitment to adipocytes instead of osteoblast lineage. In addition, they found that osteoclast-mediated bone resorption increases in *Fgf21* transgenic mice and suggested that FGF21 may promote osteoclastogenesis by increasing RANKL expression level in osteocytes (Wei et al., 2012). Charoenphandhu et al. (2017) and Hao et al. (2018) sequentially confirmed the deterioration effect of FGF21 on skeletal and the indirect influence of FGF21 on osteoclasts in humans and rats. Wang X. et al. (2015) discovered that FGF21 mediates a liver-osteoclast communication via insulin-like growth factor binding protein 1 (IGFBP1). FGF21 enhances the expression of IGFBP1 mainly in the liver, and then IGFBP1 is released into the bloodstream, promotes RANKL-induced osteoclastogenesis via combination with Integrin β1 receptor, further activates RANKL-induced NFATc1 expression (Wang X. et al., 2015). Furthermore, miR-100 was identified as the upstream regulator of *Fgf21*, miR-100 overexpression reduces FGF21 levels in serum and liver, thus inhibiting osteoclast-mediated bone resorption and partially restoring the bone phenotype in OVX-operated mice (Zhou et al., 2019). Nevertheless, none of these studies investigated the direct effects of muscle-derived FGF21 on bone and bone-muscle crosstalk.

The effects of FGF21 on myogenesis. Recently, attention is turned to the autocrine function of myokine FGF21. Evidence showed that FGF21 requires other factors to trigger its harmful function in muscle. Oost et al. (2019) demonstrated that *Fgf21* is dispensable for muscle mass maintenance under normal conditions, while it is necessary to induce muscle atrophy and weakness in a starvation state via enhancing mitophagic flux mediated by activation of mitophagy protein BCL2/adenovirus E1B interacting protein 3 (BNIP3). Reduction of the important pro-fusion protein optic atrophy protein 1 (OPA1) is related to aging-related muscle atrophy, Tezze et al. (2017) found that in double muscle-specific *Opa1/Fgf21* knockout mice, *Fgf21* deletion could partially rescue the muscle loss caused by OPA1 deficiency. These observations suggested a harmful effect of FGF21 on muscle. Nevertheless, FGF21 administration cannot inhibit the FGF19 function, which induces muscle hypertrophy (Benoit et al., 2017). Furthermore, FGF21 was found to induce cell cycle exit in C2C12 myoblasts by suppressing the cell cycle-related protein by p21, which is activated by p53 (Liu S. et al., 2017; Liu et al., 2017b). In addition, Liu et al. (2017a) suggested that FGF21 enhances myogenesis through PAX3 activation, and it could promote formation of aerobic myofibers via the FGF21-sirtuin-AMPK-peroxisome proliferative activated receptor, gamma coactivator 1 alpha (PGC1α) pathway *in vitro* and *in vivo*. The effect of FGF21 on myogenesis is obscure, and scientists should focus on deciphering these effects to discover novel therapeutic intervention strategies aimed at treating musculoskeletal diseases.

FGF21 in bone-muscle crosstalk during aging. FGF21 was found to increase with age, and reported to be negatively associated with BMD (Hao et al., 2018; Lee et al., 2020). The mechanism behind this may be attributed to BMSCs preferring to form adipocytes over osteoblasts or osteoclasts enhancing its bone resorption via FGF21-IGFBP1 axis (Wei et al., 2012; Wang X. et al., 2015); however, Lee et al. (2020) rejected the second half of the hypothesis and demonstrated that age-related bone loss caused by FGF21 is irrelevant to the FGF21-IGFBP1 axis. Further, serum FGF21 was reportedly positively associated with sarcopenia (Hanks et al., 2015; Tezze et al., 2017). The major shortcoming of this research regarding the relationship between FGF21 with BMD and muscle mass is the cross-sectional study design, as it cannot conclude a causal relationship between age-related changes in FGF21 and bone or muscle loss in the elderly. Therefore, further research is required to investigate whether FGF21 can be used as a potential target to treat osteosarcopenia, and the causal correlation should be explored.

β-*aminoisobutyric acid*

BAIBA refers to β-aminoisobutyric acid, which has two enantiomers, L-BAIBA and D-BAIBA, like every other amino acid except for glycine. BAIBA was found in urine and reported as a myokine generated during exercise or from muscle-PGC-1α-over-expressing mice. It is a catalysate of branched chain amino acid valine and thymine, exhibiting effects on browning white adipose tissue and promoting β-oxidation of fatty acid in liver (Roberts et al., 2014). Reports have shown that BAIBA improves metabolism dependent on PPAR and leptin (Kammoun and Febbraio, 2014; Roberts et al., 2014). As a newly discovered exercise-induced myokine, it has attracted many scientists to study its mysterious role in bone-muscle crosstalk.

The effects of BAIBA on osteogenesis. Kitase et al. (2018) found that BAIBA, especially L-BAIBA, could protect young osteocytes from reactive oxygen species (ROS)-induced cell death by protecting mitochondrial morphology and function, and reduce bone loss in a hind-limb unloading model. Subsequently, Zhu X.W. et al. (2018) demonstrated that appropriate low doses of BAIBA either promotes proliferation or enhances the expression of osteogenic transcription factor RUNX2 and differentiation markers OPG, osteopontin, and ALP in MC3T3-E1 osteoprogenitor cells. Meanwhile, they declared that moderate ROS production by NAD(P)H oxidase 4 might explain the BAIBA stimulatory effect on an osteoblast cell line (Zhu X.W. et al., 2018). Recently, Wang et al. (2020) illustrate that BAIBA is

positively associated with BMD in young, healthy women. The correlation is disrupted after the occurrence of a fracture or during an obese state, mainly due to interference caused by medical treatments and cytokines released by obese subjects. Research regarding the effects of BAIBA on bone is far from enough, whether it can affect formation or function of osteoclasts remains to be studied, and its physiological dosages for bone formation also need to be determined.

The effects of BAIBA on myogenesis. Very few BAIBA functional studies on muscle exist. Scientists found that BAIBA could prevent loss of extensor digitorum longus (EDL) and soleus muscle function in unloading hind-limb male mice (Kitase et al., 2018). While BAIBA increases the male EDL muscle mass only, it indicated that gains in muscle mass are unnecessary for improved muscle function and gender specific hormone expression of female mice might account for unaffected muscle phenotype (Kitase et al., 2018). Furthermore, the only *in vitro* study on the effects of BAIBA on muscle reported that BAIBA prevents hyperlipidemia-induced insulin resistance and palmitate-induced inflammation in a C2C12 myoblast cell line (Jung et al., 2015). Although it was widely recognized that insulin resistance and muscle inflammation are two mainly harmful factors to muscle mass and function, further research is required to investigate the direct effect of BAIBA on myogenesis (Cleasby et al., 2016).

BAIBA in bone-muscle crosstalk during aging. Reactive oxygen species-induced osteocyte cell death could be rescued by BAIBA treatment. To our knowledge, increased ROS can lead to aging, therefore BAIBA, which protects cells from ROS injury, may be a profoundly effective osteoporosis treatment (Hamrick and McGee-Lawrence, 2018). The protective effect of BAIBA on osteocytes decreases with age; to further elucidate the underlying mechanism, researchers compared not only the ability of skeletal muscle to produce BAIBA in different-aged mice but also the expression of BAIBA receptor-Mas-related G-protein-coupled receptor type D (MRGPRD) in young and aged osteocytes (Kitase et al., 2018). Interestingly, Kitase et al. (2018) demonstrated that decreasing level of MRGPRD in osteocyte membranes could account for the compromised effect of BAIBA on aged osteocytes, although BAIBA production increases in aged skeletal muscle. Further investigations should be conducted to explore methods to improve MRGPRD expression in osteocytes. Further, the detailed role of BAIBA in osteosarcopenia deserves exploration.

Meteorin-like

Meteorin-like is a small protein molecule reported to regulate glucose metabolism, thermogenesis, and inflammation (Ushach et al., 2018). Scientists using *Pgc-1α* splice isoform *Pgc-1α4* muscle-specific transgenic mice reported that METRNL is released by muscle after exercise; in addition, they found adipocytes can also release METRNL during cold stimulation (Rao et al., 2014). METRNL recruits eosinophils to secret IL-4/IL-13, activating macrophages to release anti-inflammatory cytokines to improve glucose homeostasis and promote white adipose tissue (WAT) browning (Rao et al., 2014). In addition, METRNL, also defined as Subfatin, appears downregulated in adipose tissue of calorie restricted rats and is highly expressed in obese-mice adipocytes and during adipogenic differentiation, thus thought to be an adipokine related to energy storage (Li et al., 2014). Moreover, METRNL was found to be an anti-inflammatory cytokine expressed in human barrier tissue and macrophages, while *Metrnl* knockout mice do not exhibit abnormal metabolism but exhibit immunity defects (Ushach et al., 2018). The reason for this phenomenon may be that, like FGF21, METRNL is weakly expressed under normal conditions and mainly plays roles in regulating immunity, it requires other factors to trigger its function regarding energy metabolism. Furthermore, research investigating the roles of METRNL in bone and muscle regulation is not well-developed, with only one study reporting that METRNL could affect Ap-1 transcription factor and inhibit mineralized nodule formation (Gong et al., 2016). No studies exist regarding the effects of METRNL on skeletal muscle mass and function, but research has shown that METRNL recruits eosinophils to activate macrophages, and eosinophil-macrophage synergy reportedly participates in repairing damaged muscle (Heredia et al., 2013; Rao et al., 2014). Therefore, METRNL supposedly affects muscle regeneration and/or myogenesis. This indicates that METRNL may function as a messenger to mediate muscle-bone crosstalk and their interplay during aging.

Osteokines

Osteocalcin

Osteocalcin (OCN), a secreted protein originating from osteoblasts, goes through sequential cleavages to split amino acid sequences, such as signal peptides, and obtains γ-carboxylate at three residues aided by a cofactor – vitamin K. There are two forms of OCN depending on the degree of carboxylation, while the under-carboxylated form is considered to function in blood circulation, which stems from an acid circumstance caused by bone matrix resorption through osteoclasts or directly released by osteoblasts during acute stress response (Battafarano et al., 2020). OCN is like hormones in biological characteristic and physiological function. Serum OCN can enter distant cells to regulate insulin resistance, glucose homeostasis, male fertility, and brain function (Li J. et al., 2016; Mizokami et al., 2017; Battafarano et al., 2020). Recently, many studies show that OCN acts as a messenger and participates in interactions between bone and muscle. OCN expression increases dramatically during bone matrix mineralization, which is considered to be a marker representing late osteogenesis. Besides, skeletal muscle, a locomotive and glycogen storage organ, is also an important target tissue of OCN.

The effects of osteocalcin on muscle

Initially, studies investigating OCN effects on skeletal muscle were limited to energy metabolism. Mera et al. (2016a) demonstrated that OCN could improve muscle to utilize glucose and fatty acids, meanwhile, they found that mice deficient in *Ocn* exhibit impaired exercise capacity and exogenous OCN administration could rescue the exercise capacity of aged mice. Furthermore, OCN could stimulate skeletal muscle to release IL-6, simultaneously IL-6 and OCN form a feed-forward axis

to amplify adaption to exercise (Mera et al., 2016a). Next, the influence of OCN on muscle mass was investigated. Using female mice in a study, to exclude the effect of testosterone, Mera et al. (2016b) found that osteocalcin signaling is necessary to maintain muscle mass in old mice by promoting protein synthesis. However, this research did not elaborate on the mechanism. Later, Liu S. et al. (2017) illustrated and confirmed that under-carboxylated OCN enhances C2C12 myoblast cell proliferation and myogenic differentiation thorough activation of the PI3K/Akt, p38, and GPRC6A-ERK1/2 signaling pathways, respectively. Moreover, several investigations on rats, healthy volunteers, or patients with hypoparathyroidism revealed that under-carboxylated OCN is positively associated with muscle mass or function (Levinger et al., 2014; Harslof et al., 2016; Lin et al., 2016). However, this experiment should be repeated in a large healthy population.

The effects of osteocalcin on bone

The effects of OCN on bone are divided into three parts. First, the controversial role in bone formation. OCN is highly expressed in mature osteoblasts and a familiar marker of bone formation, however, unexpectedly, $Ocn^{-/-}$ mice exhibit increased bone mass (Li J. et al., 2016). Bodine and Komm (1999) found an OCN receptor coupled with a Gi-protein in a human osteoblast cell line and confirmed that OCN could suppress bone formation. However, the specific mechanism has not been clarified. Second, the role in bone mineralization. OCN has a strong affinity for Ca^{2+} and hydroxyapatite and reportedly promotes bone mineral maturity in *Ocn* knockout mice; furthermore, hydroxyapatite crystal growth is suppressed by OCN in certain studies (Neve et al., 2013). Third, the role in bone resorption, besides recruiting osteoclasts and enhancing its chemotaxis, OCN fragments can also promote osteoclastogenesis (Neve et al., 2013; Li J. et al., 2016). Mera et al. (2016a) further demonstrated that OCN could stimulate skeletal muscle release IL-6, subsequently increasing the expression of RANKL in osteoblasts and decreasing the decoy receptor of *Rankl*, in other words, OCN enhances bone resorption mediated by IL-6 released from muscle. The detailed mechanism should be elucidated, and researchers should distinguish the functional component between the fragments or carboxylation status.

Osteocalcin in bone-muscle crosstalk during aging

It is widely recognized that sex hormones and brain function decline with age. Studies reported positive association between serum OCN and testosterone, meanwhile low OCN is related to impaired brain cognition and microstructure (Puig et al., 2016; Zhong et al., 2016). Therefore, although the results regarding OCN and age are controversial, we prefer the theory suggesting plasma OCN levels decrease with age (Mera et al., 2016a; Diemar et al., 2020). Nevertheless, many cross-sectional investigations revealed that OCN is negatively associated with BMD (Kim et al., 2010; Ling et al., 2016). The effects of OCN may be blurred by diverse subtypes, which may explain the contradictory results between age-related bone loss and age-related decreases in OCN, and its deleterious function on bone. Thus, further study is required to confirm whether OCN can be used as a treatment for osteoporosis and sarcopenia.

Sclerostin

Sclerostin is a glycoprotein released by osteocytes and recognized as a member of Dan/Cerberus family of bone morphogenetic protein (BMP) antagonists. Sclerostin primarily originates from mature osteocytes, but is also observed in the cardio-cerebral vascular system, lung, and kidney, with only the mRNA expression detected in the latter tissues (Delgado-Calle et al., 2017; Holdsworth et al., 2019). Sclerostin not only couples with BMP to suppress BMP-induced phosphorylation of Smad but also impairs the canonical Wnt pathway through competitive combination with LDL receptor related protein 5/6 (LRP5/6), the co-receptor of the Wnt pathway (Winkler et al., 2003; Fijalkowski et al., 2016). In addition, the binding of sclerostin to LRP5/6 requires the "molecular chaperone" LRP4; consequently, mutations in sclerostin or *Lrp4* produce similar abnormal phenotype (Fijalkowski et al., 2016).

The effects of sclerostin on muscle

Sclerostin may play an important role in muscle mass modulation. von Maltzahn et al. (2012) reported that the Wnt signaling pathway is engaged in the differentiation of muscle stem cells. Moreover, Kim S.P. et al. (2017) showed that $Sost^{-/-}$ mice exhibit increased lean body mass in older animals with *P*-value of 0.06, while over-expressing sclerostin by an adeno-associated virus revealed the opposite body composition phenotype in $Sost^{-/-}$ mice, which showed an increase in body fat mass and a small, but significant reduction in lean body mass. Further, circulating sclerostin levels are higher in low muscle mass subjects than healthy controls (Kim et al., 2019). In addition, Huang et al. (2017) found that sclerostin could suppress WNT3a mediated crosstalk between MLO-Y4 osteocytes and muscle cells (C2C12) by regulating the Wnt/β-catenin pathway. While a sclerostin inhibitor enhances muscle regeneration, it can also restore muscle function in cancer induced muscle weakness, but it cannot prevent soleus muscle atrophy in rodents after spinal cord injury, possibly because low expression of *Lrp5/Lrp6* was observed in the rat soleus (Phillips et al., 2018; Hesse et al., 2019). A detailed mechanism of action regarding muscle function regulation by sclerostin should be explored further.

The effects of sclerostin on bone

SOST genetic mutation-induced high bone mass was reported in the 1950s, but the pathogenesis of the skeletal disease, named Sclerosteosis, was identified in 2001 (Van Buchem et al., 1955). Moreover, other modifications in or near *SOST* can cause abnormal BMD, such as Van Buchem disease (Holdsworth et al., 2019). In addition, sclerostin transgenic mice exhibit osteopenia (Winkler et al., 2003). Sclerostin is the second emerging therapeutic target, besides PTH, to promote bone anabolism. Several osteogenic activities, such as mechanical load or intermittent PTH administration, can influence serum sclerostin levels (Keller and Kneissel, 2005; Robling et al., 2008). Besides impairing the canonical Wnt pathway and BMP signaling pathway in bone formation, sclerostin was reported to regulate differentiation and mineralization of osteogenic lineage cells via a matrix extracellular phosphoglycoprotein (MEPE)-acidic serine aspartate-rich MEPE-associated motif

(ASARM)-dependent mechanism (Atkins et al., 2011). Moreover, labeling osteoblasts with tamoxifen-inducible lineage-tracing strategies, researchers found that sclerostin inhibition could re-activate quiescent bone lining cells, but the underlying mechanism requires further investigation (Kim S.W. et al., 2017). Sclerostin not only affects the activities of osteogenic lineage cells within the bone microenvironment but also promotes bone resorption in a RANKL-dependent pathway in an autocrine manner (Carvalho et al., 2011).

Sclerostin in bone-muscle crosstalk during aging

Serum sclerostin levels ensue with aging, and osteoclasts are also a source of aging-related sclerostin increase (Mirza et al., 2010). It has been reported that osteoclast cultures from old mice produce more sclerostin than from young mice, suggesting that sclerostin may contribute to decreased bone formation in the elderly (Ota et al., 2013). However, Reppe et al. (2015) demonstrated that osteoporosis patients exhibit lower sclerostin levels than healthy controls. The relationship between sclerostin and bone mass is intriguing, since sclerostin inhibits bone formation and is produced by bone cells. There is a functional negative feedback between sclerostin and formation of mature osteocytes. Furthermore, Chang et al. (2014) found that LRP4 acts as an anchor to trap sclerostin in the local bone environment. Genetic deletion of *Lrp4* increases bone mass despite rising serum sclerostin, which indicated that circulating sclerostin level cannot reflect local bone turnover (Chang et al., 2014). Despite the ambiguous relationship between sclerostin level and aged-related osteoporosis, sclerostin inhibitor was found to increase bone mass and strength in the early stages of treatment in a pre-clinical study, although the effects were significantly reduced after prolonged treatment. Meanwhile, ablation of *Sost* increases lean body mass in elderly animals (Kim S.P. et al., 2017). In addition, it has been reported that diabetes is associated with increased risk of sarcopenia. Medeiros et al. (2020) reported on a study involving hemodialysis patients with diabetes and illustrated that sclerostin proportion is higher in patients with type 2 diabetes mellitus compared to healthy controls, possibly indicating that a positive relationship between sclerostin and sarcopenia exists. Thus, sclerostin may play an active role in age-related bone-muscle crosstalk.

OPG/RANKL/RANK

Receptor Activator of Nuclear Factor κB Ligand, abbreviated as RANKL, is a transmembrane protein located in osteocytes and osteoblasts. When talking about RANKL, it is necessary to introduce the OPG/RANKL/RANK system together. It is well known that bone formation and bone resorption are cyclical, dynamically balanced processes, but the molecular mechanisms that link bone formation and resorption were not substantially improved until 1997 (Simonet et al., 1997; Khosla, 2001). The identification of the OPG/RANKL/RANK system presented a new era in the history of bone biology. RANK is a tumor necrosis factor (TNF) receptor superfamily protein in osteoclasts, it can bind to RANKL to activate major molecules in downstream signaling pathways, such as nuclear factor kappa B (NF-κB) and colony-stimulating factor 1 receptor, thus driving differentiation of pre-osteoclasts to osteoclasts (Chung et al., 2014). Besides RANK, OPG also binds to RANKL, unlike other receptor proteins, it is a soluble receptor which suppresses osteoclast activation. Dysfunction of the OPG/RANKL/RANK axis can cause osteoporosis (Dufresne et al., 2018). In addition, RANK is reportedly expressed in skeletal muscle, while dysfunction of the OPG/RANKL/RANK axis induces various muscle phenotype, therefore, the OPG/RANKL/RANK axis presents a new avenue for the investigation of bone-muscle interplay (Dufresne et al., 2018).

The effects of OPG/RANKL/RANK on muscle

RANKL-RANK interaction can activate NF-κB, a pro-inflammation pathway, which can inhibit myogenic differentiation and enhance the expression of the ubiquitin proteasome system to induce muscle atrophy. Anti-RANKL treatment can shift macrophages into the M2 phenotype and inhibit the activation of NF-κB in Duchenne muscular dystrophy, thus protecting muscle from chronic inflammation and improving its mechanical properties (Hamoudi et al., 2019). In dystrophic mdx mice, *Rank* knockout rescues muscle strength, but is less effective than full-length OPG-Fc treatment. This may because while full-length OPG-Fc suppresses the RANK-RANKL combination, it also activates sarco/endoplasmic reticulum Ca^{2+} ATPase to regulate Ca^{2+} homeostasis in dystrophic EDL through another pathway (Dufresne et al., 2018). Moreover, Bonnet et al. (2019) observed that RANKL inhibitor Dmab could rescue muscle function in humans. Recently, Hamoudi et al. (2020) reveal that *Opg* knockout mice displays selective atrophy of fast-twitch-type IIb myofibers, while C2C12 myotubes exhibit reduced cross section area when exposed to RANKL, they further confirmed that the OPG/RANKL/RANK axis is involved in muscle function regulation.

The effects of OPG/RANKL/RANK on bone

The study of the OPG/RANKL/RANK system on bone began with the identification of OPG. Simonet et al. (1997) found that OPG is a TNF receptor molecule in the rat intestine, and over-expressing OPG in mice show a predominant decrease in osteoclasts (Khosla, 2001). Hormone deficiency and long-term use of glucocorticoids induced abnormal bone resorption are due to changes in RANKL or OPG expression (Singh et al., 2018). Traditionally, the OPG/RANKL/RANK axis reportedly plays a role in osteoclastogenesis. However, scientists found that OPG/RANKL/RANK has an entirely new role in regulating bone metabolism. Zhang et al. (2016) illustrated that *Opg* ablated mice show increased adipocytes, while BMSCs from these mice prefer adipogenesis via enhanced expression of adipogenic transcription marker, Pparγ. Recently, RANK is found to play a role in osteoclast-to-osteoblast crosstalk via EVs released from osteoclasts to induce reverse RANKL signaling, leading to increased osteogenesis and mineralization (Ikebuchi et al., 2018).

OPG/RANKL/RANK in bone-muscle crosstalk during aging

The imbalance between bone formation and bone resorption leads to age-related osteoporosis (Yang et al., 2019). Much attention has been paid to the role of the OPG/RANKL/RANK axis in this process. Researchers found that RANK, RANKL,

and RANKL/OPG ratio increase in the bone marrow with age, while the bone protective factor OPG decreases with age (Chung et al., 2014; Zhang et al., 2016). However, Piemontese et al. (2017) found that OPG increase with age in femoral marrow plasma, but it's not as obvious as RANKL, indicating that the RANKL/OPG ratio would increase with age. Furthermore, Singh et al. (2018) demonstrated high serum RANKL/OPG ratio in adult mice, and IL-3 could improve the RANKL/OPG ratio and act as a potent medicine to treat osteoporosis. Therefore, changes in the RANKL/OPG ratio are more appropriate as a determinant of bone mass than individual changes in protein levels, such as RANKL or OPG alone. As for muscle, the relationship between RANKL/OPG/RANK and muscle atrophy has been reported, while the relationship with sarcopenia was rarely reported. Bonnet et al. (2019) observed that RANKL inhibitor Dmab could rescue muscle function in postmenopausal women, as well as in osteo-sarcopenic *Pparb*$^{-/-}$ mice. This suggests that the OPG/RANKL/RANK axis may be an existing and feasible method to treat osteoporosis and sarcopenia together.

SKELETAL MUSCLE-DERIVED EV-microRNAs

EV-microRNAs of Skeletal Muscle Engaged in Bone-Muscle Crosstalk

Skeletal muscle, a force generator in motion, also an essential endocrine organ, continually releases myokines and EVs to regulate organic metabolism and homeostasis.

A considerable amount of EVs circulate in the bloodstream, and muscle-derived EVs make up 1–5% of total EVs in circulation (Guescini et al., 2015). Guescini et al. (2015) illustrated that muscle-specific microRNAs enclosed in EVs are released into the blood during exercise, and 60–65% of the muscular EVs are CD81 positive. During moderate exercise, contracting muscle can strengthen bone quality and prolong lifespan. However, few studies reported that muscular EVs act on bone. Xu Q. et al. (2018) reported that EVs from C2C12 myoblasts or myotubes promote MC3T3-E1 cell osteogenic differentiation via the β-catenin signaling pathway, and miR-27a-3p is the major functional factor. Furthermore, miR-27a was found to enhance myoblast differentiation (Huang et al., 2012; Chen et al., 2014) and miR-27a mimic could rescue chronic kidney disease-induced muscle atrophy (Wang et al., 2017). This indicates that miR-27a in muscle-derived EVs might function in bone and muscle crosstalk. In addition, besides bone formation, muscular EVs also exert a negative effect on osteoclast formation and its mitochondrial metabolism, the latter is necessary for mature osteoclast resorption (Takafuji et al., 2020).

EV-microRNAs of Skeletal Muscle in Bone-Muscle Crosstalk During Aging

Intensity and frequency of exercise are reduced in most elderly people, and senescent cell-derived EVs alter their cargo, contributing to age-related decline in somatic function. Alpha-sarcoglycan, an integral membrane glycoprotein, which specially localized to the sarcolemma acts as a typical marker of muscular EVs (Ervasti et al., 1990; Guescini et al., 2015). Recently, an intriguing study demonstrates that miR-34a is highly expressed in aged mouse skeletal muscle and serum EVs. Furthermore, Fulzele et al. (2019) reported that alpha-sarcoglycan-positive EVs and EVs from oxidative stress treated C2C12 cells all exhibit that miR-34a increases with age, and these EVs could home to bone marrow, leading to BMSC senescence by repressing SIRT1 expression. Elevated miR-34a in the aging muscle can account for muscle metabolic dysfunction, while decreased SIRT1 activity in aging muscles is associated with impaired muscle performance (Mohamed et al., 2014; Kukreti and Amuthavalli, 2020). Yang et al. (2020) reported that miR-29b-3p is increased in the plasma of aging mice and humans, differentiated atrophic C2C12 myotube could release miR-29b-3p-loaded EVs to induce neuronal dysfunction. miR-29b was shown to contribute to several types of muscle atrophy (Li et al., 2017). Moreover, regarding bone metabolism, miR-29b-3p was found to decrease in osteocytes under mechanical loading. Transfection of miR-29b-3p in osteocytes reduces IGF-1 production, thus suppressing osteoblast differentiation (Zeng et al., 2019). Future research should investigate whether miR-29b-3p in muscle-derived EVs acts as a critical factor in bone-muscle crosstalk during aging. Research should look into whether muscle-specific microRNAs enclosed in muscular EVs, which are influenced by exercise, such as miR-1, miR-133a, can be used for osteosarcopenia treatment (Guescini et al., 2015).

EV-microRNAs OF BONE CELLS ENGAGED IN BONE-MUSCLE CROSSTALK

Most scientists focused on the influence of muscle on bone mass, and sometimes on the effects of osteokines on muscle, while no studies directly investigated the influence of EVs secreted by bone on muscle. Herein, we summarize several microRNAs, which appear altered in senescent bone cell-derived EVs, reported to influence bone metabolism and regulate muscle metabolism.

A subset of differentially expressed EV-microRNAs among young and aging BMSCs were found recently (Davis et al., 2017; Umezu et al., 2017; Su et al., 2019). We summarize and select several from 65 age-dependent altered microRNAs, including miR-10a/10b-5p/15b/17-5p/182-5p/183-5p/185/186/196a-5p/20a/221/24/28-5p/31a-5p/328/365/374/411/467e-5p/487a/99b etc. By consulting articles regarding bone metabolism and myogenesis, we screen out four downregulated and seven upregulated microRNAs in aging BMSC-derived exosomes.

The downregulated microRNAs include miR-24, miR-328, miR-365, and miR-374. The commonality between these microRNAs downregulated in aging BMSC-EVs is that they reportedly benefit myogenesis and bone formation, or at least myogenesis. Sun et al. (2008) demonstrated that ectopic expression of miR-24 promotes the expression of myogenic differentiation markers in C2C12 myoblasts. Furthermore, miR-365 and miR-374 were reported to accelerate cardiomyocyte

hypertrophy (Lee et al., 2017; Wu et al., 2017). Besides myogenesis, bone formation is also regulated by these two microRNAs. Concretely, miR-365 overexpression could improve the expression of *Runx2* in MC3T3-E1 cells and rescue dexamethasone-induced osteogenesis suppression; it can also suppress bone resorption via decreasing osteoclast number (Franceschetti et al., 2014; Xu et al., 2017). Regarding miR-374, Ge et al. (2018) found that miR-374 expression is significantly increased in fractured mice and verified that miR-374 improves MSC osteogenesis via PTEN using miR-374 transgenic and knockout model. Moreover, miR-328 may play an important role in bone-muscle crosstalk in aging. Liu D. et al. (2018) verified that apoptosis-deficient *MRL/lpr* and *Casp3*$^{-/-}$ mice show impaired osteogenesis capability of BMSCs. Further, they found that circulating apoptotic bodies treatment maintains bone homeostasis of *MRL/lpr* and *Casp3*$^{-/-}$ mice and improves the osteopenia phenotype of ovariectomized mice. Interestingly, Liu D. et al. (2018) found that miR-328 is a functional factor in apoptotic bodies. Lately, miR-328 was reportedly decreased in the plasma of the sarcopenia group in the elderly (Wu et al., 2017).

The upregulated microRNAs include miR-15b, miR-17, miR-20a, miR-186, miR-221, miR-31a-5p, and miR-99b. miR-15b was reported to be a negative regulator of myoblast differentiation via SET-domain containing 3 (SETD3) (Zhao et al., 2019). In addition, Fang et al. (2019) found that miR-15b could repress BMSC osteogenesis, while others revealed contrasting result that miR-15b has a positive effect on osteogenic differentiation, therefore, further research is required to determine if miR-15b is a potential target. miR-17 and miR-20a belong to the miR-17-92 cluster, which is reported to suppress myogenesis by reducing the expression of enigma homolog 1 (*Enh1*), then inhibiting myogenic regulatory factor (MRF) and E protein binding to the myogenesis genes (Qiu et al., 2016; Vimalraj et al., 2014). Moreover, Fang et al. (2016) found that silencing miR-17 could improve the micro-architecture of trabecular bones. Meanwhile, miR-17 and miR-20a were reported to enhance BMSC adipogenesis (An et al., 2016; Zhu E. et al., 2018). Nevertheless, Zhou et al. (2014) had shown that miR-17-92 cluster heterozygous mice exhibit worse trabecular micro-architecture than wild-type controls. Consequently, scientists should investigate whether miR-17 and miR-20a can act as a cluster enclosed in EVs to influence bone and muscle phenotype together in aging. Combined with the negative effect of miR-186 on rat BMSC osteogenesis and the inhibitory action on the final myogenesis differentiation step by influencing myogenin translation, we deduce that miR-186 may be the driving factor in bone-muscle crosstalk during aging (Antoniou et al., 2014; Xiao J. et al., 2020). Furthermore, the increased miR-221 in aged-BMSC may also function in osteosarcopenia, because it was reported that ectopic overexpression of miR-221 in skeletal muscle satellite cells inhibits myotube formation and miR-221 was found to be a negative regulator of bone formation (Zhang et al., 2017; Liu B. et al., 2018; Gan et al., 2020). Xu R. et al. (2018) reported aged BMSCs express high levels of miR-31a-5p leading to bias lineage fate of BMSCs to adipocytes through AT-rich sequence binding protein 2 (SATB2), aged BMSCs also release miR-31a-5p enriched EVs to its microenvironment, inducing increase in osteoclast number and function via the RhoA pathway. Moreover, age-dependent increases in miR-31 can inhibit the dystrophin response to loading, and cause muscles of aged rats more susceptible to injury after disuse (Hughes et al., 2018). Whether these above molecules can participate in age-related bone-muscle crosstalk or not requires further research. Furthermore, we were inspired to investigate whether miR-188, which appears increased in aging BMSCs, can be released through EVs to regulate aging muscle phenotype, since miR-188 was reportedly elevated in a muscular dystrophy dog model (Li et al., 2015; Shibasaki et al., 2019). Zacharewicz et al. (2014, 2020) reported that miR-99b displays a negative age-dependent association with protein synthesis in skeletal muscle. Next, they verified that overexpression of miR-99b in human primary myotubes could inhibit protein synthesis via regulatory-associated protein of mTOR (RPTOR). As for bone, Franceschetti et al. (2014) performed a microRNA array during osteoclastogenesis and found that miR-99b inhibition decreases both osteoclast number and size. Considering the effects of miR-99b on muscle and osteoclasts, we hypothesize that miR-99b might become a new target of osteosarcopenia in the elderly.

Besides BMSCs, aged osteoclasts were found to liberate EVs unloading enhanced expression of miR-214-3p comparing with the young. Increasing miR-214-3p not only directly promotes osteoclast formation but it's also enclosed in osteoclast-derived EVs, then leading to impaired bone formation (Li D. et al., 2016). However, miR-214 was found to positively regulate C2C12 myoblasts proliferation and differentiation and reported to be an important participant in muscle metabolism (Feng et al., 2011). Overall, whether miR-214 can serve as a reasonable target to treat age-related osteoporosis and sarcopenia or not needs further exploration. In addition, Davis et al. (2017) collected bone marrow interstitial fluid from mice at two age stages and found that miR-183-5p increases with age in bone-derived EVs and is endocytosed by BMSCs, and finally suppresses osteogenic differentiation and induce BMSCs senescence. However, research is required on its function in muscle metabolism.

CONCLUSION AND FUTURE DIRECTIONS

There is much literature on bone and muscle crosstalk although, many key issues need to be addressed. Previous studies mainly focused on simple unidirectional communications between bone and muscle, little has reported their age-related reciprocal interactions. We outline age-related changes in the secretome and EV-microRNAs of bone and muscle, and aim to find out their common pathogenic factors and shared therapeutic targets. However, the study of age-related bone-muscle crosstalk is relatively complex, many uncharted fields still need to be explored.

Extracellular vesicles unloading many potential bioactive molecules act as information-transmitters between cells. Besides microRNAs, long non-coding RNA (LncRNA) is also enriched in EVs. No studies have reported its role in bone-muscle crosstalk in

aging, thus researches on age-related LncRNA changes in BMSCs and muscle, together with their related LncRNA functional studies will provide a niche for further investigation (Nie et al., 2015; Li et al., 2018). Scientists can investigate whether aged bone cells can enclose LncRNA, such as Bmncr, within EVs to regulate musculoskeletal metabolism. Such studies will help to find efficient therapeutic applications in age-related musculoskeletal diseases.

AUTHOR CONTRIBUTIONS

CH wrote the manuscript and designed the figures. WH, JH, KC, MH, MY, and XL revised the manuscript. CL provided critical feedback and helped to shape the manuscript. All authors listed have made a substantial contribution to the work.

FUNDING

This work was supported by the National Key R&D Program of China (Grant 2019YFA0111900), the National Natural Science Foundation of China (Grants 81922017, 81873669, and 81802209), the Hunan Province Natural Science Foundation of China (Grant 2018JJ3863), the Innovation Driven Project of Central South University (Grant 20170033010017), and the Talent Plan of Xiangya Hospital in Central South University (Grants 35 and 41).

REFERENCES

Alibhai, F. J., Lim, F., Yeganeh, A., DiStefano, P. V., Binesh-Marvasti, T., Belfiore, A., et al. (2020). Cellular senescence contributes to age-dependent changes in circulating extracellular vesicle cargo and function. *Aging Cell* 19:e13103. doi: 10.1111/acel.13103

An, X., Ma, K., Zhang, Z., Zhao, T., Zhang, X., Tang, B., et al. (2016). miR-17, miR-21, and miR-143 enhance adipogenic differentiation from porcine bone marrow-derived mesenchymal stem cells. *DNA Cell Biol.* 35, 410–416. doi: 10.1089/dna.2015.3182

Antoniou, A., Mastroyiannopoulos, N., Uney, J., and Phylactou, L. (2014). miR-186 inhibits muscle cell differentiation through myogenin regulation. *J. Biol. Chem.* 289, 3923–3935. doi: 10.1074/jbc.M113.507343

Atkins, G. J., Rowe, P. S., Lim, H. P., Welldon, K. J., Ormsby, R., Wijenayaka, A. R., et al. (2011). Sclerostin is a locally acting regulator of late-osteoblast/preosteocyte differentiation and regulates mineralization through a MEPE-ASARM-dependent mechanism. *J. Bone Miner. Res.* 26, 1425–1436. doi: 10.1002/jbmr.345

Battafarano, G., Rossi, M., Marampon, F., Minisola, S., and Del Fattore, A. (2020). Bone control of muscle function. *Int. J. Mol. Sci.* 21:1178. doi: 10.3390/ijms21041178

Benoit, B., Meugnier, E., Castelli, M., Chanon, S., Vieille-Marchiset, A., Durand, C., et al. (2017). Fibroblast growth factor 19 regulates skeletal muscle mass and ameliorates muscle wasting in mice. *Nat. Med.* 23, 990–996. doi: 10.1038/nm.4363

Binkley, N., and Buehring, B. (2009). Beyond FRAX: it's time to consider sarco-osteopenia. *J. Clin. Densitomet.* 12, 413–416. doi: 10.1016/j.jocd.2009.06.004

Bodine, P. V., and Komm, B. S. (1999). Evidence that conditionally immortalized human osteoblasts express an osteocalcin receptor. *Bone* 25, 535–543. doi: 10.1016/S8756-3282(99)00213-6

Bonnet, N., Bourgoin, L., Biver, E., Douni, E., and Ferrari, S. (2019). RANKL inhibition improves muscle strength and insulin sensitivity and restores bone mass. *J. Clin. Investig.* 129, 3214–3223. doi: 10.1172/JCI125915

Boström, P., Wu, J., Jedrychowski, M. P., Korde, A., Ye, L., Lo, J. C., et al. (2012). A PGC1-α-dependent myokine that drives brown-fat-like development of white fat and thermogenesis. *Nature* 481, 463–468. doi: 10.1038/nature10777

Bowser, M., Herberg, S., Arounleut, P., Shi, X., Fulzele, S., Hill, W. D., et al. (2013). Effects of the activin A-myostatin-follistatin system on aging bone and muscle progenitor cells. *Exp. Gerontol.* 48, 290–297. doi: 10.1016/j.exger.2012.11.004

Carvalho, D. P. D., Wijenayaka, A. R., Kogawa, M., Lim, H. P., Bonewald, L. F., Findlay, D. M., et al. (2011). Sclerostin stimulates osteocyte support of osteoclast activity by a RANKL-dependent pathway. *PLoS One* 6:e25900. doi: 10.1371/journal.pone.025900

Chang, J. S., Kim, T. H., Nguyen, T. T., Park, K.-S., Kim, N., and Kong, I. D. (2017). Circulating irisin levels as a predictive biomarker for sarcopenia: a cross-sectional community-based study. *Geriatr. Gerontol. Intern.* 17, 2266–2273. doi: 10.1111/ggi.13030

Chang, J. S., and Kong, I. D. (2020). Irisin prevents dexamethasone-induced atrophy in C2C12 myotubes. *Pflugers Arch.* 472, 495–502. doi: 10.1007/s00424-020-02367-4

Chang, M. K., Kramer, I., Huber, T., Kinzel, B., Guth-Gundel, S., Leupin, O., et al. (2014). Disruption of Lrp4 function by genetic deletion or pharmacological blockade increases bone mass and serum sclerostin levels. *Proc. Natl. Acad. Sci. U.S.A.* 111, E5187–E5195. doi: 10.1073/pnas.1413828111

Charoenphandhu, N., Suntornsaratoon, P., Krishnamra, N., Sa-Nguanmoo, P., Tanajak, P., Wang, X., et al. (2017). Fibroblast growth factor-21 restores insulin sensitivity but induces aberrant bone microstructure in obese insulin-resistant rats. *J. Bone Mineral Metab.* 35, 142–149. doi: 10.1007/s00774-016-0745-z

Chen, X., Huang, Z., Chen, D., Yang, T., and Liu, G. (2014). Role of microRNA-27a in myoblast differentiation. *Cell Biol. Intern.* 38, 266–271. doi: 10.1002/cbin.10192

Chen, Y. S., Guo, Q., Guo, L. J., Liu, T., Wu, X. P., Lin, Z. Y., et al. (2017). GDF8 inhibits bone formation and promotes bone resorption in mice. *Clin. Exper. Pharmacol. Physiol.* 44, 500–508. doi: 10.1111/1440-1681.12728

Chen, Z., Zhang, Y., Zhao, F., Yin, C., Yang, C., Wang, X., et al. (2020). Recombinant Irisin prevents the reduction of osteoblast differentiation induced by stimulated microgravity through increasing beta-Catenin expression. *Int. J. Mol. Sci.* 21:1259. doi: 10.3390/ijms21041259

Chung, P. L., Zhou, S., Eslami, B., Shen, L., LeBoff, M. S., and Glowacki, J. (2014). Effect of age on regulation of human osteoclast differentiation. *J. Cell. Biochem.* 115, 1412–1419. doi: 10.1002/jcb.24792

Cleasby, M. E., Jamieson, P. M., and Atherton, P. J. (2016). Insulin resistance and sarcopenia: mechanistic links between common co-morbidities. *J. Endocrinol.* 229, R67–R81. doi: 10.1530/JOE-15-0533

Colaianni, G., Cuscito, C., Mongelli, T., Oranger, A., Mori, G., Brunetti, G., et al. (2014). Irisin enhances osteoblast differentiation in vitro. *Intern. J. Endocrinol.* 2014:902186. doi: 10.1155/2014/902186

Colaianni, G., Cuscito, C., Mongelli, T., Pignataro, P., Buccoliero, C., Liu, P., et al. (2015). The myokine irisin increases cortical bone mass. *Proc. Natl. Acad. Sci. U.S.A.* 112, 12157–12162. doi: 10.1073/pnas.1516622112

Colaianni, G., Mongelli, T., Cuscito, C., Pignataro, P., Lippo, L., Spiro, G., et al. (2017). Irisin prevents and restores bone loss and muscle atrophy in hind-limb suspended mice. *Sci. Rep.* 7:2811. doi: 10.1038/s41598-017-02557-8

Dankbar, B., Fennen, M., Brunert, D., Hayer, S., Frank, S., Wehmeyer, C., et al. (2015). Myostatin is a direct regulator of osteoclast differentiation and its inhibition reduces inflammatory joint destruction in mice. *Nat. Med.* 21, 1085–1090. doi: 10.1038/nm.3917

Das, D. K., Graham, Z. A., and Cardozo, C. P. (2020). Myokines in skeletal muscle physiology and metabolism: recent advances and future perspectives. *Acta Physiol.* 228:e13367. doi: 10.1111/apha.13367

Davis, C., Dukes, A., Drewry, M., Helwa, I., Johnson, M. H., Isales, C. M., et al. (2017). MicroRNA-183-5p increases with age in bone-derived extracellular vesicles, suppresses bone marrow stromal (Stem) cell proliferation, and induces stem cell senescence. *Tissue Eng. Part A* 23, 1231–1240. doi: 10.1089/ten.tea.2016.0525

Delgado-Calle, J., Sato, A. Y., and Bellido, T. (2017). Role and mechanism of action of sclerostin in bone. *Bone* 96, 29–37. doi: 10.1016/j.bone.2016.10.007

Deng, Z., Luo, P., Lai, W., Song, T., Peng, J., and Wei, H. K. (2017). Myostatin inhibits eEF2K-eEF2 by regulating AMPK to suppress protein synthesis. *Biochem. Biophys. Res. Commun.* 494, 278–284. doi: 10.1016/j.bbrc.2017.10.040

Diemar, S. S., Mollehave, L. T., Quardon, N., Lylloff, L., Thuesen, B. H., Linneberg, A., et al. (2020). Effects of age and sex on osteocalcin and bone-specific alkaline phosphatase-reference intervals and confounders for two bone formation markers. *Arch. Osteoporos.* 15:26. doi: 10.1007/s11657-020-00715-6

Dufresne, S. S., Boulanger-Piette, A., Bosse, S., Argaw, A., Hamoudi, D., Marcadet, L., et al. (2018). Genetic deletion of muscle RANK or selective inhibition of RANKL is not as effective as full-length OPG-fc in mitigating muscular dystrophy. *Acta Neuropathol. Commun.* 6:31. doi: 10.1186/s40478-018-0533-1

Ervasti, J. M., Ohlendieck, K., Kahl, S. D., Gaver, M. G., and Campbell, K. P. (1990). Deficiency of a glycoprotein component of the dystrophin complex in dystrophic muscle. *Nature* 345, 315–319. doi: 10.1038/345315a0

Fang, S., Chen, L., Chen, H., Li, Y., Luo, H., Hu, D., et al. (2019). MiR-15b ameliorates SONFH by targeting Smad7 and inhibiting osteogenic differentiation of BMSCs. *Eur. Rev. Med. Pharmacol. Sci.* 23, 9761–9771.

Fang, T., Wu, Q., Zhou, L., Mu, S., and Fu, Q. (2016). miR-106b-5p and miR-17-5p suppress osteogenic differentiation by targeting Smad5 and inhibit bone formation. *Exper. Cell Res.* 347, 74–82. doi: 10.1016/j.yexcr.2016.07.010

Feng, Y., Cao, J. H., Li, X. Y., and Zhao, S. H. (2011). Inhibition of miR-214 expression represses proliferation and differentiation of C2C12 myoblasts. *Cell Biochem. Funct.* 29, 378–383. doi: 10.1002/cbf.1760

Fijalkowski, I., Geets, E., Steenackers, E., Van Hoof, V., Ramos, F. J., Mortier, G., et al. (2016). A novel domain-specific mutation in a sclerosteosis patient suggests a role of LRP4 as an anchor for sclerostin in human bone. *J. Bone Miner. Res.* 31, 874–881. doi: 10.1002/jbmr.2782

Franceschetti, T., Dole, N., Kessler, C., Lee, S., and Delany, A. (2014). Pathway analysis of microRNA expression profile during murine osteoclastogenesis. *PLoS One* 9:e107262. doi: 10.1371/journal.pone.0107262

Fulzele, S., Mendhe, B., Khayrullin, A., Johnson, M., Kaiser, H., Liu, Y., et al. (2019). Muscle-derived miR-34a increases with age in circulating extracellular vesicles and induces senescence of bone marrow stem cells. *Aging* 11, 1791–1803. doi: 10.18632/aging.101874

Gan, K., Dong, G., Wang, N., and Zhu, J. (2020). miR-221-3p and miR-222-3p downregulation promoted osteogenic differentiation of bone marrow mesenchyme stem cells through IGF-1/ERK pathway under high glucose condition. *Diabetes Res. Clin. Pract.* 167:108121. doi: 10.1016/j.diabres.2020.108121

Ge, J., Lin, J., Hong, H., Sun, Y., Li, Y., and Zhang, C. (2018). MiR-374b promotes osteogenic differentiation of MSCs by degrading PTEN and promoting fracture healing. *Eur. Rev. Med. Pharmacol. Sci.* 22, 3303–3310.

Gong, W., Liu, Y., Wu, Z., Wang, S., Qiu, G., and Lin, S. (2016). Meteorin-like shows unique expression pattern in bone and its overexpression inhibits osteoblast differentiation. *PLoS One* 11:e0164446. doi: 10.1371/journal.pone.0164446

Grube, L., Dellen, R., Kruse, F., Schwender, H., Stühler, K., and Poschmann, G. (2018). Mining the secretome of C2C12 muscle cells: data dependent experimental approach to analyze protein secretion using label-free quantification and peptide based analysis. *J. Proteom. Res.* 17, 879–890. doi: 10.1021/acs.jproteome.7b00684

Guescini, M., Canonico, B., Lucertini, F., Maggio, S., Annibalini, G., Barbieri, E., et al. (2015). Muscle releases alpha-sarcoglycan positive extracellular vesicles carrying miRNAs in the bloodstream. *PLoS One* 10:e0125094. doi: 10.1371/journal.pone.0125094

Hamoudi, D., Bouredji, Z., Marcadet, L., Yagita, H., Landry, L. B., Argaw, A., et al. (2020). Muscle weakness and selective muscle atrophy in osteoprotegerin-deficient mice. *Hum. Mol. Genet.* 29, 483–494. doi: 10.1093/hmg/ddz312

Hamoudi, D., Marcadet, L., Piette Boulanger, A., Yagita, H., Bouredji, Z., Argaw, A., et al. (2019). An anti-RANKL treatment reduces muscle inflammation and dysfunction and strengthens bone in dystrophic mice. *Hum. Mol. Genet.* 28, 3101–3112. doi: 10.1093/hmg/ddz124

Hamrick, M. W., and McGee-Lawrence, M. E. (2018). Blocking bone loss with l-BAIBA. *Trends Endocrinol. Metab.* 29, 284–286. doi: 10.1016/j.tem.2018.03.005

Hamrick, M. W., Shi, X., Zhang, W., Pennington, C., Thakore, H., Haque, M., et al. (2007). Loss of myostatin (GDF8) function increases osteogenic differentiation of bone marrow-derived mesenchymal stem cells but the osteogenic effect is ablated with unloading. *Bone* 40, 1544–1553. doi: 10.1016/j.bone.2007.02.012

Hanks, L. J., Gutierrez, O. M., Bamman, M. M., Ashraf, A., McCormick, K. L., and Casazza, K. (2015). Circulating levels of fibroblast growth factor-21 increase with age independently of body composition indices among healthy individuals. *J. Clin. Transl. Endocrinol.* 2, 77–82. doi: 10.1016/j.jcte.2015.02.001

Hao, R. H., Gao, J. L., Li, M., Huang, W., Zhu, D. L., Thynn, H. N., et al. (2018). Association between fibroblast growth factor 21 and bone mineral density in adults. *Endocrine* 59, 296–303. doi: 10.1007/s12020-017-1507-y

Harslof, T., Sikjaer, T., Mosekilde, L., Langdahl, B. L., and Rejnmark, L. (2016). Correlations between changes in undercarboxylated osteocalcin and muscle function in hypoparathyroidism. *Inter. J. Endocrinol. Metab.* 14:e38440. doi: 10.5812/ijem.38440

Heredia, J. E., Mukundan, L., Chen, F. M., Mueller, A. A., Deo, R. C., Locksley, R. M., et al. (2013). Type 2 innate signals stimulate fibro/adipogenic progenitors to facilitate muscle regeneration. *Cell* 153, 376–388. doi: 10.1016/j.cell.2013.02.053

Hesse, E., Schroder, S., Brandt, D., Pamperin, J., Saito, H., and Taipaleenmaki, H. (2019). Sclerostin inhibition alleviates breast cancer-induced bone metastases and muscle weakness. *JCI Insight* 5:543. doi: 10.1172/jci.insight.125543

Holdsworth, G., Roberts, S. J., and Ke, H. Z. (2019). Novel actions of sclerostin on bone. *J. Mol. Endocrinol.* 62, R167–R185. doi: 10.1530/JME-18-0176

Huang, J., Romero-Suarez, S., Lara, N., Mo, C., Kaja, S., Brotto, L., et al. (2017). Crosstalk between MLO-Y4 osteocytes and C2C12 muscle cells is mediated by the Wnt/beta-catenin pathway. *JBMR Plus* 1, 86–100. doi: 10.1002/jbm4.10015

Huang, Z., Chen, X., Yu, B., He, J., and Chen, D. (2012). MicroRNA-27a promotes myoblast proliferation by targeting myostatin. *Biochem. Biophys. Res. Commun.* 423, 265–269. doi: 10.1016/j.bbrc.2012.05.106

Hughes, D. C., Marcotte, G. R., Baehr, L. M., West, D. W. D., Marshall, A. G., Ebert, S. M., et al. (2018). Alterations in the muscle force transfer apparatus in aged rats during unloading and reloading: impact of microRNA-31. *J. Physiol.* 596, 2883–2900. doi: 10.1113/JP275833

Huh, J. Y., Dincer, F., Mesfum, E., and Mantzoros, C. S. (2014). Irisin stimulates muscle growth-related genes and regulates adipocyte differentiation and metabolism in humans. *Int. J. Obes.* 38, 1538–1544. doi: 10.1038/ijo.2014.42

Huh, J. Y., Panagiotou, G., Mougios, V., Brinkoetter, M., Vamvini, M. T., Schneider, B. E., et al. (2012). FNDC5 and irisin in humans: I. Predictors of circulating concentrations in serum and plasma and II. mRNA expression and circulating concentrations in response to weight loss and exercise. *Metabolism* 61, 1725–1738. doi: 10.1016/j.metabol.2012.09.002

Ibanez, L., Ferrandiz, M. L., Brines, R., Guede, D., Cuadrado, A., and Alcaraz, M. J. (2014). Effects of Nrf2 deficiency on bone microarchitecture in an experimental model of osteoporosis. *Oxid. Med. Cell Longev.* 2014:726590. doi: 10.1155/2014/726590

Ikebuchi, Y., Aoki, S., Honma, M., Hayashi, M., Sugamori, Y., Khan, M., et al. (2018). Coupling of bone resorption and formation by RANKL reverse signalling. *Nature* 561, 195–200. doi: 10.1038/s41586-018-0482-7

Itoh, N. (2014). FGF21 as a hepatokine, adipokine, and myokine in metabolism and diseases. *Front. Endocrinol.* 5:107. doi: 10.3389/fendo.2014.00107

Jung, T. W., Hwang, H. J., Hong, H. C., Yoo, H. J., Baik, S. H., and Choi, K. M. (2015). BAIBA attenuates insulin resistance and inflammation induced by palmitate or a high fat diet via an AMPK-PPARdelta-dependent pathway in mice. *Diabetologia* 58, 2096–2105. doi: 10.1007/s00125-015-3663-z

Kadota, T., Fujita, Y., Yoshioka, Y., Araya, J., Kuwano, K., and Ochiya, T. (2018). Emerging role of extracellular vesicles as a senescence-associated secretory phenotype: Insights into the pathophysiology of lung diseases. *Mol. Aspects Med.* 60, 92–103. doi: 10.1016/j.mam.2017.11.005

Kammoun, H. L., and Febbraio, M. A. (2014). Come on BAIBA light my fire. *Cell Metab.* 19, 1–2. doi: 10.1016/j.cmet.2013.12.007

Keller, H., and Kneissel, M. (2005). SOST is a target gene for PTH in bone. *Bone* 37, 148–158. doi: 10.1016/j.bone.2005.03.018

Khosla, S. (2001). Minireview: the OPG/RANKL/RANK system. *Endocrinology* 142, 5050–5055. doi: 10.1210/endo.142.12.8536

Kim, H., Wrann, C. D., Jedrychowski, M., Vidoni, S., Kitase, Y., Nagano, K., et al. (2018). Irisin mediates effects on bone and fat via alphaV integrin receptors. *Cell* 175, 1756–1768.e17. doi: 10.1016/j.cell.2018.10.025

Kim, J. A., Roh, E., Hong, S. H., Lee, Y. B., Kim, N. H., Yoo, H. J., et al. (2019). Association of serum sclerostin levels with low skeletal muscle mass: the Korean Sarcopenic Obesity Study (KSOS). *Bone* 128:115053. doi: 10.1016/j.bone.2019.115053

Kim, S. M., Kim, K. M., Kim, B. T., Joo, N. S., Kim, K. N., and Lee, D. J. (2010). Correlation of undercarboxylated osteocalcin (ucOC) concentration and bone

density with age in healthy Korean women. *J. Korea. Med. Sci.* 25, 1171–1175. doi: 10.3346/jkms.2010.25.8.1171

Kim, S. P., Frey, J. L., Li, Z., Kushwaha, P., Zoch, M. L., Tomlinson, R. E., et al. (2017). Sclerostin influences body composition by regulating catabolic and anabolic metabolism in adipocytes. *Proc. Natl. Acad. Sci. U.S.A.* 114, E11238–E11247. doi: 10.1073/pnas.1707876115

Kim, S. W., Lu, Y., Williams, E. A., Lai, F., Lee, J. Y., Enishi, T., et al. (2017). Sclerostin antibody administration converts bone lining cells into active osteoblasts. *J. Bone Miner. Res.* 32, 892–901. doi: 10.1002/jbmr.3038

Kitase, Y., Vallejo, J. A., Gutheil, W., Vemula, H., Jähn, K., Yi, J., et al. (2018). β-aminoisobutyric Acid, l-BAIBA, is a muscle-derived osteocyte survival factor. *Cell Rep.* 22, 1531–1544. doi: 10.1016/j.celrep.2018.01.041

Kukreti, H., and Amuthavalli, K. (2020). MicroRNA-34a causes ceramide accumulation and effects insulin signaling pathway by targeting ceramide kinase (CERK) in aging skeletal muscle. *J. Cell. Biochem.* 121, 3070–3089. doi: 10.1002/jcb.29312

Lee, J., Park, J., Kim, Y. H., Lee, N. H., and Song, K. M. (2019). Irisin promotes C2C12 myoblast proliferation via ERK-dependent CCL7 upregulation. *PLoS One* 14:e0222559. doi: 10.1371/journal.pone.0222559

Lee, J., Song, D., Park, J., Kim, J., Cho, C., and Kim, D. (2017). miR-374 promotes myocardial hypertrophy by negatively regulating vascular endothelial growth factor receptor-1 signaling. *BMB Rep.* 50, 208–213. doi: 10.5483/BMBRep.2017.50.4.165

Lee, N. K., Sowa, H., Hinoi, E., Ferron, M., Ahn, J. D., Confavreux, C., et al. (2007). Endocrine regulation of energy metabolism by the skeleton. *Cell* 130, 456–469. doi: 10.1016/j.cell.2007.05.047

Lee, S. Y., Fam, K. D., Chia, K. L., Yap, M. M. C., Goh, J., Yeo, K. P., et al. (2020). Age-related bone loss is associated with FGF21 but not IGFBP1 in healthy adults. *Exper. Physiol.* 105, 622–631. doi: 10.1113/EP088351

Levinger, I., Scott, D., Nicholson, G. C., Stuart, A. L., Duque, G., McCorquodale, T., et al. (2014). Undercarboxylated osteocalcin, muscle strength and indices of bone health in older women. *Bone* 64, 8–12. doi: 10.1016/j.bone.2014.03.008

Li, C. J., Cheng, P., Liang, M. K., Chen, Y. S., Lu, Q., Wang, J. Y., et al. (2015). MicroRNA-188 regulates age-related switch between osteoblast and adipocyte differentiation. *J. Clin. Invest.* 125, 1509–1522. doi: 10.1172/JCI77716

Li, C. J., Xiao, Y., Yang, M., Su, T., Sun, X., Guo, Q., et al. (2018). Long noncoding RNA Bmncr regulates mesenchymal stem cell fate during skeletal aging. *J. Clin. Invest.* 128, 5251–5266. doi: 10.1172/JCI99044

Li, D., Liu, J., Guo, B., Liang, C., Dang, L., Lu, C., et al. (2016). Osteoclast-derived exosomal miR-214-3p inhibits osteoblastic bone formation. *Nat. Commun.* 7:10872. doi: 10.1038/ncomms10872

Li, J., Zhang, H., Yang, C., Li, Y., and Dai, Z. (2016). An overview of osteocalcin progress. *J. Bone Miner. Metab.* 34, 367–379. doi: 10.1007/s00774-015-0734-7

Li, G., Zhang, L., Wang, D., AIQudsy, L., Jiang, J. X., Xu, H., et al. (2019). Muscle-bone crosstalk and potential therapies for sarco-osteoporosis. *J.Cell. Biochem.* 120, 14262–14273. doi: 10.1002/jcb.28946

Li, J., Chan, M., Yu, Y., Bei, Y., Chen, P., Zhou, Q., et al. (2017). miR-29b contributes to multiple types of muscle atrophy. *Nat. Commun.* 8:15201. doi: 10.1038/ncomms15201

Li, Z.-Y., Zheng, S.-L., Wang, P., Xu, T.-Y., Guan, Y.-F., Zhang, Y.-J., et al. (2014). Subfatin is a novel adipokine and unlike meteorin in adipose and brain expression. *CNS Neurosci. Therapeut.* 20, 344–354. doi: 10.1111/cns.12219

Lin, X., Hanson, E., Betik, A. C., Brennan-Speranza, T. C., Hayes, A., and Levinger, I. (2016). Hindlimb immobilization, but not castration, induces reduction of undercarboxylated osteocalcin associated with muscle atrophy in rats. *J. Bone Miner. Res.* 31, 1967–1978. doi: 10.1002/jbmr.2884

Ling, Y., Gao, X., Lin, H., Ma, H., Pan, B., and Gao, J. (2016). A common polymorphism rs1800247 in osteocalcin gene was associated with serum osteocalcin levels, bone mineral density, and fracture: the Shanghai Changfeng Study. *Osteoporos. Intern.* 27, 769–779. doi: 10.1007/s00198-015-3244-5

Liu, B., Shi, Y., He, H., Cai, M., Xiao, W., Yang, X., et al. (2018). miR-221 modulates skeletal muscle satellite cells proliferation and differentiation. *Vitro Cell. Dev. Biol. Anim.* 54, 147–155. doi: 10.1007/s11626-017-0210-x

Liu, D., Kou, X., Chen, C., Liu, S., Liu, Y., Yu, W., et al. (2018). Circulating apoptotic bodies maintain mesenchymal stem cell homeostasis and ameliorate osteopenia via transferring multiple cellular factors. *Cell Res.* 28, 918–933. doi: 10.1038/s41422-018-0070-2

Liu, S., Gao, F., Wen, L., Ouyang, M., Wang, Y., Wang, Q., et al. (2017). Osteocalcin induces proliferation via positive activation of the PI3K/Akt, P38 MAPK pathways and promotes differentiation through activation of the GPRC6A-ERK1/2 pathway in C2C12 myoblast cells. *Cell. Physiol. Biochem.* 43, 1100–1112. doi: 10.1159/000481752

Liu, X., Wang, Y., Hou, L., Xiong, Y., and Zhao, S. (2017a). Fibroblast growth factor 21 (FGF21) promotes formation of aerobic myofibers via the FGF21-SIRT1-AMPK-PGC1alpha pathway. *J. Cell. Physiol.* 232, 1893–1906. doi: 10.1002/jcp.25735

Liu, X., Wang, Y., Zhao, S., and Li, X. (2017b). Fibroblast growth factor 21 promotes C2C12 cells myogenic differentiation by enhancing cell cycle exit. *Biomed. Res. Int.* 2017:1648715. doi: 10.1155/2017/1648715

Ma, Y., Qiao, X., Zeng, R., Cheng, R., Zhang, J., Luo, Y., et al. (2018). Irisin promotes proliferation but inhibits differentiation in osteoclast precursor cells. *FASEB J.* 32, 5813–5823. doi: 10.1096/fj.201700983RR

Mahmoodnia, L., Sadoughi, M., Ahmadi, A., and Kafeshani, M. (2016). Relationship between serum irisin, glycemic indices, and renal function in type 2 diabetic patients. *J. Ren. Injury Prevent.* 6, 88–92. doi: 10.15171/jrip.2017.17

McPherron, A. C., Lawler, A. M., and Lee, S. J. (1997). Regulation of skeletal muscle mass in mice by a new TGF-beta superfamily member. *Nature* 387, 83–90. doi: 10.1038/387083a0

Medeiros, M. C., Rocha, N., Bandeira, E., Dantas, I., Chaves, C., Oliveira, M., et al. (2020). Serum sclerostin, body composition, and sarcopenia in hemodialysis patients with diabetes. *Intern. J. Nephrol.* 2020:4596920. doi: 10.1155/2020/4596920

Mera, P., Laue, K., Ferron, M., Confavreux, C., Wei, J., Galán-Díez, M., et al. (2016a). Osteocalcin signaling in myofibers is necessary and sufficient for optimum adaptation to exercise. *Cell Metab.* 23, 1078–1092. doi: 10.1016/j.cmet.2016.05.004

Mera, P., Laue, K., Wei, J., Berger, J. M., and Karsenty, G. (2016b). Osteocalcin is necessary and sufficient to maintain muscle mass in older mice. *Mol. Metab.* 5, 1042–1047. doi: 10.1016/j.molmet.2016.07.002

Mirza, F. S., Padhi, I. D., Raisz, L. G., and Lorenzo, J. A. (2010). Serum sclerostin levels negatively correlate with parathyroid hormone levels and free estrogen index in postmenopausal women. *J. Clin. Endocrinol. Metab.* 95, 1991–1997. doi: 10.1210/jc.2009-2283

Mizokami, A., Kawakubo-Yasukochi, T., and Hirata, M. (2017). Osteocalcin and its endocrine functions. *Biochem. Pharmacol.* 132, 1–8. doi: 10.1016/j.bcp.2017.02.001

Mohamed, J. S., Wilson, J. C., Myers, M. J., Sisson, K. J., and Alway, S. E. (2014). Dysregulation of SIRT-1 in aging mice increases skeletal muscle fatigue by a PARP-1-dependent mechanism. *Aging* 6, 820–834. doi: 10.18632/aging.100696

Morissette, M. R., Stricker, J. C., Rosenberg, M. A., Buranasombati, C., Levitan, E. B., Mittleman, M. A., et al. (2009). Effects of myostatin deletion in aging mice. *Aging Cell* 8, 573–583. doi: 10.1111/j.1474-9726.2009.00508.x

Neve, A., Corrado, A., and Cantatore, F. P. (2013). Osteocalcin: skeletal and extra-skeletal effects. *J. Cell. Physiol.* 228, 1149–1153. doi: 10.1002/jcp.24278

Nie, M., Deng, Z. L., Liu, J., and Wang, D. Z. (2015). Noncoding RNAs, emerging regulators of skeletal muscle development and diseases. *Biomed. Res. Intern.* 2015:676575. doi: 10.1155/2015/676575

Oost, L. J., Kustermann, M., Armani, A., Blaauw, B., and Romanello, V. (2019). Fibroblast growth factor 21 controls mitophagy and muscle mass. *J. Cachexia Sarcopenia Muscle* 10, 630–642. doi: 10.1002/jcsm.12409

Ota, K., Quint, P., Ruan, M., Pederson, L., Westendorf, J. J., Khosla, S., et al. (2013). Sclerostin is expressed in osteoclasts from aged mice and reduces osteoclast-mediated stimulation of mineralization. *J. Cell. Biochem.* 114, 1901–1907. doi: 10.1002/jcb.24537

Perie, L., Parente, A., Brun, C., Magnol, L., Pelissier, P., and Blanquet, V. (2016). Enhancement of C2C12 myoblast proliferation and differentiation by GASP-2, a myostatin inhibitor. *Biochem. Biophys. Rep.* 6, 39–46. doi: 10.1016/j.bbrep.2016.03.001

Phillips, E. G., Beggs, L. A., Ye, F., Conover, C. F., Beck, D. T., Otzel, D. M., et al. (2018). Effects of pharmacologic sclerostin inhibition or testosterone administration on soleus muscle atrophy in rodents after spinal cord injury. *PLoS One* 13:e0194440. doi: 10.1371/journal.pone.0194440

Piemontese, M., Almeida, M., Robling, A. G., Kim, H. N., Xiong, J., Thostenson, J. D., et al. (2017). Old age causes de novo intracortical bone remodeling and porosity in mice. *JCI Insight* 2:e93771. doi: 10.1172/jci.insight.93771

Poggioli, T., Vujic, A., Yang, P., Macias-Trevino, C., Uygur, A., Loffredo, F. S., et al. (2016). Circulating growth differentiation factor 11/8 levels decline with age. *Circ. Res.* 118, 29–37. doi: 10.1161/CIRCRESAHA.115.307521

Puig, J., Blasco, G., Daunis-i-Estadella, J., Moreno, M., Molina, X., Alberich-Bayarri, A., et al. (2016). Lower serum osteocalcin concentrations are associated with brain microstructural changes and worse cognitive performance. *Clin. Endocrinol.* 84, 756–763. doi: 10.1111/cen.12954

Qiao, X., Nie, Y., Ma, Y., Chen, Y., Cheng, R., Yin, W., et al. (2016). Irisin promotes osteoblast proliferation and differentiation via activating the MAP kinase signaling pathways. *Sci. Rep.* 6:18732. doi: 10.1038/srep21053

Qin, Y., Peng, Y., Zhao, W., Pan, J., Ksiezak-Reding, H., Cardozo, C., et al. (2017). Myostatin inhibits osteoblastic differentiation by suppressing osteocyte-derived exosomal microRNA-218: a novel mechanism in muscle-bone communication. *J. Biol. Chem.* 292, 11021–11033. doi: 10.1074/jbc.M116.770941

Qiu, H., Liu, N., Luo, L., Zhong, J., Tang, Z., Kang, K., et al. (2016). MicroRNA-17-92 regulates myoblast proliferation and differentiation by targeting the ENH1/Id1 signaling axis. *Cell Death Differ.* 23, 1658–1669. doi: 10.1038/cdd.2016.56

Ran, N., Gao, X., Dong, X., Li, J., Lin, C., Geng, M., et al. (2020). Effects of exosome-mediated delivery of myostatin propeptide on functional recovery of mdx mice. *Biomaterials* 236:119826. doi: 10.1016/j.biomaterials.2020.119826

Rana, K. S., Arif, M., Hill, E. J., Aldred, S., Nagel, D. A., Nevill, A., et al. (2014). Plasma irisin levels predict telomere length in healthy adults. *Age* 36, 995–1001. doi: 10.1007/s11357-014-9620-9

Rao, R. R., Long, J. Z., White, J. P., Svensson, K. J., Lou, J., Lokurkar, I., et al. (2014). Meteorin-like is a hormone that regulates immune-adipose interactions to increase beige fat thermogenesis. *Cell* 157, 1279–1291. doi: 10.1016/j.cell.2014.03.065

Rebbapragada, A., Benchabane, H., Wrana, J. L., Celeste, A. J., and Attisano, L. (2003). Myostatin signals through a transforming growth factor beta-like signaling pathway to block adipogenesis. *Mol. Cell. Biol.* 23, 7230–7242. doi: 10.1128/MCB.23.20.7230-7242.2003

Reginster, J. Y., Beaudart, C., Buckinx, F., and Bruyère, O. (2016). Osteoporosis and sarcopenia: two diseases or one? *Curr. Opin. Clin. Nutr. Metab. Care* 19, 31–36. doi: 10.1097/MCO.0000000000000230

Reppe, S., Noer, A., Grimholt, R. M., Halldórsson, B. V., Medina-Gomez, C., Gautvik, V. T., et al. (2015). Methylation of bone SOST, its mRNA, and serum sclerostin levels correlate strongly with fracture risk in postmenopausal women. *J. Bone Miner. Res.* 30, 249–256. doi: 10.1002/jbmr.2342

Reza, M. M., Sim, C. M., Subramaniyam, N., Ge, X., Sharma, M., Kambadur, R., et al. (2017a). Irisin treatment improves healing of dystrophic skeletal muscle. *Oncotarget* 8, 98553–98566. doi: 10.18632/oncotarget.21636

Reza, M. M., Subramaniyam, N., Sim, C. M., Ge, X., Sathiakumar, D., McFarlane, C., et al. (2017b). Irisin is a pro-myogenic factor that induces skeletal muscle hypertrophy and rescues denervation-induced atrophy. *Nat. Commun.* 8:1104. doi: 10.1038/s41467-017-01131-0

Roberts, L. D., Bostrom, P., O'Sullivan, J. F., Schinzel, R. T., Lewis, G. D., Dejam, A., et al. (2014). beta-Aminoisobutyric acid induces browning of white fat and hepatic beta-oxidation and is inversely correlated with cardiometabolic risk factors. *Cell Metab.* 19, 96–108. doi: 10.1016/j.cmet.2013.12.003

Robling, A. G., Niziolek, P. J., Baldridge, L. A., Condon, K. W., Allen, M. R., Alam, I., et al. (2008). Mechanical stimulation of bone in vivo reduces osteocyte expression of Sost/sclerostin. *J. Biol. Chem.* 283, 5866–5875. doi: 10.1074/jbc.M705092200

Rodriguez, J., Vernus, B., Chelh, I., Cassar-Malek, I., Gabillard, J. C., Hadj Sassi, A., et al. (2014). Myostatin and the skeletal muscle atrophy and hypertrophy signaling pathways. *Cell Mol. Life Sci.* 71, 4361–4371. doi: 10.1007/s00018-014-1689-x

Ruan, Q., Huang, Y., Yang, L., Ruan, J., Gu, W., Zhang, X., et al. (2019). The effects of both age and sex on irisin levels in paired plasma and cerebrospinal fluid in healthy humans. *Peptides* 113, 41–51. doi: 10.1016/j.peptides.2019.01.004

Severinsen, M. C. K., and Pedersen, B. K. (2020). Muscle-organ crosstalk: the emerging roles of myokines. *Endocr. Rev.* 41, 594–609. doi: 10.1210/endrev/bnaa016

Shan, T., Liang, X., Bi, P., and Kuang, S. (2013). Myostatin knockout drives browning of white adipose tissue through activating the AMPK-PGC1alpha-Fndc5 pathway in muscle. *FASEB J.* 27, 1981–1989. doi: 10.1096/fj.12-225755

Shibaguchi, T., Maeoka, T., Yoshihara, T., Naito, H., Goto, K., Yoshioka, T., et al. (2018). Age-related changes in myostatin expression in rat skeletal muscles. *J. Phys. Fitness Sports Med.* 7, 221–227. doi: 10.7600/jpfsm.7.221

Shibasaki, H., Imamura, M., Arima, S., Tanihata, J., Kuraoka, M., Matsuzaka, Y., et al. (2019). Characterization of a novel microRNA, miR-188, elevated in serum of muscular dystrophy dog model. *PLoS One* 14:e0211597. doi: 10.1371/journal.pone.0211597

Simonet, W. S., Lacey, D. L., Dunstan, C. R., Kelley, M., Chang, M. S., Lüthy, R., et al. (1997). Osteoprotegerin: a novel secreted protein involved in the regulation of bone density. *Cell* 89, 309–319. doi: 10.1016/S0092-8674(00)80209-3

Singh, K., Piprode, V., Mhaske, S. T., Barhanpurkar-Naik, A., and Wani, M. R. (2018). IL-3 differentially regulates membrane and soluble rankl in osteoblasts through metalloproteases and the JAK2/STAT5 pathway and improves the RANKL/OPG ratio in adult mice. *J. Immunol.* 200, 595–606. doi: 10.4049/jimmunol.1601528

Siriett, V., Platt, L., Salerno, M. S., Ling, N., Kambadur, R., and Sharma, M. (2006). Prolonged absence of myostatin reduces sarcopenia. *J. Cell. Physiol.* 209, 866–873. doi: 10.1002/jcp.20778

Steensberg, A., van Hall, G., Osada, T., Sacchetti, M., Saltin, B., and Klarlund Pedersen, B. (2000). Production of interleukin-6 in contracting human skeletal muscles can account for the exercise-induced increase in plasma interleukin-6. *J. Physiol.* 529(Pt 1), 237–242. doi: 10.1111/j.1469-7793.2000.00237.x

Storlino, G., Colaianni, G., Sanesi, L., Lippo, L., Brunetti, G., Errede, M., et al. (2020). Irisin prevents disuse-induced osteocyte apoptosis. *J. Bone Miner. Res.* 35, 766–775. doi: 10.1002/jbmr.3944

Su, T., Xiao, Y., Xiao, Y., Guo, Q., Li, C., Huang, Y., et al. (2019). Bone marrow mesenchymal stem cells-derived exosomal MiR-29b-3p regulates aging-associated insulin resistance. *ACS Nano* 13, 2450–2462. doi: 10.1021/acsnano.8b09375

Sun, L., Sun, S., Zhao, X., Zhang, J., Guo, J., Tang, L., et al. (2019). Inhibition of myostatin signal pathway may be involved in low-intensity pulsed ultrasound promoting bone healing. *J. Med. Ultrason.* 46, 377–388. doi: 10.1007/s10396-019-00962-2

Sun, Q., Zhang, Y., Yang, G., Chen, X., Zhang, Y., Cao, G., et al. (2008). Transforming growth factor-beta-regulated miR-24 promotes skeletal muscle differentiation. *Nucleic Acids Res.* 36, 2690–2699. doi: 10.1093/nar/gkn032

Szulc, P., Schoppet, M., Goettsch, C., Rauner, M., Dschietzig, T., Chapurlat, R., et al. (2012). Endocrine and clinical correlates of myostatin serum concentration in men–the STRAMBO study. *J. Clin. Endocrinol. Metab.* 97, 3700–3708. doi: 10.1210/jc.2012-1273

Takafuji, Y., Tatsumi, K., Ishida, M., Kawao, N., Okada, K., and Kaji, H. (2020). Extracellular vesicles secreted from mouse muscle cells suppress osteoclast formation: roles of mitochondrial energy metabolism. *Bone* 134:115298. doi: 10.1016/j.bone.2020.115298

Tezze, C., Romanello, V., Desbats, M. A., Fadini, G. P., Albiero, M., Favaro, G., et al. (2017). Age-associated loss of OPA1 in muscle impacts muscle mass, metabolic homeostasis, systemic inflammation, and epithelial senescence. *Cell Metab.* 25, 1374–1389.e6. doi: 10.1016/j.cmet.2017.04.021

Umezu, T., Imanishi, S., Azuma, K., Kobayashi, C., Yoshizawa, S., Ohyashiki, K., et al. (2017). Replenishing exosomes from older bone marrow stromal cells with miR-340 inhibits myeloma-related angiogenesis. *Blood Adv.* 1, 812–823. doi: 10.1182/bloodadvances.2016003251

Ushach, I., Arrevillaga-Boni, G., Heller, G. N., Pone, E., Hernandez-Ruiz, M., Catalan-Dibene, J., et al. (2018). Meteorin-like/Meteorin-beta is a novel immunoregulatory cytokine associated with inflammation. *J. Immunol.* 201, 3669–3676. doi: 10.4049/jimmunol.1800435

Van Buchem, F. S., Hadders, H. N., and Ubbens, R. (1955). An uncommon familial systemic disease of the skeleton: hyperostosis corticalis generalisata familiaris. *Acta Radiol.* 44, 109–120. doi: 10.3109/00016925509170789

Vaynman, S., Ying, Z., and Gomez-Pinilla, F. (2004). Hippocampal BDNF mediates the efficacy of exercise on synaptic plasticity and cognition. *Eur. J. Neurosci.* 20, 2580–2590. doi: 10.1111/j.1460-9568.2004.03720.x

Vimalraj, S., Partridge, N., and Selvamurugan, N. (2014). A positive role of microRNA-15b on regulation of osteoblast differentiation. *J. Cell. Physiol.* 229, 1236–1244. doi: 10.1002/jcp.24557

von Maltzahn, J., Chang, N. C., Bentzinger, C. F., and Rudnicki, M. A. (2012). Wnt signaling in myogenesis. *Trends Cell Biol.* 22, 602–609. doi: 10.1016/j.tcb.2012.07.008

Wang, B., Zhang, C., Zhang, A., Cai, H., Price, S. R., and Wang, X. H. (2017). MicroRNA-23a and MicroRNA-27a mimic exercise by ameliorating CKD-Induced muscle atrophy. *J. Am. Soc. Nephrol.* 28, 2631–2640. doi: 10.1681/ASN.2016111213

Wang, D. T., Yang, Y. J., Huang, R. H., Zhang, Z. H., and Lin, X. (2015). Myostatin activates the ubiquitin-proteasome and autophagy-lysosome systems contributing to muscle wasting in chronic kidney disease. *Oxid. Med. Cell Longev.* 2015:684965. doi: 10.1155/2015/684965

Wang, X., Wei, W., Krzeszinski, J. Y., Wang, Y., and Wan, Y. (2015). A Liver-bone endocrine relay by IGFBP1 promotes osteoclastogenesis and mediates FGF21-induced bone resorption. *Cell Metab.* 22, 811–824. doi: 10.1016/j.cmet.2015.09.010

Wang, Z., Bian, L., Mo, C., Shen, H., Zhao, L. J., Su, K. J., et al. (2020). Quantification of aminobutyric acids and their clinical applications as biomarkers for osteoporosis. *Commun. Biol.* 3:39. doi: 10.1038/s42003-020-0766-y

Wei, W., Dutchak, P. A., Wang, X., Ding, X., Wang, X., Bookout, A. L., et al. (2012). Fibroblast growth factor 21 promotes bone loss by potentiating the effects of peroxisome proliferator-activated receptor gamma. *Proc. Natl. Acad. Sci. U.S.A.* 109, 3143–3148. doi: 10.1073/pnas.1200797109

Weilner, S., Schraml, E., Wieser, M., Messner, P., Schneider, K., Wassermann, K., et al. (2016). Secreted microvesicular miR-31 inhibits osteogenic differentiation of mesenchymal stem cells. *Aging Cell* 15, 744–754. doi: 10.1111/acel.12484

White, T. A., and LeBrasseur, N. K. (2014). Myostatin and sarcopenia: opportunities and challenges – a mini-review. *Gerontology* 60, 289–293. doi: 10.1159/000356740

Winkler, D. G., Sutherland, M. K., Geoghegan, J. C., Yu, C., Hayes, T., Skonier, J. E., et al. (2003). Osteocyte control of bone formation via sclerostin, a novel BMP antagonist. *EMBO J.* 22, 6267–6276. doi: 10.1093/emboj/cdg599

Wu, H., Wang, Y., Wang, X., Li, R., and Yin, D. (2017). MicroRNA-365 accelerates cardiac hypertrophy by inhibiting autophagy via the modulation of Skp2 expression. *Biochem. Biophys. Res. Commun.* 484, 304–310. doi: 10.1016/j.bbrc.2017.01.108

Wu, L. F., Zhu, D. C., Wang, B. H., Lu, Y. H., He, P., Zhang, Y. H., et al. (2018). Relative abundance of mature myostatin rather than total myostatin is negatively associated with bone mineral density in Chinese. *J. Cell. Mol. Med.* 22, 1329–1336. doi: 10.1111/jcmm.13438

Xiao, J., Qin, S., Li, W., Yao, L., Huang, P., Liao, J., et al. (2020). Osteogenic differentiation of rat bone mesenchymal stem cells modulated by MiR-186 via SIRT6. *Life Sci.* 253:117660. doi: 10.1016/j.lfs.2020.117660

Xiao, Y. Z., Yang, M., Xiao, Y., Guo, Q., Huang, Y., Li, C. J., et al. (2020). Reducing hypothalamic stem cell senescence protects against aging-associated physiological decline. *Cell Metab.* 31, 534–548.e5. doi: 10.1016/j.cmet.2020.01.002

Xin, C., Liu, J., Zhang, J., Zhu, D., Wang, H., Xiong, L., et al. (2016). Irisin improves fatty acid oxidation and glucose utilization in type 2 diabetes by regulating the AMPK signaling pathway. *Intern. J. Obes.* 40, 443–451. doi: 10.1038/ijo.2015.199

Xu, D., Gao, Y., Hu, N., Wu, L., and Chen, Q. (2017). miR-365 ameliorates dexamethasone-induced suppression of osteogenesis in MC3T3-E1 cells by targeting HDAC4. *Intern. J. Mol. Sci.* 18:977. doi: 10.3390/ijms18050977

Xu, L., Shen, L., Yu, X., Li, P., Wang, Q., and Li, C. (2020). Effects of irisin on osteoblast apoptosis and osteoporosis in postmenopausal osteoporosis rats through upregulating Nrf2 and inhibiting NLRP3 inflammasome. *Exp. Ther. Med.* 19, 1084–1090. doi: 10.3892/etm.2019.8313

Xu, Q., Cui, Y., Luan, J., Zhou, X., Li, H., and Han, J. (2018). Exosomes from C2C12 myoblasts enhance osteogenic differentiation of MC3T3-E1 pre-osteoblasts by delivering miR-27a-3p. *Biochem. Biophys. Res. Commun.* 498, 32–37. doi: 10.1016/j.bbrc.2018.02.144

Xu, R., Shen, X., Si, Y., Fu, Y., Zhu, W., Xiao, T., et al. (2018). MicroRNA-31a-5p from aging BMSCs links bone formation and resorption in the aged bone marrow microenvironment. *Aging Cell* 17:e12794. doi: 10.1111/acel.12794

Yan, J., Liu, H. J., Guo, W. C., and Yang, J. (2018). Low serum concentrations of Irisin are associated with increased risk of hip fracture in Chinese older women. *Joint Bone Spine* 85, 353–358. doi: 10.1016/j.jbspin.2017.03.011

Yang, C., Yang, W., Wong, Y., Wang, K., Teng, Y., Chang, M., et al. (2020). Muscle atrophy-related myotube-derived exosomal microRNA in neuronal dysfunction: Targeting both coding and long noncoding RNAs. *Aging Cell* 19:e13107. doi: 10.1111/acel.13107

Yang, M., Guo, Q., Peng, H., Xiao, Y. Z., Xiao, Y., Huang, Y., et al. (2019). Kruppel-like factor 3 inhibition by mutated lncRNA Reg1cp results in human high bone mass syndrome. *J. Exp. Med.* 216, 1944–1964. doi: 10.1084/jem.20181554

Yang, M., Li, C. J., Sun, X., Guo, Q., Xiao, Y., Su, T., et al. (2017). MiR-497 195 cluster regulates angiogenesis during coupling with osteogenesis by maintaining endothelial Notch and HIF-1α activity. *Nat. Commun.* 8:16003. doi: 10.1038/ncomms16003

Ye, W., Wang, J., Lin, D., and Ding, Z. (2020). The immunomodulatory role of irisin on osteogenesis via AMPK-mediated macrophage polarization. *Int. J. Biol. Macromol.* 146, 25–35. doi: 10.1016/j.ijbiomac.2019.12.028

Zacharewicz, E., Della Gatta, P., Reynolds, J., Garnham, A., Crowley, T., Russell, A., et al. (2014). Identification of microRNAs linked to regulators of muscle protein synthesis and regeneration in young and old skeletal muscle. *PLoS One* 9:e114009. doi: 10.1371/journal.pone.0114009

Zacharewicz, E., Kalanon, M., Murphy, R., Russell, A., and Lamon, S. (2020). MicroRNA-99b-5p downregulates protein synthesis in human primary myotubes. *Am. J. Physiol. Cell Physiol.* 319, C432–C440. doi: 10.1152/ajpcell.00172.2020

Zeng, Q., Wang, Y., Gao, J., Yan, Z., Li, Z., Zou, X., et al. (2019). miR-29b-3p regulated osteoblast differentiation via regulating IGF-1 secretion of mechanically stimulated osteocytes. *Cell. Mol. Biolo. Lett.* 24:11. doi: 10.1186/s11658-019-0136-2

Zhang, L., Liu, M., Zhou, X., Liu, Y., Jing, B., Wang, X., et al. (2016). Role of osteoprotegerin (OPG) in bone marrow adipogenesis. *Cell. Physiol. Biochem.* 40, 681–692. doi: 10.1159/000452580

Zhang, N., Chim, Y. N., Wang, J., Wong, R. M. Y., Chow, S. K. H., and Cheung, W. H. (2020). Impaired fracture healing in sarco-osteoporotic mice can be rescued by vibration treatment through myostatin suppression. *J. Orthop. Res.* 38, 277–287. doi: 10.1002/jor.24477

Zhang, Y., Gao, Y., Cai, L., Li, F., Lou, Y., Xu, N., et al. (2017). MicroRNA-221 is involved in the regulation of osteoporosis through regulates RUNX2 protein expression and osteoblast differentiation. *Am. J. Transl. Res.* 9, 126–135.

Zhao, M., Xie, J., Shu, W., Wang, H., Bi, J., Jiang, W., et al. (2019). MiR-15b and miR-322 inhibit SETD3 expression to repress muscle cell differentiation. *Cell Death Dis.* 10:183. doi: 10.1038/s41419-019-1432-5

Zhong, N., Xu, B., Cui, R., Xu, M., Su, J., Zhang, Z., et al. (2016). Positive correlation between serum osteocalcin and testosterone in male hyperthyroidism patients with high bone turnover. *Exper. Clin. Endocrinol. Diabetes* 124, 452–456. doi: 10.1055/s-0042-107944

Zhou, L., Song, H. Y., Gao, L. L., Yang, L. Y., Mu, S., and Fu, Q. (2019). MicroRNA-100-5p inhibits osteoclastogenesis and bone resorption by regulating fibroblast growth factor 21. *Intern. J. Mol. Med.* 43, 727–738. doi: 10.3892/ijmm.2018.4017

Zhou, M., Ma, J., Chen, S., Chen, X., and Yu, X. (2014). MicroRNA-17-92 cluster regulates osteoblast proliferation and differentiation. *Endocrine* 45, 302–310. doi: 10.1007/s12020-013-9986-y

Zhu, E., Zhang, J., Zhou, J., Yuan, H., Zhao, W., and Wang, B. (2018). miR-20a-5p promotes adipogenic differentiation of murine bone marrow stromal cells via targeting Kruppel-like factor 3. *J. Mol. Endocrinol.* 60, 225–237. doi: 10.1530/JME-17-0183

Zhu, X. W., Ding, K., Dai, X. Y., and Ling, W. Q. (2018). beta-aminoisobutyric acid accelerates the proliferation and differentiation of MC3T3-E1 cells via moderate activation of ROS signaling. *J. Chin. Med. Assoc.* 81, 611–618. doi: 10.1016/j.jcma.2017.12.005

Conflict of Interest: The authors declare that the research was conducted in the absence of any commercial or financial relationships that could be construed as a potential conflict of interest.

Copyright © 2020 He, He, Hou, Chen, Huang, Yang, Luo and Li. This is an open-access article distributed under the terms of the Creative Commons Attribution License (CC BY). The use, distribution or reproduction in other forums is permitted, provided the original author(s) and the copyright owner(s) are credited and that the original publication in this journal is cited, in accordance with accepted academic practice. No use, distribution or reproduction is permitted which does not comply with these terms.

frontiers in Cell and Developmental Biology

REVIEW
published: 15 December 2020
doi: 10.3389/fcell.2020.601224

Recent Advances of Osterix Transcription Factor in Osteoblast Differentiation and Bone Formation

Qian Liu[1,2], Mao Li[2], Shiyi Wang[3], Zhousheng Xiao[4], Yuanyuan Xiong[1,5] and Guangwei Wang[1,2]**

[1] Key Laboratory of Brain and Neuroendocrine Diseases, College of Hunan Province, Hunan University of Medicine, Huaihua, China, [2] Biomedical Research Center, Hunan University of Medicine, Huaihua, China, [3] XiangYa School of Medicine, Central South University, Changsha, China, [4] Department of Medicine, University of Tennessee Health Science Center, Memphis, TN, United States, [5] Department of Neurosurgery, The Second Affiliated Hospital of Nanchang University, Nanchang, China

OPEN ACCESS

Edited by:
Jiake Xu,
University of Western Australia, Australia

Reviewed by:
Xinli Zhang,
University of California, Los Angeles, United States
Shiwu Dong,
Third Military Medical University, China

***Correspondence:**
Guangwei Wang
guangwei_wang323@outlook.com
Yuanyuan Xiong
xiongyuanyuan_pub@126.com

Specialty section:
This article was submitted to Molecular Medicine, a section of the journal Frontiers in Cell and Developmental Biology

Received: 31 August 2020
Accepted: 23 November 2020
Published: 15 December 2020

Citation:
Liu Q, Li M, Wang S, Xiao Z, Xiong Y and Wang G (2020) Recent Advances of Osterix Transcription Factor in Osteoblast Differentiation and Bone Formation. Front. Cell Dev. Biol. 8:601224. doi: 10.3389/fcell.2020.601224

With increasing life expectations, more and more patients suffer from fractures either induced by intensive sports or other bone-related diseases. The balance between osteoblast-mediated bone formation and osteoclast-mediated bone resorption is the basis for maintaining bone health. Osterix (Osx) has long been known to be an essential transcription factor for the osteoblast differentiation and bone mineralization. Emerging evidence suggests that Osx not only plays an important role in intramembranous bone formation, but also affects endochondral ossification by participating in the terminal cartilage differentiation. Given its essentiality in skeletal development and bone formation, Osx has become a new research hotspot in recent years. In this review, we focus on the progress of Osx's function and its regulation in osteoblast differentiation and bone mass. And the potential role of Osx in developing new therapeutic strategies for osteolytic diseases was discussed.

Keywords: osterix, osteoblast differentiation, therapy, osteolytic diseases, bone

INTRODUCTION

Nearly two decades ago, osterix (Osx) was first discovered by Nakashima et al. (2002). Osx, also known as Sp7, is a zinc finger-containing osteoblast-specific transcription factor belonging to the SP/KLF family (Nakashima et al., 2002; Suske et al., 2005). Its subcellular localization is restricted to the nucleus (Nakashima et al., 2002). Osx is expressed in osteoblast-lineage cells, chondrocytes and also overexpressed in various cancer tissues (Qu et al., 2019). The Osx protein is highly conserved between human and mouse with an overall amino acid sequence identity of 95%. The transcription factor Osx induces the expression of a slew of mature osteoblast genes such as collagen type-I a1 (Col1a1), Osteonectin, Osteopontin, Osteocalcin, and Bone sialoprotein (Bsp) which are all necessary for productive osteoblasts during the creation of ossified bone (Renn and Winkler, 2009). In humans, several genome-wide association studies have demonstrated a correlation between Osx's certain polymorphisms and decreased bone mineral density in children and adults, and clinical

researches revealed that Osx is associated with age-related osteoporosis (Calabrese et al., 2017; Kemp et al., 2017; Qaseem et al., 2017). This review aims to discuss the role of Osx in bone formation and bone mass control, signaling pathway network of Osx regulation, as well as Osx potential value in developing new therapeutic strategies for osteolytic diseases.

THE STRUCTURE OF Osx

Human Osx is located at chromosome 12q13.13 while in mice, it's located in chromosome 15q (Nakashima et al., 2002). The initial research found that Osx gene consists of three exons and two introns, with exon2 contains the 5′UTR and encodes a small part of amino acids, while exon3 contains the 3′UTR and encodes most of the protein (Nakashima et al., 2002; Gao et al., 2004). The Osx gene has a TATA-less promoter, and Osx regulates its own promoter through a tandem repeat CCACCC element in its proximal promoter (Barbuto and Mitchell, 2013). The Osx mRNA transcript is an approximately 3.2 kb sequence and three alternatively spliced mRNA variants have been identified with 5′RACE experiments (Gao et al., 2004). Because of the absence of initiation codon in the exon1 and the same coding sequence between the transcript type I and type II, they eventually translated into the identical protein products (Gao et al., 2004). Therefore, the Osx protein can exist as either the long isoform α with 431 residues, derived from the transcript type I and II, or a short isoform β with 413 residues, derived from the transcript type III. As a result, protein β lacks the first 18 N-terminal amino acids compared to protein α, and both isoforms can be visualized on an immunoblot as bands at approximately 45 and 43 kDa, respectively (Milona et al., 2003; Gao et al., 2004; Ramazzotti et al., 2019). The difference between these two protein isoforms is the absence or presence of exon2. In addition, the amino acid sequence of the protein translated by Osx transcription factor was as high as 95%, in which a transcriptional activation domain (TAD) rich in proline and serine at N-terminal (Gao et al., 2004). Osx protein is a sequence-specific DNA binding protein. Its DNA-binding domain is located at the C-terminus and contains three C2H2-type zinc finger domains, which binds to SP1 and EKLF consensus sequences and to other G/C-rich sequences in the target genes (Nakashima et al., 2002). The schematic diagram of the Osx gene genome structure, mRNA transcript and its protein isoforms was shown in **Figure 1**.

THE FUNCTION OF Osx IN CONTROLLING BONE FORMATION

Up to now, it has been shown that Osx is specifically expressed in osteoblasts and osteocytes and, albeit at lower levels, in prehypertrophic and hypertrophic chondrocytes, while not expressed in osteoclasts (Xing et al., 2019). Osx not only plays a vital role in the differentiation, maturation or function of bone cells through the regulation of different genes, but also shows the potential role in the bone micro-environment. The schematic diagrams were summarized in **Figure 2**.

The Function of Osx in Osteoblasts

Osx has been confirmed to be involved in osteoblast differentiation, maturation and activity (Ramazzotti et al., 2019). It was reported that osteoblast differentiation does not occur at all in Osx-null embryos (Fu et al., 2010; Zhou et al., 2010). These studies demonstrated that Osx is essential for embryonic skeletal development. In Osx-deficient mice, the differentiation of runt-related transcription factor 2 (Runx2) expressing precursor cells was arrested and unable to express osteoblast markers (Zhou et al., 2010). When the vector expressing Osx was transfected into C2C12 and C3H10T1/2 cells, Osteocalcin RNA was obviously induced by Osx in these two cell types and Col1a1 gene expression was activated in C2C12 cells (Nakashima et al., 2002). Inactivation of Osx mice by CAG-CreER postnatally resulted in an arrest of osteoblast differentiation and of new bone formation, revealing that Osx also plays an indispensable functional role in postnatal skeletal growth and homeostasis (Zhou et al., 2010). An Osx mutation in zebrafish or medaka, belonging to non-mammals, resulted in a general delay in osteoblast maturation or severe bone defects and larval lethality (Azetsu et al., 2017; Niu et al., 2017; Yu et al., 2017), which established a key role of Osx for bone formation in non-mammalian species.

The Function of Osx in Osteocytes

Osx is necessary for the maturation and function of osteocytes postnatally (Baek and Kim, 2011; Klein-Nulend et al., 2013). Osx postnatal mutants appeared morphological osteocyte abnormalities, unlike normal osteocytes, and the expression levels of proteins encoded by "mineralization-related genes," such as Dmp1, Phex, and Sost, were significantly reduced (Zhou et al., 2010). The number of osteocytes close to both periosteum and endosteum was decreased and osteocytes were also markedly deformed. The mineralization process was seriously compromised in the Osx postnatal mutants. In both EMSA experiments and intact cells, Osx interacted with a specific site in the sclerostin promoter and activated this promoter in transfection assays, suggesting that Osx is also a player in mature osteocytes (Zhou et al., 2010).

The Function of Osx in Chondrocytes

The role of Osx in chondrocytes was first reported by Omoteyama and Takagi (2010). They investigated the *in vitro* effects of Osx gene silencing in the chondrogenic cell line ATDC5. Osx's shRNA down-regulated the expression of type X collagen (Col X), distal-less homeobox 5 (Dlx5) and alkaline phosphatase (Alp) mRNA, attenuated Alp enzyme activity, which suggests that Osx is involved in chondrogenic gene activation and chondrocyte differentiation. As for the *in vivo* effects, in Osx null mutants, there is no abnormality in the cellular organization of the cartilage growth plate (Nakashima et al., 2002). However, endochondral ossification completely stopped at the hypertrophic stage in chondrocyte-specific Osx conditional KO mice, even resulting in postnatal lethality combined with respiratory insufficiency (Omoteyama and Takagi, 2010; Oh et al., 2012). Massive accumulation of calcified

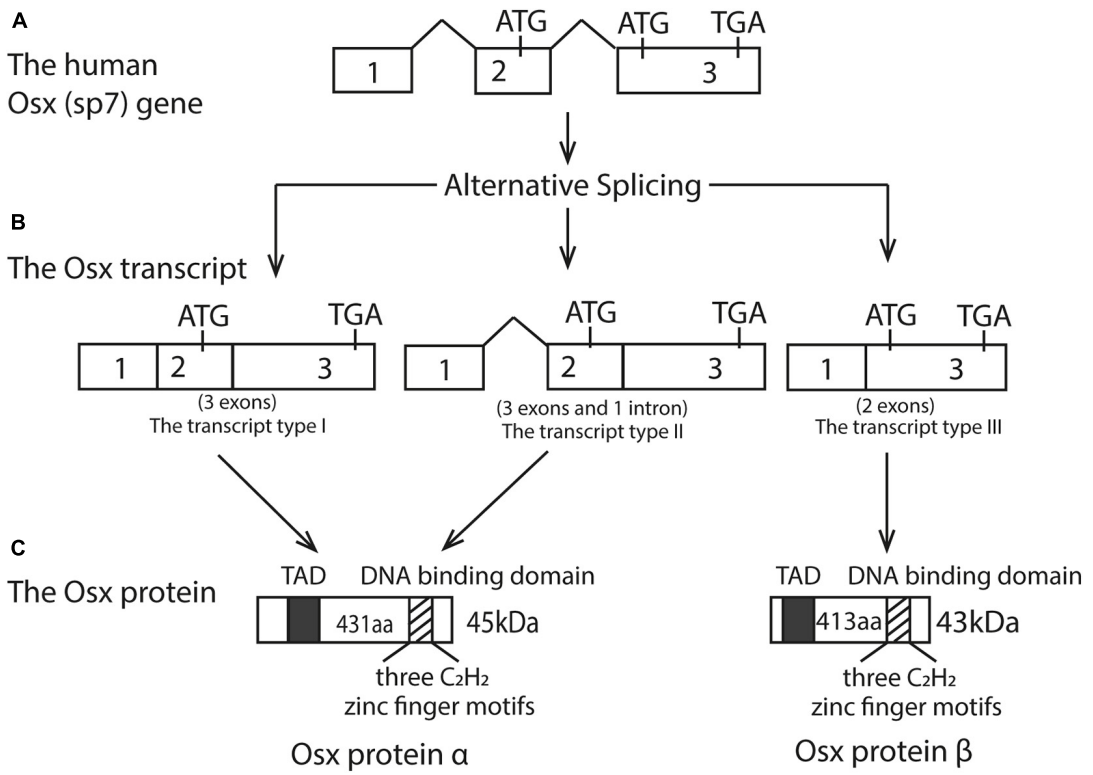


FIGURE 1 | Structure of the Osx gene, its three transcripts, and two protein isoforms. **(A)** Human Osx (sp7) gene; **(B)** The Osx transcripts; **(C)** The Osx protein isoforms. Open boxes represent exons and the thick line represents introns. Three alternatively spliced mRNA isoform were obtained. Because of the absence of initiation codon in the exonl and the same coding sequence between the transcript type I and type II, they eventually translated into the identical protein products. The transcript type III translated into a short protein isoforms with 413 aa. These two protein isoforms differ by the absence or presence of exon2. Therefore, Osx protein B lacks the first 18 N-terminal amino acids compared to Osx protein α. The black box represents N-terminal transcriptional activation domain (TAD) rich in proline and serine. The striped box represents the DNA binding domain containing three C2H2 zinc finger motifs near the C-terminal.

cartilage and diminishment of bone trabecula were observed in Osx-floxed mice with the Col2a1-Cre-ERT2 transgene, which was caused by a delay in the development of hypertrophic chondrocytes and their conversion to osteoblasts (Zhou et al., 2010; Xing et al., 2019).

The Function of Osx in Osteoclasts

Although Osx is not expressed in osteoclasts, a number of scientific studies have suggested that Osx has different effects on osteoclasts. Receptor activator of NF-kappaB ligand (Rankl) signaling is the major determinant of osteoclast formation and activation, while osteoprotegerin (Opg) protects bone from excessive resorption by binding to Rankl. Their relative concentration is of great significance for bone mass and strength. A research conducted by Cao et al. (2005) found that the decrease of osteolysis was followed by Osx gene transfection, but the transfection of Osx did not inhibit Rankl expression. However, Zhou et al. (2010) have shown that the ratio of Opg/Rankl expression in long bones was increased in the Osx postnatal mutants. Consequently, the fewer overall number and size of osteoclasts was observed in Osx postnatal-null long bones. This contradicted result declared that more studies about the mechanisms of Osx's inhibiting effect on osteoclasts are necessary. Cytokines like interleukin-8 (IL-8) and parathyroid hormone-related protein (PTHrP) can cause bone destruction by inducing osteoclast differentiation and activation, they were also increased by Osx over-expression (Yao et al., 2019). An essential transcriptional factor for osteoclast differentiation named nuclear factor of activated T cells 1 (NFATc1) was also studied. It forms a complex with Osx and activates Osx-dependent Col1a 1 promoter, suggesting that Osx has different effects on osteoclasts (Koga et al., 2005; Canalis et al., 2020).

The Promising Role of Osx in the Complex Communications Among Different Bone Cells and Its Role in the Bone Micro-Environment

The achievement and maintenance of a healthy and stable bone mass is accomplished through a close crosstalk among bone cells. Increasing evidences have shown that Osx not only performs multiple functions in different bone cells, but also participates in the cross-talk among them. Sclerostin (Sost) and Dickkopf-related protein 1 (Dkk1) are predominantly expressed in osteocytes, they exhibit a suppressive effect on osteoblast activity and function by antagonizing the Wingless-type and

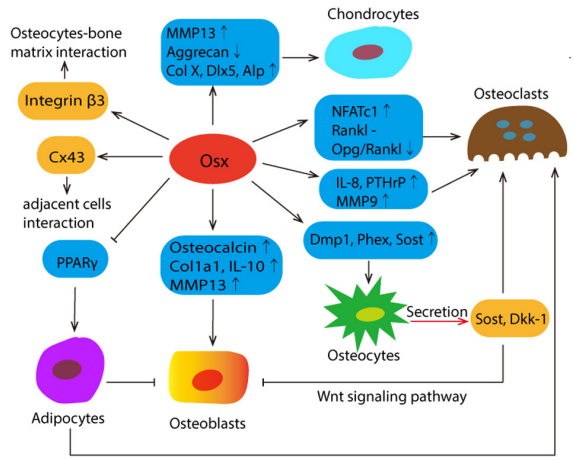


FIGURE 2 | The schematic summary of Osx's mission in the complex communications among different bone cells and its potential role in bone micro-environment. Osx affects the differentiation, maturation and function by regulating the different target genes, which were presented in the blue box. Osx directly controls the expression of integrin β3, which plays a mediating role in osteocyte-bone matrix interaction. The most abundant gap junction protein Connexin43 (Cx43) was significantly regulated by Osx positively. Osx decreases osteoblast activity by stimulating the expression of sclerostin (Sost) and Wnt signaling pathway inhibitor Dickkopf-related protein 1 (Dkk1). Both of them are predominantly expressed in osteocytes. And Sost also functions as a secreted osteoclast-derived BMP antagonist to promotes osteoclast differentiation. In addition, Osx represses adipogenesis by negatively regulating PPARγ expression and transcriptional activity, and adipocytes suppress osteoblasts and promote bone resorption by the recruitment of osteoclasts.

Int (Wnt) signaling pathway. Osx decreases osteoblast activity by stimulating the expression of Sost and Dkk1. As a secreted osteoclast-derived BMP antagonist, Sost not only inhibits osteoblast differentiation but also promotes osteoclast differentiation (Kusu et al., 2003). In addition to this, Osx can activate the Sost promoter and specifically bind to a DNA fragment located within the promoter (Cao et al., 2015; Zhang Z. H. et al., 2020). The osteocytes are surrounded by a non-organized pericellular matrix and integrins play a mediating role in osteocyte-bone matrix interaction. Osx directly controls the expression of integrin β3, which regulates corticalization for longitudinal bone growth (Moon et al., 2018). Osteoblasts and osteoclasts can communicate with each other. Osteoclasts produce factors called clastokines controlling osteoblasts during the bone remodeling cycle. Matrix metalloproteinase-9 (MMP9), predominantly produced by osteoclasts in bone, have an important function at the injured bone absorption, healing and bone remodeling after dental implant placement. It was reported that MMP9 initiates osteoclasts by removing collagen from the demineralized bone (Liu et al., 2004; Chen et al., 2018; Zhang H. et al., 2020). MMP9 is the target of Osx, in which Osx is recruited to the MMP9 promoter and binds to the CCAAT regulatory element of MMP9 promoter. Correspondingly, it has been clearly demonstrated that osteoblasts also affect the activity of osteoclasts, and Osx participates in the cross-talk between them by up-regulating factors expressed in osteoblasts such as Matrix metalloproteinase-13 (MMP13) (Hayami et al., 2011; Nakatani et al., 2016). MMP13 is expressed in hypertrophic chondrocyte and osteoblast. It contributes significantly to differentiation of osteoblast. Meanwhile, MMP13 also plays a significant role in differentiation and activation of osteoclast (Hayami et al., 2011; Pivetta et al., 2011; Nakatani et al., 2016). In osteoblasts, Osx activates the MMP13 promoter activity in a dose-dependent manner (Zhang et al., 2012). These studies suggested that Osx is involved in the interaction of osteoblast and osteoclast by mediating different factors. As the most abundant gap junction protein in bone cells, Connexin43 (Cx43) participates in the communication between adjacent cells, as well as cells and extracellular environment (Chen et al., 2019). It was reported that Cx43 expression was significantly repressed by the addition of shRNA against Osx, whereas overexpression of Osx resulted in enhanced Cx43 expression. Further studies have proven that Osx can directly occupy the promoter region of Cx43 and subsequently increases Cx43 promoter activity in a dose-dependent manner (Han et al., 2016a; Chen et al., 2019). Recent studies have shown that bone marrow adipocytes not only suppress osteoblasts, but also promote bone resorption by the recruitment of osteoclasts, and Osx represses adipogenesis by negatively regulating PPARγ expression and transcriptional activity (Han et al., 2016b; Li et al., 2018b).

Osx PROMOTES OSTEOGENESIS THROUGH THE REGULATION OF DOWNSTREAM FACTORS

The essential role of Osx in osteoblast differentiation is attributed to its ability to regulate the expression of various osteoblast markers such as Bsp, fibromodulin, Osteocalcin, Dkk1 and Col1a1, etc. (Wu et al., 2007; Ortuno et al., 2013; Yang et al., 2016; Niu et al., 2017). In addition to these target genes previously discovered, several novel downstream targets of Osx have been identified. Zinc finger and BTB domain containing 16 (Zbtb16), a downstream target gene of Osx, functions as a late marker of osteoblastic differentiation and regulates osteogenesis of human multipotent mesenchymal stromal cells (Onizuka et al., 2016). Fibrillin-2 and periostin are also identified to be target candidates of Osx in osteoblast differentiation (Lee et al., 2017). Besides, Osx regulates corticalization by controlling integrin β3 expression directly (Moon et al., 2018). Osx increases the promoter activity of Cx43 by directly interacting with the Cx43 promoter and subsequently upregulates the expression level of Cx43. As a result, the expression and transcriptional activity of Cx43 were considerably affected by Osx (Han et al., 2016a).

It is generally recognized that the canonical Osx pathway usually involves binding to GC-box DNA elements to regulate the transcription of target genes. Osx is able to activate Bsp promoter reporter in a dose-dependent manner, and one GC-rich site is required for Bsp promoter activation by Osx directly (Yang et al., 2016). Contrary to expectation, it has been reported that Osx acts as a transcriptional co-activator in the distal-less homeobox (Dlx) regulatory complex that binds to AT-rich motifs (Hojo et al., 2016). It's obvious from this point

that Osx can also form complexes with other transcription factors to co-regulate downstream target genes. Osx can also interact with Runx2 to coordinately activate the expression of the various genes, and their synergistic effects achieve significantly higher expression levels than those obtained with the individual expression vectors. Col1a1, Sost, Ectonucleotide pyrophosphatase/phosphodiesterase 1(Enpp1) and the novel gene unique cartilage matrix-associated protein (Ucma) have been reported to be their coordinated target genes (Ortuno et al., 2013; Lee Y. J. et al., 2015; Pérez-Campo et al., 2016; Gao M. et al., 2018). The interaction of Osx and Runx2 in the regulation of these promoters is mediated by Osx's enhancer regions adjacent to Sp1 and Runx2 DNA-binding sites, thereby synergistically regulating those downstream genes transcription.

More notably, both Runx2 and Osx are induced by Zn^{2+} influx, and they transcriptionally regulated ZIP1 expression which further leads to induction of Zn^{2+} influx contributing to a positive feed-forward zinc-Runx2/Osx-ZIP1 regulation loop during osteogenic differentiation (Karieb and Fox, 2012; Fu et al., 2018). NFATc1 forms a complex with Osx and activates Osx-dependent Col1a 1 promoter, however it does not activate Runx2-dependent transcription. Furthermore, transcriptional regulators such as p300, Brg1 or NO66 have been shown to interact with Osx and regulate its transcriptional activity (Ortuño et al., 2010; Sinha et al., 2014). It is noteworthy that Osx and NO66 histone demethylase control the chromatin of its target genes, in which Osx acts as a molecular switch for the formation of an active chromatin state during osteoblast differentiation, whereas NO66 suppresses gene through histone demethylation and/or formation of a repressor complex. Osx and NO66 work together to achieve multi-layered control of the chromatin structure of target genes (Sinha et al., 2010; Sinha et al., 2014).

The investigation of downstream targets of Osx contributes to elucidate its molecular mechanism affecting osteoblast differentiation and bone formation, thereby further promoting the exploration of new regulatory mechanisms involving Osx. The Osx direct and indirect downstream targeting molecules for osteoblastic differentiation and their mode of action (MOA) were sumarized in **Table 1**.

TABLE 1 | The Osx direct and indirect downstream targeting molecules for osteoblastic differentiation and their mode of action (MOA).

Target genes	MOA of Osx	Functions	Reference(s)
Bsp	By binding to specific GC-rich site directly	Up-regulation	Yang et al., 2016
Fibromodulin	By binding to specific GC-rich site directly	Up-regulation	Ortuño et al., 2010
Sost	By binding to specific GC-rich site directly and activating Sost expression with Runx2 in a co-ordinated manner	Up-regulation	Yang et al., 2010; Pérez-Campo et al., 2016
Periostin	By binding to specific GC-rich site directly	Up-regulation	Lee et al., 2017
Osteocalcin	By binding to the CCAAT sequence directly	Up-regulation	Niger et al., 2011
Dkk1	By enhancing Dkk1 expression directly	Up-regulation	Cao et al., 2015
Col1a1	By binding the Sp1 boxes directly or forming a complex with NFATc1 to upregulate the Col1a 1 expression indirectly	Up-regulation	Koga et al., 2005; Ortuno et al., 2013
Col1a2	By binding to the second GC-rich site directly	Up-regulation	Yano et al., 2014
Col5a1	By binding to GC-rich sequence directly	Up-regulation	Wu et al., 2010a,b
Col5a3	By binding to GC-rich sequence directly	Up-regulation	Wu et al., 2010a,b
Zbtb16	By binding to the SP1-binding site directly	Up-regulation	Onizuka et al., 2016
Integrin β3	By binding to the integrin β3 promoter directly	Up-regulation	Moon et al., 2018
Cx43	By binding to the promoter region of Cx43 directly	Up-regulation	Han et al., 2016a
Vascular endothelial growth factor (VEGF)	By binding to the promoter directly or regulating gene expression of VEGF with HIF-1α cooperatively	Up-regulation	Chen et al., 2012; Tang et al., 2012
MMP13	By binding to the GC-rich sequence directly	Up-regulation	Zhang et al., 2012
MMP9	By binding to the CCAAT sequence directly	Up-regulation	Yao et al., 2019
ZIP1	By regulating gene ZIP1 expression of VEGF with Runx2 cooperatively	Up-regulation	Fu et al., 2018
Ucma	By binding to Sp1-binding sites directly	Up-regulation	Lee Y. J. et al., 2015
Enpp1	By binding to Sp1-binding sites directly	Up-regulation	Gao M. et al., 2018
Fibrillin-2	Unknown	Down-regulation	Lee et al., 2017

THE SIGNALING PATHWAYS CONTROL Osx EXPRESSION

There are two main pathways which cause in the induction of Osx gene expression, indirectly or directly (Ramazzotti et al., 2019). We will discuss these two signaling pathways in detail below. The overview of crosstalk pathways associated with Osx were showed in **Figure 3**.

Runx2-Dependent Pathways

It has been extensively recognized that Osx functions as downstream of Runx2, since the latter is expressed in mesenchymal cells of Osx KO mice while Osx expression is not observed in the absence of Runx2 (Komori, 2018). For the Runx2-dependent pathway, it is usually activated by bone morphogenic protein (BMP) signals (Li et al., 2017, 2018a; Lee et al., 2019). Interestingly, Osx was also first discovered as a BMP2 induced gene (Lee et al., 2003). BMP2 plays a unique role in mesenchymal stem cells (MSCs) differentiation by controlling the transition from progenitors to $Runx^{2+}$ Osx^{+} cells. Osx expression is not regulated by the orchestration of the BMP signaling pathways directly and specifically but eventually by crucial transcriptional factors (Matsubara et al., 2008). BMP2 is proved to activate Runx2 through Smad signaling and Runx2 in turn up-regulates Osx expression, in which Runx2 directly binds to Osx promoter

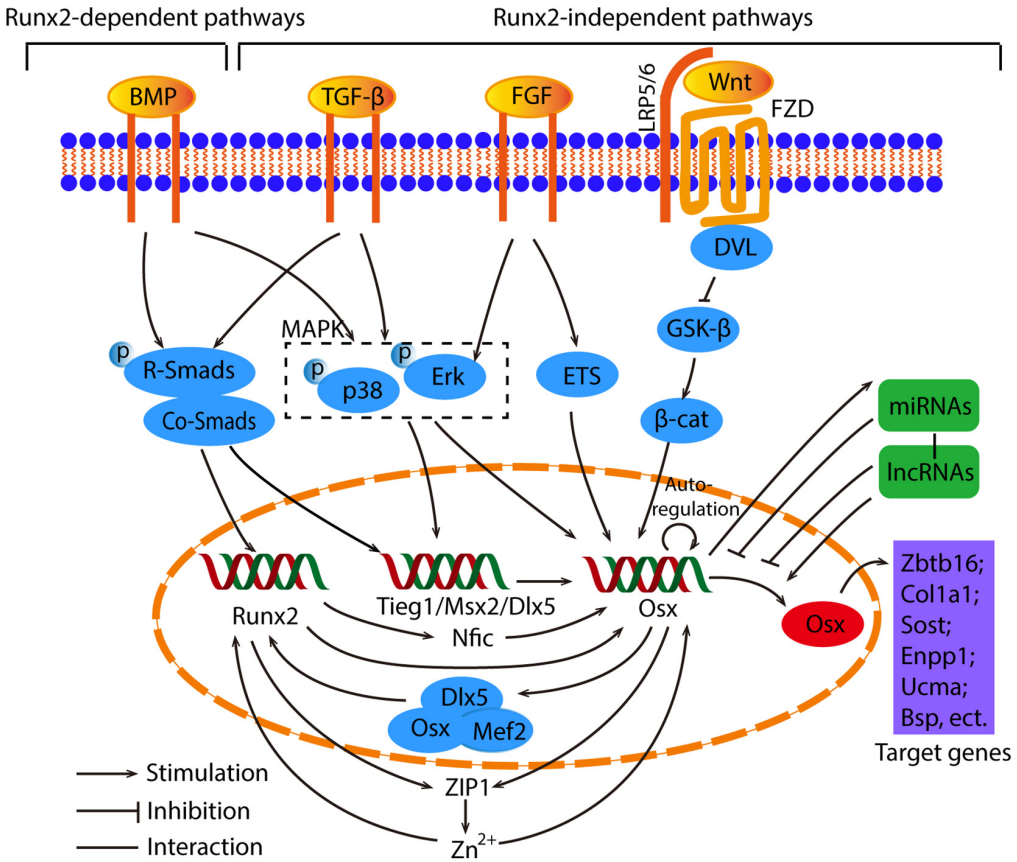


FIGURE 3 | The overview of crosstalk pathways associated with Osx. The signaling pathways that control Osx expression can be divided into Runx2-dependent and Runx2-independent pathways. In regard to the Runx2 dependent pathways, the BMP/Smads/Runx2 is the canonical pathway, and Runx2 regulates Osx by Nfic, ZIP1 indirectly or upregulate Osx directly. Meanwhile, Osx cooperate with Dlx5 and Mef2 to control Runx2 reversely. As for the Runx2-independent pathway, they are induced by BMP, TGF-β and FGF, then activate Smads, MAPK or ETS to regulate Osx directly or indirectly. The Wnt/β-catenin signaling is involved in the suppression of Osx. What's more, Osx has the capability of auto-regulation. Osx are also controlled by miRNAs and lncRNAs in an epigenetic manner. Generally, miRNAs act as negative regulators and Osx conversely stimulates miRNAs. Different lncRNAs regulate Osx positively or negatively. Eventually, Osx promotes osteogenesis through the regulation of downstream factors such as Zbtb16, Col1a1, Sost, etc.

region and regulates Osx promoter activity (Xiao et al., 2004; Pérez-Campo et al., 2016; Takarada et al., 2016). Nuclear factor I-C (Nfic), expressed in human osteoblasts and osteoblast-like cell lines, was found to be a new candidate gene that participate in osteogenic differentiation. It acts as an intermediary transducer between Runx2 and Osx in the BMP2 signaling pathway where Runx2 is upstream of Nfic and Nfic directly controls Osx expression (Lee et al., 2014; Zhang et al., 2015; Lee et al., 2018). Osx is localized on the enhancer region in primary osteoblasts, and can form an enhanceosome with Dlx5 and myocyte enhancer factor 2 (Mef2) to synergistically activate an osteoblast-specific enhancer of Runx2, demonstrating that Osx is also involved in the regulation of Runx2 expression (Kawane et al., 2014). These suggest that the regulation between Osx and Runx2 works like a positive loop indirectly.

Runx2-Independent Pathways

Despite both Runx2 and Osx control bone mineralization and MSCs differentiation, the bone phenotype of Osx-deficient mice differ from that of Runx2-deficient mice (Nakashima et al., 2002; Caparros-Martin et al., 2013), indicating their distinctive functions during the process of bone formation. Osx could even bind and stimulate the upstream CCACCC site in its promoter to regulate its own expression, forming a positive feedback mechanism (Barbuto and Mitchell, 2013). It has been shown that BMP2 and Msh homeobox 2 (Msx2) induced Osx expression in Runx2-deficient mesenchymal cells, and the knockdown of Msx2 blocked the induction of Osx in the Runx2-deficient MSCs, which indicates that BMP2 regulates Osx expression through Msx2 independently of Runx2 (Matsubara et al., 2008). Similarly, a novel factor necessary for optimal expression of Osx in osteoblasts, namely TGFβ-induced early gene 1 (Tieg1), is also required for BMP2 and TGFβ-mediated Osx expression. It directly regulates the expression of Osx by binding to its proximal promoter (Subramaniam et al., 2016; Rajamannan, 2019).

According to reports, MAPK is also involved in the BMP2-induced Osx expression (Sun et al., 2018). BMP2-mediated enhancement of Osx mRNA transcription is achieved through

the activation of Dlx5 by p38 and extracellular signal-regulated kinase (Erk)-mediated phosphorylation. During this process, the Dlx5 binds to the Osx promoter and recruits p300, a co-activator, to increase the stability of Osx (Lee et al., 2003; Choi et al., 2011a; Xiao et al., 2015; Abdallah et al., 2018). Based on the studies of the signaling pathways related to MAPK, the mechanism of osteoporosis treatment is being further understood. For example, a significant decreases in the protein levels of Runx2 and Osx under Erk1/2, p38, or c-Jun-N-terminal kinase (JNK) signaling inhibitor treatment in β-tricalcium phosphate (β-TCP)/Mg-Zn composite can be observed easily, indicating that Mg^{2+} in Mg-Zn extract promotes osteogenic differentiation via p38 MAPK-regulated Osx (Wang Z. et al., 2020).

The wingless-related integration site (Wnt) pathway modulates bone formation through the control of progenitor cells proliferation and differentiation (Sun et al., 2016; Jing et al., 2018; Yang et al., 2020). The Wnt1 class activates the canonical Wnt signaling pathway by binding to lipoprotein receptor-related protein 5 and 6 (LRP5/6). And the canonical Wnt signaling pathway increases the stability and accumulation of β-catenin in the cytoplasm, therefore facilitating the entry of β-catenin into the nucleus to promote target genes Osx transcription (Liu et al., 2015; Nemoto et al., 2016; Shi et al., 2016). A process in the developing facial skeleton was investigated and showed that Osx is a transcriptional target of the fibroblast growth factors (FGFs) pathway. Its manipulation has an immediate and strong effect on Osx expression and FGFs directly activate Osx expression via a shared intronic *cis*-regulatory module. The activity of the FGFs pathway was modulated by Wnt/β-Catenin pathway, and the interactions between FGFs and Wnt/β-Catenin signaling pathways were mediated by ETS factors (Felber et al., 2015). Wnt3a upregulates Osx expression through activation of p38 MAPK in dental follicle cells, but p38 MAPK signaling has no crosstalk with phosphorylation of the glycogen synthase kinase-3β (GSK3β) and accumulation or translocation of β-catenin (Sakisaka et al., 2016). Osx can synchronously work with HIF-1α to further inhibit β-catenin activity. Similarly, Osx suppresses the activity of the canonical Wnt signaling pathway in osteoblasts by activating the Wnt antagonist Dkk1 (Cao et al., 2015).

OTHER FACTORS IN THE BONE MICROENVIRONMENT INTERACT WITH Osx

The secretion of hormones and cytokines in the bone microenvironment has a significant effect on the differentiation of osteoblasts and osteoclasts. And these molecules interact with Osx to influence osteogenic differentiation, which provides new avenues to develop therapeutic strategies for osteolytic diseases.

It is well-known that estrogen (ER) deficiency has clearly been established as seminal mechanism in the pathogenesis of osteoporosis (Farr et al., 2019). The lack of estrogen leads to disorders in the regulation of cytokines, growth factors and humoral factors in the bone microenvironment. And the molecular mechanism for the role of ER in bone cells is being unraveled gradually. Interestingly, it has been certificated that ER exert its function of promoting osteogenic differentiation by elevating Osx expression (Han et al., 2020). Parathyroid hormone (PTH) has been proved to increase the Osx expression levels (Yang et al., 2019). Secretion of melatonin is regulated by the suprachiasmatic nucleus of the hypothalamus. Recently, several findings have demonstrated that melatonin regulates Osx expression through inhibition of the ubiquitin-proteasome system, and therefore increases Osx-mediated Alp activity, matrix mineralization, and transcriptional activity. Furthermore, the occupancy of Osx at the promoter of the Bsp gene is also enhanced by melatonin. Researchers believe that melatonin may be a potent osteogenic agent in the treatment of osteoporosis (Machida et al., 2006; Han et al., 2017; Choi et al., 2018; Zhou et al., 2020). Another hormone neuropeptide Y, produced by osteoblasts and other peripheral tissues, was also proved to directly promote osteogenic differentiation of MC3T3-E1 cells by upregulating Osx *in vitro* (Zhang B. et al., 2020).

The bone is the third most common site of metastasis for a wide range of solid tumors. When metastatic cancer cells invade the bone, the crosstalk between tumor cells and the bone microenvironment disrupts the bone homeostasis. It was reported that galectin-3, a tumor-secreted sugar-binding protein, regulates the expression of Osx, thereby remodeling bone in the bone microenvironment niche (Nakajima et al., 2014). Opn released from cancer stem cells acts as a stimulator of osteogenesis by regulating Osx (Kim et al., 2019). In addition, expressions of two cytokines, interleukin-8 (IL-8) and parathyroid hormone-related protein (PTHrP), that cause bone destruction by inducing osteoclast differentiation and activation, were increased by Osx over-expression. On the contrary, there is low IL-8 and PTHrP expression in the tumors with Osx-knockdown cells (Yao et al., 2019). Interleukin-10 (IL-10), a cytokine that directly increases osteoblast differentiation and inhibits osteoclast differentiation, is able to up-regulate Osx gene expression in osteoblasts via mitogen-activated protein kinase (MAPK) pathway (Rios-Arce et al., 2020). These results demonstrated that Osx has potential regulatory effects on various molecules in the bone microenvironment.

miRNAs AND lncRNAs REGULATE Osx EXPRESSION

Osx Is Regulated by lncRNAs in an Epigenetic Manner

Long non-coding RNAs (lncRNAs), a novel subset of non-protein-coding RNAs with longer than 200 nucleotides was established to regulate Osx epigenetically (Wu J. et al., 2018; Wu R. et al., 2018; Jiang et al., 2019; Wang et al., 2019). It was found that the regulation of osteoblast activity by lnc-ob1 is dependent on Osx. lnc-ob1 binds Suz12, a subunit of the Polycomb Repressive Complex 2, to control H3K27me3 methylation at the Osx promoter, thereby effectively regulating the Osx mRNA levels and protein levels (Sun et al., 2019). A recent report illustrated a novel mechanism of Osx during the osteogenic differentiation, that is, lncRNAs regulate Osx expression via a Runx2-independent pathway. Overexpression or knockdown of lncRNA ODIR1(Osteogenic differentiation

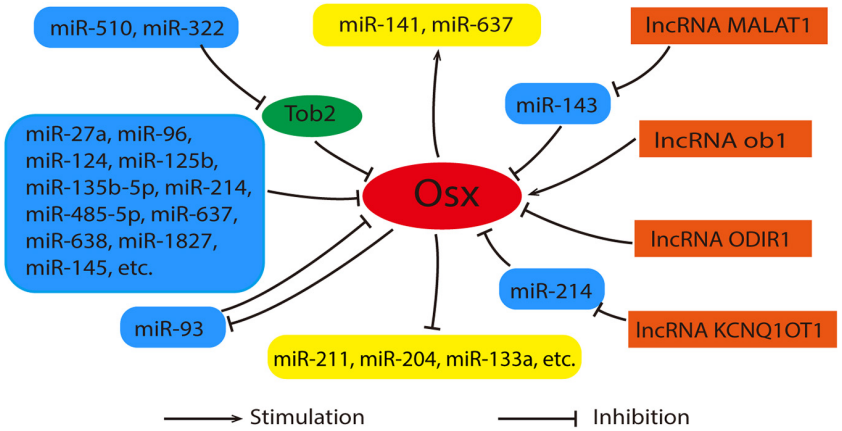


FIGURE 4 | Relationships between Osx, miRNAs and lncRNAs. Generally, miRNAs act as inhibitors during the regulation of Osx. These miRNAs were listed in the left with blue. Among them, miR-322 and rmiR-510 promote Osx expression via the inhibition of Tob2 indirectly. Meanwhile, Osx also has feedback effects on the miRNAs expression positively or negatively. These miRNAs were listed in the middle with yellow. lncRNAs (orange) control the expression of Osx in an direct or indirect manner. As for the indirect way, miRNAs can serve as their intermediary.

inhibitory regulator 1) significantly reduced or increased the expression levels of the mRNA and protein level of Osx in the osteogenic differentiation of MSCs while Runx2 was not altered, which strongly indicates that lncRNA ODIR1-mediated Osx expression is not dependent on Runx2. Further research showed that lncRNA ODIR1 inhibits Osx transcription by altering the modification of histone marks on Osx promoter. Increased expression level of F-box protein 25 (FBXO25) by knockdown of lncRNA ODIR1 in human umbilical cord-derived MSCs promoted H2BK120 mono-ubiquitylation which stimulated H3K4 trimethylation, and then the transcription level of Osx was elevated, in which both H2BK120ub and H3K4me3 form a loose chromatin structure and induce Osx expression (He et al., 2019). Consequently, these studies demonstrated that Osx has become a key regulator for researching the mechanism of lncRNAs involved in osteogenic differentiation, and it would be performed to develop novel therapeutic strategies for osteoporosis.

miRNAs Participate in Epigenetic Regulation of Osx During Osteogenic Differentiation

As an important post-transcriptional regulator, microRNAs (miRNAs) participate in the osteogenic differentiation of MSCs by targeting multiple genes including Runx2, Dlx, Smad4, etc. (Landgraf et al., 2007; Huang et al., 2016). It has been proved that miR-27a and miR-96 etc. regulate osteogenesis by targeting Osx (As shown in **Figure 4**) (Zhang et al., 2011; Shi et al., 2013; Zhang et al., 2018; Jiao et al., 2019). They suppress osteogenic differentiation by decreasing Osx expression directly. Recently, Liu et al. (2020) have certified that Osx serves as the direct target of miR-1827 and the inhibitive effect on osteogenic differentiation of miR-1827 amplification was reversed by Osx overexpression. In addition to this, some miRNAs indirectly regulated the expression of Osx via other genes. miR-322 and miR-510 promoted Osx expression via the inhibition of Tob2, a negative regulator of osteogenesis that bound and mediated the degradation of Osx mRNA (Gamez et al., 2013; Wang et al., 2017). Interestingly, a study revealed that Osx also has feedback effects on the miRNAs expression. It was reported that miRNA-93 is able to form a feedback loop with Osx to regulate osteoblast mineralization (Yang et al., 2012). The details were shown in **Figure 4**.

lncRNAs Interact With miRNAs to Regulate Osx

Since both miRNAs and lncRNAs have such vital functions in Osx-mediated osteogenic differentiation, is there a possibility that lncRNAs interact with miRNAs to regulate Osx? Some experimental findings correlate with this point of view. In human bone marrow-derived MSCs, lncRNA Metastasis-associated lung adenocarcinoma transcript-1 (MALAT1) is able to increase Osx expression by competitively binding to miR-143 and inhibit its expression, since miR-143 inhibits Osx expression (Gao Y. et al., 2018). Recently, it has been also reported that lncRNA KCNQ1OT1 promotes osteogenic differentiation of bone marrow mesenchymal stem cells (BMSCs) by sponging miR-214 as a competing endogenous RNA via regulating BMP2/Smad pathway (Wang et al., 2019). Obviously, the new molecular mechanism of the interaction between Osx, miRNAs and lncRNAs in regulation of osteogenic differentiation of BMSCs still remains to be explored. For intuitive description, **Figure 4** shows the relationships between Osx, miRNAs and lncRNAs clearly.

POST-TRANSLATIONAL MODIFICATIONS ARE IMPORTANT FOR Osx ACTIVITY

Post-translational modification is a key cellular event in controlling the activities of Osx during osteogenic differentiation.

Osteoblast activity is augmented in ubiquitin ligase-deficient mice that generate adult onset osteosclerosis with increased bone

mass, indicating that the ubiquitin-proteasome system plays a role in osteoblast differentiation. Generally speaking, proteins are ubiquitinated and then degraded by proteasome. Further studies demonstrated that ubiquitination of Osx plays a key role in osteoblast differentiation. K58 and K230 were first identified to be the ubiquitination sites of Osx by Co-IP assays and protein stability assays (Peng et al., 2013). Subsequently, it has been illustrated that ring finger type E3 ubiquitin ligases Cbl-b and c-Cbl enhance ubiquitin-proteasome-mediated degradation of Osx by reducing the protein stability of Osx in BMP2-stimulated C2C12 cells (Choi et al., 2015). However, Cbl-b and c-Cbl did not affect the protein levels of other osteogenic transcription factors such as Dlx3, Dlx5, and Msx2. These results suggest that Cbl-b and c-Cbl specifically regulate the function of Osx during osteoblast differentiation. CHIP, another novel post-translational regulator of Osx, plays an important role in the regulation of Osx in protein levels in osteoblast precursor cells upon treatment with tumor necrosis factor-α (TNF-α). Unlike the previous description, CHIP mediates the inhibition of Osx by TNF-α in K55 and K386 ubiquitination sites of Osx (Xie and Gu, 2015).

Phosphorylation is widely recognized as an important regulatory pathway in skeletal development and maintenance. Osx can be regulated post-translationally by protein kinase-mediated phosphorylation including NFATc1, protein kinase B (Akt), kinase glycogen synthase kinase-3 (GSK-3), Peptidyl-prolyl isomerase 1 (Pin1) and Erk, etc. in osteoblast differentiation (Koga et al., 2005; Choi et al., 2011b; Qi et al., 2015). Akt is a member of serine/threonine-specific protein kinase that phosphorylates Osx and its activation increases protein stability, osteogenic and transcriptional activity of Osx (You et al., 2011). Mammalian GSK-3, consisting of two isoforms GSK-3α and GSK-3β, plays a vital role in the functional regulation of Osx through phosphorylation modification. Interestingly, different GSK-3 isoforms phosphorylate Osx in a different manner, although the catalytic domains of them exhibit 97% sequence homology. Particularly, GSK-3α phosphorylated Osx at Ser76/80 sites and up-regulated the osteogenic activity of Osx, whereas GSK-3β increased the stability and transactivation activity of Osx through phosphorylation of the newly identified site S422 (Xu et al., 2015). Similarly, the phosphorylation of Ser76/80 of Osx is also important for Pin1 interaction and function (Lee S. H. et al., 2015). What's more, p38-mediated phosphorylation of Osx at Ser-73/77 enhanced the recruitment of coactivators and then transcriptionally active complexes formed. Further study showed that p38-mediated phosphorylation of Osx increases its interaction with the transcriptional coactivators p300 and Brg1 (Ortuño et al., 2010).

Like phosphorylation, acetylation is a universal modification of proteins by increasing or decreasing the DNA binding and transcriptional activity of transcription factors. CREB binding protein (CBP) co-transfection contributing to Osx acetylation significantly delayed Osx degradation and conversely, histone deacetylase 4 (HDAC4) co-transfection involved in the deacetylation of Osx significantly accelerated Osx degradation. CBP interacts with Osx as a transcription coactivator *in vivo*, resulting in acetylation of the two lysine residues at the C-terminus of Osx. Further studies have shown that Osx acetylation increases its binding to the promoter of the target genes such as Alp, Bsp, Col1a1 and Osteocalcin (Lu et al., 2016). These facts demonstrated that acetylation of Osx enhances its stability and transcription activity. And Osx activity is required for the osteogenic differentiation of C2C12 cells. Therefore, Osx acetylation is necessary to promote osteoblast differentiation. Recently, the effect of Osx acetylation on the osteogenic differentiation of vascular smooth muscle cells (VSMCs) was also studied. After the knockdown of the histone deacetylase Hdac9, the expression of Osx mRNA remained unchanged while the protein expression level was significantly enhanced and then resulted in the enhancement of VSMCs calcification *in vitro*. This process may be mediated by acetylation of Osx (He et al., 2020). It has been confirmed that both endogenous and exogenous Osx protein can be acetylated. Generally, acetylation inhibits DNA binding when the acetylation sites are located in the DNA binding domain, and if they are adjacent to the DNA binding domain, DNA binding is activated. A recent study has identified K307 and K312 as the acetylation sites of Osx (Lu et al., 2016). Among them, K307 is close to the C2H2 DNA binding domain of Osx (from amino acids 309 to 376), while K312 is located at the N-terminus of Osx's DNA-binding domain. It is necessary to take further exploration for understanding of the structural changes of Osx after acetylation and the signal pathway networks about acetylation or deacetylation of Osx, as well as any crosstalk between acetylation and other post-translational modifications.

DNA methylation has been a hot topic of epigenetic studies in the bone development system. The CpG dinucleotides of the Osx promoter regions were unmethylated in osteogenic cell lines transcribing but methylated in non-osteogenic cell lines, suggesting that DNA methylation plays an important role in cell type-specific expression of Osx (Lee et al., 2006; Sepulveda et al., 2017a). DNA demethylation is accompanied by activation of the Osx gene during osteoblast differentiation, which involves the release of DNA methyltransferases from the Osx promoter (Sepulveda et al., 2017b).

THE POTENTIAL EFFICACY OF Osx FOR THE TREATMENT OF OSTEOLYTIC DISEASES

In the normal physiological circumstances, bone resorption by osteoclasts and bone formation by osteoblasts maintain a healthy balance. Once the balance of this coupled process is broken, the molecular characteristics of the bone microenvironment change. As a result, osteolytic lesions occur, eliciting severe bone pain and fractures.

Osteoporosis is an osteolytic disease resulted from imbalance in bone homeostasis. It is well-known that estrogen (ER) therapy can significantly achieve anti-fracture efficacy, especially for postmenopausal women (Farr et al., 2019). Osx is also involved in osteoporosis treatment. However, ER therapy is usually accompanied by increased risk of breast, ovarian and endometrial cancer, which eventually leads to its diminished application clinically. In addition, as the only drug stimulating bone

formation approved by Food and Drug Administration (FDA), Parathyroid hormone (PTH) has been proved to increase the Osx expression levels. However, it is related to osteosarcoma and can only be used for 2 years (Arumugam et al., 2019; Yang et al., 2019). Therefore, big efforts are underway to investigate new drugs or find serendipitous effects with old drugs in order to gain better therapy efficacy and minimize potential harms of long-term drug exposure (Stringhetta-Garcia et al., 2016; Qaseem et al., 2017; Haryati et al., 2018; Farr et al., 2019; Yoon et al., 2019). Besides, some natural extracts have been identified to promote osteogenic differentiation via Osx in the treatment of osteoporosis (Choi et al., 2016; Yashan et al., 2017; Wang et al., 2018; Chai et al., 2019; El-Makawy et al., 2020). They positively regulate the transcriptional expression and enhance the activity of Osx via different signaling pathways. Recent research has illustrated that the initial anabolic response after mechanical loading is based on the activation and proliferation of Osx lineage cells, but not the differentiation of progenitor cells (Zannit and Silva, 2019). Low intensity pulsed ultrasound (LIPUS) has been proven successful recoveries from non-unions, delayed unions and fracture of the bone in both animal experiments and clinical treatments. The underlying mechanism revealed that LIPUS-mediated mechanism of osteogenic differentiation may be achieved via upregulation of BMP2 expression and through activation of the BMP/Smad canonical pathway, and then increased Osx expression (Maung et al., 2020).

In addition to osteoporosis, Osx may be an attractive therapeutic target for the control of other osteolytic diseases such as osteosarcoma and bone metastasis of cancers. The expression of Osx was decreased in murine osteosarcoma cells compared with normal mouse osteoblasts. The transfection of Osx into K7M2 cells altered the osteolytic morphology of the tumors. More specifically, the expression of Osx suppressed the osteolytic phenotype (Cao et al., 2005). Decreased Osx expression would result in decreased osteoblast differentiation and increased osteoclast activity leading to lytic destruction as the tumor cells invade the normal bone. Multiple myeloma (MM) is a malignancy to involve the skeleton with patients developing osteolytic bone lesions. A proteasome inhibitor and immunomodulatory drug bortezomib has been introduced in the therapy of MM. when treatment with 10 nM of bortezomib, an increase of Osx RNA transcription both in normal and MM osteoblasts were observed. In the myeloma microenvironment, bortezomib has the ability to stimulate osteoblast differentiation by increasing Osx levels during osteogenesis and inhibit osteoclast differentiation by reducing the induction of osteoclast marker genes and proteins like NFATc1 (De Matteo et al., 2010; Kim et al., 2018; Wang H. et al., 2020). On the contrary, another proteasome inhibitor and immunomodulatory drug named lenalidomide induces osteoblast differentiation by inhibiting the secretion of osteoclastogenic factors which reflects the inhibitory effect exerted on osteogenic cells, but have no effect on Runx2 and Osx transcription (De Matteo et al., 2010). There is a strong nuclear expression of Osx in osteoid osteomas and osteoblastomas, while the expression of Osx in chondromyxoid fibromas and chondroblastomas are negative generally, which represent a novel marker in assessing chondroblastic and osteoblastic lineage differentiation of bone tumors (Dancer et al., 2010). The potential role of Osx in chondroblastoma are required to be explored indeeply.

TABLE 2 | The treatment for different osteolytic diseases by targeting Osx.

Drug and trials	Disease or cells	Mechanisms	References
Estrogen (ER)	Osteoporosis	By elevating the expressions of Runx2 and Osx	Han et al., 2020
Parathyroid hormone (PTH)	Dental pulp stem cells	By activating Erk and p38 signaling pathways and elevating Osx expression	Ge et al., 2020
Pseudoshikonin I	C2C12 cells	By stimulating Osx and Runx2 via the Akt and Pka signaling pathways	Choi et al., 2018
Gushukang (GSK)	Osteoporosis	By enhancing BMP2/Smads signaling pathway and elevating Osx expression	Chai et al., 2019
Strength training and Raloxifene	Osteopenia	By stimulating/reducing the genesis and activity of osteoblasts/osteoclasts	Stringhetta-Garcia et al., 2016
Turnip bioactive lipids	Osteoporosis	By activating Osx and suppressing Cathepsin K and TNF-α signaling	El-Makawy et al., 2020
Remifentanil	C2C12 cells	By upregulating Osx and Runx2 expression.	Yoon et al., 2019
Low intensity pulsed ultrasound(LIPUS)	Periosteum-derived cells	By upregulating Osx expression through activation of the BMP/Smad canonical pathway	Maung et al., 2020
Bortezomib	Multiple myeloma	By increasing Osx expression and synthesizing the final differentiation markers in osteogenesis	De Matteo et al., 2010
Lenalidomide	Multiple myeloma	By inhibiting the secretion of osteoclastogenic factors exerting on osteogenic cells negatively and no effect on Runx2 and Osx transcription	De Matteo et al., 2010

Obviously, these studies suggest that Osx has become one of the few downstream specific transcription factors directly regulated by ER or other alternative drugs in the treatment of osteolytic diseases as shown in **Table 2**. And Osx might be a therapeutic target for osteosarcoma and other osteolytic diseases. Therefore, we would conclude that Osx-mediated mechanism of osteogenic differentiation points out the direction for exploitation of novel bone disease therapy strategies.

CONCLUSION

Overall, the current literatures have demonstrated that Osx plays a critical role in osteogenesis differentiation. In the last 10 years, the mechanism of Osx in osteoblast differentiation and bone formation are further understood. The efforts in designing new drugs steadily increased due to the recognition that the significance of bone health. Noteworthy, Osx is involved in the complex communications among different bone cells and plays a role in the bone micro-environment. What's more, Osx plays an

important role in the treatment of osteolytic diseases. And Osx may be an attractive therapeutic target for the control of other osteolytic diseases. As more and more key genes and regulatory mechanisms of osteolytic diseases are discovered, medication of osteolytic diseases with new mechanisms is foreseeable in the future. We believe that the research on Osx and osteolytic diseases in the future will mainly focus on the following aspects: (1) The interaction between bone formation-related protein and Osx during osteogenic differentiation as well as their underlying molecular mechanisms remains to be further studied; (2) The new molecular mechanism of Osx regulated by miRNAs and lncRNAs remains to be explored, which may provide a potential target for the treatment of osteoporosis;(3) More effective and safer Osx-targeted drugs are needed to be further developed for the treatment of osteolytic diseases.

AUTHOR CONTRIBUTIONS

GW and YX conceived of this review. QL drafted this manuscript and designed the figures. ML conducted the literature investigation. All the authors provided the critical feedback, contributed to the discussion on the manuscript writing and revising, and approved the manuscript.

FUNDING

This work was received financial support from the National Natural Science Foundation of China (NSFC) (No. 81670809) and the Science and Technology Research Fund of Hunan Provincial Education Department.

REFERENCES

Abdallah, B. M., Alzahrani, A. M., and Kassem, M. (2018). Secreted Clusterin protein inhibits osteoblast differentiation of bone marrow mesenchymal stem cells by suppressing ERK1/2 signaling pathway. *Bone* 110, 221–229. doi: 10.1016/j.bone.2018.02.018

Arumugam, B., Vishal, M., Shreya, S., Malavika, D., Rajpriya, V., He, Z., et al. (2019). Parathyroid hormone-stimulation of Runx2 during osteoblast differentiation via the regulation of lnc-SUPT3H-1:16 (RUNX2-AS1:32) and miR-6797-5p. *Biochimie* 158, 43–52. doi: 10.1016/j.biochi.2018.12.006

Azetsu, Y., Inohaya, K., Takano, Y., Kinoshita, M., Tasaki, M., and Kudo, A. (2017). The sp7 gene is required for maturation of osteoblast-lineage cells in medaka (*Oryzias latipes*) vertebral column development. *Dev. Biol.* 431, 252–262. doi: 10.1016/j.ydbio.2017.09.010

Baek, W. Y., and Kim, J. E. (2011). Gene alterations by osteoblast-specific transcription factor osterix in postnatal bone formation. *Osteoporosis* 9, 51–56.

Barbuto, R., and Mitchell, J. (2013). Regulation of the osterix (Osx, Sp7) promoter by osterix and its inhibition by parathyroid hormone. *J. Mol. Endocrinol.* 51, 99–108. doi: 10.1530/jme-12-0251

Calabrese, G. M., Mesner, L. D., Stains, J. P., Tommasini, S. M., Horowitz, M. C., Rosen, C. J., et al. (2017). Integrating GWAS and co-expression network data identifies bone mineral density genes SPTBN1 and MARK3 and an osteoblast functional module. *Cell Syst.* 4, 46–59.e4.

Canalis, E., Schilling, L., Eller, T., and Yu, J. (2020). Nuclear factor of activated T cells 1 and 2 are required for vertebral homeostasis. *J. Cell. Physiol.* 235, 8520–8532. doi: 10.1002/jcp.29696

Cao, Y., Zhou, Z., de Crombrugghe, B., Nakashima, K., Guan, H., Duan, X., et al. (2005). Osterix, a transcription factor for osteoblast differentiation, mediates antitumor activity in murine osteosarcoma. *Cancer Res.* 65, 1124–1128. doi: 10.1158/0008-5472.Can-04-2128

Cao, Z., Liu, R., Zhang, H., Liao, H., Zhang, Y., Hinton, R. J., et al. (2015). Osterix controls cementoblast differentiation through downregulation of Wnt-signaling via enhancing DKK1 expression. *Int. J. Biol. Sci.* 11, 335–344. doi: 10.7150/ijbs.10874

Caparros-Martin, J., Aglan, M., Temtamy, S., Martinez-Glez, V., Valencia, M., Tenorio, J., et al. (2013). "OSX/SP7 mutations and osteogenesis imperfecta," in *Osteogenesis Imperfecta: A Translational Approach to Brittle Bone Disease*, eds J. R. Shapiro, P. H. Byers, F. H. Glorieux, and P. Sponsellor (Amsterdam: Elsevier), 173–179. doi: 10.1016/B978-0-12-397165-4.00018-6

Chai, S., Wan, L., Wang, J. L., Huang, J. C., and Huang, H. X. (2019). Gushukang inhibits osteocyte apoptosis and enhances BMP-2/Smads signaling pathway in ovariectomized rats. *Phytomedicine* 64:153063. doi: 10.1016/j.phymed.2019.153063

Chen, D., Tian, W., Li, Y., Tang, W., and Zhang, C. (2012). Osteoblast-specific transcription factor Osterix (Osx) and HIF-1α cooperatively regulate gene expression of vascular endothelial growth factor (VEGF). *Biochem. Biophys. Res. Commun.* 424, 176–181. doi: 10.1016/j.bbrc.2012.06.104

Chen, X., Wang, Z., Duan, N., Zhu, G., Schwarz, E. M., and Xie, C. (2018). Osteoblast-osteoclast interactions. *Connect. Tissue Res.* 59, 99–107. doi: 10.1080/03008207.2017.1290085

Chen, Y., Chen, M., Xue, T., Li, G., Wang, D., Shang, P., et al. (2019). Osteocytic connexin 43 channels affect fracture healing. *J. Cell. Physiol.* 234, 19824–19832. doi: 10.1002/jcp.28581

Choi, Y. H., Gu, Y. M., Oh, J. W., and Lee, K. Y. (2011a). Osterix is regulated by Erk1/2 during osteoblast differentiation. *Biochem. Biophys. Res. Commun.* 415, 472–478. doi: 10.1016/j.bbrc.2011.10.097

Choi, Y. H., Han, Y., Jin, S. W., Lee, G. H., Kim, G. S., Lee, D. Y., et al. (2018). Pseudoshikonin I enhances osteoblast differentiation by stimulating Runx2 and Osterix. *J. Cell. Biochem.* 119, 748–757. doi: 10.1002/jcb.26238

Choi, Y. H., Han, Y., Lee, S. H., Jin, Y. H., Bahn, M., Hur, K. C., et al. (2015). Cbl-b and c-Cbl negatively regulate osteoblast differentiation by enhancing ubiquitination and degradation of Osterix. *Bone* 75, 201–209. doi: 10.1016/j.bone.2015.02.026

Choi, Y. H., Jeong, H. M., Jin, Y.-H., Li, H., Yeo, C.-Y., and Lee, K.-Y. (2011b). Akt phosphorylates and regulates the osteogenic activity of Osterix. *Biochem. Biophys. Res. Commun.* 411, 637–641. doi: 10.1016/j.bbrc.2011.07.009

Choi, Y. H., Kim, G. S., Choi, J. H., Jin, S. W., Kim, H. G., Han, Y., et al. (2016). Ethanol extract of *Lithospermum erythrorhizon* Sieb. et Zucc. promotes osteoblastogenesis through the regulation of Runx2 and Osterix. *Int. J. Mol. Med.* 38, 610–618. doi: 10.3892/ijmm.2016.2655

Dancer, J. Y., Henry, S. P., Bondaruk, J., Lee, S., Ayala, A. G., de Crombrugghe, B., et al. (2010). Expression of master regulatory genes controlling skeletal development in benign cartilage and bone forming tumors. *Hum. Pathol.* 41, 1788–1793. doi: 10.1016/j.humpath.2010.06.008

De Matteo, M., Brunetti, A. E., Maiorano, E., Cafforio, P., Dammacco, F., and Silvestris, F. (2010). Constitutive down-regulation of Osterix in osteoblasts from myeloma patients: in vitro effect of Bortezomib and Lenalidomide. *Leuk. Res.* 34, 243–249. doi: 10.1016/j.leukres.2009.07.017

El-Makawy, A. I., Ibrahim, F. M., Mabrouk, D. M., Abdel-Aziem, S. H., Sharaf, H. A., and Ramadan, M. F. (2020). Efficiency of turnip bioactive lipids in treating osteoporosis through activation of Osterix and suppression of Cathepsin K and TNF-alpha signaling in rats. *Environ. Sci. Pollut. Res. Int.* 27, 20950–20961. doi: 10.1007/s11356-020-08540-7

Farr, J. N., Rowsey, J. L., Eckhardt, B. A., Thicke, B. S., Fraser, D. G., Tchkonia, T., et al. (2019). Independent roles of estrogen deficiency and cellular senescence in the pathogenesis of osteoporosis: evidence in young adult mice and older humans. *J. Bone Miner. Res.* 34, 1407–1418. doi: 10.1002/jbmr.3729

Felber, K., Elks, P. M., Lecca, M., and Roehl, H. H. (2015). Expression of osterix is regulated by FGF and Wnt/beta-catenin signalling during Osteoblast differentiation. *PLoS One* 10:e0144982. doi: 10.1371/journal.pone.0144982

Fu, H., Doll, B., Mcnelis, T., and Hollinger, J. O. (2010). Osteoblast differentiation in vitro and in vivo promoted by Osterix. *J. Biomed. Mater. Res. A* 83A, 770–778. doi: 10.1002/jbm.a.31356

Fu, X., Li, Y., Huang, T., Yu, Z., Ma, K., Yang, M., et al. (2018). Runx2/Osterix and zinc uptake synergize to orchestrate osteogenic differentiation and citrate

containing bone apatite formation. *Adv. Sci.* 5:1700755. doi: 10.1002/advs.201700755

Gamez, B., Rodriguez-Carballo, E., Bartrons, R., Rosa, J. L., and Ventura, F. (2013). MicroRNA-322 (miR-322) and its target protein Tob2 modulate Osterix (Osx) mRNA stability. *J. Biol. Chem.* 288, 14264–14275. doi: 10.1074/jbc.M112.432104

Gao, M., Su, Q., Liang, T., Ma, J., and Zou, X. (2018). Transcriptional activation of ENPP1 by osterix in osteoblasts and osteocytes. *Eur. Cell. Mater.* 36, 1–14. doi: 10.22203/ecm.v036a01

Gao, Y., Jheon, A., Nourkeyhani, H., Kobayashi, H., and Ganss, B. (2004). Molecular cloning, structure, expression, and chromosomal localization of the human Osterix (SP7) gene. *Gene* 341, 101–110. doi: 10.1016/j.gene.2004.05.026

Gao, Y., Xiao, F., Wang, C., Wang, C., Cui, P., Zhang, X., et al. (2018). Long noncoding RNA MALAT1 promotes osterix expression to regulate osteogenic differentiation by targeting miRNA-143 in human bone marrow-derived mesenchymal stem cells. *J. Cell. Biochem.* 119, 6986–6996. doi: 10.1002/jcb.26907

Ge, X., Li, Z., Jing, S., Wang, Y., Li, N., Lu, J., et al. (2020). Parathyroid hormone enhances the osteo/odontogenic differentiation of dental pulp stem cells via ERK and P38 MAPK pathways. *J. Cell. Physiol.* 235, 1209–1221. doi: 10.1002/jcp.29034

Han, K., Wang, F., Yu, M., and Xu, B. (2020). Estrogen promotes osteogenic differentiation of bone marrow stem cells in patients with postmenopausal osteoporosis by elevating the expressions of Runx-2 and Osterix. *Panminerva Med.* doi: 10.23736/s0031-0808.19.03791-1 [Epub ahead of print].

Han, Y., Cho, D. H., Chung, D. J., and Lee, K. Y. (2016a). Osterix plays a critical role in BMP4-induced promoter activity of connexin43. *Biochem. Biophys. Res. Commun.* 478, 683–688. doi: 10.1016/j.bbrc.2016.08.007

Han, Y., Kim, C. Y., Cheong, H., and Lee, K. Y. (2016b). Osterix represses adipogenesis by negatively regulating PPARgamma transcriptional activity. *Sci. Rep.* 6:35655. doi: 10.1038/srep35655

Han, Y., Kim, Y. M., Kim, H. S., and Lee, K. Y. (2017). Melatonin promotes osteoblast differentiation by regulating Osterix protein stability and expression. *Sci. Rep.* 7:5716. doi: 10.1038/s41598-017-06304-x

Haryati, A. H., Jamia, J., Nor, A., Khairana, H., Noor, M. S., Norazlina, M., et al. (2018). Demethylbelamcandaquinone B (Dmcq B) is the active compound of *Marantodes pumilum* var. alata (Blume) Kuntze with osteoanabolic activities. *Molecules* 23:1686. doi: 10.3390/molecules23071686

Hayami, T., Kapila, Y. L., and Kapila, S. (2011). Divergent upstream osteogenic events contribute to the differential modulation of MG63 cell osteoblast differentiation by MMP-1 (collagenase-1) and MMP-13 (collagenase-3). *Matrix Biol.* 30, 281–289. doi: 10.1016/j.matbio.2011.04.003

He, P., Yu, H., Jiang, L., Chen, Z., Wang, S., Macrae, V. E., et al. (2020). Hdac9 inhibits medial artery calcification through down-regulation of Osterix. *Vasc. Pharmacol.* 132:106775. doi: 10.1016/j.vph.2020.106775

He, S., Yang, S., Zhang, Y., Li, X., Gao, D., Zhong, Y., et al. (2019). LncRNA ODIR1 inhibits osteogenic differentiation of hUC-MSCs through the FBXO25/H2BK120ub/H3K4me3/OSX axis. *Cell Death Dis.* 10:947. doi: 10.1038/s41419-019-2148-2

Hojo, H., Ohba, S., He, X., Lai, L. P., and McMahon, A. P. (2016). Sp7/Osterix is restricted to bone-forming vertebrates where it acts as a Dlx co-factor in osteoblast specification. *Dev. Cell* 37, 238–253. doi: 10.1016/j.devcel.2016.04.002

Huang, C., Geng, J., Wei, X., Zhang, R., and Jiang, S. (2016). MiR-144-3p regulates osteogenic differentiation and proliferation of murine mesenchymal stem cells by specifically targeting Smad4. *FEBS Lett.* 590, 795–807. doi: 10.1002/1873-3468.12112

Jiang, Y., Wu, W., Jiao, G., Chen, Y., and Liu, H. (2019). LncRNA SNHG1 modulates p38 MAPK pathway through Nedd4 and thus inhibits osteogenic differentiation of bone marrow mesenchymal stem cells. *Life Sci.* 228, 208–214. doi: 10.1016/j.lfs.2019.05.002

Jiao, W., Zhang, D., Wang, D., Xu, R., Tang, L., Zhao, M., et al. (2019). MicroRNA-638 inhibits human aortic valve interstitial cell calcification by targeting Sp7. *J. Cell. Mol. Med.* 23, 5292–5302. doi: 10.1111/jcmm.14405

Jing, H., Su, X., Gao, B., Shuai, Y., Chen, J., Deng, Z., et al. (2018). Epigenetic inhibition of Wnt pathway suppresses osteogenic differentiation of BMSCs during osteoporosis. *Cell Death Dis.* 9:176. doi: 10.1038/s41419-017-0231-0

Karieb, S., and Fox, S. W. (2012). Zinc modifies the effect of phyto-oestrogens on osteoblast and osteoclast differentiation in vitro. *Br. J. Nutr.* 108, 1736–1745. doi: 10.1017/S0007114511007355

Kawane, T., Komori, H., Liu, W., Moriishi, T., Miyazaki, T., Mori, M., et al. (2014). Dlx5 and mef2 regulate a novel runx2 enhancer for osteoblast-specific expression. *J. Bone Miner. Res.* 29, 1960–1969. doi: 10.1002/jbmr.2240

Kemp, J. P., Morris, J. A., Medina-Gomez, C., Forgetta, V., and Evans, D. M. (2017). Identification of 153 new loci associated with heel bone mineral density and functional involvement of GPC6 in osteoporosis. *Nat. Genet.* 49, 1468–1475. doi: 10.1038/ng.3949

Kim, D., Ko, Y., Park, M., Kim, B., Sohn, H., and Lim, W. (2019). Regulation of osteosclerosis by inoculated Cd133(+) PC3 Cells in bone-marrow microenvironmental niches. *JBMR Plus* 3:e10189. doi: 10.1002/jbm4.10189

Kim, S. H., Kim, M. O., Kim, H. J., Neupane, S., Kim, H. J., Lee, J. H., et al. (2018). Bortezomib prevents ovariectomy-induced osteoporosis in mice by inhibiting osteoclast differentiation. *J. Bone Miner. Metab.* 36, 537–546. doi: 10.1007/s00774-017-0871-2

Klein-Nulend, J., Bakker, A. D., Bacabac, R. G., Vatsa, A., and Weinbaum, S. (2013). Mechanosensation and transduction in osteocytes. *Bone* 54, 182–190. doi: 10.1016/j.bone.2012.10.013

Koga, T., Matsui, Y., Asagiri, M., Kodama, T., and Takayanagi, H. (2005). NFAT and Osterix cooperatively regulate bone formation. *Nat. Med.* 11, 880–885. doi: 10.1038/nm1270

Komori, T. (2018). Runx2, an inducer of osteoblast and chondrocyte differentiation. *Histochem. Cell Biol.* 149, 313–323. doi: 10.1007/s00418-018-1640-6

Kusu, N., Laurikkala, J., Imanishi, M., Usui, H., Konishi, M., Miyake, A., et al. (2003). Sclerostin is a novel secreted osteoclast-derived bone morphogenetic protein antagonist with unique ligand specificity. *J. Biol. Chem.* 278, 24113–24117. doi: 10.1074/jbc.M301716200

Landgraf, P., Rusu, M., Sheridan, R., Sewer, A., Iovino, N., Aravin, A., et al. (2007). A mammalian microRNA expression atlas based on small RNA library sequencing. *Cell* 129, 1401–1414. doi: 10.1016/j.cell.2007.04.040

Lee, D. S., Choung, H. W., Kim, H. J., Gronostajski, R. M., Yang, Y. I., Ryoo, H. M., et al. (2014). NFI-C regulates osteoblast differentiation via control of osterix expression. *Stem Cells* 32, 2467–2479. doi: 10.1002/stem.1733

Lee, D. S., Roh, S. Y., and Park, J. C. (2018). The Nfic-osterix pathway regulates ameloblast differentiation and enamel formation. *Cell Tissue Res.* 374, 531–540. doi: 10.1007/s00441-018-2901-3

Lee, H., Min, S., Song, Y., Park, Y. H., and Park, J. B. (2019). Bone morphogenetic protein-7 upregulates genes associated with osteoblast differentiation, including collagen I, Sp7 and IBSP in gingiva-derived stem cells. *Exp. Ther. Med.* 18, 2867–2876. doi: 10.3892/etm.2019.7904

Lee, J. Y., Lee, Y. M., Kim, M. J., Choi, J. Y., Park, E. K., Kim, S. Y., et al. (2006). Methylation of the mouse DIx5 and Osx gene promoters regulates cell type-specific gene expression. *Mol. Cells* 22, 182–188.

Lee, M. H., Kwon, T. G., Park, H. S., Wozney, J. M., and Ryoo, H. M. (2003). BMP-2-induced Osterix expression is mediated by Dlx5 but is independent of Runx2. *Biochem. Biophys. Res. Commun.* 309, 689–694. doi: 10.1016/j.bbrc.2003.08.058

Lee, S. H., Jeong, H. M., Han, Y., Cheong, H., Kang, B. Y., and Lee, K. Y. (2015). Prolyl isomerase Pin1 regulates the osteogenic activity of Osterix. *Mol. Cell. Endocrinol.* 400, 32–40. doi: 10.1016/j.mce.2014.11.017

Lee, S. J., Lee, E. H., Park, S. Y., and Kim, J. E. (2017). Induction of fibrillin-2 and periostin expression in Osterix-knockdown MC3T3-E1 cells. *Gene* 596, 123–129. doi: 10.1016/j.gene.2016.10.018

Lee, Y. J., Park, S. Y., Lee, S. J., Boo, Y. C., Choi, J. Y., and Kim, J. E. (2015). Ucma, a direct transcriptional target of Runx2 and Osterix, promotes osteoblast differentiation and nodule formation. *Osteoarthr. Cartil.* 23, 1421–1431. doi: 10.1016/j.joca.2015.03.035

Li, Y., Hu, W., Han, G., Lu, W., Jia, D., Hu, M., et al. (2018a). Involvement of bone morphogenetic protein-related pathways in the effect of aucubin on the promotion of osteoblast differentiation in MG63cells. *Chem. Biol. Interact.* 283, 51–58. doi: 10.1016/j.cbi.2018.02.005

Li, Y., Jin, D., Xie, W., Wen, L., Chen, W., Xu, J., et al. (2018b). PPAR-γ and Wnt regulate the differentiation of MSCs into adipocytes and osteoblasts respectively. *Curr. Stem Cell Res. Ther.* 13, 185–192. doi: 10.2174/1574888x12666171012141908

Li, Z., Wang, W., Xu, H., Ning, Y., Fang, W., Liao, W., et al. (2017). Effects of altered CXCL12/CXCR4 axis on BMP2/Smad/Runx2/Osterix axis and osteogenic gene expressions during osteogenic differentiation of MSCs. *Am. J. Transl. Res.* 9, 1680–1693.

Liu, B., Wu, S., Han, L., and Zhang, C. (2015). beta-catenin signaling induces the osteoblastogenic differentiation of human pre-osteoblastic and bone marrow stromal cells mainly through the upregulation of osterix expression. *Int. J. Mol. Med.* 36, 1572–1582. doi: 10.3892/ijmm.2015.2382

Liu, L., He, F. M., Li, L. L., and Hu, J. A. (2004). [The expression of MMP-9, MMP-2 in the remodeling bone tissue around implant during unloaded period]. *Hua Xi Kou Qiang Yi Xue Za Zhi* 22, 325–327.

Liu, L., Zeng, D., Chen, Y., Zhou, J., Liao, Y., and Shi, B. (2020). Microarc oxidation surface of titanium implants promote osteogenic differentiation by activating ERK1/2-miR-1827-Osterix. *In Vitro Cell. Dev. Biol. Anim.* 56, 296–306. doi: 10.1007/s11626-020-00444-7

Lu, J., Qu, S., Yao, B., Xu, Y., Jin, Y., Shi, K., et al. (2016). Osterix acetylation at K307 and K312 enhances its transcriptional activity and is required for osteoblast differentiation. *Oncotarget* 7, 37471–37486. doi: 10.18632/oncotarget.9650

Machida, M., Dubousset, J., Yamada, T., Kimura, J., Saito, M., Shiraishi, T., et al. (2006). Experimental scoliosis in melatonin-deficient C57BL/6J mice without pinealectomy. *J. Pineal Res.* 41, 1–7. doi: 10.1111/j.1600-079X.2005.00312.x

Matsubara, T., Kida, K., Yamaguchi, A., Hata, K., Ichida, F., Meguro, H., et al. (2008). BMP2 regulates Osterix through Msx2 and Runx2 during osteoblast differentiation. *J. Biol. Chem.* 283, 29119–29125. doi: 10.1074/jbc.M801774200

Maung, W. M., Nakata, H., Miura, M., Miyasaka, M., Kim, Y. K., Kasugai, S., et al. (2020). Low intensity pulsed ultrasound stimulates osteogenic differentiation of periosteal cells in vitro. *Tissue Eng. Part A*. doi: 10.1089/ten.TEA.2019.0331 [Epub ahead of print].

Milona, M. A., Gough, J. E., and Edgar, A. J. (2003). Expression of alternatively spliced isoforms of human Sp7 in osteoblast-like cells. *BMC Genomics* 4:43. doi: 10.1186/1471-2164-4-43

Moon, Y. J., Yun, C.-Y., Choi, H., Kim, J. R., Park, B.-H., and Cho, E.-S. (2018). Osterix regulates corticalization for longitudinal bone growth via integrin β3 expression. *Exp. Mol. Med.* 50, 1–11. doi: 10.1038/s12276-018-0119-9

Nakajima, K., Kho, D. H., Yanagawa, T., Harazono, Y., Gao, X., Hogan, V., et al. (2014). Galectin-3 inhibits osteoblast differentiation through notch signaling. *Neoplasia* 16, 939–949. doi: 10.1016/j.neo.2014.09.005

Nakashima, K., Zhou, X., Kunkel, G., Zhang, Z., Deng, J. M., Behringer, R. R., et al. (2002). The novel zinc finger-containing transcription factor osterix is required for osteoblast differentiation and bone formation. *Cell* 108, 17–29. doi: 10.1016/s0092-8674(01)00622-5

Nakatani, T., Chen, T., and Partridge, N. C. (2016). MMP-13 is one of the critical mediators of the effect of HDAC4 deletion on the skeleton. *Bone* 90, 142–151. doi: 10.1016/j.bone.2016.06.010

Nemoto, E., Sakisaka, Y., Tsuchiya, M., Tamura, M., Nakamura, T., Kanaya, S., et al. (2016). Wnt3a signaling induces murine dental follicle cells to differentiate into cementoblastic/osteoblastic cells via an osterix-dependent pathway. *J. Periodontal. Res.* 51, 164–174. doi: 10.1111/jre.12294

Niger, C., Lima, F., Yoo, D. J., Gupta, R. R., Buo, A. M., Hebert, C., et al. (2011). The transcriptional activity of osterix requires the recruitment of Sp1 to the osteocalcin proximal promoter. *Bone* 49, 683–692. doi: 10.1016/j.bone.2011.07.027

Niu, P., Zhong, Z., Wang, M., Huang, G., Xu, S., Hou, Y., et al. (2017). Zinc finger transcription factor Sp7/Osterix acts on bone formation and regulates col10a1a expression in zebrafish. *Sci. Bull.* 62, 174–184. doi: 10.1016/j.scib.2017.01.009

Oh, J. H., Park, S. Y., de Crombrugghe, B., and Kim, J. E. (2012). Chondrocyte-specific ablation of Osterix leads to impaired endochondral ossification. *Biochem. Biophys. Res. Commun.* 418, 634–640. doi: 10.1016/j.bbrc.2012.01.064

Omoteyama, K., and Takagi, M. (2010). The effects of Sp7/Osterix gene silencing in the chondroprogenitor cell line, ATDC5. *Biochem. Biophys. Res. Commun.* 403, 242–246. doi: 10.1016/j.bbrc.2010.11.023

Onizuka, S., Iwata, T., Park, S. J., Nakai, K., Yamato, M., Okano, T., et al. (2016). ZBTB16 as a downstream target gene of Osterix regulates osteoblastogenesis of human multipotent mesenchymal stromal cells. *J. Cell. Biochem.* 117, 2423–2434. doi: 10.1002/jcb.25634

Ortuño, M. J., Ruiz-Gaspà, S., Rodríguez-Carballo, E., Susperregui, A. R., Bartrons, R., Rosa, J. L., et al. (2010). p38 regulates expression of osteoblast-specific genes by phosphorylation of Osterix. *J. Biol. Chem.* 285, 31985–31994. doi: 10.1074/jbc.M110.123612

Ortuno, M. J., Susperregui, A. R., Artigas, N., Rosa, J. L., and Ventura, F. (2013). Osterix induces Col1a1 gene expression through binding to Sp1 sites in the bone enhancer and proximal promoter regions. *Bone* 52, 548–556. doi: 10.1016/j.bone.2012.11.007

Peng, Y., Shi, K., Wang, L., Lu, J., Li, H., Pan, S., et al. (2013). Characterization of Osterix protein stability and physiological role in osteoblast differentiation. *PLoS One* 8:e56451. doi: 10.1371/journal.pone.0056451

Pérez-Campo, F. M., Santurtún, A., García-Ibarbia, C., Pascual, M. A., Valero, C., Garcés, C., et al. (2016). Osterix and RUNX2 are transcriptional regulators of sclerostin in human bone. *Calcif. Tissue Int.* 99, 302–309. doi: 10.1007/s00223-016-0144-4

Pivetta, E., Scapolan, M., Pecolo, M., Wassermann, B., Abu-Rumeileh, I., Balestreri, L., et al. (2011). MMP-13 stimulates osteoclast differentiation and activation in tumour breast bone metastases. *Breast Cancer Res.* 13:R105. doi: 10.1186/bcr3047

Qaseem, A., Forciea, M. A., McLean, R. M., Denberg, T. D., and Clinical Guidelines Committee of the American College of Physicians, (2017). Treatment of low bone density or osteoporosis to prevent fractures in men and women: a clinical practice guideline update from the American college of physicians. *Ann. Intern. Med.* 166, 818–839. doi: 10.7326/m15-1361

Qi, J., Hu, K. S., and Yang, H. L. (2015). Roles of TNF-α, GSK-3β and RANKL in the occurrence and development of diabetic osteoporosis. *Int. J. Clin. Exp. Pathol.* 8, 11995–12004.

Qu, S., Wu, J., Bao, Q., Yao, B., Duan, R., Chen, X., et al. (2019). Osterix promotes the migration and angiogenesis of breast cancer by upregulation of S100A4 expression. *J. Cell. Mol. Med.* 23, 1116–1127. doi: 10.1111/jcmm.14012

Rajamannan, N. M. (2019). TIEG1 is upregulated in Lrp5/6-mediated valve osteogenesis. *J. Cell. Biochem.* 120, 3362–3366. doi: 10.1002/jcb.27606

Ramazzotti, G., Fiume, R., Chiarini, F., Campana, G., Ratti, S., Billi, A. M., et al. (2019). Phospholipase C-β1 interacts with cyclin E in adipose- derived stem cells osteogenic differentiation. *Adv. Biol. Regul.* 71, 1–9. doi: 10.1016/j.jbior.2018.11.001

Renn, J., and Winkler, C. (2009). Osterix-mCherry transgenic medaka for in vivo imaging of bone formation. *Dev. Dyn.* 238, 241–248. doi: 10.1002/dvdy.21836

Rios-Arce, N. D., Dagenais, A., Feenstra, D., Coughlin, B., Kang, H. J., Mohr, S., et al. (2020). Loss of interleukin-10 exacerbates early Type-1 diabetes-induced bone loss. *J. Cell. Physiol.* 235, 2350–2365. doi: 10.1002/jcp.29141

Sakisaka, Y., Kanaya, S., Nakamura, T., Tamura, M., Shimauchi, H., and Nemoto, E. (2016). p38 MAP kinase is required for Wnt3a-mediated osterix expression independently of Wnt-LRP5/6-GSK3β signaling axis in dental follicle cells. *Biochem. Biophys. Res. Commun.* 478, 527–532. doi: 10.1016/j.bbrc.2016.07.076

Sepulveda, H., Aguilar, R., Prieto, C. P., Bustos, F., Aedo, S., Lattus, J., et al. (2017a). Epigenetic signatures at the RUNX2-P1 and Sp7 gene promoters control osteogenic lineage commitment of umbilical cord-derived mesenchymal stem cells. *J. Cell. Physiol.* 232, 2519–2527. doi: 10.1002/jcp.25627

Sepulveda, H., Villagra, A., and Montecino, M. (2017b). Tet-mediated DNA demethylation is required for SWI/SNF-dependent chromatin remodeling and histone-modifying activities that trigger expression of the Sp7 osteoblast master gene during mesenchymal lineage commitment. *Mol. Cell. Biol.* 37:e00177–17. doi: 10.1128/MCB.00177-17

Shi, K., Lu, J., Zhao, Y., Wang, L., Li, J., Qi, B., et al. (2013). MicroRNA-214 suppresses osteogenic differentiation of C2C12 myoblast cells by targeting Osterix. *Bone* 55, 487–494. doi: 10.1016/j.bone.2013.04.002

Shi, L., Cai, G., Shi, J., Guo, Y., Chen, D., Chen, D., et al. (2016). Ossification of the posterior ligament is mediated by osterix via inhibition of the β-catenin signaling pathway. *Exp. Cell Res.* 349, 53–59. doi: 10.1016/j.yexcr.2016.09.019

Sinha, K. M., Yasuda, H., Coombes, M. M., Dent, S. Y., and de Crombrugghe, B. (2010). Regulation of the osteoblast-specific transcription factor Osterix by NO66, a Jumonji family histone demethylase. *EMBO J.* 29, 68–79. doi: 10.1038/emboj.2009.332

Sinha, K. M., Yasuda, H., Zhou, X., and de Crombrugghe, B. (2014). Osterix and NO66 histone demethylase control the chromatin of Osterix target genes during osteoblast differentiation. *J. Bone Miner. Res.* 29, 855–865. doi: 10.1002/jbmr.2103

Stringhetta-Garcia, C. T., Singulani, M. P., Santos, L. F., Louzada, M. J., Nakamune, A. C., Chaves-Neto, A. H., et al. (2016). The effects of strength training and

raloxifene on bone health in aging ovariectomized rats. *Bone* 85, 45–54. doi: 10.1016/j.bone.2015.11.023

Subramaniam, M., Pitel, K. S., Withers, S. G., Drissi, H., and Hawse, J. R. (2016). TIEG1 enhances Osterix expression and mediates its induction by TGFbeta and BMP2 in osteoblasts. *Biochem. Biophys. Res. Commun.* 470, 528–533. doi: 10.1016/j.bbrc.2016.01.112

Sun, C., Yuan, H., Wang, L., Wei, X., Williams, L., Krebsbach, P. H., et al. (2016). FAK promotes Osteoblast progenitor cell proliferation and differentiation by enhancing Wnt signaling. *J. Bone Miner. Res.* 31, 2227–2238. doi: 10.1002/jbmr.2908

Sun, X., Yang, X., Zhao, Y., Li, Y., and Guo, L. (2018). Effects of 17beta-estradiol on mitophagy in the murine MC3T3-E1 osteoblast cell line is mediated via G protein-coupled estrogen receptor and the ERK1/2 signaling pathway. *Med. Sci. Monit.* 24, 903–911. doi: 10.12659/msm.908705

Sun, Y., Cai, M., Zhong, J., Yang, L., Xiao, J., Jin, F., et al. (2019). The long noncoding RNA lnc-ob1 facilitates bone formation by upregulating Osterix in osteoblasts. *Nat. Metab.* 1, 485–496. doi: 10.1038/s42255-019-0053-8

Suske, G., Bruford, E., and Philipsen, S. (2005). Mammalian SP/KLF transcription factors: bring in the family. *Genomics* 85, 551–556. doi: 10.1016/j.ygeno.2005.01.005

Takarada, T., Nakazato, R., Tsuchikane, A., Fujikawa, K., Iezaki, T., Yoneda, Y., et al. (2016). Genetic analysis of Runx2 function during intramembranous ossification. *Development* 143, 211–218. doi: 10.1242/dev.128793

Tang, W., Yang, F., Li, Y., de Crombrugghe, B., Jiao, H., Xiao, G., et al. (2012). Transcriptional regulation of vascular endothelial growth factor (VEGF) by osteoblast-specific transcription factor Osterix (Osx) in osteoblasts. *J. Biol. Chem.* 287, 1671–1678. doi: 10.1074/jbc.M111.288472

Wang, C. G., Liao, Z., Xiao, H., Liu, H., Hu, Y. H., Liao, Q. D., et al. (2019). LncRNA KCNQ1OT1 promoted BMP2 expression to regulate osteogenic differentiation by sponging miRNA-214. *Exp. Mol. Pathol.* 107, 77–84. doi: 10.1016/j.yexmp.2019.01.012

Wang, H., Cui, Y., Luan, J., Zhou, X., Li, C., Li, H., et al. (2017). MiR-5100 promotes osteogenic differentiation by targeting Tob2. *J. Bone Miner. Metab.* 35, 608–615. doi: 10.1007/s00774-016-0799-y

Wang, H., Zhang, H., Srinivasan, V., Tao, J., Sun, W., Lin, X., et al. (2020). Targeting Bortezomib to bone increases its bone anabolic activity and reduces systemic adverse effects in mice. *J. Bone Miner. Res.* 35, 343–356. doi: 10.1002/jbmr.3889

Wang, Q., Zhao, Y., Sha, N., Zhang, Y., Li, C., Zhang, H., et al. (2018). The systemic bone protective effects of Gushukang granules in ovariectomized mice by inhibiting osteoclastogenesis and stimulating osteoblastogenesis. *J. Pharmacol. Sci.* 136, 155–164. doi: 10.1016/j.jphs.2018.01.007

Wang, Z., Liu, Q., Liu, C., Tan, W., Tang, M., Zhou, X., et al. (2020). Mg(2+) in beta-TCP/Mg-Zn composite enhances the differentiation of human bone marrow stromal cells into osteoblasts through MAPK-regulated Runx2/Osx. *J. Cell. Physiol.* 235, 5182–5191. doi: 10.1002/jcp.29395

Wu, J., Zhao, J., Sun, L., Pan, Y., Wang, H., and Zhang, W. B. (2018). Long non-coding RNA H19 mediates mechanical tension-induced osteogenesis of bone marrow mesenchymal stem cells via FAK by sponging miR-138. *Bone* 108, 62–70. doi: 10.1016/j.bone.2017.12.013

Wu, L., Wu, Y., Lin, Y., Jing, W., Nie, X., Qiao, J., et al. (2007). Osteogenic differentiation of adipose derived stem cells promoted by overexpression of osterix. *Mol. Cell. Biochem.* 301, 83–92. doi: 10.1007/s11010-006-9399-9

Wu, R., Ruan, J., Sun, Y., Liu, M., Sha, Z., Fan, C., et al. (2018). Long non-coding RNA HIF1A-AS2 facilitates adipose-derived stem cells (ASCs) osteogenic differentiation through miR-665/IL6 axis via PI3K/Akt signaling pathway. *Stem Cell Res. Ther.* 9:48. doi: 10.1186/s13287-018-1082-z

Wu, Y. F., Matsuo, N., Sumiyoshi, H., and Yoshioka, H. (2010a). Sp7/Osterix is involved in the up-regulation of the mouse pro-α1(V) collagen gene (Col5a1) in osteoblastic cells. *Matrix Biol.* 29, 701–706. doi: 10.1016/j.matbio.2010.09.002

Wu, Y. F., Matsuo, N., Sumiyoshi, H., and Yoshioka, H. (2010b). Sp7/Osterix up-regulates the mouse pro-alpha3(V) collagen gene (Col5a3) during the osteoblast differentiation. *Biochem. Biophys. Res. Commun.* 394, 503–508. doi: 10.1016/j.bbrc.2010.02.171

Xiao, W.-l., Zhang, D.-z., Fan, C.-h., and Yu, B.-j. (2015). Intermittent stretching and osteogenic differentiation of bone marrow derived mesenchymal stem cells via the p38MAPK-osterix signaling pathway. *Cell. Physiol. Biochem.* 36, 1015–1025. doi: 10.1159/000430275

Xiao, Z. S., Hjelmeland, A. B., and Quarles, L. D. (2004). Selective deficiency of the "Bone-related" Runx2-II unexpectedly preserves osteoblast-mediated skeletogenesis. *J. Biol. Chem.* 279, 20307–20313. doi: 10.1074/jbc.m401109200

Xie, J., and Gu, J. (2015). Identification of C-terminal Hsp70-interacting protein as a mediator of tumour necrosis factor action in osteoblast differentiation by targeting osterix for degradation. *J. Cell. Mol. Med.* 19, 1814–1824. doi: 10.1111/jcmm.12553

Xing, W., Godwin, C., Pourteymoor, S., and Mohan, S. (2019). Conditional disruption of the osterix gene in chondrocytes during early postnatal growth impairs secondary ossification in the mouse tibial epiphysis. *Bone Res.* 7:24. doi: 10.1038/s41413-019-0064-9

Xu, Y., Yao, B., Shi, K., Lu, J., Jin, Y., Qi, B., et al. (2015). Phosphorylation of Serine422 increases the stability and transactivation activities of human Osterix. *FEBS Lett.* 589, 857–864. doi: 10.1016/j.febslet.2015.02.021

Yang, B., Li, S., Chen, Z., Feng, F., He, L., Liu, B., et al. (2020). Amyloid β peptide promotes bone formation by regulating Wnt/β-catenin signaling and the OPG/RANKL/RANK system. *FASEB J.* 34, 3583–3593. doi: 10.1096/fj.201901550R

Yang, F., Tang, W., So, S., de Crombrugghe, B., and Zhang, C. (2010). Sclerostin is a direct target of osteoblast-specific transcription factor osterix. *Biochem. Biophys. Res. Commun.* 400, 684–688. doi: 10.1016/j.bbrc.2010.08.128

Yang, L., Cheng, P., Chen, C., He, H.-B., Xie, G.-Q., Zhou, H.-D., et al. (2012). miR-93/Sp7 function loop mediates osteoblast mineralization. *J. Bone Miner. Res.* 27, 1598–1606. doi: 10.1002/jbmr.1621

Yang, M., Arai, A., Udagawa, N., Zhao, L., Nishida, D., Murakami, K., et al. (2019). Parathyroid hormone shifts cell fate of a leptin receptor-marked stromal population from adipogenic to osteoblastic lineage. *J. Bone Miner. Res.* 34, 1952–1963. doi: 10.1002/jbmr.3811

Yang, Y., Huang, Y., Zhang, L., and Zhang, C. (2016). Transcriptional regulation of bone sialoprotein gene expression by Osx. *Biochem. Biophys. Res. Commun.* 476, 574–579. doi: 10.1016/j.bbrc.2016.05.164

Yano, H., Hamanaka, R., Nakamura-Ota, M., Adachi, S., Zhang, J. J., Matsuo, N., et al. (2014). Sp7/Osterix induces the mouse pro-α2(I) collagen gene (Col1a2) expression via the proximal promoter in osteoblastic cells. *Biochem. Biophys. Res. Commun.* 452, 531–536. doi: 10.1016/j.bbrc.2014.08.100

Yao, B., Wang, J., Qu, S., Liu, Y., Jin, Y., Lu, J., et al. (2019). Upregulated osterix promotes invasion and bone metastasis and predicts for a poor prognosis in breast cancer. *Cell Death Dis.* 10:28. doi: 10.1038/s41419-018-1269-3

Yashan, Y., Yunxia, L., and Hong, Z. (2017). Clinical study on the effects of Gushukang capsules in treating glucocorticoid induced osteoporosis. *Chin. J. Osteoporos.* 23, 795–799.

Yoon, J. Y., Kim, T. S., Ahn, J. H., Yoon, J. U., Kim, H. J., and Kim, E. J. (2019). Remifentanil promotes osteoblastogenesis by upregulating Runx2/osterix expression in preosteoblastic C2C12 cells. *J. Dent. Anesth. Pain Med.* 19, 91–99. doi: 10.17245/jdapm.2019.19.2.91

You, H. C., Jeong, H. M., Jin, Y. H., Li, H., Yeo, C. Y., and Lee, K. Y. (2011). Akt phosphorylates and regulates the osteogenic activity of Osterix. *Biochem. Biophys. Res. Commun.* 411, 637–641. doi: 10.1016/j.bbrc.2011.07.009

Yu, T., Graf, M., Renn, J., Schartl, M., Larionova, D., Huysseune, A., et al. (2017). A vertebrate-specific and essential role forosterixin osteogenesis revealed by gene knockout in the teleost medaka. *Development* 144, 265–271. doi: 10.1242/dev.139550

Zannit, H. M., and Silva, M. J. (2019). Proliferation and activation of osterix-lineage cells contribute to loading-induced periosteal bone formation in mice. *JBMR Plus* 3:e10227. doi: 10.1002/jbm4.10227

Zhang, B., Zhang, X., Xiao, J., Zhou, X., Chen, Y., and Gao, C. (2020). Neuropeptide Y upregulates Runx2 and osterix and enhances osteogenesis in mouse MC3T3E1 cells via an autocrine mechanism. *Mol. Med. Rep.* 22, 4376–4382. doi: 10.3892/mmr.2020.11506

Zhang, C., Tang, W., and Li, Y. (2012). Matrix metalloproteinase 13 (MMP13) is a direct target of osteoblast-specific transcription factor osterix (Osx) in osteoblasts. *PLoS One* 7:e50525. doi: 10.1371/journal.pone.0050525

Zhang, H., Jiang, Y., Qin, C., Liu, Y., Ho, S. P., and Feng, J. Q. (2015). Essential role of osterix for tooth root but not crown dentin formation. *J. Bone Miner. Res.* 30, 742–746. doi: 10.1002/jbmr.2391

Zhang, H., Liu, L., Jiang, C., Pan, K., Deng, J., and Wan, C. (2020). MMP9 protects against LPS-induced inflammation in osteoblasts. *Innate Immun.* 26, 259–269. doi: 10.1177/1753425919887236

Zhang, J. F., Fu, W., He, M. L., Wang, H., Wang, W. M., Yu, S. C., et al. (2011). MiR-637 maintains the balance between adipocytes and osteoblasts by directly targeting Osterix. *Mol. Biol. Cell* 22, 3955–3961. doi: 10.1091/mbc.e11-04-0356

Zhang, S. Y., Gao, F., Peng, C. G., Zheng, C. J., and Wu, M. F. (2018). miR-485-5p promotes osteoporosis via targeting Osterix. *Eur. Rev. Med. Pharmacol. Sci.* 22, 4792–4799. doi: 10.26355/eurrev_201808_15613

Zhang, Z. H., Jia, X. Y., Fang, J. Y., Chai, H., Huang, Q., She, C., et al. (2020). Reduction of SOST gene promotes bone formation through the Wnt/beta-catenin signalling pathway and compensates particle-induced osteolysis. *J. Cell. Mol. Med.* 24, 4233–4244. doi: 10.1111/jcmm.15084

Zhou, X., Zhang, Z., Feng, J. Q., Dusevich, V. M., Sinha, K., Zhang, H., et al. (2010). Multiple functions of Osterix are required for bone growth and homeostasis in postnatal mice. *Proc. Natl. Acad. Sci. U.S.A.* 107, 12919–12924. doi: 10.1073/pnas.0912855107

Zhou, Y., Wang, C., Si, J., Wang, B., Zhang, D., Ding, D., et al. (2020). Melatonin up-regulates bone marrow mesenchymal stem cells osteogenic action but suppresses their mediated osteoclastogenesis via MT(2) -inactivated NF-κB pathway. *Br. J. Pharmacol.* 177, 2106–2122. doi: 10.1111/bph.14972

Conflict of Interest: The authors declare that the research was conducted in the absence of any commercial or financial relationships that could be construed as a potential conflict of interest.

Copyright © 2020 Liu, Li, Wang, Xiao, Xiong and Wang. This is an open-access article distributed under the terms of the Creative Commons Attribution License (CC BY). The use, distribution or reproduction in other forums is permitted, provided the original author(s) and the copyright owner(s) are credited and that the original publication in this journal is cited, in accordance with accepted academic practice. No use, distribution or reproduction is permitted which does not comply with these terms.

frontiers in Cell and Developmental Biology

ORIGINAL RESEARCH
published: 15 December 2020
doi: 10.3389/fcell.2020.601188

Antenatal Corticosteroid Therapy Attenuates Angiogenesis Through Inhibiting Osteoclastogenesis in Young Mice

Yu Chai[1,2†], Jianwen Su[1,2†], Weisheng Hong[1,2], Runjiu Zhu[1,2], Caiyu Cheng[1,2], Lei Wang[1,2], Xianrong Zhang[1,2] and Bin Yu[1,2*]*

[1] Division of Orthopaedic Surgery, Department of Orthopaedics, Nanfang Hospital, Southern Medical University, Guangzhou, China, [2] Guangdong Provincial Key Laboratory of Bone and Cartilage Regenerative Medicine, Nanfang Hospital, Southern Medical University, Guangzhou, China

Antenatal corticosteroid therapy (ACT) has been shown to reduce morbidity and mortality rates in preterm delivery, but the fetus is more likely to face the risk of low bone mineralization and low fetal linear growth. However, the mechanism of ACT inducing low bone mineralization remains largely unknown. Pre-osteoclasts, which play an important role in angiogenesis and osteogenesis, are specifically regulating type H vessels ($CD31^{hi}Emcn^{hi}$) and vessel formation by secreting platelet-derived growth factor-BB (PDGF-BB). We find that the number of pre-osteoclasts and POC-secreted PDGF-BB is dramatically decreased in ACT mice, contributing to the reduction in type H vessels and bone mineralization during the mouse offspring. Quantitative analyses of micro-computed tomography show that the ACT mice have a significant reduction in the mass of trabecular bone relative to the control group. Mononuclear pre-osteoclasts in trabecular bone decreased in ACT mice, which leads to the amount of PDGF-BB reduced and attenuates type H vessel formation. After sorting the Rank+ osteoclast precursors using flow cytometry, we show that the enhancer of zeste homolog 2 (Ezh2) expression is decreased in Rank+ osteoclast precursors in ACT mice. Consistent with the flow data, by using small molecule Ezh2 inhibitor GSK126, we prove that Ezh2 is required for osteoclast differentiation. Downregulating the expression of Ezh2 in osteoclast precursors would reduce PDGF-BB production. Conditioned medium from osteoclast precursor cultures treated with GSK126 inhibited endothelial tube formation, whereas conditioned medium from vehicle group stimulated endothelial tube formation. These results indicate Ezh2 expression of osteoclast precursors is suppressed after ACT, which reduced the pre-osteoclast number and PDGF-BB secretion, thus inhibiting type H vessel formation and ACT-associated low bone mineralization.

Keywords: ACT, angiogenesis, osteoclastogenesis, EZH2, pre-osteoclasts

OPEN ACCESS

Edited by:
Changjun Li,
Central South University, China

Reviewed by:
Bo Gao,
Fourth Military Medical University, China
Hao Chen,
The First Affiliated Hospital of Soochow University, China
Bo Hu,
Shanghai Changzheng Hospital, China

***Correspondence:**
Bin Yu
yubin@smu.edu.cn
Xianrong Zhang
xianrongzh@smu.edu.cn

† These authors have contributed equally to this work

Specialty section:
This article was submitted to Molecular Medicine, a section of the journal Frontiers in Cell and Developmental Biology

Received: *31 August 2020*
Accepted: *09 October 2020*
Published: *15 December 2020*

Citation:
Chai Y, Su J, Hong W, Zhu R, Cheng C, Wang L, Zhang X and Yu B (2020) Antenatal Corticosteroid Therapy Attenuates Angiogenesis Through Inhibiting Osteoclastogenesis in Young Mice. Front. Cell Dev. Biol. 8:601188. doi: 10.3389/fcell.2020.601188

INTRODUCTION

Antenatal corticosteroid therapy (ACT) is widely used for several types of pregnancy disorders, including preparing the fetal lung for impending preterm birth, congenital adrenal hyperplasia, multiple pregnancies, and placenta previa (Young et al., 1980; Morales et al., 1986; Bloom et al., 2001; Maryniak et al., 2014), but animal and human studies link corticosteroids to smaller birth size and suppression of fetal bone turnover at birth in corticosteroid-exposed infants (Bloom et al., 2001; Murphy et al., 2008). Even more, a randomized clinical trial shows strong evidence that lower birth weight is highly relative to lower peak bone mass in ACT patients (Godfrey et al., 2011). Our previous researches show that antenatal corticosteroid exposure could impair bone development and angiogenesis and reduce the peak bone mass during the adult offspring (Sliwa et al., 2010; Cheng et al., 2014; Zhang et al., 2016; Chen et al., 2018; Su et al., 2020). The mechanism underlying ACT suppression of angiogenesis and osteogenesis in relation to lower peak bone mass and growth retardation remains unknown. Pre-osteoclasts, the immature osteoclast precursor cells, are well known to promote angiogenesis of type H vessels through the release of platelet-derived growth factor-BB (PDGF-BB) (Xie et al., 2014). Angiogenesis is coupling with the osteogenesis, participating in bone modeling and remodeling during the whole lifespan (Brandi and Collin-Osdoby, 2006; Seeman, 2009; Teti, 2011). During new vessel growth, the concentration of angiogenesis factors, such as PDGF-BB from pre-osteoclasts, in local environment must be secreted precisely to induce formation of new vessels (Bronckaers et al., 2014; Nassiri and Rahbarghazi, 2014). Corticosteroids are known to inhibit angiogenesis and decrease pre-osteoclasts (Buckley and Humphrey, 2018), suggesting that corticosteroids may impact pre-osteoclasts secreting angiogenesis factors, which support angiogenesis (Pufe et al., 2003; Weinstein, 2010; Yang et al., 2018).

Enhancer of zeste homolog 2 (EZH2), which is the methyltransferase subunit of the polycomb repressive complex 2 (PRC2), deposits the heterochromatic mark H3K27me3 that silences gene expression (Margueron and Reinberg, 2011). Evidence from different groups demonstrates that Ezh2 plays an important role in bone growth and bone remodeling (Dudakovic et al., 2015). Ezh2 was shown to epigenetically repress the osteoclast inhibitory factor IRF8, and Ezh2 also can play epigenetic and cytoplasmic roles during osteoclast differentiation by suppressing MafB transcription and regulating early phases of RANKL signaling (McCabe et al., 2012; Dudakovic et al., 2016; Fang et al., 2016; Hemming et al., 2017). Because osteoclastogenesis can be mediated by the Ezh2, we explored the Ezh2 playing a critical role in osteoclastogenesis during ACT.

Therefore, in this study, we further investigated the role of Ezh2-mediated osteoclastogenesis during the ACT. We demonstrated that antenatal corticosteroid exposure decreases osteoclastogenesis and angiogenesis by suppressing Ezh2 expression in osteoclast precursors, which cause the pre-osteoclast number and pre-osteoclast-derived PDGF-BB decrease in bone, leading to the reduced angiogenesis and bone mass in bone.

RESULTS

ACT Decreases Bone Volume and Angiogenesis in Long Bone

Bone modeling and remodeling are coupling with angiogenesis and osteogenesis by a specific vessel subtype, type H vessel, during offspring (Kusumbe et al., 2014; Ramasamy et al., 2014). Our group's previous finding has shown the adverse effect of ACT on the long bone in fetal mice. We then tested whether long bone osteogenesis and angiogenesis are being retreated or not. Femora were harvested from 12-week-old mouse of ACT, and bone architecture of the femoral bone was measured by micro-computed tomography (μCT). A significant reduction in the mass of trabecular bone was observed in ACT mice relative to control mice (**Figure 1A**). The ACT mice exhibited reduced trabecular bone volume (BV/TV) and number (Tb. N) and greater trabecular bone separation (Tb. Sp) compared with control littermates in female mice (**Figures 1B,D,E**). No significant differences were observed in trabecular thickness (Tb. Th) (**Figure 1C**). Together, these data revealed that ACT has adverse effects on bone architecture.

We then detected type H vessels ($CD31^{hi}Emcn^{hi}$), which have been recognized as osteogenesis-coupling neovessels responsible for new bone formation in femur of ACT mice. A decrease in $CD31^{hi}Emcn^{hi}$ blood vessels in primary spongiosa in femora of ACT mice (**Figures 1F–H**) is detected by immunofluorescence staining relative to control mice. A similar reduction in bone surface OCN+ osteoblasts in the same region was also observed in the ACT mice (**Figures 1I,J**). Therefore, ACT reduces type H vessel, which is highly associated with impaired bone formation in mouse offspring.

Pre-osteoclast Number and Its Synthesis of PDGF-BB Decreased in ACT Mice

It has been previously reported that pre-osteoclasts produced PDGF-BB to couple angiogenesis and osteogenesis during bone modeling and remodeling. Excessive GCs could decrease pre-osteoclasts and its synthesis of PDGF-BB (Andrae et al., 2008; Xie et al., 2014). In adult glucocorticoid-induced osteoporosis mouse models, osteoclasts were shown to have increased resorption in early phase due to enhanced survival of osteoclasts, but suppression of bone resorption in late phase due to the glucocorticoid suppression of osteoclast differentiation (Jia et al., 2006). But how ACT shows effects on osteoclastogenesis in ACT mice remains unknown. We examined the effect of ACT on the number of pre-osteoclasts and synthesis of PDGF-BB. The number of mononuclear Trap+ pre-osteoclasts was significantly decreased in 12-week-old ACT mice relative to the control mice (**Figures 2A,B**). To further document the loss of pre-osteoclast number with ACT, Rank+ osteoclast precursors were analyzed by flow cytometry and found dramatically decreased in ACT group relative to the control mice (**Figures 2E–J**). Immunofluorescence staining showed that the double-positive staining ($TRAP^{+}$. PDGF-BB+) percent was decreased in ACT mice relative to the control mice by 12 weeks old (**Figures 2C,D**). Overall, our results

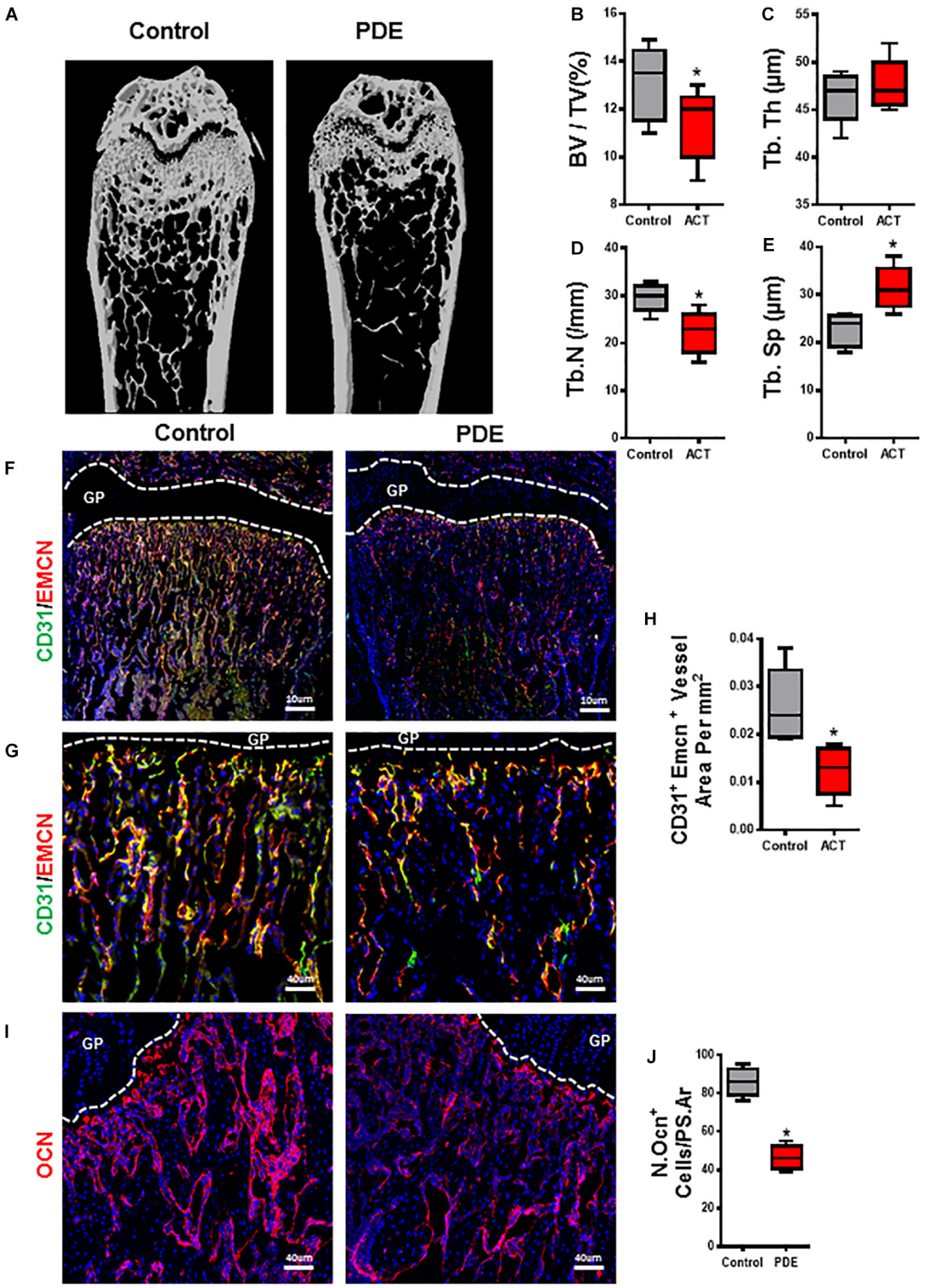


FIGURE 1 | Prenatal dexamethasone exposure decreases bone volume and angiogenesis in long bone. Representative μCT images of distal femur in 12-week-old female mouse offspring are shown in panel **(A)**. Quantitative analyses of femoral microstructural parameters of female mouse offspring including trabecular bone volume fraction (BV/TV) **(B)**, trabecular number (Tb. N) **(C)**, trabecular thickness (Tb. Th) **(D)**, and trabecular separation (Tb. Sp) **(E)**. **(F,G)** Representative images of double-immunofluorescence staining for CD31 (green) and endomucin (Emcn, red) in femoral metaphysis from 12-week-old female offspring. DAPI stains nuclei blue. Images in panel **(F)** are lower power with boxes outlining the area of higher power in panel **(G)**. Quantification of the relative fluorescence area of $CD31^{+}Emcn^{+}$ cells per tissue area in femoral metaphysis ($CD31^{+}Emcn^{+}$ area per mm^2) **(H)**. **(I)** Representative images of immunofluorescence staining for osteocalcin (red) and **(J)** quantitative analysis of $osteocalcin^{+}$ cells in femoral metaphysis from 12-week-old female offspring. DAPI stains nuclei blue. *$p < 0.05$.

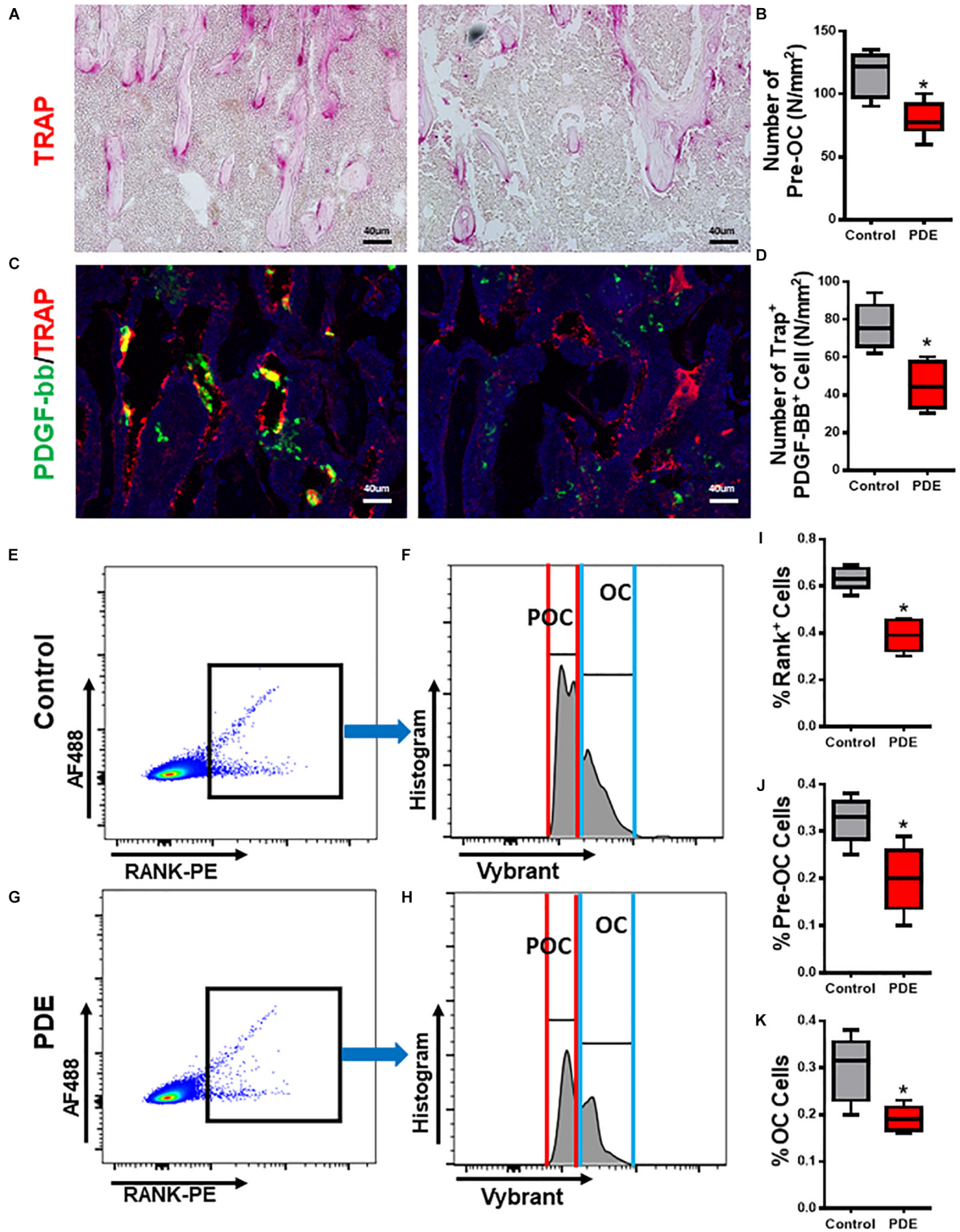


FIGURE 2 | Pre-osteoclast number and its synthesis of PDGF-BB decreased in ACT mice. **(A,C)** Representative TRAP staining (magenta) images **(A)** and immunofluorescence images of TRAP (red) and PDGF-BB (green) costaining (yellow) **(C)** in femoral metaphysis from 12-week-old female offspring. DAPI stains nuclei blue. Scale bar = 40 μm. **(B,D)** Quantitative analysis of the N. POCs **(B)** and the N. TARP^{+} PDGF-BB^{+} cells **(D)** in distal femur. **(E–H)** Representative flow cytometry plots showing the sorting profile used to separate POCs and OCs in femoral bone from 12-week-old female mouse offspring. RANK^{+} cells with 1-2 nuclei (POCs) and greater than three nuclei (OCs) are sorted for gene expression analysis. **(I–K)** Quantitative analysis of the percentage of RANK^{+} cells **(I)**, POCs **(J)**, and OCs **(K)** in distal femur. *$p < 0.05$.

indicate that ACT could inhibit osteoclastogenesis and decrease PDGF-BB secretion from pre-osteoclast.

Prenatal Dexamethasone Exposure Decreases Ezh2 Expression in Osteoclast Precursors and Attenuates Osteoclastogenesis

Enhancer of zeste homolog 2 has been mentioned playing an important role in osteoclast differentiation by silencing the negative regulator IRF8 (Fang et al., 2016) and plays epigenetic and cytoplasmic roles during osteoclast differentiation by suppressing MafB transcription and regulating early phases of RANKL signaling. To investigate whether the effect of ACT on osteoclast differentiation is being mediated by Ezh2, we sorted the Rank+ osteoclast precursors and analyzed the Ezh2 expression (**Figures 3A,B**). The number of Rank+ osteoclast precursors decreased in the ACT mice group relative to the control mice (**Figures 2I–K**), and Ezh2 mRNA expression level (**Figure 3C**) and protein level (**Figure 3E**) were decreased; MafB mRNA level was upregulated in ACT mice (**Figure 3D**).

Ezh2 Plays a Critical Role in Osteoclastogenesis by Activating Osteoclast Regulators and Represses the Osteoclast Inhibitory Factors

To further demonstrate whether Ezh2 plays an important role in osteoclastogenesis, we treated primary bone marrow-derived monocytes (BMMs) (osteoclast precursors) with Ezh2 methyltransferase domain inhibitor GSK126. We showed the inhibitory effects of GSK126 on RANKL-induced differentiation of Trap+ multinucleated osteoclasts (**Figure 4A**). To our surprise, GSK126 did not alter the Ezh2 mRNA and protein levels (**Figures 4B,C**), but effectively decreased the cellular levels of H3K27me3 (**Figure 4C**). Consistent with other research finding, GSK126 reduced RANKL-mediated upregulation of critical early osteoclast regulators NFATC1, Rank, Catk, and ITGB3 (**Figures 4D–G**). These results support a role for Ezh2 in osteoclast differentiation, and GSK126 could suppress osteoclastogenesis by inhibiting Ezh2 catalytic activity. Furthermore, effective osteoclastogenesis also requires downregulating of transcriptional repressors, such as IRF8, BCL6, or Mafb, which is against the differentiation program. GSK126 could prevent the downregulation of osteoclast inhibitory factors Mafb and Irf8 (**Figures 4H,I**). Together, we find that Ezh2 plays a critical role in osteoclastogenesis and mediates repression of OCL-negative regulators.

Loss of Ezh2 Suppresses Osteoclast Precursors PDGF-BB Expression and Bone Vasculature in ACT Mice

It has been proved that pre-osteoclasts are the major source of PDGF-BB. And in the ACT mouse model, Ezh2 expression was dramatically decreased in osteoclast precursors and attenuated the osteoclastogenesis process. Not only the number of pre-osteoclast, but also the PDGF-BB protein level was decreased in Trap+ mononuclear pre-osteoclasts of ACT mice. In order to investigate the effect of Ezh2 on osteoclast-mediated coupling angiogenesis in ACT mouse model, we perform a cotreated experiment. After treating the osteoclast precursors with GSK126 and MCSF/RANKL, the PDGF-BB mRNA level and protein level were decreased in osteoclast precursors (**Figures 5D,E**). Matrigel tube formation assays with endothelial precursor cells plus GSK126 POC-conditioned medium demonstrated suppressed tube formation rate relative to the control POC-conditioned medium (**Figures 5A–C**). Together, ACT disrupts angiogenesis and osteogenesis coupling by repression Ezh2 expression in POC and causes POC number, and POC-secreted PDGF-BB dramatically decreased, which was associated with low bone mass and growth retardation in ACT mice.

DISCUSSION

Multiple doses of glucocorticoids are in widespread use in obstetric practice to accelerate the maturation of fetal cardiovascular systems when facing preterm delivery, as well as to provide treatment for congenital adrenal hyperplasia of the fetus or asthma of pregnant women (Maryniak et al., 2014). Prenatal dexamethasone exposure has persisting "programming" effects on offspring in rodents and other model species (de Vries et al., 2007). ACT could impair bone development and angiogenesis and reduces the peak bone mass during the adult offspring (Godfrey et al., 2011). The mechanism underlying ACT suppression of angiogenesis and osteogenesis in relation to lower peak bone mass and growth retardation remains unknown. Because the dose of dexamethasone used in human pregnancy varies from 0.02 $mg{\cdot}kg^{-1}$ per day for congenital adrenal hyperplasia (Meyer-Bahlburg et al., 2004) to 0.5 $mg{\cdot}kg^{-1}$ per day for indicated preterm labor (Bloom et al., 2001; Peaceman et al., 2005), it is important to use a proper dose of dexamethasone. In animal research, a much lower therapeutic dose of dexamethasone (0.03 $mg{\cdot}kg^{-1}$ every second day) could induce loss of trabecular bone and retardation of bone growth in developmental piglets (Tomaszewska et al., 2013). Our previous work found that the intrauterine growth retardation rate is dose-dependent (Xu et al., 2011). Dose conversion between mice and human (conversion factor is 0.08) (Reagan-Shaw et al., 2008) and prenatal treatment with dexamethasone in mice at (1.2 $mg{\cdot}kg^{-1}$ per day) in this study are comparable with those prescribed for pregnant women (0.1–0.2 $mg{\cdot}kg^{-1}$). Recent studies indicated that prenatal dexamethasone treatment at (1 $mg{\cdot}kg^{-1}$ per day) induced an adverse effect on long bone development. We undertook this study to investigate the effect of prenatal dexamethasone exposure on fetal bone development and clarify the underlying mechanisms. Our data show that ACT treatment could impact the osteoclastogenesis, angiogenesis, and osteogenesis during bone development by reducing Ezh2 expression in osteoclast precursors, which plays a critical role in osteoclast precursors differentiating into pre-osteoclast. With the decreased number of pre-osteoclasts of ACT mice, the PDGF-BB protein, secreted by pre-osteoclasts, dramatically decreased and impacted the type H vessel formation.

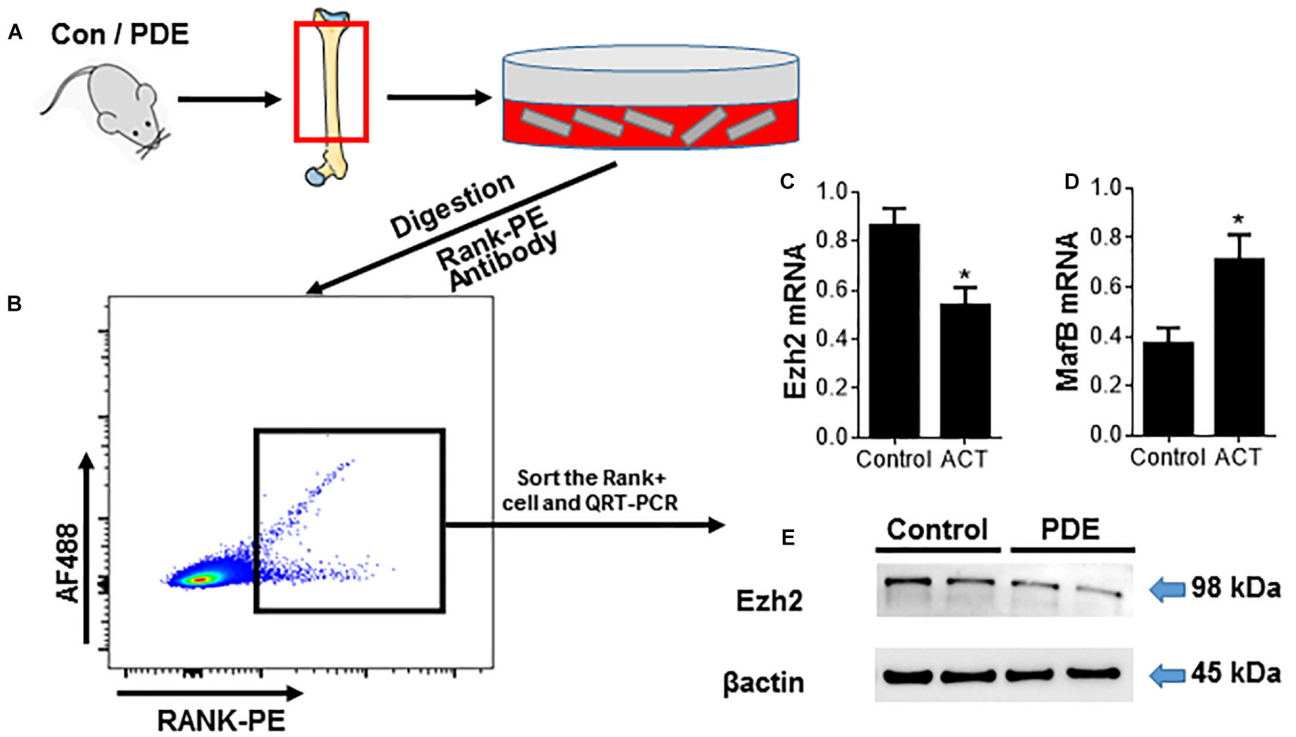


FIGURE 3 | Prenatal dexamethasone exposure decreases Ezh2 expression in osteoclast precursors and attenuates osteoclastogenesis. **(A)** Diagram showing the procedure for the isolation of OCs from femoral metaphysis (see the detailed description in section "Materials and Methods"). **(B–E)** RANK+ cells were isolated from femoral metaphyses using the same method as in **Figure 2**. **(B)** Representative flow cytometry plots showing the sorting profile used to separate POCs and OCs in femoral bone from 12-week-old female mouse offspring. Quantitative RT-PCR analyses of Ezh2 **(C)** and MafB **(D)** mRNA expression and Western blot analysis of Ezh2 **(E)** protein expression in the sorted cells are shown. β-Actin serves as control to ensure appropriate loading. $^*p < 0.05$.

Angiogenesis is coupled with bone formation in these processes for proper bone homeostasis (Brandi and Collin-Osdoby, 2006; Portal-Nunez et al., 2012); reduced angiogenesis impacts the osteogenesis by decreasing BNM transport nutrients, oxygen, minerals, and metabolic wastes, which are essential for maintaining proper osteoblastic bone matrix synthesis and mineralization (Choi et al., 2002; Percival and Richtsmeier, 2013). During the bone modeling and remodeling, osteoclast bone resorption is coupled with osteoblast bone formation. Endocrine and paracrine factors from osteoblast and osteoclast could induce migration and differentiation of the osteoblast/osteoclast precursors. In response to stimulation with MCSF and RANKL, macrophages and monocytes commit to the osteoclast lineage as $TRAP^+$ mononuclear cells, which is defined as pre-osteoclast (Del Fattore et al., 2012). Pre-osteoclasts secrete PDGF-BB to stimulate migration and angiogenesis of endothelial progenitor cells (EPCs) and MSCs (Fiedler et al., 2004; Wang et al., 2012). Pre-osteoclasts subsequently fuse to form $TRAP^+$ multinuclear cells (osteoclasts). Growth factors, transforming growth factor-β, and insulin-like growth factor-1, are released from the bone matrix during osteoclast bone resorption to recruit BMSCs to the same zone, differentiated into osteoblast for new bone formation.

It is being increasingly proven that histone methylation of bivalent promoters in central to the progression of RANKL-induced osteoclast differentiation by both activating (Yasui et al., 2011; Nakamura et al., 2017) and repressing (Fang et al., 2016) selected important gene promoters in osteoclast precursors. Ezh2-directed H3k27me3 chromatin repression of developmental genes is a key to the cellular differentiation and cellular senescence (Margueron and Reinberg, 2011; Li et al., 2017). Recent reports have shown that Ezh2 could regulate a subset of anti-inflammatory and pro-osteoclastogenic genes during interferon-γ-mediated macrophage activation. Also Ezh2 activity and total cellular H3K27me3 levels are upregulated during the initial 12 to 24 h of RANKL-induced pre-osteoclasts (Adamik et al., 2020). Ezh2 could repress the expression of osteoclast inhibitory factors MafB, Arg1, and Irf8. In our study, we demonstrated that ACT could repress the Ezh2 expression in osteoclast precursors and attenuated the osteoclastogenesis in ACT mice. The MafB and Irf8 mRNA expression level is upregulated after treating osteoclast precursors with GSK126 (Ezh2 specific inhibitor), which represses the osteoclastogenesis. To our knowledge, it is the first time that we find the pre-osteoclasts and PDGF-BB derived from pre-osteoclast decreased in the ACT mice model and caused the type H vessel decrease, which leads to dysfunction of osteogenesis. Nevertheless, a limitation of our study that cannot be neglected is that we failed to explore the mechanism of Ezh2 downregulated by ACT.

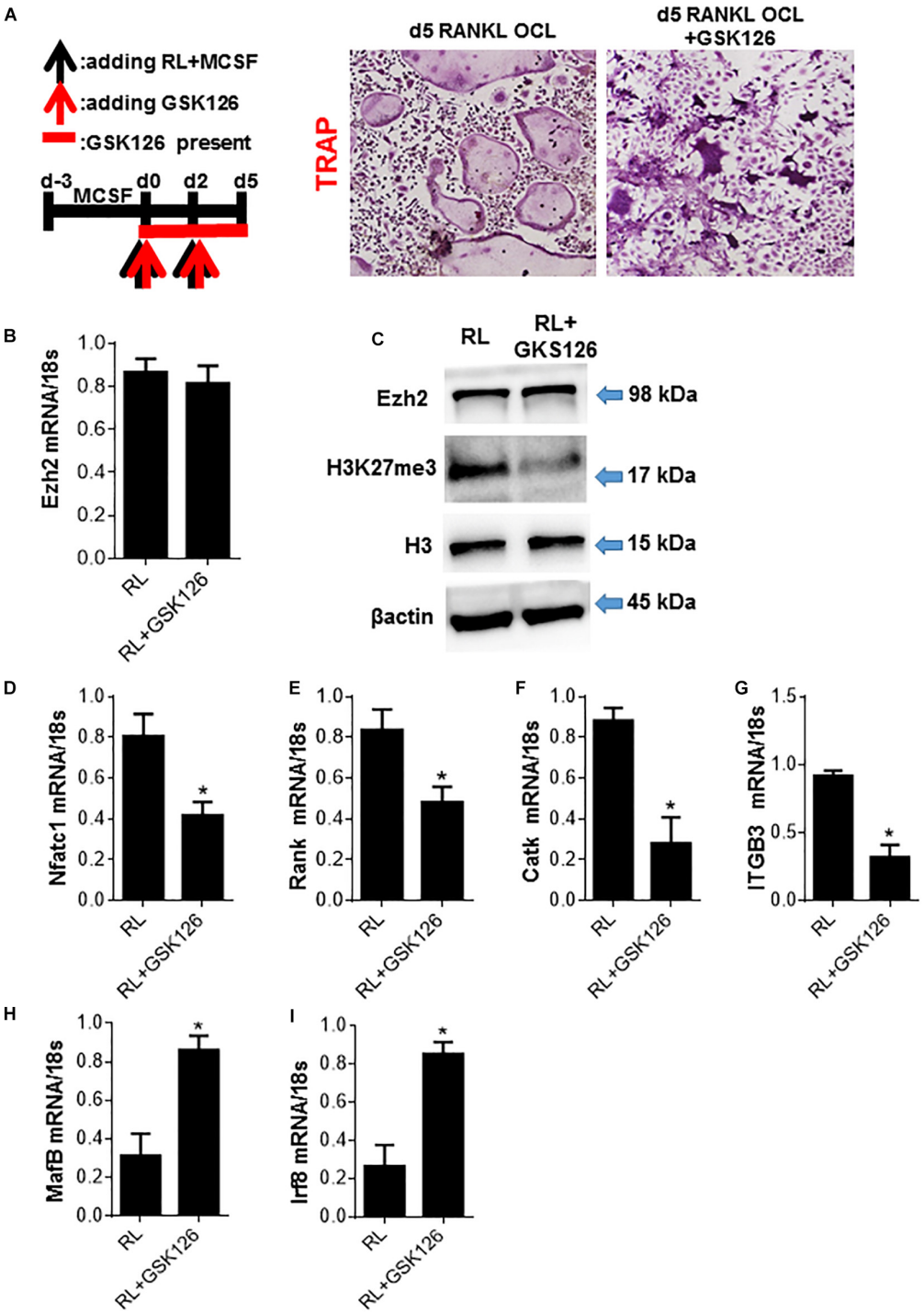


FIGURE 4 | Ezh2 plays a critical role in osteoclastogenesis by activating osteoclast regulators and repress the osteoclast inhibitory factors. BMMs were cultured with MCSF for 3 days (days 3 to 0) to form OCL precursors (OCLp) before addition of RANKL/MCSF at day 0 to generate OCL. **(A)** OCLp were cultured with RANKL/MCSF in the presence of the indicated concentrations of GSK126 for 5 days. TRAP+ OCL formed were analyzed by microscopy (representative images on left) and the counts for multinucleated ($n \geq 3$) TRAP+ OCL/well graphed (right). GSK126 (10 μM) was added at the indicated time intervals during the processes of OCLp and OCL (day 4) formation, and representative images and counts for multinucleated ($n \geq 3$) TRAP+ OCL/well are shown. **(B)** OCLp (day 0) or stimulated with RANKL/MCSF ± GSK126 (10 μM; GSK) for 5 days were analyzed for Ezh2 mRNA by quantitative PCR (qPCR). **(C)** OCLp cultures (day 0) or after stimulation with RANKL/MCSF ± GSK126 (10 μM) for 1 day were analyzed for total cellular levels of Ezh2, H3K27me3, H3, and β-actin by WB. **(D–G)** OCLp (day 0) or after stimulation with RANKL/MCSF ± GSK126 (10 μM) for 5 days were analyzed for the expression of OCL-specific genes NFATc1, RANK, CatK, ITGB3 by qPCR. **(H,I)** OCLp (day 0) or after stimulation with RANKL/MCSF ± GSK126 (10 μM) for 1 day were analyzed for the expression of OCL-negative regulators MafB and Irf8 by qPCR. WB analyses show representative of three independent experiments and error bars in mRNA experiments represent SEM for 4 biological replicates. *$p < 0.05$.

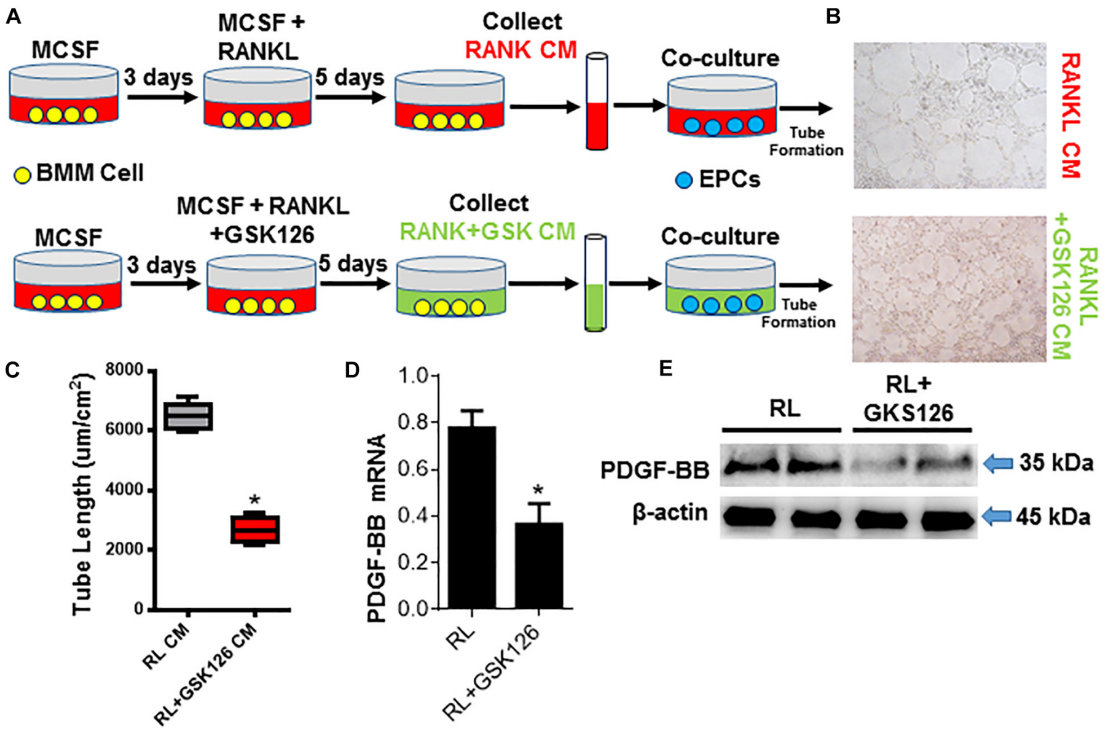


FIGURE 5 | Loss of Ezh2 suppress osteoclast precursors PDGF-BB expression and bone vasculature in ACT mice. **(A)** Diagram showing the procedure for the collection of condition media of OCs under denoted conditions and the co-culture with the EPCs. **(B,C)** Representative images **(B)** and tube length **(C)** from Matrigel endothelial tube formation assay with addition of OCLp (red) and after stimulation with RANKL/MCSF ± GSK126 (10 μM) (green) culture media. **(D,E)** Quantification of Pdgfb mRNA by real-time PCR **(D)** and total cellular levels of PDGF-BB and β-actin by WB **(E)**. mRNA normalized to GAPDH. *$p < 0.05$.

Therefore, further study is necessary to unravel the cellular and molecular mechanisms of how ACT regulates Ezh2 expression in osteoclast precursor.

MATERIALS AND METHODS

Animals

This study was conducted in accordance with the Guide for the Care and Use of Laboratory Animals of Nanfang Hospital Southern Medical University. The protocol was approved by the Animal Care and Use Committee of Nanfang Hospital. Pathogen-free mice were maintained under standard conditions in a 12-h light and 12-h dark cycle, at 25°C ± 3°C, with a relative humidity of 40 to 60% and with food and tap water available *ad libitum*. ACT during GD 12 to 14 was applied according to the procedure previously described (Chen et al., 2018). Briefly, virgin C57BL/6 female mice at 10 to 12 weeks old were mated with male mice overnight. The day of the presence of a vaginal plug was set as GD 0; the pregnant mice were randomly assigned to the ACT group or vehicle treatment (control) group. To construct ACT mice model, dexamethasone sodium phosphate (Cat. 2392-39-4, Tianxin, China) was injected subcutaneously (1.2 mg kg^{-1} per day) during GD 12 to 14. To construct the vehicle control of ACT model, pregnant mice were treated with the same amount of vehicle (normal saline) daily during GD 12–14. The pregnant mice were housed individually in cages with freely available food and water. Two female offspring were selected randomly from each litter for postnatal bone development investigation. Femora from female mice offspring at 12 weeks old were dissected for further analysis.

μCT Analysis

Femora from 12-week-old mice offspring were dissected free of soft tissue, fixed and stored in 70% ethanol, and imaged using a μCT specimen scanner (Scanco Medical, AG, Switzerland). The scan was performed using an X-ray energy of 55 kVp and current of 145 mA, with a voxel size of 9 μm and an integration time of 400 ms. Cross-sectional images of the distal femur were used to perform three-dimensional histomorphometric analysis of trabecular bone. The sample area selected for analyses was of 2-mm length of the metaphyseal secondary spongiosa, originating 1.0 mm below the epiphyseal growth plate and extending caudally.

Histochemistry

Femora of mice offspring at 12 weeks old were fixed in 4% paraformaldehyde, decalcified in 0.5 M ethylenediaminetetraacetic acid (pH 8.0), and then followed by paraffin embedding or frozen embedding. Serial longitudinal sections (4 μm thick) were cut. For detecting the alkaline phosphatase activity in bone, TRAP staining was performed on

the deparaffinized and rehydrated sections using a leukocyte alkaline phosphatase kit (Cat. 387A-1KT, Sigma-Aldrich, United States). The $TRAP^+$ multinucleated cells containing at least three nuclei were identified as osteoclasts under light microscope (Olympus, BX53). The $TRAP^+$ cells per square millimeter of metaphyseal area (N. mm^{-2}) in the area from 0 to 0.5 mm below growth plate were quantified.

Immunofluorescence

For immunofluorescence staining, frozen sections were incubated in blocking buffer [3% bovine serum albumin in phosphate-buffered saline (PBS) with Triton X-100 (PBST)] for 1 h at room temperature and incubated with primary antibodies overnight at 4°C. The primary antibodies for immunostaning include osteocalcin (M173, Takara, 1:200), CD31 (FAB3629G-100, R&D Systems, 1:100), endomucin (Emcn, SC-65495, Santa Cruz, 1:100), and PDGF-BB (sc-365805, Santa Cruz, 1:100). Sections were washed three times in PBS and then incubated with secondary antibodies for 1 h at room temperature. The secondary antibodies for immunostaning include 488-conjugated secondary antibody (703-546-155, Jackson ImmunoResearch, 1:200) and 594-conjugated secondary antibody (712-586-153, Jackson ImmunoResearch, 1:200). Nuclei were counterstained with DAPI (S2110, Solarbio, China). Images were captured using a fluorescence microscope (Olympus, BX53, Japan). Positively stained area or relative staining intensity was measured in the area from 0 to 0.5 mm below growth plate.

Cell Sorting and Flow Cytometry Analysis

For flow cytometric analysis and sorting of mouse $RANK^+$ MSPCs from femoral metaphysis, we dissected the femora free of soft tissues from mice offspring at 12 weeks old. The epiphysis was removed, and the bones were cut into small pieces and digested in the protease solution for 20 min. Cells within the supernatant were collected for flow cytometry. Cell numbers were determined after removal of red blood cells with ACK Lysis Buffer (CS0001, Leagene, China). Cells were then sorted according to side scatter and RANK-PE fluorescence at $>10^3$ log Fl-1 (RANK-PE) fluorescence. FACS was performed using a 5-laser Beckman FACS system (MoFlo XDF, Beckman, United States). Flow cytometric analyses were performed using FlowJo software (BD Life Sciences, San Jose, CA, United States). The primary antibody used was RANK-PE (12-6612-82, Thermo Fisher Scientific, 5 $\mu L/10^6$ cells).

Western Blotting

Western blotting was performed according to standard protocols using the following antibodies directed toward Ezh2 (5246S; Cell Signaling Technology), GAPDH (ET1601-4; HuaBio), PDGF-BB (sc-365805, Santa Cruz), and β-actin (85316, Sigma). Nuclear and cytoplasmic protein separations were performed using the Nuclear Extract Kit (Active Motif, 40010). Signals were developed by ECL (MilliporeSigma, Burlington, MA, United States) and visualized by Tanon chemiluminescence apparatus. Protein densitometry was quantified by ImageJ software (National Institutes of Health, Bethesda, MD, United States).

TABLE 1 | qPCR primers for mouse mRNA analysis.

Gene	Forward primer (5′→3′)	Reverse primer (5′→3′)
mEzh2	TACATCCCTTCCATGCAACA	TCCCTCCAGATGCTGGTAAC
mNfatc1	TGGAGAAGCAGAGCACAGAC	GCGGAAAGGTGGTATCTCAA
mRank	GTGGAAATAAGGAGTCCTCAG	CACCGTCTTCTGGAACCATC
mCatk	AATACGTGCAGCAGAACGGAGGC	CTCGTTCCCCACAGGAATCTCTCTGTAC
mMafB	GAGCAGGTGTGACTCACGAT	TGGCTAGTGGGTAGCTGTTG
mIrf8	CTACCTGACAGCAGGGTGGT	GGCATACAGCTGCTCTACCTG
mPdgf-bb	ACCCAGAAGACTGTGGATGG	CACATT-GGGGGTAGGAACAC
mItgb3	CCACACGAGGCGTGAACTC	CTTCAGGTTACATCGGGGTGA

OCL Differentiation and TRAP Staining

Primary BMM cells were expanded in αMEM with MCSF (20 ng/mL) (R&D Systems, Minneapolis, MN, United States) for 3 days (days 3 to 0) to generate OCLp. Then RANKL (10 ng/mL) (R&D Systems) and MCSF (10 ng/mL) were used at day 0 to differentiate OCL for 4 to 5 days. In some cases, BMMs were transduced with lentivirus particles for the first day (days 3 to 2) of MCSF generation of OCLp. OCL was fixed with 37% formaldehyde for 15 min, washed with ddH_2O, and stained using leukocyte acid phosphatase kit (Sigma-Aldrich, 387A-1KT) following the manufacturer's instructions. $TRAP^+$ multinucleated cells with three or more nuclei were counted as OCL. All OCL formation experiments were scored from four to five independent wells.

Quantitative Real-Time Polymerase Chain Reaction

POCs were incubated with prednisolone 10^{-6} M alone or with either RU486, GRsiRNA, or tumor necrosis factor α or prednisolone 10^{-7} M alone for 24 h. Total RNA for quantitative real-time (qRT)-polymerase chain reaction (PCR) was extracted from the cells using Trizol reagent (Invitrogen, Carlsbad, CA, United States) according to the manufacturer's protocol. RNA purity was tested by measuring the absorbance at 260 and 280 nm. For qRT-PCR, cDNA was prepared with random primers using the SuperScript First-Strand Synthesis System (Invitrogen) and analyzed with SYBR Green Master Mix (Qiagen, Valencia, CA, United States) in the thermal cycler with two sets of primers specific for each targeted gene. Relative expression was calculated for each gene by the $2^{-\Delta\Delta Ct}$ method, with GAPDH for normalization. The quantitative PCR primers are listed in **Table 1**.

In vitro Tube Formation Assay

Culture media was collected from POC cultures in the presence of RANKL (10 ng/mL) (R&D Systems) and MCSF (10 ng/mL) or in addition to GSK126 (Selleck; S7061) for 5 days. In a separate culture, EPCs were seeded in endothelial progenitor outgrowth cell growth medium (BioChain, Newark, CA, United States; Z7030033). Tube formation assays were performed by using

Matrigel Matrix basement membrane (Corning, Corning, NY, United States; 356230) as reported. Briefly, 50 μL of Matrigel was added into 96-well culture plates and incubated at 37°C for 30 min to allow the gel to solidify. We then seeded EPCs (2×10^4 cells/well) on polymerized Matrigel in plates and cultured the cells with the collected POC conditioned medium mixed with the endothelial cell culture medium in a ratio of 1:1. Two groups of cells were incubated in medium with RANKL and MCSF or additional GSK126. After incubation at 37°C for 4 h, we observed tube formation by microscopy and measured the cumulative tube lengths.

Statistics

All quantitative data were presented as mean ± SEM. For comparisons between two groups, independent Student *t* test was performed. For multiple comparisons, one-way analysis of variance with Bonferroni *post hoc* test was used. Statistical analysis was performed using SPSS, version 20 software (IBM Corp.). Significant level was defined as $P < 0.05$.

DATA AVAILABILITY STATEMENT

The raw data supporting the conclusions of this article will be made available by the authors, without undue reservation.

ETHICS STATEMENT

The animal study was reviewed and approved by Animal Care and Use Committee of Nanfang Hospital.

AUTHOR CONTRIBUTIONS

BY and XZ designed the research and drafted, revised, and approved the manuscript. YC and JS acquired the data. RZ, CC, and WH analyzed the data. All authors read and approved the final manuscript.

FUNDING

This study was supported by grants from the National Natural Science Foundation of China (No. 81573515 to XZ), The Major Program of National Natural Science Foundation of China (No. 81830079 to BY), China Postdoctoral Science Foundation (Grant number: 2020M672720), Natural Science Foundation of Guangdong (Grant number: 2019A1515011778), President Foundation of Nanfang Hospital, Southern Medical University (Grant number: 2019Z011), and Outstanding Youths Development Scheme of Nanfang Hospital, Southern Medical University 2018J012.

REFERENCES

Adamik, J., Pulugulla, S. H., Zhang, P., Sun, Q., Lontos, K., Macar, D. A., et al. (2020). EZH2 supports osteoclast differentiation and bone resorption via epigenetic and cytoplasmic targets. *J. Bone Miner. Res.* 35, 181–195. doi: 10.1002/jbmr.3863

Andrae, J., Gallini, R., and Betsholtz, C. (2008). Role of platelet-derived growth factors in physiology and medicine. *Genes Dev.* 22, 1276–1312. doi: 10.1101/gad.1653708

Bloom, S. L., Sheffield, J. S., McIntire, D. D., and Leveno, K. J. (2001). Antenatal dexamethasone and decreased birth weight. *Obstet. Gynecol.* 97, 485–490. doi: 10.1016/s0029-7844(00)01206-0

Brandi, M. L., and Collin-Osdoby, P. (2006). Vascular biology and the skeleton. *J. Bone Miner. Res.* 21, 183–192. doi: 10.1359/JBMR.050917

Bronckaers, A., Hilkens, P., Martens, W., Gervois, P., Ratajczak, J., Struys, T., et al. (2014). Mesenchymal stem/stromal cells as a pharmacological and therapeutic approach to accelerate angiogenesis. *Pharmacol. Ther.* 143, 181–196. doi: 10.1016/j.pharmthera.2014.02.013

Buckley, L., and Humphrey, M. B. (2018). Glucocorticoid-induced osteoporosis. *N. Engl. J. Med.* 379, 2547–2556. doi: 10.1056/NEJMcp1800214

Chen, Z., Zhao, X., Li, Y., Zhang, R., Nie, Z., Cheng, X., et al. (2018). Course-, dose-, and stage-dependent toxic effects of prenatal dexamethasone exposure on long bone development in fetal mice. *Toxicol. Appl. Pharmacol.* 351, 12–20. doi: 10.1016/j.taap.2018.05.005

Cheng, X., Wang, G., Lee, K. K., and Yang, X. (2014). Dexamethasone use during pregnancy: potential adverse effects on embryonic skeletogenesis. *Curr. Pharm. Des.* 20, 5430–5437. doi: 10.2174/1381612820666140205144534

Choi, I. H., Chung, C. Y., Cho, T. J., and Yoo, W. J. (2002). Angiogenesis and mineralization during distraction osteogenesis. *J. Korean Med. Sci.* 17, 435–447. doi: 10.3346/jkms.2002.17.4.435

de Vries, A., Holmes, M. C., Heijnis, A., Seier, J. V., Heerden, J., Louw, J., et al. (2007). Prenatal dexamethasone exposure induces changes in nonhuman primate offspring cardiometabolic and hypothalamic-pituitary-adrenal axis function. *J. Clin. Invest.* 117, 1058–1067. doi: 10.1172/JCI30982

Del Fattore, A., Teti, A., and Rucci, N. (2012). Bone cells and the mechanisms of bone remodelling. *Front. Biosci.* 4, 2302–2321. doi: 10.2741/543

Dudakovic, A., Camilleri, E. T., Riester, S. M., Paradise, C. R., Gluscevic, M., O'Toole, T. M., et al. (2016). Enhancer of zeste homolog 2 inhibition stimulates bone formation and mitigates bone loss caused by ovariectomy in skeletally mature mice. *J. Biol. Chem.* 291, 24594–24606. doi: 10.1074/jbc.M116.740571

Dudakovic, A., Camilleri, E. T., Xu, F., Riester, S. M., McGee-Lawrence, M. E., Bradley, E. W., et al. (2015). Epigenetic control of skeletal development by the histone methyltransferase Ezh2. *J. Biol. Chem.* 290, 27604–27617. doi: 10.1074/jbc.M115.672345

Fang, C., Qiao, Y., Mun, S. H., Lee, M. J., Murata, K., Bae, S., et al. (2016). Cutting edge: EZH2 promotes osteoclastogenesis by epigenetic silencing of the negative regulator IRF8. *J. Immunol.* 196, 4452–4456. doi: 10.4049/jimmunol.1501466

Fiedler, J., Etzel, N., and Brenner, R. E. (2004). To go or not to go: migration of human mesenchymal progenitor cells stimulated by isoforms of PDGF. *J. Cell. Biochem.* 93, 990–998. doi: 10.1002/jcb.20219

Godfrey, K. M., Inskip, H. M., and Hanson, M. A. (2011). The long-term effects of prenatal development on growth and metabolism. *Semin. Reprod. Med.* 29, 257–265. doi: 10.1055/s-0031-1275518

Hemming, S., Cakouros, D., Codrington, J., Vandyke, K., Arthur, A., Zannettino, A., et al. (2017). EZH2 deletion in early mesenchyme compromises postnatal bone microarchitecture and structural integrity and accelerates remodeling. *FASEB J.* 31, 1011–1027. doi: 10.1096/fj.201600748R

Jia, D., O'Brien, C. A., Stewart, S. A., Manolagas, S. C., and Weinstein, R. S. (2006). Glucocorticoids act directly on osteoclasts to increase their life span and reduce bone density. *Endocrinology* 147, 5592–5599. doi: 10.1210/en.2006-0459

Kusumbe, A. P., Ramasamy, S. K., and Adams, R. H. (2014). Coupling of angiogenesis and osteogenesis by a specific vessel subtype in bone. *Nature* 507, 323–328. doi: 10.1038/nature13145

Li, C., Chai, Y., Wang, L., Gao, B., Chen, H., Gao, P., et al. (2017). Programmed cell senescence in skeleton during late puberty. *Nat. Commun.* 8:1312. doi: 10.1038/s41467-017-01509-0

Margueron, R., and Reinberg, D. (2011). The Polycomb complex PRC2 and its mark in life. *Nature* 469, 343–349. doi: 10.1038/nature09784

Maryniak, A., Ginalska-Malinowska, M., Bielawska, A., and Ondruch, A. (2014). Cognitive and social function in girls with congenital adrenal hyperplasia – influence of prenatally administered dexamethasone. *Child Neuropsychol.* 20, 60–70. doi: 10.1080/09297049.2012.745495

McCabe, M. T., Ott, H. M., Ganji, G., Korenchuk, S., Thompson, C., Van Aller, G. S., et al. (2012). EZH2 inhibition as a therapeutic strategy for lymphoma with EZH2-activating mutations. *Nature* 492, 108–112. doi: 10.1038/nature11606

Meyer-Bahlburg, H. F., Dolezal, C., Baker, S. W., Carlson, A. D., Obeid, J. S., and New, M. I. (2004). Cognitive and motor development of children with and without congenital adrenal hyperplasia after early-prenatal dexamethasone. *J. Clin. Endocrinol. Metab.* 89, 610–614. doi: 10.1210/jc.2002-021129

Morales, W. J., Diebel, N. D., Lazar, A. J., and Zadrozny, D. (1986). The effect of antenatal dexamethasone administration on the prevention of respiratory distress syndrome in preterm gestations with premature rupture of membranes. *Am. J. Obstet. Gynecol.* 154, 591–595. doi: 10.1016/0002-9378(86)90607-1

Murphy, K. E., Hannah, M. E., Willan, A. R., Hewson, S. A., Ohlsson, A., Kelly, E. N., et al. (2008). Multiple courses of antenatal corticosteroids for preterm birth (MACS): a randomised controlled trial. *Lancet* 372, 2143–2151. doi: 10.1016/S0140-6736(08)61929-7

Nakamura, S., Koyama, T., Izawa, N., Nomura, S., Fujita, T., Omata, Y., et al. (2017). Negative feedback loop of bone resorption by NFATc1-dependent induction of Cadm1. *PLoS One* 12:e0175632. doi: 10.1371/journal.pone.0175632

Nassiri, S. M., and Rahbarghazi, R. (2014). Interactions of mesenchymal stem cells with endothelial cells. *Stem Cells Dev.* 23, 319–332. doi: 10.1089/scd.2013.0419

Peaceman, A. M., Bajaj, K., Kumar, P., and Grobman, W. A. (2005). The interval between a single course of antenatal steroids and delivery and its association with neonatal outcomes. *Am. J. Obstet. Gynecol.* 193(3 Pt 2), 1165–1169. doi: 10.1016/j.ajog.2005.06.050

Percival, C. J., and Richtsmeier, J. T. (2013). Angiogenesis and intramembranous osteogenesis. *Dev. Dyn.* 242, 909–922. doi: 10.1002/dvdy.23992

Portal-Nunez, S., Lozano, D., and Esbrit, P. (2012). Role of angiogenesis on bone formation. *Histol. Histopathol.* 27, 559–566. doi: 10.14670/HH-27.559

Pufe, T., Scholz-Ahrens, K. E., Franke, A. T., Petersen, W., Mentlein, R., Varoga, D., et al. (2003). The role of vascular endothelial growth factor in glucocorticoid-induced bone loss: evaluation in a minipig model. *Bone* 33, 869–876. doi: 10.1016/j.bone.2003.08.002

Ramasamy, S. K., Kusumbe, A. P., Wang, L., and Adams, R. H. (2014). Endothelial Notch activity promotes angiogenesis and osteogenesis in bone. *Nature* 507, 376–380. doi: 10.1038/nature13146

Reagan-Shaw, S., Nihal, M., and Ahmad, N. (2008). Dose translation from animal to human studies revisited. *FASEB J.* 22, 659–661. doi: 10.1096/fj.07-9574LSF

Seeman, E. (2009). Bone modeling and remodeling. *Crit. Rev. Eukaryot. Gene Expr.* 19, 219–233. doi: 10.1615/critreveukargeneexpr.v19.i3.40

Sliwa, E., Dobrowolski, P., and Piersiak, T. (2010). Bone development of suckling piglets after prenatal, neonatal or perinatal treatment with dexamethasone. *J. Anim. Physiol. Anim. Nutr.* 94, 293–306. doi: 10.1111/j.1439-0396.2008.00909.x

Su, J., Chai, Y., Ji, Z., Xie, Y., Yu, B., and Zhang, X. (2020). Cellular senescence mediates the detrimental effect of prenatal dexamethasone exposure on postnatal long bone growth in mouse offspring. *Stem Cell Res. Ther.* 11:270. doi: 10.1186/s13287-020-01790-9

Teti, A. (2011). Bone development: overview of bone cells and signaling. *Curr. Osteoporos. Rep.* 9, 264–273. doi: 10.1007/s11914-011-0078-8

Tomaszewska, E., Dobrowolski, P., and Puzio, I. (2013). Morphological changes of the cartilage and bone in newborn piglets evoked by experimentally induced glucocorticoid excess during pregnancy. *J. Anim. Physiol. Anim. Nutr.* 97, 785–796. doi: 10.1111/j.1439-0396.2012.01319.x

Wang, H., Yin, Y., Li, W., Zhao, X., Yu, Y., Zhu, J., et al. (2012). Over-expression of PDGFR-beta promotes PDGF-induced proliferation, migration, and angiogenesis of EPCs through PI3K/Akt signaling pathway. *PLoS One* 7:e30503. doi: 10.1371/journal.pone.0030503

Weinstein, R. S. (2010). Glucocorticoids, osteocytes, and skeletal fragility: the role of bone vascularity. *Bone* 46, 564–570. doi: 10.1016/j.bone.2009.06.030

Xie, H., Cui, Z., Wang, L., Xia, Z., Hu, Y., Xian, L., et al. (2014). PDGF-BB secreted by preosteoclasts induces angiogenesis during coupling with osteogenesis. *Nat. Med.* 20, 1270–1278. doi: 10.1038/nm.3668

Xu, D., Chen, M., Pan, X. L., Xia, L. P., and Wang, H. (2011). Dexamethasone induces fetal developmental toxicity through affecting the placental glucocorticoid barrier and depressing fetal adrenal function. *Environ. Toxicol. Pharmacol.* 32, 356–363. doi: 10.1016/j.etap.2011.08.003

Yang, P., Lv, S., Wang, Y., Peng, Y., Ye, Z., Xia, Z., et al. (2018). Preservation of type H vessels and osteoblasts by enhanced preosteoclast platelet-derived growth factor type BB attenuates glucocorticoid-induced osteoporosis in growing mice. *Bone* 114, 1–13. doi: 10.1016/j.bone.2018.05.025

Yasui, T., Hirose, J., Tsutsumi, S., Nakamura, K., Aburatani, H., and Tanaka, S. (2011). Epigenetic regulation of osteoclast differentiation: possible involvement of Jmjd3 in the histone demethylation of Nfatc1. *J. Bone Miner. Res.* 26, 2665–2671. doi: 10.1002/jbmr.464

Young, B. K., Klein, S. A., Katz, M., Wilson, S. J., and Douglas, G. W. (1980). Intravenous dexamethasone for prevention of neonatal respiratory distress: a prospective controlled study. *Am. J. Obstet. Gynecol.* 138, 203–209. doi: 10.1016/0002-9378(80)90036-8

Zhang, X., Shang-Guan, Y., Ma, J., Hu, H., Wang, L., Magdalou, J., et al. (2016). Mitogen-inducible gene-6 partly mediates the inhibitory effects of prenatal dexamethasone exposure on endochondral ossification in long bones of fetal rats. *Br. J. Pharmacol.* 173, 2250–2262. doi: 10.1111/bph.13506

Conflict of Interest: The authors declare that the research was conducted in the absence of any commercial or financial relationships that could be construed as a potential conflict of interest.

Copyright © 2020 Chai, Su, Hong, Zhu, Cheng, Wang, Zhang and Yu. This is an open-access article distributed under the terms of the Creative Commons Attribution License (CC BY). The use, distribution or reproduction in other forums is permitted, provided the original author(s) and the copyright owner(s) are credited and that the original publication in this journal is cited, in accordance with accepted academic practice. No use, distribution or reproduction is permitted which does not comply with these terms.

frontiers in Cell and Developmental Biology

REVIEW
published: 21 December 2020
doi: 10.3389/fcell.2020.600181

Obesity and Bone Health: A Complex Link

*Jing Hou[1], Chen He[1], Wenzhen He[1], Mi Yang[1,2,3], Xianghang Luo[1,2,3] and Changjun Li[1,2,3]**

[1] Department of Endocrinology, Endocrinology Research Center, The Xiangya Hospital of Central South University, Changsha, China, [2] National Clinical Research Center for Geriatric Disorders (Xiangya Hospital), Changsha, China, [3] Key Laboratory of Organ Injury, Aging and Regenerative Medicine of Hunan Province, Changsha, China

So far, the connections between obesity and skeleton have been extensively explored, but the results are inconsistent. Obesity is thought to affect bone health through a variety of mechanisms, including body weight, fat volume, bone formation/resorption, proinflammatory cytokines together with bone marrow microenvironment. In this review, we will mainly describe the effects of adipokines secreted by white adipose tissue on bone cells, as well as the interaction between brown adipose tissue, bone marrow adipose tissue, and bone metabolism. Meanwhile, this review also reviews the evidence for the effects of adipose tissue and its distribution on bone mass and bone-related diseases, along with the correlation between different populations with obesity and bone health. And we describe changes in bone metabolism in patients with anorexia nervosa or type 2 diabetes. In summary, all of these findings show that the response of skeleton to obesity is complex and depends on diversified factors, such as mechanical loading, obesity type, the location of adipose tissue, gender, age, bone sites, and secreted cytokines, and that these factors may exert a primary function in bone health.

Keywords: obesity, adipose tissue, bone health, bone remodeling, bone-related diseases

OPEN ACCESS

Edited by:
Chunyi Wen,
Hong Kong Polytechnic University, Hong Kong

Reviewed by:
Liu Yang,
Xijing Hospital, Fourth Military Medical University, China
Jeffrey Gimble,
Obatala Sciences, United States

***Correspondence:**
Changjun Li
lichangjun@csu.edu.cn

Specialty section:
This article was submitted to Molecular Medicine, a section of the journal Frontiers in Cell and Developmental Biology

Received: *29 August 2020*
Accepted: *30 November 2020*
Published: *21 December 2020*

Citation:
Hou J, He C, He W, Yang M, Luo X and Li C (2020) Obesity and Bone Health: A Complex Link. Front. Cell Dev. Biol. 8:600181. doi: 10.3389/fcell.2020.600181

INTRODUCTION

Bone is a living tissue with metabolic functions. The size and shape of bones are accurately modeled and reshaped over a lifetime to ensure skeletal structure and integrity (Xie et al., 2014; Li et al., 2017). During bone remodeling, bone can coordinate the activities of osteoblasts, osteocytes, and osteoclasts, thus maintaining the dynamic coupling balance of bone metabolism, in which osteoblasts (bone formation) and osteoclasts (bone resorption) play pivotal roles in bone metabolism. Bone marrow mesenchymal stem cells (BMSCs) have the ability to differentiate into osteoblasts and adipocytes, which is also a dynamic balance (Li et al., 2015; Li C.J. et al., 2018). In addition, bones exhibit the characteristics of endocrine organs, which secrete a variety of hormones to participate in the endocrine cycle throughout the body. For instance, bone can secrete estrogen, androgens, follicle suppressant and other sex hormones to participate in the reproductive process, cellular senescence, and osteoporosis (OP). Moreover, bone marrow fat cells can also secrete a series of adipokine including adiponectin, leptin through autocrine, and paracrine, which play an important regulatory role in local and systemic metabolism of bone marrow. There are however many metabolic osteopathy, including OP, bone tumor, and inflammatory arthritis, where this fine equilibrium is disrupted (Sun et al., 2019).

Overweight and obesity are identified as abnormal or excessive fat accumulation that can lead to impaired health. Body mass index (BMI) is a simple ratio of height to weight that is often used to distinguish between overweight and obesity adults. The WHO defines overweight as having a BMI of 25 to <30 kg/m^2 and obesity as ≥30 kg/m^2. In addition, obesity can be divided into three grades, namely obese class I (30 to <35 kg/m^2), class II (35 to <40 kg/m^2), and class III (≥40 kg/m^2) (Barba et al., 2004; Di Angelantonio et al., 2016). However, the diversity of Asian countries is mainly manifested in ethnic and cultural subgroups, degree of urbanization, social and economic conditions, and nutritional transformation. And compared with white people of the same age, sex, and BMI, Asians typically have a higher percentage of body fat. Therefore, the BMI cut-off points for overweight and obesity may be more applicable in Asian countries (Barba et al., 2004). Overweight and obesity are associated with risk and prognosis for certain disease states (Dalamaga and Christodoulatos, 2015).

The prevalence of obesity and obesity-related diseases is on the rise worldwide due to the socioeconomic and demographic transitions. The link between adiposity and bone health has been extensively studied, but the impact of obesity on bones has long been a subject of debate. This review will discuss the correlation between adiposity and bone-related diseases from multiple perspectives.

EXTRAMEDULLARY ADIPOSE TISSUE AND BONE

Adipose tissue consists mainly of fat cells that have accumulated in large numbers, which are divided into fat lobules by thin layers of loose connective tissue and widely distributed in the subcutaneous and around the internal organs. It is not only involved in body construction and energy storage, but is also a vital endocrine organ. Adipose tissue has an effect on insulin sensitivity, blood pressure level, endothelial function, fibrinolytic activity and inflammatory response, and participates in a variety of important pathophysiological processes.

Adipose tissue exerts a primary function in obesity and related diseases. According to different functions, adipose tissue can be divided into white adipose tissue (WAT), brown adipose tissue (BAT), and beige adipose tissue. WAT is an energy-storing tissue that regulates energy metabolism by secreting cytokines and hormones. Excessive accumulation of WAT in the body can cause obesity and obesity-related diseases. BAT, however, is an energy-consuming organization that is involved in non-shivering heat and diet-induced heat production. Both thermogenic mechanisms are due to the exclusive expression of uncoupled protein-1 (UCPl) in the mitochondria of brown fat cells, resulting in the uncoupling of fatty acids and ATP oxidation, ultimately causing energy dissipation in the form of heat (Del Mar Gonzalez-Barroso et al., 2001; Carobbio et al., 2017; Huang et al., 2020). Thus, BAT can be capable of fighting obesity. Beige fat is more widely distributed than the typical brown fat, which is concentrated in the interscapular storage of rodents and in the supraclavicular and mediastinal areas of humans (Frontini and Cinti, 2010; Wiedmann et al., 2017). Beige fat also possesses an innate ability to metabolize energy as heat release by non-shivering thermogenesis (Zhang et al., 2018).

Leptin Secreted by White Adipose Tissue and Bone

White adipose tissue has a main endocrine function secreting many adipokines, especially leptin and adiponectin. These latest findings suggest that adipokines are closely related to metabolic diseases such as obesity, insulin resistance and diabetes, and play an important regulatory role in bone disease (Conde et al., 2011). Particularly, leptin and adiponectin have been shown to act directly on certain bone cells, including BMSCs, osteoblasts, and osteoclasts. Consistent evidence suggests that leptin has a direct anabolic effect on osteoblasts. Astudillo et al. (2007) observed that leptin can promote the proliferation of bone marrow stromal cells, differentiation into osteoblasts, and form mineralized nodules, but prevent the differentiation into adipocytes. Thomas (1999) have also shown that leptin leads to dose-dependent increases in mRNA and protein levels of alkaline phosphatase (ALP), osteocalcin (OC), and type I collagen. Gordeladze et al. (2002) found that continuous exposure of leptin to ilium osteoblasts contributed to collagen synthesis, cell differentiation, and *in vitro* mineralization, together with cell survival and transition to preosseous cells.

Additionally, leptin may increase local bone mass and may contribute to the link between bone formation and bone resorption. Holloway et al. (2002) found that after adding human macrophage colony stimulating factor (HM-CSF) and human soluble NF-Kappab ligand receptor activator (sRANKL) to bone culture, leptin can inhibit the formation of human peripheral blood mononuclear cells (PBMCs) and mouse spleen cells to osteoclasts. Leptin increased mRNA and protein expression of osteoprotegerin (OPG, a protein that inhibits osteoclast formation) in PBMC, suggesting that its inhibition may be realized through the RANKL/RANK/OPG pathway (Holloway et al., 2002). Leptin effectively attenuated trabecular bone loss, trabecular structure change and periosteal bone formation. Leptin also significantly reduced RANKL mRNA levels which mainly regulates osteoclast development in cultured human bone marrow stromal cells (Burguera et al., 2001; Reid et al., 2018).

In addition to having a direct anabolic effect on osteoblasts, leptin also indirectly affects bones. Numerous studies have shown that in mice lacking leptin or leptin receptors, spinal trabecular volume increases, vertebral bone mass increases, while femur bone mass decreases and femur bone marrow fat increases sharply (Ducy et al., 2000; Steppan et al., 2000; Hamrick et al., 2004). Remarkably, Steppan et al. (2000) found, compared with the control group, leptin administration significantly increased femur length, systemic bone area, bone mineral density (BMD) and bone mineral content in leptin-deficient mice (ob/ob mice). This conclusion has been confirmed in other studies as well (Hamrick et al., 2005; Bartell et al., 2011; Philbrick et al., 2017). In summary, the role of leptin in skeleton remains a highly controversial area.

Adiponectin Secreted by White Adipose Tissue and Bone

Adiponectin, the most common adipokine in plasma, has important metabolic and anti-inflammatory effects and is rapidly becoming a valuable marker for treatment in metabolic diseases. The role of adiponectin in certain bone cells including osteoblasts and osteoclasts, has been extensively studied. Human adiponectin promoted bone formation of primary human maxillary BMSCs through the APPL1-P38 MAPK pathway (Pu et al., 2016). Also, adiponectin induced osteogenesis of MSCs through adipoR1-mediated phosphorylation of P38 MAPK. Then, p38 MAPK phosphorylated c-Jun, which enhanced COX-2 (cyclooxygenase-2) expression and ultimately lead to an increase in BMP2 expression (bone morphogenetic protein 2, a strong osteogenic cytokine) (Lee et al., 2009; Huang et al., 2010). Similarly, Luo et al. (2005) demonstrated that adiponectin promoted osteoblastic proliferation, leading to increased alkaline phosphatase (ALP) activity, generation of type I collagen and OC, and increase in mineralized substrates in a dose-dependent and time-dependent manner. The increase of ALP, type I collagen, and OC is a marker of osteoblast differentiation and maturation, while matrix mineralization is a marker of osteoblastic phenotype. This study also provided evidence that adiponectin induced the proliferation and differentiation of human osteoblasts, which was realized through AdipoR/JNK pathway, while the differentiation was realized through AdipoR/P38 pathway (Sowa et al., 2002; Nöth et al., 2003; Luo et al., 2005).

Adiponectin also directly regulates osteoclast function. Adiponectin down-regulated expression of osteoclast regulators such as acid tartrate – resistant phosphatase and cathepsin K. Adiponectin also enhanced osteoclast apoptosis and reduced osteoclast precursor cells survival/proliferation (Tu et al., 2011; Pal China et al., 2018).

Significantly, like leptin, *in vivo* studies showed that the regulation of bone metabolism by adiponectin is also contradictory. Several studies reported that compared with wild-type mice, adiponectin knockout mice showed lower bone mineralization and bone density (Shinoda et al., 2006; Naot et al., 2016). But, others have shown that lack of adiponectin exert a protective effect on skeleton. Pal China et al. (2018) found KO mice prevented trabecular bone loss in mice caused by ovariectomy, and showed better bone quality (Williams et al., 2009). Taken together, the data from *in vitro* and *in vivo* studies fail to provide any definitive conclusions about the relationship between leptin, adiponectin and bone. And, white adipocytes can not only synthesize and secrete hormones including adiponectin and leptin, but also secrete proinflammatory factors such as TNF-α, IL-6, which may negatively regulate bone metabolism, further complicating the relationship between obesity and bone (Fruhbeck et al., 2001).

Brown Adipose Tissue and Bone

It is well known that BAT not only exists in newborns, but also exists in adults, and gradually decreases with age. In fact, Ponrartana et al. (2012) have observed a significant correlation between BAT volume and cross-sectional bone size, regardless of gender. Moreover, recent findings suggest that BAT activity is positively correlated with skeletal metabolism. In contrast, some previous studies have shown that BAT can secrete fibroblast growth factor 21 (FGF21) and increase plasma FGF21 levels. Wei et al. showed that in animal models, transgenic mice overexpressing FGF21 had a lower bone mass phenotype, while mice given the drug dose of FGF21 also had a lower bone mass, because of reduced bone formation and significantly increased bone absorption (Wei et al., 2012). Also, Fazeli et al. (2015) found that FGF21 was negatively correlated with trabecular microstructural parameters, such as trabecular number (TbN), in patients with anorexia nervosa (AN). Recently, plasma FGF21 level was found to be negatively correlated with bone density in femoral neck and Ward's triangle of hip region (Hao et al., 2018). Taken together, these data reveal that FGF21 is a major negative regulator of bone mass.

Interestingly, as an endocrine organ, bone can also secrete a variety of bioactive substances to control energy metabolism in adipose tissue. OC, a small molecular protein secreted by osteoblasts, is a classic indicator of bone formation. Li Q. et al. (2018) verified the specific role of OC in thermogenesis of brown adipocytes. Their study showed that the OC signaling pathway directly promoted the activation of the Gprc6a Tcf7 Ucp1 promoter through the positive feedback of the interaction between the Wnt3a Tcf7 and the WNT/β-catenin pathway (Li Q. et al., 2018).

In addition, bone regulates browning and energy metabolism via the expression of peroxisome proliferator-activated receptor (PPAR) in mature osteoblasts and osteocytes. Several studies have confirmed that, in bone, PPAR plays a negative regulatory role in bone formation by inhibiting osteoblast generation and promoting osteoclast activity. Specific ablation of PPAR in mature osteoblasts and osteocyte mice (OCY-PPAR-/-) was found to induce high-bone mass and low fat mass phenotypes, as well as increase fat browning and energy comsumption. Moreover, Ocy-PPARγ-/- could partly prevent the dysmetabolism caused by high fat intake (Brun et al., 2017). Interestingly, BMP7 levels were also higher in Ocy-PPARγ-/- mice in conditioned medium and serum. BMP7, derived from osteocytes, is believed to promote browning and reduce steatosis through endocrine mechanisms (Kinoshita et al., 2007; Sugimoto et al., 2007; Tseng et al., 2008; Boon et al., 2013).

Collectively, these results indicate that bone and adipose tissue can interact to regulate bone metabolism and energy metabolism, which provides a new idea for the exploration and development of treatment methods for bone-related diseases.

BONE MARROW ADIPOCYTES AND BONE

Bone marrow adipose tissue (BMAT), which accounts for about 8% of total fat mass, is an important fat depot in the adult body and exerts a significant function in bone homeostasis and energy metabolism throughout the body (Tencerova et al., 2019). BMAT is thought to be negatively correlated with bone density and bone integrity, so it may be an important regulator of bone turnover

(Fazeli et al., 2013). Studies have shown that BMAT in the lumbar spine is an independent predictive factor of fracture (Wehrli et al., 2000). BMAT is distinct from WAT and BAT. Excessive accumulation of lipids interferes with the normal function of cells and tissues, a condition known as lipotoxicity (Carobbio et al., 2017; Piccolis et al., 2019). Lipotoxicity is caused primarily by bone marrow fat through the secretion of adipokines and free fatty acids (mainly palmitate). In bone marrow, lipotoxicity is mainly manifested by the toxic effect of palmitate on bone cells, especially osteoblasts (Al Saedi et al., 2020). Exposure to adipocyte secretory factors can reduce the ability of BMSC to differentiate into bone cells, but also promote fat formation, a phenomenon that may be explained by a variety of mechanisms, including oxidative stress and proinflammatory mediators (TNF-α and IL-6) and adipokines (Horowitz et al., 2017; Singh et al., 2018). Furthermore, Elbaz et al. (2010) observed that, by co-culturing normal human osteoblasts (NHOst) with pre-differentiation adipocytes in the absence of a fatty acids synthase inhibitor (cerulenin), the differentiation and functional levels of NHOst were significantly reduced due to the lower mineralization and decreased expression of ALP, osterix, OC, and Runx2 (Elbaz et al., 2010). Actually, some evidences, indicates that palmitate has negative effects on osteoblast differentiation, bone nodule formation and mineralization.

Apart from BMSC and osteoblasts, osteoclasts are also affected by bone marrow fat to increase bone resorption and decrease bone mass (Singh et al., 2018). Takeshita et al. (2014) found that, during the differentiation of marrow stromal cells into adipocytes, RANKL expression was induced, along with the down-regulation of osteoprotegerin. The early adipogenic transcription factors C/EBPβ and C/EBPδ could bind to the RANKL promoter and ultimately stimulate RANKL gene transcription (Takeshita et al., 2014; Paccou et al., 2015; Hardouin et al., 2016).

Overall, these findings point to metabolic differences between bone marrow fat and peripheral fat that may be related to the development of therapeutic strategies for metabolic bone disease.

ANOREXIA NERVOSA, OBESITY, AND BONE

Anorexia nervosa is a major mental disorder that mainly affects women. Patients are unable to maintain normal weight due to extreme self-imposed starvation, which is typical of chronic malnutrition (Kaye et al., 2020). Bone loss is almost the most common feature in many comorbidities associated with this disease.

Interestingly, compared with normal-weight women, anorexic patients showed less subcutaneous adipose tissue (SAT) and visceral adipose tissue (VAT), but more BMAT (Bredella et al., 2009). Previous studies have shown that increased BMAT level has clinical significance and is related to bone density and bone strength. In the above content, we mentioned that bone marrow fat can inhibit bone formation and promote bone resorption. In addition, marrow fat content increased in elderly patients with OP and was inversely correlated with bone density in healthy white women, and also in obese women (Justesen et al., 2001; Shen et al., 2007; Bredella et al., 2011b). Similarly, in ovariectomy animals, loss of bone mass was often accompanied by abnormal accumulation of bone marrow fat (Bredella et al., 2009; Li S. et al., 2018; Beekman et al., 2019). Given the negative correlation between marrow fat and BMD, BMAT may be an important risk factor for low bone density and increased fracture risk in patients with AN. For example, increased BMAT and decreased bone density and bone strength were observed in AN in women and adolescents (Singhal et al., 2018; Fazeli et al., 2019). Moreover, bone marrow fat in L4 vertebral body, femoral metaphyseal and diaphyseal increased markedly in women with AN. Importantly, marrow fat content had a highly significant negative association with BMD in multiple bone sites including the lumbar spine, hip and whole body (Bredella et al., 2009). One reason may be that osteoblasts and fat cells are derived from the mesenchymal stem cells in the bone marrow, the increased adipogenic differentiation may lead to a decreased osteogenic differentiation in BMSCs.

However, studies have shown that in patients recovering from AN, BMAT levels in L4 vertebrae are similar to those in healthy controls (Fazeli et al., 2012). BMAT positively correlated with VAT in overweight/obese women, while no such association was observed in underweight women (Bredella et al., 2011b; Polineni et al., 2020). These data may indicate that BMAT is a dynamic depot, which may play different roles under the condition of insufficient and adequate nutrition. In addition, since hypercortisolemia and hypoestrogenism are both characteristics of AN, these factors may result in marrow adiposity (Putignano et al., 2001). In summary, during chronic starvation, while other fat stores are used as energy sources, this adipose tissue storage is retained, suggesting that it may have significant functions. And, studying this paradox may lead to a better understanding of the function of bone marrow fat.

TYPE 2 DIABETES, OBESITY AND BONE

Diabetes is a chronic disease characterized by neuropathy, nephropathy and retinopathy, with type 2 diabetes mellitus (T2DM) as the predominant type. The patient presents primarily with insulin resistance, and relative insulin deficiency (Compston, 2018; Su et al., 2019). This has been accompanied by a sharp rise in the incidence of obesity, an important determinant of type 2 diabetes. Abnormal accumulation of fat both inside and outside adipose tissue not only results in structural and functional disorders (insulin resistance) of adipose tissue itself, but also affects muscles, liver, and pancreas (Tsatsoulis et al., 2013; de Araujo et al., 2017). The bone disease of type 2 diabetes remains a mystery because the mechanism by which diabetes affects the bone is multifactorial, including factors such as obesity, hyperinsulinemia and insulin-like growth factors (IGFs). The effect of insulin on bone metabolism is controversial. Studies *in vitro* have reported that insulin signals in osteoblasts can promote bone absorption (Ferron et al., 2010). Consistent with *in vitro* results, Srikanthan et al. also confirmed that insulin resistance, especially hyperinsulinemia, may adversely affect femoral neck strength (Srikanthan et al., 2014). However,

other *in vivo* studies show that insulin stimulates osteoblasts to proliferate and increases the histologic markers of bone formation (Shanbhogue et al., 2016). Furthermore, in the early stages of diabetes, obesity and hyperinsulinemia often occur together, and it is challenging to identify the unique contribution of obesity and hyperinsulinemia to bone health.

It is believed that IGFs is associated with the pathogenesis of diabetic complications. In addition, serum IGF-I level was decreased in patients with poor blood glucose control (Thrailkill, 2000; Kanazawa et al., 2012). IGF I is thought to have anabolic effects on bone. Circulating IGF-I activates bone remodeling and plays an anabolic role in bone tissue (Johansson et al., 1992; Zhang et al., 2002). Some clinical studies have suggested that low serum IGF-I level is related to a higher risk of fractures independent of BMD in patients with type 2 diabetes (Ardawi et al., 2013; Miyake et al., 2017). Serum IGF-I level was found to be significantly negatively correlated with the prevalence of vertebral fractures in postmenopausal women with type 2 diabetes (Kanazawa et al., 2011, 2018). Based on the above evidence, the reduced serum IGF-I may be involved in diabetes-induced bone fragility and can be used to assess the risk of fracture in patients with T2DM.

In addition to the factors described above, the effects of hypoglycemic drugs on bone metabolism should also be taken into account. Most studies have shown that sulfonylureas and metformin have protective or neutral effects on fracture risk (Vestergaard et al., 2005; Kahn et al., 2006; Monami et al., 2008; Borges et al., 2011). In contrast, thiazolidinediones activate PPARγ, which in turn stimulate adipogenesis and inhibit osteogenesis (Gimble et al., 1996; Lecka-Czernik, 2017). Studies have reported an increased risk of fracture in patients taking thiazolidinedione (Dormuth et al., 2009; Zhu et al., 2014). Incretin hormones are considered to have the potential to treat type 2 diabetes. For instance, glucagon-like peptide-1 (GLP-1) targets primarily pancreatic β cells, where it stimulates insulin production, which helps control blood glucose levels (Baggio and Drucker, 2007). More recently, there has been growing evidence that incretins may also be beneficial for skeletal strength. GLP-1 plays a key role in bone homeostasis, inhibiting bone resorption and stimulating bone formation in response to nutrient intake (Shanbhogue et al., 2016). Indeed, GLP-1 receptor knockdown in mice can result in dramatic changes in trabecular and cortical microstructures, as well as adverse effects on bone tissue material properties (Mabilleau et al., 2013; Mansur et al., 2015, 2016). Thus, the effect on bone health should be considered when selecting hypoglycemic drugs to avoid inducing or exacerbating fractures and bone diseases in patients.

OBESITY AND BONE-RELATED DISEASES

Osteoporosis

Osteoporosis is a skeletal metabolic disorder with multiple causes, characterized by bone loss, microstructure degeneration, increased brittleness, reduced bone strength, and increased risk of fracture. Therefore, OP seriously affects the quality of life and living standards of patients (Khaliq et al., 2016; Pagnotti et al., 2019; Yang et al., 2019).

Bone mineral density is a commonly used indicator in the diagnosis of OP, which is performed by dual energy X-ray bone absorptiometry (DEXA). In addition, BMD can also be used to track changes in OP and evaluate the efficacy of OP drugs.

Numerous studies strongly suggest that, abdominal obesity, hypertension, dyslipidemia and dysglycemia are all considered as components of metabolic syndrome (MS) and are closely related to OP (Muka et al., 2015). Obesity may lead to an increase in bone density because it is associated with higher 17β-estradiol levels and higher mechanical loads, which may protect bones (Nelson and Bulun, 2001). Qiao et al. (2020) observed that adult obese patients had higher BMD in the lumbar spine and femoral neck than those of healthy weight. In general, obesity is negatively correlated with femoral neck OP, suggesting that obesity is a protective factor for OP (Qiao et al., 2020). Kim et al. (2010) found, however, that after adjusting for confounders, bone density was significantly lower in men over 40 and in postmenopausal women with MS. Moreover, the BMD decreased with the increase of MS components. Among MS indicators, waist circumference as a diagnostic criterion for abdominal obesity is the most critical factor leading to this negative correlation. Waist circumference was an important contributor in this association, suggesting that visceral fat may contribute to bone loss. The negative correlation between fat mass and bone density further supports this hypothesis, especially in men (Kim et al., 2010). Furthermore, pro-inflammatory molecules TNF- and IL-6 released from visceral fat play a key role in regulating bone resorption and participating in the pathogenesis of OP (Nanes, 2004; Roy et al., 2016).

Vitamin D is known to play a major role in the development and maintenance of bones and muscles in the body because of its ability to regulate the absorption of calcium and phosphorus. Low levels of vitamin D in the body are considered a potential risk factor for OP and bone fractures. Serum vitamin D deficiency prevents the intestinal tract from absorbing Ca^{2+} from diet, eventually leading to elevated levels of parathyroid hormone (PTH) secretion. Oversecretion of PTH induces osteoclast formation, inhibits osteogenesis, and maintains optimal blood calcium and phosphorus levels required for metabolic processes and neuromuscular function (Roy, 2013). Recent studies have found that the serum 25(OH)D of obese people is lower than that of normal weight people, which is negatively correlated with body weight, BMI, and fat mass (Fassio et al., 2018).

It is worth noting that recently, Li et al. proposed that obesity may lead to low serum 25(OH)D, high serum leptin and high bone density (Snijder et al., 2005; Konradsen et al., 2008; Felson, 2010). In this context, femoral neck and spine BMD were positively correlated with BMI and fat mass index. Recombinant human (Rh) leptin in the treatment of BMSCs significantly facilitated bone formation. In addition, leptin down-regulated CYP24A1 and up-regulated CYP27B1, CYP27A1, and VDR, all of which play key roles in vitamin D metabolism In summary, this study confirmed the relationship between obesity, vitamin D metabolism and osteoblastic development, and the

direct effect of leptin on vitamin D metabolism and osteoblastic differentiation of BMSCs may protect bone under the effect of low serum 25(OH)D in obese people (Lim et al., 2019; Li J. et al., 2020).

Fractures

Osteoporosis, sarcopenia, and obesity are commonly associated with aging. Obviously, fall-related injuries and fractures are the major causes of disability and death among the elderly, seriously affecting their quality of life and survival (Rapp et al., 2010; Sanchez-Riera et al., 2014).

Studies have shown that fat accumulation may contribute to the deterioration of muscle and bone, thereby promoting the development of sarcopenia and OP (Ilich et al., 2014). Additionally, more and more studies have confirmed that sarcopenia is not only closely related to low bone density, but also an important risk factor for fractures (Tarantino et al., 2015).

Obesity was previously deemed to be a protective factor for OP or brittle fractures because patients affected by obesity have more soft tissue to protect bone tissue. That is, the positive impact of mechanical load caused by body weight. But recent research suggests that obesity may increase the risk of certain fractures types (Cao and Picklo, 2015; Scott et al., 2016). Obesity may be a protective factor for hip fracture in adults and significantly reduce the risk of hip fracture (Tang et al., 2013). This view was driven in part by the positive correlation between BMD and BMI. Similar results were seen in obese patients with proximal femoral and vertebral fractures (De Laet et al., 2005).

The association between obesity and fracture in postmenopausal women may be site-dependent. Compared with normal/underweight women, obesity may prevent hip and pelvic fractures, but it increases the risk of proximal humerus fractures. Some non-spinal fractures, such as proximal humerus fractures, upper leg fractures, and ankle fractures, are at higher risk (Compston et al., 2011; Prieto-Alhambra et al., 2012).

In principle, obesity does not completely prevent fractures, and there are some specific site effects on fractures. In fact, obese people are more likely to fall and break bones than people of normal weight. Especially when BMI is over 30, obesity has limited protection against fractures and may even increase the risk of fractures (Kang et al., 2015).

Osteoarthritis

Osteoarthritis (OA) is the most common degenerative joint disease that affects any joint in the elderly, especially the knee joint. OA is characterized by the progressive deterioration of articular cartilage and structural changes throughout synovial joints, such as synovial membrane, knee meniscus, adipose tissue, periarticular ligaments, and subchondral bone (Brandt, 2006; Loeser et al., 2012; Hunter and Bierma-Zeinstra, 2019). Clinical and animal studies have revealed that age-related OA is related to many factors including age, sex, trauma, and obesity. Among these factors, obesity is one of the most influential and modifiable risk factors (Bijlsma et al., 2011).

Actually, a growing body of evidence suggests a strong link between obesity and inflammation. Adipose tissue has been shown to regulate inflammatory immune responses in cartilage People and animals affected by obesity exhibit higher serum levels of TNF-α, IL-1 and IL-6, all from macrophages in adipose tissue (Park et al., 2005; Ding, 2011). In parallel, the levels of TNF-α, IL-1 and IL-6 in synovial fluid, synovial membrane, subchondral bone and cartilage in patients with OA were increased, confirming their important roles in the pathogenesis of OA TNF-α, IL-6, and IL-1 are the cytokines produced by adipose tissue to directly and negatively regulate cartilage. In addition, TNF-α, IL-1, and IL-6 can promote the formation of other factors, matrix metalloproteinases (MMPs) and prostaglandins, while restrain the synthesis of proteoglycans and type II collagen. Therefore, they play an important role in OA cartilage matrix degradation and bone resorption. Moreover, TNF-α, IL-1, and IL-6 may indirectly cause OA by regulating adiponectin and leptin secreted by fat cells (Koskinen et al., 2011; Wang and He, 2018; Tu et al., 2019).

Reyes et al. (2016) subsequently found that being overweight or obese increased the risk of OA in all three joint areas (knees, hips, and hands), especially the knees. Overweight, class I obesity and class II obesity increased the risk of knee OA by 2-, 3. 1-, and 4.7-fold, respectively (Reyes et al., 2016).

Adipokines represent a new class of compounds that are currently considered to be key molecules involved in the pathogenesis of rheumatic diseases (Felson and Chaisson, 1997; Scotece et al., 2011; Gremese et al., 2014; Feng et al., 2019). Resistin is an adipokines closely related to obesity, local low-level inflammation and MS (Rong et al., 2019). Alissa et al. (2020) recently found that serum resistin levels were higher in patients with primary knee arthritis than in healthy controls. In addition, elevated serum resistin levels were positively correlated with indicators of obesity, markers of inflammation, and WOMAC Index (an indicator of the severity of OA symptoms) (Alissa et al., 2020). Furthermore, Koskinen et al. (2011) believed that the combination of leptin and IL-1 could promote the production of MMP-1, MMP-3, and MMP-13 in human OA cartilage. The effect of leptin on MMP-1, MMP-3, and MMP-13 was mediated by transcription factor NF-κβ, and protein kinase C and MAP kinase pathways. Leptin concentration in synovial fluid was also positively correlated with MMP-1 and MMP-3 levels in patients with OA (Koskinen et al., 2011). The results showed that leptin had catabolic effect on OA joints by increasing the production of MMP in cartilage (Bao et al., 2010).

In addition, adiponectin has been reported to be involved in the pathophysiological process of OA. Kang et al. (2010) reported that the total amount of nitric oxide (NO) and the levels of MMP-1, MMP-3, and MMP-13 were increased in adiponectin stimulated OA chondrocytes compared with unstimulated cells. NO is one of the main mediators of pro-inflammatory cytokines acting on chondrocytes and also regulates different cartilage functions, including chondrocyte phenotypic loss, apoptosis, and extracellular matrix degradation (Otero et al., 2007). In this study, adiponectin increased the expression of MMPs and iNOS in human OA chondrocytes through AMPK and JNK pathways, leading to the degradation of OA cartilage matrix (Kang et al., 2010).

In summary, obesity not only increases the incidence of OA, especially in weight-bearing joints such as knee joints,

but also is related to non-weight-bearing joints such as finger joints and wrist OA, suggesting that these metabolic mediators lead to an increase in the incidence of OA in obese patients. This may be because obesity increases the mechanical load of articular cartilage, leading to its degradation, and fatty tissue secretes metabolic factors (such as IL-1, TNF-A, adiponectin, and leptin), leading to an increased prevalence of OA in obese people (Oliveria et al., 1999; Grotle et al., 2008; Kalichman and Kobyliansky, 2009).

Rheumatoid Arthritis

Rheumatoid arthritis (RA), the most common form of inflammatory arthritis, is a chronic systemic autoimmune disease characterized by aggressive symmetrical inflammation of multiple joints (Kobayashi et al., 2010; Miossec, 2013; Minamino et al., 2020). Epidemiological studies have shown that about 90% of RA patients develop bone erosion within 2 years of onset, resulting in joint deformity or even disability. Therefore, RA has brought a heavy burden and great pain to affected families, patients and even the whole society (Nam et al., 2017).

Overweight/obesity is associated with higher rates of chronic autoimmune diseases and inflammatory diseases, including type 2 diabetes and RA (Zhang et al., 2014). There is evidence that an increase in BMI is associated with an increased risk of RA (Feng et al., 2019). As mentioned above, adipokines such as adiponectin and visfatin have also been reported to play a key role in the pathophysiology of autoimmune diseases (Coelho et al., 2013). It has now been well established that patients with RA show higher plasma adiponectin, leptin, and visfatin levels compared with healthy controls (Otero et al., 2006). Visfatin is a proinflammatory mediator that induces the production of TNF-α, IL-1, IL-6, IL-8, and MMPs, which are typical manifestations of RA joint inflammation (Brentano et al., 2007). Similarly, adiponectin stimulated fibroblast-like synoviocytes (FLS) in patients with RA to produce IL-6, IL-8, and PGE2 (Choi et al., 2009; Lee and Bae, 2018). In addition, adiponectin increased the production of VEGF and MMPs in RA FLS, which may induce inflammation and joint destruction (Lee et al., 2014; Choi et al., 2020; **Figure 1**).

Previous studies have shown that the frequency of circulating T follicular helper cells (Tfh) is significantly increased in RA patients, which is positively correlated with disease activity and anti-CCP autoantibody levels (Liu et al., 2012, 2015). RA FLSs stimulated by AD (adiponectin) promoted the production of Tfh cells. In addition, intra-articular injection of AD aggravated synovitis and increased the frequency of Tfh cells in CIA mice treated with AD (Nurieva et al., 2008; Liu et al., 2020).

Obesity is not only prevalent in RA patients, but also associated with disease activity. Obesity reduces the chance of RA remission and negatively affects disease activity and outcomes reported by patients during treatment (Liu et al., 2017). Lee and Bae (2018) observed that the levels of circulating adiponectin and visfatin in RA patients were significantly higher than those in the control group. The levels of visfatin in 28 joints were positively correlated with disease activity score and CRP level (Lee and Bae, 2018).

OBESITY TYPE AND BONE

On the one hand, obesity is divided into peripheral obesity and abdominal obesity according to the distribution of fat in the body. Abdominal fat is made up of abdominal wall fat (SAT) and abdominal fat (VAT), also known as central obesity, visceral obesity. Previous studies have shown that adipokins are associated with bone metabolism, and that central obesity can lead to osteopenia or OP because bone density decreases with an increase in waist-to-hip ratio, an index of central obesity (Mitsuyo et al., 2007). In one study, whole body bone mineral content was positively correlated with HOMA-IR and negatively correlated with the percentage of trunk fat, which is a good representative of visceral fat, suggesting that abdominal obesity may have an adverse effect on systemic bone parameters (Krishnan et al., 2018).

Local fat is increasingly recognized as a determinant of bone density, and this association may be mediated by adipocytokines (Vicente et al., 2009). Russell et al. (2010) proposed that VAT was a negative predictor of spine BMD, apparent BMD, systemic BMD and bone mineral content for obese adolescent girls aged 12–18 years (Katzmarzyk et al., 2012). Importantly, VAT/SAT, adipokines, cytokines, E-selectin, and adiponectin were negative predictors of bone density, while leptin was positive. Consequently, VAT is an independent negative determining factor of bone density in obesity (Jurimae et al., 2008; Agbaht et al., 2009; Russell et al., 2010; Bredella et al., 2011a).

On the other hand, according to the different obesity phenotypes, it can be divided into normal metabolic healthy BMI, metabolic healthy obesity and metabolic abnormal obesity (Karelis et al., 2004; Dobson et al., 2016). Marques Loureiro et al. (2019) observed significantly increased deficiencies of calcium, phosphorus, vitamin D, and PTH in the metabolically unhealthy obese (MUHO) group compared to the metabolically healthy obese (MHO) group. In summary, the MUHO phenotype presents a higher risk of bone metabolism-related changes, which may contribute to the development of metabolic bone disease (Marques Loureiro et al., 2019; **Figure 2**).

DIFFERENT POPULATIONS WITH OBESITY AND BONE

Children and Adolescents

While childhood obesity has always been a major health problem, its prevalence has been on the rise. In addition, childhood obesity may be associated with multiple complications, such as hyperinsulinemia, hypertension, MS, and non-alcoholic fatty liver disease (NAFLD; Oh et al., 2016). Childhood obesity may affect the growth patterns of children and adolescents, according to several studies Children influenced by obesity may develop accelerated skeletal maturity and advanced bone age beyond their actual age (Johnson et al., 2012; Marcovecchio and Chiarelli, 2013). A study of 232 children (aged 6–15 years) found that the prevalence of advanced bone age increased significantly with increased body weight, height, BMI, and waist circumference percentiles (Oh et al., 2020).

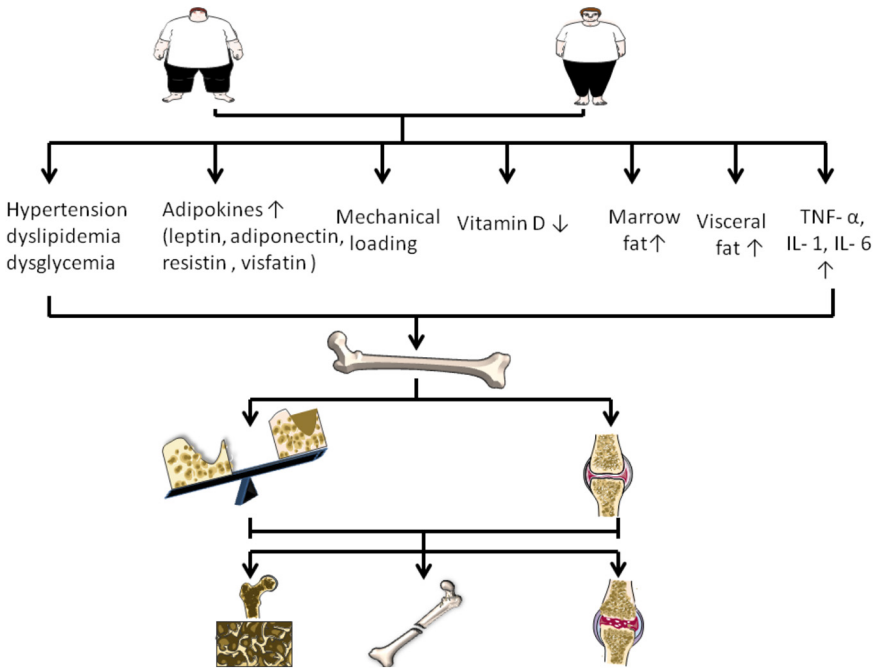


FIGURE 1 | Changes of various factors caused by obesity on the regulation of bone disease. Obesity can increase mechanical load, visceral fat and bone marrow fat. In addition, obesity is associated with increased adipokines, increased TNF – or, IL-1, IL- 6, decreased vitamin D, and accompanied by hypertension, dyslipidemia, and dysglycemia. They regulate bone disease by affecting bone formation, bone resorption, and cartilage.

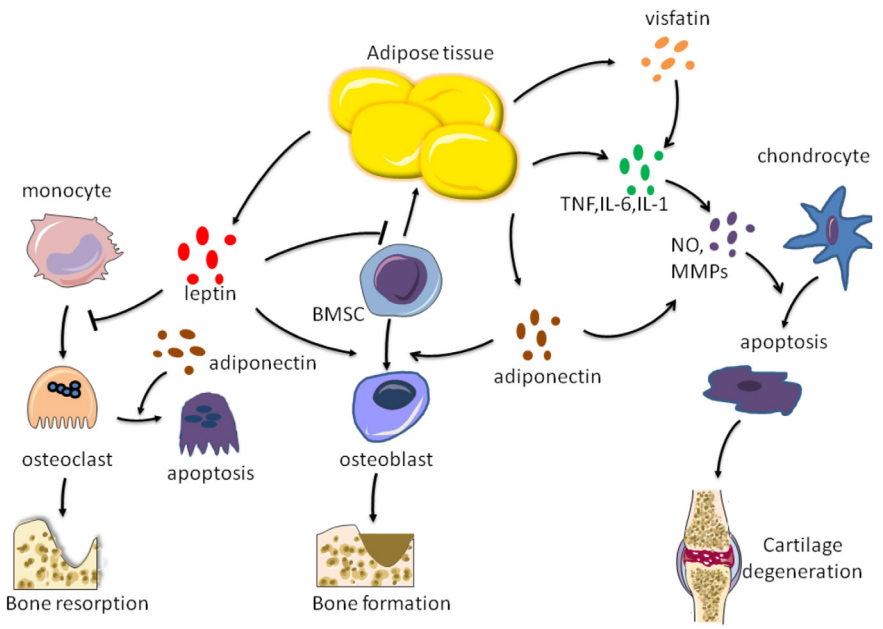


FIGURE 2 | Effects of factors secreted by adipose tissue on bone metabolism. Adipose tissue can secrete leptin, adiponectin, visfatin, TNF-*a,* IL-6, and IL-1 These factors act on chondrocytes, osteoblasts, osteoclasts, respectively, to regulate bone formation and resorption, as well as cartilage degradation.

Instead, a study of young people with an average age of 10–17 confirmed that obese children and adolescents had higher bone mass and density than their normal-weight peers (Chaplais et al., 2018).

Notably, Zhao et al. (2020) recently found that obesity had no benefit for BMD in Chinese children aged 0-5 years. t BMD was positively correlated with age, height/length, and inversely with BMI. The BMD gradually increased in the range within 21.2kg,

but began to gain slowly and even decreased when the body weight exceeded 21.2kg (Zhao et al., 2020).

As noted above, although there have been several studies on the effects of fat mass on skeletal health in normal weight and obese adolescents, the results remain controversial.

Postmenopausal Women

Osteoporosis is considered a major public health problem for postmenopausal women. Low estrogen levels lead to rapid bone loss in women five to seven years after menopause (Kanis et al., 2008). Actually, some evidences, indicated that age and BMI were important factors influencing BMD. The BMD of obese postmenopausal women was higher than that of normal size women, and the reduction of BMD of obese women can be delayed by weight bearing (Méndez et al., 2013).

At the same time, Cherif et al. also observed that the left femur, right femur, total hip joint, and overall bone density were higher in obese women (Cherif et al., 2018).

In addition, adipokines secreted by fat are considered as potential pathophysiological factors of OP. Several studies have shown that leptin has significant effects on bone growth and bone metabolism through central and peripheral pathways, and may be involved in the occurrence of various bone diseases (Chen and Yang, 2015). Studies have shown a positive correlation between leptin levels and BMI. And higher BMI is associated with higher bone density. However, obesity had no effect on adiponectin and resistin secretion in postmenopausal women with OP, so leptin was the only one of the adipokines studied to be considered as a protective factor for bone tissue in postmenopausal women (Pasco et al., 2001; Glogowska-Szelag et al., 2019).

Thus, the above results indicate that, adiposity may be beneficial to bone density in postmenopausal women. The protective effect of high body weight and BMI may be due to hormonal influences in the body. Postmenopausal women affected by obesity have more adipose tissue and more estrogen conversion, resulting in higher estrogen levels in their bodies.

Elderly Patients With Obesity

Obesity, sarcopenia, and OP are common chronic diseases in the elderly. Sarcopenia is a newly discovered age-related disease related to lipid metabolism and insulin resistance. The main diagnostic criteria for sarcopenia are reduced skeletal muscle mass, muscle strength, and function. Older people continue to lose muscle mass as they age, while body fat, especially visceral fat, tends to rise, known as "sarcopenic obesity" (SO; Stenholm et al., 2008; Arango-Lopera et al., 2013). A recent study found that women with SO were more easy to show elevated blood glucose, while men with SO were more likely to present with OP and dyslipidemia (Du et al., 2019). On the other hand, muscles secrete a set of cytokines called myokines, thereby regulating bone metabolism. Myostatin, as a key myokine, has been reported for its effect on bone. Myostatin can inhibit osteogenic differentiation of BMSCs, as well as osteoblast differentiation and mineralization (Hamrick et al., 2007; Chen et al., 2017). Likewise, myostatin may inhibit osteogenesis by activating the RANKL signaling pathway, thus showing an adverse impact on bone mass (Saad, 2020). In addition, myostatin itself is an important autocrine/paracrine factor that inhibits skeletal muscle growth (Rodriguez et al., 2014; Cui et al., 2020). Thus, inhibition or blocking of the myostatin signaling pathway may provide potential therapeutic targets for a number of diseases, particularly in sarcopenia and OP.

Several studies have reported the links between BMD and body fat and lean mass. When body weight was stratified into lean body mass and fat mass, the increase in BMD was more pronounced for lean body mass, whereas fat mass was only beneficial for men and premenopausal women. Santos et al. also observed a more direct relationship between lean body mass and bone density (total bone density, femur, and spine), while sarcopenia was associated with OP. Obesity was more likely to be a protective factor for OP in old subjects aged 80 and over (Santos et al., 2018). At the same time, Barrera et al. demonstrated the beneficial effects of high BMI on femoral neck bone density in older adults. Men and women with a BMI of more than 30 kg/m^2 had about a 33% risk of bone mass loss compared to those with a normal BMI (Barrera et al., 2004). In particular, obese people were reported to have higher bone density, but they also showed damaged bone microstructures and different fall patterns (Compston, 2013; Ilich et al., 2016).

HIGH-FAT DIET INDUCED OBESITY AND BONE

Conclusions about the relationship between obesity and bone in humans rely on statistical correlations or models, rather than controlled trials. Therefore, the establishment of obesity mouse model is helpful to study the effect of high-fat diet (HFD)-induced obesity on bone metabolism. Studies have shown that obese animals burn the same amount of energy, no matter how much fat is in their diet (Brown et al., 2003; Tortoriello et al., 2004; Relling et al., 2006). The mice provided a model for studying the relationship between body size, obesity and skeletal characteristics. High fat intake in rodents leads to obesity, and several studies have shown a strong link between bone size, strength and body size. However, mice are not always reliable indicators of human pathophysiology. Human can enjoy more colorful life style, more abundant food and more complicated living environment. Moreover, patients with obesity often have multiple complications, not just weight gain. These factors make the relationship between obesity and bone more complex in humans than in mice.

Cancellous Bone

The effects of a high-fat diet on cancellous bone in rodents have been shown to be harmful. Previous studies have reported that after 4, 8, and 12 weeks of HFD treatment, the trabecular density of 6-week-old male C57BL/6J mice decreased with the increase of adipocytes and trabecular degeneration. In addition, in obese mice, serum leptin levels were associated with bone trabeculae, but not cortical bone density, while adiponectin and total cholesterol levels were not associated with bone mass (Fujita et al., 2012). Scheller et al. (2016) also noted that bone trabecular volume fraction, bone mineral content, and quantity decreased after 12, 16, or 20 weeks of high-fat feeding compared

with normal rat chow (ND) controls, and only partial recovery after weight loss.

In addition, Inzana et al. (2013) found that femoral cancellous metaphyseal bones were more susceptible to adverse effects of high-fat diet before bone maturation, and had poor recovery ability after dietary correction (low-fat diet, LFD).

A recent study conducted by Tian et al. showed that the bone mass of femoral trabecular bone in C57BL/6J mice increased significantly after 8 weeks of HFD, but decreased significantly at 16 and 24 weeks (Tian et al., 2017). In other words, after short-term feeding, HFD may show a positive effect on bone mass, however, after long-term feeding, bone mass was significantly decreased in HFD mice.

Cortical Bone

However, the effects of diet induced obesity on cortical bone in rodents are less clear, with positive, negative, and neutral results reported. The femoral cortical thickness and cross-sectional area of 4-week old male mice were increased after feeding HFD-DAG (Diacylglycerol). HFD-DAG had obvious promoting effect on bone and bone metabolism (Choi et al., 2015). In addition, Silva et al. recently suggested that a high-fat diet had beneficial effects on most femoral size and skeletal mechanical properties, as well as radius size and stiffness (Silva et al., 2019). However, Ionova-Martin et al. found that femur strength, hardness, and toughness were significantly lower in both young and adult mice fed HFD than in the control group (Ionova-Martin et al., 2011).

In contrast, Cao et al. concluded that feeding mice HFD for 14 weeks reduced proximal tibial cancellous bone mass in young mice, but had no effect on cortical bone mass (Cao et al., 2009). Halade et al. (2011) also revealed that mice fed corn oil (CO) for 6 months showed a 66% reduction in distal femoral trabecular volume fraction, with no significant effect on cortical bone. To sum up, in the above studies, the effect of HFD on cortical bone was not as significant as that on cancellous bone.

It is generally believed that age-related OP has three main processes. The first and most important process is reduction of trabecular bone, the second is continuous bone resorption on the cortical surface, and the third is cortical bone loss (Chen et al., 2009). Similarly, the above studies indicate that the most significant change in obesity-related bone loss is the reduction of femoral trabecular bone Combined, these results suggest that HFD could regulate the changes of trabecular and cortical bone in different ways. This may be due to the fact that cancellous bone generally responds more strongly to diet or drug therapy, physiological conditions, or aging than cortical bone, because cancellous bone is more active in remodeling because of its larger surface to volume ratio than cortical bone (Morgan et al., 2008). On the other hand, bearing capacity and mechanical stress are important factors in determining cortical bone mass, while trabecular bone density is affected by sex maturation related hormones (Mora et al., 1994).

Bone Formation/Resorption

In addition to affecting bone structure, HFD can also have significant effects on cell function. Bone mass reflects the balance between bone formation and bone resorption and is involved in the coordination and regulation of the number and activity of osteoblasts and osteoclasts at the cellular level. The RANKL/RANK/OPG signaling pathway plays a major role in this regulation. A previous study showed that the expression of RANKL, the ratio of RANKL to OPG, and the level of serum TRAP in osteoblasts from HFD mice were increased, suggesting that HFD can promote osteoclast activity and bone resorption (Cao et al., 2009). Notably, Halade et al. reported that in mice fed HFD, the accumulation of bone marrow adipocytes resulted in significantly higher levels of pro-inflammatory factors, leading to increased bone resorption. In addition, increased expression of osteoclast-specific cathepsin K and RANKL and decreased osteoblast-specific RUNX2/Cbfa1 in CO-feeding mice also supported bone resorption (Halade et al., 2011).

Furthermore, Shu et al. (2015) revealed that the lower trabecular volume, but increased osteoclast numbers could be found in the femoral metaphyseal sections of HFD-fed mice after 3, 6, and 12 weeks. The elevated osteoclast precursor frequency, increased osteoclast formation, and bone resorption activity, along with increased osteoclastogenic regulators such as RANKL, TNF, and PPARγ were seen in bone marrow cells from HFD-fed mice. But, osteoblast function was also increased after 12 weeks of HFD (Shu et al., 2015). A possible explanation is that mechanical load of body weight stimulates bone formation, reduces apoptosis, and enhances proliferation and differentiation of osteoblasts and osteocytes. Therefore, it was not surprising that bone formation rates and osteoblast numbers increased in this study, since HFD mice were significantly heavier than the control group (Bonewald and Johnson, 2008). In conclusion, it is reasonable to believe that the bone loss caused by HFD is mainly related to the promotion of osteoclast differentiation and activity by changing the bone marrow microenvironment.

Based on these findings, the effect of HFD is bipolar and may be the result of a combination of body weight, fat mass, bone formation/absorption, pro-inflammatory mediators and bone marrow microenvironment. Obesity initially has a beneficial effect on bones, possibly due to anabolic effects that increase mechanical load. However, due to the development of metabolic complications including systemic inflammation, the second stage is followed by a reduction in bone formation (Lecka-Czernik et al., 2015). As mentioned above, these results may support the idea that as obesity rises, the benefits for bone health are diminishing.

CONCLUSION

In conclusion, obesity or overweight is strictly related to bone metabolism, although the correlation has not yet been fully unified. Adipose tissue interacts with bone by secreting various cytokines, so as to regulate bone health. Meanwhile BMAT also exerts a crucial impact on bone density and bone microstructure. In addition, human obesity is a complex problem that involves not only excessive fat intake but also other nutrient consumption imbalances such as vitamin D, calcium and phosphorus, which are known to affect bone metabolism, further making it difficult to determine the impact of obesity on human bone health.

Moreover, while BMI is closely related to the gold standard of body fat, it does not distinguish between lean and fat mass, nor does it provide an indication of the distribution of body fat. The loss of muscle mass in the elderly means that BMI is also less accurate at predicting body fat in this group. Therefore, determining whether obesity causes changes in bone mass based on BMI is less accurate. Central obesity measures, including waist circumference, waist-to-height ratio and waist-to-hip ratio, are better predictors of visceral obesity, bone-related disease and mortality than BMI. Simply put, all of these findings indicate that skeletal response to obesity has either a positive or negative effect on bone, suggesting that the influence of obesity on bone metabolism is intricate and depend on diverse factors, such as mechanical load by the weight, obesity type, the location of adipose tissue, gender, age, and bone sites, along with secreted cytokines, these factors may play a major function for bone health. The effects of obesity on bone metabolism and bone microstructure involve these multiple factors, which may exert different regulatory mechanisms and ultimately affect the skeletal health. The investigation of the relationship between obesity and bone is conducive to finding new targets for the treatment of bone-related diseases, including OP, fractures, RA, and OA.

AUTHOR CONTRIBUTIONS

JH wrote the manuscript. CH, WH, and MY revised the manuscript. CL and XL were responsible for the guidance and supervision. All authors contributed to the article and approved the submitted version.

FUNDING

This work was supported by the National Key R&D Program of China (grant 2019YFA0111900), the National Natural Science Foundation of China (grants 81922017, 81873669, and 81802209), the Hunan Province Natural Science Foundation of China (grant 2018JJ3863), the Innovation Driven Project of Central South University (grant 20170033010017), and the Talent Plan of Xiangya Hospital in Central South University (grants 35 and 41).

REFERENCES

Agbaht, K., Gurlek, A., Karakaya, J., and Bayraktar, M. (2009). Circulating adiponectin represents a biomarker of the association between adiposity and bone mineral density. *Endocrine* 35, 371–379. doi: 10.1007/s12020-009-9158-2

Al Saedi, A., Goodman, A. C., Myers, D. E., Hayes, A., and Duque, G. (2020). Rapamycin affects palmitate-induced lipotoxicity in osteoblasts by modulating apoptosis and autophagy. *J. Gerontol. A Biol. Sci. Med. Sci.* 75, 58–63. doi: 10.1093/gerona/glz149

Alissa, E. M., Alzughaibi, L. S., and Marzouki, Z. M. (2020). Relationship between serum resistin, body fat and inflammatory markers in females with clinical knee osteoarthritis. *Knee* 27, 45–50. doi: 10.1016/j.knee.2019.12.009

Arango-Lopera, V. E., Arroyo, P., Gutierrez-Robledo, L. M., Perez-Zepeda, M. U., and Cesari, M. (2013). Mortality as an adverse outcome of sarcopenia. *J. Nutr. Health Aging* 17, 259–262. doi: 10.1007/s12603-012-0434-0

Ardawi, M. S., Akhbar, D. H., Alshaikh, A., Ahmed, M. M., Qari, M. H., Rouzi, A. A., et al. (2013). Increased serum sclerostin and decreased serum IGF-1 are associated with vertebral fractures among postmenopausal women with type-2 diabetes. *Bone* 56, 355–362. doi: 10.1016/j.bone.2013.06.029

Astudillo, P., Ríos, S., Pastenes, L., Pino, A. M., and Rodríguez, J. P. (2007). Increased adipogenesis of osteoporotic human-mesenchymal stem cells (MSCs) characterizes by impaired leptin action . *J. Cell. Biochem.* 103, 1054–1065. doi: 10.1002/jcb.21516

Baggio, L. L., and Drucker, D. J. (2007). Biology of incretins: GLP-1 and GIP. *Gastroenterology* 132, 2131–2157. doi: 10.1053/j.gastro.2007.03.054

Bao, J. P., Chen, W. P., Feng, J., Hu, P. F., Shi, Z. L., and Wu, L. D. (2010). Leptin plays a catabolic role on articular cartilage. *Mol. Biol. Rep.* 37, 3265–3272. doi: 10.1007/s11033-009-9911-x

Barba, C., Cavalli-Sforza, T., Cutter, J., Darnton-Hill, I., Deurenberg, P., Deurenberg-Yap, M., et al. (2004). Appropriate body-mass index for Asian populations and its implications for policy and intervention strategies. *Lancet* 363, 157–163. doi: 10.1016/s0140-6736(03)15268-3

Barrera, G., Bunout, D., Gattas, V., de la Maza, M. P., Leiva, L., and Hirsch, S. (2004). A high body mass index protects against femoral neck osteoporosis in healthy elderly subjects. *Nutrition* 20, 769–771. doi: 10.1016/j.nut.2004.05.014

Bartell, S. M., Rayalam, S., Ambati, S., Gaddam, D. R., Hartzell, D. L., Hamrick, M., et al. (2011). Central (ICV) leptin injection increases bone formation, bone mineral density, muscle mass, serum IGF-1, and the expression of osteogenic genes in leptin-deficient ob/ob mice. *J. Bone Miner. Res.* 26, 1710–1720. doi: 10.1002/jbmr.406

Beekman, K. M., Zwaagstra, M., Veldhuis-Vlug, A. G., van Essen, H. W., den Heijer, M., Maas, M., et al. (2019). Ovariectomy increases RANKL protein expression in bone marrow adipocytes of C3H/HeJ mice. *Am. J. Physiol. Endocrinol. Metab.* 317, E1050–E1054.

Bijlsma, J. W. J., Berenbaum, F., and Lafeber, F. P. J. G. (2011). Osteoarthritis: an update with relevance for clinical practice. *Lancet* 377, 2115–2126. doi: 10.1016/s0140-6736(11)60243-2

Bonewald, L. F., and Johnson, M. L. (2008). Osteocytes, mechanosensing and Wnt signaling. *Bone* 42, 606–615. doi: 10.1016/j.bone.2007.12.224

Boon, M. R., van den Berg, S. A., Wang, Y., van den Bossche, J., Karkampouna, S., Bauwens, M., et al. (2013). BMP7 activates brown adipose tissue and reduces diet-induced obesity only at subthermoneutrality. *PLoS One* 8:e74083. doi: 10.1371/journal.pone.0074083

Borges, J. L., Bilezikian, J. P., Jones-Leone, A. R., Acusta, A. P., Ambery, P. D., Nino, A. J., et al. (2011). A randomized, parallel group, double-blind, multicentre study comparing the efficacy and safety of Avandamet (rosiglitazone/metformin) and metformin on long-term glycaemic control and bone mineral density after 80 weeks of treatment in drug-naive type 2 diabetes mellitus patients. *Diabetes Obes. Metab.* 13, 1036–1046. doi: 10.1111/j.1463-1326.2011.01461.x

Brandt, K. D. (2006). Yet more evidence that osteoarthritis is not a cartilage disease. *Ann. Rheum. Dis.* 65, 1261–1264. doi: 10.1136/ard.2006.058347

Bredella, M. A., Fazeli, P. K., Miller, K. K., Misra, M., Torriani, M., Thomas, B. J., et al. (2009). Increased bone marrow fat in anorexia nervosa. *J. Clin. Endocrinol. Metab.* 94, 2129–2136. doi: 10.1210/jc.2008-2532

Bredella, M. A., Torriani, M., Ghomi, R. H., Thomas, B. J., Brick, D. J., Gerweck, A. V., et al. (2011a). Determinants of bone mineral density in obese premenopausal women. *Bone* 48, 748–754. doi: 10.1016/j.bone.2010.12.011

Bredella, M. A., Torriani, M., Ghomi, R. H., Thomas, B. J., Brick, D. J., Gerweck, A. V., et al. (2011b). Vertebral bone marrow fat is positively associated with visceral fat and inversely associated with IGF-1 in obese women. *Obesity (Silver Spring)* 19, 49–53. doi: 10.1038/oby.2010.106

Brentano, F., Schorr, O., Ospelt, C., Stanczyk, J., Gay, R. E., Gay, S., et al. (2007). Pre-B cell colony-enhancing factor/visfatin, a new marker of inflammation in rheumatoid arthritis with proinflammatory and matrix-degrading activities. *Arthritis Rheum.* 56, 2829–2839. doi: 10.1002/art.22833

Brown, J. L., Spicer, M. T., and Spicer, L. J. (2003). Effect of high-fat diet on body composition and hormone responses to glucose tolerance tests. *Endocrine* 19, 327–332. doi: 10.1385/endo:19:3:327

Brun, J., Berthou, F., Trajkovski, M., Maechler, P., Foti, M., and Bonnet, N. (2017). Bone regulates browning and energy metabolism through mature osteoblast/osteocyte PPARgamma expression. *Diabetes* 66, 2541–2554. doi: 10.2337/db17-0116

Burguera, B., Hofbauer, L. C., Thomas, T., Gori, F., Evans, G. L., Khosla, S., et al. (2001). Leptin reduces ovariectomy-induced bone loss in rats. *Endocrinology* 142, 3546–3553. doi: 10.1210/endo.142.8.8346

Cao, J. J., and Picklo, M. J. Sr. (2015). Involuntary wheel running improves but does not fully reverse the deterioration of bone structure of obese rats despite decreasing adiposity. *Calcif. Tissue Int.* 97, 145–155. doi: 10.1007/s00223-015-9992-6

Cao, J. J., Gregoire, B. R., and Gao, H. (2009). High-fat diet decreases cancellous bone mass but has no effect on cortical bone mass in the tibia in mice. *Bone* 44, 1097–1104. doi: 10.1016/j.bone.2009.02.017

Carobbio, S., Pellegrinelli, V., and Vidal-Puig, A. (2017). Adipose tissue function and expandability as determinants of lipotoxicity and the metabolic syndrome. *Adv. Exp. Med. Biol.* 960, 161–196. doi: 10.1007/978-3-319-48382-5_7

Chaplais, E., Naughton, G., Greene, D., Dutheil, F., Pereira, B., Thivel, D., et al. (2018). Effects of interventions with a physical activity component on bone health in obese children and adolescents: a systematic review and meta-analysis. *J. Bone Miner. Metab.* 36, 12–30. doi: 10.1007/s00774-017-0858-z

Chen, H., Zhou, X., Emura, S., and Shoumura, S. (2009). Site-specific bone loss in senescence-accelerated mouse (SAMP6): a murine model for senile osteoporosis. *Exp. Gerontol.* 44, 792–798. doi: 10.1016/j.exger.2009.09.009

Chen, X. X., and Yang, T. (2015). Roles of leptin in bone metabolism and bone diseases. *J. Bone Miner. Metab.* 33, 474–485. doi: 10.1007/s00774-014-0569-7

Chen, Y. S., Guo, Q., Guo, L. J., Liu, T., Wu, X. P., Lin, Z. Y., et al. (2017). GDF8 inhibits bone formation and promotes bone resorption in mice. *Clin. Exp. Pharmacol. Physiol.* 44, 500–508. doi: 10.1111/1440-1681.12728

Cherif, R., Mahjoub, F., Sahli, H., Cheour, E., Vico, L., Sakly, M., et al. (2018). Positive Association of Obesity and insulin resistance with bone mineral density in Tunisian postmenopausal women. *J. Clin. Densitom.* 21, 163–171. doi: 10.1016/j.jocd.2017.05.015

Choi, H. M., Doss, H. M., and Kim, K. S. (2020). Multifaceted physiological roles of adiponectin in inflammation and diseases. *Int. J. Mol. Sci.* 21:1219. doi: 10.3390/ijms21041219

Choi, H. M., Lee, Y. A., Lee, S. H., Hong, S. J., Hahm, D. H., Choi, S. Y., et al. (2009). Adiponectin may contribute to synovitis and joint destruction in rheumatoid arthritis by stimulating vascular endothelial growth factor, matrix metalloproteinase-1, and matrix metalloproteinase-13 expression in fibroblast-like synoviocytes more than proinflammatory mediators. *Arthritis Res. Ther.* 11:R161.

Choi, H. S., Park, S. J., Lee, Z. H., and Lim, S. K. (2015). The effects of a high fat diet containing diacylglycerol on bone in C57BL/6J mice. *Yonsei Med. J.* 56, 951–960. doi: 10.3349/ymj.2015.56.4.951

Coelho, M., Oliveira, T., and Fernandes, R. (2013). Biochemistry of adipose tissue: an endocrine organ. *Arch. Med. Sci.* 9, 191–200. doi: 10.5114/aoms.2013.33181

Compston, J. (2013). Obesity and fractures. *Joint Bone Spine* 80, 8–10. doi: 10.1016/j.jbspin.2012.07.016

Compston, J. (2018). Type 2 diabetes mellitus and bone. *J. Intern. Med.* 283, 140–153.

Compston, J. E., Watts, N. B., Chapurlat, R., Cooper, C., Boonen, S., Greenspan, S., et al. (2011). Obesity is not protective against fracture in postmenopausal women: GLOW. *Am. J. Med.* 124, 1043–1050. doi: 10.1016/j.amjmed.2011.06.013

Conde, J., Scotece, M., Gomez, R., Lopez, V., Gomez-Reino, J. J., and Gualillo, O. (2011). Adipokines and osteoarthritis: novel molecules involved in the pathogenesis and progression of disease. *Arthritis* 2011:203901.

Cui, Y., Yi, Q., Sun, W., Huang, D., Zhang, H., Duan, L., et al. (2020). Molecular basis and therapeutic potential of myostatin on bone formation and metabolism in orthopedic disease. *Biofactors* 71, 4361–4371.

Dalamaga, M., and Christodoulatos, G. S. (2015). Adiponectin as a biomarker linking obesity and adiposopathy to hematologic malignancies. *Horm. Mol. Biol. Clin. Investig.* 23, 5–20.

de Araujo, I. M., Salmon, C. E., Nahas, A. K., Nogueira-Barbosa, M. H., Elias, J. Jr., and de Paula, F. J. (2017). Marrow adipose tissue spectrum in obesity and type 2 diabetes mellitus. *Eur. J. Endocrinol.* 176, 21–30. doi: 10.1530/eje-16-0448

De Laet, C., Kanis, J. A., Oden, A., Johanson, H., Johnell, O., Delmas, P., et al. (2005). Body mass index as a predictor of fracture risk: a meta-analysis. *Osteoporos. Int.* 16, 1330–1338.

Del Mar Gonzalez-Barroso, M., Ricquier, D., and Cassard-Doulcier, A. M. (2001). The human uncoupling protein−1 gene (UCP1): present status and perspectives in obesity research. *Obes. Rev.* 1, 61–72. doi: 10.1046/j.1467-789x.2000.00009.x

Di Angelantonio, E., Bhupathiraju, S. N., Wormser, D., Gao, P., Kaptoge, S., de Gonzalez, A. B., et al. (2016). Body-mass index and all-cause mortality: individual-participant-data meta-analysis of 239 prospective studies in four continents. *Lancet* 388, 776–786.

Ding, C. (2011). Metabolic triggered inflammation in osteoarthritis. *Osteoarthritis Cartilage* 41, 90–91. doi: 10.1016/j.semarthrit.2011.06.009

Dobson, R., Burgess, M. I., Sprung, V. S., Irwin, A., Hamer, M., Jones, J., et al. (2016). Metabolically healthy and unhealthy obesity: differential effects on myocardial function according to metabolic syndrome, rather than obesity. *Int. J. Obes. (Lond.)* 40, 153–161. doi: 10.1038/ijo.2015.151

Dormuth, C. R., Carney, G., Carleton, B., Bassett, K., and Wright, J. M. (2009). Thiazolidinediones and fractures in men and women. *Arch. Intern. Med.* 169, 1395–1402. doi: 10.1001/archinternmed.2009.214

Du, Y., Wang, X., Xie, H., Zheng, S., Wu, X., Zhu, X., et al. (2019). Sex differences in the prevalence and adverse outcomes of sarcopenia and sarcopenic obesity in community dwelling elderly in East China using the AWGS criteria. *BMC Endocr. Disord.* 19:109. doi: 10.1186/s12902-019-0432-x

Ducy, P., Amling, M., Takeda, S., Priemel, M., Schilling, A. F., Beil, F. T., et al. (2000). Leptin inhibits bone formation through a hypothalamic relay: a central control of bone mass. *Cell* 100, 197–207. doi: 10.1016/s0092-8674(00)81558-5

Elbaz, A., Wu, X., Rivas, D., Gimble, J. M., and Duque, G. (2010). Inhibition of fatty acid biosynthesis prevents adipocyte lipotoxicity on human osteoblasts in vitro. *J. Cell. Mol. Med.* 14, 982–991. doi: 10.1111/j.1582-4934.2009.00751.x

Fassio, A., Idolazzi, L., Rossini, M., Gatti, D., Adami, G., Giollo, A., et al. (2018). The obesity paradox and osteoporosis. *Eat. Weight Disord.* 23, 293–302.

Fazeli, P. K., Bredella, M. A., Freedman, L., Thomas, B. J., Breggia, A., Meenaghan, E., et al. (2012). Marrow fat and preadipocyte factor-1 levels decrease with recovery in women with anorexia nervosa. *J. Bone Miner. Res.* 27, 1864–1871. doi: 10.1002/jbmr.1640

Fazeli, P. K., Faje, A. T., Bredella, M. A., Polineni, S., Russell, S., Resulaj, M., et al. (2019). Changes in marrow adipose tissue with short-term changes in weight in premenopausal women with anorexia nervosa. *Eur. J. Endocrinol.* 180, 189–199. doi: 10.1530/eje-18-0824

Fazeli, P. K., Faje, A. T., Cross, E. J., Lee, H., Rosen, C. J., Bouxsein, M. L., et al. (2015). Serum FGF-21 levels are associated with worsened radial trabecular bone microarchitecture and decreased radial bone strength in women with anorexia nervosa. *Bone* 77, 6–11. doi: 10.1016/j.bone.2015.04.001

Fazeli, P. K., Horowitz, M. C., MacDougald, O. A., Scheller, E. L., Rodeheffer, M. S., Rosen, C. J., et al. (2013). Marrow fat and bone–new perspectives. *J. Clin. Endocrinol. Metab.* 98, 935–945.

Felson, D. T., and Chaisson, C. E. (1997). Understanding the relationship between body weight and osteoarthritis. *Baillieres Clin. Rheumatol.* 11, 671–681. doi: 10.1016/s0950-3579(97)80003-9

Felson, T. (2010). Effect of weight and body mass index on bone mineral density in men and women: the Framingham study. *J. Bone Miner. Res.* 8, 567–573. doi: 10.1002/jbmr.5650080507

Feng, X., Xu, X., Shi, Y., Liu, X., Liu, H., Hou, H., et al. (2019). Body mass index and the risk of rheumatoid arthritis: an updated dose-response meta-analysis. *Biomed. Res. Int.* 2019:3579081.

Ferron, M., Wei, J., Yoshizawa, T., Fattore, A. Del, DePinho, R. A., Teti, A., et al. (2010). Insulin signaling in osteoblasts integrates bone remodeling and energy metabolism. *Cell* 142, 296–308. doi: 10.1016/j.cell.2010.06.003

Frontini, A., and Cinti, S. (2010). Distribution and development of brown adipocytes in the murine and human adipose organ. *Cell Metab.* 11, 253–256. doi: 10.1016/j.cmet.2010.03.004

Fruhbeck, G., Gomez-Ambrosi, J., Muruzabal, F. J., and Burrell, M. A. (2001). The adipocyte: a model for integration of endocrine and metabolic signaling in energy metabolism regulation. *Am. J. Physiol. Endocrinol. Metab.* 280, E827–E847.

Fujita, Y., Watanabe, K., and Maki, K. (2012). Serum leptin levels negatively correlate with trabecular bone mineral density in high-fat diet-induced obesity mice. *J. Musculoskelet. Neuronal Interact.* 12, 84–94.

Gimble, J. M., Robinson, C. E., Wu, X., Kelly, K. A., Rodriguez, B. R., Kliewer, S. A., et al. (1996). Peroxisome proliferator-activated receptor-gamma activation by thiazolidinediones induces adipogenesis in bone marrow stromal cells. *Mol. Pharmacol.* 50, 1087–1094.

Glogowska-Szelag, J., Kos-Kudla, B., Marek, B., Nowak, M., and Sieminska, L. (2019). Assessment of selected adipocytokines in obese women with postmenopausal osteoporosis. *Endokrynol. Pol.* 70, 478–483. doi: 10.5603/ep.a2019.0043

Gordeladze, J. O., Drevon, C. A., Syversen, U., and Reseland, J. E. (2002). Leptin stimulates human osteoblastic cell proliferation, de novo collagen synthesis, and mineralization: impact on differentiation markers, apoptosis, and osteoclastic signaling. *J. Cell. Biochem.* 85, 825–836. doi: 10.1002/jcb.10156

Gremese, E., Tolusso, B., Gigante, M. R., and Ferraccioli, G. (2014). Obesity as a risk and severity factor in rheumatic diseases (autoimmune chronic inflammatory diseases). *Front. Immunol.* 5:576. doi: 10.3389/fimmu.2014.00576

Grotle, M., Hagen, K. B., Natvig, B., Dahl, F. A., and Kvien, T. K. (2008). Obesity and osteoarthritis in knee, hip and/or hand: an epidemiological study in the general population with 10 years follow-up. *BMC Musculoskelet. Disord.* 9:132. doi: 10.1186/1471-2474-9-132

Halade, G. V., Jamali, A. El, Williams, P. J., Fajardo, R. J., and Fernandes, G. (2011). Obesity-mediated inflammatory microenvironment stimulates osteoclastogenesis and bone loss in mice. *Exp. Gerontol.* 46, 43–52. doi: 10.1016/j.exger.2010.09.014

Hamrick, M. W., Della-Fera, M. A., Choi, Y. H., Pennington, C., Hartzell, D., and Baile, C. A. (2005). Leptin treatment induces loss of bone marrow adipocytes and increases bone formation in leptin-deficient ob/ob mice. *J. Bone Miner. Res.* 20, 994–1001. doi: 10.1359/jbmr.050103

Hamrick, M. W., Pennington, C., Newton, D., Xie, D., and Isales, C. (2004). Leptin deficiency produces contrasting phenotypes in bones of the limb and spine. *Bone* 34, 376–383. doi: 10.1016/j.bone.2003.11.020

Hamrick, M. W., Shi, X., Zhang, W., Pennington, C., Thakore, H., Haque, M., et al. (2007). Loss of myostatin (GDF8) function increases osteogenic differentiation of bone marrow-derived mesenchymal stem cells but the osteogenic effect is ablated with unloading. *Bone* 40, 1544–1553. doi: 10.1016/j.bone.2007.02.012

Hao, R. H., Gao, J. L., Li, M., Huang, W., Zhu, D. L., Thynn, H. N., et al. (2018). Association between fibroblast growth factor 21 and bone mineral density in adults. *Endocrine* 59, 296–303. doi: 10.1007/s12020-017-1507-y

Hardouin, P., Rharass, T., and Lucas, S. (2016). Bone marrow adipose tissue: to be or not to be a typical adipose tissue? *Front. Endocrinol. (Lausanne)* 7:85. doi: 10.3389/fendo.2016.00085

Holloway, W. R., Collier, F. M., Aitken, C. J., Myers, D. E., Hodge, J. M., Malakellis, M., et al. (2002). Leptin inhibits osteoclast generation. *J. Bone Miner. Res.* 17, 200–209. doi: 10.1359/jbmr.2002.17.2.200

Horowitz, M. C., Berry, R., Holtrup, B., Sebo, Z., Nelson, T., Fretz, J. A., et al. (2017). Bone marrow adipocytes. *Adipocyte* 6, 193–204.

Huang, C. Y., Lee, C. Y., Chen, M. Y., Tsai, H. C., Hsu, H. C., and Tang, C. H. (2010). Adiponectin increases BMP-2 expression in osteoblasts via AdipoR receptor signaling pathway. *J. Cell. Physiol.* 224, 475–483. doi: 10.1002/jcp.22145

Huang, Y., Xiao, Y., Liu, Y., Guo, M., Guo, Q., Zhou, F., et al. (2020). MicroRNA-188 regulates aging-associated metabolic phenotype. *Aging Cell* 19:e13077.

Hunter, D. J., and Bierma-Zeinstra, S. (2019). Osteoarthritis. *Lancet* 393, 1745–1759.

Ilich, J. Z., Kelly, O. J., and Inglis, J. E. (2016). Osteosarcopenic obesity syndrome: what is it and how can it be identified and diagnosed? *Curr. Gerontol. Geriatr. Res.* 2016:7325973.

Ilich, J. Z., Kelly, O. J., Inglis, J. E., Panton, L. B., Duque, G., and Ormsbee, M. J. (2014). Interrelationship among muscle, fat, and bone: connecting the dots on cellular, hormonal, and whole body levels. *Ageing Res. Rev.* 15, 51–60. doi: 10.1016/j.arr.2014.02.007

Inzana, J. A., Kung, M., Shu, L., Hamada, D., Xing, L. P., Zuscik, M. J., et al. (2013). Immature mice are more susceptible to the detrimental effects of high fat diet on cancellous bone in the distal femur. *Bone* 57, 174–183. doi: 10.1016/j.bone.2013.08.003

Ionova-Martin, S. S., Wade, J. M., Tang, S., Shahnazari, M., Ager, J. W. III, Lane, N. E., et al. (2011). Changes in cortical bone response to high-fat diet from adolescence to adulthood in mice. *Osteoporos. Int.* 22, 2283–2293. doi: 10.1007/s00198-010-1432-x

Johansson, A. G., Lindh, E., and Ljunghall, S. (1992). Insulin-like growth factor I stimulates bone turnover in osteoporosis. *Lancet* 339:1619. doi: 10.1016/0140-6736(92)91889-g

Johnson, W., Stovitz, S. D., Choh, A. C., Czerwinski, S. A., Towne, B., and Demerath, E. W. (2012). Patterns of linear growth and skeletal maturation from birth to 18 years of age in overweight young adults. *Int. J. Obes. (Lond.)* 36, 535–541.

Jurimae, J., Jurimae, T., Leppik, A., and Kums, T. (2008). The influence of ghrelin, adiponectin, and leptin on bone mineral density in healthy postmenopausal women. *J. Bone Miner. Metab.* 26, 618–623. doi: 10.1007/s00774-008-0861-5

Justesen, J., Stenderup, K., Ebbesen, E. N., Mosekilde, L., Steiniche, T., and Kassem, M. (2001). Adipocyte tissue volume in bone marrow is increased with aging and in patients with osteoporosis. *Biogerontology* 2, 165–171.

Kahn, S. E., Haffner, S. M., Heise, M. A., Herman, W. H., Holman, R. R., Jones, N. P., et al. (2006). Glycemic durability of rosiglitazone, metformin, or glyburide monotherapy. *N. Engl. J. Med.* 355, 2427–2443. doi: 10.1056/nejmoa066224

Kalichman, L., and Kobyliansky, E. (2009). Hand osteoarthritis in Chuvashian population: prevalence and determinants. *Rheumatol. Int.* 30, 85–92. doi: 10.1007/s00296-009-0920-9

Kanazawa, I., Notsu, M., Miyake, H., Tanaka, K., and Sugimoto, T. (2018). Assessment using serum insulin-like growth factor-I and bone mineral density is useful for detecting prevalent vertebral fractures in patients with type 2 diabetes mellitus. *Osteoporos. Int.* 29, 2527–2535. doi: 10.1007/s00198-018-4638-y

Kanazawa, I., Yamaguchi, T., and Sugimoto, T. (2011). Serum insulin-like growth factor-I is a marker for assessing the severity of vertebral fractures in postmenopausal women with type 2 diabetes mellitus. *Osteoporos. Int.* 22, 1191–1198. doi: 10.1007/s00198-010-1310-6

Kanazawa, I., Yamaguchi, T., and Sugimoto, T. (2012). Effects of intensive glycemic control on serum levels of insulin-like growth factor-I and dehydroepiandrosterone sulfate in type 2 diabetes mellitus. *J. Endocrinol. Invest.* 35, 469–472.

Kang, D. H., Guo, L. F., Guo, T., Wang, Y., Liu, T., Feng, X. Y., et al. (2015). Association of body composition with bone mineral density in northern Chinese men by different criteria for obesity. *J. Endocrinol. Invest.* 38, 323–331. doi: 10.1007/s40618-014-0167-5

Kang, E. H., Lee, Y. J., Kim, T. K., Chang, C. B., Chung, J. H., Shin, K., et al. (2010). Adiponectin is a potential catabolic mediator in osteoarthritis cartilage. *Arthritis Res. Ther.* 12:R231.

Kanis, J. A., Burlet, N., Cooper, C., Delmas, P. D., Reginster, J. Y., Borgstrom, F., et al. (2008). European guidance for the diagnosis and management of osteoporosis in postmenopausal women. *Osteoporos. Int.* 19, 399–428. doi: 10.1007/s00198-008-0560-z

Karelis, A. D., Brochu, M., and Rabasa-Lhoret, R. (2004). Can we identify metabolically healthy but obese individuals (MHO)? *Diabetes Metab.* 30, 569–572. doi: 10.1016/s1262-3636(07)70156-8

Katzmarzyk, P. T., Barreira, T. V., Harrington, D. M., Staiano, A. E., Heymsfield, S. B., and Gimble, J. M. (2012). Relationship between abdominal fat and bone mineral density in white and African American adults. *Bone* 50, 576–579. doi: 10.1016/j.bone.2011.04.012

Kaye, W. H., Wierenga, C. E., Bischoff-Grethe, A., Berner, L. A., Ely, A. V., Bailer, U. F., et al. (2020). Neural insensitivity to the effects of hunger in women remitted from anorexia nervosa. *Am. J. Psychiatry.* 177, 601–610. doi: 10.1176/appi.ajp.2019.19030261

Khaliq, A., Sayed, S. A., and Mahmood, A. (2016). Evaluating the risk of osteoporosis through bone mass density. *J. Ayub Med. Coll. Abbottabad* 28, 730–733.

Kim, H. Y., Choe, J. W., Kim, H. K., Bae, S. J., Kim, B. J., Lee, S. H., et al. (2010). Negative association between metabolic syndrome and bone mineral density in Koreans, especially in men. *Calcif. Tissue Int.* 86, 350–358. doi: 10.1007/s00223-010-9347-2

Kinoshita, K., Iimuro, Y., Otogawa, K., Saika, S., Inagaki, Y., Nakajima, Y., et al. (2007). Adenovirus-mediated expression of BMP-7 suppresses the development of liver fibrosis in rats. *Gut* 56, 706–714. doi: 10.1136/gut.2006.092460

Kobayashi, H., Giles, J. T., Polak, J. F., Blumenthal, R. S., Leffell, M. S., Szklo, M., et al. (2010). Increased prevalence of carotid artery atherosclerosis in rheumatoid arthritis is artery-specific. *J. Rheumatol.* 37, 730–739. doi: 10.3899/jrheum.090670

Konradsen, S., Ag, H., Lindberg, F., Hexeberg, S., and Jorde, R. (2008). Serum 1,25-dihydroxy vitamin D is inversely associated with body mass index. *Eur. J. Nutr.* 47, 87–91. doi: 10.1007/s00394-008-0700-4

Koskinen, A., Vuolteenaho, K., Nieminen, R., Moilanen, T., and Moilanen, E. (2011). Leptin enhances MMP-1, MMP-3 and MMP-13 production in human

osteoarthritic cartilage and correlates with MMP-1 and MMP-3 in synovial fluid from OA patients. *Clin. Exp. Rheumatol.* 29, 57–64.

Krishnan, S., Anderson, M. P., Fields, D. A., and Misra, M. (2018). Abdominal obesity adversely affects bone mass in children. *World J. Clin. Pediatr.* 7, 43–48. doi: 10.5409/wjcp.v7.i1.43

Lecka-Czernik, B. (2017). Diabetes, bone and glucose-lowering agents: basic biology. *Diabetologia* 60, 1163–1169. doi: 10.1007/s00125-017-4269-4

Lecka-Czernik, B., Stechschulte, L. A., Czernik, P. J., and Dowling, A. R. (2015). High bone mass in adult mice with diet-induced obesity results from a combination of initial increase in bone mass followed by attenuation in bone formation; implications for high bone mass and decreased bone quality in obesity. *Mol. Cell. Endocrinol.* 410, 35–41. doi: 10.1016/j.mce.2015.01.001

Lee, H. W., Sang, Y. K., Kim, A. Y., Lee, E. J., Choi, J. Y., and Kim, J. B. (2009). Adiponectin stimulates osteoblast differentiation through induction of COX2 in mesenchymal progenitor cells. *Stem Cells* 27, 2254–2262. doi: 10.1002/stem.144

Lee, Y. A., Ji, H. I., Lee, S. H., Hong, S. J., Yang, H. I., Yoo, M. Chul, et al. (2014). The role of adiponectin in the production of IL-6, IL-8, VEGF and MMPs in human endothelial cells and osteoblasts: implications for arthritic joints. *Exp. Mol. Med.* 46:e72. doi: 10.1038/emm.2013.141

Lee, Y. H., and Bae, S.-C. (2018). Circulating adiponectin and visfatin levels in rheumatoid arthritis and their correlation with disease activity: a meta-analysis. *Int. J. Rheum. Dis.* 21, 664–672. doi: 10.1111/1756-185x.13038

Li, C. J., Chai, Y., Wang, L., Gao, B., Chen, H., Gao, P., et al. (2017). Programmed cell senescence in skeleton during late puberty. *Nat. Commun.* 8:1312.

Li, C. J., Cheng, P., Liang, M. K., Chen, Y. S., Lu, Q., Wang, J. Y., et al. (2015). MicroRNA-188 regulates age-related switch between osteoblast and adipocyte differentiation. *Sci. Found. China* 125, 22–22.

Li, C. J., Xiao, Y., Yang, M., Su, T., Sun, X., Guo, Q., et al. (2018). Long noncoding RNA Bmncr regulates mesenchymal stem cell fate during skeletal aging. *J. Clin. Invest.* 128, 5251–5266. doi: 10.1172/jci99044

Li, J., Gao, Y., Yu, T., Lange, J. K., LeBoff, M. S., Gorska, A., et al. (2020). Obesity and leptin influence vitamin D metabolism and action in human marrow stromal cells. *J. Steroid. Biochem. Mol. Biol.* 198:105564. doi: 10.1016/j.jsbmb.2019.105564

Li, Q., Hua, Y., Yang, Y., He, X., Zhu, W., Wang, J., et al. (2018). T cell factor 7 (TCF7)/TCF1 feedback controls osteocalcin signaling in brown adipocytes independent of the wnt/beta-catenin pathway. *Mol. Cell. Biol.* 38:e00562-17.

Li, S., Jiang, H., Wang, B., Gu, M., Zhang, N., Liang, W., et al. (2018). Effect of leptin on marrow adiposity in ovariectomized rabbits assessed by proton magnetic resonance spectroscopy. *J. Comput. Assist. Tomogr.* 42, 588–593. doi: 10.1097/rct.0000000000000725

Lim, H. S., Byun, D. W., Suh, K. I., Park, H. K., Kim, H. J., Kim, T. H., et al. (2019). Is there a difference in serum vitamin D levels and bone mineral density according to body mass index in young adult women? *J. Bone Metab.* 26, 145–150. doi: 10.11005/jbm.2019.26.3.145

Liu, R., Li, X., Zhang, Z., Zhou, M., Sun, Y., Su, D., et al. (2015). Allogeneic mesenchymal stem cells inhibited T follicular helper cell generation in rheumatoid arthritis. *Sci. Rep.* 5:12777.

Liu, R., Wu, Q., Su, D., Che, N., Chen, H., Geng, L., et al. (2012). A regulatory effect of IL-21 on T follicular helper-like cell and B cell in rheumatoid arthritis. *Arthritis Res. Ther.* 14:R255.

Liu, R., Zhao, P., Zhang, Q., Che, N., Xu, L., Qian, J., et al. (2020). Adiponectin promotes fibroblast-like synoviocytes producing IL-6 to enhance T follicular helper cells response in rheumatoid arthritis. *Clin. Exp. Rheumatol.* 38, 11–18.

Liu, Y., Hazlewood, G. S., Kaplan, G. G., Eksteen, B., and Barnabe, C. (2017). Impact of obesity on remission and disease activity in rheumatoid arthritis: a systematic review and meta-analysis. *Arthritis Care Res. (Hoboken)* 69, 157–165. doi: 10.1002/acr.22932

Loeser, R. F., Goldring, S. R., Scanzello, C. R., and Goldring, M. B. (2012). Osteoarthritis: a disease of the joint as an organ. *Arthritis Rheum.* 64, 1697–1707. doi: 10.1002/art.34453

Luo, X. H., Guo, L. J., Yuan, L. Q., Xie, H., and Liao, E. Y. (2005). Adiponectin stimulates human osteoblasts proliferation and differentiation via the MAPK signaling pathway. *Chin. J. Osteoporos.* 309, 99–109. doi: 10.1016/j.yexcr.2005.05.021

Mabilleau, G., Mieczkowska, A., Irwin, N., Flatt, P. R., and Chappard, D. (2013). Optimal bone mechanical and material properties require a functional glucagon-like peptide-1 receptor. *J. Endocrinol.* 219, 59–68. doi: 10.1530/joe-13-0146

Mansur, S. A., Mieczkowska, A., Bouvard, B., Flatt, P. R., Chappard, D., Irwin, N., et al. (2015). Stable incretin mimetics counter rapid deterioration of bone quality in type 1 diabetes mellitus. *J. Cell. Physiol.* 230, 3009–3018. doi: 10.1002/jcp.25033

Mansur, S. A., Mieczkowska, A., Flatt, P. R., Bouvard, B., Chappard, D., Irwin, N., et al. (2016). A new stable GIP-oxyntomodulin hybrid peptide improved bone strength both at the organ and tissue levels in genetically-inherited type 2 diabetes mellitus. *Bone* 87, 102–113. doi: 10.1016/j.bone.2016.04.001

Marcovecchio, M. L., and Chiarelli, F. (2013). Obesity and growth during childhood and puberty. *World Rev. Nutr. Diet.* 106, 135–141. doi: 10.1159/000342545

Marques Loureiro, L., Lessa, S., Mendes, R., Pereira, S., Saboya, C. J., and Ramalho, A. (2019). Does the metabolically healthy obese phenotype protect adults with class III obesity from biochemical alterations related to bone metabolism? *Nutrients* 11:2125. doi: 10.3390/nu11092125

Méndez, J. P., Rojano-Mejía, D., Pedraza, J., Coral-Vázquez, R. M., Soriano, R., García-García, E., et al. (2013). Bone mineral density in postmenopausal Mexican-Mestizo women with normal body mass index, overweight, or obesity. *Menopause* 20, 568–572.

Minamino, H., Katsushima, M., Yoshida, T., Hashimoto, M., Fujita, Y., Shirakashi, M., et al. (2020). Increased circulating adiponectin is an independent disease activity marker in patients with rheumatoid arthritis: a cross-sectional study using the KURAMA database. *PLoS One* 15:e0229998. doi: 10.1371/journal.pone.0229998

Miossec, P. (2013). Rheumatoid arthritis: still a chronic disease. *Lancet* 381, 884–886. doi: 10.1016/s0140-6736(12)62192-8

Mitsuyo, K., Soko, S., and Solomon, D. H. (2007). Bone mineral density in adults with the metabolic syndrome: analysis in a population-based U.S. sample. *J. Clin. Endocrinol. Metab.* 92, 4161–4164. doi: 10.1210/jc.2007-0757

Miyake, H., Kanazawa, I., and Sugimoto, T. (2017). Decreased serum insulin-like growth factor-i is a risk factor for non-vertebral fractures in diabetic postmenopausal women. *Intern. Med.* 56, 269–273. doi: 10.2169/internalmedicine.56.7416

Monami, M., Cresci, B., Colombini, A., Pala, L., Balzi, D., Gori, F., et al. (2008). Bone fractures and hypoglycemic treatment in type 2 diabetic patients: a case-control study. *Diabetes Care* 31, 199–203. doi: 10.2337/dc07-1736

Mora, S., Goodman, W. G., Loro, M. L., Roe, T. F., Sayre, J., and Gilsanz, V. (1994). Age-related changes in cortical and cancellous vertebral bone density in girls: assessment with quantitative CT. *AJR Am. J. Roentgenol.* 162, 405–409. doi: 10.2214/ajr.162.2.8310936

Morgan, E. F., Barnes, G. L., and Einhorn, T. A. (2008). "Chapter 1–the bone organ system : form and function," in *Osteoporosis*, eds R. Marcus, D. Feldman, and J. Kelsey (Boston, MA: Elsevier Academic Press).

Muka, T., Trajanoska, K., Jong, K. D., Ling, O., Uitterlinden, A. G., Hofman, A., et al. (2015). The association between metabolic syndrome, bone mineral density, hip bone geometry and fracture risk: the Rotterdam study. *PLoS One* 10:e0129116. doi: 10.1371/journal.pone.0129116

Nam, J. L., Takase-Minegishi, K., Ramiro, S., Chatzidionysiou, K., Smolen, J. S., van der Heijde, D., et al. (2017). Efficacy of biological disease-modifying antirheumatic drugs: a systematic literature review informing the 2016 update of the EULAR recommendations for the management of rheumatoid arthritis. *Ann. Rheum. Dis.* 76, 1113–1136. doi: 10.1136/annrheumdis-2016-210713

Nanes, M. S. (2004). Tumor necrosis factor-alpha: molecular and cellular mechanisms in skeletal pathology. *Gene* 321, 1–15. doi: 10.1016/s0378-1119(03)00841-2

Naot, D., Watson, M., Callon, K. E., Tuari, D., Musson, D. S., Choi, A. J., et al. (2016). Reduced bone density and cortical bone indices in female adiponectin-knockout mice. *Endocrinology* 157, 3550–3561. doi: 10.1210/en.2016-1059

Nelson, L. R., and Bulun, S. E. (2001). Estrogen production and action. *J. Am. Acad. Dermatol.* 45(Suppl. 3), S116–S124.

Nöth, U., Tuli, R., Seghatoleslami, R., Howard, M., Shah, A., Hall, D. J., et al. (2003). Activation of p38 and Smads mediates BMP-2 effects on human trabecular bone-derived osteoblasts. *Exp. Cell Res.* 291, 201–211. doi: 10.1016/s0014-4827(03)00386-0

Nurieva, R. I., Chung, Y., Hwang, D., Yang, X. O., Kang, H. S., Ma, L., et al. (2008). Generation of T follicular helper cells is mediated by interleukin-21

but independent of T helper 1, 2, or 17 cell lineages. *Immunity* 29, 138–149. doi: 10.1016/j.immuni.2008.05.009

Oh, M. S., Kim, S., Jang, J. H., Park, J. Y., Kang, H. S., Lee, M. S., et al. (2016). Associations among the degree of nonalcoholic fatty liver disease, metabolic syndrome, degree of obesity in children, and parental obesity. *Pediatr. Gastroenterol. Hepatol. Nutr.* 19, 199–206. doi: 10.5223/pghn.2016.19.3.199

Oh, M. S., Kim, S., Lee, J., Lee, M. S., Kim, Y. J., and Kang, K. S. (2020). Factors associated with advanced bone age in overweight and obese children. *Pediatr. Gastroenterol. Hepatol. Nutr.* 23, 89–97. doi: 10.5223/pghn.2020.23.1.89

Oliveria, S. A., Felson, D. T., Cirillo, P. A., Reed, J. I., and Walker, A. M. (1999). Body weight, body mass index, and incident symptomatic osteoarthritis of the hand, hip, and knee. *Epidemiology* 10, 161–166. doi: 10.1097/00001648-199903000-00013

Otero, M., Lago, R., Gomez, R., Lago, F., Dieguez, C., Gomez-Reino, J. J., et al. (2006). Changes in plasma levels of fat-derived hormones adiponectin, leptin, resistin and visfatin in patients with rheumatoid arthritis. *Ann. Rheum. Dis.* 65, 1198–1201. doi: 10.1136/ard.2005.046540

Otero, M., Lago, R., Gomez, R., Lago, F., Gomez-Reino, J. J., and Gualillo, O. (2007). Phosphatidylinositol 3-kinase, MEK-1 and p38 mediate leptin/interferon-gamma synergistic NOS type II induction in chondrocytes. *Life Sci.* 81, 1452–1460. doi: 10.1016/j.lfs.2007.09.007

Paccou, J., Hardouin, P., Cotten, A., Penel, G., and Cortet, B. (2015). The role of bone marrow fat in skeletal health: usefulness and perspectives for clinicians. *J. Clin. Endocrinol. Metab.* 100, 3613–3621. doi: 10.1210/jc.2015-2338

Pagnotti, G. M., Styner, M., Uzer, G., Patel, V. S., Wright, L. E., Ness, K. K., et al. (2019). Combating osteoporosis and obesity with exercise: leveraging cell mechanosensitivity. *Nat. Rev. Endocrinol.* 15, 339–355. doi: 10.1038/s41574-019-0170-1

Pal China, S., Sanyal, S., and Chattopadhyay, N. (2018). Adiponectin signaling and its role in bone metabolism. *Cytokine* 112, 116–131. doi: 10.1016/j.cyto.2018.06.012

Park, H. S., Park, J. Y., and Yu, R. (2005). Relationship of obesity and visceral adiposity with serum concentrations of CRP, TNF-alpha and IL-6. *Diabetes Res. Clin. Pract.* 69, 29–35. doi: 10.1016/j.diabres.2004.11.007

Pasco, J. A., Henry, M. J., Kotowicz, M. A., Collier, G. R., Ball, M. J., Ugoni, A. M., et al. (2001). Serum leptin levels are associated with bone mass in nonobese women. *J. Clin. Endocrinol. Metab.* 86, 1884–1887. doi: 10.1210/jc.86.5.1884

Philbrick, K. A., Wong, C. P., Branscum, A. J., Turner, R. T., and Iwaniec, U. T. (2017). Leptin stimulates bone formation in ob/ob mice at doses having minimal impact on energy metabolism. *J. Endocrinol.* 232, 461–474. doi: 10.1530/joe-16-0484

Piccolis, M., Bond, L. M., Kampmann, M., Pulimeno, P., Chitraju, C., Jayson, C. B. K., et al. (2019). Probing the global cellular responses to lipotoxicity caused by saturated fatty acids. *Mol. Cell* 74, 32–44.e8.

Polineni, S., Resulaj, M., Faje, A. T., Meenaghan, E., Bredella, M. A., Bouxsein, M., et al. (2020). Red and white blood cell counts are associated with bone marrow adipose tissue, bone mineral density, and bone microarchitecture in premenopausal women. *J. Bone Miner. Res.* 35, 1031–1039. doi: 10.1002/jbmr.3986

Ponrartana, S., Aggabao, P. C., Hu, H. H., Aldrovandi, G. M., Wren, T. A., and Gilsanz, V. (2012). Brown adipose tissue and its relationship to bone structure in pediatric patients. *J. Clin. Endocrinol. Metab.* 97, 2693–2698. doi: 10.1210/jc.2012-1589

Prieto-Alhambra, D., Premaor, M. O., Avilés, F. Fina, Hermosilla, E., Martinez-Laguna, D., Carbonell-Abella, C., et al. (2012). The association between fracture and obesity is site-dependent: a population-based study in postmenopausal women. *J. Bone Min. Res.* 27, 294–300. doi: 10.1002/jbmr.1466

Pu, Y., Wu, H., Lu, S., Hu, H., Li, D., Wu, Y., et al. (2016). Adiponectin promotes human jaw bone marrow stem cell osteogenesis. *J. Dent. Res.* 95, 769–775. doi: 10.1177/0022034516636853

Putignano, P., Dubini, A., Toja, P., Invitti, C., Bonfanti, S., Redaelli, G., et al. (2001). Salivary cortisol measurement in normal-weight, obese and anorexic women: comparison with plasma cortisol. *Eur. J. Endocrinol.* 145, 165–171. doi: 10.1530/eje.0.1450165

Qiao, D., Li, Y., Liu, X., Zhang, X., Qian, X., Zhang, H., et al. (2020). Association of obesity with bone mineral density and osteoporosis in adults: a systematic review and meta-analysis. *Public Health* 180, 22–28. doi: 10.1016/j.puhe.2019.11.001

Rapp, K., Cameron, I. D., Kurrle, S., Klenk, J., Kleiner, A., Heinrich, S., et al. (2010). Excess mortality after pelvic fractures in institutionalized older people. *Osteoporos. Int.* 21, 1835–1839. doi: 10.1007/s00198-009-1154-0

Reid, I. R., Baldock, P. A., and Cornish, J. (2018). Effects of Leptin on the skeleton. *Endocr. Rev.* 39, 938–959. doi: 10.1210/er.2017-00226

Relling, D. P., Esberg, L. B., Fang, C. X., Johnson, W. T., Murphy, E. J., Carlson, E. C., et al. (2006). High-fat diet-induced juvenile obesity leads to cardiomyocyte dysfunction and upregulation of Foxo3a transcription factor independent of lipotoxicity and apoptosis. *J. Hypertens.* 24, 549–561. doi: 10.1097/01.hjh.0000203846.34314.94

Reyes, C., Leyland, K. M., Peat, G., Cooper, C., Arden, N. K., and Prieto-Alhambra, D. (2016). Association between overweight and obesity and risk of clinically diagnosed knee, hip, and hand osteoarthritis: a population-based Cohort study. *Arthritis Rheumatol.* 68, 1869–1875. doi: 10.1002/art.39707

Rodriguez, J., Vernus, B., Chelh, I., Cassar-Malek, I., Gabillard, J. C., Hadj Sassi, A., et al. (2014). Myostatin and the skeletal muscle atrophy and hypertrophy signaling pathways. *Cell. Mol. Life Sci.* 71, 4361–4371. doi: 10.1007/s00018-014-1689-x

Rong, B., Feng, R., Liu, C., Wu, Q., and Sun, C. (2019). Reduced delivery of epididymal adipocyte-derived exosomal resistin is essential for melatonin ameliorating hepatic steatosis in mice. *J. Pineal Res.* 66:e12561. doi: 10.1111/jpi.12561

Roy, B. (2013). Biomolecular basis of the role of diabetes mellitus in osteoporosis and bone fractures. *World J. Diabetes* 4, 101–113. doi: 10.4239/wjd.v4.i4.101

Roy, B., Curtis, M. E., Fears, L. S., Nahashon, S. N., and Fentress, H. M. (2016). Molecular mechanisms of obesity-induced osteoporosis and muscle atrophy. *Front. Physiol.* 7:439. doi: 10.3389/fphys.2016.00439

Russell, M., Mendes, N., Miller, K. K., Rosen, C. J., Lee, H., Klibanski, A., et al. (2010). Visceral fat is a negative predictor of bone density measures in obese adolescent girls. *J. Clin. Endocrinol. Metab.* 95, 1247–1255. doi: 10.1210/jc.2009-1475

Saad, F. A. (2020). Novel insights into the complex architecture of osteoporosis molecular genetics. *Ann. N. Y. Acad. Sci.* 1462, 37–52. doi: 10.1111/nyas.14231

Sanchez-Riera, L., Carnahan, E., Vos, T., Veerman, L., Norman, R., Lim, S. S., et al. (2014). The global burden attributable to low bone mineral density. *Ann. Rheum. Dis.* 73, 1635–1645.

Santos, V. R. D., Christofaro, D. G. D., Gomes, I. C., Junior, I. F. F., and Gobbo, L. A. (2018). Relationship between obesity, sarcopenia, sarcopenic obesity, and bone mineral density in elderly subjects aged 80 years and over. *Rev. Bras. Ortop.* 53, 300–305. doi: 10.1016/j.rboe.2017.09.002

Scheller, E. L., Khoury, B., Moller, K. L., Wee, N. K. Y., Khandaker, S., Kozloff, K. M., et al. (2016). Changes in skeletal integrity and marrow adiposity during high-fat diet and after weight loss. *Front. Endocrinol.* 7:102. doi: 10.3389/fendo.2016.00102

Scotece, M., Conde, J., Gomez, R., Lopez, V., Lago, F., Gomez-Reino, J. J., et al. (2011). Beyond fat mass: exploring the role of adipokines in rheumatic diseases. *ScientificWorldJournal* 11, 1932–1947. doi: 10.1100/2011/290142

Scott, D., Chandrasekara, S. D., Laslett, L. L., Cicuttini, F., Ebeling, P. R., and Jones, G. (2016). Associations of sarcopenic obesity and dynapenic obesity with bone mineral density and incident fractures over 5-10 years in community-dwelling older adults. *Calcif. Tissue Int.* 99, 30–42. doi: 10.1007/s00223-016-0123-9

Shanbhogue, V. V., Mitchell, D. M., Rosen, C. J., and Bouxsein, M. L. (2016). Type 2 diabetes and the skeleton: new insights into sweet bones. *Lancet Diabetes Endocrinol.* 4, 159–173. doi: 10.1016/s2213-8587(15)00283-1

Shen, W., Chen, J., Punyanitya, M., Shapses, S., Heshka, S., and Heymsfield, S. B. (2007). MRI-measured bone marrow adipose tissue is inversely related to DXA-measured bone mineral in Caucasian women. *Osteoporos. Int.* 18, 641–647. doi: 10.1007/s00198-006-0285-9

Shinoda, Y., Yamaguchi, M., Ogata, N., Akune, T., Kubota, N., Yamauchi, T., et al. (2006). Regulation of bone formation by adiponectin through autocrine/paracrine and endocrine pathways. *J. Cell. Biochem.* 99, 196–208. doi: 10.1002/jcb.20890

Shu, L., Beier, E., Sheu, T., Zhang, H., Zuscik, M. J., Puzas, E. J., et al. (2015). High-fat diet causes bone loss in young mice by promoting osteoclastogenesis through alteration of the bone marrow environment. *Calcif. Tissue Int.* 96, 313–323. doi: 10.1007/s00223-015-9954-z

Silva, M. J., Eekhoff, J. D., Patel, T., Kenney-Hunt, J. P., Brodt, M. D., Steger-May, K., et al. (2019). Effects of high-fat diet and body mass on bone morphology and

mechanical properties in 1100 advanced intercross mice. *J. Bone Miner. Res.* 34, 711–725. doi: 10.1002/jbmr.3648

Singh, L., Tyagi, S., Myers, D., and Duque, G. (2018). Good, bad, or ugly: the biological roles of bone marrow fat. *Curr. Osteoporos. Rep.* 16, 130–137. doi: 10.1007/s11914-018-0427-y

Singhal, V., Tulsiani, S., Campoverde, K. J., Mitchell, D. M., Slattery, M., Schorr, M., et al. (2018). Impaired bone strength estimates at the distal tibia and its determinants in adolescents with anorexia nervosa. *Bone* 106, 61–68. doi: 10.1016/j.bone.2017.07.009

Snijder, M. B., Dam, R. M. V., Visser, M., Deeg, D. J. H., and Lips, P. (2005). Adiposity in relation to vitamin D status and parathyroid hormone levels: a population-based study in older men and women. *J. Clin. Endocrinol. Metab.* 90, 4119–4123. doi: 10.1210/jc.2005-0216

Sowa, H., Kaji, H., Yamaguchi, T., Sugimoto, T., and Chihara, K. (2002). Smad3 promotes alkaline phosphatase activity and mineralization of osteoblastic MC3T3-E1 cells. *J. Bone Miner. Res.* 17, 1190–1199. doi: 10.1359/jbmr.2002.17.7.1190

Srikanthan, P., Crandall, C. J., Miller-Martinez, D., Seeman, T. E., Greendale, G. A., Binkley, N., et al. (2014). Insulin resistance and bone strength: findings from the study of midlife in the United States. *J. Bone Miner. Res.* 29, 796–803. doi: 10.1002/jbmr.2083

Stenholm, S., Harris, T. B., Rantanen, T., Visser, M., Kritchevsky, S. B., and Ferrucci, L. (2008). Sarcopenic obesity: definition, cause and consequences. *Curr. Opin. Clin. Nutr. Metab. Care* 11, 693–700. doi: 10.1097/mco.0b013e328312c37d

Steppan, C. M., Crawford, D. T., Chidsey-Frink, K. L., Ke, H. Z., and Swick, A. G. (2000). Leptin is a potent stimulator of bone growth in ob/ob mice. *Regul. Pept.* 92, 73–78. doi: 10.1016/s0167-0115(00)00152-x

Su, T., Xiao, Y., Xiao, Y., Guo, Q., Li, C., Huang, Y., et al. (2019). Bone marrow mesenchymal stem cells-derived exosomal mir-29b-3p regulates aging-associated insulin resistance. *ACS Nano* 13, 2450–2462.

Sugimoto, H., Yang, C., Lebleu, V. S., Soubasakos, M. A., and Kalluri, R. (2007). BMP-7 functions as a novel hormone to facilitate liver regeneration. *FASEB J.* 21, 256–264. doi: 10.1096/fj.06-6837com

Sun, X., Guo, Q., Wei, W., Robertson, S., Yuan, Y., and Luo, X. (2019). Current progress on microRNA-based gene delivery in the treatment of osteoporosis and osteoporotic fracture. *Int. J. Endocrinol.* 2019:6782653.

Takeshita, S., Fumoto, T., Naoe, Y., and Ikeda, K. (2014). Age-related marrow adipogenesis is linked to increased expression of RANKL. *J. Biol. Chem.* 289, 16699–16710. doi: 10.1074/jbc.m114.547919

Tang, X., Liu, G., Kang, J., Hou, Y., Jiang, F., Yuan, W., et al. (2013). Obesity and risk of hip fracture in adults: a meta-analysis of prospective cohort studies. *PLoS One* 8:e55077. doi: 10.1371/journal.pone.0055077

Tarantino, U., Piccirilli, E., Fantini, M., Baldi, J., Gasbarra, E., and Bei, R. (2015). Sarcopenia and fragility fractures: molecular and clinical evidence of the bone-muscle interaction. *J. Bone Joint Surg. Am.* 97, 429–437. doi: 10.2106/jbjs.n.00648

Tencerova, M., Okla, M., and Kassem, M. (2019). Insulin signaling in bone marrow adipocytes. *Curr. Osteoporos. Rep.* 17, 446–454. doi: 10.1007/s11914-019-00552-8

Thomas, T. (1999). Leptin acts on human marrow stromal cells to enhance differentiation to osteoblasts and to inhibit differentiation to adipocytes. *Endocrinology* 140, 1630–1638. doi: 10.1210/endo.140.4.6637

Thrailkill, K. M. (2000). Insulin-like growth factor-I in diabetes mellitus: its physiology, metabolic effects, and potential clinical utility. *Diabetes Technol. Ther.* 2, 69–80. doi: 10.1089/152091599316775

Tian, L., Wang, C., Xie, Y., Wan, S., Zhang, K., and Yu, X. (2017). High fructose and high fat exert different effects on changes in trabecular bone micro-structure. *J. Nutr. Health Aging* 22, 361–370. doi: 10.1007/s12603-017-0933-0

Tortoriello, D. V., McMinn, J., and Chua, S. C. (2004). Dietary-induced obesity and hypothalamic infertility in female DBA/2J mice. *Endocrinology* 145, 1238–1247. doi: 10.1210/en.2003-1406

Tsatsoulis, A., Mantzaris, M. D., Bellou, S., and Andrikoula, M. (2013). Insulin resistance: an adaptive mechanism becomes maladaptive in the current environment - an evolutionary perspective. *Metabolism* 62, 622–633. doi: 10.1016/j.metabol.2012.11.004

Tseng, Y. H., Kokkotou, E., Schulz, T. J., Huang, T. L., Winnay, J. N., Taniguchi, C. M., et al. (2008). New role of bone morphogenetic protein 7 in brown adipogenesis and energy expenditure. *Nature* 454, 1000–1004. doi: 10.1038/nature07221

Tu, M., Yang, M., Yu, N., Zhen, G., Wan, M., Liu, W., et al. (2019). Inhibition of cyclooxygenase-2 activity in subchondral bone modifies a subtype of osteoarthritis. *Bone Res.* 7:29.

Tu, Q., Zhang, J., Dong, L. Q., Saunders, E., Luo, E., Tang, J., et al. (2011). Adiponectin inhibits osteoclastogenesis and bone resorption via APPL1-mediated suppression of Akt1. *J. Biol. Chem.* 286, 12542–12553. doi: 10.1074/jbc.m110.152405

Vestergaard, P., Rejnmark, L., and Mosekilde, L. (2005). Relative fracture risk in patients with diabetes mellitus, and the impact of insulin and oral antidiabetic medication on relative fracture risk. *Diabetologia* 48, 1292–1299. doi: 10.1007/s00125-005-1786-3

Vicente, G., James, C., Mo, A. O., Lee, D. C., Dorey, F. J., and Mittelman, S. D. (2009). Reciprocal relations of subcutaneous and visceral fat to bone structure and strength. *J. Clin. Endocrinol. Metab.* 94, 3387–3393. doi: 10.1210/jc.2008-2422

Wang, T., and He, C. (2018). Pro-inflammatory cytokines: the link between obesity and osteoarthritis. *Cytokine Growth Factor Rev.* 44, 38–50. doi: 10.1016/j.cytogfr.2018.10.002

Wehrli, F. W., Hopkins, J. A., Hwang, S. N., Song, H. K., and Haddad, J. G. (2000). Cross-sectional study of osteopenia with quantitative MR imaging and bone densitometry. *Radiology* 217, 527–538. doi: 10.1148/radiology.217.2.r00nv20527

Wei, W., Dutchak, P. A., Wang, X., Ding, X., Wang, X., Bookout, A. L., et al. (2012). Fibroblast growth factor 21 promotes bone loss by potentiating the effects of peroxisome proliferator-activated receptor gamma. *Proc. Natl. Acad. Sci. U.S.A.* 109, 3143–3148. doi: 10.1073/pnas.1200797109

Wiedmann, N. M., Stefanidis, A., and Oldfield, B. J. (2017). Characterization of the central neural projections to brown, white, and beige adipose tissue. *FASEB J.* 31, 4879–4890. doi: 10.1096/fj.201700433r

Williams, G. A., Wang, Y., Callon, K. E., Watson, M., Lin, J. M., Lam, J. B., et al. (2009). In vitro and in vivo effects of adiponectin on bone. *Endocrinology* 150, 3603–3610.

Xie, H., Cui, Z., Wang, L., Xia, Z., Hu, Y., Xian, L., et al. (2014). PDGF-BB secreted by preosteoclasts induces CD31hiEmcnhi vessel subtype in coupling osteogenesis. *Nat. Med.* 20, 1270–1278. doi: 10.1038/nm.3668

Yang, M., Guo, Q., Peng, H., Xiao, Y. Z., Xiao, Y., Huang, Y., et al. (2019). Kruppel-like factor 3 inhibition by mutated lncRNA Reg1cp results in human high bone mass syndrome. *J. Exp. Med.* 216, 1944–1964. doi: 10.1084/jem.20181554

Zhang, F., Hao, G., Shao, M., Nham, K., An, Y., Wang, Q., et al. (2018). An adipose tissue atlas: an image-guided identification of human-like bat and beige depots in rodents. *Cell Metab.* 27, 252–262.e3.

Zhang, M., Xuan, S., Bouxsein, M. L., von Stechow, D., Akeno, N., Faugere, M. C., et al. (2002). Osteoblast-specific knockout of the insulin-like growth factor (IGF) receptor gene reveals an essential role of IGF signaling in bone matrix mineralization. *J. Biol. Chem.* 277, 44005–44012. doi: 10.1074/jbc.m208265200

Zhang, Y., Liu, J., Yao, J., Ji, G., Qian, L., Wang, J., et al. (2014). Obesity: pathophysiology and intervention. *Nutrients* 6, 5153–5183.

Zhao, Y., Qin, R., Ma, X., Qin, Z., Yang, Z., Hong, H., et al. (2020). Adiposity is not beneficial to bone mineral density in 0-5 year old Chinese children: the Jiangsu bone health study. *Obes. Res. Clin. Pract.* 14, 39–46. doi: 10.1016/j.orcp.2019.10.011

Zhu, Z. N., Jiang, Y. F., and Ding, T. (2014). Risk of fracture with thiazolidinediones: an updated meta-analysis of randomized clinical trials. *Bone* 68, 115–123. doi: 10.1016/j.bone.2014.08.010

Conflict of Interest: The authors declare that the research was conducted in the absence of any commercial or financial relationships that could be construed as a potential conflict of interest.

Copyright © 2020 Hou, He, He, Yang, Luo and Li. This is an open-access article distributed under the terms of the Creative Commons Attribution License (CC BY). The use, distribution or reproduction in other forums is permitted, provided the original author(s) and the copyright owner(s) are credited and that the original publication in this journal is cited, in accordance with accepted academic practice. No use, distribution or reproduction is permitted which does not comply with these terms.

frontiers in Cell and Developmental Biology

REVIEW
published: 22 December 2020
doi: 10.3389/fcell.2020.598263

Communications Between Bone Marrow Macrophages and Bone Cells in Bone Remodeling

Kaixuan Chen[1], *Yurui Jiao*[1], *Ling Liu*[1], *Mei Huang*[1], *Chen He*[1], *Wenzhen He*[1], *Jing Hou*[1], *Mi Yang*[1], *Xianghang Luo*[1,2,3] *and Changjun Li*[1,2,3]*

[1] Department of Endocrinology, Endocrinology Research Center, The Xiangya Hospital of Central South University, Changsha, China, [2] National Clinical Research Center for Geriatric Disorders, Xiangya Hospital, Changsha, China, [3] Key Laboratory of Organ Injury, Aging and Regenerative Medicine of Hunan Province, Changsha, China

The mammalian skeleton is a metabolically active organ that continuously undergoes bone remodeling, a process of tightly coupled bone resorption and formation throughout life. Recent studies have expanded our knowledge about the interactions between cells within bone marrow in bone remodeling. Macrophages resident in bone (BMMs) can regulate bone metabolism via secreting numbers of cytokines and exosomes. This review summarizes the current understanding of factors, exosomes, and hormones that involved in the communications between BMMs and other bone cells including mensenchymal stem cells, osteoblasts, osteocytes, and so on. We also discuss the role of BMMs and potential therapeutic approaches targeting BMMs in bone remodeling related diseases such as osteoporosis, osteoarthritis, rheumatoid arthritis, and osteosarcoma.

Keywords: macrophages, intracellular communication, macrophage-derived exosome, bone remodeling, bone diseases

OPEN ACCESS

Edited by:
Mario Antonio Bianchet, Johns Hopkins University, United States

Reviewed by:
Bin Tang, Southern University of Science and Technology, China
Zhongyu Liu, Third Affiliated Hospital of Sun Yat-sen University, China
Junichi Kikuta, Osaka University, Japan

***Correspondence:**
Changjun Li
lichangjun@csu.edu.cn

Specialty section:
This article was submitted to Molecular Medicine, a section of the journal Frontiers in Cell and Developmental Biology

Received: *24 August 2020*
Accepted: *27 November 2020*
Published: *22 December 2020*

Citation:
Chen K, Jiao Y, Liu L, Huang M, He C, He W, Hou J, Yang M, Luo X and Li C (2020) Communications Between Bone Marrow Macrophages and Bone Cells in Bone Remodeling. Front. Cell Dev. Biol. 8:598263. doi: 10.3389/fcell.2020.598263

INTRODUCTION

Macrophages are diverse, multifunctional, and plastic cells that regulate tissue homeostasis under physiological conditions and in various pathophysiological processes according to the surrounding environment.

Macrophages can be divided into circulating and resident macrophages. During embryonic development, macrophages are also the first emerged cells of the nascent immune system and they would infiltrate various developing organs to differentiate into tissue-resident macrophages, such as bone-resident macrophages (Wynn et al., 2013). Current knowledge of bone-resident macrophages (Michalski and McCauley, 2017) is limited. Osteal macrophages are a subset of bone-resident macrophages and are f4/80 positive and trap negative. Close to the bone surface, osteal macrophages are adjacent to osteoblasts, regulate bone formation, and are closely related to the osteogenic differentiation of mesenchymal stem cells. One characteristic of this group of myeloid cells is that although they share a common precursor with osteoclasts, they have different markers on their surfaces from osteoclasts. Communications between macrophages and other bone cells play an important role in bone tissue homeostasis and new bone formation. In this review, we focus primarily on the effects of macrophages on other bone cells. Extracellular vesicles are a group of cell-derived heterogeneous membranous structures that facilitate cell-cell communications. Hence, we discussed the potential contribution of the new-found microRNAs and alarmins contained in macrophage-derived extracellular vesicles in maintaining bone homeostasis in the context of bone stromal regulation. In the end, we further explained the role of macrophages in bone remodeling-related bone diseases and described the relationship between macrophages and bone tumors such as osteosarcoma.

This review focuses on the presence of macrophages in endosseous tissue, revealing the important role of macrophages in bone physiology and pathology.

MACROPHAGES

The Occurrence and Function of Macrophages

Since Elie Metchnikoff first translated macrophages into Greek "big eaters," macrophages are primarily known for their phagocytosis in inflammation and immunity (Gordon, 2008). Macrophages are differentiated immune cells with heterogeneity and plasticity. They are activated under different environmental signals and participate in diverse functions (Das et al., 2014, 2015; Jafarnezhad-Ansariha et al., 2018). Macrophage is often referred to as polarization. Different subtypes of macrophages have been derived from the simple M1/M2 classification, according to the environment, transcription factors, and cytokines secreted by macrophages. According to the expression of marker in macrophage surface, M1/M2 are currently also called "M1-like" and "M2-like" (Biswas and Mantovani, 2010), but in this review, we still only use M1 and M2 to represent.

M1 or classical activation of macrophages is an important inflammatory responser. Polarized M1 can produce high levels of reactive oxygen species (ROS), nitric oxide (NO), and pro-inflammatory cytokines such as interleukin IL-1, IL-2, IL-6, IL-12, TNF-α, and IFN-γ, which are involved in enhancing the host's defense response (Mosser, 2003; Genin et al., 2015). However, excessive stimulation of M1 macrophages can lead to tissue damage and autoimmune diseases (Mosser and Edwards, 2008). M2 macrophages mainly present in the subsiding phase of inflammation and are responsible for the production of anti-inflammatory cytokines and the clearance of apoptotic cells. Exposure to anti-inflammatory cytokines (IL-4, IL-10, and IL-13) or IL-1 receptor ligands or immune complexes and toll-like receptors (TLRs) can lead to M2 macrophage polarization (Mantovani et al., 2004; Guihard et al., 2012; Woo et al., 2015). M2 can produce anti-inflammatory cytokines such as chemokines ligands 18 (CCL-18), CCL-22, IL-10, and a small amount of IL-12 family members (Mosser and Edwards, 2008; Guo et al., 2019). In addition, M2 macrophages can produce a large number of osteogenic growth factors such as BMP-2 bone morphogenetic protein-2, a subclass of the TGF-β family and a potent promoter to osteogenic differentiation of MSCs (Champagne et al., 2002; Li et al., 2018), TGF-β (Assoian et al., 1987), osteopontin (Takahashi et al., 2004), and 1,25-dihydroxy-vitamin D3 (Kreutz et al., 1993). M2 can be further subdivided into M2a, M2c, and M2d by different signal activation, cell surface markers, and their functions (**Figure 1**) (Mosser and Edwards, 2008; Jetten et al., 2014; Murray et al., 2014; Roszer, 2015; Ogle et al., 2016; Arora et al., 2018).

Moreover, macrophages can also be divided into circulating and tissue-resident types. Tissue-resident macrophages are a diverse family of cells found in most organs (such as liver kupffer cells and alveolar macrophages in the lungs). Based on the origin, tissue-resident macrophages can be divided into two subsets. One derives from the yolk sac and another population originates from hematopoietic progenitors and circulating monocytes (**Figure 1**) (Heideveld and van den Akker, 2017). Tissue-resident macrophages express a large number of cell surface receptors, growth factors, proinflammatory and anti-inflammatory cytokines, and many other cell products (Jamalpoor et al., 2018). Most damage-related factors are first sensed by the resident macrophages, which become tense and recruit more macrophages when activated. Resident and recruited macrophages respond to their local environment and activate specific transcriptional programs that drive macrophages to a range of different phenotypes, from pro-inflammatory M1 macrophages to anti-inflammatory M2 macrophages (Xue et al., 2014; Juhas et al., 2018). Tissue damage caused by external (damage, chemicals, infection) and internal triggers (DNA damage, immune response) or by lack (nutrients, oxygen) and excess (sugar, cholesterol) factors may induce macrophage activation, sequentially lead to a disruption of the delicate balance between bone formation and resorption.

One Subset of Bone-Resident Macrophages—Osteal Macrophages

Bone macrophage includes bone marrow macrophage (erythroblastic island macrophage, hematopoietic stem cell niche macrophage), osteoclast and osteal macrophages which also named osteomacs. Osteal macrophages were found in both periosteum and endosseous tissue, which support osteoblastic function and maintain bone homeostasis (Winkler et al., 2010; Cho et al., 2014b; Raggatt et al., 2014; Miron et al., 2016; Michalski and McCauley, 2017). Osteal macrophages account for about one sixth of the total cells in bone tissue (Chang et al., 2008), they present in resting bone tissue and increase in active bone anabolism sites. Osteal macrophages are a unique subset of bone-resident macrophages, close to the bone surface, f4/80 positive and trap-negative (Geissmann et al., 2010), adjacent to bone-forming cells (osteoblasts), dormant cells, and osteoclasts. The osteoblasts on the inner surface of cortical bone were mostly covered by f4/80$^+$, CD68$^+$, mac-3$^+$, and trap-macrophages and be regulated by osteomacs (Chang et al., 2008; Batoon et al., 2019).

CSF-1 (colony stimulating factor 1) and various molecular markers are required for the proliferation and differentiation of mononuclear phagocyte progenitor cells to monocytes, osteal macrophages, and osteoclasts. Previous studies have shown that osteomacs on and in the periosteum are highly expressed with the mature macrophage marker CD169, which can be distinguished from osteoclasts (Mohsenzadegan et al., 2015; Batoon et al., 2019). So far, there is no unique marker between osteal cells and other bone macrophage subsets, but it is known osteal cells that in endosteum do not express ER-HR3 antigen which can be distinguished (Wu et al., 2016; Kaur et al., 2017).

COMMUNICATIONS BETWEEN MACROPHAGES AND BONE CELLS

Bone is a kind of mineralized connective tissue, which plays the role of movement, support, and protection of soft tissues, storage of calcium and phosphorus, and preservation of bone marrow

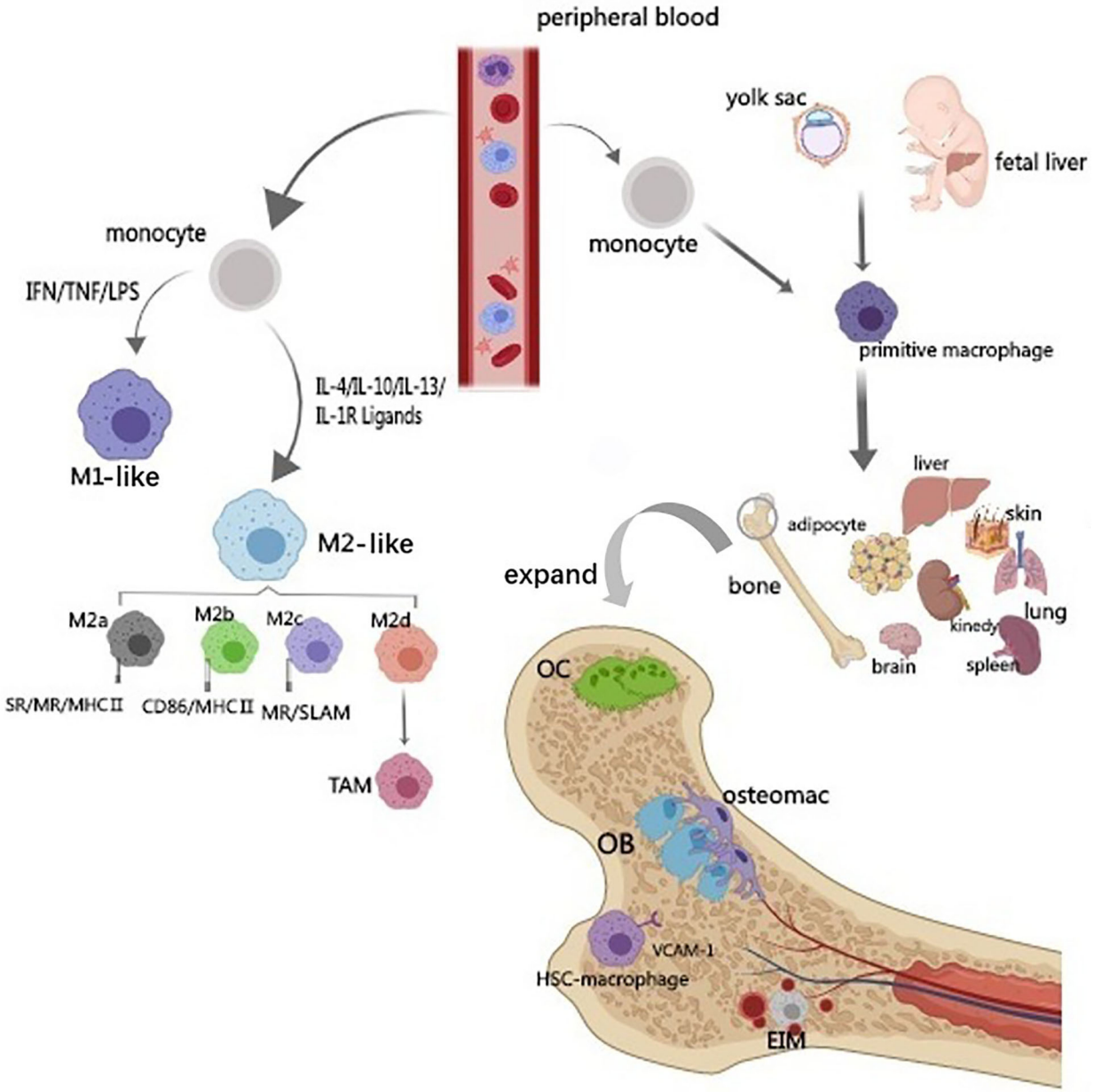


FIGURE 1 | Origin and classification of macrophages. The diagram illustrates the source and classification of macrophages. Circulating macrophages are classified into M1 and M2 types according to their activators and functions. M2-type can be further subdivided into M2a, M2c, and M2d by different signal activation, cell surface markers and their functions. Based on the origin, tissue-resident macrophages can be divided into two subsets. One derives from the yolk sac and another population originates from hematopoietic progenitors and circulating monocytes. Bone macrophage includes bone marrow macrophage (erythroblastic island macrophage, hematopoietic stem cell niche macrophage), osteoclast and osteal macrophages (osteomacs).

(Robling et al., 2006; Datta et al., 2008). Bone tissue is composed of roughly two parts: the dense layer and the spongy layer. The dense layer consists primarily of bone cells that make up the outermost layer of bone and functions primarily to support structural stability of the body and movement. The spongy layer is a trabecular, highly vascularized network of bone that houses the red and white marrow and is a hotbed of hematopoietic blood (Le et al., 2017). Despite bone is inert in appearance, it is a highly dynamic organ, constantly absorbed by osteoclasts and regenerated by osteoblasts, by which old bone is replaced by new bone. The equilibrium state of bone resorption and formation is regulated by local and systemic factors including cells, hormones,

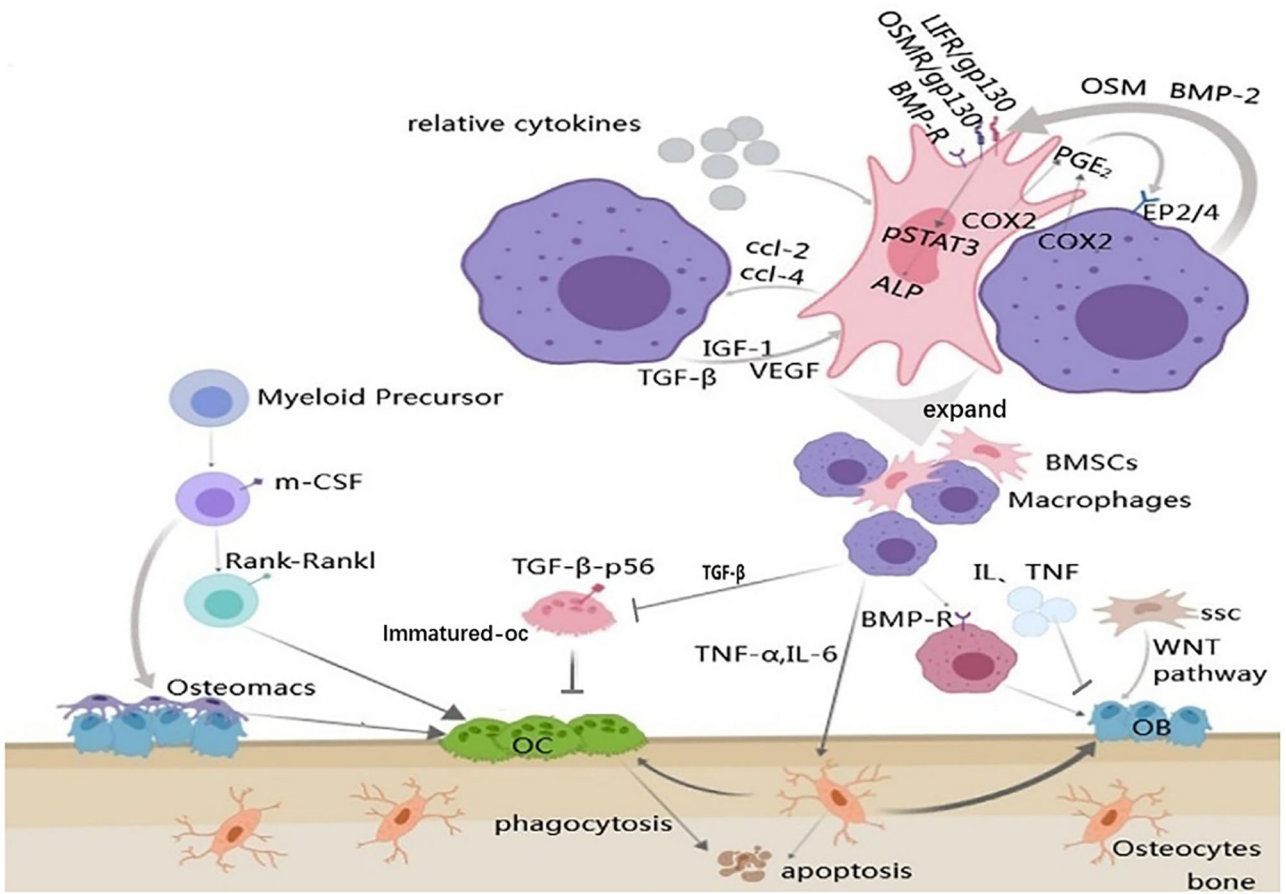


FIGURE 2 | Communications between macrophages and bone remodeling cells. Arrow represents "stimulatory modification;" the gray triangle means "enlarged display;" the arrow with a line means "suppress." Cell-cell communication between MSCs and macrophages results in the production of PGE2 and through the EP2/4 receptors to produce OSM. OSM acts on the MSCs via the gp130 receptors to activate STAT3 phosphorylation. Macrophage can also release BMP-2 to active the osteoblast differentiation genes, such as ALP, via the BMP-R in MSCs. MSCs can produce CCL-2 and CCL-4 to regulate macrophages and in reverse, this process is under the control of the macrophages; The differentiation of osteoblasts is regulated by variety of aspects including macrophages, osteocytes, inflammatory mediators and MSCs; Osteoclasts and osteomacs can derive from the same myeloid precursor, but it's unknown if the osteomac is a kind of the osteoclast precursors. Besides, macrophages mediate the growth of osteoclasts through various cytokines; Osteocytes apoptosis is under the regulation of macrophages.

cytokines, etc. Here we focus on the relationship between bone derived macrophages and bone remodeling related cells.

Macrophage and BMSCs

Champagne is the first one to propose the mechanism by which macrophages contribute to osteogenic differentiation of bone marrow mesenchymal stem cells (BMSCs). In their study, the conditioned medium of the inactive J774A.1 mouse macrophage cell line was used for experiments, and it was found that the activity of alkaline phosphatase in human bone marrow mesenchymal stem cells was enhanced by the mediation of BMP-2 (**Figure 2**) (Champagne et al., 2002; Jamalpoor et al., 2018). A subsequent study co-cultured inactive human monocytes and human bone marrow mesenchymal stem cells (hbMSCs) and found that monocytes promoted MSC proliferation and increased expression of osteocalcin and osteopontin (Pirraco et al., 2013). Osteomacs regulate maintenance and proliferation of Nestin-positive MSC. These MSC express a variety of HSC retention factors and it is thought that macrophages talk to MSC via unknown secreted factors, excluding IL-1, IL-10, TNF-α, and insulin like growth factor 1 (IGF-1) (Heideveld and van den Akker, 2017). Nicolaidou et al. found that the number of macrophages in culture was positively correlated with bone formation when they co-culture human peripheral blood mononuclear cells (PBMCs) with hbMSCs (Nicolaidou et al., 2012). This process requires direct cell-cell contact to produce a soluble factor that induces STAT3 phosphorylation, known as oncostatin M (OSM). OSM is bound by two receptor complexes, consisting of a gp130 subunit and a leukemia suppressor receptor (LIFR). OSM gene deletion altered bone healing in the tibial injury model in mice. *In vitro* studies have described the stimulating effect of OSM produced by macrophages on the mineralization activity and differentiation of osteoblasts (Sims and Quinn, 2014). This

process also depends on prostaglandin E2 (PGE2) and cox-2 (COX2) (Nicolaidou et al., 2012). Cell-cell contact between MSCs and macrophages produces PGE2 and induces OSM production through EP2/4 receptor on macrophages. Then OSM activates STAT3 phosphorylation through OSM and LIF receptors (**Figure 2**) (Nicolaidou et al., 2012; Horwood, 2016). Guihard also found the OSM signaling pathway. However, when hbMSCs were cultured in the conditioned medium of mononuclear cells treated with IL-4 or IL-10, there was no enhanced osteogenesis found and no OSM secretion detected (Guihard et al., 2012). Found in the study of inducing bone formation through bone Ti implants, the osteogenic differentiation of BMSCs could be changed by shifting the macrophage phenotype. Excessive polarization in the M1 direction leads to prolonged inflammation, while excessive polarization in the M2 direction leads to enhanced osteogenesis around Ti implants greatly (Wang et al., 2018). In contrast to the above studies, the effects of M0, M1, and M2 mouse bone marrow macrophages on osteogenic differentiation of mouse bone marrow mesenchymal stem cells have been studied. It was noted that all the macrophage subtypes could promote bone formation, and the M1-type macrophages had the greatest effect on bone formation (Lu et al., 2017). Studies have found that M1 macrophages increase the early and middle osteogenesis of MSCs, but do not increase matrix mineralization, while M2 macrophages co-culture can lead to increasing matrix mineralization. Moreover, it was found that the production of OSM increased in M1 culture and the production of BMP-2 increased in M2 co-culture, suggesting that different factors may be the driving factors for MSC differentiation in M1 and M2 cultures (Zhang et al., 2017).

In the co-culture model, MSCs significantly inhibited the production of LPS-induced pro-inflammatory cytokines (TNF-α, IL-1β, and IL-6) through iNOS and COX2-dependent pathways, and increased the secretion of IL-10 in macrophages by enhancing the production of PGE2 (Maggini et al., 2010). Experiments have proved that co-culture of MSCs and macrophages can significantly inhibit M1-macrophage polarization and induce M2 polarization (Kim and Hematti, 2009; Cho et al., 2014a). Human and mouse bone marrow mesenchymal stem cells secrete a large number of chemokines, including CCL-2 and CCL-4 (Seebach et al., 2014), which are the main chemokines for monocytes and macrophages (Mantovani et al., 2004). Combining INF-γ with another pro-inflammatory cytokine (TNF-β, IL-1β) activates bone marrow mesenchymal stem cells in damaged or inflammatory tissue, leading to increased secretion of various chemokines (**Figure 2**) (Ren et al., 2008). This MSC-mediated macrophage recruitment and macrophage phenotypic regulation may promote tissue regeneration (Bernardo and Fibbe, 2013).

Macrophage and Osteoblasts

The purest form of bone formation is intramembrane ossification, in which the bone matrix is formed and deposited directly by osteoblasts. *In vivo*, osteal cells occur in multiple stages of intramembranous bone healing and form a unique canopy structure on mature osteoblasts. Osteal cells are in direct contact with stromal production and mineralized osteoblasts. Moreover, osteomacs promoted osteoblast differentiation, through the OSM-mediated tyrosine phosphorylation and interaction between the STAT3 and Yes-associated protein 1 (YAP1) (Wang et al., 2020). Depletion of osteomacs significantly inhibited the formation of new bone, however, specific enlargement of osteomacs resulted in a significant increase in new mineralized substrates (Raggatt et al., 2014). In MAFIA mice (a macrophage Fas-induced apoptosis mouse model), the bone transformation rate is significantly reduced (Cho et al., 2014b). TNF-α released by activated macrophages can stimulate osteoblast chemotactic effect *in vitro*, and can inhibit osteoblast differentiation in rheumatoid arthritis patients (Sun et al., 2018). IL-6 inhibits osteoblast differentiation and disrupts the balance of normal bone turnover (Harmer et al., 2018). Osteoblasts are derived from a subtype of skeleton stem cells (SSC) which belongs to bone marrow mesenchymal stem cells (Fierro et al., 2017). The WNT pathway is a major pathway for the transformation of SSC into osteoblasts. Macrophage-derived BMP-2 plays a critical role in inducing ossification by inducing alkaline phosphatase production through the signaling cascade of Wnt and Wnt/LRP5 in osteoblasts (Rawadi et al., 2003; Jamalpoor et al., 2018). Treatment of macrophages with BMP-2 antibody can prevent osteogenesis (Champagne et al., 2002). The conditioned medium collected from the BMP-2-stimulated macrophages also accelerated the osteogenic differentiation of the BMSC (Wei et al., 2018). In addition, BMP-2 affects the migration, recruitment and the differentiation of macrophages (Pardali et al., 2018).In addition to WNT, the macrophage derived-BMP can bind to the BMP receptor, which causes the dimerization of BMP-R and the phosphorylation of Smad proteins. Then, the phosphorylated molecule activates Runx2 to up-regulate OB activity and differentiation (**Figure 2**) (Kawabata et al., 1998). In a study of xenografts about deproteinized bovine bone matrix (DBBM), it was found that IL-10 released by macrophages can promote the osteogenic response of osteoblasts induced by macrophages (Shi et al., 2018).

Macrophage and Osteoclasts

Osteal macrophages and osteoclasts are derived from myeloid progenitor cell precursors and can be stimulated by many of the same cytokines to function. But it must be emphasized that the osteomacs are not osteoclasts, because osteoclasts do not contain F4/80 Ag at all. Osteoclasts activated by pro-inflammatory stimuli may produce pre-osteoclast cytokines, including IL-6 and IL-1, which can promote the differentiation and/or function of osteoclasts. Therefore, osteoporosis may provide some candidate cellular mechanisms to explain why chronic inflammation and systemic infection often lead to osteopenia/osteoporosis (Chang et al., 2008). The generation of macrophage-derived osteoclasts can be activated by M-CSF and RANKL, and the blocking of the RANKL signaling pathway may prevent the progression of osteoporosis in mice (Jin et al., 2019). Macrophages can produce TGF-β1, which is essential for bone metabolism. NF-kB, composed of subunits such as p65, is a downstream transcription factor of the RANKL-RANKL signaling pathway (Park et al.,

TABLE 1 | Macrophage-derived exosomes in bone metabolism.

Cell of origin	Types	Mediators	Main biological effects	References
Bone marrow macrophage	Exosomes	Undetected	Promote osteogenesis	Wei et al., 2019
	MicroRNAs	mir-21	Promote tendon cell formation and fibrosis by decreasing Smad7	Cui et al., 2019
			Interfere the PTEN/PI3K/AKT signaling pathway to regulate the biological behavior of cells	Zheng et al., 2017; Yang et al., 2018
		mir-155	Promote the secretion of inflammatory cytokines	Stanczyk et al., 2008; Heymans et al., 2013; Ying et al., 2017
		mir-5106	Inhibit the genes SIK2 and SIK3 to promote bone formation	Xiong et al., 2020
	Alarmins	Annexins	Induce bone resorption and help macrophages to work	Li et al., 2005; D'Souza et al., 2012; Stukes et al., 2016; McArthur et al., 2020; Xia et al., 2020; Xiong et al., 2020
		Galectins	Act on the differentiation of various bone cells	Andersen et al., 2003; Shimura et al., 2005; Nakajima et al., 2014; Weilner et al., 2016; Simon et al., 2017; Iacobini et al., 2018
		HSP; fibronectin	Functions through osteoblasts and osteoclasts.	Moursi et al., 1996; Koh et al., 2009; Gramoun et al., 2010; Notsu et al., 2016; Nakamura et al., 2019

2017). Nuclear factor of activated T cells cytoplasmic 1 (NFATc1) is a master regulator of osteoclast differentiation (Okamoto and Takayanagi, 2011). Some studies have shown that TGF-β1 directly down-regulates NFATc1 activity by blocking the p65 in the receptor activator and then inhibits the generation and bone resorption of osteoclasts (**Figure 2**) (Tokunaga et al., 2020). Recently, the role of the NEMO protein (a core component of the NF-kB signaling pathway) in mouse bone marrow macrophages was investigated that if the lysine-270 (NEMO-Lys270) in NEMO protein was mutated to Ala, the NF-kB signal in bone marrow macrophages would lose control, leading to the accelerated production of osteoclasts (Adapala et al., 2020). What's more, studies have found that the overexpression of cr6 interaction factor-1 (Crif1) in mouse BMSCs can increase the secretion of RANKL through the cAMP/PKA pathway, and then combine with RANK on macrophages to promote the formation of osteoclasts *in vitro* (Xiang et al., 2020).

Macrophage and Osteocytes

Osteocytes account for 90–95% of all bone cells and are the most abundant and long-lived cells (Franz-Odendaal et al., 2006). Activated macrophages can induce the production of pro-inflammatory cytokines such as IL-1, IL-6, and TNF-α, which may play a significant role in inflammatory bone loss. Activated fibroblast growth factor-23 secreted by osteocytes after activation induced by IL-1 and TNF-α may cause hypophosphatemia during sepsis. TNF-α attracts osteoclasts by inducing osteocyte apoptosis (Tan et al., 2006). IL-1 may cause the decrease of bone cell activity through the NF-kB/RANKL signaling pathway, and soluble IL-6 can increase osteocyte-mediated osteoclastic differentiation by activating JAK2 and RANKL during normal bone growth and bone remodeling (Wu et al., 2017; Yang and Yang, 2019). It was reported that purified osteocytes can express a much higher amount of RANKL, which bind with mouse bone marrow macrophage and support osteoclast differentiation (Elango et al., 2018). Inflammation is thought to be highly correlated with bone cell apoptosis. If macrophages in part of the femoral head are polarized to the M1 phenotype and up-regulate a large number of inflammatory mediators, they can promote bone cell apoptosis and accelerate femoral head necrosis (**Figure 2**) (Jin et al., 2020).

In summary, bone formation relies on the interaction of a variety of cells which reminded above and other cytokines including HIF-1α (Karshovska et al., 2020)and CSF-1 (Alexander et al., 2011; Raggatt et al., 2014)to maintain the dynamic balance of the skeletal environment.

MACROPHAGE-DERIVED EXOSOMES (VESICLES) REGULATE BONE METABOLISM

Intercellular communication is a key biological process that enables cells to coordinate their responses spatially and temporally to physiological changes. A fresh member of the intercellular communication system is the extracellular vesicle (EVs) (Théry, 2011) which is a small membrane derived phospholipid bilayer with a diameter between 30 and 2,000 nm. A vital class of EVs is exosomes (released by exocytosis, 30–150 nm diameter) (Colombo et al., 2014), has gained closely attention.

Recent studies have shown that macrophage-derived EVs play an important role in maintaining stability of the bone environment and bone remodeling (**Table 1**). In the study of BMP-2/macrophage-derived exosomes implantation of titanium nanotube, BMP2/macrophage-derived exosomes dramatically increased the expression of osteogenesis-related genes (ALP, osteopontin, Runx2, BMP-2, and BMP-7). Furthermore,

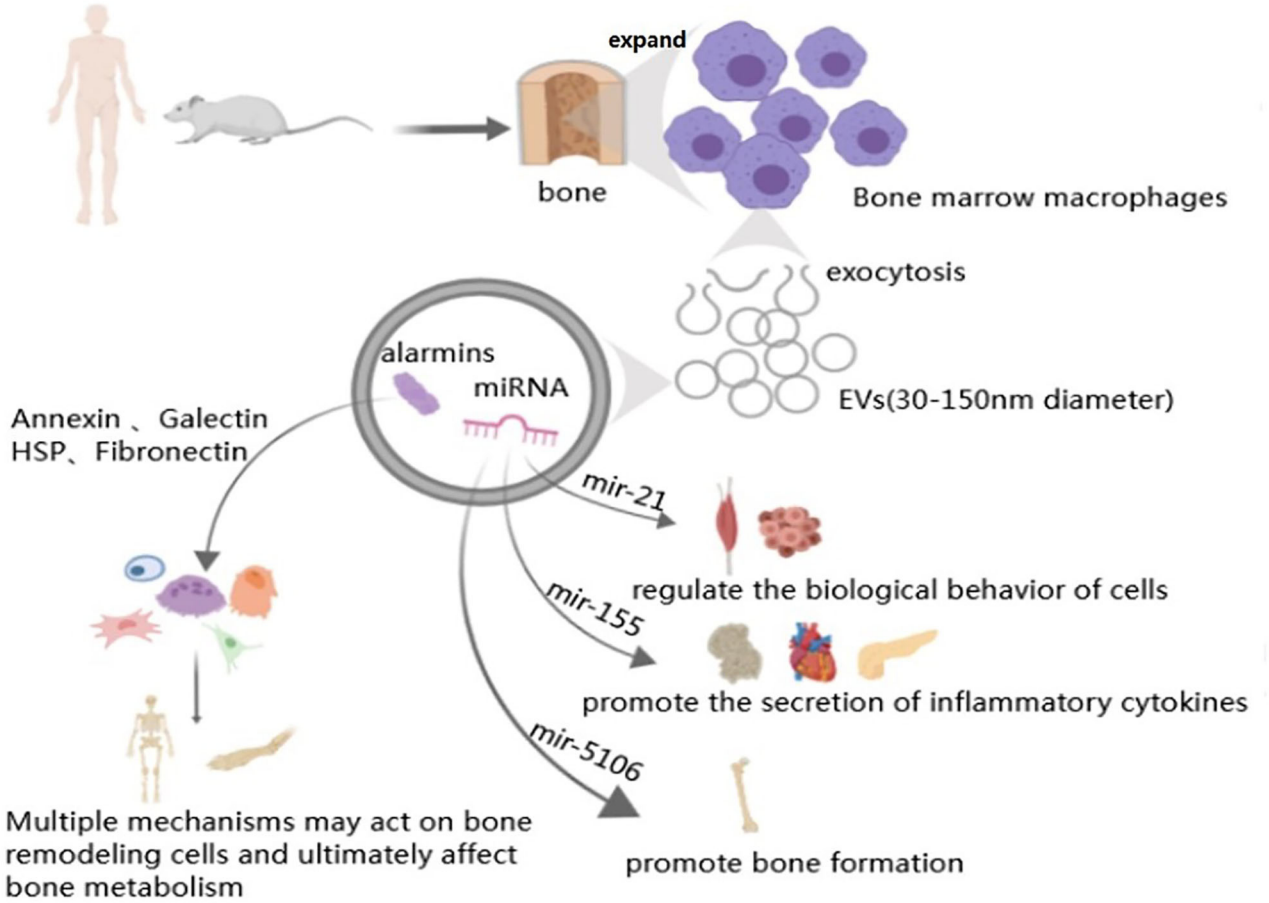


FIGURE 3 | Macrophage-derived exosomes in bone metabolism. Arrow represents "stimulatory modification;" the gray triangle means "enlarged display." The structure of macrophage derived exosomes is phospholipid bilayer with a diameter between 30 and 150 nm. Macrophage derived exosomes contain miRNAs (such as mir-21, mir-155, and mir-5106) and alarmins (such as Annexin, Galectin, HSP, and Fibronectin), all of them can through diverses signal pathways or release relative cytokines to participate in variety organs metabolism, including bone remodeling.

exosome-encapsulated nanotubes activated autophagy of hBMSCs and altered the secretion of cytokines associated with bone remodeling. All of these indicate the pro-osteogenic role of the BMP-2/macrophage-derived exosomes (Wei et al., 2019). And studies have found that after tendon injury, the development of the fibrotic healing response impairs the function of the tendon and restricts the movement of the tendon. MicroRNAs are a same category of small, single-stranded non-coding RNAs discovered in diverse organisms, which can regulate the expression of mRNAs (Yang et al., 2017). Studies have found that exosome miR-21-5p secreted by bone marrow macrophages activates and promotes tendon cell fibrosis fiber formation by inhibiting the expression of Smad7 (Cui et al., 2019). After induction into M2 macrophages, murine bone marrow derived macrophages can secrete miR-21, interfere with the normal signal of the PTEN/PI3K/AKT signaling pathway, and thus regulate the biological behavior of a variety of tumors, including osteosarcoma (**Figure 3**) (Zheng et al., 2017; Yang et al., 2018). This finding serves as a potential target for the prevention and treatment of tendon adhesion and bone tumors. Bone marrow macrophage-derived miR-155 can be induced to release by the activators of pro-inflammatory M1 phenotype macrophages (LPS, IFN-α) and promote the secretion of inflammatory cytokines such as TNF-α, IL-12, thereby aggravating the inflammatory response in RA (Stanczyk et al., 2008), diabetes (Ying et al., 2017), and heart disease (**Figure 3**) (Heymans et al., 2013). The latest studies found that M2-type macrophages derived from mouse bone marrow macrophages enriched miR-5106. M2D-Exo containing miR-5106 can promote osteogenic differentiation of bone marrow mesenchymal stem cells and accelerate fracture healing *in vivo* by inhibiting the expression of osteogenic related genes SIK2 and SIK3 (**Figure 3**) (Xiong et al., 2020). Unexpectedly, compared to exosomes from M0 and M2, exosomes from M1 have a stronger stimulating effect on the proliferation, osteogenesis, and adipogenic differentiation of BMSCS and all three types of exosomes had an adverse effect on the chondrogenic differentiation of BMMSCs (Xia et al., 2020). The above findings indicate that the exact mechanisms of

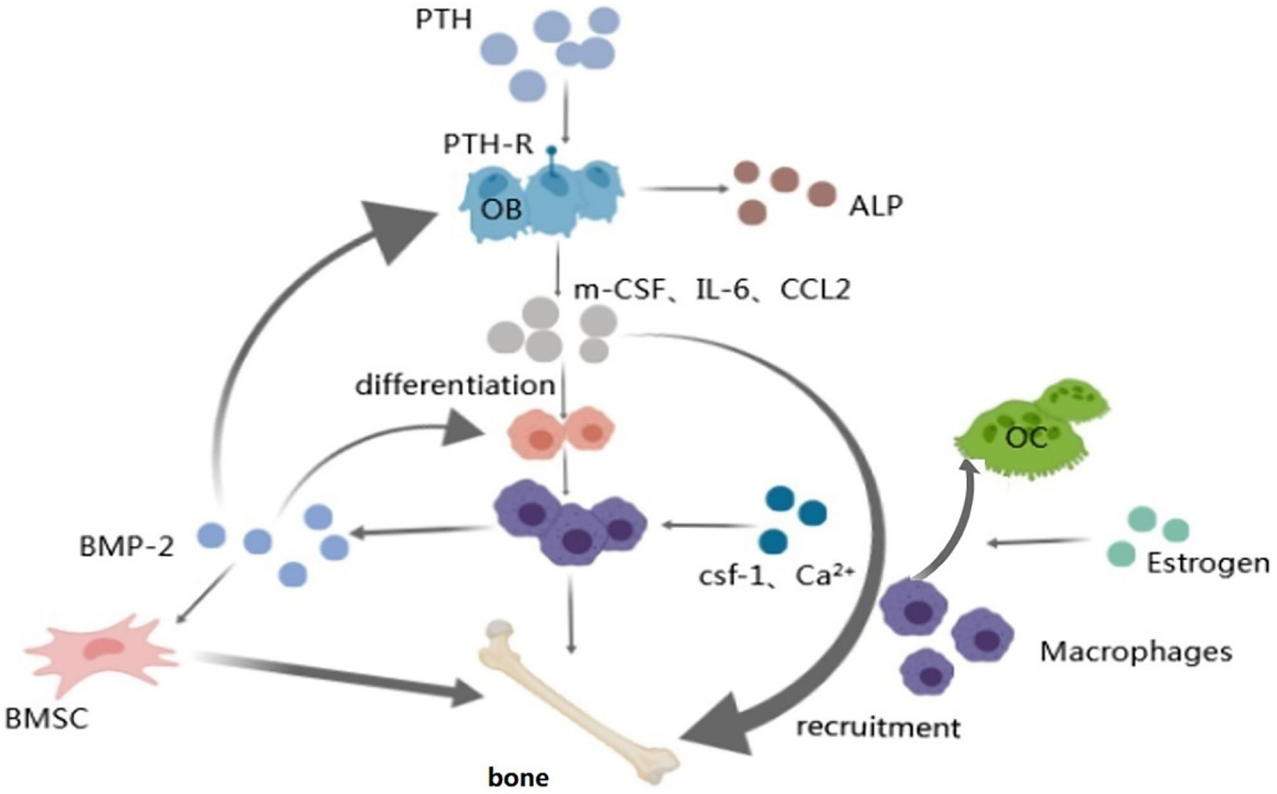


FIGURE 4 | Macrophage and regulatory hormones and factors. Arrow represents "stimulatory modification;" the gray triangle means "enlarged display." Macrophages play a part in the anabolic response to intermittent PTH therapy via osteoblasts which can secrete factors (IL-6, etc.) that promote the differentiation and recruitment of macrophages; Worthy to be mentioned the work of CSF-1 and Ca^{2+} on macrophages; Macrophage-derived BMP-2 has effect on BMSCs, osteoblasts and macrophages via BMP-R to accelerate the osteogenic differentiation so as to make bone metabolism balance; Estrogen regulates bone homeostasis mainly through osteoblasts and osteoclasts. Estrogen mainly affects the activity of macrophages by interfering with the macrophage-mediated osteoclast formation process.

the macrophage-derived EVs still need to be further investigated and could be used as an effective therapeutic strategy for tissue regeneration.

Proteomic studies have shown that macrophage-derived EVs contain a large number of alarmins (one of endogenous molecules) (**Figure 3**). Annexins can stimulate bone resorption (Li et al., 2005), improve the phagocytic efficiency of macrophage (Stukes et al., 2016), which is related to Multiple myeloma (MM) (D'Souza et al., 2012) and play an auxiliary role of macrophages in infected tissues (Silva et al., 2019; McArthur et al., 2020; Sanches et al., 2020). Galectins mainly affect the differentiation of bone marrow stromal cells (Andersen et al., 2003), osteoblast, osteoclast (Shimura et al., 2005; Nakajima et al., 2014; Simon et al., 2017; Iacobini et al., 2018) and the osteogenesis of mesenchymal stem cells (Weilner et al., 2016). What's more, HSP-60 (Koh et al., 2009), HSP-70 (Notsu et al., 2016; Nakamura et al., 2019) and fibronectin are also primarily concerned with osteoblasts (Moursi et al., 1996) and osteoclasts (Gramoun et al., 2010) to come into play (**Table 1**).

Macrophages play a critical role in bone remodeling as a source of vehicle-carried alarmins. In conclusion, future studies should be more detailed to determine the contribution of the macrophage-derived exosomes.

The body's regulatory agents are complex and poorly understood, and future efforts would be made to unravel them (**Figure 4**).

MACROPHAGE AND BONE REMODELING-RELATED BONE DISEASES

Tissue homeostasis requires a tight tissue system of various cell types to maintain. If the balance is disrupted, the progression of abnormal disease states may continue. Macrophages are involved in the development of many diseases with various phenotypes, but the direct link between macrophage function and bone-related diseases has not been thoroughly studied.

Osteoporosis

Osteoporosis is a common disease characterized by the destruction of bone mass and microstructure, resulting in brittle fractures. The characterize of age-related osteoporosis is reduced bone formation and increased marrow fat accumulation (Li et al., 2015). People with osteoporosis are under a 40% lifetime risk of fractures, most often in the spine, hip or wrist. As the aging of the population, postmenopausal osteoporosis, in particular,

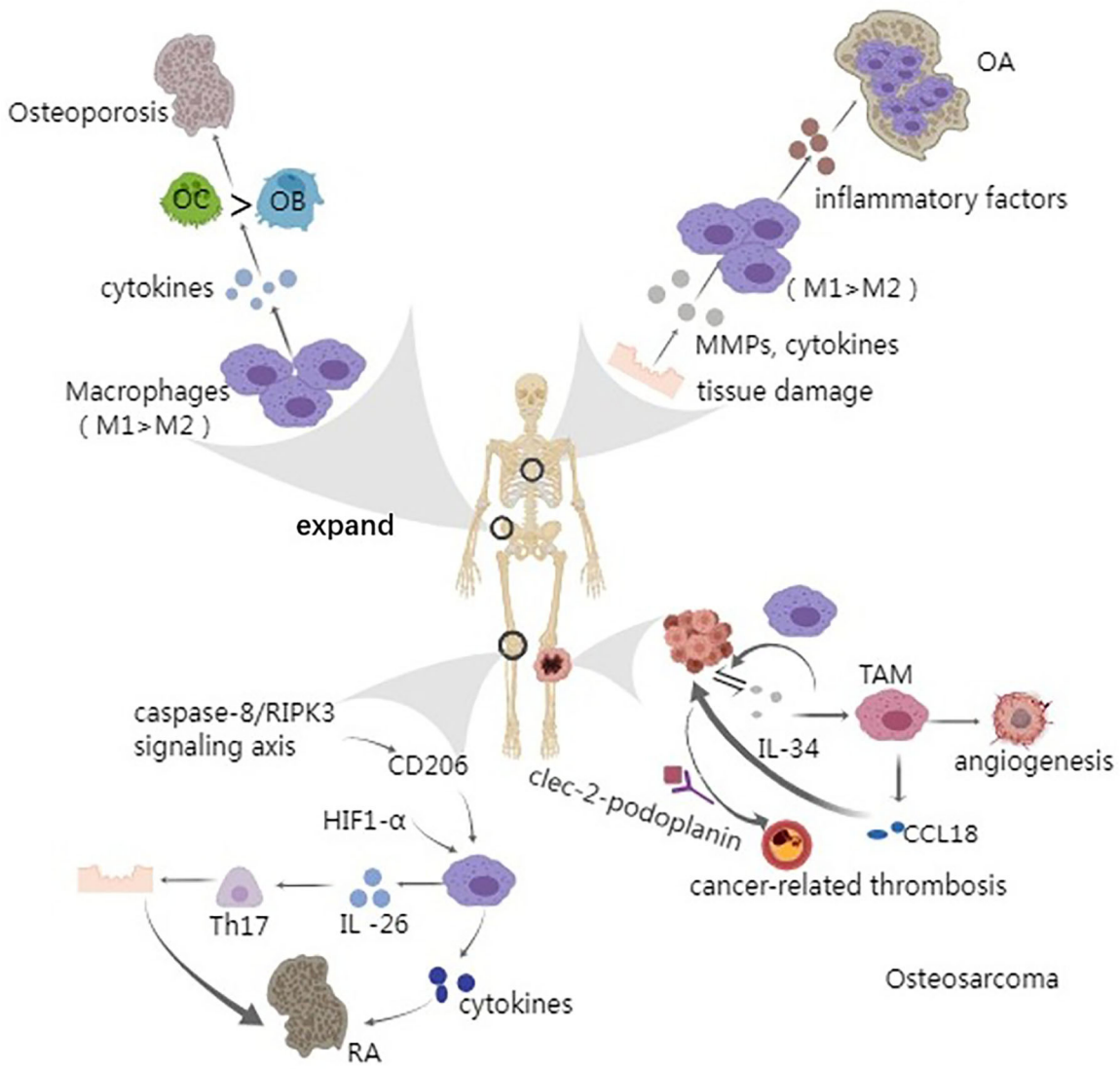


FIGURE 5 | Macrophage and bone remodeling related diseases. Arrow represents "stimulatory modification;" the gray triangle means "enlarged display." Osteoporosis is an age-related bone disease to some extent. The release and accumulation of proinflammatory cytokines can active osteoclasts and thus greatly accelerate the process of osteoporosis; The patients of osteoarthritis have a vital inducer that is tissue damage which can release various cytokines, leading to the imbalance between M1 and M2 macrophages. Usually, the quantity of M1 prevails, leading to the aggravation of OA; Caspase-8/RIPK3 signaling pathway and HIF1-α have been found to play a role in regulating macrophages, through CD206 and glycolysis, respectively. Besides, macrophages can secret IL-26, an inducer of Th17 cells which can cause autoimmune tissue damage; Osteosarcoma always occurs in the metaphyseal region of the long bone and the growth and metastasis of tumor cells have a closely relationship with IL-34 and CCL18. Moreover, tumor cell-derived IL-34 stimulates the angiogenesis of TAM. Cancer-related thrombosis could be made by the interaction of clec-2-podoplanin and the ectopic expression of podoplanin in patient's macrophages is the inducer, leading to the severe complications.

will further increase (Rachner et al., 2011). In addition, the 12-month mortality rate for osteoporotic hip and spinal fractures is up to 20%, and the incidence of fracture complications such as pneumonia or thromboembolic disease increases due to chronic fixation (Center et al., 1999).

Aging is usually accompanied by an irreversible recession in physiological functions. Age-associated metabolic dysfunction includes, but is not limited to, increased fat mass accumulation and insulin sensitivity deterioration (Huang et al., 2020). Aging is usually accompanied by a decrease in M2-type macrophages and an increase in proinflammatory factors, which promote the M1 transformation of the macrophage phenotype to aggravate the symptom. A study of transplanted bone marrow from 4-week-old mice into 12-month-old mice found improved fracture healing in older mice, which was attributed to younger inflammatory cells participating in the repair process (Xing et al., 2010). Cytokines secreted by macrophages related to osteoclasts including IL-1, IL-6, IL-18,

IL-23, IL-27, and TNF-α may promote osteoclast differentiation and activation in an inflammatory state (**Figure 5**) (Yang and Yang, 2019). As mentioned, macrophages regulate osteoclasts and osteoblasts mainly through inflammatory cytokines to mediate the occurrence of osteoporosis.

In addition to inflammatory response, latest studies have identified new regulatory mechanisms of macrophages in osteoporosis. They employed mice BMMs modified for over expression or inhibition of miR-128 levels to determine its effect on osteoclast differentiation. *In vitro* experiments showed that miR-128 may play a regulatory role in BMMs through miR-128/SIRT1/NF-kB signaling axis, and over expression or inhibition of miR-128 can significantly increase or decrease the occurrence of macrophage-derived osteoclasts, respectively (Shen et al., 2020). Further studies found that miR-506-3p can selectively inhibit NFATc1 in RANKL-induced activated rat BMMs, further reduce the release of bone resorption enzymes, thus relieving osteolysis (Dinesh et al., 2020). What's more, both the smo-GLI1/2 axis (Hh ligands permitting the activation of Hh signal transducer smoothened (SMO) and transmitting intracellular signaling through transcription factors of the GLI family)in the Hedgehog (Hh) signaling pathway (Kohara et al., 2020) and delphinidin (Imangali et al., 2020) can mediate the regulation of osteoclasts by macrophages.

The new studies provide an important basis for the treatment of senile osteoporosis by preventing osteoclast formation which derived from macrophages, but the exact mechanism of macrophages in osteoporosis has yet to be investigated.

Osteoarthritis

Osteoarthritis (Murray et al., 2014), the most common form of joint disease, is characterized by cartilage destruction, synovial fibrosis, osteophyte (osteophyte at the edge of the joint) formation and pain, and sometimes swelling of certain joints such as the knee, hip, hand, and spine (Hügle and Geurts, 2017). Depending on the world health organization (WHO), the prevalence of OA worldwide exceeds 150 million (Harrell et al., 2019). The exact mechanism of OA appears to be the result of complex interactions among mechanical, cellular, and immune factors. Synovitis has turned out to be found in the early and late stages of most patients with OA (Sellam and Berenbaum, 2010), and the accumulation of macrophages in the synovium is a feature of synovitis (Sun et al., 2016).

The high proportion of M2 macrophages in the synovial tissues has certain clinical diagnostic significance for OA (Chen et al., 2020), and the pro-inflammatory M1 macrophages are also increased significantly (Sun et al., 2017). Some studies have confirmed that macrophages play an important role in the occurrence of OA through inflammatory factors, cytokines and proteins, whether it is inflammatory or mechanical injury (Bondeson et al., 2010). Since M1 macrophages are considered to be pro-inflammatory while M2 macrophages are anti-inflammatory, the degree of imbalance between M1 and M2 macrophages in OA is related to the severity of OA (Xue et al., 2019). In OA, potential mediators (MMPs, cytokines, and growth factors due to cartilage injury) leak into synovial fluid through damaged cartilage and activate synovial macrophages. Subsequently, the proinflammatory cytokines, catabolism, and anabolic factors are released, which induce osteophyte formation (**Figure 5**) (Liu-Bryan, 2013). OA was induced by intra articular injection of collagenase (collagenase-induced osteoarthritis (CIOA) and surgical medial meniscus instability (DMM) and the result showed that compared with M2 macrophages, M1 polarization of synovial macrophages was increased in the CIOA and DMM circu;amodels (Zhang et al., 2018). All above studies indicate that M1 macrophages are potential therapeutic targets for OA therapy.

Rheumatoid Arthritis

Rheumatoid arthritis (RA) is a chronic immune-mediated inflammatory disease that affects nearly 1% of the world's population. It mainly affects synovial tissue, cartilage, and bone, leading to delayed joint damage, pain, swelling, and stiffness (McInnes and Schett, 2011). RA patients are at a higher risk of serious infection, respiratory disease, osteoporosis, cardiovascular disease, cancer, and death than the general population.

The exact pathogenesis of RA is unknown, but the activated macrophages play an important role in the pathogenesis. Caspase-8 is a promoter of apoptosis and an inhibitor of cell necrosis. Studies have found that the caspase-8/RIPK3 signaling axis is involved in maintaining stability of macrophages in synovial tissues, thereby limiting arthritis. The lack of caspase-8 in mouse synovium macrophage reduces the expression of CD206, resulting the inadequate of caspase-8-deficient macrophages to endocytosis of cellular debris caused by joint inflammation, thereby failing to control subsequent inflammation (**Figure 5**) (Dominguez et al., 2017). IL-34 is a pleiotropic cytokine and it's expression is associated with inflammatory diseases involving excessive proliferation of monocytes/macrophages (Ushach and Zlotnik, 2016). The plasma concentration of IL-34 in synovial fluid and serum is low (Nandi et al., 2012; Tian et al., 2013), but in rheumatoid arthritis, the content of IL-34 is dramatically increased, hence it's level is a useful biomarker for predicting the progression of rheumatoid arthritis (Ding et al., 2015; Liu et al., 2018; Ge et al., 2019). IL-34 and CSF-1R act in combination on mononuclear cell line (THP-1) can through a series of reactions to promote the production of helper T (Th17) cells, which is the main driver of autoimmune tissue damage, especially RA (Kuwabara et al., 2017). Additional data indicated that mononuclear/macrophage-derived IL−26 stimulation is also an important inducer of Th17 cells in RA (**Figure 5**) (Kragstrup et al., 2018). In addition, scientists have found that increasing the amount of anti-inflammatory macrophages by decreasing FLIP (flice-like inhibitory protein, highly expressed in RA synovial macrophages) in macrophages may be an effective treatment for suppressing inflammation (Huang et al., 2017). What's more, it is now becoming clear that metabolic pathways are the characteristic of rheumatoid arthritis and they may be the potential therapeutic targets (Sanchez-Lopez et al., 2019). Glycolysis is the preferred source of ATP under anoxic conditions (Epstein et al., 2017). Inflammatory joints are usually in a severe hypoxia environment, which results in the synovial fluid hypoxia inducing factor 1 α (HIF1-α) generation

increases. The HIF1-α can inhibit the progression of glycolysis to stimulate the production of IL-1 and other pro-inflammatory cytokines by macrophages (**Figure 5**) (Tannahill et al., 2013), thus to accelerate the incidence of RA, increase oxidative damage and cartilage erosion (Hua and Dias, 2016).

Osteosarcoma

Osteosarcoma is the most common primary malignant bone tumor. It can occur in any bone but most seen in the metaphyseal region of the long bone, and initially presents as progressive pain and/or swelling. Risk factors are various (Harrison and Schwartz, 2017) and this tumor tend to involve the lung (Kelleher and O'Sullivan, 2017).

Both cancer cells and immune cells can secrete various interleukins such as IL-34 (Franzè et al., 2020), which can increase the recruitment of M2 macrophages and promote the growth and metastasis of osteosarcoma (Ségaliny et al., 2015). There is increasing evidences that IL-34 promotes tumorigenesis through autocrine and paracrine mechanisms. In the autocrine pathway, IL-34 interacts with the M-CSF receptor on cancer cells to activate signaling pathways, stimulate the growth, and spread of cancer cells and increase their resistance to chemotherapy drugs (**Figure 5**) (Baghdadi et al., 2016). In the paracrine pathway, IL-34 produced by tumor cells and/or immune cells triggers M-CSF1-R signaling in tumor-associated macrophages (TAMs), thereby promoting recruitment of TAM to the tumor area, facilitating the formation of new blood vessels and the exosmosis of immunosuppressive cells (**Figure 5**) (Mantovani et al., 2017). CCL-18 (c-c motif chemokine ligand 18) is an element secreted by TAM. Studies have shown that CCL-18 can be the activator of the EP300/UCA1/Wnt/hy-catenin pathway and promote the proliferation and migration of OS cells (**Figure 5**) (Su et al., 2019). Patients with cancer have an increased risk of thromboembolism. Platelet-activated receptor c-type lectin-like receptor 2 (clec-2) is almost specifically expressed in human platelets/megakaryocytes. The endogenous ligand podoplanin is a membrane protein. Patients with osteosarcoma may have ectopic expression of podoplanin in macrophages, and the interaction of clec-2-podoplanin stimulates the formation of cancer-related thrombosis, thus aggravating the patient's condition (**Figure 5**) (Suzuki-Inoue, 2019). The exact mechanism of osteosarcoma is still unknown, but recent studies on macrophages may provide new methods for clinical treatment and prevention of complications in patients with osteosarcoma.

Bisphosphonates, PTH, estrogen, or selective estrogen receptor modulators (SERMs) and calcitonin have been used to treat osteoporosis. Non-steroidal anti-inflammatory drugs are commonly used in rheumatoid. Moreover, surgical treatment is considered the first choice for the treatment of OA and osteosarcoma. But long-term use of PTH/bisphosphonates can increase the risk of severe side effects (osteosarcoma, mandibular necrosis, and atypical femoral fractures). Surgical treatment is unsuitable for the patients who cannot tolerate it. Thus, it seems that new treatments for common bone diseases are especially important in terms of conservative treatment. At present, we have known that bone tissue macrophages can communicate with a variety of cells in the bone by secreting of a series of hormones, cytokines, and exosomes. They mediate bone remodeling in various aspects and provides a new direction for clinical treatments.

CONCLUSIONS AND FUTURE DIRECTIONS

Current knowledge of macrophages has been outlined, including their polarization, support for bone formation, potential role in bone biology, and regulation of bone metastasis. Osteal macrophages construct the cell canopy structure at the bone reconstruction site, anabolic cytokines promote bone formation and coordinate the coupling between osteoclasts and osteoblasts. However, the study of osteal macrophages is a relatively new research field, and many important and puzzling research problems still exist. The identification of specific markers of osteal macrophages remains to be explored, and the mice with specific Cre expression in BMMs/osteal macrophages is also expected to provide greater convenience for scientific research.

The potential role of microRNAs and protein profiles in exosomes, secreted by bone-resident macrophages, remains the critical issues. The prospect of improving patient outcomes and designing new therapeutic approaches are the eventual goals by better understanding the change of macrophages in the state of aging and figuring out the effects of the change on bone remodeling related diseases. Presently, new treatments targeting macrophages mainly focus on mediating the inflammatory response while lack the specific methods targeting the communications of bone-resident macrophages and other cells. Thus, validation of the role of macrophages in human bone disease requires further investigation. Targeting bone-resident macrophages may be a powerful tool for the treatment of bone remodeling related diseases.

AUTHOR CONTRIBUTIONS

CL conceived the presented idea and supervised the written of this work. KC wrote the manuscript with supports from CL, XL, MH, YJ, CH, WH, JH, LL, and MY. All authors discussed the results and contributed to the final manuscript.

FUNDING

This work was supported by the National Key R&D Program of China (Grant No. 2019YFA0111900), the National Natural Science Foundation of China (Grants 81922017, 81873669, and 81802209), the Hunan Province Natural Science Foundation of China (Grant 2018JJ3863), the Innovation Driven Project of Central South University (Grant 20170033010017), and the Talent Plan of Xiangya Hospital in Central South University (Grants 35 and 41).

REFERENCES

Adapala, N. S., Swarnkar, G., Arra, M., Shen, J., Mbalaviele, G., Ke, K., et al. (2020). Inflammatory osteolysis is regulated by site-specific ISGylation of the scaffold protein NEMO. *Elife.* 9:e56095. doi: 10.7554/eLife.56095

Alexander, K. A., Chang, M. K., Maylin, E. R., Kohler, T., Müller, R., Wu, A. C., et al. (2011). Osteal macrophages promote *in vivo* intramembranous bone healing in a mouse tibial injury model. *J. Bone Miner. Res.* 26, 1517–1532. doi: 10.1002/jbmr.354

Andersen, H., Jensen, O. N., Moiseeva, E. P., and Eriksen, E. F. (2003). A proteome study of secreted prostatic factors affecting osteoblastic activity: galectin-1 is involved in differentiation of human bone marrow stromal cells. *J. Bone Miner. Res.* 18, 195–203. doi: 10.1359/jbmr.2003.18.2.195

Arora, S., Dev, K., Agarwal, B., Das, P., and Syed, M. A. (2018). Macrophages: their role, activation and polarization in pulmonary diseases. *Immunobiology* 223, 383–396. doi: 10.1016/j.imbio.2017.11.001

Assoian, R. K., Fleurdelys, B. E., Stevenson, H. C., Miller, P. J., Madtes, D. K., Raines, E. W., et al. (1987). Expression and secretion of type beta transforming growth factor by activated human macrophages. *Proc. Natl. Acad. Sci. U.S.A.* 84, 6020–6024. doi: 10.1073/pnas.84.17.6020

Baghdadi, M., Wada, H., Nakanishi, S., Abe, H., Han, N., Putra, W. E., et al. (2016). Chemotherapy-induced IL34 enhances immunosuppression by tumor-associated macrophages and mediates survival of chemoresistant lung cancer cells. *Cancer Res.* 76, 6030–6042. doi: 10.1158/0008-5472.CAN-16-1170

Batoon, L., Millard, S. M., Wullschleger, M. E., Preda, C., Wu, A. C., Kaur, S., et al. (2019). $CD169^{+}$ macrophages are critical for osteoblast maintenance and promote intramembranous and endochondral ossification during bone repair. *Biomaterials* 196, 51–66. doi: 10.1016/j.biomaterials.2017.10.033

Bernardo, M. E., and Fibbe, W. E. (2013). Mesenchymal stromal cells: sensors and switchers of inflammation. *Cell Stem Cell* 13, 392–402. doi: 10.1016/j.stem.2013.09.006

Biswas, S. K., and Mantovani, A. (2010). Macrophage plasticity and interaction with lymphocyte subsets: cancer as a paradigm. *Nat. Immunol.* 11, 889–896. doi: 10.1038/ni.1937

Bondeson, J., Blom, A. B., Wainwright, S., Hughes, C., Caterson, B., and van den Berg, W. B. (2010). The role of synovial macrophages and macrophage-produced mediators in driving inflammatory and destructive responses in osteoarthritis. *Arthritis Rheum.* 62, 647–657. doi: 10.1002/art.27290

Center, J. R., Nguyen, T. V., Schneider, D., Sambrook, P. N., and Eisman, J. A. (1999). Mortality after all major types of osteoporotic fracture in men and women: an observational study. *Lancet* 353, 878–882. doi: 10.1016/S0140-6736(98)09075-8

Champagne, C. M., Takebe, J., Offenbacher, S., and Cooper, L. F. (2002). Macrophage cell lines produce osteoinductive signals that include bone morphogenetic protein-2. *Bone* 30, 26–31. doi: 10.1016/S8756-3282(01)00638-X

Chang, M. K., Raggatt, L. J., Alexander, K. A., Kuliwaba, J. S., Fazzalari, N. L., Schroder, K., et al. (2008). Osteal tissue macrophages are intercalated throughout human and mouse bone lining tissues and regulate osteoblast function *in vitro* and *in vivo*. *J. Immunol.* 181, 1232–1244. doi: 10.4049/jimmunol.181.2.1232

Chen, Z., Ma, Y., Li, X., Deng, Z., Zheng, M., and Zheng, Q. (2020). The immune cell landscape in different anatomical structures of knee in osteoarthritis: a gene expression-based study. *Biomed. Res. Int.* 2020:9647072. doi: 10.1155/2020/9647072

Cho, D. I., Kim, M. R., Jeong, H. Y., Jeong, H. C., Jeong, M. H., Yoon, S. H., et al. (2014a). Mesenchymal stem cells reciprocally regulate the M1/M2 balance in mouse bone marrow-derived macrophages. *Exp. Mol. Med.* 46:e70. doi: 10.1038/emm.2013.135

Cho, S. W., Soki, F. N., Koh, A. J., Eber, M. R., Entezami, P., Park, S. I., et al. (2014b). Osteal macrophages support physiologic skeletal remodeling and anabolic actions of parathyroid hormone in bone. *Proc. Natl. Acad. Sci. U.S.A.* 111, 1545–1550. doi: 10.1073/pnas.1315153111

Colombo, M., Raposo, G., and Théry, C. (2014). Biogenesis, secretion, and intercellular interactions of exosomes and other extracellular vesicles. *Annu. Rev. Cell Dev. Biol.* 30, 255–289. doi: 10.1146/annurev-cellbio-101512-122326

Cui, H., He, Y., Chen, S., Zhang, D., Yu, Y., and Fan, C. (2019). Macrophage-derived miRNA-containing exosomes induce peritendinous fibrosis after tendon injury through the miR-21-5p/Smad7 pathway. *Mol. Ther. Nucl. Acids* 14, 114–130. doi: 10.1016/j.omtn.2018.11.006

Das, A., Ganesh, K., Khanna, S., Sen, C. K., and Roy, S. (2014). Engulfment of apoptotic cells by macrophages: a role of microRNA-21 in the resolution of wound inflammation. *J. Immunol.* 192, 1120–1129. doi: 10.4049/jimmunol.1300613

Das, A., Sinha, M., Datta, S., Abas, M., Chaffee, S., Sen, C. K., and Roy, S. (2015). Monocyte and macrophage plasticity in tissue repair and regeneration. *Am. J. Pathol.* 185, 2596–2606. doi: 10.1016/j.ajpath.2015.06.001

Datta, H. K., Ng, W. F., Walker, J. A., Tuck, S. P., and Varanasi, S. S. (2008). The cell biology of bone metabolism. *J. Clin. Pathol.* 61, 577–587. doi: 10.1136/jcp.2007.048868

Dinesh, P., Kalaiselvan, S., Sujitha, S., and Rasool, M. (2020). miR-506-3p alleviates uncontrolled osteoclastogenesis via repression of RANKL/NFATc1 signaling pathway. *J. Cell. Physiol.* 235, 9497–9509. doi: 10.1002/jcp.29757

Ding, R., Li, P., Song, D., Zhang, X., and Bi, L. (2015). Predictors of response to TNF-α antagonist therapy in Chinese rheumatoid arthritis. *Clin. Rheumatol.* 34, 1203–1210. doi: 10.1007/s10067-015-2973-3

Dominguez, S., Montgomery, A. B., Haines, G. K. 3rd, Bloomfield, C. L., and Cuda, C. M. (2017). The caspase-8/RIPK3 signaling axis in antigen presenting cells controls the inflammatory arthritic response. *Arthritis Res. Ther.* 19:224. doi: 10.1186/s13075-017-1436-4

D'Souza, S., Kurihara, N., Shiozawa, Y., Joseph, J., Taichman, R., Galson, D. L., et al. (2012). Annexin II interactions with the annexin II receptor enhance multiple myeloma cell adhesion and growth in the bone marrow microenvironment. *Blood* 119, 1888–1896. doi: 10.1182/blood-2011-11-393348

Elango, J., Sanchez, C., de Val, J., Henrotin, Y., Wang, S., Motaung, K., et al. (2018). Cross-talk between primary osteocytes and bone marrow macrophages for osteoclastogenesis upon collagen treatment. *Sci. Rep.* 8:5318. doi: 10.1038/s41598-018-23532-x

Epstein, T., Gatenby, R. A., and Brown, J. S. (2017). The Warburg effect as an adaptation of cancer cells to rapid fluctuations in energy demand. *PLoS ONE* 12:e0185085. doi: 10.1371/journal.pone.0185085

Fierro, F. A., Nolta, J. A., and Adamopoulos, I. E. (2017). Concise review: stem cells in osteoimmunology. *Stem Cells* 35, 1461–1467. doi: 10.1002/stem.2625

Franzè, E., Stolfi, C., Troncone, E., Scarozza, P., and Monteleone, G. (2020). Role of interleukin-34 in cancer. *Cancers* 12:252. doi: 10.3390/cancers12010252

Franz-Odendaal, T. A., Hall, B. K., and Witten, P. E. (2006). Buried alive: how osteoblasts become osteocytes. *Dev. Dyn.* 235, 176–190. doi: 10.1002/dvdy.20603

Ge, Y., Huang, M., and Yao, Y. M. (2019). Immunomodulation of interleukin-34 and its potential significance as a disease biomarker and therapeutic target. *Int. J. Biol. Sci.* 15, 1835–1845. doi: 10.7150/ijbs.35070

Geissmann, F., Manz, M. G., Jung, S., Sieweke, M. H., Merad, M., and Ley, K. (2010). Development of monocytes, macrophages, and dendritic cells. *Science* 327, 656–661. doi: 10.1126/science.1178331

Genin, M., Clement, F., Fattaccioli, A., Raes, M., and Michiels, C. (2015). M1 and M2 macrophages derived from THP-1 cells differentially modulate the response of cancer cells to etoposide. *BMC Cancer* 15:577. doi: 10.1186/s12885-015-1546-9

Gordon, S. (2008). Elie Metchnikoff: father of natural immunity. *Eur. J. Immunol.* 38, 3257–3264. doi: 10.1002/eji.200838855

Gramoun, A., Azizi, N., Sodek, J., Heersche, J. N., Nakchbandi, I., and Manolson, M. F. (2010). Fibronectin inhibits osteoclastogenesis while enhancing osteoclast activity via nitric oxide and interleukin-1β-mediated signaling pathways. *J. Cell. Biochem.* 111, 1020–1034. doi: 10.1002/jcb.22791

Guihard, P., Danger, Y., Brounais, B., David, E., Brion, R., Delecrin, J., et al. (2012). Induction of osteogenesis in mesenchymal stem cells by activated monocytes/macrophages depends on oncostatin M signaling. *Stem Cells.* 30, 762–772. doi: 10.1002/stem.1040

Guo, Y., Cao, W., and Zhu, Y. (2019). Immunoregulatory functions of the IL-12 family of cytokines in antiviral systems. *Viruses* 11:772. doi: 10.3390/v11090772

Harmer, D., Falank, C., and Reagan, M. R. (2018). Interleukin-6 interweaves the bone marrow microenvironment, bone loss, and multiple myeloma. *Front. Endocrinol.* 9:788. doi: 10.3389/fendo.2018.00788

Harrell, C. R., Markovic, B. S., Fellabaum, C., Arsenijevic, A., and Volarevic, V. (2019). Mesenchymal stem cell-based therapy of osteoarthritis: current

knowledge and future perspectives. *Biomed. Pharmacother.* 109, 2318–2326. doi: 10.1016/j.biopha.2018.11.099

Harrison, D. J., and Schwartz, C. L. (2017). Osteogenic sarcoma: systemic chemotherapy options for localized disease. *Curr. Treat. Options Oncol.* 18:24. doi: 10.1007/s11864-017-0464-2

Heideveld, E., and van den Akker, E. (2017). Digesting the role of bone marrow macrophages on hematopoiesis. *Immunobiology* 222, 814–822. doi: 10.1016/j.imbio.2016.11.007

Heymans, S., Corsten, M. F., Verhesen, W., Carai, P., van Leeuwen, R. E., Custers, K., et al. (2013). Macrophage microRNA-155 promotes cardiac hypertrophy and failure. *Circulation* 128, 1420–1432. doi: 10.1161/CIRCULATIONAHA.112.001357

Horwood, N. J. (2016). Macrophage polarization and bone formation: a review. *Clin. Rev. Allergy Immunol.* 51, 79–86. doi: 10.1007/s12016-015-8519-2

Hua, S., and Dias, T. H. (2016). Hypoxia-inducible factor (HIF) as a target for novel therapies in rheumatoid arthritis. *Front. Pharmacol.* 7:184. doi: 10.3389/fphar.2016.00184

Huang, Q. Q., Birkett, R., Doyle, R. E., Haines, G. K., Perlman, H., Shi, B., et al. (2017). Association of increased F4/80(high) macrophages with suppression of serum-transfer arthritis in mice with reduced FLIP in myeloid cells. *Arthritis Rheumatol.* 69, 1762–1771. doi: 10.1002/art.40151

Huang, Y., Xiao, Y., Liu, Y., Guo, M., Guo, Q., Zhou, F., et al. (2020). MicroRNA-188 regulates aging-associated metabolic phenotype. *Aging Cell.* 19:e13077. doi: 10.1111/acel.13077

Hügle, T., and Geurts, J. (2017). What drives osteoarthritis?-synovial versus subchondral bone pathology. *Rheumatology* 56, 1461–1471. doi: 10.1093/rheumatology/kew389

Iacobini, C., Blasetti Fantauzzi, C., Bedini, R., Pecci, R., Bartolazzi, A., Amadio, B., et al. (2018). Galectin-3 is essential for proper bone cell differentiation and activity, bone remodeling and biomechanical competence in mice. *Metab. Clin. Exp.* 83, 149–158. doi: 10.1016/j.metabol.2018.02.001

Imangali, N., Phan, Q. T., Mahady, G., and Winkler, C. (2020). The dietary anthocyanin delphinidin prevents bone resorption by inhibiting Rankl-induced differentiation of osteoclasts in a medaka (Oryzias latipes) model of osteoporosis. *J. Fish Biol.* doi: 10.1111/jfb.14317. [Epub ahead of print].

Jafarnezhad-Ansariha, F., Yekaninejad, M. S., Jamshidi, A. R., Mansouri, R., Vojdanian, M., Mahmoudi, M., et al. (2018). The effects of β-D-mannuronic acid (M2000), as a novel NSAID, on COX1 and COX2 activities and gene expression in ankylosing spondylitis patients and the murine monocyte/macrophage, J774 cell line. *Inflammopharmacology* 26, 375–384. doi: 10.1007/s10787-017-0386-4

Jamalpoor, Z., Asgari, A., Lashkari, M. H., Mirshafiey, A., and Mohsenzadegan, M. (2018). Modulation of macrophage polarization for bone tissue engineering applications. *Iran. J. Allergy Asthma Immunol.* 17, 398–408. doi: 10.18502/ijaai.v17i5.298

Jetten, N., Verbruggen, S., Gijbels, M. J., Post, M. J., De Winther, M. P., and Donners, M. M. (2014). Anti-inflammatory M2, but not pro-inflammatory M1 macrophages promote angiogenesis *in vivo*. *Angiogenesis* 17, 109–118. doi: 10.1007/s10456-013-9381-6

Jin, H., Yao, L., Chen, K., Liu, Y., Wang, Q., Wang, Z., et al. (2019). Evodiamine inhibits RANKL-induced osteoclastogenesis and prevents ovariectomy-induced bone loss in mice. *J. Cell. Mol. Med.* 23, 522–534. doi: 10.1111/jcmm.13955

Jin, S., Meng, C., He, Y., Wang, X., Zhang, Q., Wang, Z., et al. (2020). Curcumin prevents osteocyte apoptosis by inhibiting M1-type macrophage polarization in mice model of glucocorticoid-associated osteonecrosis of the femoral head. *J. Orthop. Res.* 38, 2020–2030. doi: 10.1002/jor.24619

Juhas, M., Abutaleb, N., Wang, J. T., Ye, J., Shaikh, Z., Sriworarat, C., Qian, Y., and Bursac, N. (2018). Incorporation of macrophages into engineered skeletal muscle enables enhanced muscle regeneration. *Nat. Biomed. Eng.* 2, 942–954. doi: 10.1038/s41551-018-0290-2

Karshovska, E., Wei, Y., Subramanian, P., Mohibullah, R., Geißler, C., Baatsch, I., et al. (2020). HIF-1α (hypoxia-inducible factor-1α) promotes macrophage necroptosis by regulating miR-210 and miR-383. *Arterioscler. Thromb. Vasc. Biol.* 40, 583–596. doi: 10.1161/ATVBAHA.119.313290

Kaur, S., Raggatt, L. J., Batoon, L., Hume, D. A., Levesque, J. P., and Pettit, A. R. (2017). Role of bone marrow macrophages in controlling homeostasis and repair in bone and bone marrow niches. *Semin. Cell Dev. Biol.* 61, 12–21. doi: 10.1016/j.semcdb.2016.08.009

Kawabata, M., Imamura, T., and Miyazono, K. (1998). Signal transduction by bone morphogenetic proteins. *Cytokine Growth Factor Rev.* 9, 49–61. doi: 10.1016/S1359-6101(97)00036-1

Kelleher, F. C., and O'Sullivan, H. (2017). Monocytes, macrophages, and osteoclasts in osteosarcoma. *J. Adolesc. Young Adult Oncol.* 6, 396–405. doi: 10.1089/jayao.2016.0078

Kim, J., and Hematti, P. (2009). Mesenchymal stem cell-educated macrophages: a novel type of alternatively activated macrophages. *Exp. Hematol.* 37, 1445–1453. doi: 10.1016/j.exphem.2009.09.004

Koh, J. M., Lee, Y. S., Kim, Y. S., Park, S. H., Lee, S. H., Kim, H. H., et al. (2009). Heat shock protein 60 causes osteoclastic bone resorption via toll-like receptor-2 in estrogen deficiency. *Bone* 45, 650–660. doi: 10.1016/j.bone.2009.06.007

Kohara, Y., Haraguchi, R., Kitazawa, R., Imai, Y., and Kitazawa, S. (2020). Hedgehog inhibitors suppress osteoclastogenesis in *in vitro* cultures, and deletion of smo in macrophage/osteoclast lineage prevents age-related bone loss. *Int. J. Mol. Sci.* 21:2745. doi: 10.3390/ijms21082745

Kragstrup, T. W., Andersen, T., Heftdal, L. D., Hvid, M., Gerwien, J., Sivakumar, P., et al. (2018). The IL-20 cytokine family in rheumatoid arthritis and spondyloarthritis. *Front. Immunol.* 9:2226. doi: 10.3389/fimmu.2018.02226

Kreutz, M., Andreesen, R., Krause, S. W., Szabo, A., Ritz, E., and Reichel, H. (1993). 1,25-dihydroxyvitamin D3 production and vitamin D3 receptor expression are developmentally regulated during differentiation of human monocytes into macrophages. *Blood* 82, 1300–1307. doi: 10.1182/blood.V82.4.1300.1300

Kuwabara, T., Ishikawa, F., Kondo, M., and Kakiuchi, T. (2017). The role of IL-17 and related cytokines in inflammatory autoimmune diseases. *Mediators Inflamm.* 2017:3908061. doi: 10.1155/2017/3908061

Le, B. Q., Nurcombe, V., Cool, S. M., van Blitterswijk, C. A., de Boer, J., and LaPointe, V. L. S. (2017). The components of bone and what they can teach us about regeneration. *Materials* 11:14. doi: 10.3390/ma11010014

Li, C. J., Cheng, P., Liang, M. K., Chen, Y. S., Lu, Q., Wang, J. Y., et al. (2015). MicroRNA-188 regulates age-related switch between osteoblast and adipocyte differentiation. *J. Clin. Invest.* 125, 1509–1522. doi: 10.1172/JCI77716

Li, C. J., Xiao, Y., Yang, M., Su, T., Sun, X., Guo, Q., et al. (2018). Long noncoding RNA Bmncr regulates mesenchymal stem cell fate during skeletal aging. *J. Clin. Invest.* 128, 5251–5266. doi: 10.1172/JCI99044

Li, F., Chung, H., Reddy, S. V., Lu, G., Kurihara, N., Zhao, A. Z., et al. (2005). Annexin II stimulates RANKL expression through MAPK. *J. Bone Miner. Res.* 20, 1161–1167. doi: 10.1359/JBMR.050207

Liu, Q., Fan, J., Bai, J., Peng, L., Zhang, T., Deng, L., et al. (2018). IL-34 promotes foam cell formation by enhancing CD36 expression through p38 MAPK pathway. *Sci. Rep.* 8:17347. doi: 10.1038/s41598-018-35485-2

Liu-Bryan, R. (2013). Synovium and the innate inflammatory network in osteoarthritis progression. *Curr. Rheumatol. Rep.* 15:323. doi: 10.1007/s11926-013-0323-5

Lu, L. Y., Loi, F., Nathan, K., Lin, T. H., Pajarinen, J., Gibon, E., et al. (2017). Pro-inflammatory M1 macrophages promote osteogenesis by mesenchymal stem cells via the COX-2-prostaglandin E2 pathway. *J. Orthop. Res.* 35, 2378–2385. doi: 10.1002/jor.23553

Maggini, J., Mirkin, G., Bognanni, I., Holmberg, J., Piazzón, I. M., Nepomnaschy, I., et al. (2010). Mouse bone marrow-derived mesenchymal stromal cells turn activated macrophages into a regulatory-like profile. *PLoS ONE* 5:e9252. doi: 10.1371/journal.pone.0009252

Mantovani, A., Marchesi, F., Malesci, A., Laghi, L., and Allavena, P. (2017). Tumour-associated macrophages as treatment targets in oncology. *Nat. Rev. Clin. Oncol.* 14, 399–416. doi: 10.1038/nrclinonc.2016.217

Mantovani, A., Sica, A., Sozzani, S., Allavena, P., Vecchi, A., and Locati, M. (2004). The chemokine system in diverse forms of macrophage activation and polarization. *Trends Immunol.* 25, 677–686. doi: 10.1016/j.it.2004.09.015

McArthur, S., Juban, G., Gobbetti, T., Desgeorges, T., Theret, M., Gondin, J., et al. (2020). Annexin A1 drives macrophage skewing to accelerate muscle regeneration through AMPK activation. *J. Clin. Invest.* 130, 1156–1167. doi: 10.1172/JCI124635

McInnes, I. B., and Schett, G. (2011). The pathogenesis of rheumatoid arthritis. *N. Engl. J. Med.* 365, 2205–2219. doi: 10.1056/NEJMra1004965

Michalski, M. N., and McCauley, L. K. (2017). Macrophages and skeletal health. *Pharmacol. Ther.* 174, 43–54. doi: 10.1016/j.pharmthera.2017.02.017

Miron, R. J., Zohdi, H., Fujioka-Kobayashi, M., and Bosshardt, D. D. (2016). Giant cells around bone biomaterials: osteoclasts or multi-nucleated giant cells? *Acta Biomater*. 46, 15–28. doi: 10.1016/j.actbio.2016.09.029

Mohsenzadegan, M., Fayazi, M. R., Abdolmaleki, M., Bakhshayesh, M., Seif, F., and Mousavizadeh, K. (2015). Direct immunomodulatory influence of IFN-β on human astrocytoma cells. *Immunopharmacol. Immunotoxicol.* 37, 214–219. doi: 10.3109/08923973.2015.1014559

Mosser, D. M. (2003). The many faces of macrophage activation. *J. Leukoc. Biol.* 73, 209–212. doi: 10.1189/jlb.0602325

Mosser, D. M., and Edwards, J. P. (2008). Exploring the full spectrum of macrophage activation. *Nat. Rev. Immunol.* 8, 958–969. doi: 10.1038/nri2448

Moursi, A. M., Damsky, C. H., Lull, J., Zimmerman, D., Doty, S. B., Aota, S., et al. (1996). Fibronectin regulates calvarial osteoblast differentiation. *J. Cell Sci.* 109, 1369–1380.

Murray, P. J., Allen, J. E., Biswas, S. K., Fisher, E. A., Gilroy, D. W., Goerdt, S., et al. (2014). Macrophage activation and polarization: nomenclature and experimental guidelines. *Immunity* 41, 14–20. doi: 10.1016/j.immuni.2014.06.008

Nakajima, K., Kho, D. H., Yanagawa, T., Harazono, Y., Gao, X., Hogan, V., et al. (2014). Galectin-3 inhibits osteoblast differentiation through notch signaling. *Neoplasia* 16, 939–949. doi: 10.1016/j.neo.2014.09.005

Nakamura, M., Notsu, K., and Nakagawa, M. (2019). Heat shock protein 60 negatively regulates the biological functions of ubiquitin-like protein MNSFβ in macrophages. *Mol. Cell. Biochem*. 456, 29–39. doi: 10.1007/s11010-018-3487-5

Nandi, S., Gokhan, S., Dai, X. M., Wei, S., Enikolopov, G., Lin, H., et al. (2012). The CSF-1 receptor ligands IL-34 and CSF-1 exhibit distinct developmental brain expression patterns and regulate neural progenitor cell maintenance and maturation. *Dev. Biol.* 367, 100–113. doi: 10.1016/j.ydbio.2012.03.026

Nicolaidou, V., Wong, M. M., Redpath, A. N., Ersek, A., Baban, D. F., Williams, L. M., et al. (2012). Monocytes induce STAT3 activation in human mesenchymal stem cells to promote osteoblast formation. *PLoS ONE* 7:e39871. doi: 10.1371/journal.pone.0039871

Notsu, K., Nakagawa, M., and Nakamura, M. (2016). Ubiquitin-like protein MNSFβ noncovalently binds to molecular chaperone HSPA8 and regulates osteoclastogenesis. *Mol. Cell. Biochem*. 421, 149–156. doi: 10.1007/s11010-016-2795-x

Ogle, M. E., Segar, C. E., Sridhar, S., and Botchwey, E. A. (2016). Monocytes and macrophages in tissue repair: implications for immunoregenerative biomaterial design. *Exp. Biol. Med*. 241, 1084–1097. doi: 10.1177/1535370216650293

Okamoto, K., and Takayanagi, H. (2011). Regulation of bone by the adaptive immune system in arthritis. *Arthritis Res. Ther*. 13:219. doi: 10.1186/ar3323

Pardali, E., Makowski, L. M., Leffers, M., Borgscheiper, A., and Waltenberger, J. (2018). BMP-2 induces human mononuclear cell chemotaxis and adhesion and modulates monocyte-to-macrophage differentiation. *J. Cell. Mol. Med*. 22, 5429–5438. doi: 10.1111/jcmm.13814

Park, J. H., Lee, N. K., and Lee, S. Y. (2017). Current understanding of RANK signaling in osteoclast differentiation and maturation. *Mol. Cells* 40, 706–713. doi: 10.14348/molcells.2017.0225

Pirraco, R. P., Reis, R. L., and Marques, A. P. (2013). Effect of monocytes/macrophages on the early osteogenic differentiation of hBMSCs. *J. Tissue Eng. Regen. Med*. 7, 392–400. doi: 10.1002/term.535

Rachner, T. D., Khosla, S., and Hofbauer, L. C. (2011). Osteoporosis: now and the future. *Lancet* 377, 1276–1287. doi: 10.1016/S0140-6736(10)62349-5

Raggatt, L. J., Wullschleger, M. E., Alexander, K. A., Wu, A. C., Millard, S. M., Kaur, S., et al. (2014). Fracture healing via periosteal callus formation requires macrophages for both initiation and progression of early endochondral ossification. *Am. J. Pathol*. 184, 3192–3204. doi: 10.1016/j.ajpath.2014.08.017

Rawadi, G., Vayssière, B., Dunn, F., Baron, R., and Roman-Roman, S. (2003). BMP-2 controls alkaline phosphatase expression and osteoblast mineralization by a Wnt autocrine loop. *J. Bone Miner. Res*. 18, 1842–1853. doi: 10.1359/jbmr.2003.18.10.1842

Ren, G., Zhang, L., Zhao, X., Xu, G., Zhang, Y., Roberts, A. I., et al. (2008). Mesenchymal stem cell-mediated immunosuppression occurs via concerted action of chemokines and nitric oxide. *Cell Stem Cell* 2, 141–150. doi: 10.1016/j.stem.2007.11.014

Robling, A. G., Castillo, A. B., and Turner, C. H. (2006). Biomechanical and molecular regulation of bone remodeling. *Annu. Rev. Biomed. Eng*. 8, 455–498. doi: 10.1146/annurev.bioeng.8.061505.095721

Roszer, T. (2015). Understanding the mysterious M2 macrophage through activation markers and effector mechanisms. *Mediators Inflamm.* 2015:816460. doi: 10.1155/2015/816460

Sanches, J. M., Branco, L. M., Duarte, G. H. B., Oliani, S. M., Bortoluci, K. R., Moreira, V., et al. (2020). Annexin A1 regulates NLRP3 inflammasome activation and modifies lipid release profile in isolated peritoneal macrophages. *Cells* 9:926. doi: 10.3390/cells9040926

Sanchez-Lopez, E., Cheng, A., and Guma, M. (2019). Can metabolic pathways be therapeutic targets in rheumatoid arthritis? *J. Clin. Med*. 8:753. doi: 10.3390/jcm8050753

Seebach, E., Freischmidt, H., Holschbach, J., Fellenberg, J., and Richter, W. (2014). Mesenchymal stroma cells trigger early attraction of M1 macrophages and endothelial cells into fibrin hydrogels, stimulating long bone healing without long-term engraftment. *Acta Biomater*. 10, 4730–4741. doi: 10.1016/j.actbio.2014.07.017

Ségaliny, A. I., Mohamadi, A., Dizier, B., Lokajczyk, A., Brion, R., Lanel, R., et al. (2015). Interleukin-34 promotes tumor progression and metastatic process in osteosarcoma through induction of angiogenesis and macrophage recruitment. *Int. J. Cancer* 137, 73–85. doi: 10.1002/ijc.29376

Sellam, J., and Berenbaum, F. (2010). The role of synovitis in pathophysiology and clinical symptoms of osteoarthritis. *Nat. Rev. Rheumatol*. 6, 625–635. doi: 10.1038/nrrheum.2010.159

Shen, G., Ren, H., Shang, Q., Zhang, Z., Zhao, W., Yu, X., et al. (2020). miR-128 plays a critical role in murine osteoclastogenesis and estrogen deficiency-induced bone loss. *Theranostics* 10, 4334–4348. doi: 10.7150/thno.42982

Shi, M., Wang, C., Wang, Y., Tang, C., Miron, R. J., and Zhang, Y. (2018). Deproteinized bovine bone matrix induces osteoblast differentiation via macrophage polarization. *J. Biomed. Mater. Res. A* 106, 1236–1246. doi: 10.1002/jbm.a.36321

Shimura, T., Takenaka, Y., Fukumori, T., Tsutsumi, S., Okada, K., Hogan, V., et al. (2005). Implication of galectin-3 in Wnt signaling. *Cancer Res*. 65, 3535–3537. doi: 10.1158/0008-5472.CAN-05-0104

Silva, J. M. D., Silva, H., Zelenski, C., Souza, J. A. M., Hueb, M., and Damazo, A. S. (2019). Analysis of macrophage subtypes and annexin A1 expression in lesions of patients with cutaneous leishmaniasis. *Rev. Soc. Bras. Med. Trop*. 52:e20190361. doi: 10.1590/0037-8682-0361-2019

Simon, D., Derer, A., Andes, F. T., Lezuo, P., Bozec, A., Schett, G., et al. (2017). Galectin-3 as a novel regulator of osteoblast-osteoclast interaction and bone homeostasis. *Bone* 105, 35–41. doi: 10.1016/j.bone.2017.08.013

Sims, N. A., and Quinn, J. M. (2014). Osteoimmunology: oncostatin M as a pleiotropic regulator of bone formation and resorption in health and disease. *Bonekey Rep*. 3:527. doi: 10.1038/bonekey.2014.22

Stanczyk, J., Pedrioli, D. M., Brentano, F., Sanchez-Pernaute, O., Kolling, C., Gay, R. E., et al. (2008). Altered expression of MicroRNA in synovial fibroblasts and synovial tissue in rheumatoid arthritis. *Arthritis Rheum*. 58, 1001–1009. doi: 10.1002/art.23386

Stukes, S., Coelho, C., Rivera, J., Jedlicka, A. E., Hajjar, K. A., and Casadevall, I. (2016). The membrane phospholipid binding protein annexin A2 promotes phagocytosis and nonlytic exocytosis of cryptococcus neoformans and impacts survival in fungal infection. *J Immunol*. 197, 1252–61. doi: 10.4049/jimmunol.1501855

Su, Y., Zhou, Y., Sun, Y. J., Wang, Y. L., Yin, J. Y., Huang, Y. J., et al. (2019). Macrophage-derived CCL18 promotes osteosarcoma proliferation and migration by upregulating the expression of UCA1. *J. Mol. Med*. 97, 49–61. doi: 10.1007/s00109-018-1711-0

Sun, A. R., Friis, T., Sekar, S., Crawford, R., Xiao, Y., and Prasadam, I. (2016). Is synovial macrophage activation the inflammatory link between obesity and osteoarthritis? *Curr. Rheumatol. Rep*. 18:57. doi: 10.1007/s11926-016-0605-9

Sun, A. R., Panchal, S. K., Friis, T., Sekar, S., Crawford, R., Brown, L., et al. (2017). Obesity-associated metabolic syndrome spontaneously induces infiltration of pro-inflammatory macrophage in synovium and promotes osteoarthritis. *PLoS ONE* 12:e0183693. doi: 10.1371/journal.pone.0183693

Sun, W., Meednu, N., Rosenberg, A., Rangel-Moreno, J., Wang, V., Glanzman, J., et al. (2018). B cells inhibit bone formation in rheumatoid arthritis by suppressing osteoblast differentiation. *Nat. Commun*. 9:5127. doi: 10.1038/s41467-018-07626-8

Suzuki-Inoue, K. (2019). Platelets and cancer-associated thrombosis: focusing on the platelet activation receptor CLEC-2 and podoplanin. *Blood* 134, 1912–1918. doi: 10.1182/blood.2019001388

Takahashi, F., Takahashi, K., Shimizu, K., Cui, R., Tada, N., Takahashi, H., et al. (2004). Osteopontin is strongly expressed by alveolar macrophages in the lungs of acute respiratory distress syndrome. *Lung* 182, 173–185. doi: 10.1007/s00408-004-0309-1

Tan, S. D., Kuijpers-Jagtman, A. M., Semeins, C. M., Bronckers, A. L., Maltha, J. C., Von den Hoff, J. W., et al. (2006). Fluid shear stress inhibits TNFalpha-induced osteocyte apoptosis. *J. Dent. Res.* 85, 905–909. doi: 10.1177/154405910608501006

Tannahill, G. M., Curtis, A. M., Adamik, J., Palsson-McDermott, E. M., McGettrick, A. F., Goel, G., et al. (2013). Succinate is an inflammatory signal that induces IL-1β through HIF-1α. *Nature* 496, 238–242. doi: 10.1038/nature11986

Théry, C. (2011). Exosomes: secreted vesicles and intercellular communications. *F1000 Biol. Rep.* 3:15. doi: 10.3410/B3-15

Tian, Y., Shen, H., Xia, L., and Lu, J. (2013). Elevated serum and synovial fluid levels of interleukin-34 in rheumatoid arthritis: possible association with disease progression via interleukin-17 production. *J. Interferon Cytokine Res.* 33, 398–401. doi: 10.1089/jir.2012.0122

Tokunaga, T., Mokuda, S., Kohno, H., Yukawa, K., Kuranobu, T., Oi, K., et al. (2020). TGFβ1 Regulates human RANKL-induced osteoclastogenesis via suppression of NFATc1 expression. *Int. J. Mol. Sci.* 21:800. doi: 10.3390/ijms21030800

Ushach, I., and Zlotnik, A. (2016). Biological role of granulocyte macrophage colony-stimulating factor (GM-CSF) and macrophage colony-stimulating factor (M-CSF) on cells of the myeloid lineage. *J. Leukoc. Biol.* 100, 481–489. doi: 10.1189/jlb.3RU0316-144R

Wang, J., Meng, F., Song, W., Jin, J., Ma, Q., Fei, D., et al.(2018). Nanostructured titanium regulates osseointegration via influencing macrophage polarization in the osteogenic environment. *Int J Nanomedicine*. 13, 4029–4043. doi: 10.2147/IJN.S163956

Wang, J., Zheng, Z., Huang, B., Wu, H., Zhang, X., Chen, Y., et al. (2020). Osteal Tissue macrophages are involved in endplate osteosclerosis through the OSM-STAT3/YAP1 signaling axis in modic changes. *J. Immunol.* 205, 968–980. doi: 10.4049/jimmunol.1901001

Wei, F., Li, M., Crawford, R., Zhou, Y., and Xiao, Y. (2019). Exosome-integrated titanium oxide nanotubes for targeted bone regeneration. *Acta Biomater.* 86, 480–492. doi: 10.1016/j.actbio.2019.01.006

Wei, F., Zhou, Y., Wang, J., Liu, C., and Xiao, Y. (2018). The immunomodulatory role of BMP-2 on macrophages to accelerate osteogenesis. *Tissue Eng. A* 24, 584–594. doi: 10.1089/ten.tea.2017.0232

Weilner, S., Keider, V., Winter, M., Harreither, E., Salzer, B., Weiss, F., et al. (2016). Vesicular Galectin-3 levels decrease with donor age and contribute to the reduced osteo-inductive potential of human plasma derived extracellular vesicles. *Aging* 8, 16–33. doi: 10.18632/aging.100865

Winkler, I. G., Sims, N. A., Pettit, A. R., Barbier, V., Nowlan, B., Helwani, F., et al. (2010). Bone marrow macrophages maintain hematopoietic stem cell (HSC) niches and their depletion mobilizes HSCs. *Blood* 116, 4815–4828. doi: 10.1182/blood-2009-11-253534

Woo, S. R., Corrales, L., and Gajewski, T. F. (2015). Innate immune recognition of cancer. *Annu. Rev. Immunol.* 33, 445–474. doi: 10.1146/annurev-immunol-032414-112043

Wu, A. C., He, Y., Broomfield, A., Paatan, N. J., Harrington, B. S., Tseng, H. W., et al. (2016). $CD169^{+}$ macrophages mediate pathological formation of woven bone in skeletal lesions of prostate cancer. *J. Pathol.* 239, 218–230. doi: 10.1002/path.4718

Wu, Q., Zhou, X., Huang, D., Ji, Y., and Kang, F. (2017). IL-6 enhances osteocyte-mediated osteoclastogenesis by promoting JAK2 and RANKL activity *in vitro*. *Cell. Physiol. Biochem.* 41, 1360–1369. doi: 10.1159/000465455

Wynn, T. A., Chawla, A., and Pollard, J. W. (2013). Macrophage biology in development, homeostasis and disease. *Nature* 496, 445–455. doi: 10.1038/nature12034

Xia, Y., He, X. T., Xu, X. Y., Tian, B. M., An, Y., and Chen, F. M. (2020). Exosomes derived from M0, M1 and M2 macrophages exert distinct influences on the proliferation and differentiation of mesenchymal stem cells. *PeerJ.* 8:e8970. doi: 10.7717/peerj.8970

Xiang, L. X., Ran, Q., Chen, L., Xiang, Y., Li, F. J., Zhang, X. M., et al. (2020). CR6-interacting factor-1 contributes to osteoclastogenesis by inducing receptor activator of nuclear factor κB ligand after radiation. *World J. Stem Cells* 12, 222–240. doi: 10.4252/wjsc.v12.i3.222

Xing, Z., Lu, C., Hu, D., Miclau, T. 3rd, and Marcucio, R. S. (2010). Rejuvenation of the inflammatory system stimulates fracture repair in aged mice. *J. Orthop. Res.* 28, 1000–1006. doi: 10.1002/jor.21087

Xiong, Y., Chen, L., Yan, C., Zhou, W., Yu, T., Sun, Y., et al. (2020). M2 Macrophagy-derived exosomal miRNA-5106 induces bone mesenchymal stem cells towards osteoblastic fate by targeting salt-inducible kinase 2 and 3. *J. Nanobiotechnol.* 18:66. doi: 10.1186/s12951-020-00622-5

Xue, J., Schmidt, S. V., Sander, J., Draffehn, A., Krebs, W., Quester, I., et al. (2014). Transcriptome-based network analysis reveals a spectrum model of human macrophage activation. *Immunity* 40, 274–288. doi: 10.1016/j.immuni.2014.01.006

Xue, Y. Z. B., Niu, Y. M., Tang, B., and Wang, C. M. (2019). PCL/EUG scaffolds with tunable stiffness can regulate macrophage secretion behavior. *Prog. Biophys. Mol. Biol.* 148, 4–11. doi: 10.1016/j.pbiomolbio.2019.05.006

Yang, D. H., and Yang, M. Y. (2019). The role of macrophage in the pathogenesis of osteoporosis. *Int. J. Mol. Sci.* 20:2093. doi: 10.3390/ijms20092093

Yang, J., Zou, Y., and Jiang, D. (2018). Honokiol suppresses proliferation and induces apoptosis via regulation of the miR-21/PTEN/PI3K/AKT signaling pathway in human osteosarcoma cells. *Int. J. Mol. Med.* 41, 1845–1854. doi: 10.3892/ijmm.2018.3433

Yang, M., Li, C. J., Sun, X., Guo, Q., Xiao, Y., Su, T., et al. (2017). MiR-497∼195 cluster regulates angiogenesis during coupling with osteogenesis by maintaining endothelial Notch and HIF-1α activity. *Nat. Commun.* 8:16003. doi: 10.1038/ncomms16003

Ying, W., Riopel, M., Bandyopadhyay, G., Dong, Y., Birmingham, A., Seo, J. B., et al. (2017). Adipose tissue macrophage-derived exosomal miRNAs can modulate *in vivo* and *in vitro* insulin sensitivity. *Cell* 171, 372–384.e12. doi: 10.1016/j.cell.2017.08.035

Zhang, H., Lin, C., Zeng, C., Wang, Z., Wang, H., Lu, J., et al. (2018). Synovial macrophage M1 polarisation exacerbates experimental osteoarthritis partially through R-spondin-2. *Ann. Rheum. Dis.* 77, 1524–1534. doi: 10.1136/annrheumdis-2018-213450

Zhang, Y., Böse, T., Unger, R. E., Jansen, J. A., Kirkpatrick, C. J., and van den Beucken, J. (2017). Macrophage type modulates osteogenic differentiation of adipose tissue MSCs. *Cell Tissue Res.* 369, 273–286. doi: 10.1007/s00441-017-2598-8

Zheng, P., Chen, L., Yuan, X., Luo, Q., Liu, Y., Xie, G., et al. (2017). Exosomal transfer of tumor-associated macrophage-derived miR-21 confers cisplatin resistance in gastric cancer cells. *J. Exp. Clin. Cancer Res.* 36:53. doi: 10.1186/s13046-017-0528-y

Conflict of Interest: The authors declare that the research was conducted in the absence of any commercial or financial relationships that could be construed as a potential conflict of interest.

Copyright © 2020 Chen, Jiao, Liu, Huang, He, He, Hou, Yang, Luo and Li. This is an open-access article distributed under the terms of the Creative Commons Attribution License (CC BY). The use, distribution or reproduction in other forums is permitted, provided the original author(s) and the copyright owner(s) are credited and that the original publication in this journal is cited, in accordance with accepted academic practice. No use, distribution or reproduction is permitted which does not comply with these terms.

frontiers in Cell and Developmental Biology

REVIEW
published: 21 January 2021
doi: 10.3389/fcell.2020.607764

Subchondral Bone Remodeling: A Therapeutic Target for Osteoarthritis

Xiaobo Zhu[1,2†], *Yau Tsz Chan*[1,3†], *Patrick S. H. Yung*[1,2], *Rocky S. Tuan*[1,3*] *and Yangzi Jiang*[1,3*]

[1] *Institute for Tissue Engineering and Regenerative Medicine, The Chinese University of Hong Kong, Hong Kong, China,* [2] *Department of Orthopaedics & Traumatology, Faculty of Medicine, The Chinese University of Hong Kong, Hong Kong, China,* [3] *School of Biomedical Sciences, The Chinese University of Hong Kong, Hong Kong, China*

There is emerging awareness that subchondral bone remodeling plays an important role in the development of osteoarthritis (OA). This review presents recent investigations on the cellular and molecular mechanism of subchondral bone remodeling, and summarizes the current interventions and potential therapeutic targets related to OA subchondral bone remodeling. The first part of this review covers key cells and molecular mediators involved in subchondral bone remodeling (osteoclasts, osteoblasts, osteocytes, bone extracellular matrix, vascularization, nerve innervation, and related signaling pathways). The second part of this review describes candidate treatments for OA subchondral bone remodeling, including the use of bone-acting reagents and the application of regenerative therapies. Currently available clinical OA therapies and known responses in subchondral bone remodeling are summarized as a basis for the investigation of potential therapeutic mediators.

Keywords: osteoarthritis, subchondral bone, cellular and molecular targets, subchondral bone remodeling, regenerative therapy, stem cells

OPEN ACCESS

Edited by:
Jiake Xu,
University of Western Australia, Australia

Reviewed by:
David M. Findlay,
University of Adelaide, Australia
Akhilesh Kumar,
Central Drug Research Institute (CSIR), India

***Correspondence:**
Yangzi Jiang
yangzjiang21@cuhk.edu.hk
Rocky S. Tuan
tuanr@cuhk.edu.hk

[†] *These authors have contributed equally to this work*

Specialty section:
This article was submitted to Molecular Medicine, a section of the journal Frontiers in Cell and Developmental Biology

Received: *18 September 2020*
Accepted: *28 December 2020*
Published: *21 January 2021*

Citation:
Zhu X, Chan YT, Yung PSH, Tuan RS and Jiang Y (2021) Subchondral Bone Remodeling: A Therapeutic Target for Osteoarthritis. Front. Cell Dev. Biol. 8:607764. doi: 10.3389/fcell.2020.607764

INTRODUCTION

Osteoarthritis (OA) affects all tissues in diarthrodial joints, including articular cartilage, subchondral cortical bone, subchondral trabecular bone, and synovium, and the resultant pathological changes lead to pain, stiffness and dysfunction of the joint. Although articular cartilage loss and degeneration has long been considered the main cause of OA, and many therapies are designed to preserve articular cartilage, growing evidence suggests that the integrity and remodeling process of subchondral bone in OA joints, as an adaptation to cartilage degradation to maintain joint tissue homeostasis, also play an important role in OA physiopathology. Understanding the mechanism of subchondral bone remodeling in OA may provide insights for the design of future therapies to tackle OA at its early stage. This review will cover the structure and function of subchondral bone; describe the key regulatory factors and pathological changes of subchondral bone in OA joints; present the potential cellular and molecular therapeutic targets in subchondral bone remodeling and related current therapies, and possible strategies for future therapeutic design.

SUBCHONDRAL BONE IN OA

Structure and Function of Subchondral Bone

Articular cartilage is the hyaline connective tissue that covers the ends of bones in the diarthrodial joint, and it serves to absorb shock from joint movement. Articular cartilage has an aneural,

avascular, and alymphatic structure composed of 65–80% water, 20–40% extracellular matrix (ECM), and 1–5% chondrocytes. The major components of ECM are collagens (mainly collagen type II) and proteoglycans (Carballo et al., 2017; Chen et al., 2017). Articular cartilage presents zonal structures from the articular surface (superficial, middle, and deep zones) to the conjunction area of subchondral bone (calcified zone), and the cell density and morphology differ in each zone (Jiang et al., 2017).

Subchondral bone refers to the bone tissue underlying the calcified cartilage and tidemark (**Figure 1**), including both subchondral cortical plate and subchondral trabecular bone. Subchondral bone plate is a thin layer of cortical bone lying immediately beneath the calcified cartilage. The physiological properties of the cortical plate are similar to the cortical bone located at other skeletal sites, providing mechanical strength to support the overlying articular cartilage, although the cortical plate is less stiff in comparison to diaphyseal cortical bone (Elastic modulus: 1.372 vs. 14 GN/m^2) (Brown and Vrahas, 1984; Burr and Gallant, 2012). Underneath the cortical bone plate lies the subchondral trabecular bone, which is more porous and metabolically active compared to the cortical plate. The trabeculae in the cancellous bone have a unique structural network that adjusts to local mechanical influences (**Figure 1A**).

The osteochondral unit in the joint, which transfers load during joint movement, consists of articular cartilage, calcified cartilage and subchondral cortical and trabecular bone (Lories and Luyten, 2011; Goldring and Goldring, 2016). The normal subchondral cortical plate has a dense structure to support articular cartilage, and there are canals (10–160 mm in diameter) in the cortical plate, allowing the exchange of nutrients and molecules between cartilage and bone (Duncan et al., 1987; Clark, 1990; Bian et al., 2016).

Articular cartilage stress distribution changes with subchondral bone expansion, and even a 1–2% incremental

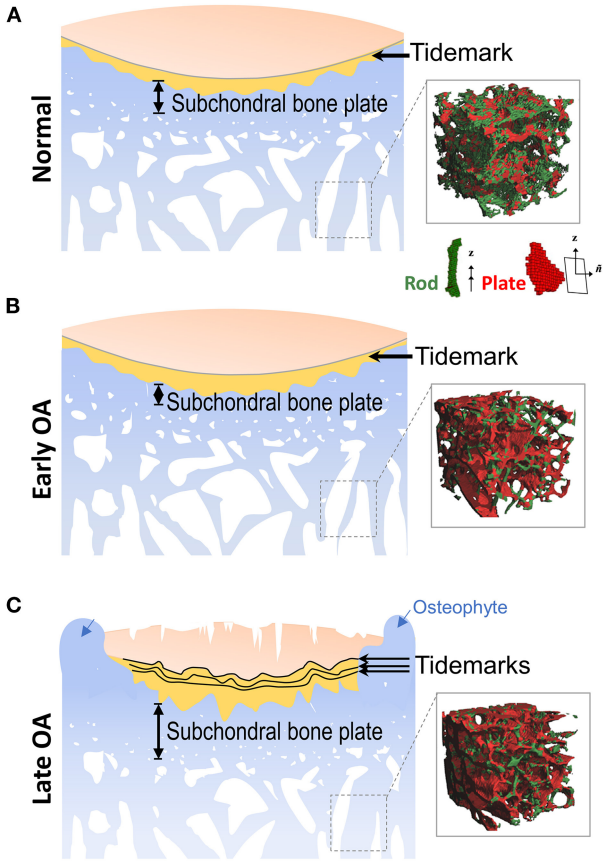


FIGURE 1 | Alterations of subchondral bone during OA progression. **(A)** Located at the ends of bones, articular cartilage provides a low friction surface for weight bearing and joint movement, and is made up of four zones: superficial zone, middle zone, deep zone, and calcified zone. In the healthy joint, the thin layer of calcified zone/cartilage (yellow) present at the bottom of the articular cartilage is separated from the upper three zones by the histological marker termed tidemark. Subchondral bone is the bone tissue lying beneath the calcified cartilage, and includes both the subchondral cortical plate and subchondral trabecular bone, although there is no precise distinction for the differences between these two structures. (Inset) Depiction of the mineralized rod and plate structures in the trabecular bone. **(B)** In early OA, when the cartilage is still intact, the thickness of subchondral cortical plate is decreased due to elevated rate of bone remodeling. At the same time, bone loss also occurs in the subchondral trabecular bone. (Inset) A drastic loss of rod-like trabeculae and mild thickening of plate-like trabeculae is also detected in early OA. **(C)** In late OA, when degenerative changes are evident in articular cartilage, the thickness of the subchondral plate is increased, and the subchondral trabecular bone becomes sclerotic. Other periarticular bone changes, such as the formation of osteophytes (blue arrows) also occurs at this stage. The amount of calcified cartilage expands and penetrates into the upper hyaline articular cartilage, with the tidemark duplicated or disrupted. (Inset) The drastic loss of rod-like trabeculae and thickening of plate-like trabeculae continue in late OA. Inset figures depicting structure of trabecular plate and rod are reprinted with permission from Chen et al. (2018).

Abbreviations: ACLT, anterior cruciate ligament transection; ADSCs, adipose-derived mesenchymal stromal cells; ALP, alkaline phosphatase; BMLs, bone marrow lesions; BMSCs, bone marrow-derived mesenchymal stromal cells; BPs, bisphosphonates; BSMs, bone substitute materials; CaP, calcium phosphate; COL1, collagen type I; COX-2, cyclooxygenase-2; CTSK, cathepsin K; Dexa, dual energy X-ray absorptiometry; DKK2, Dickkopf-2; DMOAD, disease-modifying osteoarthritis drug; DMP1, dentin matrix acidic phosphoprotein 1; ECM, extracellular matrix; EGFR, epidermal growth factor receptor; FAK, focal adhesion kinase; HTO, high tibial osteotomy; ICOAP, intermittent and constant osteoarthritis pain; ICRS, International Cartilage Repair Society; IGF1, insulin-like growth factor 1; IKDC, International Knee Documentation Committee; KJD, knee joint distraction; KL, Kellgren-Lawrence; KOOS, Knee Injury and Osteoarthritis Outcome Score; MACI, matrix induced autologous chondrocyte implantation; MMX, medial meniscectomy; MMP, metalloproteinase; MRI, magnetic resonance imaging; MSCs, mesenchymal stem cells; mTOR, mammalian target of rapamycin; mTORC1, mechanistic target of rapamycin complex 1; OA, osteoarthritis; OCN, osteocalcin; ODF, osteoclast differentiation factor; OPG, osteoprotegerin; OPGL, osteoprotegerin ligand; ON, osteonecrosis; PBMCs, peripheral blood mononuclear cells; PDGF-BB, platelet-derived growth factor-BB; PGE2, prostaglandin E2; PLR, perilacunar/canalicular remodeling; RANK, receptor activator of nuclear factor kappa-B; PTH, parathyroid hormone; PTHrP, parathyroid hormone related peptide; RAL, Raloxifene; RANKL, receptor activator of nuclear factor kappa-B ligand; SERMs, selective estrogen receptor modulators; SMSCs, synovium-derived mesenchymal stromal cells; SrR, strontium ranelate; TGFβ1, transforming growth factor β1; TKA, total knee arthroplasty; TRAP, tartrate-resistant acid phosphatase; UC-MSCs, umbilical cord-derived mesenchymal stromal cells; VAS, visual analog scale; VEGF, vascular endothelial growth factor; WOMAC, Western Ontario and McMaster Universities Arthritis Index; YAP, Yes-associated protein.

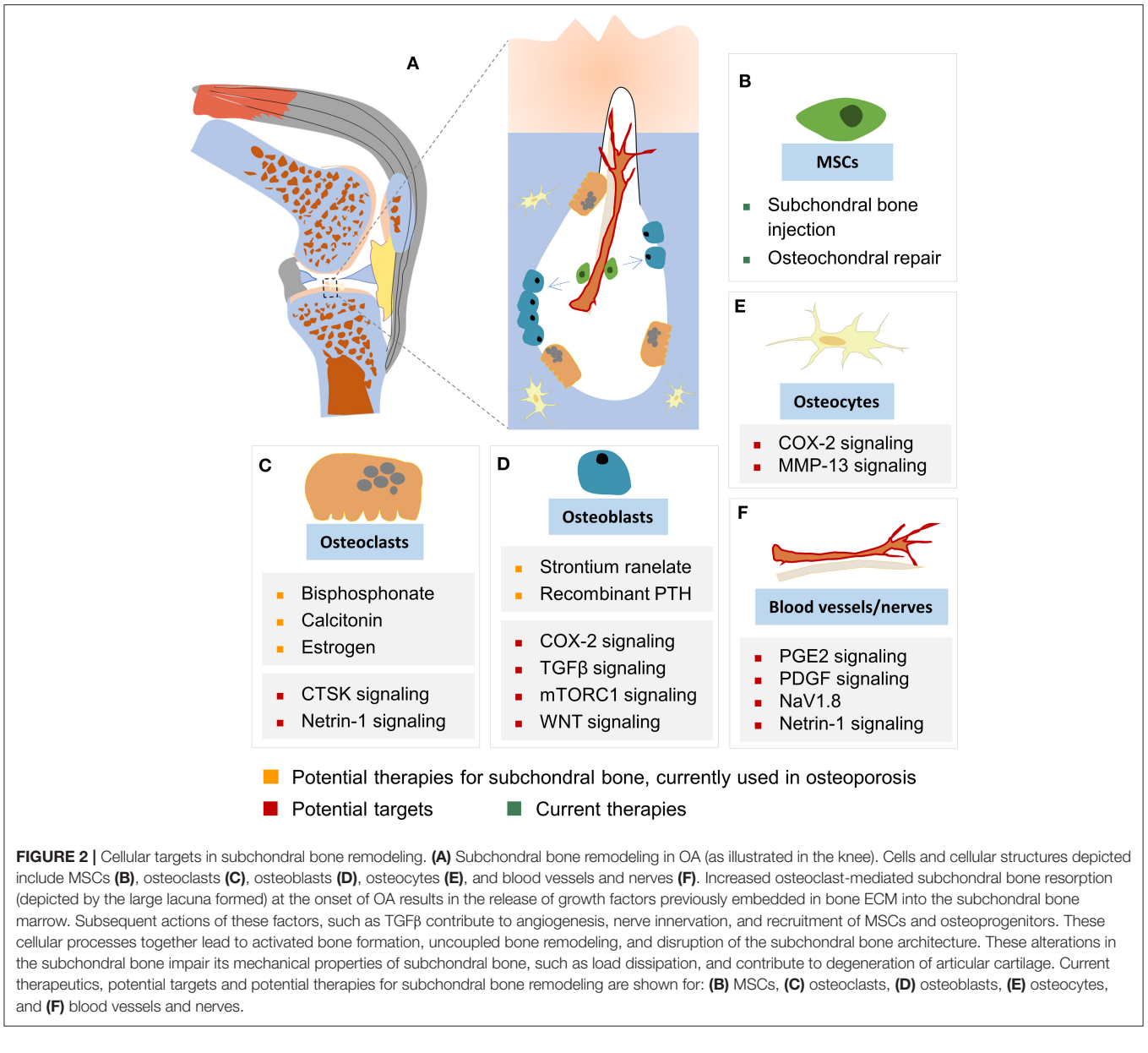


FIGURE 2 | Cellular targets in subchondral bone remodeling. **(A)** Subchondral bone remodeling in OA (as illustrated in the knee). Cells and cellular structures depicted include MSCs **(B)**, osteoclasts **(C)**, osteoblasts **(D)**, osteocytes **(E)**, and blood vessels and nerves **(F)**. Increased osteoclast-mediated subchondral bone resorption (depicted by the large lacuna formed) at the onset of OA results in the release of growth factors previously embedded in bone ECM into the subchondral bone marrow. Subsequent actions of these factors, such as TGFβ contribute to angiogenesis, nerve innervation, and recruitment of MSCs and osteoprogenitors. These cellular processes together lead to activated bone formation, uncoupled bone remodeling, and disruption of the subchondral bone architecture. These alterations in the subchondral bone impair its mechanical properties of subchondral bone, such as load dissipation, and contribute to degeneration of articular cartilage. Current therapeutics, potential targets and potential therapies for subchondral bone remodeling are shown for: **(B)** MSCs, **(C)** osteoclasts, **(D)** osteoblasts, **(E)** osteocytes, and **(F)** blood vessels and nerves.

increase in the size of the subchondral bone could significantly increase stress to articular cartilage, as estimated by a recent human tibia data based computer-simulated model (Zhen et al., 2013). Upon injury or degeneration, the integrity of the osteochondral unit is breached, and the crosstalk between cartilage and subchondral bone is increased; the osteochondral unit is consequently altered and reshaped by the dynamic mechanical environment and biological microenvironment. Recently, Chen et al. (2020) reported a horizontal fissure at the osteochondral interface in obese OA patients, characterized by irregular cartilage erosion, fibro-granulation tissue infiltration, presence of free cartilage/bone debris and rupture of microcapillaries at the interface within the osteochondral unit. This represents a new type of OA pathological features, where neurovascular invasions were also identified in the degenerative osteochondral tissues (Li et al., 2013) (**Figures 1B**, **2A**).

Subchondral Bone in OA Joints

In OA joints, subchondral bone undergoes remarkable changes in both composition and structural organization, and has adverse effects on the overlying articular cartilage (**Figure 1**). With a bone scan (^{99m}Tc pyrophosphate) and tetracycline labeling, Radin et al. (1984) provided early direct evidence that subchondral bone remodeling was significantly enhanced in response to mechanical loading in a rabbit model of hindlimb loading, and it preceded the fibrillation of the overlying articular cartilage (Radin et al., 1984). More histopathological features in osteoarthritic subchondral bone were then identified and

discussed, including microdamage, bone marrow edema/lesions and bone cysts (Goldring and Goldring, 2016).

"Bone marrow edema" was termed and used about three decades ago, when Wilson et al. (1988) detected and localized regions of increased signal intensity in the subchondral bone of OA patients, with MRI based fluid-sensitive magnetic resonance sequences. However, histological examination of the subchondral bone in the anatomical edema sites revealed that local fat necrosis, marrow fibrosis and vascular changes were associated with microfractures of the trabecular bone, but not associated with edema (Leydet-Quilici et al., 2010). In current practice, people termed this pathological feature as bone marrow lesions (BMLs) in subchondral bone. Today, the different types and stages of BMLs can be identified by the radiological response to two MRI sequences, the fast spin-echo proton density (PDFS)-weighted and T1-weighted spin echo. Two major types of BMLs were designated based on the MRI readouts: BML1 represents an early-stage of the structural alteration in subchondral bone, which is detectable only by PDFS sequence, and BML2 is considered as a relatively more degenerative stage in the lesion sites, which is detectable by both PDFS and T1 sequence (Muratovic et al., 2016). Therefore, it appears that BMLs are correlated to the severity of OA progression (Taljanovic et al., 2008; Tanamas et al., 2010).

Subchondral bone cyst, also known as intra-osseous lesion, is another pathological feature often found in the load-bearing regions of the arthritic joints, but the exact pathogenesis of cyst formation is still unclear. Mechanical instability and overload may be the major cause. McErlain et al. (2012) created mechanically unstable OA models in rat knees by anterior cruciate ligament transection (ACLT) and partial medial meniscectomy (MMX); 75% of the knees developed subchondral bone cysts in 4 weeks, and all knees had subchondral bone cysts in 12 weeks. Moreover, enhanced bone turnover was also identified in human OA subchondral bone. Chen et al. (2015) examined cellular composition of human OA subchondral bone cysts and showed that the number of osteoclasts, osteoprogenitors (osterix$^+$), osteoblasts (osteocalcin$^+$, OCN$^+$), and SOX9$^+$ cells were higher in bone cyst sites than those in peri-cyst sites, suggesting enhanced bone turnover and abnormal bone remodeling.

Recently, the fine microarchitecture alterations of OA subchondral trabecular bone have been imaged and analyzed by advanced high-resolution micro-CT and MRI imaging systems. Liu et al. (2008) examined 71 human trabecular bone samples, and found that healthy trabecular bone consists of a network of rod-like and plate-like trabeculae microstructure (**Figure 1A**, right panel). Healthy subchondral trabecular bone displayed an even distribution of rod-like and plate-like trabeculae, and in human OA tibial plateau, a dramatic loss of rod-like trabeculae and thickening of plate-like trabeculae were identified using a novel microstructural analysis method, based on individual trabecula segmentation (**Figures 1B,C**, right panels) (Chen et al., 2018). Interestingly, in the same study, Chen et al. (2018) discovered that subchondral trabecular bone underneath the intact cartilage shared a similar phenotype with that underneath the severely damaged cartilage, which implied that the alterations of subchondral bone in early OA could precede cartilage degeneration.

SUBCHONDRAL BONE REMODELING IN OA

Alterations in OA subchondral bone represent their adaptation to the changes of local biomechanical and biological signals, and are mediated by different types of bone cells (Goldring, 2009). These cell-regulatory adaptations conform to Wolff's law that the distribution and material properties of bone are dynamically determined by the applied load (Frost, 1994). Accordingly, when bone is subjected to increased loading, a number of bone properties change, including an expanding subchondral bone cross-sectional area, changes in bone mass, and remodeling of the trabeculae network (Teichtahl et al., 2015). Adult skeleton is constantly renewed during lifetime by bone remodeling, whereby mature bone tissue is removed from the skeleton (bone resorption) and new bone tissue is formed (bone formation). Bone remodeling controls the reshaping or replacement of bone following injuries, and this principle also applies to the subchondral bone, where increased bone resorption and alterations in its microarchitecture have been identified in both rheumatoid arthritis and OA (Li et al., 2014). Osteoclasts, mononuclear cells, osteoblasts, and osteocytes are the major cell types that participate in bone remodeling (Sims et al., 2015).

Cells in Subchondral Bone Remodeling

Osteoclasts and Osteoclastogenesis in Subchondral Bone Resorption

Osteoclasts (tartrate-resistant acid phosphatase positive, TRAP$^+$) are multinucleated cells that originate from bone marrow myeloid progenitor cells (TRAP$^-$), and are the major cell type responsible for bone resorption (Teitelbaum, 2000; Katsimbri, 2017). During osteoclastogenesis, progenitor cells (TRAP$^-$) are recruited to specific sites on bone surface, and differentiate to pre-osteoclast (TRAP$^+$, mononucleated cells) and fuse to form multinucleated mature osteoclasts. Mature osteoclasts form a sealing zone on bone surface, and release hydrogen ions and catalytic enzymes for bone dissolution.

Osteoclasts are involved in arthritic bone diseases (Schett et al., 2005). Interestingly, peripheral blood mononuclear cells (PBMCs) from OA patients showed a higher level of osteoclastogenesis. Durand et al. (2013) isolated PBMCs from 140 OA patients, which were differentiated into osteoclasts for 3 weeks. OA-PBMCs generated more osteoclasts, and showed higher bone resorption rate when cultured on top of bovine cortical bone slides, compared to healthy controls (Durand et al., 2013). RANKL (receptor activator of nuclear factor kappa-B ligand, also known as osteoprotegerin ligand, osteoclast differentiation factor), exerts its function by binding to its receptor RANK on the surface of osteoclast precursors, and is one of the key regulators of osteoclastogenesis (Borciani et al., 2020). Increased osteoclast population was also observed in subchondral bone plates of OA patients (Jaiprakash et al., 2012).

The remodeling events in the subchondral bone in OA are not uniform across the joint because of different load-bearing conditions, and the remodeling rates may also vary with disease progression. For instance, active bone remodeling was found in bone cysts, but not in non-cyst areas, where the cyst cavity was created by activated osteoclasts, and bone formation was enhanced by osteoprogenitors ($Osterix^+$) and osteoblasts (OCN^+) (Chen et al., 2015). The high rate of subchondral bone resorption in OA is probably caused by increased osteoclast population and activity, and decreased cell apoptosis in a resorption cycle (Jaiprakash et al., 2012).

One of the key enzymes expressed by osteoclasts for bone resorption is cathepsin K (CTSK). Ctsk knockout mice ($Ctsk^{-/-}$) maintained cartilage volume and structure in OA surgical model of destabilization of the medial meniscus (DMM model), although the $TRAP^+$ osteoclast population in subchondral bone was increased in both wild type and $Ctsk^{-/-}$ mice (Soki et al., 2018), and the subchondral bone was also preserved in OA $Ctsk^{-/-}$ mice (Soki et al., 2018).

Mononuclear Cells in Subchondral Bone Reversal Phase

There is a reversal phase in bone remodeling cycle between bone resorption and bone formation, and so far little is known about it (Jensen et al., 2014; Sims and Martin, 2020). Reversal phase is a step to prepare the bone surface for bone formation, including clearing away the resorption debris and stimulating MSC proliferation, lineage commitment toward pre-osteoblast, differentiation and migration. Mononuclear cells are observed on the newly-resorbed bone surface, and are believed as the key cellular players in reversal phase, thus termed as reversal cells. These mononuclear cells are thought to be originated from hemopoietic-lineage mononuclear phagocytes, and with the possibility from osteoblast-lineage cells (Tran Van et al., 1982; Delaisse, 2014; Sims et al., 2015). The exact role of reversal cells is still under investigation, however, it is possible that the reversal phase might be the key therapeutic window to regulate subchondral bone remodeling in OA.

Osteoblasts, Osteoblastogenesis, and Subchondral Bone Sclerosis

Osteoblasts are differentiated from mesenchymal cells, and undergo four maturational stages - preosteoblasts, osteoblasts, bone-lining cells, and osteocytes, and contribute to bone formation (Clarke, 2008; Katsimbri, 2017). In OA, osteoblast phenotype and cell activity shift in the subchondral bone. Alkaline phosphatase (ALP) activity, releasing of RANKL (Kwan Tat et al., 2008), OCN, transforming growth factor β1 (TGFβ1) (Abed et al., 2017), insulin-like growth factor 1 (IGF1) (Hilal et al., 1998), and vascular endothelial growth factor (VEGF) (Corrado et al., 2013) are elevated in OA subchondral bone osteoblasts compared to normal osteoblasts, and the elevation of biofactors also induces a cascade of down-stream events, including sclerosis (Wang et al., 2013), osteoclastogenesis, and angiogenesis.

One of the most pronounced alterations in OA subchondral bone is sclerosis, which is usually found in the late stage of OA. A sclerotic subchondral bone has several structural characteristics, including the increased bone volume and density, thickening of subchondral bone plate, increased trabecular thickness, and decreased trabecular separation (**Figure 1C**). The microarchitecture of sclerotic subchondral trabeculae is transformed from rod-like into more plate-like (**Figure 1C**, right panel) (Li et al., 2013). Importantly, although bone volume and density are increased in sclerotic subchondral bone, the degree of mineralization is inadequate. The material stiffness of OA subchondral bone is therefore decreased, which may exaggerate cartilage degeneration upon joint loading (Li and Aspden, 1997). One possible explanation for subchondral bone sclerosis is that OA subchondral bone is actively being remodeled, and there is active recruitment of bone marrow and subchondral bone-resident progenitor cells and their induction toward osteogenesis; however, new bone formation and maturation are significantly impaired by the OA microenvironment (Bianco et al., 2018). Specifically, the mineralization ability of osteoblasts is reduced in the OA sclerotic subchondral cortical plate and trabecular bone tissues (Sanchez et al., 2008). The exact pathological mechanism is still under investigation. One of the possible reason is that OA sclerotic subchondral bone osteoblasts produce abnormal collagen type I (COL1), and both an aberrant formation of collagen type I homotrimer and a higher ratio of COL1A1 to COL1A2 have been reported (Bailey et al., 2002; Couchourel et al., 2009). Hypomineralization has also been found in OA sclerotic subchondral bone. One of the underlying molecular mechanisms is the elevated expression level of TGFβ in human OA subchondral bone osteoblasts, which may induce the expression of dickkopf-2 (DKK2), an inhibitor of mineralization (Chan et al., 2011). Recently, Sanchez et al. (2018) compared the secretome from human osteoblasts isolated from non-sclerotic and sclerotic areas, and identified 12 proteins about normal osteoblast function and mineralization that were significantly reduced in the osteoblasts from sclerotic subchondral bone.

Osteocytes

The role of osteocytes in OA subchondral bone is incompletely understood. As terminally differentiated osteoblasts embedded in bone matrix, osteocytes function as one type of mechanosensing cells (Robling and Bonewald, 2020), *via* mechanoloading-sensitive expression of RANKL to regulate osteoclastogenesis (Tatsumi et al., 2007; Nakashima et al., 2011; Xiong et al., 2011). Recent studies have also revealed a critical role for osteocyte-intrinsic TGFβ signaling in remodeling their surrounding bone matrix, a process termed perilacunar/canalicular remodeling (PLR), by which osteocytes sense the mechanical alterations, and resorb surrounding bone matrix by producing matrix metalloproteinases (MMPs), cathepsin and other proteolytic enzymes dynamically (Dole et al., 2017). Breakdown of PLR in subchondral bone osteocytes could induce an OA-like phenotype, even in the non-injured knee (Mazur et al., 2019), suggesting the important role of osteocytes in subchondral bone.

Bone Extracellular Matrix

Bone ECM is produced by osteoblasts, and compositionally consists of mineral, water, collagen and noncollagenous proteins

and lipids; the proportion of each component varies depending on species, age and site (Boskey and Robey, 2013). The osteoid matrix located at the endosteum of the bone is the newly secreted unmineralized matrix which then undergoes mineralization during osteogenesis, and collagen type I serves as the scaffold for the deposition of hydroxyapatite crystals in osteoid mineralization. The mechanical properties of bone are a function of the hardness of the mineralized ECM and the flexibility of organic components of the ECM. Bone ECM is the body's reservoir of minerals, macromolecules, and bioactive factors. It is the primary source of calcium, phosphate, and magnesium ions for maintenance of general physiological functions, including the maintenance of bone homeostasis. Bioactive factors are released into the marrow microenvironment upon bone resorption, and subsequently contribute to the recruitment and differentiation of stem/progenitor cells, such as mesenchymal stem cells (MSCs), during bone formation (Crane and Cao, 2014). For instance, bone matrix-derived IGF1 could stimulate osteoblastic differentiation of MSCs by activating mammalian target of rapamycin (mTOR), thus maintaining proper bone microarchitecture and mass (Xian et al., 2012). TGFβs are also abundant in bone ECM (TGFβ1, 188 ng/g; TGFβ2, 14 ng/g) (Hering et al., 2001), and activation of the TGFβ signaling pathway has been confirmed in OA subchondral bone, resulting in recruitment of MSCs and enhancement of bone formation (Zhen et al., 2013). In this manner, the subchondral bone ECM also participates in the regulation of bone homeostasis during OA bone remodeling.

CURRENT AND POTENTIAL THERAPIES FOR OA SUBCHONDRAL BONE REMODELING

The subchondral cortical bone and subchondral cancellous bone respond differently at early and late stages of OA (**Figure 1**) (Burr and Gallant, 2012; Goldring and Goldring, 2016). Subchondral bone plate thickness decreased at the early stage of OA (Intema et al., 2010), and elevation of bone resorption markers are found in the progressive OA patients (Bettica et al., 2002; Bolbos et al., 2008), accompanied by cartilage degeneration and enhanced vascularization in the subchondral bone (Bellido et al., 2010). At late stage of OA, subchondral sclerosis was reported with a 15% increase in bone mineral density and up to 30% increase in bone volume, accompanied by reduced mineralization (Hannan et al., 1993; Arden et al., 1996; Sanchez et al., 2008). Although there is no specific therapeutic treatment designed for subchondral bone remodeling, several bone-acting reagents are being investigated and pursued for their potential in regulating subchondral bone in OA patients (**Figure 2**).

Inhibiting Osteoclasts in Subchondral Bone

Bisphosphonates

Bisphosphonates (BPs) are the most commonly used prescription drug for prevention and treatment of osteoporosis. BP binds to bone calcium and is released from the acidified bone surface, which is taken up by osteoclasts, and inhibits osteoclast activity by inducing osteoclast apoptosis (Coxon et al., 2008; Rogers et al., 2011). BPs have the potential to be used as OA subchondral bone regulating agents. For example, alendronate and zoledronate were reported to relieve subchondral bone pathological changes, thus effectively protecting the articular cartilage in OA animal models (Zhu et al., 2013; Lampropoulou-Adamidou et al., 2014). Clinically, the therapeutic effect of BPs for OA patients is controversial (Laslett et al., 2012; Cai et al., 2020). One up-to-date meta-analysis of randomized controlled trials involving 3,013 patients showed that BPs did not significantly improve OA in pain and structural and functional aspects compared to placebo (Vaysbrot et al., 2018). However, BPs may be suitable for OA patients with high bone turnover (Vaysbrot et al., 2018). A recent report by Hayes et al. (2020) suggested an early preventive effect of BPs for a subpopulation of OA patients (Hayes et al., 2020). Hayes et al. (2020) identified 346 BP responsive end-users from 1,977 eligible women, and in this cluster of patients, administration of BPs showed a protective effect against radiographic knee OA progression. The administration of BPs was particularly effective as early prevention for non-overweight patients, but less effective for those with more advanced disease or with higher weight-bearing stress (Hayes et al., 2020). These results suggest that BPs have the potential to be used as a prevention intervention for some early OA patients by regulating subchondral bone remodeling. Apart from subchondral bone, certain type of BPs, such as chlodronate, was also shown to have a protective effect on cartilage, acting *via* a purinergic receptor pathway (Rosa et al., 2014).

Calcitonin

Calcitonin is a 32-amino acid hormone produced by parafollicular cells of the thyroid gland that can inhibit osteoclast activity in bone. Similar to BPs, calcitonin also shows the capacity to prevent the loss of subchondral trabecular bone in an animal model (Behets et al., 2004), and exhibits chondro-protective effect in animal OA models (Wen et al., 2016). However, a recent Phase III clinical trial reported that the administration of calcitonin did not provide reproducible improvements on joint space width and pain relief (Karsdal et al., 2015). Moreover, due to the risk of cancer with long-term use of calcitonin, the European Medicines Agency concluded that the benefits of calcitonin could not outweigh their risks in the treatment of osteoporosis (European Medicines Agency, 2020). The application of calcitonin in OA subchondral bone remodeling should be further investigated and assessed.

Estrogen

Estrogen is important for bone development and health, and it regulates bone homeostasis by inhibiting osteoclast activation and inducing osteoclast apoptosis. Although estrogen has not been specifically subjected to randomized clinical trial for OA, some promising results provide support that estrogen has the potential to regulate OA-associated subchondral bone remodeling. One cross-sectional clinical study reported that elderly women with estrogen administration had a lower prevalence of knee OA–related subchondral bone attrition and subchondral bone edema-like lesions than those without

estrogen administration (Carbone et al., 2004). Another cross-sectional study involving 4,366 white women found that estrogen replacement therapy can result in a lower risk of hip OA (Nevitt et al., 1996). Therefore, estrogen, estrogenic compounds, and selective estrogen receptor modulators (SERMs) may also be suitable for OA prevention in the postmenopausal patient cluster. There are also additional animal studies supporting this concept. Raloxifene (RAL), a commonly used drug for postmenopausal osteoporosis, could inhibit subchondral bone resorption, improve subchondral bone micro-architecture, and retard patellofemoral joint OA progression in ovariectomized rats (Bei et al., 2020). Another anti-postmenopausal osteoporosis drug, Tibolone, was also evidenced to increase serum ALP level and attenuated the development of knee OA in ovariectomized rats (Yang et al., 2014).

Regulating Osteogenesis

Strontium Ranelate

Strontium ranelate (SrR), a bone-acting agent that has long been used as an anti-osteoporosis drug, was recently tested in clinic as a potential disease-modifying OA drug (DMOAD) to target subchondral bone. Strontium is a chemical analog of calcium that binds to bone and can enhance pre-osteoblast maturation, stimulate OPG production in osteoblasts, and inhibit osteoclast formation by regulating RANKL (Atkins et al., 2009; Tat et al., 2011). Interestingly, it was also found that SrR could enhance the cartilage matrix production rate of human chondrocytes *in vitro* (Henrotin et al., 2001).

A Phase III large international study, the SEKOIA trial (ISRCTN41323372), consisting of 1,371 OA patients over 50 years old with joint space width 2.5–5 mm who were treated with 1 g/day ($n = 558$), 2 g/day ($n = 566$), or placebo ($n = 559$) of SrR, reported structural and beneficial effects in the 1 g and 2 g /day groups, and symptomatic benefits in the 2 g/day group at 3 years (Reginster et al., 2013). Further follow-up also indicated improvement in pain and physical functions (Bruyere et al., 2014). The significance of the findings from this trial is the direct support of the possibility to target subchondral bone as early OA intervention. The remaining concerns of this drug are its side effects on the cardiovascular system that limit its applications, and the unclear patient subpopulation profile to identify proper responders.

Recombinant Human Parathyroid Hormone, Teriparatide

Recombinant human parathyroid hormone (PTH or teriparatide) has anabolic effects on bone formation by acting on osteoblasts, and has been approved to treat osteoporosis. In addition, emerging evidence suggested that PTH and parathyroid hormone related peptide (PTHrP) could directly influence articular cartilage homeostasis and bone growth (Chang et al., 2009; Sampson et al., 2011). Currently, there is no completed randomized clinical trial for treating OA with teriparatide. A Phase II clinical trial is under way to study the chondroprotective effect of teriparatide on participants with knee OA (NCT03072147), and the results on subchondral bone will be very relevant.

Osteocytes

No current therapy is available to specifically target osteocytes.

Other Components: Vascularization, Innervation

No current therapy is available.

FUTURE THERAPEUTIC TARGETS

Therapeutic Target: Inhibiting Osteoclasts

Cathepsin K Inhibitor

CTSK is an osteolytic protease involved in bone resorption and cartilage degradation by degrading bone matrix proteins. In OA, as subchondral bone remodeling exhibits aberrantly activated bone resorption, the CTSK pathway has been considered a potential therapeutic target. Administration of the CTSK inhibitor, SB-553484, delayed OA progression in a canine model (Connor et al., 2009). Another novel selective CTSK inhibitor, MIV-711, was recently developed for OA treatment, and showed promising protection against subchondral bone loss (both plate and trabecular bone) and partial alleviation of cartilage deterioration in early OA in rabbit and canine OA models (Lindstrom et al., 2018). In a Phase II clinical trial of MIV-711, although there was no impact on pain relief, effective reduction of bone resorption and cartilage volume loss was observed (Conaghan et al., 2020). Odanacatib is the only candidate CTSK inhibitor for human use, which is supported by the results from Phase III clinical trials, and exhibits high therapeutic efficacy in postmenopausal osteoporosis patients (Mcclung et al., 2019). However, the pharmaceutical company has discontinued development of Odanacatib due to adverse cardio-cerebrovascular effects and other concerns (Mullard, 2016).

Therapeutic Target: Regulating Osteoblasts

TGFβ

TGFβ signaling is one of the key pathways that regulate bone development and remodeling (Kegelman et al., 2020). A high level of TGFβ1 activation was found in both human and mouse OA subchondral bone, which led to subchondral bone abnormality, including increased number of osteoblastic cells, enhanced subchondral bone sclerosis, and angiogenesis. Inhibition of TGFβ1 pathway *via* blocking TGFβ1 receptor (SB-505124) or neutralizing TGFβ1 in subchondral bone with neutralizing antibody (1D11) attenuated OA progression and rescued both articular cartilage from degeneration and subchondral bone from sclerosis (Zhen et al., 2013). Interestingly, researchers from the same group also reported that halofuginone, a natural quinazolinone alkaloid found in the Chinese herb *Dichroa febrifuga*, showed similar TGFβ1 inhibition effects in OA mouse models (Cui et al., 2016), suggesting that halofuginone may have potential therapeutic effect on regulating subchondral bone in OA. Another Chinese herbal extract isolated from the plant *Artemisia annua,* Artesunate, also inhibited subchondral bone TGFβ/Smad signaling pathway and restored the coupled bone remodeling in an ACLT-induced mice OA model (Li et al., 2019) (**Table 1**).

TABLE 1 | Potential targets of subchondral bone remodeling for OA under investigation.

OA phase	Potential target	Possible drug	References
Early	Estrogen/Estrogen receptor	Raloxifene; Tibolone	Yang et al., 2014; Bei et al., 2020
	TGFβ	Halofuginone; Artesunate	Cui et al., 2016; Li et al., 2019
	COX2/PEG2	NSAIDs	Massicotte et al., 2002; Tu et al., 2019
Early-Late	PDGF; VEGF	Bevacizumab	Nagai et al., 2014
	H-Type ($CD31^{high}Emcn^{high}$) vessel	Defactinib	Kusumbe et al., 2014; Hu et al., 2020
N/A	YAP	Verteporfin	Zhang et al., 2020

Wnt

Canonical signaling *via* β-catenin is involved in bone remodeling and regulates joint development and disease, including subchondral bone (Huang et al., 2018). Activation of Wnt/β-catenin signaling has been found in OA subchondral bone, and inhibition of Wnt in osteoblasts by overexpression of its natural antagonist Dkk1, decreased OA phenotype, suggesting Wnt signaling as a possible pharmacological target for subchondral bone remodeling in OA (Funck-Brentano et al., 2014).

mTORC1

A newly discovered subchondral bone regulator is the mechanistic target of rapamycin complex 1 (mTORC1), a crucial element of the mTOR pathway. mTORC1 is overactivated in pre-osteoblasts in OA subchondral bone in both human and mice models. Lin et al. (2019) demonstrated that mTORC1 activation in pre-osteoblasts resulted in aberrant subchondral bone formation, and specific inhibition of mTORC1 pathway in pre-osteoblast could alleviate subchondral bone sclerosis and cartilage deterioration. Pharmacologic inhibition of mTOR pathway could be a possible target option for early stage OA treatment by regulating subchondral bone remodeling (Chan et al., 2011; Lin et al., 2019).

Other Chinese Herbs

Cai et al. (2018) reported that Magnoflorine, an herbal extract from *Pachygone ovata*, stimulated osteoblast proliferation and mineralization *in vitro* (25 μg /ml), and attenuated the degeneration of cartilage in early stage OA in a guinea pig spontaneous OA model. The drug delivery method consisted of 50 ng purified magnoflorine mixed with 2 μl hyaluronic acid gel to achieve sustained drug release *in situ* (Cai et al., 2018).

Therapeutic Target: Osteocytes

Apart from osteoblasts and osteoclasts, emerging evidence suggests that the matrix-embedded osteocytes also play essential roles in bone remodeling, particularly in arthritic subchondral bone. Tu et al. (2019) reported that osteocytes in subchondral bone expressed high level of cyclooxygenase-2 (COX-2) during the development of OA in a spontaneous OA model (STR/Ort mice), where there was no significant changes in the number of tartrate-resistant acid phosphatase (TRAP)-positive osteoclasts, supporting the importance of osteocytes in early OA subchondral bone remodeling. Specifically, in this STR/Ort mice OA model, the high level of COX-2 expression in osteocytes gave rise to abnormal subchondral bone formation, and accelerated cartilage degeneration at the onset of OA. Application of COX-2 inhibitors to animals at 12.5–25% of the clinical application dosage for 4 weeks resulted in normalization of the microstructure of subchondral bone and relief of cartilage degeneration in mice; a similar effect was also found in a rheumatoid arthritis mice model (TNF-α transgenic RA mice). This important piece of pre-clinical evidence suggested a treating window for bone remodeling during the development of arthritis, and the current clinical available COX-2 inhibitors could also manage the subchondral bone remodeling *via* regulating the osteocytes (Tu et al., 2019).

In addition, subchondral bone osteocyte-derived matrix metallopeptidase 13 (MMP13) was also identified as a regulator of articular cartilage health, by affecting PLR of osteocytes. Mazur et al. (2019) established a MMP13 knockout mouse model with a Cre recombinase driven dentin matrix acidic phosphoprotein 1 (DMP1) promoter to specifically ablate osteocyte MMP13, without affecting chondrocyte derived MMP13. The depletion of osteocyte MMP13 increased both cortical and subchondral bone mass, and suppressed PLR during OA development in animals. Results from this study provided insights on the important contribution of osteocyte derived MMP13 to PLR during OA development, and on the dynamic crosstalk between subchondral bone osteocytes and cartilage (Mazur et al., 2019).

Other Therapeutic Targets: Vascularization and Nerve Innervation

The vasculature in bone is indispensable for skeletal development and homeostasis. Osteogenesis is coupled with angiogenesis during bone modeling and remodeling (Brandi and Collin-Osdoby, 2006; Kusumbe et al., 2014; Xie et al., 2014). The role of angiogenesis in subchondral bone has been studied recently with genetic mouse models. Su et al. (2020) used transgenic mice to prove that overexpression of platelet-derived growth factor-BB (PDGF-BB) in preosteoclast spontaneously recapitulated the OA-like phenotype in subchondral bone by enhancing both angiogenesis and subchondral bone remodeling; meanwhile, conditional PDGF-BB knockout could effectively prevent surgically-induced OA progression (Su et al., 2020). These results suggested that subchondral bone angiogenesis is one of the key processes in subchondral bone remodeling and may be considered as a potential target. Besides intrinsically inhibiting subchondral bone vascularization, exogenous drugs targeting subchondral bone angiogenesis have also been studied. For example, bevacizumab (a VEGF antibody), halofuginone (inhibiting phosphorylation of Smad2/3 and TGFβ) and

defactinib (inhibitor of focal adhesion kinase, FAK) all showed promising beneficial effects against OA in animal models *via* inhibition of subchondral vascularization (Cui et al., 2016; Lu et al., 2018; Wu et al., 2020).

Nerves often grow along new blood vessels into subchondral bone structures that are normally not innervated, which is also a feature of OA pathogenesis (**Figure 2A**), and may be related to pain (Mapp and Walsh, 2012). Recently, in a study of the role of osteoclast-initiated subchondral bone remodeling in sensory innervation and OA pain, Zhu et al. (2019) showed that osteoclast-initiated aberrant subchondral bone remodeling induced sensory innervation *via* subchondral osteoclast-derived Netrin-1, resulting in enhanced subchondral bone sensory nerve growth. This sensory innervation and OA pain could be attenuated by either inhibiting subchondral osteoclasts (by means of gene knockout in DMP1-Rankl Flox mice or treatment with alendronate), or deleting Netrin1 in osteoclast-lineage cells (by means of knockout in Trap-Netrin1 flox mice) (Zhu et al., 2019). Our group has recently reported the role of NGF/TrkA signaling pathway in calcification of human healthy articular chondrocyte, representing another mechanism operating on the other side of the cartilage tidemark that regulates OA subchondral remodeling (Jiang and Tuan, 2019). Another osteoblast-secreted inflammatory mediator, prostaglandin E2 (PGE2), was also found to be increased in OA subchondral bone and sensory innervation. PGE2 activates an ion channel protein, Nav1.8, and inhibition of PEG2 production or Nav1.8 function with a selective Nav1.8 sodium channel blocker A-803467 could attenuate OA (Zhu et al., 2020). Taken together, these observations provide insights on the linkage between sensory innervation and OA subchondral bone remodeling (Zhu et al., 2020).

That angiogenesis/vascularization and nerve innervation appear to play functional roles in subchondral bone remodeling during OA progression suggests that they are potential therapeutic targets for the development of OA drugs (**Figure 2F**).

Regenerative Therapy

Regenerative therapies, including stem cell-based therapies are actively investigated for OA treatment. There are Phase I/II clinical trials of using bone marrow derived MSCs/BMSCs (Gupta et al., 2016; Shapiro et al., 2017), adipose tissue derived MSCs/ADSCs (Song et al., 2018; Lu et al., 2019), and other allogeneically derived MSCs (Matas et al., 2019) to treat OA knees (**Table 2**). For instance, two Phase II clinical trials showed that intra-articular injections of human ADSCs (5×10^7 cells) exhibited the improvement in both pain relief and cartilage volume (Song et al., 2018; Lu et al., 2019). However, the favorable results reported are primarily focused on pain relief and functional improvement but few tissue regeneration and subchondral bone reestablishment, and the application is with the strict condition of administrative DOSES (Donor, Origin tissue, Separation method, Exhibited cell characteristics associated with behavior, and Site of delivery), i.e., cell derivation, cell number, harvesting method, sites of delivery (Murray et al., 2019) and frequency (Kim et al., 2019).

Regenerative therapy also represents an emerging strategy to enhance the subchondral bone health, particularly at the early stage of disease that could prevent OA progression. Subchondroplasty is a recently developed, clinically-used surgical treatment using bioactive materials, e.g., calcium phosphate, as bone substitute materials (BSMs), to fill the subchondral bone marrow lesions. The BSMs used for subchondroplasty are injectable, and are engineered products that have similar mechanical properties as the surrounding trabecular bone, thereby providing a bioactive scaffold for local subchondral bone remodeling, and preventing further damage to the osteochondral tissue (Farr and Cohen, 2013; Colon et al., 2015). Another approach is to use cell-based therapy to regenerate the osteochondral defects before it progresses to OA. Autologous chondrocytes (Brittberg et al., 1994; Peterson et al., 2010) and adult stem cells such as cartilage derived-progenitors (Jiang et al., 2016), bone marrow derived-MSCs (Wakitani et al., 2002, 2007; Kuroda et al., 2007) are the most frequently used cell types with satisfactory tissue repair results in clinical studies and applications (Jiang et al., 2017) (**Table 2**).

Tissue engineering constitutes a major strategy in regenerative therapy, i.e., to repair the tissue with exogenous cells, biomaterials, and/or bioactive factors. Another strategy is to enhance and push the limit of a tissue's self-healing capacity. Subchondral bone has a certain degree of self-repair ability in healthy joints. This healing capacity has been reported in different animal models, dependent on age and species (Pfeifer et al., 2017), size and site of the defect (Fisher et al., 2015; Orth et al., 2016), and is the foundation of the well-established surgical technique of microfracture. Microfracture has been used to treat small to medium sized cartilage/osteochondral defects by creating perpendicular channels into the subchondral bone plate and allowing the bone marrow to seep into the defect area (Pan et al., 2009). The cartilage repair/resurfacing resulting from this type of marrow stimulation techniques is thought to be partially due to the recruitment and local differentiation of bone marrow-derived MSCs, which act as a key player in subchondral bone remodeling and osteochondral homeostasis. We have previously established the application of a bioactive scaffold that achieved fast healing of subchondral bone in a rabbit osteochondral defect model. Interestingly, articular cartilage resurfacing was observed in the fast healing subchondral bone groups without any other additional treatments (Jiang et al., 2013). A subchondral remodeling step thus appears to take place in advance of cartilage repair in osteochondral healing, and the quality of cartilage generated from the marrow stimulation techniques is dependent on the healing speed and quality of subchondral bone remodeling (Chen et al., 2011; Jiang et al., 2013).

In this manner, a practical regenerative approach for OA is to enhance the performance of the subchondral bone by introducing additional bone marrow derived MSCs, to maintain osteochondral tissue homeostasis and prevent further cartilage loss. Some exciting results from a series of clinical trials have just been released by Hernigou et al. (2018, 2020a,b) (**Table 3**), with clinical data of up to 15 years of follow-ups. Patients with different OA conditions (moderate to advanced OA, 60 cases; advanced OA, 140 cases; OA secondary to knee osteonecrosis related to corticosteroids, 30 cases) were recruited. These patients have comparable clinical symptom in bilateral knees, and were

TABLE 2 | Stem cell-based therapy for cartilage/osteochondral defect and OA.

Disease condition	Cell sources	Sample size and group	Placebo/ Control	Follow-up	Route of administration	Main results	Study group
Cartilage defect	Autologous Chondrocytes	23 patients (13 femoral condyle defect due to trauma; 3 osteochondritis dissecans; 6 chondromalacia patellae; 1 traumatic origin)	N/A	39 months (16–66 months)	Autologous chondrocyte implantation	Transplants eliminated knee locking and reduced pain and swelling after surgery. Two-year follow-up showed that 14 (14/16) patients with femoral condylar transplants had good-to-excellent results. Three-year follow-up showed that 2 (2/7) patients with patellar transplants had excellent or good results.	Brittberg et al., 1994
		224 patients	N/A	12.8 years (10–20 year)		92% of the patients were satisfied with the treatment effect, and 74% of the patients reported same or better status as previous years. Improved clinical outcome, better life quality, and high activity level were reported.	Peterson et al., 2010
	CDPCs	15 patients	N/A	12 months	MACI, mini-arthrotomy	The cartilage defects (6–13 cm^2) were completely repaired. Knee function (IKDC scores and Lysholm scores) was significantly improved.	Jiang et al., 2016
	BMSCs	24 patients; BMSCs ($n = 12$), Placebo ($n = 12$)	Cell-free collagen gel sheet	10.5 months (28–95 weeks)	Implantation at the time of HTO	Arthroscopic and histological grading scores were significantly improved, but no significant clinical improvement.	Wakitani et al., 2002
		3 patients	N/A	27 months	Transplantation surgery	The cartilage defects were repaired, and clinical symptoms were improved.	Wakitani et al., 2007
		1 patient	N/A	12 months	Arthroscopic surgery	The defect was recovered with hyaline-like cartilage tissue, and clinical symptoms were improved.	Kuroda et al., 2007
	SMSCs	10 patients (Symptomatic single cartilage lesion in femoral condyle)	N/A	52 months (37–80 months)	Arthroscopic surgery	The MRI score and Lysholm score were significantly improved compared to pre-surgery.	Sekiya et al., 2015
		5 patients (Symptomatic knee chondral lesions; 1.5-3.0 cm^2)	N/A	24 months	Mini-arthrotomy	The defects were successfully repaired. And the VAS, Lysholm, and KOOS scores were significantly improved compared to pre-surgery.	Shimomura et al., 2018
Osteoarthritis	Bone marrow aspirate concentrate (BMAC)	25 patients (bilateral knee OA); BMACs into one knee joint and placebo into the contralateral knee	Sterile saline	6 months	Intra-articular injection	The pain relief (VAS scores and ICOAP scores) was significant compared to the baseline, but was non-significant compared to the saline treated contralateral knee.	Shapiro et al., 2017; Phase I
	BMSCs	60 patients; Cohort1: BMSCs dose1(2.5×10^7 cells; $n = 10$), Placebo ($n = 5$); Cohort2: BMSCs dose2 (5×10^7 cells; $n = 10$), Placebo ($n = 5$); Cohort3: BMSCs dose3 (7.5×10^7 cells; $n = 10$), Placebo ($n = 5$); Cohort4: BMSCs dose4 (1.5×10^8 cells; $n = 10$), Placebo ($n = 5$)	PLASMA-LYTE A (a multiple electrolytes injection)	12 months	Intra-articular injection	The lowest dose cohort (Cohort1; 2.5×10^7 cells) showed a trend toward improvement in all parameters including VAS, WOMAC and ICOAP cores (though non-significant compared to the placebo group), while other higher doses cohorts neither showed significant symptomatic relief, nor showed acceptable safety.	Gupta et al., 2016; Phase II
	ADSCs	52 patients; ADSCs group ($n = 26$); Placebo ($n = 26$)	1% sodium Hyaluronic acid	12 months	Intra-articular injection	ADSCs group showed significant improvement in joint (WOMAC scores) and cartilage volume (MRI quantification) in comparison with both baseline and placebo group.	Lu et al., 2019; Phase IIb

(Continued)

TABLE 2 | Continued

Disease condition	Cell sources	Sample size and group	Placebo/ Control	Follow-up	Route of administration	Main results	Study group
		18 patients; ADSCs low-dose: (1×10^7 cells; $n = 6$); ADSCs mid-dose: (2×10^7 cells; $n = 6$); ADSCs high-dose: (5×10^7 cells; $n = 6$)	N/A	24 months	Intra-articular injection	ADSCs group with different dosage all showed significant improvement in joint function (WOMAC scores), life quality (SF-36 scores) and cartilage volume (MRI quantification). The high dose group (5×10^7 cells) exhibited the highest improvement.	Song et al., 2018; Phase I/II
		24 patients; ADSCs group (1×10^8 cells; $n = 12$); Placebo ($n = 12$)	Sterile saline	6 months	Intra-articular injection	ADSCs group showed a significant functional improvement and pain relief in comparison with baseline, without cartilage volume changes at 6 months' follow-up.	Lee et al., 2019; Phase IIb
		30 patients; ADSCs single-injection group: (1×10^8 cells; $n = 10$); ADSCs twice-injection group: (1×10^8 cells, injection at baseline and 6 months; $n = 10$); Control group: ($n = 10$)	Conservative management	12 months	Intra-articular injection	The pain, function, and life quality of both treatment groups were significantly improved compared to the control group.	Freitag et al., 2019; Phase II
	UC-MSCs	26 patients; Single-dose UC-MSCs (20×10^6 cells, $n = 9$); Repeated-dose UC-MSCs (20×10^6 cells, twice a year, $n = 9$); Placebo ($n = 8$)	Hyaluronic acid	12 months	Intra-articular injection	Pain (WOMAC-A, pain scores) and function (WOMAC-C, function scores) were significantly improved in comparison with placebo group. Repeated-dose UC-MSCs (20×10^6cells, twice a year) exhibited a superior effect to placebo group and single-dose group.	Matas et al., 2019; Phase I/II
		6 patients (KL grade 3 and ICRS cartilage defect grade 4); Low-dose group ($1.15–1.25 \times 10^7$cells; $n = 3$) High-dose group ($1.65–2.0 \times 10^7$cells; $n = 3$)	N/A	7 years	Intra-articular injection	The improved clinical outcomes were stable over 7 years of follow-up. The histological findings at 1 year showed hyaline-like cartilage. MRI at 3 years showed persistence of the regenerated cartilage. No cases of osteogenesis or tumorigenesis was observed over 7 years.	Park et al., 2017; Phase I/II

ADSCs, adipose-derived mesenchymal stromal cells; BMSCs, Bone marrow-derived mesenchymal stromal cells; CDPCs, Cartilage derived progenitor cells; HTO, High tibial osteotomy; ICOAP, intermittent and constant osteoarthritis pain; ICRS, International Cartilage Repair Society; IKDC, International Knee Documentation Committee; KL, Kellgren-Lawrence; KOOS, Knee Injury and Osteoarthritis Outcome Score; MACI, matrix induced autologous chondrocyte implantation; MRI, magnetic resonance imaging; SMSCs, synovium-derived mesenchymal stromal cells; UC-MSCs, umbilical cord-derived mesenchymal stromal cells; VAS, visual analog scale; WOMAC, Western Ontario and McMaster Universities Arthritis Index.

TABLE 3 | Clinical results of subchondral bone MSC therapy for OA patients.

Bilateral clinical study		OA condition before treatment	No. of Knees	Age/Gender	Treatment details	Clinical results		References
						Short-term follow-up	Long-term follow-up	
1	MSC subchondral bone injection	Bilateral knee osteoarthritis	60	61 y (48–72 y) 25M/35F	5,727 BMSCs/mL; 20 mL total (10 mL in medial tibial plateau; 10 mL in medial femoral condyle)	Knee score (2 years): 79.3 ± 12; Elevated K-L score (2 years): 2/60	Yearly arthroplasty incidence: 1.3%; TKA incidence: 20% (12/60)	Hernigou et al., 2020a
	MSC IA injection		60		5,727 BMSCs/mL; 20 mL into joint	Knee score (2 years): 64 ± 21; Elevated K-L score (2 years): 11/60	Yearly arthroplasty incidence: 4.6%; TKA incidence: 70% (42/60)	
2	MSC subchondral bone injection	Planned for staged-bilateral TKA for medial osteoarthritis; "comparable" pain in both knees	140	75.4 y (65–90 y) 53M/87F	7,800 BMSCs/mL; 20 mL total (10 mL in medial tibia plateau; 10 mL in femoral condyle)	Average BML size (before treatment): 3.4 cm^3 (0.4–6.9) Average BML size (2 years): 2.1 cm^3 (1.2–5.7)	TKA incidence: 18% (25/140)	Hernigou et al., 2020b
	TKA		140		TKA	Average BML size: N/A	TKA revision incidence: 15% (21/140)	
3	MSC subchondral bone injection	Bilateral osteoarthritis; secondary to knee ON related to corticosteroids	30	28 y (18–40 y) 12M/18F	6,500 BMSCs/mL; 40 mL (10 mL in medial tibial plateau; 10 mL in medial femoral condyle; 10 mL in lateral tibial plateau; 10 mL in lateral femoral condyle)	Knee score (3 mo): 81.3 ± 12	TKA incidence: 10% (3/30)	Hernigou et al., 2018
	TKA		30		TKA	Knee score (3 mo): 79 ± 21	TKA revision rate: 20% (6/30); re-revision: (2/6)	

MSCs, mesenchymal stem cells; IA, intra-articular injection; BMLs, bone marrow lesions; TKA, total knee arthroplasty; ON, osteonecrosis.

randomized to accept subchondral bone MSC therapy or other surgical treatments. The subchondral bone MSC therapy was delivered to one knee, while the other knee was treated with either intraarticular MSC injection ($n = 60$) or total knee arthroplasty (TKA, $n = 140$) (**Table 3**, Study 1 and Study 2). These results showed that: (i) precise delivery of MSCs to subchondral bone could postpone TKA in OA patients for more than 10 years; (ii) subchondral bone MSC therapy achieved similar clinical scores as TKA knees in short and long-term follow ups; and (iii) subchondral bone MSC therapy could effectively reduce the size of BMLs in OA patients, and postpone or prevent the first TKA surgery in young patients with secondary osteonecrosis related to corticosteroids (**Table 3**, Study 3).

The exact injection site and optimal delivery technique for bone marrow concentrate/MSC are of high significance for these studies. Surgeons used fluoroscopy to direct the trocar to subchondral bone marrow lesions, reaching a distance of 5 mm distal from the tidemark to avoid perforating the cartilage and to keep the calcified cartilage intact; such an approach ensures precise delivery of MSCs to the injury sites of subchondral bone in clinical practice. Delivery sites (subchondral bone *vs.* intraarticular) of MSCs are also of importance: 20% of the knees (12 in 60) in the subchondral implantation group underwent TKA at a mean of 14 years (range, 9–16 years), while 70% of the knees (42 in 60) in the intra-articular implantation group underwent TKA at a mean of 7 years (range, 3–14 years) (Hernigou et al., 2020a).

OA SUBTYPES AND THERAPEUTIC TARGETS

OA is a heterogeneous and multifactorial disease, and the disease is described and categorized into subtypes on the basis of pathological mechanisms and clinical phenotypes. Defining the OA subtypes is clinically relevant to provide insights into the pathological process as well as to generate future therapeutic guidelines for specific patient groups. For example, Sun et al. (2018) subcategorized OA patients into two groups, $pEGFR^{high}$ and $pEGFR^{low}$, according to the level of expression of phosphorylated epidermal growth factor receptor (pEGFR) in cartilage (Sun et al., 2018). Inhibition of EGFR signaling pathway in murine chondrocytes by gene knockout or using the EGFR inhibitor Gefitinib was found to attenuate cartilage degeneration in mouse OA model. These findings suggest a rationale for exploration of Gefitinib as a potential intervention therapeutic to treat OA patients in the $pEGFR^{high}$ subgroup.

Herrero-Beaumont et al. (2017) characterized four subtypes of OA, including biomechanical, osteoporotic, metabolic, and inflammatory OA. Karsdal et al. (2014) proposed six potential OA subtypes, including low-grade autoimmunity, inflammation, genetic, hormonal, metabolic and mechanotransduction subtypes, and categorized the drivers of OA into at least three different types based on the most active or affected joint tissues, including cartilage, bone and inflamed synovium. Recent work based on transcriptomic profiles of peripheral blood

mononuclear cells identified two OA subtypes, a degenerative subtype, and an inflammation related subtype (Zhao et al., 2018). Presented below is a discussion of potential OA subtypes on the basis of current reported pathology and intervention studies and clinical findings on the response profile of subchondral bone remodeling.

Profile of the OA Subchondral Bone Remodeling Responders

Four potential OA subtype are proposed: (1) responders to bone-acting agents; (2) responders to NSAIDs (Bingham et al., 2006); (3) responders to MSC-subchondral bone/regenerative therapy; and (4) responders to mechanical stimuli.

Responders to Bone-Acting Agents

Bone acting agents that are reported to be beneficial for OA patients include estrogen (Carbone et al., 2004), BPs (Carbone et al., 2004; Hayes et al., 2020), and SrR (Reginster et al., 2013; Bruyere et al., 2014). Effective responders to estrogen and BPs are mostly postmenopausal women at early stage of OA, and non-overweight; administration of estrogen or BPs reduced radiographic knee OA progression, and is correlated to less subchondral bone lesions (Carbone et al., 2004; Hayes et al., 2020). Responders to SrR are generally early OA patients from both genders over 50 years old with joint space width 2.5–5 mm from the SEKOIA clinical trial (ISRCTN41323372) (Reginster et al., 2013; Bruyere et al., 2014). It is noteworthy that while estrogen could prevent subchondral bone lesions, reduction of knee pain was not observed (Carbone et al., 2004); thus, using bone-acting agents for subchondral bone remodeling is more likely to be a preventive step at the very early phase of OA.

Responders to NSAIDs

OA patients are reported to have different types of subchondral bone osteoblast behavior, characterized by difference in endogenous production levels of PGE2 (Massicotte et al., 2002; Kwan Tat et al., 2008), i.e., low PGE2 OA [L-OA] or high PGE2 OA [H-OA] (Massicotte et al., 2002). The L-OA osteoblasts produce higher level of RANKL and exhibit a lower ratio of OPG/RANKL compared with healthy subchondral bone osteoblasts, suggesting that L-OA osteoblasts may play a causal role in subchondral bone resorption in certain subtypes of OA (Kwan Tat et al., 2008). In addition, Tu et al. (2019) identified another subchondral bone responder subtype as COX-2^+ OA and COX-2^- OA in animal models, according to expression level of COX-2 in subchondral bone, and the elevated levels of COX-2 in subchondral bone accelerated cartilage degeneration at the onset of OA. These patients with $PGE2^{high}$/COX-2^+ subchondral bone osteoblast are highly likely to be the responders to NSAIDs.

Responders to MSC (Subchondral Bone Application) and Regenerative Therapy

From the patient inclusion criteria of subchondroplasty and the cell-based therapies (**Table 2**), it is clear that regenerative therapies are the frontline choices to bone marrow lesions (Hernigou et al., 2020a), osteochondral defects, and injuries (Brittberg et al., 1994; Wakitani et al., 2002, 2007; Kuroda et al., 2007; Peterson et al., 2010; Jiang et al., 2016).

Hernigou et al. provided a wide spectrum patient profile for MSC-based therapy for subchondral bone remodeling to prevent OA development and minimize TKA (**Table 3**). In the 140-case study, patients scheduled for TKA who were administrated subchondral injection of BMSCs reported good joint preservation results after 15 years of follow up (Hernigou et al., 2020b). In the young osteonecrosis patients, 96% of those who received subchondral bone MSC injection showed postponement of the first TKA for more than 10 years, while a 20% revision rate was found in the TKA treatment group (Hernigou et al., 2018). Subchondral bone MSCs treatment was found to be applicable for both early and late stage OA in terms of subchondral bone remodeling and joint preservation. These investigators also found that: (i) persistent BML larger than 3 cm^3 after MSC therapy was an independent risk factor for TKA; and (ii) incidence rates of arthroplasty were higher for young patients and for patients with severe malalignment (hip-knee-ankle angle $< 170°$) (Hernigou et al., 2020b). In other words, responders to MSC subchondral bone injection were most likely individuals whose BML was no larger than 3 cm^3 and without lower limb malalignment.

Responders to Mechanical Stimuli

Two obvious effective management strategies for OA related to mechanical stimuli are weight loss and exercise, both of which are recommended by the American College of Rheumatology (Kolasinski et al., 2020). A pre-clinical study showed that body weight-supported treadmill training (lower than 60% loading in the joint) is more efficient in maintaining cartilage integrity and attenuating subchondral bone loss and remodeling than treadmill training alone (Hao et al., 2020). Weight loss and exercise are therefore highly beneficial for early OA patients.

Lower limb malalignment alters the stress distribution across the knee, resulting in altered bone remodeling in tibiofemoral joint, and is a major contributor to severity of OA. Patients with malalignment are mechanical stimuli responders, and the conditions can be attenuated by correction of malalignment. The subchondral bone remodeling before and after osteotomy or other malalignment correction surgeries can be observed by bone scintigraphy, which measures reflects alterations in the metabolic activity of bone (Kraus et al., 2009), dual energy X-ray absorptiometry (Dexa), and MRI.

Knee joint distraction (KJD) is a surgical procedure involving the gradual separation of the two joint surfaces by an external fixator frame (Intema et al., 2011). Interestingly, separation and mechanical unloading of OA affected joint surfaces could reduce tissue wear and tear. Intema et al. (2011) reported a decrease in subchondral bone density on the OA affected compartment after KJD for 12 months, delaying the progression of late OA. Goh et al. (2019) recently reviewed the role of KJD in OA management and summarized available supportive evidence for the beneficial outcomes. Therefore, KJD could be a promising, clinically available therapy for OA patients, based on the reduction of mechanical stimuli to prevent OA development. In addition, exoskeletons have also shown promise in modifying

the biomechanical environment of the knee in OA patients (Mcgibbon et al., 2017).

Future Targets Under Investigation

Several new cellular and molecular targets of OA subchondral bone remodeling have been recently reported in pre-clinical animal studies, including TGFβ, PGE2/Cox2, vascularization, and mechanical sensor proteins (**Figure 2**). These mechanistic studies are investigated with small animals, and the targets and their possible pharmacological manipulation are summarized in **Table 1**. Among these, the known OA subchondral bone regulatory signaling pathways of estrogen, TGFβ, and COX2/PEG2 have been discussed in previous sections. Additional details on the regulators of the vascular and mechanical responses in OA subchondral bone are provided below.

Increased vascularization of subchondral bone and the invasion into osteochondral junction are important pathological characteristics of OA (Suri et al., 2007). The vascularization in subchondral bone is one of the potential targets. In the arthritic joint, VEGF signaling contributes to bone resorption and destruction *via* recruitment and activation osteoclasts (Matsumoto et al., 2002). Administration of bevacizumab, a neutralizing VEGF antibody, either intra-articularly (1 mL; 25 mg/mL; 3 weeks) or intravenously (5 mg/kg; 2 weeks), has been confirmed to attenuate OA in a rabbit model (Nagai et al., 2014). Su et al. (2020) discovered that preosteoclast-derived PDGF-BB enhanced the H type vessel numbers in OA subchondral bone (Kusumbe et al., 2014; Su et al., 2020). In addition, Hu et al. (2020) reported that H-type vessels and MSCs were coordinated in a positive feedback loop *via* focal adhesion kinase (FAK) signaling in MSCs, subsequently causing aberrant bone formation in ACLT-induced murine OA subchondral bone (Hu et al., 2020); furthermore, the FAK inhibitor defactinib effectively suppressed the positive loop between H type vessels and MSCs, and alleviated OA in mice (Hu et al., 2020) (**Table 1**).

As both cartilage and bone are mechanical sensitive joint tissues, the mechanosensitive pathway in subchondral bone represents another potential target. The expression of the mechanosensing molecule, Yes-associated protein (YAP), in human knee joint articular cartilage was positively correlated with cartilage ECM stiffness. In OA mouse cartilage, YAP expression was aberrantly increased, and conditional knockout of YAP protected against cartilage degeneration. Intra-articular administration of Verteporfin, a YAP-selective inhibitor, also lowered the expression of YAP and alleviated cartilage degeneration in DMM-induced murine OA model (Zhang et al., 2020). Wang et al. (2020) recently identified PIEZO1 as the major skeletal mechanosensor or mechanostat protein that tunes bone homeostasis. Mice deficient in Piezo1 gene expression in osteoblastic cells, while showing loss of bone mass and spontaneous fractures with increased bone resorption, are resistant to further bone loss and bone resorption due to mechanical unloading, suggesting that PIEZO1 in osteoblasts controls osteoblast-osteoclast crosstalk in response to mechanical forces. PIEZO1 regulates the YAP-dependent expression of collagen types II and IX, which in turn regulate osteoclast differentiation and bone remodeling. Additional support is provided by the findings of Zhou et al. (2020) who also reported that Piezo1/2 could regulate bone formation by mediating mechanotransduction *via* the NFAT/YAP1/ß-catenin axis in mice (Zhou et al., 2020). The manner and approach of regulating the mechano-modulatory factors and cellular activities in OA subchondral bone thus requires further exploration. Definitive classification of the nature of impairment of mechanoresponsive pathways in subchondral bone would be helpful to identify new subtypes of OA patients.

CONCLUSION

In summary, we have provided a review of the key cellular and molecular players in subchondral bone remodeling, and the changes that accompany the pathogenesis of OA in the articular joint. These factors and associated pathways are potential targets for development of OA therapies focused on subchondral bone remodeling. Brief profiles of the different types of OA responders to subchondral bone remodeling are presented, based on available clinical therapies. Finally, we have also summarized the novel mediators of OA subchondral bone remodeling that are currently under investigation.

AUTHOR CONTRIBUTIONS

YJ: conceptual design. YC, XZ, and YJ: data mining and collection. XZ, YJ, and YC: manuscript preparation. YJ, RT, and PY: manuscript editing. PY, RT, and YJ: data interpretation. All authors contributed to the article and approved the submitted version.

FUNDING

This study was supported by the National Key R&D Program of China (2019YFA0111900 to YJ).

ACKNOWLEDGMENTS

The authors acknowledge the research support of The Chinese University of Hong Kong.

REFERENCES

Abed, E., Delalandre, A., and Lajeunesse, D. (2017). Beneficial effect of resveratrol on phenotypic features and activity of osteoarthritic osteoblasts. *Arthritis Res. Ther.* 19:151. doi: 10.1186/s13075-017-1365-2

Arden, N. K., Griffiths, G. O., Hart, D. J., Doyle, D. V., and Spector, T. D. (1996). The association between osteoarthritis and osteoporotic fracture: the Chingford study. *Br. J. Rheumatol.* 35, 1299–1304. doi: 10.1093/rheumatology/35.12.1299

Atkins, G. J., Welldon, K. J., Halbout, P., and Findlay, D. M. (2009). Strontium ranelate treatment of human primary osteoblasts promotes an osteocyte-like

phenotype while eliciting an osteoprotegerin response. *Osteoporos. Int.* 20, 653–664. doi: 10.1007/s00198-008-0728-6

Bailey, A. J., Sims, T. J., and Knott, L. (2002). Phenotypic expression of osteoblast collagen in osteoarthritic bone: production of type I homotrimer. *Int. J. Biochem. Cell. Biol.* 34, 176–182. doi: 10.1016/S1357-2725(01)00107-8

Behets, C., Williams, J. M., Chappard, D., Devogelaer, J. P., and Manicourt, D. H. (2004). Effects of calcitonin on subchondral trabecular bone changes and on osteoarthritic cartilage lesions after acute anterior cruciate ligament deficiency. *J. Bone Miner. Res.* 19, 1821–1826. doi: 10.1359/JBMR.040609

Bei, M. J., Tian, F. M., Xiao, Y. P., Cao, X. H., Liu, N., Zheng, Z. Y., et al. (2020). Raloxifene retards cartilage degradation and improves subchondral bone micro-architecture in ovariectomized rats with patella baja-induced - patellofemoral joint osteoarthritis. *Osteoarthr. Cartil.* 28, 344–355. doi: 10.1016/j.joca.2019.06.014

Bellido, M., Lugo, L., Roman-Blas, J. A., Castaneda, S., Caeiro, J. R., Dapia, S., et al. (2010). Subchondral bone microstructural damage by increased remodelling aggravates experimental osteoarthritis preceded by osteoporosis. *Arthritis Res. Ther.* 12:R152. doi: 10.1186/ar3103

Bettica, P., Cline, G., Hart, D. J., Meyer, J., and Spector, T. D. (2002). Evidence for increased bone resorption in patients with progressive knee osteoarthritis: longitudinal results from the Chingford study. *Arthritis Rheum.* 46, 3178–3184. doi: 10.1002/art.10630

Bian, W., Lian, Q., Li, D., Wang, J., Zhang, W., Jin, Z., and Qiu, Y. (2016). Morphological characteristics of cartilage-bone transitional structures in the human knee joint and CAD design of an osteochondral scaffold. *Biomed. Eng. Online* 15:82. doi: 10.1186/s12938-016-0200-3

Bianco, D., Todorov, A., Cengic, T., Pagenstert, G., Scharen, S., Netzer, C., et al. (2018). Alterations of subchondral bone progenitor cells in human knee and hip osteoarthritis lead to a bone sclerosis phenotype. *Int. J. Mol. Sci.* 19:475. doi: 10.3390/ijms19020475

Bingham, C. O. III, Buckland-Wright, J. C., Garnero, P., Cohen, S. B., Dougados, M., Adami, S., et al. (2006). Risedronate decreases biochemical markers of cartilage degradation but does not decrease symptoms or slow radiographic progression in patients with medial compartment osteoarthritis of the knee: results of the two-year multinational knee osteoarthritis structural arthritis study. *Arthritis Rheum.* 54, 3494–3507. doi: 10.1002/art.22160

Bolbos, R. I., Zuo, J., Banerjee, S., Link, T. M., Ma, C. B., Li, X., et al. (2008). Relationship between trabecular bone structure and articular cartilage morphology and relaxation times in early OA of the knee joint using parallel MRI at 3 T. *Osteoarthr. Cartil.* 16, 1150–1159. doi: 10.1016/j.joca.2008.02.018

Borciani, G., Montalbano, G., Baldini, N., Cerqueni, G., Vitale-Brovarone, C., and Ciapetti, G. (2020). Co-culture systems of osteoblasts and osteoclasts: simulating *in vitro* bone remodeling in regenerative approaches. *Acta Biomater.* 108, 22–45. doi: 10.1016/j.actbio.2020.03.043

Boskey, A. L., and Robey, P. G. (2013). "The composition of bone," in *Primer on the Metabolic Bone Diseases and Disorders of Mineral Metabolism*, ed. C. J. Rosen. 8th ed. (Hoboken, NJ: American Society for Bone and Mineral Research), 49–58.

Brandi, M. L., and Collin-Osdoby, P. (2006). Vascular biology and the skeleton. *J. Bone Miner. Res.* 21, 183–192. doi: 10.1359/JBMR.050917

Brittberg, M., Lindahl, A., Nilsson, A., Ohlsson, C., Isaksson, O., and Peterson, L. (1994). Treatment of deep cartilage defects in the knee with autologous chondrocyte transplantation. *N. Engl. J. Med.* 331, 889–895. doi: 10.1056/NEJM199410063311401

Brown, T. D., and Vrahas, M. S. (1984). The apparent elastic modulus of the juxtarticular subchondral bone of the femoral head. *J. Orthop. Res.* 2, 32–38. doi: 10.1002/jor.1100020106

Bruyere, O., Reginster, J. Y., Bellamy, N., Chapurlat, R., Richette, P., Cooper, C., et al. (2014). Clinically meaningful effect of strontium ranelate on symptoms in knee osteoarthritis: a responder analysis. *Rheumatology* 53, 1457–1464. doi: 10.1093/rheumatology/keu018

Burr, D. B., and Gallant, M. A. (2012). Bone remodelling in osteoarthritis. *Nat. Rev. Rheumatol.* 8, 665–673. doi: 10.1038/nrrheum.2012.130

Cai, G., Aitken, D., Laslett, L. L., Pelletier, J. P., Martel-Pelletier, J., Hill, C., et al. (2020). Effect of intravenous zoledronic acid on tibiofemoral cartilage volume among patients with knee osteoarthritis with bone marrow lesions: a randomized clinical Trial. *JAMA* 323, 1456–1466. doi: 10.1001/jama.2020.2938

Cai, Z., Feng, Y., Li, C., Yang, K., Sun, T., Xu, L., et al. (2018). Magnoflorine with hyaluronic acid gel promotes subchondral bone regeneration and attenuates cartilage degeneration in early osteoarthritis. *Bone* 116, 266–278. doi: 10.1016/j.bone.2018.08.015

Carballo, C. B., Nakagawa, Y., Sekiya, I., and Rodeo, S. A. (2017). Basic science of articular cartilage. *Clin. Sports Med.* 36, 413–425. doi: 10.1016/j.csm.2017.02.001

Carbone, L. D., Nevitt, M. C., Wildy, K., Barrow, K. D., Harris, F., Felson, D., et al. (2004). The relationship of antiresorptive drug use to structural findings and symptoms of knee osteoarthritis. *Arthritis Rheum.* 50, 3516–3525. doi: 10.1002/art.20627

Chan, T. F., Couchourel, D., Abed, E., Delalandre, A., Duval, N., and Lajeunesse, D. (2011). Elevated Dickkopf-2 levels contribute to the abnormal phenotype of human osteoarthritic osteoblasts. *J. Bone Miner. Res.* 26, 1399–1410. doi: 10.1002/jbmr.358

Chang, J. K., Chang, L. H., Hung, S. H., Wu, S. C., Lee, H. Y., Lin, Y. S., et al. (2009). Parathyroid hormone 1-34 inhibits terminal differentiation of human articular chondrocytes and osteoarthritis progression in rats. *Arthritis Rheum.* 60, 3049–3060. doi: 10.1002/art.24843

Chen, H., Chevrier, A., Hoemann, C. D., Sun, J., Ouyang, W., and Buschmann, M. D. (2011). Characterization of subchondral bone repair for marrow-stimulated chondral defects and its relationship to articular cartilage resurfacing. *Am. J. Sports Med.* 39, 1731–1740. doi: 10.1177/0363546511403282

Chen, L., Yao, F., Wang, T., Li, G., Chen, P., Bulsara, M., et al. (2020). Horizontal fissuring at the osteochondral interface: a novel and unique pathological feature in patients with obesity-related osteoarthritis. *Ann. Rheum. Dis.* 79, 811–818. doi: 10.1136/annrheumdis-2020-216942

Chen, S., Fu, P., Wu, H., and Pei, M. (2017). Meniscus, articular cartilage and nucleus pulposus: a comparative review of cartilage-like tissues in anatomy, development and function. *Cell Tissue Res.* 370, 53–70. doi: 10.1007/s00441-017-2613-0

Chen, Y., Hu, Y., Yu, Y. E., Zhang, X., Watts, T., Zhou, B., et al. (2018). Subchondral trabecular rod loss and plate thickening in the development of osteoarthritis. *J. Bone Miner. Res.* 33, 316–327. doi: 10.1002/jbmr.3313

Chen, Y., Wang, T., Guan, M., Zhao, W., Leung, F. K., Pan, H., et al. (2015). Bone turnover and articular cartilage differences localized to subchondral cysts in knees with advanced osteoarthritis. *Osteoarthr. Cartil.* 23, 2174–2183. doi: 10.1016/j.joca.2015.07.012

Clark, J. M. (1990). The structure of vascular channels in the subchondral plate. *J. Anat.* 171, 105–115.

Clarke, B. (2008). Normal bone anatomy and physiology. *Clin. J. Am. Soc. Nephrol.* 3, S131–S139. doi: 10.2215/CJN.04151206.

Colon, D. A., Yoon, B. V., Russell, T. A., Cammisa, F. P., and Abjornson, C. (2015). Assessment of the injection behavior of commercially available bone BSMs for Subchondroplasty(R) procedures. *Knee* 22, 597–603. doi: 10.1016/j.knee.2015.06.017

Conaghan, P. G., Bowes, M. A., Kingsbury, S. R., Brett, A., Guillard, G., Rizoska, B., et al. (2020). Disease-modifying effects of a novel cathepsin K inhibitor in osteoarthritis: a randomized controlled trial. *Ann. Intern. Med.* 172, 86–95. doi: 10.7326/M19-0675

Connor, J. R., Lepage, C., Swift, B. A., Yamashita, D., Bendele, A. M., Maul, D., et al. (2009). Protective effects of a cathepsin K inhibitor, SB-553484, in the canine partial medial meniscectomy model of osteoarthritis. *Osteoarthr. Cartil.* 17, 1236–1243. doi: 10.1016/j.joca.2009.03.015

Corrado, A., Neve, A., and Cantatore, F. P. (2013). Expression of vascular endothelial growth factor in normal, osteoarthritic and osteoporotic osteoblasts. *Clin. Exp. Med.* 13, 81–84. doi: 10.1007/s10238-011-0170-5

Couchourel, D., Aubry, I., Delalandre, A., Lavigne, M., Martel-Pelletier, J., Pelletier, J. P., et al. (2009). Altered mineralization of human osteoarthritic osteoblasts is attributable to abnormal type I collagen production. *Arthritis Rheum.* 60, 1438–1450. doi: 10.1002/art.24489

Coxon, F. P., Thompson, K., Roelofs, A. J., Ebetino, F. H., and Rogers, M. J. (2008). Visualizing mineral binding and uptake of bisphosphonate by osteoclasts and non-resorbing cells. *Bone* 42, 848–860. doi: 10.1016/j.bone.2007.12.225

Crane, J. L., and Cao, X. (2014). Bone marrow mesenchymal stem cells and TGF-beta signaling in bone remodeling. *J. Clin. Invest.* 124, 466–472. doi: 10.1172/JCI70050

Cui, Z., Crane, J., Xie, H., Jin, X., Zhen, G., Li, C., et al. (2016). Halofuginone attenuates osteoarthritis by inhibition of TGF-beta activity and H-type vessel formation in subchondral bone. *Ann. Rheum. Dis.* 75, 1714–1721. doi: 10.1136/annrheumdis-2015-207923

Delaisse, J.-M. (2014). The reversal phase of the bone-remodeling cycle: cellular prerequisites for coupling resorption and formation. *Bonekey Rep.* 3, 1–8. doi: 10.1038/bonekey.2014.56

Dole, N. S., Mazur, C. M., Acevedo, C., Lopez, J. P., Monteiro, D. A., Fowler, T. W., et al. (2017). Osteocyte-intrinsic TGF-beta signaling regulates bone quality through perilacunar/canalicular remodeling. *Cell. Rep.* 21, 2585–2596. doi: 10.1016/j.celrep.2017.10.115

Duncan, H., Jundt, J., Riddle, J. M., Pitchford, W., and Christopherson, T. (1987). The tibial subchondral plate. A scanning electron microscopic study. *J. Bone Joint Surg. Amb.* 69, 1212–1220. doi: 10.2106/00004623-198769080-00015

Durand, M., Komarova, S. V., Bhargava, A., Trebec-Reynolds, D. P., Li, K., Fiorino, C., et al. (2013). Monocytes from patients with osteoarthritis display increased osteoclastogenesis and bone resorption: the *in vitro* osteoclast differentiation in arthritis study. *Arthritis Rheum.* 65, 148–158. doi: 10.1002/art.37722

European Medicines Agency (2020) *Science Medicines Health*. Available online at: https://www.ema.europa.eu/en/medicines/human/referrals/calcitonin (accessed November 15, 2020).

Farr, J. II., and Cohen, S. B. (2013). Expanding applications of the subchondroplasty procedure for the treatment of bone marrow lesions observed on magnetic resonance imaging. *Operat Tech Sports Med.* 21, 138–143. doi: 10.1053/j.otsm.2013.03.006

Fisher, M. B., Belkin, N. S., Milby, A. H., Henning, E. A., Bostrom, M., Kim, M., et al. (2015). Cartilage repair and subchondral bone remodeling in response to focal lesions in a mini-pig model: implications for tissue engineering. *Tissue Eng. Part A* 21, 850–860. doi: 10.1089/ten.tea.2014.0384

Freitag, J., Bates, D., Wickham, J., Shah, K., Huguenin, L., Tenen, A., et al. (2019). Adipose-derived mesenchymal stem cell therapy in the treatment of knee osteoarthritis: a randomized controlled trial. *Regen. Med*. 14, 213–230. doi: 10.2217/rme-2018-0161

Frost, H. M. (1994). Wolff's Law and bone's structural adaptations to mechanical usage: an overview for clinicians. *Angle Orthod.* 64, 175–188.

Funck-Brentano, T., Bouaziz, W., Marty, C., Geoffroy, V., Hay, E., and Cohen-Solal, M. (2014). Dkk-1-mediated inhibition of Wnt signaling in bone ameliorates osteoarthritis in mice. *Arthritis Rheumatol.* 66, 3028–3039. doi: 10.1002/art.38799

Goh, E. L., Lou, W. C. N., Chidambaram, S., and Ma, S. (2019). The role of joint distraction in the treatment of knee osteoarthritis: a systematic review and quantitative analysis. *Orthop. Res. Rev.* 11, 79–92. doi: 10.2147/ORR.S211060

Goldring, S. R. (2009). Role of bone in osteoarthritis pathogenesis. *Med. Clin. N. Am.* 93, 25–35, xv. doi: 10.1016/j.mcna.2008.09.006

Goldring, S. R., and Goldring, M. B. (2016). Changes in the osteochondral unit during osteoarthritis: structure, function and cartilage-bone crosstalk. *Nat. Rev. Rheumatol.* 12, 632–644. doi: 10.1038/nrrheum.2016.148

Gupta, P. K., Chullikana, A., Rengasamy, M., Shetty, N., Pandey, V., Agarwal, V., et al. (2016). Efficacy and safety of adult human bone marrow-derived, cultured, pooled, allogeneic mesenchymal stromal cells (Stempeucel): preclinical and clinical trial in osteoarthritis of the knee joint. *Arthritis Res. Ther.* 18:301. doi: 10.1186/s13075-016-1195-7

Hannan, M. T., Anderson, J. J., Zhang, Y., Levy, D., and Felson, D. T. (1993). Bone mineral density and knee osteoarthritis in elderly men and women. The Framingham Study. *Arthritis Rheum.* 36, 1671–1680. doi: 10.1002/art.1780361205

Hao, X., Wang, S., Zhang, J., and Xu, T. (2020). Effects of body weight-supported treadmill training on cartilage-subchondral bone unit in the rat model of posttraumatic osteoarthritis. *J. Orthop. Res.* 2020, 1–9. doi: 10.1002/jor.24791

Hayes, K. N., Giannakeas, V., and Wong, A. K. O. (2020). Bisphosphonate use is protective of radiographic knee osteoarthritis progression among those with low disease severity and being non-overweight: data from the Osteoarthritis Initiative. *J. Bone Miner. Res.* 35, 2318–2326. doi: 10.1002/jbmr.4133

Henrotin, Y., Labasse, A., Zheng, S. X., Galais, P., Tsouderos, Y., Crielaard, J. M., et al. (2001). Strontium ranelate increases cartilage matrix formation. *J. Bone Miner. Res.* 16, 299–308. doi: 10.1359/jbmr.2001.16.2.299

Hering, S., Isken, E., Knabbe, C., Janott, J., Jost, C., Pommer, A., et al. (2001). TGFbeta1 and TGFbeta2 mRNA and protein expression in human bone samples. *Exp. Clin. Endocrinol. Diabetes* 109, 217–226. doi: 10.1055/s-2001-15109

Hernigou, P., Auregan, J. C., Dubory, A., Flouzat-Lachaniette, C. H., Chevallier, N., and Rouard, H. (2018). Subchondral stem cell therapy versus contralateral total knee arthroplasty for osteoarthritis following secondary osteonecrosis of the knee. *Int. Orthop.* 42, 2563–2571. doi: 10.1007/s00264-018-3916-9

Hernigou, P., Bouthors, C., Bastard, C., Flouzat Lachaniette, C. H., Rouard, H., and Dubory, A. (2020a). Subchondral bone or intra-articular injection of bone marrow concentrate mesenchymal stem cells in bilateral knee osteoarthritis: what better postpone knee arthroplasty at fifteen years? A randomized study. *Int. Orthop*. doi: 10.1007/s00264-020-04687-7. [Epub ahead of print].

Hernigou, P., Delambre, J., Quiennec, S., and Poignard, A. (2020b). Human bone marrow mesenchymal stem cell injection in subchondral lesions of knee osteoarthritis: a prospective randomized study versus contralateral arthroplasty at a mean fifteen year follow-up. *Int. Orthop*. doi: 10.1007/s00264-020-04571-4. [Epub ahead of print].

Herrero-Beaumont, G., Roman-Blas, J. A., Bruyere, O., Cooper, C., Kanis, J., Maggi, S., et al. (2017). Clinical settings in knee osteoarthritis: pathophysiology guides treatment. *Maturitas* 96, 54–57. doi: 10.1016/j.maturitas.2016.11.013

Hilal, G., Martel-Pelletier, J., Pelletier, J. P., Ranger, P., and Lajeunesse, D. (1998). Osteoblast-like cells from human subchondral osteoarthritic bone demonstrate an altered phenotype *in vitro*: possible role in subchondral bone sclerosis. *Arthritis Rheum.* 41, 891–899. doi: 10.1002/1529-0131(199805)41:5<891::AID-ART17>3.0.CO;2-X

Hu, Y., Wu, H., Xu, T., Wang, Y., Qin, H., Yao, Z., et al. (2020). Defactinib attenuates osteoarthritis by inhibiting positive feedback loop between H-type vessels and MSCs in subchondral bone. *J. Orthop. Translat.* 24, 12–22. doi: 10.1016/j.jot.2020.04.008

Huang, J., Zhao, L., and Chen, D. (2018). Growth factor signalling in osteoarthritis. *Growth Fact.* 36, 187–195. doi: 10.1080/08977194.2018.1548444

Intema, F., Sniekers, Y. H., Weinans, H., Vianen, M. E., Yocum, S. A., Zuurmond, A. M., et al. (2010). Similarities and discrepancies in subchondral bone structure in two differently induced canine models of osteoarthritis. *J. Bone Miner. Res.* 25, 1650–1657. doi: 10.1002/jbmr.39

Intema, F., Van Roermund, P. M., Marijnissen, A. C., Cotofana, S., Eckstein, F., Castelein, R. M., et al. (2011). Tissue structure modification in knee osteoarthritis by use of joint distraction: an open 1-year pilot study. *Ann. Rheum. Dis.* 70, 1441–1446. doi: 10.1136/ard.2010.142364

Jaiprakash, A., Prasadam, I., Feng, J. Q., Liu, Y., Crawford, R., and Xiao, Y. (2012). Phenotypic characterization of osteoarthritic osteocytes from the sclerotic zones: a possible pathological role in subchondral bone sclerosis. *Int. J. Biol. Sci.* 8, 406–417. doi: 10.7150/ijbs.4221

Jensen, P. R., Andersen, T. L., Pennypacker, B. L., Duong, L. T., and Delaiss,é, J. M. (2014). The bone resorption inhibitors Odanacatib and Alendronate affect post-osteoclastic events differently in Ovariectomized rabbits. *Calcif. Tissue Int.* 94, 212–222. doi: 10.1007/s00223-013-9800-0

Jiang, Y., Cai, Y., Zhang, W., Yin, Z., Hu, C., Tong, T., et al. (2016). Human cartilage-derived progenitor cells from committed chondrocytes for efficient cartilage repair and regeneration. *Stem Cells Transl. Med.* 5, 733–744. doi: 10.5966/sctm.2015-0192

Jiang, Y., Chen, L., Zhang, S., Tong, T., Zhang, W., Liu, W., et al. (2013). Incorporation of bioactive polyvinylpyrrolidone-iodine within bilayered collagen scaffolds enhances the differentiation and subchondral osteogenesis of mesenchymal stem cells. *Acta Biomater.* 9, 8089–8098. doi: 10.1016/j.actbio.2013.05.014

Jiang, Y., Lin, H., and Tuan, R. S. (2017). "Overview: state of the art and future prospectives for cartilage repair," in *Cartilage Volume 3: Repair Strategies and Regeneration,* eds. S. Grässel, and A. Aszódi (Chem: Springer), 1–34.

Jiang, Y., and Tuan, R. S. (2019). Role of NGF-TrkA signaling in calcification of articular chondrocytes. *FASEB J.* 33, 10231–10239. doi: 10.1096/fj.201900970

Karsdal, M. A., Byrjalsen, I., Alexandersen, P., Bihlet, A., Andersen, J. R., Riis, B. J., et al. (2015). Treatment of symptomatic knee osteoarthritis with oral salmon calcitonin: results from two phase 3 trials. *Osteoarthr. Cartil.* 23, 532–543. doi: 10.1016/j.joca.2014.12.019

Karsdal, M. A., Christiansen, C., Ladel, C., Henriksen, K., Kraus, V. B., and Bay-Jensen, A. C. (2014). Osteoarthritis–a case for personalized health care? *Osteoarthr. Cartil.* 22, 7–16. doi: 10.1016/j.joca.2013.10.018

Katsimbri, P. (2017). The biology of normal bone remodelling. *Eur. J. Cancer Care* 26:e12740. doi: 10.1111/ecc.12740

Kegelman, C. D., Coulombe, J. C., Jordan, K. M., Horan, D. J., Qin, L., Robling, A. G., et al. (2020). YAP and TAZ mediate osteocyte perilacunar/canalicular remodeling. *J. Bone Miner. Res.* 35, 196–210. doi: 10.1002/jbmr.3876

Kim, S. H., Ha, C. W., Park, Y. B., Nam, E., Lee, J. E., and Lee, H. J. (2019). Intra-articular injection of mesenchymal stem cells for clinical outcomes and cartilage repair in osteoarthritis of the knee: a meta-analysis of randomized controlled trials. *Arch. Orthop. Trauma Surg.* 139, 971–980. doi: 10.1007/s00402-019-03140-8

Kolasinski, S. L., Neogi, T., Hochberg, M. C., Oatis, C., Guyatt, G., Block, J., et al. (2020). 2019 American college of rheumatology/arthritis foundation guideline for the management of osteoarthritis of the hand, hip, and knee. *Arthritis Rheumatol.* 72, 220–233. doi: 10.1002/art.41142

Kraus, V. B., Mcdaniel, G., Worrell, T. W., Feng, S., Vail, T. P., Varju, G., et al. (2009). Association of bone scintigraphic abnormalities with knee malalignment and pain. *Ann. Rheum. Dis.* 68, 1673–1679. doi: 10.1136/ard.2008.094722

Kuroda, R., Ishida, K., Matsumoto, T., Akisue, T., Fujioka, H., Mizuno, K., et al. (2007). Treatment of a full-thickness articular cartilage defect in the femoral condyle of an athlete with autologous bone-marrow stromal cells. *Osteoarthr. Cartil.* 15, 226–231. doi: 10.1016/j.joca.2006.08.008

Kusumbe, A. P., Ramasamy, S. K., and Adams, R. H. (2014). Coupling of angiogenesis and osteogenesis by a specific vessel subtype in bone. *Nature* 507, 323–328. doi: 10.1038/nature13145

Kwan Tat, S., Pelletier, J. P., Lajeunesse, D., Fahmi, H., Lavigne, M., and Martel-Pelletier, J. (2008). The differential expression of osteoprotegerin (OPG) and receptor activator of nuclear factor kappaB ligand (RANKL) in human osteoarthritic subchondral bone osteoblasts is an indicator of the metabolic state of these disease cells. *Clin. Exp. Rheumatol.* 26, 295–304.

Lampropoulou-Adamidou, K., Dontas, I., Stathopoulos, I. P., Khaldi, L., Lelovas, P., Vlamis, J., et al. (2014). Chondroprotective effect of high-dose zoledronic acid: an experimental study in a rabbit model of osteoarthritis. *J. Orthop. Res.* 32, 1646–1651. doi: 10.1002/jor.22712

Laslett, L. L., Dore, D. A., Quinn, S. J., Boon, P., Ryan, E., Winzenberg, T. M., et al. (2012). Zoledronic acid reduces knee pain and bone marrow lesions over 1 year: a randomised controlled trial. *Ann. Rheum. Dis.* 71, 1322–1328. doi: 10.1136/annrheumdis-2011-200970

Lee, W. S., Kim, H. J., Kim, K. I., Kim, G. B., and Jin, W. (2019) Intra-articular injection of autologous adipose tissue-derived mesenchymal stem cells for the treatment of knee osteoarthritis: a phase IIb, randomized, placebo-controlled clinical trial. *Stem Cells Transl. Med.* 8, 504–511. doi: 10.1002/sctm.18-0122

Leydet-Quilici, H., Le Corroller, T., Bouvier, C., Giorgi, R., Argenson, J. N., Champsaur, P., et al. (2010). Advanced hip osteoarthritis: magnetic resonance imaging aspects and histopathology correlations. *Osteoarthr. Cartil.* 18, 1429–1435. doi: 10.1016/j.joca.2010.08.008

Li, B., and Aspden, R. M. (1997). Composition and mechanical properties of cancellous bone from the femoral head of patients with osteoporosis or osteoarthritis. *J. Bone Miner. Res.* 12, 641–651. doi: 10.1359/jbmr.1997.12.4.641

Li, G., Ma, Y., Cheng, T. S., Landao-Bassonga, E., Qin, A., Pavlos, N. J., et al. (2014). Identical subchondral bone microarchitecture pattern with increased bone resorption in rheumatoid arthritis as compared to osteoarthritis. *Osteoarthr. Cartil.* 22, 2083–2092. doi: 10.1016/j.joca.2014.08.015

Li, G., Yin, J., Gao, J., Cheng, T. S., Pavlos, N. J., Zhang, C., et al. (2013). Subchondral bone in osteoarthritis: insight into risk factors and microstructural changes. *Arthritis Res. Ther.* 15:223. doi: 10.1186/ar4405

Li, Y., Mu, W., Xu, B., Ren, J., Wahafu, T., Wuermanbieke, S., et al. (2019). Artesunate, an anti-malaria agent, attenuates experimental osteoarthritis by inhibiting bone resorption and CD31(hi)Emcn(hi) vessel formation in subchondral bone. *Front. Pharmacol.* 10:685. doi: 10.3389/fphar.2019.00685

Lin, C., Liu, L., Zeng, C., Cui, Z. K., Chen, Y., Lai, P., et al. (2019). Activation of mTORC1 in subchondral bone preosteoblasts promotes osteoarthritis by stimulating bone sclerosis and secretion of CXCL12. *Bone Res.* 7:5. doi: 10.1038/s41413-018-0041-8

Lindstrom, E., Rizoska, B., Tunblad, K., Edenius, C., Bendele, A. M., Maul, D., et al. (2018). The selective cathepsin K inhibitor MIV-711 attenuates joint pathology in experimental animal models of osteoarthritis. *J. Transl. Med.* 16:56. doi: 10.1186/s12967-018-1425-7

Liu, X. S., Sajda, P., Saha, P. K., Wehrli, F. W., Bevill, G., Keaveny, T. M., et al. (2008). Complete volumetric decomposition of individual trabecular plates and rods and its morphological correlations with anisotropic elastic moduli in human trabecular bone. *J. Bone Miner. Res.* 23, 223–235. doi: 10.1359/jbmr.071009

Lories, R. J., and Luyten, F. P. (2011). The bone-cartilage unit in osteoarthritis. *Nat. Rev. Rheumatol.* 7, 43–49. doi: 10.1038/nrrheum.2010.197

Lu, J., Zhang, H., Cai, D., Zeng, C., Lai, P., Shao, Y., et al. (2018). Positive-feedback regulation of subchondral H-type vessel formation by chondrocyte promotes osteoarthritis development in mice. *J. Bone Miner. Res.* 33, 909–920. doi: 10.1002/jbmr.3388

Lu, L., Dai, C., Zhang, Z., Du, H., Li, S., Ye, P., et al. (2019). Treatment of knee osteoarthritis with intra-articular injection of autologous adipose-derived mesenchymal progenitor cells: a prospective, randomized, double-blind, active-controlled, phase IIb clinical trial. *Stem Cell Res. Ther.* 10:143. doi: 10.1186/s13287-019-1248-3

Mapp, P. I., and Walsh, D. A. (2012). Mechanisms and targets of angiogenesis and nerve growth in osteoarthritis. *Nat. Rev. Rheumatol.* 8, 390–398. doi: 10.1038/nrrheum.2012.80

Massicotte, F., Lajeunesse, D., Benderdour, M., Pelletier, J. P., Hilal, G., Duval, N., et al. (2002). Can altered production of interleukin-1beta, interleukin-6, transforming growth factor-beta and prostaglandin E(2) by isolated human subchondral osteoblasts identify two subgroups of osteoarthritic patients. *Osteoarthr. Cartil.* 10, 491–500. doi: 10.1053/joca.2002.0528

Matas, J., Orrego, M., Amenabar, D., Infante, C., Tapia-Limonchi, R., Cadiz, M. I., et al. (2019). Umbilical cord-derived mesenchymal stromal cells (MSCs) for knee osteoarthritis: repeated MSC dosing is superior to a single MSC dose and to hyaluronic acid in a controlled randomized phase I/II trial. *Stem Cells Transl. Med.* 8, 215–224. doi: 10.1002/sctm.18-0053

Matsumoto, Y., Tanaka, K., Hirata, G., Hanada, M., Matsuda, S., Shuto, T., et al. (2002). Possible involvement of the vascular endothelial growth factor-Flt-1-focal adhesion kinase pathway in chemotaxis and the cell proliferation of osteoclast precursor cells in arthritic joints. *J. Immunol.* 168, 5824–5831. doi: 10.4049/jimmunol.168.11.5824

Mazur, C. M., Woo, J. J., Yee, C. S., Fields, A. J., Acevedo, C., Bailey, K. N., et al. (2019). Osteocyte dysfunction promotes osteoarthritis through MMP13-dependent suppression of subchondral bone homeostasis. *Bone Res.* 7:34. doi: 10.1038/s41413-019-0070-y

Mcclung, M. R., O'donoghue, M. L., Papapoulos, S. E., Bone, H., Langdahl, B., Saag, K. G., et al. (2019). Odanacatib for the treatment of postmenopausal osteoporosis: results of the LOFT multicentre, randomised, double-blind, placebo-controlled trial and LOFT Extension study. *Lancet Diabetes Endocrinol.* 7, 899–911. doi: 10.1016/S2213-8587(19)30346-8

McErlain, D. D., Ulici, V., Darling, M., Gati, J. S., Pitelka, V., Beier, F., et al. (2012). An *in vivo* investigation of the initiation and progression of subchondral cysts in a rodent model of secondary osteoarthritis. *Arthritis Res. Ther.* 14:R26. doi: 10.1186/ar3727

Mcgibbon, C. A., Brandon, S. C. E., Brookshaw, M., and Sexton, A. (2017). Effects of an over-ground exoskeleton on external knee moments during stance phase of gait in healthy adults. *Knee* 24, 977–993. doi: 10.1016/j.knee.2017.04.004

Mullard, A. (2016). Merck &Co. drops osteoporosis drug odanacatib. *Nat. Rev. Drug Discov.* 15:669. doi: 10.1038/nrd.2016.207

Muratovic, D., Cicuttini, F., Wluka, A., Findlay, D., Wang, Y., Otto, S., et al. (2016). Bone marrow lesions detected by specific combination of MRI sequences are associated with severity of osteochondral degeneration. *Arthritis Res. Ther.* 18, 1–11. doi: 10.1186/s13075-016-0953-x

Murray, I. R., Chahla, J., Safran, M. R., Krych, A. J., Saris, D. B. F., Caplan, A. I., et al. (2019). International expert consensus on a cell therapy communication tool: DOSES. *J. Bone Joint Surg. Am.* 101, 904–911. doi: 10.2106/JBJS.18.00915

Nagai, T., Sato, M., Kobayashi, M., Yokoyama, M., Tani, Y., and Mochida, J. (2014). Bevacizumab, an anti-vascular endothelial growth factor antibody, inhibits osteoarthritis. *Arthritis Res. Ther.* 16:427. doi: 10.1186/s13075-014-0427-y

Nakashima, T., Hayashi, M., Fukunaga, T., Kurata, K., Oh-Hora, M., Feng, J. Q., et al. (2011). Evidence for osteocyte regulation of bone homeostasis through RANKL expression. *Nat. Med.* 17, 1231–1234. doi: 10.1038/nm.2452

Nevitt, M. C., Cummings, S. R., Lane, N. E., Hochberg, M. C., Scott, J. C., Pressman, A. R., et al. (1996). Association of estrogen replacement therapy with the risk of osteoarthritis of the hip in elderly white women. Study of osteoporotic fractures research group. *Arch. Intern. Med.* 156, 2073–2080. doi: 10.1001/archinte.1996.00440170081009

Orth, P., Duffner, J., Zurakowski, D., Cucchiarini, M., and Madry, H. (2016). Small-diameter awls improve articular cartilage repair after microfracture treatment in a translational animal model. *Am. J. Sports Med.* 44, 209–219. doi: 10.1177/0363546515610507

Pan, J., Zhou, X., Li, W., Novotny, J. E., Doty, S. B., and Wang, L. (2009). *In situ* measurement of transport between subchondral bone and articular cartilage. *J. Orthop. Res.* 27, 1347–1352. doi: 10.1002/jor.20883

Park, Y. B., Ha, C. W., Lee, C. H., Yoon, Y. C., and Park, Y. G. (2017). Cartilage regeneration in osteoarthritic patients by a composite of allogeneic umbilical cord blood-derived mesenchymal stem cells and hyaluronate hydrogel: results from a clinical trial for safety and proof-of-concept with 7 years of extended follow-up. *Stem Cells Transl. Med.* 6, 613–621. doi: 10.5966/sctm.2016-0157

Peterson, L., Vasiliadis, H. S., Brittberg, M., and Lindahl, A. (2010). Autologous chondrocyte implantation: a long-term follow-up. *Am. J. Sports Med.* 38, 1117–1124. doi: 10.1177/0363546509357915

Pfeifer, C. G., Fisher, M. B., Saxena, V., Kim, M., Henning, E. A., Steinberg, D. A., et al. (2017). Age-dependent subchondral bone remodeling and cartilage repair in a minipig defect model. *Tissue Eng. Part C Methods* 23, 745–753. doi: 10.1089/ten.tec.2017.0109

Radin, E. L., Martin, R. B., Burr, D. B., Caterson, B., Boyd, R. D., and Goodwin, C. (1984). Effects of mechanical loading on the tissues of the rabbit knee. *J. Orthop. Res.* 2, 221–234. doi: 10.1002/jor.1100020303

Reginster, J. Y., Badurski, J., Bellamy, N., Bensen, W., Chapurlat, R., Chevalier, X., et al. (2013). Efficacy and safety of strontium ranelate in the treatment of knee osteoarthritis: results of a double-blind, randomised placebo-controlled trial. *Ann. Rheum. Dis.* 72, 179–186. doi: 10.1136/annrheumdis-2012-202231

Robling, A. G., and Bonewald, L. F. (2020). The osteocyte: new insights. *Annu. Rev. Physiol.* 82, 485–506. doi: 10.1146/annurev-physiol-021119-034332

Rogers, M. J., Crockett, J. C., Coxon, F. P., and Monkkonen, J. (2011). Biochemical and molecular mechanisms of action of bisphosphonates. *Bone* 49, 34–41. doi: 10.1016/j.bone.2010.11.008

Rosa, R. G., Collavino, K., Lakhani, A., Delve, E., Weber, J. F., Rosenthal, A. K., et al. (2014). Clodronate exerts an anabolic effect on articular chondrocytes mediated through the purinergic receptor pathway. *Osteoarthr. Cartil.* 22, 1327–1336. doi: 10.1016/j.joca.2014.07.009

Sampson, E. R., Hilton, M. J., Tian, Y., Chen, D., Schwarz, E. M., Mooney, R. A., et al. (2011). Teriparatide as a chondroregenerative therapy for injury-induced osteoarthritis. *Sci. Transl. Med.* 3:101ra193. doi: 10.1126/scitranslmed.3002214

Sanchez, C., Deberg, M. A., Bellahcene, A., Castronovo, V., Msika, P., Delcour, J. P., et al. (2008). Phenotypic characterization of osteoblasts from the sclerotic zones of osteoarthritic subchondral bone. *Arthritis Rheum.* 58, 442–455. doi: 10.1002/art.23159

Sanchez, C., Mazzucchelli, G., Lambert, C., Comblain, F., Depauw, E., and Henrotin, Y. (2018). Comparison of secretome from osteoblasts derived from sclerotic versus non-sclerotic subchondral bone in OA: a pilot study. *PLoS ONE* 13:e0194591. doi: 10.1371/journal.pone.0194591

Schett, G., Hayer, S., Zwerina, J., Redlich, K., and Smolen, J. S. (2005). Mechanisms of disease: the link between RANKL and arthritic bone disease. *Nat. Clin. Pract. Rheumatol.* 1, 47–54. doi: 10.1038/ncprheum0036

Sekiya, I., Muneta, T., Horie, M., and Koga, H. (2015). Arthroscopic Transplantation of synovial stem cells improves clinical outcomes in knees with cartilage defects. *Clin. Orthop. Relat. Res.* 473, 2316–2326. doi: 10.1007/s11999-015-4324-8

Shapiro, S. A., Kazmerchak, S. E., Heckman, M. G., Zubair, A. C., and O'Connor, M. I. (2017). A prospective, single-blind, placebo-controlled trial of bone marrow aspirate concentrate for knee osteoarthritis. *Am. J. Sports Med.* 45, 82–90. doi: 10.1177/0363546516662455

Shimomura, K., Yasui, Y., Koizumi, K., Chijimatsu, R., Hart, DA., Yonetani, Y., et al. (2018). First-in-human pilot study of implantation of a scaffold-free tissue-engineered construct generated from autologous synovial mesenchymal stem cells for repair of knee chondral lesions. *Am. J. Sports Med.* 46, 2384–2393. doi: 10.1177/0363546518781825

Sims, N. A., and Martin, T. J. (2020). Osteoclasts provide coupling signals to osteoblast lineage cells through multiple mechanisms. *Annu. Rev. Physiol.* 82, 507–529. doi: 10.1146/annurev-physiol-021119-034425

Sims, N. A., Martin, T. J., and Quinn, J. M. W. (2015). "Coupling: the influences of immune and bone cells," in *Osteoimmunology: Interactions of the Immune and Skeletal Systems,* eds. J. Lorenzo, M. C. Horowitz, Y. Choi, H. Takayanagi, and G. Schett. 2 ed. (London: Academic Press), 169–185.

Soki, F. N., Yoshida, R., Paglia, D. N., Duong, L. T., Hansen, M. F., and Drissi, H. (2018). Articular cartilage protection in Ctsk(-/-) mice is associated with cellular and molecular changes in subchondral bone and cartilage matrix. *J. Cell. Physiol.* 233, 8666–8676. doi: 10.1002/jcp.26745

Song, Y., Du, H., Dai, C., Zhang, L., Li, S., Hunter, D. J., et al. (2018). Human adipose-derived mesenchymal stem cells for osteoarthritis: a pilot study with long-term follow-up and repeated injections. *Regen. Med.* 13, 295–307. doi: 10.2217/rme-2017-0152

Su, W., Liu, G., Liu, X., Zhou, Y., Sun, Q., Zhen, G., et al. (2020). Angiogenesis stimulated by elevated PDGF-BB in subchondral bone contributes to osteoarthritis development. *JCI Insight* 5:135446. doi: 10.1172/jci.insight.135446

Sun, H., Wu, Y., Pan, Z., Yu, D., Chen, P., Zhang, X., et al. (2018). Gefitinib for epidermal growth factor receptor activated osteoarthritis subpopulation treatment. *EBioMedicine* 32, 223–233. doi: 10.1016/j.ebiom.2018.06.002

Suri, S., Gill, S. E., Massena De Camin, S., Wilson, D., Mcwilliams, D. F., and Walsh, D. A. (2007). Neurovascular invasion at the osteochondral junction and in osteophytes in osteoarthritis. *Ann. Rheum. Dis.* 66, 1423–1428. doi: 10.1136/ard.2006.063354

Taljanovic, M. S., Graham, A. R., Benjamin, J. B., Gmitro, A. F., Krupinski, E. A., Schwartz, S. A., et al. (2008). Bone marrow edema pattern in advanced hip osteoarthritis: quantitative assessment with magnetic resonance imaging and correlation with clinical examination, radiographic findings, and histopathology. *Skeletal Radiol.* 37, 423–431. doi: 10.1007/s00256-008-0446-3

Tanamas, S. K., Wluka, A. E., Pelletier, J. P., Pelletier, J. M., Abram, F., Berry, P. A., et al. (2010). Bone marrow lesions in people with knee osteoarthritis predict progression of disease and joint replacement: a longitudinal study. *Rheumatology* 49, 2413–2419. doi: 10.1093/rheumatology/keq286

Tat, S. K., Pelletier, J. P., Mineau, F., Caron, J., and Martel-Pelletier, J. (2011). Strontium ranelate inhibits key factors affecting bone remodeling in human osteoarthritic subchondral bone osteoblasts. *Bone* 49, 559–567. doi: 10.1016/j.bone.2011.06.005

Tatsumi, S., Ishii, K., Amizuka, N., Li, M., Kobayashi, T., Kohno, K., et al. (2007). Targeted ablation of osteocytes induces osteoporosis with defective mechanotransduction. *Cell. Metab.* 5, 464–475. doi: 10.1016/j.cmet.2007.05.001

Teichtahl, A. J., Wluka, A. E., Wijethilake, P., Wang, Y., Ghasem-Zadeh, A., and Cicuttini, F. M. (2015). Wolff's law in action: a mechanism for early knee osteoarthritis. *Arthritis Res. Ther.* 17:207. doi: 10.1186/s13075-015-0738-7

Teitelbaum, S. L. (2000). Bone resorption by osteoclasts. *Science* 289, 1504–1508. doi: 10.1126/science.289.5484.1504

Tran Van, P., Vignery, A., and Baron, R. (1982). An electron-microscopic study of the bone-remodeling sequence in the rat. *Cell Tissue Res.* 225, 283–292. doi: 10.1007/BF00214682

Tu, M., Yang, M., Yu, N., Zhen, G., Wan, M., Liu, W., et al. (2019). Inhibition of cyclooxygenase-2 activity in subchondral bone modifies a subtype of osteoarthritis. *Bone Res.* 7:29. doi: 10.1038/s41413-019-0071-x

Vaysbrot, E. E., Osani, M. C., Musetti, M. C., Mcalindon, T. E., and Bannuru, R. R. (2018). Are bisphosphonates efficacious in knee osteoarthritis? A meta-analysis of randomized controlled trials. *Osteoarthr. Cartil.* 26, 154–164. doi: 10.1016/j.joca.2017.11.013

Wakitani, S., Imoto, K., Yamamoto, T., Saito, M., Murata, N., and Yoneda, M. (2002). Human autologous culture expanded bone marrow mesenchymal cell transplantation for repair of cartilage defects in osteoarthritic knees. *Osteoarthr. Cartil.* 10, 199–206. doi: 10.1053/joca.2001.0504

Wakitani, S., Nawata, M., Tensho, K., Okabe, T., Machida, H., and Ohgushi, H. (2007). Repair of articular cartilage defects in the patello-femoral joint with autologous bone marrow mesenchymal cell transplantation: three case reports involving nine defects in five knees. *J. Tissue Eng. Regen. Med.* 1, 74–79. doi: 10.1002/term.8

Wang, L., You, X., Lotinun, S., Zhang, L., Wu, N., and Zou, W. (2020). Mechanical sensing protein PIEZO1 regulates bone homeostasis via osteoblast-osteoclast crosstalk. *Nat. Commun.* 11:282. doi: 10.1038/s41467-019-14146-6

Wang, T., Wen, C. Y., Yan, C. H., Lu, W. W., and Chiu, K. Y. (2013). Spatial and temporal changes of subchondral bone proceed to microscopic articular cartilage degeneration in guinea pigs with spontaneous osteoarthritis. *Osteoarthr. Cartil.* 21, 574–581. doi: 10.1016/j.joca.2013.01.002

Wen, Z. H., Tang, C. C., Chang, Y. C., Huang, S. Y., Lin, Y. Y., Hsieh, S. P., et al. (2016). Calcitonin attenuates cartilage degeneration and nociception in an experimental rat model of osteoarthritis: role of TGF-beta in chondrocytes. *Sci. Rep.* 6:28862. doi: 10.1038/srep28862

Wilson, A. J., Murphy, W. A., Hardy, D. C., and Totty, W. G. (1988). Transient osteoporosis: transient bone marrow edema? *Radiology* 167, 757–760. doi: 10.1148/radiology.167.3.3363136

Wu, H., Xu, T., Chen, Z., Wang, Y., Li, K., Chen, P. S., et al. (2020). Specific inhibition of FAK signaling attenuates subchondral bone deterioration and articular cartilage degeneration during osteoarthritis pathogenesis. *J. Cell. Physiol.* 235, 8653–8666. doi: 10.1002/jcp.29709

Xian, L., Wu, X., Pang, L., Lou, M., Rosen, C. J., Qiu, T., et al. (2012). Matrix IGF-1 maintains bone mass by activation of mTOR in mesenchymal stem cells. *Nat. Med.* 18, 1095–1101. doi: 10.1038/nm.2793

Xie, H., Cui, Z., Wang, L., Xia, Z., Hu, Y., Xian, L., et al. (2014). PDGF-BB secreted by preosteoclasts induces angiogenesis during coupling with osteogenesis. *Nat. Med.* 20, 1270–1278. doi: 10.1038/nm.3668

Xiong, J., Onal, M., Jilka, R. L., Weinstein, R. S., Manolagas, S. C., and O'brien, C. A. (2011). Matrix-embedded cells control osteoclast formation. *Nat. Med.* 17, 1235–1241. doi: 10.1038/nm.2448

Yang, P. Y., Tang, C. C., Chang, Y. C., Huang, S. Y., Hsieh, S. P., Fan, S. S., et al. (2014). Effects of tibolone on osteoarthritis in ovariectomized rats: association with nociceptive pain behaviour. *Eur. J. Pain* 18, 680–690. doi: 10.1002/j.1532-2149.2013.00406.x

Zhang, X., Cai, D., Zhou, F., Yu, J., Wu, X., Yu, D., et al. (2020). Targeting downstream subcellular YAP activity as a function of matrix stiffness with Verteporfin-encapsulated chitosan microsphere attenuates osteoarthritis. *Biomaterials* 232:119724. doi: 10.1016/j.biomaterials.2019.119724

Zhao, K., Lin, J., Wu, B., Sun, G., An, C., Paul, M. E., et al. (2018). Diagnosis of osteoarthritis subtypes with blood biomarkers. *bioRxiv [Preprint]*. doi: 10.1101/366047

Zhen, G., Wen, C., Jia, X., Li, Y., Crane, J. L., Mears, S. C., et al. (2013). Inhibition of TGF-beta signaling in mesenchymal stem cells of subchondral bone attenuates osteoarthritis. *Nat. Med.* 19, 704–712. doi: 10.1038/nm.3143

Zhou, T., Gao, B., Fan, Y., Liu, Y., Feng, S., Cong, Q., et al. (2020). Piezo1/2 mediate mechanotransduction essential for bone formation through concerted activation of NFAT-YAP1-ss-catenin. *Elife* 9:e52779. doi: 10.7554/eLife.52779.sa2

Zhu, J., Zhen, G., An, S., Wang, X., Wan, M., Li, Y., et al. (2020). Aberrant subchondral osteoblastic metabolism modifies NaV1.8 for osteoarthritis. *Elife* 9:e57656. doi: 10.7554/eLife.57656

Zhu, S., Chen, K., Lan, Y., Zhang, N., Jiang, R., and Hu, J. (2013). Alendronate protects against articular cartilage erosion by inhibiting subchondral bone loss in ovariectomized rats. *Bone* 53, 340–349. doi: 10.1016/j.bone.2012.12.044

Zhu, S., Zhu, J., Zhen, G., Hu, Y., An, S., Li, Y., et al. (2019). Subchondral bone osteoclasts induce sensory innervation and osteoarthritis pain. *J. Clin. Invest.* 129, 1076–1093. doi: 10.1172/JCI121561

Conflict of Interest: The authors declare that the research was conducted in the absence of any commercial or financial relationships that could be construed as a potential conflict of interest.

Copyright © 2021 Zhu, Chan, Yung, Tuan and Jiang. This is an open-access article distributed under the terms of the Creative Commons Attribution License (CC BY). The use, distribution or reproduction in other forums is permitted, provided the original author(s) and the copyright owner(s) are credited and that the original publication in this journal is cited, in accordance with accepted academic practice. No use, distribution or reproduction is permitted which does not comply with these terms.

frontiers in Cell and Developmental Biology

REVIEW
published: 21 January 2021
doi: 10.3389/fcell.2020.627893

Regulatory Role of the RNA N^6-Methyladenosine Modification in Immunoregulatory Cells and Immune-Related Bone Homeostasis Associated With Rheumatoid Arthritis

Danping Fan[1,2†], *Ya Xia*[3†], *Cheng Lu*[4†], *Qinbin Ye*[3], *Xiaoyu Xi*[3], *Qiong Wang*[5], *Zheng Wang*[6], *Chengyuan Wang*[7*] and *Cheng Xiao*[1,2,8*]

[1] Institute of Clinical Medicine, China-Japan Friendship Hospital, Beijing, China, [2] Graduate School of Peking Union Medical College, Chinese Academy of Medical Sciences/Peking Union Medical College, Beijing, China, [3] School of Traditional Chinese Medicine, Beijing University of Chinese Medicine, Beijing, China, [4] Institute of Basic Research in Clinical Medicine, China Academy of Chinese Medical Sciences, Beijing, China, [5] Clinical Medical School (China-Japan Friendship Hospital), Beijing University of Chinese Medicine, Beijing, China, [6] Laboratory for Bone and Joint Diseases, RIKEN Center for Integrative Medical Sciences, Tokyo, Japan, [7] Department of Plastic Surgery, China-Japan Friendship Hospital, Beijing, China, [8] Department of Emergency, China-Japan Friendship Hospital, Beijing, China

Rheumatoid arthritis (RA) is a systemic autoimmune disease for which the etiology has not been fully elucidated. Previous studies have shown that the development of RA has genetic and epigenetic components. As one of the most highly abundant RNA modifications, the N^6-methyladenosine (m^{6}A) modification is necessary for the biogenesis and functioning of RNA, and modification aberrancies are associated with various diseases. However, the specific functions of m^{6}A in the cellular processes of RA remain unclear. Recent studies have revealed the relationship between m^{6}A modification and immune cells associated with RA. Therefore, in this review, we focused on discussing the functions of m^{6}A modification in the regulation of immune cells and immune-related bone homeostasis associated with RA. In addition, to gain a better understanding of the progress in this field of study and provide the proper direction and suggestions for further study, clinical application studies of m^{6}A modification were also summarized.

Keywords: RNA N^6-methyladenosine, immunoregulatory cells, bone homeostasis, rheumatoid arthritis, epigenetics

OPEN ACCESS

Edited by:
Changjun Li,
Central South University, China

Reviewed by:
Huabing Li,
Shanghai Jiao Tong University School of Medicine, China
Wen Zhou,
Harvard Medical School, United States

***Correspondence:**
Chengyuan Wang
zryhyyent@126.com
Cheng Xiao
xc2002812@126.com

[†]These authors have contributed equally to this work

Specialty section:
This article was submitted to Molecular Medicine, a section of the journal Frontiers in Cell and Developmental Biology

Received: *10 November 2020*
Accepted: *22 December 2020*
Published: *21 January 2021*

Citation:
Fan D, Xia Y, Lu C, Ye Q, Xi X, Wang Q, Wang Z, Wang C and Xiao C (2021) Regulatory Role of the RNA N^6-Methyladenosine Modification in Immunoregulatory Cells and Immune-Related Bone Homeostasis Associated With Rheumatoid Arthritis. Front. Cell Dev. Biol. 8:627893. doi: 10.3389/fcell.2020.627893

INTRODUCTION

Rheumatoid arthritis (RA) is a systemic autoimmune disease characterized by inflammatory changes in the joints synovial tissue, bone and cartilage of joints, with changes in extra-articular sites occurring less frequently (Scherer et al., 2020), substantially burdening both individuals and society (Cross et al., 2014). The etiology of RA has not been fully elucidated, but is thought to be associated with autoimmunity, infection, and provoking environmental factors. Recently, it has become evident that RA can occur due to genetic and epigenetic components. Previous genealogical studies and modern molecular-genetic investigations have also confirmed the involvement of genetic factors in the development of RA (Sparks and Costenbader, 2014). However, genetic heterogeneity does not appear to explain all the features of RA. Thus, investigations of epigenetic

factors and mechanisms correlated with RA progression and response to treatment are increasingly significant (Glant et al., 2014; McGee and Hargreaves, 2019).

Epigenetics is the study of heritable changes in gene expression that do not involve alterations in the DNA/RNA sequence, including DNA methylation, histone, and RNA modifications (Arguello et al., 2019; McGee and Hargreaves, 2019). First reported in the 1970s, the reversible methylation of N^6-methyladenosine (m^{6}A) is the most prevalent internal messenger RNA (mRNA) modification in eukaryotes including mammals, plants, *Drosophila* and yeast, as well as in viruses with a nuclear phase (Fu et al., 2014). This modification is installed by N^6-adenosine methyltransferase. A 70 kD S-adenosyl-L-methionine (SAM)-binding subunit, also called MT-A70 (METTL3), was identified as one component of the m^{6}A methyltransferase complexes in mammalian cells. Recent studies have characterized this complex, which comprises METTL3, METTL14 and Wilms tumor 1 associated protein (WTAP). METTL14 and METTL3 are two active methyltransferases that form a heterodimer to catalyze m^{6}A RNA methylation, while WTAP interacts with this complex and substantially affects mRNA methylation inside cells but not *in vitro*. Knockdowns of these methyltransferases affect mouse embryonic stem cell differentiation (Fu et al., 2014). Since 2011, two m^{6}A RNA demethylases of fat mass and obesity-associated (FTO) protein and AlkB homolog 5 (ALKBH5) have been discovered that are involved in mammalian development, RNA metabolism and fertility (Jia et al., 2011; Fu et al., 2014). These findings reveal the first examples that RNA modification is reversible and indicate their regulatory effects on mRNA and specific non-coding RNAs that contain m^{6}A (Coker et al., 2019). Subsequent profiling of m^{6}A distributions in mammalian transcriptomes and the recent mapping of the yeast m^{6}A methylome in the meiotic state further confirm the dynamic nature of m^{6}A modification (Cao et al., 2016). In addition, various studies have shown that m^{6}A is preferentially centered around stop codon and at 3′untranslated regions (3′UTRs), as well as in long internal exons and at transcription start sites (TSSs). RNA-binding proteins has been shown to be affected by m^{6}A, such as heterogeneous nuclear ribonucleoprotein G (HNRNPG). HNRNPG is a new m^{6}A reader protein that can recognize a motif exposed by m^{6}A modification through a low-complexity region (Liu et al., 2017). Furthermore, the protein human YTH domain family 2 (YTHDF2) was recently demonstrated to specifically recognize m^{6}A-methylated mRNA and accelerate the decay of the bound mRNA (Chen et al., 2018). The results of these studies indicate that chemical modifications of m^{6}A are common and important in a variety of biological processes.

Recent studies have demonstrated m^{6}A modification is necessary for the biogenesis and functions of RNA, and modification aberrancies have been associated with various pathological process, such as obesity, systemic lupus erythematosus, and carcinogenesis (Wang et al., 2017; Wei et al., 2017; Li L. et al., 2018). In addition, m^{6}A modification has been recognized as crucial regulator in the immune response and in immune cells. Thus, selectively altered m^{6}A levels along with other types of immunotherapies may be effective management strategies in various of immunological diseases, such as RA. In this review, we focus on discussing the functions of m^{6}A modification in regulating the innate and adaptive immune response, especially in immune cells and immune-related bone homeostasis associated with RA. In addition, we also summarize clinical application studies of m^{6}A modification to gain a better understanding of the progress in this area and provide proper direction and suggestions for its further study.

m^{6}A WRITERS, ERASERS, AND READERS

As mentioned above, m^{6}A modification is one of the most highly abundant RNA modifications and is involved in the etiology of various immune diseases, such as systemic lupus erythematosus and RA (Wei et al., 2017; Li L. et al., 2018). The results of numerous studies have revealed that m^{6}A modification commonly occurs at the consensus motif RRACH (R = A or G; H = A, C or U) (Roundtree and He, 2016). Furthermore, m^{6}A modification can interfere with RNA processing, splicing, export, degradation, and translation through the methyltransferase (m^{6}A writers), demethylase enzymes (m^{6}A erasers), and readers proteins (Chen et al., 2019). The potential molecular functions of m^{6}A RNA modification are presented in **Figure 1**.

m^{6}A Writers

m^{6}A mRNA methylation is catalyzed by a multisubunit writer complex' comprising a METTL3-METTL14 heterodimer and many additional adaptor proteins (Shulman and Stern-Ginossar, 2020). METTL3 was earlier identified as a SAM-binding component of "writer complex" and exhibited catalytic function by itself (Bokar et al., 1997). METTL3 knockdown can reduce m^{6}A peaks and promote the apoptosis of HeLa and HepG2 cells (Dominissini et al., 2012; Liu et al., 2014). METTL3 located in nucleus and cytoplasm were observed, which is consistent with early findings showing that cytosolic extracts also possessed methyltransferase activity (Harper et al., 1990). As an allosteric activator, METTL14 forms a stable hetero complex with METTL3 and binds to the target RNA. Liu et al. showed that METTL14 knockdown decreased m^{6}A levels in HeLa and 293FT cells (Liu et al., 2014). The other known writer complex also includes the WTAP, ZC3H13, RBM15 or RBM15B, and VIRMA subunits. WTAP is a splicing factor that can binds to the METTL3-METTL14 heterodimer and regulates the deposition of m^{6}A inside cells (Liu et al., 2014). ZC3H13 maintains the nuclear localization of the complex, and RBM15/15B and VIRMA are regarded as providing additional specificity (Patil et al., 2016; Knuckles et al., 2018; Yue et al., 2018).

Except for the canonical writer complex, several other enzymes have been shown to act as methyltransferases of m^{6}A, such as METTL16, MAT2A, ZCCHC4, METTL15 and PCIF1 (Pendleton et al., 2017; Akichika et al., 2019; Boulias et al., 2019; Ma et al., 2019; Sun et al., 2019; van Tran et al., 2019). Because the m^{6}A modified positions generated by these enzymes have not been shown to be associated with immunity, this review focuses on the canonical writer complex of m^{6}A mRNA modification.

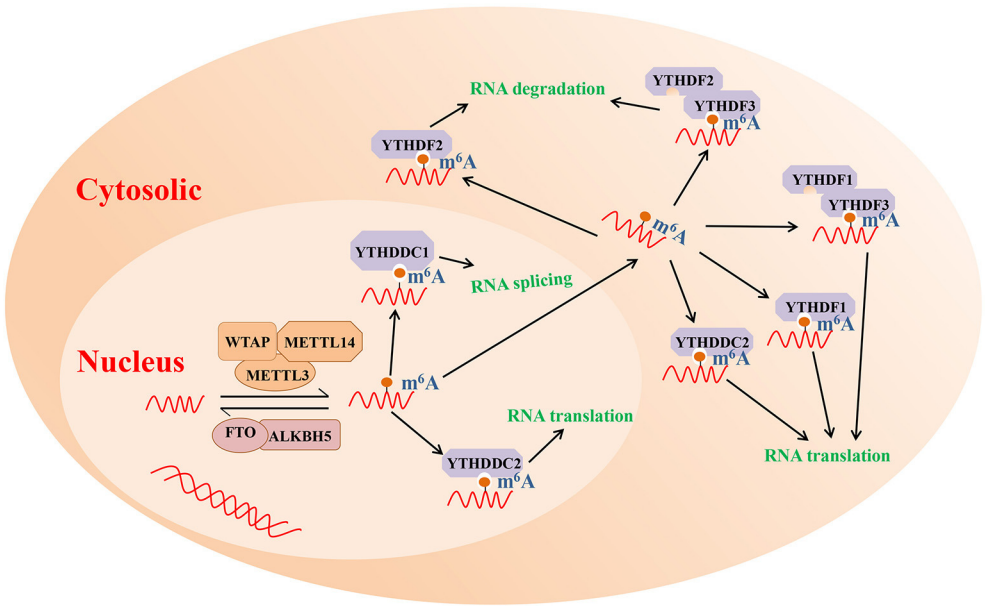


FIGURE 1 | The potential molecular functions of m^{6}A RNA modification. m^{6}A modification is a reversible process mediated by its regulatory proteins, including the writers (MELTT3, METTL14, WTAP, etc.), erasers (FTO, ALKBH5, etc.), and readers (YTHDF1, YTHDF2, YTHDF3, etc.). ALKBH5, Alk B homolog 5; FTO, fat mass and obesity-associated protein; m^{6}A, N^6-methyladenosine; METTL3, methyltransferase like 3; METTL14, methyltransferase like 14; WTAP, Wilms tumor 1 associated protein; YTHDF1, YTH domain family 1; YTHDF2, YTH domain family 2; YTHDF3, YTH domain family 3.

m^{6}A Erasers

Two enzymes, FTO and ALKBH5, have been suggested to remove m^{6}A from mRNA, indicating that m^{6}A is a dynamically reversible modification of RNA. As the first identified RNA demethylase, FTO was discovered in 2011 and was important in reigniting investigations of m^{6}A (Jia et al., 2011). FTO is a member of the non-heme Fe^{II}/α-KG-dependent dioxygenase AlkB family of proteins, which also includes ABH1 to ABH8 (Kurowski et al., 2003; Gerken et al., 2007), and previous research revealed that FTO probably demethylates both m^{6}A and terminal m^{6}Am (Mauer et al., 2017; Wei et al., 2018). ALKBH5 was the second demethylase identified and specifically demethylates m^{6}A (Zheng et al., 2013). Although m^{6}A erasers allow for the dynamic and signal-dependent regulation of m^{6}A levels, various studies have demonstrated that FTO and ALKBH5 has different intracellular localization patterns and tissue specificity. FTO is highly expressed in cerebral and adipose tissue, while ALKBH5 is highly abundant in the testes (Zheng et al., 2013). Thus, demethylation that occurs in some tissues may be regulated only by FTO or ALKBH5, indicating that the potential effects of RNA demethylation in more physiological contexts need to be further studied.

m^{6}A Readers

The m^{6}A methylation or demethylation modification of target RNA occurs under the action of "writers" and "erasers," respectively, altering the secondary or tertiary structure of RNA. The m^{6}A-binding protein referred to as an m^{6}A "reader" recognizes and preferentially binds to the m^{6}A-modified RNA. For m^{6}A modifications to exerts biological function, RNAs with m^{6}A modifications need to be recognized by different "readers" to exert different downstream effects.

Members of the YT521-b homology (YTH) family are the primary "readers" that identified to date. In mammals, YTH domain-containing proteins that bind to m^{6}A-modified RNAs are divided into five classes as follows. YTHDF1 interacts with initiation factors and promotes the binding of target RNAs to ribosomes, enhancing mRNA translation and protein synthesis (Zhuang et al., 2019). YTHDF2 selectively binds m^{6}A-modified mRNA and then recruits it to the mRNA attenuation site to induce the degradation of transcription products. For example, (Du et al., 2016; Park et al., 2019), YTHDF2 triggers the adenylation and decay of m^{6}A-modified mRNA by binding to the SH domain of the CNOT1 subunit in its N-terminal region, promoting its recruitment to the adenylase complex. Alternatively, YTHDF2 forms a complex with HRSP12 and RNaseP/MRP to mediate the cleavage of the m^{6}A-modified RNA in the nucleus. Interestingly, YTHDF3 has been reported to have bidirectional activity, enhancing RNA translation when interacting with YTHDF1, while binding to YTHDF2 can promote RNA degradation (Shi et al., 2017). These three YTHDF family member proteins are primarily localized to the cytosol and have paralogs that are highly similar. YTHDC1 facilitates mRNA splicing (Xiao et al., 2016) and mRNA production in the nucleus (Roundtree et al., 2017). YTHDC2, which exhibits both cytosolic and nuclear expression, can promote the translation efficiency of target RNA (Mao et al., 2019). In addition to YTH readers, several other binding proteins have shown to bind to m^{6}A-modified

RNA, such as IGF2BPs, HNRNPA2B1, and EIF3 (Alarcón et al., 2015; Meyer et al., 2015; Huang et al., 2018).

m^{6}A DETECTION METHODS

At present, numerous technologies involved in quantifying m^{6}A levels and m^{6}A modified transcripts have been developed to understand the phenotypes caused by the deletion of proteins associated with m^{6}A modification and how m^{6}A-modified transcripts are affected at the molecular level. According to their detection performance, these technologies can be classified as semiquantitative, quantitative, and localization-detecting methods (Chen et al., 2019).

Semiquantitative detection methods include dot blotting, immuno-Northern blotting and assay exploiting the methylation-specific sensitivity of MazF RNA endonucleases, which are applied to detect the presence of m^{6}A modification. Dot blots are used to measure the global change in m^{6}A levels using antibodies that specifically bind to the m^{6}A site. Although this method has the advantages of being simple and fast, when m^{6}A RNA fragments are small, its sensitivity is low (Zhu et al., 2019). Immuno-northern blotting is used for various types of RNA as it does not require RNA fragmentation prior to analysis. Thus, immuno-northern blotting is another technique used for the semi-quantitative detection of m^{6}A modifications. This method is characterized by its high specificity, sensitivity, and quantitative capability (Mishima et al., 2015). MAZTER-seq takes advantage of the ability of the MazF RNase to cleave RNA at unmethylated ACA motifs but not at their methylated counterparts. This method was the first to provide systematic quantitative profiling of m^{6}A at single-nucleotide resolution, but it only detects approximately 16–25% of mammalian m^{6}A-modified sites due to its specificity (Garcia-Campos et al., 2019; Zhang Z. et al., 2019).

Unlike semi-quantitative methods, quantitative detection strategies include the electrochemical immunosensor method, photo-crosslink-based quantitative proteomics, and support vector machine-based method, which can be used to determine the levels of m^{6}A RNA. In the electrochemical immunosensor approach, an anti-m^{6}A antibody is used to recognize and capture the m^{6}A-5′-triphosphate. Subsequently, silver nanoparticles and amine-PEG3-biotin functionalized SiO_2 nanospheres (Ag@SiO_2) are used to amplify the signal, after which phos-tag-biotin has the crucial function of connecting m^{6}ATP and Ag@SiO_2. This method is inexpensive, simple, and highly specific and sensitive (Yin et al., 2017). Photo-crosslinkers are widely used to stabilize protein-RNA interactions and can be combined with quantitative proteomics to measure m^{6}A RNA levels. In addition, diazirine-containing RNA probes have also been synthesized and used to improve the efficiency of photo-crosslinkers (Arguello et al., 2017). The support vector machine-based method is a computational method proposed by Chen et al. to predict m^{6}A sites within RNA strands using high-throughput sequencing data, a method is suitable for identifying m^{6}A sites in plants (Chen et al., 2016).

At present, researchers have developed several methods to detect the specific locations of m^{6}A sites within RNA. In combination with RNA immunoprecipitation (IP) whole-transcriptome sequencing, m^{6}A levels and isoform-characterization sequencing (m^{6}A-LAIC-seq) was invented by Molinie et al. to quantify m^{6}A contents. However, although this method can be used to detect the m^{6}A levels in each gene, it cannot analyze the methylation of a single modified nucleotide (Molinie et al., 2016). The use of m^{6}A-seq provided the first global view of m^{6}A-modified transcripts through transcriptome-wide sequencing and comparing m^{6}A-antibody enriched regions to the input. This method has been widely used, promoting the identification of modified transcripts and demonstrating that m^{6}A is a dynamically reversible modification enriched near stop codons and in 3′-UTRs (Dominissini et al., 2012; Meyer et al., 2012). However, the m^{6}A-seq method can only localize m^{6}A sites in RNA in 100–200 nt long regions and lacks single-base-resolution because of non-specific antibody binding. m^{6}A-CLIP/IP and miCLIP are additional ultraviolet crosslinking strategies that can be used to determine the m^{6}A site at a nucleotide-specific level and provide single-base resolution (Ke et al., 2015; Linder et al., 2015; Grozhik et al., 2017). In addition to the aforementioned methods, HRM analysis is another simple technique that can be used for m^{6}A specific site detection as well as to screen knockout/knockdown strain libraries to identify genes contributing to the formation of a specific m^{6}A nucleoside (Zhu et al., 2019).

m^{6}A MODIFICATION IN CELLS INVOLVED IN RA

As an autoimmune disease, RA is characterized by the infiltration of multiple type of immune cells and their secreted inflammatory mediators in synovial tissue (Feldmann et al., 1996). Both innate and adaptive immune cells are involved in the pathogenesis of RA. Many studies have shown that macrophages cannot only engulf and kill pathogenic microorganisms but also secrete a variety of inflammatory factors to participate in the pathogenic process of RA. Furthermore, during the pathogenesis of RA, a variety of factors disrupt the equilibrium of M1/M2 macrophages, resulting in a skew toward M1-pro-inflammatory macrophages (Fukui et al., 2017; Sun et al., 2017; Siouti and Andreakos, 2019). In addition, a large number of dendritic cells (DCs) migrate to synovial tissues and fluids and highly express MHC and co-stimulators in patients with RA (Thomas et al., 1994). Macrophages and DCs act as specialized antigen presenting cells (APCs) to stimulate the T cell response (Mulherin et al., 1996; Leung et al., 2002; Merad et al., 2013). In RA patients, abnormal T cell activation is involved in the onset of RA and greatly contributes to joint destruction. Thus, the homeostasis of immune cells is crucial to maintaining health. Moreover, in the pathological condition of RA, bone homeostasis, involving bone formation mediated by osteoblasts and bone resorption regulated by osteoclasts, is disrupted. Due to the important role of m^{6}A modifications in immune regulation, below we have summarized the dramatical effects of m^{6}A

TABLE 1 | m^{6}A modification in PBMCs of RA patients.

m^{6}A component	Regulation	Samples and conditions	References
ALKBH5, FTO, YTHDF2	Down regulation	79 RA patients and 61 healthy controls	Luo et al., 2020
METTL3	Up regulation	47 RA patients and 30 healthy controls	(Wang J. et al., 2019)

AKBH5, Alk B homolog 5; FTO, fat mass and obesity-associated protein; METTL3, methyltransferase-like 3; RA, rheumatoid arthritis; YTHDF2, YTH domain family 2.

modifications in different immunoregulatory cells and on bone homeostasis associated with RA.

m^{6}A Modification in Peripheral Blood Mononuclear Cells (PBMCs)

Accumulating evidence have shown that immune system dysfunctions, such as the abnormal activation of T cells, B lymphocytes, mast cells, neutrophils and macrophages contributes to promoting the onset of RA and is involved in the mechanisms of RA (Cascão et al., 2010; Klareskog et al., 2013). **Table 1** lists a number of studies describing m^{6}A modifications in PBMCs associated with RA that involved m^{6}A writers, erasers and readers. Luo et al. assessed ALKBH5, FTO and YTHDF2 mRNA expression in PBMCs from RA patients using quantitative real-time polymerase chain reaction, with the global m^{6}A content measured using an m^{6}A RNA methylation quantification kit. The results showed that the mRNA expression of ALKBH5, FTO and YTHDF2 was lower in PBMCs from RA patients than in controls. After standard treatment, ALKBH5 mRNA levels were increased in RA patients. In addition, FTO expression is associated with some common markers for RA disease activity, including disease activity score 28 (DAS28), immunoglobulin G (IgG), complement 3 (C3), and the lymphocyte-to-monocyte ratio (LMR). YTHDF2 mRNA expression was shown to be correlated with L%, N%, RBC, NLR, and LMR. Moreover, logistic regression analysis suggested that reduced ALKBH5, FTO, and YTHDF2 expression in PBMCs is a risk factor for RA (Luo et al., 2020). Another study revealed that METTL3 expression is significantly increased in the PBMCs of RA patients (Wang J. et al., 2019). As a long-term autoimmune disease of unknown etiology, it is crucial to identify a biomarker signature that can predict joint damage at an early stage, which will support more informed clinical decisions on the most appropriate treatment strategies for individual patients. Although the exact mechanisms by which m^{6}A modifications in PBMCs affect RA have not been fully elucidated, the results of the above studies suggested that the "writers," "erasers" and "readers" of m^{6}A modifications may serve as biomarkers for the diagnosis of RA.

m^{6}A-Mediated Regulation of Macrophage Activation and Polarization

Macrophages are a subset of mononuclear phagocytic cells. During the RA progression, macrophages play distinct roles in the innate immunity function that causes inflammation. Activated macrophages are classified as two types and exhibit different polarization states based on the presence of pathogens and the expression of cytokines in the microenvironment. M1 macrophages, or classically activated macrophages, secret principally proinflammatory cytokines such as tumor necrosis factor (TNF)-α and interleukin (IL)-1 and cause joint erosion. M2 macrophages, or alternatively activated macrophages, can produce anti-inflammatory cytokines mainly including transforming growth factor (TGF)-β and IL-10 contributing to vasculogenesis, tissue remodeling and repair (Kinne et al., 2000). Mechanistically, macrophage polarization is regulated by a variety of signaling molecules and associated pathways, such as nuclear factor kappa-B (NF-κB) and the janus kinase/signal transducer and activator of transcription (JAK/STAT) signaling pathway, which are all associated with RA (Kubo et al., 2018; Li H. et al., 2018). Recently, m^{6}A modification has been shown to alter the mRNA levels of specific signaling molecules and affect the polarization state of macrophages. *In vitro*, macrophages are typically activated by pathogenic factors, leading to the phosphorylation and translocation of the transcription factor NF-κB. When METTL3 is overexpressed, the nuclear translocation of phosphorylated NF-κB in cells is inhibited. Wang et al. found that METTL3 inhibits the activation of phor-bol 12-myristate 13-acetate (PMA)-induced macrophage-like cells (pTHP-1 cells) and attenuates the lipopolysaccharide (LPS)-induced inflammatory response in pTHP-1 macrophages through the NF-κB signaling pathway (Wang J. et al., 2019). METTL3-mediated m^{6}A modification also facilitates the expression of STAT1 by enhancing mRNA stability, thereby altering the polarization type of macrophages. Moreover, METTL3 silencing significantly suppresses IFNγ-induced M1 macrophage polarization while promoting the expression of M2 macrophage marker genes (Liu Y. et al., 2019), indicating METTL3 potentially serving as an anti-inflammatory target in RA.

As an m^{6}A erasers, FTO affects both the phosphorylation of NF-κB and the expression of STAT1 during macrophage polarization. Following FTO depletion, both the phosphorylation levels of several elements in the NF-κB signaling pathway and the mRNA stability of STAT are decreased, resulting in macrophage activation being blocked (Gu et al., 2020). As an m^{6}A-binding protein, YTHDF2 may be involved in the above processes. The primary function of YTHDF2 is to selectively bind to m^{6}A-modified mRNA and recruit it to the mRNA decay site to induce transcription product degradation. Furthermore, YTHDF2 participates in regulating the LPS-stimulated macrophage inflammatory response. Yu et al. found that YTHDF2 knockdown could increase the expression and stability of MAP2K4 and MAP4K4 mRNA through stabilizing the mRNA transcripts, which activate MAPK and NF-κB signaling pathways, promote proinflammatory cytokines expression and aggravate the inflammatory response in LPS-induced RAW264.7 macrophages cells. (Yu et al., 2019). In view of the important role of macrophages in RA, although there was no study about m^{6}A in macrophages related to RA directly such as macrophages from

collagen-induced arthritis model, these findings *in vitro* provide new directions for epigenetic studies in the pathogenesis of RA.

m^{6}A-Mediated Regulation of Dendritic Cell Activation and Function

As professional antigen presenting cells, DCs connect the innate and adaptive immune responses. Activated DCs have the striking ability to capture and present antigens and can express major histocompatibility complexes and co-stimulating molecules to activate T cells. DCs and T cells interactions consolidate the generation of an autoimmune response in RA. In RA patients, DCs are recruited to joint synovial fluid and tissues in high concentration, and synovial DCs are generally mature and NF-κB is overexpression (Cheung and McInnes, 2017; Wehr et al., 2019). Furthermore, compared with healthy controls DCs, CD1c$^+$ DCs from RA secrete increased amounts of proinflammatory cytokines such as IL-1β, IL-6, IL-12 and IL-23, which are crucial players in the pathogenesis of RA (Lebre et al., 2008). Recent study confirmed that METTL3-mediated m^{6}A modification increases the expression of CD40, CD80, and Tirap mRNA both *in vivo* and *in vitro*. The up-regulated CD40 and CD80 are conducive to the capacity of DCs that presents antigens and stimulate T cells (**Figure 2**). Higher Tirap expression enhances Toll-like receptor (TLR4)/NF-κB signaling pathway in DCs and increase the secretion of IL-6 and IL-12 (Wang H. et al., 2019). CC-chemokine receptor 7 (CCR7) stimulation is well known to induce DCs to migrate into lymph nodes in a unique manner, which is essential for initiating protective immunity and maintaining immune homeostasis (Förster et al., 2008; Seth et al., 2011). A long non-coding RNA lnc-Dpf3 has been reported to be involved in this mechanism (Liu J. et al., 2019). Following CCR7 stimulation, m^{6}A modification of lnc-Dpf3 is down-regulated. Moreover, m^{6}A can be recognized on lnc-Dpf3 by YTHDF2, but not YTHDF1. CCR7 stimulation down-regulates the recognition of lnc-Dpf3 by YTHDF2 and then reduces its degradation. The two effects described above increase the expression of lnc-Dpf3, which then interacts with the transcription factor hypoxia inducible factor 1-α (HIF-1α) to inhibit the HIF-1α-dependent glycolysis. HIF-1α-dependent glycolysis is one of the metabolic pathways that promotes maturation and migration of DCs Which ultimately prevents the amplification of inflammatory responses (Guak et al., 2018; Liu J. et al., 2019). At present, the study about m^{6}A modification in synovial DCs from RA is rare, but the above findings may provide new ideas for epigenetic researches of RA in the future.

m^{6}A Regulation of T Cell Homeostasis

T cell is one of the key regulators of synovial inflammation and recognized as a contributor to the progressive joint destruction that is a hallmark of RA, which has both stimulatory and inhibitory effects and plays a destructive or a protective role in bone metabolism in a context-and subtype-dependent manner (McInnes and Schett, 2011). Several studies have shown that mRNA methylation due to m^{6}A modification is crucial for maintaining T cell homeostasis, which is essential to maintain the size of the T cell pool and lay the foundation for adaptive immunity. Physiologically, members of the suppressor of cytokine signaling (SOCS) protein family are important

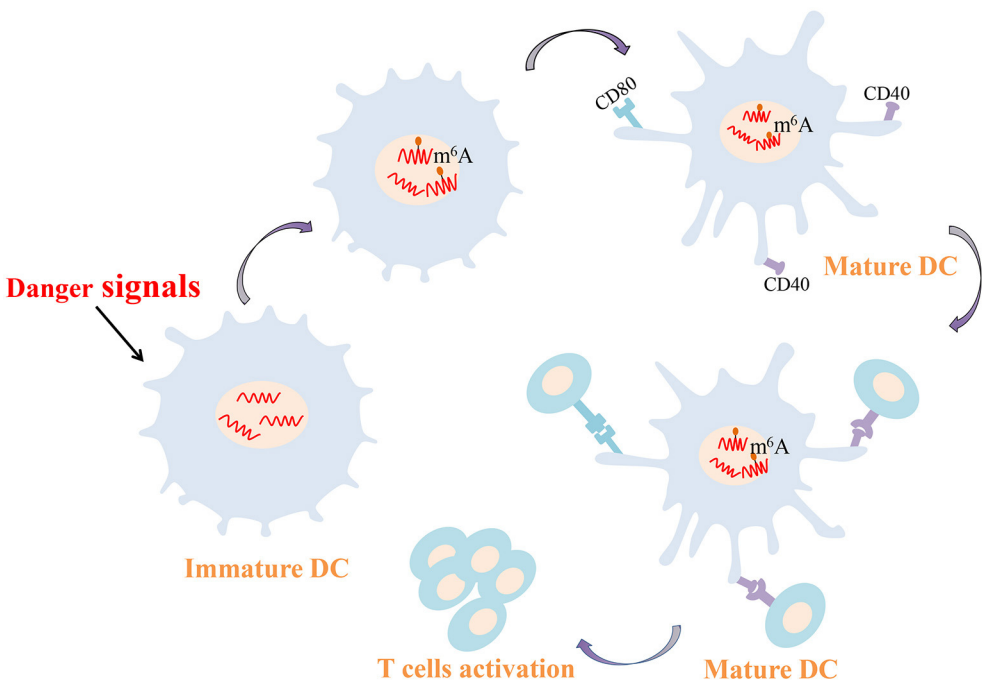


FIGURE 2 | m^{6}A-mediated regulation of dendritic cell. m^{6}A modification increases the expression of CD40 and CD80 conducive to the capacity of DCs that presents antigens and stimulates T cells. DCs, dendritic cells; m^{6}A, N^6-methyladenosine.

inhibitors of the JAK-STAT signaling pathway, including SOCS1, SOCS3, and CISH. SOCS1 is a significant negative regulator of IL-7, while SOCS3 and CISH inhibit STAT5 phosphorylation and T cell proliferation (Yoshimura et al., 2007; Palmer and Restifo, 2009). METTL3 has been reported to affect the stability and expression of SOCS1, SOCS3 and CISH mRNA in cells to regulate the balance between TCR-mediated ERK/AKT signaling and IL-7-mediated JAK-STAT signaling to control T cell homeostasis (Li et al., 2017; Furlan et al., 2019) (**Figure 3**).

T cells are complex lymphocytes, and there can be subpopulations of these cells with different developmental stages or functions. In RA, type 1 T helper (Th1)-cell and Th17-cell subsets have important pathogenic roles and are major contributors to synovial inflammation as well as to cartilage and bone destruction. And a disrupted balance between Th1 and Th2 has been thought to driven the pathology of organ in RA (Kobezda et al., 2014). Compared to wild-type naive T cells, fewer Th1 and Th17 cells and more Th2 cells are present during cell differentiation among naive T cells lacking METTL3, while Tregs remained unchanged. The specific absence of METTL3 in Tregs leads to the increased expression of SOCS, which inhibits the IL2-STAT5 signaling pathway (Li et al., 2017; Tong et al., 2018) an essential pathway for maintaining the immunosuppressive function of Tregs. It may be considered that m^{6}A is an important regulatory factor for helper T cell differentiation and to maintain the functions of various T cells.

In addition, previous study revealed that autoimmune arthritis occurred with a wide spectrum among HIV-infected patients (Lawson and Walker-Bone, 2012). It had been observed that RA was worsening with antiretroviral therapy in the era of highly active antiretroviral therapy, which might reveal a pivotal role of CD4$^+$ T lymphocytes in the pathogenesis of RA (Siva and Brasington, 2001). At present, m^{6}A modification has been shown to be involved in the antiviral mechanism of T cells and hosts. Kennedy and Lichinchi et al. suggested that posttranscriptional m^{6}A modification and the YTHDF1-3 protein are positive regulators of HIV-1 infection. The overexpression of YTHDF1-3 protein in CD4+ T cells increased viral replication as well as the expression of HIV-1 viral protein (Kennedy et al., 2016; Lichinchi et al., 2016). In contrast, Tirumuru et al. showed that YTHDF1-3 is an inhibitor and reduced HIV-1 reverse transcription to inhibit HIV-1 infection in CD4$^+$ T cells after its overexpression (Tirumuru et al., 2016). This discrepancy may be due to the different detection methods or different roles of YTHDF1-3 in different cell lines. In summary, m^{6}A methylation may indirectly regulate the antiviral effect of the host by regulating T cells. As T cells regulate the entire adaptive immune response and have crucial roles in RA, the above findings open new avenues of investigation into the function of m^{6}A in RA and further suggest that T cell-specific delivery of m^{6}A-modifying agents might be an effective treatment to alleviate RA.

m^{6}A Modification in Immune-Related Bone Homeostasis

Bone is composed of a highly calcified intercellular stroma, namely, bone matrix, and varieties of cells. Bones are in a constant state of transition from old to new. In the process of physiological reconstruction, osteogenesis and osteolysis are in a state of dynamic equilibrium. Osteogenesis promotes the growth, repair, and reconstruction of bone, which is primarily performed by osteoblasts. Under specific conditions, bone dissolves to release Ca^{2+}, maintaining a constant level of blood calcium. The dissolution of bone is called osteolysis and is primarily performed by osteoclasts. Osteoclasts absorb bone tissues through enzymatic degradation and participate in bone reconstruction and blood calcium balance. RA is characterized by synovitis, with the infiltration numerous inflammatory cells. Due to the expression of proinflammatory cytokines in inflammatory synovial cells, osteoclast differentiation is promoted, while osteoblast function is inhibited. If this condition persists, the bone balance will be

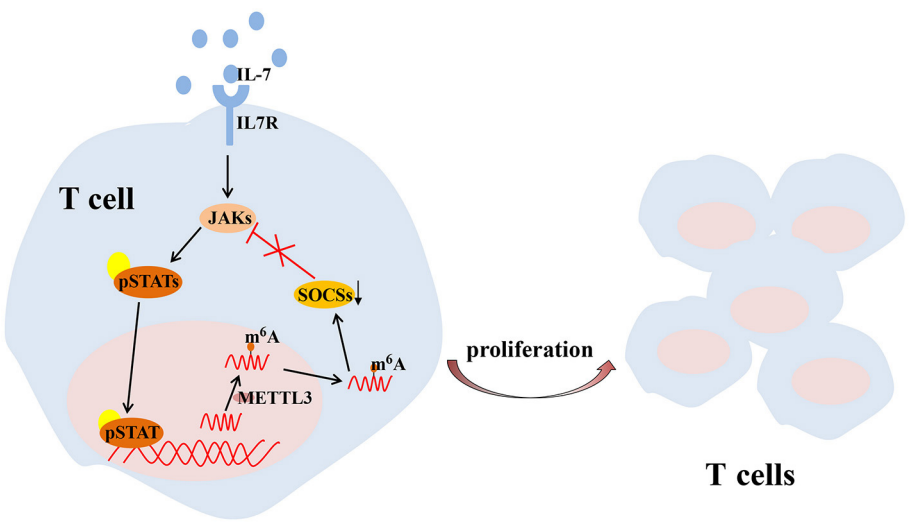


FIGURE 3 | METTL3-mediated m^{6}A mRNA methylation controls T cell proliferation by targeting IL-7/STAT/SOCS pathway. IL-7, interleukin 7; m^{6}A, N^6-methyladenosin; METTL3, methyltransferase like 3; SOCS, suppressor of cytokine signaling; STAT, signal transducer and activator of transcription.

disrupted and then lead to the destruction of bone and articular cartilage (Karmakar et al., 2010; Baum and Gravallese, 2014; Schett, 2017).

Several experiments have shown the importance of m^{6}A modification in bone remodeling. Abnormal changes of m^{6}A machinery proteins, including "writer," "eraser" and "reader," lead to the impaired differentiation and dysfunction of osteocytes. For example, the absence of METTL3 in bone marrow mesenchymal stem cells (BMSCs) reduces the expression of parathyroid hormone receptor-1 (Pth1r) in mammals by inhibiting the Parathyroid hormone (PTH)/Pth1r signaling pathway, thereby blocking the synthesis of parathyroid hormone. These deletions tilt parathyroid hormone-induced osteogenic differentiation toward adipogenic differentiation, leading to bone loss and excessive bone marrow fat (Wu et al., 2018). The deletion of METTL3 in BMSCs can also inhibit osteoblast differentiation by limiting the expression of vascular endothelial growth factor A (Vegfa) and its spliceosomes associated with bone formation (Tian et al., 2019). However, it has been reported that METTL3 overexpression *in vitro* significantly reduces the expression of osteogenic related genes (Mi et al., 2020). These results indicate that either too high or too low METTL3 expression may be detrimental to osteoblast differentiation. Osteoblast differentiation is also dependent on the regulation of FTO. Studies have shown that miR-22-3p and miR-149-3p modulate the osteoblast differentiation of BMSCs by targeting FTO (Li et al., 2019; Zhang et al., 2020). Mice with a global loss of FTO or a selective lack FTO in osteoblasts exhibit bone loss (Sachse et al., 2018; Zhang Q. et al., 2019). Li et al. established an osteoclastogenesis model using RANKL-induced RAW264.7 cells and observed that m^{6}A level and METTL3 expression were increased during osteoclast differentiation. METTL3 knockdown resulted in an increased size of osteoclasts, but the bone-resorbing ability of osteoclasts was decreased. The mechanism associated with this process involved Atp6v0d2 mRNA degradation mediated by YTHDF2 and Traf6 mRNA nuclear export (Li et al., 2020). In addition, the abnormal differentiation and activation of osteoclasts can also cause bone homeostasis disorders, leading to various bone resorptive diseases. Knocking down METTL3 in preosteoclast expands the volume of mature osteoclasts, while the amount and the capacity of bone

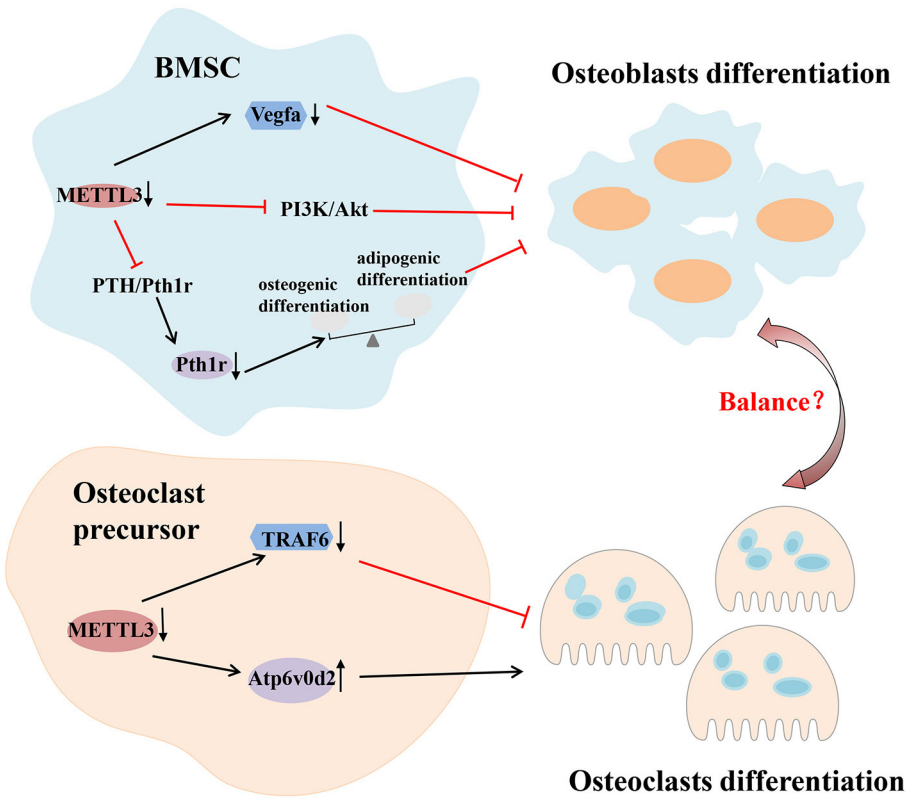


FIGURE 4 | m^{6}A modification in immune-related bone homeostasis. Deletion of METTL3 in BMSCs can inhibit osteoblast differentiation by inhibiting the PTH/Pth1r, PI3K/Akt signaling pathway and limiting the expression of vascular endothelial growth factor A (Vegfa). As for osteoclast, METTL3 regulates the differentiation and function of osteoclast through different mechanisms which involve Atp6v0d2 mRNA degradation mediated by YTHDF2 and Traf6 mRNA nuclear export. Akt, protein kinase B; Atp6v0d2, V-type proton ATPase subunit d 2; BMSCs, bone marrow mesenchymal stem cells; METTL3, methyltransferase like 3; PI3K, phosphoinositide-3-kinase; PTH, parathyroid hormone; Pth1r, parathyroid hormone 1 receptor; Traf6, tumor necrosis factor receptor-associated factor 6; YTHDF2, YTH domain family 2.

resorption are reduced (Li et al., 2020). Therefore, the stability of METTL3 is essential for physiological bone remodeling (**Figure 4**).

Inflammation is destructive to normal bone remodeling in RA. Due to the effect of m^{6}A on bone remodeling, the unique role of m^{6}A in the inflammatory environment on bone remodeling has been gradually recognized. In the inflammatory environment, METTL3 knockdown inhibits the transcription and protein levels of osteoblast factors, including Runx2, Sp7, Alpl, and Col1a1 while phosphorylation of the Smad1/5/9 complex is inhibited. Thus, insufficient Runx2 is recruited in the nucleus to activate osteogenic gene expression, resulting in the negative regulation of osteogenic differentiation (Zhang Y. et al., 2019). In another study, METTL3 silencing was shown to inhibit inflammatory responses and extracellular matrix (ECM) synthesis in chondrocytes treated with IL-1β, decreasing the chondrocyte apoptosis (Liu Q. et al., 2019). Rheumatic immune diseases eventually destroy the normal structure and function of bones, and the roles of methylation in immunity and bone remodeling has been demonstrated. Therefore, additional studies should be conducted to uncover the effects of m^{6}A in RA.

m^{6}A Modification Regulates Cytokines and Cytokine receptors Signaling

Cytokines are small molecular polypeptides or glycoproteins that are primarily synthesized and secreted by immune cells. And cytokines can act on immune cells. Cytokines mediate intercellular interactions between cells and are involved in regulating the immune and inflammatory responses. Among them, inflammatory cytokines, including TNF-α, IL-6, TGF-β, and IL-10, have the closest association with the occurrence and development of RA (Feldmann et al., 1996). LPS is a recognized inducer of inflammatory responses. After adding LPS, increased mRNA levels of IL-6, IL-12, and TNF-α in preosteoblasts indicates a successful induction of inflammatory environment. Knocking down METTL3 can increase the expression of these inflammatory factors (Zhang Y. et al., 2019). In general, the combination of YTHDF2 and m^{6}A modification leads to mRNA degradation, which can reduce the expression of proinflammatory cytokines. Thus, the deletion of YTHDF2 results in increased TNF-α, IL-1β, IL-6, and IL-12 expression in macrophages. Interestingly, YTHDF2 deletion does not directly affect the stability of these cytokines but rather dose so by promoting the phosphorylation of their upstream molecules p65, P38, and ERK (Yu et al., 2019). In the section on the m^{6}A-mediated regulation of T cell homeostasis, we noted that SOCS protein family members inhibit IL-7 receptor signaling and negatively regulate T cell homeostasis proliferation. Not coincidentally, the degradation and expression level of SOCS mRNA can change in response to m^{6}A markers (Li et al., 2017). In addition, the secretion of proinflammatory cytokines aids in controlling the inflammatory response influences the activity of bone cells, METTL3 knockdown can inhibits osteoblast differentiation via YTHDF2 involvement and activates the inflammatory response by regulating MAPK signaling in LPS-induced inflammation (Zhang Y. et al., 2019).

As an autoimmune disease, RA is related to the overexpression of proinflammatory cytokines and the abnormal up-regulation of cytokines is prevalent in RA patients (Gao et al., 2018). It has been proved that interferons (IFNs), acting as a subgroup of cytokines, can make crucial effects on regulating immunology, as well as modulating the dynamic balance of bone matrix. Type I IFNs consist of a multi-gene family including IFN-α and IFN-β. IFN-α has the ability to activate osteoblast differentiation and inhibits osteoclast fusion to maintain bone matrix integrity. Meanwhile, IFN-β exerts effects of suppressing osteoblast-mediated bone remodeling and inhibiting osteoclast differentiation to attenuate bone resorption (Deng et al., 2020). DEAD-box (DDX) helicases have been shown to demethylate m^{6}A-modified transcripts to participate in type I IFNs activation by recruiting ALKBH5. This process enhances the preservation of transcripts in the nucleus to inhibit the production of type I IFNs, ultimately inhibiting the antiviral innate immune response (Zheng et al., 2017). However, another study where METTL3 was knocked down appears to have shown the opposite effect, indicating that m^{6}A is a negative regulator of the type I IFNs response (Winkler et al., 2019). Do these two mechanisms work together to regulate type I IFNs production and further play a role in RA? Further studies are needed to elucidate these questions.

m^{6}A MODIFICATION IN CLINICAL APPLICATION

As a refractory disease, it is essential to develop drugs that can target the molecules associated with RA. Novel RNA-targeted therapeutics, which are poised to offer high efficacy and specificity, provide inherent advantages and have shown convincing prospects in the treatment of various diseases (Dori and Soreq, 2006; Crooke et al., 2018; Scoles and Pulst, 2018; Tsimikas, 2018). The involvement of m^{6}A-based medication in various immune and bone cells associated with RA has promoted extensive research efforts in m^{6}A-based therapy. As previously mentioned, RNA processing, splicing, export, degradation, and translation can be interfered with by m^{6}A modification through the activity of "writer," "eraser," and "reader" protein making it possible that developing inhibitors or promoters of "writers," "erasers," and "readers" to control the disease progression. In **Table 2**, we have summarized several inhibitors have been discovered via natural product analyses, chemical synthesis or biochemical- or cell-based small molecule compound library screening.

Until now, the target of inhibitors is almost FTO. In 2012, Chen and colleagues identified several small-molecule inhibitors of human FTO demethylase and observed that the natural product rhein could competitively bind to the FTO active site *in vitro* for the first time (Chen et al., 2012). Meclofenamic acid (MA) is a non-steroidal, anti-inflammatory drug that was identified as a highly selective inhibitor of FTO, which could compete with FTO for m^{6}A-containing substrate binding over ALKBH5 (Huang et al., 2015). N-(5-Chloro-2,4-dihydroxyphenyl)-1-phenylcyclobutanecarboxamide

TABLE 2 | Inhibitors and mechanisms of FTO discovered to date.

Inhibitors' name	Experimental subject (*in vivo*/*in vitro*)	Mechanisms of inhibitors	References
Rhein	BE (2)-C cells	Competitively binds to the FTO active site *in vitro*	Chen et al., 2012
Meclofenamic acid	HeLa cells	Competes with FTO on m^{6}A-containing substrate binding over ALKBH5	Huang et al., 2015
N-CDPCB, 1a	3T3-L1 cells	An antiparallel β-sheet and the L1 loop of FTO sandwich N-CDPCB	He et al., 2015
CHTB	3T3-L1 cells	CHTB can bind to the FTO active site	Qiao et al., 2016
Entacapone	DIO mice/Hep-G2 cells	Directly bound to FTO and inhibited FTO activity *in vitro*	Peng et al., 2019
Radicicol	— —	Adopts an L-shaped conformation in the FTO binding site and occupies the same position as N-CDPCB	Wang et al., 2018

CHTB, 4-chloro-6-(6′-chloro-7′-hydroxy-2′,4′,4′-trimethyl-chroman-2′-yl)benzene-1,3-diol; DIO, diet-induced obese; FTO, fat mass and obesity associated protein; N-CDPCB, 1a, N-(5-Chloro-2,4-dihydroxyphenyl)-1-phenylcyclobutanecarboxamide; "— —" indicates that there are no corresponding animals and cells used in the literature we cited.

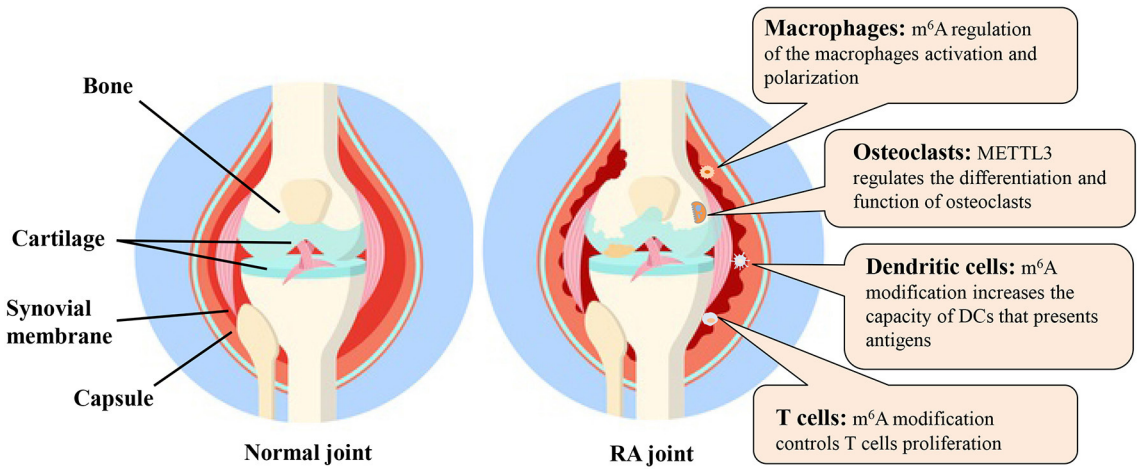


FIGURE 5 | The m^{6}A modification and possible molecular mechanisms in various cells related to RA. DC, dendritic cell; m^{6}A, N^6-methyladenosine; METTL3, methyltransferase like 3; RA, rheumatoid arthritis.

(N-CDPCB, 1a) and 4-chloro-6-(6′-chloro-7′-hydroxy-2′,4′,4′-trimethyl-chroman-2′-yl) benzene-1,3-diol (CHTB) are the other inhibitors that bind FTO and were identified by virtual screening. The crystal structure of N-CDPCB, CHTB complexes with FTO show that N-CDPCB is sandwiched between an antiparallel β-sheet and the L1 loop of FTO as well as that CHTB can bind the FTO active site (He et al., 2015; Qiao et al., 2016). Furthermore, a previous study also observed that entacapone can directly bind to FTO and inhibit FTO activity *in vitro* (Peng et al., 2019). Radicicol, a nature compound, was also shown to be a potent inhibitor of FTO that can adopt an L-shaped conformation in the FTO binding site and occupy the same position as N-CDPCB (Wang et al., 2018).

Since METTL3 up-regulation and ALKBH5 and YTHDF2 down-regulation contribute to the progression of RA, METTL3, ALKBH5, and YTHDF2 may also be targeted for treatment. Indeed, Bedi et al. identified two series of adenine derivatives *in silico* by high-throughput docking of METTL3 and identified two compounds showing good ligand efficiency (Bedi et al., 2020). Although the inhibitors of METTL3, ALKBH5, and YTHDF2 are not available so far, these findings offer novel research directions.

DISCUSSION AND FURTHER PERSPECTIVES

In this review, we briefly described the "writers," "readers" and "erasers" of m^{6}A and various detection methods for m^{6}A modification. The m^{6}A modification and relevant molecular mechanisms in various cells related to RA were also discussed (**Figure 5**). Although the field of m^{6}A modification has become increasingly attractive, many research challenges and knowledge gaps remain.

Recently, analytical technology innovations have greatly promoted the study of m^{6}A RNA modification. However, the selection and optimization of the laboratory technology m^{6}A

measurements in clinical practice remains an open problem. The application of these techniques in practical clinical m^{6}A RNA is rare. Moreover, in addition to better detection sensitivity and accuracy, comprehensive detection and mapping the same biological sample with different modifications are desirable. Challenges pertaining to the needs of tools for deciphering the functions of m^{6}A RNA modification will continue to stimulate the development of analytical methods and software.

The results of a growing number of preclinical studies have suggested that m^{6}A modification is especially crucial in a variety of pathological and physiological conditions of immune and bone cells. We speculate that the potential primary effect of m^{6}A modification in RA may be achieved through the regulation of different immune and bone cells. However, we observed that the percentage of m^{6}A studies focused on RA is small. Mo et al. conducted a large-scale genome-wide association study to identify m^{6}A-associated SNPs that affecting RA progression identifying 37 m^{6}A-SNPs related to RA and 27 of them were verified to affect expression of 24 local genes in different RA cells or tissues (Mo et al., 2018). This result revealed the potential roles of m^{6}A-SNPs in RA. Indeed, synovial hyperplasia is a hallmark in RA and is the primary contributor to the formation of an invasive pannus. In the progression of RA, synovial inflammation is dominated by the infiltration of immune cells into synovial tissue and by joint effusions rich in leukocytes compared to osteoarthritis (Scherer et al., 2020). Earlier studies of epigenetic changes in RA have demonstrated that differential DNA methylation genes can alter gene expression in fibroblast-like synoviocytes (FLS) and play a crucial role in RA pathogenesis (Karouzakis et al., 2009; Nakano et al., 2013). Thus, studies of m^{6}A modification regarding synovial cells and tissues should be carried out in the future. In addition, as RA is a systemic and intricate disease, the mechanisms of m^{6}A modification in RA require further investigation. Up to now, most of the conclusions in this field were based on the deletion of one of m^{6}A machinery components. Therefore, determining how to bridge gaps between phenotype, specific methylated mRNAs and molecular mechanisms continues to be a major challenge. Furthermore, since the majority of essential components of m^{6}A writers and erasers were deleted to conduct immunological phenotypes studies, a straightforward strategy is to identify the m^{6}A readers such as YTHDF1 and YTHDF2, that can drive the observed phenotypes and determine whether the deletion of individual or multiple m^{6}A readers can recapitulate these effects (Shulman and Stern-Ginossar, 2020). Recently, a study found that the YTHDF1-3, cytosolic m^{6}A-binding proteins, could undergo liquid-liquid phase separation (LLPS) in cells. And this LLPS is markedly enhanced by mRNAs that contain multiple, but not single, m^{6}A residues (Ries et al., 2019; Wang et al., 2020). Under the stress conditions, different RNAs and RNA-binding proteins form phase-separated, membraneless granules in cells. Stress granules (SGs) are RNA-protein granules that play crucial roles in epigenetic and post-transcriptional regulations. Fu et al. studied the localization of m^{6}A-modified mRNAs and m^{6}A-binding proteins, YTHDF proteins, in mammalians cells. They revealed that YTHDF proteins played an important role in SG formation (Fu and Zhuang, 2020). These findings may provide new ideas for m^{6}A modification research.

In terms of the clinical application of m^{6}A modification, the most important question may involve the development of drugs, as m^{6}A-based drugs are currently scarce and poorly understood. There are only a limited number of inhibitors associated with FTO that have been identified, but their effects have only been experimentally verified, and an evaluation of their effectiveness and safety remains to be resolved. More importantly, there are no m^{6}A-based drugs for RA at present. Thus, additional studies are needed to advance the application of m^{6}A-based approaches for RA.

AUTHOR CONTRIBUTIONS

CX designed the framework of the review. DF, YX, and CL wrote the manuscript. QY and XX contributed in figure designing. QW and ZW contributed to the literature research. CW and CX revised and approved the manuscript. All authors contributed to the article and approved the submitted version.

FUNDING

This work was supported by the National Natural Science Foundation of China [Nos. 82073677, 81673844, 81873223, and 82074269].

REFERENCES

Akichika, S., Hirano, S., Shichino, Y., Suzuki, T., Nishimasu, H., Ishitani, R., et al. (2019). Cap-specific terminal N (6)-methylation of RNA by an RNA polymerase II-associated methyltransferase. *Science* 363:aav0080. doi: 10.1126/science.aav0080

Alarcón, C. R., Goodarzi, H., Lee, H., Liu, X., Tavazoie, S., and Tavazoie, S. F. (2015). HNRNPA2B1 is a mediator of m(6)A-dependent nuclear RNA processing events. *Cell* 162, 1299–1308. doi: 10.1016/j.cell.2015.08.011

Arguello, A. E., DeLiberto, A. N., and Kleiner, R. E. (2017). RNA chemical proteomics reveals the N(6)- methyladenosine (m(6)A)-regulated protein-RNA interactome. *J. Am. Chem. Soc.* 139, 17249–17252. doi: 10.1021/jacs.7b09213

Arguello, A. E., Leach, R. W., and Kleiner, R. E. (2019). *In vitro* selection with a site-specifically modified RNA library reveals the binding preferences of N(6)-methyladenosine reader proteins. *Biochemistry* 58, 3386–3395. doi: 10.1021/acs.biochem.9b00485

Baum, R., and Gravallese, E. M. (2014). Impact of inflammation on the osteoblast in rheumatic diseases. *Curr. Osteoporos. Rep.* 12, 9–16. doi: 10.1007/s11914-013-0183-y

Bedi, R. K., Huang, D., Eberle, S. A., Wiedmer, L., and Sled,z, P., Caflisch, A. (2020). Small-molecule inhibitors of METTL3, the major human epitranscriptomic writer. *ChemMedChem.* 15, 744–748. doi: 10.1002/cmdc.202000011

Bokar, J. A., Shambaugh, M. E., Polayes, D., Matera, A. G., and Rottman, F. M. (1997). Purification and cDNA cloning of the AdoMet-binding subunit of the human mRNA (N^6-adenosine)-methyltransferase. *RNA* 3, 1233–1247.

Boulias, K., Toczydłowska-Socha, D., Hawley, B. R., Liberman, N., Takashima, K., Zaccara, S., et al. (2019). Identification of the m(6)Am methyltransferase PCIF1 reveals the location and functions of m(6)Am in the transcriptome. *Mol. Cell.* 75, 631–643.e8. doi: 10.1016/j.molcel.2019.06.006

Cao, G., Li, H. B., Yin, Z., and Flavell, R. A. (2016). Recent advances in dynamic m^{6}A RNA modification. *Open Biol.* 6:160003. doi: 10.1098/rsob.160003

Cascão, R., Rosário, H. S., Souto-Carneiro, M. M., and Fonseca, J. E. (2010). Neutrophils in rheumatoid arthritis: more than simple final effectors. *Autoimmun Rev.* 9, 531–535. doi: 10.1016/j.autrev.2009.12.013

Chen, B., Ye, F., Yu, L., Jia, G., Huang, X., Zhang, X., et al. (2012). Development of cell-active **N^6**-methyladenosine RNA demethylase FTO inhibitor. *J. Am. Chem. Soc.* 134, 17963–17971. doi: 10.1021/ja3064149

Chen, B., Yuan, B. F., and Feng, Y. Q. (2019). Analytical methods for deciphering RNA modifications. *Anal. Chem.* 91, 743–756. doi: 10.1021/acs.analchem.8b04078

Chen, M., Wei, L., Law, C. T., Tsang, F. H., Shen, J., Cheng, C. L., et al. (2018). RNA **N^6**-methyladenosine methyltransferase-like 3 promotes liver cancer progression through YTHDF2-dependent posttranscriptional silencing of SOCS2. *Hepatology* 67, 2254–2270. doi: 10.1002/hep.29683

Chen, W., Feng, P., Ding, H., and Lin, H. (2016). Identifying N (6)-methyladenosine sites in the Arabidopsis thaliana transcriptome. *Mol. Genet. Genomics* 291, 2225–2229. doi: 10.1007/s00438-016-1243-7

Cheung, T. T., and McInnes, I. B. (2017). Future therapeutic targets in rheumatoid arthritis? *Semin. Immunopathol.* 39, 487–500. doi: 10.1007/s00281-017-0623-3

Coker, H., Wei, G., and Brockdorff, N. (2019). m^{6}A modification of non-coding RNA and the control of mammalian gene expression. *Biochim. Biophys. Acta Gene Regul. Mech.* 1862, 310–318. doi: 10.1016/j.bbagrm.2018.12.002

Crooke, S. T., Witztum, J. L., Bennett, C. F., and Baker, B. F. (2018). RNA-targeted therapeutics. *Cell Metab.* 27, 714–739. doi: 10.1016/j.cmet.2018.03.004

Cross, M., Smith, E., Hoy, D., Carmona, L., Wolfe, F., Vos, T., et al. (2014). The global burden of rheumatoid arthritis: estimates from the global burden of disease 2010 study. *Ann. Rheum. Dis.* 73, 1316–1322. doi: 10.1136/annrheumdis-2013-204627

Deng, Z., Hu, W., Ai, H., Chen, Y., and Dong, S. (2020). The dramatic role of IFN family in aberrant inflammatory osteolysis. *Curr. Gene Ther.* 21, 1–18. doi: 10.2174/1566523220666201127114845

Dominissini, D., Moshitch-Moshkovitz, S., Schwartz, S., Salmon-Divon, M., Ungar, L., Osenberg, S., et al. (2012). Topology of the human and mouse m^{6}A RNA methylomes revealed by m^{6}A-seq. *Nature* 485, 201–206. doi: 10.1038/nature11112

Dori, A., and Soreq, H. (2006). Neuromuscular therapeutics by RNA-targeted suppression of ACHE gene expression. *Ann. NY Acad. Sci.* 1082, 77–90. doi: 10.1196/annals.1348.004

Du, H., Zhao, Y., He, J., Zhang, Y., Xi, H., Liu, M., et al. (2016). YTHDF2 destabilizes m(6)A-containing RNA through direct recruitment of the CCR4-NOT deadenylase complex. *Nat. Commun.* 7:12626. doi: 10.1038/ncomms12626

Feldmann, M., Brennan, F. M., and Maini, R. N. (1996). Role of cytokines in rheumatoid arthritis. *Annu. Rev. Immunol.* 14, 397–440. doi: 10.1146/annurev.immunol.14.1.397

Förster, R., Davalos-Misslitz, A. C., and Rot, A. (2008). CCR7 and its ligands: balancing immunity and tolerance. *Nat. Rev. Immunol.* 8, 362–371. doi: 10.1038/nri2297

Fu, Y., Dominissini, D., Rechavi, G., and He, C. (2014). Gene expression regulation mediated through reversible m^{6}A RNA methylation. *Nat. Rev. Genet.* 15, 293–306. doi: 10.1038/nrg3724

Fu, Y., and Zhuang, X. (2020). m(6)A-binding YTHDF proteins promote stress granule formation. *Nat. Chem. Biol.* 16, 955–963. doi: 10.1038/s41589-020-0524-y

Fukui, S., Iwamoto, N., Takatani, A., Igawa, T., Shimizu, T., Umeda, M., et al. (2017). M1 and M2 Monocytes in rheumatoid arthritis: a contribution of imbalance of M1/M2 monocytes to osteoclastogenesis. *Front. Immunol.* 8:1958. doi: 10.3389/fimmu.2017.01958

Furlan, M., Galeota, E., de Pretis, S., Caselle, M., and Pelizzola, M. (2019). m^{6}A-dependent RNA dynamics in T cell differentiation. *Genes* 10, 1–9. doi: 10.3390/genes10010028

Gao, J., Kong, R., Zhou, X., Ji, L., Zhang, J., and Zhao, D. (2018). MiRNA-126 expression inhibits IL-23R mediated TNF-α or IFN-γ production in fibroblast-like synoviocytes in a mice model of collagen-induced rheumatoid arthritis. *Apoptosis* 23, 607–615. doi: 10.1007/s10495-018-1474-7

Garcia-Campos, M. A., Edelheit, S., Toth, U., Safra, M., Shachar, R., Viukov, S., et al. (2019). Deciphering the "m(6)A Code" via antibody-independent quantitative profiling. *Cell* 178, 731–747.e16. doi: 10.1016/j.cell.2019.06.013

Gerken, T., Girard, C. A., Tung, Y. C., Webby, C. J., Saudek, V., Hewitson, K. S., et al. (2007). The obesity-associated FTO gene encodes a 2-oxoglutarate-dependent nucleic acid demethylase. *Science* 318, 1469–1472. doi: 10.1126/science.1151710

Glant, T. T., Mikecz, K., and Rauch, T. A. (2014). Epigenetics in the pathogenesis of rheumatoid arthritis. *BMC Med.* 12:35. doi: 10.1186/1741-7015-12-35

Grozhik, A. V., Linder, B., Olarerin-George, A. O., and Jaffrey, S. R. (2017). Mapping m(6)A at individual-nucleotide resolution using crosslinking and immunoprecipitation (miCLIP). *Methods Mol. Biol.* 1562, 55–78. doi: 10.1007/978-1-4939-6807-7_5

Gu, X., Zhang, Y., Li, D., Cai, H., Cai, L., and Xu, Q. (2020). **N^6**-methyladenosine demethylase FTO promotes M1 and M2 macrophage activation. *Cell Signal.* 69:109553. doi: 10.1016/j.cellsig.2020.109553

Guak, H., Al, H. S., Ma, E. H., Aldossary, H., Al-Masri, M., Won, S. Y., et al. (2018). Glycolytic metabolism is essential for CCR7 oligomerization and dendritic cell migration. *Nat. Commun.* 9:2463. doi: 10.1038/s41467-018-04804-6

Harper, J. E., Miceli, S. M., Roberts, R. J., and Manley, J. L. (1990). Sequence specificity of the human mRNA **N^6**-adenosine methylase *in vitro*. *Nucleic Acids Res.* 18, 5735–5741. doi: 10.1093/nar/18.19.5735

He, W., Zhou, B., Liu, W., Zhang, M., Shen, Z., Han, Z., et al. (2015). Identification of a novel small-molecule binding site of the fat mass and obesity associated protein (FTO). *J. Med. Chem.* 58, 7341–7348. doi: 10.1021/acs.jmedchem.5b00702

Huang, H., Weng, H., Sun, W., Qin, X., Shi, H., Wu, H., et al. (2018). Recognition of RNA N(6)-methyladenosine by IGF2BP proteins enhances mRNA stability and translation. *Nat. Cell Biol.* 20, 285–295. doi: 10.1038/s41556-018-0045-z

Huang, Y., Yan, J., Li, Q., Li, J., Gong, S., Zhou, H., et al. (2015). Meclofenamic acid selectively inhibits FTO demethylation of m^{6}A over ALKBH5. *Nucleic Acids Res.* 43, 373–384. doi: 10.1093/nar/gku1276

Jia, G., Fu, Y., Zhao, X., Dai, Q., Zheng, G., Yang, Y., et al. (2011). **N^6**-methyladenosine in nuclear RNA is a major substrate of the obesity-associated FTO. *Nat. Chem. Biol.* 7, 885–887. doi: 10.1038/nchembio.687

Karmakar, S., Kay, J., and Gravallese, E. M. (2010). Bone damage in rheumatoid arthritis: mechanistic insights and approaches to prevention. *Rheum. Dis. Clin. North Am.* 36, 385–404. doi: 10.1016/j.rdc.2010.03.003

Karouzakis, E., Gay, R. E., Michel, B. A., Gay, S., and Neidhart, M. (2009). DNA hypomethylation in rheumatoid arthritis synovial fibroblasts. *Arthritis Rheum.* 60, 3613–3622. doi: 10.1002/art.25018

Ke, S., Alemu, E. A., Mertens, C., Gantman, E. C., Fak, J. J., Mele, A., et al. (2015). A majority of m^{6}A residues are in the last exons, allowing the potential for 3′ UTR regulation. *Genes Dev.* 29, 2037–2053. doi: 10.1101/gad.269415.115

Kennedy, E. M., Bogerd, H. P., Kornepati, A. V., Kang, D., Ghoshal, D., Marshall, J. B., et al. (2016). Posttranscriptional m^{6}A Editing of HIV-1 mRNAs enhances viral gene expression. *Cell Host Microbe.* 19, 675–685. doi: 10.1016/j.chom.2016.04.002

Kinne, R. W., Bräuer, R., Stuhlmüller, B., Palombo-Kinne, E., and Burmester, G. R. (2000). Macrophages in rheumatoid arthritis. *Arthritis Res.* 2, 189–202. doi: 10.1186/ar86

Klareskog, L., Lundberg, K., and Malmström, V. (2013). Autoimmunity in rheumatoid arthritis: citrulline immunity and beyond. *Adv Immunol.* 118, 129–158. doi: 10.1016/B978-0-12-407708-9.00003-0

Knuckles, P., Lence, T., Haussmann, I. U., Jacob, D., Kreim, N., Carl, S. H., et al. (2018). Zc3h13/Flacc is required for adenosine methylation by bridging the mRNA-binding factor Rbm15/Spenito to the m(6)A machinery component Wtap/Fl(2)d. *Genes Dev.* 32, 415–429. doi: 10.1101/gad.309146.117

Kobezda, T., Ghassemi-Nejad, S., Mikecz, K., Glant, T. T., and Szekanecz, Z. (2014). Of mice and men: how animal models advance our understanding of T-cell function in RA. *Nat. Rev. Rheumatol.* 10, 160–170. doi: 10.1038/nrrheum.2013.205

Kubo, S., Nakayamada, S., Sakata, K., Kitanaga, Y., Ma, X., Lee, S., et al. (2018). Janus kinase inhibitor baricitinib modulates human innate and adaptive immune system. *Front. Immunol.* 9:1510. doi: 10.3389/fimmu.2018.01510

Kurowski, M. A., Bhagwat, A. S., Papaj, G., and Bujnicki, J. M. (2003). Phylogenomic identification of five new human homologs of the DNA repair enzyme AlkB. *BMC Genomics* 4:48. doi: 10.1186/1471-2164-4-48

Lawson, E., and Walker-Bone, K. (2012). The changing spectrum of rheumatic disease in HIV infection. *Br. Med. Bull.* 103, 203–221. doi: 10.1093/bmb/lds022

Lebre, M. C., Jongbloed, S. L., Tas, S. W., Smeets, T. J., McInnes, I. B., and Tak, P. P. (2008). Rheumatoid arthritis synovium contains two subsets of CD83-DC-LAMP- dendritic cells with distinct cytokine profiles. *Am. J. Pathol.* 172, 940–950. doi: 10.2353/ajpath.2008.070703

Leung, B. P., Conacher, M., Hunter, D., McInnes, I. B., Liew, F. Y., and Brewer, J. M. (2002). A novel dendritic cell-induced model of erosive inflammatory arthritis: distinct roles for dendritic cells in T cell activation and induction of local inflammation. *J. Immunol.* 169, 7071–7077. doi: 10.4049/jimmunol.169.12.7071

Li, D., Cai, L., Meng, R., Feng, Z., and Xu, Q. (2020). METTL3 modulates osteoclast differentiation and function by controlling RNA stability and nuclear export. *Int. J. Mol. Sci.* 21:1660. doi: 10.3390/ijms21051660

Li, H., Jiang, T., Li, M. Q., Zheng, X. L., and Zhao, G. J. (2018). Transcriptional regulation of macrophages polarization by microRNAs. *Front. Immunol.* 9:1175. doi: 10.3389/fimmu.2018.01175

Li, H. B., Tong, J., Zhu, S., Batista, P. J., Duffy, E. E., Zhao, J., et al. (2017). m(6)A mRNA methylation controls T cell homeostasis by targeting the IL-7/STAT5/SOCS pathways. *Nature* 548, 338–342. doi: 10.1038/nature23450

Li, L. J., Fan, Y. G., Leng, R. X., Pan, H. F., and Ye, D. Q. (2018). Potential link between m(6)A modification and systemic lupus erythematosus. *Mol. Immunol.* 93, 55–63. doi: 10.1016/j.molimm.2017.11.009

Li, Y., Yang, F., Gao, M., Gong, R., Jin, M., Liu, T., et al. (2019). miR-149-3p regulates the switch between adipogenic and osteogenic differentiation of BMSCs by targeting FTO. *Mol. Ther. Nucleic Acids* 17, 590–600. doi: 10.1016/j.omtn.2019.06.023

Lichinchi, G., Gao, S., Saletore, Y., Gonzalez, G. M., Bansal, V., Wang, Y., et al. (2016). Dynamics of the human and viral m^{6}A RNA methylomes during HIV-1 infection of T cells. *Nat. Microbiol.* 1:16011. doi: 10.1038/nmicrobiol.2016.11

Linder, B., Grozhik, A. V., Olarerin-George, A. O., Meydan, C., Mason, C. E., and Jaffrey, S. R. (2015). Single-nucleotide-resolution mapping of m^{6}A and m^{6}Am throughout the transcriptome. *Nat. Methods* 12, 767–772. doi: 10.1038/nmeth.3453

Liu, J., Yue, Y., Han, D., Wang, X., Fu, Y., Zhang, L., et al. (2014). A METTL3-METTL14 complex mediates mammalian nuclear RNA **N^6**-adenosine methylation. *Nat. Chem. Biol.* 10, 93–95. doi: 10.1038/nchembio.1432

Liu, J., Zhang, X., Chen, K., Cheng, Y., Liu, S., Xia, M., et al. (2019). CCR7 Chemokine receptor-inducible inc-Dpf3 restrains dendritic cell migration by inhibiting HIF-1α-mediated glycolysis. *Immunity* 50, 600–615.e15. doi: 10.1016/j.immuni.2019.01.021

Liu, N., Zhou, K. I., Parisien, M., Dai, Q., Diatchenko, L., and Pan, T. (2017). **N^6**-methyladenosine alters RNA structure to regulate binding of a low-complexity protein. *Nucleic Acids Res.* 45, 6051–6063. doi: 10.1093/nar/gkx141

Liu, Q., Li, M., Jiang, L., Jiang, R., and Fu, B. (2019). METTL3 promotes experimental osteoarthritis development by regulating inflammatory response and apoptosis in chondrocyte. *Biochem. Biophys. Res. Commun.* 516, 22–27. doi: 10.1016/j.bbrc.2019.05.168

Liu, Y., Liu, Z., Tang, H., Shen, Y., Gong, Z., Xie, N., et al. (2019). The N(6)-methyladenosine (m(6)A)-forming enzyme METTL3 facilitates M1 macrophage polarization through the methylation of STAT1 mRNA. *Am. J. Physiol. Cell Physiol.* 317, C762–C775. doi: 10.1152/ajpcell.00212.2019

Luo, Q., Gao, Y., Zhang, L., Rao, J., Guo, Y., Huang, Z., et al. (2020). Decreased ALKBH5, FTO, and YTHDF2 in peripheral blood are as risk factors for rheumatoid arthritis. *Biomed. Res. Int.* 2020:5735279. doi: 10.1155/2020/5735279

Ma, H., Wang, X., Cai, J., Dai, Q., Natchiar, S. K., Lv, R., et al. (2019). N(6-)methyladenosine methyltransferase ZCCHC4 mediates ribosomal RNA methylation. *Nat. Chem. Biol.* 15, 88–94. doi: 10.1038/s41589-018-0184-3

Mao, Y., Dong, L., Liu, X. M., Guo, J., Ma, H., Shen, B., et al. (2019). m(6)A in mRNA coding regions promotes translation via the RNA helicase-containing YTHDC2. *Nat. Commun.* 10:5332. doi: 10.1038/s41467-019-13317-9

Mauer, J., Luo, X., Blanjoie, A., Jiao, X., Grozhik, A. V., Patil, D. P., et al. (2017). Reversible methylation of m(6)A(m) in the 5′ cap controls mRNA stability. *Nature* 541, 371–375. doi: 10.1038/nature21022

McGee, S. L., and Hargreaves, M. (2019). Epigenetics and exercise. *Trends Endocrinol. Metab.* 30, 636–645. doi: 10.1016/j.tem.2019.06.002

McInnes, I. B., and Schett, G. (2011). The pathogenesis of rheumatoid arthritis. *N. Engl. J. Med.* 365, 2205–2219. doi: 10.1056/NEJMra1004965

Merad, M., Sathe, P., Helft, J., Miller, J., and Mortha, A. (2013). The dendritic cell lineage: ontogeny and function of dendritic cells and their subsets in the steady state and the inflamed setting. *Annu. Rev. Immunol.* 31, 563–604. doi: 10.1146/annurev-immunol-020711-074950

Meyer, K. D., Patil, D. P., Zhou, J., Zinoviev, A., Skabkin, M. A., Elemento, O., et al. (2015). 5′ UTR m(6)A promotes cap-independent translation. *Cell* 163, 999–1010. doi: 10.1016/j.cell.2015.10.012

Meyer, K. D., Saletore, Y., Zumbo, P., Elemento, O., Mason, C. E., and Jaffrey, S. R. (2012). Comprehensive analysis of mRNA methylation reveals enrichment in 3′ UTRs and near stop codons. *Cell* 149, 1635–1646. doi: 10.1016/j.cell.2012.05.003

Mi, B., Xiong, Y., Yan, C., Chen, L., Xue, H., Panayi, A. C., et al. (2020). Methyltransferase-like 3-mediated **N^6**-methyladenosine modification of miR-7212-5p drives osteoblast differentiation and fracture healing. *J. Cell Mol. Med.* 24, 6385–6396. doi: 10.1111/jcmm.15284

Mishima, E., Jinno, D., Akiyama, Y., Itoh, K., Nankumo, S., Shima, H., et al. (2015). Immuno-northern blotting: detection of RNA modifications by using antibodies against modified nucleosides. *PLoS ONE* 10:e0143756. doi: 10.1371/journal.pone.0143756

Mo, X. B., Zhang, Y. H., and Lei, S. F. (2018). Genome-wide identification of N(6)-methyladenosine (m(6)A) SNPs associated with rheumatoid arthritis. *Front Genet.* 9:299. doi: 10.3389/fgene.2018.00299

Molinie, B., Wang, J., Lim, K. S., Hillebrand, R., Lu, Z. X., Van Wittenberghe, N., et al. (2016). m(6)A-LAIC-seq reveals the census and complexity of the m(6)A epitranscriptome. *Nat. Methods* 13, 692–698. doi: 10.1038/nmeth.3898

Mulherin, D., Fitzgerald, O., and Bresnihan, B. (1996). Synovial tissue macrophage populations and articular damage in rheumatoid arthritis. *Arthritis Rheum.* 39, 115–124. doi: 10.1002/art.1780390116

Nakano, K., Whitaker, J. W., Boyle, D. L., Wang, W., and Firestein, G. S. (2013). DNA methylome signature in rheumatoid arthritis. *Ann. Rheum. Dis.* 72, 110–117. doi: 10.1136/annrheumdis-2012-201526

Palmer, D. C., and Restifo, N. P. (2009). Suppressors of cytokine signaling (SOCS) in T cell differentiation, maturation, and function. *Trends Immunol.* 30, 592–602. doi: 10.1016/j.it.2009.09.009

Park, O. H., Ha, H., Lee, Y., Boo, S. H., Kwon, D. H., Song, H. K., et al. (2019). Endoribonucleolytic cleavage of m(6)A-containing RNAs by RNase P/MRP complex. *Mol. Cell* 74, 494–507.e8. doi: 10.1016/j.molcel.2019.02.034

Patil, D. P., Chen, C. K., Pickering, B. F., Chow, A., Jackson, C., Guttman, M., et al. (2016). m(6)A RNA methylation promotes XIST-mediated transcriptional repression. *Nature* 537, 369–373. doi: 10.1038/nature19342

Pendleton, K. E., Chen, B., Liu, K., Hunter, O. V., Xie, Y., Tu, B. P., et al. (2017). The U6 snRNA m(6)A methyltransferase METTL16 regulates SAM synthetase intron retention. *Cell* 169, 824–835.e14. doi: 10.1016/j.cell.2017.05.003

Peng, S., Xiao, W., Ju, D., Sun, B., Hou, N., Liu, Q., et al. (2019). Identification of entacapone as a chemical inhibitor of FTO mediating metabolic regulation through FOXO1. *Sci. Transl. Med.* 11:aau7116. doi: 10.1126/scitranslmed.aau7116

Qiao, Y., Zhou, B., Zhang, M., Liu, W., Han, Z., Song, C., et al. (2016). A novel inhibitor of the obesity-related protein FTO. *Biochemistry* 55, 1516–1522. doi: 10.1021/acs.biochem.6b00023

Ries, R. J., Zaccara, S., Klein, P., Olarerin-George, A., Namkoong, S., Pickering, B. F., et al. (2019). m(6)A enhances the phase separation potential of mRNA. *Nature* 571, 424–428. doi: 10.1038/s41586-019-1374-1

Roundtree, I. A., and He, C. (2016). RNA epigenetics—chemical messages for posttranscriptional gene regulation. *Curr. Opin. Chem. Biol.* 30, 46–51. doi: 10.1016/j.cbpa.2015.10.024

Roundtree, I. A., Luo, G. Z., Zhang, Z., Wang, X., Zhou, T., Cui, Y., et al. (2017). YTHDC1 mediates nuclear export of N(6)-methyladenosine methylated mRNAs. *Elife* 6, 1–28. doi: 10.7554/eLife.31311

Sachse, G., Church, C., Stewart, M., Cater, H., Teboul, L., Cox, R. D., et al. (2018). FTO demethylase activity is essential for normal bone growth and bone mineralization in mice. *Biochim. Biophys. Acta Mol. Basis. Dis.* 1864, 843–850. doi: 10.1016/j.bbadis.2017.11.027

Scherer, H. U., Häupl, T., and Burmester, G. R. (2020). The etiology of rheumatoid arthritis. *J. Autoimmun.* 110:102400. doi: 10.1016/j.jaut.2019.102400

Schett, G. (2017). Autoimmunity as a trigger for structural bone damage in rheumatoid arthritis. *Mod. Rheumatol.* 27, 193–197. doi: 10.1080/14397595.2016.1265907

Scoles, D. R., and Pulst, S. M. (2018). Oligonucleotide therapeutics in neurodegenerative diseases. *RNA Biol.* 15, 707–714. doi: 10.1080/15476286.2018.1454812

Seth, S., Oberdörfer, L., Hyde, R., Hoff, K., Thies, V., Worbs, T., et al. (2011). CCR7 essentially contributes to the homing of plasmacytoid dendritic cells to lymph nodes under steady-state as well as inflammatory conditions. *J. Immunol.* 186, 3364–3372. doi: 10.4049/jimmunol.1002598

Shi, H., Wang, X., Lu, Z., Zhao, B. S., Ma, H., Hsu, P. J., et al. (2017). YTHDF3 facilitates translation and decay of N(6)-methyladenosine-modified RNA. *Cell Res.* 27, 315–328. doi: 10.1038/cr.2017.15

Shulman, Z., and Stern-Ginossar, N. (2020). The RNA modification N(6)-methyladenosine as a novel regulator of the immune system. *Nat. Immunol.* 21, 501–512. doi: 10.1038/s41590-020-0650-4

Siouti, E., and Andreakos, E. (2019). The many facets of macrophages in rheumatoid arthritis. *Biochem. Pharmacol.* 165, 152–169. doi: 10.1016/j.bcp.2019.03.029

Siva, C., and Brasington, R. D. (2001). Worsening of arthritis with antiretroviral therapy: the coexistence of rheumatoid arthritis and human immunodeficiency virus infection revisited. *J. Clin. Rheumatol.* 7, 42–46. doi: 10.1097/00124743-200102000-00010

Sparks, J. A., and Costenbader, K. H. (2014). Genetics, environment, and gene-environment interactions in the development of systemic rheumatic diseases. *Rheum. Dis. Clin. North Am.* 40, 637–657. doi: 10.1016/j.rdc.2014.07.005

Sun, H., Zhang, M., Li, K., Bai, D., and Yi, C. (2019). Cap-specific, terminal N(6)-methylation by a mammalian m(6)Am methyltransferase. *Cell Res.* 29, 80–82. doi: 10.1038/s41422-018-0117-4

Sun, W., Zhang, H., Wang, H., Chiu, Y. G., Wang, M., Ritchlin, C. T., et al. (2017). Targeting notch-activated M1 macrophages attenuates joint tissue damage in a mouse model of inflammatory arthritis. *J. Bone Miner Res.* 32, 1469–1480. doi: 10.1002/jbmr.3117

Thomas, R., Davis, L. S., and Lipsky, P. E. (1994). Rheumatoid synovium is enriched in mature antigen-presenting dendritic cells. *J. Immunol.* 152, 2613–2623.

Tian, C., Huang, Y., Li, Q., Feng, Z., and Xu, Q. (2019). Mettl3 regulates osteogenic differentiation and alternative splicing of Vegfa in bone marrow mesenchymal stem cells. *Int. J. Mol. Sci.* 20:551. doi: 10.3390/ijms20030551

Tirumuru, N., Zhao, B. S., Lu, W., Lu, Z., He, C., and Wu, L. (2016). N^6-methyladenosine of HIV-1 RNA regulates viral infection and HIV-1 Gag protein expression. *Elife*. 5:e15528. doi: 10.7554/eLife.15528

Tong, J., Cao, G., Zhang, T., Sefik, E., Amezcua, V. M., Broughton, J. P., et al. (2018). m^{6}A mRNA methylation sustains Treg suppressive functions. *Cell Res.* 28, 253–256. doi: 10.1038/cr.2018.7

Tsimikas, S. (2018). RNA-targeted therapeutics for lipid disorders. *Curr. Opin. Lipidol.* 29, 459–466. doi: 10.1097/MOL.0000000000000549

van Tran, N., Ernst, F., Hawley, B. R., Zorbas, C., Ulryck, N., Hackert, P., et al. (2019). The human 18S rRNA m^{6}A methyltransferase METTL5 is stabilized by TRMT112. *Nucleic Acids Res.* 47, 7719–7733. doi: 10.1093/nar/gkz619

Wang, H., Hu, X., Huang, M., Liu, J., Gu, Y., Ma, L., et al. (2019). Mettl3-mediated mRNA m(6)A methylation promotes dendritic cell activation. *Nat. Commun.* 10:1898. doi: 10.1038/s41467-019-09903-6

Wang, J., Wang, L., Diao, J., Shi, Y. G., Shi, Y., Ma, H., et al. (2020). Binding to m(6)A RNA promotes YTHDF2-mediated phase separation. *Protein Cell* 11, 304–307. doi: 10.1007/s13238-019-00660-2

Wang, J., Yan, S., Lu, H., Wang, S., and Xu, D. (2019). METTL3 Attenuates LPS-induced inflammatory response in macrophages via NF-κB signaling pathway. *Mediators Inflamm.* 2019: 3120391. doi: 10.1155/2019/3120391

Wang, R., Han, Z., Liu, B., Zhou, B., Wang, N., Jiang, Q., et al. (2018). Identification of natural compound radicicol as a potent FTO inhibitor. *Mol. Pharm.* 15, 4092–4098. doi: 10.1021/acs.molpharmaceut.8b00522

Wang, S., Sun, C., Li, J., Zhang, E., Ma, Z., Xu, W., et al. (2017). Roles of RNA methylation by means of N(6)-methyladenosine (m(6)A) in human cancers. *Cancer Lett.* 408, 112–120. doi: 10.1016/j.canlet.2017.08.030

Wehr, P., Purvis, H., Law, S. C., and Thomas, R. (2019). Dendritic cells, T cells and their interaction in rheumatoid arthritis. *Clin. Exp. Immunol.* 196, 12–27. doi: 10.1111/cei.13256

Wei, J., Liu, F., Lu, Z., Fei, Q., Ai, Y., He, P. C., et al. (2018). Differential m(6)A, m(6)A(m), and m(1)A demethylation mediated by FTO in the Cell nucleus and cytoplasm. *Mol Cell.* 71, 973–985.e5. doi: 10.1016/j.molcel.2018.08.011

Wei, W., Ji, X., Guo, X., and Ji, S. (2017). Regulatory Role of N(6) -methyladenosine (m(6) A) methylation in RNA processing and human diseases. *J. Cell Biochem.* 118, 2534–2543. doi: 10.1002/jcb.25967

Winkler, R., Gillis, E., Lasman, L., Safra, M., Geula, S., Soyris, C., et al. (2019). m(6)A modification controls the innate immune response to infection by targeting type I interferons. *Nat. Immunol.* 20, 173–182. doi: 10.1038/s41590-018-0275-z

Wu, Y., Xie, L., Wang, M., Xiong, Q., Guo, Y., Liang, Y., et al. (2018). Mettl3-mediated m(6)A RNA methylation regulates the fate of bone marrow mesenchymal stem cells and osteoporosis. *Nat. Commun.* 9:4772. doi: 10.1038/s41467-018-06898-4

Xiao, W., Adhikari, S., Dahal, U., Chen, Y. S., Hao, Y. J., Sun, B. F., et al. (2016). Nuclear m(6)A reader YTHDC1 regulates mRNA splicing. *Mol. Cell* 61, 507–519. doi: 10.1016/j.molcel.2016.01.012

Yin, H., Wang, H., Jiang, W., Zhou, Y., and Ai, S. (2017). Electrochemical immunosensor for N6-methyladenosine detection in human cell lines based on biotin-streptavidin system and silver-SiO(2) signal amplification. *Biosens. Bioelectron.* 90, 494–500. doi: 10.1016/j.bios.2016.10.066

Yoshimura, A., Naka, T., and Kubo, M. (2007). SOCS proteins, cytokine signalling and immune regulation. *Nat. Rev. Immunol.* 7, 454–465. doi: 10.1038/nri2093

Yu, R., Li, Q., Feng, Z., Cai, L., and Xu, Q. (2019). m^{6}A reader YTHDF2 regulates LPS-induced inflammatory response. *Int. J. Mol. Sci.* 20: 1323. doi: 10.3390/ijms20061323

Yue, Y., Liu, J., Cui, X., Cao, J., Luo, G., Zhang, Z., et al. (2018). VIRMA mediates preferential m(6)A mRNA methylation in 3′UTR and near stop codon and associates with alternative polyadenylation. *Cell Discov.* 4:10. doi: 10.1038/s41421-018-0019-0

Zhang, Q., Riddle, R. C., Yang, Q., Rosen, C. R., Guttridge, D. C., Dirckx, N., et al. (2019). The RNA demethylase FTO is required for maintenance of bone mass and functions to protect osteoblasts from genotoxic damage. *Proc. Natl. Acad. Sci. U.S.A.* 116, 17980–17989. doi: 10.1073/pnas.1905489116

Zhang, X., Wang, Y., Zhao, H., Han, X., Zhao, T., Qu, P., et al. (2020). Extracellular vesicle-encapsulated miR-22-3p from bone marrow mesenchymal stem cell promotes osteogenic differentiation via FTO inhibition. *Stem Cell Res. Ther.* 11:227. doi: 10.1186/s13287-020-01707-6

Zhang, Y., Gu, X., Li, D., Cai, L., and Xu, Q. (2019). METTL3 Regulates osteoblast differentiation and inflammatory response via Smad signaling and MAPK signaling. *Int. J. Mol. Sci.* 21:199. doi: 10.3390/ijms21010199

Zhang, Z., Chen, L. Q., Zhao, Y. L., Yang, C. G., Roundtree, I. A., Zhang, Z., et al. (2019). Single-base mapping of m(6)A by an antibody-independent method. *Sci. Adv.* 5:eaax0250. doi: 10.1126/sciadv.aax0250

Zheng, G., Dahl, J. A., Niu, Y., Fedorcsak, P., Huang, C. M., Li, C. J., et al. (2013). ALKBH5 is a mammalian RNA demethylase that impacts RNA metabolism and mouse fertility. *Mol. Cell* 49, 18–29. doi: 10.1016/j.molcel.2012.10.015

Zheng, Q., Hou, J., Zhou, Y., Li, Z., and Cao, X. (2017). The RNA helicase DDX46 inhibits innate immunity by entrapping m(6)A-demethylated antiviral transcripts in the nucleus. *Nat. Immunol.* 18, 1094–1103. doi: 10.1038/ni.3830

Zhu, W., Wang, J. Z., Xu, Z., Cao, M., Hu, Q., Pan, C., et al. (2019). Detection of **N^6**-methyladenosine modification residues (review). *Int. J. Mol. Med.* 43, 2267–2278. doi: 10.3892/ijmm.2019.4169

Zhuang, M., Li, X., Zhu, J., Zhang, J., Niu, F., Liang, F., et al. (2019). The m^{6}A reader YTHDF1 regulates axon guidance through translational control of Robo3.1 expression. *Nucleic Acids Res.* 47, 4765–4777. doi: 10.1093/nar/gkz157

Conflict of Interest: The authors declare that the research was conducted in the absence of any commercial or financial relationships that could be construed as a potential conflict of interest.

Copyright © 2021 Fan, Xia, Lu, Ye, Xi, Wang, Wang, Wang and Xiao. This is an open-access article distributed under the terms of the Creative Commons Attribution License (CC BY). The use, distribution or reproduction in other forums is permitted, provided the original author(s) and the copyright owner(s) are credited and that the original publication in this journal is cited, in accordance with accepted academic practice. No use, distribution or reproduction is permitted which does not comply with these terms.

frontiers in Cell and Developmental Biology

ORIGINAL RESEARCH
published: 21 January 2021
doi: 10.3389/fcell.2020.613891

Low Dose BMP2-Doped Calcium Phosphate Graft Promotes Bone Defect Healing in a Large Animal Model

Tie Liu[1,2†], Wen Fang[2,3†], Gang Wu[4], Yining Li[2,5], Janak L. Pathak[6] and Yuelian Liu[4*]*

[1] *Department of Oral Implantology, The Affiliated Hospital of Stomatology, School of Stomatology, Zhejiang University School of Medicine, Hangzhou, China,* [2] *Key Laboratory of Oral Biomedical Research of Zhejiang Province, Hangzhou, China,* [3] *Department of Periodontology, The Affiliated Hospital of Stomatology, School of Stomatology, Zhejiang University School of Medicine, Hangzhou, China,* [4] *Department of Oral Implantology and Prosthetic Dentistry, Academic of Dentistry Amsterdam (ACTA), VU Universiteit Amsterdam and University of Amsterdam, Amsterdam, Netherlands,* [5] *Department of Oral Pathology, The Affiliated Hospital of Stomatology, School of Stomatology, Zhejiang University School of Medicine, Hangzhou, China,* [6] *Guangzhou Key Laboratory of Basic and Applied Research of Oral Regenerative Medicine, Affiliated Stomatology Hospital of Guangzhou Medical University, Guangzhou, China*

OPEN ACCESS

Edited by:
Jiake Xu, University of Western Australia, Australia

Reviewed by:
Dietmar W. Werner Hutmacher, Queensland University of Technology, Australia
Katharina Schmidt-Bleek, Charité – Universitätsmedizin Berlin, Germany

***Correspondence:**
Janak L. Pathak
j.pathak@gzhmu.edu.cn
Yuelian Liu
y.liu@acta.nl

† These authors have contributed equally to this work and share first authorship

Specialty section:
This article was submitted to Molecular Medicine, a section of the journal Frontiers in Cell and Developmental Biology

Received: *04 October 2020*
Accepted: *21 December 2020*
Published: *21 January 2021*

Citation:
Liu T, Fang W, Wu G, Li Y, Pathak JL and Liu Y (2021) Low Dose BMP2-Doped Calcium Phosphate Graft Promotes Bone Defect Healing in a Large Animal Model. Front. Cell Dev. Biol. 8:613891. doi: 10.3389/fcell.2020.613891

Background: Bone grafts are in high demand due to the increase in the cases of bone defects mainly caused by trauma, old age, and disease-related bone damages. Tissue-engineered calcium phosphate (CaP) biomaterials match the major inorganic contents of bone, thereby could be the potential bone graft substitute. However, CaP-bone grafts lack the osteoinductivity that is vital for effective bone regeneration. In this study, we aimed to test the bone defect healing potential of biomimetically fabricated low dose BMP2-doped CaP (BMP2.BioCaP) grafts in a large animal model.

Methods: Low dose BMP2 was doped internally (BMP2-int.BioCaP) or on the surface of CaP (BMP2-sur.BioCaP) grafts during the fabrication process. Our previous study showed the robust bone regenerative potential of BMP2-int.BioCaP and BMP2-sur.BioCaP grafts in the rat ectopic model. In this study, we investigated the bone defect healing potential of BMP2.BioCaP grafts in sheep humerus/femoral defects, as well as compared with that of autologous bone graft and clinically used deproteinized bovine bone (DBB) xenograft.

Results: Different ways of BMP2 doping did not affect the surface morphology and degradation properties of the graft materials. Micro-CT and histology results showed robustly higher bone defect-healing potential of the BMP2.BioCaP grafts compared to clinically used DBB grafts. The bone defect healing potential of BMP2.BioCaP grafts was as effective as that of the autologous bone graft. Although, BMP2-int.BioCaP doped half the amount of BMP2 compared to BMP2-sur.BioCaP, its' bone defect healing potential was even robust. The BMP2.BioCaP grafts showed less immunogenicity compared to BioCaP or DBB grafts. The volume density of blood vessel-like and bone marrow-like structures in both BMP2.BioCaP graft groups were in a similar extent to the autologous group. Meticulous observation of higher magnification histological images showed active bone regeneration and remodeling during bone defect healing in BMP2.BioCaP graft groups.

Conclusion: The robust bone regenerative potential of BMP2.BioCaP grafts in the ectopic model and *in-situ* bone defects in small and large animals warrant the pre-clinical studies on large animal critical-sized segmental bone defects.

Keywords: bone regeneration, BioCaP graft, BMP2, osteoinduction, bone defect healing

INTRODUCTION

Large bone defects caused by trauma, fracture, tumor resection, infection, and congenital malformation substantially impact patient health and quality of life (Greenwald et al., 2001; Huang et al., 2016; Kumar et al., 2016). The global bone graft substitutes market was valued at US$ 2.9 Bn in 2019 and is anticipated to expand at a Compound Annual Growth Rate of ∼3% from 2020 to 2030 (Transperancy Market Research Report, 2020). Bone defect reconstruction is a complex biological process that involves proper bone grafts, a supply of precursor cells and growth factors, vascularization, immunomodulation, and osteogenesis (Greenwald et al., 2001; Huang et al., 2016). Therefore, the reconstruction of large bone defects is still a challenge for orthopedic and craniomaxillofacial surgeons. To treat a large bone defect, a functional bone graft must be implanted. Autografts are regarded as the gold standard for repairing bone defects; (Jung et al., 2003; Ferreira et al., 2013) however, their application is limited due to low graft availability and donor site morbidity (Nkenke et al., 2004). Alternative bone grafts such as allografts and xenografts are clinically used for critical size bone defect healing. Limited source, immunotoxicity, and risk of infection are the main limitations of these alternative bone grafts (Van Der Stok et al., 2011; Sun et al., 2019). Bone tissue engineering approaches are focused on developing novel biomaterials that address the limitations of conventional autogenic, allogenic, or xenogenic bone grafts.

The tissue-engineered ideal bone graft should be biocompatible, osteoconductive, osteoinductive, angiogenic, non-immunogenic, and biodegradable (Haugen et al., 2019). Recent advances in bone tissue engineering had developed 3D-prinetd biomaterial-based patient-specific scaffolds with enhanced biological and mechanical properties (Zhang et al., 2019). Synthetic scaffolds in combination with bioactive molecules or stem cells has shown promising potential for large size bone defect healing (Ho-Shui-Ling et al., 2018). Bone ingrowth pattern in synthetic scaffold directly correlates with the pore scale morphology and physical properties of the scaffolds (Jones et al., 2009). The primary inorganic component of bone is calcium phosphate (CaP), mainly the hydroxyapatite. CaP-based biomaterials including hydroxyapatite and beta-tricalcium phosphate had shown promising potential to be used as a bone graft (Samavedi et al., 2013). So far developed CaP-based bone grafts are reported to be biocompatible and osteoconductive, but they lack osteoinductivity. Doping osteogenic and/or angiogenic growth factors such as BMP2, VEGF, or FGF in biomaterials improves the bone regenerative potential of the bone grafts (Chim et al., 2013; Chen R. et al., 2016). Emerging pieces of literature had reported a robust bone defect healing potential of BMP2-loaded biomaterials (Selvig et al., 2002; Rao et al., 2013; Oortgiesen et al., 2014; Halloran et al., 2020). Although the Food and Drug Administration (FDA) approved usage of recombinant human BMP-2 (rhBMP-2) during spinal fusion surgery, tibial shaft repair, and maxillary sinus reconstructive surgery, series of systemic adverse effects were experienced during clinical application (Zhang et al., 2015; Halloran et al., 2020). Such systemic adverse effects of BMP2 applied for bone regeneration are mainly due to the burst released high dose BMP2 (James et al., 2016). Reducing the dose of doped BMP2 in graft materials and maintaining the slow and sustained release of low dose BMP2 in the defect site could minimize the systemic adverse effects of the BMP2. Moreover, the traditional CaP bone graft materials lack biomimicry and physicochemical properties required for bone defect healing (Fernandez-Yague et al., 2015). To overcome the above-mentioned issues, we had developed the BMP2-doped biomimetic CaP (BMP2.BioCaP) granules as a bone graft substitute with a robust bone defect healing potential (Liu et al., 2017; Wang et al., 2019).

The bone defect healing potential of the majority of the artificial bone grafts is usually tested in small animal models, which cannot represent the exact bone remodeling and bone properties in the human body. Large animal models, including sheep, dogs, and pigs, provide insights on the bone defect healing potential of artificial bone grafts in tibial and femoral bone defects with relevant clinical similarities to human bone defects (Weigand et al., 2017; Mcgovern et al., 2018). However, the differences in types of bone defects, animal models, surgical methods, and fixation procedures used in literature to test bone defect healing potential of bone grafts make it difficult to draw conclusions for clinical translation (Reichert et al., 2012). Among the large animal models, sheep bone properties and bone-remodeling rate are comparatively close to the human bone (Mcgovern et al., 2018; Hettwer et al., 2019). Moreover, sheep are less aggressive and easy to handle and house (Pearce et al., 2007; Reichert et al., 2012; Ingavle et al., 2019). Our previous studies had shown the bone defect healing potential of BMP2.BioCaP grafts alone or in combination with DBB in ectopic and critical size bone defects in murine models (Liu et al., 2014; Wang et al., 2017, 2019). Interestingly, BMP2.BioCaP grafts in the combination of DBB healed sheep humeral/femoral bone defect as effectively as the autologous bone graft (Liu et al., 2017). However, the bone defect healing potential of BMP2.BioCaP bone grafts alone in a large animal model has not been investigated yet.

Different methods of BMP2-doping incorporate the distinctive concentrations of BMP2 in bone grafts and affect the bioactivity of the grafts contrarily. We had developed BioCaP with an internal or surface biomimetic coating of BMP2. The

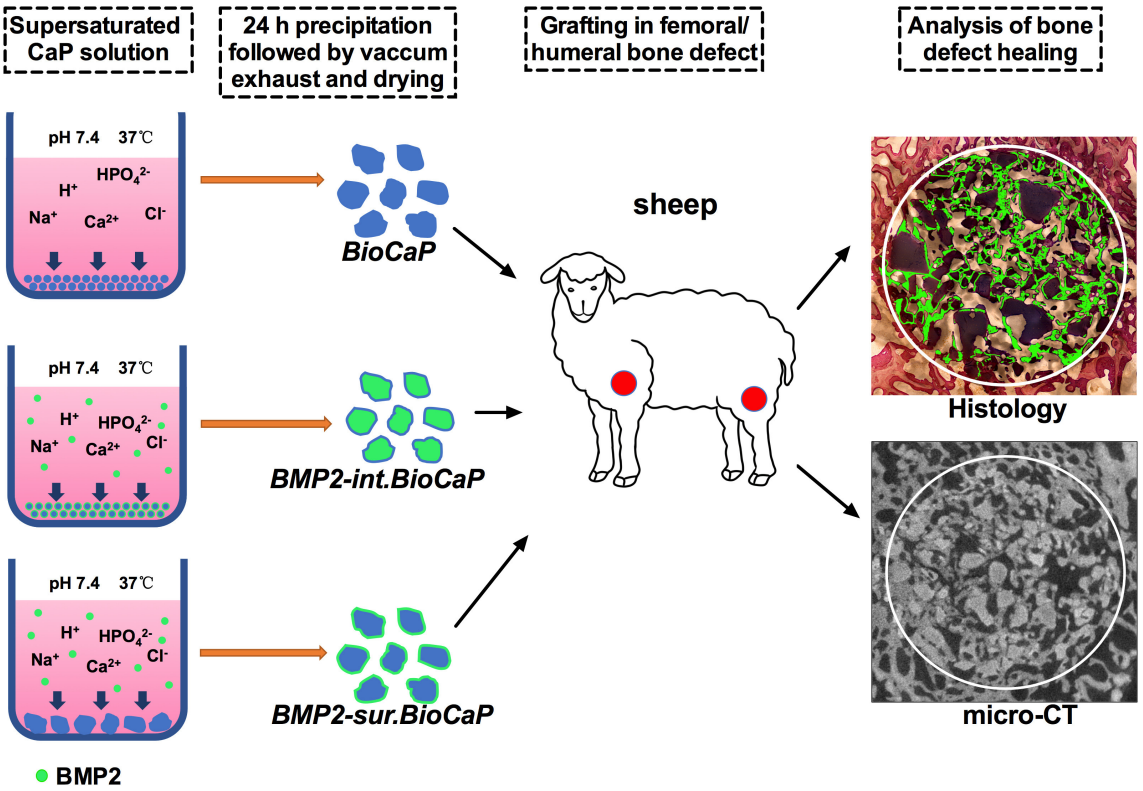


FIGURE 1 | Scheme of BMP2.BioCaP preparation and sheep femoral/humeral bone defect healing potential analysis.

internal or surface biomimetic coating of BMP2 osteogenically functionalizes the BioCaP grafts as indicated by the robust bone regeneration in ectopic transplantation (Liu et al., 2014). Moreover, BMP2 release from the bone graft is mainly controlled by the cellular activity around the graft. In this study, we aimed to further investigate the bone defect healing potential of BMP2.BioCaP grafts in a large animal model (sheep) as indicated in **Figure 1**. We also compared the bone defect-repairing efficacy of BMP2.BioCaP grafts with that of autologous bone graft and clinically used deproteinized bovine bone (DBB) xenograft. BMP2.BioCaP grafts (BMP2 internally or on surface coating) promoted bone defect healing in sheep as effectively as the autologous graft.

MATERIALS AND METHODS

Fabrication of Biomimetic Calcium Phosphate (BioCaP) Granules

Since the incubation of biomaterials in 5-fold concentrated simulated body fluid can deposit a CaP layer resembling the *in vivo* surface structure, this method is named as a biomimetic coating (Lin et al., 2020). BioCaP granule was fabricated by refining a well-established biomimetic mineralization process (Wang et al., 2019). Briefly, a CaP solution (200 mM HCl, 20 mM $CaCl_2{\cdot}2H_2O$, 680 mM NaCl, and 10 mM Na_2HPO_4) buffered by TRIS (250 mM) to a pH of 7.4 was incubated in a shaking water bath (50 agitations/min) at 37°C for 24 h. For sterilization, the CaP solution was filtered with the vacuum filter (0.22-μm pore) before buffering. Precipitation was retrieved and gently washed by Milli-Q water, strongly filtered and compressed to a block using a vacuum exhaust filtering method with a vacuum filter (0.22-μm pore, Corning, NY, USA) and an air pump. After drying in air circulation at room temperature for 2 h, the hardened block was ground and filtered through metallic mesh filters to obtain BioCaP granules with a size of 0.25–1.0 mm. All the procedures were performed under aseptic conditions.

Biomimetic Coating to Fabricate BMP2.BioCaP Grafts

BioCaP granules are osteoconductive but lack osteoinductive properties. A low dose of BMP2 was incorporated in BioCaP granules to obtain osteoconductive and osteoinductive BMP2.BioCaP graft materials. BMP-2 (INFUSE® Bone Graft, Medtronic, USA) was introduced into the CaP solution at a final concentration of 0.2 μg/ml before buffering and co-precipitated into the interior of BioCaP (BMP2-int.BioCaP), viz. the internally-incorporation mode. The doses of BMP2 and CaP solution were determined based on the results of our previous studies (Liu et al., 2014; Wei et al., 2019).

The superficial BMP2 coating was deposited on BioCaP granules according to the well-established biomimetic mineralization approach to obtain BMP2-sur.BioCaP (Liu

et al., 2014). Briefly, 0.58 g of BioCaP granules (size: 0.25–1 mm) was incubated in the coating solution [40 mM HCl, 4 mM $CaCl_2 \cdot 2H_2O$, 136 mM NaCl, 2 mM Na_2HPO_4, and 50 mM TRIS (pH 7.4); total volume of 150 ml] containing 1 μg/ml BMP2 in a shaking water bath (50 agitations/min) at 37°C for 24 h.

Quantification of Incorporated BMP-2

The amount of incorporated BMP-2 was determined by a commercially available BMP2 enzyme-linked immunosorbent assay (ELISA) kit (PeproTech, London, UK). BMP2-int.BioCaP and BMP2-sur.BioCaP (0.05 g/sample) were dissolved in 1 ml 0.5 M EDTA (pH 8.0) for 10 min in a 100-rpm stirrer. The ELISA assay was performed according to the manufacturer's instructions ($n = 6$/group). The BioCaP without BMP2 incorporation was used as a control.

Surface Characteristics and Protein Distribution in BioCaP Grafts

The morphology and surface characteristics of BMP2.BioCaP grafts were visualized in a scanning electron microscope (SEM, XL20, FEI Company, the Netherlands), under an accelerating voltage of 10 kV using sputter-coated with gold. To analyze the pattern of BMP2 protein distribution in BMP2.BioCaP, FITC-BSA was used as a mimic of BMP2 to incorporate in BioCaP and visualized under a fluorescence microscope as described previously (Liu et al., 2014).

In vivo BMP2.BioCaP Grafting in Bone Defect of Large Animal Model

Twelve Australian sheep (4 years old female, 40–50 kg body weight) were purchased from the Military Veterinary Institute, Quartermaster University of PLA, Changchun, China and housed at the Animal facility of Zhejiang University, Zhejiang, China. This study adapted the 4 years age sheep and defect model based on the previous literature (Nuss et al., 2006; Kobayashi et al., 2010; Liu et al., 2017). Sheep were anesthetized by administering Sumianxin II (0.3 ml/kg,) with the addition of penicillium (5×10^4 U/kg) and atropine (0.03 mg/kg) at 30 min before surgery. Local anesthesia (1% lidocaine with 1:100,000 adrenaline) and skin disinfection (0.5% iodophor solution) were applied to the proximal part of femoral diaphysis or proximal diaphysis of humerus or distal epiphysis of humerus. Six implantation sites/sheep were randomly chosen. Cylindrical defects (8 mm diameter and 13 mm deep) were created in the cancellous bone anatomical sites (proximal part of femoral diaphysis or proximal diaphysis of humerus or distal epiphysis of humerus) as described previously (Nuss et al., 2006; Liu et al., 2017). These implantation sites were assigned to the six experiment groups according to a randomization protocol (Wang et al., 2012). A total of 72 defect areas were used in this study with 36 each for 4 and 8 weeks (6 defects/group). This study was approved by the Ethical Committee of the School of Stomatology, Zhejiang University. All the animal experiments were carried out according to the ethics laws and regulations of P.R. China. Throughout the study, the sheep were treated following the ARRIVE guidelines. The following six groups were established to analyze the critical-sized bone defect healing potential of BMP2.BioCaP grafts.

TABLE 1 | Graft materials implanted in different experimental groups.

Group	Graft material (volume/graft)	Loaded BMP2/graft
(i) No graft	-	-
(ii) Autologous bone	0.65 cc	
(iii) DBB	0.65 cc (0.35 g)	-
(iv) BioCaP	0.65 cc (0.58 g)	-
(v) BMP2-sur.BioCaP	0.65 cc (0.58 g)	19.28 μg
(vi) BMP2-int.BioCaP	0.65 cc (0.58 g)	9.95 μg

(i) No graft (Negative control)
(ii) Autologous bone graft (Positive control)
(iii) DBB graft, bovine bone (Bio-Oss®) (Clinical standard control)
(iv) BioCaP graft
(v) BMP2-sur.BioCaP graft
(vi) BMP2-int.BioCaP graft

The amount of graft and incorporated BMP2 used in each group is elaborated in **Table 1**. In the case of autograft, the autologous bone was harvested during the creation of the defect and minced to 0.25–1 mm chips using a rongeur. After implantation of grafts, the Geistlich Bio-Gide® membrane (Geistlich Biomaterials, Wolhuser, Switzerland) was used to cover the defect. All sheep were allowed to walk in the confined plain grassland. One week after surgery all the sheep showed normal mobility. All the sheep exhibited good health and all the surgical implant sites healed well without any significant wound complication. No visual signs of inflammation or adverse host tissue reaction were observed. After 4 or 8 weeks of grafting, sheep were sacrificed by an overdose of intramuscular veterinary Sumianxin II (Jilin Huamu Animal Health Product, Jilin Province, China) injection. Bone grafts with surrounding tissues were retrieved and processed for histological and micro-CT analysis.

Micro Computed Tomography (Micro CT) Imaging and Quantification

Retrieved grafts with surrounding tissues were fixed in a 10% neutral buffered formalin solution and embedded into an MMA block as described previously (Liu et al., 2005; Wu et al., 2011). Three-dimensional distribution of BMP2.BioCaP graft with bone tissues in the bone defects was measured with a high-resolution micro CT system (μCT 40, Scanco Medical AG, Brüttisellen, Switzerland). Each specimen of the bone defect cylinder was positioned vertically and scanned with an isotropic spatial resolution of 18 μm and the beam energy 70 kV source voltage, 113 μA current, and an 18 μm isotropic voxel size. The specimens were mounted in cylindrical specimen holders (polyetherimide; outer diameter: 35.0 mm, wall thickness: 1.0 mm) and secured with synthetic foam to make sure the bone defect cylinder was vertical. The integration time of 750 ms was used to minimize noise. The system was equipped

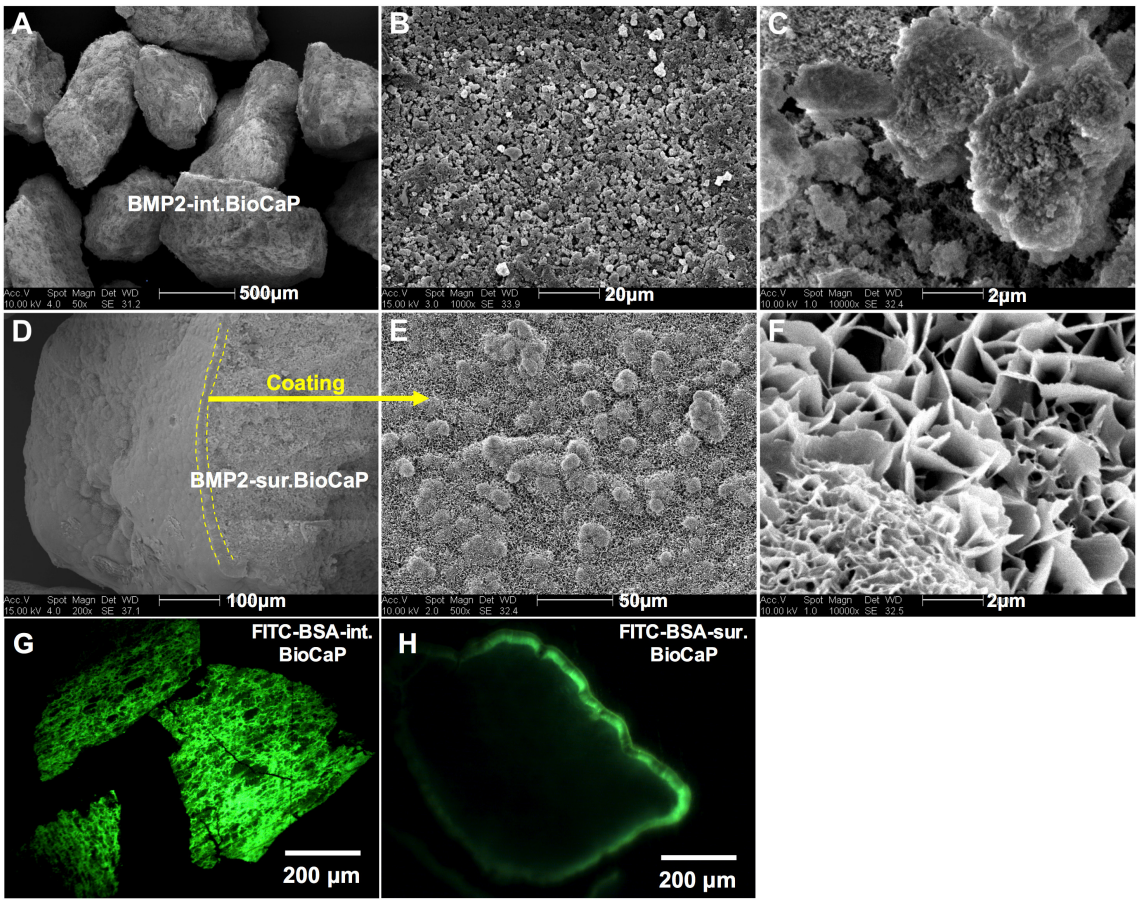


FIGURE 2 | Surface characteristic and morphology of BMP2.BioCaP grafts. Representative SEM images of BMP2-int.BioCaP **(A–C)** and BMP2-sur.BioCaP **(D–F)** from lower to higher magnification. Representative fluorescence images of FITC-BSA-int.BioCaP **(G)**, and FITC-BSA-sur.BioCaP **(H)**, showing the protein loading and distribution pattern.

with an aluminum filter and a correction algorithm to minimize beam-hardening artifacts (Mulder et al., 2006).

The gray values of each specimen, which depends on the radiopacity of the scanned material were converted into the degree of mineralization with the analysis software (Scanco Medical AG). Newly formed bone was distinguished from bone graft materials using the novel "onion-peeling" algorithm (Scanco Medical AG) (Schulten et al., 2013). Briefly, a low threshold of 560 mg hydroxyapatite (HA)/cm^3 was used to discriminate bone tissue from connective tissue and bone marrow. The gray values were scaled from 1 to 1,000 and the threshold was set at 200 to distinguish bone graft materials from newly formed bone tissue. These two thresholds were calculated by averaging the thresholds resolved in three slices of three samples by two blinded observers. Using this approach, we measured the bone volume/total volume in the bone grafts.

Histological Procedures

Retrieved grafts with surrounding tissues were fixed and embedded into an MMA block as described previously (Liu et al., 2005; Wu et al., 2011). The tissue embedded blocks were trimmed and sawn vertically to the long axis into 10–12 slices of 600 µm thickness at an interval of 1 mm applying a systematic random-sampling strategy (Gundersen and Jensen, 1987). Slices of each sample were separately mounted on plexiglass holders and polished. The slices were surface-stained with McNeal's tetrachrome, basic fuchsine, and toluidine blue (Wu et al., 2011) and examined with a light microscope with a digital camera (Leica, Wetzlar, Germany).

Histomorphometric Analysis

In addition to a subjective histological description, 10 slices of each graft were used for quantitative histomorphometric analysis including the volume of newly formed bone, bone marrow-like structure, remaining BioCaP, and the volume density of multinucleated giant cells (MGCs). The surface area (S) of a component per slice was obtained by two blinded observers using the point-counting technique in the whole area of 8 mm diameter of each slice (Cruz-Orive and Weibel, 1990). The interval between the two slices was 1 mm. Therefore, the volume (V) of a component is defined as $V = \sum_{n=1}^{10} (Sn \times 1)$.

TABLE 2 | Amount of BMP2 loaded in two type of BMP2.BioCaP grafts.

Sample number	Loaded BMP2 in BMP2-sur.BioCaP/graft (μg)	Loaded BMP2 in BMP2-int.BioCaP/graft (μg)
1	19.89	10.03
2	19.90	9.40
3	20.08	11.35
4	19.10	9.30
5	18.84	8.20
6	17.90	11.40
Average	**19.28**	**9.95**

The volume density of MGCs was normalized to the volume of BioCaP or DBB. The volume density of MGCs (Va) is defined as its volume (Vb) per unit volume of graft materials (Vc): Va = Vb/Vc. To evaluate the degradation of BioCaP granules, the volume of BioCaP before implantation (time 0, as control) was evaluated by the same histological method. Six chemically fixed and plastic-embedded samples (0.58 g of BioCaP granules per sample) were specifically reserved for this purpose.

Statistical Analysis

All data are presented as mean ± standard deviation (SD). Data were compared using one way analysis of variance (ANOVA), and Bonferroni's correction was used for *post-hoc* comparison. The significance level was set at $p < 0.05$.

RESULTS

In-vitro Characterization

BMP2.BioCaP grafts with random shape and 0.25–1.00 mm size were successfully synthesized. BMP2-int.BioCaP showed a homogeneous rough surface (**Figures 2A–C**). BMP2-sur.BioCaP showed the crystalline surface (**Figures 2D–F**). SEM images indicate that the biomimetic technique of BMP2 incorporation in BioCaP to develop BMP2.BioCaP graft did not affect the surface morphology (**Figures 2A,F**). The internal protein incorporation technique ensured the homogenous distribution of protein (green color) in the outer and inner part of the BioCaP (**Figure 2G**). In surface protein incorporated BioCaP, the protein was localized only on the periphery of the graft (**Figure 2H**). ELISA results indicated that BMP2-sur.BioCaP loaded 2 times higher dose of BMP2 (19.28 μg vs. 9.95 μg) compared to BMP2-int.BioCaP graft (**Table 2**).

Micro-CT Analysis

Figure 3 shows the micro-CT images of bone defects after 4 weeks of surgery. An almost empty defect was observed in the no graft group. The homogeneous distribution of graft materials was observed in all other groups (**Figure 3**). **Figure 4** shows the micro-CT images of bone defects after 8 weeks of surgery. The newly formed bone was observed in the periphery of the no graft group. In the autologous bone graft group, newly formed bone was observed in the center and periphery with some empty area. This empty area might be the result of faster degradation properties of autologous bone graft. In the synthetic bone graft groups, the faded white color indicates the newly formed bone and the sharp white color indicates the remaining graft materials (**Figure 4**). In DBB and BioCaP group, the defect area was mainly covered by graft materials and with a meager amount of newly formed bone. BMP2-sur.BioCaP and BMP2-int.BioCaP group showed a comparatively bigger area of newly formed bone.

Histological Analysis

Figures 5A–F represents the McNeal's tetrachrome, basic fuchsine, and toluidine blue stained histological images of tissue sections from bone defects at week 4. Histological images showed an empty defect in no graft group (**Figure 5A**). The newly formed bone surrounding the autologous graft was observed in the autologous bone graft group (**Figure 5B**). The newly formed bone was hardly observed in the DBB and BioCaP group (**Figures 5C,D**). Homogeneous distribution of newly formed bone surrounding the graft and in space between graft materials was observed in BMP2-sur.BioCaP and BMP2-int.BioCaP group. **Figures 5A1–F1** represents the histological images of tissue sections from bone defects at week 8. Histological images from 8 weeks showed a higher amount of newly formed bone in all the groups compared to images from 4 weeks of the respective group (**Figures 5A1–F1**). This result indicates the active bone regeneration process during bone defect healing. Newly formed bone was spotted only in the periphery of the defect in no graft group (**Figure 5A1**). The autologous bone graft group mainly showed newly formed bone with almost no remaining graft materials (**Figure 5B1**). Big areas of empty spaces were noticed in the autologous bone graft group, possibly due to the faster degradation nature of the autologous bone graft. The newly formed bone surrounding the graft material was also observed in the DBB and BioCaP group (**Figures 5C1,D1**). However, the area covered by newly formed bone in DBB or BioCaP group was less compared to BMP2.BioCaP or autologous group. This indicates the lack of osteoinductive properties in DBB or BioCaP grafts. A robust amount of new bone was formed surrounding the graft materials and in spaces between the graft materials in BMP2-sur.BioCaP and BMP2-int.BioCaP groups (**Figures 5E1,F1**). The results of histology images are per the results of micro-CT images (**Figures 3–5**).

Active Bone Regeneration and Bone Remodeling in BMP2.BioCaP Graft Groups

Figure 6 represents the higher magnification histological images of bone defects at week 4. No graft group was mainly covered with fibrous tissues at week 4. Robust osteogenesis around the graft and in space between the grafts was observed in the autologous bone graft group. DBB and BioCaP group showed sporadic thin layers of newly formed bone around the graft materials and in space between the grafts. Both the BMP2.BioCaP graft groups showed robust bone regeneration throughout the defect compared to the DBB or BioCaP group. **Figure 7** represents the higher magnification histological images of bone defects at week 8. Newly formed bone was hardly observed in the no graft group. The autologous graft group showed big areas

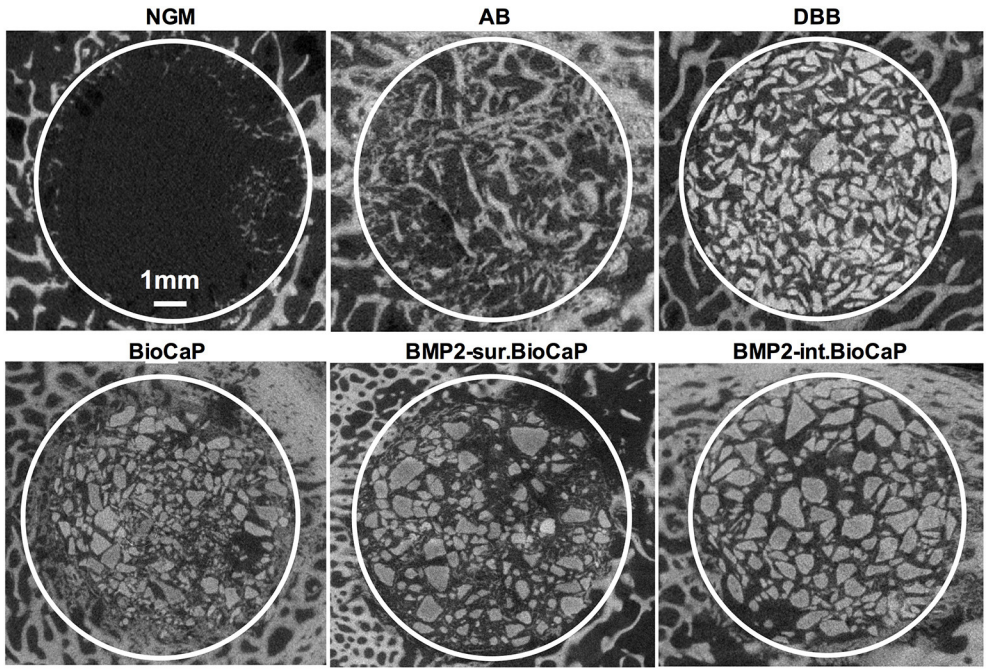


FIGURE 3 | Micro-CT images showing newly formed bone and grafted biomaterials in the defect site after 4 weeks of grafting.

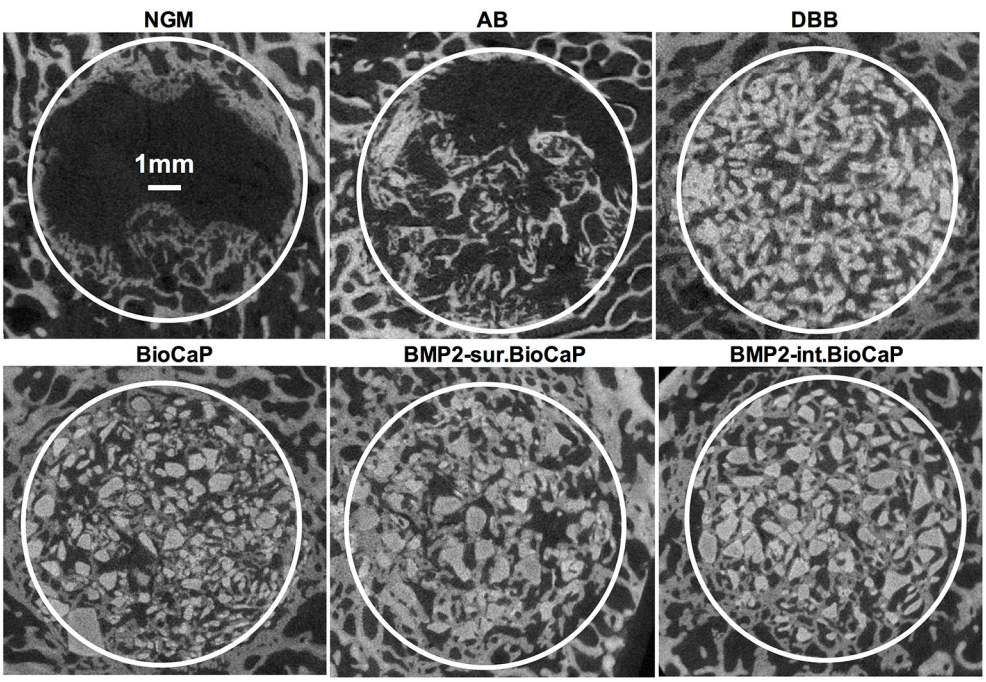


FIGURE 4 | Micro-CT images showing newly formed bone and grafted biomaterials in the defect site after 8 weeks of grafting.

of newly formed bone but no graft material was left. BMP2-sur.BioCaP and BMP2-int.BioCaP groups showed phenomenal bone regeneration compared to DBB or BioCaP group. All the groups with higher bone regeneration showed the woven bone. BMP2.BioCaP group showed the higher area with trabecular bone appearance, indicating active bone remodeling of woven bone in these groups. In both time points (week 4 and 8), it was difficult to recognize coating around the BMP2.BioCaP, indicating complete degradation of coating possibly by the effect of biological fluid or/and multinucleated giant cells.

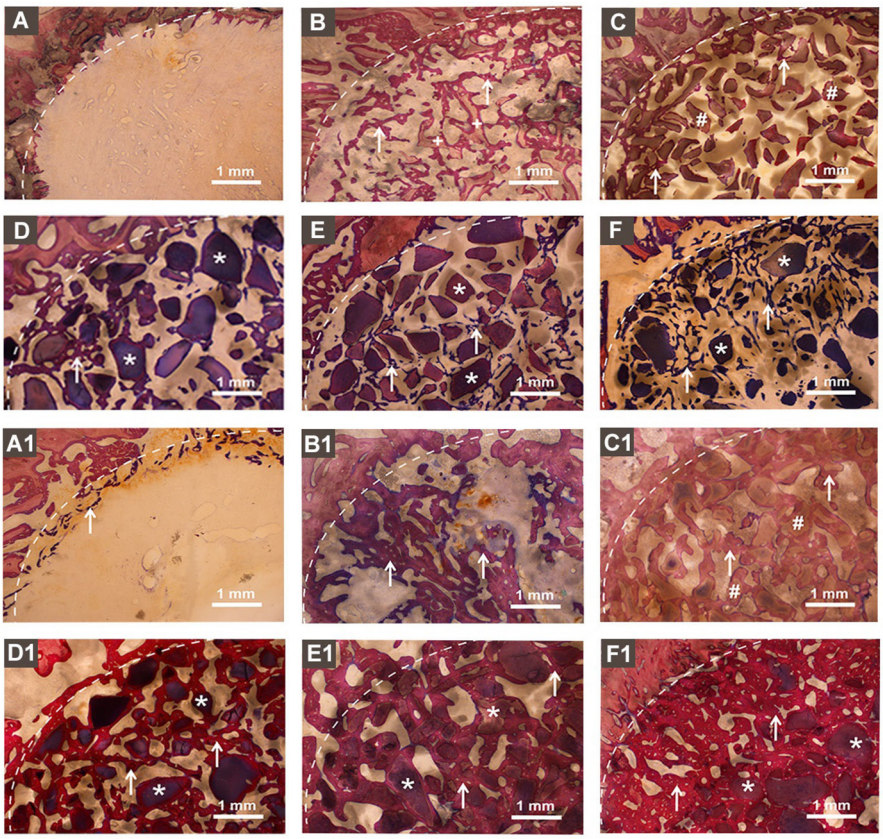


FIGURE 5 | Histological images in showing newly formed bone and remaining bone grafts. **(A)** no graft, **(B)** autologous bone, **(C)** DBB, **(D)** BioCaP, **(E)** BMP2-sur.BioCaP, and **(F)** BMP2-int.BioCaP after 4 weeks of grafting. **(A1)** no graft, **(B1)** autologous bone, **(C1)** DBB, **(D1)** BioCaP, **(E1)** BMP2-sur.BioCaP-group, and **(F1)** BMP2-int.BioCaP after 8 weeks of grafting. White dot line: demarcation between native bone and newly formed bone; white stars: remaining graft materials; +: remaining autologous bone; #: remaining DBB.

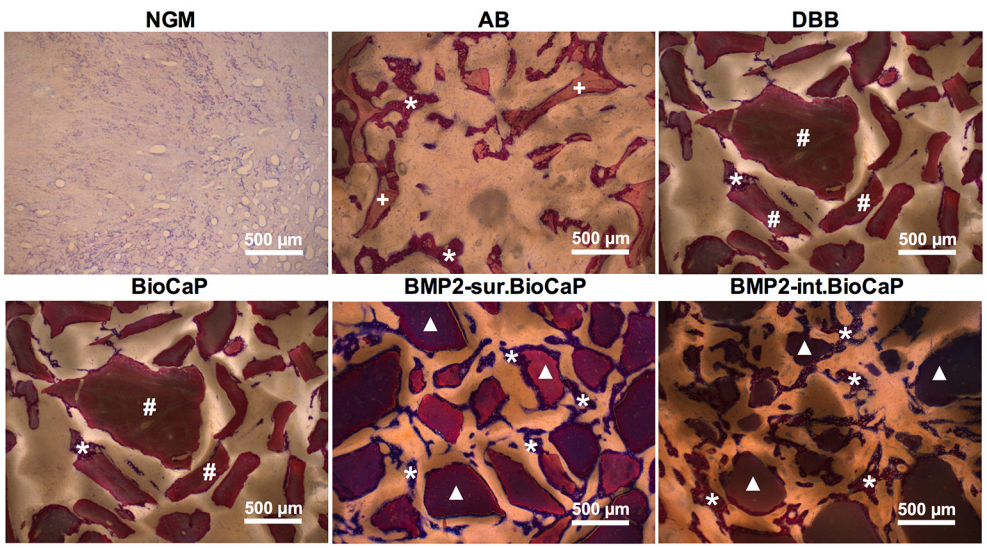


FIGURE 6 | Histological images in higher magnification showing newly formed bone and grafted biomaterials in the defect site after 4 weeks of grafting. White stars: remaining graft materials; +: remaining autologous bone; #: remaining DBB.

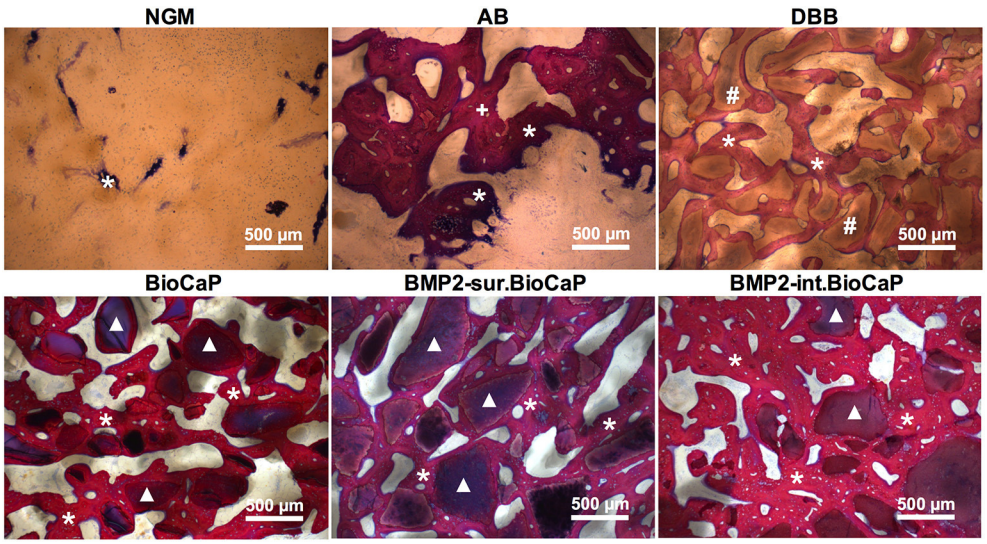


FIGURE 7 | Histological images in higher magnification showing newly formed bone and grafted biomaterials in the defect site after 8 weeks of grafting. White stars: newly formed bone; +: remaining autologous bone; #: remaining DBB.

Further high-resolution magnification of histological images indicated active bone regeneration and bone remolding activities at week 4 and 8. Representative histological images of BMP2.BioCaP grafts showed the presence of abundant cells, mainly mononuclear immune cells in the space between the graft materials (**Supplementary Figure 1**). At week 8, the number of mononuclear immune cells was reduced drastically. Chondrocytes and hypertrophic chondrocytes-like cells were observed in the newly formed bone area indicating the active endochondral ossification. Lining osteoblasts were observed on the surface of the newly formed bone. Moreover, osteocytes in lacunae and osteoids were observed inside the newly formed bone at week 8. Similarly, active multinucleated cells on the surface of newly formed bone indicate the active bone remodeling process during bone defect healing (**Supplementary Figure 2**). Bone marrow-like structures and blood vessel-like structures were observed in the space between the graft materials. Osteoclast-resorbed and bio-actively-degraded irregular edges were observed in the DBB, BioCaP, or BMP2.BioCaP grafts.

Quantitative Micro-CT and Histomorphometric Analysis

Quantitative micro-CT analysis was performed to analyze bone volume/total volume in the site of the defects at week 4 and 8 (**Figure 8A**). BMP2-int.BioCaP group at week 8 showed higher bone volume/total volume compared to DBB and BioCaP grafts. Bone volume/total volume in BMP2-sur.BioCaP and BMP2-int.BioCaP groups was to a similar extent to that of autologous bone graft group. Histomorphometric analysis was performed to quantify the volume density of newly formed bone, bone marrow-like structure, blood vessel-like structure, multinucleated giant cells, and graft material degradation % in the different materials grafted bone defects. Except in the no graft group, all other groups showed a higher volume density of newly formed bone at week 8 compared to the respective group at week 4 (**Figure 8B**). This result revealed that bone formation significantly increased with the implantation duration. The autologous bone group showed a significantly higher volume density of newly formed bone compared to DBB or BioCaP group at week 4 and 8. BMP2-sur.BioCaP and BMP2-int.BioCaP group showed 3.3-, and 3.7-fold higher volume density of newly formed bone respectively at week 4 compared to the DBB group. BMP2-sur.BioCaP and BMP2-int.BioCaP group had a similar degree volume density of newly formed bone with the autologous bone graft group at week 4 and 8. BMP2-int.BioCaP but not BMP2-sur.BioCaP enhanced bone regeneration compared to the BioCaP group at week 8, indicating the better osteoinductive properties of BMP2-int.BioCaP grafts. The results of quantitative micro-CT analysis on newly formed bone were in accordance with the results from the histomorphometric analysis (**Figures 8A,B**).

There was no bone marrow-like structure in the no graft group at week 4 and 8. In all other groups, the quantitative evaluation revealed a robust increase in the volume density of bone marrow-like structures at week 8 compared to the respective group at week 4. There was no difference in the volume density of bone marrow-like structures among the groups at week 4 (**Figure 8C**). The autologous graft group showed the highest volume density of bone marrow-like structures at week 8. BioCaP, BMP2-sur.BioCaP, or BMP2-int.BioCaP group showed a higher volume density of bone marrow-like structures compared to the DBB group at week 8. BioCaP and BMP2.BioCaP groups showed an almost similar degree of the volume density of bone marrow-like structures to the autologous group at week 8 (**Figure 8C**).

There was no significant difference in the volume density of newly formed blood vessel-like structures among the groups at week 4 or 8 (**Supplementary Figure 3A**). Multinucleated giant cells were hardly visualized in the no graft or autologous group at week 4 and 8. In the remaining four groups, the volume density of multinucleated giant cells significantly was reduced at week 8 compared to the respective group at week 4 (**Figure 8D**).

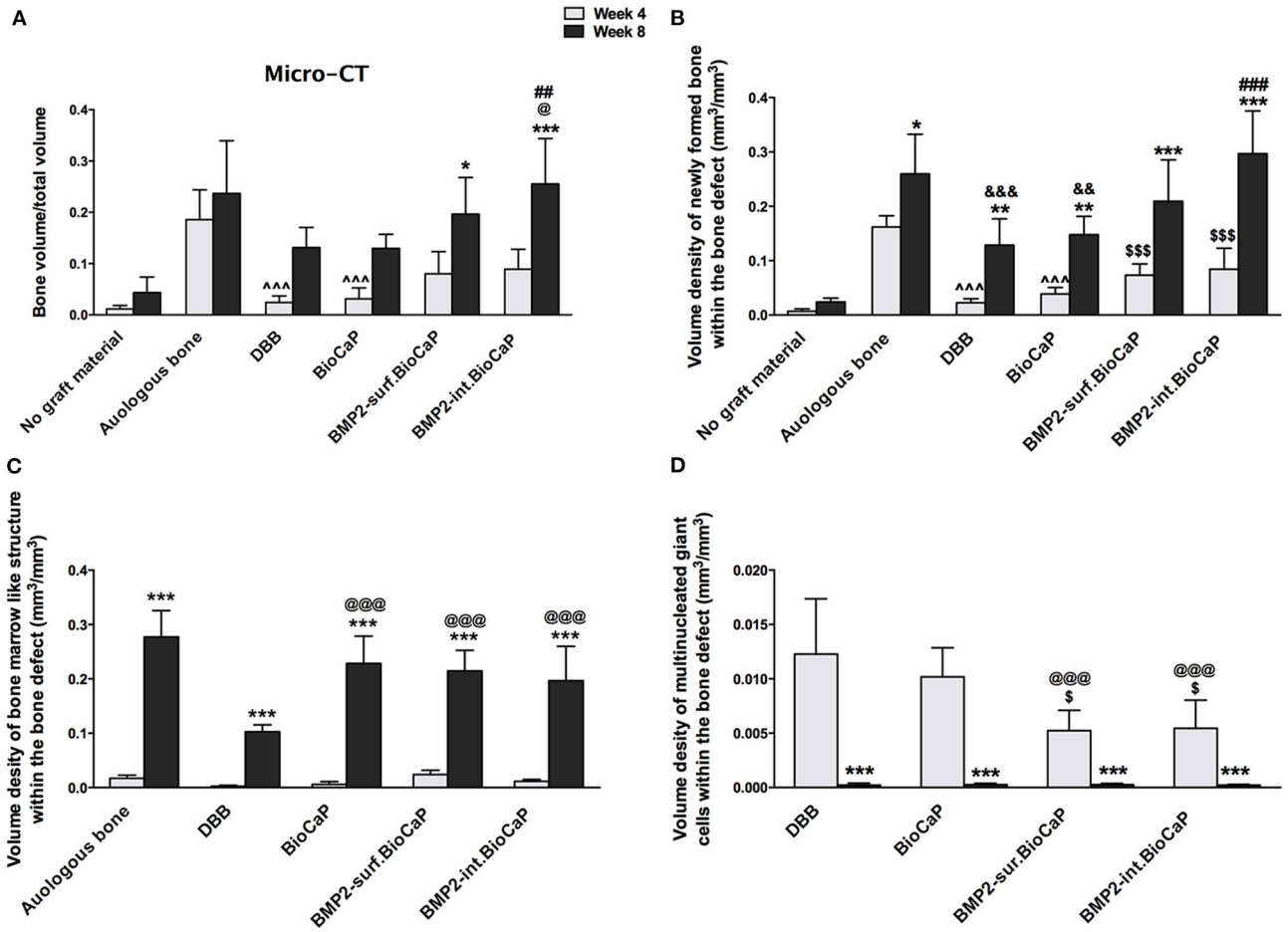


FIGURE 8 | (A) Bone volume/Total volume of newly formed bone analyzed from micro-CT data. Volume density of: **(B)** newly formed bone, **(C)** bone marrow-like structures, and **(D)** multinucleated giant cells analyzed form histological images. Data are presented as mean ± SD ($n = 6$). Significant difference compared to respective week 4-group, $^{*}p < 0.05$, $^{**}p < 0.01$, and $^{***}p < 0.001$; compared to BioCaP week 4-group, $^{\$}p < 0.05$ and $^{\$\$\$}p < 0.001$; compared to DBB week 8-group or week 4-group, $^{@}p < 0.05$, $^{@@@}p < 0.001$; compared to BioCaP week 8-group, $^{\#\#}p < 0.01$, $^{\#\#\#}p < 0.001$; compared to autologous bone week 4-group, $^{\wedge\wedge\wedge}p < 0.001$; compared to autologous bone week 8-group, $^{\&\&}p < 0.01$, $^{\&\&\&}p < 0.001$.

BMP2-sur.BioCaP or BMP2-int.BioCaP group showed a less volume density of multinucleated giant cells compared to DBB or BioCaP group at week 4, indicating less immunogenicity of BMP2.BioCaP grafts. In the autologous group, there was excessive degradation of graft materials at week 4 and almost no graft material was left at week 8. Among the other groups, there was no difference in the graft materials degradation % at week 4 and week 8 (**Supplementary Figure 3B**). The results of this study indicate the osteoconductive, robust osteoinductive, less immunogenic, and phenomenal bone regenerative potential of BMP2-sur.BioCaP and BMP2-int.BioCaP grafts. BMP2-int.BioCaP graft showed better bone defect healing potential than BMP2-sur.BioCaP.

DISCUSSION

Bone grafts are the second most implanted grafts due to the increase in the cases of bone defects mainly caused by trauma, old-age, and disease-related bone damages. Due to limited sources and other shortcomings of the autografts, allografts, or xenografts, the tissue-engineered biomaterials are being developed as an optional source of the bone grafts for clinical use. Advances in biomaterials had led to the development of osteogenic/angiogenic growth factors loaded tissue-engineered bone grafts. However, osteogenic bioactivity, biosafety, and local/systemic adverse effects are still key issues of synthetic bone grafts that need to be addressed. In this study, we tested the bone defect healing potential of biomimetically fabricated BMP2.BioCaP grafts (BMP2-sur.BioCaP and BMP2-int.BioCaP) in sheep humerus and femoral bone defects.

BMP2-sur.BioCaP and BMP2-int.BioCaP grafts doped ∼1000 and 500-fold less BMP2, respectively than used in clinics for bone regeneration (Block and Achong, 2006; Liu et al., 2017). Both Bone grafts showed robustly higher bone defect-healing potential compared to clinically used DBB grafts. The bone defect healing potential of BMP2.BioCaP grafts was as effective as that of the autologous bone graft. Although, BMP2-int.BioCaP graft doped half the amount of BMP2 compared to BMP2-sur.BioCaP graft, the bone defect healing potential of BMP2-int.BioCaP was even robust. Different ways of BMP2 doping did not affect

the surface morphology and degradation properties of the graft materials. The BMP2.BioCaP grafts showed less immunogenicity compared to BioCaP or DBB bone grafts. Bone defect sites were healed well without any significant wound complication, signs of inflammation, or adverse host tissue reactions. Our findings indicate the possibility of clinical application of biomimetically fabricated BMP2.BioCaP grafts.

Bone graft biomaterials directly interact with the precursor cells and affect cellular activity and differentiation (Gao et al., 2017). Similarly, the graft material-mediated immunogenicity modulates immune cells' function regulating inflammation in bone defect milieu (Chen Z. T. et al., 2016). Chemical remnants in grafts used for material synthesis can induce graft-related immunogenicity. Biomimetically synthesized biomaterials minimize the immunogenicity and graft material-related local/systemic adverse effects (Greenwald et al., 2001; Fernandez-Yague et al., 2015; Sun et al., 2019; Green et al., 2020). In this study, BMP2.BioCaP grafts were synthesized biomimetically as we reported previously (Liu et al., 2014, 2017; Wang et al., 2017, 2019). BMP2.BioCaP grafts showed less immunogenicity compared to DBB or BioCaP grafts as indicated by the fewer numbers of multinucleated giant immune cells around in BMP2.BioCaP grafts. Foreign body multinucleated giant cells resorb the graft materials and also remodel newly formed bone (Milde et al., 2015; Barbeck et al., 2017). Higher immunogenicity of graft materials triggered the formation of multinucleated cells and inflammatory cascade (Barbeck et al., 2017). In this study, the volume density of multinucleated giant cells was significantly higher in the DBB or BioCaP group compared to BMP2.BioCaP groups at week 4. This result is in accordance with the result from the previous study of ectopic and *in-situ* implantation of BMP2.BioCaP grafts (Liu et al., 2014, 2017). Since, there was no significant difference in the graft materials degradation among the DBB, BioCaP, or BMP2.BioCaP groups, the higher volume density of multinucleated giant cells in DBB or BioCaP might be associated with a higher degree of inflammation.

BMP2.BioCaP grafts give slow and sustained release of low dose BMP2 in the defect area and this release is mainly cellular activity-dependent (Liu et al., 2017). The robust bone regenerative and less immunogenic properties of BMP2.BioCaP grafts might be the effect of this BMP2 release phenomenon. Moreover, slow and sustained release of low dose BMP2 in the defect area might be responsible for the well-healed bone defects without any significant wound complication, signs of inflammation, or adverse host tissue reactions.

Active bone regeneration and bone remodeling are essential for the graft-mediated effective bone defect healing. Recruitment of osteogenic/endothelial precursor cells and immune cells to the graft material is inevitable for bone regeneration and remodeling process (Shi et al., 2016). BMP2.BioCaP graft group showed higher numbers of progenitor cells and immune cells at week 4. The density of immune cells and progenitor cells around the graft materials and newly formed bone was drastically reduced during week 8 of bone defect healing compared to week 4. This indicates the importance of early recruited progenitor cells and immune cells on bone defect healing. During bone defect healing, precursor cells undergo chondrogenic differentiation forming the cartilaginous soft callus that subsequently transfers to the mineralized-bone matrix via endochondral ossification (Nilsson Hall et al., 2020). In this study, we observed chondrocytes and hypertrophic chondrocyte-like structures in or nearby the newly formed bone. This result indicates the endogenous bone regenerative potential of BMP2.BioCaP grafts via endochondral ossification. A prominent number of osteoblast-like lining cells and multinucleated osteoclast-like cells on the surface of the newly formed bone in the BMP2.BioCaP grafts group indicate active bone remodeling. Moreover, A similar extent of the volume density of newly formed bone, bone marrow-like structure, and blood vessel-like structures in BMP2.BioCaP graft groups compared to that in autologous graft group suggests a highly active bone regenerative and bone remodeling potential of BMP2.BioCaP grafts during bone defect healing.

In this study, we analyzed the bone defect healing potential of BMP2.BioCaP grafts in a large animal model. Furthermore, we compared the bone defect healing potential of BMP2.BioCaP graft with the gold standard autologous bone graft and clinically used DBB bone graft. The bone defect healing potential of BMP2.BioCaP grafts was robustly superior compared to BioCaP or DBB graft, and as effective as that of autologous bone graft. Week 4 is the initial stage of new bone formation in the defects of the large animal model as shown by presence of precursor cells and a small amount of newly formed bone in BMP2.BioCaP and autologous bone graft groups. At week 8, the newly formed in mainly woven bone, which requires to undergo the major remodeling for 6–12 months to convert into real load-bearing bone (Hettwer et al., 2019). The use of femoral bone defect in 4 years old adult sheep model allowed us to investigate the biocompatibility, degradation, and bone regenerative potential of the BMP2.BioCaP grafts (Nuss et al., 2006). However, the bone volume, osteoid volume, and mineral apposition rate of 9–10 years old sheep resembles those of 60–70 years humans (Turner, 2001). Therefore, the preclinical study, using segmental bone defect in old age sheep analyzing the major bone remodeling for 6–12 months (Reichert et al., 2009; Hettwer et al., 2019), is further required to understand the bone defect healing potential of BMP2.BioCaP grafts. Early mechanical stimulation is necessary for timely bone defect healing (Tufekci et al., 2018). The current study lacks the role of mechanical stimulation in BMP2.BioCaP-mediated bone defect healing in sheep. The limitation of BMP2.BioCaP graft is the small size of each graft granule (0.25–1.0 mm) that is not suitable to graft in extra-large bone defect and load-bearing site such as segmental bone defects. It is difficult to custom design BMP2.BioCaP granules-based bone graft with a specific shape and certain mechanical strength. However, the biomimetic coating of BMP2.BioCaP on the surface of CaP-based 3D-printed scaffolds could osteogenically functionalize the large size bone grafts designed for critical size bone defects (Lin et al., 2020).

CONCLUSIONS

Biomimetically fabricated BMP2.BioCaP grafts reduce the clinical dose BMP2. BMP2.BioCaP grafts showed biocompatibility and robust bone regenerative potential in the ectopic model and in *in-situ* bone defects of small and large animals. Our results warrant the pre-clinical studies in critical

size segmental bone defect of large animals to access the bone defect healing potential of BMP2.BioCaP grafts.

DATA AVAILABILITY STATEMENT

The original contributions presented in the study are included in the article/**Supplementary Materials**, further inquiries can be directed to the corresponding authors.

ETHICS STATEMENT

The animal study was reviewed and approved by the Ethical Committee of School of Stomatology, Zhejiang University.

AUTHOR CONTRIBUTIONS

TL, WF, JP, and YL: study concept, design, and data interpretation. YL and TL: data acquisition and analysis. TL and WF: experiment and manuscript writing. GW: BMP2.BioCaP preparation and manuscript editing. All authors read and approved the submitted version.

FUNDING

This study was supported by National Natural Science Foundation of China (81500891), Zhejiang Provincial Natural Science Foundation of China (LQ15H140001), Osteology grant (2008-015), KNAW grant (08CDP043, 09CDP036, and 11CDP011), and High-Level University Construction Talents of Guangzhou Medical University of China (B185006003014 and B195002003017).

ACKNOWLEDGMENTS

We thank Daniel Wismeijer for his scientific input on the design of this project.

SUPPLEMENTARY MATERIAL

The Supplementary Material for this article can be found online at: https://www.frontiersin.org/articles/10.3389/fcell.2020.613891/full#supplementary-material

Supplementary Figure 1 | Histological images showing active bone regeneration process during 4 and 8 weeks of grafting in the BMP2-sur.BioCaP group. White star: newly formed bone; white triangle: remaining graft; black arrow: mononuclear immune cells; yellow arrow: chondrocytes and hypertrophic chondrocytes-like cells; green arrow: osteoblast lining cells.

Supplementary Figure 2 | Histological images showing active multinucleated giant cells, bone marrow-like, and blood vessel-like structures. White star: newly formed bone; white triangle: remaining graft; black arrow: active osteoclasts; yellow arrow: chondrocytes and hypertrophic chondrocytes-like cells; green arrow: osteoblast lining cells; pink arrow: resorbed graft material by active osteoclasts; M: bone marrow-like structure; V: blood vessel-like structure.

Supplementary Figure 3 | Quantitative analysis of volume density of blood vessels like structure **(A)**, and graft material degradation (%) **(B)**. Data are presented as mean ± SD ($n = 6$).

REFERENCES

Barbeck, M., Booms, P., Unger, R., Hoffmann, V., Sader, R., Kirkpatrick, C. J., et al. (2017). Multinucleated giant cells in the implant bed of bone substitutes are foreign body giant cells-New insights into the material-mediated healing process. *J. Biomed. Mater. Res. Part A* 105, 1105–1111. doi: 10.1002/jbm.a.36006

Block, M. S., and Achong, R. (2006). Bone morphogenetic protein for sinus augmentation. *Atlas Oral Maxillofac. Surg. Clin. North Am.* 14, 99–105. doi: 10.1016/j.cxom.2005.11.002

Chen, R., Wang, J., and Liu, C. S. (2016). Biomaterials act as enhancers of growth factors in bone regeneration. *Adv. Funct. Mater.* 26, 8810–8823. doi: 10.1002/adfm.201603197

Chen, Z. T., Klein, T., Murray, R. Z., Crawford, R., Chang, J., Wu, C. T., et al. (2016). Osteoimmunomodulation for the development of advanced bone biomaterials. *Materials Today* 19, 304–321. doi: 10.1016/j.mattod.2015.11.004

Chim, S., Tickner, J., Chow, S., Kuek, V., Guo, B., Zhang, G., et al. (2013). Angiogenic factors in bone local environment. *Cytokine Growth Factor Rev.* 24, 297–310. doi: 10.1016/j.cytogfr.2013.03.008

Cruz-Orive, L. M., and Weibel, E. R. (1990). Recent stereological methods for cell biology: a brief survey. *Am. J. Physiol.* 258, 148–156. doi: 10.1152/ajplung.1990.258.4.L148

Fernandez-Yague, M. A., Abbah, S. A., Mcnamara, L., Zeugolis, D. I., Pandit, A., and Biggs, M. J. (2015). Biomimetic approaches in bone tissue engineering: integrating biological and physicomechanical strategies. *Adv. Drug Deliv. Rev.* 84, 1–29. doi: 10.1016/j.addr.2014.09.005

Ferreira, J. R., Padilla, R., Urkasemsin, G., Yoon, K., Goeckner, K., Hu, W. S., et al. (2013). Titanium-enriched hydroxyapatite-gelatin scaffolds with osteogenically differentiated progenitor cell aggregates for calvaria bone regeneration. *Tissue Eng. Part A* 19, 1803–1816. doi: 10.1089/ten.tea.2012.0520

Gao, C., Peng, S., Feng, P., and Shuai, C. (2017). Bone biomaterials and interactions with stem cells. *Bone Res* 5:17059. doi: 10.1038/boneres.2017.59

Green, D. W., Stamboulis, A., and Ben-Nissan, B. (2020). Specifiable biomimetic microsponges for timed release of crystal entrapped biomolecules useful in bone repair. *J. Mater. Chem. B* 8, 7143–7148. doi: 10.1039/D0TB01491E

Greenwald, A. S., Boden, S. D., Goldberg, V. M., Khan, Y., Laurencin, C. T., Rosier, R. N., et al. (2001). Bone-graft substitutes: facts, fictions, and applications. *J. Bone Joint Surg. Am.* 83, 98–103. doi: 10.2106/00004623-200100022-00007

Gundersen, H. J., and Jensen, E. B. (1987). The efficiency of systematic sampling in stereology and its prediction. *J. Microsc.* 147, 229–263. doi: 10.1111/j.1365-2818.1987.tb02837.x

Halloran, D., Durbano, H. W., and Nohe, A. (2020). Bone morphogenetic protein-2 in development and bone homeostasis. *J. Dev. Biol* 8:19. doi: 10.3390/jdb8030019

Haugen, H. J., Lyngstadaas, S. P., Rossi, F., and Perale, G. (2019). Bone grafts: which is the ideal biomaterial? *J. Clin. Periodontol.* 46, 92–102. doi: 10.1111/jcpe.13058

Hettwer, W., Horstmann, P. F., Bischoff, S., Gullmar, D., Reichenbach, J. R., Poh, P. S. P., et al. (2019). Establishment and effects of allograft and synthetic bone graft substitute treatment of a critical size metaphyseal bone defect model in the sheep femur. *APMIS* 127, 53–63. doi: 10.1111/apm.12918

Ho-Shui-Ling, A., Bolander, J., Rustom, L. E., Johnson, A. W., Luyten, F. P., and Picart, C. (2018). Bone regeneration strategies: engineered scaffolds, bioactive molecules and stem cells current stage and future perspectives. *Biomaterials* 180, 143–162. doi: 10.1016/j.biomaterials.2018.07.017

Huang, R. L., Kobayashi, E., Liu, K., and Li, Q. (2016). Bone graft prefabrication following the *in vivo* bioreactor principle. *EBioMedicine* 12, 43–54. doi: 10.1016/j.ebiom.2016.09.016

Ingavle, G. C., Gionet-Gonzales, M., Vorwald, C. E., Bohannon, L. K., Clark, K., Galuppo, L. D., et al. (2019). Injectable mineralized microsphere-loaded composite hydrogels for bone repair in a sheep bone defect model. *Biomaterials* 197, 119–128. doi: 10.1016/j.biomaterials.2019.01.005

James, A. W., Lachaud, G., Shen, J., Asatrian, G., Nguyen, V., Zhang, X., et al. (2016). A review of the clinical side effects of bone morphogenetic protein-2. *Tissue Eng. Part B Rev.* 22, 284–297. doi: 10.1089/ten.teb.2015.0357

Jones, A. C., Arns, C. H., Hutmacher, D. W., Milthorpe, B. K., Sheppard, A. P., and Knackstedt, M. A. (2009). The correlation of pore morphology, interconnectivity and physical properties of 3D ceramic scaffolds with bone ingrowth. *Biomaterials* 30, 1440–1451. doi: 10.1016/j.biomaterials.2008.10.056

Jung, R. E., Glauser, R., Scharer, P., Hammerle, C. H., Sailer, H. F., and Weber, F. E. (2003). Effect of rhBMP-2 on guided bone regeneration in humans. *Clin. Oral Implants Res*. 14, 556–568. doi: 10.1034/j.1600-0501.2003.00921.x

Kobayashi, H., Turner, A. S., Seim, H. B. III, Kawamoto, T., and Bauer, T. W. (2010). Evaluation of a silica-containing bone graft substitute in a vertebral defect model. *J. Biomed. Mater. Res. A* 92, 596–603. doi: 10.1002/jbm.a.32397

Kumar, B. P., Venkatesh, V., Kumar, K. A., Yadav, B. Y., and Mohan, S. R. (2016). Mandibular reconstruction: overview. *J. Maxillofac. Oral Surg*. 15, 425–441. doi: 10.1007/s12663-015-0766-5

Lin, X., Chen, J., Liao, Y., Pathak, J. L., Li, H., and Liu, Y. (2020). Biomimetic calcium phosphate coating as a drug delivery vehicle for bone tissue engineering: a mini-review. *Coatings* 10:1118. doi: 10.3390/coatings10111118

Liu, T., Wu, G., Zheng, Y., Wismeijer, D., Everts, V., and Liu, Y. (2014). Cell-mediated BMP-2 release from a novel dual-drug delivery system promotes bone formation. *Clin. Oral Implants Res*. 25, 1412–1421. doi: 10.1111/clr.12283

Liu, T., Zheng, Y., Wu, G., Wismeijer, D., Pathak, J. L., and Liu, Y. (2017). BMP2-coprecipitated calcium phosphate granules enhance osteoinductivity of deproteinized bovine bone, and bone formation during critical-sized bone defect healing. *Sci. Rep*. 7:41800. doi: 10.1038/srep41800

Liu, Y., De Groot, K., and Hunziker, E. B. (2005). BMP-2 liberated from biomimetic implant coatings induces and sustains direct ossification in an ectopic rat model. *Bone* 36, 745–757. doi: 10.1016/j.bone.2005.02.005

Mcgovern, J. A., Griffin, M., and Hutmacher, D. W. (2018). Animal models for bone tissue engineering and modelling disease. *Dis. Model. Mech*. 11:dmm033084. doi: 10.1242/dmm.033084

Milde, R., Ritter, J., Tennent, G. A., Loesch, A., Martinez, F. O., Gordon, S., et al. (2015). Multinucleated giant cells are specialized for complement-mediated phagocytosis and large target destruction. *Cell Rep*. 13, 1937–1948. doi: 10.1016/j.celrep.2015.10.065

Mulder, L., Koolstra, J. H., and Van Eijden, T. M. (2006). Accuracy of MicroCT in the quantitative determination of the degree and distribution of mineralization in developing bone. *Acta Radiol*. 47, 882–883. doi: 10.1080/02841850600854944

Nilsson Hall, G., Mendes, L. F., Gklava, C., Geris, L., Luyten, F. P., and Papantoniou, I. (2020). Developmentally engineered callus organoid bioassemblies exhibit predictive *in vivo* long bone healing. *Adv. Sci*. 7:1902295. doi: 10.1002/advs.201902295

Nkenke, E., Weisbach, V., Winckler, E., Kessler, P., Schultze-Mosgau, S., Wiltfang, J., et al. (2004). Morbidity of harvesting of bone grafts from the iliac crest for preprosthetic augmentation procedures: a prospective study. *Int. J. Oral Maxillofac. Surg*. 33, 157–163. doi: 10.1054/ijom.2003.0465

Nuss, K. M., Auer, J. A., Boos, A., and Von Rechenberg, B. (2006). An animal model in sheep for biocompatibility testing of biomaterials in cancellous bones. *BMC Musculoskelet. Disord*. 7:67. doi: 10.1186/1471-2474-7-67

Oortgiesen, D. A., Walboomers, X. F., Bronckers, A. L., Meijer, G. J., and Jansen, J. A. (2014). Periodontal regeneration using an injectable bone cement combined with BMP-2 or FGF-2. *J. Tissue Eng. Regen. Med*. 8, 202–209. doi: 10.1002/term.1514

Pearce, A. I., Richards, R. G., Milz, S., Schneider, E., and Pearce, S. G. (2007). Animal models for implant biomaterial research in bone: a review. *Eur. Cell. Mater* 13, 1–10. doi: 10.22203/eCM.v013a01

Rao, S. M., Ugale, G. M., and Warad, S. B. (2013). Bone morphogenetic proteins: periodontal regeneration. *N. Am. J. Med. Sci*. 5, 161–168. doi: 10.4103/1947-2714.109175

Reichert, J. C., Cipitria, A., Epari, D. R., Saifzadeh, S., Krishnakanth, P., Berner, A., et al. (2012). A tissue engineering solution for segmental defect regeneration in load-bearing long bones. *Sci. Transl. Med*. 4:141ra193. doi: 10.1126/scitranslmed.3003720

Reichert, J. C., Saifzadeh, S., Wullschleger, M. E., Epari, D. R., Schutz, M. A., Duda, G. N., et al. (2009). The challenge of establishing preclinical models for segmental bone defect research. *Biomaterials* 30, 2149–2163. doi: 10.1016/j.biomaterials.2008.12.050

Samavedi, S., Whittington, A. R., and Goldstein, A. S. (2013). Calcium phosphate ceramics in bone tissue engineering: a review of properties and their influence on cell behavior. *Acta Biomater*. 9, 8037–8045. doi: 10.1016/j.actbio.2013.06.014

Schulten, E. A., Prins, H. J., Overman, J. R., Helder, M. N., Ten Bruggenkate, C. M., and Klein-Nulend, J. (2013). A novel approach revealing the effect of a collagenous membrane on osteoconduction in maxillary sinus floor elevation with beta-tricalcium phosphate. *Eur. Cell. Mater*. 25, 215–228. doi: 10.22203/eCM.v025a16

Selvig, K. A., Sorensen, R. G., Wozney, J. M., and Wikesjo, U. M. (2002). Bone repair following recombinant human bone morphogenetic protein-2 stimulated periodontal regeneration. *J. Periodontol*. 73, 1020–1029. doi: 10.1902/jop.2002.73.9.1020

Shi, J., Sun, J., Zhang, W., Liang, H., Shi, Q., Li, X., et al. (2016). Demineralized bone matrix scaffolds modified by CBD-SDF-1alpha promote bone regeneration via recruiting endogenous stem cells. *ACS Appl. Mater. Interfaces* 8, 27511–27522. doi: 10.1021/acsami.6b08685

Sun, X., Liu, C., Shi, Y., Li, C., Sun, L., Hou, L., et al. (2019). The assessment of xenogeneic bone immunotoxicity and risk management study. *Biomed. Eng. Online* 18:108. doi: 10.1186/s12938-019-0729-z

Transperancy Market Research Report (2020). Bone Graft Substitutes Market. (Albany, NY:Transparency Market Research).

Tufekci, P., Tavakoli, A., Dlaska, C., Neumann, M., Shanker, M., Saifzadeh, S., et al. (2018). Early mechanical stimulation only permits timely bone healing in sheep. *J. Orthop. Res*. 36, 1790–1796. doi: 10.1002/jor.23812

Turner, A. S. (2001). Animal models of osteoporosis–necessity and limitations. *Eur. Cell. Mater*. 1, 66–81. doi: 10.22203/eCM.v001a08

Van Der Stok, J., Van Lieshout, E. M. M., El-Massoudi, Y., Van Kralingen, G. H., and Patka, P. (2011). Bone substitutes in the Netherlands - a systematic literature review. *Acta Biomater*. 7, 739–750. doi: 10.1016/j.actbio.2010.07.035

Wang, D., Liu, Y., Liu, Y., Yan, L., Zaat, S. A. J., Wismeijer, D., et al. (2019). A dual functional bone-defect-filling material with sequential antibacterial and osteoinductive properties for infected bone defect repair. *J. Biomed. Mater. Res. A* 107, 2360–2370. doi: 10.1002/jbm.a.36744

Wang, D., Tabassum, A., Wu, G., Deng, L., Wismeijer, D., and Liu, Y. (2017). Bone regeneration in critical-sized bone defect enhanced by introducing osteoinductivity to biphasic calcium phosphate granules. *Clin. Oral Implants Res*. 28, 251–260. doi: 10.1111/clr.12791

Wang, J., Zheng, Y., Zhao, J., Liu, T., Gao, L., Gu, Z., et al. (2012). Low-dose rhBMP2/7 heterodimer to reconstruct peri-implant bone defects: a micro-CT evaluation. *J. Clin. Periodontol*. 39, 98–105. doi: 10.1111/j.1600-051X.2011.01807.x

Wei, L. F., Teng, F., Deng, L. Q., Liu, G. F., Luan, M. Y., Jiang, J., et al. (2019). Periodontal regeneration using bone morphogenetic protein 2 incorporated biomimetic calcium phosphate in conjunction with barrier membrane: a pre-clinical study in dogs. *J. Clin. Periodontol*. 46, 1254–1263. doi: 10.1111/jcpe.13195

Weigand, A., Beier, J. P., Schmid, R., Knorr, T., Kilian, D., Gotzl, R., et al. (2017). Bone tissue engineering under xenogeneic-free conditions in a large animal model as a basis for early clinical applicability. *Tissue Eng. Part A* 23, 208–222. doi: 10.1089/ten.tea.2016.0176

Wu, G., Hunziker, E., Zheng, Y., Wismeijer, D., and Liu, Y. (2011). Functionalization of deproteinized bovine bone with a coating-incorporated depot of BMP-2 renders the material efficiently osteoinductive and suppresses foreign-body reactivity. *Bone* 49, 1323–1330. doi: 10.1016/j.bone.2011.09.046

Zhang, L., Yang, G., Johnson, B. N., and Jia, X. (2019). Three-dimensional (3D) printed scaffold and material selection for bone repair. *Acta Biomater*. 84, 16–33. doi: 10.1016/j.actbio.2018.11.039

Zhang, M., Sara, J. D., Wang, F. L., Liu, L. P., Su, L. X., Zhe, J., et al. (2015). Increased plasma BMP-2 levels are associated with atherosclerosis burden and coronary calcification in type 2 diabetic patients. *Cardiovasc. Diabetol*. 14:64. doi: 10.1186/s12933-015-0214-3

Conflict of Interest: The authors declare that the research was conducted in the absence of any commercial or financial relationships that could be construed as a potential conflict of interest.

Copyright © 2021 Liu, Fang, Wu, Li, Pathak and Liu. This is an open-access article distributed under the terms of the Creative Commons Attribution License (CC BY). The use, distribution or reproduction in other forums is permitted, provided the original author(s) and the copyright owner(s) are credited and that the original publication in this journal is cited, in accordance with accepted academic practice. No use, distribution or reproduction is permitted which does not comply with these terms.

frontiers in Cell and Developmental Biology

ORIGINAL RESEARCH
published: 04 March 2021
doi: 10.3389/fcell.2021.628139

Downregulation of Macrophage-Specific Act-1 Intensifies Periodontitis and Alveolar Bone Loss Possibly via TNF/NF-κB Signaling

Janak L. Pathak[1†], Ying Fang[1†], Yunxin Chen[1], Zhitong Ye[1], Xueqi Guo[1], Yongyong Yan[1], Jun Zha[1], Dongliang Liang[1], Xiuxian Ke[1], Luxi Yang[1], Wenchao Zhong[1], Lijing Wang[1,2] and Liping Wang[1*]*

[1] Guangzhou Key Laboratory of Basic and Applied Research of Oral Regenerative Medicine, Affiliated Stomatology Hospital of Guangzhou Medical University, Guangzhou, China, [2] Vascular Biology Research Institute, School of Life Sciences and Biopharmaceutics, Guangdong Pharmaceutical University, Guangzhou, China

OPEN ACCESS

Edited by:
Changjun Li,
Central South University, China

Reviewed by:
Yanheng Zhou,
Peking University Hospital of Stomatology, China
Kai Sheng,
Central South University, China

***Correspondence:**
Liping Wang
wangliplj@126.com
Lijing Wang
2018991265@gzhmu.edu.cn

[†] These authors have contributed equally to this work and share first authorship

Specialty section:
This article was submitted to Molecular Medicine, a section of the journal Frontiers in Cell and Developmental Biology

Received: 11 November 2020
Accepted: 15 February 2021
Published: 04 March 2021

Citation:
Pathak JL, Fang Y, Chen Y, Ye Z, Guo X, Yan Y, Zha J, Liang D, Ke X, Yang L, Zhong W, Wang L and Wang L (2021) Downregulation of Macrophage-Specific Act-1 Intensifies Periodontitis and Alveolar Bone Loss Possibly via TNF/NF-κB Signaling. Front. Cell Dev. Biol. 9:628139. doi: 10.3389/fcell.2021.628139

Periodontitis is a chronic inflammatory oral disease that affects almost half of the adult population. NF-κB activator 1 (Act1) is mainly expressed in immune cells, including macrophages, and modulates immune cells' function to regulate inflammation in inflammatory diseases. Macrophages play a vital role in the pathophysiology of periodontitis. However, the effect of macrophage-specific Act1 on periodontitis has not been investigated yet. This study aims to unravel the role of macrophage-specific Act1 on the pathophysiology of periodontitis. The expression of Act1 in healthy and periodontitis periodontal tissue was confirmed by immunohistochemistry. Macrophage-specific Act1 expression downregulated (anti-Act1) mice were developed by inserting anti-Act1 antisense oligonucleotides after the CD68 promoter of C57BL/6 mice. Ligature-induced periodontitis (LIP) was induced in anti-Act1 mice and wildtype mice. Micro-CT, histology, and TRAP staining analyzed the periodontal tissue status, alveolar bone loss, and osteoclast numbers. Immunohistochemistry, RT-qPCR, and ELISA analyzed the inflammatory cells infiltration, expression of inflammatory cytokines, and M1/M2 macrophage polarization. mRNA sequencing of *in vitro* bacterial lipopolysaccharide (LPS)-treated peritoneal macrophages analyzed the differentially expressed genes in anti-Act1 mice during inflammation. Anti-Act1 mice showed aggravated periodontitis and alveolar bone loss compared to wildtype. Periodontitis-affected periodontal tissue (PAPT) of anti-Act1 mice showed a higher degree of macrophage infiltration, and M1 macrophage polarization compared to wildtype. Levels of pro-inflammatory cytokines (IL-1β, IL-6, and TNFα), and macrophage activity-related factors (CCL2, CCL3, and CCL4) were robustly high in PAPT of anti-Act1 mice compared to wildtype. mRNA sequencing and KEGG analysis showed activated TNF/NF-κB signaling in LPS-treated macrophages from anti-Act1 mice. *In vitro* studies on LPS-treated peritoneal macrophages from anti-act1 mice showed a higher

degree of cell migration and expression of inflammatory cytokines, macrophage activity-related factors, M1 macrophage-related factors, and TNF/NF-κB signaling related P-p65 protein. In conclusion, downregulation of macrophage-specific Act1 aggravated periodontitis, alveolar bone loss, macrophage infiltration, inflammation, and M1 macrophage polarization. Furthermore, LPS-treated macrophages from anti-Act1 mice activated TNF/NF-κB signaling. These results indicate the distinct role of macrophage-specific Act1 on the pathophysiology of periodontitis possibly via TNF/NF-κB signaling.

Keywords: periodontitis, NF-κB activator 1, macrophages, inflammation, alveolar bone loss

INTRODUCTION

Periodontitis is a bacterially induced chronic inflammatory disease of the periodontium (Darveau, 2010). Periodontitis affects more than half of the adult population in China, the United States, and Europe (Holtfreter et al., 2010; Hu et al., 2011; Eke et al., 2012; Zhang et al., 2014). Disrupted interaction between the host immune defense mechanism and the oral microorganisms are frequently observed in periodontitis (Hajishengallis, 2014). In periodontitis, pro-inflammatory cytokines produced by immune cells amplify inflammation cascades in the surrounding tissues that eventually cause tissue destruction and tooth loss (Darveau, 2010; Vos et al., 2012). Currently available therapeutic interventions for periodontitis only alleviate the disease intensity and progression rather than the complete cure of the disease (Graziani et al., 2017). Therefore, novel cost-effective therapeutic approaches to treat periodontitis are in high demand. Due to the complex nature of the disease, the molecular mechanisms involved in periodontitis pathophysiology are still not clear. Therefore, an in-depth study of the molecular mechanisms and signaling pathways involved in periodontitis is essential to establish novel therapeutic targets for cost-effective treatments.

Various cell signaling molecules play role in immune cell-mediated inflammation modulation. Li et al. (2000) reported the role of NF-κB activator 1 (Act1) in inflammation modulation in 2000. Act1 is an intracellular protein with a molecular weight of 60 kD containing 574 amino acids and mainly expressed by macrophages, B cells, and T Cells (Qian et al., 2002; Novatchkova et al., 2003). A notable feature of Act1 is that it contains a TRAF6 binding sequence. Act1 mediates the ubiquitination of TRAF6 through its U-box region, and then activates the TAK1 kinase and IKK kinase complex, thereby activating the transcription factor NF-κB (Liu et al., 2009). Act1 regulates inflammation by modulating immune cell functions in a disease-specific manner. In autoimmune encephalomyelitis and allergic lung inflammation mouse models, the Act1 knockout inhibits IL-17-mediated inflammation (Swaidani et al., 2009). Act1 knockout (KO) mice show high numbers of peripheral B cells eventually leading to lymphadenopathy, splenomegaly, hyperglobulinemia, and increased autoantibodies (Qian et al., 2008). The role of macrophage-specific Act1 in inflammatory disease periodontitis is still unknown.

In the early period of periodontitis, macrophages play an important role in the immune response of periodontitis by controlling the pathogenicity of periodontal biofilm and activating adaptive immunity (Sima et al., 2019). In addition, macrophages and osteoclasts have a similar origin, and under inflammatory conditions, macrophages can transform to M1 phenotype and osteoclasts (Kubatzky et al., 2018; Pereira et al., 2018). M1 type macrophages produce pro-inflammatory cytokines and aggravate periodontitis (Yang et al., 2018). While M2 macrophages produce anti-inflammatory cytokines to alleviate periodontitis (Veloso et al., 2020). Clinical and animal studies had reported the role of a higher periodontal M1/M2 macrophages ratio in the pathophysiology of periodontitis (Yang et al., 2018; Zhu et al., 2019; Veloso et al., 2020). However, the role of Act1 on M1 and M2 macrophage polarization during inflammatory conditions such as periodontitis has not been investigated yet.

In this study, we aimed to investigate the role of macrophage-specific Act1 on periodontitis pathophysiology. We developed ligature-induced periodontitis (LIP) in macrophage-specific Act1 expression downregulated (anti-Act1) mice and extensively analyzed the disease status, inflammation, and alveolar bone loss. We analyzed the mRNA sequencing in bacterial lipopolysaccharide (LPS)-treated peritoneal macrophages from anti-Act1 mice to investigate the differential expression of migration and inflammation-related genes. Cell migration and proinflammatory cytokines release in LPS-treated peritoneal macrophages from anti-Act1 mice were further analyzed *in vitro*. Our results revealed that the downregulation of macrophage-specific Act1 aggravates periodontitis, alveolar bone loss, inflammation, M1-polarization, and TNF/NF-κB signaling.

MATERIALS AND METHODS

Human Gingival Tissues Collection

Human gingiva, including sulcus/pocket epithelium and underlying connective tissue, were obtained from healthy controls ($n = 6$) during the wisdom tooth extraction. Patients with periodontitis with alveolar bone loss were confirmed by radiography and clinical observation. Gingival tissues from periodontitis patients ($n = 6$) were obtained during the treatment procedure of periodontitis. Patients and healthy controls' clinical

TABLE 1 | Clinical characteristics and periodontal status of healthy controls and periodontitis patients.

Gender/age	Simplified oral hygiene index (OHI-S)	Bleeding index (BI)	Tooth mobility (TM)	Probing depth (PD)/mm	Gingival recession (GR)/mm	Attachment loss (AL)/mm	Furcation index (FI)	Degree of periodontitis
Female/65	2	0–1	0	2	0	0	0	–
Male/65	2	0–1	0	2	0	0	0	–
Male/44	1	0	0	1–2	0	0	0	–
Female/43	1	0	0	2	0	0	0	–
Female/42	1–2	0–1	0	2	0	0	0	–
Male/40	1	0	0	2	0	0	0	–
Female/67	4	4	III°	6–8	4	4–6	II–III°	+++
Male/67	4	4	III°	6–8	4	4–6	II–III°	+++
Female/64	3	3–4	III°	7–8	3–4	5–7	III°	+++
Male/51	4	4	III°	8	4	6	III°	+++
Female/45	3	3	III°	7–8	3	5–6	II–III°	+++
Male/27	3	2–3	III°	6–7	2–3	4–5	II–III°	+++

$^{+++}$*specifies severe periodontitis.*

characteristics and demographics are summarized in **Table 1**. Written informed consent was obtained from each participant. The Medical Ethics Committee of the Affiliated Stomatology Hospital of Guangzhou Medical University approved all protocols dealing with patients.

Development of Anti-Act1 Mice

Wildtype mice were purchased from Guangdong Medical Animal Experiment Center (Guangdong, China). Anti-Act1 mice were obtained from Prof. Lijing Wang's lab, Vascular Biology Research Institute, School of Life Sciences and Biopharmaceutics, Guangdong Pharmaceutical University, Guangzhou 510006, China. Anti-Act1 mice were developed by inserting anti-Act1 antisense oligonucleotides after the CD68 promoter of C57BL/6 mice (Wang et al., 2019). CD68 promoter-based insertion of antisense oligonucleotides confirms mononuclear macrophage-specific antisense function. Antisense was used to cover the region from 100 bp before the ATG start region of the Act1 gene to 200 bp after ATG to establish C57BL/6 background antisense-Act1 (anti-Act1) gene-modified mice, which ultimately inhibits the transcription of the Act1 gene. The development of macrophage-specific anti-Act1 mice is illustrated in **Supplementary Figure 1**. Insertion of antisense was confirmed by PCR using forward primer: 5′-CTGGTGCAGACAGCCTAGCTG-3′; reverse primer: 5′-CCTGCGAGCTAAAGT CCTGGA-3′. The PCR product was separated in agarose gel electrophoresis and visualized using a gel imager (Gel Doc^{TM} XR+, BIO-RAD). The knockdown of macrophage-specific Act1 gene expression was confirmed by RT-qPCR in peritoneal macrophages. Primers used for RT-qPCR of Act1 are listed in **Table 2**.

Development of Ligature-Induced Periodontitis in Mice

A total of 50 wildtype C57/B16 and 50 anti-Act1 mice (8 weeks old, male, ∼25 g body weight) were used in this study. The Experimental Animal Ethics Committee of Guangzhou Medical University approved all animal care and study protocols (GY2020-001). Ligation-induced periodontitis was developed as described previously (Abe and Hajishengallis, 2013). Briefly, the mice were anesthetized by Isoflurane (RWD, Shenzhen, China) and fixed prone on the animal-specific fixed plate. The oral cavity was disinfected with 75% ethanol. A 5-0 silk thread (Johnson & Johnson, United States) was ligated around the left upper second molar and fixed with a surgical knot. All the knots were placed on the palatal side. After the ligation was completed, the mouse's tongue was slightly pulled out of the mouth and placed in a warmer place until the mouse wakes up. The mice were fed with normal chow and free drinking water. The silk thread fixation was examined every day after the ligation. If the silk threads were loose or the thread knots were incomplete, mice were excluded from the experiment. The day of ligation was

TABLE 2 | Primer used for RT-pPCR.

Gene	Primer sequence (5′–3′)
Act1	Forward: TCCCGTGGAGGTTGATGAATC
	Reverse: TCAGGGTGCCTTCTAAAGAAACT
Il-6	Forward: CTGCAAGAGACTTCCATCCAG
	Reverse: AGTGGTATAGACAGGTCTGTTGG
Il-1β	Forward: GAAATGCCACCTTTTGACAGTG
	Reverse: TGGATGCTCTCATCAGGACAG
Tnf-α	Forward: TGTCTCAGCCTCTTCTCATT
	Reverse: TGATCTGAGTGTGAGGGTCT
Ccl2	Forward: TTAAAAACCTGGATCGGAACCAA
	Reverse: GCATTAGCTTCAGATTTACGGGT
Ccl3	Forward: TTCTCTGTACCATGACACTCTGC
	Reverse: CGTGGAATCTTCCGGCTGTAG
Ccl4	Forward: TTCCTGCTGTTTCTCTTACACCT
	Reverse: CTGTCTGCCTCTTTTGGTCAG
Gapdh	Forward: GTGAAGGTCGGTGTGAACGG
	Reverse: TCCTGGAAGATGGTGATGGG

considered as day 0. After 7 days of ligation, mice were sacrificed by cervical dislocation. Periodontal tissue samples were collected and analyzed for changes in the pathophysiology of periodontitis.

Histology

For histology and immunohistochemistry, the left upper jaw, including teeth, periodontal tissues, and alveolar bone, was separated and the blood was washed out with PBS. The specimens were immediately fixed in 4% paraformaldehyde at room temperature for 16 h and immersed in 10% EDTA (pH 7.4) for 24 days for decalcification. Decalcified specimens were dehydrated and embedded in paraffin. Tissue sections of 3 μm thickness were obtained using a rotary microtome (Thermo Scientific™ HM 325, Thermo Fisher Scientific, Waltham, MA, United States). Tissue sections were stained with hematoxylin and eosin (H&E) staining. Images were captured using a light microscope (DM4000B-LED/DFC450, Leica, Wetzlar, Germany). The distance from the enamel-cementum boundary to the alveolar crest (CEJ-ABC) between the maxillary first and second molars was measured as a net bone loss on tissue sections, using Image J software (Wang et al., 2015).

Immunohistochemistry

Heat-induced antigen retrieval was performed in the tissue section as described previously (Xiao et al., 2017). Methanol containing 3% H_2O_2 was added on top of the tissue section for 20 min to block the endogenous peroxidase. Tissue sections were then blocked with 10% bovine serum albumin (BSA) and incubated with primary antibodies: anti-Act1 (bs6202R, BIOSS, China), anti-CD34 (ab81289, Abcam, Cambridge, United Kingdom), anti-CD45 (20103-1-AP, Proteintech, United States), anti-F4/80(70076, CST, United States) or isotope controls for overnight at 4°C. After 3 times washing with PBS, tissue sections were incubated with a corresponding anti-rabbit/anti-mouse secondary antibody for 30 min at 37°C. Mayer's hematoxylin was used as a counterstaining. Finally, all stained sections were dehydrated through a series of graded alcohol baths of increasing concentration, cleared in xylene, and mounted with coverslips. Stained tissue sections were visualized under a microscope (DM4000B-LED/DFC450, Leica, Wetzlar, Germany), and images were captured. The visual fields between the first molar and the second molar were photographed. The number of immunostaining-positive cells was counted in the entire area of each image.

TRAP Staining

To visualize the osteoclasts, tissue sections were stained using a tartrate acid phosphatase (TRAP) kit (G1050, Servicebio, Wuhan, China). TRAP-stained histological tissue sections were examined under a microscope, and images of predefined areas were captured. TRAP-positive osteoclasts in the alveolar bone tissue section between the first molar and the second molar were counted.

Micro CT Analysis

The left maxillary specimens fixed with paraformaldehyde were scanned by SkyScan1172 (Bruker-Micro-CT, Kontich, Belgium). The voxel resolution of the scanned volumes was 10 μm. Three-dimensional reconstruction was performed by SkyScan CTvox software after scanning. The SkyScan Dataviewer software was used to measure the buccal and palatal bone resorption heights of the maxillary second molars (Abe and Hajishengallis, 2013). The CEJ-ABC was regarded as the bone resorption height. The area of the same size at the bifurcation of the maxillary second molar was measured by SkyScan Dataviewer and CTAn software (version 1.17.7.2) for bone mineral density (BMD) analysis.

Flow Cytometry Analysis

The cell suspension was prepared from mice periodontal tissue, including gingiva, periodontal ligament, and a part of alveolar bone as described previously (Wang L. et al., 2020). The cell suspension was used for flow cytometry analysis (Mizraji et al., 2013). Prior to the test, cells were counted and cell viability was evaluated by the Zombie NIR™ Fixable Viability Kit (423105,Biolegend, Beijing, China). Cells were stained with 1 μg of PE anti-mouse F4/80 (123110, BioLegend, San Diego, CA, United States) solution, FITC anti-mouse/human CD11b (101206, BioLegend, San Diego, CA, United States), PerCP/Cyanine5.5 anti-mouse CD16/32 (101324, BioLegend, San Diego, CA, United States), APC anti-mouse CD206 (141707, BioLegend, San Diego, CA, United States) or anti-rabbit IgG per 1×10^6 cells for 30 min on ice in the dark. After two times washing with PBS, the cells were resuspended in 300 μl PBS and transferred to flow tubes. Flow cytometry analysis was performed using the FACSAria III Cell Sorter (BD Biosciences, San Jose, CA, United States). The mononuclear cells were sorted using anti-CD11b. From mononuclear cells, macrophages were sorted using anti-F4/80. And from macrophages, M1 and M2 macrophages were sorted using CD16/32 and CD 206, respectively.

Real-Time qPCR Analysis

The left maxillary specimen was kept in a dry cryotube, immersed in liquid nitrogen, and stored at −80°C. Frozen tissue was poured into a mortar pre-cooled with liquid nitrogen-containing 1 ml of lysis solution added with 1% β-thioethanol and quickly ground into the lysate. Total RNA was isolated from the lysate using the PureLink™ RNA Mini kit (Cat no.12183018A, Thermo Fisher Scientific, United States). RNA concentration and quality were measured in the NanoDrop spectrophotometer (NanoDrop2000, Wilmington, DE, United States). Total RNA was reverse-transcribed using Takara PrimeScript™ RT Master Mix in T100 Thermal Cycler (Bio-Rad, United States). Expressions of specific genes were analyzed by real-time qPCR (RT-qPCR) using Takara TB-Green Premix Ex Taq in the LightCycler RT-qPCR system (LC-480 II, Roche, Switzerland). Gapdh was used as a reference housekeeping gene. The $2^{-\Delta\Delta}$Ct method was used to analyze the relative mRNA expression levels. The primers used for RT-qPCR are listed in **Table 2**.

mRNA Sequencing

Peritoneal macrophage from wildtype and anti-Act1 mice was isolated and cultured as described previously

(Pineda-Torra et al., 2015). The macrophages were treated with 100 ng/ml bacterial LPS (tlrl-pglps LPS-PG, InvivoGen, United States) for 24 h to mimic *in vivo* inflammatory milieu. The cultures were used for RNA sequencing. Total RNA was extracted from peritoneal macrophage cell culture using the Trizol kit (Invitrogen, Carlsbad, CA, United States), according to the manufacturer's protocol. The RNA concentration was determined using Qubit, and the RNA amount and purity of each sample was assessed with a NanoDrop spectrophotometer. RNA was isolated in 40 μl of DEPC water and stored at −80°C. Briefly, RNA-seq libraries were prepared by using the Illumina Truseq^{TM} RNA sample prep Kit and were sequenced using an Illumina HiSeq. Cutadapt was used to obtain paired-end reads (Kechin et al., 2017). The reads were aligned with Hisat2 (v 2.1.0) to GRCm38 with default parameters (Kim et al., 2015). Only the data matched to the reference genome were used for subsequent analysis. The mapped reads of each sample were assembled using StringTie (Pertea et al., 2015). Then, the transcriptome from all samples was merged to reconstruct a comprehensive transcriptome using Perl scripts. After the final transcriptome was generated, StringTie (Pertea et al., 2015) and Ballgown (Frazee et al., 2015) were used to estimate the expression levels of all transcripts. Traditional singular enrichment analysis (SEA) was used for the enrichment analysis of Kyoto Encyclopedia of Genes and Genomes (KEGG) pathways (Rodriguez et al., 2016). The enrichment *p*-value calculation was performed with Fisher's exact test.

Enzyme-Linked Immunosorbent Assay

Enzyme-linked immunosorbent assay (ELISA) was performed to measure the protein expression in periodontal tissue protein extract, conditioned medium of mice macrophages culture, and mice macrophages cell lysates. The macrophages were treated with 100 ng/ml LPS for 24 h. The periodontal tissue cell lysate was prepared as described previously (Wang L. et al., 2020). Mice peritoneal macrophages were isolated as described previously (Kheirandish et al., 2018). On the first day of macrophages culture, 100 ng/ml LPS was added. After 24 h of LPS treatment, conditioned medium (CM) was collected, and attached cells in the culture harvested for cell lysate preparation. The protein levels of IL-6, IL-1β, and TNF-a in periodontal tissue protein extract and CM were measured by mouse ELISA Standard Kit (RayBiotech, Atlanta, United States). The protein levels of CD16/32, CD206, and MCP-I in cell lysates were measured by Mouse ELISA Standard Kit (Cusabio, Wuhan, China).

Western Blot Analysis

Cell lysates from peritoneal macrophages treated with 100 ng/ml LPS for 24 h were prepared using RIPA buffer containing protease PMSF and phosphatase inhibitor. The protein samples (20 μl) were separated by 10% SDS-PAGE and transferred onto polyvinylidene fluoride (PVDF) membranes (EMD Millipore, Billerica, MA, United States). PVDF membranes were blocked with 5% reconstituted dry milk at 37°C for 2 h and incubated with the primary antibody p-65 (1:10000 dilution, Cell Signaling Technology, Beverly, MA, United States), phosphorylated P-p65 (1:10000 dilution, Cell Signaling Technology) at 4°C overnight, followed by secondary antibodies (1:5000 dilution, Cell Signaling Technology) at room temperature for 1 h. Membranes were washed three times with TBS with 0.05% Tween-20. An enhanced chemiluminescence detection system BLT GelView 6000 Pro (BioLight, Guangdong, China) detected the immunoreactive protein bands. Protein expression levels were evaluated using β-actin as a loading control.

Macrophage Migration Assay

Cell migration assay was performed using Transwell chambers (8.0 μm pore size; Corning, United States). The peritoneal macrophages were trypsinized and cell suspension (1×10^6/ml) in DMEM medium with 10% FBS was prepared. Cell suspension (200 μl) was added in the upper chamber and add 700 μl of DMEM medium containing 10% FBS to the lower chamber to culture for 2 h. The upper chamber was replaced with the DMEM, 100 ng/ml LPS, and no FBS. The lower chamber was replaced with DMEM containing 10% FBS serum. After 24 h incubation, non-migrated cells in the upper chamber were removed with a cotton swab, and migrated cells were fixed in 4% paraformaldehyde and stained with 0.5% crystal violet. Photographs were taken randomly from five fields of each membrane. The number of invading cells was expressed as the average number of cells per microscopic field over five fields.

Statistical Analysis

All data are presented as mean ± standard deviation (SD). Statistical analysis was performed using GraphPad Prism 7.0 statistical software (GraphPad, San Diego, CA, United States). For where appropriate (comparison of two groups only), two-tailed *t*-tests were done. $p < 0.05$ was considered to indicate a statistically significant difference.

RESULTS

The Expression of Act1 in Periodontal Tissues and Macrophages

We examined the expression of Act1 in human gingival tissues from patients with periodontitis and age and sex-matched healthy individuals. Both periodontitis and healthy gingiva showed a similar extent of Act1 expression (**Figures 1A,B**). We further tested the expression pattern of Act1 in periodontal tissue of healthy and periodontitis mice. The result of Act1 expression in periodontal tissue of healthy and periodontitis mice was per the results from human gingiva (**Figures 1A–C**). Meticulous examination of histological images indicated that the Act1 is mainly expressed in the epithelium of healthy human gingiva and mice periodontitis-affected periodontal tissue (PAPT) (**Figure 1A**). However, Act1 expression was observed in both the epithelium and connective tissue of human gingiva and mice PAPT during periodontitis (**Figure 1A**).

We analyzed the macrophage-specific Act1 expression in human gingival tissue during periodontitis. Act1 was expressed

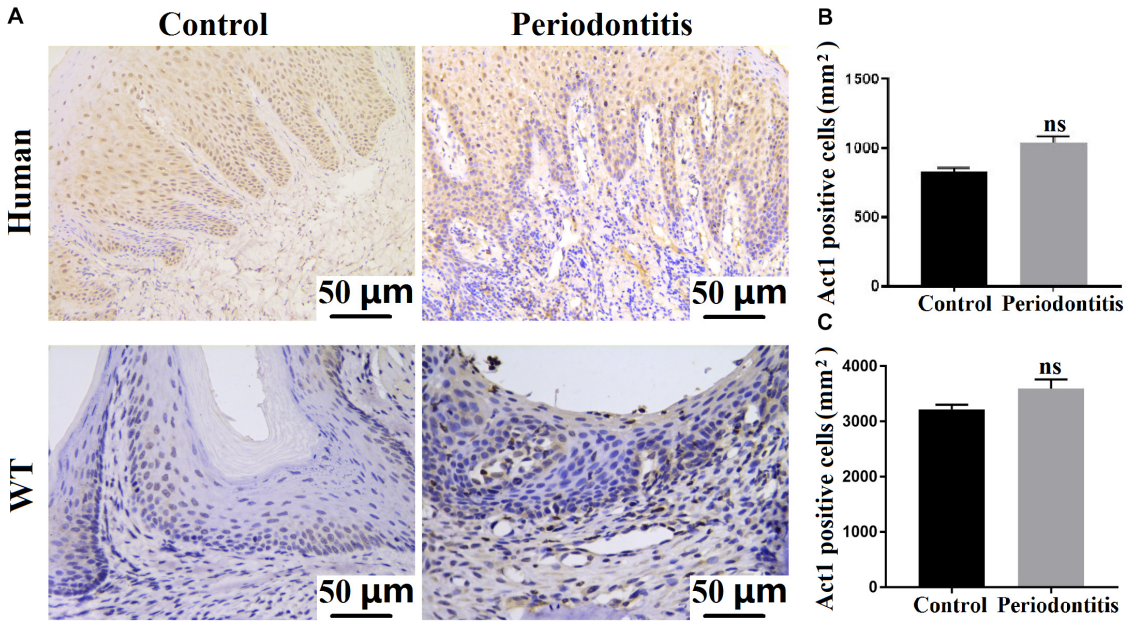


FIGURE 1 | Act1 is expressed in healthy and periodontitis gingival tissue. **(A)** Representative immunohistochemistry images of healthy/periodontitis gingival tissue (human and mice) show Act1 expression. Quantitative analysis of Act1 positive cells in healthy and periodontitis human gingival tissue **(B)**, and mice periodontal tissue **(C)**. Data are presented as mean ± SD ($n = 6$). WT, wildtype.

in macrophages infiltrated in gingiva during periodontitis (**Supplementary Figure 2A**). Immunofluorescence staining of mice peritoneal macrophages showed Act1 expression (**Supplementary Figure 2B**). Immunohistochemistry of mice PAPT also showed robust macrophage-infiltration (**Supplementary Figure 2C**).

Knockdown of Macrophage-Specific Act1 Aggravates Periodontitis

Act1 had been reported to play a vital role in various inflammatory diseases (Pisitkun et al., 2010; Swaidani et al., 2011; Doyle et al., 2012; Wang et al., 2013; Sakamuri et al., 2016). Furthermore, our results indicated Act1 expression in macrophages infiltrated in gingiva and PAPT during periodontitis. Therefore, we further analyzed the role of macrophage-specific Act1 in the pathophysiology of periodontitis. The expression of Act-1 in macrophages of anti-Act1 mice was downregulated by twofold (**Supplementary Figure 1B**). We induced periodontitis in wildtype and anti-Act1 mice and extensively analyzed the role of macrophage-specific Act1 in the pathophysiology of periodontitis.

Micro-CT images of periodontitis maxilla showed a higher degree of periodontal tissue and alveolar bone loss in anti-Act1 mice compared to wildtype mice (**Figure 2A**). CEJ-ABC distance increases with the degree of periodontitis. The CEJ-ABC distance in anti-Act1 periodontitis mice was 1.3-fold higher compared to wildtype periodontitis mice (**Figure 2B**). Alveolar bone mineral density was decreased by twofold in anti-Act1 periodontitis mice compared to wildtype periodontitis mice (**Figure 2C**). H&E stained histological images of PAPT showed a higher degree of periodontal tissue and alveolar bone loss in anti-Act1 periodontitis mice compared to wildtype periodontitis mice (**Figure 2D**). The gingival epithelium was intact in PAPT of wildtype mice. But, the gingival epithelium was degraded in PAPT anti-Act1 mice (**Figure 2D**). The result of periodontal tissue destruction and alveolar bone loss from histological analysis supports the findings from the micro-CT analysis. Moreover, the CEJ-ABC distance analysis from histological images was per the result analyzed from micro-CT images (**Figure 2E**). Higher osteoclast activity is responsible for alveolar bone loss during periodontitis. TRAP staining in PAPT histological tissue section revealed robustly higher numbers of osteoclasts in the anti-Act1 periodontitis-group (**Figure 2F**). Quantitative analysis of osteoclasts in the histological tissue section showed twofold higher numbers of osteoclasts in the anti-Act1 periodontitis mice compared to wildtype periodontitis mice (**Figure 2G**).

Knockdown of Macrophage-Specific Act1 Stimulates Macrophage Infiltration in PAPT

Angiogenesis in periodontal tissue is increased during periodontitis. CD34 expressing newly formed blood vessels were observed in PAPT of wildtype and anti-Act1 periodontitis mice (**Figure 3A**). However, there was no difference in microvessel density between these two groups (**Figure 3B**). Leukocyte infiltration in periodontal tissue is frequently observed in periodontitis. A similar degree of leukocyte infiltration was observed in PAPT of wildtype and anti-Act1 mice (**Figures 3A,C**). Macrophages are the key immune cells

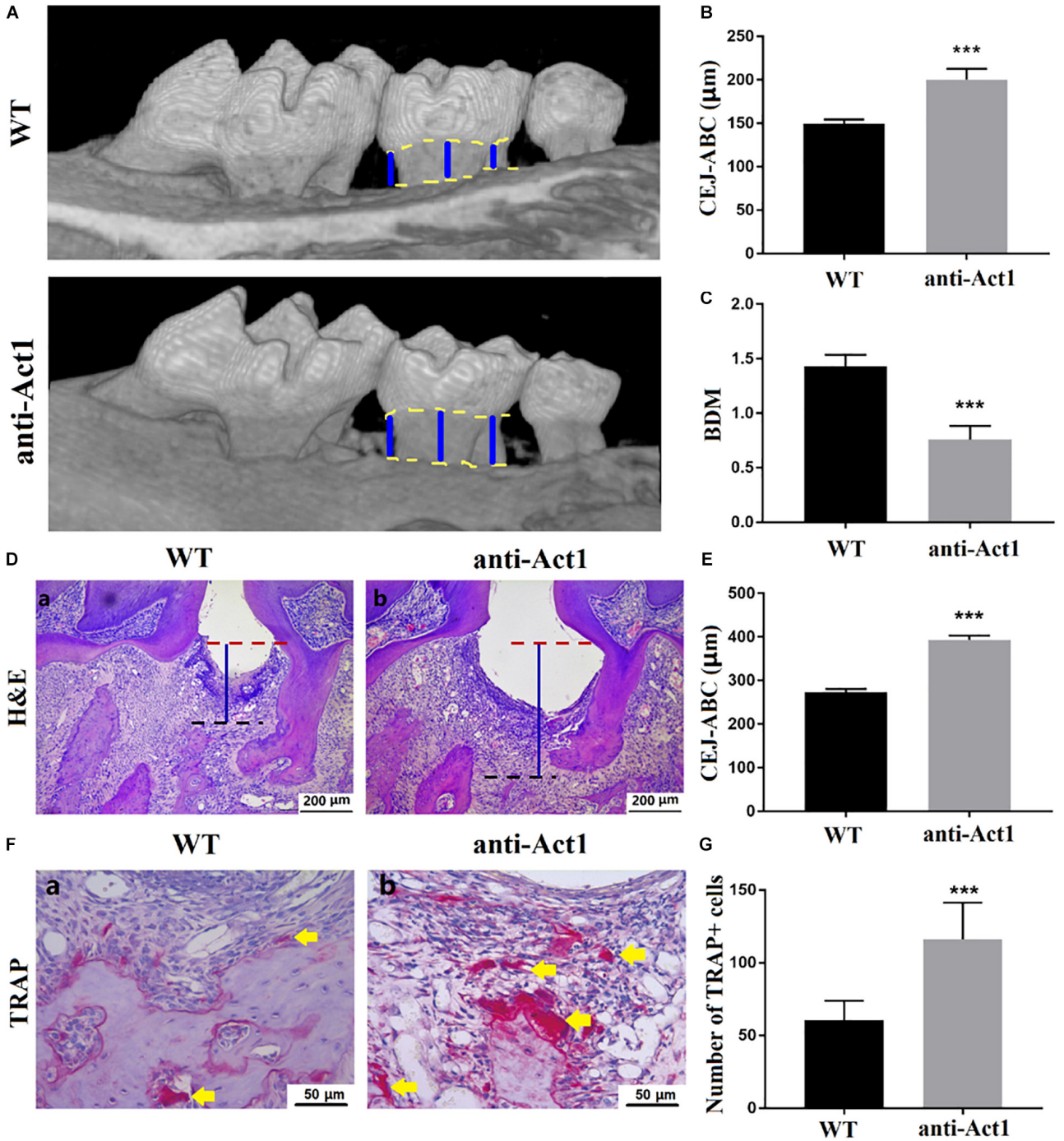


FIGURE 2 | Periodontitis and alveolar bone loss were aggravated in anti-Act1 mice compared to wildtype. **(A)** Micro-CT images of the healthy and periodontitis-affected maxilla of wildtype and anti-Act1 mice. Quantitative analysis of CEJ-ABC distance **(B)**, BMD **(C)** from micro-CT images. **(D)** H&E stained histological images of PAPT of wild-type and anti-Act1 mice. **(E)** Quantitative analysis of CEJ-ABC distance from histological images. **(F)** TRAP stained histological images of PAPT of wild-type and anti-Act1 mice. **(G)** Quantitative analysis of osteoclasts in PAPT. Data are presented as mean ± SD ($n = 6$). The significant difference between the groups, ***$P < 0.001$. CEJ, cement-enamel junction; ABC, alveolar bone crest; Red dot line, CEJ level; Black dot line, ABC level; blue line, CEJ-ABC distance; yellow arrow, osteoclasts; WT, wild-type; and BMD, bone mineral density.

involved in the pathophysiology of periodontitis. The number of macrophages infiltrated in PAPT was robustly high (twofold) in anti-Act1 mice compared to wildtype (**Figures 3A,D**). FACs analysis of mononuclear cells from PAPT also showed higher numbers (1.2-fold) of macrophages in PAPT of anti-Act1 mice compared to wildtype (**Figures 3E,F**).

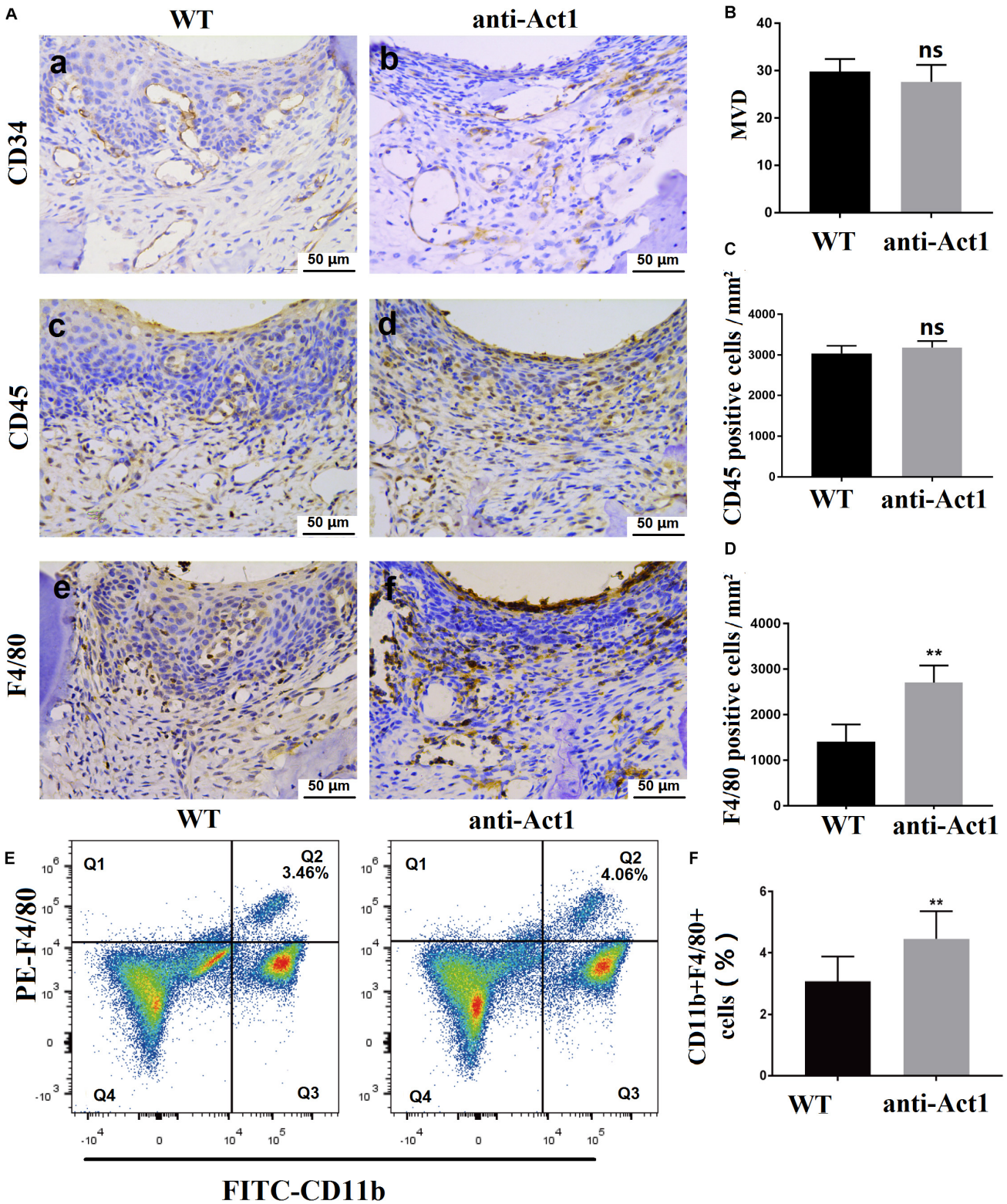


FIGURE 3 | Macrophage infiltration in PAPT was enhanced in anti-Act1 mice compared to wildtype. **(A)** Immunohistochemistry images of PAPT. Quantitative analysis of CD34 expressing MVD **(B)**, CD45 expressing pan leucocytes **(C)**, and F4/80 expressing macrophages **(D)**, $n = 6$. **(E)** FACs images of macrophages sorting using FITC-CD11b and PE-F4/80. **(F)** Quantitative FACs data. Calculated the ratio of CD11b + F4/80+ cells, $n = 8$. The significant difference between the groups, $^{**}P < 0.01$, ns, not significant. MVD, Microvessel density; WT, wildtype.

Anti-Act1 Mice Show Higher Expression of Proinflammatory Cytokines and Macrophage Migration-Specific Factors in PAPT

RT-qPCR of total RNA from PAPT tissue showed 2.3-fold higher expression of Il-6 in the anti-Act1 group compared to wildtype (**Figure 4A**). There was no significant difference on the mRNA expression of Il-1β between these groups (**Figure 4B**). Tnfα expression was 2.0-fold higher in PAPT of anti-Act1 mice compared to wildtype (**Figure 4C**). Ccl2, Ccl3, and Ccl4 are the macrophage migration markers. PAPT of anti-Act1 mice showed robustly higher mRNA expression of macrophage migration markers compared to wildtype (**Figures 4D–F**). Monocyte chemotactic protein 1 (MCP1 or CCL2), macrophage inflammatory protein 1 (MIP-1α or CCL3), and MIP-1β (CCL4) are crucial for macrophage migration/invasion and immune responses toward infection and inflammation. The expression of Ccl2, Ccl3, and Ccl4 in PAPT of anti-Act1 mice was, respectively, 2. 0-, 5. 0-, and 3.2-fold higher compared to wild type (**Figures 4D–F**). This result indicates the inflammation modulatory activity of macrophage-specific Act1 in periodontitis.

LPS-Treated Peritoneal Macrophages From Anti-Act1 Mice Show the Differential mRNAs Expression Pattern

mRNA sequencing was performed to analyze the effect of Act1 knockdown on differential expression of mRNAs in macrophages during inflammation. Peritoneal macrophages from anti-Act1 and wildtype mice were treated with LPS to mimic *in vivo* inflammatory conditions. A total of 1,344 mRNAs were differentially upregulated and 846 were differentially downregulated in LPS-treated macrophages from Act-1

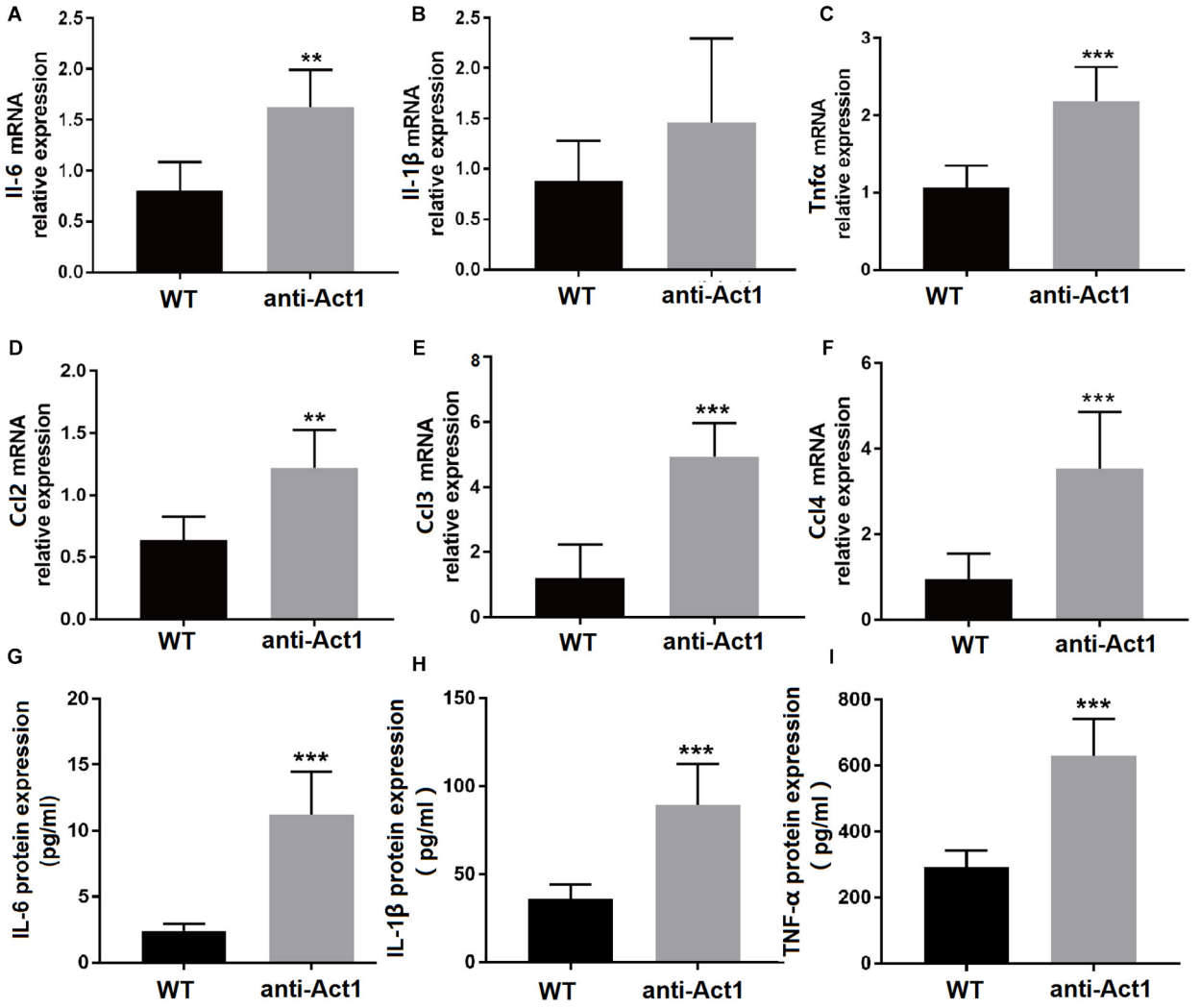


FIGURE 4 | (A–F) mRNA level expression of inflammatory cytokines and macrophage migration-related factors in PAPT of wildtype and anti-Act1 mice. **(G–I)** Protein level expression of inflammatory cytokines in PAPT of wildtype and anti-Act1 mice. Data are presented as mean ± SD ($n = 6$). The significant difference between the groups, $^{**}P < 0.01$, $^{***}P < 0.001$. WT, wildtype.

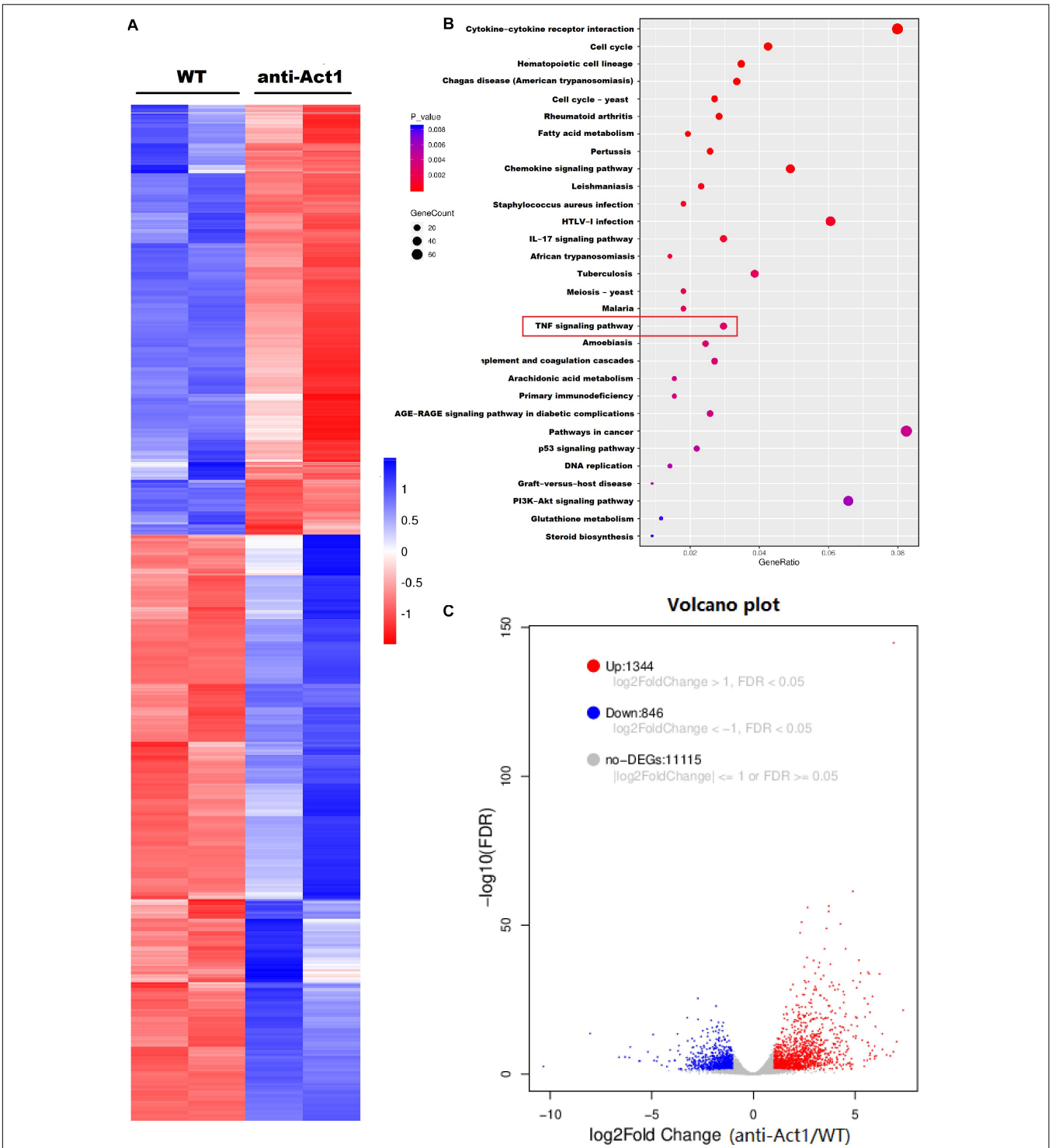


FIGURE 5 | Lipopolysaccharide -treated peritoneal macrophages from wildtype and anti-Act1 mice showed a differential expression of 2190 mRNAs. **(A)** Heat map, **(B)** KEGG pathway analysis, and **(C)** Volcano map showing differentially expressed mRNAs. Red color intensity indicates upregulation, and blue color intensity indicates the downregulation of mRNA expression.

knockdown mice compared to macrophages from wildtype mice (**Figure 5A**). **Figure 5B** indicates the KEGG pathway analysis from differentially expressed mRNAs identifying the affected signaling pathways. TNF-signaling plays a vital role in inflammation modulation in periodontitis via NF-κB signaling (Van Quickelberghe et al., 2018; Yang et al., 2020).

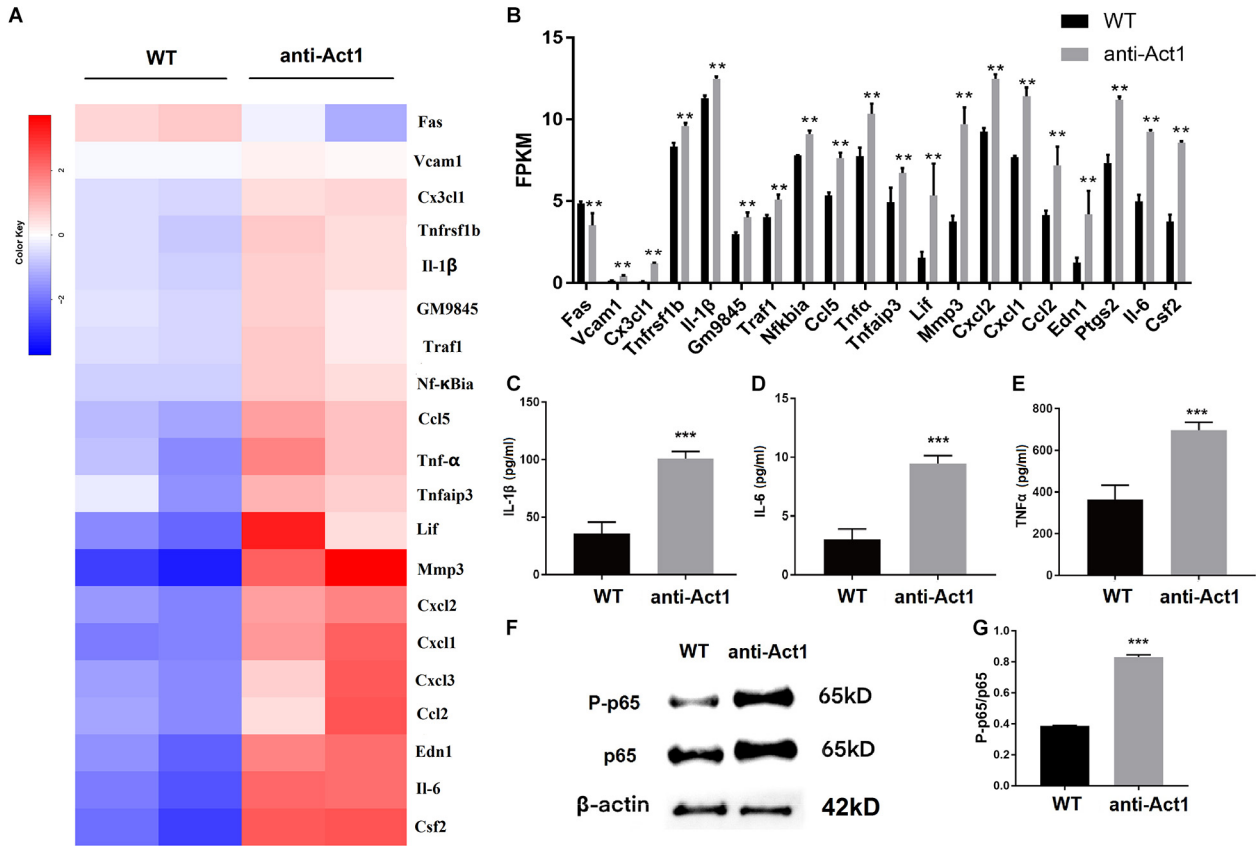


FIGURE 6 | Lipopolysaccharide -treated peritoneal macrophages from anti-Act1 mice differentially upregulate the mRNA expression of TNF-NF-κB signaling pathway-related proteins. **(A)** Heat map, and **(B)** bar figures showing differentially upregulated mRNAs. **(C–E)** Protein level expressions of inflammatory cytokines in LPS-treated peritoneal macrophages from wildtype and anti-Act1 mice (measured by ELISA), $n = 6$. **(F)** Representative western bolt images of p65 and P-p65 expression. **(G)** Quantification of western blots ($n = 3$). Data are presented as mean ± SD ($n = 6$). The significant difference between the groups, $^{**}P < 0.01$, $^{***}P < 0.001$. WT, wildtype. Red color intensity indicates upregulation, and blue color intensity indicates the downregulation of gene expression.

The TNF-signaling pathway was among the top 30 pathways detected in KEGG analysis indicating its' role in macrophage-specific Act1-mediated modulation of inflammation. **Figure 5C** illustrates the Volcano plot of non-affected as well as differentially expressed genes between LPS-treated macrophages from anti-Act1 and wildtype mice.

LPS-Treated Macrophages From Anti-Act1 Mice Express a Higher Level of Inflammatory Cytokines

Based on the result from KEGG analysis, the differential gene expression of TNF-signaling-related proteins was further analyzed (**Figure 6**). Most of the TNF-signaling-related genes including, *Tnfα, Il6, Il-1β, and Ccl2* were differentially upregulated in LPS-treated macrophages from anti-Act1 mice compared to wildtype (**Figures 6A,B**). ELISA in conditioned medium from macrophage culture with LPS showed 2. 5-, 3. 0-, and 2.0-fold higher expression of IL-1β, IL-6, and TNFα in the anti-Act1 group compared to wildtype (**Figures 6C–E**). Western blot analysis showed robustly high expression of NF-κB related p65 and P-p65 protein in LPS-treated macrophages from anti-Act1 mice compared to wildtype (**Figures 6F,G**). These findings support the results from the RT-qPCR and ELISA analysis in PAPT from anti-Act1 and wildtype mice (**Figure 4**). These results indicate increased M1 macrophage polarization in the Act1-knockdowned group during the inflammation.

LPS-Treatment Enhances Migration and M1-Polarization of Macrophages From Anti-Act1 Mice

Macrophage infiltration in gingiva and periodontal tissue plays a vital role in the pathophysiology of periodontitis. LPS-treated anti-Act1 peritoneal macrophages showed a higher rate of migration compared to wildtype macrophages (**Figures 7A,B**). Macrophage migration-related MCP-1 protein (CCL2) expression was also enhanced by 1.8-fold in LPS-treated anti-Act1 peritoneal macrophages compared to wildtype (**Figure 7C**). This result was in accordance with the *Mcp-1* mRNA expression in PAPT of anti-Act1 mice (**Figure 4D**) and mRNA sequencing data from LPS-treated macrophages from anti-Act1 mice (**Figures 6A,B**).

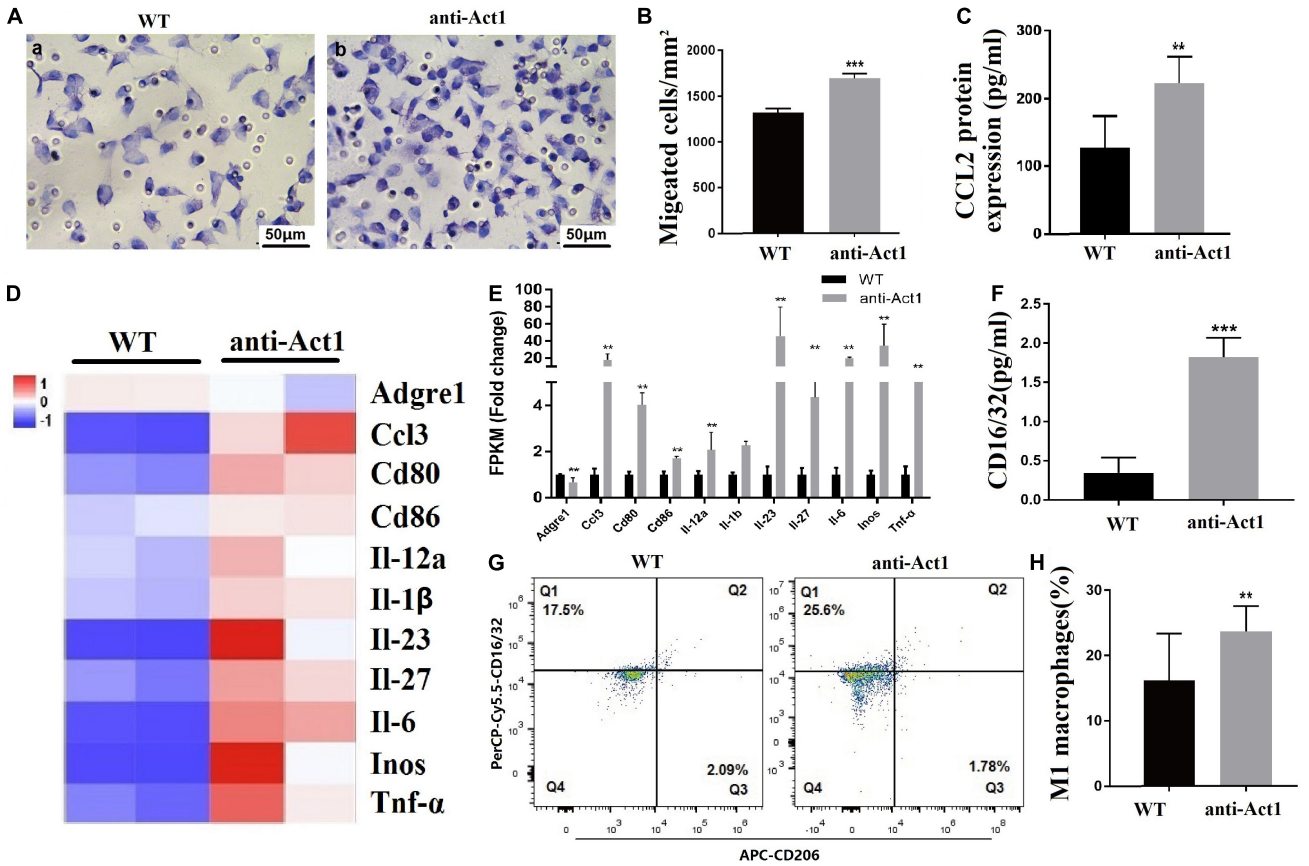


FIGURE 7 | Lipopolysaccharide -treated peritoneal macrophages from anti-Act1 mice showed higher migration and M1-polarization. **(A)** Representative images of macrophage migration. **(B)** Quantitative analysis of macrophage migration, $n = 3$. **(C)** CCL2 protein expression (ELISA, $n = 6$). Heat map **(D)**, and bar figures of differentially expressed macrophage M1-polarization-related genes **(E)**. **(F)** CD16/32 protein level expression analyzed by ELISA, $n = 6$. **(G)** FACs images of mice periodontal macrophages sorting using CD16/32 specific antibody. **(H)** Quantitative FACs data, $n = 6$. The significant difference between the groups, $^{**}P < 0.01$, $^{***}P < 0.001$. WT, wildtype. Red color intensity indicates upregulation, and blue color intensity indicates the downregulation of gene expression.

M1 macrophages are inflammatory in nature and produce proinflammatory cytokines, including, IL-1β, IL-6, and TNFα (Yuan et al., 2017; Yang et al., 2018; Hasegawa et al., 2019). Since expression levels of inflammatory cytokines were robustly upregulated in PAPT of anti-Act1 mice and LPS-treated anti-Act1 peritoneal macrophages, we further examined the M1-macrophage polarization. mRNA sequencing data showed differentially upregulated M1-macrophage related genes (**Figures 7D,E**). ELISA in cell lysate showed 5.0-fold higher expression of M1 macrophage marker CD16/32 in LPS-treated anti-Act1 peritoneal macrophages compared to that of wildtype (**Figure 7F**). FACs analysis of F4/80 positive macrophages from PAPT showed a higher number of M1 macrophages in anti-Act1 mice compared to wildtype mice (**Figures 7G,H**). In contrast, M2 macrophage-related genes were downregulated or remained unchanged in LPS-treated anti-Act1 peritoneal macrophages (**Supplementary Figures 3A,B**). Moreover, the protein expression of M2 macrophage marker CD206 in PAPT of anti-Act1 mice was reduced compared to wildtype (**Supplementary Figure 3C**).

DISCUSSION

The global prevalence rate of severe periodontitis is ∼10% (Kassebaum et al., 2014). The macrophages are a key immune cell that regulates the pathophysiology of periodontitis (Sima et al., 2019). Act1 is an intracellular signaling molecule that modulates inflammation in various diseases (Pisitkun et al., 2010; Swaidani et al., 2011; Doyle et al., 2012; Sakamuri et al., 2016). However, the role of macrophage-specific Act1 on the pathophysiology of periodontitis has not been investigated yet. In this study, we developed macrophage-specific Act1 expression inhibited mice and analyzed its role in the pathophysiology of mice periodontitis. These Anti-Act1 mice showed severe periodontitis and alveolar bone loss compared to wildtype. Macrophage infiltration, levels of inflammatory cytokines such as IL-6, IL-1β, and TNFα, and M1 macrophage polarization were enhanced in anti-Act1 periodontitis mice compared to wildtype periodontitis mice. Furthermore, TNF/NF-κB signaling was induced in macrophages from anti-Act1 mice under inflammatory conditions. These results confirmed the involvement of macrophage-specific Act1

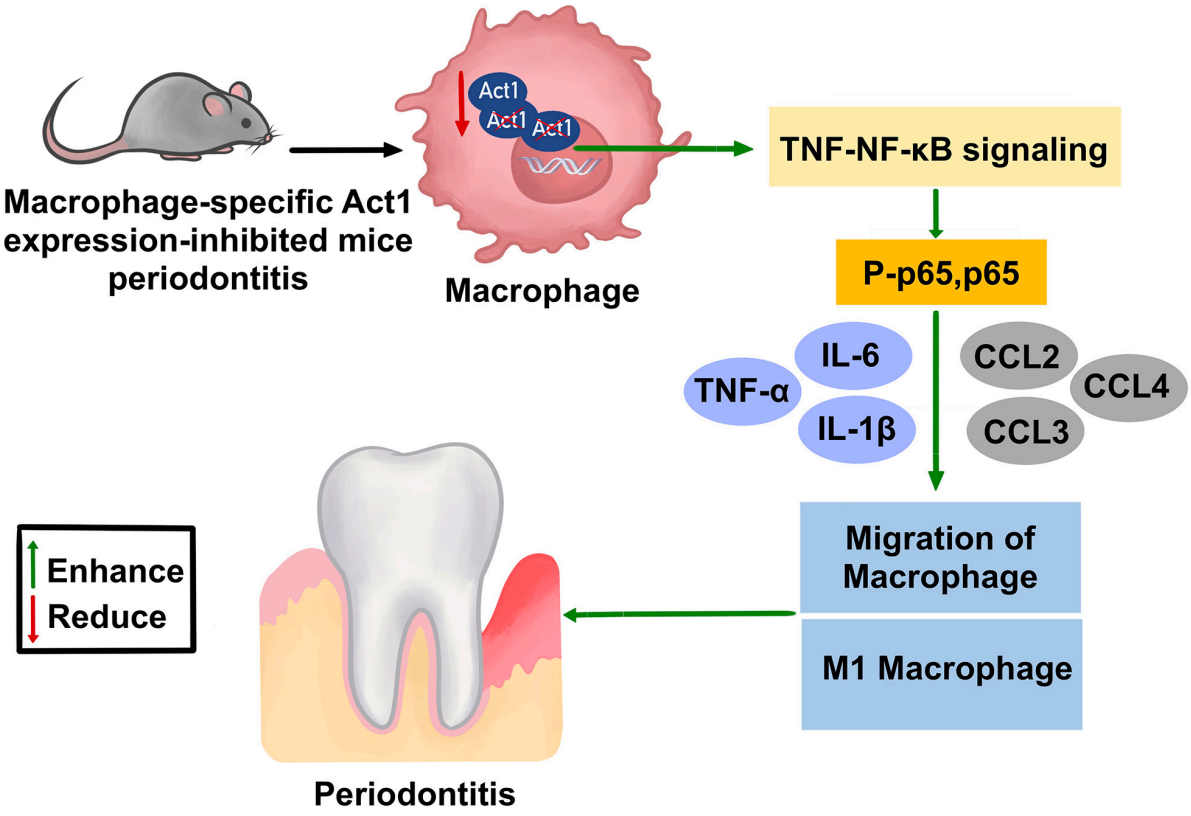


FIGURE 8 | Effect of macrophage-specific downregulation of Act1 on the pathophysiology of mice periodontitis.

on the pathophysiology of periodontitis possibly via regulating inflammation and M1 macrophage polarization (**Figure 8**).

Act1 was expressed in both healthy and periodontitis oral tissue in humans and mice. Act1 is expressed in various tissues, including the brain, heart, kidney, skeletal muscle, and bone marrow (Li et al., 2000; Xia et al., 2002). Alveolar bone resorption, periodontal tissue degeneration, higher CEJ-ABC, severe alveolar bone loss, and an increased number of osteoclasts were observed in anti-Act1 periodontitis mice compare to wildtype periodontitis mice. A higher degree of angiogenesis and infiltration of leucocyte/macrophages in PAPT have been reported in severe cases of periodontitis (Shi et al., 2008; Parisi et al., 2018; Wang L. et al., 2020; Zhang Z. et al., 2020). In this study, a similar extent of neo-vasculogenesis and leucocyte infiltration was observed in anti-Act1 and wildtype LIP mice. However, macrophage infiltration was highly enhanced in PAPT of anti-Act1 mice compared to wildtype. M1 macrophage polarization is associated with the severity of periodontitis (He et al., 2020; Wang L. et al., 2020). In this study, M1 macrophage polarization was enhanced in PAPT of anti-Act1 mice compared to wildtype. M1 macrophages release the pro-inflammatory cytokines amplifying inflammation in the PAPT milieu (He et al., 2020; Wang L. et al., 2020). The higher levels of pro-inflammatory cytokines in PAPT aggravate periodontitis and alveolar bone loss (Fredriksson et al., 2002; Azuma et al., 2014; Sakalauskiene et al., 2016; Wang D. et al., 2020). Chemotactic molecules CCL2, CCL3, and CCL4 play roles in the infiltration of macrophages and other immune cells in PAPT (Repeke et al., 2010; Parisi et al., 2018). In this study, levels of inflammatory cytokines IL-6, IL-1β, TNFα, and chemotactic molecules CCL2, CCL3, and CCL4 were robustly higher in PAPT of anti-Act1 mice than wildtype. Furthermore, levels of inflammatory cytokines, such as IL-6, IL-1β, and TNFα, and the expression of M1 macrophage polarization related genes were enhanced in macrophages from anti-Act1 mice under the inflammatory condition *in vitro*. These results further confirm the role of macrophage-specific Act-1 on periodontitis via immune modulation, inflammation regulation, and immune cell migration.

NF-κB regulates periodontal inflammation and the pathophysiology of periodontitis (Francis et al., 2020). TNF/NF-κB signaling also plays a role in the pathophysiology of various inflammatory diseases (Liedtke and Trautwein, 2012; Kunz, 2013; Sayegh et al., 2019). mRNA sequencing of LPS-treaded macrophages from anti-Act1 mice showed upregulation of TNF/NF-κB signaling related genes, including Tnfα, Il-1β, Ccl2, and Nfkbia. KEGG analysis revealed the activation of TNF/NF-κB signaling in LPS-treated macrophages from anti-Act1 mice. Shreds of literature had reported that the activated TNF/NF-κB signaling enhances M1-macrophage polarization (Liu et al., 2017; Lu et al., 2020; Zhang H. et al., 2020). Inflammation triggers M1 macrophage polarization and M1 macrophages further release proinflammatory cytokines thereby amplifying inflammation

in a vicious fashion in the periodontitis milieu. This M1 macrophage-induced inflammation could be responsible for the abrogated periodontitis in anti-Act1 mice. Elevated levels of proinflammatory cytokines in periodontal tissue affect the osteoblast activity that might partly contribute to the alveolar bone loss (Lacey et al., 2009). The reports from the literature and results of this study indicate the role of macrophage-specific Act1 on the pathophysiology of periodontitis possibly via TNF/NF-κB signaling-mediated M1 macrophage polarization.

Act1 regulates the function of various other cells, including epithelial cells, B cells, and T cells. Overexpression of Act1 leads to the activation of NF-κB and JNK signaling in epithelial cells (Qian et al., 2002). Act1 is a negative regulator in T cell and B cell (Zhang et al., 2018). Shreds of literature had reported the role of Act1 in various inflammatory diseases (Qian et al., 2007, 2008; Li, 2008; Swaidani et al., 2009; Kang et al., 2010; Zhang et al., 2018). Compared with IL-17-stimulated wild-type mice, Act1-deficient mice have reduced recruitment of neutrophils to the airways and Act1 deficiency in epithelial cells reduces the phenotype of allergic lung inflammation (Swaidani et al., 2009). The deficiency of Act1 leads to the development of Sjögren's syndrome (Qian et al., 2008). In mouse models of experimental autoimmune encephalomyelitis (EAE) and asthma, the lack of Act1 leads to resistance to IL-17-mediated inflammation (Qian et al., 2007; Kang et al., 2010). Although Act1 is necessary for IL-17-mediated inflammation, Act1-deficient mice develop spontaneous SLE and Sjögren-like diseases (Li, 2008; Zhang et al., 2018). However, the role of Act1 in periodontitis and periodontitis-related inflammation has not been reported so far. This is the first study to report the role of macrophage-specific Act1 on the pathophysiology of periodontitis. Aggravated inflammation, alveolar bone loss, macrophage infiltration, and M1-macrophage polarization in anti-Act1 periodontitis mice also indicate the possible role of macrophage-specific Act-1 on bone and cartilage degenerative inflammatory diseases such as osteoarthritis, rheumatoid arthritis, and osteoporosis.

In this study, we developed LIP in macrophage-specific Act1 expression inhibited mice to investigate the role of macrophage-specific Act1 on the pathophysiology of periodontitis. Periodontal degeneration, alveolar bone loss, levels of inflammatory cytokines, immune cell infiltration, and M1 macrophage polarization in PAPT were extensively studied. *In vitro* studies related to macrophage infiltration, M1 macrophage polarization, mRNA sequencing, and inflammation were performed in macrophages from anti-Act1 mice to further validate the results from *in vivo* studies. Our results show that the macrophage-specific Act1 knockdown aggravates periodontitis possibly via activation of TNF/NF-κB signaling. The results of this study suggest the macrophage-specific Act1 as a possible target to treat periodontitis. However, future studies focusing on the pathophysiology of periodontitis in macrophage-specific Act1 overexpressed mice are necessary to prove this hypothesis. A limitation of this study is the lack of molecular mechanism of TNF/NF-κB activation in macrophages from anti-Act1 mice under inflammatory conditions. Currently, we are developing macrophage-specific Act1 transgenic mice to further investigate the role of macrophage-specific Act1 on the pathophysiology of periodontitis and underlying molecular mechanisms.

CONCLUSION

Act1 is expressed in both healthy and periodontitis human gingival tissue as well as healthy and periodontitis periodontal tissue of mice. Downregulation of macrophage-specific Act1 in mice aggravated periodontitis, alveolar bone loss, and macrophage infiltration and M1 polarization. Anti-Act1 periodontitis mice showed a higher number of osteoclasts, and elevated level of pro-inflammatory cytokines and macrophage activity-related factors. Moreover, the LPS-treated macrophages from anti-Act1 mice activated TNF/NF-κB signaling and P-p65 expression. These results indicate the distinct role of macrophage-specific Act1 on the pathophysiology of periodontitis. Our findings warrant further studies to unravel the molecular mechanisms involved in macrophage-specific Act1-mediated regulation of periodontitis.

DATA AVAILABILITY STATEMENT

RNAseq data was uploaded to NCBI SRA database (SRA accession: PRJNA702259), https://www.ncbi.nlm.nih.gov/bioproject/PRJNA702259/.

ETHICS STATEMENT

The studies involving human participants were reviewed and approved by the Medical Ethics Committee of the Affiliated Stomatology Hospital of Guangzhou Medical University. The patients/participants provided their written informed consent to participate in this study. The animal study was reviewed and approved by the Experimental Animal Ethics Committee of Guangzhou Medical University.

AUTHOR CONTRIBUTIONS

LJW, LPW, YF, and JP: study design. YC, ZY, XG, and YY: experimental conduct. JZ, YC, DL, XK, and LY: animal work. JZ, JP, YC, DL, LY, and WZ: data collection, analysis, and interpretation. YC and JP: manuscript preparation. All authors approved the final version of the manuscript.

FUNDING

This study was supported by the project of Guangzhou Science and Technology Bureau (202002030301), Department of Education of Guangdong Province (2018KTSCX186), and high-level university construction funding of Guangzhou Medical University (02-412-B205002-1003018, 02-410-B205001293, B185006003014, and B195002003017). The funding bodies

played no role in the design of the study and collection, analysis, and interpretation of data, and in writing the manuscript.

SUPPLEMENTARY MATERIAL

The Supplementary Material for this article can be found online at: https://www.frontiersin.org/articles/10.3389/fcell.2021.628139/full#supplementary-material

Supplementary Figure 1 | (A) Scheme of macrophage-specific downregulation of Act1 in anti-Act1 mice. **(B)** Image PCR-product gel run showing a successful insertion of Act1 antisense oligonucleotides in anti-Act1 mice. **(C)** RT-qPCR data showing reduced Act-1 expression in macrophages from anti-Act1 mice. Data are presented as mean ± SD ($n = 6$). The significant difference between the groups, $^{***}P < 0.001$. WT, wildtype.

Supplementary Figure 2 | The expression pattern of Act1 in periodontal tissues and macrophages. Representative image of immunofluorescence staining showing the Act1 expression in macrophages in healthy human gingival tissue sections **(A)**, and peritoneal macrophages of wildtype mice **(B)**. **(C)** Macrophage infiltration in PAPT of wildtype mice. Act1-Alexa 488: green fluorescence, F4/80-Alexa 594: red fluorescence, CD68-Alexa 594: red fluorescence, DAPE: blue fluorescence, white arrow: Act1 is expressed in macrophages.

Supplementary Figure 3 | (A) Heat map showing differential expression of M2 macrophage related genes. **(B)** Quantification of the expression level of M2 macrophage related genes from mRNA-seq data. **(C)** CD206 protein level expression in PAPT analyzed by ELISA, $n = 6$. Data are presented as mean ± SD. The significant difference between the groups, $^{*}P < 0.05$. WT, wildtype.

REFERENCES

Abe, T., and Hajishengallis, G. (2013). Optimization of the ligature-induced periodontitis model in mice. *J. Immunol. Methods* 394, 49–54. doi: 10.1016/j.jim.2013.05.002

Azuma, M. M., Samuel, R. O., Gomes-Filho, J. E., Dezan-Junior, E., and Cintra, L. T. (2014). The role of IL-6 on apical periodontitis: a systematic review. *Int. Endod. J.* 47, 615–621. doi: 10.1111/iej.12196

Darveau, R. P. (2010). Periodontitis: a polymicrobial disruption of host homeostasis. *Nat. Rev. Microbiol.* 8, 481–490. doi: 10.1038/nrmicro2337

Doyle, M. S., Collins, E. S., Fitzgerald, O. M., and Pennington, S. R. (2012). New insight into the functions of the interleukin-17 receptor adaptor protein Act1 in psoriatic arthritis. *Arthritis Res. Ther.* 14:226. doi: 10.1186/ar4071

Eke, P. I., Dye, B. A., Wei, L., Thornton-Evans, G. O., Genco, R. J., and CDC Periodontal Disease Surveillance Workgroup (2012). Prevalence of periodontitis in adults in the United States: 2009 and 2010. *J. Dent. Res.* 91, 914–920. doi: 10.1177/0022034512457373

Francis, M., Gopinathan, G., Salapatas, A., Nares, S., Gonzalez, M., Diekwisch, T. G. H., et al. (2020). SETD1 and NF-kappaB regulate periodontal inflammation through H3K4 trimethylation. *J. Dent. Res.* 99, 1486–1493. doi: 10.1177/0022034520939029

Frazee, A. C., Pertea, G., Jaffe, A. E., Langmead, B., Salzberg, S. L., and Leek, J. T. (2015). Ballgown bridges the gap between transcriptome assembly and expression analysis. *Nat. Biotechnol.* 33, 243–246. doi: 10.1038/nbt.3172

Fredriksson, M., Bergstrom, K., and Asman, B. (2002). IL-8 and TNF-alpha from peripheral neutrophils and acute-phase proteins in periodontitis. *J. Clin. Periodontol.* 29, 123–128. doi: 10.1034/j.1600-051x.2002.290206.x

Graziani, F., Karapetsa, D., Alonso, B., and Herrera, D. (2017). Nonsurgical and surgical treatment of periodontitis: how many options for one disease? *Periodontol. 2000* 75, 152–188. doi: 10.1111/prd.12201

Hajishengallis, G. (2014). Immunomicrobial pathogenesis of periodontitis: keystones, pathobionts, and host response. *Trends Immunol.* 35, 3–11. doi: 10.1016/j.it.2013.09.001

Hasegawa, T., Kikuta, J., Sudo, T., Matsuura, Y., Matsui, T., Simmons, S., et al. (2019). Identification of a novel arthritis-associated osteoclast precursor macrophage regulated by FoxM1. *Nat. Immunol.* 20, 1631–1643. doi: 10.1038/s41590-019-0526-7

He, D., Liu, F., Cui, S., Jiang, N., Yu, H., Zhou, Y., et al. (2020). Mechanical load-induced H2S production by periodontal ligament stem cells activates M1 macrophages to promote bone remodeling and tooth movement via STAT1. *Stem Cell Res. Ther.* 11:112.

Holtfreter, B., Kocher, T., Hoffmann, T., Desvarieux, M., and Micheelis, W. (2010). Prevalence of periodontal disease and treatment demands based on a german dental survey (DMS IV). *J. Clin. Periodontol.* 37, 211–219. doi: 10.1111/j.1600-051x.2009.01517.x

Hu, D. Y., Hong, X., and Li, X. (2011). Oral health in China–trends and challenges. *Int. J. Oral Sci.* 3, 7–12. doi: 10.4248/ijos11006

Kang, Z., Altuntas, C. Z., Gulen, M. F., Liu, C., Giltiay, N., Qin, H., et al. (2010). Astrocyte-restricted ablation of interleukin-17-induced Act1-mediated signaling ameliorates autoimmune encephalomyelitis. *Immunity* 32, 414–425. doi: 10.1016/j.immuni.2010.03.004

Kassebaum, N. J., Bernabe, E., Dahiya, M., Bhandari, B., Murray, C. J., and Marcenes, W. (2014). Global burden of severe periodontitis in 1990-2010: a systematic review and meta-regression. *J. Dent. Res.* 93, 1045–1053. doi: 10.1177/0022034514552491

Kechin, A., Boyarskikh, U., Kel, A., and Filipenko, M. (2017). cutPrimers: a new tool for accurate cutting of primers from reads of targeted next generation sequencing. *J. Comput. Biol.* 24, 1138–1143. doi: 10.1089/cmb.2017.0096

Kheirandish, F., Mosaffa, N., Tarahi, M. J., and Fallahi, S. (2018). Olive (*Olea europaea*) leaf extract alters the cytokine profile of leishmania major-infected macrophages: new insight into the underlying mechanism. *Parasite Immunol.* 40:e12520. doi: 10.1111/pim.12520

Kim, D., Langmead, B., and Salzberg, S. L. (2015). HISAT: a fast spliced aligner with low memory requirements. *Nat. Methods* 12, 357–360. doi: 10.1038/nmeth.3317

Kubatzky, K. F., Uhle, F., and Eigenbrod, T. (2018). From macrophage to osteoclast–how metabolism determines function and activity. *Cytokine* 112, 102–115. doi: 10.1016/j.cyto.2018.06.013

Kunz, M. (2013). Lupus erythematosus. part I: epidemiology, genetics and immunology. *J. Dtsch. Dermatol. Ges.* 11, 709–719. doi: 10.1111/ddg.12165

Lacey, D. C., Simmons, P. J., Graves, S. E., and Hamilton, J. A. (2009). Proinflammatory cytokines inhibit osteogenic differentiation from stem cells: implications for bone repair during inflammation. *Osteoarthritis Cartilage* 17, 735–742. doi: 10.1016/j.joca.2008.11.011

Li, X. (2008). Act1 modulates autoimmunity through its dual functions in CD40L/BAFF and IL-17 signaling. *Cytokine* 41, 105–113. doi: 10.1016/j.cyto.2007.09.015

Li, X., Commane, M., Nie, H., Hua, X., Chatterjee-Kishore, M., Wald, D., et al. (2000). Act1, an NF-kappa B-activating protein. *Proc. Natl. Acad. Sci. U.S.A* 97, 10489–10493. doi: 10.1073/pnas.160265197

Liedtke, C., and Trautwein, C. (2012). The role of TNF and fas dependent signaling in animal models of inflammatory liver injury and liver cancer. *Eur. J. Cell Biol.* 91, 582–589. doi: 10.1016/j.ejcb.2011.10.001

Liu, C., Qian, W., Qian, Y., Giltiay, N. V., Lu, Y., Swaidani, S., et al. (2009). Act1, a U-box E3 ubiquitin ligase for IL-17 signaling. *Sci. Signal.* 2:ra63. doi: 10.1126/scisignal.2000382

Liu, C. P., Zhang, X., Tan, Q. L., Xu, W. X., Zhou, C. Y., Luo, M., et al. (2017). NF-kappaB pathways are involved in M1 polarization of RAW 264.7 macrophage by polyporus polysaccharide in the tumor microenvironment. *PLoS One* 12:e0188317. doi: 10.1371/journal.pone.0188317

Lu, Z., Li, X., Yang, P., Mu, G., He, L., Song, C., et al. (2020). Heparin-binding protein enhances NF-kappaB pathway-mediated inflammatory gene transcription in M1 macrophages via lactate. *Inflammation* 44, 48–56. doi: 10.1007/s10753-020-01263-4

Mizraji, G., Segev, H., Wilensky, A., and Hovav, A. H. (2013). Isolation, processing and analysis of murine gingival cells. *J. Vis. Exp.* 77:e50388.

Novatchkova, M., Leibbrandt, A., Werzowa, J., Neubuser, A., and Eisenhaber, F. (2003). The STIR-domain superfamily in signal transduction, development and

immunity. *Trends Biochem. Sci.* 28, 226–229. doi: 10.1016/s0968-0004(03)00067-7

Parisi, L., Gini, E., Baci, D., Tremolati, M., Fanuli, M., Bassani, B., et al. (2018). Macrophage polarization in chronic inflammatory diseases: killers or builders? *J. Immunol. Res.* 2018:8917804.

Pereira, M., Petretto, E., Gordon, S., Bassett, J. H. D., Williams, G. R., and Behmoaras, J. (2018). Common signalling pathways in macrophage and osteoclast multinucleation. *J. Cell Sci.* 131:jcs216267.

Pertea, M., Pertea, G. M., Antonescu, C. M., Chang, T. C., Mendell, J. T., and Salzberg, S. L. (2015). StringTie enables improved reconstruction of a transcriptome from RNA-seq reads. *Nat. Biotechnol.* 33, 290–295.

Pineda-Torra, I., Gage, M., De Juan, A., and Pello, O. M. (2015). Isolation, culture, and polarization of murine bone marrow-derived and peritoneal macrophages. *Methods Mol. Biol.* 1339, 101–109. doi: 10.1007/978-1-4939-2929-0_6

Pisitkun, P., Claudio, E., Ren, N., Wang, H., and Siebenlist, U. (2010). The adaptor protein CIKS/ACT1 is necessary for collagen-induced arthritis, and it contributes to the production of collagen-specific antibody. *Arthritis Rheum.* 62, 3334–3344. doi: 10.1002/art.27653

Qian, Y., Giltiay, N., Xiao, J., Wang, Y., Tian, J., Han, S., et al. (2008). Deficiency of Act1, a critical modulator of B cell function, leads to development of Sjogren's syndrome. *Eur. J. Immunol.* 38, 2219–2228. doi: 10.1002/eji.200738113

Qian, Y., Liu, C., Hartupee, J., Altuntas, C. Z., Gulen, M. F., Jane-Wit, D., et al. (2007). The adaptor Act1 is required for interleukin 17-dependent signaling associated with autoimmune and inflammatory disease. *Nat. Immunol.* 8, 247–256. doi: 10.1038/ni1439

Qian, Y., Zhao, Z., Jiang, Z., and Li, X. (2002). Role of NF kappa B activator Act1 in CD40-mediated signaling in epithelial cells. *Proc. Natl. Acad. Sci. U.S.A.* 99, 9386–9391. doi: 10.1073/pnas.142294499

Repeke, C. E., Ferreira, S. B. Jr., Claudino, M., Silveira, E. M., De Assis, G. F., Avila-Campos, M. J., et al. (2010). Evidences of the cooperative role of the chemokines CCL3, CCL4 and CCL5 and its receptors CCR1+ and CCR5+ in RANKL+ cell migration throughout experimental periodontitis in mice. *Bone* 46, 1122–1130. doi: 10.1016/j.bone.2009.12.030

Rodriguez, J. C., Gonzalez, G. A., Fresno, C., Llera, A. S., and Fernandez, E. A. (2016). Improving information retrieval in functional analysis. *Comput. Biol. Med.* 79, 10–20. doi: 10.1016/j.compbiomed.2016.09.017

Sakalauskiene, J., Giedrimiene, D., Gleiznys, D., Gleiznys, A., Gleizniene, R., and Vitkauskiene, A. (2016). Peripheral blood leukocytes interleukin-1 beta (IL-1beta) cytokine hyper-reactivity in chronic periodontitis. *Med. Sci. Monit.* 22, 4323–4329. doi: 10.12659/msm.898422

Sakamuri, S., Higashi, Y., Sukhanov, S., Siddesha, J. M., Delafontaine, P., Siebenlist, U., et al. (2016). TRAF3IP2 mediates atherosclerotic plaque development and vulnerability in ApoE(-/-) mice. *Atherosclerosis* 252, 153–160. doi: 10.1016/j.atherosclerosis.2016.05.029

Sayegh, S., El Atat, O., Diallo, K., Rauwel, B., Degboe, Y., Cavaignac, E., et al. (2019). Rheumatoid synovial fluids regulate the immunomodulatory potential of adipose-derived mesenchymal stem cells through a TNF/NF-kappaB-dependent mechanism. *Front. Immunol.* 10:1482. doi: 10.3389/fimmu.2019.01482

Shi, D., Meng, H., Xu, L., Zhang, L., Chen, Z., Feng, X., et al. (2008). Systemic inflammation markers in patients with aggressive periodontitis: a pilot study. *J. Periodontol.* 79, 2340–2346. doi: 10.1902/jop.2008.080192

Sima, C., Viniegra, A., and Glogauer, M. (2019). Macrophage immunomodulation in chronic osteolytic diseases-the case of periodontitis. *J. Leukoc. Biol.* 105, 473–487. doi: 10.1002/jlb.1ru0818-310r

Swaidani, S., Bulek, K., Kang, Z., Gulen, M. F., Liu, C., Yin, W., et al. (2011). T cell-derived Act1 is necessary for IL-25-mediated Th2 responses and allergic airway inflammation. *J. Immunol.* 187, 3155–3164. doi: 10.4049/jimmunol.1002790

Swaidani, S., Bulek, K., Kang, Z., Liu, C., Lu, Y., Yin, W., et al. (2009). The critical role of epithelial-derived Act1 in IL-17- and IL-25-mediated pulmonary inflammation. *J. Immunol.* 182, 1631–1640. doi: 10.4049/jimmunol.182.3.1631

Van Quickelberghe, E., De Sutter, D., Van Loo, G., Eyckerman, S., and Gevaert, K. (2018). A protein-protein interaction map of the TNF-induced NF-kappaB signal transduction pathway. *Sci. Data* 5:180289.

Veloso, P., Fernandez, A., Terraza-Aguirre, C., Alvarez, C., Vernal, R., Escobar, A., et al. (2020). Macrophages skew towards M1 profile through reduced CD163 expression in symptomatic apical periodontitis. *Clin. Oral Investig.* 24, 4571–4581. doi: 10.1007/s00784-020-03324-2

Vos, T., Flaxman, A. D., Naghavi, M., Lozano, R., Michaud, C., Ezzati, M., et al. (2012). Years lived with disability (YLDs) for 1160 sequelae of 289 diseases and injuries 1990-2010: a systematic analysis for the Global Burden of disease study 2010. *Lancet* 380, 2163–2196.

Wang, C., Wu, L., Bulek, K., Martin, B. N., Zepp, J. A., Kang, Z., et al. (2013). The psoriasis-associated D10N variant of the adaptor Act1 with impaired regulation by the molecular chaperone hsp90. *Nat. Immunol.* 14, 72–81. doi: 10.1038/ni.2479

Wang, D., Hu, B., Hu, C., Zhu, F., Liu, X., Zhang, J., et al. (2020). Clinical characteristics of 138 hospitalized patients with 2019 novel coronavirus–infected pneumonia in Wuhan, China. *JAMA* 323, 1061–1069. doi: 10.1001/jama.2020.1585

Wang, J., Li, L., Li, B., Lu, X., Wang, L., and Yang, Y. (2019). Targeted suppression of macrophage Act1 inhibits the lung metastasis of melanoma cells in mice. *Chin. J. Comp. Med.* 29, 1–6.

Wang, L., Guan, N., Jin, Y., Lin, X., and Gao, H. (2015). Subcutaneous vaccination with *Porphyromonas gingivalis* ameliorates periodontitis by modulating Th17/Treg imbalance in a murine model. *Int. Immunopharmacol.* 25, 65–73. doi: 10.1016/j.intimp.2015.01.007

Wang, L., Zheng, J., Pathak, J. L., Chen, Y., Liang, D., Yang, L., et al. (2020). SLIT2 overexpression in periodontitis intensifies inflammation and alveolar bone loss, possibly via the activation of MAPK pathway. *Front. Cell Dev. Biol.*8:593. doi: 10.3389/fcell.2020.00593

Xia, Y. F., Li, Y. D., Li, X., and Geng, J. G. (2002). Identification of alternatively spliced Act1 and implications for its roles in oncogenesis. *Biochem. Biophys. Res. Commun.* 296, 406–412. doi: 10.1016/s0006-291x(02)00887-2

Xiao, E., Mattos, M., Vieira, G. H. A., Chen, S., Correa, J. D., Wu, Y., et al. (2017). Diabetes enhances IL-17 expression and alters the oral microbiome to increase its pathogenicity. *Cell Host Microbe* 22:120-128.e4.

Yang, B., Sun, H., Xu, X., Zhong, H., Wu, Y., and Wang, J. (2020). YAP1 inhibits the induction of TNF-α-stimulated bone-resorbing mediators by suppressing the NF-κB signaling pathway in MC3T3-E1 cells. *J. Cell. Physiol.* 235, 4698–4708. doi: 10.1002/jcp.29348

Yang, J., Zhu, Y., Duan, D., Wang, P., Xin, Y., Bai, L., et al. (2018). Enhanced activity of macrophage M1/M2 phenotypes in periodontitis. *Arch. Oral Biol.* 96, 234–242. doi: 10.1016/j.archoralbio.2017.03.006

Yuan, H., He, J., Zhang, G., Zhang, D., Kong, X., and Chen, F. (2017). Osteoclast stimulatory transmembrane protein induces a phenotypic switch in macrophage polarization suppressing an M1 pro-inflammatory state. *Acta Biochim. Biophys. Sin.* 49, 935–944. doi: 10.1093/abbs/gmx092

Zhang, C. J., Wang, C., Jiang, M., Gu, C., Xiao, J., Chen, X., et al. (2018). Act1 is a negative regulator in T and B cells via direct inhibition of STAT3. *Nat. Commun.* 9:2745.

Zhang, H., Cao, N., Yang, Z., Fang, X., Yang, X., Li, H., et al. (2020). Bilobalide alleviated dextran sulfate sodium-induced experimental colitis by inhibiting M1 macrophage polarization through the NF-kappaB signaling pathway. *Front. Pharmacol.* 11:718. doi: 10.3389/fphar.2020.00718

Zhang, Q., Li, Z., Wang, C., Shen, T., Yang, Y., Chotivichien, S., et al. (2014). Prevalence and predictors for periodontitis among adults in China, 2010. *Glob. Health Action* 7:24503. doi: 10.3402/gha.v7.24503

Zhang, Z., Shuai, Y., Zhou, F., Yin, J., Hu, J., Guo, S., et al. (2020). PDLSCs regulate angiogenesis of periodontal ligaments via VEGF transferred by exosomes in periodontitis. *Int. J. Med. Sci.* 17, 558–567. doi: 10.7150/ijms.40918

Zhu, L. F., Li, L., Wang, X. Q., Pan, L., Mei, Y. M., Fu, Y. W., et al. (2019). M1 macrophages regulate TLR4/AP1 via paracrine to promote alveolar bone destruction in periodontitis. *Oral Dis.* 25, 1972–1982. doi: 10.1111/odi.13167

Conflict of Interest: The authors declare that the research was conducted in the absence of any commercial or financial relationships that could be construed as a potential conflict of interest.

Copyright © 2021 Pathak, Fang, Chen, Ye, Guo, Yan, Zha, Liang, Ke, Yang, Zhong, Wang and Wang. This is an open-access article distributed under the terms of the Creative Commons Attribution License (CC BY). The use, distribution or reproduction in other forums is permitted, provided the original author(s) and the copyright owner(s) are credited and that the original publication in this journal is cited, in accordance with accepted academic practice. No use, distribution or reproduction is permitted which does not comply with these terms.

frontiers in Cell and Developmental Biology

ORIGINAL RESEARCH
published: 09 April 2021
doi: 10.3389/fcell.2021.646386

Src Homology 2 Domain-Containing Protein Tyrosine Phosphatase Promotes Inflammation and Accelerates Osteoarthritis by Activating β-Catenin

Tenghui Tao[1], Danni Luo[1], Chenghao Gao[1], Hui Liu[1], Zehua Lei[1], Wenbin Liu[1], Chuankun Zhou[1], Dahu Qi[1], Zhenhan Deng[2], Xuying Sun[1] and Jun Xiao[1]**

[1] Department of Orthopedics, Tongji Hospital, Tongji Medical College, Huazhong University of Science and Technology, Wuhan, China, [2] Department of Sports Medicine, The First Affiliated Hospital of Shenzhen University, Shenzhen Second People's Hospital, Shenzhen, China

OPEN ACCESS

Edited by:
Changjun Li,
Central South University, China

Reviewed by:
Yurui Jiao,
Central South University, China
Ling Liu,
Central South University, China

***Correspondence:**
Xuying Sun
Xuying_Sun@hust.edu.cn
Jun Xiao
Jun_Xiao@hust.edu.cn

Specialty section:
This article was submitted to Molecular Medicine, a section of the journal Frontiers in Cell and Developmental Biology

Received: 26 December 2020
Accepted: 18 March 2021
Published: 09 April 2021

Citation:
Tao T, Luo D, Gao C, Liu H, Lei Z, Liu W, Zhou C, Qi D, Deng Z, Sun X and Xiao J (2021) Src Homology 2 Domain-Containing Protein Tyrosine Phosphatase Promotes Inflammation and Accelerates Osteoarthritis by Activating β-Catenin. Front. Cell Dev. Biol. 9:646386. doi: 10.3389/fcell.2021.646386

Osteoarthritis (OA) is a chronic articular disease characterized by cartilage degradation, subchondral bone remodeling and osteophyte formation. Src homology 2 domain-containing protein tyrosine phosphatase (SHP2) has not been fully investigated in the pathogenesis of OA. In this study, we found that SHP2 expression was significantly increased after interleukin-1β (IL-1β) treatment in primary mouse chondrocytes. Inhibition of SHP2 using siRNA reduced MMP3, MMP13 levels, but increased AGGRECAN, COL2A1, SOX9 expression *in vitro*. On the contrary, overexpression of SHP2 exerted the opposite results and promoted cartilage degradation. Mechanistically, SHP2 activated Wnt/β-catenin signaling possibly through directly binding to β-catenin. SHP2 also induced inflammation through activating Mitogen-activated protein kinase (MAPK) and nuclear factor κB (NF-κB) pathways. Our *in vivo* studies showed that SHP2 knockdown effectively delayed cartilage destruction and reduced osteophyte formation in the mouse model of OA induced by destabilization of the medial meniscus (DMM). Altogether, our study identifies that SHP2 is a novel and potential therapeutic target of OA.

Keywords: SHP2, osteoarthritis, chondrocytes, β-catenin, MAPK, NF-κB

INTRODUCTION

Osteoarthritis (OA) is the most common chronic joint disorder characterized by increased pain and joint dysfunction. It was once regarded as a disease of purely mechanical cartilage degradation. However, increased research and knowledge have revealed it to be a complex condition affecting the whole joint (Glyn-Jones et al., 2015). The pathology of OA includes the loss of articular cartilage, hypertrophic differentiation of chondrocytes, subchondral bone remodeling, synovial inflammation, and osteophyte formation (Li et al., 2018). In such inflammatory condition, terminally differentiated hypertrophic chondrocytes abnormally release several kinds of growth

factors, cathepsins, and matrix metalloproteases (MMPs), which disturb the coordinated coupling between osteoclastogenesis and matrix remodeling at the chondro-osseous front, leading to cartilage degradation (Naski et al., 1998; Uusitalo et al., 2000; Stickens et al., 2004; Nakashima et al., 2011). The most well-known mechanisms of OA include the increased expression of matrix-degrading enzymes like MMPs, a disintegrin and metalloproteinases (ADAMTS), and the degradation of COL2A1 (collagen, type II, alpha 1) and AGGRECAN (Hollander et al., 1995; Lark et al., 1995; Neuhold et al., 2001; Glasson et al., 2005). Recently, an increasing amount of new molecules have been reported to be responsible for the degeneration of articular cartilage, such as tyrosine kinase Fyn, complement C5, Yes-associated protein, and hypoxia-inducible factor-2α. Dysregulation of these proteins is correlated with abnormal signaling pathways, such as the Wnt, Mitogen-activated protein kinase (MAPK), and nuclear factor κB (NF-κB) pathway (Wang et al., 2011; Deng et al., 2018; Li et al., 2018). However, the exact molecular mechanisms crucial for OA remain to be fully elucidated, because there is still a lack of effective targets for the treatment of such disease. Exploring new pathogenic factors and accurate signaling pathways will pave the way and provide new strategies for developing novel medications for the disease.

SHP2, encoded by *Ptpn11*, is a ubiquitously expressed Src homology 2 domain-containing protein tyrosine phosphatase, which has been proved to be involved in several kinds of bone diseases (Kamiya et al., 2014). Mesenchymal stem cell (MSC)-specific SHP2 knock-out mice develop a distinct increased number of terminally differentiated chondrocytes, accompanied by severe chondrodysplasia and completely blocked osteogenesis, resulting in various skeletal defects including postnatal growth retardation, delayed closure of the skull, pectus carinatum, and limb deformity. Consistently, the MAPK and protein kinase B (Akt) signal pathways are also suppressed (Lapinski et al., 2013). Conditional knockout of SHP2 in osteoclasts significantly suppresses receptor activator of nuclear factor (NF)-κB ligand (RANKL)-mediated signaling and impairs osteoclast (OCL) precursor cells differentiation or maturation (Zhou et al., 2015). These studies strongly indicate the vital role of SHP2 in bone remodeling. Besides, several studies have been conducted about SHP2 in OA. For example, one study revealed that long non-coding RNA named MM2P can prevent SHP2-mediated dephosphorylation of STAT3, the activation of which promotes transcription of chondrocyte-specific protein *Sox9* and contributes to cartilage repairment (Bai et al., 2020). Recently, Keisuke reported that the *Ptpn11* gene is up-regulated in fibroblast-like synoviocytes of rheumatoid arthritis (RA) compared to that of OA (Maeshima et al., 2016). However, the effect of SHP2 on OA progress remains elusive.

In our study, we found SHP2 is accumulated in the primary chondrocytes after IL-1β stimulation. We further investigated the role of SHP2 in OA by regulating SHP2 expression both *in vitro* and *in vivo*. The results demonstrated that inhibition of SHP2 alleviated the cartilage destruction in chondrocytes by targeting β-catenin signaling. Consistently, SHP2 knockdown delayed cartilage degradation in OA animal model. This study provided a potential novel therapeutic target for treating OA.

MATERIALS AND METHODS

Reagents and Antibodies

Recombinant mouse IL-1β was purchased from R&D Systems (Minneapolis, MN, United States). Lipofectamine 3000 reagent was obtained from Invitrogen (Waltham, MA, United States). Anti-SHP2, β-catenin, p38, p-p38, extracellular signal-regulated kinase (ERK), p-ERK, c-Jun N-terminal kinase (JNK), p-JNK, p65, p-p65, IκBα, p-IκBα, IκB kinase (IKK)-β and p-IKKα/β antibodies were supplied by Cell Signaling Technology (Beverly, MA, United States). MMP3, MMP13 and p-β-catenin(Y142) antibodies were obtained from Abcam (Cambridge, United Kingdom). p-β-catenin(S33/37/141), COL2A1, and AGGRECAN antibodies were purchased from Abclonal (Wuhan, China). GAPDH antibody was purchased from Boster (Wuhan, China) and secondary antibodies were obtained from the Jackson lab.

Isolation and Culture of Primary Chondrocytes

Knee joint cartilages were dissected from newborn mice (5-days-old) to harvest the primary chondrocytes. After digestion with 0.2% trypsin for 30 min, cartilage pieces were purified and digested with 0.25% collagenase II dissolved in Dulbecco's Modified Eagle Medium (DMEM)/F12 (Hyclone, United States) culture medium at 37°C for 6–8 h. The released chondrocytes were resuspended and cultured in DMEM/F12 supplemented with 10% fetal bovine serum (FBS) (Gibco, Waltham, United States), 100 units/ml penicillin and 100 μg/ml streptomycin at 37°C in an incubator. Cells were plated onto 10 cm plates and grown to approximately 80% confluences before each experiment.

Small Interfering RNA and Plasmid Transfections

Transfections were performed using Lipofectamine 3000 reagent. Chondrocytes were plated onto six-well plates. For siRNA transfection, 50 pM siRNA (RiboBio, Guangzhou, China) or scrambled siRNAs, 5 μL of Lipofectamine 3000, 250 μL of Opti-MEM, and 2 mL of complete medium were mixed and added to each well. The siRNA (sequence 5′-GAACCTTCATTGTGATTGA-3′) targeting mouse SHP2 was purchased from RiboBio (Guangzhou, China). For SHP2 or active form of β-catenin (β-cat-S33Y) overexpression, chondrocytes were transfected with 1 μg SHP2 overexpression plasmids (OriGene, Rockville, MD, United States) or β-cat-S33Y in 2 mL complete medium, added with 5 μL Lipofectamine 3000 and 250 μL Opti-MEM. 48 h after transfection, chondrocytes were harvested and subjected to different experiments. The efficiency of knockdown or overexpression was confirmed by RT-qPCR and western blot.

Cell Proliferation Analysis

Primary chondrocytes were plated onto 96-well plates for SHP2 siRNA or over-expressed plasmid transfection and then were stimulated with IL-1β for 24 h. All tests were performed in

triplicate and cell proliferation was measured by Cell Counting Kit-8 Assay (CCK-8, TargetMol). To measure the proliferation rate, cells were cultured in the CCK-8 culture medium for 1 h, and then were subjected to absorbance measurement at 450 nm using a microplate reader (Bio Tek, United States).

Flow Cytometry

An Annexin V-FITC Apoptosis Detection Kit (Keygentec, China) was applied to determine the apoptosis rates following the manufacturer's instructions. Briefly, Collected chondrocytes were suspended in binding buffer in a concentration of 1×10^5 cells/ml and were stained with 5 μl Annexin V-FITC and 10 μl PI for 15 min in the darkroom. The results were analyzed using a flow cytometer (Becton Dickinson, United States).

Cell Migration Assay

A two-well Ibidi silicone culture insert (Ibidi, Martinsried, Germany) was set onto the middle of the well in 12-well plates, and 70 μL chondrocyte suspension with 5×10^5 cells were seeded onto each well of the chamber. After cell attachment, the silicone insert was carefully removed, leaving a 500-μm cell-free gap. The chondrocytes were incubated for 24 h in the presence or absence of IL-1β, and images were captured at different time points using Nikon inverted microscope (Nikon, Tokyo, Japan).

Animal Model

Animals were purchased from the Experimental Animal Center of Tongji Hospital, Huazhong University of Science and Technology. All the experiments were approved by the Ethics Committee on Animal Experimentation of the hospital. 12-weeks-old male C57BL/6J mice were used to induce OA by the destabilized medial meniscus (DMM) surgery which was performed as previously described (Glasson et al., 2007). To conduct animal experiments, a total of forty-eight mice were randomly divided into four groups: (1) Sham group: sham-operated mice administered with Ad-shControl adenoviruses (n = 6 for both 8 and 12 weeks); (2) Sham + Ad-shSHP2 group: sham-operated mice treated with Ad-shSHP2 adenoviruses (n = 6 for both 8 and 12 weeks); (3) DMM + Ad-shControl group: DMM-operated mice administered with Ad-shControl adenoviruses (n = 6 for both 8 and 12 weeks); (4) DMM + Ad-shSHP2 group: DMM-operated mice administered with Ad-shSHP2 adenoviruses (n = 6 for both 8 and 12 weeks). Half of the mice were sacrificed 8 weeks after surgery, and the other half were sacrificed 12 weeks after surgery. To perform the surgery, the mice were anesthetized and the right knee was prepared before surgery. Then, the joint capsule was opened and the fat pad was removed to expose the medial menisco-tibial ligament under the microscope. The ligament was cut before suturing the joint capsule and skin wound. In sham-operated groups, only the joint capsule was opened, while other tissues remained intact. The knees were dissected at 8 or 12 weeks after surgery, respectively after sacrificing. To knock down SHP2 *in vivo*, shRNA was designed and mixed by Vigene Biosciences Inc. (Shandong, China). 10 μL Ad-shSHP2 or Ad-shControl adenoviruses (1×10^9 plaque-forming units [PFUs]) were injected into the right knee joint cavity 1 week after DMM surgery using a 33G needle (Hamilton, Bonaduz, GR, Switzerland) once a week for 8 or 12 weeks after surgery.

RNA Extraction and RT-qPCR

Total RNA was extracted from cultured chondrocytes using TRIzol reagent (Takara Bio, Japan) according to the manufacturer's descriptions. 0.5–1 μg RNA was used to synthesize cDNA using Revert Aid First Strand cDNA synthesis Kit (Toyobo, Osaka, Japan). Templates were amplified using the SYBR Green Quantitative PCR Protocol (TaKaRa, Shiga, Japan) to determine mRNA levels. All primer sequences used are listed below: *Shp2*, 5′-AGAGGGAAGAGCAAATGTGTCA –3′ (sense), 5′-CTGTGTTTCCTTGTCCGACCT-3′ (antisense); *Axin2*, 5′-ATGAGTAGCGCCGTGTTAGTG-3′ (sense), 5′-GGGCATAGGTTTGGTGGACT-3′ (antisense); *Lef1*, 5′-GCCACCGATGAGATGATCCC-3′ (sense), 5′-TTGATGTCGGCTAAGTCGCC-3′ (antisense); *Tcf4*, 5′-GATGGGACTCCCTATGACCAC-3′ (sense), 5′-GAAAGGGTTCCTGGATTGCCC-3′ (antisense); *Aggrecan*, 5′-AGGTGTCGCTCCCCAACTAT-3′ (sense), 5′-CTTCACAGCGGTAGATCCCAG-3′ (antisense); *Col2a1*, 5′-CTTCACAGCGGTAGATCCCAG-3′ (sense), 5′-ACCAGGGGAACCACTCTCAC (antisense); *Mmp3*, 5′-ACTCCCTGGGACTCTACCAC-3′ (sense), 5′-GGTACCACGAGGACATCAGG-3′ (antisense); *Mmp13*, 5′-TGATGGACCTTCTGGTCTTCTGG-3′ (sense), 5′-CATCCACATGGTTGGGAAGTTCT-3′ (antisense); *Gapdh*, 5′-CTCCCACTCTTCCACCTTCG-3′ (sense), 5′-TTGCTGTAGCCGTATTCATT-3′ (antisense); *Sox9*, 5′-CAGCCCCTTCAACCTTCCTC-3′ (sense), 5′-TGATGGTCAGCGTAGTCGTATT-3′ (antisense); *Col10a1*, 5′-TTCTGCTGCTAATGTTCTTGACC-3′ (sense), 5′-GGGATGAAGTATTGTGTCTTGGG-3′ (antisense). The relative mRNA levels of target genes were calculated using the $2^{-\Delta\Delta Cq}$ method.

Western Blotting Analysis

Cultured chondrocytes were lysed by ice-cold RIPA lysis buffer (Boster, Wuhan) containing 1% protease and phosphatase inhibitor for 30 min. Then, the cell lysates were immediately configurated at 10,000 g at 4°C for 30 min. Equal amounts of protein were loaded on SDS-PAGE (10–15%) for electrophoresis, and then the proteins were transferred to polyvinylidene fluoride (PVDF) membranes. Each membrane was blocked with 5% non-fat milk in Tris-buffered saline with 0.1% Tween 20 buffer (TBST) for 1 h and then incubated with primary antibodies overnight at 4°C on a shaker. After incubation with horseradish peroxidase-conjugated secondary antibodies for 1 h, proteins were visualized by an enhanced chemiluminescence kit (Thermo Fisher Scientific, Waltham, MA, United States) in the ChemiDoc XRS System (Bio-Rad Laboratories, Hercules, CA, United States). Proteins were quantified using Image lab software and the targeted protein levels were normalized to GAPDH or relative total proteins.

Co-immunoprecipitation

The interactions of SHP2 with β-catenin proteins were detected in primary chondrocytes. Cells were lysed in lysis buffer (20 mM Tris, pH 7.5, 150 mM NaCl, 1% Triton, and 10% glycerol) containing 1% protease and phosphatase inhibitor. Lysates were pre-cleared with the control IgG for 1 h to remove any proteins

that bind non-specifically to immunoprecipitation components. Then, the primary antibodies or relative IgG, and the protein A/G beads were added to the lysates, and the mixture was incubated overnight at 4°C for immunoprecipitation. After being rinsed five times with lysis buffer, the immunoprecipitates were boiled in the loading buffer and then were subjected to western blotting.

Micro-Computed Tomography

After euthanasia, the right knee joints of the mice were harvested and fixed in 4% formaldehyde for 48 h. High-resolution micro-computed tomography (μCT, Scanco Medical, Bassersdorf, Switzerland) was used to analyze the subchondral bone structures at 15 μm resolution, 70 kVP and 112 μA x-ray energy. The three-dimensional images were reconstructed according to the manufacturer's instructions. The parameters of Bone volume per unit total volume (BV/TV), Trabecular number (Tb.N), trabecular separation (Tb.Sp) and trabecular thickness (Tb.Th) were evaluated using the μCT system software.

Histopathological and Immunocytochemical Analysis

After scanning, the tissues were fixed in 4% paraformaldehyde for 2 days and decalcified in 10% EDTA (pH 7.4) for 4 weeks. Subsequently, the tissues were embedded in paraffin and sectioned continuously at 5 μm thickness for hematoxylin and eosin (HE), toluidine blue and Safranin O/Fast Green staining. The images were taken and scored for degree of articular cartilage damage according to the Osteoarthritis Research Association (OARSI) histopathology scoring system in a blind manner (Glasson et al., 2010). For DAB or immunofluorescence staining, sections were deparaffinized, hydrated, and blocked with BSA containing 0.1% Triton X-100 for 1 h at room temperature. After incubation with primary antibodies against MMP3 (1:100), MMP13 (1:100), SHP2 (1:100), COL2A1 (1:200), AGGRECAN (1:100) overnight at 4°C, the sections were incubated with HRP-conjugated secondary antibodies and counterstained with hematoxylin or corresponded fluorescence secondary antibodies. Finally, all the images were taken under a microscope.

Immunofluorescence

The co-expression analysis of SHP2 and β-catenin in chondrocytes were performed by immunofluorescence staining. After being fixed in 4% paraformaldehyde and permeabilized in 0.2% Triton X-100, the chondrocytes were incubated with primary antibodies against β-catenin (1:100) and SHP2 (1:100) overnight at 4°C. The cells were subsequently incubated with anti-mouse and anti-rabbit secondary antibodies for 1 h. Finally, all images were captured using a fluorescence microscope.

Statistical Analysis

All data were presented as means ± SEM. Statistical analyses were conducted using GraphPad Prism v. 5.0 (Graphpad Software Inc., San Diego, CA, United States). All experiments were independently repeated at least three times. One-way ANOVA followed by LSD's *post hoc* tests were used to test the differences among groups. The student's *t*-test was used to assess statistically significant differences in the data between groups. Values of $P < 0.05$ were considered statistically significant.

RESULTS

SHP2 Expression Is Increased in Primary Chondrocytes After IL-1β Treatment and in Mouse OA Cartilage

To investigate the role of SHP2 in OA, cultured chondrocytes were exposed to different concentrations of IL-1β (0, 1, 5, 10, 20 ng/ml) to mimic OA model *in vitro*. Matrix-degrading enzyme MMP13 and MMP3 were gradually increased, while Col2a1 level was decreased upon IL-1β treatment in a dose-dependent manner, indicating a successful induction of inflammation in chondrocytes. Subsequently, SHP2 was elevated gradually by IL-1β (**Figure 1A**). Besides, the mRNA levels of *Shp2* were also increased after 5 and 20 ng/ml IL-1β treatment for 24 h although no obvious significance was observed at 1 and 10 ng/ml after IL-1β treatment (**Figure 1B**). We thus treated chondrocytes using 5 ng/ml IL-1β for different time points. Results showed MMP13 level increased within 24 h exposure but was slightly decreased at 48 h, SHP2 expression showed the same trend, MMP3 level elevated while COL2A1 decreased time-dependently within 48 h of treatment (**Figure 1C**). The mRNA level of *Shp2* was up-regulated in a time-dependently manner but was statistically significant at 24 and 48 h after IL-1β treatment (**Figure 1D**). Furthermore, we assessed the expression of SHP2 in the articular cartilage of DMM and Sham-operated mice by immunofluorescence staining, and the result revealed that SHP2 was strongly elevated in OA cartilage compared with the sham-operated mice (**Figure 1E**). Our data demonstrated that SHP2 was up-regulated both *in vivo* and *in vitro* in OA pathogenesis.

SHP2 Regulates IL-1β–Induced Chondrocyte Destruction *in vitro*

To further investigate the effect of SHP2 on IL-1β–induced chondrocyte destruction, SHP2 was knocked down using siRNA or overexpressed using plasmid in mice chondrocytes. The efficiency of SHP2 knockdown and overexpression was verified by qPCR and western blotting (**Figures 2A,B,I,J**). Subsequently, we performed CCK8 assays, flow cytometry and cell migration assays to test cell function. Results showed chondrocytes stimulated with IL-1β (5 ng/ml) for 24 h markedly increased the apoptotic rates which was not significantly influenced by SHP2 knockdown or overexpression (**Supplementary Figures 1A–D**). Furthermore, SHP2 knockdown or overexpression has no effect on chondrocyte viability (**Supplementary Figures 1E,F**). Cell migration assays showed scratch distances were not altered in SHP2 knockdown or overexpressed chondrocytes (**Supplementary Figures 1G–J**). These results suggested SHP2 had no significant effect on chondrocyte apoptosis, proliferation or migration. We then evaluated the role of SHP2 in IL-1β–induced chondrocyte degeneration. Downregulation of SHP2 decreased the elevation of MMP3 and MMP13 induced by IL-1β in both protein and mRNA levels (**Figures 2A,C,D**). *Aggrecan*, *Col2a1*, *Sox9*, and *Col10a1* levels were also tested by qPCR. The results showed that SHP2 knockdown increased *Aggrecan*, *Col2a1* and *Sox9* mRNA level, but decreased *Col10a1* mRNA level after IL-1β treatment in chondrocytes (**Figures 2E–H**). Furthermore, SHP2 overexpression distinctly increased the elevation of levels

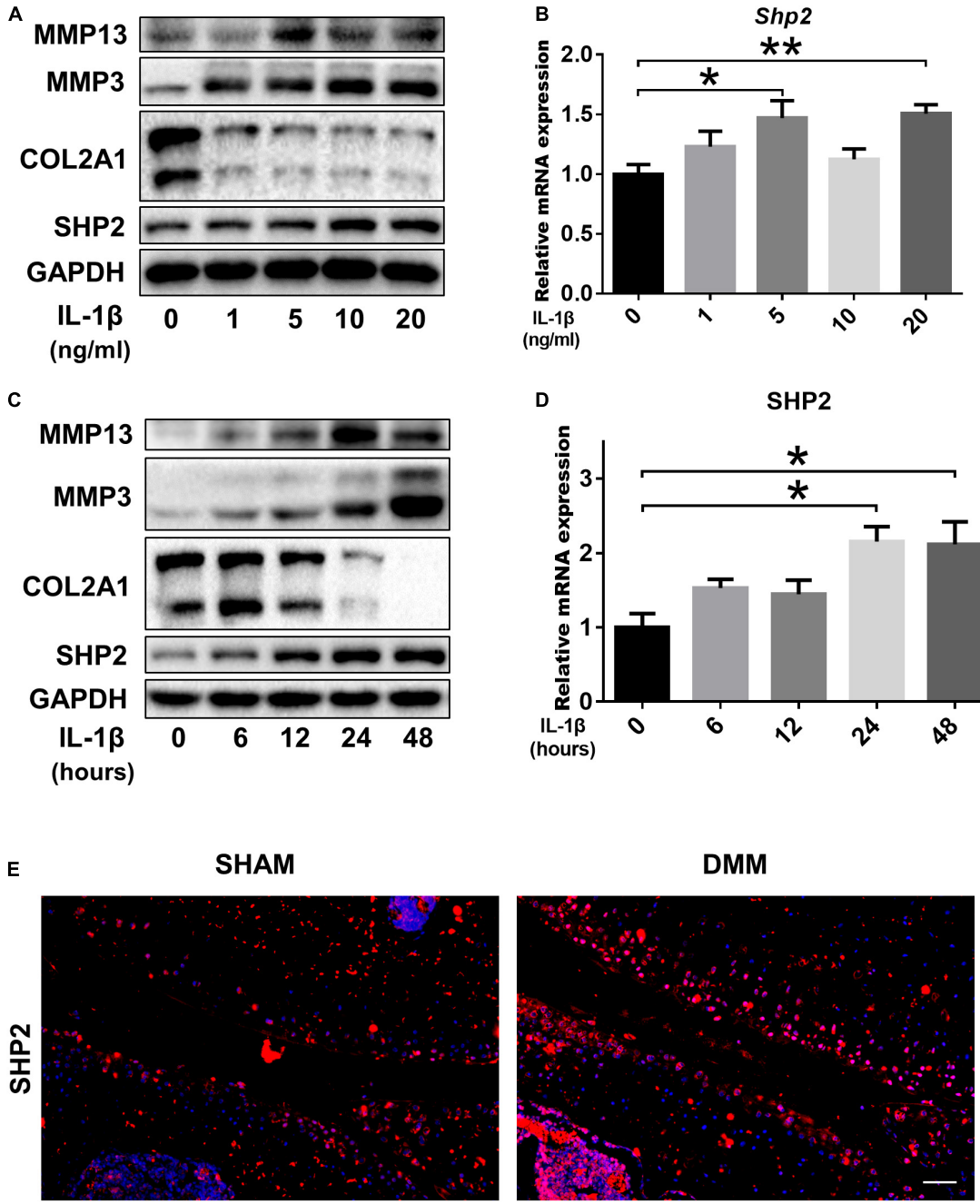


FIGURE 1 | SHP2 expression is increased in primary chondrocytes after IL-1β treatment and in mouse OA cartilage. **(A)** Representative western blot of MMP3, MMP13, COL2A1, SHP2, and **(B)** mRNA level of *Shp2* determined by qRT-PCR in chondrocytes after stimulation with various doses of IL-1β for 24 h. **(C)** Representative western blot of MMP3, MMP13, COL2A1, SHP2, and **(D)** mRNA level of *Shp2* determined by qRT-PCR in chondrocytes after stimulation with 5 ng/ml IL-1β for different time points. $^{*}P < 0.05$, $^{**}P < 0.01$ versus chondrocytes without IL-1β treatment. **(E)** Representative immunofluorescence images of SHP2 in articular cartilage in DMM and Sham mice, scale bar = 100 μm.

of MMP3 and MMP13 induced by IL-1β in protein and mRNA (**Figures 2I,K,L**). Consistently, *Aggrecan*, *Col2a1*, *Sox9* mRNA levels were reduced and *Col10a1* mRNA level was increased in chondrocytes exposed to IL-1β (**Figures 2M–P**). In short, our data displayed that SHP2 aggravated IL-1β–induced chondrocyte destruction *in vitro*.

SHP2 Interacts With β-Catenin in Chondrocytes and Activates Wnt/β-Catenin Pathway

Accumulating data identified that canonical Wnt/β-catenin signaling plays an important role in modulating the pathogenesis

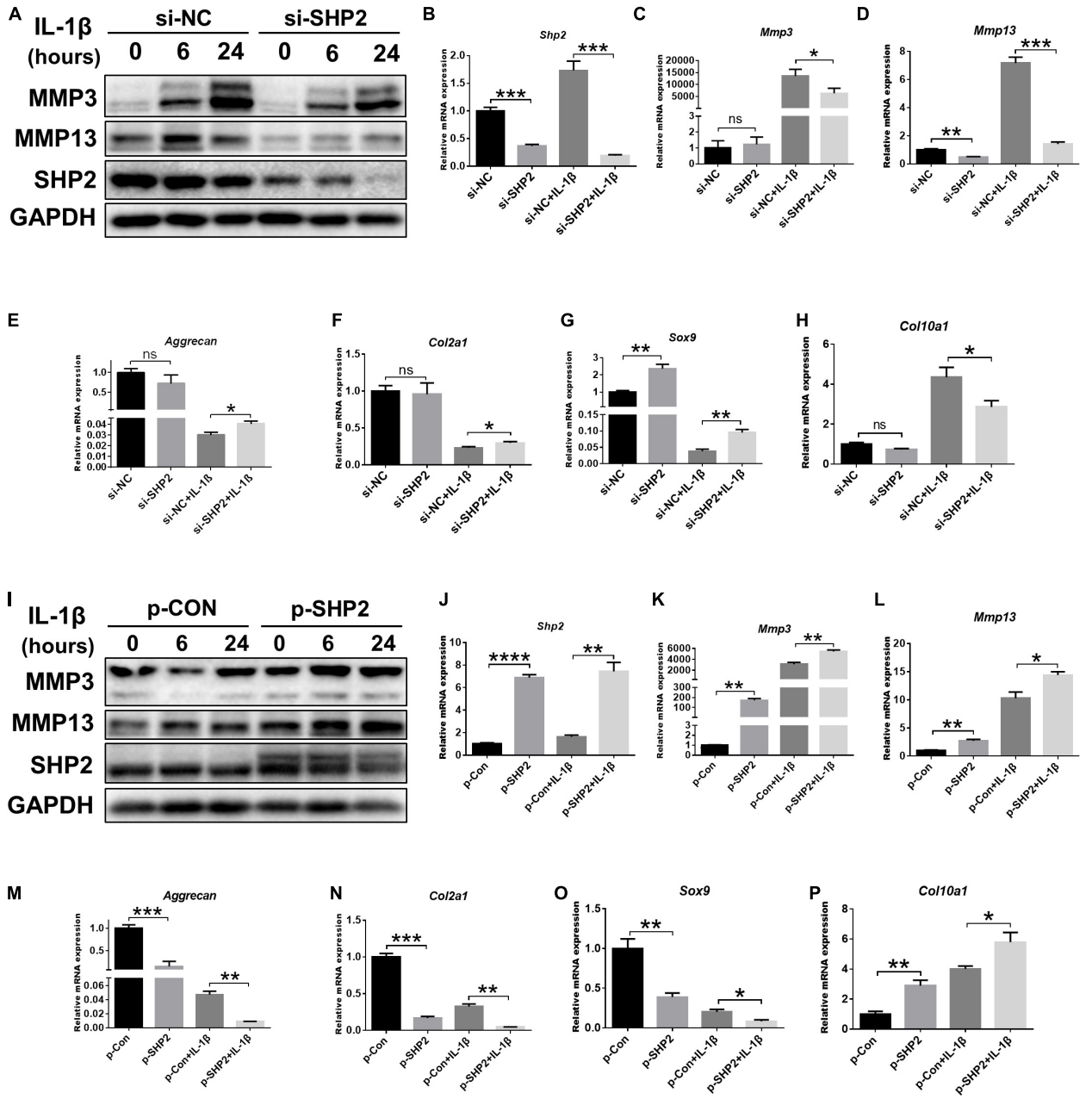


FIGURE 2 | SHP2 regulates IL-1β–induced cartilage destruction *in vitro*. **(A)** Representative western blot of MMP3, MMP13 and SHP2 after chondrocytes were transfected with si-NC or si-SHP2 for 48 h and then were treated with IL-1β (5 ng/ml) for indicated time points. **(B–H)** mRNA levels of *Shp2*, *Mmp3*, *Mmp13*, *Aggrecan*, *Col2a*, *Sox9,* and *Col10a1* were shown in chondrocytes that were transfected with si-NC or si-SHP2 for 48 h and then were treated with IL-1β (5 ng/mL) for 24 h. $^{*}P < 0.05$, $^{**}P < 0.01$, $^{***}P < 0.001$ versus si-NC transfected chondrocytes. **(I)** Representative western blot of MMP3, MMP13 and SHP2 after chondrocytes transfected with control plasmid (p-CON) or SHP2 (p-SHP2) overexpressed plasmid for 48 h and then incubated with or without IL-1β (5 ng/ml) for indicated time points. **(J–P)** mRNA levels of *Shp2*, *Mmp3*, *Mmp13*, *Aggrecan*, *Col2a1*, *Sox9,* and *Col10a1* were shown in chondrocytes transfected with p-CON or p-SHP2 plasmids for 48 h and then stimulated with IL-1β (5 ng/mL) for 24 h. $^{*}P < 0.05$, $^{**}P < 0.01$, $^{***}P < 0.001$, $^{****}P < 0.0001$ versus p-CON transfected chondrocytes.

of OA (Wu et al., 2010; Bouaziz et al., 2015; Zhou et al., 2017). Activation of β-catenin resulted in the development of an OA-like phenotype (Zhu et al., 2009), while inhibition of β-catenin signaling in articular chondrocytes contributes to cartilage destruction (Zhu et al., 2008). Other studies found that SHP2 and β-catenin proteins can form a complex and SHP2 increased β-catenin accumulation by inhibiting glycogen synthase kinase 3β (GSK-3β)–mediated β-catenin degradation in liver cancer (Biswas et al., 2006; Xiang et al., 2017). To unveil the possible mechanism by which SHP2 promotes OA progression,

we treated primary chondrocytes with IL-1β and found that IL-1β suppressed phosphorylated β-catenin at S33/37/141 sites, induced β-catenin phosphorylation at Y142, and increased total β-catenin expression at 6 and 12 h after IL-1β treatment. Although the expression of total β-catenin was slightly decreased 24 h after IL-1β treatment (**Figure 3A**). Downregulation of SHP2 by siRNA remarkably reduced β-catenin expression at 6 and 24 h after IL-1β treatment. However, the phosphorylated site at Y142 of β-catenin was not significantly changed in SHP2-downregulated cells after IL-1β treatment, indicating that SHP2 did not specifically dephosphorylate this site (**Figure 3B**). On the contrary, SHP2 overexpression promoted the expression of β-catenin (**Figure 3D**). To confirm SHP2 induced overexpression of matrix-degrading enzymes was indeed through β-catenin, we transfected mouse chondrocytes with plasmids expressing an active form of β-catenin with a mutation on the S33 site (β-cat-S33Y) (Ming et al., 2012). Overexpression of β-cat-S33Y prominently reversed the downregulation of MMP13 and MMP3 caused by SHP2 knockdown at 24 h after IL-1β treatment (**Figure 3C**). Additionally, the interaction of SHP2 and β-catenin in the primary chondrocytes was identified by co-immunoprecipitation (CO-IP) (**Figures 4A,B**). Besides, double staining for β-catenin and SHP2 was also performed and SHP2 colocalized with β-catenin in chondrocytes (**Figure 4C**). We further examined the target genes of the canonical Wnt/β-catenin pathway such as *Axin2*, *Lef1,* and *Tcf4*. In accordance with the β-catenin expression, the mRNA levels of these genes were attenuated by knocking down SHP2, but were increased significantly after SHP2 overexpression in chondrocytes (**Figures 4D,E**). Together, our results suggested that SHP2 activated Wnt/β-catenin signaling in chondrocytes.

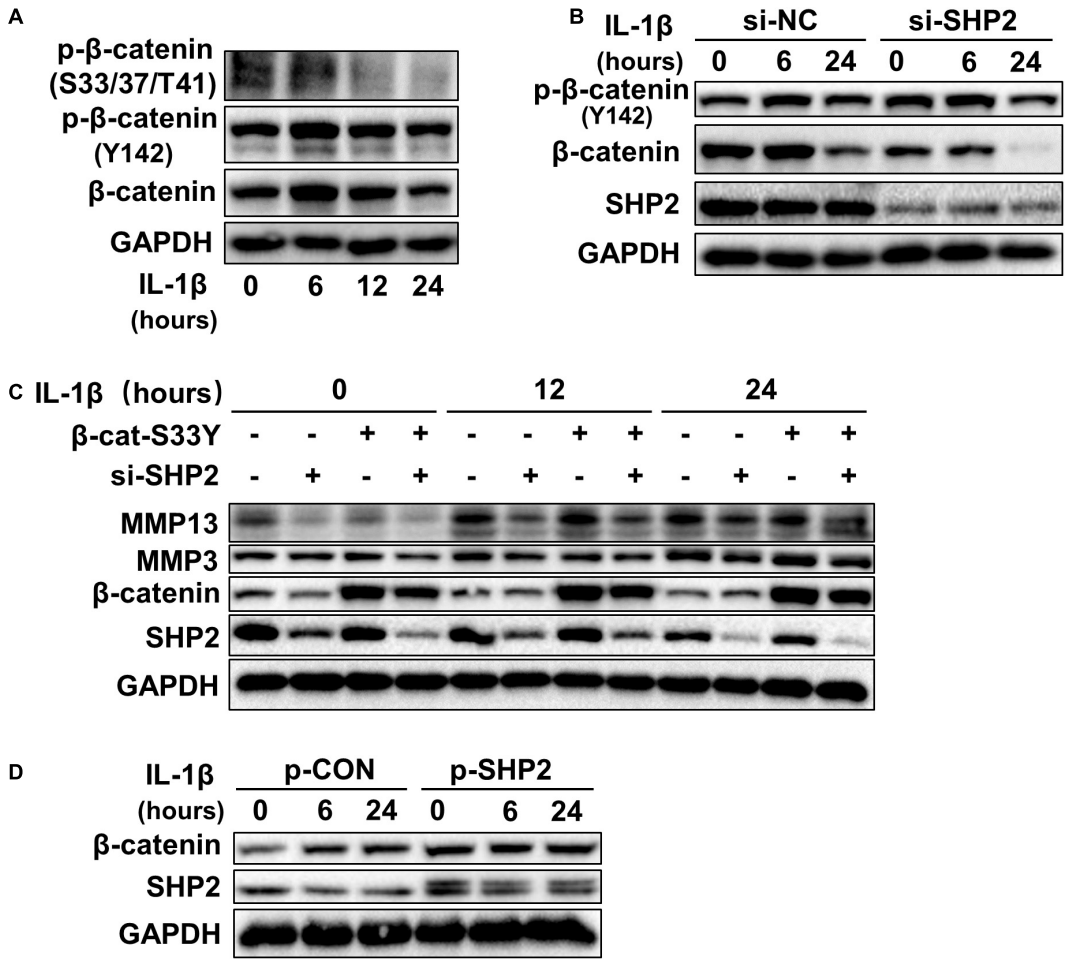


FIGURE 3 | SHP2 activates Wnt/β-catenin in chondrocytes. **(A)** Representative western blot of p-β-catenin (S33/37/T41), p-β-catenin (Y142) and β-catenin, in chondrocytes incubated with IL-1β of 5 ng/ml for the indicated time points. **(B)** Representative western blot of p-β-catenin (Y142), β-catenin and SHP2 in chondrocytes incubated with IL-1β (5 ng/ml) for indicated time points after si-NC or si-SHP2 transfection for 48 h. **(C)** Representative western blot of MMP3, MMP13, β-catenin, and SHP2 in chondrocytes incubated with IL-1β (5 ng/ml) for indicated time points after siRNA or active form of β-catenin (β-cat-S33Y) transfection with for 48 h. **(D)** Representative western blot of β-catenin and SHP2 in chondrocytes incubated with IL-1β (5 ng/ml) for the indicated time points after p-CON or p-SHP2 transfection for 48 h.

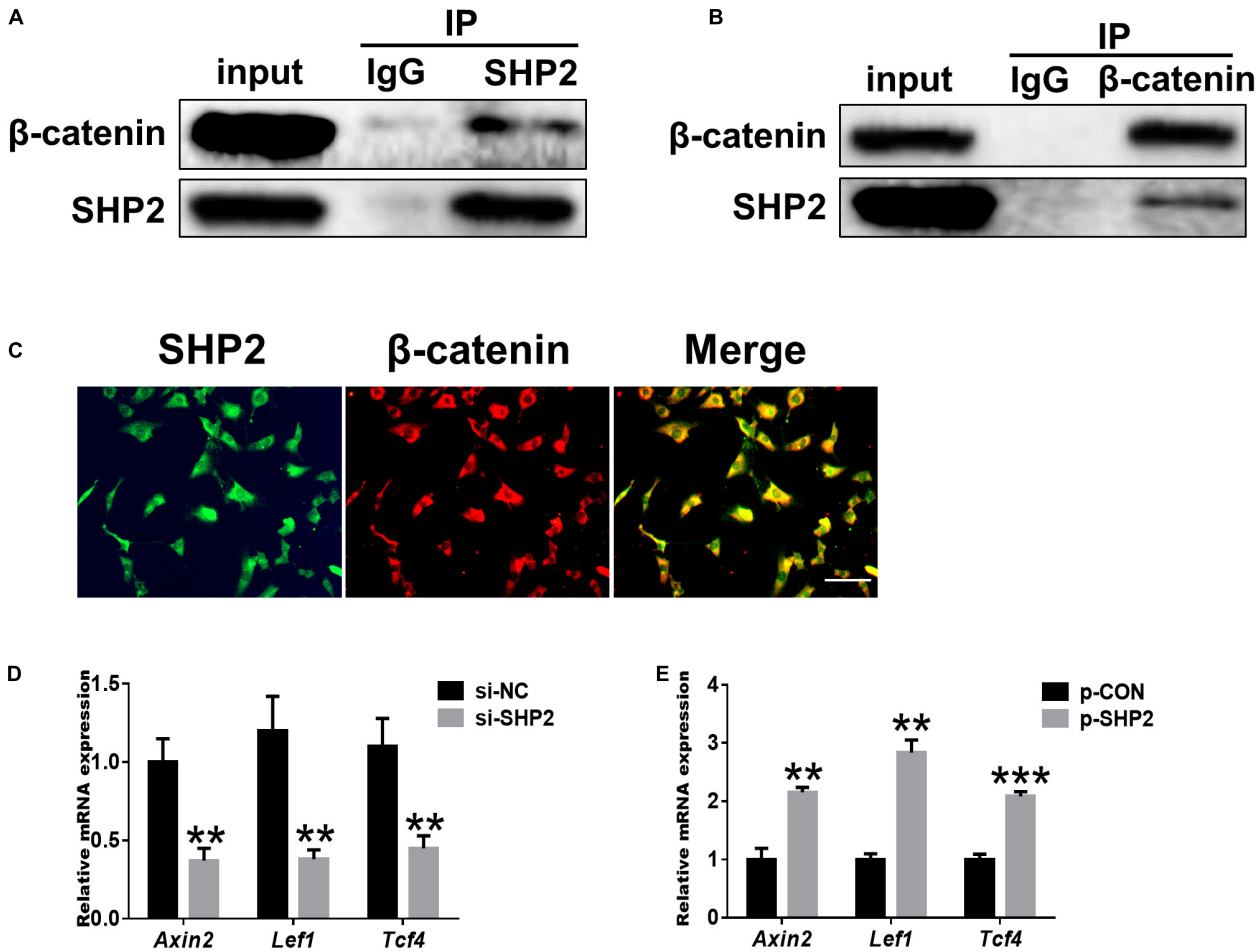


FIGURE 4 | SHP2 interacts with β-catenin and activates Wnt/β-catenin target genes. **(A)** β-catenin was co-immunoprecipitated with an anti-SHP2 antibody and **(B)** SHP2 was co-immunoprecipitated with an anti-β-catenin antibody in chondrocytes. **(C)** Immunofluorescence image for SHP2 and β-catenin cellular localization in chondrocytes. Scale bar, 100 μm. **(D)** Relative mRNA levels of three Wnt/β-catenin targets *Axin2*, *Lef1*, and *Tcf4* in chondrocytes after si-NC or si-SHP2 transfection. **(E)** Relative mRNA levels of three Wnt/β-catenin targets *Axin2*, *Lef1*, and *Tcf4* in chondrocytes after p-CON or p-SHP2 transfection. $n = 3$, $^{**}P < 0.01$, $^{***}P < 0.001$ versus si-NC or p-CON transfected chondrocytes.

SHP2 Promotes MAPK and NF-κB Signaling Pathways

The MAPK and NF-κB signaling pathways, widely involved in OA pathophysiology through various effects, are activated in osteoarthritic chondrocytes during aging and inflammation (Chang et al., 2019; Wongwichai et al., 2019). Hence, to investigate whether SHP2 influences IL-1β induced cartilage degradation via NF-κB and MAPK signaling pathways, we examined the phosphorylation levels of components of the MAPK and NF-κB pathways in chondrocytes. As shown in **Figures 5A,B**, the phosphorylated JNK, ERK, p38 protein levels were diminished in IL-1β stimulated chondrocytes following SHP2 siRNA transfection. The NF-κB pathway-related proteins were also tested. Phosphorylated IKKβ, p65 and IκBα were apparently decreased (**Figures 5C,D**). In contrast, overexpression of SHP2 significantly elevated the level of phosphorylated JNK, ERK, and p38 induced by IL-1β (**Figures 6A,B**). Phosphorylated IKKβ, p65, and IκBα were also increased after SHP2 overexpression (**Figures 6C,D**). These results implicated that SHP2 induced inflammation by activating MAPK and NF-κB signaling pathways.

Knockdown of SHP2 Attenuates Cartilage Degradation in DMM Model

To explore the possible association between SHP2 and OA *in vivo*, the mice OA model was induced by destabilized medial meniscus (DMM) surgery. A week after surgery, mice were intra-articular injected weekly with Ad-shControl or Ad-shSHP2 adenovirus both in sham-operated and DMM groups. Eight or twelve weeks after surgery, hematoxylin and eosin (HE), Safranin O/Fast Green, Toluidine blue staining and Immuno-histochemical staining were performed to assess the histomorphology differences among these groups. The efficiency of SHP2 knockdown in the cartilage was confirmed

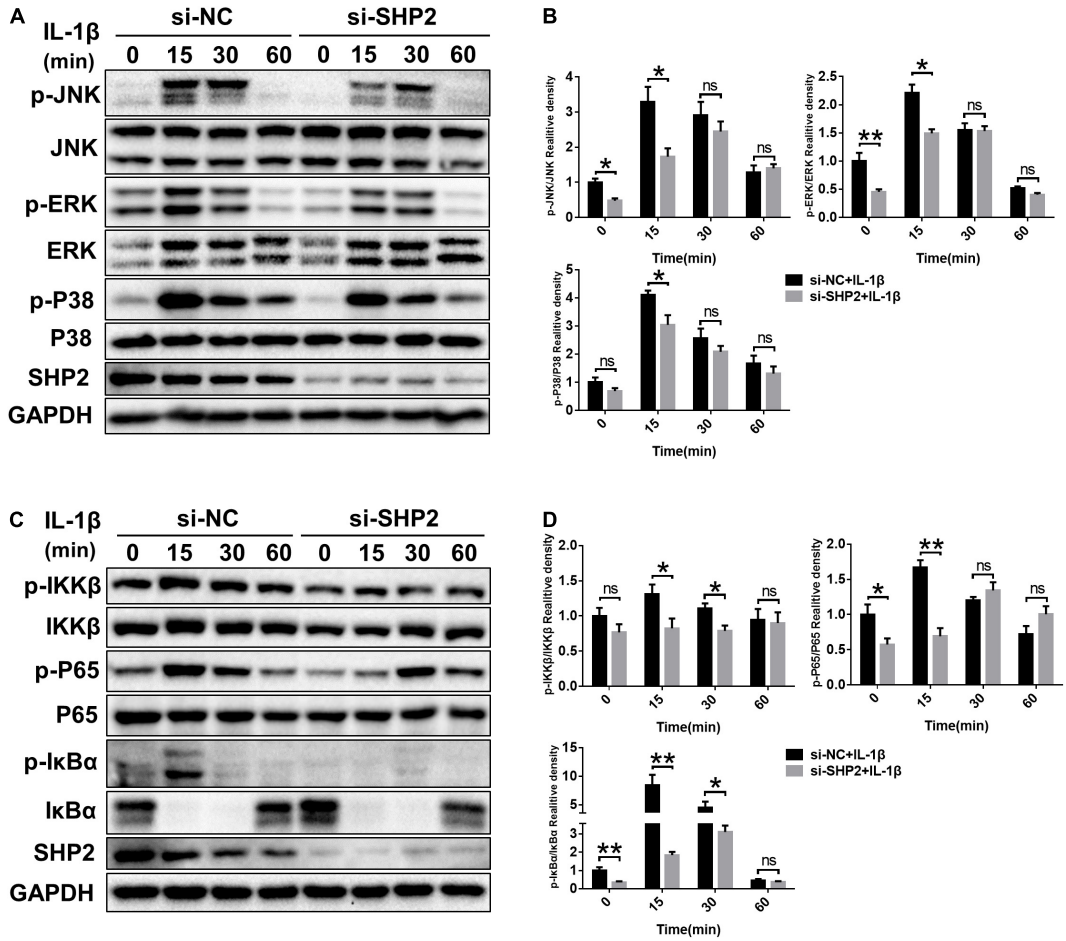


FIGURE 5 | SHP2 knockdown inhibits MAPK and NF-κB signaling pathways. Chondrocytes were transfected with siRNA for 48 h, and then stimulated with IL-1β for indicated time points. **(A)** Representative western blot and **(B)** quantification of the effect of SHP2 silencing on phosphorylated p38, JNK, ERK in chondrocytes. **(C)** Representative western blot and **(D)** quantification of the effect of SHP2 silencing on phosphorylated p65, IKKβ, and IκBα in chondrocytes. *$P < 0.05$, **$P < 0.01$ versus cells transfected with si-NC and without IL-1β treatment.

by SHP2 staining (**Figure 7A**). Data showed DMM group developed moderate cartilage destruction at 8 weeks after surgery. However, knockdown of SHP2 (Ad-shSHP2) dramatically alleviated cartilage degradation as demonstrated by Safranin O and Toluidine blue staining, with significantly lower OARSI grades at 8 weeks after DMM surgery (**Figures 7B,C**). In addition, the expression of MMP3 and MMP13 were significantly decreased in the DMM + shSHP2 group compared with the DMM + shControl group, while the levels of COL2A1 and AGGRECAN were significantly increased (**Figures 7D,E**). μCT was applied to view the osteophyte formation and determine the effects of SHP2 on the structure of tibial subchondral bone in these mice. More osteophytes were seen in DMM + Ad-shControl group, and SHP2 depletion reduced osteophyte formation at 8 weeks after surgery (**Figure 7F**). Also, we tested the effect of SHP2 in DMM model 12 weeks after surgery. Although osteophyte formation at 12 weeks seems to be less pronounced than that at 8 weeks after surgery in DMM + Ad-shControl group, SHP2 knockdown still ameliorated osteophyte formation and osteoarthritis progress (**Figures 8A–F**). The parameters of BV/TV, Tb.Th, and Tb.Sp were evaluated. Interestingly, SHP2 knockdown remarkably decreased BV/TV in sham-operated mice both at 8 and 12 weeks after surgery in subchondral bone, but no differences were seen in Tb.N, Tb.Th, and Tb.Sp. However, the difference in BV/TV was not observed between DMM + Ad-shSHP2 and DMM + Ad-shControl groups at 8 and 12 weeks after surgery (**Supplementary Figure 2**). The above results illustrated that inhibition of SHP2 reversed cartilage degradation and osteophyte formation *in vivo* without significantly affecting tibial subchondral bone remodeling in mice.

DISCUSSION

Degeneration of the articular cartilage is the main pathological feature of OA joints, which leads to cartilage damage, subchondral bone remodeling, and osteophyte formation (Loeser et al., 2012). To date, there is still no effective treatment

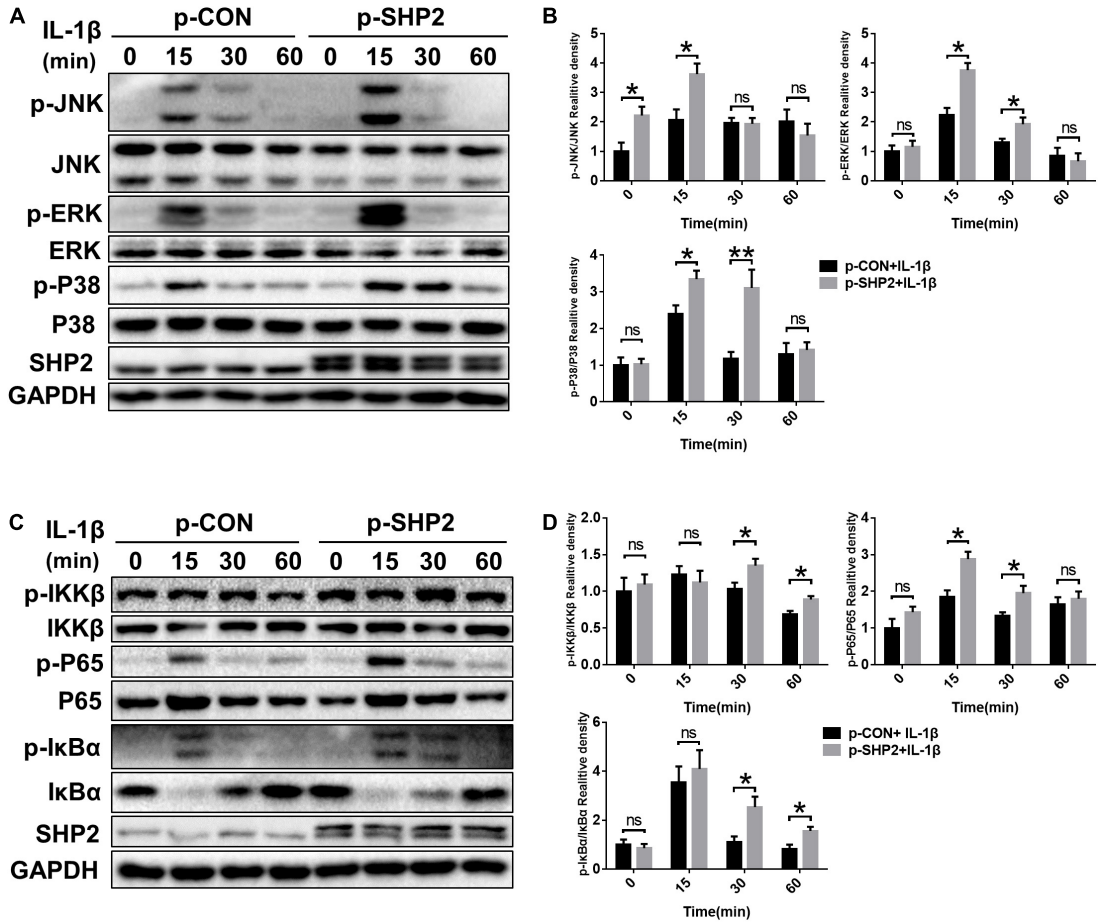


FIGURE 6 | SHP2 overexpression activates MAPK and NF-κB Signaling Pathways. Chondrocytes were transfected with p-CON or p-SHP2 overexpression plasmid for 48 h, and then stimulated with IL-1β for indicated time points. **(A)** Representative western blot and **(B)** quantification of the effect of SHP2 overexpression on phosphorylated p38, JNK, ERK in chondrocytes. **(C)** Representative western blot and **(D)** quantification of the effect of SHP2 overexpression on phosphorylated p65, IKKβ, and IκBα in chondrocytes. *$P < 0.05$, **$P < 0.01$ versus cells transfected with p-CON and without IL-1β treatment.

for OA. In the past 20 years, SHP2 has been reported to participate in developmental diseases, such as Noonan syndrome, metachondromatosis, and malignancies such as juvenile myelomonocytic leukemia (Zhang et al., 2015). For example, two studies focused on the upregulation of SHP2 in cancer and concomitant enhancement in tumor invasion (Chauhan et al., 2000; Sturla et al., 2011). Therefore, we aim to identify the association between SHP2 and OA. In the present study, we found SHP2 expression was significantly induced by IL-1β treatment. By loss-of-function and gain-of-function studies in chondrocytes, we found that SHP2 apparently affected MMP3, MMP13, AGGRECAN, COL2A1, SOX9, and COL10A1 expression. These results strongly suggested SHP2 play an important role in cartilage degeneration. However, we found SHP2 had no significant effect on chondrocyte apoptosis, proliferation or migration, indicating the effect of SHP2 on cartilage degeneration was not through influencing chondrocyte function.

The canonical Wnt/β-catenin signal axis has been involved in the pathogenesis of OA (Corr, 2008). Researchers concluded that activation of the Wnt/β-catenin pathway resulted in articular chondrocytes degradation toward catabolism and loss of structure and function. Several studies demonstrated the relation between SHP2 and β-catenin. Ilse Timmerman et al. reported that SHP2 regulated the restoration of endothelial cell adhesion junctions by regulating β-catenin phosphorylation (Timmerman et al., 2012). However, how SHP2 regulate β-catenin was not studied in cartilage. Our data recognized a targeted β-catenin in OA progression. SHP2 knockdown reduced β-catenin level accompanied by decreased levels of target genes such as *Axin2*, *LEF1,* and *TCF4*. The interaction of SHP2 and β-catenin was identified by co-immunoprecipitation and double immune-staining. Besides, constitute activation of β-catenin reversed the decrease of catabolic enzymes MMP3 and MMP13 induced by knockdown of SHP2 after IL-1β stimulation in primary chondrocytes, showing that β-catenin was a direct target of SHP2 to induce chondral degeneration. Notably, as SHP2 is a protein tyrosine phosphatase, we found p-β-catenin (Y142) was not altered by SHP2. Therefore, we speculated Y142 site of β-catenin may not be the specific dephosphorylated site for SHP2 to interact

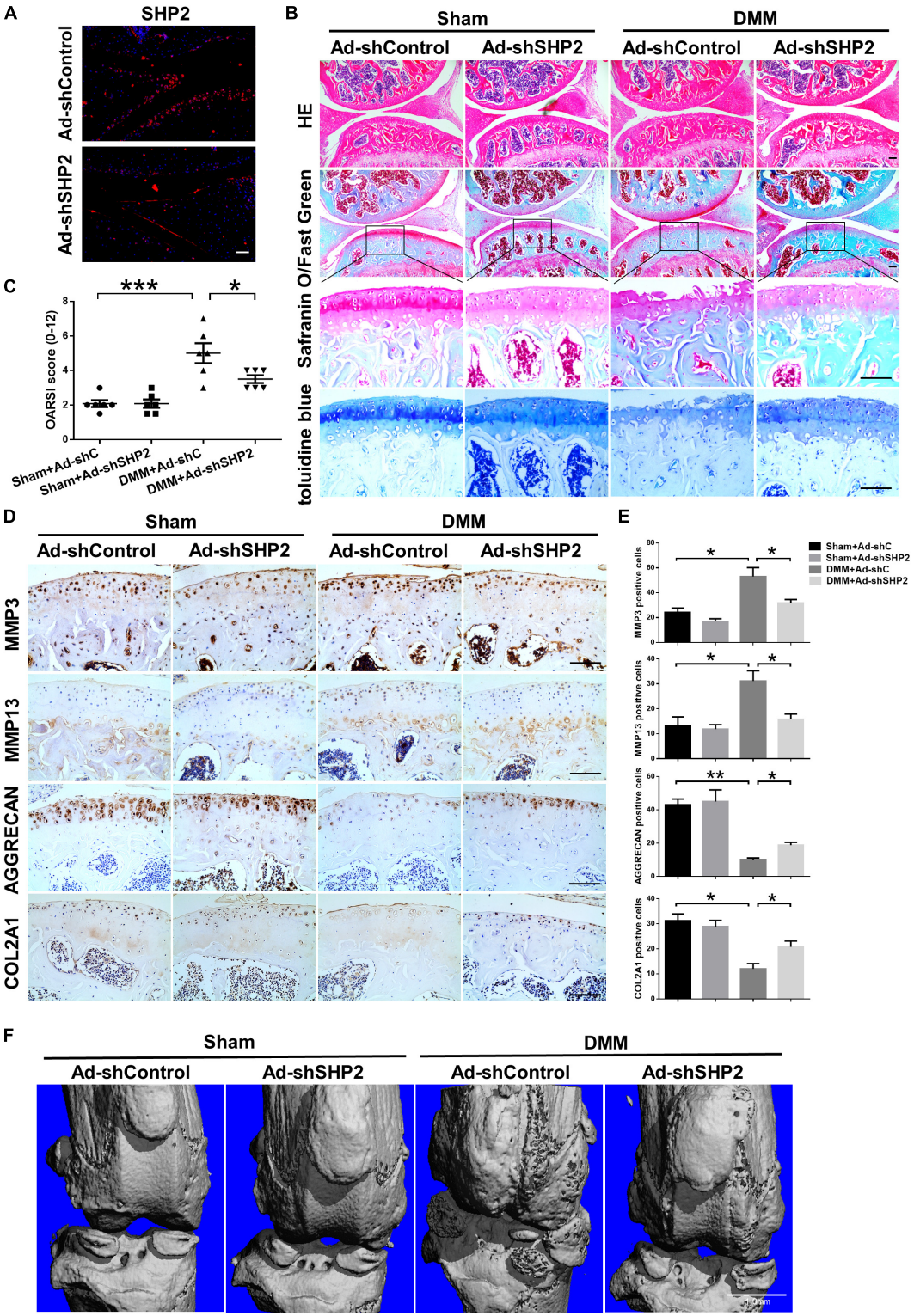


FIGURE 7 | Knockdown of SHP2 prevents cartilage destruction at 8 weeks after DMM surgery. **(A)** Immunofluorescence image of SHP2 after mice were intra-articular injected with Ad-shControl and Ad-shSHP2 virus 8 weeks after DMM surgery, scale bar = 100 μm. **(B)** HE, Safranin O/Fast Green, and toluidine blue staining and **(C)** OARSI grades of knee joints from Ad-shControl and Ad-shSHP2 mice at 8 weeks after DMM surgery. Scale bars, 100 μm, $^{*}P < 0.05$, $^{***}P < 0.001$ versus Sham + Ad-shC or DMM + Ad-shC group. **(D,E)** Immunostaining images and quantification of MMP3, MMP13, AGGRECAN, and COL2A1 in the joint cartilage of control and SHP2 knockdown mice at 8 weeks after DMM surgery. $^{*}P < 0.05$, $^{**}P < 0.01$ versus Sham + Ad-shC or DMM + Ad-shC group. $n = 6$. Scale bars, 100 μm. **(F)** Representative micro-CT images of the knee joints in each group. $n = 6$. Scale bar, 1.0 mm.

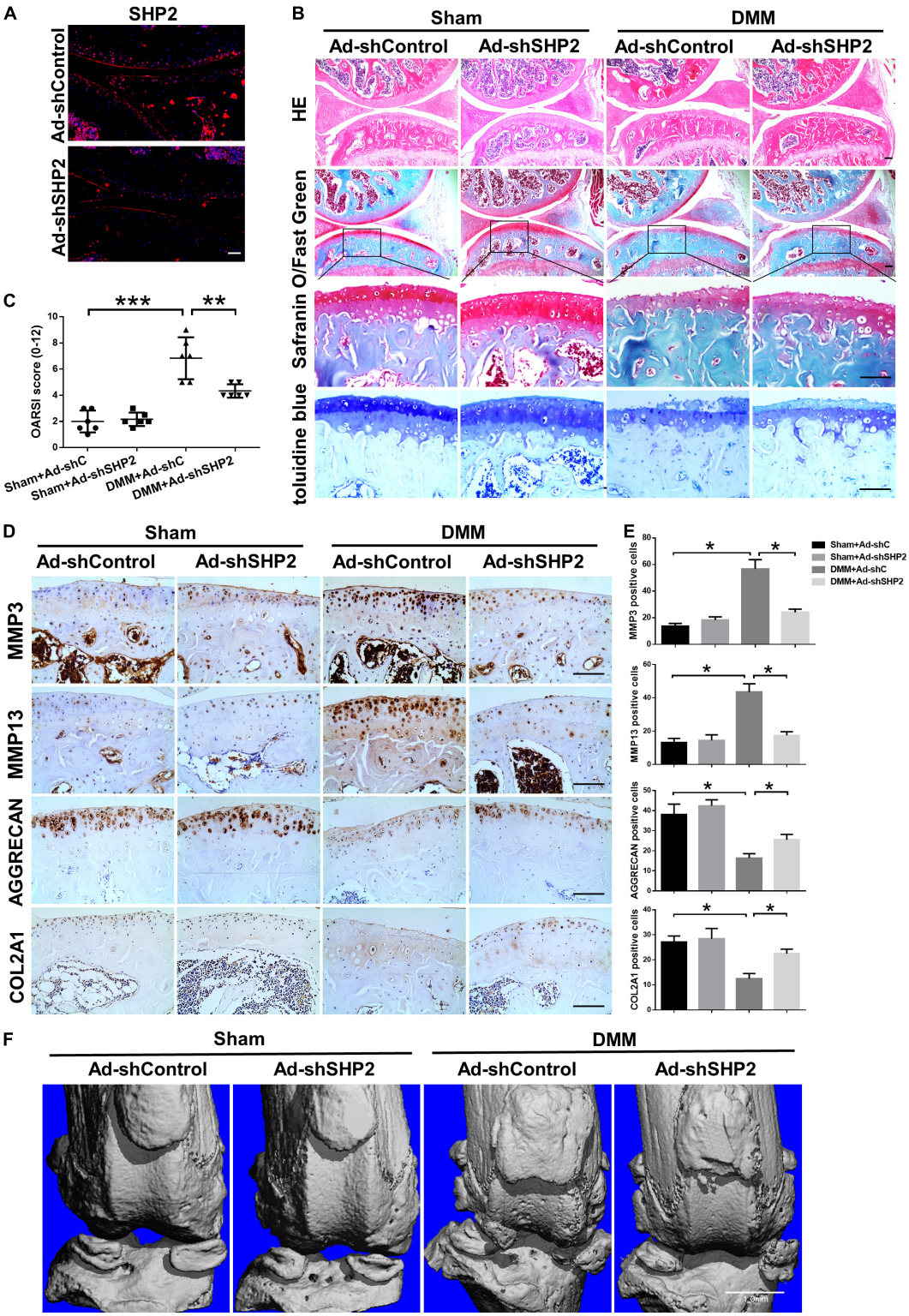


FIGURE 8 | Knockdown of SHP2 prevents cartilage destruction at 12 weeks after DMM surgery. **(A)** Immunofluorescence image of SHP2 after mice were intra-articular injected with Ad-shControl and Ad-shSHP2 virus 12 weeks after DMM surgery, scale bar = 100 μm. **(B)** HE, Safranin O/Fast Green, and toluidine blue staining and **(C)** OARSI grades of knee joints from Ad-shControl and Ad-shSHP2 mice at 12 weeks after DMM surgery. Scale bars, 100 μm, $^{**}P < 0.01$, $^{***}P < 0.001$ versus Sham + Ad-shC or DMM + Ad-shC group. **(D,E)** Immunostaining images and quantification of MMP3, MMP13, AGGRECAN, and COL2A1 in the joint cartilage of control and SHP2 knockdown mice at 12 weeks after DMM surgery. $^{*}P < 0.05$ versus Sham + Ad-shC or DMM + Ad-shC group. $n = 6$. Scale bars, 100 μm. **(F)** Representative u-CT images of the knee joints in each group. $n = 6$. Scale bar, 1.0 mm.

with. Further investigations need to be performed to recognize the specific dephosphorylation site of SHP2 on β-catenin.

The inflammation status in cartilage or periarticular tissues is mostly attributed to MAPK and NF-κB pathways whose hyperactivation directly initiate and target articular cartilage and subchondral bone, causing cartilage degeneration and subchondral bone formation. Previous studies have shown SHP2 mediated MAPK and NF-κB activation (Zou et al., 2007; Heun et al., 2019; Niogret et al., 2019; Liu et al., 2020). However, whether SHP2 regulated these signaling in OA pathogenesis was not fully elucidated. Our data found that inhibition of SHP2 impaired MAPK and NF-κB pathways while overexpression of SHP2 significantly activated MAPK and NF-κB pathways after IL-1β exposure, indicated SHP2 indeed regulate inflammation status *in vitro*. This may be one of the mechanisms for a better understanding of the potential role of SHP2 in OA initiation and progression. Surprisingly, SHP2 knockdown or overexpression, have a significant impact on cartilage degeneration such as altered MMP3, MMP13 level and downstream MAPK, NF-κB pathways without IL-1β treatment (see IL-1β 0 h treatment). This may attribute to that SHP2 knockdown or overexpression already affected β-catenin signaling at baseline levels (**Figures 3B,D**). Altered β-catenin further affect downstream OA-like phenotype (**Figure 2A**) and MAPK, NF-κB pathways (**Figures 5A–D**). The similar phenomenon was not seen in our DMM models, where knockdown of SHP2 by intra-articular injection of Ad-shSHP2 robustly prevented cartilage degradation compared with the control both at 8 and 12 weeks after DMM surgery, but not in sham-operated mice. Since *in vivo* researches are much more complicated than *in vitro*, it is normal to see some of the inconsistency in different models. Accordingly, MMP3 and MMP13 levels decreased in Ad-shSHP2 injected mice confirmed its role in catabolic enzymes, the increased AGGRECAN and COL2A1 levels further proved its protective role in OA pathogenesis after SHP2 knockdown.

Interestingly, osteophyte formation was not so obvious as 8 weeks results, this maybe explained that the osteophyte formation rate was alleviated as time went by in all groups but SHP2 knockdown still has a beneficial effect on osteophyte formation at 12 weeks after surgery. Unlike cartilage degeneration process, most degenerated chondrocytes are hypertrophic differentiated and are kind of "irreversible" in OA pathogenesis. Osteophyte formation was a result of sclerosis of the subchondral bone, which should be faster to be alleviated. The current study found the subchondral bone mass was not significantly altered after SHP2 reduction as shown by μCT although SHP2 knockdown remarkably decreased BV/TV in sham-operated mice both at 8 and 12 weeks after surgery in subchondral bone, no differences were seen in Tb.N, Tb.Th, and Tb.Sp. Collectively, our results indicated that increased SHP2 is important for the initiation and progression of OA, SHP2 knockdown ameliorated cartilage degeneration.

Consistent with *in vitro* studies, there were some limitations of this study. First, the effect of overexpressing SHP2 *in vivo* was not detected although the *in vitro* results were shown in the present study, future researches will be conducted to see these results. Second, it would be more convincing if chondrocytes-specific SHP2 deletion mice can be used. However, since the construction and breeding of these mice are very time-consuming, we will extend this to animal models in the future.

Given the facts above, our study identified that SHP2 played a vital role in the degeneration of articular cartilage in OA. SHP2 knockdown protected cartilage from degradation during OA pathogenesis via suppressing the Wnt/β-catenin pathway, MAPK and NF-κB signaling pathways. These proved SHP2 might be a promising therapeutic target for OA.

DATA AVAILABILITY STATEMENT

The original contributions presented in the study are included in the article/**Supplementary Material**, further inquiries can be directed to the corresponding author/s.

ETHICS STATEMENT

The animal study was reviewed and approved by the Ethics Committee on Animal Experimentation of Tongji Hospital, Huazhong University of Science and Technology. Written informed consent was obtained from the owners for the participation of their animals in this study.

AUTHOR CONTRIBUTIONS

JX and XS designed the study. TT performed most of the experiments. DL, CG, HL, and ZL helped with the DMM surgery. WL, CZ, and DQ helped inject the mice. ZD analyzed some of the data. All authors provided editorial comments.

FUNDING

This study was supported by the National Natural Science Foundation of China (Nos. 81974350 and 81772396) and the Natural Science Foundation of Hubei Province (No. 2020CFA019).

ACKNOWLEDGMENTS

We thank Dr. Ke Chen in Department of Urology, Tonji Hospital, Tongji Medical College, Huazhong University of Science and Technology for providing β-cat-S33Y plasmid.

SUPPLEMENTARY MATERIAL

The Supplementary Material for this article can be found online at: https://www.frontiersin.org/articles/10.3389/fcell.2021.646386/full#supplementary-material

Supplementary Figure 1 | The impact of SHP2 on cell migration, proliferation and apoptosis. Chondrocytes were seeded onto each well after transfection for 48 h, and then chondrocytes were incubated with or without IL-1β (5 ng/mL) for 24 h. **(A,B)** An apoptosis detection kit was used to detect chondrocytes apoptosis by flow cytometry after si-NC or si-SHP2 transfection. Data are means ± SEM of three independent experiments; $^*P < 0.05$ versus the control group. **(C,D)** Chondrocytes apoptosis by flow cytometry after p-Con or p-SHP2 transfection. Data are means ± SEM of three independent experiments; $^*P < 0.05$ versus the control group. **(E,F)** The proliferation of chondrocytes was detected by CCK-8 assay. **(G–J)** The scratch-wound assay and Quantitative data revealed the impacts of transfection with SHP2 siRNA or overexpression plasmid on the migration of chondrocytes. Scale bar, 100 μm. Data are means ± SEM of three independent experiments; $^*P < 0.05$ versus the control group.

Supplementary Figure 2 | The effect of SHP2 on subchondral bone quality in mice. **(A)** μCT parameters of BV/TV, Tb. N, Tb. Th and Tb. Sp of subchondral bone in each group of mice 8 weeks after DMM surgery. $n = 6$, $^*P < 0.05$ versus Sham+Ad−shControl group. **(B)** uCT parameters of BV/TV, Tb. N, Tb. Th and Tb. Sp of subchondral bone in each group of mice 12 weeks after DMM surgery. $n = 6$, $^*P < 0.05$ versus Sham+Ad−shControl group.

REFERENCES

Bai, J., Zhang, Y., Zheng, X., Huang, M., Cheng, W., Shan, H., et al. (2020). LncRNA MM2P-induced, exosome-mediated transfer of Sox9 from monocyte-derived cells modulates primary chondrocytes. *Cell Death Dis*. 11:763. doi: 10.1038/s41419-020-02945-5

Biswas, P., Canosa, S., Schoenfeld, D., Schoenfeld, J., Li, P., Cheas, L. C., et al. (2006). PECAM-1 affects GSK-3beta-mediated beta-catenin phosphorylation and degradation. *Am. J. Pathol*. 169, 314–324. doi: 10.2353/ajpath.2006.051112

Bouaziz, W., Funck-Brentano, T., Lin, H., Marty, C., Ea, H. K., Hay, E., et al. (2015). Loss of sclerostin promotes osteoarthritis in mice via beta-catenin-dependent and -independent Wnt pathways. *Arthritis Res. Ther*. 17:24. doi: 10.1186/s13075-015-0540-6

Chang, S. H., Mori, D., Kobayashi, H., Mori, Y., Nakamoto, H., Okada, K., et al. (2019). Excessive mechanical loading promotes osteoarthritis through the gremlin-1-NF-kappaB pathway. *Nat. Commun*. 10:1442. doi: 10.1038/s41467-019-09491-5

Chauhan, D., Pandey, P., Hideshima, T., Treon, S., Raje, N., Davies, F. E., et al. (2000). SHP2 mediates the protective effect of interleukin-6 against dexamethasone-induced apoptosis in multiple myeloma cells. *J. Biol. Chem*. 275, 27845–27850. doi: 10.1074/jbc.M003428200

Corr, M. (2008). Wnt-beta-catenin signaling in the pathogenesis of osteoarthritis. *Nat. Clin. Pract. Rheumatol*. 4, 550–556. doi: 10.1038/ncprheum0904

Deng, Y., Lu, J., Li, W., Wu, A., Zhang, X., Tong, W., et al. (2018). Reciprocal inhibition of YAP/TAZ and NF-kappaB regulates osteoarthritic cartilage degradation. *Nat. Commun*. 9:4564. doi: 10.1038/s41467-018-07022-2

Glasson, S. S., Askew, R., Sheppard, B., Carito, B., Blanchet, T., Ma, H. L., et al. (2005). Deletion of active ADAMTS5 prevents cartilage degradation in a murine model of osteoarthritis. *Nature* 434, 644–648.

Glasson, S. S., Blanchet, T. J., and Morris, E. A. (2007). The surgical destabilization of the medial meniscus (DMM) model of osteoarthritis in the 129/SvEv mouse. *Osteoarthritis Cartilage* 15, 1061–1069. doi: 10.1016/j.joca.2007.03.006

Glasson, S. S., Chambers, M. G., Van Den Berg, W. B., and Little, C. B. (2010). The OARSI histopathology initiative – recommendations for histological assessments of osteoarthritis in the mouse. *Osteoarthritis Cartilage* 18(Suppl. 3), S17–S23. doi: 10.1016/j.joca.2010.05.025

Glyn-Jones, S., Palmer, A. J. R., Agricola, R., Price, A. J., Vincent, T. L., Weinans, H., et al. (2015). Osteoarthritis. *Lancet* 386, 376–387. doi: 10.1016/s0140-6736(14)60802-3

Heun, Y., Pircher, J., Czermak, T., Bluem, P., Hupel, G., Bohmer, M., et al. (2019). Inactivation of the tyrosine phosphatase SHP-2 drives vascular dysfunction in sepsis. *EBioMedicine* 42, 120–132. doi: 10.1016/j.ebiom.2019.03.034

Hollander, A. P., Pidoux, I., Reiner, A., Rorabeck, C., Bourne, R., and Poole, A. R. (1995). Damage to type II collagen in aging and osteoarthritis starts at the articular surface, originates around chondrocytes, and extends into the cartilage with progressive degeneration. *J. Clin. Invest*. 96, 2859–2869.

Kamiya, N., Kim, H. K., and King, P. D. (2014). Regulation of bone and skeletal development by the SHP-2 protein tyrosine phosphatase. *Bone* 69, 55–60. doi: 10.1016/j.bone.2014.08.015

Lapinski, P. E., Meyer, M. F., Feng, G. S., Kamiya, N., and King, P. D. (2013). Deletion of SHP-2 in mesenchymal stem cells causes growth retardation, limb and chest deformity, and calvarial defects in mice. *Dis. Model Mech*. 6, 1448–1458. doi: 10.1242/dmm.012849

Lark, M. W., Bayne, E. K., and Lohmander, L. S. (1995). Aggrecan degradation in osteoarthritis and rheumatoid arthritis. *Acta Orthop. Scand. Suppl*. 266, 92–97.

Li, K., Zhang, Y., Zhang, Y., Jiang, W., Shen, J., Xu, S., et al. (2018). Tyrosine kinase fyn promotes osteoarthritis by activating the beta-catenin pathway. *Ann. Rheum. Dis*. 77, 935–943. doi: 10.1136/annrheumdis-2017-212658

Liu, Y. N., Guan, Y., Shen, J., Jia, Y. L., Zhou, J. C., Sun, Y., et al. (2020). Shp2 positively regulates cigarette smoke-induced epithelial mesenchymal transition by mediating MMP-9 production. *Respir. Res*. 21:161. doi: 10.1186/s12931-020-01426-9

Loeser, R. F., Goldring, S. R., Scanzello, C. R., and Goldring, M. B. (2012). Osteoarthritis: a disease of the joint as an organ. *Arthritis Rheum*. 64, 1697–1707.

Maeshima, K., Stanford, S. M., Hammaker, D., Sacchetti, C., Zeng, L. F., Ai, R., et al. (2016). Abnormal PTPN11 enhancer methylation promotes rheumatoid arthritis fibroblast-like synoviocyte aggressiveness and joint inflammation. *JCI Insight* 1:e86580. doi: 10.1172/jci.insight.86580

Ming, M., Wang, S., Wu, W., Senyuk, V., Le Beau, M. M., Nucifora, G., et al. (2012). Activation of Wnt/β-catenin protein signaling induces mitochondria-mediated apoptosis in hematopoietic progenitor cells. *J. Biol. Chem*. 287, 22683–22690. doi: 10.1074/jbc.M112.342089

Nakashima, T., Hayashi, M., Fukunaga, T., Kurata, K., Oh-Hora, M., Feng, J. Q., et al. (2011). Evidence for osteocyte regulation of bone homeostasis through RANKL expression. *Nat. Med*. 17, 1231–1234. doi: 10.1038/nm.2452

Naski, M. C., Colvin, J. S., Coffin, J. D., and Ornitz, D. M. (1998). Repression of hedgehog signaling and BMP4 expression in growth plate cartilage by fibroblast growth factor receptor 3. *Development* 125, 4977–4988.

Neuhold, L. A., Killar, L., Zhao, W., Sung, M. L., Warner, L., Kulik, J., et al. (2001). Postnatal expression in hyaline cartilage of constitutively active human collagenase-3 (MMP-13) induces osteoarthritis in mice. *J. Clin. Invest*. 107, 35–44.

Niogret, C., Miah, S. M. S., Rota, G., Fonta, N. P., Wang, H., Held, W., et al. (2019). Shp-2 is critical for ERK and metabolic engagement downstream of IL-15 receptor in NK cells. *Nat. Commun*. 10:1444. doi: 10.1038/s41467-019-09431-3

Stickens, D., Behonick, D. J., Ortega, N., Heyer, B., Hartenstein, B., Yu, Y., et al. (2004). Altered endochondral bone development in matrix metalloproteinase 13-deficient mice. *Development* 131, 5883–5895. doi: 10.1242/dev.01461

Sturla, L. M., Zinn, P. O., Ng, K., Nitta, M., Kozono, D., Chen, C. C., et al. (2011). Src homology domain-containing phosphatase 2 suppresses cellular senescence in glioblastoma. *Br. J. Cancer* 105, 1235–1243. doi: 10.1038/bjc.2011.345

Timmerman, I., Hoogenboezem, M., Bennett, A. M., Geerts, D., Hordijk, P. L., and van Buul, J. D. (2012). The tyrosine phosphatase SHP2 regulates recovery of endothelial adherens junctions through control of beta-catenin phosphorylation. *Mol. Biol. Cell* 23, 4212–4225. doi: 10.1091/mbc.E12-01-0038

Uusitalo, H., Hiltunen, A., Soderstrom, M., Aro, H. T., and Vuorio, E. (2000). Expression of cathepsins B, H, K, L, and S and matrix metalloproteinases 9 and 13 during chondrocyte hypertrophy and endochondral ossification in mouse fracture callus. *Calcif. Tissue Int*. 67, 382–390. doi: 10.1007/s002230001152

Wang, Q., Rozelle, A. L., Lepus, C. M., Scanzello, C. R., Song, J. J., Larsen, D. M., et al. (2011). Identification of a central role for complement in osteoarthritis. *Nat. Med*. 17, 1674–1679. doi: 10.1038/nm.2543

Wongwichai, T., Teeyakasem, P., Pruksakorn, D., Kongtawelert, P., and Pothacharoen, P. (2019). Anthocyanins and metabolites from purple rice inhibit IL-1beta-induced matrix metalloproteinases expression in human articular

chondrocytes through the NF-kappaB and ERK/MAPK pathway. *Biomed. Pharmacother*. 112:108610. doi: 10.1016/j.biopha.2019.108610

Wu, Q., Zhu, M., Rosier, R. N., Zuscik, M. J., O'Keefe, R. J., and Chen, D. (2010). Beta-catenin, cartilage, and osteoarthritis. *Ann. N. Y. Acad. Sci*. 1192, 344–350. doi: 10.1111/j.1749-6632.2009.05212.x

Xiang, D., Cheng, Z., Liu, H., Wang, X., Han, T., Sun, W., et al. (2017). Shp2 promotes liver cancer stem cell expansion by augmenting beta-catenin signaling and predicts chemotherapeutic response of patients. *Hepatology* 65, 1566–1580. doi: 10.1002/hep.28919

Zhang, J., Zhang, F., and Niu, R. (2015). Functions of Shp2 in cancer. *J. Cell. Mol. Med*. 19, 2075–2083. doi: 10.1111/jcmm.12618

Zhou, Y., Mohan, A., Moore, D. C., Lin, L., Zhou, F. L., Cao, J., et al. (2015). SHP2 regulates osteoclastogenesis by promoting preosteoclast fusion. *FASEB J*. 29, 1635–1645. doi: 10.1096/fj.14-260844

Zhou, Y., Wang, T., Hamilton, J. L., and Chen, D. (2017). Wnt/beta-catenin signaling in osteoarthritis and in other forms of arthritis. *Curr. Rheumatol. Rep*. 19:53. doi: 10.1007/s11926-017-0679-z

Zhu, M., Chen, M., Zuscik, M., Wu, Q., Wang, Y. J., Rosier, R. N., et al. (2008). Inhibition of beta-catenin signaling in articular chondrocytes results in articular cartilage destruction. *Arthritis Rheum*. 58, 2053–2064. doi: 10.1002/art.23614

Zhu, M., Tang, D., Wu, Q., Hao, S., Chen, M., Xie, C., et al. (2009). Activation of beta-catenin signaling in articular chondrocytes leads to osteoarthritis-like phenotype in adult beta-catenin conditional activation mice. *J. Bone Miner. Res*. 24, 12–21. doi: 10.1359/jbmr.080901

Zou, G. M., Hu, W. Y., and Wu, W. (2007). TNF family molecule LIGHT regulates chemokine CCL27 expression on mouse embryonic stem cell-derived dendritic cells through NF-kappaB activation. *Cell. Signal*. 19, 87–92. doi: 10.1016/j.cellsig.2006.05.025

Conflict of Interest: The authors declare that the research was conducted in the absence of any commercial or financial relationships that could be construed as a potential conflict of interest.

Copyright © 2021 Tao, Luo, Gao, Liu, Lei, Liu, Zhou, Qi, Deng, Sun and Xiao. This is an open-access article distributed under the terms of the Creative Commons Attribution License (CC BY). The use, distribution or reproduction in other forums is permitted, provided the original author(s) and the copyright owner(s) are credited and that the original publication in this journal is cited, in accordance with accepted academic practice. No use, distribution or reproduction is permitted which does not comply with these terms.

frontiers in Cell and Developmental Biology

ORIGINAL RESEARCH
published: 26 May 2021
doi: 10.3389/fcell.2021.675503

CGRP Regulates the Age-Related Switch Between Osteoblast and Adipocyte Differentiation

Hang Li[1,2†], Jian Qu[1,2†], Haihong Zhu[1,2], Jiaojiao Wang[1,2], Hao He[3], Xinyan Xie[1,2], Ren Wu[4] and Qiong Lu[1,2*]*

[1] Department of Pharmacy, The Second Xiangya Hospital of Central South University, Changsha, China, [2] Institute of Clinical Pharmacy, Central South University, Changsha, China, [3] Department of Vascular Surgery, The Second Xiangya Hospital of Central South University, Changsha, China, [4] Department of Orthopedics, The Second Xiangya Hospital of Central South University, Changsha, China

OPEN ACCESS

Edited by:
Changjun Li,
Central South University, China

Reviewed by:
Ye Xiao,
Central South University, China
Gaofeng Xiong,
University of Kentucky, United States

***Correspondence:**
Qiong Lu
christy_luq@csu.edu.cn
Ren Wu
wurenraul@csu.edu.cn

† These authors have contributed equally to this work

Specialty section:
This article was submitted to Molecular Medicine, a section of the journal Frontiers in Cell and Developmental Biology

Received: *03 March 2021*
Accepted: *03 May 2021*
Published: *26 May 2021*

Citation:
Li H, Qu J, Zhu H, Wang J, He H, Xie X, Wu R and Lu Q (2021) CGRP Regulates the Age-Related Switch Between Osteoblast and Adipocyte Differentiation. Front. Cell Dev. Biol. 9:675503. doi: 10.3389/fcell.2021.675503

Osteoporosis is a chronic age-related disease. During aging, bone marrow-derived mesenchymal stem cells (BMSCs) display increased adipogenic, along with decreased osteogenic, differentiation capacity. The aim of the present study was to investigate the effect of calcitonin gene-related peptide (CGRP) on the osteogenic and adipogenic differentiation potential of BMSC-derived osteoblasts. Here, we found that the level of CGRP was markedly lower in bone marrow supernatant from aged mice compared with that in young mice. *In vitro* experiments indicated that CGRP promoted the osteogenic differentiation of BMSCs while inhibiting their adipogenic differentiation. Compared with vehicle-treated controls, aged mice treated with CGRP showed a substantial promotion of bone formation and a reduction in fat accumulation in the bone marrow. Similarly, we found that CGRP could significantly enhance bone formation in ovariectomized (OVX) mice *in vivo*. Together, our results suggested that CGRP may be a key regulator of the age-related switch between osteogenesis and adipogenesis in BMSCs and may represent a potential therapeutic strategy for the treatment of age-related bone loss.

Keywords: CGPR, osteoporosis, BMSCs, osteogenic, adipogenic, age-related

INTRODUCTION

Osteoporosis is a chronic disease caused by the breakdown of bone homeostasis, with elderly and postmenopausal women being the populations most at risk of developing this condition (NIH Consensus Development Panel on Osteoporosis Prevention, Diagnosis, and Therapy, 2001; Rachner et al., 2011). Age-related bone loss and osteoporosis have been associated with reduced numbers of osteoblasts and increased numbers of adipocytes (Idris et al., 2009; Yu and Wang, 2016). It is known that bone marrow mesenchymal stem cells (BMSCs) have the potential to differentiate into osteoblasts, adipocytes, and osteoclasts, thereby playing an important role in bone formation (Li et al., 2016; Chen et al., 2018; Peng et al., 2019). Overall, bone homeostasis depends on the balance between the osteogenic and adipogenic differentiation of BMSCs (Li et al., 2015;

Lv et al., 2018). Age-related osteoporosis results from reduced osteogenic differentiation and increased adipogenic differentiation of BMSCs in elderly patients (Shen et al., 2012; Childs et al., 2015; Li et al., 2017).

Calcitonin gene-related peptide (CGRP), a member of the calcitonin protein family, is a 37-amino acid peptide generated through the alternative splicing of primary transcripts of the calcitonin gene (Amara et al., 1982; Rosenfeld et al., 1983; Naot and Cornish, 2008). In humans and mice, CGRP exists as two isoforms—α-CGRP and β-CGRP—which are encoded by the *CALCA* and *CALCB* genes, respectively. In mice, α-CGRP is highly expressed in the central nervous system and peripheral nervous system, while β-CGRP is expressed in the enteric nervous system (Sternini, 1992; Russell et al., 2014). In addition, in mice, the *Calca* gene has been shown to affect bone remodeling; however, the underlying mechanism remains unclear (Schinke et al., 2004).

CGRP is a neuropeptide that is released from sensory nerve endings and can also be found in bone cells and endothelial cells (Russell et al., 2014). There is evidence that CGRP is involved in the regulation of cell proliferation and differentiation, and may also be important for connecting the systems involved in bone metabolism (Bjurholm et al., 1988; Chattergoon et al., 2005; Thievent et al., 2005; Zhang et al., 2016; Xu et al., 2019). Additionally, studies have confirmed that CGRP can promote osteogenesis and inhibit osteoclast formation (Imai et al., 1997; Villa et al., 2003; Yoo et al., 2014). However, few studies have investigated the roles of CGRP in the age-related switch between osteoblast and adipocyte differentiation in bone marrow. Consequently, the aim of this study was to investigate whether CGRP is associated with increased bone formation and inhibition of adipocyte accumulation in age-related bone loss.

In the current study, we show that the level of CGRP in mouse bone marrow-derived supernatant decreases with aging. Furthermore, we found that CGRP not only promotes the osteogenic differentiation of BMSCs but also inhibits their adipogenic differentiation and senescence. Importantly, we demonstrate that exogenous application of CGRP can accelerate bone formation in aged and OVX mice *in vivo*, implying that CGRP may be a potential therapeutic target for the prevention of osteoporosis.

MATERIALS AND METHODS

Mice

C57BL/6JN mice were purchased from Hunan Slaccas Jingda (Changsha, China). Two-month-old female C57BL/6JN mice underwent bilateral ovarian resection to establish the OVX model. For *in vitro* CGRP treatment experiments, 12-month-old OVX mice and sham-operated mice were injected with CGRP (10 mg/kg) *via* the tail vein three times weekly for 1 month. Mice treated with 1 × PBS were used as controls. All mice were maintained in the specific-pathogen-free facility of the Laboratory Animal Research Center of Central South University. The mice were kept under a 12 h/12 h light: dark

TABLE 1 | Primer pairs in this study.

Name	Sequence (5′-3′)	Amplicon size (bp)
Gdpd2-F	CCAGCAAGTGCGACTGTATCT	185
Gdpd2-R	GACCAGGAGAGAGACGACCA	
Igf1-F	CTGGACCAGAGACCCTTTGC	269
Igf1-R	GGACGGGGACTTCTGAGTCTT	
Fgf9-F	ATGGCTCCCTTAGGTGAAGTT	104
Fgf9-R	TCATTTAGCAACACCGGACTG	
Wnt10b-F	GCGGGTCTCCTGTTCTTGG	71
Wnt10b-R	CCGGGAAGTTTAAGGCCCAG	
Gli2-F	GGGACTCTTTAGCCTCGCAG	158
Gli2-R	CCACAGGGTTGAGGTAGTCAT	
Rspo2-F	CCAAGGCAACCGATGGAGAC	100
Rspo2-R	TCGGCTGCAACCATTGTCC	
Jag1-F	CCTCGGGTCAGTTTGAGCTG	150
Jag1-R	CCTTGAGGCACACTTTGAAGTA	
Sox2-F	GCGGAGTGGAAACTTTTGTCC	157
Sox2-R	CGGGAAGCGTGTACTTATCCTT	
Igfbp3-F	CCAGGAAACATCAGTGAGTCC	101
Igfbp3-R	GGATGGAACTTGGAATCGGTCA	
Igf2-F	GTGCTGCATCGCTGCTTAC	222
Igf2-R	ACGTCCCTCTCGGACTTGG	
Bmp8a-F	AGTCTCTGGTCAGTACCACAG	160
Bmp8a-R	TGTTTACGCAGGATGACATTGTT	
Bmp4-F	ATTCCTGGTAACCGAATGCTG	89
Bmp4-R	CCGGTCTCAGGTATCAAACTAGC	
Id4-F	CAGTGCGATATGAACGACTGC	72
Id4-R	GACTTTCTTGTTGGGCGGGAT	
Bmp6-F	AGAAGCGGGAGATGCAAAAGG	211
Bmp6-R	GACAGGGCGTTGTAGAGATCC	
Acvr2a-F	GCGTTCGCCGTCTTTCTTATC	108
Acvr2a-R	GTTGGTTCTGTCTCTTTCCCAAT	
Pth1r-F	CAGGCGCAATGTGACAAGC	125
Pth1r-R	TTTCCCGGTGCCTTCTCTTTC	
Lrp5-F	ACGTCCCGTAAGGTTCTCTTC	172
Lrp5-R	GCCAGTAAATGTCGGAGTCTAC	
Hdac5-F	AGCACCGAGGTAAAGCTGAG	91
Hdac5-R	GCTGTGGGAGGGAATGGTT	
Hey1-F	GCGCGGACGAGAATGGAAA	231
Hey1-R	TCAGGTGATCCACAGTCATCTG	
Dlk1-F	AGTGCGAAACCTGGGTGTC	148
Dlk1-R	GCCTCCTTGTTGAAAGTGGTCA	
Tmem119-F	CCTACTCTGTGTCACTCCCG	212
Tmem119-R	CACGTACTGCCGGAAGAAATC	
Fam20c-F	GATGTGACGCGGGATAAGAAG	100
Fam20c-R	GCTCGGTGGAACAGTAGTAGG	
Gja1-F	ACAGCGGTTGAGTCAGCTTG	106
Gja1-R	GAGAGATGGGGAAGGACTTGT	
Tgfbr3-F	GGTGTGAACTGTCACCGATCA	125
Tgfbr3-R	GTTTAGGATGTGAACCTCCCTTG	
Col1a1-F	GCTCCTCTTAGGGGCCACT	103
Col1a1-R	CCACGTCTCACCATTGGGG	
Ift80-F	AGCTGTGTGGGTTGGACTAC	107
Ift80-R	AGCTTGACTATTAGGCTGGTTTC	
Hmga2-F	GAGCCCTCTCCTAAGAGACCC	106

(Continued)

TABLE 1 | Continued

Name	Sequence (5'-3')	Amplicon size (bp)
Hmga2-R	TTGGCCGTTTTTCTCCAATGG	
Ptgs2-F	TGTGACTGTACCCGGACTGG	233
Ptgs2-R	TGCACATTGTAAGTAGGTGGAC	
Vgf-F	AAGGATGACGGCGTACCAGA	114
Vgf-R	TGCCTGCAACAGTACCGAG	
Per2-F	GAAAGCTGTCACCACCATAGAA	101
Per2-R	AACTCGCACTTCCTTTTCAGG	
Acads-F	TGGCGACGGTTACACACTG	231
Acads-R	GTAGGCCAGGTAATCCAAGCC	
Fabp3-F	ACCTGGAAGCTAGTGGACAG	106
Fabp3-R	TGATGGTAGTAGGCTTGGTCAT	
Prkab2-F	ACCATCTCTATGCACTGTCCA	86
Prkab2-R	CAGCGTGGTGACATACTTCTT	
Dgat1-F	TCCGTCCAGGGTGGTAGTG	199
Dgat1-R	TGAACAAAGAATCTTGCAGACGA	
Hdac6-F	TCCACCGGCCAAGATTCTTC	109
Hdac6-R	CAGCACACTTCTTTCCACCAC	
Egr2-F	GCCAAGGCCGTAGACAAAATC	154
Egr2-R	CCACTCCGTTCATCTGGTCA	
Apmap-F	CCTTGCCATTCCCCTACTTGG	116
Apmap-R	ACTTCGTATTTGGATGCAGAACA	
FABP4-F	AAGGTGAAGAGCATCATAACCCT	133
FABP4-R	TCACGCCTTTCATAACACATTCC	
PPARGγ-F	TCGCTGATGCACTGCCTATG	103
PPARGγ-R	GAGAGGTCCACAGAGCTGATT	
β-actin-F	GGCTGTATTCCCCTCCATCG	154
β-actin-R	CCAGTTGGTAACAATGCCATGT	

cycle and had adequate access to food and water. All animal care protocols and experiments were reviewed and approved by the Animal Care and Use Committee of the Laboratory Animal Research Center at The Second Xiangya Hospital of Central South University.

Isolation and Culture of BMSCs

BMSCs were isolated as previously described (Picke et al., 2018). Briefly, the femora and tibiae of four 7-day-old mice were cut and digested with Liberase DL (26 U/mL) (Roche) in a water bath at 37°C for 2 h. The cell suspension was centrifugated at 1,000 rpm for 5 min at 4°C, resuspended in 1 mL of α-MEM containing 1% penicillin/streptomycin and 10% FBS, and then cultured in a 10-cm culture dish. The medium was replaced every other day and $CD11b^+$ cells were cleared using anti-CD11b antibody-coated magnetic beads.

Osteogenic Differentiation and Mineralization Assay

Isolated BMSCs were digested with 0.25% trypsin and diluted to 1×10^7 cells/mL. Then, 200 μL of the cell suspension was plated in 6-well plates at a density of 2×10^6 cells/well. At 80% confluence, the medium was replaced with osteogenic induction medium containing 10% FBS, 1% penicillin/streptomycin, 0.1 mM dexamethasone, 10 mM β-glycerol phosphate, and 50 mM ascorbate. The osteogenic induction medium was renewed every 3 days for 21 days. The cells were subsequently fixed in 4% paraformaldehyde and stained with 2% Alizarin Red S (Sigma-Aldrich). The Alizarin Red S was dissolved in cetylpyridinium chloride solution and quantified by spectrophotometry at 540 nm.

Adipogenic Differentiation Assay

Isolated BMSCs were plated in 6-well plates at 2.5×10^6 cells/well in adipogenic differentiation medium containing 10% FBS, 1% penicillin/streptomycin, 0.5 mM 3-isobutyl-1-methylxanthine, 1 μM dexamethasone, and 5 μg/mL insulin. The adipogenic induction medium was renewed every 3 days for 14 days. The cells were then fixed in 4% paraformaldehyde and stained with Oil Red solution (Sigma-Aldrich). The dye was solubilized in isopropanol and the absorption at 540 nm was measured using a BioTek Epoch microplate spectrophotometer (BioTek Instruments).

Enzyme-Linked Immunosorbent Assay (ELISA)

Bone marrow was separated, centrifuged at 1,000 rpm for 10 min, and then the supernatant was transferred to a new centrifuge tube. ELISA was performed using a CGPR (rat, mouse) EIA-Kit (K-01509, Phoenix Pharmaceuticals) according to the manufacturer's instructions.

Quantitative Real-Time PCR Analysis

Total RNA (1 μg) isolated from CGRP-treated BMSCs was treated with gDNA Eraser to remove residual genomic DNA and then reverse-transcribed into cDNA using the PrimeScript RT reagent Kit (Takara, Japan). Real-time PCR analysis was performed with SYBR Green (Takara, Japan) in an Applied Biosystems QuantStudio 3 Real-Time PCR System (Applied Biosystems). The amplification reactions were performed in a 96-well plate and consisted of 40 cycles of 95°C for 5 s and 60°C for 30 s. The relative transcript levels of target genes were quantified using the $2^{-\Delta\Delta Ct}$ method with beta-actin serving as the internal control. The primer sequences are listed in **Table 1**.

Micro-CT Analysis

Micro-computed tomography (micro-CT) analysis was performed as previously reported (Li et al., 2015; Yang et al., 2019). The femora of mice from both the CGRP treatment group and the control group were isolated, fixed in 4% formaldehyde for 24 h, and then scanned by X-ray microtomography (Skyscan 1172, Bruker) at a pixel size of 13.98 μm. For the distal femur, the region-of-interest (ROI) was defined from 0.215 to 1.72 mm below the growth plate. The bone volume as a fraction of total bone volume (BV/TV), trabecular thickness (Tb. Th), trabecular number (Tb. N), and trabecular separation (Tb. Sp) were measured.

Immunohistochemistry and Tartrate-Resistant Acid Phosphatase (TRAP) Staining

The femora were decalcified with 0.5 M EDTA for 1–2 weeks and then embedded in paraffin. The paraffin-embedded femora were sectioned (4 μm) using a RM2135 rotary microtome (Leica Geosystems). Sections were roasted at 60°C in an oven for 2 h, dewaxed with dimethyl benzene, dehydrated with alcohol, and treated with an antigen retrieval solution. The sections were subsequently washed with 1 × TTBS, blocked with 5% goat serum, and incubated with an anti-osteocalcin primary antibody (diluted 1:500; Cat# M041, Takara) overnight at 4°C. The next day, the sections were washed with 1 × TTBS, incubated with biotinylated secondary antibody (anti-mouse,1:200; Cat# PV9000, Beijing Zhongshan Jinqiao Biotechnology Co. Ltd.) for 1 h, washed with 1 × TTBS, and counterstained with hematoxylin (Sigma–Aldrich) for immunohistochemical analysis. An inverted fluorescence microscope was used for imaging. For TRAP staining, an Osteoclast Staining Kit (Sigma–Aldrich) was used according to the manufacturer's instructions. The number of osteoblasts on the bone surface and osteoclast number per bone perimeter were measured in the femora.

β-Galactosidase Staining

BMSCs were washed with 1 × PBS and fixed in 4% formaldehyde for 30 min. Cell senescence was assessed using a β-Galactosidase Staining Kit (Cell Signaling Technology, 9860) according to the manufacturer's instructions. The percentage of senescent cells was determined using ImageJ software.

Statistical Analysis

Data were analyzed by unpaired, two-tailed, Student's *t*-tests or one-way or two-way analysis of variance (ANOVA) followed by Bonferroni's post-test using GraphPad Prism 7.0 software. All data are presented as means ± SEM. A p-value < 0.05 was considered statistically significant.

RESULTS

CGRP Levels Were Decreased in the Bone Marrow Supernatant of Mice During Aging

CGRP is a 37-residue neuropeptide primarily expressed in the central and peripheral nervous systems (Emeson et al., 1989, 1992). That CGRP plays a vital role in bone metabolism is supported by evidence showing that the lack of CGRP results in reduced bone formation and impaired bone regeneration in mice (Schinke et al., 2004; Appelt et al., 2020). To assess the expression of *Calca* (encoding α-CGRP) in bone tissue during aging, we conducted RT-qPCR analysis on total RNA extracted from the bone tissue of mice at 3, 6, 9, 12, 15, 18, 21, and 24 months of age (n = 5 per age group). We found that the *Calca* level was significantly decreased during aging (**Figure 1A**). CGRP is thought to be a secreted neuropeptide that is released from sensory nerve endings (Tsujikawa et al., 2007). To assess the CGRP levels in bone marrow, we collected bone marrow supernatant from male C57BL/6JN mice aged 3, 12, and 24 months (n = 5 per age group) and measured CGRP levels by ELISA. As shown in **Figure 1B**, CGRP levels were lower in aged mice than in young mice. Given the vital role of CGRP in bone metabolism (Irie et al., 2002; Schinke et al., 2004; Appelt et al., 2020) and that CGRP has been reported to stimulate the proliferation and osteogenic differentiation of rat-derived BMSCs (Liang et al., 2015), we subsequently hypothesized that CGRP may be involved in regulating BMSC functions during the aging process in mice.

CGRP Treatment Promoted BMSC Osteogenic Differentiation and Reduced BMSC Senescence

To evaluate the effect of CGRP on the osteogenic differentiation potential of BMSCs, we isolated BMSCs from femoral and

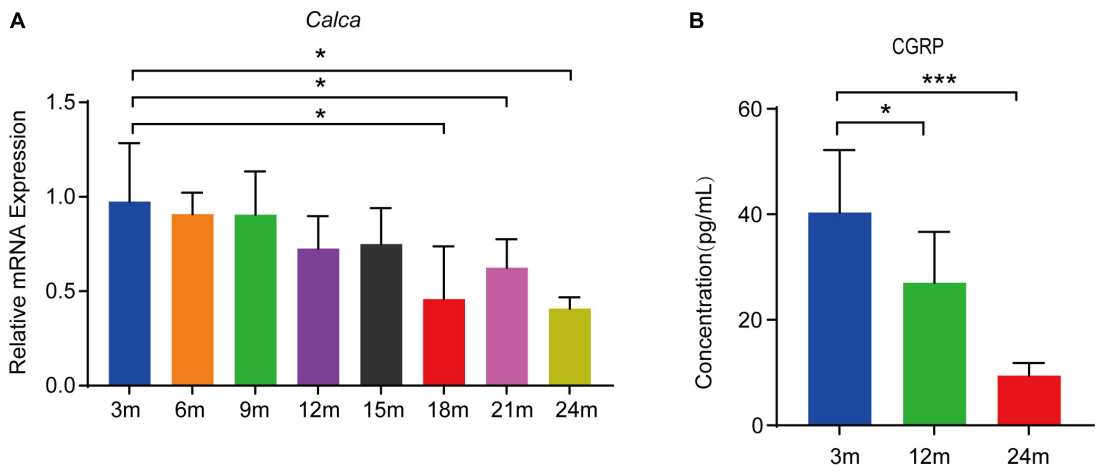


FIGURE 1 | CGRP levels were decreased in the bone marrow supernatant of mice during aging. **(A)** RT-qPCR analysis of the mRNA level of *Calca* in bone tissue of mice at 3, 6, 9, 12, 15, 18, 21, and 24 months of age (n = 5 per age group). **(B)** The relative levels of CGRP in bone marrow supernatant were measured by ELISA. $^{*}P < 0.05$, $^{***}P < 0.001$.

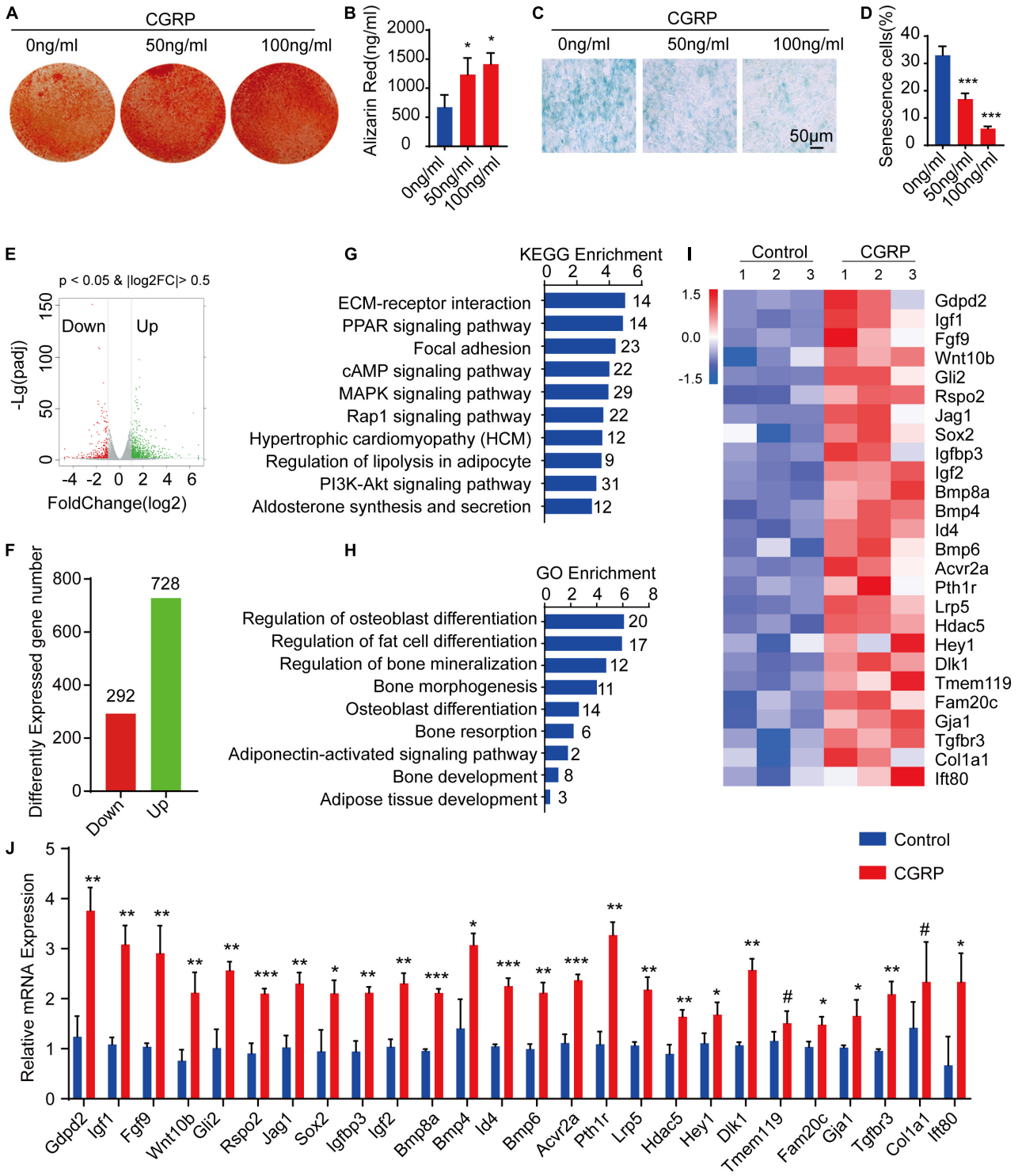


FIGURE 2 | CGRP induced the osteogenic differentiation of bone marrow-derived stem cells (BMSCs) and reduced BMSC senescence. **(A)** Representative images of Alizarin Red staining and **(B)** quantitative analysis of matrix mineralization in BMSCs treated with or without CGRP. **(C)** Representative images of beta-galactosidase staining and **(D)** quantitative analysis of the percentage of senescent cells in BMSCs treated with or without CGRP. **(E)** Volcano map and **(F)** histogram of differentially expressed genes between the CGRP treatment and control groups. Red spots represent downregulated genes and green spots represent upregulated genes. **(G)** Enrichment of differentially expressed genes was tested using Kyoto Encyclopedia of Genes and Genomes (KEGG) pathway analysis and **(H)** Gene Ontology (GO) analysis. **(I)** A heatmap of the mRNA-seq profile of BMSCs treated with or without CGRP. Fold-change ≥ 2.0. **(J)** RT-qPCR analysis of gene expression levels in BMSCs treated with or without CGRP. Scale bar, 50 μm. Data are presented as means ± SEM. $^{*}P < 0.05$, $^{**}P < 0.01$,$^{***}P < 0.001$.

tibial bone marrow of mice and cultured them first in a complete medium, and then in an osteogenesis induction medium containing CGRP at 0, 50, or 100 ng/mL. Alizarin Red staining and quantitative analysis of calcium content indicated that the ability of BMSCs to form mineralized nodules was enhanced in the CGRP treatment group compared with that in the control group (**Figures 2A,B**). A similar result was obtained for BMSCs transfected with a CGRP expression plasmid (**Supplementary Figures 1A,B**). In mice, the capacity of BMSCs to differentiate into osteoblasts is known to decrease with age. Consequently, we next measured the effect of CGRP on BMSC senescence by β-galactosidase staining. As expected, the percentage of senescent cells (β-galactosidase^{+}) was significantly lower in the CGRP treatment group than in the control group (**Figures 2C,D**). To determine the mechanism underlying the effect of CGRP on osteogenic differentiation of BMSCs and BMSC senescence, we performed RNA-seq to identify differences in mRNA expression levels between the CGRP treatment group and the control group. A total of 1,020 differentially expressed mRNAs (log2 fold-change ≥ 2) were identified (**Figures 2E,F**). Using Kyoto Encyclopedia of Genes and Genomes (KEGG) pathway and Gene Ontology (GO) enrichment analyses of the differentially expressed genes (**Figures 2G,H**), we identified several biological processes involved in osteogenic and fat cell differentiation (**Figure 2H**). Analysis of a heatmap depicting the differentially expressed genes involved in the regulation of osteoblast differentiation demonstrated that almost all of these genes, including *Gdpd2*, *Igf1*, *Fgf9*, *Wnt10b*, *Gli2*, *Rspo2*, *Jag1*, *Sox2*, *Igfbp3*, *Igf2*, *Bmp4*, *Bmp6*, *Bmp8a*, *Id4*, *Acvr2a*, *Pth1r*, *Lrp5*, *Hdac5*, *Hey1*, *Dlk1*, *Tmem119*, *Fam20c*, *Gja1*, *Tgfbr3*, *Col1a1*, and *Ift80*, were markedly upregulated in the CGRP treatment group compared with that in the control group (**Figure 2I**). The result of the RNA-seq was further confirmed by RT-qPCR analysis (**Figure 2J**). Combined, the results showed that CGRP treatment dose-dependently increased the osteogenic differentiation potential of BMSCs and reduced BMSC senescence.

CGRP Inhibited the Adipogenic Differentiation of BMSCs

BMSCs are multipotent stem cells capable of differentiating into multiple lineages, including osteoblasts and adipocytes (Pittenger et al., 1999; James, 2013). The differentiation potential of BMSCs is influenced by multiple factors, such as injury. Given our above results showing that CGRP can induce the osteogenic differentiation of BMSCs and reduce BMSC senescence, we then tested whether CGRP treatment could also affect the adipogenic differentiation capacity of BMSCs. To evaluate this possibility *in vitro*, BMSCs were cultured in an adipogenesis induction medium containing CGRP at 0, 50, or 100 ng/mL. Oil Red O staining results showed that there were fewer lipid droplets and their size was reduced in CGRP-treated BMSCs compared with that in control BMSCs (**Figures 3A,B**). We obtained a similar result in BMSCs transfected with a CGRP expression plasmid (**Supplementary Figures 1C,D**). Next, we

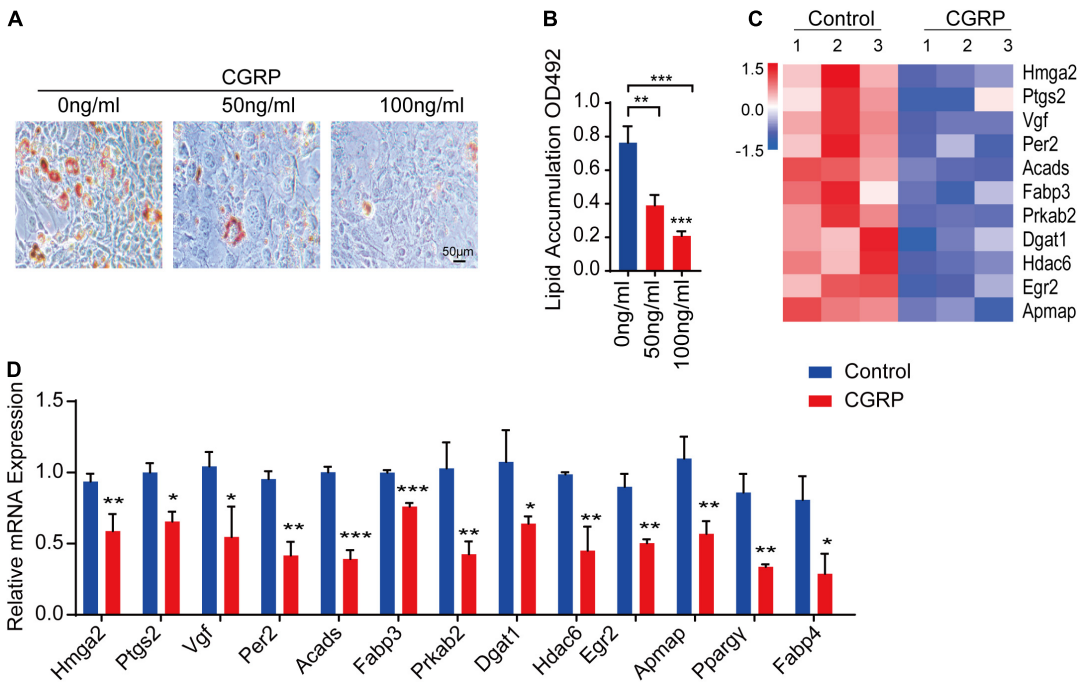


FIGURE 3 | CGRP inhibited the adipogenic differentiation of bone marrow-derived stem cells (BMSCs). **(A)** Representative images of Oil Red O staining and **(B)** quantitative analysis of lipid droplet formation in BMSCs treated with or without CGRP. **(C)** A heatmap of the mRNA-seq profile of BMSCs treated with or without CGRP. Fold change ≥ 2.0. **(D)** RT-qPCR analysis of gene expression levels in BMSCs treated with or without CGRP. Scale bar, 50 μm. Data are presented as means ± SEM. $^{*}P < 0.05$, $^{**}P < 0.01$,$^{***}P < 0.001$.

identified genes involved in promoting adipogenesis that were differentially expressed between the CGRP treatment group and the control group. Heatmap analysis showed that, compared with control BMSCs, the expression of *Hmga2*, *Ptgs2*, *Vgf*, *Per2*, *Acads*, *Fabp3*, *Prkab2*, *Dgat1*, *Hdac6*, *Egr2*, and *Apmap* was markedly downregulated in those treated with CGRP (**Figure 3C**). RT-qPCR analysis further confirmed the RNA-seq results (**Figure 3D**). These data indicated that CGRP treatment downregulated the expression of adipogenesis-related genes and inhibited the adipogenic differentiation capacity of BMSCs.

CGRP Treatment Promoted Bone Formation in Aged Mice

To evaluate whether CGRP could promote bone formation in aged mice *in vivo*, 12-month-old male C57BL/6JN mice (n = 5) were administered CGRP (10 mg/kg) or 1 × PBS *via* tail vein injection three times weekly (**Figure 4A**). After 1 month, the bone phenotype of the mice in both groups was analyzed. The results showed that bone mass, BV, Tb. Th, and Tb. N were markedly higher, and the Tb. Sp lower, in mice treated with CGRP when compared with those treated with PBS (**Figures 4B–F**). Hematoxylin and eosin (H&E) staining results showed that, compared with PBS-treated mice, those treated with CGRP had fewer adipocytes, and the area occupied by them was smaller (**Figures 4G,H**). Moreover, the number of osteocalcin^{+} osteoblasts on the trabecular surface was also higher in mice treated with CGRP compared with that of the control group (**Figures 4I,J**). These results suggested that CGRP treatment induced osteoblast differentiation and promoted bone formation in aged mice.

CGRP Treatment Promoted Bone Formation in OVX Mice

The OVX rodent model is well-established as a means for investigating osteoporosis and osteoporotic therapies (Mathavan et al., 2015). Here, to test the effect of CGRP on bone formation in OVX mice, we generated a model of postmenopausal osteoporosis *via* bilateral ovarian resection in 2-month-old female C57BL/6JN mice (n = 12/group). One month after the operation, CGRP (10 mg/kg) or 1 × PBS (10 mg/kg) was administered into mice of the OVX and sham operation groups *via* tail vein injection and ovarian injections three

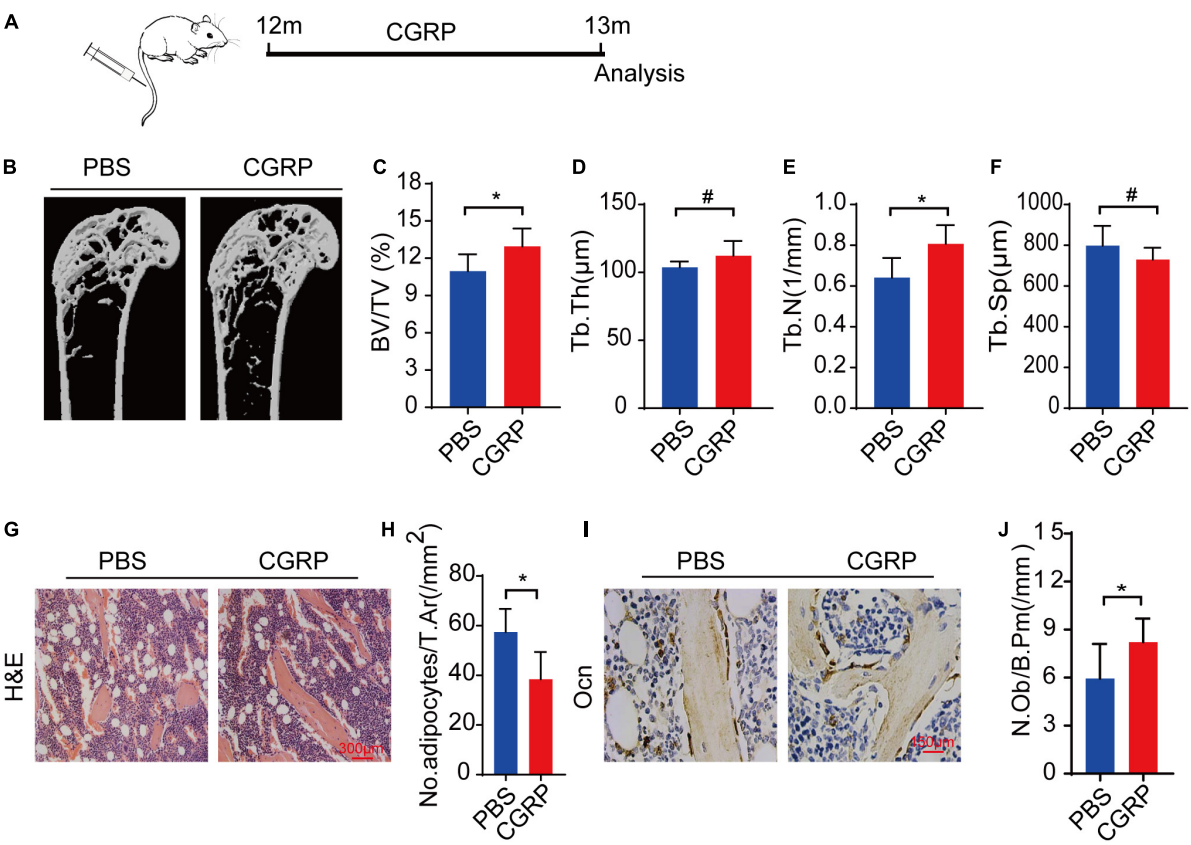


FIGURE 4 | CGRP treatment promoted bone formation in aged mice. **(A)** A schematic representation of the injection protocol (CGRP or 1 × PBS *via* the tail vein) in aged mice. **(B)** Representative micro-computed tomographs (n = 6/group) and **(C–F)** quantitative analysis of bone volume as a fraction of total bone volume (BV/TV), trabecular thickness (Tb. Th), trabecular number (Tb. N), and trabecular separation (Tb. Sp) of femora from CGRP-treated and control mice. **(G)** Representative images of hematoxylin and eosin staining and **(H)** quantitative analysis of the number and area of adipocytes in the bone marrow of CGRP-treated and control mice. **(I)** Representative images of osteocalcin (OCN) staining and **(J)** quantification of osteoblast bone surface density (N.Ob/B.Pm) in the femora of CGRP-treated and control mice. Scale bars, 150 μm. Data are presented as means ± SEM. *P < 0.05. # means no statistical significance.

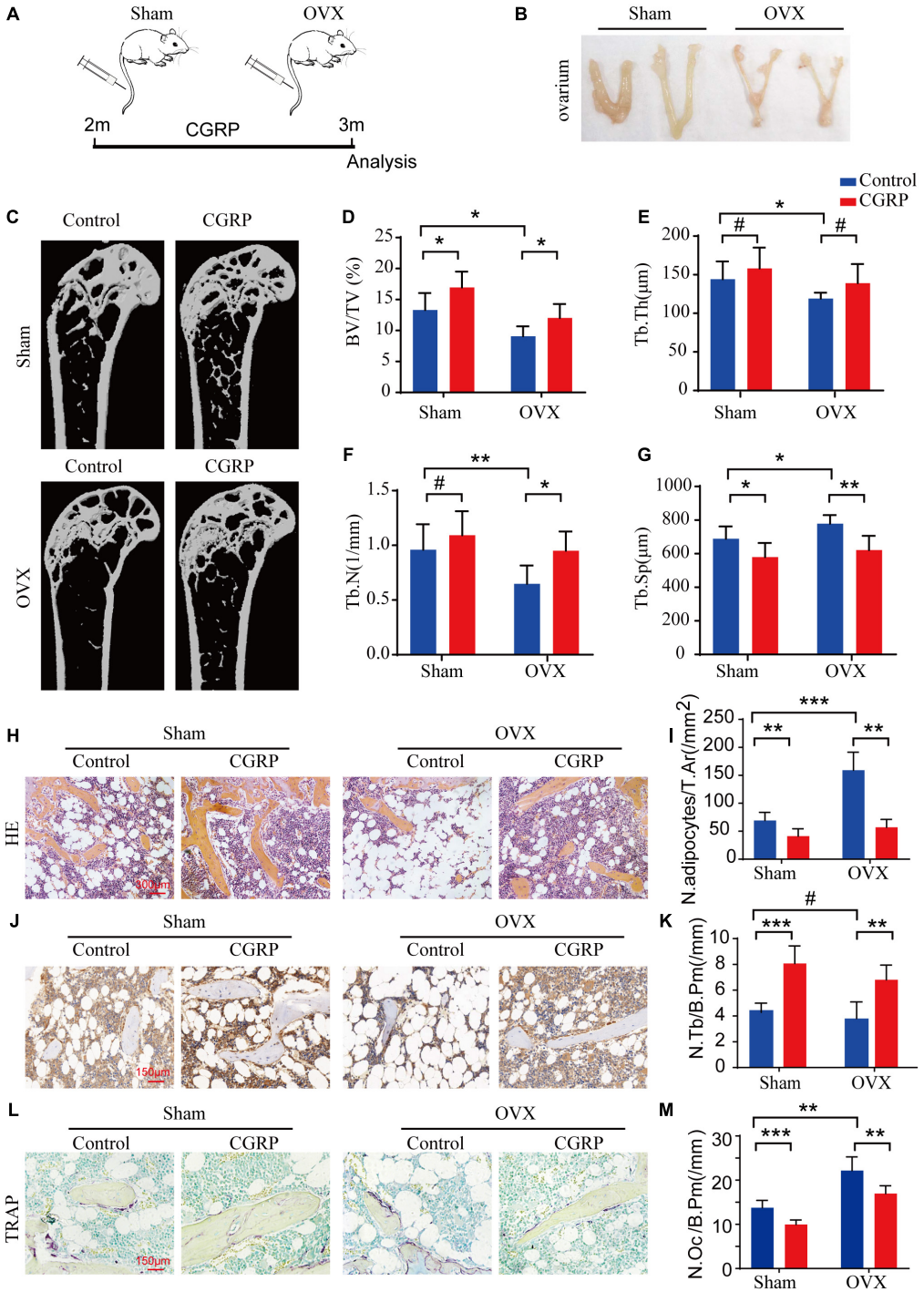


FIGURE 5 | CGRP treatment promoted bone formation in ovariectomized (OVX) mice. **(A)** A schematic representation of the injection protocol (CGRP or 1 × PBS *via* the tail vein) for OVX and control (sham-operated) mice. **(B)** Representative images of the ovaries of OVX and control (sham-operated) mice treated with or without CGRP. **(C)** Representative micro-computed tomographs (n = 6/group) and **(D–G)** quantitative analysis of bone volume as a fraction of total bone volume (BV/TV), trabecular thickness (Tb. Th), trabecular number (Tb. N), and trabecular separation (Tb. Sp) of femora from OVX and control (sham-operated) mice treated with or without CGRP. **(H)** Representative images of hematoxylin and eosin staining and **(I)** quantitative analysis of the number and area of adipocytes in the bone marrow of OVX and control (sham-operated) mice treated with or without CGRP. Scale bar, 300 μm. **(J)** Representative images of osteocalcin (OCN) staining and **(K)** quantification of osteoblast bone surface density (N.Ob/B.Pm) in the femora of OVX and control (sham-operated) mice treated with or without CGRP. **(L)** Representative images of tartrate-resistant acid phosphatase (TRAP) staining and **(M)** quantification of osteoclast bone surface density (N.Oc/B.Pm) in the femora of OVX and control (sham-operated) mice treated with or without CGRP. Scale bar, 150 μm. Data are presented as means ± SEM. $^{*}P < 0.05$, $^{**}P < 0.01$, $^{***}P < 0.001$. # means no statistical significance.

times weekly (**Figures 5A,B**). We found that the BV and Tb. Th were markedly reduced in the OVX group compared with those in the sham operation group, indicating that the model of postmenopausal osteoporosis had been successfully generated (**Figures 5C–G**). Moreover, bone mass, BV, Tb. Th, and Tb. N were markedly increased, while the Tb. Sp. was reduced, in CGRP-treated mice from both the OVX and sham operation groups compared with that in PBS-treated mice from both groups (**Figure 5C–G**). Additionally, when compared with control mice, CGRP-treated mice from the OVX and sham operation groups displayed fewer adipocytes and smaller adipocyte-containing areas in the bone marrow (**Figures 5H,I**), as well as greater numbers of osteocalcin$^+$ osteoblasts and alkaline phosphatase$^+$ osteoprogenitors on the bone surfaces (**Figures 5J,K**). In contrast, CGRP-treated mice from the OVX and sham operation groups had fewer TRAP$^+$ osteoclasts on the bone surfaces (**Figures 5L,M**), which was consistent with the results of previous *in vitro* studies (Wang et al., 2010). Taken together, these results suggested that CGRP can promote bone formation in both aged and osteoporotic (OVX) mice, and suggest a potential approach for the treatment of age-related osteoporosis.

DISCUSSION

Osteoporosis is a chronic, age-related disease that seriously affects the quality of life of both the elderly and postmenopausal women (Rachner et al., 2011). Owing to the aging of the world's population, it is increasingly important to understand the role of neuropeptides and their receptors in the aging process (Naot and Cornish, 2008). In the elderly, BMSCs have a greater capacity to differentiate along adipocytic lineages than along osteoblastic lineages, leading to the gradual accumulation of fat and the loss of bone (Bartel, 2004). Here, we demonstrated that CGRP is involved in the shift in BMSC cell lineage commitment, which leads to increased osteogenic differentiation and reduced adipogenic differentiation of BMSCs. Furthermore, we demonstrated for the first time that systemic CGRP administration can reduce fat accumulation, as well as promote bone formation, in both aged and OVX mice, likely by acting on BMSCs.

CGRP can reportedly regulate BMSC lineage commitment (Villa et al., 2003; Wang et al., 2010; Naot et al., 2019). In addition, several studies have shown that CGRP levels are influenced by age, and that these age-related changes can affect osteogenesis (Imai and Matsusue, 2002; Villa et al., 2003; Niedermair et al., 2020). These results are consistent with those reported here. We found that the level of CGRP in bone marrow supernatants was inversely proportional to age. Furthermore, CGRP treatment enhanced the ability of BMSCs to form mineralized nodules and significantly reduced the percentage of senescent BMSCs. Given the interaction between osteogenesis and adipogenesis, we further examined the role of CGRP in adipogenic differentiation, and report for the first time that CGRP can inhibit the adipogenic differentiation of BMSCs. These results indicated that CGRP regulates BMSC lineage commitment during aging and contributes to age-related bone formation.

It has recently been suggested that CGRP is a key neuropeptide in bone metabolism. Niedermair et al. (2020) demonstrated that CGRP regulates the bone remodeling properties of osteoblasts and osteoclasts in an age-dependent manner. Further, Mi et al. (2021) reported that CGRP can increase the endothelial progenitor cell population in the endothelial differentiation of BMSCs *in vitro*, thereby promoting bone regeneration in a rat model of distraction osteogenesis. In addition, it has been shown that CGRP can enhance BMP2 signal transduction, the expression of related osteogenic genes, and mineralization *in vitro* (Tuzmen and Campbell, 2018). He et al. (2016) reported that CGRP can maintain bone mass by stimulating osteoblast differentiation and inhibiting RANKL-induced osteoclastogenesis and bone resorption. CGRP has also been indicated to serve as a protective mechanism against particle-induced osteolysis (Kauther et al., 2011). However, to date, no work has reported on the role of CGRP in the regulation of BMSC function. In the present study, we defined a new mechanism through which CGRP regulates the BMSC switch in the bone. We further identified biological processes involved in both osteogenic and adipocyte differentiation and found that CGRP treatment led to a significant upregulation of the expression of almost all osteogenesis-related genes. Furthermore, based on the decrease in the expression level of adipogenesis-related genes, we reasoned that CGRP might suppress adipogenesis.

These results suggested that CGRP influences the direction of BMSC differentiation by regulating the expression of related genes, thereby providing a neuropeptide-mediated link to the age-related transition between osteoblast and adipocyte differentiation. During the aging process, the level of CGRP and the expression of osteogenic-related genes in the bone marrow decreases, whereas that of lipid-related genes increases. Consequently, BMSCs tend to differentiate into adipocytes, leading to a reduction in the number of osteoblasts and an increase in that of adipocytes, resulting in age-related bone loss. Here, we identified a new mechanism through which CGRP regulates the differentiation of BMSCs during aging. Relatively few studies have investigated the role of CGRP in bone metabolism *in vivo*. Here, *via* the delivery of CGRP to BMSCs by tail vein injection, we confirmed *in vivo* that CGRP can promote the osteogenic differentiation of BMSCs and inhibit fat accumulation in the bone marrow. The results of bone histomorphometry in the CGRP-treated group were significantly better than those in the control group in both aged and OVX mice. *In vitro* and *in vivo* experiments both confirmed that CGRP can promote the osteogenic differentiation and inhibit the adipogenic differentiation of BMSCs.

With the aging of the world's population, age-related osteoporosis has become a serious public health issue (Curtis and Safford, 2012). However, most drugs currently used to treat osteoporosis are aimed at inhibiting bone resorption without promoting bone formation, and most are accompanied by severe side effects (Hu et al., 2020). In this study, we identified a new neuropeptide that may serve as potential therapeutic target for

the treatment of osteoporosis. To date, CGRP has been applied in the treatment of several diseases, such as migraine, diabetes, and liver damage, as well as for cardioprotection (Kroeger et al., 2009; Yuan et al., 2017; Guo et al., 2018, 2020), suggesting that CGRP can be used safely and effectively in the treatment of age-related osteoporosis.

CONCLUSION

In conclusion, our findings support that the age-related changes in CGRP levels regulate BMSC differentiation. Our results revealed a novel mechanism underlying age-related bone loss and provide a potential therapeutic strategy to treat age-related osteoporosis.

DATA AVAILABILITY STATEMENT

The raw data supporting the conclusions of this article will be made available by the authors, without undue reservation.

ETHICS STATEMENT

All animal care protocols and experiments were reviewed and approved by the Animal Care and Use Committee of the Laboratory Animal Research Center at the Second Xiangya Hospital of Central South University. All mice were maintained in the specific pathogen–free facility of the Laboratory Animal Research Center at Central South University.

AUTHOR CONTRIUTIONS

QL conceived the study. HL and RW drafted the manuscript. HZ and JW designed the figures. XX and JQ designed the tables. QL and RW revised the manuscript. All the authors were involved in the critical revision of the manuscript and approved the final version.

FUNDING

This work was supported by the Natural Science Foundation of Hunan Province (2020JJ4799), the China National Key R&D Program (Nos. 2020YFC2009000 and 2020YFC2009001), and the Natural Science Foundation of Changsha (KQ2007051).

SUPPLEMENTARY MATERIAL

The Supplementary Material for this article can be found online at: https://www.frontiersin.org/articles/10.3389/fcell.2021.675503/full#supplementary-material

REFERENCES

Amara, S. G., Jonas, V., Rosenfeld, M. G., Ong, E. S., and Evans, R. M. (1982). Alternative RNA processing in calcitonin gene expression generates mRNAs encoding different polypeptide products. *Nature* 298, 240–244. doi: 10.1038/298240a0

Appelt, J., Baranowsky, A., Jahn, D., Yorgan, T., Kohli, P., Otto, E., et al. (2020). The neuropeptide calcitonin gene-related peptide alpha is essential for bone healing. *EBioMedicine* 59:102970. doi: 10.1016/j.ebiom.2020.102970

Bartel, D. P. (2004). MicroRNAs: genomics, biogenesis, mechanism, and function. *Cell* 116, 281–297. doi: 10.1016/s0092-8674(04)00045-5

Bjurholm, A., Kreicbergs, A., Brodin, E., and Schultzberg, M. (1988). Substance P- and CGRP-immunoreactive nerves in bone. *Peptides* 9, 165–171. doi: 10.1016/0196-9781(88)90023-x

Chattergoon, N. N., D'Souza, F. M., Deng, W., Chen, H., Hyman, A. L., Kadowitz, P. J., et al. (2005). Antiproliferative effects of calcitonin gene-related peptide in aortic and pulmonary artery smooth muscle cells. *Am. J. Physiol. Lung Cell Mol. Physiol.* 288, L202–L211. doi: 10.1152/ajplung.00064.2004

Chen, X., Zhi, X., Wang, J., and Su, J. (2018). RANKL signaling in bone marrow mesenchymal stem cells negatively regulates osteoblastic bone formation. *Bone Res.* 6:34. doi: 10.1038/s41413-018-0035-6

Childs, B. G., Durik, M., Baker, D. J., and van Deursen, J. M. (2015). Cellular senescence in aging and age-related disease: from mechanisms to therapy. *Nat. Med.* 21, 1424–1435. doi: 10.1038/nm.4000

Curtis, J. R., and Safford, M. M. (2012). Management of osteoporosis among the elderly with other chronic medical conditions. *Drugs Aging* 29, 549–564. doi: 10.2165/11599620-000000000-00000

Emeson, R. B., Hedjran, F., Yeakley, J. M., Guise, J. W., and Rosenfeld, M. G. (1989). Alternative production of calcitonin and CGRP mRNA is regulated at the calcitonin-specific splice acceptor. *Nature* 341, 76–80. doi: 10.1038/341076a0

Emeson, R. B., Yeakley, J. M., Hedjran, F., Merillat, N., Lenz, H. J., and Rosenfeld, M. G. (1992). Posttranscriptional regulation of calcitonin/CGRP gene expression. *Ann. N. Y. Acad. Sci.* 657, 18–35.

Guo, Y., Chen, H., Jiang, Y., Yuan, Y., Zhang, Q., Guo, Q., et al. (2020). CGRP regulates the dysfunction of peri-implant angiogenesis and osseointegration in streptozotocin-induced diabetic rats. *Bone* 139:115464. doi: 10.1016/j.bone.2020.115464

Guo, Z., Liu, N., Chen, L., Zhao, X., and Li, M. R. (2018). Independent roles of CGRP in cardioprotection and hemodynamic regulation in ischemic postconditioning. *Eur. J. Pharmacol.* 828, 18–25. doi: 10.1016/j.ejphar.2018.03.031

He, H., Chai, J., Zhang, S., Ding, L., Yan, P., Du, W., et al. (2016). CGRP may regulate bone metabolism through stimulating osteoblast differentiation and inhibiting osteoclast formation. *Mol. Med. Rep.* 13, 3977–3984. doi: 10.3892/mmr.2016.5023

Hu, Q., Long, C., Wu, D., You, X., Ran, L., Xu, J., et al. (2020). The efficacy and safety of ipriflavone in postmenopausal women with osteopenia or osteoporosis: a systematic review and meta-analysis. *Pharmacol. Res.* 159:104860. doi: 10.1016/j.phrs.2020.104860

Idris, A. I., Sophocleous, A., Landao-Bassonga, E., Canals, M., Milligan, G., Baker, D., et al. (2009). Cannabinoid receptor type 1 protects against age-related osteoporosis by regulating osteoblast and adipocyte differentiation in marrow stromal cells. *Cell Metab.* 10, 139–147. doi: 10.1016/j.cmet.2009.07.006

Imai, S., and Matsusue, Y. (2002). Neuronal regulation of bone metabolism and anabolism: calcitonin gene-related peptide-, substance P-, and tyrosine hydroxylase-containing nerves and the bone. *Microsc. Res. Tech.* 58, 61–69. doi: 10.1002/jemt.10119

Imai, S., Rauvala, H., Konttinen, Y. T., Tokunaga, T., Maeda, T., Hukuda, S., et al. (1997). Efferent targets of osseous CGRP-immunoreactive nerve fiber before and after bone destruction in adjuvant arthritic rat: an ultramorphological study on their terminal-target relations. *J. Bone Miner Res.* 12, 1018–1027. doi: 10.1359/jbmr.1997.12.7.1018

Irie, K., Hara-Irie, F., Ozawa, H., and Yajima, T. (2002). Calcitonin gene-related peptide (CGRP)-containing nerve fibers in bone tissue and their involvement in bone remodeling. *Microsc. Res. Tech.* 58, 85–90. doi: 10.1002/jemt.10122

James, A. W. (2013). Review of signaling pathways governing MSC osteogenic and adipogenic differentiation. *Scientifica (Cairo)* 2013, 684736. doi: 10.1155/2013/684736

Kauther, M. D., Bachmann, H. S., Neuerburg, L., Broecker-Preuss, M., Hilken, G., Grabellus, F., et al. (2011). Calcitonin substitution in calcitonin deficiency reduces particle-induced osteolysis. *BMC Musculoskelet Disord.* 12:186. doi: 10.1186/1471-2474-12-186

Kroeger, I., Erhardt, A., Abt, D., Fischer, M., Biburger, M., Rau, T., et al. (2009). The neuropeptide calcitonin gene-related peptide (CGRP) prevents inflammatory liver injury in mice. *J. Hepatol.* 51, 342–353. doi: 10.1016/j.jhep.2009.03.022

Li, C. J., Cheng, P., Liang, M. K., Chen, Y. S., Lu, Q., Wang, J. Y., et al. (2015). MicroRNA-188 regulates age-related switch between osteoblast and adipocyte differentiation. *J. Clin. Invest.* 125, 1509–1522. doi: 10.1172/JCI77716

Li, H., Liu, P., Xu, S., Li, Y., Dekker, J. D., Li, B., et al. (2017). FOXP1 controls mesenchymal stem cell commitment and senescence during skeletal aging. *J. Clin. Invest.* 127, 1241–1253. doi: 10.1172/JCI89511

Li, K. C., Chang, Y. H., Yeh, C. L., and Hu, Y. C. (2016). Healing of osteoporotic bone defects by baculovirus-engineered bone marrow-derived MSCs expressing MicroRNA sponges. *Biomaterials* 74, 155–166. doi: 10.1016/j.biomaterials.2015.09.046

Liang, W., Zhuo, X., Tang, Z., Wei, X., and Li, B. (2015). Calcitonin gene-related peptide stimulates proliferation and osteogenic differentiation of osteoporotic rat-derived bone mesenchymal stem cells. *Mol. Cell Biochem.* 402, 101–110. doi: 10.1007/s11010-014-2318-6

Lv, Y. J., Yang, Y., Sui, B. D., Hu, C. H., Zhao, P., Liao, L., et al. (2018). Resveratrol counteracts bone loss via mitofilin-mediated osteogenic improvement of mesenchymal stem cells in senescence-accelerated mice. *Theranostics* 8, 2387–2406. doi: 10.7150/thno.23620

Mathavan, N., Turunen, M. J., Tagil, M., and Isaksson, H. (2015). Characterising bone material composition and structure in the ovariectomized (OVX) rat model of osteoporosis. *Calcif. Tissue Int.* 97, 134–144. doi: 10.1007/s00223-015-9991-7

Mi, J., Xu, J., Yao, H., Li, X., Tong, W., Li, Y., et al. (2021). Calcitonin gene-related peptide enhances distraction osteogenesis by increasing angiogenesis. *Tissue Eng. Part A* 27, 87–102. doi: 10.1089/ten.TEA.2020.0009

Naot, D., and Cornish, J. (2008). The role of peptides and receptors of the calcitonin family in the regulation of bone metabolism. *Bone* 43, 813–818. doi: 10.1016/j.bone.2008.07.003

Naot, D., Musson, D. S., and Cornish, J. (2019). The activity of peptides of the calcitonin family in bone. *Physiol. Rev.* 99, 781–805. doi: 10.1152/physrev.00066.2017

Niedermair, T., Schirner, S., Lasheras, M. G., Straub, R. H., and Grassel, S. (2020). Absence of alpha-calcitonin gene-related peptide modulates bone remodeling properties of murine osteoblasts and osteoclasts in an age-dependent way. *Mech. Ageing Dev.* 189:111265. doi: 10.1016/j.mad.2020.111265

NIH Consensus Development Panel on Osteoporosis Prevention, Diagnosis, and Therapy (2001). Osteoporosis prevention, diagnosis, and therapy. *JAMA* 285, 785–795. doi: 10.1001/jama.285.6.785

Peng, H., Yang, M., Guo, Q., Su, T., Xiao, Y., and Xia, Z. Y. (2019). Dendrobium officinale polysaccharides regulate age-related lineage commitment between osteogenic and adipogenic differentiation. *Cell Prolif.* 52:e12624. doi: 10.1111/cpr.12624

Picke, A. K., Campbell, G. M., Bluher, M., Krugel, U., Schmidt, F. N., Tsourdi, E., et al. (2018). Thy-1 (CD90) promotes bone formation and protects against obesity. *Sci. Transl. Med.* 10:eaao6806. doi: 10.1126/scitranslmed.aao6806

Pittenger, M. F., Mackay, A. M., Beck, S. C., Jaiswal, R. K., Douglas, R., Mosca, J. D., et al. (1999). Multilineage potential of adult human mesenchymal stem cells. *Science* 284, 143–147. doi: 10.1126/science.284.5411.143

Rachner, T. D., Khosla, S., and Hofbauer, L. C. (2011). Osteoporosis: now and the future. *Lancet* 377, 1276–1287. doi: 10.1016/S0140-6736(10)62349-5

Rosenfeld, M. G., Mermod, J. J., Amara, S. G., Swanson, L. W., Sawchenko, P. E., Rivier, J., et al. (1983). Production of a novel neuropeptide encoded by the calcitonin gene via tissue-specific RNA processing. *Nature* 304, 129–135. doi: 10.1038/304129a0

Russell, F. A., King, R., Smillie, S. J., Kodji, X., and Brain, S. D. (2014). Calcitonin gene-related peptide: physiology and pathophysiology. *Physiol. Rev.* 94, 1099–1142. doi: 10.1152/physrev.00034.2013

Schinke, T., Liese, S., Priemel, M., Haberland, M., Schilling, A. F., Catala-Lehnen, P., et al. (2004). Decreased bone formation and osteopenia in mice lacking alpha-calcitonin gene-related peptide. *J. Bone Miner Res.* 19, 2049–2056. doi: 10.1359/JBMR.040915

Shen, W., Chen, J., Gantz, M., Punyanitya, M., Heymsfield, S. B., Gallagher, D., et al. (2012). MRI-measured pelvic bone marrow adipose tissue is inversely related to DXA-measured bone mineral in younger and older adults. *Eur. J. Clin. Nutr.* 66, 983–988. doi: 10.1038/ejcn.2012.35

Sternini, C. (1992). Enteric and visceral afferent CGRP neurons. Targets of innervation and differential expression patterns. *Ann. N. Y. Acad. Sci.* 657, 170–186. doi: 10.1111/j.1749-6632.1992.tb22766.x

Thievent, A., Sena, S., Parlakian, A., Breuzard, G., Beley, A., Rochette, L., et al. (2005). Potential role of the neuropeptide CGRP in the induction of differentiation of rat hepatic portal vein wall. *Peptides* 26, 1567–1572. doi: 10.1016/j.peptides.2005.02.015

Tsujikawa, K., Yayama, K., Hayashi, T., Matsushita, H., Yamaguchi, T., Shigeno, T., et al. (2007). Hypertension and dysregulated proinflammatory cytokine production in receptor activity-modifying protein 1-deficient mice. *Proc. Natl. Acad. Sci. U.S.A.* 104, 16702–16707. doi: 10.1073/pnas.0705974104

Tuzmen, C., and Campbell, P. G. (2018). Crosstalk between neuropeptides SP and CGRP in regulation of BMP2-induced bone differentiation. *Connect Tissue Res.* 59(Suppl. 1), 81–90. doi: 10.1080/03008207.2017.1408604

Villa, I., Dal Fiume, C., Maestroni, A., Rubinacci, A., Ravasi, F., and Guidobono, F. (2003). Human osteoblast-like cell proliferation induced by calcitonin-related peptides involves PKC activity. *Am. J. Physiol. Endocrinol. Metab.* 284, E627–E633. doi: 10.1152/ajpendo.00307.2002

Wang, L., Shi, X., Zhao, R., Halloran, B. P., Clark, D. J., Jacobs, C. R., et al. (2010). Calcitonin-gene-related peptide stimulates stromal cell osteogenic differentiation and inhibits RANKL induced NF-kappaB activation, osteoclastogenesis and bone resorption. *Bone* 46, 1369–1379. doi: 10.1016/j.bone.2009.11.029

Xu, Y., Xia, M., Chen, T., Yang, Y., Fu, G., Ji, P., et al. (2019). Inferior alveolar nerve transection disturbs innate immune responses and bone healing after tooth extraction. *Ann. N. Y. Acad. Sci.* 1448, 52–64. doi: 10.1111/nyas.14120

Yang, M., Guo, Q., Peng, H., Xiao, Y. Z., Xiao, Y., Huang, Y., et al. (2019). Kruppel-like factor 3 inhibition by mutated lncRNA Reg1cp results in human high bone mass syndrome. *J. Exp. Med.* 216, 1944–1964. doi: 10.1084/jem.20181554

Yoo, Y. M., Kwag, J. H., Kim, K. H., and Kim, C. H. (2014). Effects of neuropeptides and mechanical loading on bone cell resorption in vitro. *Int. J. Mol. Sci.* 15, 5874–5883. doi: 10.3390/ijms15045874

Yu, B., and Wang, C. Y. (2016). Osteoporosis: the result of an 'aged' bone microenvironment. *Trends Mol. Med.* 22, 641–644. doi: 10.1016/j.molmed.2016.06.002

Yuan, H., Lauritsen, C. G., Kaiser, E. A., and Silberstein, S. D. (2017). CGRP monoclonal antibodies for migraine: rationale and progress. *BioDrugs* 31, 487–501. doi: 10.1007/s40259-017-0250-5

Zhang, Y., Xu, J., Ruan, Y. C., Yu, M. K., O'Laughlin, M., Wise, H., et al. (2016). Implant-derived magnesium induces local neuronal production of CGRP to improve bone-fracture healing in rats. *Nat. Med.* 22, 1160–1169. doi: 10.1038/nm.4162

Conflict of Interest: The authors declare that the research was conducted in the absence of any commercial or financial relationships that could be construed as a potential conflict of interest.

Copyright © 2021 Li, Qu, Zhu, Wang, He, Xie, Wu and Lu. This is an open-access article distributed under the terms of the Creative Commons Attribution License (CC BY). The use, distribution or reproduction in other forums is permitted, provided the original author(s) and the copyright owner(s) are credited and that the original publication in this journal is cited, in accordance with accepted academic practice. No use, distribution or reproduction is permitted which does not comply with these terms.

frontiers in Cell and Developmental Biology

CORRECTION
published: 22 June 2021
doi: 10.3389/fcell.2021.715740

Corrigendum: CGRP Regulates the Age-Related Switch Between Osteoblast and Adipocyte Differentiation

Hang Li[1,2†], Jian Qu[1,2†], Haihong Zhu[1,2], Jiaojiao Wang[1,2], Hao He[3], Xinyan Xie[1,2], Ren Wu[4] and Qiong Lu[1,2*]*

[1] Department of Pharmacy, The Second Xiangya Hospital of Central South University, Changsha, China, [2] Institute of Clinical Pharmacy, Central South University, Changsha, China, [3] Department of Vascular Surgery, The Second Xiangya Hospital of Central South University, Changsha, China, [4] Department of Orthopedics, The Second Xiangya Hospital of Central South University, Changsha, China

Keywords: CGPR, osteoporosis, BMSCs, osteogenic, adipogenic, age-related

OPEN ACCESS

Edited and reviewed by:
Frontiers in Cell and Developmental Biology Editorial Office, Frontiers Media SA, Switzerland

***Correspondence:**
Qiong Lu
christy_luq@csu.edu.cn
Ren Wu
wurenraul@csu.edu.cn

[†] These authors have contributed equally to this work

Specialty section:
This article was submitted to Molecular Medicine, a section of the journal Frontiers in Cell and Developmental Biology

Received: *27 May 2021*
Accepted: *28 May 2021*
Published: *22 June 2021*

Citation:
Li H, Qu J, Zhu H, Wang J, He H, Xie X, Wu R and Lu Q (2021) Corrigendum: CGRP Regulates the Age-Related Switch Between Osteoblast and Adipocyte Differentiation. Front. Cell Dev. Biol. 9:715740. doi: 10.3389/fcell.2021.715740

A Corrigendum on

CGRP Regulates the Age-Related Switch Between Osteoblast and Adipocyte Differentiation
by Li, H., Qu, J., Zhu, H., Wang, J., He, H., Xie, X., et al. (2021). Front. Cell Dev. Biol. 9:675503. doi: 10.3389/fcell.2021.675503

In the published article, there was an error regarding the affiliation(s) for Qiong Lu. It should be Qiong Lu[1,2*] instead of Qiong Lu[2,3*].

The authors apologize for this error and state that this does not change the scientific conclusions of the article in any way. The original article has been updated.

Copyright © 2021 Li, Qu, Zhu, Wang, He, Xie, Wu and Lu. This is an open-access article distributed under the terms of the Creative Commons Attribution License (CC BY). The use, distribution or reproduction in other forums is permitted, provided the original author(s) and the copyright owner(s) are credited and that the original publication in this journal is cited, in accordance with accepted academic practice. No use, distribution or reproduction is permitted which does not comply with these terms.

frontiers in Cell and Developmental Biology

REVIEW
published: 10 June 2021
doi: 10.3389/fcell.2021.683457

Bone-Derived Modulators That Regulate Brain Function: Emerging Therapeutic Targets for Neurological Disorders

*Hongzhen Chen[1,2], Dewei Shang[2], Yuguan Wen[2] and Chao Liang[1]**

[1] Department of Biology, Southern University of Science and Technology, Shenzhen, China, [2] Department of Pharmacy, The Affiliated Brain Hospital of Guangzhou Medical University, Guangzhou, China

Bone has traditionally been regarded as a structural organ that supports and protects the various organs of the body. Recent studies suggest that bone also acts as an endocrine organ to regulate whole-body metabolism. Particularly, homeostasis of the bone is shown to be necessary for brain development and function. Abnormal bone metabolism is associated with the onset and progression of neurological disorders. Recently, multiple bone-derived modulators have been shown to participate in brain function and neurological disorders, including osteocalcin, lipocalin 2, and osteopontin, as have bone marrow-derived cells such as mesenchymal stem cells, hematopoietic stem cells, and microglia-like cells. This review summarizes current findings regarding the roles of these bone-derived modulators in the brain, and also follows their involvement in the pathogenesis of neurological disorders. The content of this review may aide in the development of promising therapeutic strategies for neurological disorders via targeting bone.

Keywords: bone, bone-derived proteins, bone marrow-derived cells, brain function, neurological disorders

OPEN ACCESS

Edited by:
Changjun Li
Central South University, China

Reviewed by:
Yangli Xie,
Daping Hospital, China
Yili Xu,
Central South University, China
Lixiong Gao,
Sixth Medical Center of PLA General Hospital, China

***Correspondence:**
Chao Liang
liangc@sustech.edu.cn

Specialty section:
This article was submitted to Molecular Medicine, a section of the journal Frontiers in Cell and Developmental Biology

Received: *21 March 2021*
Accepted: *18 May 2021*
Published: *10 June 2021*

Citation:
Chen H, Shang D, Wen Y and Liang C (2021) Bone-Derived Modulators That Regulate Brain Function: Emerging Therapeutic Targets for Neurological Disorders. Front. Cell Dev. Biol. 9:683457. doi: 10.3389/fcell.2021.683457

INTRODUCTION

The brain is a complex and powerful organ consisting of a great variety of nerve tissues that plays essential roles in coordinating body homeostasis (Qin et al., 2016). The brain also directly and indirectly regulates almost all body behaviors, including executive and cognitive functions, immunity, reproduction, and glucose metabolism, through neuroendocrine signaling (Elenkov et al., 2000; Kane and Engle, 2002; Kauffman et al., 2007; Jia et al., 2020). Meanwhile, the brain is influenced by the feedback effects from other organs. A famous example is the microbiota-gut-brain axis (Vuotto et al., 2020). Gut microbes can affect brain functions by multiple mechanisms, such as neural, immunoregulation, and endocrine pathways. Indeed, disturbances in the intestinal microbiota balance contribute to the onset and progression of central nervous system diseases (Logsdon et al., 2018).

Bone is a hard tissue viewed as a scaffold to support and protect the various organs of the body and, historically, has been regarded as an "independent" organ (Buckwalter et al., 1996). However, in recent years, bone has proven to be an endocrine organ. Osteocalcin (OCN), a hormone secreted by osteoblasts, was reported to take part in systemic body regulation by acting on adipose tissue, muscle, pancreas, and male gonads (Wei et al., 2014;

Kover et al., 2015; Sabek et al., 2015; De Toni et al., 2016a,b; Gao J. et al., 2016; Khrimian et al., 2017; Cristina Diaz-Franco et al., 2019).

Although bone and brain tissue seem apparently unrelated, both clinical and experimental research have proposed a bilateral dependence of the two organs (Otto et al., 2020). A large number of well-established studies indicate that the brain can influence bone metabolism by several pathways, including (a) secretion of hypothalamic peptides that directly regulate bone, (b) transduction of neuronal signals that act on bone through the sympathetic nervous system, and (c) transduction of hypothalamic neuroendocrine signals that act on bone via the pituitary (Quiros-Gonzalez and Yadav, 2014; Dimitri and Rosen, 2017). However, the roles of bone-derived modulators in the regulation of brain development and function are often underestimated.

Increasing studies have shown that bone can exert regulation on the brain by secreting various molecules, several of which are essential to brain homeostasis (Chamouni et al., 2015). Abnormal bone metabolism may also contribute to the occurrence and development of neurodegenerative and neuropsychiatric disorders (Downey et al., 2017; Yuan et al., 2019). Patients with neurological disorders, the second main cause of death worldwide in 2016, still have no access to effective treatments (Feigin et al., 2019). These unexpected and remarkable discoveries provide a new perspective to explore how bone regulates brain function, and an opportunity to develop promising therapeutic methods for neurological disorders via targeting bone.

The purpose of this review is to provide a detailed overview of the bone-derived modulators that have the capability to regulate brain functions, and to summarize the current knowledge about the relevance of the bone-derived modulators in the pathogenesis of neurological disorders.

IMPACT OF BONE-DERIVED MODULATORS ON THE BRAIN

Bone mainly regulates brain development, function, and pathophysiology by secreting various proteins, including OCN, lipocalin-2 (LCN2), and osteopontin (OPN) (**Figure 1**), and providing cells such as bone-derived mesenchymal stem cells (BMSCs), hematopoietic stem cells, and microglia-like cells (Otto et al., 2020).

OCN

OCN, also known as bone gamma-carboxyglutamate protein, is exclusively secreted by osteoblasts and decarboxylated by osteoclasts into undercarboxylated OCN, which is an active molecule acting as an endocrine hormone (Price et al., 1976; Mizokami et al., 2017). In the peripheral, OCN binds to the G protein-coupled receptor family C group 6 member A (Gprc6a) to exert endocrine functions, including regulating insulin secretion and testosterone production, and promoting muscle adaptation to exercise (Mizokami et al., 2017). OCN was discovered to transverse the blood-brain barrier (BBB), inhibit γ-aminobutyric acid (GABA) synthesis, and enhance monoamine neurotransmitters synthesis by binding specifically to neurons in the hippocampus, brainstem, and midbrain (Oury et al., 2013; Khrimian et al., 2017). G protein-coupled receptor 158 (Gpr158) was the first receptor that was discovered in the brain for OCN and is expressed in the somatosensory, motor, and auditory areas of the cortex, and in the piriform cortex, the retro-splenial area, and the ventral tegmental area. Behavioral experiments discovered that, compared with wild-type littermates, adult mice lacking OCN exhibited a substantial increase in anxiety-like behavior and had a major deficit in memory and learning (Nakazawa et al., 2002; Oury et al., 2013). Administration of OCN to the OCN-lacking mice reduced anxiety-like behavior and improved their memory and learning capabilities (Villeda et al., 2014). Moreover, maternal OCN was required for the fetal brain to regulate the progression of neurogenesis and prevent neuronal apoptosis, and it was necessary for optimal memory and spatial in the adult offspring (Oury et al., 2013).

LCN2

Another bone-derived hormone, LCN2, also known as 24p3 and neutrophil gelatinase-associated lipocalin, is an osteoblast-enriched glycoprotein (Borregaard and Cowland, 2006). LCN2 was previously thought to be exclusively secreted by adipose tissue, but increasing evidence suggests that bone is the predominant organ expressing LCN2, with tenfold or higher expression levels compared with adipose tissue (Soukas et al., 2000; Yan et al., 2007; Mosialou et al., 2017). Similar to OCN, LCN2 was discovered to participate in energy metabolism by regulating insulin secretion and improving glucose tolerance and insulin sensitivity (Yan et al., 2007). Recently, LCN2 was found to activate the anorexigenic pathway by binding to the melanocortin 4 receptor in the paraventricular nucleus and ventromedial neurons of the hypothalamus after crossing the BBB (Ste Marie et al., 2000; Liu et al., 2003; Mosialou et al., 2017). Furthermore, studies reported that LCN2 was involved in direct neurotoxic effects by interacting with the LCN2 receptor on neurons and increasing the sensitivity of neurons to cell death evoked by oxidative stress, nitric oxide, and tumor necrosis factor (Devireddy et al., 2005; Tong et al., 2005; Nelson et al., 2008; Mucha et al., 2011). LCN2 also enhanced neuronal motility and inflammatory responses through activation of the JAK2, STAT3 and NF-kB pathways to upregulate expression of C-X-C motif chemokine 10 (Yan et al., 2007; Bauer et al., 2008; Lee et al., 2012). These findings indicate that LCN2 can influence the development of the central nervous system and its neuropathology by regulating neuronal cell death, migration, and morphology.

OPN

OPN is a secreted matricellular protein that was originally discovered in bone and was later shown to be expressed in various tissues including kidney, epithelial linings, skeletal muscle, mammary, and brain (Franzen and Heinegard, 1985; Yokosaki et al., 2005; Clemente et al., 2016). OPN was reported to play important roles in tissue remodeling, immune regulation, and biomineralization by binding to multiple receptors, including

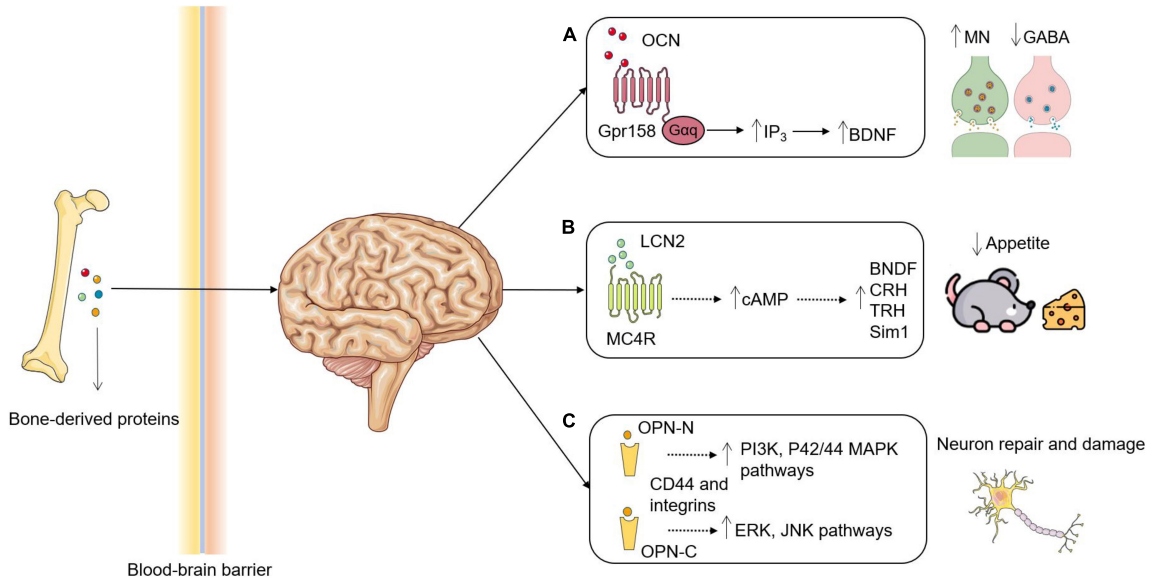


FIGURE 1 | Roles of bone-derived proteins in brain functions. **(A)** OCN is decarboxylated and secreted by osteoblasts and enters the circulation to act as an endocrine hormone. OCN transverses the BBB, where it binds to Gpr158 in the brain to increase the synthesis of BDNF through upregulating IP3 and eventually results in promoting MN synthesis and inhibiting GABA production. **(B)** LCN2 is secreted by osteoblasts and binds to MC4R in the hypothalamus after crossing the BBB. Activation of MC4R by LCN2 induces cAMP and promotes the synthesis of BDNF, CRH, TRH and Sim1 to suppress appetite. **(C)** The proteases cleavage may generate two OPN fragments: OPN-N and OPN-C. OPN-N binds with integrins to activate PI3K and P42/44 MAPK pathways leading to a protective role, whereas OPN-C binds with CD44 to activate ERK and JNK pathways leading to a detrimental role. OCN, Osteocalcin; BBB, blood-brain barrier; Gpr158, G protein-coupled receptor 158; BDNF, brain-derived neurotrophic factor; IP3, inositol triphosphate; MN, monoamine neurotransmitters; Gαq, guanine nucleotide-binding protein α-q; LCN2, lipocalin-2; MC4R, melanocortin 4 receptor; cAMP, cyclic adenosine monophosphate; CRH, corticotropin releasing hormone; TRH, thyrotropin-releasing hormone; Sim1, single-minded homolog 1; OPN, osteopontin. OPN-N/C, N/C-terminal fragment of OPN. Figures were produced using Servier Medical Art, modified.

various integrins (αvβ1, αvβ3, αvβ5, αvβ6, α4β1, α5β1, α8β1, and α9β1) and CD44 (Lin and Yang-Yen, 2001; Yokosaki et al., 2005). In bone, OPN was thought to promote bone resorption by anchoring osteoclasts to the mineral matrix of bones (Reinholt et al., 1990; Yoshitake et al., 1999; Ishijima et al., 2001). Patients with high serum OPN concentrations had low bone mineral density (Cho et al., 2013; Filardi et al., 2019). Interestingly, OPN was discovered to exert conflicting functions in the brain. Several studies demonstrated that OPN protected neurons and promoted repair in acute brain injuries and neurodegenerative diseases by coordinating inflammatory responses, anti-apoptotic actions, BBB maintenance, and chemotaxis and proliferation of nerve cells (Denhardt et al., 2001; Lin and Yang-Yen, 2001; Mazzali et al., 2002; Zhou et al., 2020). In contrast, other studies suggested that OPN served as a proinflammatory cytokine, recruiting harmful inflammatory cells to lesion sites and contributing to neurological diseases (Chabas et al., 2001; Maetzler et al., 2007; Rentsendorj et al., 2018). A possible explanation for the above conflicting findings is that OPN formed different fragments after proteases cleavage, which could bind to distinct receptors (CD44 and integrins) to activate different signaling pathways and cell responses (Boggio et al., 2016). OPN has been reported to activate P42/44 MAPK and PI3K pathways to exerts neuroprotective function, whereas activation of JNK and ERK pathways evokes detrimental neuroinflammation by upregulating the expression of proinflammatory cytokines (Meller et al., 2005; Wang et al., 2019).

Bone Marrow-Derived Cells

Bone marrow, a tissue with a malleable and sponge-like texture, plays an active role in the body by producing various types of cells, such as hematopoietic stem cells, microglia-like cells and BMSCs. For hematopoietic stem cells, they have been demonstrated to act on the brain by secreting cytokines and hematopoietic growth factors, which can inhibit apoptosis, increase neurogenesis and also promote the migration of bone marrow-derived microglia-like cells into the brain (Sanchez-Ramos et al., 2008). Bone marrow-derived microglia-like cells have potential therapy against AD through phagocytic clearance of protein aggregates and cellular debris to maintain homeostasis in the brain (Arandjelovic and Ravichandran, 2015). Additionally, BMSCs are pluripotent stem cells and have been proved to migrate to areas afflicted by neurological insults or neurodegeneration (Borlongan et al., 2011). When compared with other types of bone marrow-derived cells, BMSCs have been widely studied because of their availability, ease of isolation and culture, powerful self-renewal, and multilineage differentiation (Grove et al., 2004; Badyra et al., 2020). The possible mechanism by which BMSCs act on brain tissue can be summarized as follows (**Figure 2**): (1) BMSCs could migrate to the injured brain areas via passing through the BBB with the help of several receptors, integrins, selectins and proteolytic enzymes. One of the critical chemoattractants for BMSCs migration is SDF-1 (stromal cell-derived factor-1). The level of SDF-1 was significantly increased under pathological conditions such as inflammation, ischemia

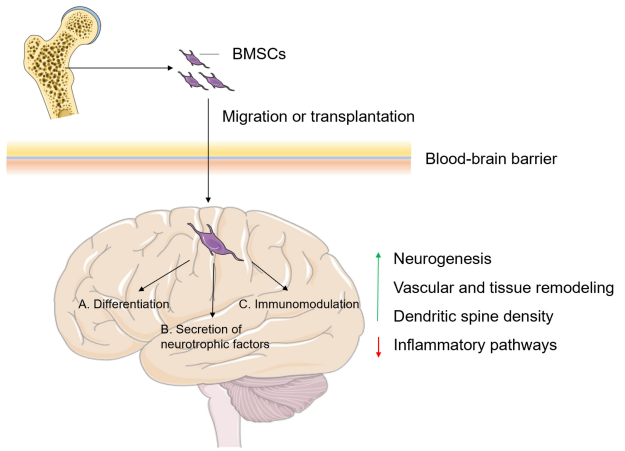


FIGURE 2 | The possible mechanisms of BMSCs involved in the regulation of brain functions. BMSCs can be transplanted directly into the injury site, or they can actively migrate to the injured site after crossing the BBB, where **(A)** they differentiate into neuronal lineages and oligodendrocytes; **(B)** elicit nerve regeneration by secreting neurotrophic factors and **(C)** act as immunomodulatory cells, eventually leading to promoted neurogenesis, vascular and tissue remodeling, and dendritic spine density and inhibited inflammatory pathways. BMSCs, bone mass-derived mesenchymal stem cells; BBB, blood-brain barrier. Figures were produced using Servier Medical Art, modified.

or hypoxic. SDF-1 bound with CXCR4 to attracting the BMSCs to migrate into the damaged region. However, only minute quantities of bone BMSCs can migrate to the brain under non-pathological conditions (Lee et al., 2015; Bang et al., 2017).; (2) BMSCs have the potential to differentiate into neuronal lineages and oligodendrocytes by forming primary neurospheres (Balasubramanian et al., 2013); (3) BMSCs are regarded as immunomodulatory cells that could effectively inhibit the inflammatory state by regulating inflammatory signaling. BMSCs also directly influence inflammation through direct cell-cell contact and secretion of soluble factors (Di Trapani et al., 2013; Gao F. et al., 2016; Simon et al., 2017); and (4) BMSCs elicit nerve regeneration by secreting nerve growth factor, glial cell-line-derived neurotrophic factor, brain-derived neurotrophic factor, and vascular endothelial growth factor (Zhang et al., 2004; Uccelli et al., 2011). BMSCs therapy may be one of the most promising treatments for neurodegeneration, as this approach has been proven to be safe and has great potential to improve the symptoms of neurological diseases (Pernia et al., 2020). In the next part, we reviewed the research progress in the application of BMSCs in the treatment of neurological disorders.

THE ROLE OF BONE-DERIVED MODULATORS IN NEURODEGENERATIVE DISEASES

Neurodegenerative diseases, a heterogeneous group of disorders, cause severe motor and cognitive impairments and are characterized by the relentlessly progressive degeneration of the functional and structural integrity of the central nervous system and peripheral nervous system (Heemels, 2016). Different neurodegenerative diseases may share the same neuropathological features, such as neuronal loss, neuroinflammation, BBB impairment, protein misfolding, and autophagy dysfunction (Menzies et al., 2015; Riek and Eisenberg, 2016; Wyss-Coray, 2016). Below, we review the roles of bone-derived modulators in neurodegenerative diseases, including Alzheimer's disease (AD) and Parkinson's disease (PD), and stroke (**Table 1**).

AD

AD, a progressive and neurodegenerative disease, is the most common cause of dementia. Initially, patients with AD often present with mild memory loss, which over time further deteriorates, resulting in the loss the of ability to live independently. The major pathologic characteristics of AD are neurofibrillary tangles and β-amyloid (Aβ) plaques (Hardy and Higgins, 1992; De Strooper and Karran, 2016). Though the pathogenesis of AD is still not clear, the excessive accumulation of Aβ plaques, which are generated by the abnormal processing of the amyloid precursor protein, is regarded as the cause of the deregulation of kinases and phosphatases that results in neuroinflammation and impairment of synaptic and neuronal function associated with the disease (Hardy and Higgins, 1992). A growing number of studies have supported that abnormal bone metabolism may participate in the pathogenesis of AD.

Clinical studies have suggested an association between circulating levels of undercarboxylated OCN and cognitive performance (Bradburn et al., 2016; Puig et al., 2016). OCN was also shown to be sufficient to rescue age-related cognitive decline and decrease anxiety-like behavior (Khrimian et al., 2017). Blood extracted from young mice, and subsequently transfused into older mice, was found to rejuvenate brain function, which indicated that young blood contained effective factors that exerted nerve repair functions (Villeda et al., 2014). Khrimian et al. (2017) reproduced this experiment and discovered that OCN was necessary for young blood to exert nerve repair function. Therefore, OCN was regarded as an anti-gerontic hormone and the lack of OCN in old blood may be related to the pathogenesis of AD. However, to date, an explicit role for OCN in AD is unclear and needs further investigation.

LCN2 has been found to be decreased in cerebrospinal fluid (CSF) but elevated in plasma of patients with mild cognitive impairment and AD. In particular, plasma LCN2 was found to be negatively corrected with clinical dementia rating scores and positively corrected with mini-mental status examination scores, and is therefore regarded as a potential marker to predict the progression from mild cognitive impairment to AD (Choi et al., 2011; Naude et al., 2012). LCN2 may also be involved in AD pathogenesis through several mechanisms. First, LCN2 contributes to the neuroinflammation leading to the pathogenesis of AD. The chronic and excessive immune response could induce the upregulation of LCN2 in the brain (Naude et al., 2012; Dong et al., 2013). The upregulation of LCN2 then promotes the migration of microglia, astrocytes, and neurons, which play an important role in neuroinflammation

TABLE 1 | Bone-derived modulators involved in neurological disorders.

Factors	Role in	Organism or model	Correlated observation	Potential action
OCN	PD	PD rats	Downregulated in CSF	Increase in dopamine synthesis; improvement in behavioral dysfunctions; reduction in the loss of tyrosine hydroxylase; improvement in astrocytic and microglial functions.
	MD	Patients with depression	Downregulated in plasma	Increase in serotonin, dopamine, and noradrenaline release and reduction in GABA release.
OPN	AD	Patients with AD	Upregulated in plasma and CSF especially in early stage AD	Protective role: Reduction in Aβ plaques. Detrimental role: No reports.
	PD	PD marmosets; patients with PD	Downregulated in substantia nigra following nigral cell degeneration; upregulated in serum and CSF	Protective role: Protects tyrosine hydroxylase positive cells against toxic. Detrimental role: *Opn* $(^{-/-})$ mice showed less death of tyrosine hydroxylase positive cells and dopaminergic fibers.
	Stroke	Patients with stroke	Upregulated in plasma	Protective role: Reduced mean infarct volume, ameliorated neurological deficits, mediated anti-inflammatory effect. Detrimental role: No reports.
LCN2	AD	Patients with AD	Upregulated in plasma but downregulated in CSF	Increase in neuroinflammation; reduction in Aβ plaque clearance; reduction in dehydrogenase activity and survival of wild-type astrocytes.
	PD	PD mice; patients with PD	Upregulated in substantia nigra; negative corrected with dopaminergic neurons	Disruption of the nigrostriatal dopaminergic projections; Involved in the induction of abnormal locomotor behaviors.
	Stroke	Patients with stroke	Upregulated in plasma especially in the acute stage	Increase in BBB permeability, neurological deficits, cerebral infarction, and infiltration of neutrophils in the acute stage. Stimulated microglia and astrocytes into potentially pro-recovery phenotypes in the later stage.
	MD	Chronic stress mice	Upregulated in the hippocampus after stress	Reduction in dendritic spines and ability to regulate neuronal excitability.
BMSCs	AD	AD mice	/	Reduction in Aβ plaques and dystrophic neurites; Increase in neovascularization.
	PD	PD mice	/	Differentiation into functional dopaminergic neurons; reduction in microglial activation and tyrosine hydroxylase-positive neuronal loss.
	Stroke	Ischemic stroke rats	/	Promoted neurogenesis and angiogenesis, inhibited neuronal apoptosis.
	MD	Depression model mice	/	Increase in hippocampal neurogenesis.

OCN, Osteocalcin; LCN2, lipocalin-2; OPN, osteopontin; BMSCs, bone mass-derived mesenchymal stem cells; AD, Alzheimer's disease; PD, Parkinson's disease; MD, Mood Disorders; CSF, cerebrospinal fluid; Aβ, β-amyloid; BBB, blood-brain barrier.

(Lee et al., 2011, 2012). Second, the upregulation of LCN2 might inhibit Aβ plaque clearance. Insulin signaling was reported to inhibit Aβ plaques and promote the transport of Aβ out of the brain (Farris et al., 2003; Talbot and Wang, 2014). Interestingly, LCN2 was demonstrated to reduce insulin sensitivity (Yan et al., 2007; Law et al., 2010). Furthermore, LCN2 might regulate the cellular response to Aβ plaques. Aβ stimulation was found to decrease dehydrogenase activity and survival of wild-type astrocytes, but these effects were negated in *Lcn2*$^{(-/-)}$ mice (Mesquita et al., 2014). Taken together, the results indicate that LCN2 may participate in the regulation of AD pathogenesis by influencing neuroinflammation, insulin signaling, and cellular responses associated with Aβ plaques. In conclusion, these studies indicate that LCN2 involve in the onset and progression of AD; therefore, control of LCN2 expression or activity may be the therapeutic target for AD.

OPN levels were found to be significantly elevated in the plasma and CSF of patients with AD (Sun et al., 2013). Similarly, Comi et al. (2010) found that OPN levels were significantly higher in patients with early stage AD and were correlated with the Mini-Mental Status score, making it a possible predictor for early AD. Moreover, Wung et al. (2007) discovered a significant increase in OPN expression in the hippocampus of patients with AD and that OPN showed positive correlation with Aβ plaques and age. Recently, OPN was also shown to have potential therapeutic effects against AD. Glatiramer acetate immunization markedly inhibited Aβ plaques and preserved cognitive function in an AD mouse model through upregulation of OPN, which regulated immunological profiles and physiological functions of macrophages to resist pathogenic factors of AD (Rentsendorj et al., 2018). Finally, OPN is known to bind with CD44 to exert its anti-apoptotic functions, which could be utilized to serve as a potential molecular checkpoint to reduce neuronal degeneration associated with AD (Lin and Yang-Yen, 2001).

Many reports have indicated the potential of BMSCs in the treatment of AD. Using a mouse model of AD, Lee et al. (2009) found that BMSC intracerebral injection promoted the reduction of Aβ through activation of microglia. Another study showed that transplantation of BMSCs overexpressing vascular endothelial growth factor into the hippocampus of AD mice promoted Aβ

clearance and neovascularization, which was accompanied by behavioral benefits and alleviation of cognitive dysfunctions. Similarly, Wu et al. (2017) showed that extracellular vesicles secreted by BMSCs were effective at improving cognitive function and reducing the Aβ deposition and number of dystrophic neurites in an APP/PS1 mouse model. Moreover, BMSCs were found to play an important role in the replenishment of neural lineages and neurogenesis in the brains of AD mice. In summary, BMSCs may treat AD via regulating angiogenesis, neurogenesis, immunomodulation and eliminating the Aβ deposition.

PD

PD is one of the most common progressive neurodegenerative disorders, characterized by motor deficits such as slowness of movement, rigidity, tremor, and postural instability (Braak et al., 2003). Neurons, and in particular dopaminergic neurons, in the PD brain gradually break down and die, leading to decreased dopamine levels, which is the primary cause of the motor symptoms of PD (Magalingam et al., 2015). The neuropathological hallmark of PD is the formation of Lewy body inclusions enriched in filamentous forms of the synaptic protein alpha-synuclein (Angot and Brundin, 2009).

The circulating levels of OCN are significantly lower in midlife than in adolescence and falling OCN levels have been demonstrated to be one of the important factors associated with age-related cognitive decline (Liu et al., 2008; Bradburn et al., 2016; Obri et al., 2018). Furthermore, OCN binds to neurons to increase dopamine synthesis, the low levels of which are associated with motor symptoms (Oury et al., 2013). Recently, a study found that OCN level was lower in CSF of 6-hydroxydopamine-induced PD rats than that in sham rats, and administration of OCN could ameliorate behavioral dysfunctions associated with PD (Guo et al., 2018). Further research showed that OCN could reduce the loss of tyrosine hydroxylase in the nigrostriatal system and regulate astrocytic and microglial functions (Guo et al., 2018). Gpr158 is the only central receptor of OCN found in the brain, but whether OCN can exert its neuroprotective efficacy in a PD rat model by binding to Gpr158 is still unknown (Khrimian et al., 2017; Cetereisi et al., 2019).

Kim et al. (2016) showed that LCN2 expression was significantly elevated in the substantia nigra of PD patients, and there was a negative correlation between LCN2 levels and dopaminergic neurons. In animal experiments, LCN expression was found to increase in the substantia nigra following injection of 6-hydroxydopamine in the medial forebrain bundle, suggesting that increased LCN2 levels may be associated with PD pathogenesis. Beyond that, LCN2 upregulation was discovered in neurotoxin-treated mouse models of PD. The dopaminergic neurotoxin, 1-methyl-4-phenyl-1,2,3,6-tetrahydropyridine (MPTP), can cause clinical symptoms similar to PD and is commonly used to induce PD mouse models (Song et al., 2021). LCN2 expression, in an MTPT induced mouse model, was found to be significantly upregulated in the brain, especially in reactive astrocytes of the substantia nigra and striatum (Kim et al., 2016). This upregulation of LCN2 was regarded as a potential pathogenic mechanism of PD, involving disruption of the nigrostriatal dopaminergic projections and induction of abnormal locomotor behaviors through neurotoxic iron accumulation and neuroinflammation (Kim et al., 2016). More importantly, they also found that gene knockout of LCN2 ameliorated the aforementioned PD symptoms in mice (Kim et al., 2016). Therefore, the development of regulatory method for LCN2 or the inhibitors of LCN2-induced neurotoxicity and neuroinflammation may be helpful for the treatment of PD.

OPN protein expression was discovered to be significantly low in marmosets after treatment with MPTP, including in the dopaminergic neurons of the substantia nigra (Iczkiewicz et al., 2006). Similarly, the same study found low OPN expression in the postmortem brains of patients with atypical parkinsonism (Iczkiewicz et al., 2006). The low expression levels of OPN following nigral cell degeneration indicated that OPN might play a central role in dopaminergic neuron survival. Further studies showed that the N-terminal fragment of OPN (OPN-N) containing arginine-glycine-aspartic acid (RGD)-peptide, an OPN fragment generated by thrombin cleavage, could protect tyrosine hydroxylase positive cells in the rat substantia nigra and primary ventral mesencephalic cultures from damage induced by 6-hydroxydopamine, lipopolysaccharide, and MPTP through its interaction with integrins, which subsequently altered glial activation (Iczkiewicz et al., 2010; Broom et al., 2015). These studies suggest that OPN can exert neuroprotective functions in PD models. In contrast, Maetzler et al. (2007) found that the level of OPN was elevated in PD patients and its absence led to reduced neurodegeneration in the MPTP mouse model. Besides, after MPTP treatment, OPN knockout mice showed less death of hydroxylase positive cells and dopaminergic fibers in the striatum compared with wild-type controls (Maetzler et al., 2007). The detrimental role of OPN in PD can be attributed to the inflammatory response. C-terminal fragment of OPN (OPN-C), another OPN fragment generated by thrombin cleavage, may be the main driver for inflammatory response. OPN-C was reported to interact with CD44 to inhibit IL-10 secretion and promote cell-cell adhesion (Weber et al., 1996). Collectively, these seemingly opposing roles of OPN in PD may be associated with the different functional domains of OPN or activation of different signaling pathways (Cappellano et al., 2021). Correctly understanding the molecular mechanism for the opposing roles of OPN will help to develop highly specific therapeutic tools via targeting OPN.

Growing evidence from experimental PD research has demonstrated that BMSC-mediated amelioration of PD is multimechanistic. Shetty et al. (2009) demonstrated that BMSCs could efficiently transdifferentiate into functional dopaminergic neurons both *in vitro* and *in vivo*. They then transplanted undifferentiated BMSCs into animal PD models and found significant behavioral improvements (Shetty et al., 2009). BMSCs were also found to have the capacity to induce neuroblasts to migrate to lesioned brain areas and enhance neurogenesis. Park et al. (2012) demonstrated that tail vein BMSC administration to PD mice increased neurogenesis in the substantia nigra and subventricular zone and also led to the differentiation of neural precursor cells into dopaminergic neurons in the substantia nigra. Furthermore, BMSCs are thought to exert their neuroprotective efficacy on dopaminergic neurons via

anti-inflammatory effects by inhibiting microglial activation. Kim et al. (2009) used LPS to induce inflammation in a rat model of PD. They found that BMSCs administration significantly decreased tyrosine hydroxylase positive neuronal loss, microglia activation, TNF-α mRNA expression, and iNOS and TNF-α secretion.

Stroke

Stroke, which is the leading cause of death and the primary reason for adult disability, can be divided into ischemic stroke and hemorrhagic stroke. Ischemic stroke is the most common type of stroke and caused by a blood clot that blocks a blood vessel in the brain. Another type of stroke is hemorrhagic stroke which is caused by the rupture of cerebral arteries (Rothwell et al., 2004; Polivka et al., 2019). Below, we reviewed the roles of LCN2, OPN and BMSCs in stroke except for OCN which has not been reported.

Plasma level of LCN2 was found to be significantly elevated in patients with ischemic stroke, especially in the early stages, and to be a risk factor for unfavorable modified Rankin scale scores, the occurrence of post-stroke infections and cardiovascular mortality (Anwaar et al., 1998; Falke et al., 2000; Hochmeister et al., 2016). In mice models of ischemic stroke induced by transient middle cerebral artery occlusion (tMCAo), serum level of LCN2 was acutely induced after tMCAo and was reduced at 48–72h post-tMCAo (Jin et al., 2014; Wang et al., 2015). The early induction of LCN2 indicated that LCN2 can be used as an early blood biomarker for stroke. Further researches showed that LCN2 deficient mice with fewer symptoms of BBB permeability, neurological deficits, cerebral infarction, and infiltration of neutrophils after tMCAo (Jin et al., 2014; Wang et al., 2015). They also revealed LCN2 promoted neuroinflammation through the activation of neutrophil infiltration, microglia/astrocytes, and the induction of pro-inflammatory cytokines and chemokines (Bi et al., 2013; Jin et al., 2014; Wang et al., 2015). Therefore, inhibiting LCN2 might be a promising therapeutic strategy to reduce post-stroke inflammation. Interestingly, Xing et al. (2014) suggested that LCN2 expressed in injured neurons may be as a "help-me" signal that stimulated microglia to increase interleukin-10 (IL-10) production and enhance phagocytosis, and stimulated astrocytes to upregulate levels of BDNF, glial fibrillary acid protein and thrombospondin-1. These studies indicate that LCN2 might play different roles during the acute and later stages of stroke.

OPN has been regarded to have a clinical and pathophysiological relevance with stroke. Carbone et al. (2015) found that the serum level of OPN was positively associated with poor outcome at day 90 after ischemic stroke, while Jing et al. (2013) showed that the serum level of thrombin-cleaved OPN could discriminate patients with ischemic stroke from healthy controls and was negatively correlated with the clinical outcome at 12 months after hospital discharge. OPN was also proposed to regulate repair processes and to protect neurons in stroke. Meller et al. (2005) showed that intracerebral ventricular OPN administration to murine stroke models could significantly reduce infarct size after tMCAo. Besides, Doyle et al. (2008) discovered that the RGD-containing peptide fragment of OPN, which was a twofold more effective neuroprotectant than the full-length OPN, was the effective peptide for OPN to treat with stroke. Similarly, Jin et al. (2016) found that OPN failed to decrease infarct volumes in the focal cerebral ischemia rat model when the RGD was replaced by arginine-alanine-alanine. They also found that the direct binding between RGD-containing peptide fragment of OPN and αvβ3 integrin might be the mechanism for OPN to mediated anti-inflammatory effect (Jin et al., 2016). These results indicate that OPN can be used as a novel biomarker, predictor and therapeutic target for stroke.

Transplantation of BMSCs is regarded as a promising therapy for stroke. Several mechanisms of BMSCs treatment for stroke are as follows. BMSCs-induced angiogenesis was considered important for neurological recovery in stroke. Bao et al. (2011) found that BMSCs transplantation could promote angiogenesis in Ischemic brain areas through stimulating Notch signaling pathway. Besides, BMSCs were also found to promote neurogenesis, inhibit neuronal apoptosis, and improve behavioral and motor function in the ischemic stroke through increasing neurotrophic expression, and differentiating into neurons and oligodendrocytes (Jahromi et al., 2015; He et al., 2017, 2019).

THE ROLE OF BONE-DERIVED MODULATORS IN MOOD DISORDERS

Mood disorders, such as mania, bipolar disorder, and depression, are heterogeneous conditions that are characterized by complex genetics, unclear pathophysiology, and variable symptomatology. A growing number of clinical investigations have shown that patients affected by mood disorders have a high incidence of bone metabolism abnormalities, which can lead to low bone mass and increased risk of fracture (Gale et al., 2012; Williams et al., 2013; Chen et al., 2016; Cheng et al., 2016). Meanwhile, alterations in bone-derived hormones can influence brain development, function, and behavior and regulate of neurotransmitter synthesis (Otto et al., 2020). Below, we outline the possible relationships between the bone-derived modulators and mood disorders.

First, significantly lower OCN levels have been found in depression patients (Aydin et al., 2011). Furthermore, OCN knockout adult mice were shown to exhibit a significant increase in anxiety-like behavior, including increased aversion to open spaces and light and deceased exploratory activity, all of which were reversed by the administration of OCN (Oury et al., 2013). Others found that OCN derived from bone was able to cross the BBB and modulate transcription factors in neurons of the VTA, DRN, MRN, and CA3 region, which increased serotonin, dopamine, and noradrenaline release and inhibited GABA release (Oury et al., 2013; Khrimian et al., 2017), resulting in a reduction in anxiety-like behavior[6,25]. These results indicate that OCN may be a promising treatment tool for depression.

Another bone-derived factor related to mood disorders is LCN2. The nervous system undergoes a variety of adaptive changes to maintain homeostasis after psychological stress (Roozendaal et al., 2009). However, disorders of the regulatory functions that maintain homeostasis may lead to affective disorders. LCN2 is regarded as an important regulatory factor

in the nervous system's response to reply stress. Mariusz and co-workers demonstrated that LCN2 was significantly upregulated in the mouse hippocampus after stress, which resulted in the loss of dendritic spines and regulation of neuronal excitability (as a result of reduced dendritic spine actin mobility), and increased anxiety (Pawlak et al., 2003; Adhikari et al., 2010; Mucha et al., 2011). Therefore, LCN2 may be a therapeutic target to combat anxiety induced by stress.

BMSCs may be also a promising strategy for mood disorders, as they promote the expression of neurotrophic factors and neurogenesis. However, studies regarding the efficacy BMSCs in animal models of mood disorders are still limited. It is known that impaired hippocampal neurogenesis is related to depression (Thomas et al., 2007). Munoz et al. (2005) demonstrated that BMSC implantation promoted hippocampal neurogenesis. Furthermore, using a mouse model of depression, Tfilin et al. (2010) found that BMSCs migrated to the CA1 and CA2 regions, and the ipsilateral dentate gyrus after intracerebroventricular injection, which improved depressive-like behavior and hippocampal neurogenesis (Tfilin et al., 2010).

POTENTIAL CLINICAL APPLICATION OF BONE-DERIVED MODULATORS IN NEUROLOGICAL DISORDERS

Until now, patients with neurological disorders, the second main cause of death worldwide in 2016, still have no access to effective treatments (Feigin et al., 2019). Therefore, there is an urgent need to develop new and effective treatments for those suffering from neurological disorders. The crosstalk between bone and brain tissues provides a new perspective to research new therapeutic approaches for neurology.

Although, as mentioned above, a growing number of bone-derived molecules have been demonstrated to affect brain function, most of these discoveries are limited to preclinical studies except for BMSCs (Otto et al., 2020). A growing number of basic research and clinical trials regarding the therapeutic effects of BMSCs in neurological diseases have shown that BMSCs have great potential to improve patient symptoms and quality of life (Badyra et al., 2020). To date, more than 20 clinical trials have been registered on the ClinicalTrials.gov[1]. However, more research is needed to evaluate different doses, methods of administration, and cell culture conditions, among others, to obtain the best therapeutic regimen for patients.

Several researchers have demonstrated that young blood could reverse age-related impairments, including loss of cognitive function and synaptic plasticity (Villeda et al., 2011, 2014; Khrimian et al., 2017). These reports indicate that young blood may contain powerful molecules that exert rejuvenating effects in the brain, several of which may have direct clinical applications.

An unexpected and remarkable discovery indicated that bone-derived OCN was necessary for young blood to exert an anti-geronic function. Khrimian et al. (2017) showed that the administration of plasma from young $Ocn^{-/-}$ mice to older mice did not improve anxiety-like behavior or cognitive function in several behavioral tests. However, improvements were found when wild-type control plasma was used. Importantly, no side effects were detected after plasma administration. Taken together with the other OCN functions presented in this review, we believe that OCN has prospective anti-geronic benefits with low side effects and high effectiveness. However, it is important to consider that the research results are limited to mice, and that future studies in humans are necessary.

[1]https://www.clinicaltrials.gov/

CONCLUSION AND FUTURE PERSPECTIVES

Since the discovery of the essential roles of bone-derived OCN in brain development and function, the number of studies regarding the regulation of the brain by bone has increased considerably. Studies have revealed that bone can influence anxiety, memory, acute stress response, and even appetite by acting on various brain regions (Oury et al., 2013). These studies reconfirm the classic principle of physiology that no single organ can develop alone (Qin et al., 2016). Future therapeutic strategies could be designed to target the crosstalk between the brain and bone.

The remarkable discoveries regarding the roles of bone-derived modulators in brain functions not only add to our knowledge of brain function-related factors but also provide revolutionary insights from the perspective of the pathophysiology of psychiatric and neurological diseases. However, the roles of bone-derived modulators in the brain are not fully known (Han et al., 2018). It has been shown that OCN and Gpr158 (OCN receptor) are not only expressed in the hippocampus and ventral tegmental area but also the motor areas, auditory and somatosensory areas of the cortex, piriform cortex, and retrosplenial area (Oury et al., 2013; Khrimian et al., 2017). However, it remains unclear whether OCN binds to Gpr158 in all of these areas to exert different functions.

LCN2 was formerly thought to be secreted exclusively by adipose tissue. However, recent research demonstrated that bone was the main organ where LCN2 was expressed (Mosialou et al., 2017). Though the role of LCN2 in the central nervous system has been extensively studied, there is little research related to the role of bone-derived LCN2 in the brain (Mucha et al., 2011; Ferreira et al., 2018). Importantly, the expression level of LCN2 in bone was at least 10-fold higher than that in adipose and other tissues, implying that bone-derived LCN2 might play the main effect in the brain (Mosialou et al., 2017).

OPN, as a double-edged sword, not only exerts a detrimental role but also exerts a protective role in neurological disorders (Cappellano et al., 2021). Therefore, it is important to study the role of OPN in the development of diseases of the central nervous system. In particular, further research is needed to determine the mechanisms involved in the opposing roles of OPN-mediated neuronal toxicity and OPN-mediated neuroprotection in the development of neurological disorders. Correctly understanding the mechanisms of these opposing roles of OPN will help to develop highly specific therapeutic tools via targeting OPN. Another interesting point is that OPN has been regarded as an

injury and repair biomarker of PD in two different respective studies (Maetzler et al., 2007; Broom et al., 2015). However, contrasting findings may both be correct because of the opposing roles of OPN in PD. We speculate that low levels of OPN may inhibit wound healing and tissue injury through immune-mediated mechanisms, whereas high levels of OPN may induce excessive tissue injury.

As we mentioned above, BMSC treatment has been widely studied both in preclinical studies and clinical trials, and has great potential to treat neurological disorders (Badyra et al., 2020). However, many aspects need to be improved to obtain the best therapeutic regimen for patients. Thus far, several types of BMSC transplantation have been established, including intravenous, intra-arterial, intrathecal, intranasal, intraspinal, intracerebroventricular, and intracerebral. Yet, thus far, there has been no consensus which method/methods are best. Though intravenous is the most common and feasible way of transplantation in the clinic, many of the cells become trapped in the lungs, which limits the therapeutic outcome of BMSCs (Agadi and Shetty, 2015). Research shows that invasive methods of transplantation may be more effective when BMSCs are transplanted directly into the injured brain (Jarocha et al., 2015). However, these invasive methods may induce more adverse reactions. Therefore, it is important to identify the best BMSC transplantation methods that are closely related to therapeutic outcome (Ben-Shaanan et al., 2008). Other aspects, including medication time and dosage, also need to be optimized in clinical trials to realize the best therapeutic regimen for patients.

Sclerostin, an osteocyte-specific glycoprotein encoded by the SOST gene, which can elevate bone resorption and reduce bone formation by inhibiting the Wnt/β-catenin pathway. Recently, several studies have shown that the Wnt/β-catenin pathway plays an important in neurogenesis, synaptic plasticity, neuronal survival, and BBB integrity (Baron and Kneissel, 2013; Williams, 2014; Shah et al., 2015; Noelanders and Vleminckx, 2017; Koide and Kobayashi, 2019). This leads us to question whether sclerostin crosses the BBB and influences brain functions via the Wnt/β-catenin pathway. Further investigations are needed to answer this and other unknowns regarding bone-derived modulators.

In the future, it will be necessary to decode the detailed regulatory network between bone and brain function. We believe that more bone-derived modulators will be identified that directly influence brain function and that these modulators could serve as potential molecular targets for the treatment of neurological disorders.

AUTHOR CONTRIBUTIONS

CL designed and supervised the manuscript. HC consulted the literature and wrote the manuscript. YW and DS provided advice on the manuscript. All authors read and agreed to publish the manuscript.

FUNDING

This work was supported by the National Natural Science Foundation Council of China (grant nos. 81922081 and 81700780).

REFERENCES

Adhikari, A., Topiwala, M. A., and Gordon, J. A. (2010). Synchronized activity between the ventral hippocampus and the medial prefrontal cortex during anxiety. *Neuron* 65, 257–269. doi: 10.1016/j.neuron.2009.12.002

Agadi, S., and Shetty, A. K. (2015). Concise review: prospects of bone marrow mononuclear cells and mesenchymal stem cells for treating status epilepticus and chronic epilepsy. *Stem Cell.* 33, 2093–2103. doi: 10.1002/stem.2029

Angot, E., and Brundin, P. (2009). Dissecting the potential molecular mechanisms underlying a-synuclein cell-to-cell transfer in Parkinson's disease. *Parkinson. Relat. Disord.* 15, S143–S147. doi: 10.1016/s1353-8020(09)70802-8

Anwaar, I., Gottsater, A., Ohlsson, K., Mattiasson, I., and Lindgarde, F. (1998). Increasing levels of leukocyte-derived inflammatory mediators in plasma and cAMP in platelets during follow-up after acute cerebral ischemia. *Cerebrovas. Dis. (Basel Switzerl.)* 8, 310–317. doi: 10.1159/000015873

Arandjelovic, S., and Ravichandran, K. S. (2015). Phagocytosis of apoptotic cells in homeostasis. *Nat. Immunol.* 16, 907–917. doi: 10.1038/ni.3253

Aydin, H., Mutlu, N., and Akbas, N. B. G. (2011). Treatment of a major depression episode suppresses markers of bone turnover in premenopausal women. *J. Psychiatr. Res.* 45, 1316–1320. doi: 10.1016/j.jpsychires.2011.04.005

Badyra, B., Sulkowski, M., Milczarek, O., and Majka, M. (2020). Mesenchymal stem cells as a multimodal treatment for nervous system diseases. *Stem Cell. Transl. Med.* 9, 1174–1189. doi: 10.1002/sctm.19-0430

Balasubramanian, S., Thej, C., Venugopal, P., Priya, N., Zakaria, Z., Sundarraj, S., et al. (2013). Higher propensity of Wharton's jelly derived mesenchymal stromal cells towards neuronal lineage in comparison to those derived from adipose and bone marrow. *Cell Biol. Int.* 37, 507–515. doi: 10.1002/cbin.10056

Bang, O. Y., Moon, G. J., Kim, D. H., Lee, J. H., Kim, S., Son, J. P., et al. (2017). Stroke induces mesenchymal stem cell migration to infarcted brain areas via CXCR4 and C-met signaling. *Transl. Stroke Res.* 8, 449–460. doi: 10.1007/s12975-017-0538-2

Bao, X., Feng, M., Wei, J., Han, Q., Zhao, H., Li, G., et al. (2011). Transplantation of Flk-1+human bone marrow-derived mesenchymal stem cells promotes angiogenesis and neurogenesis after cerebral ischemia in rats. *Eur. J. Neurosci.* 34, 87–98. doi: 10.1111/j.1460-9568.2011.07733.x

Baron, R., and Kneissel, M. (2013). WNT signaling in bone homeostasis and disease: from human mutations to treatments. *Nat. Med.* 19, 179–192. doi: 10.1038/nm.3074

Bauer, M., Eickhoff, J. C., Gould, M. N., Mundhenke, C., Maass, N., and Friedl, A. (2008). Neutrophil gelatinase-associated lipocalin (NGAL) is a predictor of poor prognosis in human primary breast cancer. *Breast Cancer Res.. Treat.* 108, 389–397. doi: 10.1007/s10549-007-9619-3

Ben-Shaanan, T. L., Ben-Hur, T., and Yanai, J. (2008). Transplantation of neural progenitors enhances production of endogenous cells in the impaired brain. *Mol. Psychiatry* 13, 222–231. doi: 10.1038/sj.mp.4002084

Bi, F., Huang, C., Tong, J., Qiu, G., Huang, B., Wu, Q., et al. (2013). Reactive astrocytes secrete lcn2 to promote neuron death. *Proc. Natl. Acad. Sci. U.S.A.* 110, 4069–4074. doi: 10.1073/pnas.1218497110

Boggio, E., Dianzani, C., Gigliotti, C. L., Soluri, M. F., Clemente, N., Cappellano, G., et al. (2016). Thrombin cleavage of osteopontin modulates its activities in human cells in vitro and mouse experimental autoimmune encephalomyelitis in vivo. *J. Immunol. Res.* 2016:9345495. doi: 10.1155/2016/9345495

Borlongan, C. V., Glover, L. E., Tajiri, N., Kaneko, Y., and Freeman, T. B. (2011). The great migration of bone marrow-derived stem cells toward the ischemic

brain: therapeutic implications for stroke and other neurological disorders. *Progr. Neurobiol.* 95, 213–228. doi: 10.1016/j.pneurobio.2011.08.005

Borregaard, N., and Cowland, J. B. (2006). Neutrophil gelatinase-associated lipocalin, a siderophore-binding eukaryotic protein. *Biometals* 19, 211–215. doi: 10.1007/s10534-005-3251-7

Braak, H., Del Tredici, K., Rub, U., De Vos, R. a. I., Jansen Steur, E. N. H., and Braak, E. (2003). Staging of brain pathology related to sporadic Parkinson's disease. *Neurobiol. Aging* 24, 197–211. doi: 10.1016/s0197-4580(02)00065-9

Bradburn, S., Mcphee, J. S., Bagley, L., Sipila, S., Stenroth, L., Narici, M. V., et al. (2016). Association between osteocalcin and cognitive performance in healthy older adults. *Age Ageing* 45, 844–849. doi: 10.1093/ageing/afw137

Broom, L., Jenner, P., and Rose, S. (2015). Increased neurotrophic factor levels in ventral mesencephalic cultures do not explain the protective effect of osteopontin and the synthetic 15-mer RGD domain against MPP plus toxicity. *Expe. Neurol.* 263, 1–7. doi: 10.1016/j.expneurol.2014.09.005

Buckwalter, J. A., Glimcher, M. J., Cooper, R. R., and Recker, R. (1996). Bone biology. II: formation, form, modeling, remodeling, and regulation of cell function. *Instruct. Cour. Lect.* 45, 387–399.

Cappellano, G., Vecchio, D., Magistrelli, L., Clemente, N., Raineri, D., Mazzucca, C. B., et al. (2021). The Yin-Yang of osteopontin in nervous system diseases: damage versus repair. *Neur. Regenerat. Res.* 16, 1131–1137. doi: 10.4103/1673-5374.300328

Carbone, F., Vuilleumier, N., Burger, F., Roversi, G., Tamborino, C., Casetta, I., et al. (2015). Serum osteopontin levels are upregulated and predict disability after an ischaemic stroke. *Eur. J. Clin. Invest.* 45, 579–586. doi: 10.1111/eci.12446

Cetereisi, D., Kramvis, I., Gebuis, T., Van Der Loo, R. J., Gouwenberg, Y., Mansvelder, H. D., et al. (2019). Gpr158 deficiency impacts hippocampal CA1 neuronal excitability, dendritic architecture, and affects spatial learning. *Front. Cell. Neurosci.* 13:465. doi: 10.3389/fncel.2019.00465

Chabas, D., Baranzini, S. E., Mitchell, D., Bernard, C. C., Rittling, S. R., Denhardt, D. T., et al. (2001). The influence of the proinflammatory cytokine, osteopontin, on autoimmune demyelinating disease. *Science (New York N. Y.)* 294, 1731–1735. doi: 10.1126/science.1062960

Chamouni, A., Schreiweis, C., and Oury, F. (2015). Bone, brain & beyond. *Rev. Endocr. Metab. Disord.* 16, 99–113. doi: 10.1007/s11154-015-9312-5

Chen, H.-J., Kuo, C.-Y., Tu, M.-S., Wang, F.-W., Chen, R.-Y., Hsueh, K.-C., et al. (2016). The incidence and risk of osteoporosis in patients with anxiety disorder: a population-based retrospective cohort study. *Medicine* 95:4912. doi: 10.1097/md.0000000000004912

Cheng, B.-H., Chen, P.-C., Yang, Y.-H., Lee, C.-P., Huang, K.-E., and Chen, V. C. (2016). Effects of depression and antidepressant medications on hip fracture: a population-based cohort study in Taiwan. *Medicine* 95:4655. doi: 10.1097/md.0000000000004655

Cho, E.-H., Cho, K.-H., Lee, H. A., and Kim, S.-W. (2013). High serum osteopontin levels are associated with low bone mineral density in postmenopausal women. *J. Kor. Med. Sci.* 28, 1496–1499. doi: 10.3346/jkms.2013.28.10.1496

Choi, J., Lee, H.-W., and Suk, K. (2011). Increased plasma levels of lipocalin 2 in mild cognitive impairment. *J. Neurol. Sci.* 305, 28–33. doi: 10.1016/j.jns.2011.03.023

Clemente, N., Raineri, D., Cappellano, G., Boggio, E., Favero, F., Soluri, M. F., et al. (2016). Osteopontin bridging innate and adaptive immunity in autoimmune diseases. *J. Immunol. Res.* 2016:7675437. doi: 10.1155/2016/7675437

Comi, C., Carecchio, M., Chiocchetti, A., Nicola, S., Galimberti, D., Fenoglio, C., et al. (2010). Osteopontin is increased in the cerebrospinal fluid of patients with Alzheimer's disease and its levels correlate with cognitive decline. *J. Alzheimers Dis.* 19, 1143–1148. doi: 10.3233/jad-2010-1309

Cristina Diaz-Franco, M., Franco-Diaz De Leon, R., and Rafael Villafan-Bernal, J. (2019). Osteocalcin-GPRC6A: an update of its clinical and biological multi-organic interactions. *Mol. Med. Rep.* 19, 15–22. doi: 10.3892/mmr.2018.9627

De Strooper, B., and Karran, E. (2016). The cellular phase of Alzheimer's disease. *Cell* 164, 603–615. doi: 10.1016/j.cell.2015.12.056

De Toni, L., Di Nisio, A., Speltra, E., Rocca, M. S., Ghezzi, M., Zuccarello, D., et al. (2016a). Polymorphism rs2274911 of GPRC6A as a novel risk factor for testis failure. *J. Clin. Endocrinol. Metab.* 101, 953–961. doi: 10.1210/jc.2015-3967

De Toni, L., Guidolin, D., De Filippis, V., Tescari, S., Strapazzon, G., Rocca, M. S., et al. (2016b). Osteocalcin and sex hormone binding globulin compete on a specific binding site of GPRC6A. *Endocrinology* 157, 4473–4486. doi: 10.1210/en.2016-1312

Denhardt, D. T., Noda, M., O'regan, A. W., Pavlin, D., and Berman, J. S. (2001). Osteopontin as a means to cope with environmental insults: regulation of inflammation, tissue remodeling, and cell survival. *J. Clin. Investigat.* 107, 1055–1061. doi: 10.1172/jci12980

Devireddy, L. R., Gazin, C., Zhu, X., and Green, M. R. (2005). A cell-surface receptor for lipocalin 24p3 selectively mediates apoptosis and iron uptake. *Cell* 123, 1293–1305. doi: 10.1016/j.cell.2005.10.027

Di Trapani, M., Bassi, G., Ricciardi, M., Fontana, E., Bifari, F., Pacelli, L., et al. (2013). Comparative study of immune regulatory properties of stem cells derived from different tissues. *Stem Cell. Dev.* 22, 2990–3002. doi: 10.1089/scd.2013.0204

Dimitri, P., and Rosen, C. (2017). The central nervous system and bone metabolism: an evolving story. *Calcif. Tissue Int.* 100, 476–485. doi: 10.1007/s00223-016-0179-6

Dong, M., Xi, G., Keep, R. F., and Hua, Y. (2013). Role of iron in brain lipocalin 2 upregulation after intracerebral hemorrhage in rats. *Brain Res.* 1505, 86–92. doi: 10.1016/j.brainres.2013.02.008

Downey, C. L., Young, A., Burton, E. F., Graham, S. M., Macfarlane, R. J., Tsapakis, E.-M., et al. (2017). Dementia and osteoporosis in a geriatric population: is there a common link? *World J. Orthop.* 8, 412–423. doi: 10.5312/wjo.v8.i5.412

Doyle, K. P., Yang, T., Lessov, N. S., Ciesielski, T. M., Stevens, S. L., Simon, R. P., et al. (2008). Nasal administration of osteopontin peptide mimetics confers neuroprotection in stroke. *J. Cereb. Blood Flow Metabol.* 28, 1235–1248. doi: 10.1038/jcbfm.2008.17

Elenkov, I. J., Wilder, R. L., Chrousos, G. P., and Vizi, E. S. (2000). The sympathetic nerve–an integrative interface between two supersystems: the brain and the immune system. *Pharmacol. Rev.* 52, 595–638.

Falke, P., Elneihoum, A. M., and Ohlsson, K. (2000). Leukocyte activation: relation to cardiovascular mortality after cerebrovascular ischemia. *Cerebrovas. Dis. (Basel Switzerl.)* 10, 97–101. doi: 10.1159/000016037

Farris, W., Mansourian, S., Chang, Y., Lindsley, L., Eckman, E. A., Frosch, M. P., et al. (2003). Insulin-degrading enzyme regulates the levels of insulin, amyloid beta-protein, and the beta-amyloid precursor protein intracellular domain in vivo. *Proc. Natl. Acad. Sci. U.S.A.* 100, 4162–4167. doi: 10.1073/pnas.0230450100

Feigin, V. L., Nichols, E., Alam, T., Bannick, M. S., Beghi, E., Blake, N., et al. (2019). Global, regional, and national burden of neurological disorders, 1990-2016: a systematic analysis for the Global Burden of Disease Study 2016. *Lancet Neurol.* 18, 459–480. doi: 10.1016/s1474-4422(18)30499-x

Ferreira, A. C., Santos, T., Sampaio-Marques, B., Novais, A., Mesquita, S. D., Ludovico, P., et al. (2018). Lipocalin-2 regulates adult neurogenesis and contextual discriminative behaviours. *Mol. Psychiatry* 23, 1031–1039. doi: 10.1038/mp.2017.95

Filardi, T., Carnevale, V., Massoud, R., Russo, C., Nieddu, L., Tavaglione, F., et al. (2019). High serum osteopontin levels are associated with prevalent fractures and worse lipid profile in post-menopausal women with type 2 diabetes. *J. Endocrinol. Investigat.* 42, 295–301. doi: 10.1007/s40618-018-0914-0

Franzen, A., and Heinegard, D. (1985). Isolation and characterization of two sialoproteins present only in bone calcified matrix. *Biochem. J.* 232, 715–724. doi: 10.1042/bj2320715

Gale, C. R., Dennison, E. M., Edwards, M., Sayer, A. A., and Cooper, C. (2012). Symptoms of anxiety or depression and risk of fracture in older people: the Hertfordshire Cohort Study. *Arch. Osteop.* 7, 59–65. doi: 10.1007/s11657-012-0080-5

Gao, F., Chiu, S. M., Motan, D. a. L., Zhang, Z., Chen, L., Ji, H. L., et al. (2016). Mesenchymal stem cells and immunomodulation: current status and future prospects. *Cell Death Dis.* 7:327. doi: 10.1038/cddis.2015.327

Gao, J., Zhong, X., Ding, Y., Bai, T., Wang, H., Wu, H., et al. (2016). Inhibition of voltage-gated potassium channels mediates uncarboxylated osteocalcin-regulated insulin secretion in rat pancreatic beta cells. *Eur. J. Pharmacol.* 777, 41–48. doi: 10.1016/j.ejphar.2016.02.060

Grove, J. E., Bruscia, E., and Krause, D. S. (2004). Plasticity of bone marrow-derived stem cells. *Stem Cell. (Dayton Ohio)* 22, 487–500. doi: 10.1634/stemcells.22-4-487

Guo, X.-Z., Shan, C., Hou, Y.-F., Zhu, G., Tao, B., Sun, L.-H., et al. (2018). Osteocalcin ameliorates motor dysfunction in a 6-hydroxydopamine-induced Parkinson's disease rat model through AKT/GSK3 beta signaling. *Front. Mol. Neurosci.* 11:343. doi: 10.3389/fnmol.2018.00343

Han, Y., You, X., Xing, W., Zhang, Z., and Zou, W. (2018). Paracrine and endocrine actions of bone-the functions of secretory proteins from osteoblasts, osteocytes, and osteoclasts. *Bone Res.* 6:19. doi: 10.1038/s41413-018-0019-6

Hardy, J. A., and Higgins, G. A. (1992). Alzheimer's disease: the amyloid cascade hypothesis. *Sci. (New York N. Y.)* 256, 184–185. doi: 10.1126/science.1566067

He, H., Zeng, Q., Huang, G., Lin, Y., Lin, H., Liu, W., et al. (2019). Bone marrow mesenchymal stem cell transplantation exerts neuroprotective effects following cerebral ischemia/reperfusion injury by inhibiting autophagy via the PI3K/Akt pathway. *Brain Res.* 1707, 124–132. doi: 10.1016/j.brainres.2018.11.018

He, X., Jiang, L., Dan, Q.-Q., Lv, Q., Hu, Y., Liu, J., et al. (2017). Bone marrow stromal cells promote neuroplasticity of cerebral ischemic rats via a phosphorylated CRMP2-mediated mechanism. *Behav. Brain Res.* 320, 494–503. doi: 10.1016/j.bbr.2016.10.027

Heemels, M.-T. (2016). Neurodegenerative diseases. *Nature* 539, 179–179. doi: 10.1038/539179a

Hochmeister, S., Engel, O., Adzemovic, M. Z., Pekar, T., Kendlbacher, P., Zeitelhofer, M., et al. (2016). Lipocalin-2 as an infection-related biomarker to predict clinical outcome in ischemic stroke. *PLoS One* 11:e0154797. doi: 10.1371/journal.pone.0154797

Iczkiewicz, J., Broom, L., Cooper, J. D., Wong, A. M. S., Rose, S., and Jenner, P. (2010). The RGD-containing peptide fragment of osteopontin protects tyrosine hydroxylase positive cells against toxic insult in primary ventral mesencephalic cultures and in the rat substantia nigra. *J. Neurochem.* 114, 1792–1804. doi: 10.1111/j.1471-4159.2010.06896.x

Iczkiewicz, J., Jackson, M. J., Smith, L. A., Rose, S., and Jenner, P. (2006). Osteopontin expression in substantia nigra in MPTP-treated primates and in Parkinson's disease. *Brain Res.* 1118, 239–250. doi: 10.1016/j.brainres.2006.08.036

Ishijima, M., Rittling, S. R., Yamashita, T., Tsuji, K., Kurosawa, H., Nifuji, A., et al. (2001). Enhancement of osteoclastic bone resorption and suppression of osteoblastic bone formation in response to reduced mechanical stress do not occur in the absence of osteopontin. *J. Exp. Med.* 193, 399–404. doi: 10.1084/jem.193.3.399

Jahromi, G. P., Pirsaraei, A. S., Sadr, S. S., Kaka, G., Jafari, M., Seidi, S., et al. (2015). Multipotent bone marrow stromal cell therapy promotes endogenous cell proliferation following ischemic stroke. *Clin. Exp. Pharmacol. Physiol.* 42, 1158–1167. doi: 10.1111/1440-1681.12466

Jarocha, D., Milczarek, O., Wedrychowicz, A., Kwiatkowski, S., and Majka, M. (2015). Continuous improvement after multiple mesenchymal stem cell transplantations in a patient with complete spinal cord injury. *Cell Transplant.* 24, 661–672. doi: 10.3727/096368915x687796

Jia, X., Liu, X.-A., Shi, Y., Yao, S., Zhong, X., Tian, Y., et al. (2020). Profiling of key brain nuclei involved in CNS control of stress and glucose homeostasis. *Biochem. Biophys. Res. Commun.* 521, 441–448. doi: 10.1016/j.bbrc.2019.10.072

Jin, M., Kim, J.-H., Jang, E., Lee, Y. M., Han, H. S., Woo, D. K., et al. (2014). Lipocalin-2 deficiency attenuates neuroinflammation and brain injury after transient middle cerebral artery occlusion in mice. *J. Cereb. Blood Flow Metab.* 34, 1306–1314. doi: 10.1038/jcbfm.2014.83

Jin, Y.-C., Lee, H., Kim, S.-W., Kim, I.-D., Lee, H.-K., Lee, Y., et al. (2016). Intranasal delivery of RGD Motif-containing osteopontin icosamer confers neuroprotection in the postischemic brain via alpha(v)beta(3) integrin binding. *Mol. Neurobiol.* 53, 5652–5663. doi: 10.1007/s12035-015-9480-z

Jing, M., Li, B., Hou, X., Shoba, J., Li, C., Liang, H., et al. (2013). OPN gene polymorphism and the serum OPN levels confer the susceptibility and prognosis of ischemic stroke in chinese patients. *Cell. Physiol. Biochem.* 32, 1798–1807. doi: 10.1159/000356613

Kane, M. J., and Engle, R. W. (2002). The role of prefrontal cortex in working-memory capacity, executive attention, and general fluid intelligence: an individual-differences perspective. *Psychonom. Bull. Rev.* 9, 637–671. doi: 10.3758/bf03196323

Kauffman, A. S., Clifton, D. K., and Steiner, R. A. (2007). Emerging ideas about kisspeptin-GPR54 signaling in the neuroendocrine regulation of reproduction. *Trends Neurosci.* 30, 504–511. doi: 10.1016/j.tins.2007.08.001

Khrimian, L., Obri, A., Ramos-Brossier, M., Rousseaud, A., Moriceau, S., Nicot, A.-S., et al. (2017). Gpr158 mediates osteocalcin's regulation of cognition. *J. Exp. Med.* 214, 2859–2873. doi: 10.1084/jem.20171320

Kim, B.-W., Jeong, K. H., Kim, J.-H., Jin, M., Kim, J.-H., Lee, M.-G., et al. (2016). Pathogenic Upregulation of glial lipocalin-2 in the Parkinsonian dopaminergic system. *J. Neurosci.* 36, 5608–5622. doi: 10.1523/jneurosci.4261-15.2016

Kim, Y.-J., Park, H.-J., Lee, G., Bang, O. Y., Ahn, Y. H., Joe, E., et al. (2009). Neuroprotective effects of human mesenchymal stem cells on dopaminergic neurons through anti-inflammatory action. *Glia* 57, 13–23. doi: 10.1002/glia.20731

Koide, M., and Kobayashi, Y. (2019). Regulatory mechanisms of sclerostin expression during bone remodeling. *J. Bone Miner. Metabol.* 37, 9–17. doi: 10.1007/s00774-018-0971-7

Kover, K., Yan, Y., Tong, P. Y., Watkins, D., Li, X., Tasch, J., et al. (2015). Osteocalcin protects pancreatic beta cell function and survival under high glucose conditions. *Biochem. Biophys. Res. Commun.* 462, 21–26. doi: 10.1016/j.bbrc.2015.04.095

Law, I. K. M., Xu, A., Lam, K. S. L., Berger, T., Mak, T. W., Vanhoutte, P. M., et al. (2010). Lipocalin-2 deficiency attenuates insulin resistance associated with aging and obesity. *Diabetes* 59, 872–882. doi: 10.2337/db09-1541

Lee, J. K., Jin, H. K., and Bae, J.-S. (2009). Bone marrow-derived mesenchymal stem cells reduce brain amyloid-beta deposition and accelerate the activation of microglia in an acutely induced Alzheimer's disease mouse model. *Neurosci. Lett.* 450, 136–141. doi: 10.1016/j.neulet.2008.11.059

Lee, S. H., Jin, K. S., Bang, O. Y., Kim, B. J., Park, S. J., Lee, N. H., et al. (2015). Differential migration of mesenchymal stem cells to ischemic regions after middle cerebral artery occlusion in rats. *PLoS One* 10:e0134920. doi: 10.1371/journal.pone.0134920

Lee, S., Kim, J.-H., Kim, J.-H., Seo, J.-W., Han, H.-S., Lee, W.-H., et al. (2011). Lipocalin-2 is a chemokine inducer in the central nervous system role of chemokine ligand 10 (CXCL10) in Lipocalin-2-induced cell migration. *J. Biol. Chem.* 286, 43855–43870. doi: 10.1074/jbc.M111.299248

Lee, S., Lee, W.-H., Lee, M.-S., Mori, K., and Suk, K. (2012). Regulation by lipocalin-2 of neuronal cell death, migration, and morphology. *J. Neurosci. Res.* 90, 540–550. doi: 10.1002/jnr.22779

Lin, Y. H., and Yang-Yen, H. F. (2001). The osteopontin-CD44 survival signal involves activation of the phosphatidylinositol 3-kinase/Akt signaling pathway. *J. Biol. Chem.* 276, 46024–46030. doi: 10.1074/jbc.M105132200

Liu, H., Kishi, T., Roseberry, A. G., Cai, X., Lee, C. E., Montez, J. M., et al. (2003). Transgenic mice expressing green fluorescent protein under the control of the melanocortin-4 receptor promoter. *J. Neurosci. Off. J. Soc. Neurosci.* 23, 7143–7154. doi: 10.1523/jneurosci.23-18-07143.2003

Liu, J.-M., Zhao, H.-Y., Ning, G., Chen, Y., Zhang, L.-Z., Sun, L.-H., et al. (2008). IGF-1 as an early marker for low bone mass or osteoporosis in premenopausal and postmenopausal women. *J. Bone Min. Metabol* 26, 159–164. doi: 10.1007/s00774-007-0799-z

Logsdon, A. F., Erickson, M. A., Rhea, E. M., Salameh, T. S., and Banks, W. A. (2018). Gut reactions: How the blood-brain barrier connects the microbiome and the brain. *Exp. Biol. Med.* 243, 159–165. doi: 10.1177/1535370217743766

Maetzler, W., Berg, D., Schalamberidze, N., Melms, A., Schott, K., Mueller, J. C., et al. (2007). Osteopontin is elevated in Parkinson's disease and its absence leads to reduced neurodegeneration in the MPTP model. *Neurobiol. Dis.* 25, 473–482. doi: 10.1016/j.nbd.2006.10.020

Magalingam, K. B., Radhakrishnan, A. K., and Haleagrahara, N. (2015). Protective mechanisms of flavonoids in Parkinson's disease. *Oxidat. Med. Cell. Longev.* 2015:314560. doi: 10.1155/2015/314560

Mazzali, M., Kipari, T., Ophascharoensuk, V., Wesson, J. A., Johnson, R., and Hughes, J. (2002). Osteopontin–a molecule for all seasons. *QJM Month. J. Associat. Phys.* 95, 3–13. doi: 10.1093/qjmed/95.1.3

Meller, R., Stevens, S. L., Minami, M., Cameron, J. A., King, S., Rosenzweig, H., et al. (2005). Neuroprotection by osteopontin in stroke. *J. Cereb. Blood Flow Metab. Off. J. Int. Soc. Cereb. Blood Flow Metabol.* 25, 217–225. doi: 10.1038/sj.jcbfm.9600022

Menzies, F. M., Fleming, A., and Rubinsztein, D. C. (2015). Compromised autophagy and neurodegenerative diseases. *Nat. Rev. Neurosci.* 16, 345–357. doi: 10.1038/nrn3961

Mesquita, S. D., Ferreira, A. C., Falcao, A. M., Sousa, J. C., Oliveira, T. G., Correia-Neves, M., et al. (2014). Lipocalin 2 modulates the cellular response to amyloid beta. *Cell Death Differentiat.* 21, 1588–1599. doi: 10.1038/cdd.2014.68

Mizokami, A., Kawakubo-Yasukochi, T., and Hirata, M. (2017). Osteocalcin and its endocrine functions. *Biochem. Pharmacol.* 132, 1–8. doi: 10.1016/j.bcp.2017.02.001

Mosialou, I., Shikhel, S., Liu, J.-M., Maurizi, A., Luo, N., He, Z., et al. (2017). MC4R-dependent suppression of appetite by bone-derived lipocalin 2. *Nature* 543, 385–390. doi: 10.1038/nature21697

Mucha, M., Skrzypiec, A. E., Schiavon, E., Attwood, B. K., Kucerova, E., and Pawlak, R. (2011). Lipocalin-2 controls neuronal excitability and anxiety by regulating dendritic spine formation and maturation. *Proc. Natl. Acad. Sci. U.S.A.* 108, 18436–18441. doi: 10.1073/pnas.1107936108

Munoz, J. R., Stoutenger, B. R., Robinson, A. P., Spees, J. L., and Prockop, D. J. (2005). Human stem/progenitor cells from bone marrow promote neurogenesis of endogenous neural stem cells in the hippocampus of mice. *Proc. Natl. Acad. Sci. U.S.A.* 102, 18171–18176. doi: 10.1073/pnas.0508945102

Nakazawa, K., Quirk, M. C., Chitwood, R. A., Watanabe, M., Yeckel, M. F., Sun, L. D., et al. (2002). Requirement for hippocampal CA3 NMDA receptors in associative memory recall. *Science (New York N. Y.)* 297, 211–218. doi: 10.1126/science.1071795

Naude, P. J. W., Csaba, N., Eiden, L. E., Ait-Ali, D., Van Der Heide, R., Engelborghs, S., et al. (2012). Lipocalin 2: novel component of proinflammatory signaling in Alzheimer's disease. *Faseb J.* 26, 2811–2823. doi: 10.1096/fj.11-202457

Nelson, A. M., Zhao, W., Gilliland, K. L., Zaenglein, A. L., Liu, W., and Thiboutot, D. M. (2008). Neutrophil gelatinase-associated lipocalin mediates 13-cis retinoic acid-induced apoptosis of human sebaceous gland cells. *J. Clin. Investigat.* 118, 1468–1478. doi: 10.1172/jci33869

Noelanders, R., and Vleminckx, K. (2017). How wnt signaling builds the brain: bridging development and disease. *Neuroscientist* 23, 314–329. doi: 10.1177/1073858416667270

Obri, A., Khrimian, L., Karsenty, G., and Oury, F. (2018). Osteocalcin in the brain: from embryonic development to age-related decline in cognition. *Nat. Rev. Endocrinol.* 14, 174–182. doi: 10.1038/nrendo.2017.181

Otto, E., Knapstein, P.-R., Jahn, D., Appelt, J., Frosch, K.-H., Tsitsilonis, S., et al. (2020). Crosstalk of brain and bone-clinical observations and their molecular bases. *Int. J. Mol. Sci.* 21:4946. doi: 10.3390/ijms21144946

Oury, F., Khrimian, L., Denny, C. A., Gardin, A., Chamouni, A., Goeden, N., et al. (2013). Maternal and offspring pools of osteocalcin influence brain development and functions. *Cell* 155, 228–241. doi: 10.1016/j.cell.2013.08.042

Park, H.-J., Shin, J. Y., Lee, B. R., Kim, H. O., and Lee, P. H. (2012). Mesenchymal Stem Cells augment neurogenesis in the subventricular zone and enhance differentiation of neural precursor cells into dopaminergic neurons in the substantia nigra of a parkinsonian model. *Cell Transplant.* 21, 1629–1640. doi: 10.3727/096368912x640556

Pawlak, R., Magarinos, A. M., Melchor, J., Mcewen, B., and Strickland, S. (2003). Tissue plasminogen activator in the amygdala is critical for stress-induced anxiety-like behavior. *Nat. Neurosci.* 6, 168–174. doi: 10.1038/nn998

Pernia, C., Tobe, B. T. D., O'donnell, R., and Snyder, E. Y. (2020). The evolution of stem cells, disease modeling, and drug discovery for neurological disorders. *Stem Cell. Dev.* 29, 1131–1141. doi: 10.1089/scd.2019.0217

Polivka, J. Jr., Polivka, J., Pesta, M., Rohan, V., Celedova, L., Mahajani, S., et al. (2019). Risks associated with the stroke predisposition at young age: facts and hypotheses in light of individualized predictive and preventive approach. *Epma J.* 10, 81–99. doi: 10.1007/s13167-019-00162-5

Price, P. A., Otsuka, A. A., Poser, J. W., Kristaponis, J., and Raman, N. (1976). Characterization of a gamma-carboxyglutamic acid-containing protein from bone. *Proc. Natl. Acad. Sci. U.S.A.* 73, 1447–1451. doi: 10.1073/pnas.73.5.1447

Puig, J., Blasco, G., Daunis-I-Estadella, J., Moreno, M., Molina, X., Alberich-Bayarri, A., et al. (2016). Lower serum osteocalcin concentrations are associated with brain microstructural changes and worse cognitive performance. *Clin. Endocrinol.* 84, 756–763. doi: 10.1111/cen.12954

Qin, Y., Pan, J., Cai, M., Yao, L., and Ji, Z. (2016). Pattern genes suggest functional connectivity of organs. *Sci. Rep.* 6:26501. doi: 10.1038/srep26501

Quiros-Gonzalez, I., and Yadav, V. K. (2014). Central genes, pathways and modules that regulate bone mass. *Arch. Biochem. Biophys.* 561, 130–136. doi: 10.1016/j.abb.2014.06.005

Reinholt, F. P., Hultenby, K., Oldberg, A., and Heinegard, D. (1990). Osteopontin–a possible anchor of osteoclasts to bone. *Proc. Natl. Acad. Sci. U.S.A.* 87, 4473–4475. doi: 10.1073/pnas.87.12.4473

Rentsendorj, A., Sheyn, J., Fuchs, D.-T., Daley, D., Salumbides, B. C., Schubloom, H. E., et al. (2018). A novel role for osteopontin in macrophage-mediated amyloid-beta clearance in Alzheimer's models. *Brain Behav. Immun.* 67, 163–180. doi: 10.1016/j.bbi.2017.08.019

Riek, R., and Eisenberg, D. S. (2016). The activities of amyloids from a structural perspective. *Nature* 539, 227–235. doi: 10.1038/nature20416

Roozendaal, B., Mcewen, B. S., and Chattarji, S. (2009). Stress, memory and the amygdala. *Nat. Rev. Neurosci.* 10, 423–433. doi: 10.1038/nrn2651

Rothwell, P. M., Coull, A. J., Giles, M. F., Howard, S. C., Silver, L. E., Bull, L. M., et al. (2004). Change in stroke incidence, mortality, case-fatality, severity, and risk factors in Oxfordshire, UK from 1981 to 2004 (Oxford Vascular Study). *Lancet (Lond. Engl.)* 363, 1925–1933. doi: 10.1016/s0140-6736(04)16405-2

Sabek, O. M., Nishimoto, S. K., Fraga, D., Tejpal, N., Ricordi, C., and Gaber, A. O. (2015). Osteocalcin effect on human beta-cells mass and function. *Endocrinology* 156, 3137–3146. doi: 10.1210/en.2015-1143

Sanchez-Ramos, J., Song, S., Cao, C., and Arendash, G. (2008). The potential of hematopoietic growth factors for treatment of Alzheimer's disease: a mini-review. *BMC Neurosci.* 9:S3. doi: 10.1186/1471-2202-9-s2-s3

Shah, A. D., Shoback, D., and Lewiecki, E. M. (2015). Sclerostin inhibition: a novel therapeutic approach in the treatment of osteoporosis. *Int. J. Womens health* 7, 565–580. doi: 10.2147/ijwh.s73244

Shetty, P., Ravindran, G., Sarang, S., Thakur, A. M., Rao, H. S., and Viswanathan, C. (2009). Clinical grade mesenchymal stem cells transdifferentiated under xenofree conditions alleviates motor deficiencies in a rat model of Parkinson's disease. *Cell Biol. Int.* 33, 830–838. doi: 10.1016/j.cellbi.2009.05.002

Simon, D. W., Mcgeachy, M. J., Bayir, H., Clark, R. S. B., Loane, D. J., and Kochanek, P. M. (2017). The far-reaching scope of neuroinflammation after traumatic brain injury. *Nat. Rev. Neurol.* 13, 171–191. doi: 10.1038/nrneurol.2017.13

Song, M. K., Lee, J. H., Kim, J., Kim, J. H., Hwang, S., Kim, Y.-S., et al. (2021). Neuroprotective effect of NXP031 in the MPTP-induced Parkinson's disease model. *Neurosci. Lett.* 740:135425. doi: 10.1016/j.neulet.2020.135425

Soukas, A., Cohen, P., Socci, N. D., and Friedman, J. M. (2000). Leptin-specific patterns of gene expression in white adipose tissue. *Genes Dev.* 14, 963–980.

Ste Marie, L., Miura, G. I., Marsh, D. J., Yagaloff, K., and Palmiter, R. D. (2000). A metabolic defect promotes obesity in mice lacking melanocortin-4 receptors. *Proc. Natl. Acad. Sci. U.S.A.* 97, 12339–12344. doi: 10.1073/pnas.220409497

Sun, Y., Yin, X. S., Guo, H., Han, R. K., He, R. D., and Chi, L. J. (2013). Elevated osteopontin levels in mild cognitive impairment and Alzheimer's disease. *Mediat. Inflamm.* 2013, 615745. doi: 10.1155/2013/615745

Talbot, K., and Wang, H.-Y. (2014). The nature, significance, and glucagon-like peptide-1 analog treatment of brain insulin resistance in Alzheimer's disease. *Alzheimers Demen.* 10, S12–S25. doi: 10.1016/j.jalz.2013.12.007

Tfilin, M., Sudai, E., Merenlender, A., Gispan, I., Yadid, G., and Turgeman, G. (2010). Mesenchymal stem cells increase hippocampal neurogenesis and counteract depressive-like behavior. *Mol. Psychiatry* 15, 1164–1175. doi: 10.1038/mp.2009.110

Thomas, R. M., Hotsenpiller, G., and Peterson, D. A. (2007). Acute psychosocial stress reduces cell survival in adult hippocampal neurogenesis without altering proliferation. *J. Neurosci.* 27, 2734–2743. doi: 10.1523/jneurosci.3849-06.2007

Tong, Z., Wu, X., Ovcharenko, D., Zhu, J., Chen, C.-S., and Kehrer, J. P. (2005). Neutrophil gelatinase-associated lipocalin as a survival factor. *Biochem. J.* 391, 441–448.

Uccelli, A., Benvenuto, F., Laroni, A., and Giunti, D. (2011). Neuroprotective features of mesenchymal stem cells. *Best Pract. Res. Clin. Haematol.* 24, 59–64. doi: 10.1016/j.beha.2011.01.004

Villeda, S. A., Luo, J., Mosher, K. I., Zou, B., Britschgi, M., Bieri, G., et al. (2011). The ageing systemic milieu negatively regulates neurogenesis and cognitive function. *Nature* 477, 90–U157. doi: 10.1038/nature10357

Villeda, S. A., Plambeck, K. E., Middeldorp, J., Castellano, J. M., Mosher, K. I., Luo, J., et al. (2014). Young blood reverses age-related impairments in cognitive function and synaptic plasticity in mice. *Nat. Med.* 20, 659–663. doi: 10.1038/nm.3569

Vuotto, C., Battistini, L., Caltagirone, C., and Borsellino, G. (2020). Gut microbiota and disorders of the central nervous system. *Neuroscientist* 26, 487–502. doi: 10.1177/1073858420918826

Wang, G., Weng, Y.-C., Han, X., Whaley, J. D., Mccrae, K. R., and Chou, W.-H. (2015). Lipocalin-2 released in response to cerebral ischaemia mediates reperfusion injury in mice. *J. Cell. Mol. Med.* 19, 1637–1645. doi: 10.1111/jcmm.12538

Wang, J., Huang, J., Zhu, M., Chen, S., Chen, C., Miao, C., et al. (2019). Osteopontin potentiates PM-induced IL-1 alpha and IL-1 beta production via the ERK/JNK

signaling pathway. *Ecotoxicol. Environ. Saf.* 171, 467–474. doi: 10.1016/j.ecoenv.2019.01.005

Weber, G. F., Ashkar, S., Glimcher, M. J., and Cantor, H. (1996). Receptor-ligand interaction between CD44 and osteopontin (Eta-1). *Science (New York N. Y.)* 271, 509–512. doi: 10.1126/science.271.5248.509

Wei, J., Hanna, T., Suda, N., Karsenty, G., and Ducy, P. (2014). Osteocalcin promotes beta-cell proliferation during development and adulthood through Gprc6a. *Diabetes* 63, 1021–1031. doi: 10.2337/db13-0887

Williams, B. O. (2014). Insights into the mechanisms of sclerostin action in regulating bone mass accrual. *J. Bone Miner. Res.* 29, 24–28. doi: 10.1002/jbmr.2154

Williams, L. J., Pasco, J. A., Jacka, F. N., Hodge, J. M., Kotowicz, M. A., and Berk, M. (2013). Quantitative Heel Ultrasound (QUS) measures of bone quality in association with mood and anxiety disorders. *J. Affect. Disord.* 146, 395–400. doi: 10.1016/j.jad.2012.09.025

Wu, C.-C., Wang, I. F., Chiang, P.-M., Wang, L.-C., Shen, C.-K. J., and Tsai, K.-J. (2017). G-CSF-mobilized bone marrow mesenchymal stem cells replenish neural lineages in Alzheimer's disease mice via CXCR4/SDF-1 chemotaxis. *Mol. Neurobiol.* 54, 6198–6212. doi: 10.1007/s12035-016-0122-x

Wung, J. K., Perry, G., Kowalski, A., Harris, P. L. R., Bishop, G. M., Trivedi, M. A., et al. (2007). Increased expression of the remodeling- and tumorigenic-associated factor osteopontin in pyramidal neurons of the Alzheimer's disease brain. *Curr. Alzheimer Res.* 4, 67–72. doi: 10.2174/156720507779939869

Wyss-Coray, T. (2016). Ageing, neurodegeneration and brain rejuvenation. *Nature* 539, 180–186. doi: 10.1038/nature20411

Xing, C., Wang, X., Cheng, C., Montaner, J., Mandeville, E., Leung, W., et al. (2014). Neuronal production of Lipocalin-2 as a help-me signal for glial activation. *Stroke* 45, 2085–2092. doi: 10.1161/strokeaha.114.005733

Yan, Q.-W., Yang, Q., Mody, N., Graham, T. E., Hsu, C.-H., Xu, Z., et al. (2007). The adipokine lipocalin 2 is regulated by obesity and promotes insulin resistance. *Diabetes* 56, 2533–2540. doi: 10.2337/db07-0007

Yokosaki, Y., Tanaka, K., Higashikawa, F., Yamashita, K., and Eboshida, A. (2005). Distinct structural requirements for binding of the integrins alphavbeta6, alphavbeta3, alphavbeta5, alpha5beta1 and alpha9beta1 to osteopontin. *Matr. Biol. J. Int. Soc. Matr. Biol.* 24, 418–427. doi: 10.1016/j.matbio.2005.05.005

Yoshitake, H., Rittling, S. R., Denhardt, D. T., and Noda, M. (1999). Osteopontin-deficient mice are resistant to ovariectomy-induced bone resorption. *Proc. Natl. Acad. Sci. U.S.A.* 96, 8156–8160. doi: 10.1073/pnas.96.14.8156

Yuan, J., Meloni, B. P., Shi, T., Bonser, A., Papadimitriou, J. M., Mastaglia, F. L., et al. (2019). The potential influence of bone-derived modulators on the progression of Alzheimer's disease. *J. Alzheimers Dis.* 69, 59–70. doi: 10.3233/jad-181249

Zhang, J., Li, Y., Chen, J., Yang, M., Katakowski, M., Lu, M., et al. (2004). Expression of insulin-like growth factor 1 and receptor in ischemic rats treated with human marrow stromal cells. *Brain Res.* 1030, 19–27. doi: 10.1016/j.brainres.2004.09.061

Zhou, Y., Yao, Y., Sheng, L., Zhang, J., Zhang, J. H., and Shao, A. (2020). Osteopontin as a candidate of therapeutic application for the acute brain injury. *J. Cell. Mol. Med.* 24, 8918–8929. doi: 10.1111/jcmm.15641

Conflict of Interest: The authors declare that the research was conducted in the absence of any commercial or financial relationships that could be construed as a potential conflict of interest.

Copyright © 2021 Chen, Shang, Wen and Liang. This is an open-access article distributed under the terms of the Creative Commons Attribution License (CC BY). The use, distribution or reproduction in other forums is permitted, provided the original author(s) and the copyright owner(s) are credited and that the original publication in this journal is cited, in accordance with accepted academic practice. No use, distribution or reproduction is permitted which does not comply with these terms.

Advantages of publishing in Frontiers

OPEN ACCESS
Articles are free to read for greatest visibility and readership

FAST PUBLICATION
Around 90 days from submission to decision

HIGH QUALITY PEER-REVIEW
Rigorous, collaborative, and constructive peer-review

TRANSPARENT PEER-REVIEW
Editors and reviewers acknowledged by name on published articles

Frontiers
Avenue du Tribunal-Fédéral 34
1005 Lausanne | Switzerland

Visit us: www.frontiersin.org
Contact us: frontiersin.org/about/contact

REPRODUCIBILITY OF RESEARCH
Support open data and methods to enhance research reproducibility

DIGITAL PUBLISHING
Articles designed for optimal readership across devices

FOLLOW US
@frontiersin

IMPACT METRICS
Advanced article metrics track visibility across digital media

EXTENSIVE PROMOTION
Marketing and promotion of impactful research

LOOP RESEARCH NETWORK
Our network increases your article's readership